The Dissertation Committee for Stephanie Anne Freeman Certifies that this is the approved version of the following dissertation:

Thermal Degradation and Oxidation of Aqueous Piperazine for Carbon Dioxide Capture

Committee:

Gary T. Rochelle, Supervisor

Jennifer Maynard

Danny Reible

Lynn Katz

James Critchfield

Thermal Degradation and Oxidation of Aqueous Piperazine for Carbon Dioxide Capture

by

Stephanie Anne Freeman, B.S.Ch.E; M.S.Ch.E.Prac.

Dissertation

Presented to the Faculty of the Graduate School of

The University of Texas at Austin

in Partial Fulfillment

of the Requirements

for the Degree of

Doctor of Philosophy

The University of Texas at Austin

May 2011

Dedication

To my parents

for always encouraging me to do more than I thought was possible

Acknowledgements

The dedication, support, and ingenuity of Prof. Gary Rochelle inspired me throughout the completion of this dissertation. Prof. Rochelle showed enormous compassion for me during my years in his group that I will be forever grateful for. His dedication to our research inspired in me the desire to strive for more and to not shy away from difficult problems that require collaboration and innovation to solve. His dedication to us, his graduate students, and his undergraduate students demonstrate his love of learning that is contagious and that we are all influenced by in his group.

I would like to thank the Luminant Carbon Management Program (LCMP) for kindly providing funding for our research group. None of my work could have been completed without the generosity of the 30+ companies that have been involved with the LCMP and the Industrial Associates Program.

I also sincerely appreciate the time and efforts of my committee members Prof. Jennifer Maynard, Prof. Danny Reible, Prof. Lynn Katz, and Dr. James (Jim) Critchfield. Dr. Jim Critchfield, as a former Rochelle Group member himself, has been an invaluable asset during my tenure here. He was always open and willing to share his 20+ years of gas treating and CO_2 capture experience with me.

To Maeve Cooney, I would like to thank you from the bottom of my heart for all your help throughout these four years. I know it can't be easy to work with over 15 PhD students day in and out but you do it with ease. You were always considerate and helpful, and I know you are appreciated.

Numerous people within the UT Austin community helped me along the way that deserve special acknowledgement. Jim Smitherman and Butch Cunningham of the UT

ChemE Machine Shop were always a tremendous help in fabricating items for the lab and were a riot to work with during recruitment weekends. Mike Ronalter of the UT Glass Shop is a genius of glass fabrication and designed and built my TOR reactors, a unique loader for $^{13}CO_2$ experiments, and fixed countless CO_2 loaders. Hector Garcia was enormously helpful in using the IC-MS/LC-MS system. Karin Keller of the UT Chemistry Department was also a priceless source of information when I was sorting through the science and art of MS. Steve Sorey and Jim Wallin of the UT Chemistry Department NMR Laboratory were always helpful in explaining NMR fundamentals to a chemical engineer trying to be a chemist. Finally, Kay Costales-Swift, Kevin Haynes, Eddie Ibarra, T Stockman, Karen Eikner, Randy Rife, Patrick Danielewski, and Tammy McDade of the UT Chemical Engineering Department were always supportive in a variety of capacities and a pleasure to work with day in and day out.

I would also like to that the graduate students that preceded me in the Rochelle Group during my residence: Dr. Eric Chen, Dr. Marcus Hilliard, Dr. Ross Dugas, Dr. Andrew Sexton, Dr. Jason Davis, Dr. Robert Tsai, Jorge Plaza, David Van Wagener, Sepideh Ziaii-Fashima, and Qing Xu. Thank you to Dr. Andrew Sexton and Dr. Jason Davis for dedicating numerous hours teaching me the nuances of the degradation and analytical methods. I would also like to acknowledge the group members that joined with me and after me: Fred Closmann, Thu Nguyen, Stuart Cohen, Peter Frailie, Alex Voice, Chao Wang, Lynn Li, Mandana Ashouri, Steven Fulk, Humera Rafique, and Omkar Namjoshi. My co-conspirator, Fred Closmann, was an invaluable resource throughout every day of my Ph.D. I always looked forward to our daily discussions of amine degradation and a million other topics. My undergraduate research assistants, Victoria Chávez, Andy Rachlin, and James Krasnov, were a huge help and I hoped learned something in the process of working on my project.

I would also like to thank my closest friends outside of the lab for supporting me: Peter Layshock, Christina Perpich, Monica Kem, Dr. Landry "Laos Lightning" Khounlavong, Misty "Misty May" Heitsch, Dr. Robert "BobbyT" Tsai, Dr. Brent "Mountain Man" Bregenzer, Tracy "T-Bird" Hawkins, Dr. Reken "Brown Magic" Patel, Dr. Andrew Heitsch, Dan Barad, and Dr. Elizabeth (Van Wagner) Dees. I also want to acknowledge all my favorite ChemE girls from the ChEetahs intramural women's flag football team that I was lucky enough to play on for three years: Captain Dr. Jamie Sutherland, Misty Heitsch, Dr. Jen Pai, Jessica Shafer, Laurene Dobrowolski, Dr. Danielle Smith, Niki Davis, Dr. Diana Snelling, Dr. Andrea Miller, Dr. Alyson Sagle, Sloane Harris, Dr. Elizabeth Costner, Amanda Lanza, Kate Collier, Tyne Johns, Julie Cushen and our patient and long-suffering coaching staff of Dr. Ross Dugas and Dr. Jason Dees. Go ChEetahs!

Finally, the most important people have yet to be thanked. My family is the most supportive and generous family someone could ask for. We've all suffered trials and tribulations in the last four years that have made us stronger and brought us together. To my parents, it is difficult to express how thankful I am for your support and encouragement through the years. I knew I could always count on you to give me some supportive words after a rough day in the lab and remind me why I was here. I sincerely thank you for all your support and I know I am fortunate to have you as my parents. To my brothers and sisters, Greg, Kathryn, and Nathan, I'd like to thank for so many years of support. To Tracy, who has been especially supportive of my years of school, I'd like to thank you for all of your encouragement. Finally, I'd also like to posthumously thank my grandparents whose love of education instilled in me a desire to better myself from a very early age.

Thermal Degradation and Oxidation of Aqueous Piperazine for Carbon Dioxide Capture

Stephanie Anne Freeman, Ph.D.

The University of Texas at Austin, 2011

Supervisor: Gary T. Rochelle

Absorption-stripping with aqueous, concentrated piperazine (PZ) is a viable retrofit technology for post-combustion CO_2 capture from coal-fired power plants. The rate of thermal degradation and oxidation of PZ was investigated over a range of temperature, CO_2 loading, and PZ concentration. At 135 to 175 °C, degradation is first order in PZ with an activation energy of 183.5 kJ/mole. At 150 °C, the first order rate constant, k_1, for thermal degradation of 8 m PZ with 0.3 mol CO_2/mol alkalinity is 6.12×10^{-9} s^{-1}. After 20 weeks of degradation at 165 °C, 74% and 63%, respectively, of the nitrogen and carbon lost in the form of PZ and CO_2 was recovered in quantifiable degradation products. N-formylpiperazine, ammonium, and N-(2-aminoethyl) piperazine account for 57% and 45% of nitrogen and carbon lost, respectively. Thermal degradation of PZ likely proceeds through S_N2 substitution reactions. In the suspected first step of the mechanism, 1-[2-[(2-aminoethyl) amino]ethyl] PZ is formed from a ring opening S_N2 reaction of PZ with H^+PZ. Formate was found to be generated during thermal degradation from CO_2 or CO_2-containing molecules.

An analysis of k_1 values was applied to a variety of amines screened for thermal stability in order to predict a maximum recommended stripper temperature. Morpholine, piperidine, PZ, and PZ derivatives were found to be the most stable with an allowable stripper temperature above 160 °C. Long-chain alkyl amines or alkanolamines such as N-(2-hydroxyethyl)ethylenediamine and diethanolamine were found to be the most unstable with an allowable stripper temperature below 120 °C.

Iron (Fe^{2+}) and stainless steel metals (Fe^{2+}, Ni^{2+}, and Cr^{3+}) were found to be only weak catalysts for oxidation of PZ, while oxidation was rapidly catalyzed by copper (Cu^{2+}). In a system with Fe^{2+} or SSM, 5 kPa O_2 in the inlet flue gas, a 55 °C absorber, and one-third residence time with O_2, the maximum loss rate of PZ is expected to 0.23 mol PZ/kg solvent in one year of operation. Under the same conditions but with Cu^{2+} present, the loss rate of PZ is predicted to be 1.23 mole PZ/kg solvent in one year of operation. Inhibitor A was found to be effective at decreasing PZ loss catalyzed by Cu^{2+}. Ethylenediamine, carboxylate ions, and amides were the only identified oxidation products. Total organic carbon analysis and overall mass balances indicate a large concentration of unidentified oxidation products.

Table of Contents

List of Tables

List of Figures

Chapter 1 – Introduction

1.1 ANTHROPOGENIC CARBON DIOXIDE (CO_2) EMISSIONS

The levels of carbon dioxide (CO_2) in the atmosphere have been steadily rising since the industrial revolution. The Intergovermental Panel on Climate Change (IPCC) recently estimated that CO_2 levels have increased 30% since pre-industrial times and are currently increasing 0.4% per year (IPCC, 2001). Primary causation for the change in atmospheric conditions and global climate change is anthropogenic CO_2 releases and deforestation (IPCC, 2001).

The CO_2 emissions from electricity generated from the combustion of coal constitute a large fraction of overall CO_2 emissions, up to 33% of across the board CO_2 emissions for 2006 (EIA, 2007a). As shown in Figure 1.1, the CO_2 emissions from electricity generation, differentiated by individual fuel sources, have increased

approximately ten times since 1949. Emissions from coal combustion are dominant as compared to petroleum or natural gas combustion. In addition, coal combustion has the largest CO_2 emissions per kilowatt of power generated at 2.10 compared to 1.97 and 1.32 for petroleum and natural gas, respectively (IPCC, 2001). In terms of GHG emissions, electricity derived from coal is the least efficient and most detrimental to our atmosphere.

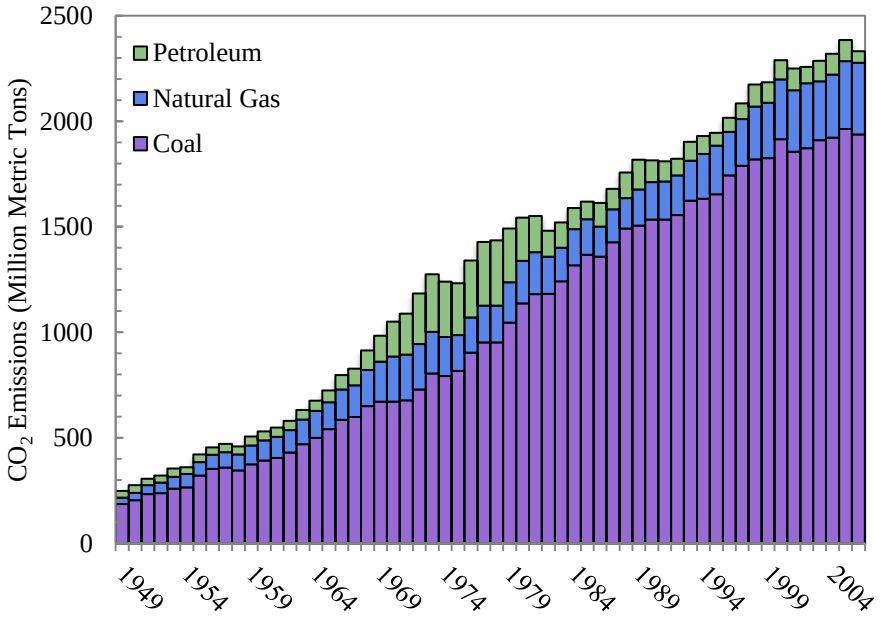

Figure 1.1: CO_2 Emissions in the US Since 1949 in the Electricity Generation Sector (EIA, 2007a)

Despite its obvious environmental disadvantages, coal continues to be a favorite method of electricity generation throughout the world, most notably in China and the US. It was estimated in 2006 that China was building a new coal-fired power plant at the rate of one every week to 10 days (Bradsher and Barboza, 2006). China is experiencing a burgeoning industrialization and newly built coal fired power plants are a large part of China's growing industrial emissions as they lead the world in annual coal production (Thieleman et al., 2007). The US has extensive coal reserves while only 49% of US

electricity is generated from coal in 2006, compared to 80% of Chinese electricity while in the same year (EIA, 2007b; Watts, 2005).

The fact that coal-fired power plants are large, stationary, point sources of CO_2 makes them the perfect candidate for a focused attempt at decreasing world-wide CO_2 emissions. With post-combustion CO_2 capture technology, for example, plants can be retrofitted with additional units that perform the needed capture of CO_2 without interfering with existing plant operations. Outside of a loss of electricity generating capacity, the power plant remains untouched and unaffected by the CO_2 control measures implemented on the waste flue gas.

1.2 CARBON DIOXIDE CAPTURE USING AMINE-BASED ABSORPTION-STRIPPING

The most promising technology for CO_2 capture is the post-combustion removal of CO_2 with an absorption-stripping system using an aqueous, amine solvent (Bottoms, 1930; Rochelle, 2009). Alkanolamines such as monoethanolamine (MEA) and diethanolamine (DEA) have been traditionally investigated for this application (Aaron and Tsouris, 2005; Bottoms, 1930; Hilliard, 2008). Other amines such as 2-amino-2-methyl-1-propanol (AMP) (Arcis et al., 2007; Mandal and Bandyopadhyay, 2006; Mandal et al., 2005; Paul and Mandal, 2006b; Reza and Trejo, 2006) and diglycolamine (DGA®) (Huntsman Corporation, 2005; Al-Juaied and Rochelle, 2006a; Al-Juaied and Rochelle, 2006b; Al-Juaied and Rochelle, 2006c; Al-Juaied, 2004) have been proposed as well. Piperazine (PZ) has been proposed as a kinetic promoter in a blend with methyldiethanolamine (MDEA) (Bishnoi, 2000; Bishnoi and Rochelle, 2000b; Bishnoi and Rochelle, 2002a; Bishnoi and Rochelle, 2002b; Derks et al., 2008; Liu et al., 1999; Paul and Mandal, 2006a; Paul and Mandal, 2006b; Zhang et al., 2001), AMP (Paul and Mandal, 2006a; Paul and Mandal, 2006b; Samanta and Bandyopadhyay, 2009; Sun et al.,

2005; Yang et al., 2010), or potassium carbonate (Cullinane and Rochelle, 2004; Cullinane and Rochelle, 2005; Cullinane and Rochelle, 2006; Oyenekan and Rochelle, 2009; Plaza et al., 2009) to enhance the rate of CO_2 absorption.

Absorption-stripping systems for CO_2 capture are based on a recycled flow of aqueous amine solution that absorbs CO_2 in the absorber and then regenerates the solvent in the stripper (Figure 1.2). Lean amine enters the top of the absorber and absorbs CO_2 while descending through the column, counter-currently contacting the flue gas. The rich amine exiting the absorber is sent to the main cross exchanger to be heated using the hot lean stream leaving the stripper. The rich solvent enters the top of the stripper and the solution flashes to release any remaining oxygen (O_2) in solution and a portion of the CO_2. The rich solution flows down the stripper and steam heating is used to desorb the captured CO_2. The stripper reboiler is heated with steam taken off of the medium pressure turbines in the coal-fired steam cycle in the power plant. This steam draw off point can be optimized, but will likely be at the intermediate pressure/low pressure (IP/LP) crossover in existing plants that are being retrofitted.

1.3 SOLVENT LOSSES IN ABSORPTION-STRIPPING SYSTEMS

Solvent losses in an absorption-stripping system can occur at multiple points in the system through different processes. As shown in Figure 1.3 below, solvent losses occur through three primary avenues: volatility, oxidation, and thermal degradation.

Volatility is the loss of volatile amine off the top of the absorber in the exiting, treated flue gas. A well-designed water wash column can be used to treat the flue gas exiting the top of the absorber to recover a majority of the amine lost through volatility and this approach can typically mitigate or completely control volatile losses. The volatility of an amine can be precisely measured using an equilibrium cell, such as is used

in the Rochelle laboratory (Nguyen et al., 2010). This path of amine loss in generally well characterized.

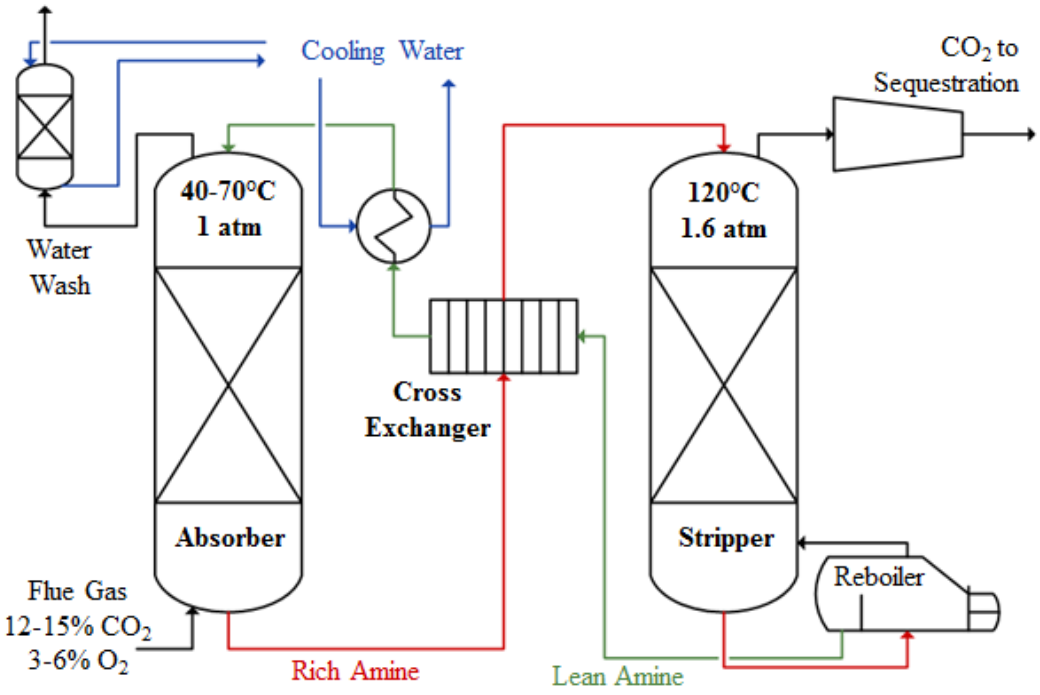

Figure 1.2: Schematic of typical amine-based absorption-stripping system for coal-fired flue gas

Oxidation is the chemical reaction of the amine with dissolved O_2 which enters the system with the flue gas. Oxidation occurs primarily in the absorber sump, absorber packing, and piping leading to the heat exchanger. Any O_2 remaining after the main cross exchanger will flash at the top of the stripper. In the absorber and absorber sump, the primary process to account for solvent loss is degradation of the amine through oxidation. Flue gas typically contains 3-5% O_2 that is carried into the absorber where it can react with the amine. The hold-up time in a sump is estimated to be 5 to 10 minutes, allowing oxidation reactions sufficient time to impact solvent loss. Research is needed into the oxidation characteristics of a specific amine in order to measure the expected loss

in this area of the system. Oxidation reactions, in general, involve fragmentation of the amine into a host of degradation products that can further react with each other, more O_2, or the amine to produce more degradation products. Oxidation of amines is not well characterized for most amines as the primary degradation products are still being identified.

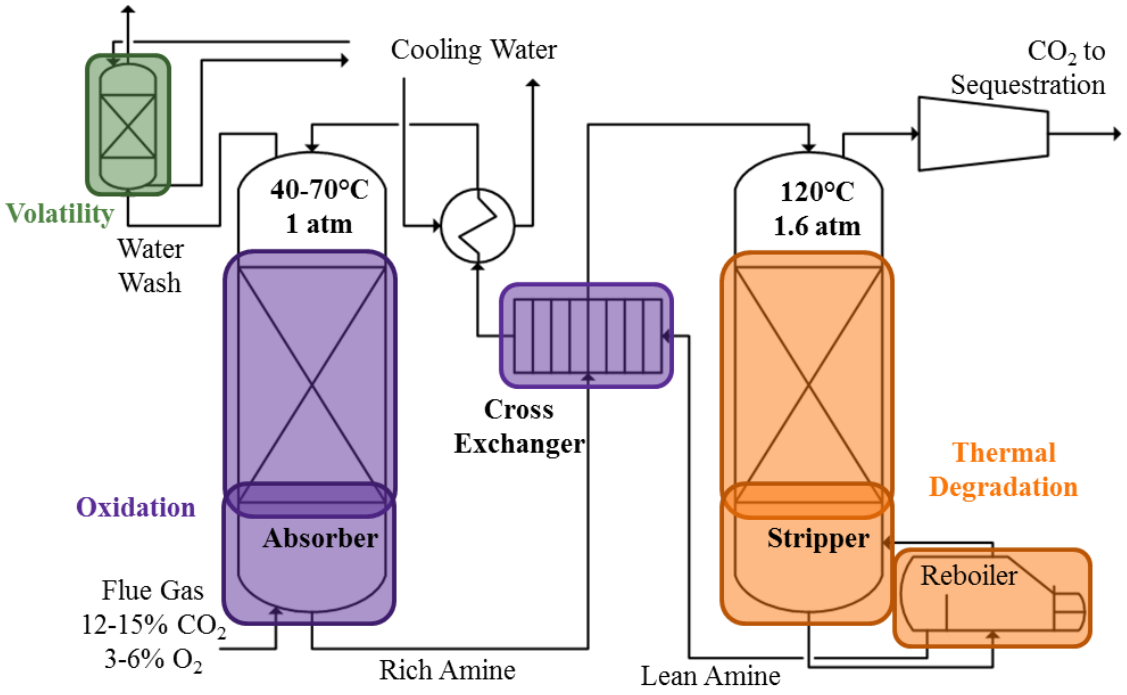

Figure 1.3: Schematic of absorption-stripping system with primary modes of amine loss highlighted

In the main cross-exchanger, the amine loss is primarily due to oxidation from any O_2 carried over from the absorber sump while there may be some thermal degradation of the rich amine as it exits the exchanger at high temperature and is fed to the stripper. This is also the primary area where the collaborative effect of oxidation and increased temperature are seen. Even with a temperature bulge in the absorber that may reach 70 °C, if any O_2 is present in the solution as it reaches the exit of the cross

exchanger, temperatures would be closer to 100 °C, and a significant effect of high temperature oxidation could be seen (Closmann and Rochelle, 2011; Plaza et al., 2009). The study of collaborative oxidation and thermal degradation, or high temperature oxidation, is area of research is decidedly lacking in that all research to date has focused on either oxidation or thermal degradation of amines separately. The collaborative effect is an important area where research is needed to fully understand the degradation characteristics of a solvent.

Thermal degradation is the reaction of an amine to degradation products based on exposure to high temperature. Stripper operating temperatures in current designs are between 100 and 120°C, significantly higher than the absorber. At these temperatures, the kinetic rates of degradation reactions that are suppressed in the absorber are elevated and cause solvent enhanced losses. Thermal degradation primarily occurs in the stripper packing (if present), stripper sump, reboiler, reclaiming system (if present) and may occur in the piping leading from the main cross exchanger to the stripper, if temperatures are high enough. If a thermal reclaiming system is used, the solvent would be subjected to high temperature degradation here as well. Novel stripper designs that do not include packing, such as flash-based designs, are still subject to thermal degradation (VanWagener and Rochelle, 2011). As with the absorber, the sump hold-up is between 5 and 10 minutes, allowing adequate time for significant amine loss.

The oxidation and thermal degradation of concentrated, aqueous PZ has not been explored previously outside of screening experiments. Preliminary tests showed enhanced resistance to both oxidation and thermal degradation, a significant advantage for this solvent (Davis, 2009; Sexton, 2008). PZ and PZ-based solvents also have advantageous kinetic rates and CO_2 capacity. The degradation characteristics of

concentrated PZ need to be fully understood before appropriate application of the solvent in pilot, demonstrate, and full scale CO_2 absorption-stripping systems.

This dissertation is focused on investigating the thermal degradation and oxidation of concentrated, aqueous PZ for use in CO_2 absorption-stripping systems. Experiments were designed to represent real systems as closely as possible

1.4 RESEARCH OBJECTIVES

The baseline solvent that has been used for CO_2 capture using aqueous amine solvents in an absorber-stripper system is MEA. This solvent has been studied extensively and has been proven at the pilot plant and demonstration level (Arnold et al., 1982; St.Clair and Simister, 1983). MEA has numerous advantageous properties such as high solubility in water, useful kinetic absorption rates, low viscosity, high heat of absorption of CO_2, ease of handling, and low cost. On the other hand, there are many disadvantages to this solvent that may prove to limit its use in industry. MEA degrades heavily at high temperatures, as found in the stripper, and in the presence of O_2, as found in the absorber (Davis, 2009; Davis and Rochelle, 2009; Sexton, 2008; Sexton and Rochelle, 2009b; Sexton and Rochelle, 2009c). MEA degrades to form heat-stable salts and polymerized products that permanently remove capacity from the solvent and increase corrosivity of the solution toward carbon steel equipment.

PZ offers a solution to some problems experienced by MEA. Preliminary investigations into PZ show a significant improvement in the areas of thermal and oxidative degradation over MEA (Davis, 2009; Sexton, 2008). Additionally, PZ has enhanced kinetic absorption rates, almost 1.5 times that of MEA (Dugas, 2008). Being a diamine, the capacity of PZ is also increased over MEA, a monoamine, which directly leads to the requirement of smaller equipment designs and less pump work. On the other

hand, PZ does have the disadvantage of high viscosity and low solubility in water, both of which create handling issues and may increase pump work.

The overall goal of this project is to explore the efficacy of concentrated, aqueous PZ as a solvent for industrial CO_2 capture applications. Since little work has been done on this subject previously, the first major hurdle is to understand the degradation characteristics of the system and discover ways to minimize solvent loss. The study of PZ degradation is a portion of a project that seeks to develop PZ as a viable solvent for CO_2 capture applications. Other parts of that project include rigorous analysis of PZ solid solubility, more extensive rate measurements, heat of absorption measurements, and eventual pilot and demonstration level projects with the help of industrial sponsors in order to evaluate the performance of the solvent.

Hilliard and Xu have measured the high and low temperature CO_2 solubility in PZ and Nguyen has measured PZ volatility over a range of conditions (Hilliard, 2008; Nguyen et al., 2010; Xu and Rochelle, 2011). With these thermodynamic properties, Frailie and Plaza have developed a thermodynamic model (Guy Fawkes model) for concentrated, aqueous PZ solutions which is useful for predicting speciation over a range of temperature and CO_2 loadings (Frailie et al., 2011; Plaza and Rochelle, 2010). Bishnoi, Cullinane, and Dugas have measured the rate of CO_2 absorption in aqueous PZ (Bishnoi and Rochelle, 2000a; Cullinane and Rochelle, 2006; Dugas, 2009). Van Wagener has utilized the Guy Fawkes model to predict the equivalent work of various stripper configurations for concentrated PZ systems (VanWagener and Rochelle, 2011).

Concentrated, aqueous PZ was identified as thermally stable in the presence of CO_2 based on a single screening experiment performed by Davis at during the course of a project focused on the thermal degradation of MEA (Davis, 2009). Davis determined PZ to be stable through a lack of degradation after 4 weeks at 135 °C, but did not identify

any degradation products. Early work on PZ oxidation as a promoter for potassium carbonate demonstrated resistance to oxidation of this blend compared to MEA (Alawode, 2005; Jones, 2003). Sexton also identified low concentration (2.5 and 5 m) aqueous PZ as stable to oxidation in the presence of up to 5 mM Fe^{2+}, but did not perform more concentrated experiments or identify any degradation products (Sexton, 2008). A few structural analogs of PZ such as 1,4-dimethylpiperazine, EDA, and substituted EDAs have been screened for thermal stability at low temperature (135 °C) with only a few degradation products identified (Eide-Haugmo et al., 2011; Lepaumier et al., 2009a).

The degradation of PZ is one important aspect to understand in the development of this solvent. The specific goals of this dissertation were split into three categories relating to thermal degradation, oxidation, or physical properties. The specific goals were as follows:

Objectives for studying PZ thermal degradation

1. Quantify the rate of PZ thermal degradation at conditions representative of the stripper, stripper sump and reboiler of a CO_2 capture system.
2. Identify and quantify degradation products from PZ thermal degradation.
3. Develop a fundamental understanding of the mechanisms that produce the primary thermal degradation products of PZ.
4. Estimate the rate of PZ loss due to thermal degradation at industrially relevant conditions.

Objectives for studying PZ oxidation

1. Quantify the rate of PZ oxidation at conditions representative of the absorber and absorber sump of a CO_2 capture system.

2. Identify and quantify degradation products of PZ oxidation.
3. Evaluate the effect of metal catalysts on the oxidative degradation of PZ.
4. Evaluate effectiveness of inhibitors in decreasing oxidation of PZ.
5. Estimate the rate of PZ loss due to oxidation at industrially relevant conditions

Objectives for studying the physical properties of PZ

1. Measure the viscosity and density of concentrated PZ solutions over a useful range of CO_2 loading, PZ concentrations, and temperature.
2. Study the PZ solid solubility in order to determine the CO_2 loading, PZ concentration, and temperature were aqueous solutions exist.

Chapter 2 - Concentrated, Aqueous Piperazine as a Solvent for CO_2 Capture

The primary purpose of this chapter is to establish concentrated, aqueous PZ as a viable solvent for post-combustion CO_2 capture from coal-fired flue gas using amine based absorption-stripping. This is achieved by describing the relevant speciation, history of the solvent, physical properties, and thermodynamic properties that would be important for designing a full scale PZ-based CO_2 capture system. From within these topics, the important advantages and disadvantages of PZ can be ascertained. Sections of this chapter are taken from a published paper where PZ was first discussed as a novel solvent (Freeman et al., 2010b).

The secondary purpose of this chapter is to serve as an overview of literature relevant to the degradation of concentrated PZ systems, but is not all inclusive. An

extensive review of literature relating to a variety of amine solvents, comparisons of kinetic rates, degradation mechanisms, and other important thermodynamic properties has been completed previously (Rochelle et al., 2001). All-encompassing reviews of literature relating to the oxidation and thermal degradation of amines have been done previously with a focus on MEA (Davis, 2009; Sexton, 2008). The degradation literature, as it particularly pertains to PZ, is expanded beyond what has been explored previously. Additional literature is included in subsequent chapters when appropriate to the subject being discussed.

2.1 PIPERAZINE (PZ) AND ITS SPECIATION

Piperazine (PZ) is a cyclic diamine with a molecular formula of $C_4H_{10}N_2$ that is crystalline in its pure anhydrous form at room temperature. When exposed to water, either in aqueous solution or absorbed from air, PZ can easily hydrate to form PZ hexahydrate ($PZ{\cdot}6H_2O$). In aqueous solution with CO_2, the two amino functions on PZ can react and create numerous PZ-based species. The PZ species present in solution, as shown in Figure 2.1, include PZ carbamate ($PZCOO^-$), PZ dicarbamate ($PZ(COO^-)_2$), protonated PZ (H^+PZ), deprotonated PZ ($H_2^{+2}PZ$), and protonated PZ carbamate (H^+PZCOO^-).

The speciation of PZ in solution is a function of the CO_2 concentration, or CO_2 loading. In the absence of CO_2 in solution, PZ exists primarily as free PZ with a small portion of H^+PZ. As the CO_2 concentration increases, $PZCOO^-$ begins to form with the H^+PZ concentration increasing and the free PZ concentration decreasing. Once a CO_2 loading of about 0.28 mole CO_2 per mole alkalinity is reached, $PZCOO^-$ reaches its maximum concentration and H^+PZ begins to level out. Leading up to this loading, the concentration of H^+PZCOO^- is steadily increasing, lagging the production of both H^+PZ

and $PZCOO^-$. After a loading of 0.28 mole CO_2 per mole alkalinity, the concentrations of H^+PZ, $PZCOO^-$, and free PZ are decreasing while H^+PZCOO^- is increasing. A loading of 0.5 mole CO_2 per mole alkalinity represents the amount of CO_2 needed in order to have half of the PZ basic groups react with CO_2 while the other half are protonated. This is essentially the maximum realistic loading. At this point, the solution is primarily made up of the zwitterion H^+PZCOO^- with a small concentration of H^+PZ present. Through the entire range of loading, the concentration of $PZ(COO^-)_2$ is very small, demonstrating that this species is not a preferred form of PZ. The concentrations of H^+PZH^+ and $PZ(COO^-)_2$ are not represented on the graph because their concentrations are nearly negligible.

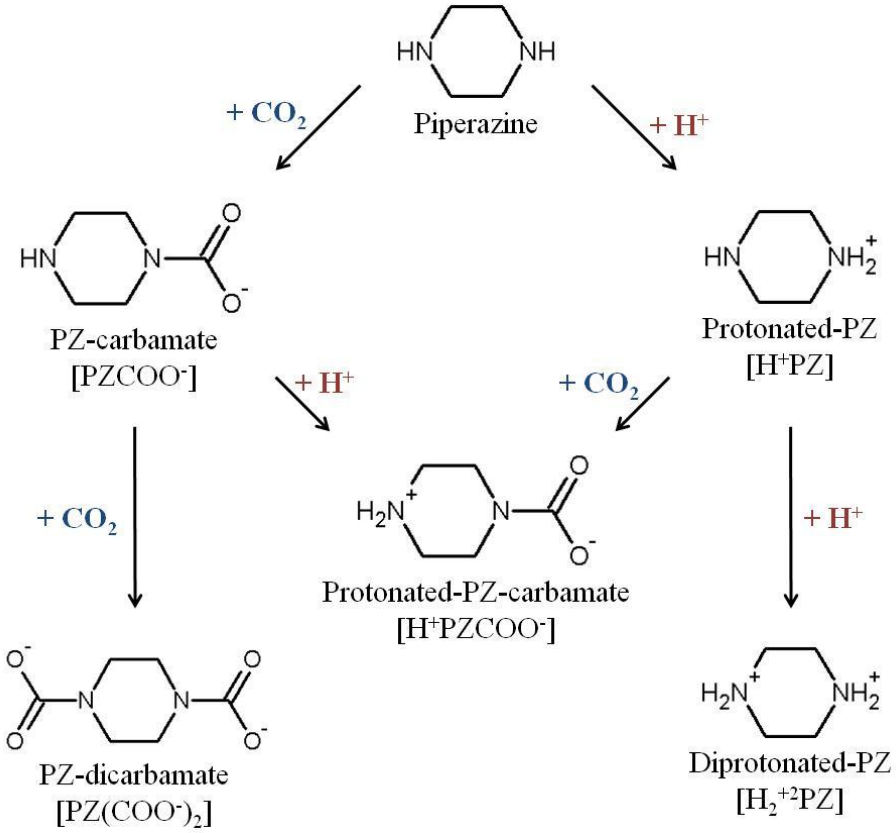

Figure 2.1: Speciation of PZ in aqueous solutions

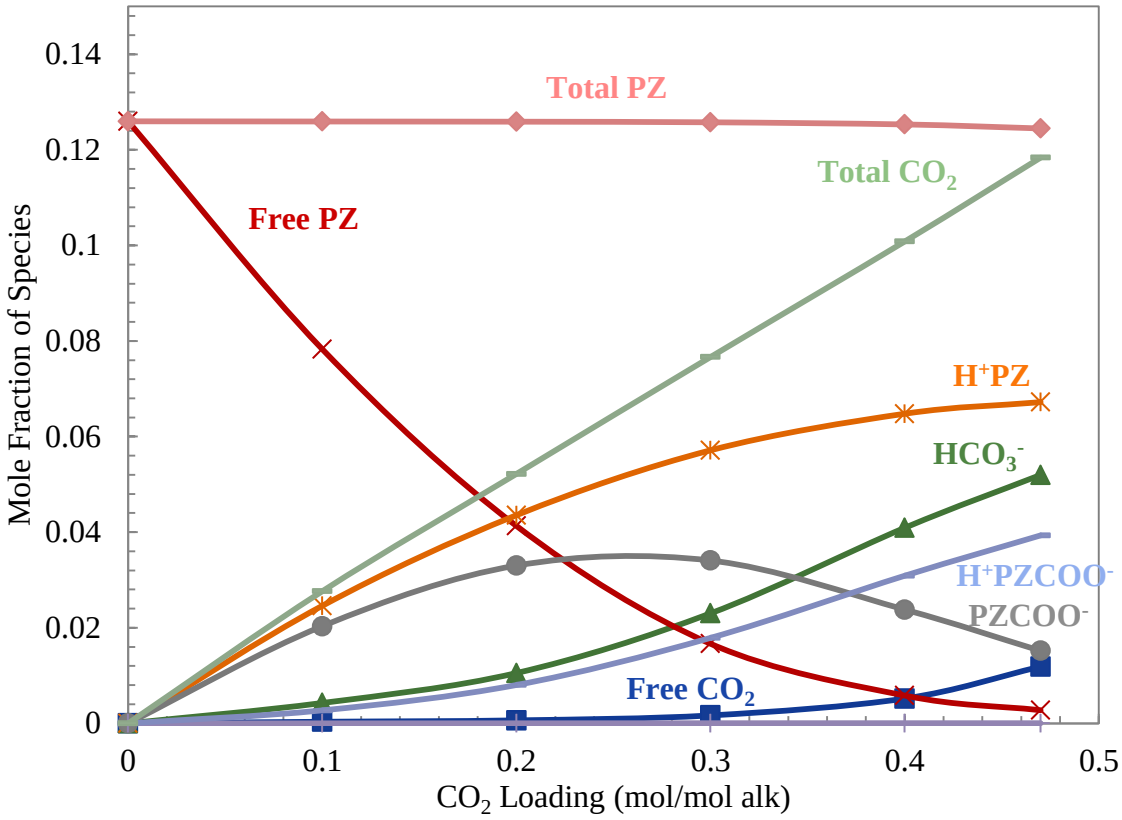

Figure 2.2: Speciation of 8 m PZ at 40°C (Frailie et al., 2011)

2.2 HISTORICAL USE OF PZ

2.2.1 PZ Used in gas treating

PZ was first identified as a possible promoter in alkanolamine solutions for use in gas treating in the 1980s (Appl et al., 1982). In gas treating, and the specific application of CO_2 capture, PZ has been identified as a kinetic promoter in amine systems with advantageous solution characteristics but diminished kinetic rates. In one of the first applications, a small concentration of PZ in combination with MDEA utilized the enhanced kinetic rate of the PZ molecule with the decreased heat of absorption of CO_2 of the tertiary amine, MDEA (Appl et al., 1982; Bishnoi and Rochelle, 2002a; Xu et al., 1992; Zhang et al., 2001). Another example is potassium carbonate ($K^+CO_3^-$)/PZ systems

where PZ enhances the overall kinetic rate of the system (Chen, 2007; Cullinane and Rochelle, 2004; Hilliard, 2008). Since its start as a kinetic promoter, the properties of PZ have been studied to determine its efficacy and usefulness in gas treating and CO_2 capture applications.

Although researchers quickly identified that PZ had enhanced reaction rates with CO_2, the limited solubility of PZ restricted its use to below 2.0 or 2.5 molal (m) in blended amine systems. Most literature available on PZ is either a blended system, where solubility issues are remediated by dilution in another solvent, or at very low PZ concentration, below the 1.9 m PZ solubility limit at room temperature.

2.2.2 Pharmaceutical use of PZ

Outside of the CO_2 capture field, PZ is a backbone molecule used in the pharmaceutical industry since 1953 in various types of stimulants (antidepressants), antihistamines, antipsychotics, and is contained in numerous recreational drugs (Mouriquand et al., 1951; White and Standen, 1953). PZ itself has anthelmintic properties and is used as a deworming agent for humans and animals with great efficacy in the form of PZ hydrate or PZ citrate (Brown and Chan, 1955; Brown and Sterman, 1954). The use of PZ as a pharmaceutical agent has also motivated more recent interest in research on the treatment of drinking water contaminated with PZ or molecules containing the PZ moiety (Burhenne et al., 1997; Dewitte et al., 2008; Dodd et al., 2006; Pietsch et al., 2001; Thabaj et al., 2007).

2.3 PHYSICAL AND THERMODYNAMIC PROPERTIES OF PZ

The physical properties of PZ have been studied since the compound was first identified. The low solubility of PZ has limited the amount of data available in literature for aqueous solutions of PZ above room temperature solubility.

2.3.1 Solid solubility of PZ

Previous authors have investigated the solid-liquid equilibrium (SLE) or solid solubility of PZ solutions. The SLE has been reported in terms of the transition temperature at which a given H_2O + PZ solution would experience a transition between the liquid or solid phase.

Bishnoi (2000) measured the SLE for unloaded PZ solutions by adding anhydrous PZ to a given amount of water and observing where crystallization occurred at a given temperature (Bishnoi, 2000). The solution was allowed to mix and reach equilibrium to allow any crystals to settle and separate from the aqueous phase. The resulting liquid was then titrated using 2 N HCl to determine the exact PZ concentration of the saturated, liquid phase. Bishnoi measured SLE for 0 to 70 °C which resulted in data for 0.5 to 40 m PZ solutions.

The Dow Chemical Company published physical property data for a group of ethylenediamines including PZ (The Dow Chemical Company, 2001). That brochure included a graph of SLE data for PZ in the form of temperatures (0 to 90 °C) and the corresponding wt % of PZ for SLE. The method of determination was not provided and data was read off of the graph manually with some inherent error. One solubility data point was also included in an MSDS published by Merck Corporation, a pharmaceutical company (Merck Corporation, 2009).

More recently, Hilliard (2008) determined solid-liquid equilibrium data for unloaded PZ solutions from heat capacity measurements on a differential scanning calorimeter (DSC) (Hilliard, 2008). The data was obtained for a wide range of PZ concentrations, from 0.5 to 40 m PZ (4.3 to 77 wt % PZ), and was calculated based on assigning the phase transition to the position of the maximum peak on the thermal profile when heating a sample from -10 to 100 °C. Finally, Muhammad and colleagues most

recently duplicated the data of Bishnoi using the same method and similar ranges of PZ concentration (Bishnoi, 2000; Muhammad et al., 2009).

All of the PZ solubility data described above is for unloaded solutions. No literature has been found that investigates SLE on the H_2O + PZ + CO_2 system. The data of the aforementioned authors can be summarized and compared on a figure showing the SLE for the H_2O + PZ system. The data from -10 to 80 °C and 0 to 0.80 weight fraction PZ is compared in Figure 2.3.

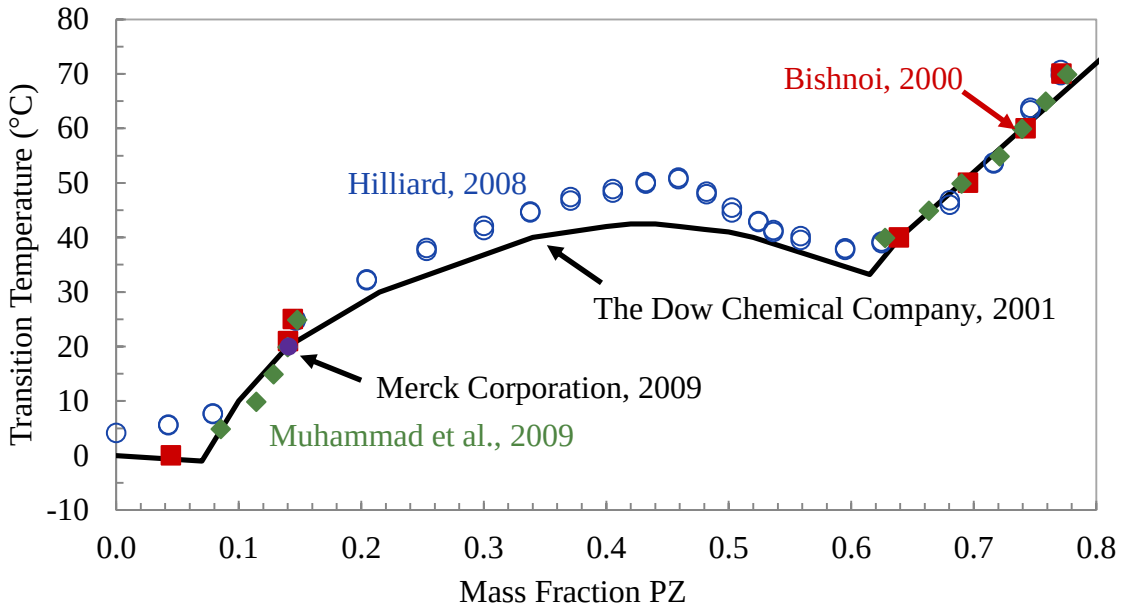

Figure 2.3: Comparison of Solid-Liquid Equilibrium Data for H_2O + PZ. Line: (The Dow Chemical Company, 2001). Data: ■, (Bishnoi, 2000); □, (Hilliard, 2008); ●, (Muhammad et al., 2009); ○, (Merck Corporation, 2009).

2.3.2 Density and viscosity of PZ solutions

There are numerous sources reporting the density and viscosity in aqueous, low concentration, unloaded PZ solutions (Cook and Lowe, 1976; Derks et al., 2005; Derks et al., 2008; Muhammad et al., 2009; Samanta and Bandyopadhyay, 2006). Physical

property data of aqueous PZ solutions loaded with CO_2 are of particular importance to this research but, unfortunately, this type of data are rare in the current literature. Chapter 4 of this thesis reports on the density and viscosity of loaded PZ solutions.

In comparison with other amine solvents of interest to CO_2 capture applications, PZ has high viscosity. The viscosity of 7, 8, 9, and 10 m PZ is compared with other amines in Figure 2.4 (Huntsman Corporation, 2005; Closmann et al., 2009). The amine concentration is plotted in units of moles alkalinity per kilogram of water in order to compare mono- and diamines on a similar basis. All of the viscosities shown in Figure 2.4 are at 40 °C and at the rich loading of the system (0.3 mole CO_2 per mole alkalinity for MDEA and MDEA/PZ blend; 0.4 mole CO_2 per mole alkalinity for PZ and DGA; 0.5 mole CO_2 per mole alkalinity for MEA).

Comparison of the viscosity on this basis demonstrates how the amine basic group affects overall viscosity. As the number of basic groups increases in a molecule, the viscosity increases in a linear direction. The viscosity of 8 m PZ is higher than that of 7 m MEA, but compared to 60 wt % DGA®, the viscosity of PZ is lower for a higher alkalinity. PZ has the advantage over DGA® of having two amine functional groups without suffering an increase in viscosity. DGA® solutions at 60 wt % are successfully used in natural gas treating (Al-Juaied and Rochelle, 2006b; Al-Juaied, 2004).

2.3.3 CO_2 solubility in PZ solutions

The solubility of CO_2 in concentrated, aqueous PZ has been studied by numerous authors in the Rochelle group. Ermatchkov and colleagues were the first to study CO_2 solubility in 1 to 4 m PZ at 40, 80, and 120 °C (313.15 to 393.15 K) (Ermatchkov et al., 2006). Hilliard measured CO_2 solubility using a low temperature vapor-liquid equilibrium cell for solutions up to 5 m PZ (Hilliard, 2008). Dugas measured CO_2

solubility using a wetted wall apparatus used to measure kinetic rates of CO_2 absorption (Dugas, 2009). As with other amines, Hilliard and Dugas both found the solubility of CO_2 in PZ to not be a function of CO_2 concentration, even up to 12 m PZ, so low PZ concentration data from other authors are still helpful (Dugas, 2009; Hilliard, 2008). A summary of CO_2 solubility gathered to date is provided in Figure 2.5 and is shown as the equilibrium partial pressure of CO_2 (P^*_{CO2}) plotted against the CO_2 loading in the liquid.

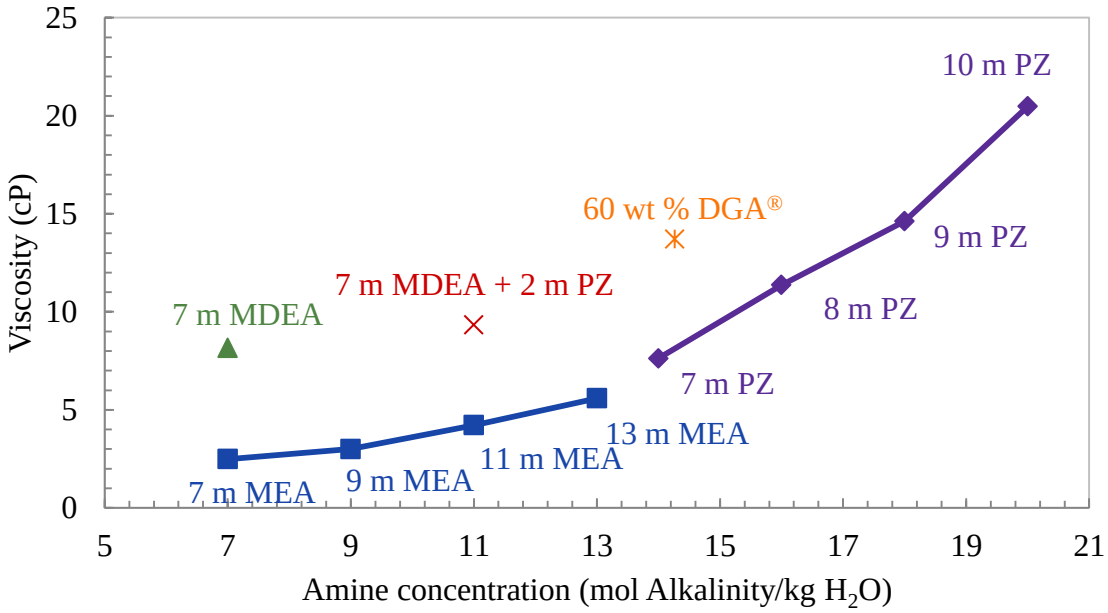

Figure 2.4: Viscosity of amine solutions at typical rich loading and 40 °C

The CO_2 solubility data for PZ were regressed by Xu cover 0.9 to 12 m PZ from 40 to 160 °C (Xu and Rochelle, 2011). The regression is the equilibrium partial pressure of CO_2 in Pa, P^*_{CO2}, in terms of temperature, T, in Kelvin, CO_2 loading, α, in mole CO_2 per mole alkalinity, and the universal gas constant, R, in kJ per mole-K, as shown in equation 2.1.

$$\mathrm{Ln}\left(P_{CO2}\right) = 35.5 - \left(91.54\frac{\mathrm{kJ}}{\mathrm{mol}}\right)\left(\frac{1}{RT}\right) - 18.0\alpha^2 + 4789\left(\frac{\alpha}{T}\right) + 9765\left(\frac{\alpha^2}{T}\right) \qquad (2.1)$$

CO_2 solubility data has been used to determine the expected rich and lean CO_2 loadings in a full-scale PZ absorption-stripping system. Based on the required partial pressure driving forces in the absorber, it is expected that the rich amine stream will have an P^*_{CO2} of 5 kPa (5000 Pa). This is to provide a small driving force between the inlet flue gas entering the bottom of the absorber with 13 to 15% CO_2, or 13 or 15 kPa (13000 to 15000 Pa). At the top of the absorber, the lean amine stream will have an P^*CO_2 of approximately 0.5 kPa (500 Pa) to provide a driving force with the gas stream exiting at 1.3 to 1.5% (130 to 150 Pa). Using the CO_2 solubility figure (Figure 2.5) with the expected P^*_{CO2} values, the expected CO_2 loadings can be determined directly. The dashed lines in Figure 2.5 indicate this procedure and show the expected lean and rich loadings of 0.31 and 0.41 mole CO_2 per mole alkalinity, respectively. These values will be used throughout this thesis as the standard CO_2 concentrations of interest.

The heat of absorption of CO_2 into an 8 m PZ solution was also estimated by Xu using the Gibbs-Helmholtz equation. The resulting expression for the heat of absorption in concentrated PZ is as follows (Equation 2.2).

$$\Delta H_{abs} = -R\frac{\partial\, \mathrm{Ln}P_{CO2}}{\partial\left(\frac{1}{T}\right)} = -R\left(-\frac{91542}{R} + 4789\alpha + 9765\alpha^2\right) \qquad (2.2)$$

2.3.4 CO_2 mass transfer rates in PZ

Mass transfer rates of CO_2 absorption into concentrated aqueous PZ were studied extensively in a wetted wall column (Dugas, 2009). The liquid-film mass transfer coefficient defined in gas-phase units, k_g', is plotted against equilibrium partial pressure of CO_2, P^*_{CO2}, for 8 m PZ and 7 m MEA at 40, 60, 80, and 100 °C in Figure 2.6 (Dugas and Rochelle, 2009). Rate data at 60, 80, and 100 °C are plotted as a function of the

equilibrium partial pressure of CO_2 at 40 °C. This x-axis provides a surrogate measurement of CO_2 loading and allows comparison of different solvents over their practical operating range.

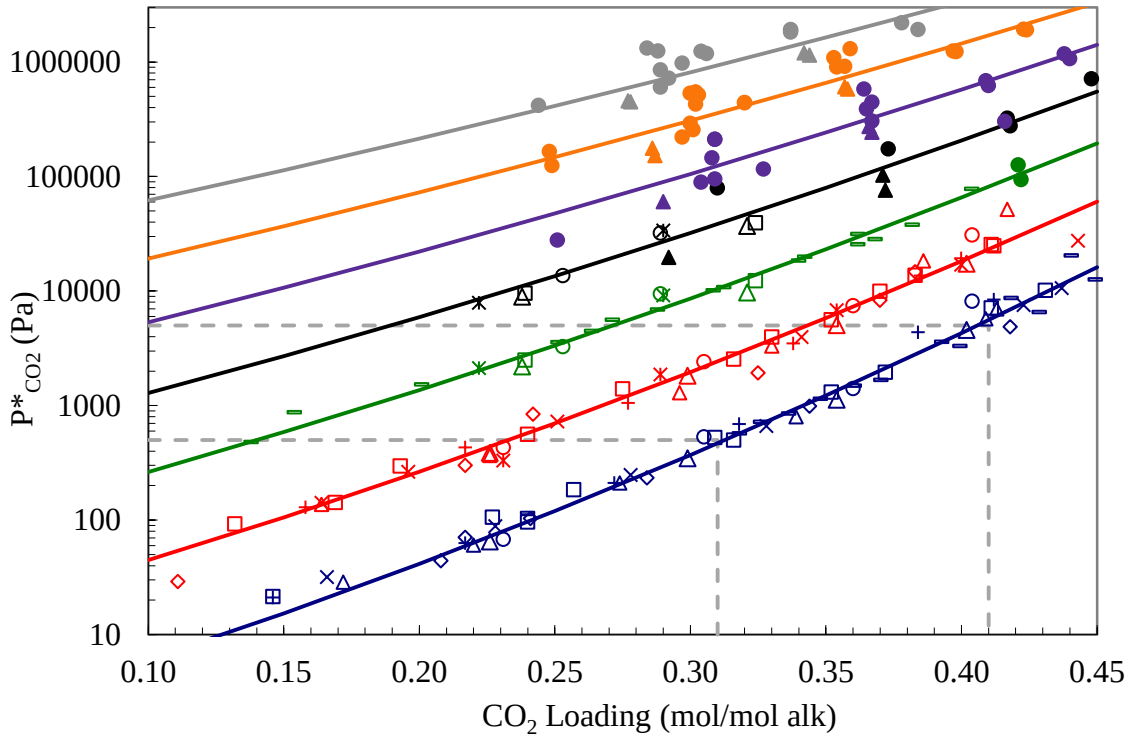

Figure 2.5: CO_2 solubility at 40 (blue), 60 (red), 80 (green), 100 (black), 120 (purple), 140 (orange), and 160 °C (gray). Data from (Dugas, 2009; Hilliard, 2008): 0.9 m, ◊; 2 m, □; 2.5 m, ×; 3.6 m, +; 5 m, Δ; 8 m, ○; 12 m *. Data from (Xu and Rochelle, 2011): 5 m, ▲; 8 m, ●. Data from (Ermatchkov et al., 2006): ─, 2 to 4 m. Lines: solid, Equation 2.1; dashed, determination of CO_2 loading range.

As demonstrated in Figure 2.6, this normalized flux, k_g', for 8 m PZ is 1.5 to 3 times greater than 7 m MEA. At 40 °C and a P^*_{CO2} of 500 Pa, the kg' for 8 m PZ and 7 m MEA are 1.98 x 10^{-6} and 7.66 x 10^{-7} mol/s-Pa-m^2, respectively. This shows that the mass transfer rate of CO_2 into concentrated PZ is twice as fast as 7 m MEA at this condition. At the higher CO_2 loading, the improvement over MEA is less distinct with the mass

transfer rate only 1.5 to 2 times faster than MEA. The same trend is observed at 60 °C. Although PZ is faster than MEA at 80 and 100 °C as well, mass transfer rates are the most important from 40 to 60 °C, the expected temperature range of the absorber.

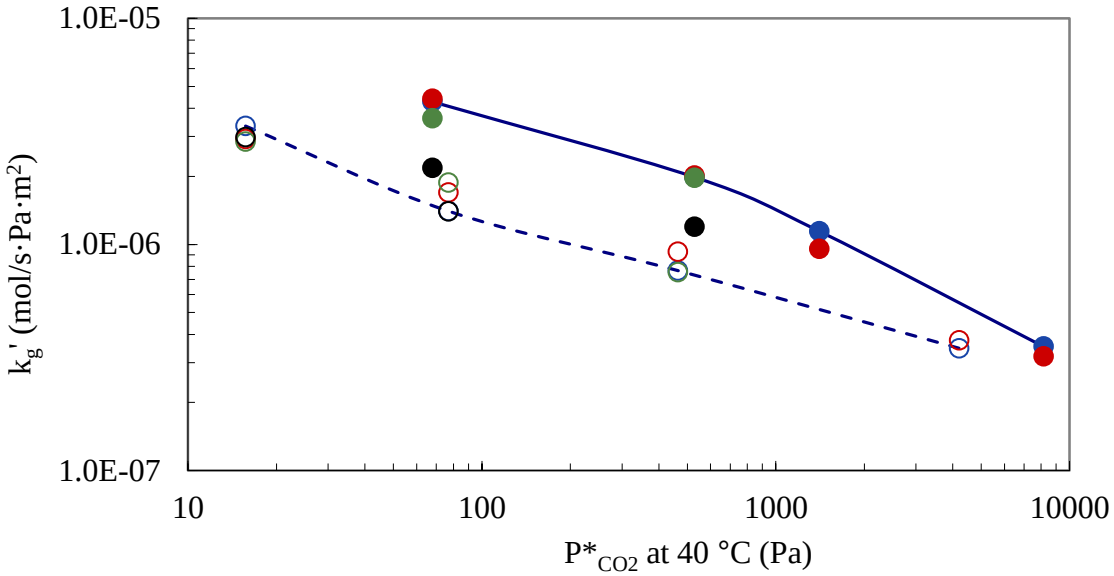

Figure 2.6: Mass transfer coefficients of 8 m PZ (filled circles) and 7 m MEA (open circles) at 40 °C (blue), 60 °C (red), 80 °C (green), and 100 °C (black) (Dugas, 2009)

2.3.5 Volatility of concentrated PZ

The volatility of PZ was measured in an equilibrium cell with hot gas FT-IR (Nguyen et al., 2010). The volatility of 8 m PZ solutions is compared to that of 5 m PZ and 7 m MEA at 40 °C in Figure 2.7. At 40 °C and atmospheric pressure, the volatility of 7 m MEA ranges from 19.0 to 64.9 ppm (MEA partial pressure of 1.93 to 6.6 Pa) over a loading range of 0.15 to 0.50 mole CO_2 per mole alkalinity. At 40 °C and atmospheric pressure, the volatility of 8 m PZ ranges from 1.07 to 7.74 ppm (PZ partial pressure of 0.11 to 0.78 Pa) over a loading range of 0.29 to 0.40 mole CO_2 per mole alkalinity. Finally, at 40 °C and atmospheric pressure, the volatility of 5 m PZ ranges from 5.53 to

50.5 ppm (PZ partial pressure of 0.56 to 5.1 Pa) over a loading range of 0 to 0.41 mole CO_2 per mole alkalinity.

At 40 °C, the volatility of PZ solutions is lower than the volatility of MEA solutions. It was anticipated that PZ would have a higher volatility than MEA because the boiling point of PZ, 146.5 °C, is lower than that of MEA, 170 °C. However, the volatility of both 5 and 8 m PZ is slightly lower at 40 °C. Modeling of PZ systems demonstrated this effect as a greatly decreased activity coefficient for PZ due to the solution non-ideality (Hilliard, 2008).

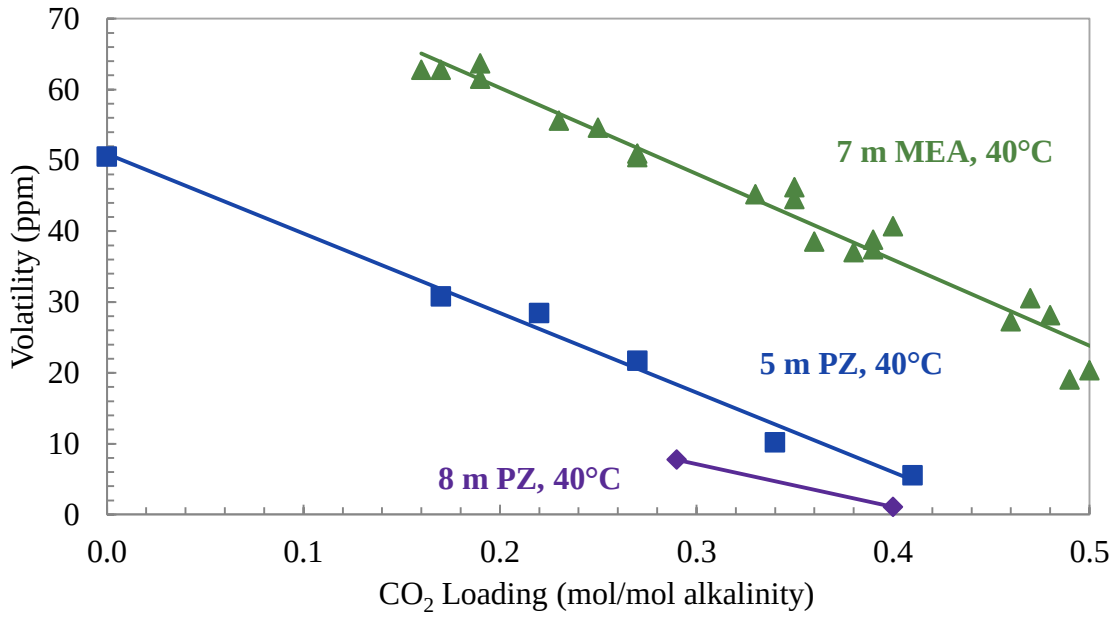

Figure 2.7: Comparison of Amine Volatility at 40 °C for 8 m PZ (♦), 5 m PZ (■), and 7 m MEA (▲) (Nguyen et al., 2010)

2.3.6 Diffusion coefficients of PZ solutions

The diffusion coefficients for N_2O and CO_2 in PZ solutions have been studied previously by various authors. Sun and colleagues measured the diffusivity of N_2O and CO_2 into water and N_2O in H_2O + PZ using a gas-liquid wetted wall contactor at

temperatures between 30 and 40 °C (303 to 313 K) and PZ concentrations between 0.23 and 0.92 kmole per m^3 (0.24 to 1.0 m PZ) (Sun et al., 2005). The diffusivity of CO_2 in H_2O + PZ was estimated using the N_2O analogy. Samanta and colleagues used the same experimental procedure as Sun and estimated the diffusivity of CO_2 in H_2O + PZ for 1.7 to 12 wt% PZ (0.21 to 1.6 m PZ), and 25 to 40 °C (298 to 313 K) (Samanta et al., 2007). Hamborg and colleagues estimated the diffusivity of CO_2 in H_2O + PZ using the N_2O analogy, as with previous authors, for 0.3 to 1.4 mole per dm^3 (0.31 to 1.6 m PZ) at 25 to 60 °C (293 to 333 K) but measured the N_2O diffusivity using a Taylor Dispersion technique which injects the solute into a laminar flow of solution rather than a wetted wall contactor (Hamborg et al., 2008). Derks (2008) also used the Taylor Dispersion technique to measure the diffusivity of the PZ molecule in a H_2O + PZ solution from 0.0008 to 1.46 mole per dm^3 PZ (0.01 to 1.48 m PZ) and 20 to 95 °C (293 to 368 K) (Derks et al., 2008).

No literature measurements have been completed for concentrated PZ or PZ solutions containing CO_2. Since real PZ-based CO_2 capture systems will include concentrations of CO_2 up to 0.45 mole CO_2 per mole alkalinity and PZ concentrations higher than 5 m, there is currently a lack of useful diffusivity data. All of the measurements for diffusivities in aqueous PZ solutions are intended for use in thermodynamic modeling of systems for design of large scale application, but the lack of CO_2 in these measurements limits their ability to predict real values. Previous modeling efforts have approximated PZ diffusion characteristics by assuming the behavior is similar to that of MEA where more data is available in literature (Dugas, 2009).

2.3.7 Heat capacity of PZ solutions

The heat capacity of concentrated, aqueous PZ solutions has not been reported in literature. Recent work has measured the heat capacity of 8, 10, and 12 m PZ solutions over a range of temperatures but has not been formally published (Rochelle, 2009a). A portion of this data is shown in Figure 2.8 to demonstrate the trends observed. Overall, the heat capacity data for PZ follows similar trends observed with other amines including an increase of heat capacity with increased temperature and a decrease of heat capacity with increased CO_2 loading and PZ concentration.

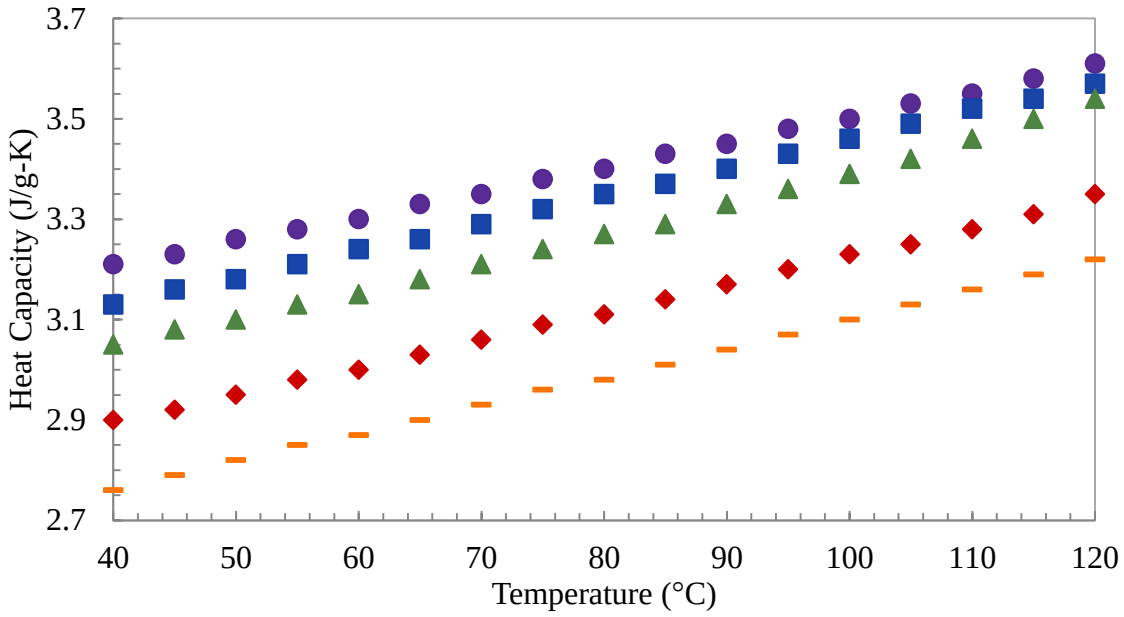

Figure 2.8: Comparison of heat capacity of concentrated PZ solutions. Data: ●, 8 m PZ with α=0.21; ■, 8 m PZ with α=0.29; ▲, 8 m PZ with α=0.40; ♦, 10 m PZ with α=0.31; ─, 12 m PZ with α=0.29 (Rochelle, 2009a)

2.3.8 Heat of absorption of PZ solutions

No studies on the heat of absorption of CO_2 into concentrated, aqueous PZ have been reported in literature prior to the publication of this work. Measurements for 8 m PZ from 0 to 0.5 mole CO_2 per mole alkalinity at 60, 80, 100, and 120 °C were made as a

part of this thesis and the results are included in Appendix F of this dissertation. The calorimeter used was not the appropriate set-up for solutions which precipitate in the absence of CO_2, so the data contains a significant portion of error.

2.4 OXIDATIVE DEGRADATION OF AMINES

The oxidative degradation, or oxidation, of amines has been investigated since the 1950s. Initial work on the topic was performed by the United States Navy during the 1950s and 1960s while investigating CO_2 scrubbers for submarine air purification (Girdler Corporation, 1950; Blachly and Ravner, 1964; Blachly and Ravner, 1965; Blachly and Ravner, 1966). Work performed by the Navy identified the first MEA oxidation products (Scheiman, 1962). Rooney and colleagues expanded the scope of oxidation research to include amines besides MEA and contributed to identifying unknown degradation products (Rooney et al., 1998).

The oxidation work in the Rochelle group began with Chi and Goff who looked at oxidation of MEA under various conditions (Chi, 2002; Goff, 2005). Goff looked extensively at oxygen mass transfer conditions in the laboratory experiments as well as inhibitors for metal catalyzed degradation. The dissertation of Sexton is the most comprehensive study of the oxidation of MEA to date (Sexton, 2008). He investigated numerous combinations of metal catalysts, inhibitors, and other additives on MEA degradation, as well as performing oxidation screening experiments on other amines, including PZ, and MEA analogs.

2.4.1 Catalyst effect of metal on amine oxidation

The connection between corrosion products and amine degradation was identified in the 1950s, indicating a link between metal-based corrosion products and degradation (Hofmeyer et al., 1956). A sub-set of oxidation research since then has been looking into

the catalytic effect of metals on the oxidation of various amines. United States Navy work performed by Blachly and Ravner included this sub-set of oxidation research after scrubber solvents were found to contain iron, nickel, chromium, and copper after use in submarines (Blachly and Ravner, 1964). Their results indicated that copper had a strong catalytic effect for enhancing MEA degradation while iron and nickel only enhanced degradation slightly. The pair also tested various oxidation inhibitors including EDTA and N,N-diethanolglycine (also known as VFS or bicine) with some success. The oxidation work of Sexton primarily looked at the effects of metals and inhibitors on the degradation characteristics of MEA (Sexton, 2008). Sexton's conclusions agree with that of Blachly and Ravner and also include the use of Inhibitors "A" and "B" to decrease MEA degradation.

2.4.2 Oxidation of PZ

One master's thesis in the Rochelle group has looked exclusively at PZ oxidation, but used gas chromatography (GC) to quantify PZ loss rather than the now preferred method of cation ion chromatography (IC) (Alawode, 2005). The high temperature used in the injection port and analytical column in the GC, up to 200 °C, was later found to over predict degradation of amines due to the thermal degradation at these temperatures (Davis, 2009). Another master's thesis focused on oxidation of PZ blended with potassium carbonate to control solubility of PZ (Jones, 2003). Although the work of Sexton was primarily focused on the degradation of MEA, one chapter of his thesis focused on low to mid-level concentration PZ experiments (Sexton, 2008). This work on PZ ranged from 2.5 to 5 m PZ and was primarily executed in the low-gas flow apparatus used by previous students (and described in detail in Chapter 3). The primary conclusion was that PZ does oxidize, but at rates significantly lower than that of MEA. The

conclusion of Sexton was that the metals tested ranked for catalyzing the most to least oxidation were: Cu > V > Fe.

2.4.3 Oxidation of PZ with other oxidants

The oxidation of amines has been studied with oxidizers other than O_2 itself in fields of environmental engineering in regards to water and wastewater treatment. Common oxidizers studied include ozone (O_3), chlorine dioxide (ClO_2) or chlorine (Cl_2).

Pietsch and colleagues found that PZ was quickly oxidized in the presence of ozone (Pietsch et al., 2001). Their ozonation studies found that PZ oxidized significantly faster than diethylamine, dimethylamine, MEA, cyclohexylamine, pyrrolidine, piperidine, or ethylenediamine (EDA) with a rate constant for PZ removal of 8.4×10^{-2} s^{-1}. Morpholine behaved similarly and EDA demonstrated the third fastest ozonation rate. The rationale of Pietsch is that the low pKa values of PZ and morpholine compared to the other amines tested allow for more non-protonated amine groups at the experimental pH of 7.0. Ozone is known to only react with non-protonated amine groups, leaving PZ and morpholine with significantly higher ozonation rates (Hoigné and Bader, 1983). Their studied also concluded that at neutral pH, the ozonation of PZ is due to the direct oxidation from the ozone molecule, not a radical mechanism.

A series of studies performed by Rosenblatt and colleagues in the late 1960s and early 1970s explored the oxidation of various amines using ClO_2 as an oxidant (Davis et al., 1972; Dennis et al., 1967; Hull et al., 1969a; Hull et al., 1969b; Hull et al., 1969c; Hull et al., 1967; Hull et al., 1969d; Rosenblatt et al., 1963; Rosenblatt et al., 1968; Rosenblatt et al., 1972; Rosenblatt et al., 1967). One study examined the oxidation of PZ with ClO_2 and found that the PZ molecule fragmented to produce EDA and formaldehyde, but an exact mechanism was not suggested (Dennis et al., 1967). Dennis

(1967) found that amines with heteroatoms attached to the β-carbon to the amine underwent oxidative fragmentation in the presence of ClO_2 while the analog without a heteroatom did not fragment.

Pietsch and colleagues also investigated the oxidation of PZ with chlorine dioxide (ClO_2) and chlorine when studying applications of chlorine-based water treatment processes for pharmaceutical agents (Pietsch et al., 2001). When treated with ClO_2, PZ showed the highest rate of oxidation of the primary and secondary amines tested. In this test, only 51% of the initial PZ remained after a typical drinking water treatment experiment. When treated with chlorine, however, minimal loss of PZ was observed, indicating that chlorine is a weaker oxidant.

2.4.4 Oxidation of compounds containing the PZ moiety

As mentioned in Section 2.2.2 above, a number of pharmaceutical agents contain the PZ moiety within a more complicated chemical structure. Fluoroquinolones are a class of synthetic antibacterial agents that are used for both humans and farm animals. A number of studies on municipal wastewater treatment have researched the oxidation of ciprofloxacin, a fluoroquinolone, as a representative antibiotic for waste water treatment aimed at removing pharmaceutical agents that propagate from hospital effluent, animal farms, and other sources (Burhenne et al., 1997; Dewitte et al., 2008; Dodd et al., 2006; Thabaj et al., 2007). These studies are notable because in most cases oxidation took place at the PZ moiety rather than any other position on the molecule and that similar products were produced in the presence of different oxidizers such as ozone (Dodd et al., 2006), potassium permanganate (Thabaj et al., 2007), or photo-induced oxidation (Burhenne et al., 1997). Multiple studies identify the oxidation products as the 3-piperazinone, EDA, 3-alcohol, N-oxide, or ammonia-derivatives of ciprofloxacin (where

the 1N connects to the rest of the ciprofloxacin molecule), shown in Figure 2.9. The oxidation of ciprofloxacin is selective for the PZ moiety and indicates the reactive nature of PZ compared to the pyridone or carboxylic acid functions contained within the same pharmaceutical molecule.

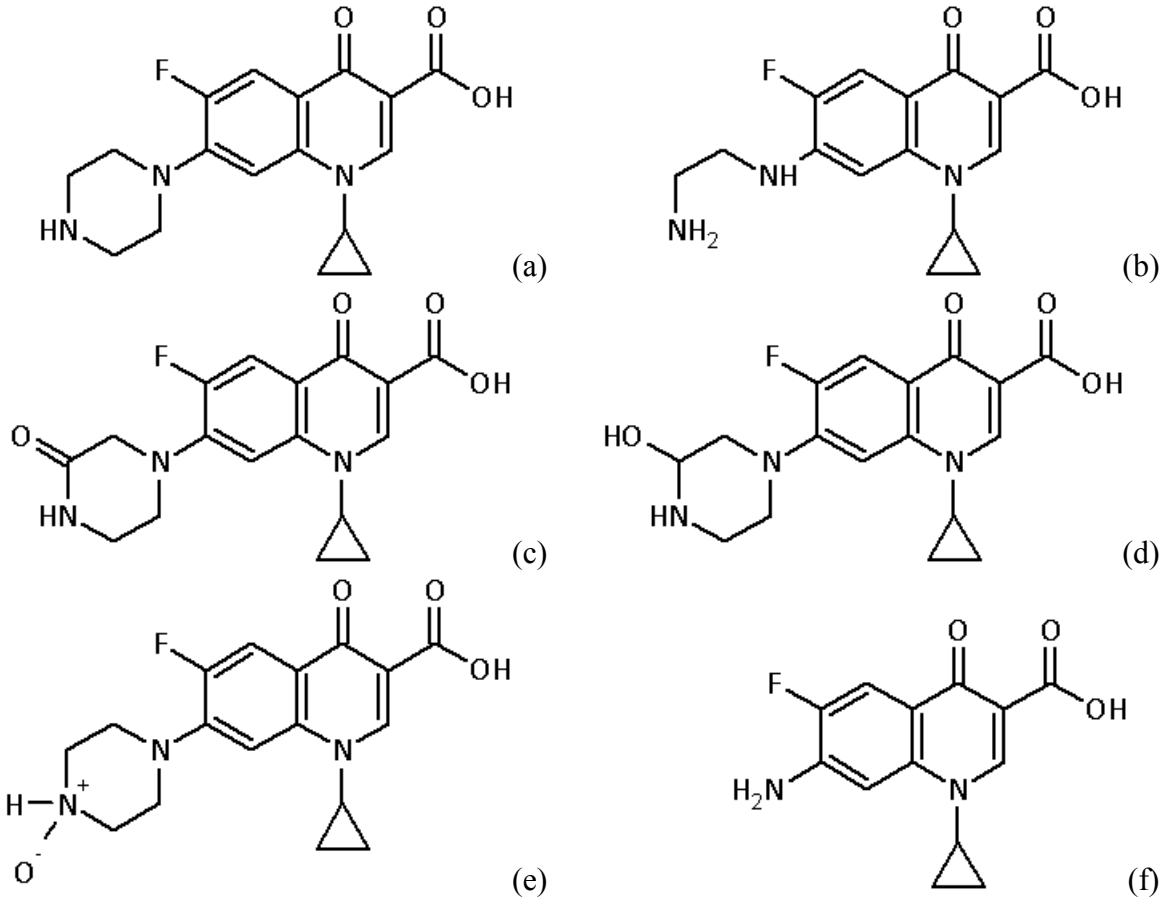

Figure 2.9: Chemical Structures of (a) Ciprofloxacin, (b) EDA derivative, (c) 3-piperazinone derivative, (d), 3-alcohol derivative, (e) N-oxide derivative, and (f) ammonia derivatives of ciprofloxacin.

2.5 THERMAL DEGRADATION OF AMINES

Thermal degradation of amines is a recent topic of interest as Reza and colleagues investigated the thermal degradation of MEA, diethanolamine (DEA), AMP, and blends

of the three amines (Reza and Trejo, 2006). The dissertation of Davis examined on thermal degradation of amines, focusing on MEA thermal degradation mechanisms and screening experiments on various amines and amine blends (Davis, 2008).

2.5.1 Thermal degradation of PZ

There is no thermal degradation data for concentrated PZ solutions available in literature outside of the Rochelle Group. The thesis work of Davis includes experiments performed on 5 m and 8 m PZ during screening experiments where the thermal degradation characteristics of a wide variety of solvents were examined (Davis, 2008). Davis found very little thermal degradation occurred at either PZ concentration at 100, 120 and 135°C. The amount of degradation detected was close to or within the system errors for the cation IC and were reported by him as essentially zero percent degradation. Along with morpholine, PZ was identified as the most thermally resistant amine screened. No degradation products were identified by Davis due to the overall lack of degradation. The thermal stability of PZ in varying conditions is still an area where much can be discovered.

Davis also screened a blend of 7 m MEA/2 m PZ for the rate of thermal degradation. PZ was found to be preferentially degraded with respect to the MEA (Davis, 2009). This has also been observed in other blends of PZ with another amine such as AMP or MDEA. In these cases, the stronger nucleophile, PZ, degrades faster even though at a lower concentration and interacts with the initial degradation products of the other, less stable amine (Closmann et al., 2009; Zhou et al., 2010)

In the degraded blend of 7 m MEA/2 m PZ, Davis identified N-(2-hydroxyethyl) ethylenediamine (HEEDA), N-(2-hydroxyethyl) imidazolidone (HEI), N-(2-aminoethyl) piperazine (AEP), and ethylenediamine (EDA) as the dominant degradation products

using cation IC-MS. HEEDA and HEI are present in MEA degradation while AEP and EDA are new products due to the presence of PZ in the blend. The suggested mechanism for producing AEP is the reaction of PZ with the oxazolidone produced during the first step of the carbamate polymerization mechanism of MEA. Given the relative concentrations of AEP and HEEDA, Davis estimated that PZ reacts up to five times faster to create AEP than MEA reacting with oxazolidone to create HEEDA, indicating the strength of PZ as a reacting nucleophile. Even in a blend with MEA, the degradation results of Davis (2009) indicate some of the characteristics of PZ thermal degradation.

2.6 CONCLUSIONS

The use of concentrated PZ as a CO_2 capture or gas treating solvent has not been previously investigated. The physical and thermodynamic properties of concentrated PZ have not been examined while a small amount of data is available for low concentration PZ without CO_2. Research into some thermodynamic characteristics of low concentration PZ and PZ in a blend has been performed. Although the low concentration work does not specifically apply to the work of this project, it provided a foundation to begin examining concentrated PZ. For properties where there is not a strong effect of amine concentration, like CO_2 solubility, the literature data can be drawn upon widely. One area where even low concentration data is not available is in the area of oxidation and thermal degradation. Widespread work on the degradation of concentrated PZ is needed to fully understand potential large scale application of this solvent. The higher price of PZ as a raw material over other amines such as MEA, DEA, or MDEA further enhances the need to understand its degradation characteristics. Understanding the degradation rates and the production of degradation products under oxidation and thermal degradation conditions is the focus of this dissertation.

Chapter 3 – Analytical Methods and Experimental Equipment

The analytical techniques methods and experimental equipment used throughout this dissertation are described in this chapter. Analytical methods are focused on liquid phase analysis for the concentration of amines, CO_2, degradation products and on the measurement of physical properties such as solid solubility, density, and viscosity. The two experimental methods used for thermal degradation and oxidation, thermal cylinders and the low gas flow reactor, are described in detail. Both the analytical techniques and the experimental equipment are described with the intention of providing enough detail to allow reproduction. Detailed description of the chemicals used including abbreviations, pseudonyms, purity, and the commercial source can be found in Appendix B of this dissertation.

3.1 Analytical Methods

3.1.1 Amine solution preparation

3.1.1.1 Preparation of concentrated, aqueous PZ solutions

Loaded solutions of PZ were prepared gravimetrically as shown in Figure 3.1 and as described previously (Hilliard, 2008; Kim et al., 2008). The calculated amounts of DDI water and anhydrous piperazine (99% pure, Fluka) were first weighed and combined in 500 mL or 1 L glass storage jar. With the cap slightly ajar, the bottle was heated with magnetic stirring until the PZ crystals have completely melted into a solution, approximately 50 °C. Meanwhile, the gas sparging column and cap are placed in a 100°C oven to warm up.

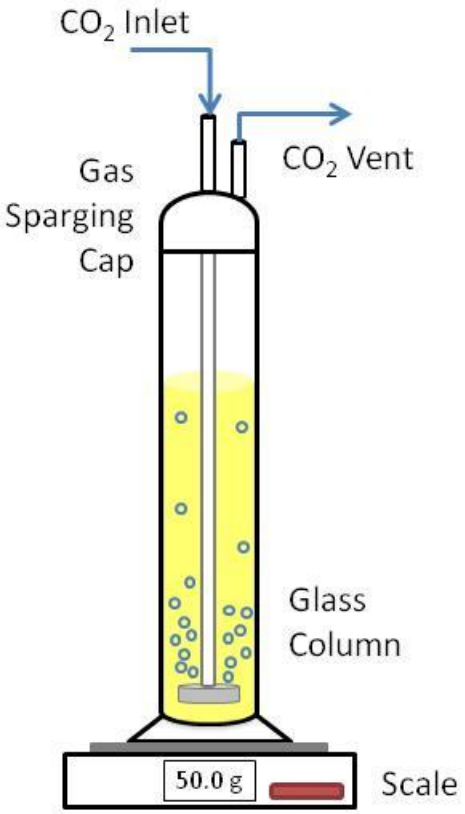

Figure 3.1: Schematic of gravimetric solution preparation

When the PZ was melted, the glass sparging column was removed from the oven and the base column was placed on the scale. The warm solution was then transferred to the column and the gas sparging cap was placed on top of the column, creating a tight seal at the top of the column. The CO_2 inlet line and CO_2 vent lines were then attached to the glass flanges on the sparging cap. Once the CO_2 lines were attached, the entire set-up was allowed to rest and settle for a few seconds. The scale was tared and once a stable zero was achieved, the CO_2 flow was started. CO_2 was sparged until the desired amount of CO_2 was absorbed by the solution, as determined gravimetrically.

Once loading was completed, the CO_2 flow was turned off. The set-up was again allowed to settle to achieve a stable final mass of CO_2 added to the solution. For disassembly, the two gas lines were removed from the cap and the cap was removed, allowing any solution to drain into the column as it was being removed. The cap was set aside and the solution was poured from the column back into the original storage bottle in which the solution was originally melted. Any PZ crystallized on the inside of the storage bottle or cap melted with the introduction of the warm, loaded PZ solution.

3.1.1.2 Preparation of non-PZ solutions

Special considerations were needed when some non-PZ solutions were made. The physical state of the amine dictated the procedure needed to prepare the solutions. Amines that were solid flakes or chunks in their pure state were created as described above for PZ. Slight heat was usually needed along with stirring to melt the starting amine. The liquid solutions were then loaded with CO_2 while warm. Amines that were liquid in their pure state were mixed with water and mixed either with a stir plate or by inverting a sealed bottle numerous times. Then, the solutions were loaded directly, without the need for heating. A few amines were not accessible in their pure form. For

example, homopiperazine (HomoPZ) and hexamethylenediamine (HMDA) are both completely solid in the bottle in their pure form. For these amines, the bottle was warmed in a water bath until the entire bottle of amine was melted into a liquid. Then, the amine was combined with water, mixed, and loaded directly. A summary of the special handling required for the amines used in this project is given in Table 3.1.

Table 3.1: Special handling required for various amines

Amine	State (at 25 °C)	Special Handling
1-Methylpiperazine (1-MPZ)	Liquid	None
2-Methylpiperazine (2-MPZ)	Solid chunks	Crush chunks with mortar and pestle, add to water, melt, and load
1,4-Dimethylpiperazine (1,4-DMPZ)	Liquid	None
trans-2,5-Dimethylpiperazine (t2,5-DMPZ)	Solid flakes	Add to water, melt, and load
Hexamethylenediamine (HDMA)	Solid	Melt, combine with water, and load
Homopiperazine (HomoPZ)	Solid	Melt, combine with water, and load
Morpholine (Morph)	Liquid	None
Piperazine (PZ)	Solid flakes	Add to water, melt, and load
Piperidine (PD)	Liquid	None
Pyrrolidine (Pyr)	Liquid	None

3.1.2 Amine titration

The concentration of total alkalinity of an amine solution was determined using acid titration at room temperature (Hilliard, 2008; Kim et al., 2008). An automatic Titrando series titrator with automatic equivalence point detection was used (Metrohm USA, Riverview, FL, USA). The software used to operate the titrator, measure, and record data was PC Control (Metrohm USA). The Titrando series titrators are potentiometric meters that measure the change in pH in a solution by measuring the

change in electric potential using a pH probe. The overall Titrando unit consists of a base unit, interchangeable dosing units, stir plate, and probe holder.

To perform a measurement, the sample of interest was diluted 300X by combining 60 mL of DDI water with 0.2 g of sample in a 100 or 250 mL beaker. A magnetic stir bar was added to the beaker. To prepare the titrator, the dosing probe was placed in the probe holder and lowered into an empty waste beaker. In the PC Control software and under the section on manual controls, the dosing unit was manually dosed twice with 5 mL of acid. This cleared the dosing line of air bubbles and readied the doser to correctly dispense the acid. Once the lines are clear of air, the pH probe was placed in the probe holder. The pH probe was rinsed with distilled water and dried delicately, avoiding pressure on the bottom membrane of the probe. The sample beaker was then placed on the stir plate and the waste beaker was removed. The probe holder was then lowered into the beaker until the bulb of the pH probe is fully submerged in the sample liquid. The dosing line was adjusted so that it stays well above the liquid line to ensure that the acid was correctly dosed in drops that fell into the liquid.

In PC Control, the acid titration method was started and the sample was titrated with 0.1 N H_2SO_4 to a pH of 2.4. The titrator automatically began stirring when the method begins. Throughout the titration, the volume of acid added and the current pH were recorded each time an increment of acid was added to the sample beaker and were displayed in the PC Control window. A typical titration curve is shown below in Figure 3.2. The Titrando has automatic equivalence point detection which judged the change in slope of the titration curve to determine if an equivalence point had been reached. The software sometimes misidentifies points along the curve other than the two known equivalence points and those points were ignored. At the end of a titration, the equivalence points detected were displayed with the amount of acid needed to reach that

point. For PZ titration, the equivalence point of interest is around a pH of 3.9. The amine concentration by titration was consistently about 2.0 % less than that from the gravimetric preparation in undegraded PZ samples.

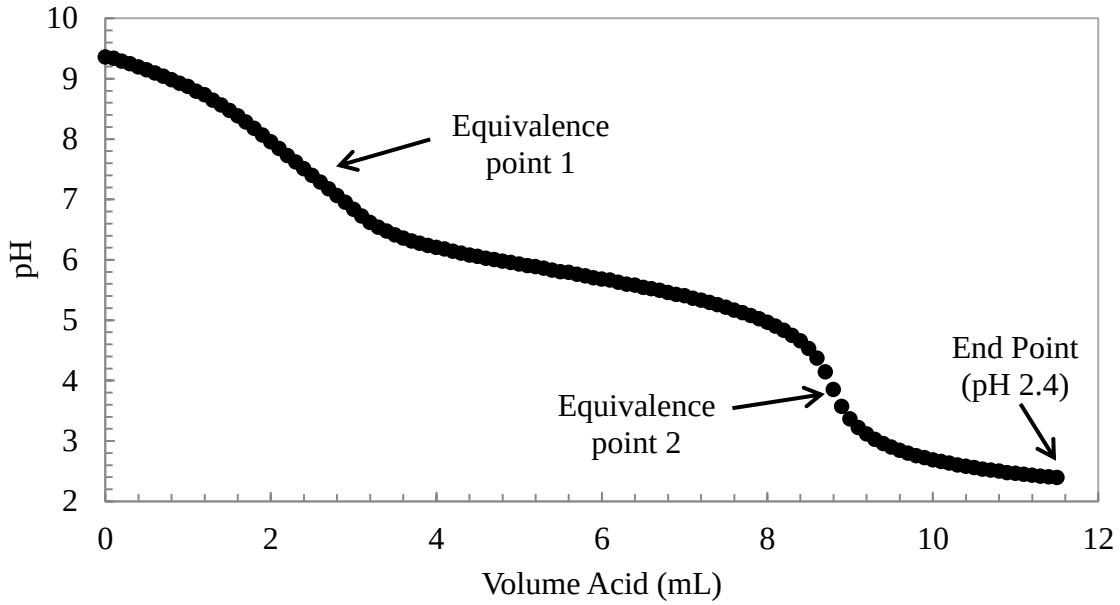

Figure 3.2: Typical acid titration curve (8 m PZ, α=0.3)

In PZ titrations, there were usually two prominent equivalence points identified. The first equivalence point represented the conversion of anhydrous PZ species into monoprotonated PZ (protonated PZ or PZH^+) (Equation 3.1).

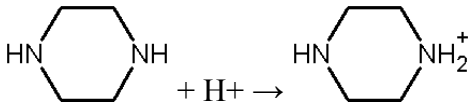

(3.1)

The second equivalence point represented the further conversion to diprotonated PZ (Equation 3.2).

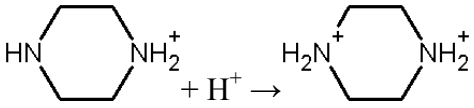

(3.2)

The equilibrium constant for an equilibrium reaction, K_a, can be defined for each of the two dominant reactions. The two protonation reactions written in reverse as deprotonations are shown in equations 3.3 and 3.4.

$$H^+PZ \rightarrow PZ + H^+ \tag{3.3}$$

$$H^+PZH^+ \rightarrow H^+PZ + H^+ \tag{3.4}$$

The K_a value for the first ($K_{a,1}$) and second deprotonation ($K_{a,2}$) an then be defined for each based upon equations 3.3 and 3.4, as shown in equations 3.5 and 3.6.

$$K_{a,1} = \frac{[PZ][H^+]}{[H^+PZ]} \tag{3.5}$$

$$K_{a,2} = \frac{[H^+PZ][H^+]}{[H^+PZH^+]} \tag{3.6}$$

Rearranging each K_a equation yields the Henderson-Hasselbalch equation relating the pH of a solution to the pKa of the species and the concentration of the species and its conjugate acid (equations 3.7 and 3.8).

$$pH = pK_{a,1} + \log\left(\frac{[PZ]}{[H^+PZ]}\right) \tag{3.7}$$

$$pH = pK_{a,2} + \log\left(\frac{[H^+PZ]}{[H^+PZH^+]}\right) \tag{3.8}$$

The measured pK_a of the first protonation, $pK_{a,1}$, ranges from 9.71 to 9.73 at 25 °C (Enea et al., 1972; Hamborg and Versteeg, 2009; Hetzer et al., 1968; Khalili et al., 2009). The measured pK_a value of the second protonation, $pK_{a,2}$, ranges from 5.33 to

5.41 at 25 °C, with Enea and colleagues reporting a value as low as 4.63 at 25 °C (Enea et al., 1972; Hamborg and Versteeg, 2009; Hetzer et al., 1968; Khalili et al., 2009). Using Equations 3.7 and 3.8, the ratio of the two pairs of species can be calculated over the range of pH experienced during the titration, as shown in Table 3.2.

Table 3.2: Change in protonated PZ species during titration

Solution pH	$\frac{[PZ]}{[H^+PZ]}$	$\frac{[H^+PZ]}{[H^+PZH^+]}$
11	15.1	251189
10	1.51	25119
9	0.151	2512
8	0.0151	251
7.5	0.00479	79.4
7	0.00151	25.1
6	0.000151	2.51
5	1.514E-05	0.251
4	1.514E-06	0.0251
3.9	1.202E-06	0.0200
3	1.514E-07	0.00251
2.4	3.802E-08	0.000631

When the first equivalence point at pH of 7.5 is reached, the concentration of PZ is only a fraction (0.000479) of the concentration of PZH^+, indicating that nearly all the PZ has been protonated once. At the second equivalence point of 3.9 pH, the concentration of PZH^+ is only a small fraction (0.02) the concentration of H^+PZH^+, indicating that most of the singly protonated PZ is now diprotonated. This second equivalence point, therefore, represented the amount of acid needed to fully protonate all of the amino groups on the PZ species.

Using the volume of acid needed to reach the equivalence point at a pH of 3.9, the concentration of total alkalinity can be calculated. It is important to make a distinction between the concentration of PZ and the total alkalinity of solution. The titration

procedure measures the total alkalinity of solution. This is true for both neat and degraded solutions. In neat solutions, however, all the alkalinity should be in the form of PZ so the calculation can proceed with this assumption. For degraded samples, the results represent the concentration of total alkalinity which carries a different, although still useful, meaning. Titrations of oxidized or thermally degraded samples result in a measure of the total alkalinity where degradation has likely decreased the PZ concentration and generated degradation products that also contain alkalinity.

The calculation of total alkalinity from the titration data is very direct and can be demonstrated assuming a case where 0.2 gram of a test sample required 8.4 mL of 0.2 N H_2SO_4 to reach a pH of 3.9. First, the amount of alkalinity in the sample can be calculated from the amount of acid added. Then, the concentration can be calculated in terms of moles of alkalinity per kilogram of solution using the original sample mass.

$$8.4\,\text{mL}\ H_2SO_4 \times \frac{0.2\,\text{mole}\ H_2SO_4}{1000\,\text{mL}} \times \frac{1\,\text{mole Alk}}{1\,\text{mole}\ H_2SO_4} = 0.00168\,\text{mole Alk}$$

$$\frac{0.00168\,\text{mole Alk}}{0.2\,\text{g soln}} \times \frac{1000\,\text{g}}{1\,\text{kg}} = 8.4\,\frac{\text{mole Alk}}{\text{kg soln}}$$

In the instance of an undegraded PZ sample, for instance those used for physical property measurements, the PZ concentration can be calculated as well if the CO_2 loading of the sample is known. Starting with the calculation demonstrated above for total alkalinity, the PZ concentration can be calculated in units of either mole PZ per kg of solution or molal. The first calculation is direct using the two amino functions in the PZ molecule.

$$\frac{0.00168\,\text{mole Alk}}{0.2\,\text{g soln}} \times \frac{1\,\text{mole PZ}}{1\,\text{mole Alk}} \times \frac{1000\,\text{g}}{1\,\text{kg}} = 4.2\,\frac{\text{mole PZ}}{\text{kg soln}}$$

To calculate the concentration in molal, the CO_2 loading must be known or estimated. When the CO_2 concentration is measured (see Section 3.1.3), the units first calculated are moles of CO_2 per kg of solution. Therefore, the CO_2 loading can be calculated directly using this value and the value calculated above for the PZ concentration.

$$CO_2 \text{ Loading} = \frac{\frac{\text{mole } CO_2}{\text{kg soln}}}{\frac{\text{mole PZ}}{\text{kg soln}} \times \frac{2 \text{ mole Alk}}{\text{mole PZ}}} = \frac{\text{mole } CO_2}{\text{mole Alk}}$$

This calculation procedure avoids the need to assume either a PZ concentration or CO_2 concentration when analyzing either set of data. Once the CO_2 concentration is calculated as a loading (units of mole CO_2 per mole alkalinity), this value can be used in the calculation of PZ concentration in molality. Continuing the example given above with an additional assumption of a CO_2 loading of 0.3 mole CO_2 per mole alkalinity, the concentration of CO_2 in the sample is then calculated in terms of the amount of water in the sample.

$$\frac{0.3 \text{ mole } CO_2}{\text{mole Alk}} \times \frac{2 \text{ mole Alk}}{\text{mole PZ}} \times \frac{8 \text{ mole PZ}}{\text{kg } H_2O} \times \frac{44.01 \text{ g } CO_2}{\text{mole } CO_2} = 211.2 \frac{\text{g } CO_2}{\text{kg } H_2O}$$

Next, the mass of CO_2 in the sample is calculated by using the sample mass and the mass fraction of CO_2 in the sample. The mass fraction is calculated by assuming a basis of 1 kg of water and a nominal PZ concentration.

$$0.2 \text{ g sample} \times \left[\frac{\left(\frac{211.2 \text{ g } CO_2}{\text{kg } H_2O} \right)}{\frac{211.2 \text{ g } CO_2}{\text{kg } H_2O} + \left(\frac{8 \text{ mole PZ}}{\text{kg } H_2O} \times \frac{86.14 \text{ g PZ}}{\text{mole PZ}} \right) + \frac{1000 \text{ g } H_2O}{\text{kg } H_2O}} \right] = 0.0222 \text{ g } CO_2$$

The mass of water in the original sample can be determined by subtracting the amount of PZ and CO_2 in the original sample. First, the mass of PZ is calculated by assuming all the alkalinity is PZ.

$$8.4\,\text{mL}\ H_2SO_4 \times \frac{0.2\,\text{mole}\ H_2SO_4}{1000\,\text{mL}} \times \frac{1\,\text{mole Alk}}{1\,\text{mole}\ H_2SO_4} \times \frac{1\,\text{mole PZ}}{2\,\text{mole Alk}} \times \frac{86.14\,\text{g PZ}}{1\,\text{mole PZ}} = 0.0724\,\text{g PZ}$$

$$(0.2\ \text{g sample}) - (0.0222\ \text{g}\ CO_2) - (0.0724\ \text{g PZ}) = 0.1052\ \text{g}\ H_2O$$

Finally, the CO_2-free molality of PZ can be calculated:

$$\frac{0.00084\,\text{mole PZ}}{0.1054\,\text{g}\ H_2O} \times \frac{1000\,\text{g}\ H_2O}{\text{kg}\ H_2O} = 7.969\,\text{m PZ}$$

Using this calculation procedure, the concentration of a single amine can be determined in terms of molality directly from a simple and quick titration procedure.

3.1.3 Total Inorganic Carbon (TIC) measurement

The concentration of CO_2 in amine solutions was determined by the measurement of the total inorganic carbon present in the sample as developed previously (Critchfield, 1988; Hilliard, 2008; Lee, 1986). A schematic of the TIC apparatus is shown in Figure 3.3. The apparatus consists of a rotameter type gas flow meter, glass injection tube with injection port and frit, two glass cylinders used as desiccant tubes, CO_2 detector, and a computer. CO_2 loading throughout this thesis is reported in units of moles CO_2 per mole alkalinity. This unit is defined for amine alkalinity, or equivalence of amine, based on the number of amino functions on the parent amine and is used for convenience in the field of CO_2 capture. This definition is not based on an alkalinity result from a titration procedure

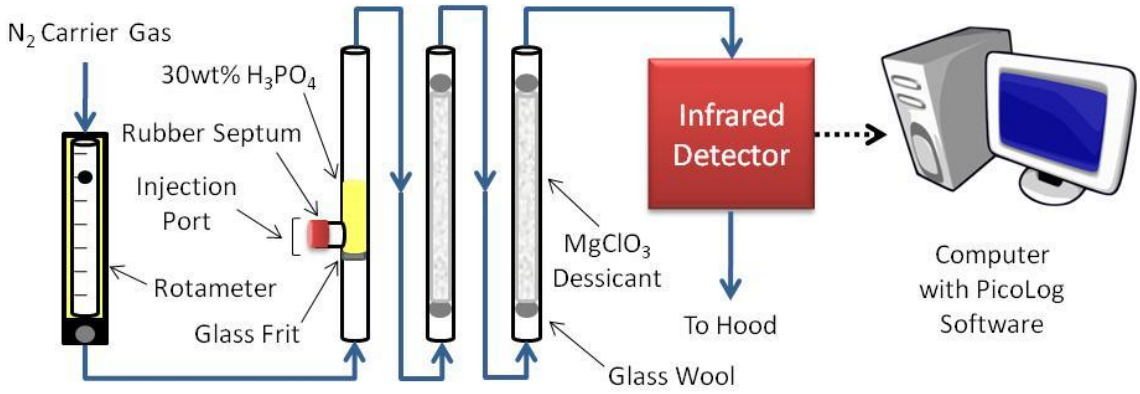

Figure 3.3: Schematic of Total Inorganic Carbon (TIC) apparatus

To set up the apparatus for use, two $^3/_8$ inch diameter glass tubes were first filled with magnesium perchlorate ($MgClO_4$) desiccant. To fill the tubes, a small ball of glass wool was placed approximately one-half inch from one end of the tube. Large pieces of desiccant were added to the tube to fill the tube until one-half inch from the other end of the tube. Another piece of glass wool was placed at the top of the tube to securely hold the desiccant in place. A new septum was placed on the injector port for each new analysis. Using a 3 mL syringe, 1 to 1.5 mL of phosphoric acid (H_3PO_4) was injected through the septum to fill the injection chamber. The nitrogen (N_2) gas was then turned on at the source and the rotameter was adjusted to achieve the desired flow rate. Usually the rotameter was maintained at a reading of 12 or 13. The rotameter was periodically checked throughout the measurements to ensure that the N_2 flow was maintained.

To begin the analysis, the samples were first gravimetrically diluted 10, 50, or 100X, depending on the expected concentration of CO_2. The dilute sample was injected into the injection port on the side of the first glass tube using a syringe pressed through the septum. This injection tube had a glass frit below the injection port that allows the carrier N_2 to pass through the frit, through the acid, and up the tube but did not allow the

acid to fall through. The injected sample entered the system in the pool of acid and was quickly acidified. This acidification released all of the CO_2 present in solution.

The released CO_2 entered the N_2 carrier gas stream that traveled through the two desiccant tubes before finally reaching the Horiba PIR 200 infrared detector (Horiba, Irvine, CA, USA). The resulting change in voltage detected by the infrared detector produces peaks that were recorded with PicoLog software (Pico Technology, Cambridgeshire, United Kingdom). The infrared detector is very sensitive to any water vapor that reaches it, so two tubes of desiccant were always used. The first tube was replaced for every run while the second tube was replaced less often, approximately every 5 to 7 runs or as needed. Not shown in Figure 3.3 is a stand that supports the three tubes on a metal plate with tube holders where the tubes can snap into place. An airtight seal is maintained with Swagelok® ultra-torr vacuum fittings (Arthur Fluids System Technologies, a Swagelok® Distributor, Austin, TX).

A calibration curve was prepared at the end of each analysis using a 1000 ppm standard inorganic carbon solution, which was a mixture of K_2CO_3 and $KHCO_3$ (Ricca Chemical Company, Arlington, TX). The TIC method quantified the CO_2, carbonate (CO_3^{-2}), bicarbonate (HCO_3^-), and carbamate ($PZCOO^-$, $PZ(COO^-)_2$, etc.) species present in solution. These species are in equilibrium in the series of reactions shown in equation 3.9 below.

$$CO_3^{2-} + 2H^+ \leftrightarrow HCO_3^- + H^+ \leftrightarrow H_2CO_3 \leftrightarrow CO_2 + H_2O \qquad (3.9)$$

Acidification shifted the equilibrium toward CO_2 which bubbles out of solution and was detected in the analyzer. CO_2 loading is reported throughout this thesis as moles of CO_2 per mole of alkalinity or moles of CO_2 per equivalence of PZ, where there are two moles of alkalinity per mole PZ.

At the end of a run, the N_2 flow was turned off at the rotameter and the source. The data recorded by PicoLog, a set of time versus voltage data, were exported to excel and saved. The first desiccant tube was removed from the apparatus and emptied. If the second desiccant tube was not wet, it remained in the apparatus for the next user. The acid in the injection port was removed using the 3 mL syringe and placed in the appropriate acid waste container. The injection port and first desiccant tube were then washed with distilled water.

In order to calculate CO_2 concentration, the areas of each peak were first calculated for the samples and the calibration peaks using trapezoidal rule integration. The area of the peaks, rather than the height or another characteristic, was used to compare samples to the calibration curve. A calibration curve was produced plotting the peak area (independent variable) versus the moles of CO_2 (dependent variable) in each calibration injection. The mass of each injection was used to calculate the moles of CO_2 from the 1000 ppm standard. The peak areas of the standards were then compared to the calibration curve to produce a value for the moles of CO_2 in each sample peak. Using the injection mass of the sample and the dilution factor, a CO_2 concentration was calculated as follows.

$$\frac{\text{mole } CO_2}{\text{g injection}} \times \underbrace{\frac{\text{g sample} + \text{g } H_2O}{\text{g sample}}}_{\text{Dilution Factor}} \times \frac{1000 \text{ g } H_2O}{\text{kg } H_2O} = \frac{\text{mole } CO_2}{\text{kg sample}}$$

If the same sample was titrated for total alkalinity, the CO_2 loading can be calculated directly with this CO_2 concentration value without the assumption of PZ concentration. From the PZ titration, the PZ concentration represented by alkalinity in units of moles of PZ (alkalinity) per kg sample can be easily calculated for a neat, non-degraded solution. This procedure would not be appropriate for degraded samples where

the titrated alkalinity represents changes to the solution and is not related to the PZ concentration after the first sample. Then, this value can be combined with the TIC result above to directly and accurately calculate the CO_2 loading.

$$\alpha = \frac{\overbrace{\left(\frac{\text{mole } CO_2}{\text{kg sample}}\right)}^{\text{Directly from TIC}}}{\underbrace{\left(\frac{\text{mole PZ}}{\text{kg sample}}\right)}_{\text{Directly from titration}} \times \left(\frac{2 \text{ mole Alk}}{1 \text{ mole PZ}}\right)} = \frac{\text{mole } CO_2}{\text{mole Alk}}$$

If the total alkalinity is known for a degraded sample, that result can also be used directly to calculate CO_2 loading. In this case, the number is direct from the amount of acid added to the titration without a conversion to PZ units. Loading can be calculated in the following case in that instance.

$$\alpha = \frac{\overbrace{\left(\frac{\text{mole } CO_2}{\text{kg sample}}\right)}^{\text{Directly from TIC}}}{\underbrace{\left(\frac{\text{mole Alk}}{\text{kg sample}}\right)}_{\text{Directly from titration}}} = \frac{\text{mole } CO_2}{\text{mole Alk}}$$

This direct calculation is the most accurate way to calculate the CO_2 loading. With this value, the titration results can then be interpreted with an accurate value for CO_2 loading to calculate amine concentration (See section 3.1.2).

Alternatively, the CO_2 loading can be calculated another way that involves assuming a PZ concentration if it is not known. The calculation uses the moles of CO_2 per kg of sample calculated above as the starting point. The overall calculation has this form below using the mass of total solution (TS) and mass of CO_2-free solution (CFS):

$$\alpha\,[=]\frac{\text{mole CO}_2}{\text{mole Alk}} = \frac{\text{mole CO}_2}{\text{kg TS}} \times \frac{\text{g TS}}{\text{g CFS}} \times \frac{\text{g CFS}}{\text{g H}_2\text{O}} \times \frac{\text{kg H}_2\text{O}}{\text{mole Alk}}$$

The two conversion factors are then based on a basis of 1000 g of TS or 1000 g of water:

$$\frac{\text{g TS}}{\text{g CFS}} = \frac{\text{g TS}}{(\text{g TS} - \text{g CO}_2)} = \frac{\text{g TS}}{\left(\text{g TS} - 2.5\,\text{mole CO}_2 \times \frac{44.01\,\text{g CO}_2}{1\,\text{mole CO}_2}\right)}$$

$$\frac{\text{g CFS}}{\text{g H}_2\text{O}} = \frac{\text{g H}_2\text{O} + \text{g PZ}}{\text{g H}_2\text{O}} = \frac{\left(1000\,\text{g H}_2\text{O} + 8\,\text{mole PZ} \times \frac{86.14\,\text{g PZ}}{1\,\text{mole PZ}}\right)}{\text{g H}_2\text{O}}$$

The last piece is the use of the PZ concentration to convert kg of H_2O to mole of alkalinity. The whole equation then looks like the following:

$$\alpha = \frac{2.5\,\text{mole CO}_2}{\text{kg TS}} \times \frac{\text{g TS}}{\left(\text{g TS} - 2.5\,\text{mole CO}_2 \times \frac{44.01\,\text{g CO}_2}{1\,\text{mole CO}_2}\right)} \times \frac{\left(1000\,\text{g H}_2\text{O} + 8\,\text{mole PZ} \times \frac{86.14\,\text{g PZ}}{1\,\text{mole PZ}}\right)}{\text{g H}_2\text{O}} \times \frac{\text{kg H}_2\text{O}}{8\,\text{mole PZ}} \times \frac{1\,\text{mole PZ}}{2\,\text{mole Alk}}$$

The result is loading in terms of moles CO_2 per mole alkalinity.

$$\alpha = \frac{\text{mole CO}_2}{\text{mole alkalinity}}$$

If you have a blend of two amines, the following changes can be made to incorporate that second amine, A2. The concentration, molecular weight, and number of alkaline groups of A2 are represented by C, MW, and N, respectively.

$$\alpha = \frac{2.5\ \text{mole}\ CO_2}{\text{kg TS}} \times \frac{\text{g TS}}{\left(\text{g TS} - 2.5\ \text{mole}\ CO_2 \times \frac{44.01\ \text{g}\ CO_2}{1\ \text{mole}\ CO_2}\right)} \times \frac{\left(1000\ \text{g}\ H_2O + 8\ \text{mole PZ} \times \frac{86.14\ \text{g PZ}}{1\ \text{mole PZ}} + \text{C mole A2} \times \frac{\text{MW g}}{1\ \text{mole A2}}\right)}{\text{g}\ H_2O} \times \left(\frac{\text{kg}\ H_2O}{8\ \text{mole PZ}} \times \frac{1\ \text{mole PZ}}{2\ \text{mole Alk}} + \frac{\text{kg}\ H_2O}{\text{C mole A2}} \times \frac{1\ \text{mole A2}}{\text{N mole Alk}}\right)$$

3.1.4 Anion Ion Chromatography (IC)

Anion IC was used to quantify negatively charged ions (anions) in solution as previously (Sexton, 2008). The types of molecules quantified include carboxylate ions (formate, acetate, glycolate, and oxalate), nitrogen containing anions (nitrite and nitrate), and tracers (sulfate and chloride). The chemical structures of molecules quantified using anion IC are shown in Figure 3.4.

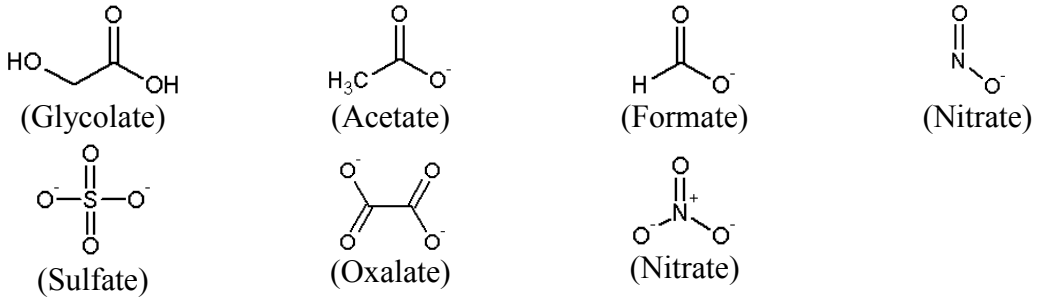

Figure 3.4: Chemical structures of molecules quantified with anion IC

3.1.4.1 Apparatus description

A Dionex ICS-3000 modular Dual RFIC Ion Chromatography System with AS autosampler is used (Dionex Corporation, Sunnyvale, CA). The eluent contains varying concentrations of KOH in analytical grade water. The separation occurred using an IonPac AG15 guard column (4 x 50 mm) and an IonPac AS15 analytical column (4 x 250

mm). Both columns contained ethylvinylbenzene cross-linked with 55% divinylbenzene resin affixed with quaternary ammonium groups as the primary separation medium. The system contained a 4-mm Anionic Self-Regenerating Suppressor (ASRS) to remove cationic species before anionic species were detected with the conductivity cell. Two carbonate removal devices were in place to remove excess carbonate species from the samples (Continuously Regenerated Anion Trap Column – CR-ATC) and the analytical water (Carbonate Removal Device – CRD). Chromeleon® software analyzed the conductivity output and controlled the entire system. The overall flow schematic of the anion IC is shown below in Figure 3.5.

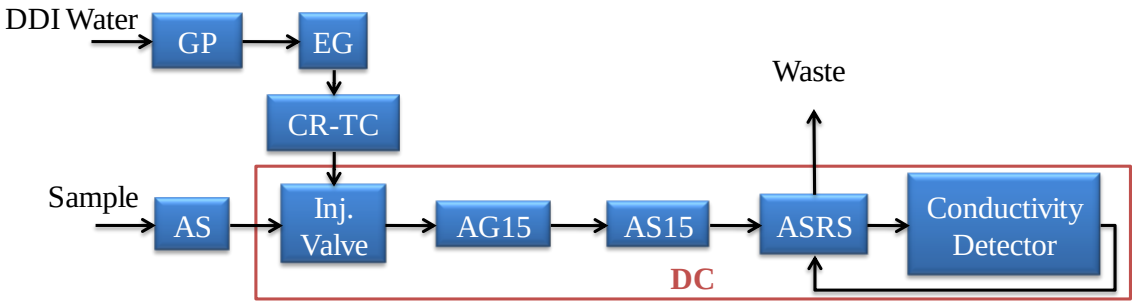

Figure 3.5: Flow schematic for the anion IC showing the AS autosampler, injection valve, AG15 guard column, AS15 analytical column, ASRS, EG eluent generator, CR-TC, DC detector compartment, and conductivity detector.

3.1.4.2 Analysis procedure

The Dionex ICS-3000 system was a dual system with two separate pumps, columns, eluents, and detectors using a common AS autosampler that holds 100 samples. The ICS-3000 system fully controlled the AS autosampler and samples in any position can be accessed by either chromatography system. The standard set-up for the ICS-3000 was to have anion IC operating in parallel with an amino acid detection method.

In Chromeleon®, a sequence was made to direct the anion IC to analyze the samples of interest. A sequence contained all the information needed for the anion IC to

determine which method to use and how much to inject of each sample. The sequence also contained an identifying name of each sample and the quantification method to be used afterward to analyze the resulting chromatogram. Sequences were generally set up with standards first and then the unknown samples with DDI placed between varying groups of samples to eliminate any cross-contamination of samples.

The flow path through the anion IC began with the samples in the autosampler. The arm of the autosampler flushed the injection needle with DDI water and then moved to the sample. The needle withdrew a small amount of sample and moved to the injection port. The sample was injected and sent through a 25 μL injection loop and then on to the ASRS suppressor. In the suppressor, the sample was passed through a channel with two membranes on opposites of the chamber, as shown in Figure 3.6 (Dionex Corporation, 2007). One membrane separated the flow path from the cathode chamber and the other from the anode chamber. In this type of suppressor, the anode membrane allowed hydronium ion (H_3O^+) from the anode chamber to enter the flow stream in order to neutralize the hydroxide present in the flow stream from the eluent KOH. At the same time, cations in the flow stream, including the potassium portion of the eluent KOH, were attracted to the cathode chamber by the electric potential applied and travel through the cathode membrane in the chamber in order to maintain electroneutrality with the H_3O^+ entering the flow stream from the anode. The result was a flow stream exiting the suppressor with only anions, which were the molecules of interest, and water formed from H_3O^+ and OH^- from KOH.

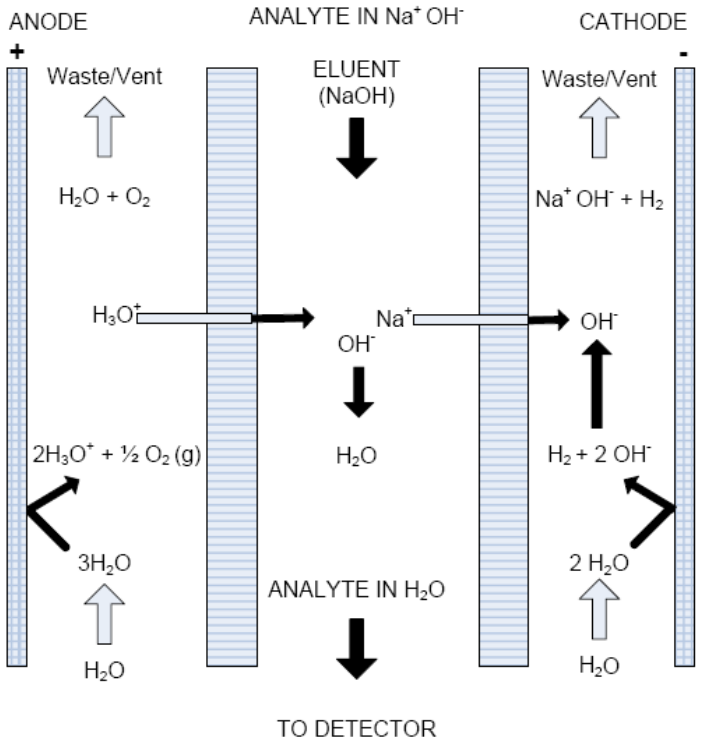

Figure 3.6: Schematic of ASRS 300 in auto-suppression mode (Source: (Dionex Corporation, 2007))

The stream exiting the suppressor was then sent through the IonPac AG15 guard column and the IonPac AS15 analytical column. The guard column was used to prevent sample contaminants from eluting onto the analytical column which would affect separation of the compounds of interest. The analytical column was where the primary separation of compounds occurs. Molecules attached to the cross-linked column internals and detached based on their adhesion properties. As the concentration of acid increased through the program, more difficult molecules to elude detached from the column internals and flowed to the detector. This difference in adhesion to the column internals was the reason for the concentration gradient in KOH. After exiting the analytical column, the flow entered the ECD. Changes in solution conductivity were detected in the

ECD and are recorded in time to create a chromatogram. As a group of anions in solution reached the detector, peaks were formed representing that specific species.

A method was used to control the various components of the system as well as adjusting the eluent gradient and setting the overall time for analysis. The primary method used for anion IC analysis was entitled "Anions.pgm". In this program, various constraints and settings were used, as shown in Table 3.3.

Table 3.3: Settings and constraints for the anion IC

Setting	Value	Units
Pressure.LowerLimit	200	Psi
Pressure.UpperLimit	3000	Psi
CellHeater	35	°C
Column_TC	30	°C
Compartment_TC	30	°C
Suppressor_Type	CSRS_4mm	-
Suppressor_Current	179	mA
Flow	1.6	mL/min

In this method, there were six minutes before each sample, indicated as negative time, which allowed the system to equilibrate to a lower KOH concentration after completion of the previous sample in preparation of the current sample. At negative six minutes, the flow rate was set at 1.6 mL/min with a 0.1 min window to decrease the concentration from 45 mM to 2 mM of KOH in preparation for the new sample. At time zero, the sample was injected and data acquisition from the electrochemical detector (ECD) was turned on. The eluent concentration remains 2 mM KOH until minute seventeen where a gradient began and increased the concentration to 45 mM by 25 minutes. The concentration then remained at 45 mM KOH until the end of the run at 35 minutes. The KOH concentration over the course of "Anions.pgm" is shown in Figure 3.7. Every analytical sample in this dissertation was analyzed using this "Anions.pgm" unless otherwise indicated. At the end of each run of samples, there was a final sample

with the "Shutdown.pgm" method. In this method, the suppressor and detector were turned off at time zero. Also, the pump flow rate was decreased to 0.2 mL/min at time zero to allow the machine to remain idle until the next time it was used.

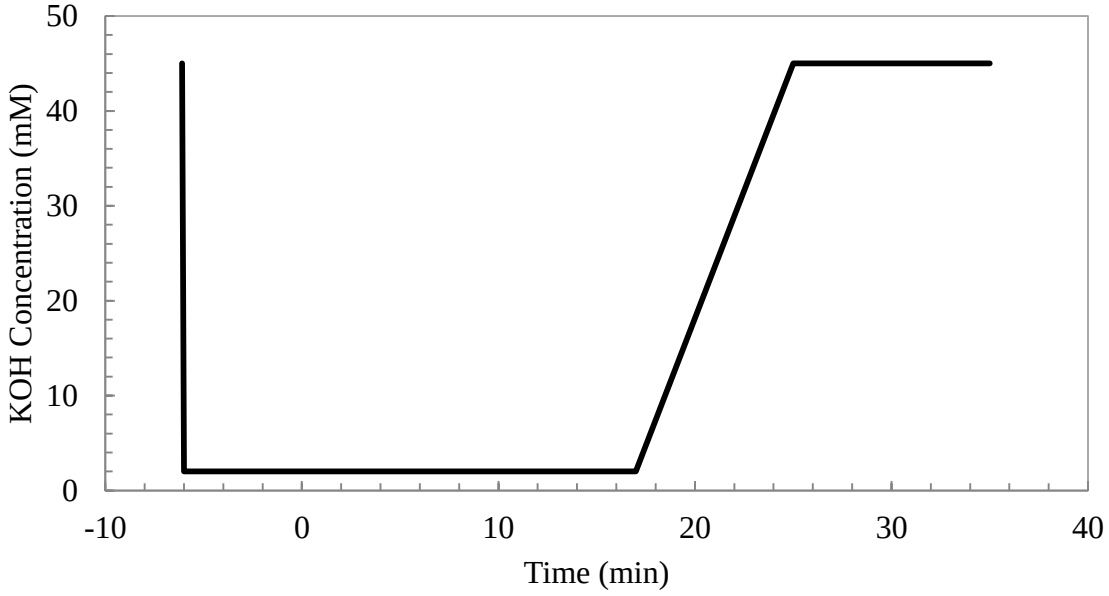

Figure 3.7: KOH gradient in anion IC method

A typical chromatogram for anion IC analysis of a thermally degraded PZ sample is shown in Figure 3.8 (TE44, t=5). A dominant formate peak can be seen at a retention time of 20.2 minutes while smaller carbonate and sulfate peaks can be seen at 25.6 and 26.9, respectively. Other peaks such as glycolate, acetate, chloride, and oxalate are not visible with this zoomed out view. Calibration curves were created in order to quantify the concentrations of species in the original sample. At least four or five calibration standards were analyzed for each anion of interest. Usually, standards were created in the range of 1 to 50 ppm for anions that are expected in low concentration such as formate, acetate, and others. The calibration curves used were always at least three different concentration standards and a quadratic regression was used to create the curve. The

calibration and quantification was performed using the quantification wizard in the Chromeleon® software. The output at the end of analysis was a ppm concentration of each analyte in the dilute sample. This ppm concentration was adjusted using the dilution factor and then converted to mmole per kg for reporting.

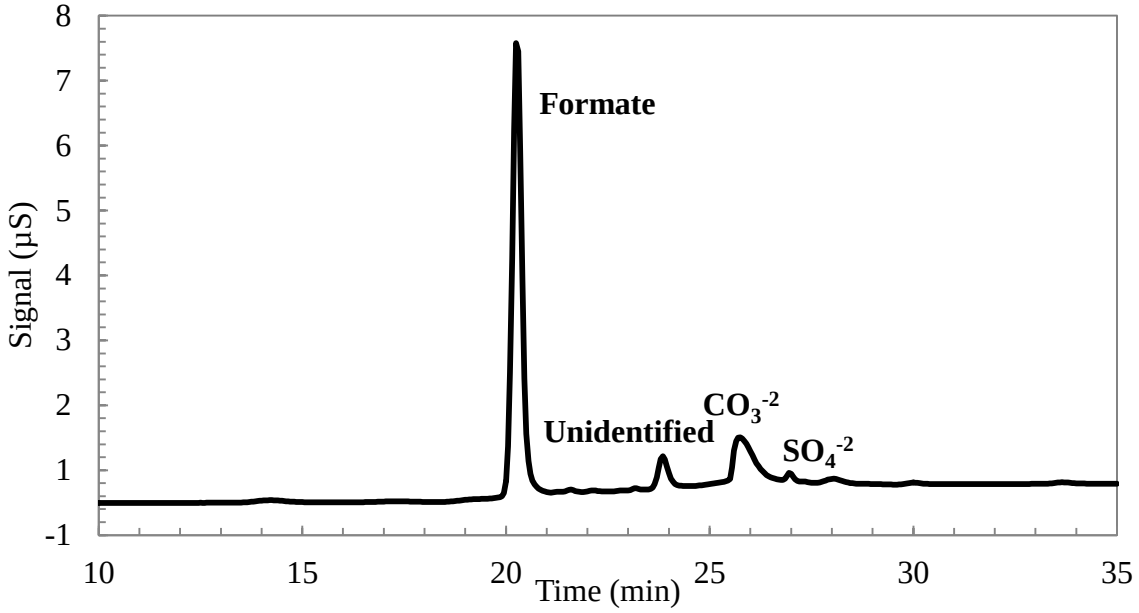

Figure 3.8: Typical anion IC chromatogram for thermally degraded PZ sample

3.1.4.3 Limitations and expected error

There was opportunity for error throughout the ICS-3000 system. The primary avenue for error being introduced into the results was through a high or unsteady baseline. When the baseline was high or had a large bulge in it, all the peak areas calculated were suspect because their areas were decreased from what they would normally be with good separation and a low baseline. This happened occasionally with the anion IC and the source of a bulge in the baseline was usually not clear. In theory, the detector should produce an additive signal where the effect of an anion on top of the

bulge was not decreased, but the size of the bulge in comparison with most anion signals makes this assumption likely not very accurate.

Error was likely introduced in the generation of the calibration curves. Standards of the anions of interest were created through serial dilution and there was always the possibility of error in this gravimetric procedure. As an estimate of this, a comparison of six calibration curves for formate performed over the course of 3.5 years are compared in Figure 3.9. Using the calibration curves shown in Figure 3.9, the concentration of formate predicted for a peak area of 3.0 µS-min ranges from 25.84 to 35.41 mmole per kg with a standard deviation of 3.35 mmole per kg, or 11% of the average of 29.96 mmole per kg. Though the system itself has undergone many changes during this time including replacing the analytical and guard columns, suppressor, and eluent generator, the relative error in the position of the calibration curves is less than 15%.

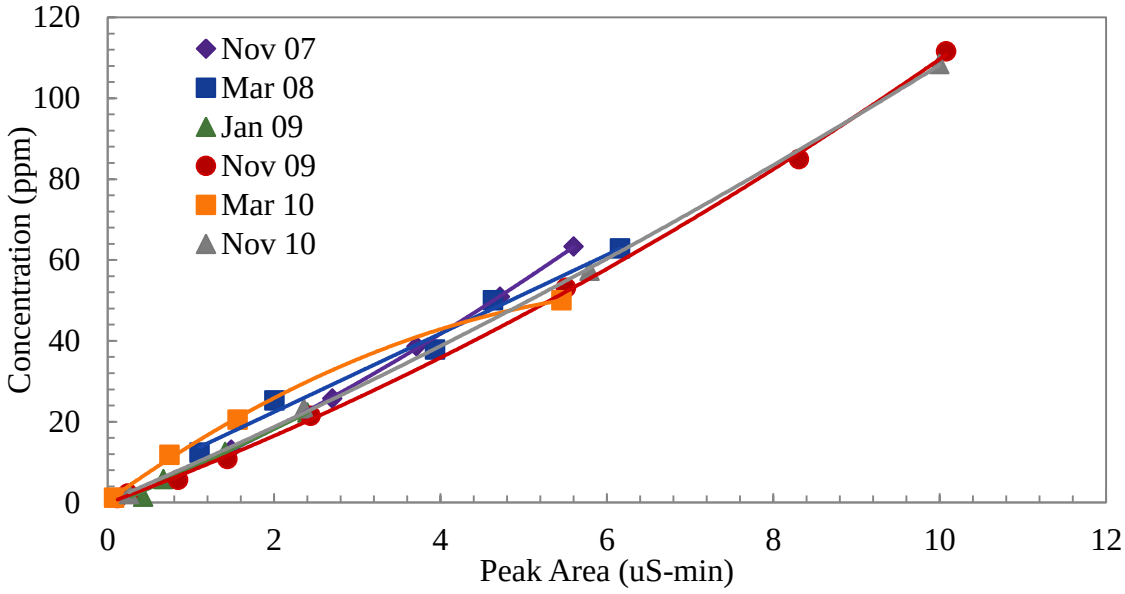

Figure 3.9: Comparison of calibration curves for formate over 3 years of operation

In order to assess the overall error of the anion IC when it is in proper working order, a random sample, the fourth time point of experiment TE51, was analyzed 18 times in a row. The measured concentration and standard deviation are shown for the three dominant peaks, formate, sulfate, and chloride, in Table 3.4 below. All three average deviations are less than 5.0%, indicating acceptable repeatability in the anion IC analysis.

Table 3.4: Assessment of error on anion IC for repeated analysis of one sample

Anion	Average Concentration mmol/kg	Standard Deviation mmol/kg	Average Deviation %
Formate	96.874	1.652	1.71
Chloride	0.103	0.00487	4.74
Sulfate	0.290	0.00368	1.27

3.1.5 Cation Ion Chromatography (IC)

Cation IC was used to identify and quantify positively charged ions (cations) in solution. The types of molecules quantified include simple cations (K^+ or Na^+), amines (PZ, EDA, 1-MPZ, HEP, and others), amides (N-formyl PZ), and polymeric amines (DETA and others). The cation IC procedure developed by Davis served as a basis of the analysis used in this work (Davis, 2009)

3.1.5.1 Apparatus description

Two separate cation IC units were used for this project. An older Dionex ICS-2500 modular Ion Chromatography System with AS-40 autosampler was initially used and then replaced with a new Dionex ICS-2100 modular IC system with AS-DV autosampler (Dionex). The method was maintained between the two instruments and the only real change was the autosampler used. For the remaining discussion, the newer ICS-2100 unit is discussed.

The flow of eluent was generated using a gradient pump that could deliver flow up to a pressure of 3000 psi. The eluent contained varying concentrations of methanesulfonic acid (MSA) in analytical grade water generated by an Eluent Generator (EG). The separation occurred in an IonPac CG17 guard column (4 x 50 mm) and an IonPac CS17 analytical column (4 x 250 mm). Both columns contained ethylvinylbenzene cross-linked with 55% divinylbenzene resin as the primary separation medium. The system also contained a 4-mm Cationic Self-Regenerating Suppressor (CSRS) to remove anionic species before cationic species finally reached the conductivity detector (CD). Chromeleon® software analyzed the conductivity output and controlled the entire system. The overall flow schematic of the cation IC is shown below in Figure 3.10.

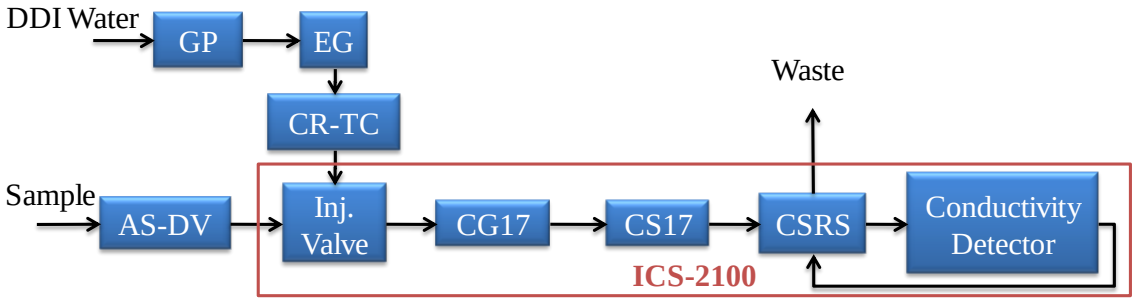

Figure 3.10: Flow schematic for the cation IC showing the AS-DV autosampler, injection valve, CG17 guard column, CS17 analytical column, CSRS, ICS-2100 housing, and conductivity detector.

The cation IC was used to quantify Na^+, K^+, NH_4^+, PZ, EDA, FPZ, 1-MPZ, 1,4-DMPZ, 2-MPZ, 2,5-DMPZ, EPZ, HEP, AEP, Mor, HomoPZ, Pyr, PD, HMI, HMDA, and other amine based degradation products. The molecular structures of the major cations quantified in this dissertation are shown below in Figure 3.11.

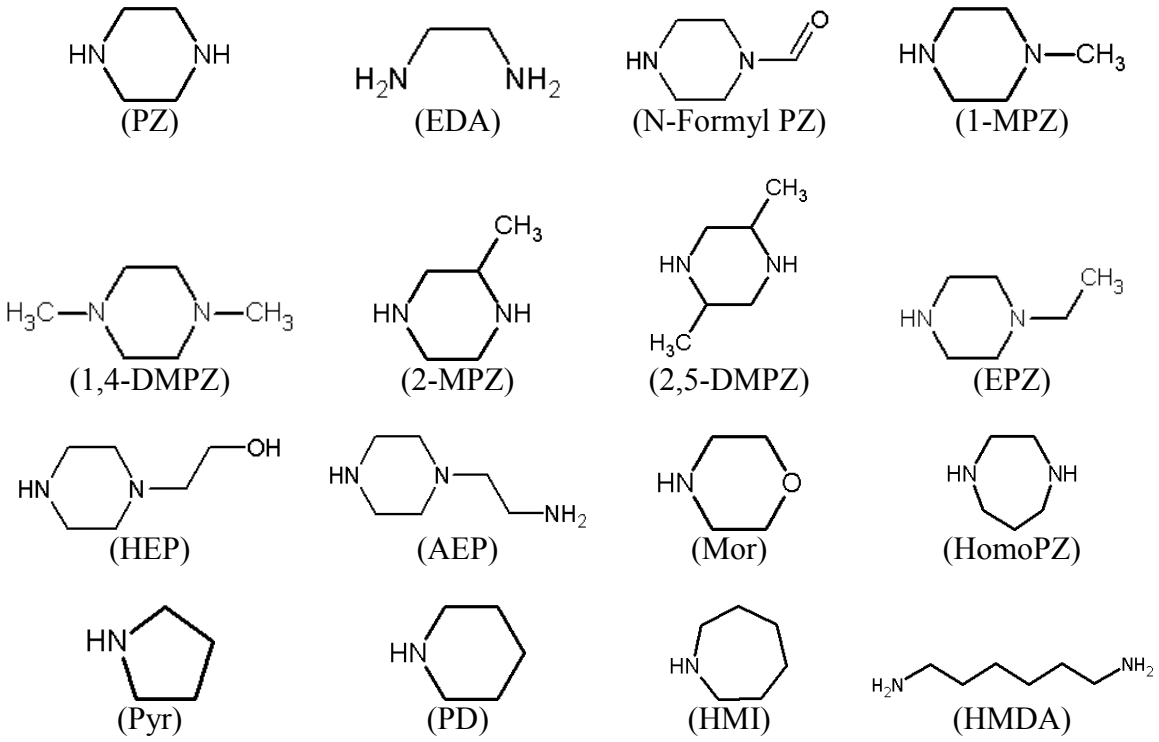

Figure 3.11: Chemical structures of molecules quantified with cation IC

3.1.5.2 Analysis procedure

The Dionex AS-DV autosampler can hold up to 50 samples, allowing high throughput of samples when needed. Samples were loaded into 5 mL sample vials with filter caps and placed into the autosampler. The autosampler was fully integrated with the Chromeleon® software and the program was written to inject only 1666 µL, or one-third of the sample volume. In this way, the sample can be injected up to three times, depending on the sequence.

In Chromeleon®, a sequence was made to direct the cation IC to analyze the samples of interested. A sequence contained all the information needed for the cation IC to know which method to use, the position of the sample in the autosampler, and how much to inject of each sample. The sequence also contained the identifying name of each

sample and the quantification file to be used afterward to analyze the resulting chromatogram. Sequences were set up with standards first and then the unknown samples with DDI placed between varying groups of samples to prevent samples from being contaminated by the previous sample.

The flow path through the cation IC begins with the samples in the autosampler. When the sample was injected, a plunger was lowered onto the top of the sample to press the filter cap downward. This allows the sample to be pushed through the filter cap and into the cation IC system. All 1667 μL of sample are injected into the system from the autosampler even though only 25 μL was injected onto the column. The first portion of the injected sample was sent to waste since it was used to flush out the line between the autosampler and the injection valve. Then, the injection valve used an injection loop to send just 25 μL of the sample to the eluent stream and onto the column. The sample was then sent to the CSRS suppressor. In the suppressor, the sample was passed through a channel with two membranes on opposite sides of the chamber, as shown in Figure 3.12 (Dionex Corporation, 2007). One membrane separated the flow path from the cathode chamber and the other from the anode chamber. In this type of suppressor, the cathode membrane allowed hydroxide from the cathode chamber to enter the flow stream in order to neutralize the proton present in the flow stream from the eluent MSA. At the same time, anions in the flow stream, including the methane sulfonate portion of MSA, were attracted to the anode chamber by the electric potential applied and travel through the anode membrane in the chamber in order to maintain electroneutrality with the hydroxide entering the flow stream. The result was a flow stream with only cations, which are the molecules of interest, and water formed from hydroxide and the proton from MSA.

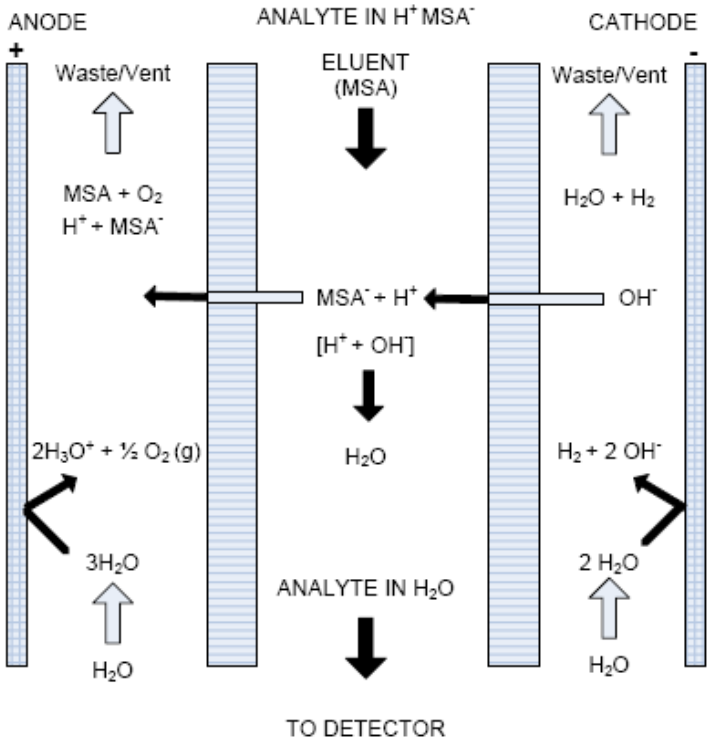

Figure 3.12: Schematic of CSRS 300 in auto-suppression mode (Source: (Dionex Corporation, 2007))

The stream that exited the suppressor was now sent through the IonPac CG17 guard column and an IonPac CS17 analytical column. The guard column was used to prevent sample contaminants from eluting onto the analytical column which would affect separation of the compounds of interest. The analytical column was where the primary separation of compounds occurs. Molecules attach to the cross-linked column internals and detach based on their adhesion properties. As the concentration of acid was increased, more difficult molecules to elute detached from the column internals and flow to the detector. This different in adhesion to the column internals was the reason for the concentration gradient in MSA. After exiting the analytical column, the flow entered the CD. Changes in solution conductivity were detected in the CD and were recorded in time

to create a chromatogram. As a group of cations in solution reached the detector, peaks were formed representing that specific species.

A method was used to control the various components of the system as well as adjusting the eluent gradient and setting the overall time for analysis. The primary method used for cation IC analysis was entitled "Jason3 Auto". In this program, various constraints and settings were used, as shown in Table 3.5.

Table 3.5: Settings and constraints for the cation IC

Setting	Value	Units
Pressure.LowerLimit	200	Psi
Pressure.UpperLimit	4000	Psi
Oven_Temperature	40	°C
Suppressor_Type	CSRS_4mm	-
Suppressor_Current	136	mA

In this method, there was three minutes before each sample, indicated as negative time, which allows the system to equilibrate after completion of the previous sample in preparation of the current sample. At negative three minutes, the flow rate was set at 1.2 mL/min with an initial concentration of 5.5 mM MSA in analytical grade water. At time zero, the sample was injected and data acquisition from the CD was turned on. At seven minutes, the gradient increased as a step change to 11 mM MSA. This eluent concentration remains until 12 minutes. Between 12 and 17 minutes, there was a gradient in the eluent concentration raising it from 11 to 38.5 mM MSA where the concentration remains for the rest of the method. The run ended at 20 minutes and the data acquisition was turned off. Each sample was analyzed using this "Jason3Auto.pgm" method unless otherwise indicated. At the end of each run of samples, the final sample was the "Shutdown.pgm" method. In this method, the suppressor and detector were turned off at

time zero. Also, the pump flow rate was decreased to 0.2 mL/min at time zero to allow the machine to remain idle until the next time it is used.

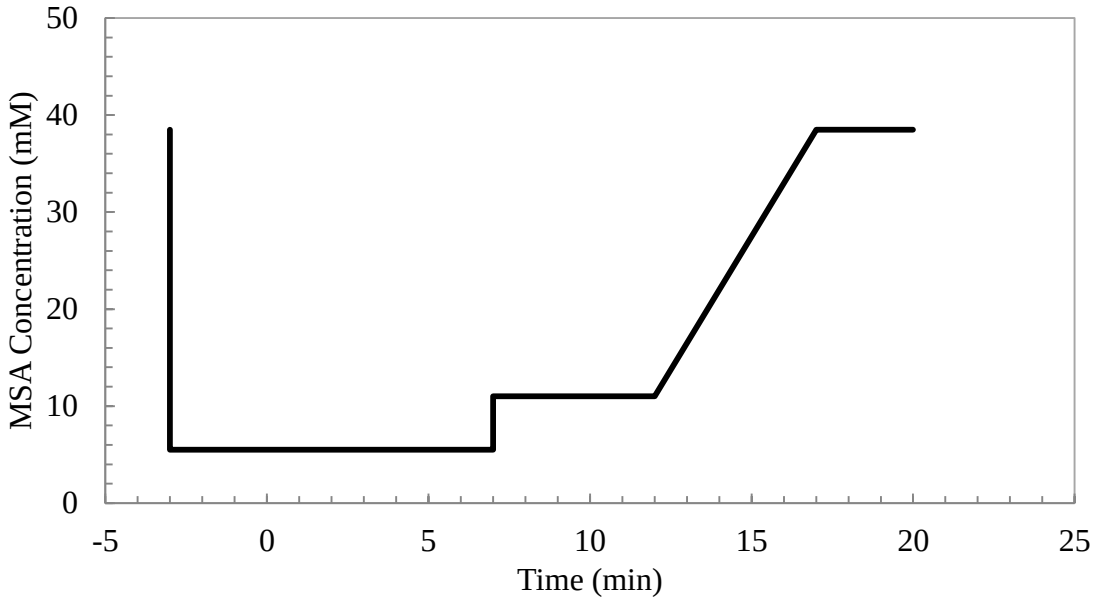

Figure 3.13: MSA gradient in cation IC method

A typical chromatogram for cation IC analysis of a thermally degraded PZ sample is shown in Figure 3.14. A dominant PZ peak can be seen at a retention time of 34.0 minutes while smaller N-formyl PZ, EDA, and AEP peaks can be seen at 15.5, 30.0, and 38.5 minutes, respectively. Calibration curves were created in order to quantify the concentrations of species in the original sample. At least four or five calibration concentrations were made for each cation of interest. Standards were created in the range of 10 to 50 ppm for amines that are expected in high concentration such as the parent amine of the given experiment. For amines that are expected in lower concentration, such as cation degradation products, calibration curves were created in the lower range of 1 to 30 ppm. The calibration curves used were always at least three different concentrations and a quadratic trendline was used. The calibration and quantification

was performed using the quantification wizard in the Chromeleon® software. The output at the end of analysis was a ppm concentration of each analyte in the dilute sample. This ppm concentration was adjusted using the dilution factor and then converted to mmole per kg for reporting.

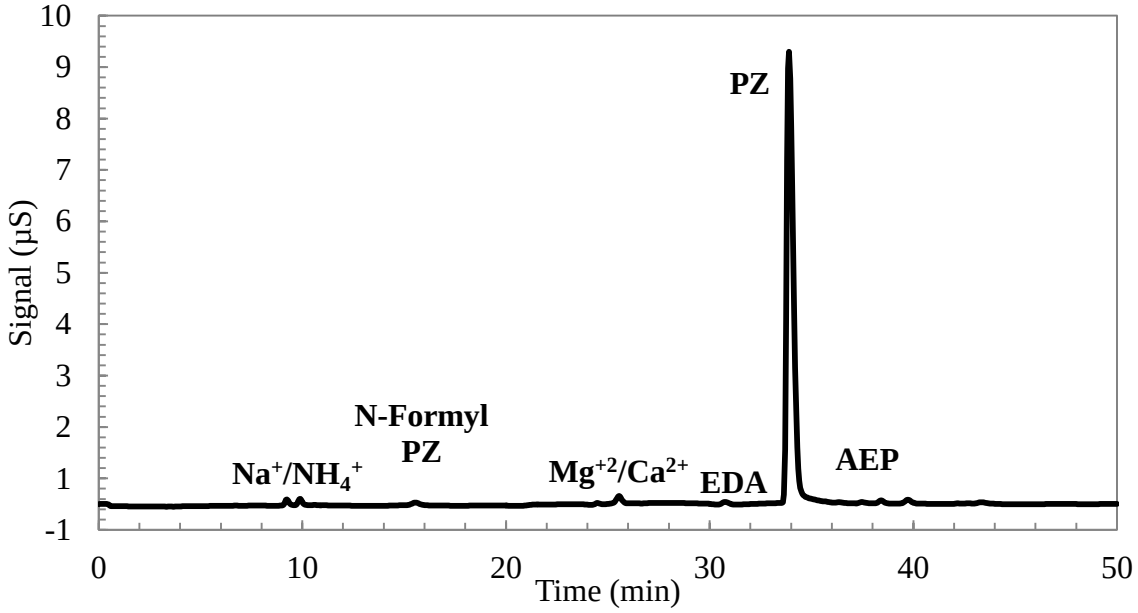

Figure 3.14: Typical cation IC chromatogram for thermally degraded PZ sample

3.1.5.3 Limitations and expected error

The primary limitation of the cation IC was the difficulty of accurately quantifying molecules that are very disparate in concentration. For example, most samples analyzed were 40 wt% in PZ (~4500 mmole per kg PZ) while amine degradation products were generated in the range of 1 to 300 mmole per kg. The large dilution needed to quantify PZ lead to the area of the degradation products being minimized. The separation of compounds was also limited by the applicability of the column, as with all types of chromatography. A CS-17 analytical and CG-17 guard column was used and particular compounds always co-elude. For example, PZ and 2-MPZ were retained

almost identically so samples containing both compounds produced a peak that could not fully resolve both compounds.

Overall, the uncertainty of the cation IC to quantify a compound of interest was less than 5%. There was error associated with every step of the analysis including the dilutions to prepare the sample, the dilutions to prepare the calibration standards, and the operation of the entire cation system that day. Overall, the system was quite accurate, but needs vigilance to ensure that the optimal operation is maintained.

In order to assess the overall error of the cation IC when it is in proper working order, a random sample, the third time point of experiment TE44, was analyzed 10 times in a row. The measured concentration and standard deviation are shown for the three dominant peaks, PZ, EDA, and NH_4^+, in Table 3.6 below. All of the average deviations are less than 5% with that of EDA and PZ being less than 0.5%, indicating superior repeatability in the cation IC.

Table 3.6: Assessment of error on cation for repeated analysis of one sample

Anion	Average Concentration mmol/kg	Standard Deviation mmol/kg	Average Deviation %
PZ	3799.5	7.9	0.21
EDA	12.06	0.04	0.35
NH4+	3.10	0.14	4.64

3.1.6 Sodium hydroxide treatment for amide quantification

Amides are molecules with a R_2N-RC=O functionality. The most basic amide is formamide (NH_3-CH=O). Amides themselves are not readily detectable with the analytical techniques employed for amines and carboxylic acids. A base hydrolysis was used to hydrolyze the amide to its corresponding carboxylic acid and amine which can be

detected as described below. This procedure was first described by Sexton who based it on the work of Koike and colleagues (Koike et al., 1987; Sexton, 2008).

Brown described how amides can be readily hydrolyzed by either acid or alkali (Brown, 1994). Water in an acidic solution or the hydroxide ion in an alkaline solution acts as a nucleophile to hydrolyze the amine to yield the corresponding carboxylic acid. An example of this hydrolysis is shown below in equation 3.10 for F PZ, a degradation product found in both oxidation and thermal degradation of PZ.

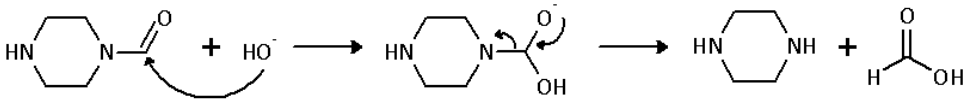

(3.10)

The concentration of total amides was determined by analyzing the hydrolyzed sample for the concentration of carboxylate anions. The increased detected in the carboxylate ions was the approximate concentration of total amides of that form (i.e. formyl amides, acetyl amides, etc.). The corresponding amine liberated from the hydrolysis was not generally used for the calculation of amide concentration because of the difficulty in detecting small changes on the cation IC. For example, an increase of 30 mmole per kg of formate was much easier to detect in a background of 20 mmole per kg of free formate compared to an increase of 30 mmole per kg of PZ in a background of 4000 mmole per kg of PZ. As mentioned in the previous section, the error in the cation IC methods can be assumed to be up to 5%, eliminating the opportunity to accurately detect small amounts of amines liberated from amides through this type of hydrolysis. In some cases where the amide concentration is sufficiently large, the increase in a particular amine was useful for determining the form of the amide originally present.

This hydrolysis was not quantitative in terms of which specific amides are present, but only quantifies the total amides of a particular carboxylic acid. Other

analytical methods are able to detect specific amides but require larger concentrations to be observed above the background in a diluted sample. Cation IC, for example, detected FPZ and gave a well separated peak around a retention time of 15 minutes on the standard "Jason3Auto.pgm" method. However, the dilution used for this technique needs to be at least 5000X, preferably 10000X, to decrease the PZ concentration to quantifiable levels. This requires at least 1-5 mmole per kg or more of FPZ to be present to produce a peak that is significant above the background at this dilution. Only highly degraded samples contain this much amide and so the hydrolysis procedure was used for all samples. Also, this hydrolysis does not take into account the possibility of multiple amide functionalities on one amine molecule. For example, two formate molecules would be liberated from the hydrolysis of N,N'-diformyl PZ. A few possible structures are listed below for PZ and EDA-based amides in Figure 3.15. These are combinations of formate, acetate, oxalate, and glycolate with both PZ and EDA, a common amine degradation product. Many more amides are possible once additional amine degradation products are generated.

The procedure for amide reversal was to treat a sample with an equal amount of 5 N NaOH and to allow the reaction to proceed overnight, at least 12 hours, before further dilution and analysis. Generally, 0.5 g or 1.0 g of each is used and the sample reacts for at least 24 hours. Tests performed on neat mixtures of loaded PZ and N-Formyl PZ showed conversion of amides within 24 hours. Thirty grams of 8 molal (m) PZ with a loading of 0.3 mole CO_2 per mole alkalinity was combined with 100 mM of N-Formyl PZ. Then, 1.0 g of this solution was treated with 1.0 g 5 N NaOH. At various time points, a sample of the treated solution was diluted 50X (to a total dilution of 100X), effectively stopping the amide reversal. The formate released during the amide reversal was then quantified using anion IC. The results are shown below in Figure 3.16. All of

the formate was released within 4 hours during this experiment. The amount of formate recovered was actually over 100% which is attributed to error in the anion IC and sample preparation. It was assumed that the FPZ standard used was not actually pure due to instability and calculations performed assumed only FPZ was present.

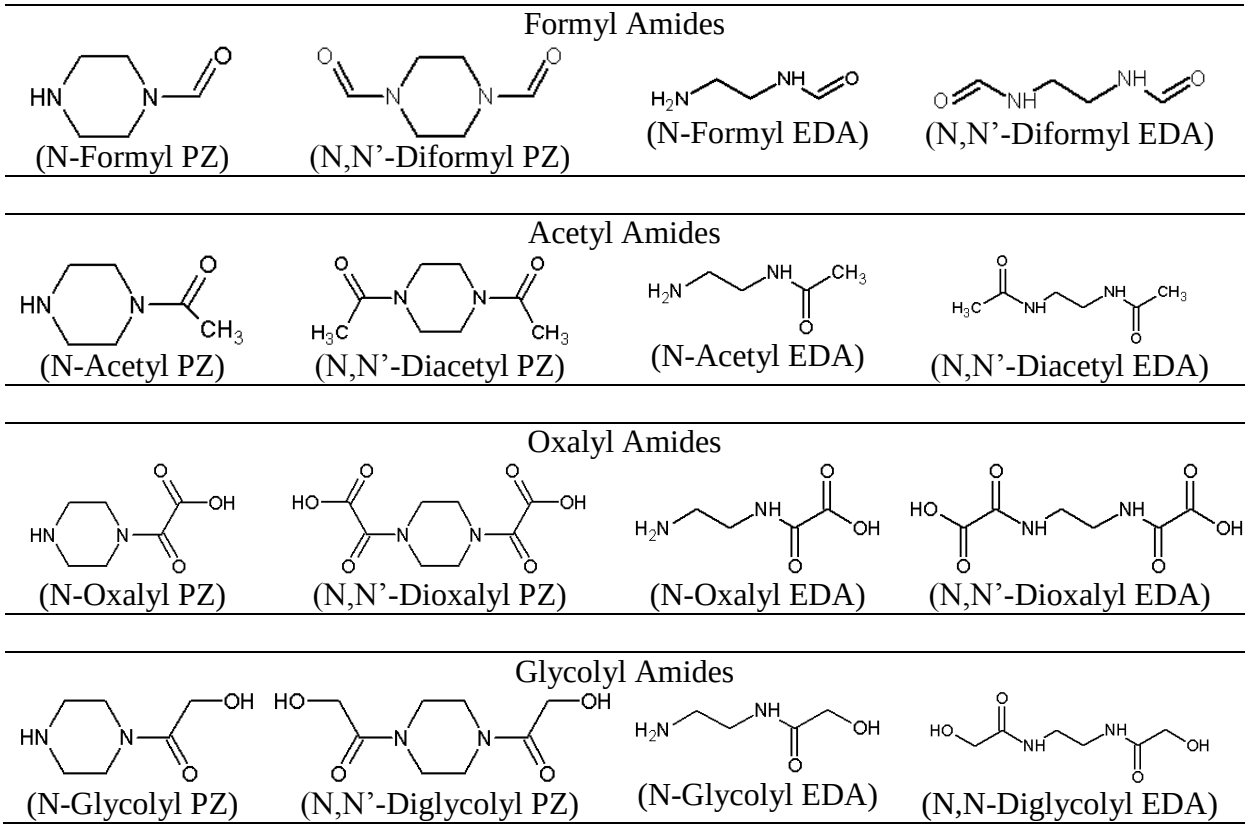

Figure 3.15: Chemical structures of possible amides in degraded solutions

The same procedure was performed on an 8 m PZ solution that was degraded for 360 hours in the Integrated Solvent Degradation Apparatus (ISDA) in order to assess the conversion of acetyl and oxalyl to their corresponding carboxylate ions (Closmann, 2011). This experimental solution was more complex than the previous test and contained a combination of both carboxylate ions (formate, acetate, and oxalate) and

amides (formyl, acetyl, and oxalyl amides) to begin with. Thirty grams of degraded PZ solution was spiked with 200 mmole per kg of FPZ and the release of carboxylate ions was observed through anion IC over the course of 48 hours. The percent of carboxylate ion released during hydrolysis is shown in Figure 3.17. The percent formate released was calculated as the increase of formate after hydrolysis compared to the 200 mmole per kg of FPZ spiked in the tested solution. The percent of acetate and oxalate released was calculated as the increase of each ion compared to the total amount released in hydrolyzed degraded PZ (without the 200 mmole per kg FPZ spike).

The anion IC results showed that the rate of reversal of acetyl and oxalyl amides was significantly slower than formyl amides. After 48 hours of hydrolysis, neither the acetate nor oxalate was fully recovered. Unfortunately, the original protocol for amide reversal only called for a 24-hour hydrolysis. This short treatment time will likely underestimate the total acetate and total oxalate, or acetyl and oxalyl amide concentrations.

3.1.7 Densitometer

3.1.7.1 Apparatus description

Density was measured using a Mettler Toledo DE40 densiometer (Mettler-Toledo, Inc., Columbus, OH). The DE40 had precise temperature control from 4 to 90 °C using a Peltier thermostat. The DE40 measured density from 0 to 3 g/cm^3 with an accuracy of 0.0001 g/cm^3. Approximately 3 mL of sample was required for each measurement and, in general, it was a destructive assay. The density was measured on neat (non-degraded) solutions due to this volume requirement.

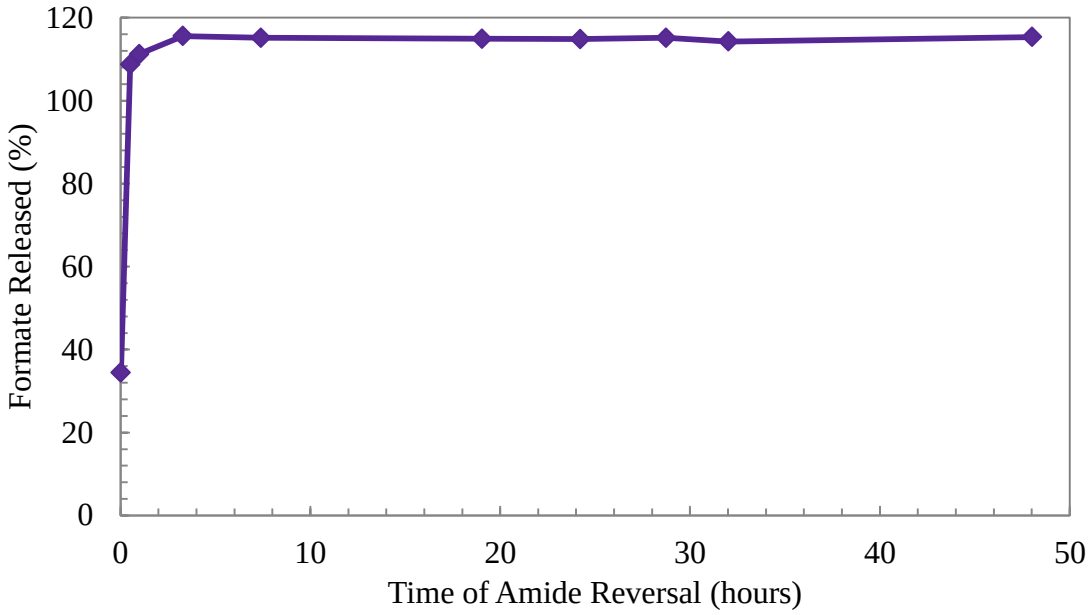

Figure 3.16: Recovery of formate during alkaline hydrolysis

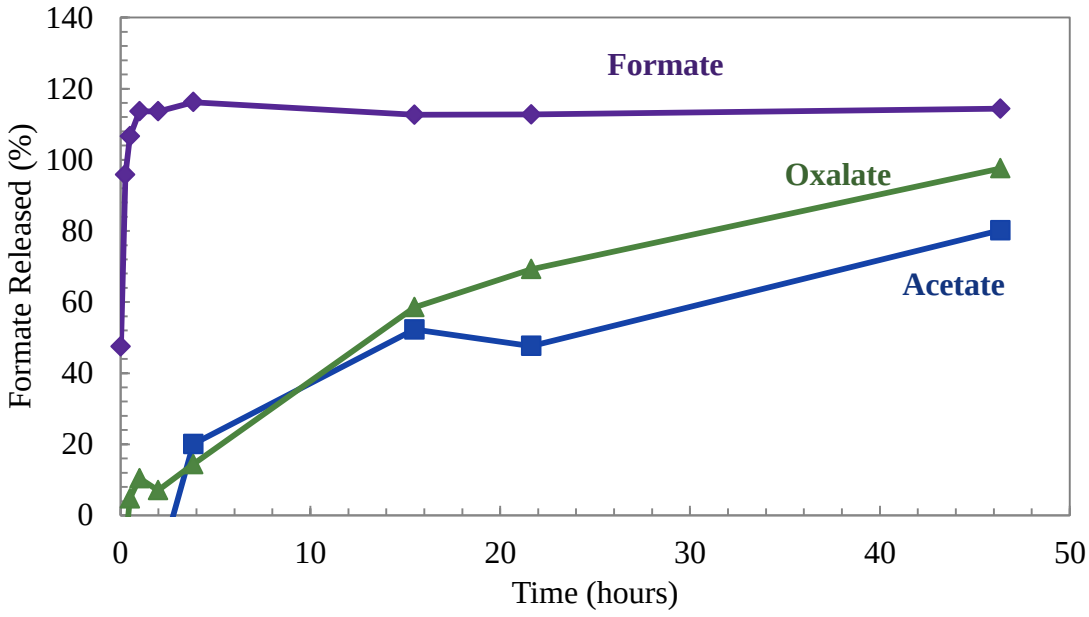

Figure 3.17: Recovery of carboxylate ions during alkaline hydrolysis of a PZ degraded for 360 hours

The DE40 measured the electromagnetically induced oscillation of a glass U-shaped tube to determine the density of a gas or liquid. The gas or liquid sample was pumped into the U-shaped tube that was contained within a thermo-conductive block, thermal insulation, and a Peltier element that maintained the U-tube temperature. A magnet was attached to the middle of the U-tube right next to a combination oscillator and vibration meter. The oscillator induced vibration in the U-tube and the period of oscillation was measured by the sensor. The frequency of oscillations was related to the calibration of air and water at each temperature to understand the characteristic frequency of oscillation of the glass tube itself. The frequency of vibration for samples was related to the mass inside the tube. A larger mass of sample inside of the U-tube would have produced a lower frequency of oscillation and, therefore, a larger the period of oscillation. The density, ρ, is related to the volume of the sample in the U-tube, V_C, the mass of the U-tube, m_C, a cell constant, K, and the period of oscillation, T, through Equation 3.11. Equation 3.11 can be rearranged in terms of ρ (Equation 3.12).

$$T = 2\pi\sqrt{\frac{\rho V_C + m_C}{K}} \tag{3.11}$$

$$\rho = \frac{K}{4\pi^2 V_C} T^2 - \frac{m_C}{V_C} \tag{3.12}$$

The value for K was determined by a two point calibration for dry air and degassed water. This constant was dependent on the type of U-tube used, the U-tube mass, and temperature. The DE40 was calibrated with air and water for each temperature of interest to determine this value of K at each experimental condition.

3.1.7.2 Analysis procedure

To measure density of a solution, the temperature of analysis was first selected by choosing the method. All the methods on the DE40 were the same except for the measurement temperature. The DE40 then needed time to reach the desired temperature and displayed "Ready" when the system was stable. To begin the analysis, the inlet tube was placed below the liquid level of the sample to be analyzed. Then, the green "Measure" button on the front of the DE40 was pressed. This activated the pump which then pulled approximately 5 mL of sample into the sample u-tube. There was excess liquid on each end of the u-tube to ensure a stable sample chamber. The DE40 then measured the density and when a stable density reading was reached, that value was displayed on the screen and the sample was pumped out of the sample tube to waste.

After the analysis of each sample, the u-tube was cleaned using three steps. After a sample was successfully analyzed, the screen on the DE40 displayed the message "Set Rinse 1 and Press Start". To begin cleaning, the inlet tube was placed below the surface of DDI water and the "Start" button was pressed. Then, the pump speed toggle was immediately pressed upward to increase the pump speed to the "Rinse" setting. This first rinse flushed the sample tube with DDI water at a fast pace to wash away any remaining amine sample. The DE40 automatically stopped at the end of this rinse cycle and the screen displayed the message "Set Rinse 2 and Press Start". Next, the inlet tube was placed below the surface of a beaker of acetone and the "Start" button was pressed. Then, the pump speed toggle was quickly set to "Rinse" and the inlet tube was lifted in and out of the acetone. This created an intermittent stream of air and acetone for this rinse cycle. When this was complete, the screen displayed the message "Set Air Purge and Press Start". For the final step, the inlet tube was placed in an empty waste beaker and the "Start" button was pressed. After 10 to 15 seconds, the pump speed toggle was

pressed downward to the "Purge" setting. The "Purge" setting reversed the direction of the pump and drew air through the desiccant on the top of the unit and pumped it through the sample u-tube to remove all moisture. The purge lasted 2 minutes and the DE40 was then ready for another sample.

3.1.7.3 Limitations and expected error

The DE40 densitometer was a very accurate apparatus yielding four decimal places on each density reading. The calibration with air and water at each temperature ensured the measurement accuracy of the system at all times. This calibration, however, must be performed at least once every few months or after long breaks in the use of the DE40 to maintain its performance. The accuracy was only guaranteed if the unit was still correctly reading the density of its standards.

A major limitation of the DE40 for the specific application to CO_2 capture solvents was that the system was at atmospheric pressure. For most amine systems, the partial pressure of CO_2 in loaded solution was significant and atmospheric heating of a solution could release CO_2 from solution. The DE40 required a very stable reading to four decimal places before registering a density measurement. For loaded solutions, this meant that readings could only be taken at temperatures below where CO_2 would bubble out of solution or in regions of lower loading. This was an additional issue with loaded, high concentration PZ solutions where the weight fraction of CO_2 can be upwards of 20% in the rich loading region.

The expected precision of this measurement was 0.0001 gram per cm^3, according to the manufacturer. A solution of 8 m PZ with 0.3 mole CO_2 per mole alkalinity has a density of approximately 1.12 gram per cm^3, which would make the expected precision

less than 0.01% of the measured value. The error could be maintained at this low level if the density of air and water was verified before each round of measurements.

3.1.8 Rheometer

3.1.8.1 Apparatus description

Viscosity was measured using a Physica MCR 301 cone and plate rheometer (Anton Paar GmbH, Graz, Austria). The apparatus had precise temperature control for measuring viscosity at temperatures ranging from -30 to 150°C through heating or cooling of the cone and plate. The apparatus was also attached to a chiller that cooled the viscometer to maintain a stable performance. The plate at the bottom of the apparatus was at a set height while the cone was attached to an arm which moved vertically up to 150 mm above the plate. A computer with the US200 software package controlled the whole system.

For well-behaved Newtonian fluids in straight, fully developed flow, the shear stress (τ) is proportional to the velocity gradient in the direction perpendicular to the direction of motion ($\partial v/\partial x$). The coefficient of proportionality is defined as the viscosity (μ). This relationship is shown in Equation 3.13.

$$\tau = \mu \frac{\partial v}{\partial x} \tag{3.13}$$

The cone and plate rheometer was used to determine viscosity by measuring the torque applied to the fluid during the rotation of the cone. The liquid sample was placed on the plate and the cone was lowered to within a defined x-distance (0.05 mm) above the plate. The cone was then rotated at specified angular speeds creating variable shear stress in the liquid. The rheometer essentially acted as a precise torque meter that determined the resistance of the fluid to rotation by being situated between the plate and cone. The

measured torque was proportional to the shear stress in the fluid and equation 3.13 was used to determine viscosity using the applied rotation speed. The viscosity was measured 10 times over a range of rotational speeds to get an accurate reading.

3.1.8.2 Analysis procedure

To determine viscosity, the CP-50 cone was first placed into the holder on the upper portion of the viscometer. In the U200 software program, a new data file was created using the "Flow Curve/CSR" option. The viscometer was set-up by choosing the experimental conditions including temperature, angular speed settings, and analysis settings. The settings used were an increase of angular speed from 100 to 1000 s^{-1} over a period of 100 seconds. The analysis involved measuring the shear stress exerted by the solution 10 times, every 10 seconds.

Once the experimental conditions were chosen, the gear box was used to initialize the instrument. In this box, the temperature was also set to match the temperature set in the "Analysis" window. Once this was done, the plate began to heat or cool to reach the experimental temperature. When the plate reached a stable experimental temperature, the zero gap was established by selecting the "Zero Gap" position for the top cone. The cone then moved down to find the zero gap that calibrates the cone at the temperature. This procedure accounted for any expansion of the bottom plate based on temperature change from the previous zero gap calibration. Then, the cone was lifted by selecting "Lift Position".

To take a measurement, 700 μL of sample was transferred onto the center of plate. The cone was then set to "Measurement Position" in the gearbox. With this command, the cone was lowered first to a "Trim Position" above the plate where any solution that was pushed outside of the edges cone was removed. When trimming was done, the cone

was finally lowered to the measurement position 0.05 mm above the plate and the measurement began by selecting the "Start Analysis" icon. After the 10 measurements were complete, the data was copied into an Excel spreadsheet. The cone was then raised to "Lift Position" and DDI water was used to clean both the cone and plate surfaces. The next sample was then transferred to the plate and the measurements continued in the same fashion.

3.1.8.3 Limitations and expected error

The Physica MCR 300 rheometer was a very accurate instrument for measuring viscosity. Anton Paar reported that it can control temperature to within 0.01 °C. The overall uncertainty of viscosity measurements was expected to be less than 1.0 %. More error was introduced when measuring the CO_2 and PZ concentrations of the experimental solutions than with the viscosity measurement.

The primary limitation of the rheometer was its inaccuracy at low viscosities. Based on experimental observation, the cone-and-plate arrangement was most accurate for liquids that were at least two to three times more viscous than water (above 2 to 3 cP). At the beginning of most analyses, the viscosity of water was measured and the rheometer consistently underestimated its value when compared to the known value for water (DIPPR, 2010). Fortunately, most amine solutions were quite viscous compared to water having about ten times the viscosity of water at room temperature. This error is apparent though for high temperature measurements when the viscosity of amine solutions was decreased.

3.1.9 Mass spectrometry coupled with Cation IC (IC-MS)

Mass spectrometry (MS) was used to determine the elemental composition of a molecule or sample of interest. In MS, a sample was ionized to create charged particles

in a gas stream. This ionized stream of particles was then subjected to electromagnetic fields that sorted the particles by their mass. A detector then measured the amount of particles of each mass and the result was a spectrum comparing the various charge-to-mass ratios (m/z) compared to the abundance of which each was found in the liquid stream. The m/z was essentially the molecular mass of a molecule plus a proton, divided by its charge of plus one. The m/z was generally just one integer higher than the molecular weight of the molecule of interest, so this technique was useful in the identification of unknown molecules in a liquid mixture. The ionization setting of the apparatus could be changed to identify neutral and positive species by using positive ionization or to detect neutral and negative species by using negative ionization depending on the desired application. When positive ionization was used, a proton was added to each molecule so neutral molecules have a positive charge and positively charged molecules receive an additional charge. Any negative charged species in solution then become neutral and were not detected.

The technique was primarily qualitative in nature and was used in this project to help identify unknown degradation products. The MS could be run using direct injection of samples or coupled with a cation IC, anion IC, or HPLC system where a sample was first separated by an analytical separation column before being analyzed by the MS. In this way, unknown peaks on cation IC, anion IC, or HPLC chromatograms could be identified specifically. This technique was also useful in the case of PZ where the high concentration of PZ can overshadow the lower concentration degradation products in direct injection techniques. In this dissertation, all MS work was cation IC-MS analysis unless otherwise noted. Direct injection analyses were performed as described previously (Davis, 2009).

3.1.9.1 Apparatus description

The IC-MS system consisted of a Dionex ICS-2100 system coupled with a Thermo Finnegan TSQ MS with a triple-stage quadrupole and electro-spray ionization (ESI) (Thermo Fisher Scientific, Waltham, MA). The chromatographic separation followed the procedure described above for cation IC. The eluent exiting the conductivity detector of the ICS-2100 was fed directly to the inlet of the ESI system of the MS. Because of this, the CSRS suppressor was not operated in recycle, or auto-suppression, mode. A N_2 tank delivered 5 psi of pressure on an auxiliary DDI water bottle to feed a slow stream of water to the back of the suppressor membrane to flush waste from the suppressor. The main method used on the cation IC had a flow rate of 0.5 mL/min and a gradient from 5.5 to 38.5 that was 50 minutes long (See appendix C for method details).

3.1.9.2 Analysis procedure

The Xcalibur® software was used to control the operation of the MS. Through the DC-MS link, Xcalibur® also controlled the Chromeleon® timebase of the cation IC. The IC-MS was operated as described previously, with a few modifications (Davis, 2009). A flow splitter was installed between the exit of the conductivity detector of the cation IC and the inlet of the ESI in order to decrease the flow rate of liquid to the MS. Better results were observed when the flow was decreased by approximately half. The valve used to split the flow was a manually controlled valve, so the exact flow rate reaching the MS was not known with precision. Also, the line bringing water from the auxiliary water bottle to the regeneration side, or back side, of the suppressor was run through the valve on the front of the ICS-2000 unit. This valve followed the behavior of the DP pump and was closed when the pump was off and opens when the pump is in use. In this way, the flow to the back of the suppressor was stopped when the system was not in use to prevent

the auxiliary water bottle from emptying and delivering air to the suppressor. The method used was very similar to the original "Jason3Auto.pgm" described above for the cation IC, except the timing was stretched out to accommodate the lower flow rate of 0.5 mL per minute. Details of the method are included in Appendix C. The shutdown method was also modified to turn off the pump at the end of a run, rather than just decreasing the flow rate to 0.2 mL per minute as done previously.

3.1.9.3 Limitations and expected error

A main limitation of the IC-MS system was the inability to distinguish between molecules with the same m/z value. This was a function of the low resolution of this particular MS where it was only possible to measure m/z ratios to the first decimal place. When trying to identify unknown degradation products, the molecular weight was a very important key, but not the entire story. As degradation products increase in size, the possibilities for what the molecules could be grow in number. For example, a peak towards the end of the chromatograms for thermally degraded PZ was identified with a molecular weight of 198 g/mole or an m/z ratio of 199. This molecular weight corresponds to three possible products that were suspected in thermal degradation of PZ, as shown in panel A of Figure 3.18. Although the molecular weights are different at the first decimal place, the MS used in this study did not have low enough resolution to differentiate between the molecules. In another case, panel B of Figure 3.18, the molecules are isomers with exactly the same molecular weight and cannot be differentiated with only MS. Usually, isomers such as these have varying retention times in chromatographic techniques and could be differentiated with retention time matching with known standards. Unfortunately, standards for complicated molecules are not always commercially available, so retention time matching was not easily done.

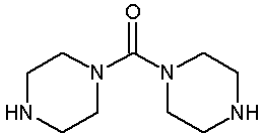

1,1’-carbonylbis-piperazine
MW: 198.2681

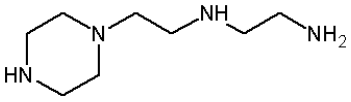

1-[2-[(2-aminoethyl)
amino]ethyl]PZ
MW: 172.2736

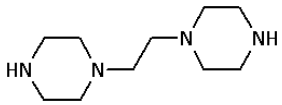

1,1'-(1,2-ethanediyl)bis-PZ
MW: 198.3115

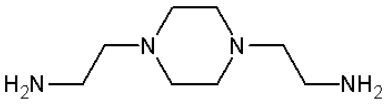

N,N’-di(2-aminoethyl)PZ
MW: 172.2736

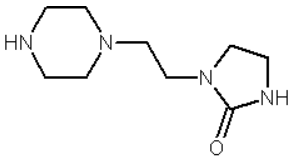

1-[2-(piperazin-1-yl)ethyl]
imidazolidin-2-one
MW: 198.2654

(A) (B)

Figure 3.18: Examples of molecules which are difficult to distinguish with IC-MS

Another limitation was the presence of Na^+ and K^+ in our samples. The samples, glassware, and IC-MS systems were all constantly exposed to low levels of Na^+ and K^+ which could act as the ionizer in the ESI process. In this way, the m/z ratio found would have been much higher than if H^+ was the ionizer, as expected. This complicated the interpretation of results when the molecular weight of the parent amine was being determined. In a similar vein, some molecules had a tendency to bunch up and attach multiple molecules to a single H^+ producing a $(2M+H)^+$ molecule instead of the expected $(M+H)^+$. Again, this made interpreting results more challenging. Finally, the destructiveness of the type of ionization used was an issue. The ESI was not a gentle ionization technique and could break apart molecules so that fragments were being

analyzed as whole molecules. In general, this was not a large issue as there was still a significant portion of the parent molecule to analyze.

3.1.10 Inductively Coupled Plasma Optical Emission Spectroscopy (ICP-OES)

3.1.10.1 Apparatus description

Inductively-Coupled Plasma Optical Emission Spectroscopy (ICP-OES) was a method for measuring the concentration of elements in solution by quantifying the absorbance of a sample over specified wavelengths. A Varian 710-ES Axial ICP-OES (Varian Inc., Palo Alto, CA) was used for this analysis. The ICP-OES was effective at measuring the concentration of multiple analytes (heavy metals and other elements) simultaneously in a single dilution. The system was controlled through ICP Expert II® software. An autosampler held all the standards and samples to be run at a given time. When being analyzed, each sample was pumped to the glass, concentric spray chamber, or nebulizer, where an argon stream nebulized the sample to be sent directly to the plasma flame. The molecules broke down in the plasma into their atoms and lose electrons, giving off optical wavelengths characteristic to each element. The emitted wavelengths were then sent to the solid state CCD detector. The plasma was created by electromagnetic induction, or time-varying magnetic fields, and created energy that broke down argon, the carrier or rarefield gas, into plasma. The plasma flame was stable and maintained at 7000 K.

For each element of interest, the three to four wavelengths with the highest intensity of absorption were measured and one argon wavelength as a background measurement. A separate calibration curve was made for each wavelength and the final concentration reported for each element was the average of the calibrated concentration of all four wavelengths. ICP-OES allowed for quick analysis of multiple metals in

solution which was especially useful for samples that contain corroded stainless steel (Fe, Cr, and Ni) or oxidation experiments where multiple metals and tracers were added (Fe, Cr, Ni, Cu, V, K, or Na).

3.1.10.2 Analysis procedure

Varian's ICP Expert II® software was used to control the apparatus, set-up the analysis sequence, and store the data. For an analysis, the exhaust fan and advanced liquid cooling supply were first turned on and the valve from the argon Dewar to the system was opened to deliver a constant supply of argon. The front of the ICP-OES had a peristaltic pump head that was used for the sampling tube and the waste tube. The autosampler had a smaller peristaltic pump used to supply a rinse solution to the autosampler probe. The default when the machine was not in use was for the rinse solution to be water, but before a run this tube was transferred to 2% HNO_3 as the rinse solution. Acid was used to rinse the autosampler sampling probe between each sample injection. These three peristaltic tubes needed to be set in their respective pump heads before the ICP-OES was turned on. The final step for preparing the ICP-OES for a run is to light the plasma. The instrument panel of ICP Expert II® was used to light the plasma. The plasma usually did not light the first time as the argon had not fully purged oxygen gas (O_2) from the system accumulated since the previous run. The plasma ignited the second time it was lit since the argon has had a chance to fully purge the system.

ICP Expert II® required a method to establish the parameters to use during the analysis and a schedule of samples. In the method, the wavelengths of interest were selected. The first wavelength of argon was always selected as a background reference. Then, for each element the three or four wavelengths that registered the most intense absorbance were selected. ICP Expert II® allowed the user to view which wavelengths of

the elements of interest overlap in the spectrum. If this occurred, the most intense wavelengths may not have been chosen for the analysis due to interference. The first four wavelengths for Fe, Cr, and Ni did not interfere with each other. The total time required for each sample increased with the total number of wavelengths chosen. When analyzing for stainless steel metals (Fe, Cr, and Ni), the first four wavelengths were selected while programs with more than three elements of interest had only the first three wavelengths selected to minimize sample volume needed and analysis time.

The ICP-OES used an autosampler containing three racks of 60 samples and one rack for 10 calibration standards. Samples were prepared by first making the desired dilution (10 – 1000X) in DDI water with 2% HNO_3. Samples were between 5 and 10 mL and stored in plastic, 15 mL falcon tubes that fit in the autosampler racks. The sample volume required depended on the total number of wavelengths to be analyzed for each sample. Calibration standards contained between 0.1 and 100 ppm of each of the metals being analyzed for and were made in DDI water with 2% HNO_3 to match sample preparation. Standards were made from commercially available 2000 ppm metal standards containing 3% HNO_3 (Fisher Scientific). Additional calibration standards were placed every 10-20 samples as a check of the system performance. A 5 or 10 ppm standard containing all the metals of interest was used for this purpose.

After a run was completed, the program automatically turned off the plasma flame and pump head for the sample and waste lines. The autosampler rinse was then transferred from 2% HNO_3 to DDI water to rinse the autosampler probe. After a few minutes of rinsing, the autosampler pump was turned off manually in ICP Expert II®. The samples were removed from the autosampler racks and the three peristaltic tubes (sample, waste, and autosampler rinse) were removed from the pump heads so they were

not stretched out and weakened in between uses. Lastly, the cooling system was turned off and the argon valve was shut in.

3.1.10.3 Limitations and expected error

ICP-OES was a fast, effective way to quantify multiple elements in solution. The primary error occurs from using a calibration curve that extended over two orders of magnitude (0.1 to 100 ppm). Gravimetric error could have occurred in preparing these standards from the 2000 ppm stock which lead to error in the predicted concentrations using the calibration curve. Another major source of error was precipitation issues frequently encountered with thermal degradation experimental samples. Also, the concentrations of metals in samples that have corroded their metal container are not known ahead of time. Therefore, knowing the appropriate dilution was difficult and the insolubility of material in the sample was used to gauge the appropriate dilution. The oxidation state of the metals was not known and some appeared to be very insoluble despite the presence of 2% HNO_3. Some solutions that had significant precipitation requiring additional dilution ended up having low concentrations of the metals of interest. The presence of solids could have damaged the ICP-OES spray chamber used to introduce the samples into the plasma. Therefore, when additional dilution was necessary to eliminate solids, the concentration of metals was at the very low end of the calibration curve.

The technology itself was considered very accurate for a multi-element solution and was designed to decrease interference from other elements. On the other hand, other methods, such as Atomic Absorption Spectroscopy (AA), were considered more accurate for a single element analysis. Since chromium, iron, and nickel were known to interact

and interfere in AA measurements, the ICP-OES was considered sufficient for the purposes of this project for a quick multi-component analysis of complicated solutions.

3.1.11 Nuclear Magnetic Resonance spectroscopy (NMR)

3.1.11.1 Background on NMR

Nuclear magnetic resonance (NMR) spectroscopy is a technique used to obtain information on the molecular structure of species in solution. NMR is used to detect molecules with non-zero spin. Stable isotopes with an odd number of protons and neutrons have an overall non-zero spin and, therefore, have a non-zero magnetic moment and angular momentum and can be detected by NMR. The most commonly used isotopes for NMR are ^{1}H and ^{13}C which are very useful for describing organic molecules.

During an NMR analysis, the sample of interest is subjected to a magnetic field and electromagnetic pulses and the result is a spectrum of peaks that are associated with individual atoms in the molecule. All molecules that are uniquely positioned within a molecule produce a separate response. Each individual atom can be assessed for the atoms it is directly connected to and what those molecules are connected to. If multiple atoms have the same relative position, they are all represented by one response on the NMR spectrum. For example, if a molecule is symmetric like PZ, there was only one unique position for all the carbons and one unique position for all the hydrogens (Figure 3.19). Each carbon in PZ is connected to another carbon, a nitrogen atom, and two hydrogen atoms. All the carbons in PZ are the same based on atomistic connectivity. In an asymmetrical molecule like $PZCOO^{-}$, there are 3 different types of hydrogen and carbon atoms because the presence of the carbamate changes the connectively associated with the two carbons (labeled C_2 in Figure 3.19) connected to the nitrogen that has the

carbamate (labeled C_3 in Figure 3.19). $PZCOO^-$ would, therefore, have three separate responses on the ^1H and ^{13}C spectrum to represent the molecule.

The unique responses on the spectrum are represented as shifts in the peaks from a reference standard, usually dioxane. Specific functional groups have common areas of the spectrum where their peaks usually shift to. It is possible, therefore, to use tables of standard peak shifts to identify the type of functional group associated with an unknown peak. For example, the C=O in a carboxylic acid or carboxylate ion has a traditional shift in the region of 10 to 13 ppm on a ^1H NMR spectrum. The details of NMR analysis has been described previously in detail (Hilliard, 2008).

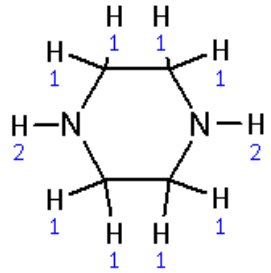

(A) Unique protons in PZ

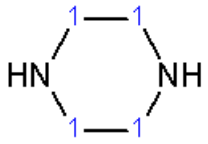

(B) Unique carbons in PZ

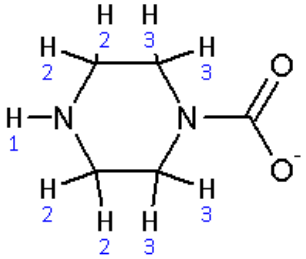

(C) Unique protons in $PZCOO^-$

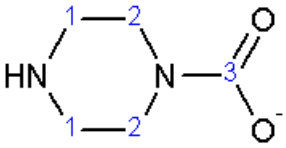

(D) Unique carbons in $PZCOO^-$

Figure 3.19: Identification of the unique protons and carbons in PZ (panels A and B) and $PZCOO^-$ (panels C and D)

Aqueous, loaded PZ solutions are complicated compared to other amines because of the speciation that exists (Section 2.1). The ^{13}C NMR spectrum for an undegraded, loaded PZ solution contains seven primary peaks associated with seven unique carbons

that are identified in Figure 3.20. In solution, equilibrium between protonated and unprotonated species occurs rapidly and ^{13}C NMR cannot differentiate between the two species. Therefore, the carbons of the protonation pairs of $PZCOO^-$ and H^+PZCOO^- or CO_3^{-2} and HCO_3^- are not unique and are represented by a single peak (Figure 3.20, panels B and D). The four types of carbon on the backbone of the PZ (C_1, C_2, C_3, and C_6) have a small downfield shift in the range of 40 to 45 ppm while the three carbons that are part of the carbonyl moiety (C_4, C_5, and C_7) have a large downfield shift and are detected in the range of 160 to 165 ppm.

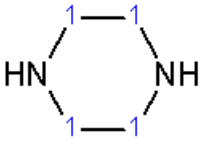

(A) Unique carbons in PZ

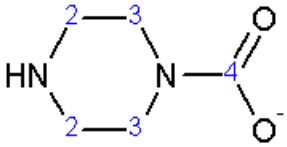

(B) Unique carbons in $PZCOO^-/H^+PZCOO^-$

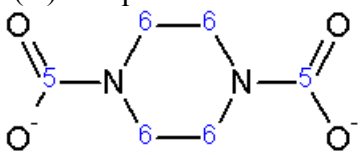

(C) Unique carbons in $(PZCOO^-)_2$

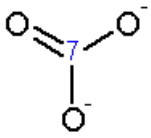

(D) Unique carbons in CO_3^{-2}/HCO_3^-

Figure 3.20: Unique carbons found in CO_2 loaded PZ solutions

In reference to this dissertation, NMR was used for two different purposes. First, NMR was used to screen for new degradation products. PZ degradation was sometimes difficult to accurately determine due to the large concentration of PZ and the detection limits of the analytical methods. NMR was used to determine if a sample only contained peaks representing PZ or if other, unidentified peaks existed. In this way, degradation of PZ could be confirmed in samples that were difficult to analyze using the other techniques described above. Secondly, ^{13}C analysis was used to analyze degradation

samples containing $^{13}CO_2$ to determine which, if any, degradation products contained the ^{13}C from $^{13}CO_2$.

3.1.11.2 Sample preparation and analysis

Samples for NMR analysis were prepared according to previous work and the recommendations of the staff of the University of Texas at Austin NMR Laboratory in the Department of Chemistry (Hilliard, 2008; Wallin and Storey, 2010). A solution was made with 10 wt% D_2O and 1 wt % dioxane with the balance being the sample of interest. Then, 2 to 3 mL of solution was carefully transferred to a 5.0 mm OD x 4.2 mm ID x 7 in NMR tube (Item No. 507-PP-7, Wilmad Glass, Vineland, NJ). When working with sensitive samples containing ^{13}C labeled CO_2, the end of the tube was sealed by Mike Ronalter of the chemistry glass shop (Ronalter, 2009).

Samples were then submitted to the NMR laboratory for analysis. NMR measurements for ^{1}H and ^{13}C NMR were performed at the NMR laboratory at the University of Texas at Austin Department of Chemistry (Wallin and Storey, 2010). The NMR laboratory used a 500 MHz Varian Inova for ^{1}H NMR, or proton NMR (Agilent Technologies, Santa Clara, CA). The NMR laboratory used the same instrument ^{13}C NMR, or carbon NMR, but at 125 MHz.

For all samples, both ^{1}H and ^{13}C analysis were performed for all samples with correlation spectroscopy (COSY). COSY results assisted during data analysis to identify which specific atoms were responsible for each peak on both spectrums.

3.1.12 High Pressure Liquid Chromatography (HPLC) and LC-MS

HPLC was used to identify and quantify nonionic species in solution. In this dissertation, the HPLC was used to quantify 2-imidazolidone (2-Imid) and look for other unidentified peaks. The same HPLC method and column described here were also

applied to the LC-MS system attached to the same MS used for IC-MS, as in Section 3.1.9. The description of the MS, ESI system, and operation of Xcalibur® in Section 3.1.9 applied to the operation of the LC-MS, except that the flow path exiting the LC separation column was fed direction into the ESI chamber during analysis. LC-MS was used in an attempt to identify the unknown peaks found during the HPLC analysis of degraded PZ samples.

3.1.12.1 Apparatus description

HPLC was performed using a Dionex UltiMate 3000 LC unit with LPG-3400SD quaternary analytical pump, WPS-3000SL analytical split-loop autosampler, TCC-3000SD thermostatted column compartment, and VWD-2100 single channel variable wavelength detector (Dionex Corporation). Separation was achieved in an Acclaim® Polar Advantage II (PA2) reversed-phase analytical column with guard column (C18, 5µm, 120Å, 4.6 x 250 mm, Dionex Corporation). The eluent contained a gradient of acetonitrile, methanol, and water during a 30 minute analysis. Samples were diluted 10-20 times in analytical grade DDI water and analyzed directly. The method was optimized for maximum separation of complicated samples. The variable wavelength ultraviolet (UV) detector scanned at 210 nm for this method and detected a variety of organic compounds that had UV responses in this range. The system also fed the flow exiting the UV detector to the evaporative light scattering detector (ELSD) for additional quantification of semi-volatile and non-volatile compounds. In the ELSD, the eluent stream containing the sample was heated and nebulized in a heated nitrogen flow. The nebulization of non-volatile and semi-volatile compounds left a particle cloud that scattered light in the detector and created the positive response. Highly volatile compounds, such as the solvent and eluent, were nebulized to a vapor phase that only

minimally scattered light. Responses on the ELSD were not been high compared to the UV detector and were not used.

3.1.12.2 Analysis procedure

The operation of the HPLC was very similar to that described previously for the anion IC operation. Chromeleon® software (Dionex Corporation) controlled the system and directed the analysis of multiple samples through the use of a sequence and by applying the appropriate method, "PA2-MeOH-ACN-2.pgm" in this case. The method contained the information regarding the injection of the sample and eluent gradient. The same 1.5 mL vials with plastic snap caps used for anion IC also fit the WPS-3000SL autosampler of the UltiMate 3000. The details of the gradient method used for HPLC analysis is shown in Figure 3.21.

The flow path for HPLC was similar to other chromatography described previously. The quaternary analytical pump was used to produce the desired concentrations and flow rate of liquid indicated by the method at a given moment. The sample was injected into the flow path of the eluent that then reached the guard column and analytical column, where the separation occurred. After exiting the analytical column, the flow brought the sample to the UV detector where the UV absorbance of a given sample in solution at 210 nm created a response. This response was recorded to produce the analytical chromatograph from which concentrations were inferred. The flow exited the UV detector and then entered the ELSD. The signal from the ELSD was also recorded for each sample. Finally, the flow exited the ELSD and any remaining condensed phase stream was sent to waste.

As with IC, calibration curves were created in order to quantify the concentrations of species in the original sample. At least four or five calibration standards were made

for each molecule of interest. The detection limit of the UV as slightly higher than with anion IC or cation IC and standards used were in the range of 0.01 to 1 wt % of the desired molecule. The calibrations were fit with quadratic regressions. The calibration curve for 2-Imid created from 0.01 to 1 wt % of the compound routinely had an r^2 value of 0.999. The calibration and quantification was performed using the quantification wizard in the Chromeleon® software. The output at the end of analysis was a weight percent of each analyte in the dilute sample. This weight percent was adjusted using the dilution factor and then converted to mmole per kg for reporting.

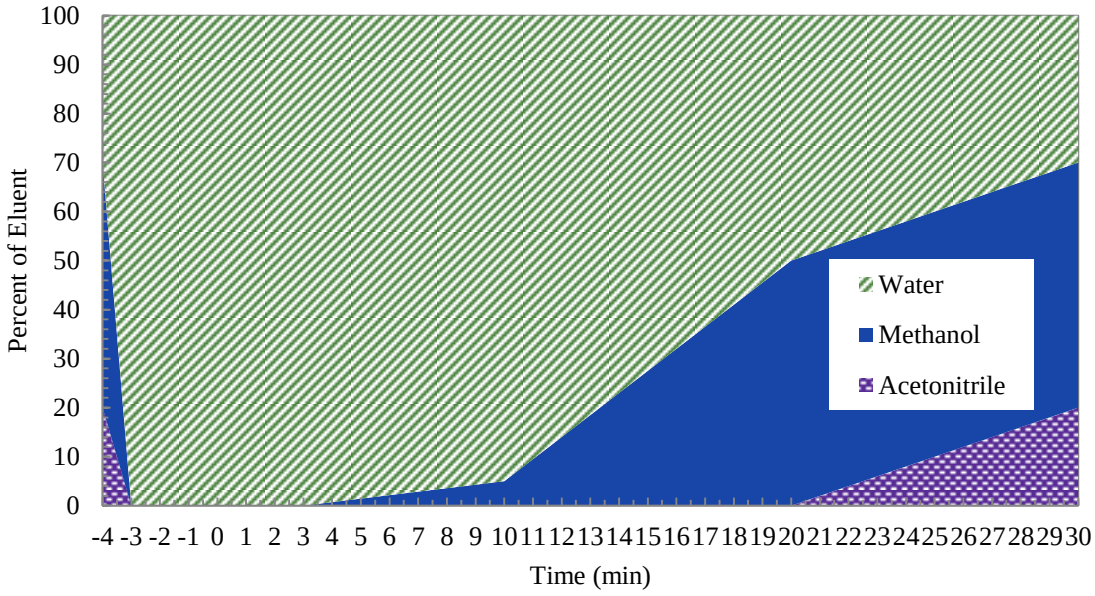

Figure 3.21: Water/methanol/acetonitrile gradient in HPLC method

3.1.12.3 Limitations and expected error

The largest sources of error in HPLC were the presence of unknown compounds, the unknown absorbance of many molecules on the UV scale, and the difficulty in optimizing the separation method. The samples analyzed were usually 10X dilutions which contained a large variety of unknown compounds. This resulted in a large number

(sometimes >30) unknown peaks that were never identified. When attempting to quantify one or more that have been identified with retention time matching of standards, the presence of so many unidentified compounds complicated the procedure. Also, the UV absorbance spectra of many of the molecules of interest were not available in literature, so it was difficult to predict or determine the identity of the unknown molecules. Finally, many variables can affect an HPLC separation and it was a challenge to fully optimize the system. For example, the flow rate, column type, guard column type, type of eluent, percentage of each eluent, dilution factor, injection amount, and temperature all affect the separation and quantification in varied ways. The system was extremely complex while the samples analyzed were more complex than standard organic chemistry lab samples. In the end, an acceptable method was found that yielded a good separation of the major compounds using a straightforward column and method. Although every variable was not exhaustively optimized, the separation was satisfactory for this analysis.

3.1.13 Total Organic Carbon (TOC) and Total Nitrogen (TN) analysis

Analysis for total organic carbon (TOC) and total nitrogen were performed using an Aurora 1030 Combustion TOC analyzer with total bound nitrogen (TN_b or TN) module (OI Analytical, College Station, TX). The TOC function is capable of quantifying 100 ppb to 30000 ppm C with precision of 1.5% relative standard deviation. Combustion of organic carbon is performed in an O_2-rich furnace where carbon is converted to CO_2 and intermediates. The gas stream then enters a catalyst chamber containing with platinum catalyst where the intermediates are converted to CO_2. The sample is sent through a scrubber to remove other contaminants and a dryer before reaching the infrared detector. For TOC, a sample size of 1 mL was used and a

calibration curve was developed from 3 to 11 mmole C per kg requiring 3000 to 4000X dilutions of the 8 m PZ samples analyzed.

For TN analysis, the same combustion chamber used for TC is used where all bound nitrogen in a liquid sample is reacted into NO_X (nitrogen trioxide (NO_3), nitrogen dioxide (NO_2), and nitric acid (NO)). After combustion in the TC combustion chamber, the gas stream is sent to a NO_X converter which contains catalyst that decreases NO_X to NO, which is then detected in the combustion analyzer. A sample size of 0.2 mL was used and a calibration curve was developed from 0.9 to 2.3 mmole N per kg requiring 8000 to 9000X dilutions of the 8 m PZ samples analyzed.

3.1.14 Amino Acid Liquid Chromatography (AA-LC)

Amino acid liquid chromatography (AA-LC) was used to observe and identify amino acids generated as degradation products. A Dionex ICS-3000 modular Dual RFIC Ion Chromatography System with AS autosampler was used (Dionex Corporation, Sunnyvale, CA). The eluent contained varying concentrations of sodium hydroxide (NaOH) and sodium acetate in analytical grade water. The separation occurred using an AminoPac PA10 guard column (4 x 50 mm) and an AminoPac PA10 analytical column (4 x 250 mm). Both columns contained hydrophobic, polymeric, pellicular, anion exchange resin according to the manufacturer. The analysis used an electrochemical detect with Ag/AgCl reference electrode that works through gold catalyzed oxidation of amino acids. Chromeleon® software analyzed the detector output and controlled the entire system.

The AA-LC analysis ran in parallel on the ICS-3000 with the anion IC technique and shared an AS autosampler. The AA-LC technique was used for screening of new compounds for this project and no specific amino acids were successfully identified or

quantified. The method was used to control the various components of the system was "Voice-1.pgm", which is provided in Appendix C. In this program, various constraints and settings were used, as shown in Table 3.7.

Table 3.7: Settings and constraints for the AA-LC

Setting	Value	Units
Pressure.LowerLimit	200	Psi
Pressure.UpperLimit	3900	Psi
pH.LowerLimit	10	-
pH.UpperLimit	13	-
Column_TC	30	°C
Compartment_TC	30	°C
Flow	0.25	mL/min

In this method, there was one minute before each sample, indicated as negative time, which allowed the system to equilibrate to the starting gradient, set the flow rate at 0.25 mL/min, and to prepare for the injection. At time zero, the sample was injected and data acquisition from the electrochemical detector (ECD) was turned on. The eluent contains water and sodium hydroxide to for the first 11 minutes. Then, sodium acetate is added until a maximum concentration of 70%, where it remained for 20 minutes. After 44 minutes, data acquisition is concluded and the flow and gradient remained constant for 30 minutes to equilibrate the cell. The eluent concentration gradient over the course of "Voice-1.pgm" is shown in Figure 3.22. At the end of each run of samples, there was a final sample with the "Shutdown.pgm" method.

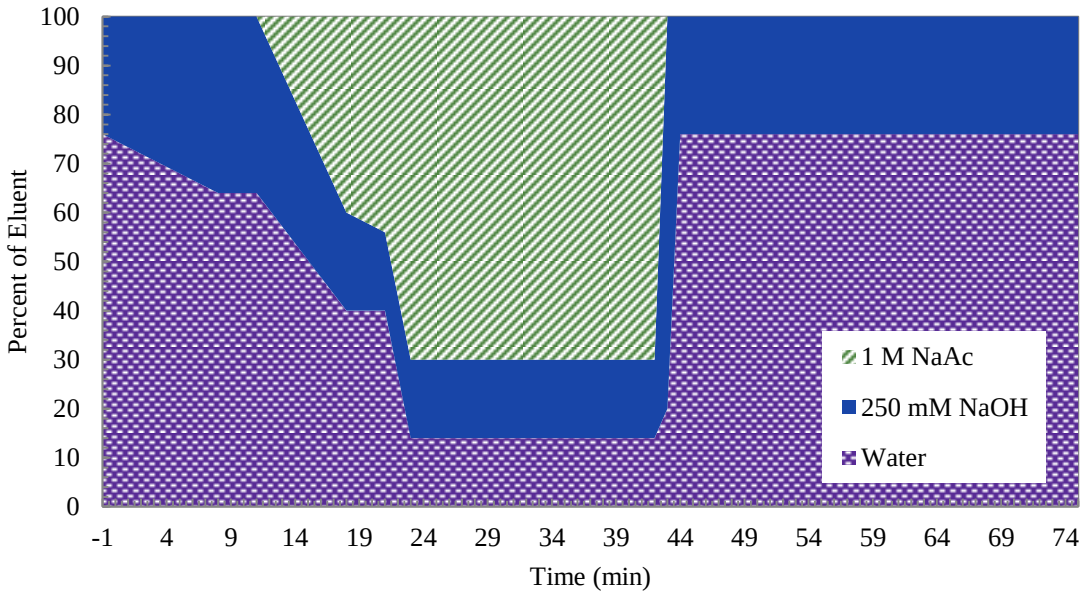

Figure 3.22: Sodium hydroxide and sodium acetate gradient in AA-LC method

3.2 EXPERIMENTAL EQUIPMENT

3.2.1 Thermal cylinders

Thermal degradation of amines was studied using thermal cylinders, formally referred to as thermal bombs (Davis, 2009). This experimental design allowed a high sample throughput due to the simple design and the Swagelok® seals maintained the solution pressure even during high temperature experiments.

3.2.1.1 Apparatus description

The thermal cylinders used were small, simple containers that sealed completely to allow amine solutions to be exposed to high temperatures under pressure. Thermal cylinders were constructed of five inches of ½-inch OD 316 stainless steel tubing with 316 stainless steel Swagelok® endcaps. The Swagelok® connection using ferrules provide an airtight seal that is rated to hold up to 2000 psi of pressure (138 bar). The simple nature of the cylinders allowed a high throughput of thermal degradation

experiments as hundreds of cylinders were constructed in a relatively short period of time and inexpensively. Cylinders were reused after the completion of each experiment but the end caps were married to a specific cylinder using engraved labeling.

3.2.1.2 Experimental procedure

Thermal degradation experiments were performed in forced convection ovens that maintain a steady high temperature. Before preparing the experimental cylinders, the oven was turned on and at the desired experimental temperature and allowed to stabilize.

The thermal cylinders all had engraved markings that indicate the cylinder number and each end separately, as indicated by the "A" and "B" in Figure 3.23. Different sets of cylinders were used that had different kinds of markings, such as "A" and "B" ends, "+" and "-" ends, or "●" and no marking ends. In each case, the sets are numbered consecutively and reused.

A group of clean thermal cylinders are prepared at the beginning of the experiment by sealing either the "B", "-"", or no marking end of each cylinder, depending on the cylinder set used. The cylinders were preferably in numerical order to simplify the experiment and in order to quickly know which experiments were in each oven at one time. Each empty cylinder was weighed with both end caps and the mass is recorded. Next, 10 mL of the amine solution being tested was pipetted into the empty cylinder through the open "A", "+", or "●" end. That end was then sealed following the instructions provided by Swagelok® (one-quarter turn past finger-tight). Each sealed cylinder was then weighed again and the full mass was recorded.

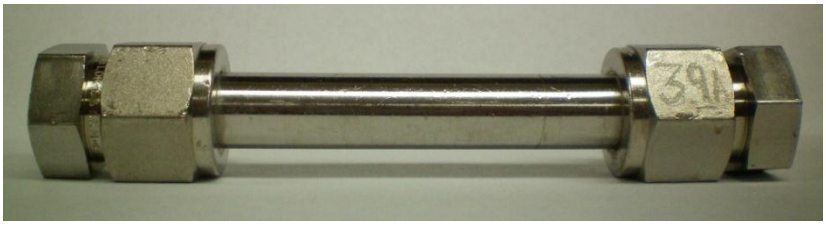

Figure 3.23: Thermal cylinder with "A" end and cylinder number (39) labeled

All of the cylinders were placed in the oven and the start time of the experiment was recorded. At each sampling time point, usually every 1 to 4 weeks, one cylinder was removed from the oven. This cylinder was allowed to cool on the bench top and then the unopened cylinder was weighed and the mass was recorded to determine if the cylinder failed. At this point, the cylinder was opened and the sample was poured into a glass sample storage vial.

The thermal cylinders failed if the seal was not properly made before placing in the oven. Once the cylinders heated up the first time, an improperly sealed cylinder would have allowed amine vapor to leave the cylinder. This usually resulted in a distinct hot amine odor and the leaking liquid left burned, black residue on the outside of the cylinder. Cylinders that lost less than 20% of their initial amine solution weight were deemed to be successful cylinders. The failing of cylinders was very dependent on temperature where high temperature experiments (175 °C) lost anywhere from one-third to half of the initial cylinders while lower temperature experiments (150 °C) usually only had one or two failures. In a typical PZ experiment, a cylinder would either lose 1-3% of its mass or completely fail with losses of 80-100% so the failures were easy to pinpoint. Any completely empty cylinders were not analyzed as part of the experimental samples. However, partially failed cylinders (0 to 80% loss) were analyzed in case the liquid still

represented the experiment well. In the experimental design, extra cylinders were prepared to allow for possible failures.

3.2.1.3 Data analysis

The main analysis performed on samples from thermal degradation experiments was liquid phase analysis for amine concentration and the production of degradation products. All thermal degradation samples were analyzed for total alkalinity, CO_2 concentration, PZ concentration (or parent amine concentration if PZ is not the parent amine), amine degradation product concentrations (cation IC), and heat stable salts or carboxylate ion concentrations (anion IC). The mass change of each cylinder was analyzed as well to ensure that each cylinder did not lose a significant amount of mass during the experiment. For most experiments, the amount of iron, nickel, and chromium was analyzed to understand the leaching of metals from the cylinders during the course of the experiment.

3.2.1.4 Special considerations – solid solubility

Numerous thermal degradation experiments were performed on amine solutions that were not aqueous solutions at room temperature or had solubility issues after degradation. Special procedures were required to properly prepare the thermal cylinders for the experiment, remove the samples at the end of the experiment, or perform dilutions for liquid analysis. Hot water was used to warm the container holding the solution, either a bottle, vial, or thermal cylinder, in nearly every case where solubility was an issue. Solutions that were insoluble at room temperature were prepared as usual and maintained on a hot plate while filling the thermal cylinders. The cylinders were then sealed as normal and the experiment started. When the experiments were complete, the cylinders were removed from the oven and allowed to cool down to room temperature in order to

measure the post experiment mass. Then, the cylinders were warmed in a beaker of water to approximately 40-50 °C. The cylinders were then removed from the hot water, excess water was removed from the outside, the cylinders were opened, and finally the solution was poured directly into a sample vial. Once the solution cooled to room temperature, it again solidified in the sample vial. When dilutions and titrations where being performed, the small sample vial was placed in a small beaker of hot water again to solubilize the solution for analysis at 40-50 °C.

A few experimental solutions were soluble at room temperature and when emptying the cylinders but then crystallized in the sample vial when analysis was needed. It was assumed that the degradation products now present in the solution contributed to the insolubility. Another phenomena observed was that solutions that should be insoluble at room temperature and pressure where able to be transferred from the cylinders to a sample vial before any crystallization. The solution is exposed to high pressure in the cylinders and even when opened, do not crystallize immediately after being exposed to atmospheric pressure. For example, the 8 m PZ experiment with a loading of 0.1 mole CO_2 per mole alkalinity (TE21) exhibited this behavior. The cylinders were filled with warm solution and degraded. When the cylinders were opened after degradation they were soluble enough to pour into the sample vials. Once in the vials, they solidified after approximately 20 minutes. The viscosity of PZ solutions helps to delay crystallization slightly. The thermal degradation experiments that had solubility issues were treated in the way indicated in Table 3.8.

3.2.2 Low gas flow reactor – Original Oxidation Reactor (OOR)

Oxidation, or oxidative degradation, of amines was studied using low gas flow reactors. The original design of the oxidation reactor has been described previously in

great detail (Goff, 2005; Sexton, 2008). In this thesis, this design is known as the original oxidation reactor (OOR).

Table 3.8: Heat requirement in preparing, sampling and analyzing thermal experiments

Expt.	Solution	Heat Requirement at Each Experimental Step		
		Filling Cylinders	Emptying Cylinders	Making dilutions
TE21	8 m PZ, α=0	Heat	Heat	Heat
TE23	8 m PZ, 0.15 mol H^+/mol alk	None	Slight heat	Heat
TE24	8 m HomoPZ, α=0.3	None	None	Heat
TE25	8 m Pyr, α=0.3	None	Slight heat	Heat
TE26	8 m PD, α=0.3	None	Slight heat	Heat
TE27	8 m HMI	None	None	Heat
TE34	8 m PZ, α=0.1	Slight heat	None	Heat
TE36	8 m HMDA, α=0.3	Slight heat	High heat	Heat
TE46	8 m PZ, α=0	Heat	Heat	Heat
TE47	8 m PZ, α=0.1	Slight heat	None	Heat
TE48	8 m PZ + 0.15 mol H^+/mol alk	None	Slight heat	Heat
TE52	8 m PZ, α=0	Heat	Heat	Heat
TE53	8 m PZ, α=0.2	Heat	Heat	Heat
TE55	8 m PZ + 0.1 mol H^+/mol alk	None	Slight heat	Heat
TE57	20 m PZ, α=0.3	None	Slight heat	None
TE58	20 m PZ, α=0.3	None	Slight heat	None
TE61	4 m PZ + 0.15 mol H^+/mol alk	Heat	Heat	Heat
TE62	12 m PZ + 0.15 mol H^+/mol alk	Heat	Heat	Heat
TE63	8 m PZ + 0.3 mol H^+/mol alk	Heat	Heat	Heat
TE65	8 m PZ + 0.1 $KHCO_3$	Heat	Heat	Heat

The OOR consists of a glass, jacketed reactor, recirculating water bath (Lauda-Brinkmann, Delran, NJ), gas pre-saturator, and mechanical agitator as shown in Figure 3.24. The reactor is a 600-mL jacketed, flat-bottomed reactor with internal diameter of 80 mm (Ace Glass, Vineland, NJ). The water bath was maintained at 55 °C for most experiments and water was circulated through the reactor jacket. The saturator was a two-piece, glass, vacuum trap placed in the 55 °C bath where the inlet gas was sparged through a column of water in order to saturate the gas at the reactor temperature. This

original design used a black, rubber stopper as the lid of the reactor. It had a central hole for the agitator and two holes near the outer edges for the inlet gas and for sampling.

Original Oxidation Reactor (OOR) Teflon Oxidation Reactor (TOR)

Figure 3.24: Overall set-up for the OOR and TOR including a water or oil bath, pre-saturator, gas inlet line, and overhead agitator

This reactor design was used successfully for many years when oxidizing amines that readily oxidize such as MEA, blends of MEA and PZ, and EDA (Goff, 2005; Rochelle, 2010b; Sexton, 2008; Zhou et al., 2010). Unfortunately, with amines that oxidize slowly, such as PZ or MDEA, the degradation of the amine was overshadowed by errors caused by the reactor design. The water balance has always been the largest issue. Water easily escapes with gas exiting the reactor through the open annular space around

the agitator shaft. A secondary issue was the use of rubber as the lid material. PZ readily absorbed into this rubber lid further confounding degradation with mechanical issues with the reactor. After oxidation experiments, the stopper would commonly be swollen with the amine and water it had absorbed. The stopper edges were also hot because of their contact with the glass reactor, adding to the swelling concern. A total of 16 oxidation experiments were performed in the OOR. The results are presented alongside those achieved with the new oxidation reactor. The reactor used was indicated to allow for interpretation of the results.

3.2.3 Low gas-flow reactor – Teflon® Oxidation Reactor (TOR)

The Teflon® Oxidation Reactor (TOR) was design specifically with PZ degradation in mind. The TOR was based on the overall design and dimensions of the OOR, but adaptations were made with the goal of achieving a more precise measurement of PZ oxidation. The main reactor body was made out of glass by Mike Ronalter of the Glass Shop at the University of Texas at Austin (Ronalter, 2009).

3.2.3.1 Reactor design

The design elements that were maintained from the OOR to the TOR were:

Internal Dimensions: The internal dimensions of the OOR were maintained in an effort to ensure that the data captured from each reactor was comparable. The ID of 80 mm and jacketed height of 160 mm were maintained.

Inlet gas: The inlet gas configuration was maintained in both reactors. The gas flow of 100 mL/min was still pre-saturated at the reactor temperature in the water bath and then fed to the top of the agitation vortex. This was kept the same primarily to have data comparability between reactors.

Jacket heating: The heating of the reactor through a water jacket was maintained. This heating method did not seem to cause any problems with the OOR operation and allowed a water bath for the inlet gas to be pre-saturated at the reactor temperature.

The major modifications over the OOR design include:

Teflon® lid: The black, rubber stopper lid of the OOR was replaced with a Teflon® (Polytetrafluoroethylene, PTFE) lid with 7 pre-drilled openings with NPT fittings. The lid required the use of a Schott-style flange connection to attach to the reactor (shown in Figure 3.25). The flange connection was O-ring grooved to accept a PTFE coated O-ring in between the flange and the smooth bottom of the lid. A stainless steel Schott-style flange clamp was the used to keep the pieces together.

Dimensional Differences: The use of a flange for the new lid required some additional height to be built into the overall height of the reactor. The jacketed portion was maintained at 160 mm, but the flange added approximately 65 mm of height, making the reactor 225 mm tall overall. This provided 65 mm of cooler glass surface and more overall gas headspace compared to the OOR. This was not ideal, but a necessity that came out of the way the glass TOR reactor body was constructed. The extra glass surface at the top of the reactor likely acted as a small condenser which helped control some vapor losses. Mike Ronalter, who constructed the glass TOR, attempted to minimize the overall height addition due to the flange.

Fritted Pre-Saturator: The vacuum trap used to saturate the inlet gas was modified with the addition of a fritted sparger rather than the open tube that originally was used. This decreased the size of the gas bubbles, hopefully achieving a better degree of saturation for a given water column height.

Oil Bath Conversion: A portion of experiments performed in the TOR were done at temperatures higher than 55 °C. To achieve these temperatures, the water bath was converted to an oil bath using dimethyl silicone oil as the circulating fluid. The tubing between the bath and reactor was changed to Tygon® silicone tubing since the original PVC tubing is not compatible with dimethyl silicone oil (Fisher Scientific Worldwide). Caution was used when adding water to the saturator since it was immersed in a bath of hot oil.

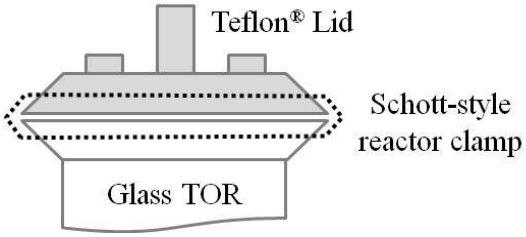

Figure 3.25: Schematic of TOR closure with Teflon® lid and Schott-style flange

3.2.3.2 Reactor set-up

The overall operation of the TOR was very similar to that of the OOR. The operation of the TOR will be described in detail since that of the OOR has been described previously (Goff, 2005; Sexton, 2008; Zhou et al., 2010).

The jacket of the reactor body was connected to the inlet and outlet lines of the recirculating portion of the water or oil bath. The lines were secured with hose clamps, even though the jacket has ringed hose connectors, because once hot fluid was flowing through the jacket, the hoses may have slipped off the connectors if not secured. The hoses were connected so that the inlet from the water bath was at the hose connection on the bottom of the reactor. This allowed fluid to fully fill the reactor jacket, rather than leaving the top portion with air.

The inlet gas to the reactor was typically 2% CO_2/ 98% O_2, except for a few experiments performed at different concentrations of CO_2 and O_2. Two sources were used for the gas: mixing the gas using flow controllers or a pre-mixed cylinder. The preferred method was to use two Brooks flow controllers connected to separate CO_2 and O_2 cylinders and connected to a controller unit. Each flow controller was sized for the appropriate flow and the controller unit was calibrated using a soap bubble flowmeter to achieve flows of 2 and 98 mL/min of CO_2 and O_2, respectively. After exiting the flow controllers, the two gas streams were combined using a ¼" Swagelok® T-union and fed into the inlet of the pre-saturator (Arthur Fluids System Technologies). When the flow meters were malfunctioning, being repaired, or otherwise unavailable, pre-mixed cylinders were used. These cylinders were blended gases containing 2% CO_2 by volume with the balance O_2 (Matheson Tri-Gas, Basking Ridge, NJ). These cylinders were used when mixing gases was not possible due to the unavailability of flow controllers. The gas line from the cylinder was sent through a rotameter and then on to the pre-saturator. The rotameter was first calibrated with the soap-bubble flowmeter to achieve a total flow of 100 mL/min to the reactor. Calibrations were performed with the presence of water in the saturator to simulate the reactor conditions as closely as possible during calibration.

A two-piece vacuum trap was used as the air saturator to allow the pieces to be separated and the water column to be refilled. The bottom piece was secured to a ring stand using a clamp and placed into the water bath. The vacuum trap was taller than the standard size of Lauda water or oil bath so only the bottom 75% of the trap was actually under fluid. DDI water was added to fill the vacuum trap and the top was placed inside. The two-piece traps had a ground glass joint that provided a secure connection upon slight heating. The inlet gas line from the flowmeters was attached using Teflon® Swagelok® connections to the smooth tube connection of the trap (top center port)

(Arthur Fluids System Technologies). The outlet (side) of the trap was then connected to the tube that enters the reactor.

There were seven predrilled holes in the Teflon® lid that accepted NPT fittings ranging from ¼ to ¾ inch (Item: 12860-18, AceGlass, Vineland, NJ). The central hole was fitted with a Teflon® ¾" male NPT to 24/40 standard taper adapter (Item: CG-1945-T-21, ChemGlass, Vineland, NJ). Then, a 10 mm Teflon® stirring bearing with 24/40 male end with an O-ring was placed in the central hole (Item: CG-2077-H-01, ChemGlass). This central hole then accepted the 8 mm agitator shaft connected to the overhead agitator (Fisher Scientific Worldwide). One of the ½" NPT openings in the lid was fitted with the same ¾" male NPT to 24/40 standard taper adaptor. A hollow Teflon® 24/40 stopper was then placed in the adaptor and secured with a 24/40 joint clip (CG-3002-05, ChemGlass). This stopper port was used for addition of water to the reactor and sampling. Two of the ¼" NPT predrilled holes were fitted with straight Teflon® ¼" male NPT to ¼" Swagelok® fittings for the inlet and outlet of the gas (Arthur Fluids Systems Technologies). The inlet fitting was bored through to allow the gas inlet ¼" OD plastic tube to be fed through the lid and positioned at the top of the agitation vortex. The outlet fitting was a Teflon® Swagelok® 90° elbow open to the environment in an attempt to direct the outlet gas, if needed, away from just leaving the reactor through the annular space surrounding the agitator. The remaining openings in the lid were not used during operation and were filled with ¼" and ¾" male NPT Teflon® solid plugs (Items: 12867-04 and 12867-18, AceGlass).

A ring stand was used with two chain clamps to keep the reactor secure and completely vertical. The alignment of the agitator was a major concern during the experimental set-up and reactor operation. The additional height of the TOR compared to the OOR added to the vibration problems traditionally experienced in oxidation

experiments. The agitator shaft was not as far inside the body of the agitator during the TOR experiments because of the increased reactor height, allowing for more vibrations. Also, the design of the TOR intentionally allowed for a smaller annular space around the agitator, making alignment and vibration of the agitator shaft an even more crucial element of the reactor set-up. The agitator shaft was placed as far inside the agitator to allow that the propellers were approximately one inch above the bottom of the reactor, as with OOR experiments. The agitator body itself was also placed very close to the top of the stirring bearing, within 0.5 cm. Experiments were all constantly monitored to ensure that the agitator did not make contact with the stirring bearing. When it did occur, some Teflon® was shaved off and ended up in the reactor solution. This was avoided when possible.

Once all the major elements of the reactor system were in place, an experiment could begin. The circulating bath was first turned on to allow the fluid to heat to the experimental temperature and begin to heat the reactor body and pre-saturator. As it heated, the hose connections were checked for leaks. Experiments in the TOR were conducted with 350 mL of amine solution, as with the OOR experiments. This volume was measured in one 100 mL and one 250 mL volumetric flask. The amine was added to the reactor either with the lid off, or through the sampling port. The mass of the amine actually entering the reactor was recorded by weighing the full flasks and the flasks containing some residue after the PZ was added to the reactor. The overall mass balance of the experiment was recorded in terms of mass entering or exiting the reactor, so all additions were recorded in terms of mass. If additives such as metals or inhibitors were to be used, they were then added to the amine solution in the reactor through the sampling port. The solution was stirred briefly at low speed to incorporate the additives. The solution itself was allowed to heat up in the reactor for approximately 10 to 20

minutes with slow agitation (<300 rpm) while other parts of the experiment set-up were completed. Once all the solution elements were added to the reactor, the top was affixed with the Teflon® O-ring in place using the stainless steel flange clamp. The clamp was made very tight to discourage water collection in between the glass flange and Teflon® lid.

Before the experiment was started, an initial sample was taken through the sampling port. Liquid samples of 3 to 5 mL were extracted through the port using a long, 5 mL glass pipet or manual pipetter with a long 10 mL tip. A piece of laboratory tape was placed vertically on the side of the reactor and the initial level (after sampling) was marked. This mark was important in order to visually observe the water balance each day. It was used as a gauge to ensure that the water level was being maintained throughout long term experiments. The temperature of the solution was taken for higher temperature experiments as well before the experiment was started. To begin the experiment, the agitator was set at 1400 rpm and the gas flow was turned on. The start time of the experiment, officially, was when the gas flow was turned on.

3.2.3.3 Reactor sampling and analysis

Daily monitoring of the TOR was required due to the delicacy of the agitator vibration and stirrer bearing set-up. Each day, the water bath was refilled to make-up for evaporation if water was the circulating fluid. The circulating bath was programmed to turn itself off when a pre-determined low liquid level was achieved. At 55 °C and with water as the circulating fluid, it took approximately 36 hours to evaporate enough liquid to initiate the automatic shut off of the bath. The alignment of the agitator in the lid was also checked daily to ensure smooth operation.

Experiments were sampled every 3 days, although some were sampled every 2 or 4 days, depending on the experimental design. The sampling procedure performed was designed to maintain the mass balance of the reactor contents as closely as possible. There were three main parts of sampling: replacing water evaporated since the last sample, taking the sample, and remarking the level. Additional steps taken on certain experiments include measuring the temperature of the reactor contents or refilling the saturator.

The first step in all sampling was to add water to the reactor to replace what has evaporated since the previous sample. Water was added to the reactor through the sampling port to reach the previous line marked on the level indicator. The exact mass of water added to the reactor was recorded. The TOR generally needed 0.15 to 0.30 gram of water per hour at 55 °C or 0.40 to 0.60 gram of water per hour at 70 °C. After the water was added, the agitator was turned on for a few seconds to mix in the newly added water. Then, the 5 mL sample was withdrawn through the sampling port using a long glass pipet and pipet bulb or a manual pipetter with a long 10 mL pipet tip. The exact mass of sample withdrawn was recorded by weighing the sample vial before and after the sample was taken. Then, the new liquid level was drawn on the level indicator on the side of the reactor. Finally, the stopper was replaced on the sampling port on the lid and the agitator was restarted.

The crucial part of the sampling procedure was that water was replaced before the sample was taken. This was done to try to make the sample as representative as possible, excluding the water evaporation since the last sample was taken. The sample should represent what has happened if no evaporation occurred, an ideal situation that cannot be yet achieved by this oxidation reactor.

One advance made in the sampling procedure was to record the amount of water added to the pre-saturator during the sampling. The loss in liquid level in the pre-saturator was assumed to be the amount of water added to the gas stream and, therefore, to the reactor itself. This liquid should be taken into account in the mass balance. In all experiments past OE20, the amount of water add to the saturator was included in the sampling procedure and included in any mass balance calculations. Previous to OE20, the saturator was topped off with water daily during the daily check and the amount was not recorded.

Chapter 4 – Density, Viscosity, and Solubility of Concentrated, Aqueous PZ and PZ Blends

The physical properties of PZ solutions that are the most important to understand for CO_2 capture systems are discussed in detail in this chapter, such as density, viscosity, and physical solubility or solid-liquid equilibrium. A majority of this chapter is excerpted from a publication that focuses on density and viscosity of PZ and the application to online monitoring of PZ based CO_2 capture systems (Freeman and Rochelle, 2011). Another previous publication also briefly touched viscosity of PZ in relation to other amine systems of interest (Freeman et al., 2010b). This chapter also includes an additional section discussing the physical solubility of PZ in aqueous solution which includes some work from a review article on PZ as a solvent (Freeman et al., 2010b). Solubility data are especially useful when operating large scale PZ systems

where insolubility anywhere in the system could be catastrophic. Finally, density and viscosity measurements for PZ blended with substituted PZs (1-MPZ, 1,4-DMPZ, and 2-MPZ) are reported over a range of conditions.

4.1 INTRODUCTION TO PHYSICAL PROPERTIES OF PZ

Amine based absorption-stripping for CO_2 capture from coal-fired power plant flue gas will be an important technology to address global climate change. Concentrated aqueous piperazine (PZ) has been identified as an attractive solvent for this process (Freeman et al., 2010a; Freeman et al., 2010b). The density and viscosity data for this solvent are needed for design calculations of fluid flow and heat transfer. Because high viscosity interferes with mass transfer and increases the size of heat exchangers, the maximum concentration of PZ in the solvent may be determined by its viscosity. Furthermore, on-line instrumentation makes it attractive to use density and viscosity measurements to infer the amine concentration and CO_2 loading. Chen and Dugas demonstrated that on-line density measurements were useful in inferring CO_2 loading of potassium carbonate promoted by PZ and monoethanolamine (MEA) solutions during pilot plant operations (Chen, 2007; Dugas, 2009).

PZ has been investigated as a CO_2 rate promoter in solvents primarily consisting of aqueous methyldiethanolamine (MDEA), 2-amino-2-methyl-1-propanol (AMP), or potassium carbonate (Bishnoi and Rochelle, 2000a; Bishnoi and Rochelle, 2000b; Bishnoi and Rochelle, 2002a; Bishnoi and Rochelle, 2002b; Cullinane and Rochelle, 2004; Cullinane and Rochelle, 2005; Cullinane and Rochelle, 2006; Derks et al., 2008; Liu et al., 1999; Oyenekan and Rochelle, 2009; Paul and Mandal, 2006b; Plaza et al., 2009; Samanta and Bandyopadhyay, 2009; Sun et al., 2005; Yang et al., 2010; Zhang et al., 2001). Concentrated PZ (40 wt %) has also been explored as a standalone solvent for

CO_2 capture (Freeman et al., 2010a; Freeman et al., 2010b; Rochelle, 2009). PZ has a low solubility in water which can prove detrimental in a large scale system and discouraged research into the solvent. The solubility of the PZ + H_2O system has been investigated previously (The Dow Chemical Company, 2001; Bishnoi and Rochelle, 2000a; Hilliard, 2008; Muhammad et al., 2009), but the effect of adding CO_2 to the system has only been researched recently (Freeman et al., 2010b; Hilliard, 2008). Large-scale CO_2 capture systems will contain a wide range of CO_2 concentrations throughout the absorber, stripper, and other unit operations; therefore, a full understanding of the effect of CO_2 concentration on the physical properties of a solvent is crucial. Previous literature on the density and viscosity of PZ solutions avoided insoluble solutions and includes data only at very low PZ concentrations (Cook and Lowe, 1976; Derks et al., 2005; Muhammad et al., 2009; Samanta and Bandyopadhyay, 2006). The concentrations of PZ studied, less than 14 wt % at 20 °C, are not useful for CO_2 capture applications since they cannot compete with the capacity of a baseline MEA solvent.

Recently, the addition of CO_2 to an aqueous solution of PZ was found to alleviate solubility concerns as PZ carbamate ($PZCOO^-$) is more soluble than anhydrous PZ itself (Freeman et al., 2010b; Hilliard, 2008). Concentrated solutions can be made without solids precipitation and have been shown to have very advantageous properties for CO_2 capture such as fast rate of CO_2 absorption, high capacity, and resistance to thermal and oxidative degradation (Freeman et al., 2010a; Freeman et al., 2010b). Physical property studies that include PZ in the presence of CO_2 report on a blended solution with another amine, such as MDEA or AMP, where PZ is added as a kinetic promoter (Derks et al., 2008). In the few studies where the PZ + H_2O + CO_2 system is investigated alone, the only properties measured and reported are CO_2 solubility, N_2O solubility, Henry's constants and diffusivities (Hilliard, 2008; Samanta et al., 2007). Literature data for the

density and viscosity of PZ solutions in the presence of CO_2 are not available outside of the author's previous work (Freeman et al., 2010b).

This study provides density and viscosity data over ranges of PZ and CO_2 concentrations applicable to CO_2 capture applications. To match with previous CO_2 capture solvent literature, solutions are analyzed at 2 to 20 molal (m) PZ and a CO_2 loading of 0 to 0.47 mole CO_2 per mole alkalinity. The data for density and viscosity are reported in SI concentration units (mole per kg), but other common units are also provided (i.e. m and CO_2 loading) for clarity to the readers in this field. The data are not all inclusive across a range of CO_2 concentrations for a given PZ concentration and are absent where PZ precipitation or CO_2 evolution occurred.

4.2 EXPERIMENTAL NOTES

PZ solutions were prepared as described in Section 3.1.1 of this dissertation for analysis of their physical properties. Alkaline titration was used to determine the PZ concentration in these samples as described in Section 3.1.2 and was determined to be within 2% of the gravimetric preparation in all cases. TIC was used to analyze for CO_2 concentration in all samples as described in Section 3.1.3.

A few modifications were made to the standard analysis procedures in order to accurately assess these properties. First, dilution series were created by making a solution of the desired PZ concentration with high loading (α=0.45) and zero loading. Intermediate loadings were created from these two CO_2 concentrations in order to have a range of loadings. Next, the 100X dilutions for TIC were made immediately after each analysis in order to capture the CO_2 concentration accurately. For a set of density or viscosity measurements, all of the loadings were analyzed at the same time and the dilutions were done immediately afterward.

The loading analysis is the most imprecise part of this study. The loading of amine solutions can change greatly due to handling, opening of bottles, or age of samples. All samples were handled carefully and analyzed immediately, but the loading of solutions inherently changed during the course of density and viscosity measurements. The error of the density and viscosity measurements is very low compared with the error in the measurement of CO_2 concentration. The estimated error in the TIC measurement is 4.0 %. Instrument errors are reported for the density meter and viscometer, but the error in CO_2 concentration overshadows them and has the most impact on the data regressions.

For both density and viscosity measurements, data are missing at low CO_2 concentration where solutions could not be analyzed due to PZ precipitation. When precipitation occurred in the rheometer, the shear stress during the 10 measurements was non-linear, producing scatter in the calculated viscosity. The shear stress was high as the samples were essentially a slurry. Data are also missing at high CO_2 concentration where CO_2 evolved from the sample. The higher temperatures of these measurements caused an increased CO_2 partial pressure leading to CO_2 evolution and instability in the measurement. This was evidenced by the production of bubbles visible in the u-tube of the DE40 or bubbles visible on the surface of the sample in the MCR 300.

For the viscosity measurements, a total of 10 measurements were taken every 10 seconds for each sample. Values reported are an average and standard deviation of these 10 instances. Percent error represented by the calculated standard deviations ranged from 0.13 % to 4.6 %. Errors were higher at higher temperatures where the value of viscosity was smaller, amplifying the standard deviation value when calculated as a percent.

Solubility or solid-liquid equilibrium measurements were based on visual observations. Aqueous solutions were prepared to cover the desired solution properties

and were allowed to equilibrate at each condition with stirring before solubility observations were made. Solutions were deemed insoluble based on the presence of any solid crystal or slurry in a given solution. The transition temperature is the temperature at which a liquid solution will first precipitate when cooled slowly. In measuring this property, a liquid solution at room temperature was heated to approximately 50 °C. For lean loadings, this caused any precipitate to melt. The temperature at which this melting occurred was noted as the approximate transition temperature and then the solution was cooled slowly. While cooling slowly, the temperature at which the solution first began to crystallize or precipitate was noted as the crystal temperature. Finally, the solution was heated again to carefully observe the temperature when the crystals fully melt and this was noted as the melting temperature. The crystal and melting temperatures demonstrated a hysteresis that was likely caused by the high viscosity of the liquid and an extended equilibrium time need to create crystals or fully melt a slurry or solid precipitate. The approximate temperature ramp for all transitions was 1 °C or less every 5 minutes.

4.3 DENSITY OF CONCENTRATED PZ

The experimental values for the density (ρ) of aqueous (PZ + CO_2) solutions as a function of PZ concentration (C_{PZ}), CO_2 concentration (C_{CO2}), and temperature (T) are listed in Table 4.1. C_{PZ} is provided in units of m (molal, mole per kg water) and mole per kg solution. C_{CO2} concentrations are given in units of mole CO_2 per mole alkalinity and mole per kg. Raw density data are provided with the units of kg per m^3, but the ratio of density to the density of water (ρ_{water}) is used throughout the proceeding discussion, which is unit less. Values for ρ_{water} over the range of 20 to 60 °C were taken from the DIPPR Database (DIPPR, 2010).

Table 4.1: Density (ρ) of Aqueous (PZ + CO_2) Solutions from 20 to 60 °C

C_{PZ}	C_{PZ}	C_{CO2}	C_{CO2}	Density, ρ (kg/m^3)		
molal	mol/kg	mol/mol alk	mol/kg	T = 20 °C	T = 40 °C	T = 60 °C
2	1.67	0.00	0.000	1006.7	999.4	989.1
	1.64	0.05	0.186	1014.6	1007.2	997.4
	1.64	0.11	0.366	1022.2	1014.8	1004.9
	1.63	0.16	0.545	1029.9	1022.4	1012.9
	1.61	0.22	0.728	1037.3	1029.9	1020.2
	1.61	0.25	0.894	1044.1	1036.5	1027.0
	1.59	0.32	1.080	1051.5	1043.8	1034.4
	1.58	0.38	1.246	1058.1	1050.5	1040.7
	1.57	0.44	1.416	1064.4	1056.7	-
	1.55	0.47	1.516	1068.8	1060.7	-
5	3.36	0.11	0.753	1049.3	-	-
	3.33	0.15	0.991	1062.2	1052.6	-
	3.25	0.22	1.433	1074.9	1065.5	1054.8
	3.21	0.28	1.780	1087.4	1078.2	1067.6
	3.16	0.35	2.216	1099.2	1090.2	1079.9
	3.11	0.40	2.504	1111.1	1102.1	1092.0
	3.06	0.46	2.822	1122.3	1113.3	1103.1
	3.03	0.50	3.023	1127.8	1118.8	1108.1
	3.01	0.53	3.182	1136.9	1127.6	-
7	4.11	0.16	1.281	1076.9	1066.1	-
	4.01	0.21	1.726	1092.3	1082.1	1070.7
	3.93	0.26	2.091	1106.1	1096.1	1085.2
	3.86	0.32	2.495	1120.6	1110.9	1100.4
	3.81	0.37	2.815	1134.1	1124.6	1114.3
	3.72	0.40	3.023	1147.3	1137.9	1127.7
	3.68	0.46	3.397	1159.6	1150.1	-
8	4.28	0.20	1.722	1100.7	1090.0	1078.5
	4.26	0.25	2.150	1116.2	1105.9	1094.9
	4.12	0.31	2.563	1130.8	1121.3	1110.7
	4.11	0.35	2.917	1145.7	1136.0	1125.7
	3.98	0.41	3.297	1160.1	1150.4	1140.2
	3.90	0.45	3.617	1173.4	1163.8	-

Table 4.1: Density (ρ) of Aqueous (PZ + CO_2) Solutions from 20 to 60 °C (Continued)

C_{PZ}	C_{PZ}	C_{CO2}	C_{CO2}	Density, ρ (kg/m^3)		
molal	mol/kg	mol/mol alk	mol/kg	T = 20 °C	T = 40 °C	T = 60 °C
9	4.68	0.15	1.453	1090.9	-	-
	4.59	0.20	1.879	1107.0	1096.1	1084.3
	4.52	0.26	2.347	1123.4	1112.8	1101.7
	4.41	0.30	2.714	1137.2	1127.0	1116.3
	4.33	0.36	3.169	1155.2	1145.3	1134.9
	4.24	0.40	3.471	1168.7	1158.9	1148.7
	4.14	0.44	3.695	1181.6	1171.7	-
10	4.80	0.25	2.436	1132.3	1121.2	1110.0
	4.73	0.31	2.875	1149.0	1138.7	1127.8
	4.69	0.36	3.343	1165.0	1154.9	1144.6
	4.41	0.41	3.726	1180.7	1170.8	1160.5
12	5.23	0.20	2.650	1121.9	1110.1	1097.8
	5.07	0.26	2.697	1139.8	1128.3	1116.7
	4.96	0.31	3.169	1156.9	1146.2	1135.3
	4.85	0.36	3.620	1173.6	1163.2	1152.7
	4.73	0.41	3.985	1189.5	1179.3	1169.0
20	6.96	0.10	1.338	1100.6	1084.7	1069.3
	6.70	0.16	2.123	1125.6	1110.8	1096.2
	6.53	0.20	2.577	1145.3	1131.3	1118.8
	6.47	0.25	3.137	1166.4	1153.7	1141.0

The ratio ρ/ρ_{water} is used to eliminate the temperature dependence of the data. At a given temperature, this ratio does not affect the trends observed. However, over a range of temperature the data collapse and the effect of C_{CO2} in relation to the effect of temperature on density is amplified. To demonstrate this effect, the temperature dependence of density and ρ/ρ_{water} are shown in Figure 4.1 for 2 and 8 m PZ (1.6 and 4.1 mole PZ per kg solution). The advantage of reporting ρ/ρ_{water} rather than density is that the effect of temperature can be minimized to focus on the effect of CO_2 concentration. This is a critical observation because the intent is to use on-line density meters in a CO_2

capture process to monitor CO_2 concentration. With regressions that eliminate the effect of temperature, the CO_2 concentration can be directly related to the density of the solution, allowing easy, inexpensive, on-line monitoring of CO_2 loading throughout a process.

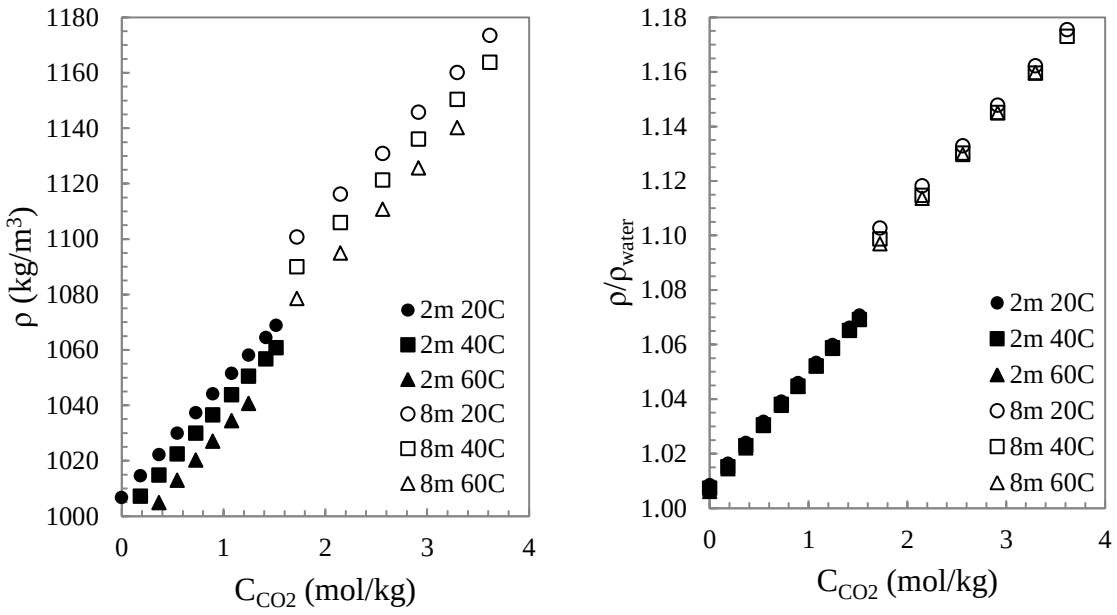

Figure 4.1: Density (ρ) (left panel) and ρ/ρ_{water} (right panel) as a function of CO_2 Concentration for aqueous PZ solutions.

All previous literature data reports density in the absence of CO_2 and only the 2 m PZ solution of this study does not precipitate in the absence of CO_2. All other density data reported in this manuscript contain CO_2. The density of 2 m PZ without CO_2 is shown along with previous literature data in Figure 4.2 (Derks et al., 2005; Muhammad et al., 2009; Samanta and Bandyopadhyay, 2006). The data of this study agree with literature values at 40 °C. At 60 °C, the data of Samanta and Bandyopadhyay (2006) appears to deviate at their highest PZ concentration while the data presented in this study agrees with that of Muhammed and colleagues (Muhammad et al., 2009).

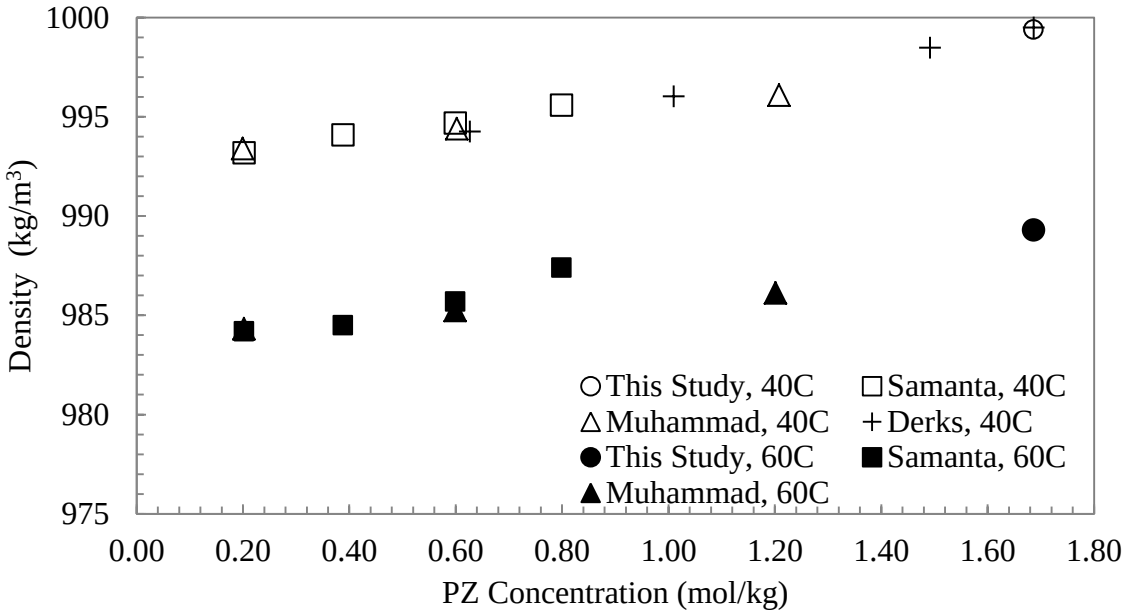

Figure 4.2: Comparison of density data for PZ without CO_2

The ρ/ρ_{water} of 2 to 20 m PZ at 40 °C are shown as a function of CO_2 concentration in Figure 4.3. Ignoring the 2 and 20 m PZ data, there is not a significant difference in the ρ/ρ_{water} of 5 to 12 m PZ when plotted in these units. The data collapse when observed in terms of ρ/ρ_{water} and C_{CO2} in units of mole per kg, rather than density (ρ) and C_{CO2} in units of mole per mole alkalinity.

The values for ρ/ρ_{water} for 5 to 12 m PZ were regressed over 20 to 60 °C using the least squares method as a function of C_{CO2} and C_{PZ}, both in terms of mole per kg. The resulting regression is

$$\frac{\rho}{\rho_{water}} = 0.0407 \cdot C_{CO2} + 0.008 \cdot C_{PZ} + 0.991 \qquad (4.1)$$

where the standard error in the two coefficients and intercept were 0.00048 kg per mole CO_2, 0.00057 kg per mole PZ, and 0.002, respectively. The average error of the total data set was 0.24 % and the maximum error was 0.78 %. The regression predicts ρ/ρ_{water}

with similar accuracy across all three temperatures as the maximum error was 0.78 %, 0.60 %, and 0.49 % for data at 20, 40, and 60 °C, respectively. The error in predicting density rather than ρ/ρ_{water} is the same given the nature of the ratio used in the regression. The average absolute deviation (AAD) of a data set is defined as

$$AAD = \frac{1}{N}\sum_{i=1}^{N}\frac{\left|y_{calc,i} - y_{expt,i}\right|}{y_{expt,i}} \tag{4.2}$$

where $y_{calc,i}$ and $y_{expt,i}$ are the calculated, or predicted, and experiment values of the dependent variable of interest, y, and N is the total number of data points. Using Equation 4.2, the AAD of Equation 4.1 with the density data for 5 to 12 m PZ at all temperatures was 0.0024, indicating that Equation 4.1 represents the data well.

The experimental ρ/ρ_{water} data at 40 °C are compared with the regression (Equation 4.1) in Figure 4.3. The prediction of Equation 4.1 is shown for 5, 8, and 12 m data to demonstrate the fit without cluttering the figure. The data for 2 and 20 m PZ were excluded from this regression but still appear in Figure 4.3 for reference. Although the regression is not intended for these PZ concentrations, a prediction for 2 and 20 m PZ yields an average error of 0.57 % and a maximum error of 1.48 %. The robustness of Equation 4.1 is demonstrated in the low error obtained when predicting data outside of the concentration ranges of data that were included in the original regression.

Only data at 40 °C are shown in Figure 4.3 for clarity and because of the importance of this temperature in the absorber side of an absorber/stripper CO_2 capture system. To encompass the entire data set, a parity plot comparing the experimental data to the predictions of ρ/ρ_{water} from Equation 4.1 for 20 to 60 °C and all PZ concentrations is shown in Figure 4.4. The data for 2 and 20 m PZ are highlighted with open points since they were not included in the regression of Equation 4.1.

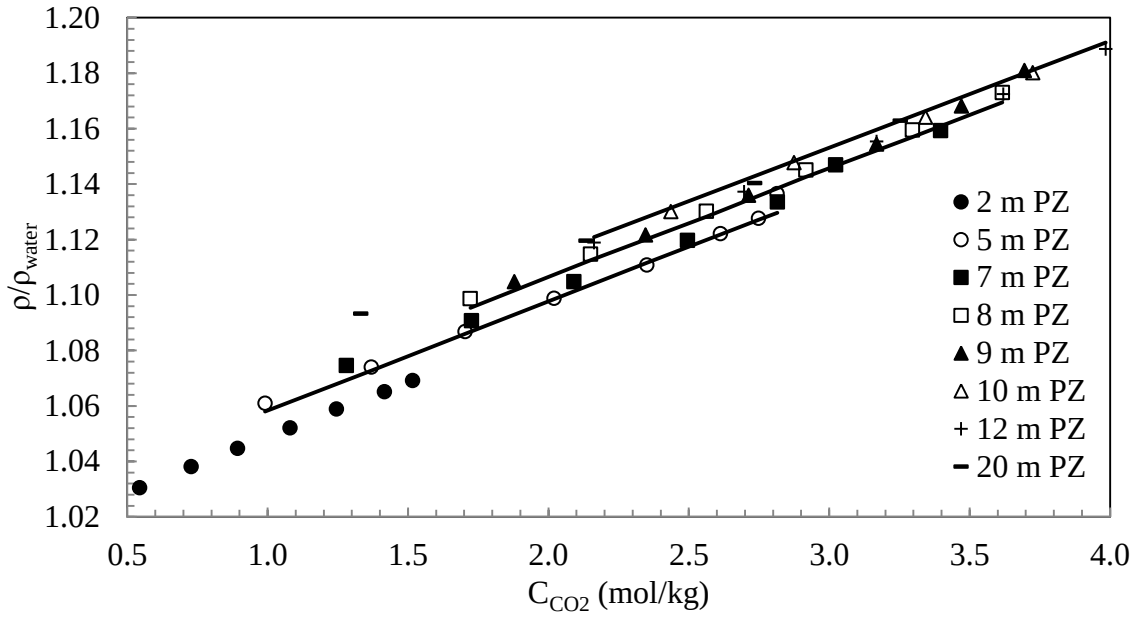

Figure 4.3: Comparison of ρ/ρ_{water} to the prediction of Equation 4.1 (solid lines; predicted for 5, 8, and 12 m PZ) at 40 °C

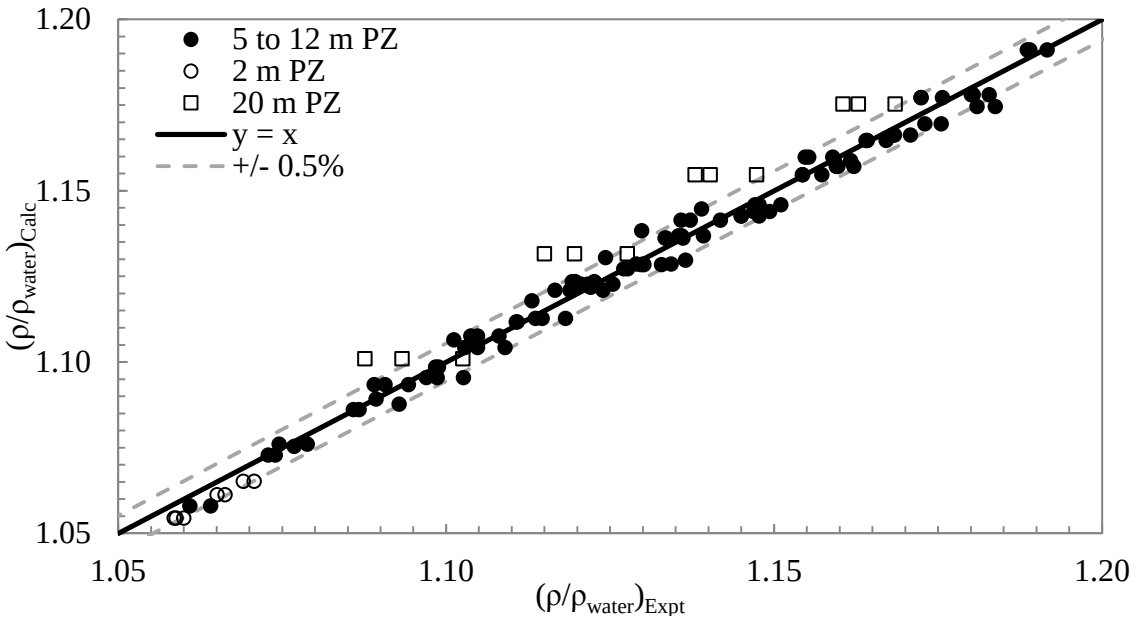

Figure 4.4: Parity plot demonstrating the accuracy of Equation 4.1 for predicting ρ/ρ_{water} from 20 to 60 °C

4.4 VISCOSITY OF CONCENTRATED PZ

The measured viscosity (μ) of aqueous (PZ + CO_2) as a function of C_{PZ}, C_{CO2}, and temperature is given in Table 4.2. As with density measurements, previous literature has only reported viscosity of aqueous PZ solutions at low concentration without CO_2. Therefore, the only data from this study that are comparable to literature is a 2 m PZ solution in the absence of CO_2. The viscosity of this solution is compared with previous data in Figure 4.5 as a function of C_{PZ} in terms of mole per kg (Derks et al., 2005; Muhammad et al., 2009; Samanta and Bandyopadhyay, 2006). The viscosity data at 40 °C are in agreement with literature values. At 60 °C, the data of Muhammed and colleagues (Muhammad et al., 2009) appear to predict lower viscosity (μ) in comparison with the current study at higher C_{PZ}. There is no literature data at 60 °C above a C_{PZ} of 1.25, so it is not clear if the literature data or the current study predicts the more correct trend. The previous section demonstrated that the current study matched the results of Muhammed and colleagues (Muhammad et al., 2009) while that of Samanta and Bandyopadhyay (Samanta and Bandyopadhyay, 2006) appeared to deviate with increasing PZ concentration at 60 °C (Figure 4.2).

An extended set of viscosity data for 8 m PZ was obtained over a wider range of temperature than the other PZ concentrations and the data are shown in Table 4.3. The importance of 8 m PZ in planned and future industrial applications called for a wider range of data and a correlation to predict viscosity for this concentration. A correlation was created from the 8 m PZ data to relate the ratio of viscosity to the viscosity of water (μ/μ_{water}) to temperature (K), C_{CO2} (mole per kg), and C_{PZ} (mole per kg), and has the form of

$$\ln\left(\frac{\mu}{\mu_{water}}\right) = a_1 + \Phi_1 + \frac{\Phi_2}{T} \tag{4.3}$$

Table 4.2: Viscosity (μ) of Aqueous (PZ + CO_2) Solutions from 25 to 60 °C

C_{PZ}	C_{PZ}	C_{CO2}	C_{CO2}	Viscosity, μ (mPa-s)		
m	mol/kg	mol/mol alk	mol/kg	25 °C	40 °C	60 °C
2	1.67	0.00	0.000	1.877 ± 0.011	1.307 ± 0.016	0.895 ± 0.016
	1.64	0.05	0.186	1.896 ± 0.007	1.334 ± 0.014	0.906 ± 0.020
	1.64	0.11	0.366	1.910 ± 0.008	1.348 ± 0.018	0.933 ± 0.020
	1.63	0.16	0.545	1.917 ± 0.008	1.371 ± 0.015	0.942 ± 0.018
	1.61	0.22	0.728	1.930 ± 0.009	1.386 ± 0.013	0.984 ± 0.017
	1.61	0.25	0.894	1.952 ± 0.006	1.414 ± 0.018	0.984 ± 0.018
	1.59	0.32	1.080	1.961 ± 0.007	1.423 ± 0.016	1.015 ± 0.017
	1.58	0.38	1.246	1.971 ± 0.010	1.439 ± 0.011	1.021 ± 0.017
	1.57	0.44	1.416	1.977 ± 0.009	1.455 ± 0.014	1.043 ± 0.029
	1.55	0.47	1.516	1.968 ± 0.013	1.468 ± 0.041	- - -
5	3.25	0.22	1.433	- - -	3.231 ± 0.012	1.946 ± 0.018
	3.21	0.28	1.780	5.336 ± 0.039	3.346 ± 0.015	2.028 ± 0.019
	3.16	0.35	2.216	5.457 ± 0.022	3.464 ± 0.007	2.144 ± 0.021
	3.11	0.40	2.504	5.872 ± 0.018	3.612 ± 0.011	2.230 ± 0.023
	3.06	0.46	2.822	5.927 ± 0.015	3.689 ± 0.014	2.309 ± 0.019
	3.03	0.50	3.023	5.941 ± 0.014	3.752 ± 0.014	2.366 ± 0.033
	3.01	0.53	3.182	6.010 ± 0.018	3.751 ± 0.010	2.502 ± 0.022
7	4.01	0.21	1.726	10.85 ± 0.053	6.347 ± 0.039	3.543 ± 0.050
	3.93	0.26	2.091	11.34 ± 0.052	6.484 ± 0.053	3.720 ± 0.058
	3.86	0.32	2.495	11.60 ± 0.000	6.929 ± 0.070	4.218 ± 0.057
	3.81	0.37	2.815	12.34 ± 0.052	7.222 ± 0.076	4.810 ± 0.216
	3.72	0.40	3.023	12.60 ± 0.047	7.617 ± 0.082	4.849 ± 0.104
	3.68	0.46	3.397	12.82 ± 0.063	7.854 ± 0.094	5.270 ± 0.243
9	4.59	0.20	1.879	20.82 ± 0.042	11.09 ± 0.088	5.659 ± 0.036
	4.52	0.26	2.347	22.03 ± 0.048	12.09 ± 0.120	6.318 ± 0.060
	4.41	0.30	2.714	23.10 ± 0.047	12.60 ± 0.105	7.562 ± 0.143
	4.33	0.36	3.169	23.99 ± 0.032	13.90 ± 0.115	8.442 ± 0.186
	4.24	0.40	3.471	25.34 ± 0.052	14.62 ± 0.132	9.162 ± 0.214
	4.14	0.44	3.695	26.72 ± 0.079	15.21 ± 0.110	10.24 ± 0.466
10	4.80	0.25	2.436	31.37 ± 0.189	16.92 ± 0.253	9.084 ± 0.069
	4.73	0.31	2.875	33.42 ± 0.220	18.08 ± 0.210	9.781 ± 0.342
	4.69	0.36	3.343	35.45 ± 0.227	19.89 ± 0.407	11.06 ± 0.237
	4.41	0.41	3.726	37.48 ± 0.352	21.18 ± 0.239	11.88 ± 0.352

Table 4.2: Viscosity (μ) of Aqueous (PZ + CO_2) Solutions from 25 to 60 °C (continued)

C_{PZ} m	C_{PZ} mol/kg	C_{CO2} mol/mol alk	C_{CO2} mol/kg	Viscosity, μ (mPa-s) 25 °C	40 °C	60 °C
12	5.23	0.20	2.650	49.35 ± 0.127	23.62 ± 0.286	10.22 ± 0.162
	5.07	0.26	2.697	52.68 ± 0.181	26.01 ± 0.213	11.78 ± 0.294
	4.96	0.31	3.169	57.22 ± 0.297	27.18 ± 0.215	13.34 ± 0.255
	4.85	0.36	3.620	60.17 ± 0.236	31.42 ± 0.413	15.11 ± 0.213
	4.73	0.41	3.985	63.22 ± 0.361	33.43 ± 0.316	18.32 ± 0.290
20	6.70	0.16	2.123	304.1 ± 0.994	95.61 ± 0.357	30.00 ± 0.176
	6.53	0.20	2.577	373.1 ± 0.994	120.3 ± 0.483	40.88 ± 0.286
	6.47	0.25	3.137	534.3 ± 2.058	138.9 ± 0.994	57.14 ± 0.420

Table 4.3: Viscosity of 8 m PZ from 20 to 70 °C

C_{PZ} mol/kg	C_{CO2} mol/mol alk	C_{CO2} mol/kg	Temperature °C	Viscosity mPa-s
4.26	0.24	2.150	20	20.30 ± 0.09
4.12	0.29	2.563	20	20.93 ± 0.08
4.11	0.35	2.917	20	22.21 ± 0.10
3.98	0.40	3.297	20	22.78 ± 0.12
4.26	0.24	2.150	25	16.50 ± 0.17
4.12	0.29	2.563	25	17.14 ± 0.13
4.11	0.35	2.917	25	18.19 ± 0.13
3.98	0.40	3.297	25	18.76 ± 0.12
4.26	0.24	2.150	30	12.93 ± 0.11
4.12	0.29	2.563	30	13.54 ± 0.13
4.11	0.35	2.917	30	14.56 ± 0.13
3.98	0.40	3.297	30	15.24 ± 0.21
4.26	0.24	2.150	40	9.460 ± 0.14
4.12	0.29	2.563	40	9.988 ± 0.17
4.11	0.35	2.917	40	10.79 ± 0.17
3.98	0.40	3.297	40	11.37 ± 0.19
4.26	0.24	2.150	50	6.586 ± 0.06
4.12	0.29	2.563	50	7.072 ± 0.07
4.11	0.35	2.917	50	7.580 ± 0.04
3.98	0.40	3.297	50	8.322 ± 0.08
4.26	0.24	2.150	60	5.351 ± 0.06
4.12	0.29	2.563	60	5.769 ± 0.06
4.11	0.35	2.917	60	6.466 ± 0.06
3.98	0.40	3.297	60	6.905 ± 0.07
4.26	0.24	2.150	70	3.919 ± 0.05
4.12	0.29	2.563	70	4.509 ± 0.05
4.11	0.35	2.917	70	4.683 ± 0.05
3.98	0.40	3.297	70	5.152 ± 0.05

where

$$\Phi_i = b_i \cdot C_{CO2} + c_i \cdot C_{PZ} + d_i \cdot C_{CO2} \cdot C_{PZ} \quad (4.4)$$

The values of the regressed parameters can be found in Table 4.4. Values for μ_{water} over the range of 20 to 70 °C were taken from the DIPPR Database (DIPPR, 2010). The resulting correlation (Equation 4.3) was able to fit all experimental μ/μ_{water} data within 2.4 %. The average absolute deviation (AAD) calculated using Equation 4.2 for the prediction of viscosity data was 0.028 indicating the data set is well represented by Equation 4.3.

Rearranging the above regression (Equation 4.3) leaves a relationship which predicts the viscosity of 8 m PZ with an average deviation of less than 3 % (maximum deviation of 6 %) (Equation 4.5).

$$\mu = \mu_{water} \cdot \exp\left(a_1 + \Phi_1 + \frac{\Phi_2}{T}\right) \quad (4.5)$$

The experimental viscosity data from Table 4.3 is compared to the prediction of Equation 4.5 in Figure 4.6. A parity plot comparing the experimental viscosity data to the values predicted using Equation 4.5 is shown in Figure 4.7 with 5 % deviation shown with dashed lines.

Table 4.4: Value of parameters in Equation 4.3

Parameter	i = 1	i = 2
a	1.723	-
b	2.63	-778
c	-1.019	355.2
d	-0.527	169.3

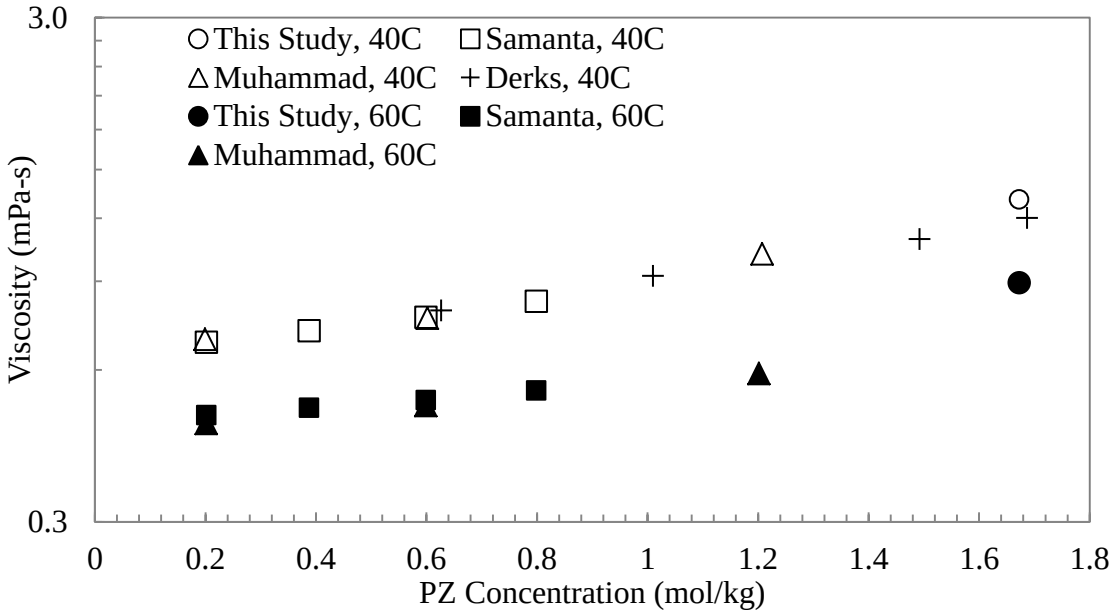

Figure 4.5: Comparison of viscosity data for PZ without CO_2

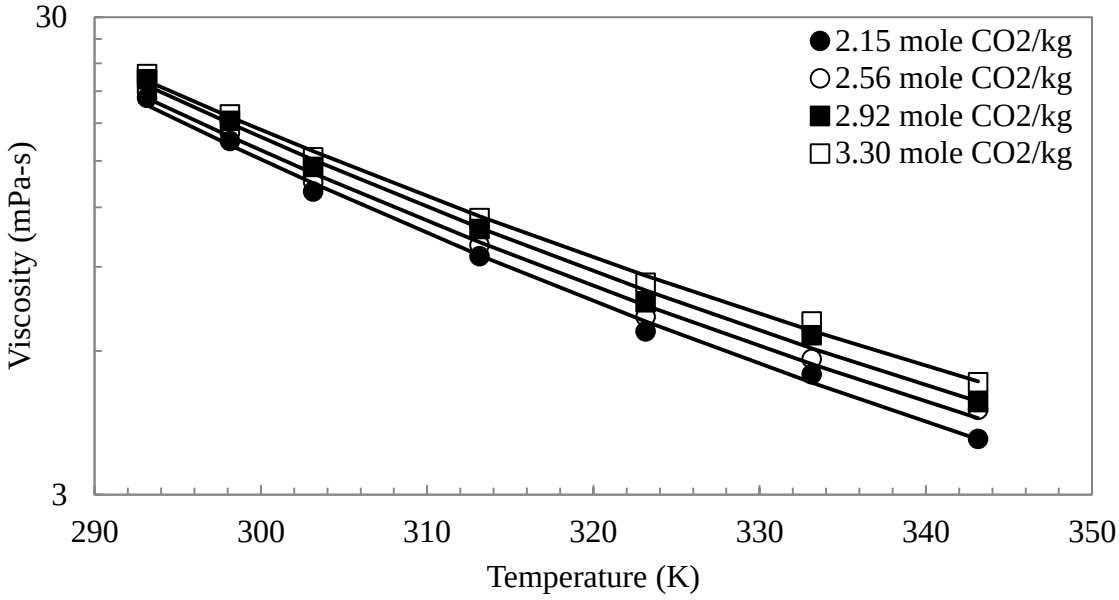

Figure 4.6: Comparison of the viscosity (μ) of 8 m PZ to the prediction of Equation 4.5 (solid lines) over a range of CO_2 concentrations

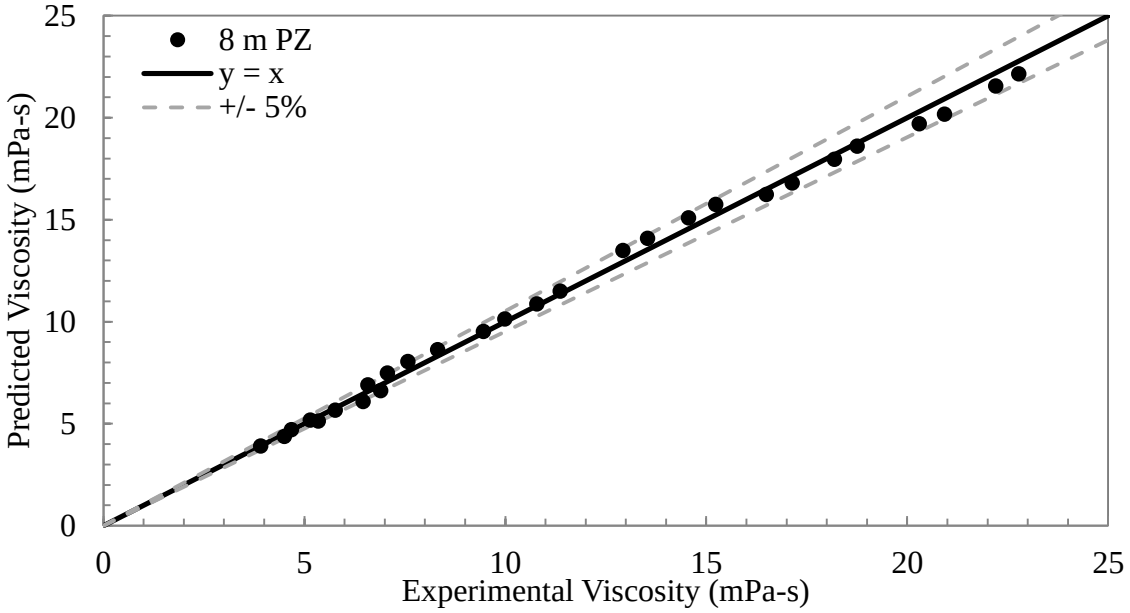

Figure 4.7: Parity plot demonstrating the accuracy of Equation 4.5 for predicting viscosity of 8 m PZ solutions at 20 to 70 °C

4.5.1 Choice of 8 m PZ based on viscosity

The viscosity of aqueous PZ increases rapidly with increased PZ concentration, as seen in the previous section. This high viscosity limits the PZ concentration applicable in CO_2 capture systems. The viscosity of 7 to 10 m PZ is compared with 7 to 13 m MEA, 7 m MDEA, 7 m MDEA / 2 m PZ, and 60wt% DGA® in Figure 4.8 (Huntsman Corporation, 2005; Closmann et al., 2009). The amine concentration is plotted in units of moles alkalinity per kilogram of water in order to compare mono- and diamines on a similar basis. All of the viscosities compared are at 40°C and at the rich loading of the system (0.3 mole CO_2 per mole alkalinity for MDEA and MDEA/PZ blend; 0.4 mole CO_2 per mole alkalinity for PZ and DGA; 0.5 mole CO_2 per mole alkalinity for MEA).

Comparison of the viscosity on this basis shows how the amine basic group affects overall viscosity. As the concentration of basic groups increases in a molecule, the viscosity increases. The viscosity of 8 m PZ is higher than that of 7 m MEA, but as

compared to 60 wt % DGA®, the viscosity of PZ is lower for a higher alkalinity. Therefore, PZ has the advantage of having two amine functional groups without suffering an increase in viscosity over DGA®. DGA® solutions at 60 wt % are successfully used in natural gas treating, which indicates that a PZ solution of a similar viscosity value should be possible (Al-Juaied and Rochelle, 2006b; Al-Juaied, 2004). The viscosity value of 8 m PZ with 0.4 mole CO_2 per mole alkalinity is one reason for the choice of 8 m PZ as the best concentrated PZ system.

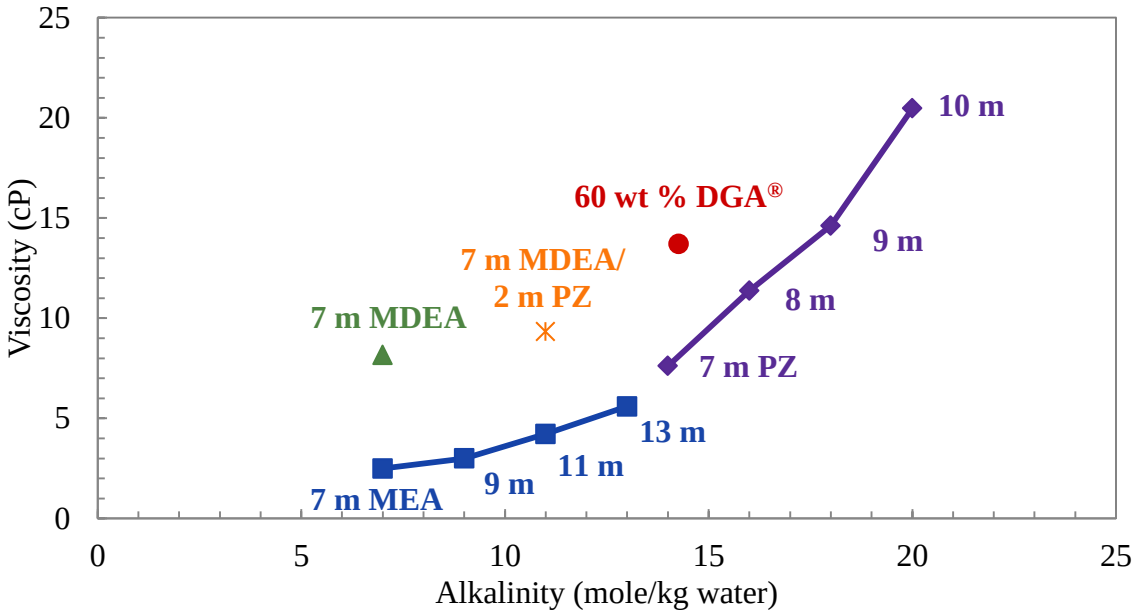

Figure 4.8: Viscosity of Amine Solutions at Typical Rich Loading and 40 °C

4.5 SOLID-LIQUID EQUILIBRIUM OF CONCENTRATED PZ

The solubility of PZ solutions is a crucial operational parameter for a concentrated PZ CO_2 capture system. In an effort to elucidate the solid-liquid equilibrium (SLE) behavior of PZ, two types of measurements were taken during this project. First, solutions with or without PZ precipitation were analyzed to understand the regions of insolubility. This was a more 'shotgun' approach to the issue of solubility by first

analyzing PZ solutions over a range of PZ concentration, CO_2 loadings (CO_2 concentrations), and temperatures. Second, transition temperatures were measured for a variety of solutions to accurate gauge the exact transition temperature for a given solution with a set PZ concentration and CO_2 loading.

4.5.1 Regions of insolubility for concentrated PZ

To examine the regions of insolubility for concentrated PZ, a database was created for all solutions that could be analyzed. Any PZ solutions that were analyzed for concentration and CO_2 loading were included in a database of solubility data. This included solutions used for other experiments (i.e. degradation experiments) or made in particular for solubility experiments. This database included only PZ solutions, no blends of PZ with other substituted PZ or other amines. Solutions were classified as soluble, where no evidence of precipitation was found, or insoluble where there was either complete precipitation, some precipitation on the bottom of the bottle, or a slurry existed. For insoluble solutions, the supernatant was generally analyzed for PZ and CO_2 concentration. This may have caused additional error since the supernatant may not accurately represent the overall solution characteristics that produced the precipitation. It would have been more accurate to heat each solution up that contained precipitate until it fully melted in order to measure the overall solution characteristics that led to insolubility. Measuring the supernatant likely led to the regions of solubility and insolubility to overlap on a few occasions.

The goal of this database was to quickly establish regions of insolubility within the typical operation range of a CO_2 capture system. The data are presented below in Figure 4.9, Figure 4.10, and Figure 4.11 as plots of CO_2 loading against PZ concentration for a given temperature. In each figure, soluble solutions are indicated with a filled point

(●) while insoluble solutions are indicated with an open point (○). The line on each figure is the prediction of the SLE for each temperature provided by the Aspen model of Hilliard (Hilliard, 2008). The data from Hilliard are provided to demonstrate that physical solubility of PZ was not correctly predicted with the early versions of PZ thermodynamic models.

The regions of insolubility for concentrated PZ are shown in Figure 4.9 at 21 °C or room temperature. The room temperature data demonstrate a few of the issues discovered when analyzing the supernatant versus the total solution. The point containing about 10 m PZ with a loading of 0.35 mole CO_2 per mole alkalinity, for example, is surrounded by soluble points and was likely analyzed with a large amount of error. The ability of the Hilliard model to predict solubility is demonstrated by the solid line in Figure 4.9. For low concentration PZ, the prediction is good but deviates with higher concentrations of PZ. This is expected since there was a dearth of high concentration PZ data available when Hilliard was modeling PZ thermodynamics.

In the insoluble regions at low loadings, the solid is predicted to be PZ hexahydrate ($PZ \cdot 6H_2O$) which represents the solution simply meeting the solubility limit of the anhydrous $PZ \cdot 6H_2O$ used to make PZ solutions, but this was not confirmed with XRD. In this region, the speciation indicates low concentrations of H^+PZ and $PZCOO^-$ in comparison to free PZ. X-ray diffraction (XRD) analysis of a solution that was overloaded and precipitated at high CO_2 loadings indicated that the precipitated crystals were protonated PZ carbamate hydrate ($H^+PZCOO^- \cdot H_2O$) (Xu, 2008). This is expected to occur in regions of rich CO_2 loading where the concentration of H^+PZCOO^- is significantly higher than free PZ, H^+PZ, or $PZCOO^-$.

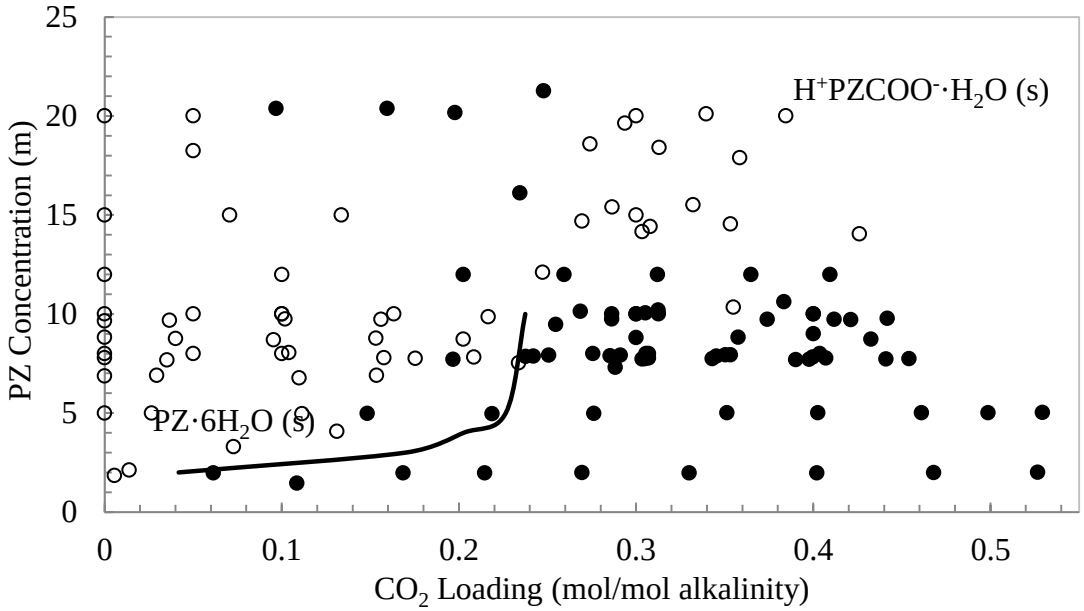

Figure 4.9: Regions of insolubility for concentrated PZ at 21 °C; data: ●, soluble solutions; ○, insoluble solutions; line: prediction of (Hilliard, 2008)

The regions of insolubility measured for 40 °C are shown in Figure 4.10. This data set includes solutions analyzed during the course of this thesis and those from the thesis of Hilliard during his measurement of vapor-liquid equilibrium (Hilliard, 2008). Hilliard performed a set of measurements at 40 °C on a variety of solutions and solutions without precipitation were required to get accurate results. Therefore, the solutions Hilliard analyzed are assumed to be free of insolubility. The predictions from Hilliard were not as extensive for 40 °C and only two points make up the predicted solubility curve in Figure 4.10. The lean loading region of insolubility at 40 °C is not as large as at room temperature, so an estimation of where $PZ \cdot 6H_2O$ is the likely precipitate is not indicated. It is still expected that rich precipitation will likely contain a majority of $H^+PZCOO^- \cdot H_2O$.

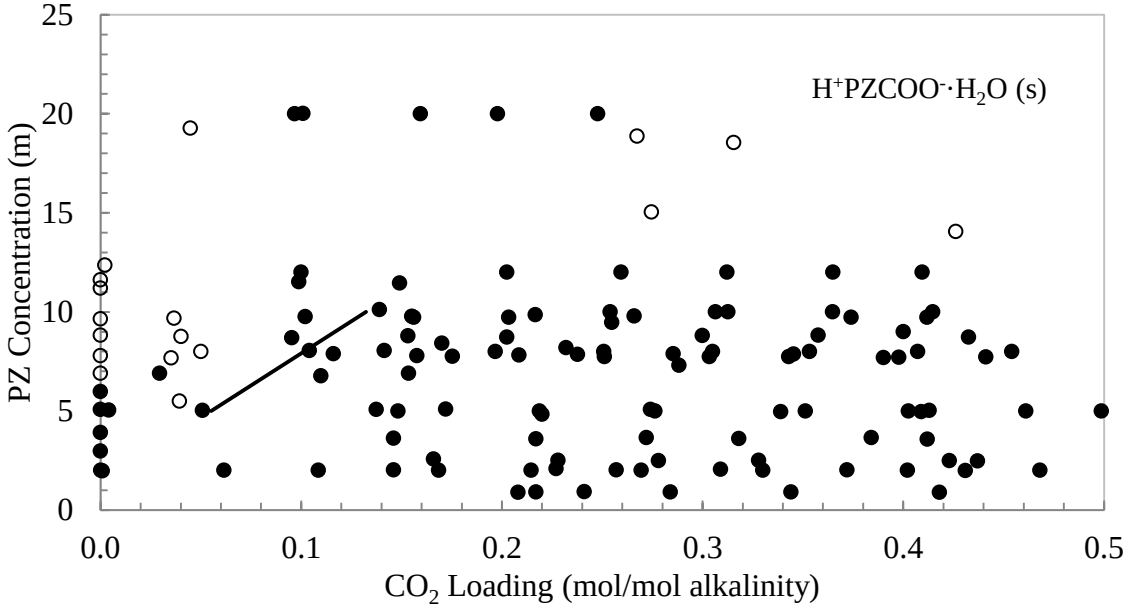

Figure 4.10: Regions of insolubility for concentrated PZ at 40 °C; data: ●, soluble solutions; ○, insoluble solutions; line: prediction of (Hilliard, 2008)

The solubility database also includes data at 60 °C which are shown in Figure 4.11. Most PZ solutions are soluble at this temperature, so there were few solutions found to be insoluble at this temperature. The Hilliard thermodynamic model did not predict SLE at this temperature so a model line is not included in Figure 4.11 (Hilliard, 2008). The solutions that were insoluble at 60 °C appear to indicate that some regions of high PZ concentration and rich loading will still not be soluble at this high temperature condition. This was not expected and would need to be investigated further to avoid precipitation in any real systems that may operate in this region. Solutions ranging from 0 to 12 m PZ were found to be completely soluble over a range of CO_2 loadings. This demonstrates that a concentrated PZ solvent will not likely experience insolubility during normal operation in a real CO_2 capture system if kept warm and not extremely rich in CO_2.

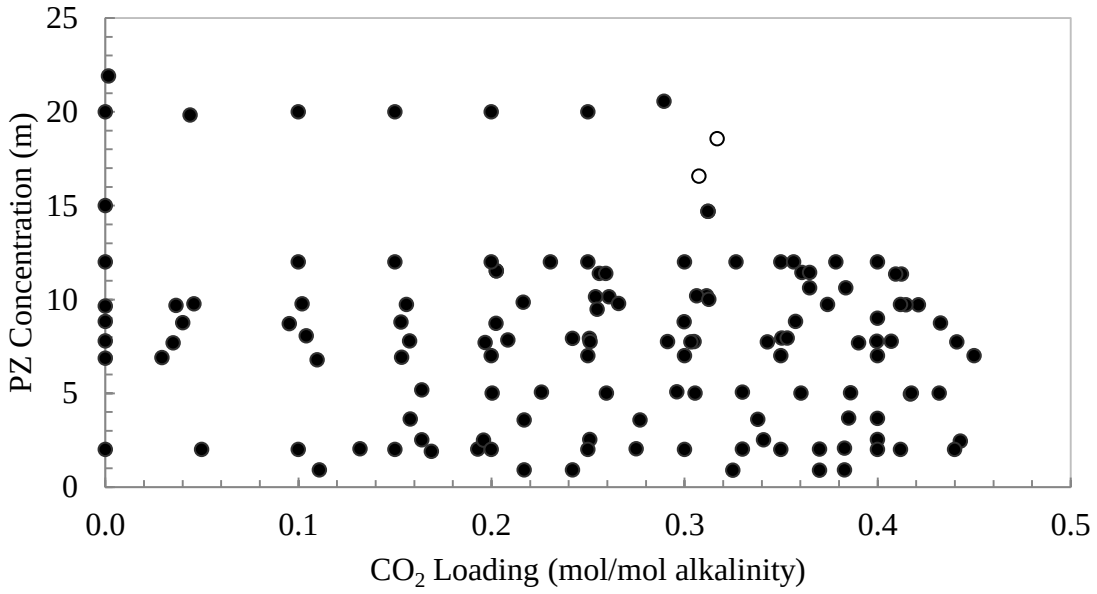

Figure 4.11: Regions of insolubility for concentrated PZ at 60 °C Data: ●, soluble solutions; ○, insoluble solutions

4.5.2 Transition temperature of concentrated PZ

One important characteristic of the SLE of concentrated PZ solutions is the transition temperature, or temperature at which a solution transitioned between liquid and solid for a given PZ concentration and CO_2 loading. This is a helpful parameter to understand in order to control a PZ solution in service and maintain a liquid solution when operating a CO_2 capture system. The transition temperature was measured as described previously and above in Section 4.2 and all values measured in this project are summarized in Table 4.5 (Freeman et al., 2010b). Provided PZ concentrations in molal are approximate while the PZ concentration in weight percent was determined from acid titration and CO_2 loading was measured with TIC.

Table 4.5: Transition temperatures for 3 to 25 m PZ

PZ Conc. m	PZ Conc. wt %	CO_2 Loading mol/mol alk	Crystal Temp °C	Melting Temp °C
3	20.4	0	29.5	31
4	25.2	0	32.0	35.5
5	30.4	0	36.0	38.5
6	34.0	0	40.0	41
7	37.3	0	41.8	43.5
7	36.4	0.029	39.5	40.5
7	35.8	0.110	36.5	37.5
7	35.1	0.153	33	34.5
8	40.1	0	43.0	45
8	39.2	0.035	40.0	41
8	39.2	0.104	38.5	39.5
8	37.7	0.158	33.0	34.5
8	37.1	0.209	26.5	29
8	36.2	0.251	18.0	22.5
8	35.5	0.303	3.0	10
8	35.0	0.343	0.0	0
9	43.2	0	43.0	44
9	42.2	0.040	40.5	41.2
9	41.1	0.095	38.0	39
9	40.3	0.153	33.5	35
9	39.4	0.202	29.0	30.5
9	40.4	0.255	21.0	24
9	38.1	0.300	7.0	15
9	37.2	0.358	0.0	0
10	45.4	0	43	44
10	44.7	0.037	40.5	41.5
10	43.6	0.102	38.5	39.5
10	42.5	0.156	35.0	36
10	41.6	0.217	27.0	31
10	40.6	0.266	18.0	23
10	38.7	0.313	5.5	13
10	38.2	0.374	0.0	0
11	49.1	0	42.5	44
12	50.0	0	41.5	42.5
12	47.2	0.1	37.0	38.5
15	56.3	0	36.0	38.5
20	61.9	0	41.5	44
25	69.4	0	49.0	55.5

The transition temperature of unloaded PZ solutions ranging from 1.0 to 20 m PZ are compared to data available in literature with up to 80 wt% PZ in Figure 4.12 (The Dow Chemical Company, 2001; Bishnoi, 2000; Corporation, ; Hilliard, 2008; Muhammad et al., 2009). The data from this study show a eutectic point at 19 m PZ (60 wt %) that was also observed in the data from The Dow Chemical Company (2001) and Hilliard (2008). The solubility of anhydrous PZ at 20 °C, or room temperature, is 14 wt % PZ, which corresponds to 1.9 m PZ. The data from this study agrees with the data from the Dow Chemical Company. The data from Hilliard (2008) over predict the transition temperature between up to a mass fraction of PZ of 0.6. The method used to obtain this data, a Differential Scanning Calorimeter (DSC), used a temperature ramp of 5 °C per minute, would may not have allowed enough time for equilibrium and even heating of the sample to correctly predict the transition point. The measurements of both Bishnoi and Muhammed did not observe the eutectic point because their methods involved allowing a known quantity of PZ to reach equilibrium at a given temperature while any precipitation settled out (Bishnoi, 2000; Muhammad et al., 2009). Then, the supernatant liquid was analyzed to provide a solubility limit at that temperature condition. The eutectic point would not be able to be observed in this way because at a range of temperatures, there would be three possible compositions of PZ in the supernatant. The data outside of the range of the eutectic point agree nicely with the data from this study and that of The Dow Chemical Company (2001).

The transition temperature of 5, 7, 8, 9, 10, and 12 m PZ solutions over a range of CO_2 loading were measured and are shown in Figure 4.13. The shape and location of the transition temperature curve does not vary significantly over the concentration range of 7 to 12 m PZ. Also, the unloaded transition temperature is nearly identical over the range of PZ concentrations.

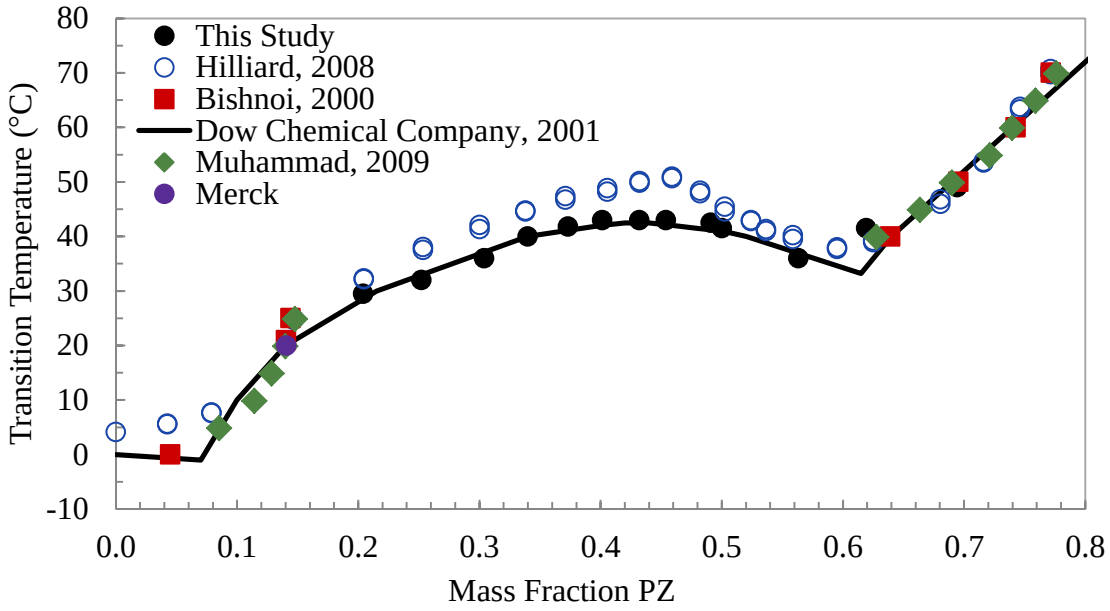

Figure 4.12: Comparison of transition temperatures of unloaded PZ

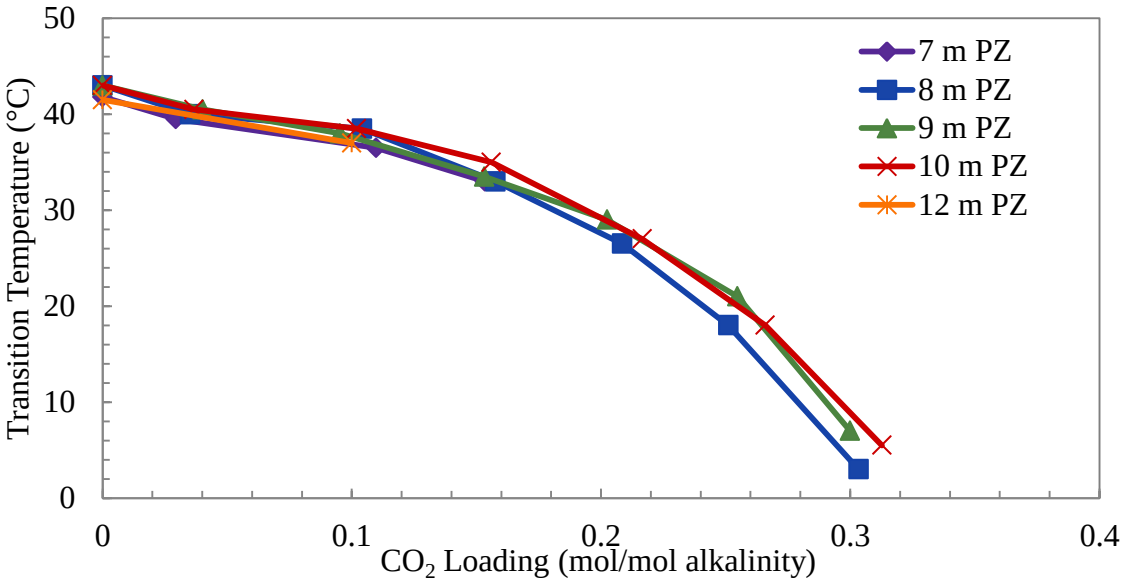

Figure 4.13: Crystal transition temperatures for 7 to 12 m PZ

As mentioned in section 4.2, two temperatures were recorded for each measurement, the crystal temperature and the melting temperature. The crystal temperature is the temperature plotted in Figure 4.13 since crystallization is the most likely concern for this system. An example of the hysteresis seen in the SLE of PZ is shown in Figure 4.14. In these measurements, the temperature at which a transition was visually observed was different depending on whether a liquid solution was cooled or a solid or slurry was heated.

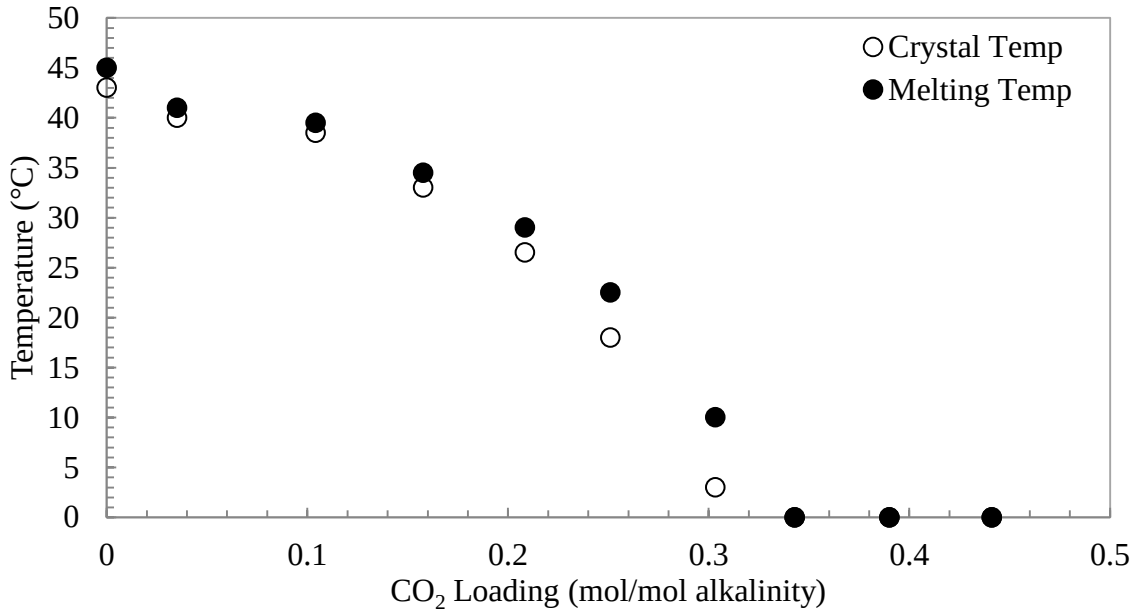

Figure 4.14: Example of hysteresis in SLE data for 8 m PZ

The solubility envelope for 8 and 10 m PZ is shown again in Figure 4.15 to highlight these two concentrations that are the most important for future industrial application. The two dashed lines at rich loadings in Figure 4.15 represent soluble PZ solutions indicating that the solubility envelope extends at least this high in CO_2 loading. These four data points represent the richest soluble solutions that were obtained at 0 and 40 °C during the solubility studies. Beneath the transition temperature line, at low

temperatures and lean CO_2 loading, a precipitate will likely be $PZ{\cdot}6H_2O$ while rich loading precipitation, as shown in the figure, has been shown to be $H^+PZCOO^-{\cdot}H_2O$ (Xu, 2008). The envelope also demonstrates that for 8 m PZ a CO_2 loading of approximately 0.25 mole CO_2 per mole of alkalinity is required to maintain a liquid solution without precipitation at room temperature (20 °C).

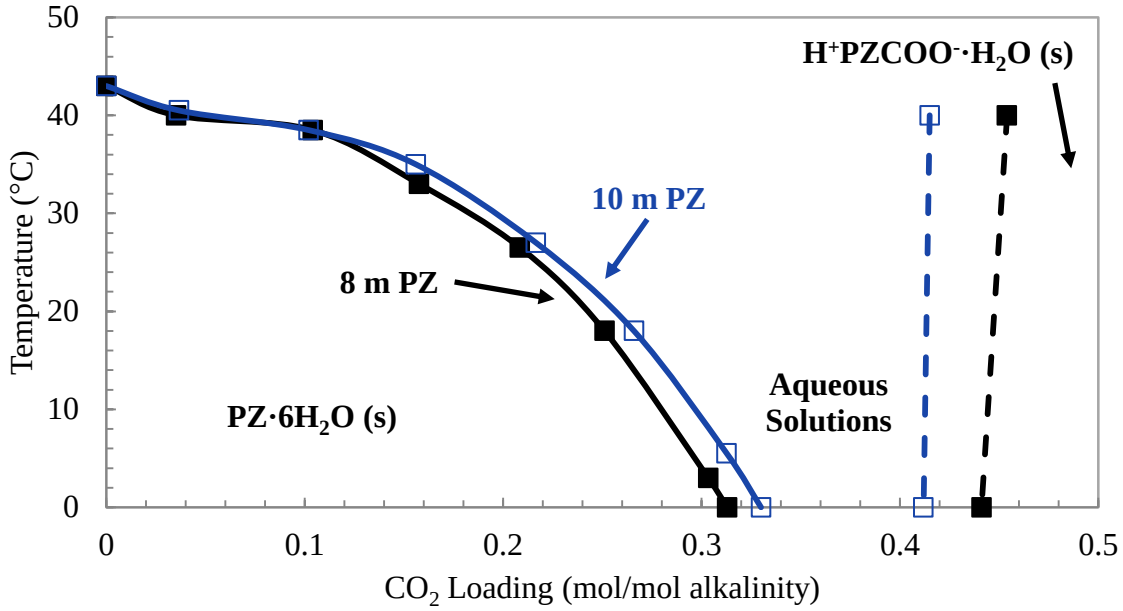

Figure 4.15: Solubility envelope for 8 and 10 m PZ

4.6 PHYSICAL PROPERTIES OF PZ BLENDS

A blend of PZ, 1-methylpiperazine (1-MPZ), and 1,4-dimethylpiperazine (1,4-DMPZ) was identified as potential novel amine system for CO_2 capture based on thermal degradation experiments. This blend is advantageous because 1-MPZ by itself was found to degrade to nearly equal parts PZ and 1,4-DMPZ, creating an equilibrium between the three molecules (see Section 7.3 for details). Because of this behavior, a blend of PZ, 1-MPZ, and 1,4-DMPZ was believed to be a good solvent because the equilibrium between the molecules would limit degradation to other amines and there was a potential cost

savings in the manufacturing of the amine blend due to decreased separation costs. One blend that was specifically identified as potentially useful was 5 m PZ / 2 m 1-MPZ / 1 m 1,4-DMPZ. The density and viscosity of this blend was measured in the same way described previously for concentrated PZ. In addition, the viscosity of 4 m PZ / 4 m 1-MPZ, 5 m PZ / 5 m 1-MPZ, and 4 m PZ / 1,4-DMPZ were each measured and are reported below. Blends of PZ with 2-MPZ were investigated as potentially favorable solvent systems as well. Densities over a range of loadings were measured for 4 m PZ / 4 m 2-MPZ and 5 m PZ / 5 m 2-MPZ.

4.6.1 Density of 5 m PZ / 2 m 1-MPZ / 1 m 1,4-DMPZ

The density of 5 m PZ / 2 m 1-MPZ / 1 m 1,4-DMPZ was measured over a range of CO_2 loadings from 0 to 0.39 and over a range of temperatures from 10 to 80 °C (283.15 to 353.15 K). Data were obtained for all solutions where precipitation and CO_2 evolution was absent. The raw data are shown in Table 4.6 while the data are plotted in Figure 4.16. The data demonstrate the expected trends of an increase of density with increasing CO_2 loading and decreasing temperature.

4.6.2 Viscosity of 5 m PZ / 2 m 1-MPZ / 1 m 1,4-DMPZ

The viscosity of a blend of 5 m PZ / 2 m 1-MPZ / 1 m 1,4-DMPZ was measured over a range of CO_2 loading from 0 to 0.39 and from 10 to 80 °C. Data were obtained for all solutions where precipitation and CO_2 evolution was absent. The raw data obtained are shown in Table 4.6 and Figure 4.17. The data demonstrate the expected trend that viscosity increases with increasing CO_2 concentration and decreasing temperature.

Table 4.6: Density and Viscosity of 5 m PZ / 2 m 1-MPZ / 1 m 1,4-DMPZ from 10 to 80 °C

CO_2 Loading mol/mol alk	CO_2 Conc. mol/kg	T °C	Density (ρ) g·cm^3	Viscosity (μ) mPa-s		
0.2	1.661	10	1.0937	42.320	±	0.042
0.23	1.900	10	1.1031	42.940	±	0.070
0.29	2.411	10	1.1221	44.240	±	0.070
0.33	2.680	10	1.1358	44.440	±	0.070
0.37	2.940	10	1.1490	44.390	±	0.088
0.39	3.105	10	1.1553	44.290	±	0.120
0.1	0.894	25	1.0553	18.030	±	0.082
0.15	1.286	25	1.0707	19.290	±	0.110
0.2	1.661	25	1.0856	20.540	±	0.178
0.23	1.900	25	1.0955	21.310	±	0.173
0.29	2.411	25	1.1147	22.790	±	0.242
0.33	2.680	25	1.1287	23.380	±	0.199
0.37	2.940	25	1.1421	23.870	±	0.200
0.39	3.105	25	1.1481	23.960	±	0.212
0	0	40	1.0117	7.420	±	0.095
0.05	0.478	40	1.0290	8.261	±	0.122
0.1	0.894	40	1.0457	9.154	±	0.148
0.15	1.286	40	1.0618	9.993	±	0.157
0.2	1.661	40	1.0772	10.900	±	0.226
0.23	1.900	40	1.0874	11.390	±	0.213
0.29	2.411	40	1.1073	12.570	±	0.206
0.33	2.680	40	1.1214	13.290	±	0.311
0.37	2.940	40	1.1347	13.680	±	0.319
0.39	3.105	40	1.1408	13.960	±	0.337
0	0	60	0.9957	3.666	±	0.125
0.05	0.478	60	1.0139	4.157	±	0.124
0.1	0.894	60	1.0317	4.698	±	0.180
0.15	1.286	60	1.0486	5.310	±	0.226
0.2	1.661	60	1.0644	5.900	±	0.243
0.23	1.900	60	1.0750	6.354	±	0.246
0.29	2.411	60	1.0951	7.045	±	0.293
0.33	2.680	60	1.1097	7.698	±	0.369
0	0	80	0.9786	2.035	±	0.051
0.05	0.478	80	0.9978	2.289	±	0.104
0.1	0.894	80	1.0165	2.628	±	0.123
0.15	1.286	80	1.0337	3.039	±	0.142
0.20	1.661	80	1.0511	3.277	±	0.160
0.23	1.900	80	1.0614	3.696	±	0.103
0.29	2.411	80	-	4.163	±	0.192
0.33	2.680	80	-	5.350	±	0.196

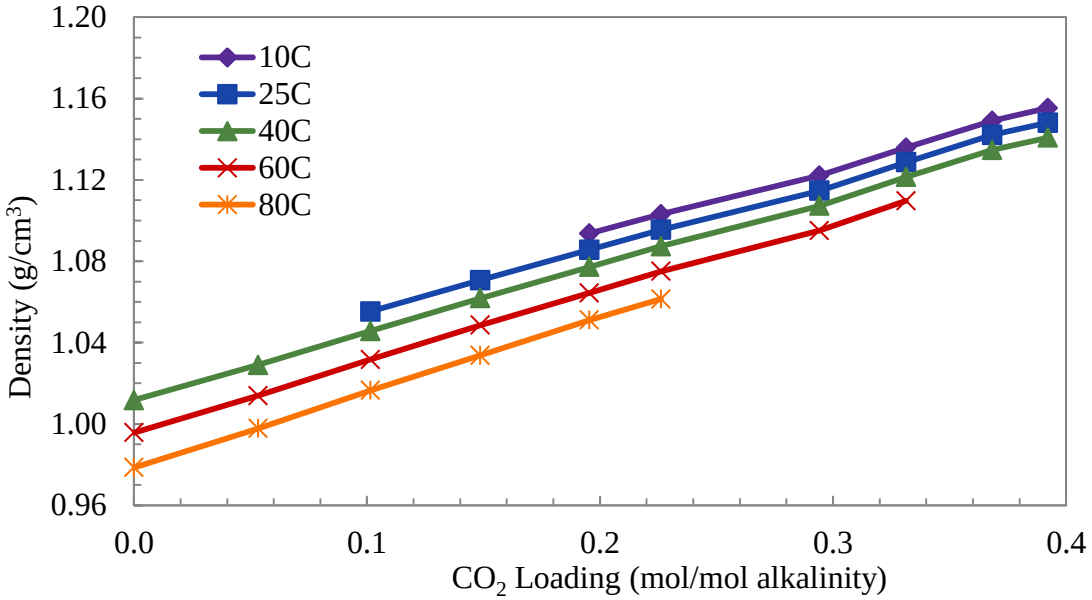

Figure 4.16: Density of 5 m PZ / 2 m 1-MPZ / 1 m 1,4-DMPZ from 10 to 80 °C

A correlation was created from the 5 m PZ / 2 m 1-MPZ / 1 m 1,4-DMPZ data to relate the ratio of viscosity to the viscosity of water (μ/μ_{water}) to temperature (K) and C_{CO2} (mol/kg) and has the form of

$$\ln\left(\frac{\mu}{\mu_{water}}\right) = \Phi_1 + \Phi_2 \cdot T + \frac{\Phi_3}{T} \tag{4.6}$$

where

$$\Phi_i = a_i + b_i \cdot C_{CO2} \tag{4.7}$$

The values of the regressed parameters can be found in Table 4.7. Values for μ_{water} over the range of 10 to 80 °C (283.15 to 353.15 K) were taken from the DIPPR Database (DIPPR, 2010). The resulting correlation (Equation 4.6) was able to fit all experimental μ/μ_{water} data within 5.1 % with an average error of only 2.0 %. The average

absolute deviation (AAD) calculated using Equation 4.2 for the prediction of viscosity data was 0.0012 indicating the data set is well represented by Equation 4.6.

Rearranging the above regression (Equation 4.6) leaves a relationship which predicts the viscosity of 5 m PZ / 2 m 1-MPZ / 1 m 1,4-DMPZ directly (Equation 4.8).

$$\mu = \mu_{water} \cdot \exp\left(\Phi_1 + \Phi_2 \cdot T + \frac{\Phi_3}{T}\right) \tag{4.8}$$

The experimental viscosity data from Table 4.6 is compared to the prediction of Equation 4.8 in Figure 4.17. A parity plot comparing the experimental viscosity data to the values predicted using Equation 4.8 is shown in Figure 4.18 with 5 % deviation shown with dashed lines.

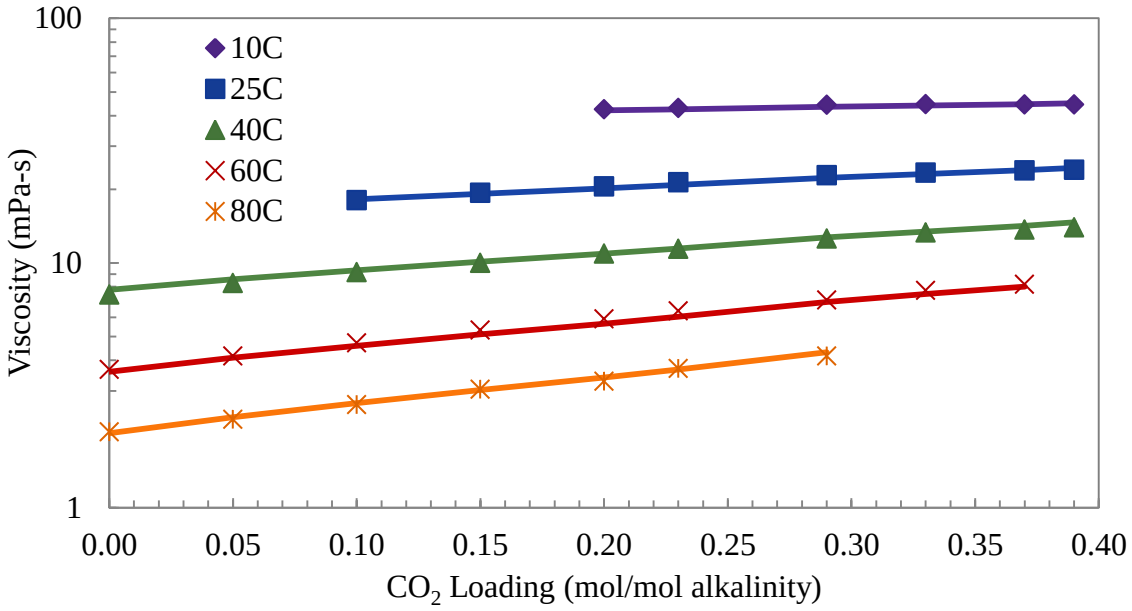

Figure 4.17: Comparison of the viscosity of 5 m PZ / 2 m 1-MPZ / 1 m 1,4-DMPZ to the prediction of Equation 4.8 (solid lines) over a range of CO_2 concentrations

Table 4.7: Value of parameters in Equation 4.6

Parameter	i = 1	i = 2	i = 3
a	-29.12	0.0379	6167.9
b	6.151	-0.00746	-1131.04

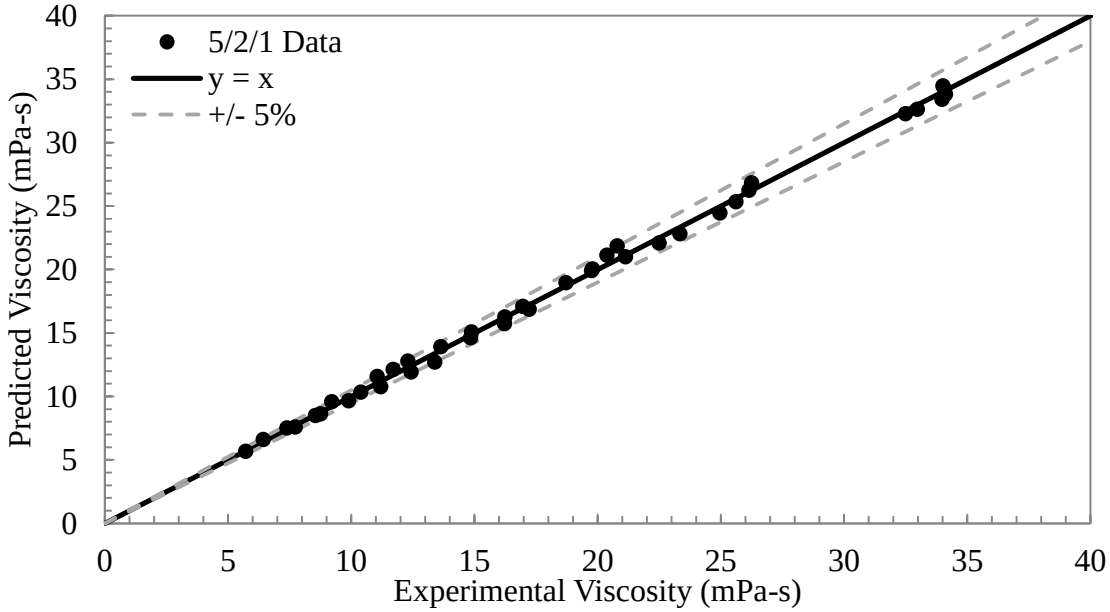

Figure 4.18: Parity plot demonstrating the accuracy of Equation 4.8 for predicting viscosity of 5 m PZ / 2 m 1-MPZ / 1 m 1,4-DMPZ solutions from 10 to 80 °C

4.6.3 Viscosity of 4 m PZ / 4 m 1-MPZ

The viscosity of the blend of 4 m PZ / 4 m 1-MPZ was measured by Cindy Tran as part of her student project that took place in the Rochelle lab. The raw viscosity data are shown in Table 4.8 while the data are shown plotted against CO_2 loading in Figure 4.19. The standard deviations in the measurement of viscosity for the data in Figure 4.19 are plotted as error bars, but the small size of the deviation is overshadowed by the data point itself in most cases. The 25 °C data set contains a large amount of error. It is likely that this error is a combination of possible solidification or the presence of slurries during measurements and the fact that an undergraduate a student took these measurements while they were first learning how to use the rheometer. The higher loading samples

appear to have successful measurements for 25 °C, indicating it is likely that the low loading samples were suffering from slurries or solidification for the lower loading samples.

Table 4.8: Viscosity of 4 m PZ / 4 m 1-MPZ from 25 to 60 °C

CO_2 Loading mol/mol alk	T °C	Viscosity (μ) mPa-s	
0.05	25	16.390	± 0.357
0.10	25	15.330	± 0.048
0.15	25	11.630	± 0.048
0.20	25	17.320	± 0.042
0.25	25	20.660	± 0.107
0.30	25	21.420	± 0.140
0.35	25	22.350	± 0.178
0.40	25	22.710	± 0.145
0.00	40	7.378	± 0.095
0.05	40	8.004	± 0.131
0.10	40	8.832	± 0.155
0.15	40	9.883	± 0.244
0.20	40	10.280	± 0.169
0.25	40	11.040	± 0.201
0.30	40	11.970	± 0.231
0.35	40	12.760	± 0.241
0.40	40	13.140	± 0.255
0.05	60	3.092	± 0.031
0.10	60	4.719	± 0.159
0.15	60	5.243	± 0.198
0.20	60	5.691	± 0.170
0.25	60	6.387	± 0.224
0.30	60	6.138	± 0.084
0.35	60	7.139	± 0.180
0.40	60	7.698	± 0.157

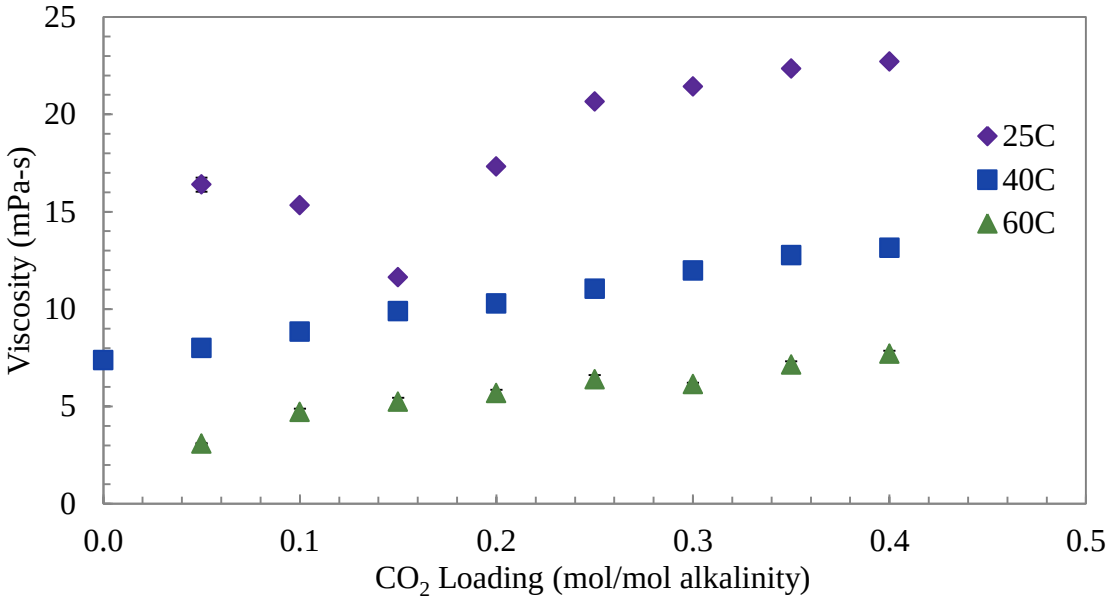

Figure 4.19: Viscosity of 4 m PZ / 4 m 1-MPZ from 25 to 60 °C

4.6.4 Viscosity of 4 m PZ / 4 m 1,4-DMPZ

The viscosity of the blend of 4 m PZ / 4 m 1,4-DMPZ was also measured by Cindy Tran as part of a student project within the Rochelle laboratory. The raw viscosity data is shown in Table 4.9 while the data are shown plotted against CO_2 loading in Figure 4.20. The standard deviation of the viscosity measurement for each data point is plotted as an error bar in Figure 4.20, but they are not visible compared to the data point itself. There are a few data points that appear to deviate from the expected trend. This is the result of basic experimental error because the measurements were performed by an undergraduate learning to use the apparatus.

4.6.5 Density of 4 m PZ + 4 m 2-MPZ

Blends of PZ with 2-MPZ were investigated as novel solvents that potentially had better solubility characteristics than concentrated PZ alone. The density of a blend of 4 m PZ + 4 m 2-MPZ was measured as part of this effort. The raw density data are shown in

Table 4.10 while the data are plotted against CO_2 loading in Figure 4.21.

Table 4.9: Viscosity of 4 m PZ + 4 m 1,4-DMPZ from 25 to 60 °C

CO_2 Loading mol/mol alk	T °C	Viscosity (μ) mPa-s		
0.10	25	19.110	±	0.032
0.15	25	21.050	±	0.071
0.20	25	22.380	±	0.079
0.25	25	23.740	±	0.070
0.30	25	24.540	±	0.097
0.35	25	24.300	±	0.082
0.10	40	9.176	±	0.069
0.15	40	10.090	±	0.099
0.20	40	11.070	±	0.082
0.25	40	12.190	±	0.166
0.30	40	13.010	±	0.099
0.35	40	13.210	±	0.120
0.10	60	4.526	±	0.086
0.15	60	5.389	±	0.160
0.20	60	6.017	±	0.162
0.25	60	5.078	±	0.021
0.30	60	6.895	±	0.030
0.35	60	6.681	±	0.296

Table 4.10: Density of 4 m PZ + 4 m 2-MPZ from 20 to 60 °C

CO_2 Loading mol/mol alk	CO_2 Conc. mol/kg	Density, ρ (g/cm^3) 20 °C	40 °C	60 °C
0.15	1.289	1.0782	1.0651	1.0531
0.18	1.728	1.0938	1.0817	1.0703
0.25	2.173	1.1088	1.0974	1.0863
0.30	2.573	1.1227	1.1119	1.1012
0.34	2.980	1.1367	1.1265	1.1160
0.39	3.373	1.1506	1.1408	1.1303

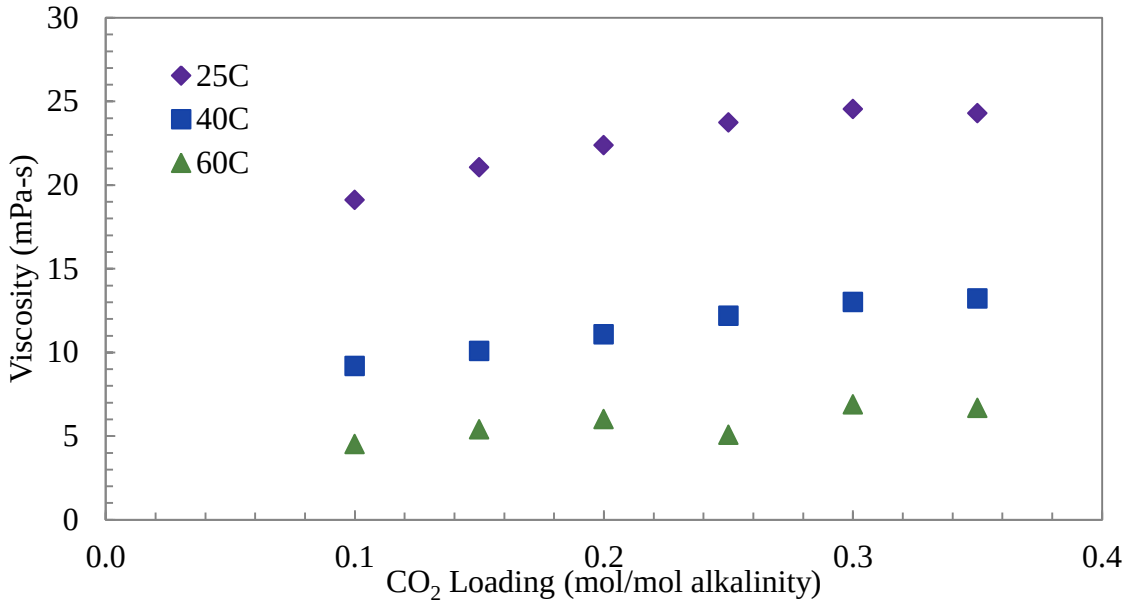

Figure 4.20: Viscosity of 4 m PZ + 4 m 1,4-DMPZ from 25 to 60 °C

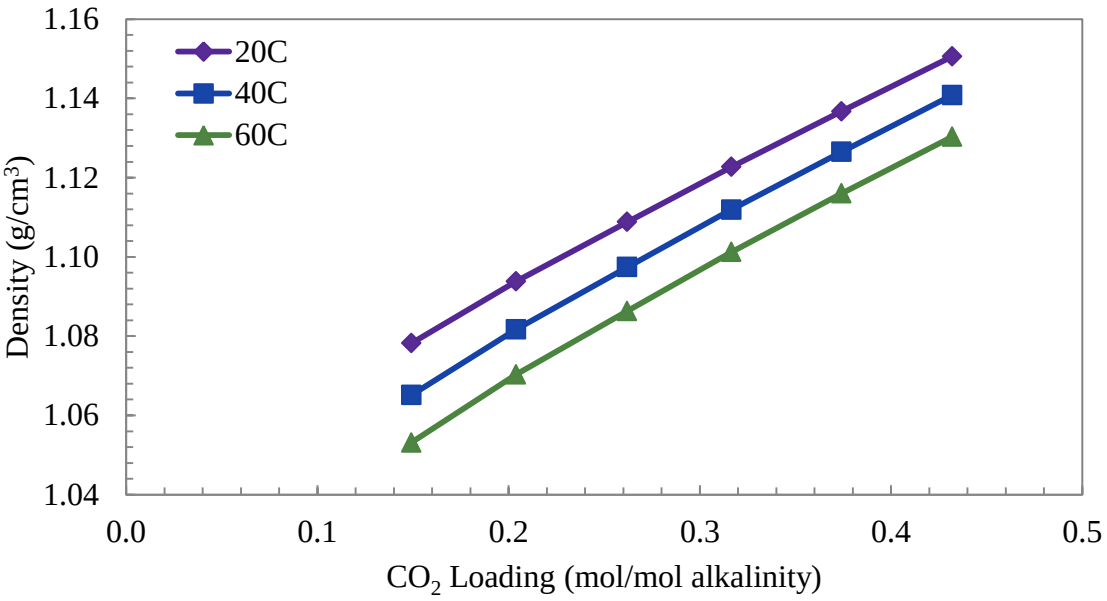

Figure 4.21: Density of 4 m PZ + 4 m 2-MPZ from 20 to 60 °C

4.6.6 Density of 5 m PZ + 5 m 2-MPZ

Another blend of interest was a 5 m PZ + 5 m 2-MPZ blend where the increased alkalinity would enhance kinetic rates of CO_2 absorption. The density of this blend was measured over a range of CO_2 loadings and temperatures. The raw density data are shown in Table 4.11 while the data are plotted against CO_2 loading in Figure 4.22.

Table 4.11: Density of 5 m PZ + 5 m 2-MPZ from 20 to 60 °C

CO_2 Loading	CO_2 Conc.	Density, ρ (g/cm^3)		
mol/mol alk	mol/kg	20 °C	40 °C	60 °C
0.078	0.782	1.0544	1.0390	1.0254
0.116	1.141	1.0749	1.0607	1.0478
0.175	1.676	1.0959	1.0827	1.0704
0.233	2.184	1.1156	1.1034	1.0915
0.302	2.747	1.1346	1.1231	1.1117
0.349	3.120	1.1530	1.1421	1.1309
0.411	3.588	1.1708	1.1604	1.1494
0.469	3.997	1.1827	1.1727	1.1615

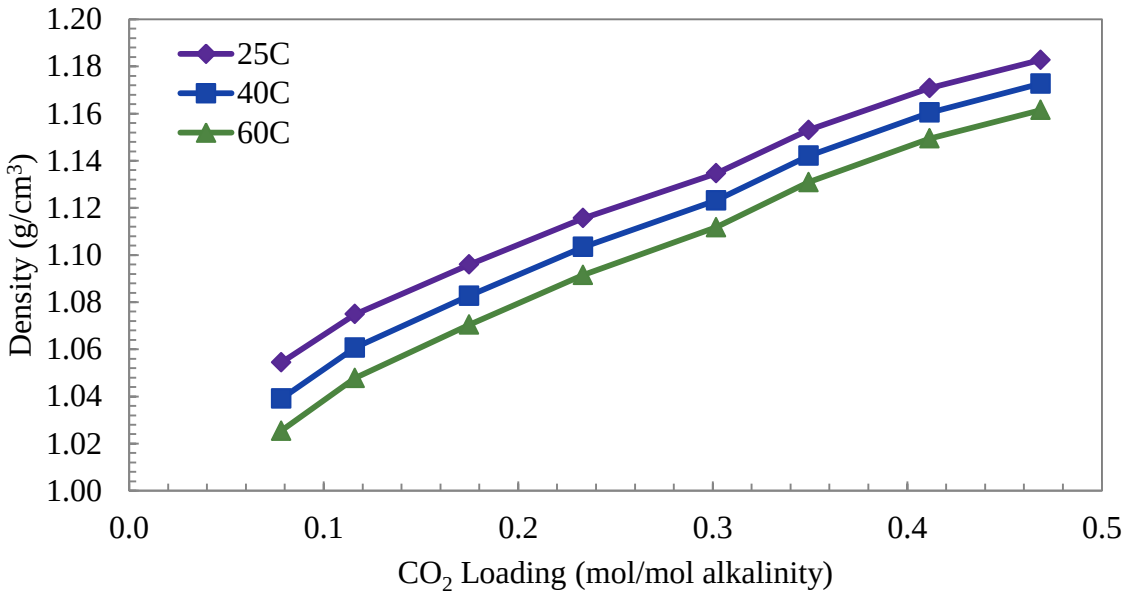

Figure 4.22: Density of 5 m PZ + 5 m 2-MPZ from 20 to 60 °C

4.6.7 Comparison of density data

The density of 4 amine solutions containing a total alkalinity of 16 m has been measured over a range of temperatures and CO_2 concentrations. A summary of the density data obtained is shown in Figure 4.23 where data for each blend at 40 °C are compared with a prediction of the density of 7 m MEA (Weiland et al., 1998). All of the PZ based solvent systems demonstrate similar density behavior and all have higher density than 7 m MEA. Density can affect pump work and fluid heat and mass transfer so a decreased density can be advantageous. On the other hand, if monitoring of CO_2 concentration through on-line density measurements is desired, the increased slope of the PZ density data can be advantageous to produce a more robust correlation where a larger and more accurate density measurement can be achieved for a given change in CO_2 loading.

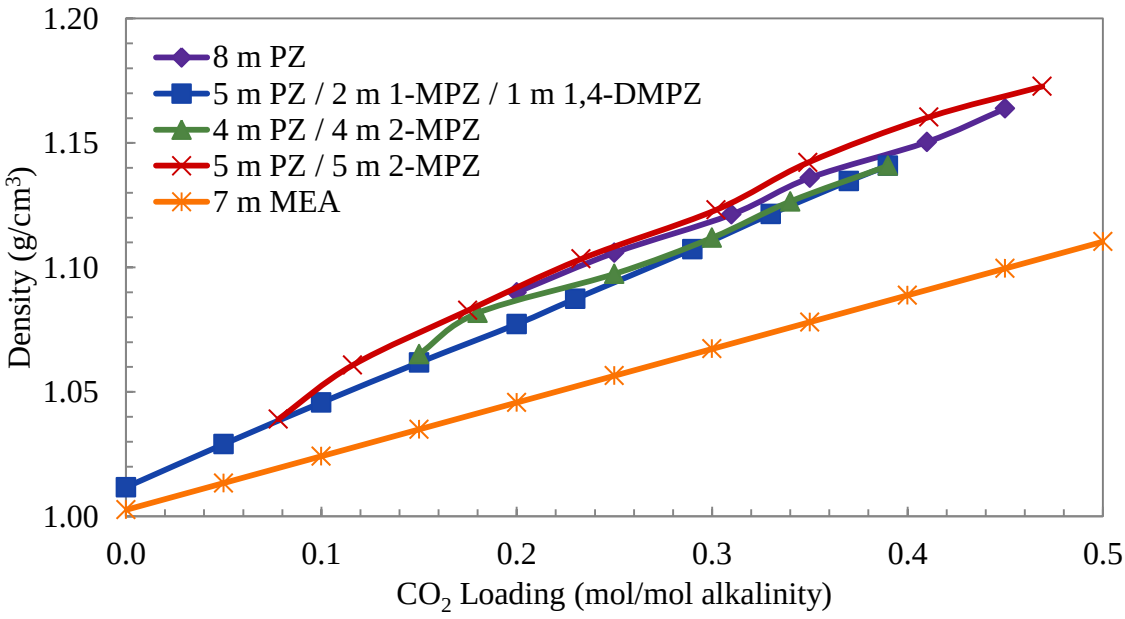

Figure 4.23: Comparison of density data for PZ based systems at 40 °C

4.6.8 Comparison of viscosity data

The viscosity of 4 amine solutions containing a total alkalinity of 16 m has been measured over a range of temperatures and CO_2 concentrations. A summary of the viscosity data obtained are shown in Figure 4.24 where data for each blend at 40 °C are compared with a prediction of the viscosity of 7 m MEA (Weiland et al., 1998). The baseline 8 m PZ solution has a lower viscosity than the three PZ blends but still significantly higher than that of MEA. This is advantageous for the concentrated PZ solvent compared to the blends, but MEA still has an advantage in this category since as increased viscosity leads to increased pumping work, decreased mass transfer, and decreased heat transfer. All of the PZ based solutions would suffer from these disadvantages compared to a MEA system.

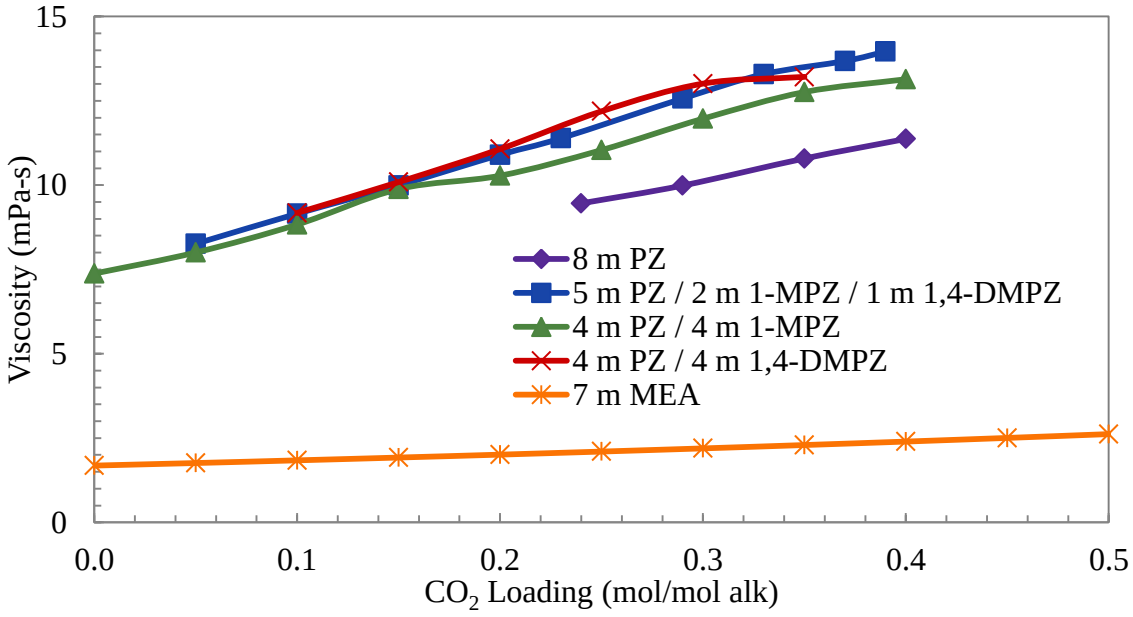

Figure 4.24: Comparison of viscosity data for PZ based systems at 40 °C

4.7 CONCLUSIONS

At 0 °C, 8 m PZ will not precipitate solids between 0.32 and 0.44 mole CO_2 per mole alkalinity. At an operating temperature of 40 °C, 8 m PZ will be an aqueous solution between 0.1 and 0.45 mole CO_2 per mole alkalinity. The room temperature (20 °C) solubility of unloaded PZ is 14 weight %, or 1.9 m PZ, while the soluble loading range is approximately 0.25 to 0.4 mole CO_2 per mole alkalinity at this temperature. Transition temperatures for concentrated PZ were measured over a range of CO_2 loading and hysteresis was observed in the temperature at which crystals formed when cooled or precipitation melted when heated.

The viscosity of 8 m PZ at 40 °C with 0.4 mole CO_2 per mole alkalinity is 11.4 cP, higher than that of 9 m MEA with 0.5 mole CO_2 per mole alkalinity (3 cP). Solutions of 60wt% DGA® with 0.4 mole CO_2 per mole alkalinity, a commercial gas treating solvent, has a viscosity 13.7 cP, even higher than PZ. The viscosity of 8 m PZ is given by Equation 4.9 in terms of the viscosity of water (cP), μ_{water}, concentration of CO_2 (mole per kg), C_{CO2}, concentration of PZ (mole per kg), C_{PZ}, and temperature (K), T.

$$\ln\left(\frac{\mu}{\mu_{water}}\right) = 1.723 + 2.63\cdot C_{CO2} - 1.019\cdot C_{PZ} - 0.527\cdot C_{CO2}\cdot C_{PZ} + \frac{-778\cdot C_{CO2} + 355.2\cdot C_{PZ} + 169.3\cdot C_{CO2}\cdot C_{PZ}}{T} \quad (4.9)$$

Density of 5 to 12 m PZ solutions was regressed in terms of the density of water, ρ_{water}, C_{CO2}, and C_{PZ}, and the resulting regression is shown in Equation 4.1. The effect of temperature on density was eliminated by including ρ_{water} at a given temperature.

$$\frac{\rho}{\rho_{water}} = 0.0407\cdot C_{CO2} + 0.008\cdot C_{PZ} + 0.991 \quad (4.1)$$

Online measurement of density and viscosity will permit accurate on-line estimates of PZ concentration and CO_2 loading. On-line viscosity and density monitors can be employed in a pilot plant, demonstration plant, or full scale CO_2 capture application as an inexpensive, easy, and effective way to continually monitor the condition of a PZ solvent. Both PZ concentration and CO_2 loading have traditionally been offline analyses that take on the order of minutes or hours to complete. Online monitoring allows for instant feedback and constant monitoring of the solvent conditions where maintaining the solution within physical solubility windows is a crucial operational concern.

The regression for viscosity was developed with only 8 m PZ data and this limits its application. Viscosity of PZ solutions is complicated and regressions across large PZ concentration ranges generally contain unacceptable levels of error for online monitoring applications. The density regression should be very robust in applications centering around 8 m PZ, the most likely concentration of concentrated PZ systems.

A blend of 4 m PZ / 4 m 2-MPZ, being developed for its beneficial physical solubility, has density less than 1% higher than an 8 m PZ solution with the same alkalinity. On the other hand, a blend of 5 m PZ / 2 m 1-MPZ / 1 m 1,4-DMPZ has up to a 3% lower density but 23% higher viscosity. All blends of PZ with substituted PZ molecules had very similar density values to PZ itself, but up to 30% higher viscosity. Blends can have advantageous characteristics, but can also result in unfavorable changes to density and viscosity.

Chapter 5 – Thermal Degradation Rate of PZ

In order to assess the thermal degradation rate of PZ as it applies to CO_2 capture applications, a number of thermal degradation experiments were conducted on concentrated, aqueous PZ. Prior work had identified PZ as a thermally resistant amine (Davis, 2009). To further explore the thermal resistance of PZ, experiments were performed that investigated the effect of temperature, PZ concentration, CO_2 concentration, and additives on the degradation rate of PZ. A first order rate constant was calculated and compared for all conditions. Portions of this chapter are excerpted from previous work (Freeman et al., 2010a).

5.1 Concentrated piperazine thermal degradation experiments

Thermal stability has been identified as a significant advantage of concentrated, aqueous PZ used for CO_2 capture applications. The temperatures chosen for PZ

degradation experiments reflect the ability of PZ to resist thermal degradation. Degradation of monoethanolamine (MEA), 2-amino-2-methyl-1-propanol (AMP), MEA blended with AMP, Morpholine (Mor), PZ, or diglycolamine® (DGA®) and other MEA structural analogs were previously studied over a range of 100 to 150 °C where significant degradation was observed at 150 °C in most cases (Davis, 2009). The screening experiment performed by Davis for 8 molal (m) PZ showed no amine loss at 135 °C after 4 weeks (Davis, 2009). Based on this data, initial experiments for PZ were performed at 150 and 175 °C. Although these temperatures are not representative of what is proposed for industrial CO_2 processes, PZ experiments were limited by time restrictions. Estimations for initial experiments showed that 72 weeks was required at 135 °C to shown measurable and significant PZ loss (10 to 15% amine loss). Any temperature less than 135 °C would have made the experiments over two years long.

The PZ concentration of interest for this dissertation is 8 m and was the focus of thermal degradation experiments. Four experiments were performed at 10 m PZ when this concentration was initially being investigated as well. Lower and higher concentrations (4 and 12 m PZ) were tested at two temperatures to determine the effect of PZ concentration on thermal degradation. Several high concentration experiments at 15 and 20 m PZ were performed to investigate the upper limit of PZ concentration and for use in thermal reclaiming modeling by other researchers. Solutions of 8 m PZ with 0 to 0.47 mole CO_2 per mole alkalinity were investigated to gauge the entire effect of CO_2 loading. A summary of the thermal degradation experiments on concentrated, aqueous PZ in the absence of other amines or additives is given in Table 5.1. Included in this table is the value of the first order rate constant, k_1, for PZ loss for each experiment. The determination of this value is described in the following section.

Table 5.1: Summary of PZ Thermal Degradation Experiments

Temp (°C)	PZ Conc. (m)	CO_2 Loading (mol/mol alk)	Experiment(s)	$k_1 \times 10^9$ (s^{-1})
135	8	0.3	TE10	1.0
	8	0.4	TE11	0.5
	10	0.3	TE1A	4.8
	10	0.4	TE1B	-
150	8	0.3	TE9, TE14	6.1
	8	0.4	TE15	7.9
	10	0.3	TE2A	8.9
	10	0.4	TE2B	6.0
	15	0.3	TE3A	-
	20	0.3	TE3B	24.2
165	4	0.3	TE49	35.5
	8	0	TE46	0.8
	8	0.1	TE47	18.4
	8	0.3	TE44	31.4
	8	0.4	TE45	40.9
	12	0.3	TE50	50.3
175	4	0.3	TE32	114
	8	0	TE21	7.0
	8	0.1	TE34	65.8
	8	0.2	TE53	78.8
	8	0.3	TE4, TE12, TE18	132
	8	0.4	TE13, TE19	171
	8	0.47	TE54	23.8
	12	0.3	TE33	156
	20	0.1	TE58	44.7
	20	0.3	TE57	168

This chapter as a whole highlights the effect of solution characteristics on the loss of PZ as the primary dependent variable. The production of degradation products will not be described in detail in each experiment in this chapter as a detailed discussion can be found in Chapter 6. Generation of formate, total formate, and ethylenediamine (EDA) will be used as representative compounds that are universally found during PZ thermal degradation. They will be used to represent the entire mix of degradation

products found in thermally degraded PZ without obscuring the main conclusions. A specific formyl amide, N-formyl PZ (FPZ), and N-(2-aminoethyl)piperazine (AEP) are generated during thermal degradation and account for a significant portion of the mass balance in many cases, but were not regularly quantified with cation IC until the end of the project. Therefore, there is not data for these compounds for all experiments. Comparisons of FPZ and AEP generation are made where data is sufficient. All of the quantified degradation products can be found in tabulated thermal degradation data contained in Appendix D

5.2 First-order rate constants analysis

It will be shown in the following section that the loss of PZ during thermal degradation is approximately first order in amine concentration at 175 °C (section 5.3.2). This observation is supported by the fact that most thermal degradation concentration profiles for PZ can be well characterized by an exponential regression. Provided the vast amount of thermal degradation data acquired in this project, an analysis was needed to investigate the PZ loss data in a simplified way in order to understand all of the data and draw meaningful conclusions that are applicable to real world situations. The method developed was the calculation and comparison of first order rate constants, k_1, for thermal degradation experiments. The calculation of k_1 assumes a first order loss in PZ as shown by the following rate equation where C_{PZ} is the concentration of PZ in any appropriate units (Equation 5.1).

$$-\frac{dC_{PZ}}{dt} = k_1 C_{PZ} \tag{5.1}$$

Equation 5.1 can be translated directly into an equation relating the fraction of PZ at any point in time, F_{PZ}, because the initial concentration will always be used as the denominator of the ratio (Equation 5.2).

$$-\frac{dF_{PZ}}{dt} = k_1 F_{PZ} \tag{5.2}$$

This assumed form of a rate expression for PZ is a differential equation that can be solved for F_{PZ} at any time point (Equation 5.3 and Equation 5.4).

$$\ln \frac{F_{PZ}}{F_{PZ,0}} = -k_1 \cdot t \tag{5.3}$$

$$F_{PZ} = F_{PZ,0} \cdot \exp(-k_1 \cdot t) \tag{5.4}$$

Each set of thermal degradation data was regressed with an exponential trendline that matched this form of the rate equation. As an example of this analysis, the PZ loss data for the degradation of 8 m PZ with 0.3 mole CO_2 per mole alkalinity at 175 °C is shown in Figure 5.1. These data are collated from multiple experiments performed with the same conditions and an exponential regression has been fit for the entire set. The regression fits the data well as evidenced by the high coefficient of determination (r^2). Based on the form of Equation 5.4, the k_1 for this set of condition is 7.97×10^{-2} wk^{-1}, or 1.32×10^{-7} s^{-1}. Raw thermal degradation data, as shown in the figure, are reported in weeks in this dissertation (Appendix D), but the k_1 will be calculated in inverse seconds (s^{-1}) for consistency with standard reaction rate reporting and previous work (Cullinane and Rochelle, 2006; Freeman et al., 2010a; Rochelle et al., 2001). The k_1 was calculated in s^{-1} for all experimental data sets obtained in this dissertation.

The rate constant, k_1, was predicted to have an Arrhenius temperature dependence with the form shown in Equation 5.5 where k_1 and the pre-exponential factor, A, have units of inverse time, the activation energy, E_A, is in kJ per mole, R is the universal gas constant, and the temperature, T, is in Kelvin. A linearized form of Equation 5.5 is shown in Equation 5.6.

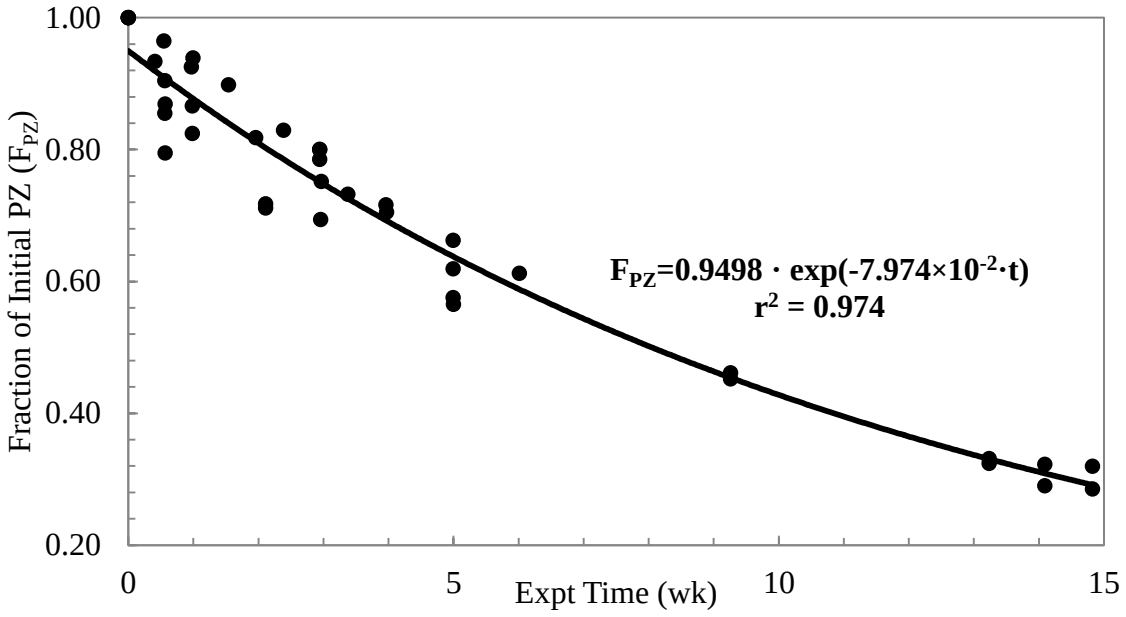

Figure 5.1: An example of the determination of k_1 value from thermal degradation of 8 m PZ with 0.3 mole CO_2 per mole alkalinity at 175 °C

$$k_1 = A \cdot \exp\left(\frac{E_A}{R} \cdot \frac{1}{T}\right) \tag{5.5}$$

$$\mathrm{Ln}(k_1) = \mathrm{Ln}(A) - \frac{E_A}{R} \cdot \frac{1}{T} \tag{5.6}$$

The Arrhenius behavior of k_1 values for PZ degradation has been confirmed. The structure of Equation 5.6 suggests a linear relationship between Ln k_1 and T^{-1}. A plot comparing the calculated k_1 value on a logarithm scale and T^{-1} for experiments with 8 m PZ with 0.3 mole CO_2 per mole alkalinity is shown in Figure 5.2. The data are plotted using Kelvin temperature units, but Celsius units are shown for clarity. The linear behavior of the data confirm that thermal degradation of concentrated PZ can be estimated accurately with a first order rate constant with Arrhenius temperature behavior. The activation energy for thermal degradation can be calculated from the slope of the linear fit shown in Figure 5.2. The activation energy for this set of data is 183.5 kJ per mole. Arrhenius temperature behavior of k_1 is observed in nearly every set of PZ

conditions and in the data from amines. Activation energies vary slightly, but the overall trends seen in the k_1 value are maintained.

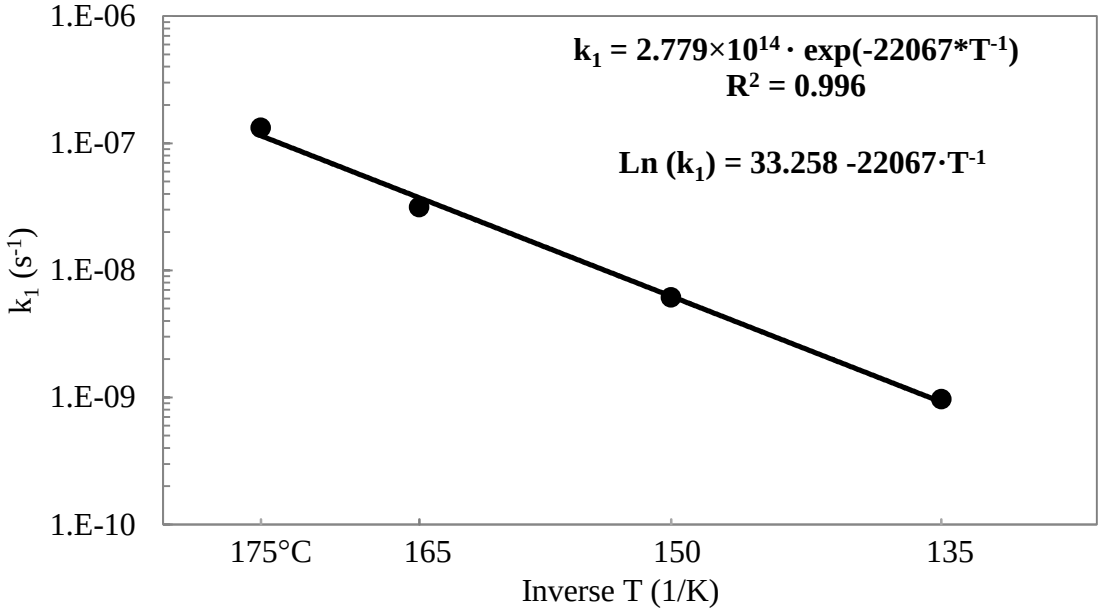

Figure 5.2: Demonstration of the Arrhenius behavior of the first order rate constant (k_1) for thermal degradation of 8 m PZ with 0.3 mole CO_2 per mole alkalinity

In chapter 7, PZ is compared with other CO_2 capture amines using this same analysis. For other amines, k_1 values are calculated using the same methodology, unless otherwise noted. For most amines discussed, the first order approximation fits well either because the data suggests the amine behavior is first order in amine loss, or because data is limited to only a few points. This overall approach allows an assessment of the tendency of an amine to degrade thermally without having to account for the length of experiment, which can vary from 4 to 72 weeks, and complex differences in degradation mechanism. This analysis is intended to be a tool to quickly assess the thermal stability of an amine in relation to other systems tested under similar conditions.

The k_1 calculation can be an oversimplification of systems where more complicated kinetics can take over beyond the initial periods of degradation. For example, this is true in the data shown in section 5.3.2.1 for rich loaded 20 m PZ. If a set of thermal degradation data demonstrated noticeably different behavior than first order in amine loss, an initial first order rate was determined and the constant was considered an apparent first order rate constant. Usually, this meant taking the first order rate using the first 10-50% of the data, based on the time scale.

For the concentrated PZ data discussed in this chapter, a first order approximation across the entire data set was used, except for aforementioned 20 m PZ experiment. The calculated k_1 values are indicated in each graph that shows PZ loss as a function of time along with exponential regressions. In this way, the derivation of k_1 for each experiment discussed is demonstrated.

5.2.1 Evaluation of error in regressed slopes and k_1 values

To assess the overall experimental error expected from the thermal degradation procedure, data from experiments with the same conditions were analyzed for repeatability and parallelism of regressed slopes used to determine k_1 values. The basis for the analysis was a student's t-test to determine if the regressed slope was the same with statistical significance for repeated experiments. For each experiment of interest, a data set was comprised of the time values (X variable) and natural log of the fraction of initial PZ ($Ln(F_{PZ})$, Y variable). Since first order behavior has been assumed for this analysis, a plot of $Ln(F_{PZ})$ against experiment time should be well fit with a linear regression. A linear regression of this nature was performed with all experimental data and k_1 values were calculated from the slope of the regression.

Three conditions during this project were repeated with multiple experiments. At 150 °C, TE9 and TE14 were both performed with 8 m PZ with 0.3 mole CO_2 per mole alkalinity. At 175 °C, TE4, TE12, and TE18 were all performed with 8 m PZ with 0.3 mole CO_2 per mole alkalinity. Finally, TE13 and TE19 were both performed with 8 m PZ with 0.4 mole CO_2 per mole alkalinity at 175 °C. The details of this statistical analysis will be shown for data from TE4, TE12, and TE18. The results will then be shown for the other two comparisons (TE9 and TE14; TE13 and TE19). The analysis performed in this section is based on the methods for comparing two straight lines using separate regression fits that has been described previously (Kleinbaum et al., 1988).

Each data set was treated separately and an independent, linear regression was made. The regressions were in the following form that relates the independent variable (X; experiment time) to the slope of the regression (m_i), the intercept (b_i), and the dependent variable (Y; $Ln(F_{PZ})$) (Equation 5.7).

$$Y = m_i X + b_i \tag{5.7}$$

A test was then performed to determine parallelism between the regressed slopes from two data sets of interest. This approach determined if two lines have the same slope with a given confidence. This translates to an estimation of the error in the calculation of k_1, since this value is derived from the regressed slope of each data set. The null hypothesis, H_0, therefore is that the slopes of two sets of data (m_1 and m_2) will be the same (Equation 5.8).

$$H_0 : m_1 = m_2 \tag{5.8}$$

A test statistic, T, for evaluating parallelism can then be defined as follows (Equation 5.9). This parameter can be used to determine if the null hypothesis is true or

false by comparing it will a t-value determined from the degrees of freedom (DOF) and desired confidence interval. Values of t are obtained from tables available in statistics literature (Kleinbaum et al, 1988). If the null hypothesis is false, the absolute value of T will be greater than the t-value based on a student's distribution (Kleinbaum et al., 1988).

$$T = \frac{m_1 - m_2}{S_{m_1 - m_2}} \tag{5.9}$$

In Equation 5.9, each slope (m_1 or m_2) is the least-squares estimate of the slope of the data while $S_{m_1 - m_2}$ is an estimate of the standard deviation of the estimated differences between the two slopes. This variable can be defined as follows (Equation 5.10).

$$S_{m_1 - m_2} = \sqrt{S^2_{P,Y/X}\left[\frac{1}{(n_1 - 1)S^2_{X_1}} + \frac{1}{(n_2 - 1)S^2_{X_2}}\right]} \tag{5.10}$$

In this equation, the variance in the X variable for both sets of data is used ($S^2_{X_1}$ and $S^2_{X_2}$) as well as $S^2_{P,Y/X}$, a pooled (P) estimate of the variance based on the mean-square error of each of the two regressions (S^2_{Y/X_1} and S^2_{Y/X_2}) and the number of data points in each set (n_1 and n_2). The pooled estimate of variance and the mean-squared error of each regression can be calculated using the follow formulas (Equation 5.11 and 5.12) (Kleinbaum et al., 1988).

$$S^2_{P,Y/X} = \frac{(n_1 - 2)\cdot S^2_{Y/X_1} + (n_2 - 2)\cdot S^2_{Y/X_2}}{n_1 + n_2 - 4} \tag{5.11}$$

$$S^2_{Y/X_i} = \frac{1}{n - 2}\sum_{i=1}^{n}\left(Y_i - Y_{i,regression}\right)^2 \tag{5.12}$$

The assumptions of this analysis are that the test statistic will be distributed with a student's t regular probability curve with a number of degrees of freedom equal to (n_1 + n_2 – 4) when the null hypothesis defined in Equation 5.8 is true (Kleinbaum et al., 1988).. A t-value will be used in this analysis that depends on the DOF (n_1 + n_2 - 4) and has 95% confidence, or a significance level of 0.05, indicated as $t_{n1+n2-4,\ 1-\alpha/2}$. The two subscripts after t indicate the DOF and confidence level to use in each particular case.

An example can be shown where the data from TE4, TE12, and TE18 are analyzed in detail. The three data sets of interest are shown in Figure 5.3 along with least-squares linear regression and the coefficient of variance (r^2) for each regression. The slope, intercept, and other pertinent data from the linear regressions are shown in Table 5.2 for reference. The sample variance in X and the residual mean-square error was been calculated for each regression.

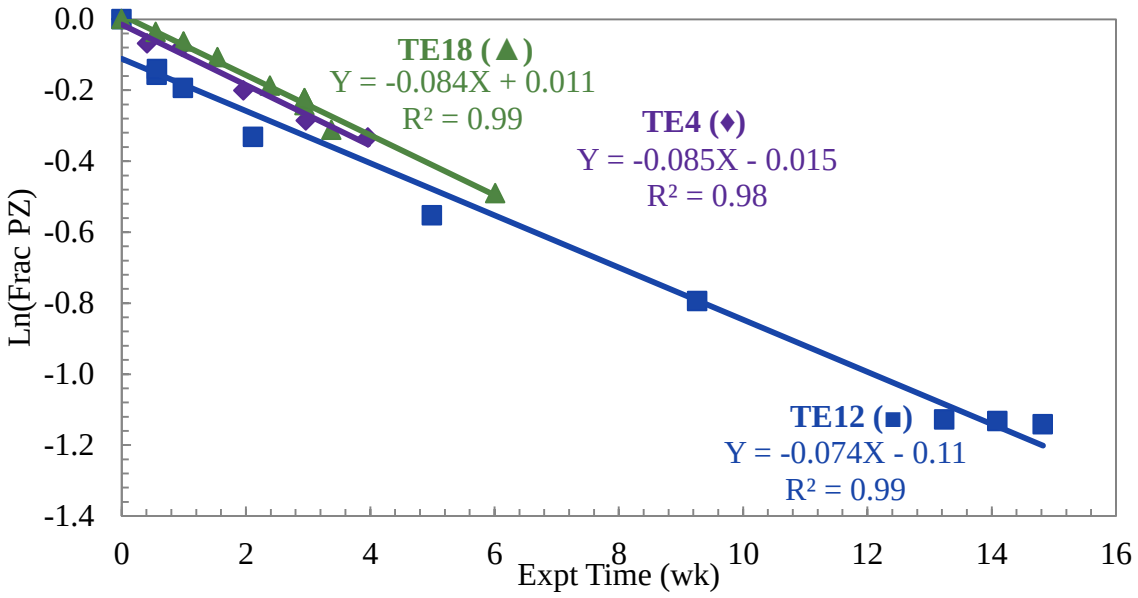

Figure 5.3: Linear regression of TE4, TE12, and TE18 for statistical analysis

Table 5.2: Details of linear regressions

Data set	Data points	Slope (wk^{-1})	Intercept	Mean of X	Sample variance ($S^2_{X_1}$)	Residual mean-square error (S^2_{Y/X_i})
TE4	6	-0.085	-0.015	1.7	2.38	0.00051
TE12	10	-0.074	-0.111	6.1	38.07	0.00350
TE18	10	-0.084	0.011	2.4	2.97	0.00091

Using the linear regression and the analysis described above, the T value for a comparison of two data sets can be calculated from Equation 5.9. This procedure has been done for the three independent pairs of TE4, TE12, and TE18 and the results are shown in Table 5.3. In all three cases, the absolute value of T is not larger than the t-value, so H_0 is not rejected. This implies that the null hypothesis is accepted since there is not sufficient evidence to reject it. This implies that with the chosen confidence interval (95%), the slopes of the three data sets are the same and indicate the overall error of the thermal degradation experiment is likely less than 5% for a standard experiment.

Table 5.3: Results for statistical comparison of parallelism of PZ loss slope for TE4, TE12, and TE18 (8 m PZ, 0.3 mole CO_2 per mole alkalinity, 175 °C)

Data set 1	TE4	TE4	TE12
Data set 2	TE12	TE18	TE18
DOF	12	12	17
α	0.05	0.05	0.05
$t_{n1+n2-4,\ 1-\alpha/2}$	$t_{12,0.975}$	$t_{12,0.975}$	$t_{17,0.975}$
t value	2.179	2.179	2.110
$S^2_{P,Y/X}$	0.00251	0.000774	0.00221
$S_{m_1-m_2}$	0.0148	0.632	0.0094
T	-0.792	-0.00138	1.149
|T|	0.792	0.00138	1.149
H_0	True	True	True

The similarity of the slopes also indicates that the k_1 value derived from the data should not contain significant error when calculated from each experiment separately. To demonstrate this, the k_1 value was calculated from the regression shown in Figure 5.3 for

each of the three experiments (TE4, TE12, and TE18). These values are shown in Table 5.4 along with the average and standard deviation that results from the three separation regressions. Finally, the k_1 value that is a result of regressing all of the data together as one data set is shown in the final row of Table 5.4. The average k_1 value determined from separate experiments is 134 ±11 s^{-1}. The low standard deviation and agreement in the regression of all of the data agrees with the t-test analysis that showed all three sets had statistically similar slopes. It is expected that all of the thermal degradation experiments suffered similar levels of experimental error, even though repeated experiments could not be performed.

Table 5.4: Comparison of error between individual and average k_1 calculations (8 m PZ, 0.3 mole CO_2 per mole alkalinity, 175 °C)

Data set or expt.	$k_1 \times 10^9$ (s^{-1})
TE4	141
TE12	122
TE18	140
Average	134
Standard deviation	11
Regression of all data	130

The same data analysis to test for parallelism in the slope of PZ loss was performed for the two remaining sets of experiments performed under the same conditions. The results are shown in Table 5.5 and in the first case, a comparison of TE9 and TE14, the null hypothesis was found to be true indicating the slopes are statistically not different with a 95% confidence. For the second comparison, TE13 and TE19, however, the null hypothesis was found to be false and the slopes of the data were determined to be statistically different. Calculation of the k_1 value for each data set along with an average value is shown in Table 5.6. The k_1 value for TE9, TE14 and the value obtained when all of the data is regressed at the same time is within the expected

deviation when the values are calculated separately and averaged. For the k_1 value of TE13 and TE19, a large deviation between the values calculated individually and the regression for the overall group of data was observed. This was expected provided the results of the student t-test. For Table 5.1 and the analysis of k_1 values in section 7.4, the value obtained from regressing all of the data simultaneously was used for the two analyses of data at 175 °C. For the final set of data comparing TE13 and TE19, the k_1 value from TE19 was used due to the higher propensity for cylinder failures and other experimental concerns with the data from TE13.

Table 5.5: Results for statistical comparison of parallelism of PZ loss slope for TE9 and TE14 (8 m PZ, 0.3 mole CO_2 per mole alkalinity, 150 °C) and TE13 and TE19 (8 m PZ, 0.4 mole CO_2 per mole alkalinity, 175 °C)

Data set 1	TE9	TE13
Data set 2	TE14	TE19
DOF	25	18
α	0.05	0.05
$t_{n1+n2-4,\ 1-\alpha/2}$	$t_{25,0.975}$	$t_{18,0.975}$
t value	2.06	2.101
$S^2_{P,Y/X}$	0.000252	0.00219
$S_{m_1-m_2}$	0.000846	0.00933
T	0.610	2.921
|T|	0.610	2.921
H_0	True	False

Table 5.6: Comparison of error between individual and average k_1 calculations

8 m PZ, 0.3 mol/mol alk, 150 °C		8 m PZ, 0.4 mol/mol alk, 175 °C	
Data set or expt.	$k_1 \times 10^9$ (s^{-1})	Data set or expt.	$k_1 \times 10^9$ (s^{-1})
TE9	5.3	TE13	126
TE14	6.1	TE19	171
Average	5.7	Average	135
Standard deviation	0.6	Standard deviation	12
Regression of all data	6.2	Regression of all data	127

5.3 PZ DEGRADATION EFFECTS

The rate of PZ degradation was assessed in terms of three primary variables: temperature, PZ concentration, and CO_2 concentration or CO_2 loading. Each of these variables was investigated independently with a series of experiments that kept the other two variables constant. Isolating the effect of each variable separately was critical as all three are interconnected in terms of degradation rates. For all of the variables, multiple sets of experiments were performed at differing conditions.

5.3.1 Effect of temperature

The effect of temperature on PZ thermal degradation was examined by degrading solutions at constant PZ and CO_2 concentrations. A summary of the experiments performed to examine temperature is given in Table 5.7. In total, nine groups of experiments were performed under similar conditions that highlighted the effect of temperature. For simplicity and to avoid repetitive reporting of data, three of the groups shown in bold text in Table 5.7 will be discussed in detail while the remaining six will not be discussed. The raw data from all experiments are provided in Appendix D to allow the interested reader to reproduce any comparisons of interest that are not described in detail.

The high temperatures of all of the PZ experiments should be noted. The intention of the experiments was not to demonstrate degradation at stripper conditions currently used for less stable amines (i.e., MEA). The resistance of PZ to thermal degradation that was identified by Davis allows higher temperature stripping with expected energy savings (Davis, 2009). As noted above, the slow degradation rate of PZ also introduced time constraints so higher temperature experiments were performed, even if not representative of temperatures expected for PZ stripping in a CO_2 capture system. The activation energy, E_A, for thermal degradation, discussed in greater detail in section

7.4, was calculated from data sets that included three or more temperatures. The activation energies for PZ systems that were calculated are included in Table 5.7.

Table 5.7: Experiment series to investigate the effect of temperature

Solution Constants	Values Tested				E_A (kJ/mol)
4 m PZ, α=0.3	-	-	165 °C	175 °C	-
8 m PZ, α=0	-	**150 °C**	**165 °C**	**175 °C**	**258.1**
8 m PZ, α=0.1	-	-	165 °C	175 °C	-
8 m PZ, α=0.3	**135 °C**	**150 °C**	**165 °C**	**175 °C**	**183.5**
8 m PZ, α=0.4	**135 °C**	**150 °C**	**165 °C**	**175 °C**	**191.4**
10 m PZ, α=0.3	135 °C	150 °C	-	-	-
10 m PZ, α=0.4	135 °C	150 °C	-	-	-
12 m PZ, α=0.3	-	-	165 °C	175 °C	-
20 m PZ, α=0.3	-	150 °C	-	175 °C	-

Previous work on the thermal degradation of numerous amines found that temperature strongly affects the degradation rate, as expected. In the case of MEA, an increase of 15 °C quadruples the loss of MEA (Davis, 2009). Arrhenius relationships between the rate constant of amine and degradation temperature were also observed for MEA, 3-amino-1-propanol, 4-amino-1-butanol, AMP, 2-amino-1-propanol, 1-amino-2-propanol, and blends of MEA with PZ, Mor, DGA, or AMP (Davis, 2009). Other degradation studies have not varied temperature so the effect on amine loss was not observed (Lepaumier et al., 2010; Lepaumier et al., 2009a; Reza and Trejo, 2006).

5.3.1.1 Effect of temperature for 8 m PZ with a lean loading (0.3 mol/mol alkalinity)

Solutions of 8 m PZ with 0.3 mole CO_2 per mole alkalinity were degraded at temperatures from 135 to 175 °C. The loss of PZ in each experiment as a fraction of the initial PZ is compared in Figure 5.4. The generation of formate, total formate, EDA, FPZ, and AEP are compared for the same experiments in Figure 5.5, Figure 5.6, Figure

5.7, Figure 5.8, and Figure 5.9, respectively. FPZ and AEP were not quantified at 150 °C.

As anticipated, thermal degradation is a strong function of temperature with the high temperature experiments at 165 and 175 °C producing significant losses of PZ. The highest temperature produced a loss of 68% of the initial PZ after 15 weeks. A decrease of 10 °C in the experimental temperature (165 °C) produced a loss of only 33% of the initial PZ, roughly half the rate. A further decrease of 15 °C in the experimental temperature (150 °C) lowers the loss to only 11% of the initial PZ. This is a 33% decrease in the loss rate of PZ for a change of 15 °C. This is a weaker temperature effect than observed for MEA where an increase of 15 °C quadrupled the loss of MEA (Davis, 2009).

The generation of degradation products in this comparison provides an example of what is typically seen with PZ thermal degradation. The generation of formate and total formate, or formyl amides, increases with temperature or PZ degradation rate. Ethylenediamine (EDA), on the other hand, seems to reach a maximum in the two high temperature experiments where even at higher degradation rates, the maximum EDA concentration does not exceed 50 to 65 mmole EDA per kg. This was observed throughout this project and is likely due to reaction of EDA into other products such as 2-imidazolidinone (2-Imid). In the low temperature experiments, the degradation rate is slower and the production of EDA has not reached its peak where further reactions of EDA limit its liquid phase concentration. FPZ and AEP are generated quickly at high temperatures, as is expected with fast thermal degradation. It is not clear why FPZ reaches a maximum value in the 175 °C. AEP was not produced at a significant rate at 135 °C.

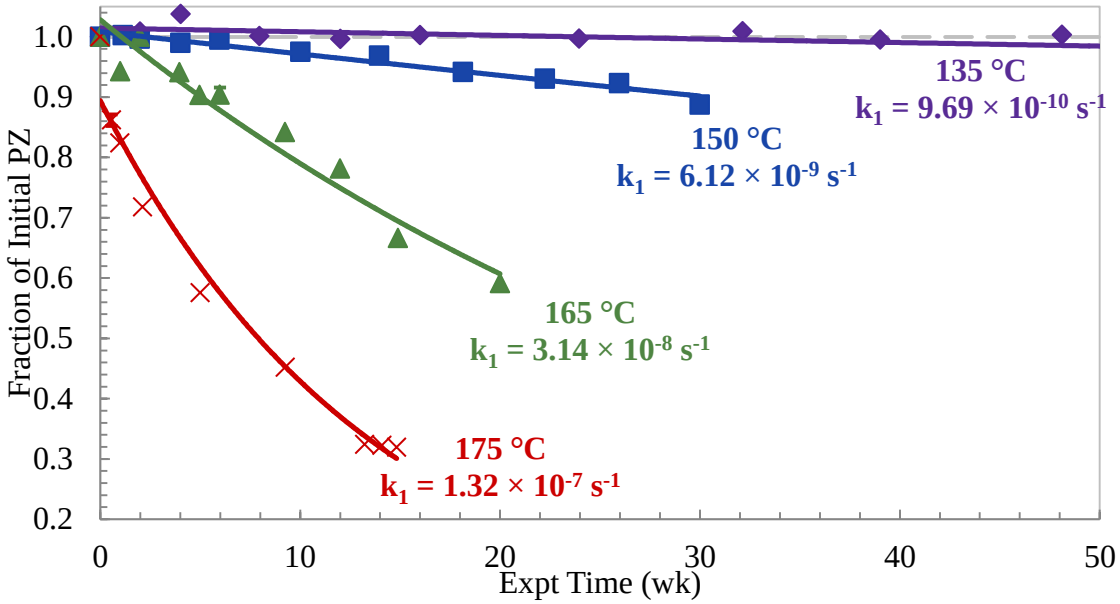

Figure 5.4: Comparison of PZ loss for 8 m PZ (α=0.3) degraded at 135 to 175 °C ×

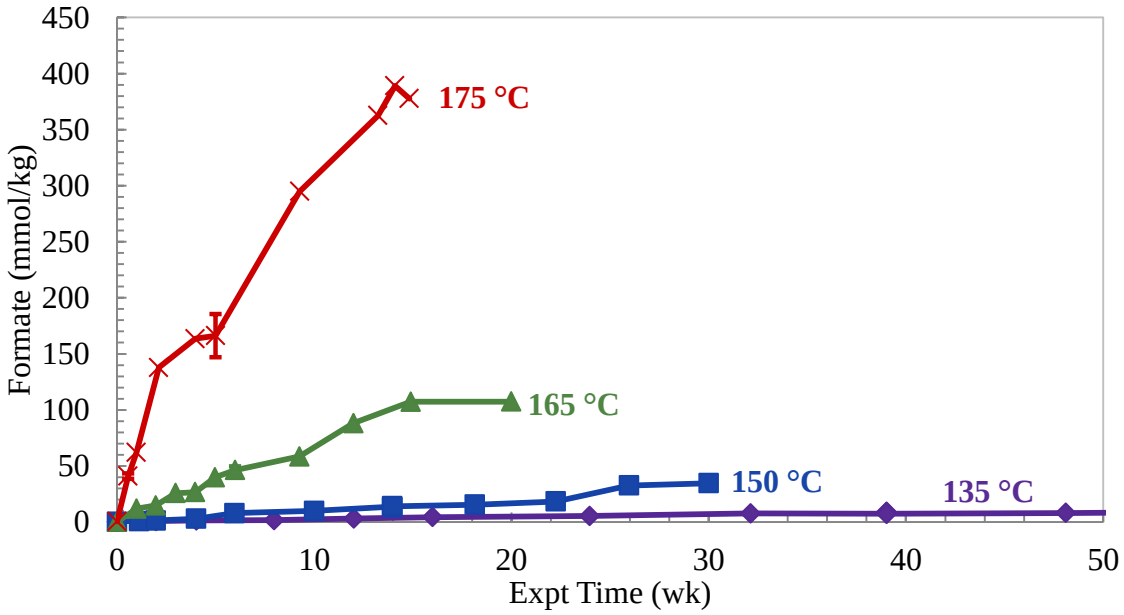

Figure 5.5: Comparison of formate generation for 8 m PZ (α=0.3) degraded at 135 to 175 °C

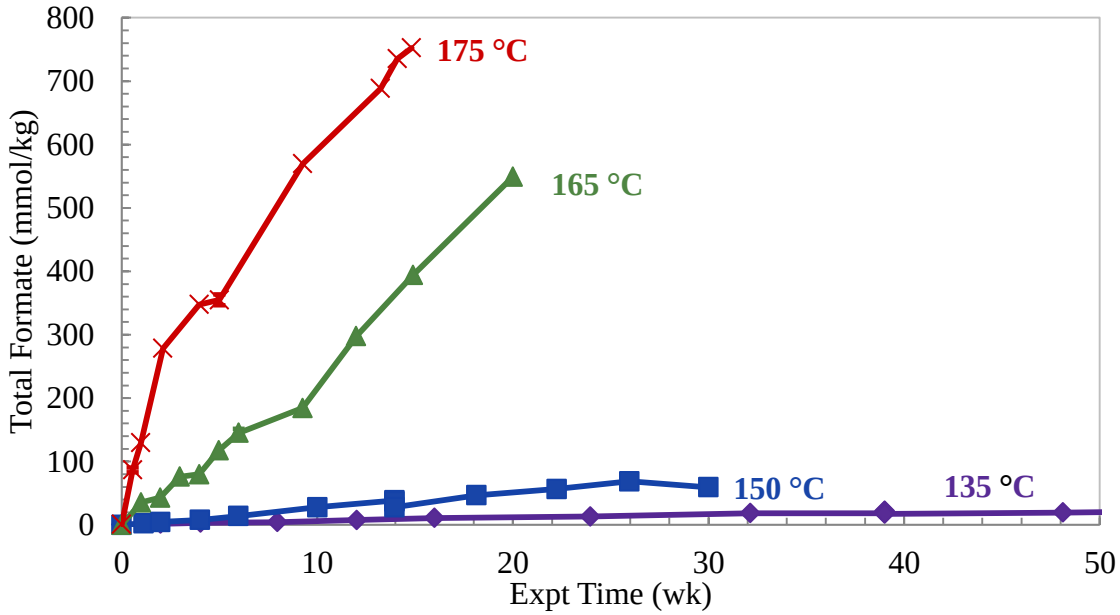

Figure 5.6: Comparison of total formate generation for 8 m PZ (α=0.3) degraded at 135 to 175 °C

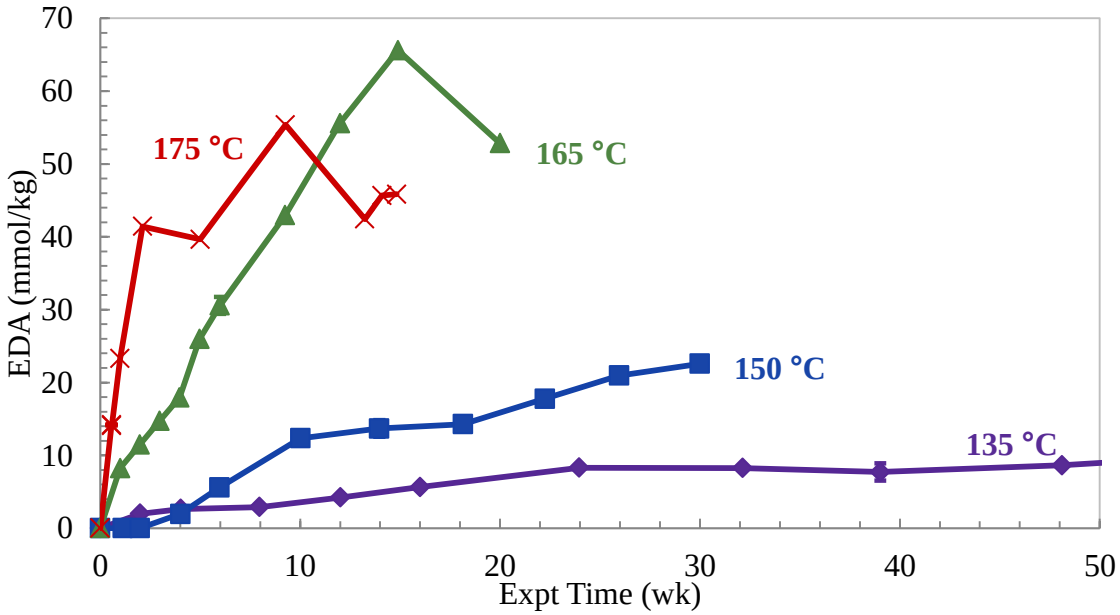

Figure 5.7: Comparison of EDA generation for 8 m PZ (α=0.3) degraded at 135 to 175 °C

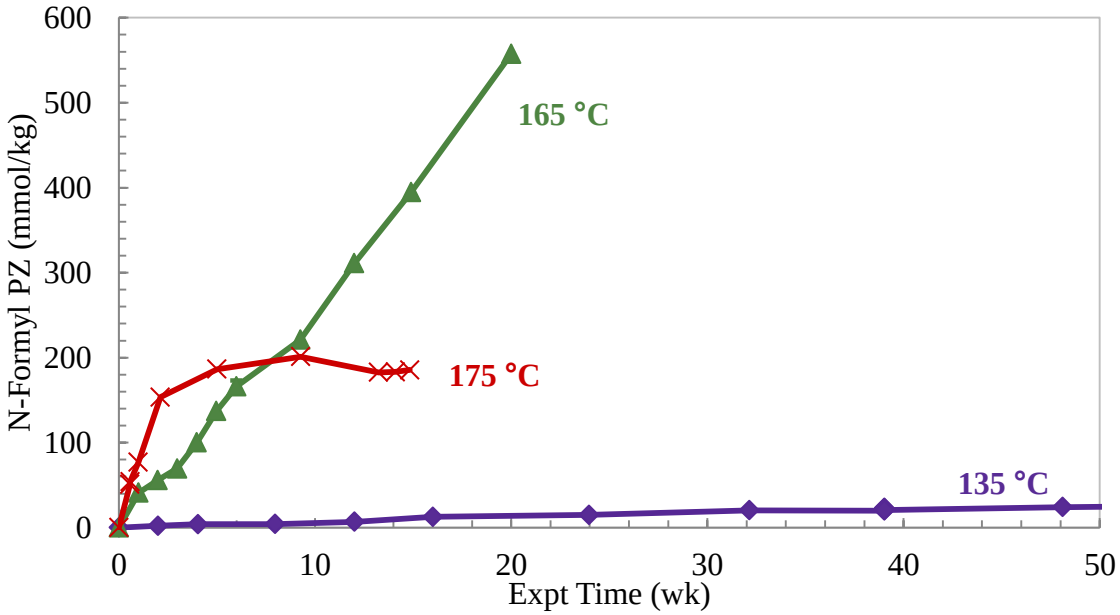

Figure 5.8: Comparison of FPZ generation for 8 m PZ (α=0.3) degraded at 135 to 175 °C

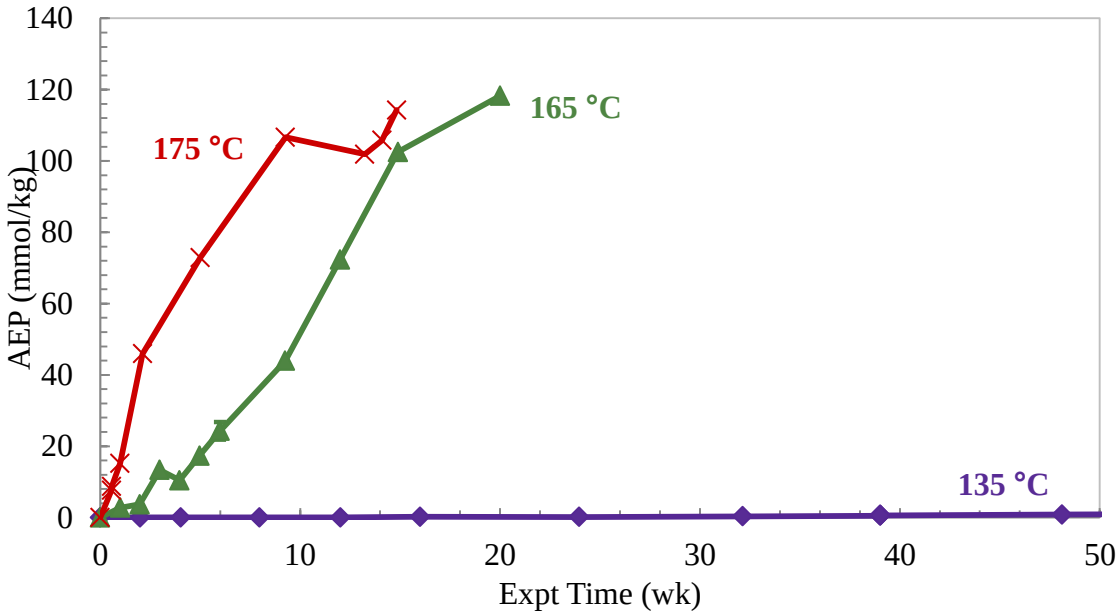

Figure 5.9: Comparison of AEP generation for 8 m PZ (α=0.3) degraded at 135 to 175 °C

5.3.1.2 Effect of temperature for 8 m PZ with a rich loading (0.4 mol/mol alkalinity)

A solution of 8 m PZ with 0.4 mole CO_2 per mole alkalinity was degraded from 135 to 175 °C, the anticipated maximum range of temperatures for the stripping section of a concentrated PZ CO_2 capture unit. Previous experiments for MEA showed that thermal degradation rates increased with increased CO_2 loading, amplifying the importance of understanding degradation on the rich portion of the system (Davis, 2009). The loss of PZ for rich loaded 8 m PZ degraded from 135 to 175 °C is compared in Figure 5.10. The generation of formate, total formate, EDA, FPZ, and AEP are compared for the same experiments in Figure 5.11, Figure 5.12, Figure 5.13, Figure 5.14, and Figure 5.15, respectively.

As with the lean loaded solutions above, temperature strongly affected PZ loss in rich loaded solutions. The highest temperature, 175 °C, produced a loss of 70% of the initial PZ after 15 weeks of degradation. A decrease in 10 °C in the experimental temperature decreased the loss by approximately one-half as only 37% of the initial PZ was lost at 165 °C after 15 weeks. A further decrease of 15 °C showed a marked decrease of 5.3 times as only 7% of the initial PZ was lost at 150 °C. This enhancement is significantly higher than that seen in MEA solutions, demonstrating that the temperature effect in PZ is highly dependent on CO_2 loading. The generation of formate, total formate, EDA, and AEP behaved similarly to the lean loaded experiments. The maximum achieved in EDA concentration in the high temperature experiments is pronounced and indicate that EDA in the liquid phase is an intermediate product of PZ thermal degradation. For FPZ, the generation rate was nearly the same for 165 and 175 °C, indicating the mechanism may not be accelerated between these temperatures with rich loading. As with the lean loaded experiments, a maximum in FPZ concentration was observed at 175 °C, but not at 165 °C.

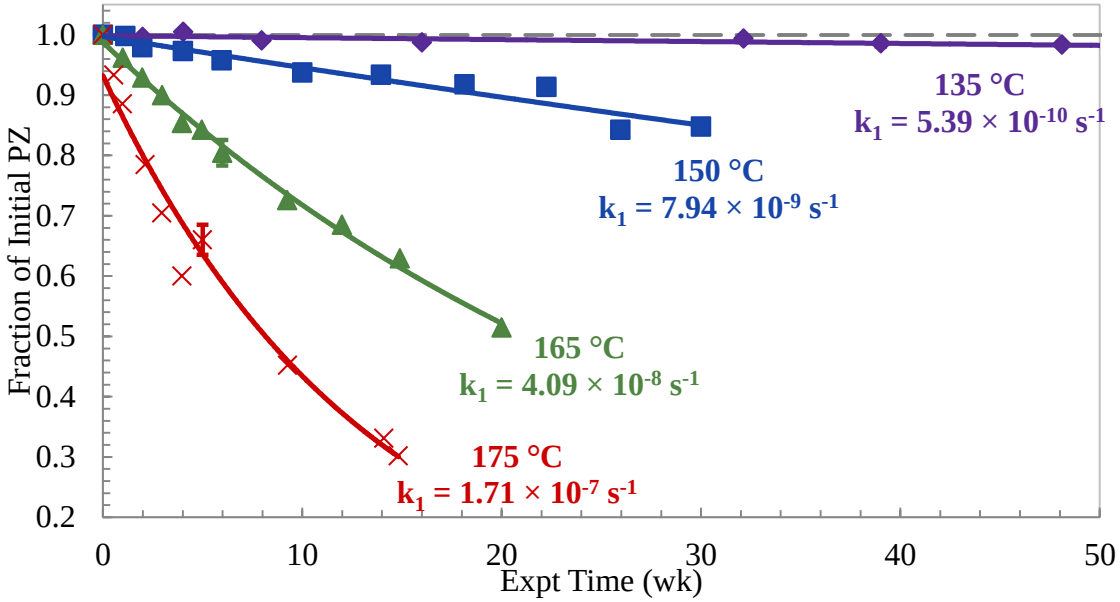

Figure 5.10: Comparison of PZ loss for 8 m PZ (α=0.4) degraded at 135 to 175 °C

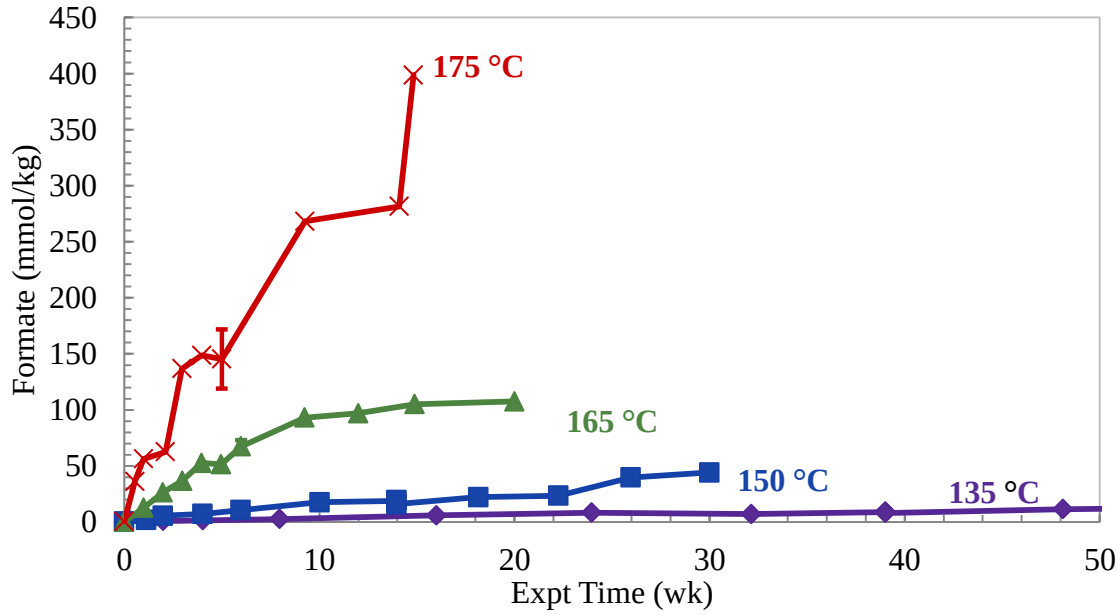

Figure 5.11: Comparison of formate generation for 8 m PZ (α=0.4) degraded at 135 to 175 °C

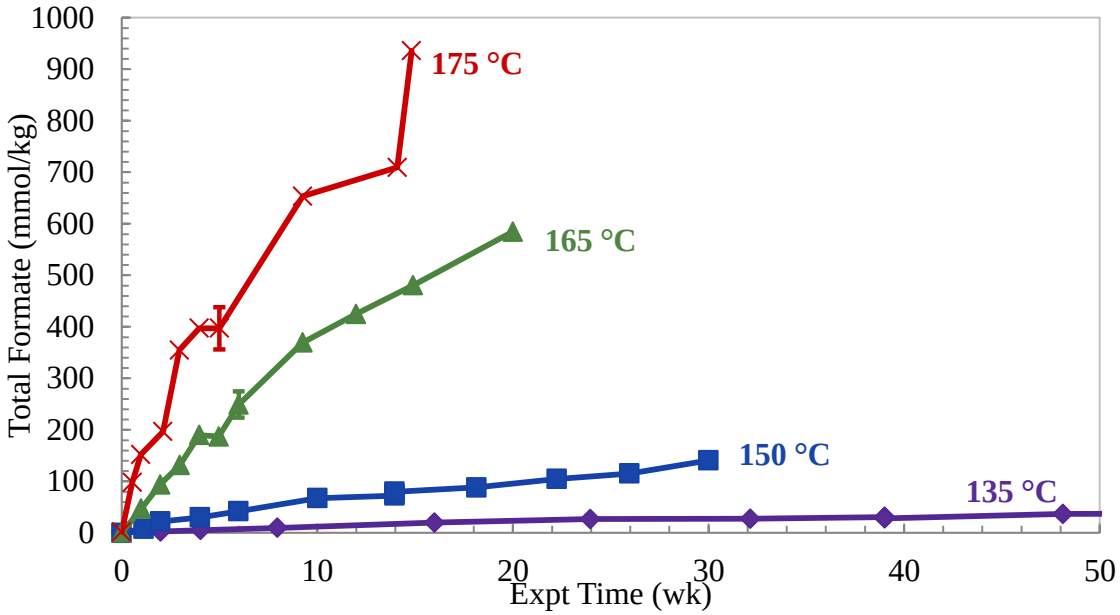

Figure 5.12: Comparison of total formate generation for 8 m PZ (α=0.4) degraded at 135 to 175 °C

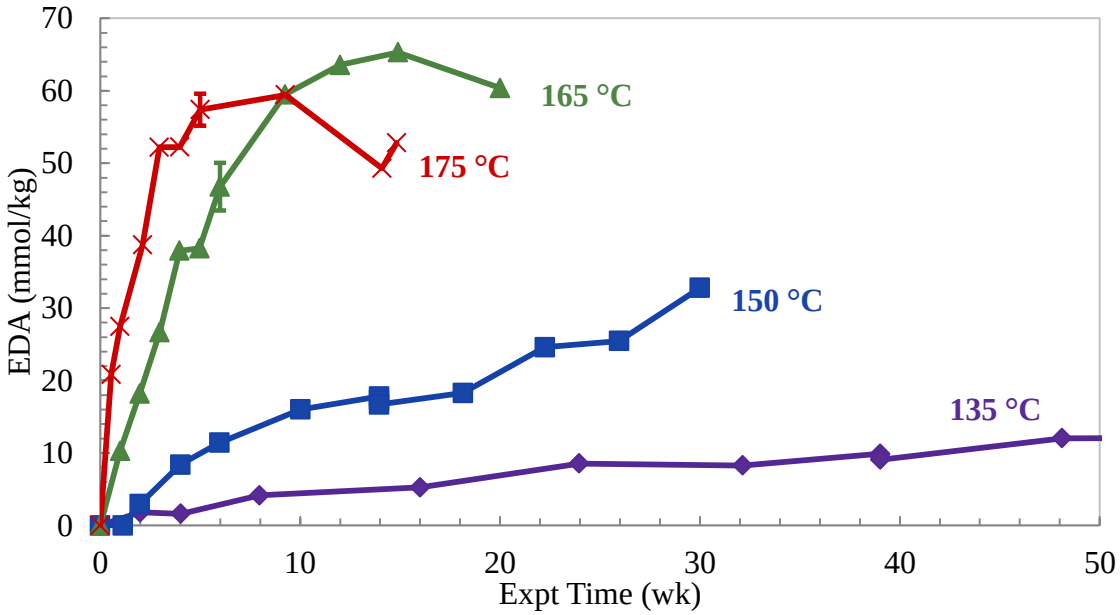

Figure 5.13: Comparison of EDA generation for 8 m PZ (α=0.4) degraded at 135 to 175 °C

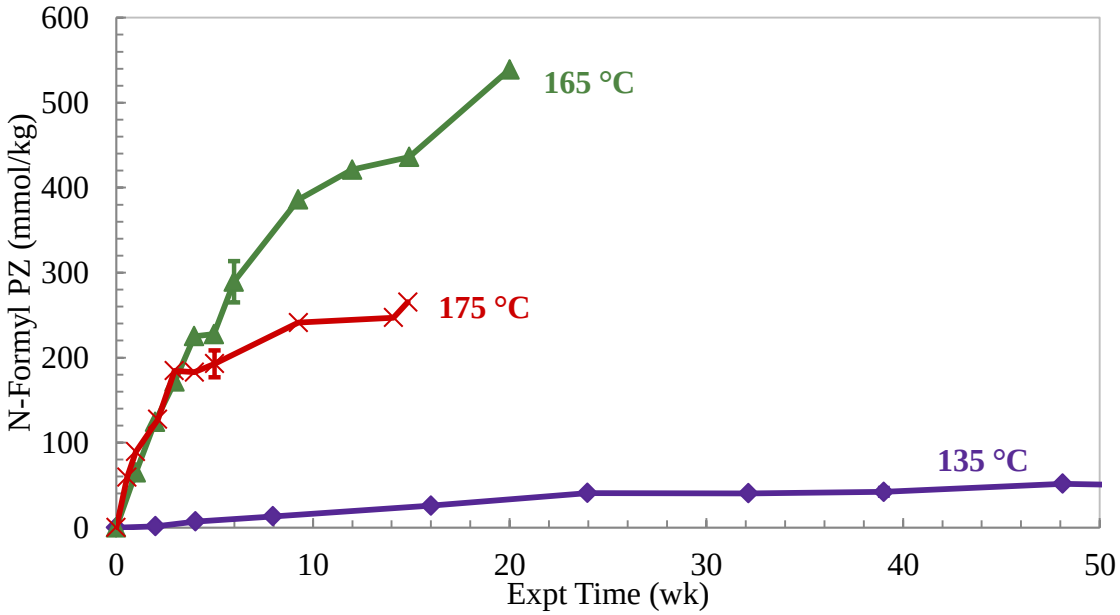

Figure 5.14: Comparison of FPZ generation for 8 m PZ (α=0.4) degraded at 135 to 175 °C

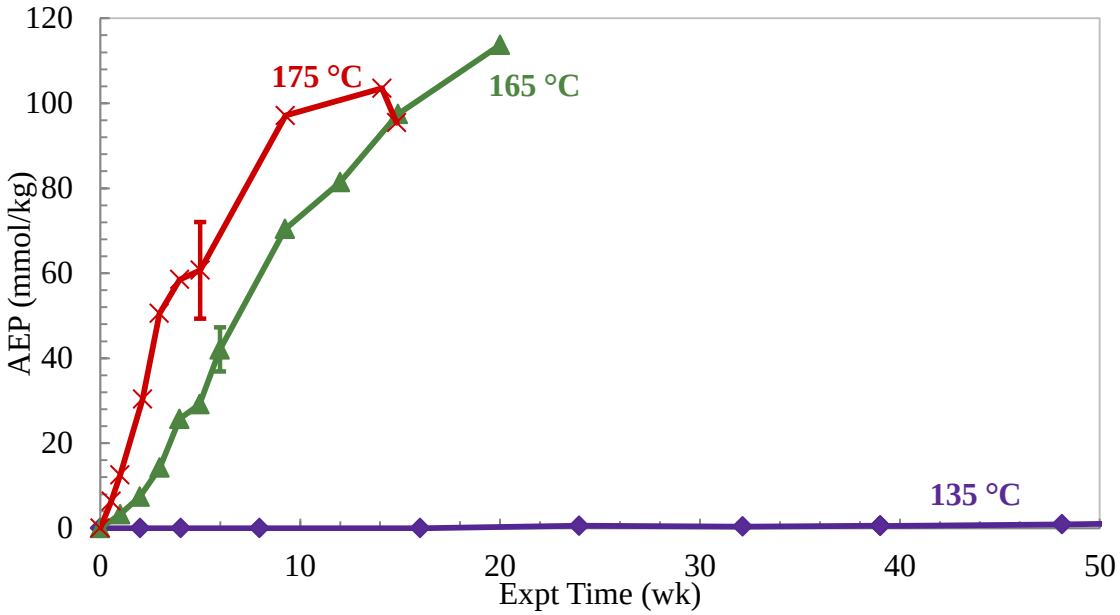

Figure 5.15: Comparison of AEP generation for 8 m PZ (α=0.4) degraded at 135 to 175 °C

5.3.1.3 Effect of temperature for unloaded 8 m PZ

Finally, unloaded 8 m PZ was examined for the effect of temperature on low rates of thermal degradation. Since very little degradation is expected for an unloaded solution, this comparison highlights the minimal effect of temperature in this case. Even though temperature is a strong catalyst, very little degradation occurs in the absence of CO_2. Therefore, it is interesting to observe that the collaborative catalytic effect of temperature and CO_2 causes the high levels of degradation seen in loaded solutions. The PZ loss for unloaded 8 m PZ is compared for degradation occurring at 150 to 175 °C in Figure 5.16. The generation of formate, total formate, and EDA in the same experiments is compared in Figure 5.17, Figure 5.18, and Figure 5.19, respectively.

The PZ loss in this case is difficult to determine with accuracy, as demonstrated by the scatter seen in Figure 5.16. Only a slight increase of PZ loss was observed with an increase in temperature because of the low overall degradation rates of unloaded PZ. The generation of degradation products behaves similarly to the loaded experiments, although at a lower magnitude in concentration. There are appreciable trends in the formate and total formate data, signifying that the detection and quantification of degradation products is more appropriate than interpreting cation IC data in low degradation environments. The generation of EDA also shows similar behavior as the loaded experiments as the two higher temperature experiments have maximums in concentration between 35 and 40 mmole EDA per kg.

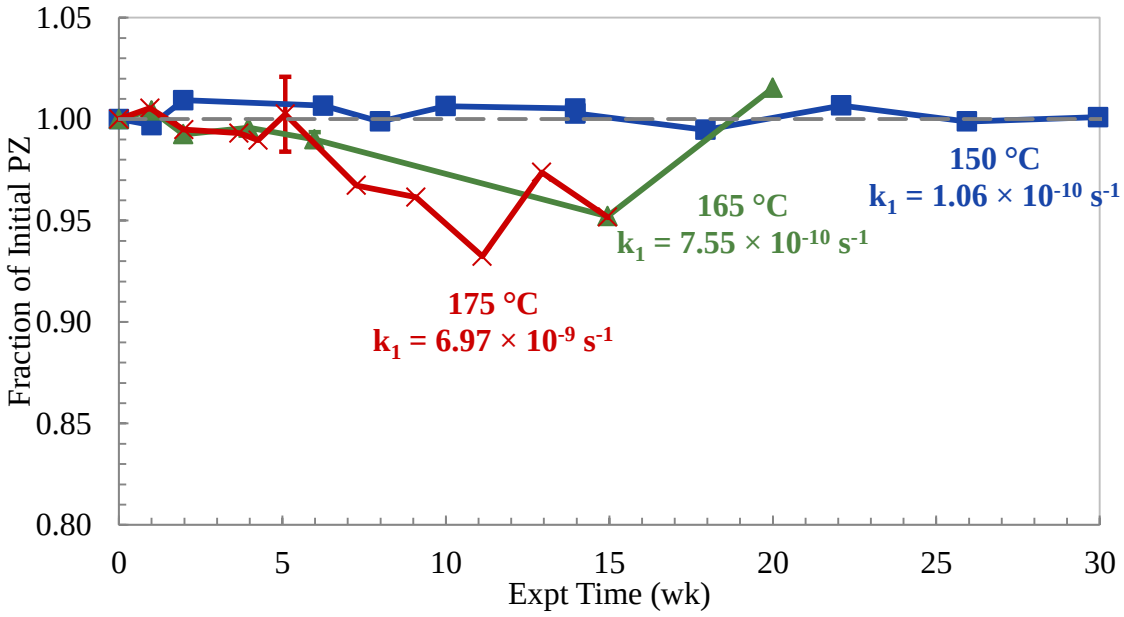

Figure 5.16: Comparison of PZ loss for 8 m PZ (α=0) degraded at 150 to 175 °C

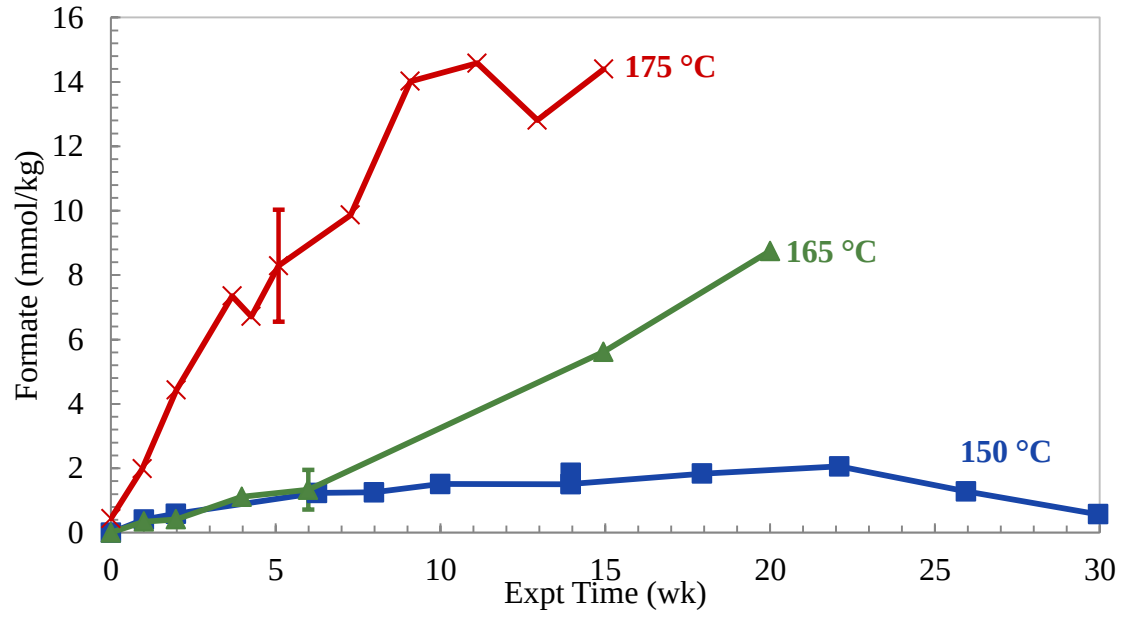

Figure 5.17: Comparison of formate generation for 8 m PZ (α=0) degraded at 150 to 175 °C

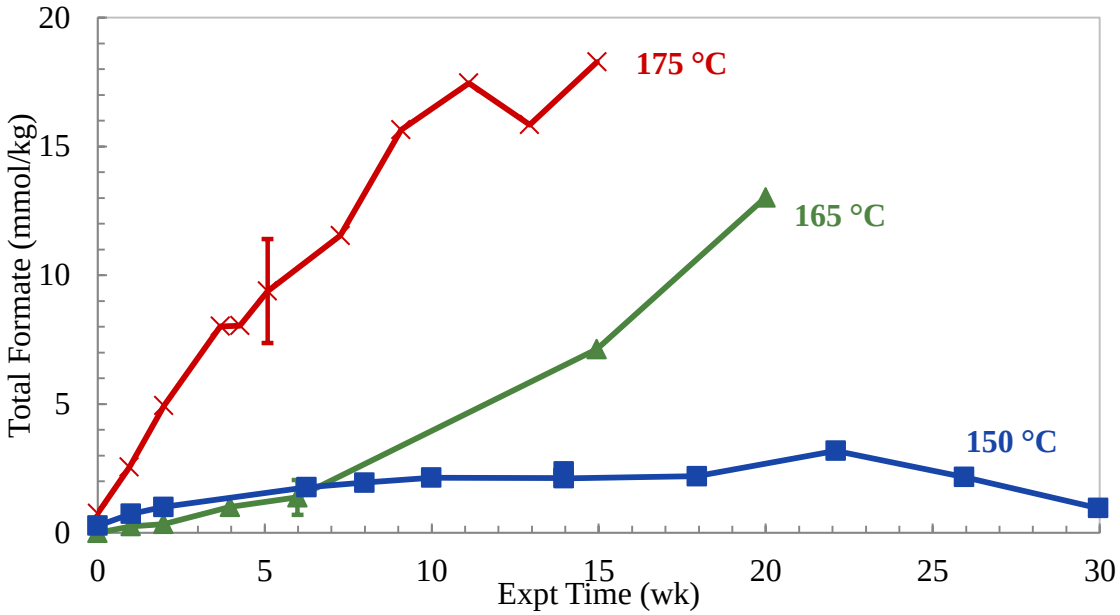

Figure 5.18: Comparison of total formate generation for 8 m PZ (α=0) degraded at 150 and 175 °C

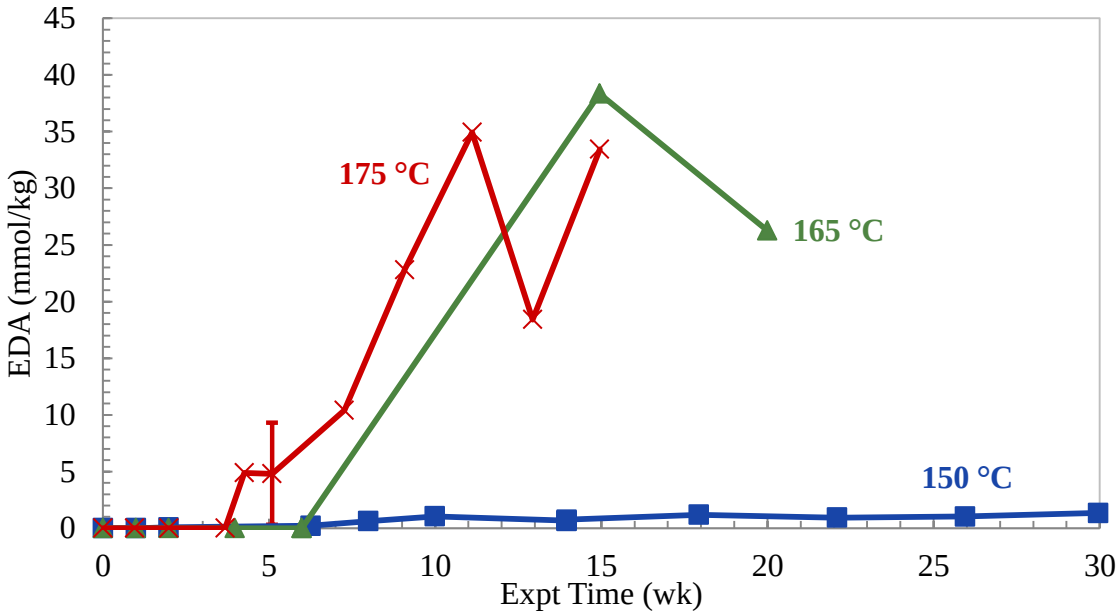

Figure 5.19: Comparison of EDA generation for 8 m PZ (α=0) degraded at 150 and 175 °C

5.3.2 Effect of PZ concentration

The effect of PZ concentration on PZ thermal degradation was examined by degrading solutions at constant temperature and CO_2 loading. A summary of the experiments performed to examine this variable is given in Table 5.8. In total, four series of experiments were performed that highlighted the effect of PZ concentration. As with temperature comparisons in the previous section, only two will be discussed in detail to eliminate unnecessary repetition of concepts (bolded text in table). All data is available in Appendix D to reproduce any desired comparison.

Table 5.8: Experiment series to investigate the effect of PZ concentration

Solution Constants	Values Tested					
150 °C, α=0.3	-	8 m PZ	10 m PZ	15 m PZ	-	20 m PZ
150 °C, α=0.4	-	8 m PZ	10 m PZ	-	-	-
165 °C, α=0.3	**4 m PZ**	**8 m PZ**	**-**	**-**	**12 m PZ**	**-**
175 °C, α=0.3	**4 m PZ**	**8 m PZ**	**-**	**-**	**12 m PZ**	**20 m PZ**

The effect of amine concentration on thermal degradation has been quantified for MEA (Davis, 2009) over a range of 3.5 to 11 m. Davis found that the loss rate was only slightly more than first order in MEA concentration, with only slight differences observed between 3.5, 7, and 11 m MEA. Other studies of the thermal degradation of amines did not vary amine concentration so the expectation for PZ was difficult to predict without experimentation (Lepaumier et al., 2010; Lepaumier et al., 2009a; Lepaumier et al., 2009b; Reza and Trejo, 2006).

5.3.2.1 Effect of PZ concentration for a lean loading (0.3 mol/mol alkalinity) at 175 °C

The effect of PZ concentration was first assessed in lean loaded solutions as 4 to 20 m PZ with 0.3 mole CO_2 per mole alkalinity was degraded at temperatures from 175 °C. The loss of PZ in each experiment as a fraction of the initial PZ is compared in

Figure 5.20. The generation of formate, total formate, and EDA are compared for the same experiments in Figure 5.21, Figure 5.22, and Figure 5.23, respectively.

There is not a significant difference in the PZ loss for 4, 8, and 12 m PZ when plotted as a fraction of the initial PZ concentration. This indicates that thermal degradation of PZ over this temperature range behaves as nearly first order in PZ concentration. There is a slight increase of the loss rate between the 8 and 12 m experiments, but as an approximation, the system is close to first order. The data for the 20 m PZ experiment, on the other hand, does not share the behavior of the lower concentration systems. The initial rate is faster in this experiment, indicating that loss may be of higher reaction order in PZ concentration than the 4 to 12 m data. This high concentration solution is 63% PZ (CO_2-free) or 53% PZ with a loading of 0.3 mole CO_2 per mole alkalinity. With this concentration of PZ, the concentration of water is becoming less significant and the activity of water may be vastly different in comparison with the 4 to 12 m PZ solutions. The speciation has also not been tested at this high level and may differ slightly due to the high PZ concentration.

The generation of all three degradation products exhibits unique behavior. For formate, less is produced in the 12 and 20 m PZ experiments than the 8 m case. This is not expected as degradation roughly increases, especially between 12 and 20 m PZ. Total formate, on the other hand, increases with increasing PZ concentration. Although 4, 8, and 12, have similar rates of thermal degradation when viewed as a fraction of the initial PZ concentration, the magnitude or PZ concentration degraded increases as the starting concentration increases. This increase translates to a higher concentration of total formate produced after degradation. The EDA concentration profiles all indicate that EDA is an intermediate degradation product, while the maximum concentration achieved is a function of the PZ starting concentration. The maximum concentration achieved

before EDA reacts to other products increases from 36 mmole per kg in the 4 m PZ experiment to over 100 mmole per kg in the 20 m PZ experiment. The time point of the maximum also occurred at nearly the same time for all four PZ concentrations. This is unlike the behavior seen in the temperature series experiments. In that case, the maximum of EDA concentration occurred later in experiments with less degradation (lower temperature). With the effect of PZ concentration, the maximum in EDA concentration occurs after 7 to 10 weeks in all four cases.

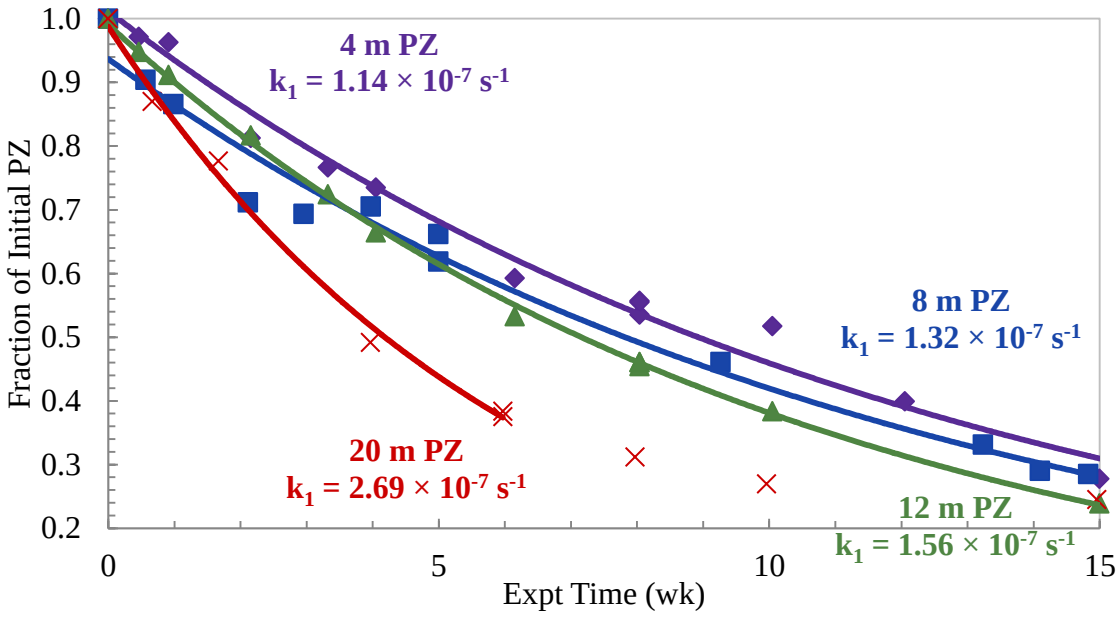

Figure 5.20: Comparison of PZ loss for lean (α=0.3) solutions degraded at 175 °C from 4 to 20 m PZ

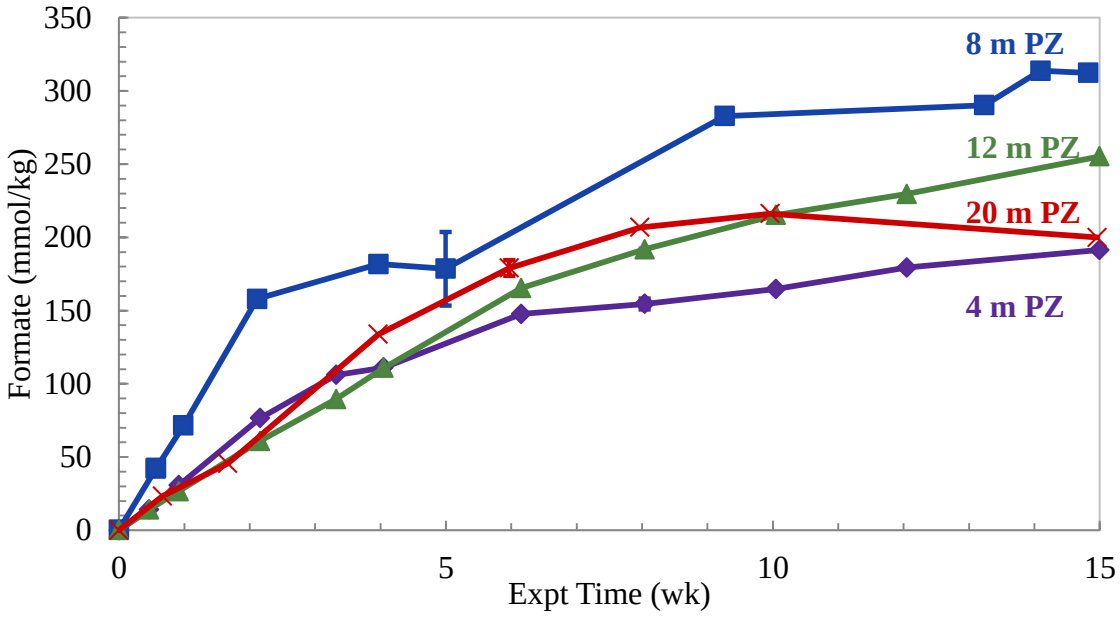

Figure 5.21: Comparison of formate generation for lean (α=0.3) solutions degraded at 175 °C from 4 to 20 m PZ

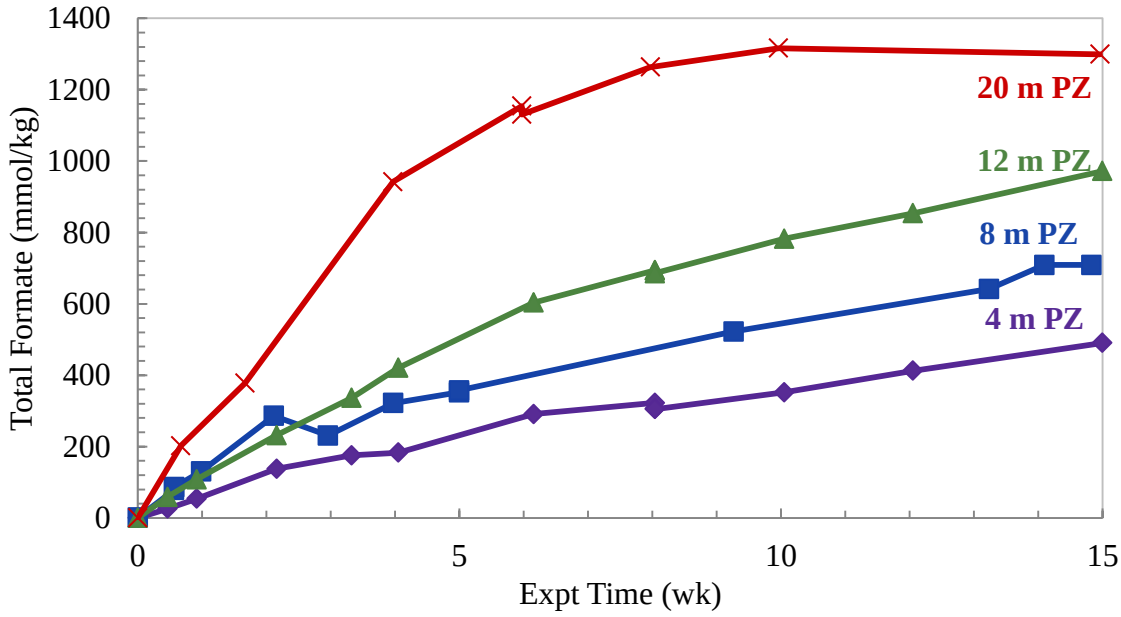

Figure 5.22: Comparison of total formate generation for lean (α=0.3) solutions degraded at 175 °C from 4 to 20 m PZ

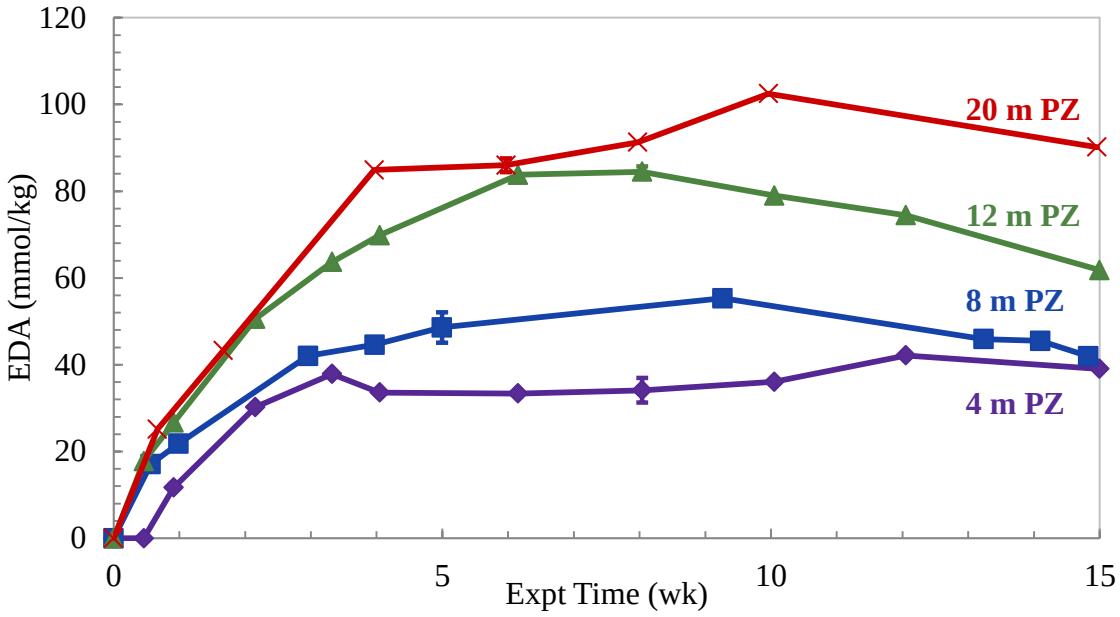

Figure 5.23: Comparison of EDA generation for lean (α=0.3) solutions degraded at 175 °C from 4 to 20 m PZ

5.3.2.2 Evaluation of error for 1st-order approximation

The data in Figure 5.20 demonstrate a small effect of PZ concentration on the loss rate of PZ between 4 to 12 m PZ. In order to determine if the effect is significant, the same t-test analysis described earlier in the chapter was performed for this set of data (section 5.2.1). The t-test was performed in the same way with the same null hypothesis described in Equation 5.7 through 5.12. The linear regressions are represented as exponential regressions in Figure 5.20. The results of the test are shown in Table 5.9 for a comparison of each of the data sets with each other.

The data for 8 m PZ was found to be statistically similar to both the 4 and 12 m PZ data sets within a confidence of 95%. The comparison of the regressed slopes for the 4 and 12 m PZ data, however, were found to disprove the null hypothesis and are statistically different with 95% confidence. This result is expected given the data discussed in the previous section. There is not a strong effect of PZ concentration in

thermal degradation of PZ in comparison to the effect of CO_2 concentration or temperature, and the behavior is slightly more than first order. The first order analysis described in section 5.2 will be used throughout this project as a basis of comparison although some amines such as concentrated PZ, may be represented more accurately with a model with slightly more than first order behavior in amine.

Table 5.9: Results for statistical comparison of parallelism of PZ loss slope for TE4, TE12, and TE18 (8 m PZ, 0.3 mole CO_2 per mole alkalinity, 175 °C)

Data set 1	4 m PZ (TE32)	8 m PZ (TE12)	4 m PZ (TE32)
Data set 2	8 m PZ (TE12)	12 m PZ (TE33)	12 m PZ (TE33)
DOF	21	21	22
α	0.05	0.05	0.05
$t_{n1+n2-4,\ 1-\alpha/2}$	$t_{21,0.975}$	$t_{21,0.975}$	$t_{22,0.975}$
t value	2.080	2.080	2.074
$S^2_{P,Y/X}$	0.00299	0.0285	0.00185
$S_{m_1-m_2}$	0.0045	0.015	0.00373
T	0.29	1.39	4.03
|T|	0.29	1.39	4.03
H_0	True	True	False

5.3.2.3 Effect of PZ concentration for a lean loading (0.3 mol/mol alkalinity) at 165 °C

The effect of PZ concentration for lean loaded solutions was also examined at a lower temperature. Solutions of 4 to 12 m PZ with 0.3 mole CO_2 per mole alkalinity were degraded at 165 °C. The PZ loss is compared for these experiments in Figure 5.24. The generation of formate, total formate, and EDA is compared for the same experiments in Figure 5.25, Figure 5.26, and Figure 5.27, respectively. Unfortunately, the 4 m PZ experiment suffered from a high rate of thermal cylinder failure and there are only three data points up to 6 weeks available.

The loss of PZ does not demonstrate the same behavior as the previous comparison at 175 °C. The 8 m PZ data has significant scatter in the earliest parts of the

data where the trend changes after 3 weeks. It is not clear if the original trend, which is similar to the 12 m PZ data, or the second trend, which behaves as the 4 m PZ data does, is the most appropriate trend. The generation of formate is the same for all three concentrations while the generation of total formate is enhanced as the PZ concentration increases. The generation of EDA is also faster in the higher PZ concentration experiments and none of the experiments reach a noticeable maximum in this time period. It is likely that as with data at 135 and 150 °C, there is not enough degradation at this point to allow for the EDA generation to accumulate and begin reacting onto other products.

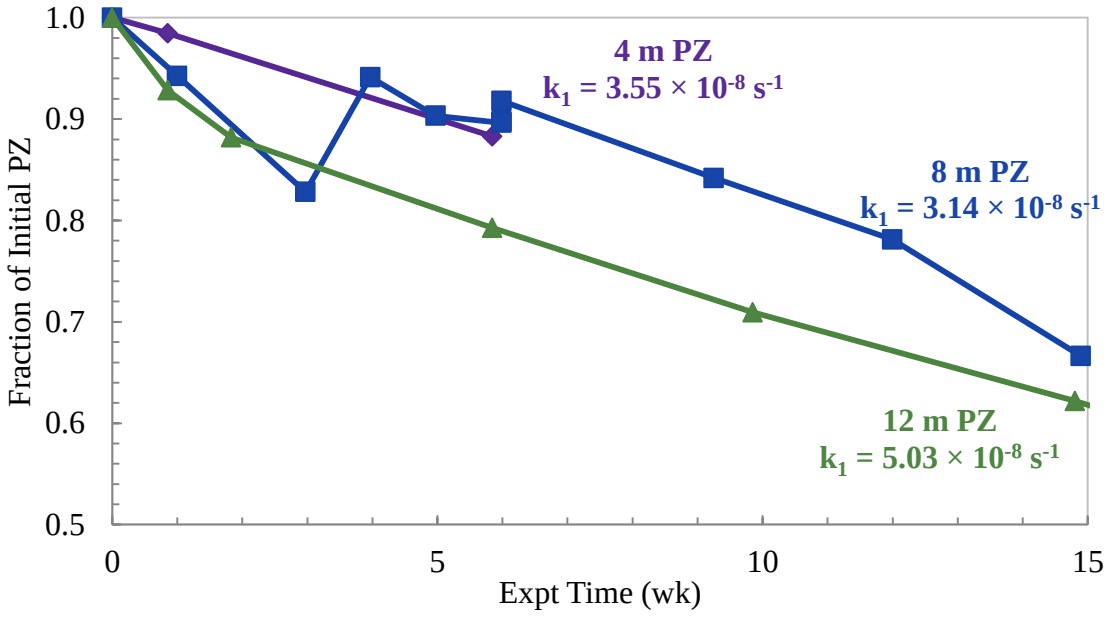

Figure 5.24: Comparison of PZ loss for lean (α=0.3) solutions degraded at 165 °C containing 4 to 12 m PZ

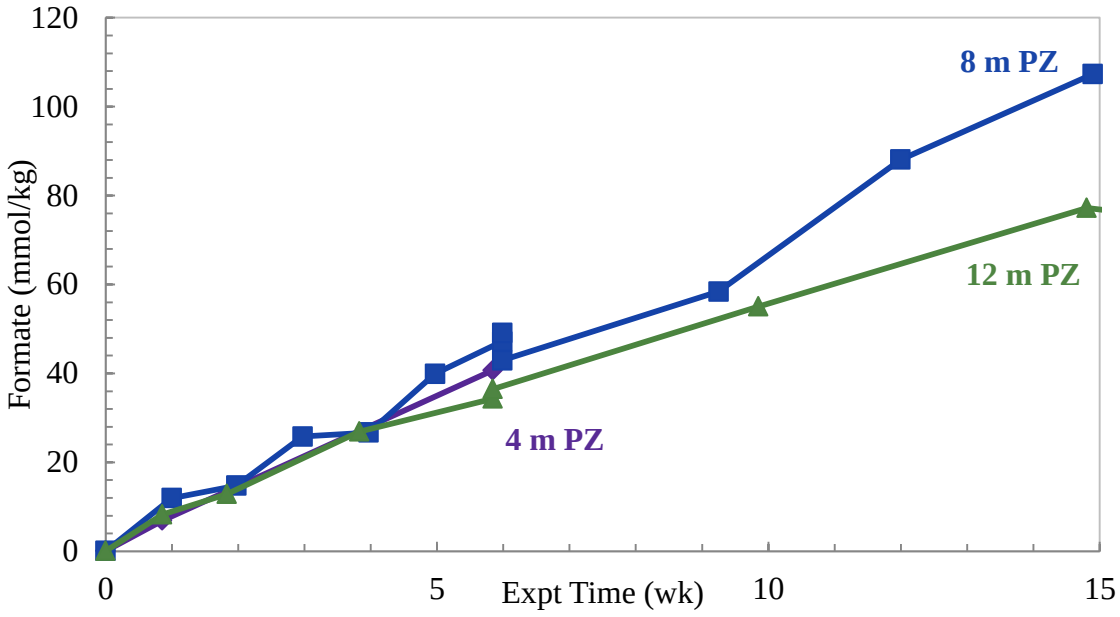

Figure 5.25: Comparison of formate generation for lean (α=0.3) solutions degraded at 165 °C containing 4 to 12 m PZ

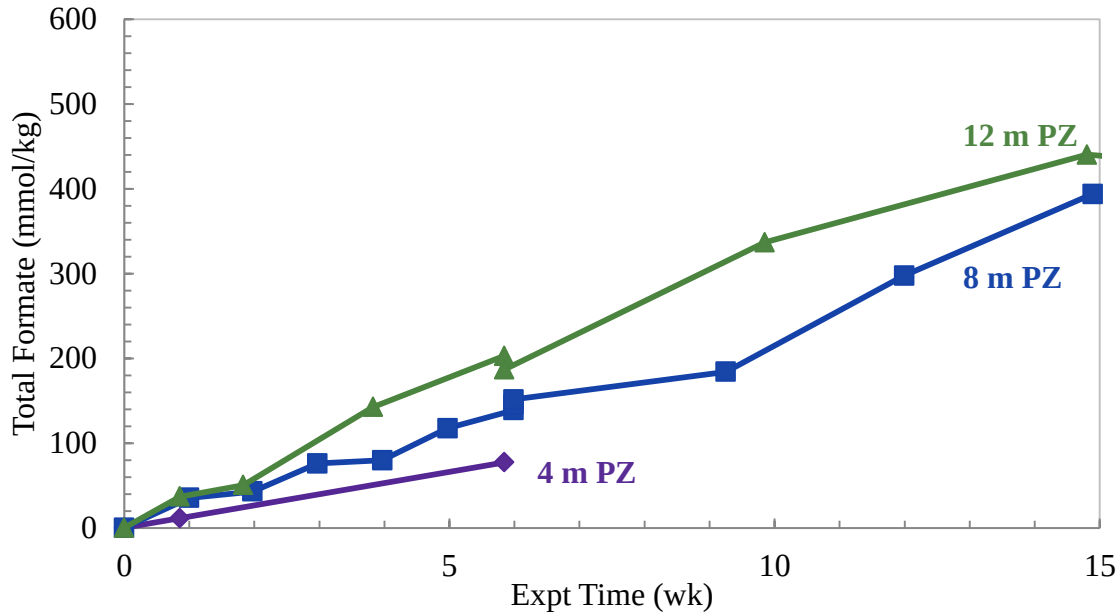

Figure 5.26: Comparison of total formate generation for lean (α=0.3) solutions degraded at 165 °C containing 4 to 12 m PZ

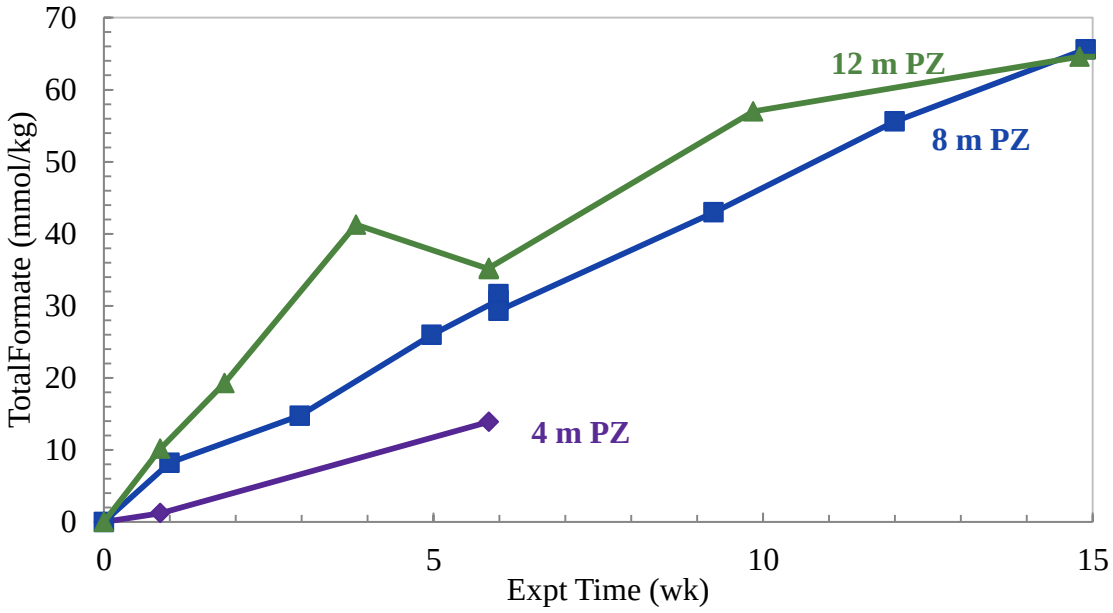

Figure 5.27: Comparison of EDA generation for lean (α=0.3) solutions degraded at 165 °C containing 4 to 12 m PZ

5.3.3 Effect of CO_2 loading

The effect of CO_2 concentration on the PZ thermal degradation was examined by degrading solutions at constant temperature and PZ concentration. A summary of the experiments performed to examine this variable is provided in Table 5.10. In total, eight groups of experiments were performed that highlighted the effect of CO_2 concentration. As with the previous two sections, only three of the eight comparisons will be discussed in detail. All data is available in Appendix D to reproduce any comparison.

Previous authors have found CO_2 to be a strong catalyst for thermal degradation of amines (Davis, 2009; Lepaumier et al., 2009a). Davis determined that degradation of MEA was approximately first order in CO_2 concentration as he observed a doubling of MEA loss with an increase of CO_2 loading from 0.2 to 0.4 with 7 m MEA at 135 °C. Lepaumier found that all of the amines tested, including MEA, AMP, diethanolamine (DEA), methyldiethanolamine (MDEA), and N-(2-hydroxyethyl)ethylenediamine

(HEEDA), demonstrated a noted increase in the level of degradation in the presence of CO_2 compared to without CO_2 (Lepaumier et al., 2009a). The catalytic effect of CO_2 on each amine was slightly different, but all showed marked increases in degradation. For HEEDA, the presence of CO_2 increased the loss of HEEDA from 1% to nearly 100% with the same temperature and experiment length (Lepaumier et al., 2009a). The effect of CO_2 on PZ thermal degradation has not been studied previously, but it was hypothesized to follow the trends found with other amines and alkanolamines.

Table 5.10: Experiment series to investigate the effect of CO_2 Loading

Solution Constants	Values Tested (mole CO_2/mole alkalinity)					
8 m PZ, 135 °C	-	-	-	0.3	0.4	-
8 m PZ, 150 °C	-	-	-	0.3	0.4	-
8 m PZ, 165 °C	**0**	**0.1**	**-**	**0.3**	**0.4**	**-**
8 m PZ, 175 °C	**0**	**0.1**	**0.2**	**0.3**	**0.4**	**0.47**
10 m PZ, 135 °C	-	-	-	0.3	0.4	-
10 m PZ, 150 °C	-	-	-	0.3	0.4	-
10 m PZ, 175 °C	-	-	-	0.3	0.4	-
20 m PZ, 175 °C	**-**	**0.1**	**-**	**0.3**	**-**	**-**

5.3.3.1 Effect of CO_2 concentration for 8 m PZ at 175 °C

The widest range of CO_2 concentrations was examined with experiments preformed on 8 m PZ at 175 °C. These experiments provide the best understanding of the effect of CO_2 concentration in thermal degradation of concentrated, aqueous PZ. The loss of PZ as a fraction of the initial PZ for experiments with initial CO_2 concentrations of 0, 0.1, 0.2, 0.3, 0.4, and 0.47 mole CO_2 per mole alkalinity are compared in Figure 5.28. The generation of formate, total formate, EDA, FPZ, and AEP for the same six experiments is compared in Figure 5.30, Figure 5.32, Figure 5.34, Figure 5.35, and Figure 5.36, respectively. Neither FPZ nor AEP were quantified in the unloaded experiment while AEP was not quantified for the 0.1 mole CO_2 per mole alkalinity.

Changes in CO_2 concentration have a complicated effect on PZ thermal degradation. In terms of PZ loss, the rate of PZ loss increases with increased CO_2 loading up to a loading of 0.3 moles CO_2 per mole alkalinity. Between 0.3 and 0.4 moles CO_2 per mole alkalinity, there is little difference in PZ loss. An increase to 0.47 moles CO_2 causes a decrease in degradation rate. Changes in CO_2 concentration, therefore, create a maximum in degradation rate between 0.3 and 0.4 moles CO_2 per mole alkalinity. The fraction of initial PZ degraded after 5 and 15 weeks at 175 °C is compared in Figure 5.29 over a range of 0 to 0.47 mole CO_2 per mole alkalinity to demonstrate this observation. The solution with 0.47 mole CO_2 per mole alkalinity has a noticeable change in rate with a lower initial rate that increases after 8 weeks of degradation. This change in rate is observable in Figure 5.29 as well as the shape of the curves at 5 and 15 weeks of degradation are different in regards to the very rich solution.

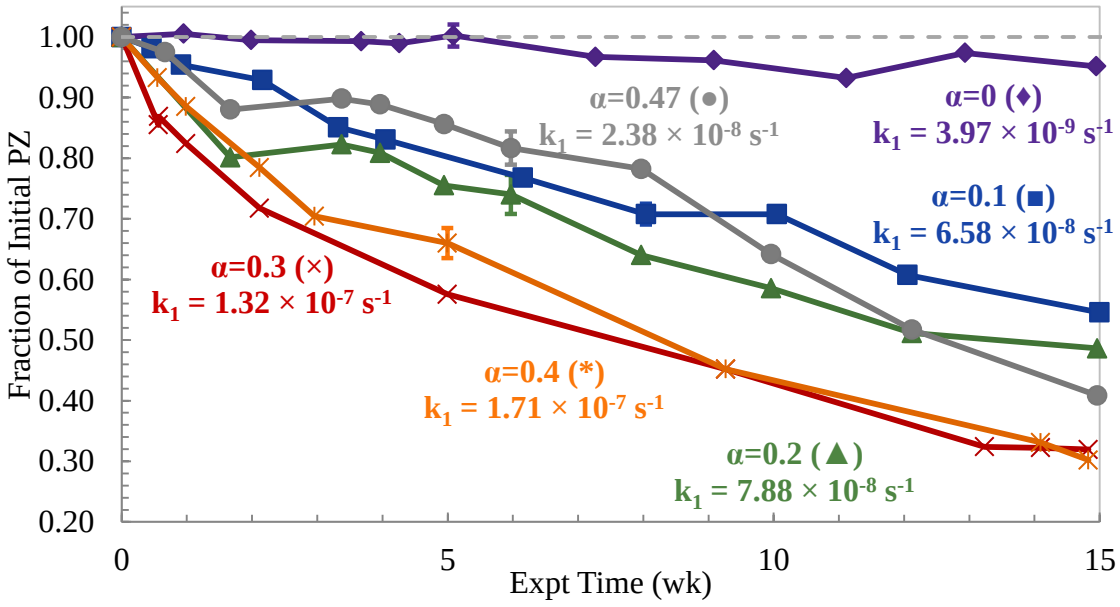

Figure 5.28: Comparison of PZ loss for 8 m PZ at 175 °C with 0 to 0.47 mole CO_2 per mole alkalinity

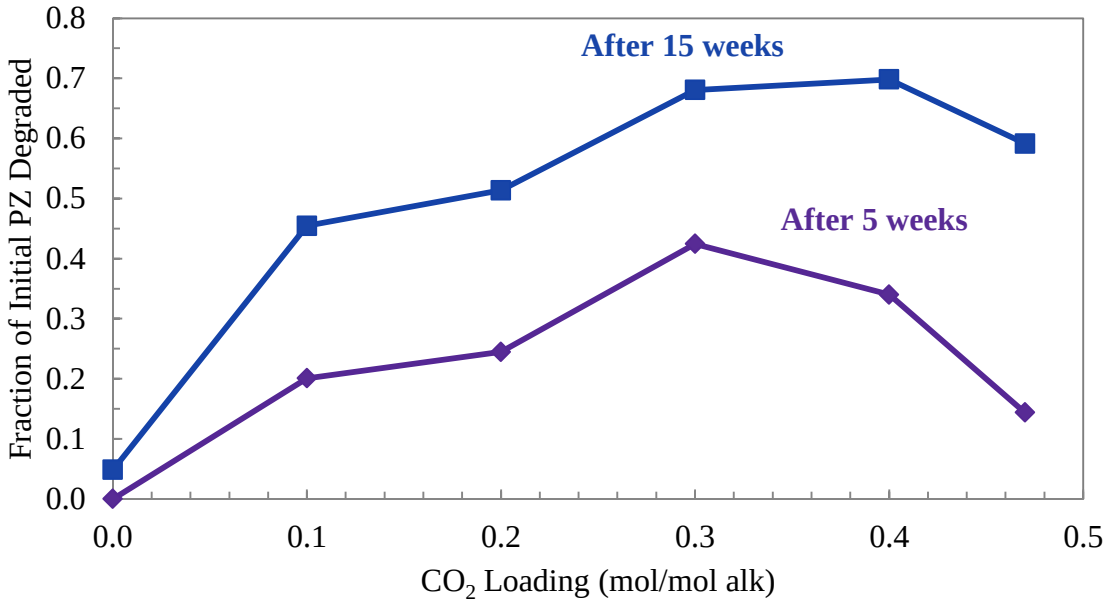

Figure 5.29: Fraction of PZ degraded after 5 and 15 weeks at 175 °C for 8 m PZ with 0 to 0.47 mole CO_2 per mole alkalinity

The generation of formate and total formate also demonstrate unique behavior with changes in CO_2 concentration. For formate, a maximum concentration is observed in the final concentration between the solutions with 0.3 and 0.4 mole CO_2 per mole alkalinity. The concentration of formate quantified after 5 and 15 weeks is compared in Figure 5.31 to demonstrate this. At both experimental times, the concentration of formate in the very rich loaded case (0.47 mole CO_2 per mole alkalinity) is lower than the rich loaded case. In the case of total formate, the concentration generated after 15 weeks of degradation increases steadily to a maximum at 0.4 mole CO_2 per mole alkalinity, then decreases in the very rich case. The concentration of total formate after 5 and 15 weeks is compared in Figure 5.33 to demonstrate this. The ratio of formate to formyl amides, therefore, does change slightly with differences in CO_2 concentration over this range. The FPZ quantified directly also has complicated behavior as 0.2 to 0.4 mole per mole

alkalinity produce similar final concentrations of FPZ while the very rich experiment produced the highest levels of FPZ.

The EDA data suggests, as with previous experiments, that EDA is an intermediate that is generated at varying initial rates, and then reacted away to form additional products. The initial rates of production can offer some clues to the effect of CO_2. The data before 5 weeks of degradation suggest that the 0.3 and 0.4 mole CO_2 per mole alkalinity experiments have the fastest EDA generation rates while the other experiments are all lower. This suggests a maximum generation rate between 0.3 and 0.4 moles CO_2 per mole alkalinity, a similar behavior as was observed with formate and total formate. Since formate and formyl amides are final products, rather than intermediates, their behavior is more readily observable. AEP was produced at similar initial rates over a range of CO_2 loadings and final concentrations that show complex behavior at very lean and very rich loadings.

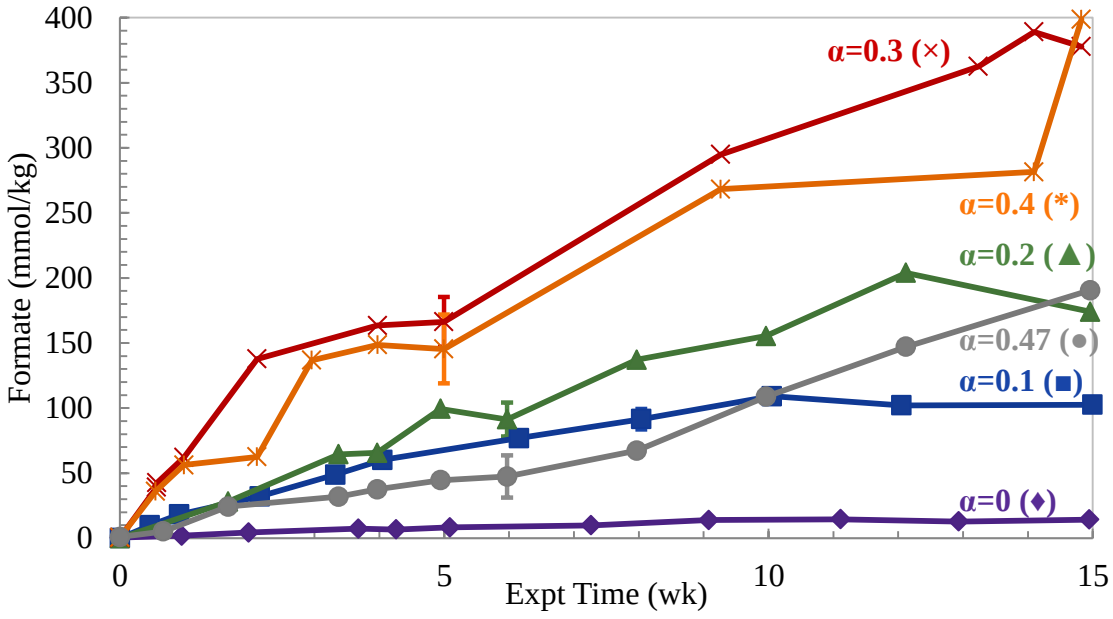

Figure 5.30: Comparison of formate generation for 8 m PZ at 175 °C with 0 to 0.47 mole CO_2 per mole alkalinity

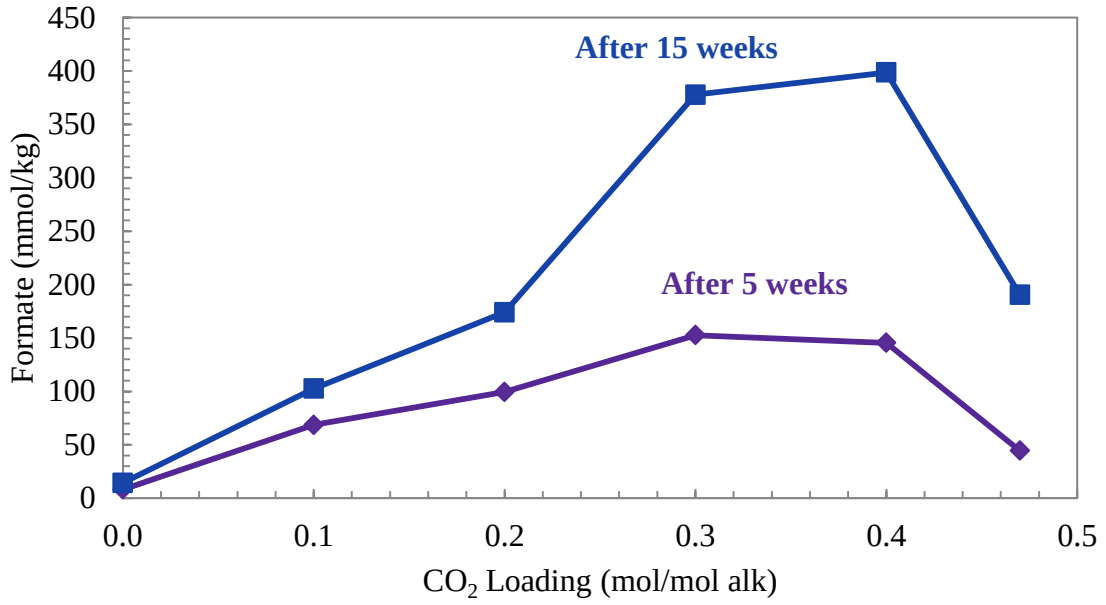

Figure 5.31: Generation of formate after 5 and 15 weeks at 175 °C for 8 m PZ with 0 to 0.47 mole CO_2 per mole alkalinity

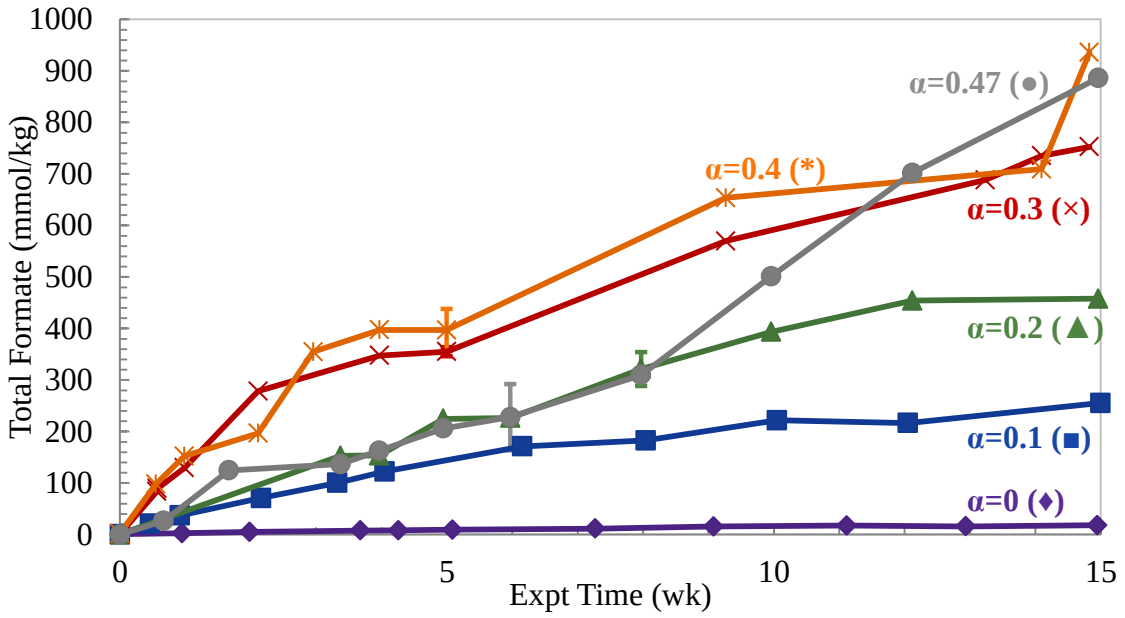

Figure 5.32: Comparison of total formate generation for 8 m PZ at 175 °C with 0 to 0.47 mole CO_2 per mole alkalinity

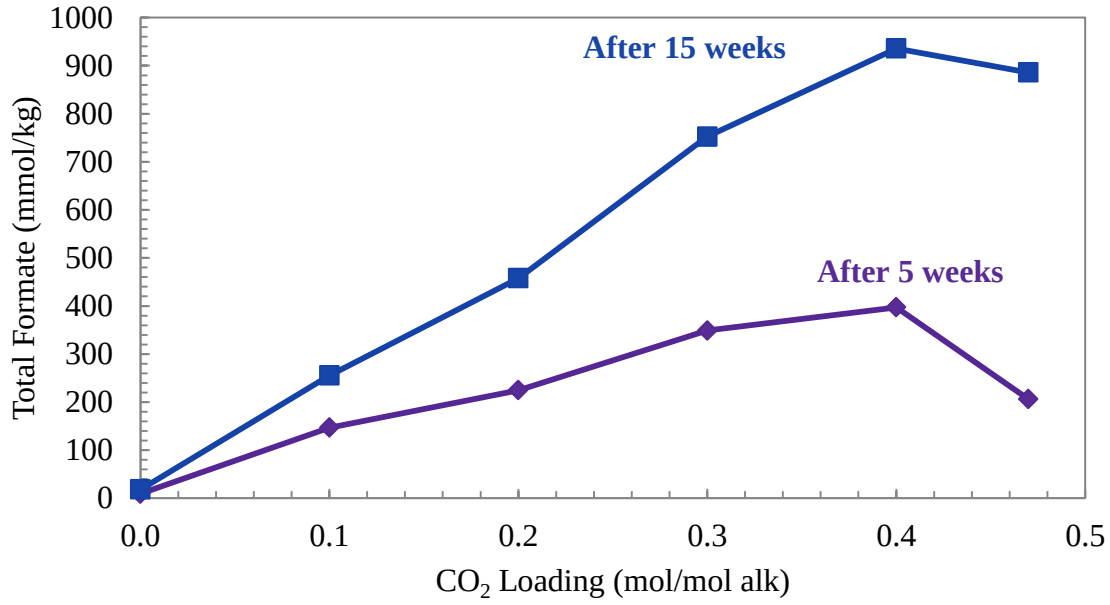

Figure 5.33: Generation of total formate after 5 and 15 weeks at 175 °C for 8 m PZ with 0 to 0.47 mole CO_2 per mole alkalinity

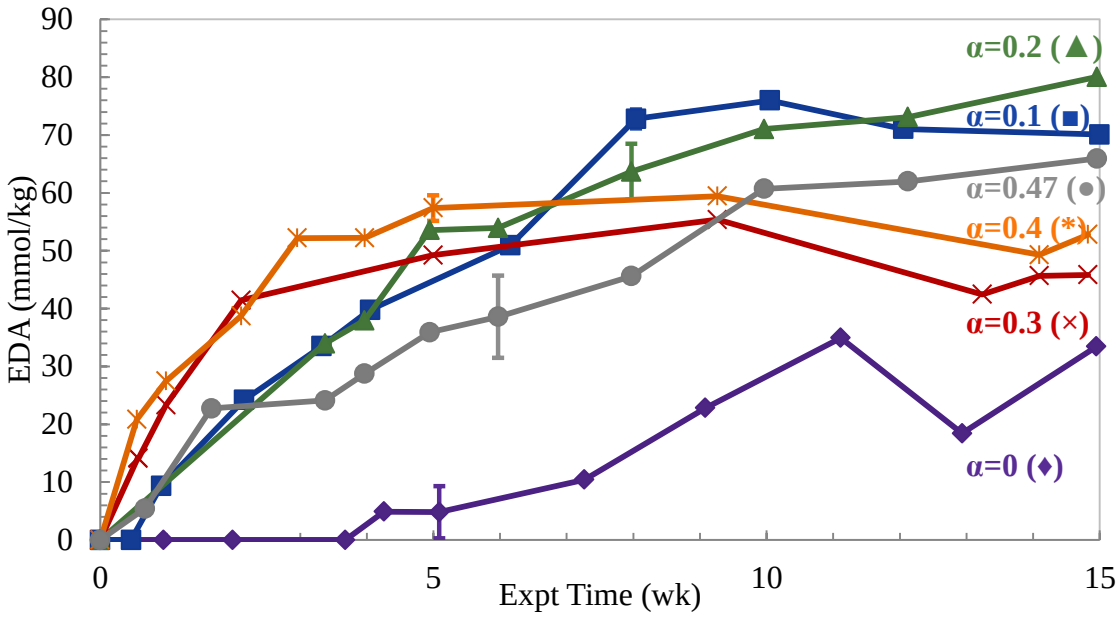

Figure 5.34: Comparison of EDA generation for 8 m PZ at 175 °C with 0 to 0.47 mole CO_2 per mole alkalinity

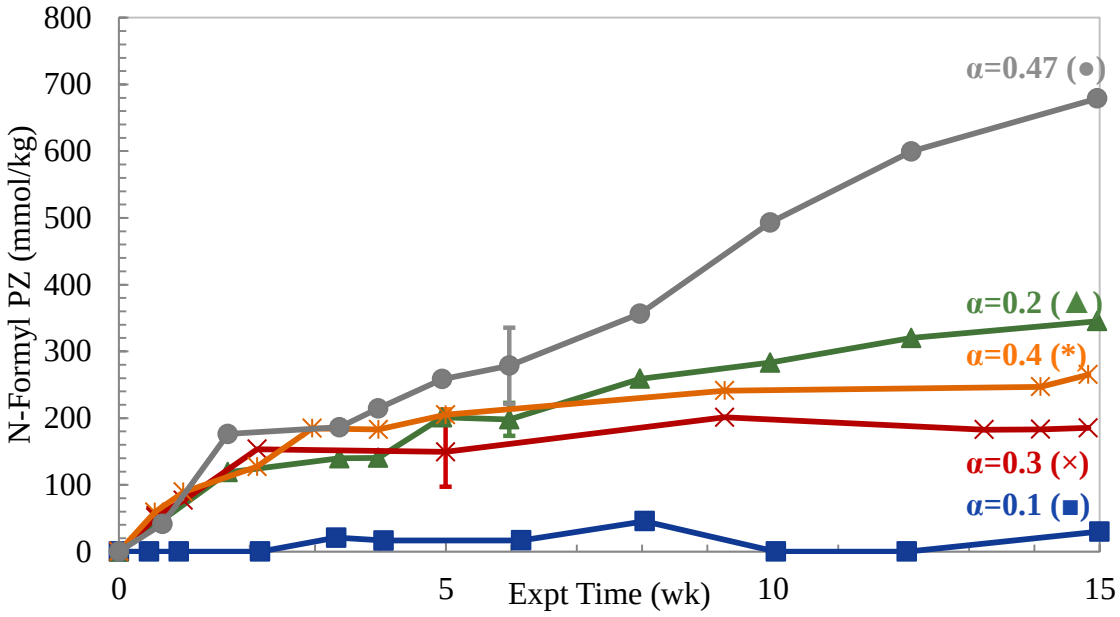

Figure 5.35: Comparison of FPZ generation for 8 m PZ at 175 °C with 0 to 0.47 mole CO_2 per mole alkalinity

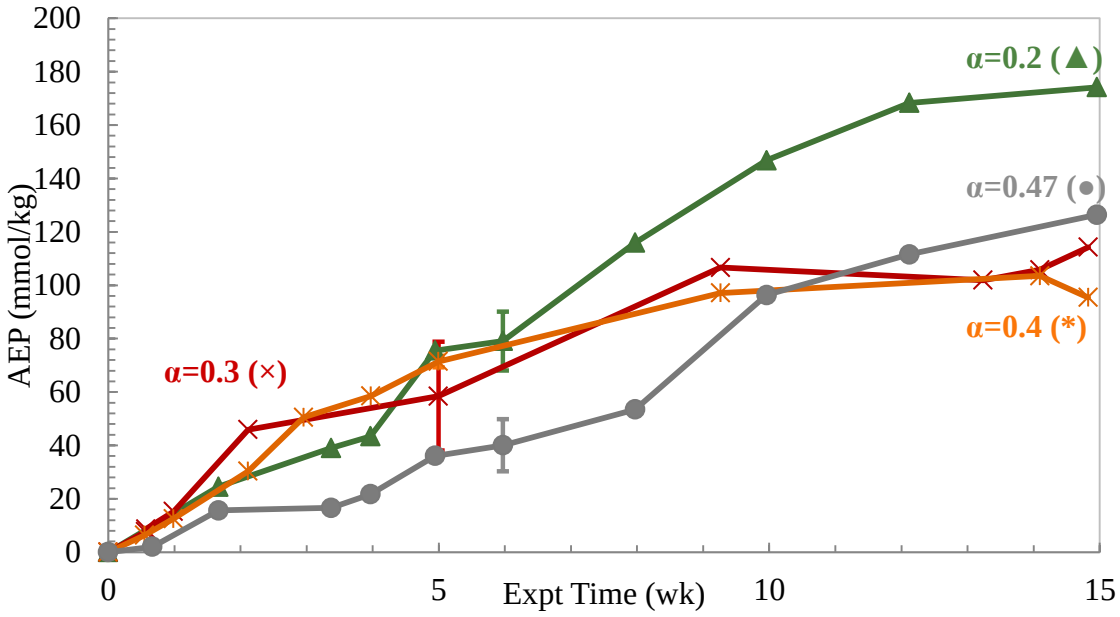

Figure 5.36: Comparison of AEP generation for 8 m PZ at 175 °C with 0 to 0.47 mole CO_2 per mole alkalinity

As the initial CO_2 concentration increases from 0 to 0.47 mole CO_2 per mole alkalinity, the rate of PZ loss and generation rates of degradation product experience a maximum rate at an intermediate CO_2 concentration. This behavior suggests a strong effect of speciation on the thermal degradation rate. The speciation predicted for 8 m PZ was discussed in section 2.1. The speciation expected for 8 m PZ at 175 °C is shown in Figure 5.37. The speciation does not show one species whose concentration matches the trend of the degradation rate, as may be expected. It is likely then, that the degradation effect is a balance of more than one active species. The concentration of $PZCOO^-$ reaches a maximum between 0.2 and 0.3 mole CO_2 per mole alkalinity while the concentration of H^+PZ is continually increasing, although slowly after 0.3 mole CO_2 per mole alkalinity. As loading increases, $PZCOO^-$ is protonated to form H^+PZCOO^- which is also likely involved with degradation as an active species. The exact cause of the degradation behavior is not known although H^+PZ, H^+PZCOO^-, and $PZCOO^-$ are all expected to be involved in the initial mechanisms for degradation. It is possible that one species, such as H^+PZ, dominates the mechanism at low loadings and then the dominant mechanisms change as the concentration of other molecules increases in solution. For example, at low loadings, H^+PZ may dominant while at loadings greater than 0.3 mole CO_2 per mole alkalinity the unprotonated molecules become more influential on the degradation mechanisms. The effect H^+PZ, in particular, is discussed in more detail in section 6.3.

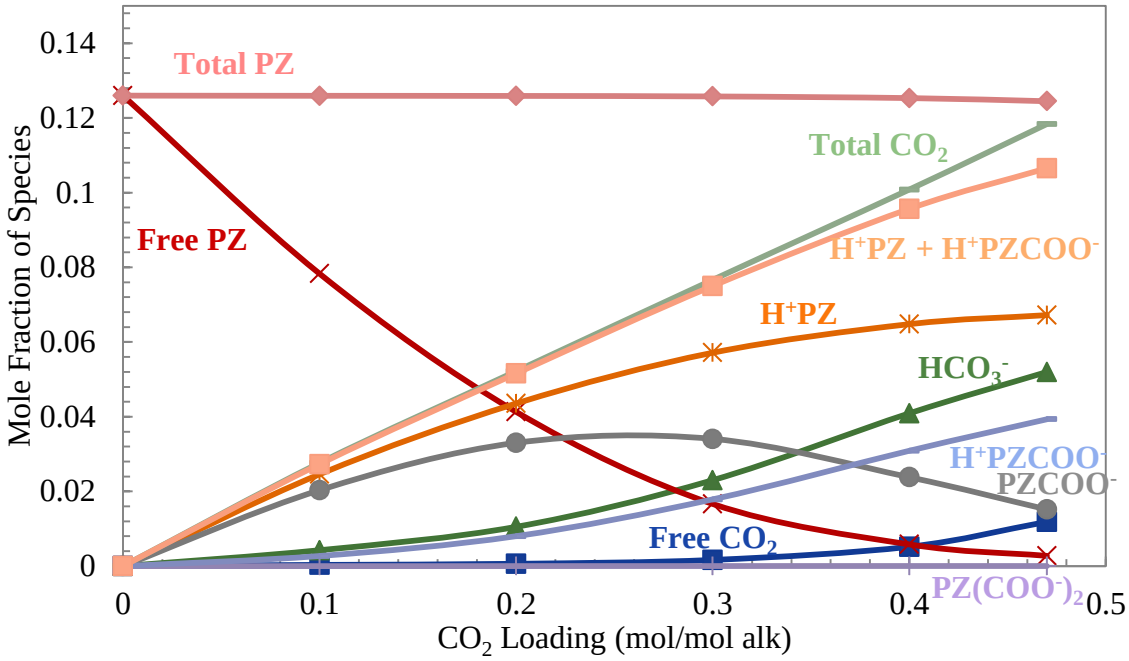

Figure 5.37: Predicted speciation of 8 m PZ at 175 °C (Frailie et al., 2011)

5.3.3.2 Effect of CO_2 concentration for 8 m PZ at 165 °C

The effect of CO_2 concentration on thermal degradation of 8 m PZ was investigated at 165 °C from 0 to 0.4 mole CO_2 per mole alkalinity. The PZ loss is compared in Figure 5.38. The generation of formate, total formate, and EDA are compared in Figure 5.39, Figure 5.40, Figure 5.41, Figure 5.42, and Figure 5.43, respectively. The rate of PZ loss increased with CO_2 loading between 0 and 0.4 mole CO_2 per mole alkalinity without a maximum being observed. The generation of formate, total formate, EDA, FPZ, and AEP all demonstrate increases in initial rate with increased loading, without a maximum being observed. At longer degradation times, the concentration differences in formate, total formate, FPZ, and AEP between the highest two loadings diminish. For EDA, maximum concentrations of 35 to 65 mmole per kg were observed and all CO_2 concentrations reached a maximum after 15 hours of degradation, mimicking the behavior observed with changes in PZ concentration.

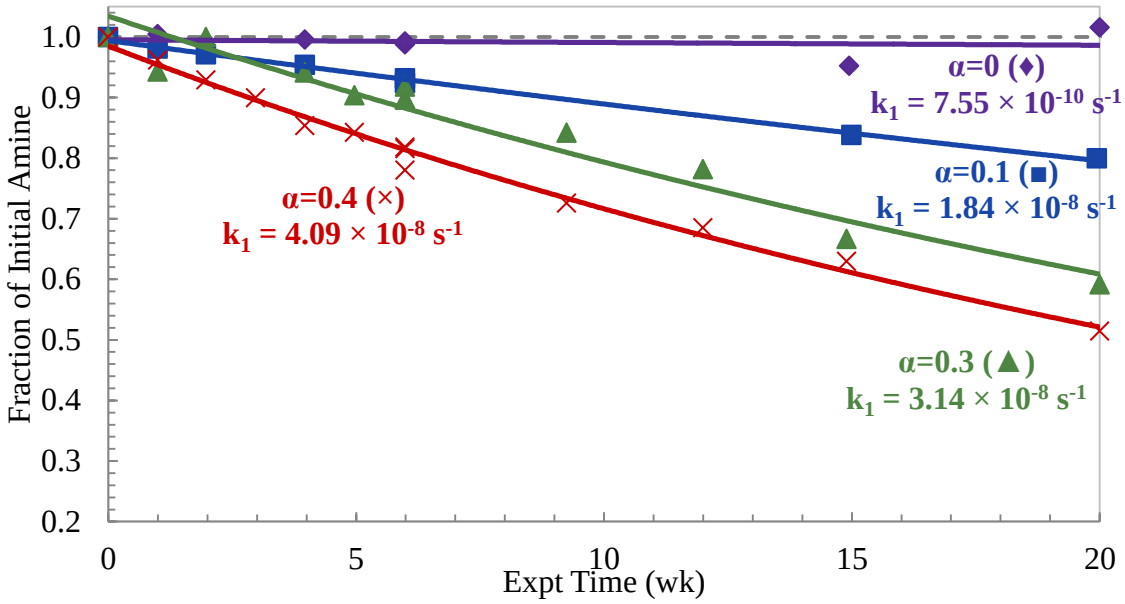

Figure 5.38: Comparison of PZ loss for 8 m PZ at 165 °C with 0 to 0.4 mole CO_2 per mole alkalinity

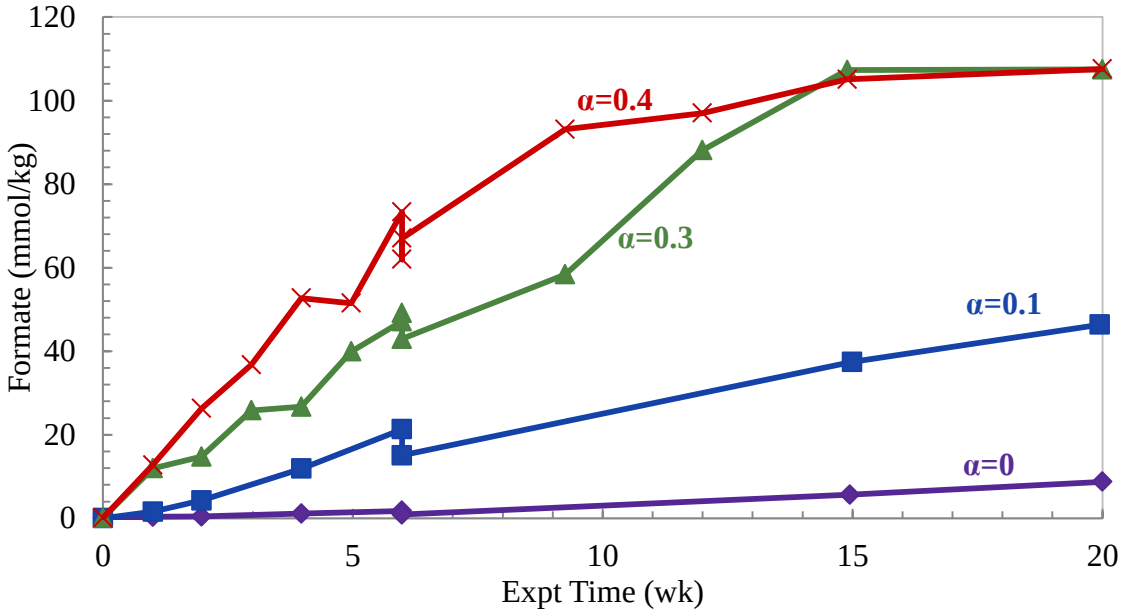

Figure 5.39: Comparison of formate generation for 8 m PZ at 165 °C with 0.3 and 0.4 mole CO_2 per mole alkalinity

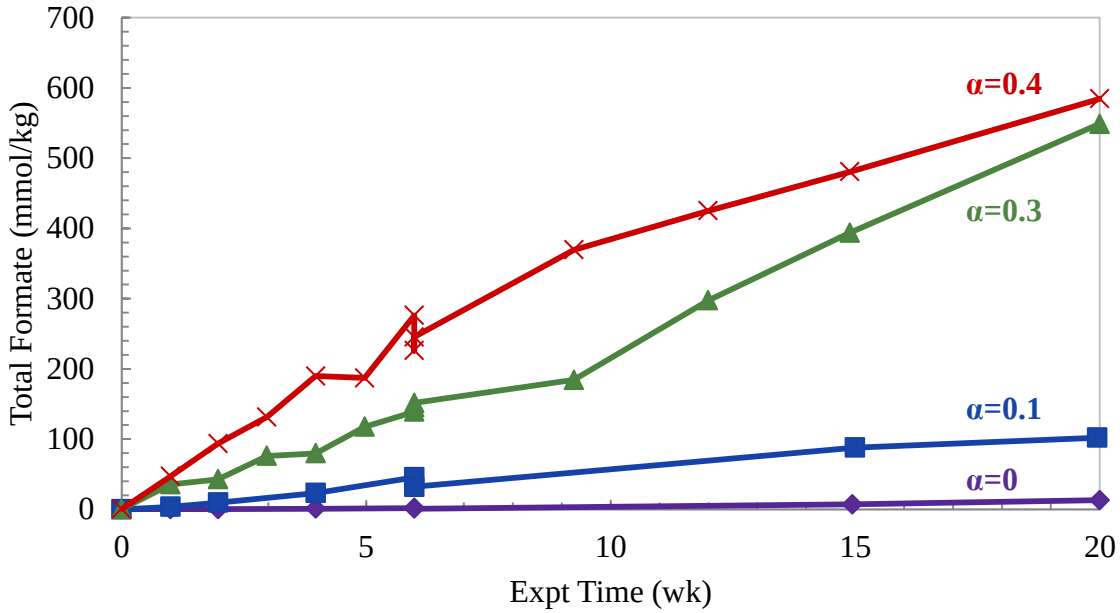

Figure 5.40: Comparison of total formate generation for 8 m PZ at 165 °C with 0.3 and 0.4 mole CO_2 per mole alkalinity

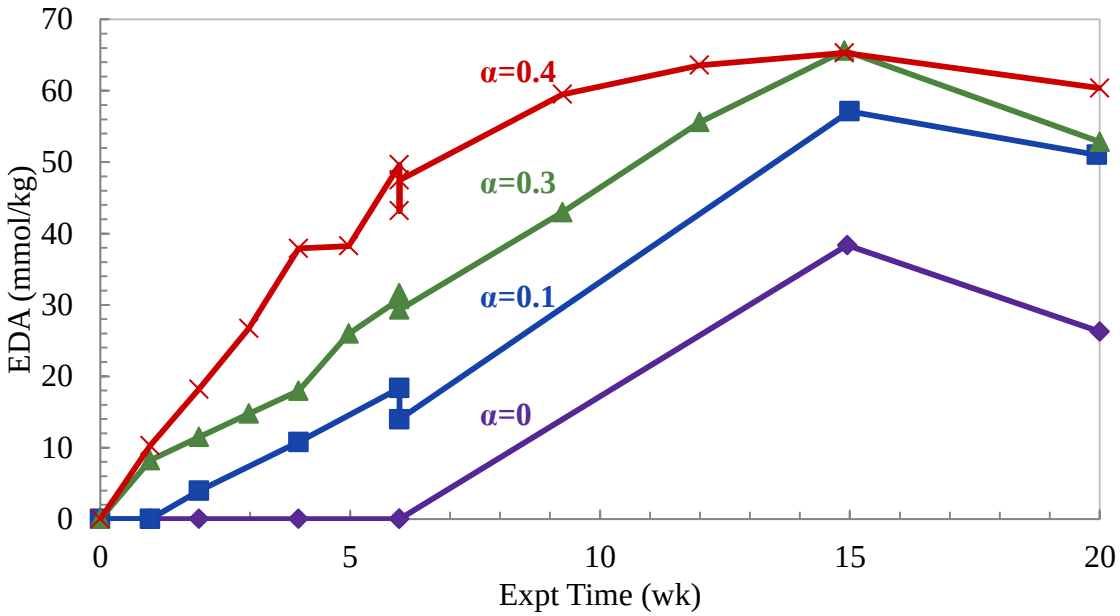

Figure 5.41: Comparison of EDA generation for 8 m PZ at 165 °C with 0.3 and 0.4 mole CO_2 per mole alkalinity

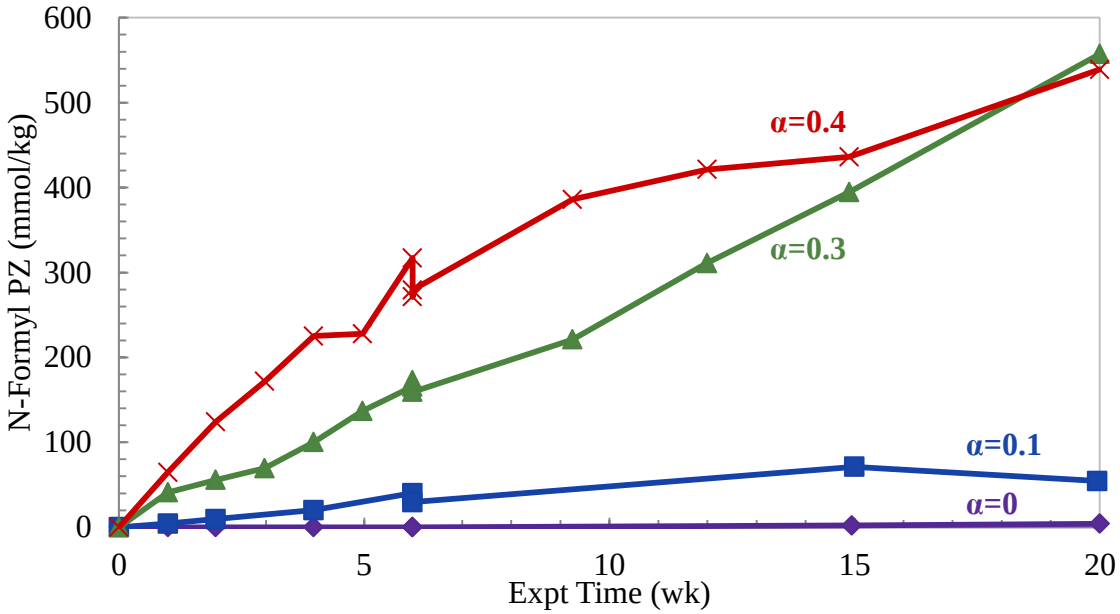

Figure 5.42: Comparison of FPZ generation for 8 m PZ at 165 °C with 0.3 and 0.4 mole CO_2 per mole alkalinity

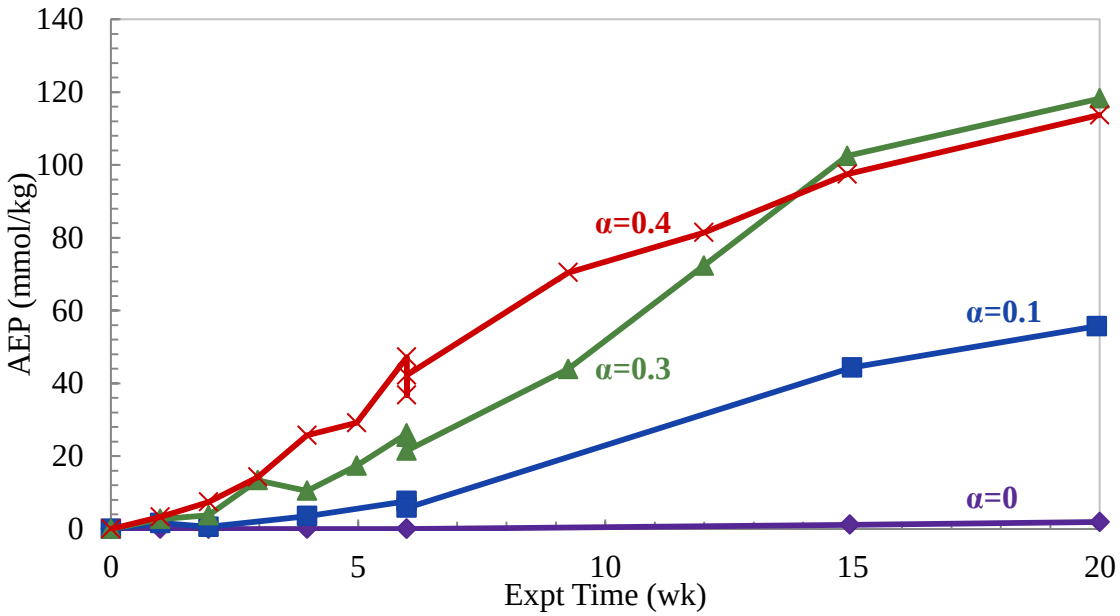

Figure 5.43: Comparison of AEP generation for 8 m PZ at 165 °C with 0.3 and 0.4 mole CO_2 per mole alkalinity

5.3.3.3 Effect of CO_2 concentration for 20 m PZ at 175 °C

The thermal degradation of 20 m PZ was measured for CO_2 loadings of 0.1 and 0.3 moles CO_2 per mole alkalinity at 175 °C. These two CO_2 concentrations were chosen because they were of interest to reclaiming activities where thermal reclaiming would concentrate the PZ concentration with the same approximately quantity of CO_2, decreasing the CO_2 loading by definition. The loss of PZ observed for these two experiments is compared in Figure 5.44. The generation of formate, total formate, and EDA are compared for the same experiments in Figure 5.45, Figure 5.46, and Figure 5.47, respectively.

As predicted, the thermal degradation of PZ and production of degradation products were significantly enhanced with increased CO_2 loading. PZ loss was doubled for an increase from 0.1 to 0.3 mole CO_2 per mole alkalinity after 15 weeks at 175 °C. Concentrations of formate and total formate more than doubled for the same increase in CO_2 concentration. FPZ and AEP generation demonstrated trends similar to that of formate and total formate, although not shown here. EDA production in these high PZ concentration experiments was not starkly different as both CO_2 loadings produced 100 to 120 mmole per kg EDA after 15 weeks. The EDA did not demonstrate an intermediate behavior, as the concentration did not decrease as in other PZ experiments, but the experiment may not have continued long enough to see this behavior.

5.3.4 Effect of additives

The effect of various additives on the thermal degradation of PZ was explored through high temperature experiments. A summary of the additive experiments is presented in Table 5.11. Thermal degradation in a real system will take place in the presence of metals, degradation products, and any solvent additives. These tests were planned to determine the effect that the presence of these molecules would have on PZ

degradation rates. The concentrations of each additive used were based on assumptions for either what would be used in industrials settings or the level expected from corrosion. For example, Inhibitor A was used at 100 mM because this is the anticipated concentration needed to deter oxidation in the absorber side of the system (Goff and Rochelle, 2006; Sexton and Rochelle, 2009a). The addition of 5 mM Cu^{2+} was used to simulate the use of a copper based corrosion inhibitor (Pearce, 1984; Reed, 1945). The addition of either 1 mM Fe^{2+} or 0.1 mM Fe^{2+}, 0.1 Ni^{2+}, and 0.6 mM Cr^{3+} was used to simulate the expected concentrations if there was corrosion in either a carbon steel or stainless steel stripper, respectively. Finally, an experiment was performed in the presence of the expected concentrations of three common degradation products in highly degraded PZ.

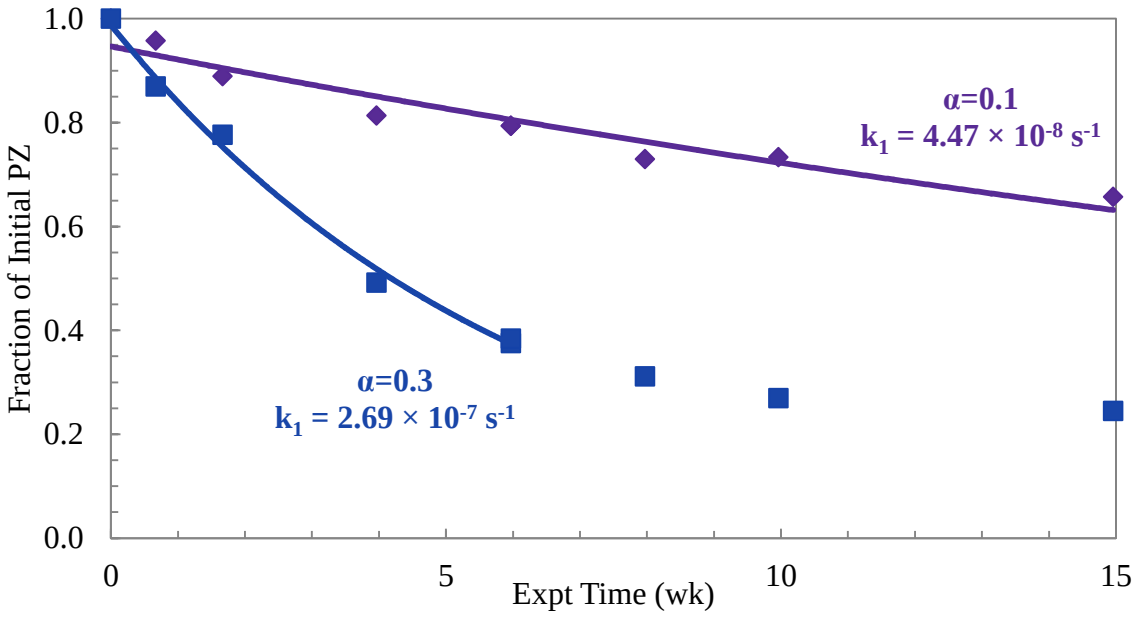

Figure 5.44: Comparison of PZ loss for 20 m PZ at 175 °C with 0.1 and 0.3 mole CO_2 per mole alkalinity

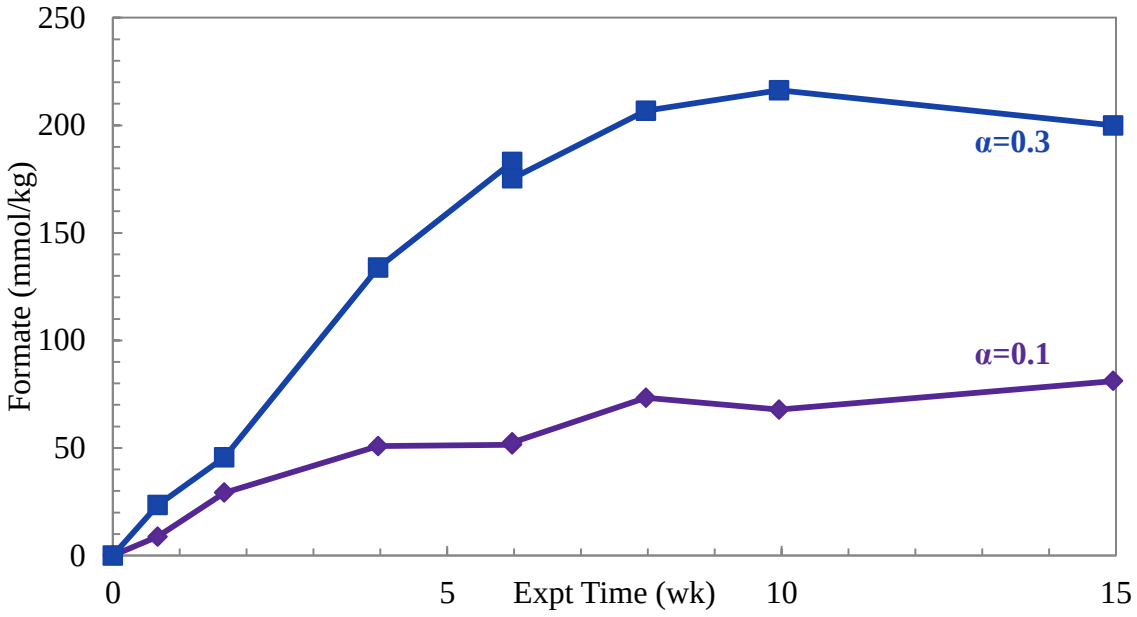

Figure 5.45: Comparison of formate generation for 20 m PZ at 175 °C with 0.1 and 0.3 mole CO_2 per mole alkalinity

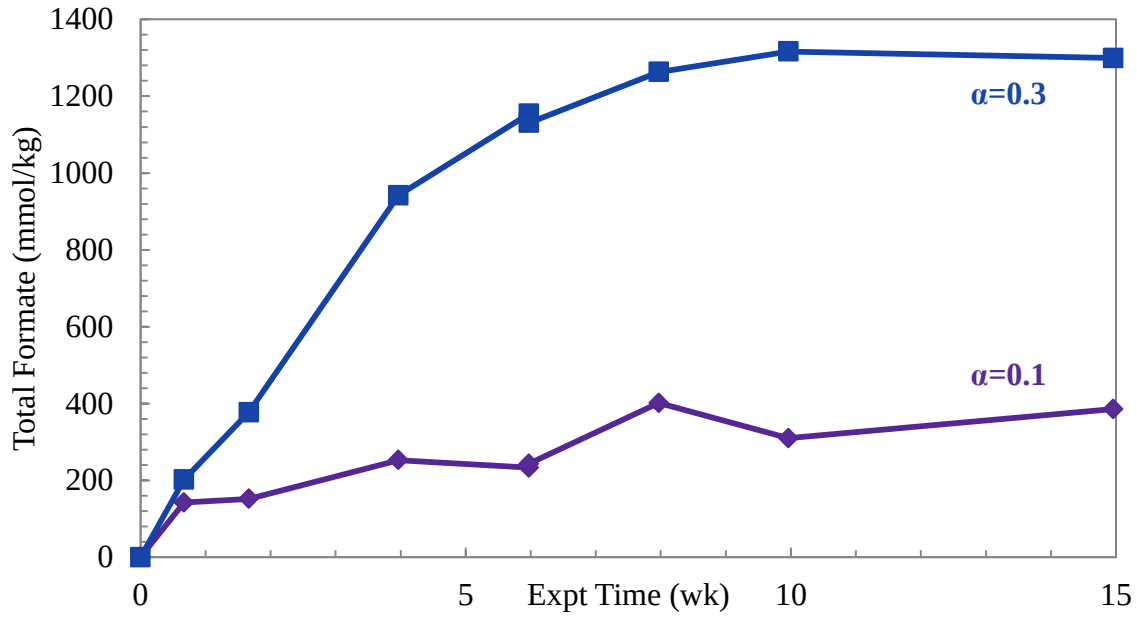

Figure 5.46: Comparison of total formate generation for 20 m PZ at 175 °C with 0.1 and 0.3 mole CO_2 per mole alkalinity

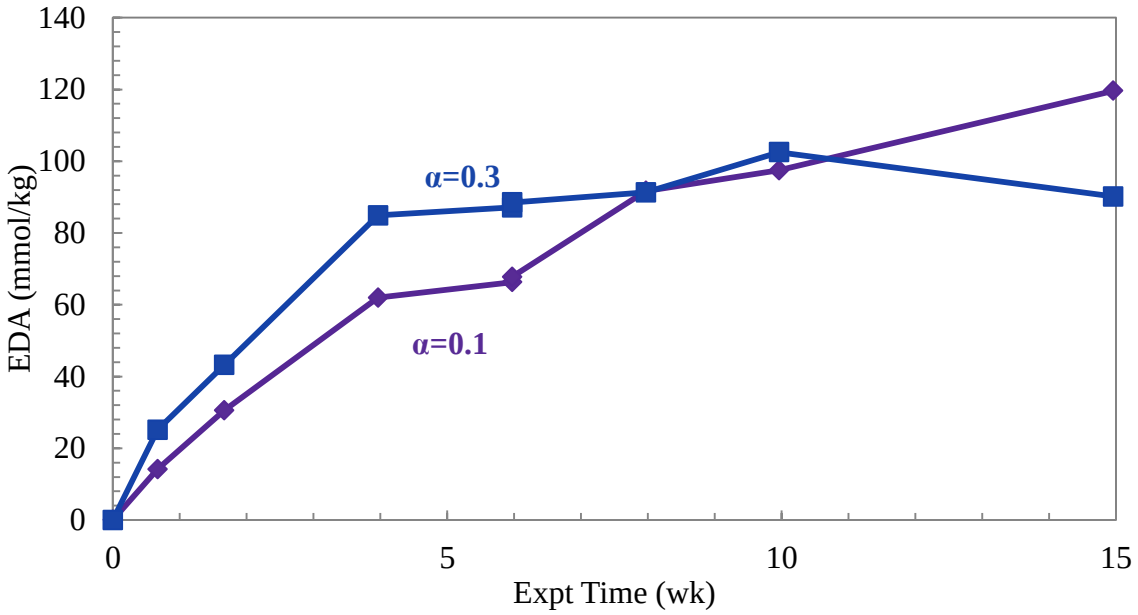

Figure 5.47: Comparison of EDA generation for 20 m PZ at 175 °C with 0.1 and 0.3 mole CO_2 per mole alkalinity

Table 5.11: Summary of PZ Thermal Degradation Experiments with Additives

Temp (°C)	PZ (m)	CO_2 Loading (mol/mol alk)	Additive (mM)	Expt.
	8	0.3	100 Inhibitor A	TE56
	8	0.3	5 Cu^{2+}, 1 Fe^{2+}	TE5
175	8	0.3	5 Cu^{2+}, 1 Fe^{2+}, 100 A	TE6
	8	0.3	0.1 Fe^{2+}, 0.1 Ni^{2+}, 0.6 Cr^{3+}	TE8
	8	0.3	1000 Formate, 100 Oxalate, 150 EDA	TE7

5.3.4.1 Addition of 100 mM Inhibitor A

Inhibitor A is an oxidation inhibitor used to minimize the effect of metal-catalyzed degradation. In chapter 9, Inhibitor A is shown to be useful at mitigating Cu^{2+}-catalyzed oxidation of concentrated PZ solutions. PZ systems are proposed to include Inhibitor A as a standard additive to decrease degradation, so the effect of this additive on thermal degradation was assessed. The thermal degradation of 8 m PZ in the presence of 100 mM Inhibitor A was investigated at 175 °C. The loss of PZ is compared between the

uninhibited and inhibited experiments in Figure 5.48. The uninhibited experiment is a set of data from three separate repeated experiments exploring thermal degradation of 8 m PZ with 0.3 mole CO_2 per mole alkalinity at 175 °C. The addition of Inhibitor A appears to decrease the loss of PZ over the course of the 15 week experiment. The error in the cation IC analysis for PZ has some scatter, but the addition of Inhibitor A decreases PZ loss by 20% as only 54% of the initial PZ is lost after 15 weeks compared to 68% in the uninhibited experiments.

The generation of total formate and EDA are shown for the same two data sets in Figure 5.49 and Figure 5.50, respectively. The generation of total formate appears to be diminished, especially in the initial portion of the experiment, while the EDA concentration is slightly higher than the uninhibited experiment. These observations follow with an overall decrease in the degradation rate of the system. With less PZ degradation, less total formate is converted. The EDA on the other hand, appears to increase in concentration rather that decrease, which is counterintuitive. This occurs because of the reaction of EDA with CO_2 to create 2-imidizolidone (2-Imid). This equilibrium is discussed in detail in section 6.4 of this thesis. With less degradation, the reaction of EDA with CO_2 occurs more slowly and EDA, therefore, builds up and appears to increase the concentration of EDA in solution compared with the baseline experiment.

The generation of total formate may occur through a free radical mechanism whose details are not yet known. Inhibitor A is thought to be a free radical or peroxide scavenger and may, therefore, inhibit formate generation during thermal degradation of PZ. With lower formate concentrations, there will be lower concentrations of FPZ and less PZ loss associated with forming FPZ. Additional oxidation products that may be produced through the free radical mechanism have not been identified.

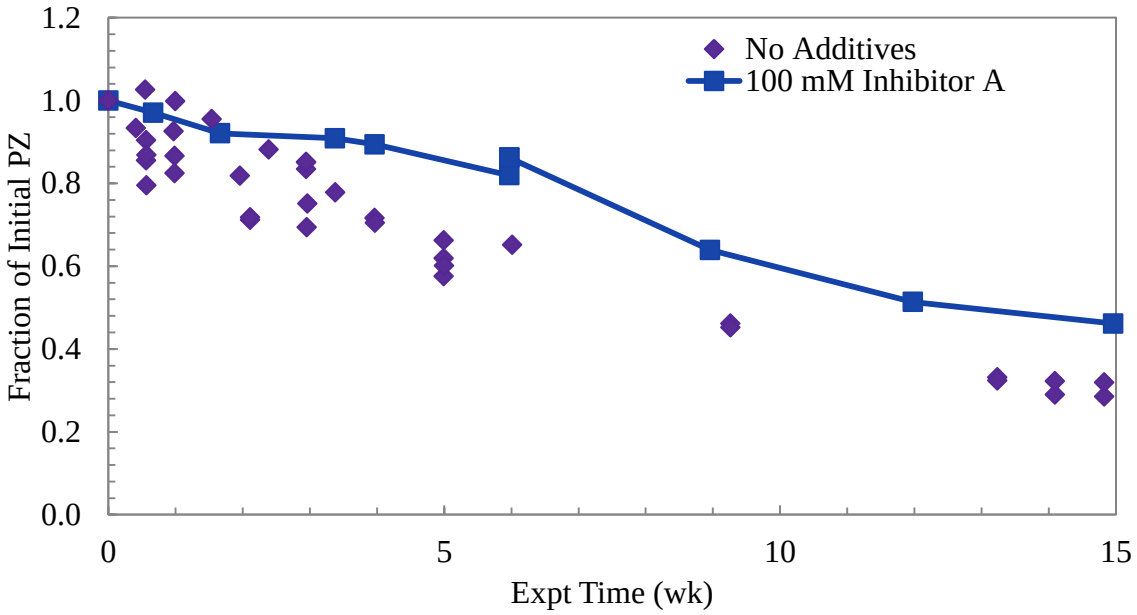

Figure 5.48: Effect of 100 mM Inhibitor A on degradation of 8 m PZ degradation with 0.3 mole CO_2 per mole alkalinity at 175 °C

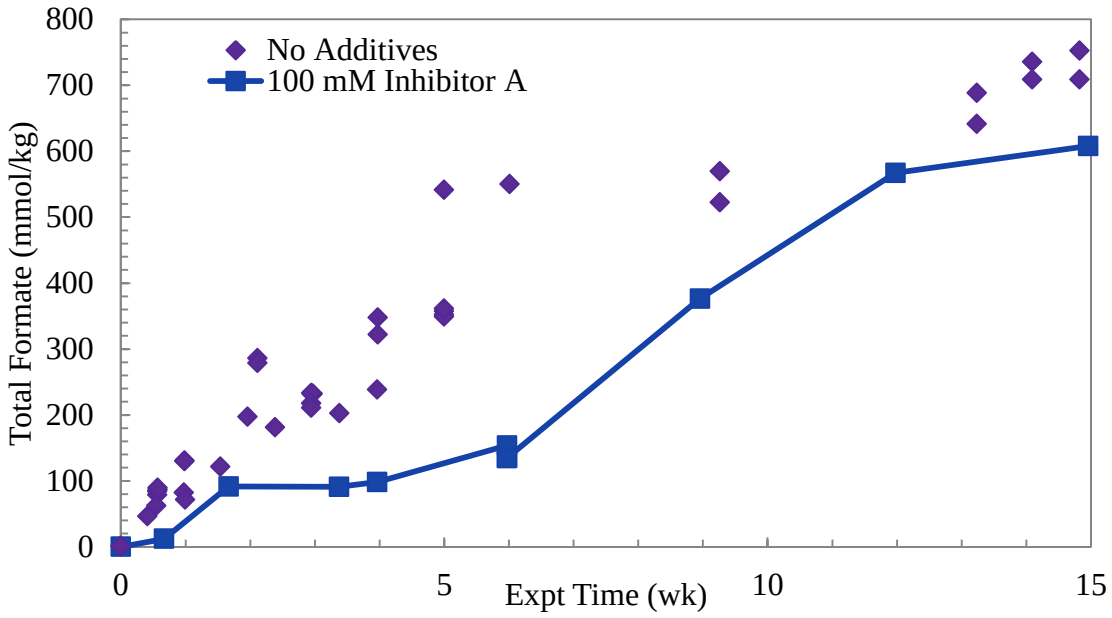

Figure 5.49: Effect of 100 mM Inhibitor A on generation of total formate during degradation of 8 m PZ with 0.3 mole CO_2 per mole alkalinity at 175 °C

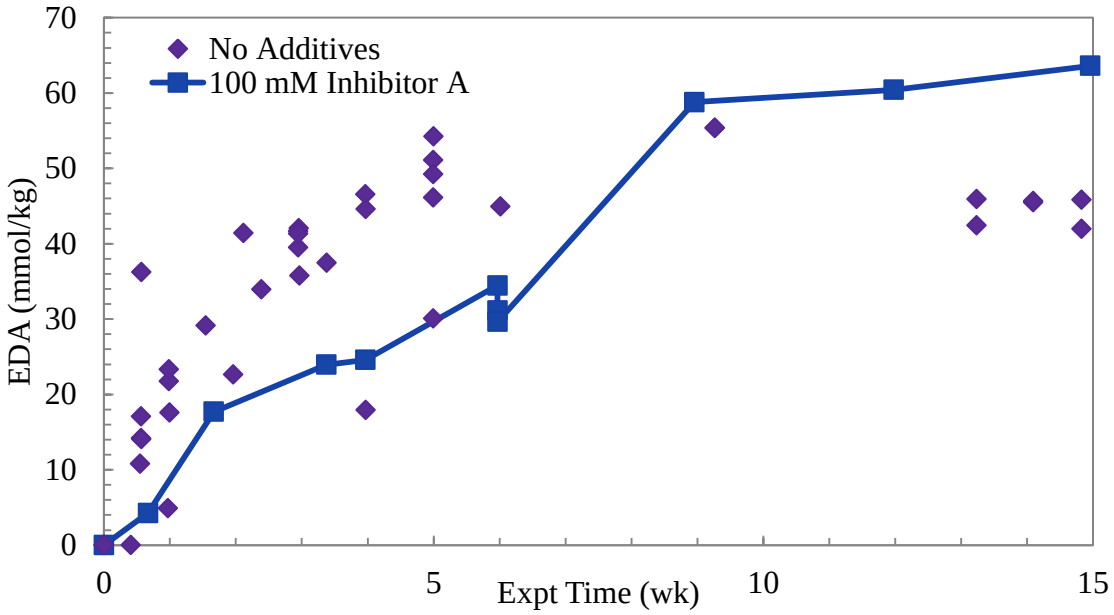

Figure 5.50: Effect of 100 mM Inhibitor A on generation of EDA during degradation of 8 m PZ with 0.3 mole CO_2 per mole alkalinity at 175 °C

The addition of Inhibitor A to a concentrated PZ solution used for CO_2 capture will not negatively affect the thermal degradation characteristics of the system. Inhibitor A caused a decrease of 20% in PZ loss in this experiment. Although different temperatures and concentrations were not tested, it does not appear that there will be an adverse effect on thermal degradation due to the presence of Inhibitor A. If any, it could cause a decrease in thermal degradation losses, which is an added advantage of the inhibitor.

5.3.4.2 Addition of 5 mM Cu^{2+} and 1 mM Fe^{2+}

To simulate a PZ solvent that is used in a carbon steel system with a Cu^{2+}-based corrosion inhibitor and a small amount of corrosion, 8 m PZ with 0.3 moles CO_2 per mole alkalinity was degraded at 175 °C in the presence of 5 mM Cu^{2+} and 1 mM Fe^{2+}. The loss of PZ for this experiment is compared with a collated set of baseline data for the

thermal degradation of 8 m PZ with 0.3 mole CO_2 per mole alkalinity at 175 °C in Figure 5.51. The generation of total formate and EDA for these experiments is compared in Figure 5.52 and Figure 5.53. Additional curves are present in this figure that will be discussed in subsequent sections.

The addition of Cu^{2+} and Fe^{2+} did not significantly affect the loss rate of PZ or the generation of total formate and EDA. The data falls in line with the baseline data without the addition of metals. It is not expected that the addition of a Cu^{2+}-based corrosion inhibitor or the accumulation of Fe^{2+} due to corrosion will accelerate thermal degradation of concentrated PZ solutions.

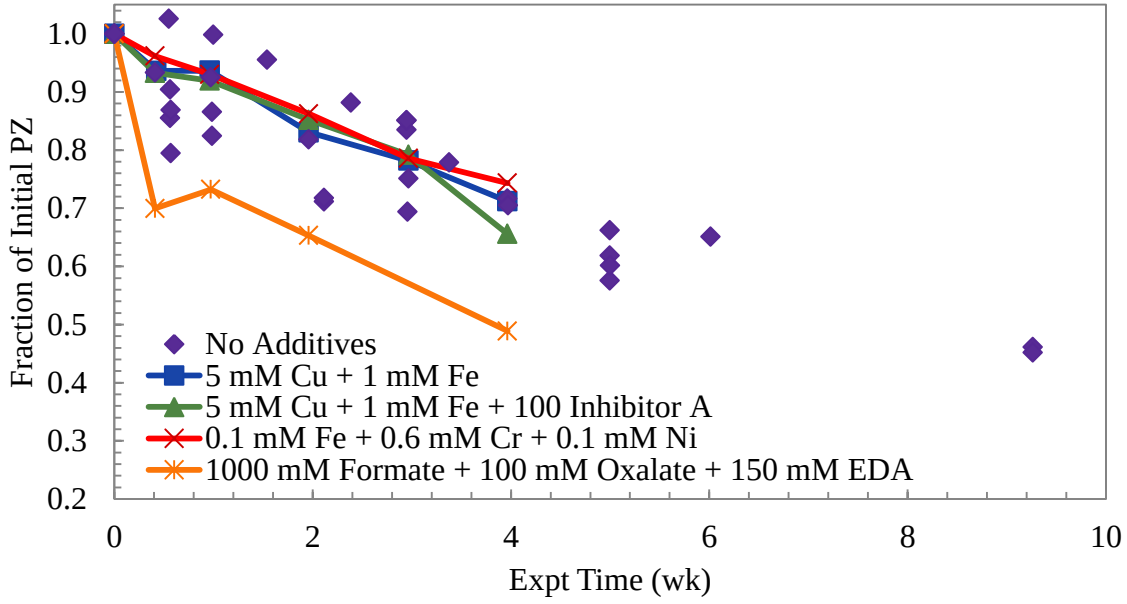

Figure 5.51: Effect of additives on the degradation of 8 m PZ with 0.3 mole CO_2 per mole alkalinity at 175 °C

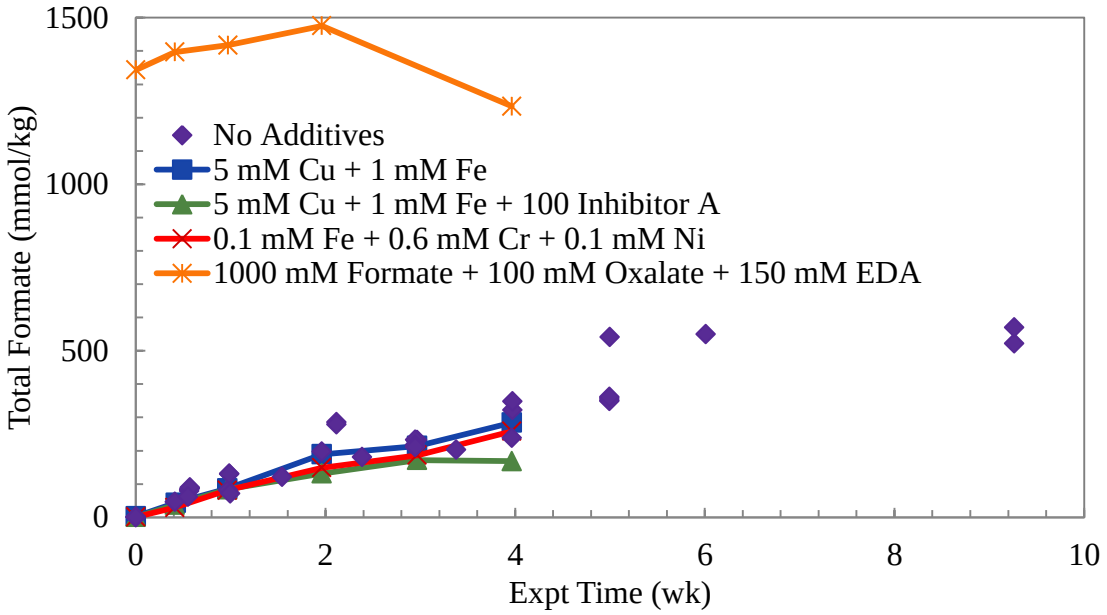

Figure 5.52: Effect of additives on the generation of total formate during degradation of 8 m PZ with 0.3 mole CO_2 per mole alkalinity at 175 °C

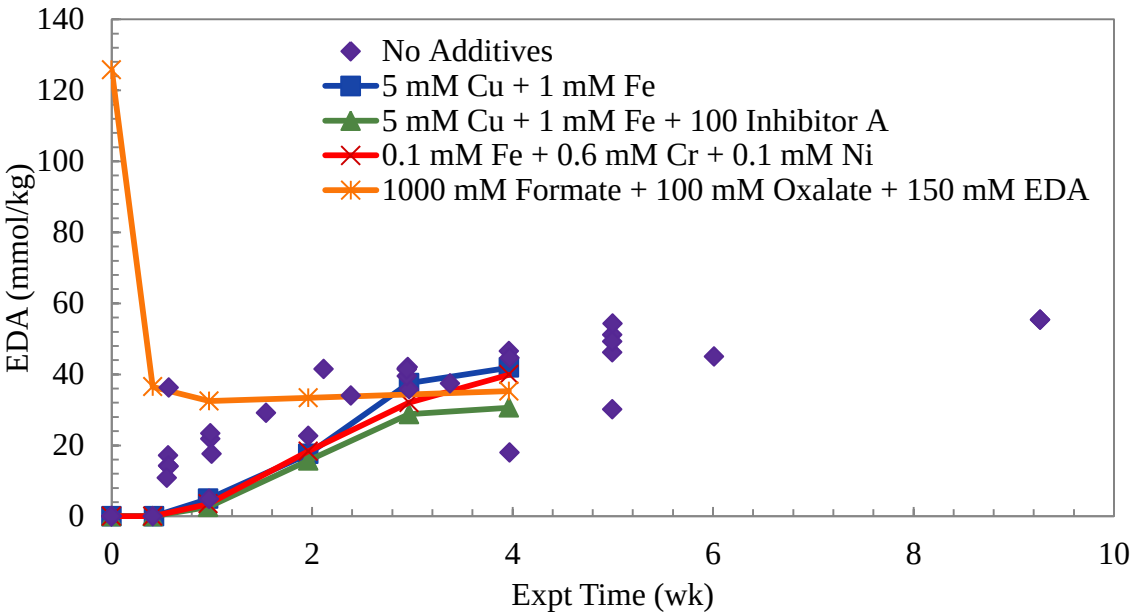

Figure 5.53: Effect of additives on the generation of EDA during degradation of 8 m PZ with 0.3 mole CO_2 per mole alkalinity at 175 °C

5.3.4.3 Addition of 5 mM Cu^{2+}, 1 mM Fe^{2+}, and 100 mM Inhibitor A

The effect of Inhibitor A on thermal degradation was confirmed through a second experiment that also simulated Fe^{2+} corrosion and the addition of a Cu^{2+}-based corrosion inhibitor. A solution of 8 m PZ with 0.3 mole CO_2 per mole alkalinity, 5 mM Cu^{2+}, 1 mM Fe^{2+}, and 100 mM Inhibitor A was degraded at 175 °C for 15 weeks. The loss of PZ, generation of total formate, and EDA production are compared with a baseline, unspiked set of data in Figure 5.51, Figure 5.52, and Figure 5.53, respectively. The solution behavior was found to be in agreement with the data in the previous two subsections as metals and Inhibitor A were not found to accelerate or inhibit thermal degradation. The rate of loss of PZ and generation of degradation products in the spiked experiment closely matched that of the unspiked condition.

5.2.4.4 Addition of 0.1 mM Fe^{2+}, 0.1 mM Ni^{2+}, and 0.6 mM Cr^{3+}

Industrial CO_2 capture systems are expected to be made from stainless steel rather than carbon steel to minimize the long term corrosive effects of amines and CO_2. The effect of metals due to stainless steel corrosion was tested by degrading 8 m PZ with 0.3 moles CO_2 per mole alkalinity at 175 °C with 0.1 mM Fe^{2+}, 0.6 mM Cr^{3+}, and 0.1 mM Ni^{2+}. The loss of PZ, generation of total formate, and EDA production are compared with a baseline, unspiked set of data in Figure 5.51, Figure 5.52, and Figure 5.53, respectively. As observed in the two previous metal spiked experiments, there was no effect from stainless steel metals on the rate of PZ loss or generation of degradation products during degradation at 175 °C.

5.3.4.5 Addition of 1000 mM Formate, 100 mM Oxalate, and 150 mM EDA

Finally, the effect of degradation products on the rate of thermal degradation was measured through the addition of formate, oxalate, and EDA, the dominant degradation

products. An 8 m PZ solution with 0.3 moles CO_2 per mole alkalinity was degraded at 175 °C in the presence of 1000 mM formate, 100 mM oxalate, and 150 mM EDA. This solution was meant to represent a highly degraded PZ solution to assess the catalytic effect of the most dominant degradation products. The loss of PZ, generation of total formate, and generation of EDA are compared with a baseline, unspiked set of data in Figure 5.51, Figure 5.52, and Figure 5.53, respectively. The equilibrium between formate and total formate is shown in Figure 5.54.

The presence of degradation products enhanced the initial loss rate for PZ. After one week, 27% of the initial PZ was degraded compared to 0-18% in the unspiked data. The rate was enhanced in the first week, but then demonstrated the same rate as seen in the unspiked experiments for the last three weeks of the experiment. The presence of formate in the initial sample created a rapid equilibrium with formyl amides, most likely N-formyl PZ (Figure 5.54). At this temperature, formate can quickly react with either PZ or EDA to form the corresponding formyl amide. This reaction with PZ could explain the high rate of loss of PZ (1200 mmole PZ per kg) after one week. EDA also rapidly reacts and reaches an equilibrium concentration of 30 to 35 mmole per kg within one week that is the same as the concentrations found in unspiked experiments. EDA is known to react quickly in solution with CO_2 to form 2-Imidazolidone (2-Imid) which is discussed in detail in section 6.5.

At the start of the experiment, the 100 mmole per kg of oxalate quickly reacted to form oxalyl amides detected in the initial sample. After the initial sample, both free oxalate and oxalyl amides reacted to an unknown product and all subsequent oxalate and oxalyl amide concentrations were less than 1 mmole per kg. It is suspected that the primary oxalyl amide was N-oxalyl piperazine and this species reacted to form N-formyl PZ or formate. Mislyuk and colleagues found that when heated, N-oxalyl PZ and N,N'-

dioxalyl PZ form N-formyl PZ and N,N'-diformyl PZ through the breaking of a C-C bond (Mislyuk et al., 1985). Górski and Kraśnicka determined that the thermal decomposition of sodium formate produced oxalate species in the presence of CO and CO_2 (Górski and Kraśnicka, 1987a). The same authors also determined that the thermal decomposition of solid, alkali oxalate compounds produced a dissociation of oxalate into CO_2 and CO_2^{-2} ion as a short lived intermediate (Górski and Kraśnicka, 1987b). A more recent study by Crossley confirmed that aqueous oxalate species thermally decompose to formate species and CO_2 at temperatures from 160-230 °C (Crossley, 1991). The decomposition of oxalate is not known under the specific conditions of this experiment, but the noticeable increase in total formate after the initial sample indicates that some or all of the oxalate ended up as formate or formyl amides. Oxalate has not been a major degradation product in any thermal degradation experiment for concentrated PZ and any production of oxalate likely ends up as formate or CO_2 species under the high temperature conditions of PZ thermal degradation.

Overall, the addition of formate, EDA and oxalate primarily affected the speciation of degradation products and their respective amides or imidazolidones, and were not found to enhance PZ thermal degradation overall.

5.3.5 Effect of the metal contamination

Previous work in literature has explored the catalytic effect of metals contamination on thermal degradation (Eide-Haugmo et al., 2011). In this work, glass cuvettes were used to line thermal degradation cylinders to prevent the contact of amine solution with the walls of the cylinders during the degradation tests. The author's hypothesis was that decreasing metals contamination would limit catalyst in solution and could potentially inhibit thermal degradation in a variety of amines. Their results

showed the same level of degradation for all amines tested except one, N-methylmonoethanolamine (MMEA) (Eide-Haugmo et al., 2011). Based on these results, concentrated PZ solutions were tested for thermal degradation with glass-lined degradation cylinders. The hypothesis was that preventing metals contamination of the amine will not change PZ stability and thermal degradation will proceed as expected at the given conditions.

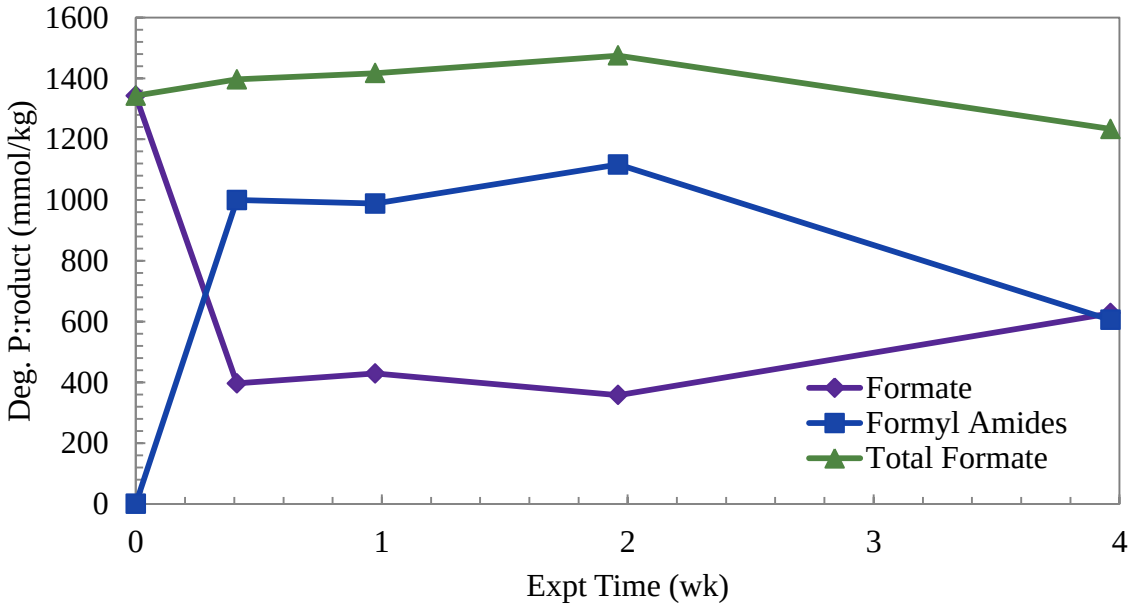

Figure 5.54: Equilibrium of formate and formyl amides in degradation of 8 m PZ at 175 °C with 1000 mM formate, 100 mM oxalate, and 150 mM EDA

With this new experimental protocol, 8 m PZ with a loading of 0.3 moles CO_2 per mole alkalinity was degraded at 175 °C for 15 weeks. The loss of PZ and generation of total formate and EDA are compared with a baseline case of thermal degradation in Figure 5.55, Figure 5.56, and Figure 5.57, respectively. As with the previous sub-section, the comparison is made with the collated thermal degradation data obtained from three experiments for 8 m PZ with 0.3 moles CO_2 per mole alkalinity degraded at 175 °C.

The concentration profiles for both PZ and degradation products indicate that the lack of metals had a nearly negligible effect on thermal degradation. The PZ loss was minimally affected, with only 1% less PZ loss observed in the glass experiment. As for degradation products, generation of total formate was decreased by 24% while EDA generation was the same as the unlined case. These measurements indicate that the mechanism responsible for the generation of formate and total formate may be sensitive to the presence of metals or may be metal catalyzed. That mechanism is discussed in greater detail in section 6.4.

The observations of Eide-Haugmo appear to be confirmed with concentrated PZ (Eide-Haugmo et al., 2011). It is important to note, however, the differences between the experimental protocols for this experiment. The cuvettes used in this experiment did not reach the top of the thermal cylinder when placed inside. That is to say, the cuvettes were too short for the standard thermal cylinders and the top of the cuvette was approximately 2 cm from the top of the cylinder. Therefore, less solution fit in the cuvette than a traditional experiment (7 mL vs. 10 mL). The extra headspace in the cylinder could have contributed to the differences seen in the figures. The CO_2 concentration in the solution would have been slightly different as the high temperature would drive CO_2 into the headspace.

Analysis of metals concentration using ICP-OES showed that there was no detectable Fe^{2+}, Ni^{2+}, or Cr^{3+}, except for one sample. The concentrations of Fe^{2+}, Ni^{2+}, and Cr^{3+} in the glass-lined experiments (TE22) are compared with two experiments with the same solution of PZ degraded in stainless steel thermal cylinders (TE12 and TE18) in Figure 5.58. The lack of metals confirms that the solutions were maintained separate from the stainless steel side walls of the solution during the glass-lined experiment.

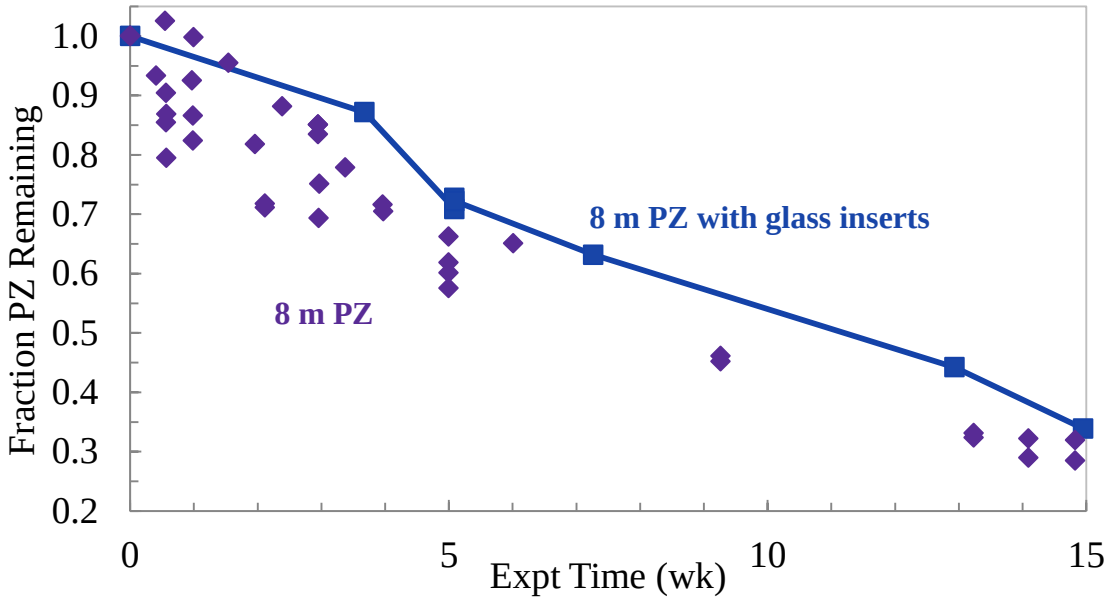

Figure 5.55: Effect of glass inserts on the degradation of 8 m PZ with 0.3 mole CO_2 per mole alkalinity at 175 °C

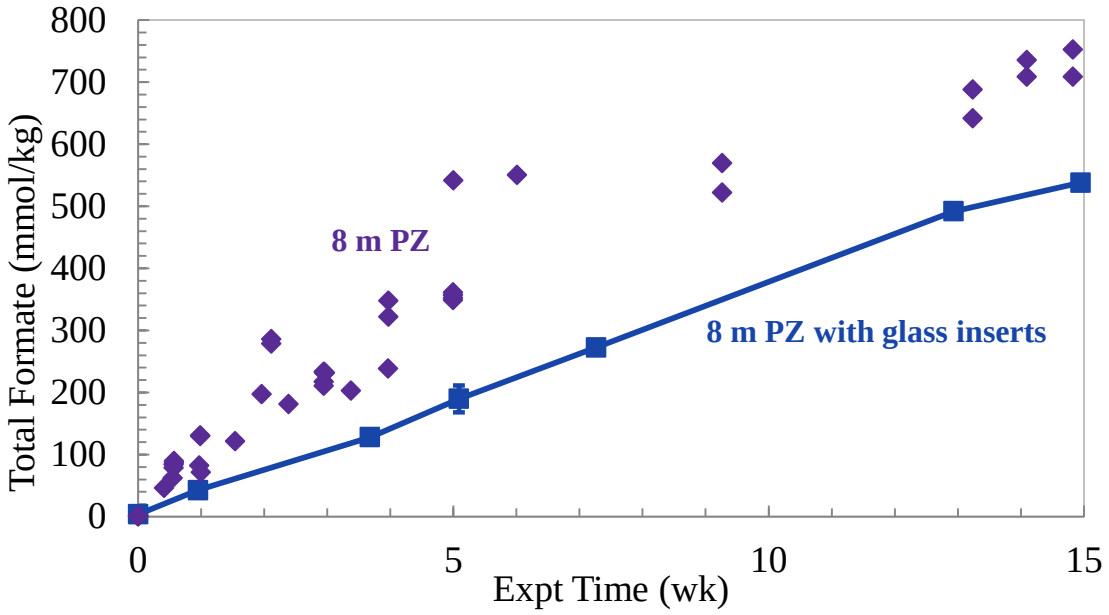

Figure 5.56: Effect of glass inserts on the generation of total formate during degradation of 8 m PZ with 0.3 mole CO_2 per mole alkalinity at 175 °C

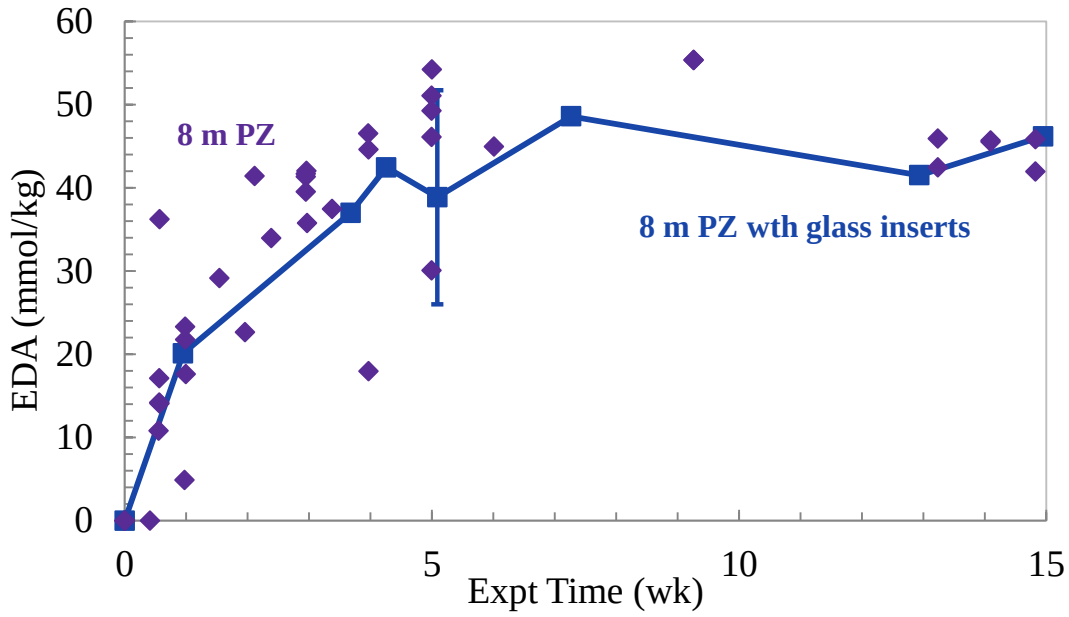

Figure 5.57: Effect of glass inserts on the generation of EDA during degradation of 8 m PZ with 0.3 mole CO_2 per mole alkalinity at 175 °C

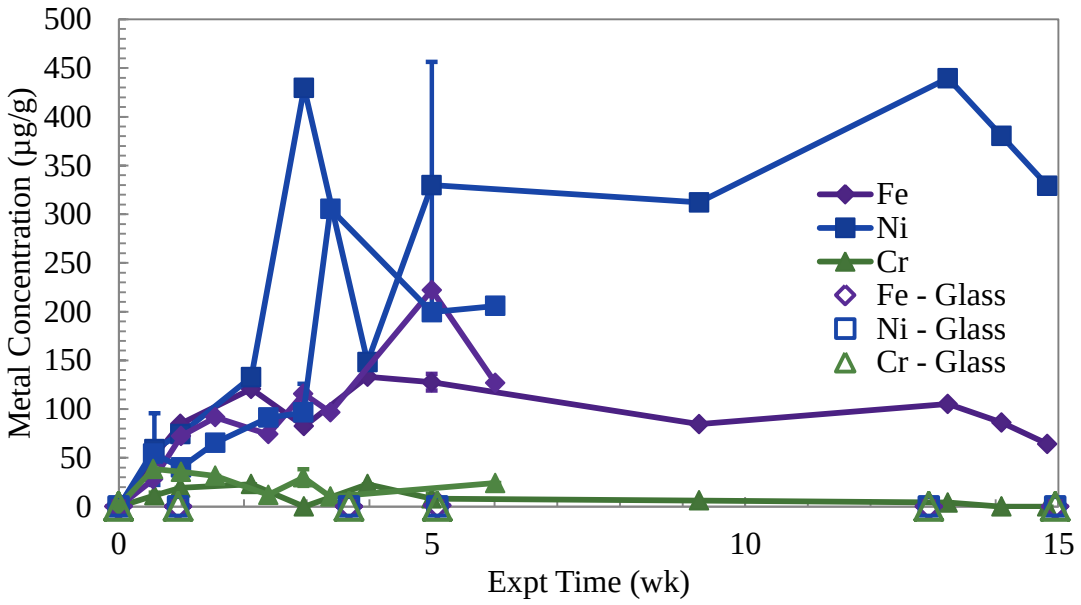

Figure 5.58: Fe^{2+}, Cr^{3+}, and Ni^{2+} concentrations for 8 m PZ with 0.3 mole CO_2 per mole alkalinity degraded at 175 °C with (open points, all sitting on x-axis) and without glass inserts (filled points).

5.3.4.1 Corrosion of stainless steel thermal cylinders

In all of the PZ thermal degradation experiments described in this chapter, no measures were taken to prevent the leaching of metals into solution, except for the experiment described in the last section. The loaded PZ solutions analyzed were exposed to the stainless steel surface for the duration of the experiment, ranging from 10 to 72 weeks, and corrosion occurred. A majority of the experimental samples were tested for metals concentration at the conclusion of the experiment using the ICP-OES as described in section 3.1.10. The corrosion tendency of PZ solutions can be assessed by analyzing the metals concentrations resulting from long-term, high temperature exposure to stainless steel.

One caveat of this analysis is the fact that the thermal cylinders were reused repetitively throughout the course of this project. Some cylinders were also used previously by other researchers and the individual histories of the cylinders were not known at the start of each experiment. When a new set of cylinders was made, it was possible to assess the fresh corrosion rate. Since the histories of the cylinders were not known with any accuracy, an estimation of the actual corrosion rate was not attempted. Instead, the tendency to corrode was assessed by comparing raw metals concentrations in solution. Also, since experimental samples are individual cylinders, there is more scatter in the metals concentration data than any other liquid phase analysis.

The concentrations of Fe^{2+}, Ni^{2+}, and Cr^{3+} during the degradation of 8 m PZ with 0.3 mole CO_2 per mole alkalinity at 150 °C are shown in Figure 5.59. This general trend in metals concentration was found for a variety of conditions where the magnitude of concentrations was similar between the three metals and all usually reached some sort of equilibrium concentration quickly where there was not more metal leached into the solution. The Fe^{2+}, Ni^{2+}, and Cr^{3+}, concentrations are compared for experiments at 135 to

175 °C in Figure 5.60, Figure 5.61, and Figure 5.62, respectively. As expected, the overall trend is that more corrosion is occurring at higher temperatures, evidenced by the increasing concentrations of metals in solution as experimental temperature increases.

The relative corrosion rate of various amines can be inferred by comparing the metals concentrations in degraded solutions. The concentration of Fe^{2+}, Ni^{2+}, and Cr^{3+} is compared for 8 m PZ with 0.3 mole CO_2 per mole alkalinity and 7 m MEA with 0.4 mole CO_2 per mole alkalinity degraded at 135 °C in Figure 5.63. MEA solutions have a higher tendency to corrode stainless steel, as shown by the high levels of metals found in degraded MEA solutions. There was 275, 15, and 32 times more Fe^{2+}, Ni^{2+}, and Cr^{3+}, respectively, found in degraded, loaded MEA than PZ. This enhanced corrosion activity may also be influenced by the fact that the MEA solutions are much more degraded at 135 °C than PZ which is thermally resistant. The limited corrosion tendency of PZ is also demonstrated when compared to the accumulation of metals in degrading EDA and 3-(methylamino)propylamine (MAPA). In Figure 5.64 the concentration of Fe^{2+} is compared for 8 m PZ with 0.3 mole CO_2 per mole alkalinity, 7 m MEA with 0.4 mole CO_2 per mole alkalinity, 8 m EDA with 0.4 mole CO_2 per mole alkalinity, and 9 m MAPA with 0.4 mole CO_2 per mole alkalinity all degraded at 135 °C (Rochelle, 2010b; Vevelstad, 2010; Zhou et al., 2010). PZ has the lowest concentration of Fe^{2+} in solution followed by MAPA, MEA, and then EDA in order of increasing tendency to corrode.

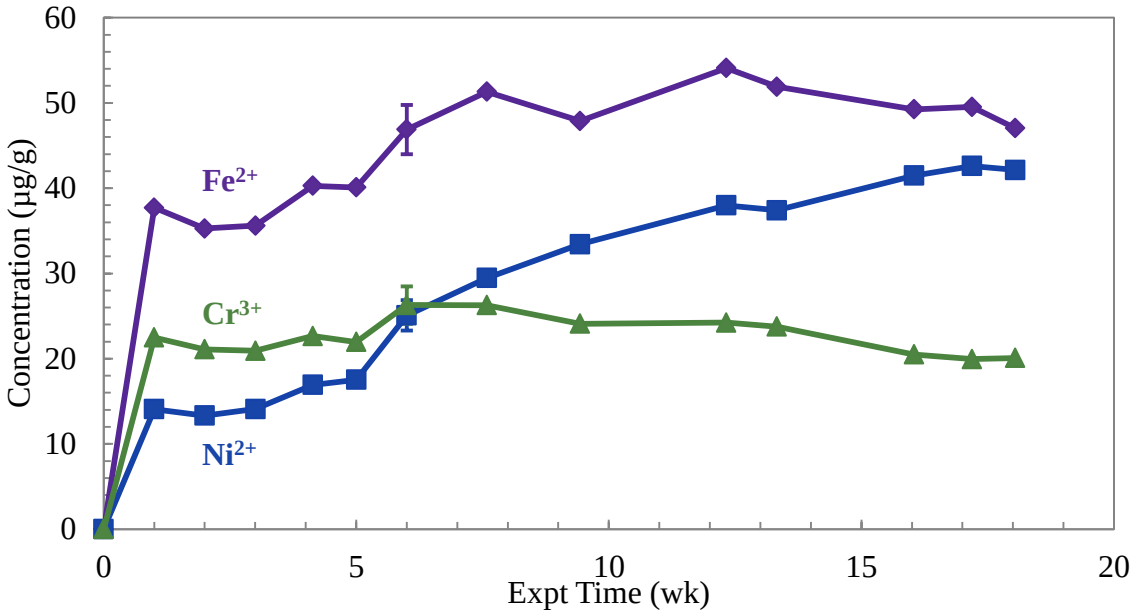

Figure 5.59: Leaching of Fe^{2+}, Ni^{2+}, and Cr^{3+} during the thermal degradation of 8 m PZ with 0.3 mole CO_2 per mole alkalinity at 150 °C

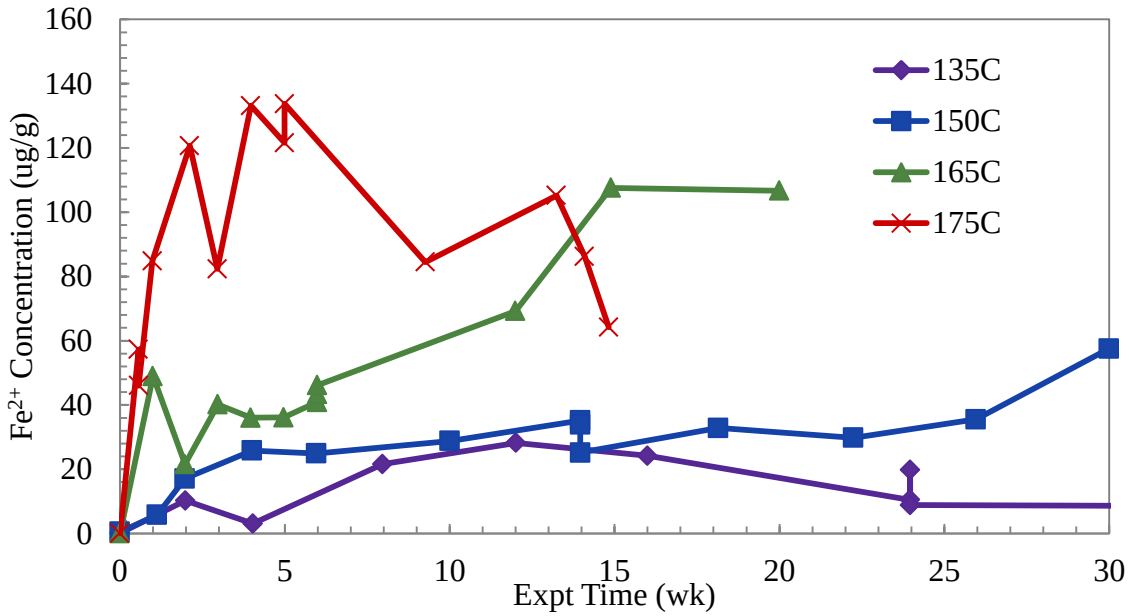

Figure 5.60: Fe^{2+} concentration for thermal degradation of 8 m PZ with 0.3 mole CO_2 per mole alkalinity degraded at 135 to 175 °C

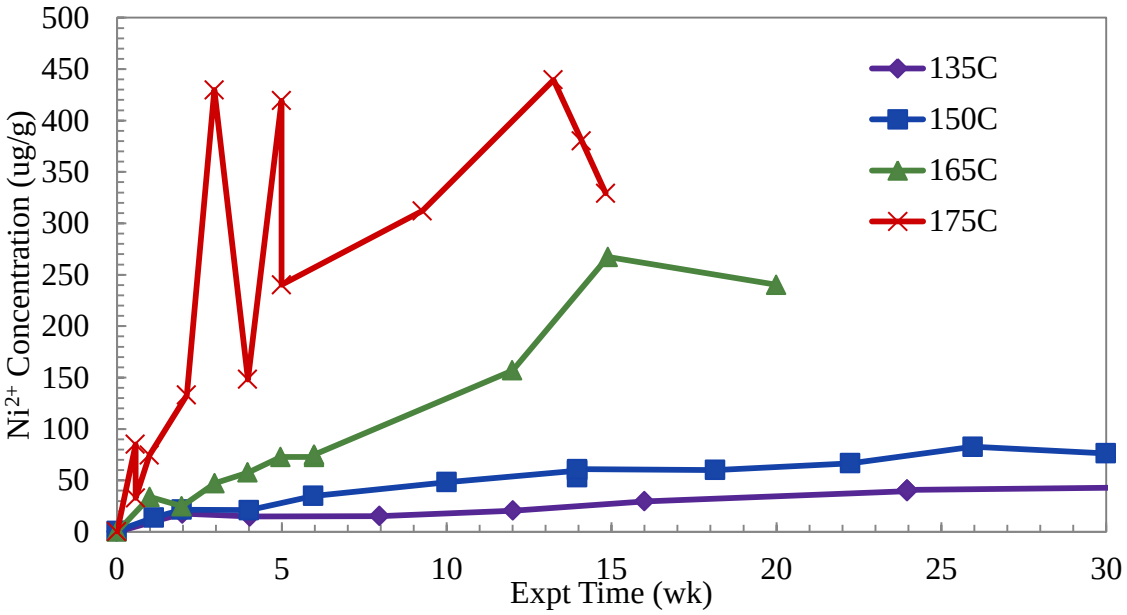

Figure 5.61: Ni^{3+} concentration for thermal degradation of 8 m PZ with 0.3 mole CO_2 per mole alkalinity degraded at 135 to 175 °C

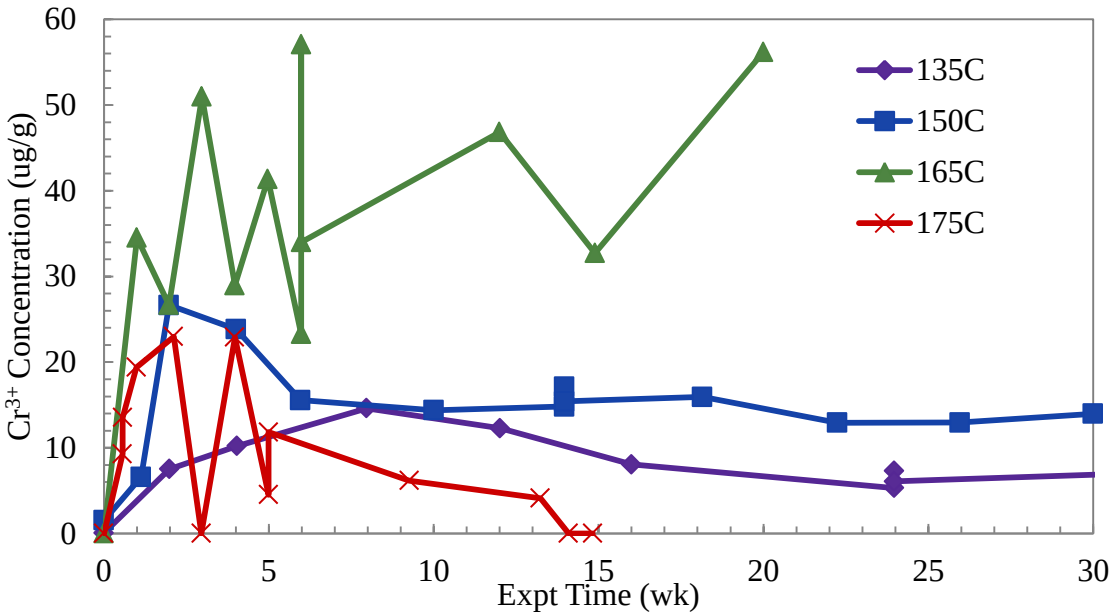

Figure 5.62: Cr^{3+} concentration for thermal degradation of 8 m PZ with 0.3 mole CO_2 per mole alkalinity degraded at 135 to 175 °C

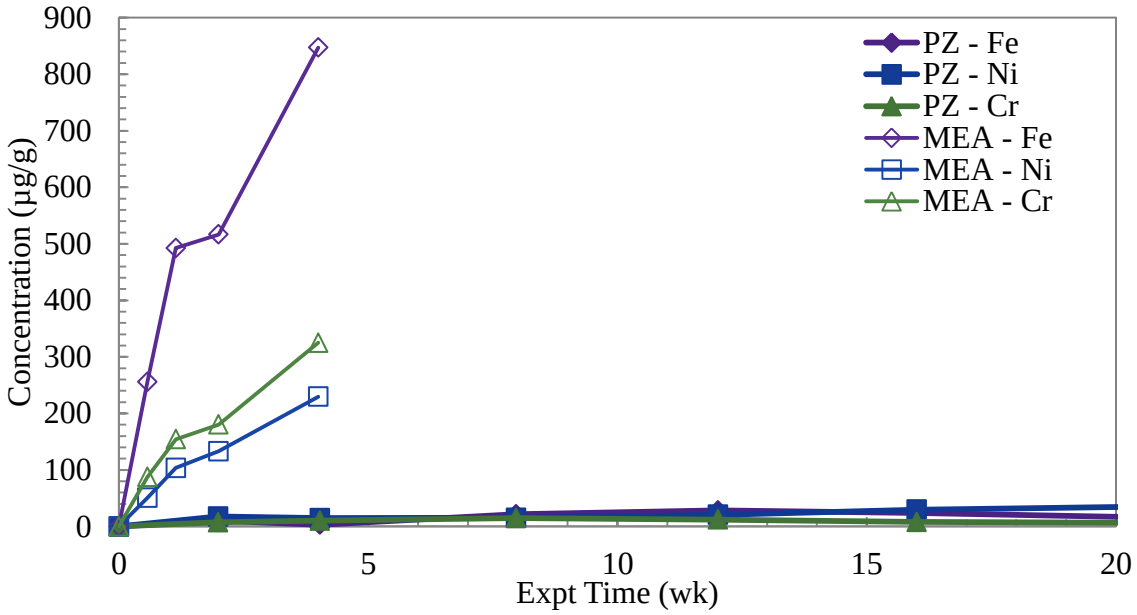

Figure 5.63: Comparison metals content for 8 m PZ with 0.3 mole CO_2 per mole alkalinity (filled points) and 7 m MEA with 0.4 mole CO_2 alkalinity (open points) degraded at 135 °C

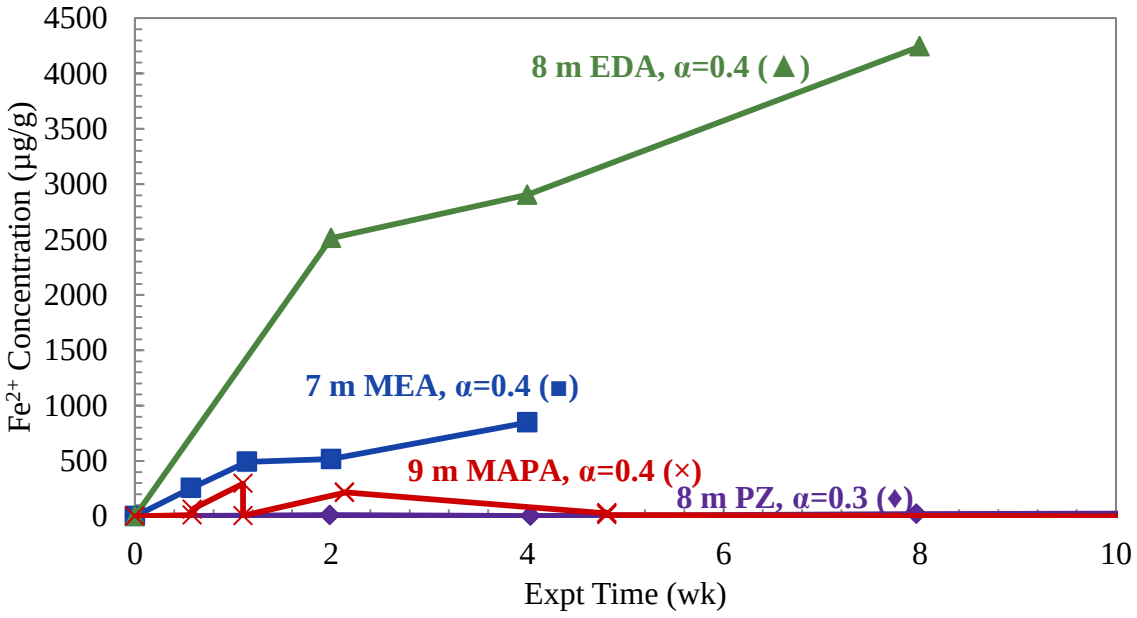

Figure 5.64: Comparison of Fe^{2+} concentration in thermally degraded solutions of PZ, MEA, EDA (Zhou et al., 2010), and MAPA (Vevelstad, 2010)

5.4 SUMMARY OF FIRST-ORDER RATE CONSTANTS FOR PZ EXPERIMENTS

The calculated k_1 values for a variety of experiments can now be compared in order to understand the global behavior of concentrated PZ during thermal degradation. The k_1 inherently changes with temperature, as demonstrated in the previous section, so the effect of CO_2 concentration and PZ concentration will be evaluated. The k_1 values for 8 m PZ over a range of CO_2 loading and temperatures are shown in Figure 5.65. For conditions with data at multiple temperatures, the linear behavior confirms Arrhenius temperature dependence for a range of loadings. For the unloaded case, the trend is impacted by the fact that at there is limited degradation occurring at 150 °C. This trend is observed throughout this project where the error in the lowest temperature measured is higher due to the confidence at which the cation IC can measure small changes of less that 5% in amine concentration.

The Arrhenius equation can be derived using a linear regression through data plotted for the logarithm of k_1 against inverse temperature. This is a linear regression through the data in Figure 5.65, for example. The Arrhenius equation for the k_1 value of 8 m PZ with 0.3 or 0.4 mole CO_2 per mole alkalinity are shown in Equations 5.13 and 5.14. For Equation 5.8, the data obtained at 135 °C were omitted from regression.

$$k_1 = 2.78\times10^{14}\cdot\exp\left(\frac{183.5\,\text{kJ}}{\text{mole}}\cdot\frac{1}{RT}\right) \tag{5.13}$$

$$k_1 = 3.19\times10^{15}\cdot\exp\left(\frac{191.4\,\text{kJ}}{\text{mole}}\cdot\frac{1}{RT}\right) \tag{5.14}$$

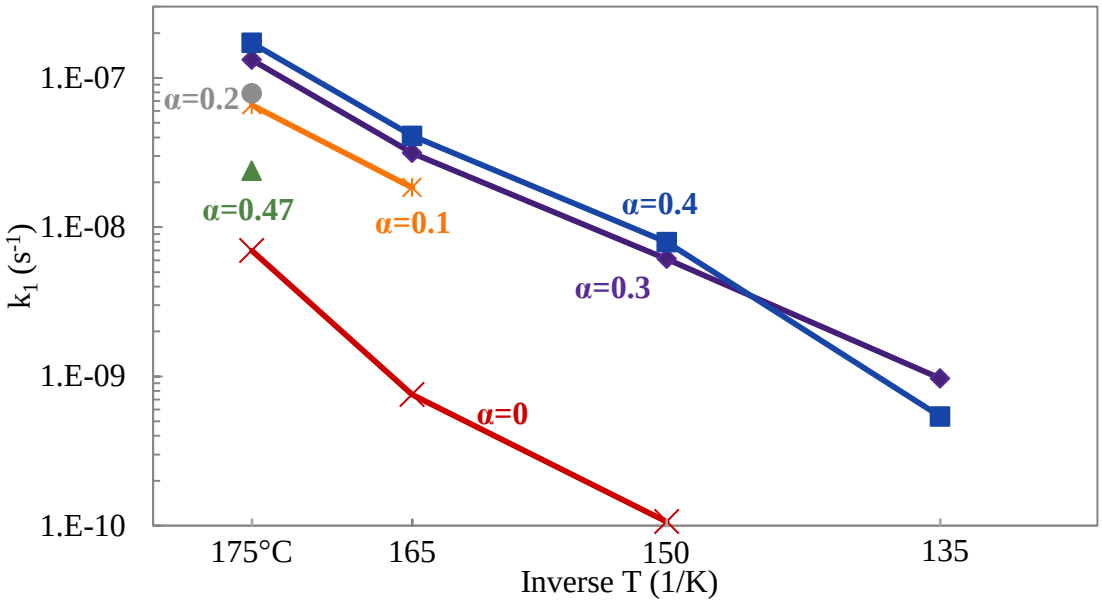

Figure 5.65: Values of k_1 for 8 m PZ with 0 to 0.47 mole CO_2 per mole alkalinity

The k_1 values for 4 to 20 m PZ at either 0.1 or 0.3 moles CO_2 per mole alkalinity are compared in Figure 5.66. For 20 m PZ with 0.3 mole CO_2 per mole alkalinity, the regression for k_1 was done over the first 6 weeks of the experiment, rather than the entire 15 weeks of data due to non-first order behavior. This value is therefore an apparent first order rate constant because more complex mechanisms are likely involved in this particular solution. As PZ concentration increases from 4 to 20 m for solutions with 0.3 mole per mole alkalinity, the k_1 value increases only a small amount. This matches data from section 5.2.2 where PZ loss was found to be only a slight function of amine concentration. The lean loaded 20 m PZ had a lower k_1 value than 8 m PZ. The speciation of 20 m PZ and activity of water are expected to be quite different in these two solutions, perhaps leading to a suppressed degradation rate in the concentrated solution. The data for 10 m PZ demonstrates enhanced error in the data at 135 °C where the degradation rate was difficult to measure accurately.

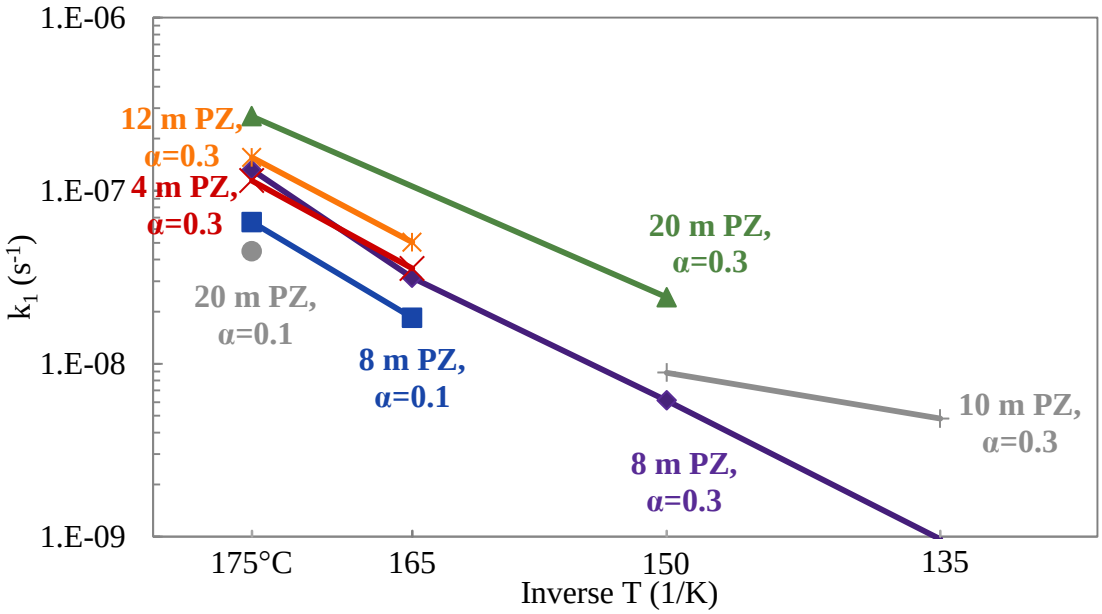

Figure 5.66: Values of k_1 for 4 to 20 m PZ with 0.1 or 0.3 mole CO_2 per mole alkalinity

The k_1 values for all experiments exploring the thermal degradation of PZ are summarized in Table 5.1. The k_1 values are presented in a simplified form ($\times 10^9$) to allow more direct comparison of values. Two experiments, TE1A and TE3B, are not included in this summary table due to difficulty in accurately quantifying a k_1 value. In the case of TE1A, 10 m PZ with 0.4 moles CO_2 per mole alkalinity was degraded at 135 °C but its degradation rate was found to be higher than a complimentary experiment at 150 °C. In the case of TE3B, 15 m PZ with 0.3 moles CO_2 per mole alkalinity was degraded but its degradation rate was found to be positive, giving a negative k_1, due to a quantified increase of PZ concentration during the experiment. Both of these experiments were done early in the project and the calculated k_1 values were determined to contain a large amount of error given the difficulty of measuring degradation rates accurately on the cation IC at low temperature.

In chapter 7, the k_1 values discussed here will be compared with that of substituted PZs, PZ structural analogs, and other CO_2 capture amines to put the PZ data in perspective. The greatest strength of concentrated PZ solvents is its thermal resistance. The stability of this solvent to high temperature allows for energy advantages that will decrease costs and extend solvent lifetimes. The comparisons in chapter 7 to other CO_2 capture amines will highlight this advantage.

5.5 CONCLUSIONS

At 150 °C, 8 m PZ with 0.3 mole CO_2 per mole alkalinity thermally degrades with a first order rate constant of 6.12×10^{-9} s^{-1}, or approximately 500 mmole PZ lost per kg solution after 30 weeks. PZ thermal degradation is approximately first order in PZ and can be described effectively with a first rate constant, k_1, with Arrhenius temperature behavior. For 8 m PZ with the expected lean loading of 0.3 mole CO per mole alkalinity, the fraction of PZ remaining (F_{PZ}) is provided by the following set of equations that include a temperature dependence of k_1.

$$F_{PZ} = F_{PZ,0} \cdot \exp(-k_1 \cdot t) \tag{5.4}$$

$$k_1 = 2.78 \times 10^{14} \cdot \exp\left(\frac{183.5\,\text{kJ}}{\text{mole}} \cdot \frac{1}{RT}\right) \tag{5.13}$$

The activation energy of the system was determined to be 183.5 kJ per mole. At the rich loading condition, 8 m PZ with 0.4 mole CO_2 per mole alkalinity experiences slightly faster PZ loss according the following equation.

$$k_1 = 3.19 \times 10^{15} \cdot \exp\left(\frac{191.4\,\text{kJ}}{\text{mole}} \cdot \frac{1}{RT}\right) \tag{5.14}$$

The activation of the rich loaded condition was determined to be 191.1 kJ per mole. Both activation energies are higher than hypothesized based on the results of Davis which found the activation energy for six MEA degradation reactions to range from 131 to 144 kJ per mole (Davis, 2009). The activation energies suggest that temperature has a stronger effect on concentrated, aqueous PZ than MEA.

At 175 °C, PZ degradation occurred at a maximum rate between 0.3 and 0.4 mole CO_2 per mole alkalinity. The degradation increased as a linear function of CO_2 loading from 0 to 0.3 mole CO_2 per mole alkalinity, and then decreased from 0.4 to 0.47 mole CO_2 per mole alkalinity. This behavior suggests that solution speciation, dictated by CO_2 loading, strongly affects thermal degradation. Model predictions of speciation at 175 °C do not indicate one species is solely responsible for this behavior, but it is rather a combination of H^+PZ, $PZCOO^-$, and H^+PZCOO^- concentrations.

On the whole, PZ loss during thermal degradation is first order in PZ loss, as is the basis of the k_1 analysis. A slight effect of increasing PZ concentration was observed that increases the k_1 value approximately 30% between 4 and 12 m PZ solutions at the same conditions (0.3 mole CO_2 per mole alkalinity, 175 °C). Highly concentrated PZ solutions do not match this behavior and degradation kinetics of more than first order was observed in 20 m PZ with 0.3 mole CO_2 per mole alkalinity. The equilibrium between the concentrations of formate and formyl amides is affected by increased PZ concentration as more amides are produced in the presence of higher concentration PZ.

The addition of 100 mM of Inhibitor A decreased PZ loss by 20%. Total formate and EDA generation also and indicated less degradation in the inhibited case. It is possible that Inhibitor A, a free radical scavenger, inhibits formation of formate. The addition of 5 mM Cu^{2+}, 0.4 mM Fe^{2+}, 0.1 mM Cr^{3+}, or 0.05 mM Ni^{2+} did not affect overall PZ loss rates or the generation of degradation products. Solutions degraded in the

absence of metals were found to have slightly repressed rates of generation of formate and formyl amides. It is likely that the mechanisms responsible for these species, potentially free radical mechanisms, are catalyzed by metals and impeded by Inhibitor A.

Concentrated PZ has decreased tendency to corrode stainless steel metals in comparison to MEA, EDA, and MAPA based on the concentration of leached metals during thermal degradation.

Chapter 6 – Thermal Degradation Products and Insights into Thermal Degradation Pathways

The degradation characteristics of concentrated PZ were discussed in Chapter 5 in terms of PZ loss and the generation of three tracer products. In this chapter, the remaining degradation products produced during those experiments will be discussed in detail including the variety of products detected and quantified, other suspected but not confirmed products, and potential reaction pathways to explain the more abundant molecules. Experiments targeted at identifying particular products or mechanisms are discussed along with experiments designed to measure basic PZ thermal degradation.

6.1 Proposed thermal degradation pathways

Thermal degradation of PZ produces a wide variety of molecules as degradation products. The chemical mechanisms involved in producing each known product are not

yet clear, but an overall set of pathways was developed that involves typical reactions and can describe the generation of the major products. This proposed set of pathways is meant for illustrative purposes and is not known at this time to be correct with complete confidence. The purpose is to suggest the types of reactions believed to be occurring and offer examples of how particular degradation products may be formed. Further research into specific reaction pathways may disprove any portion of the mechanism.

The thermal degradation of concentrated PZ can be described as proceeding with four types of reactions: secondary S_N2 type substitution reactions, elimination reactions, urea generation, and formate generation from CO_2-containing molecules. The S_N2 label indicates a reaction that is nucleophilic, bimolecular (2 molecules) substitution (McMurry, 2000). Nucleophilic substitutions, as described by S_N2 reactions, are believed to be the most prominent type of degradation reaction due to the strong nucleophilic nature of PZ and its substituted products. In the S_N2 reactions of PZ, the α-carbon to an amino function or protonated amino function is subject to attack that can occur at either secondary or tertiary amines. The pathway for formate generation is the least clear mechanism of those discussed and the general attributes of the mechanism will be discussed, rather than specific reactions.

It should be noted that the influence of speciation on all of the reactions discussed is currently unknown. The reactions described below that include attacking reactive sites or functional groups being attacked should be considered as just the active site discussed, while the rest of the molecule may be in a difference form. For example, in Equation 6.1 where PZ is shown attacking the α-carbon to a protonated PZ, it is just the amino group of the attacking PZ and the protonated amino group that are of interest to the reaction. The reaction may actually proceed with free amino group on either $PZCOO^-$ or H^+PZ while the attacked protonated amino function could be on H^+PZ, H^+PZH^+, or H^+PZCOO^-,

because all exist in a CO_2-loaded solution. Reactions likely occur with any combination of the molecules present, with the rate of reaction being dependent on the individual reacting species. Overall, a particular pair may dominate, such as PZ and H^+PZ, but all of the species are likely involved in quick reaction and equilibrium steps. All of the following reactions are proposed and the effect of speciation is a large consideration when discussing the degradation of loaded, concentrated PZ.

6.1.1 Secondary S_N2 type substitution reactions

S_N2 substitution reactions of PZ and its related molecules probably account for a large portion of the degradation products. The first step in high temperature degradation of PZ is most likely the attack of H^+PZ at the α-carbon by another PZ molecule that proceeds through an intermediate complex. The product is 1-[2-[(2-aminoethyl) amino]ethyl] PZ (AEAEPZ), as shown in equation 6.1. The exact form of the intermediate complex is not known and this is a suggested form. Further S_N2 reactions will not include any hypothesized intermediate complexes.

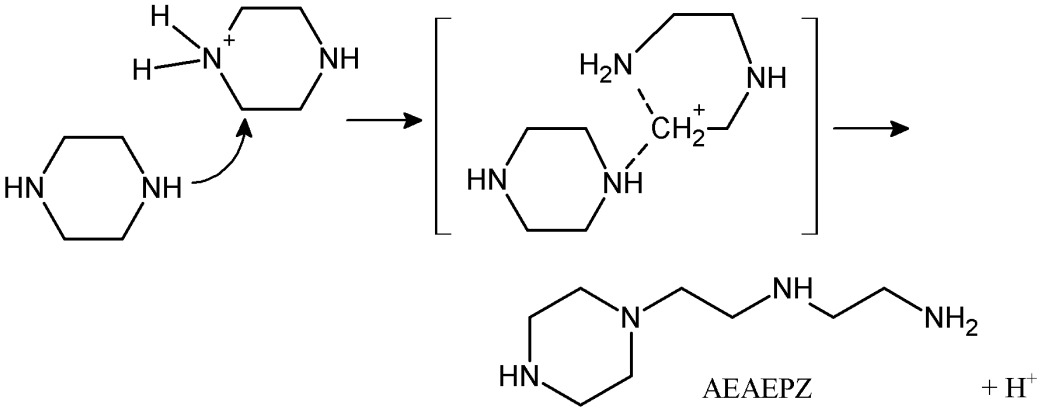

(6.1)

In the presence of CO_2, AEAEPZ should react with CO_2 in solution to produce its internal urea. It is believed that both of these molecules are present in solution and exist

in equilibrium based on the observation of other cyclic ureas in solution (see section 6.5). This equilibrium is shown in Equation 6.2.

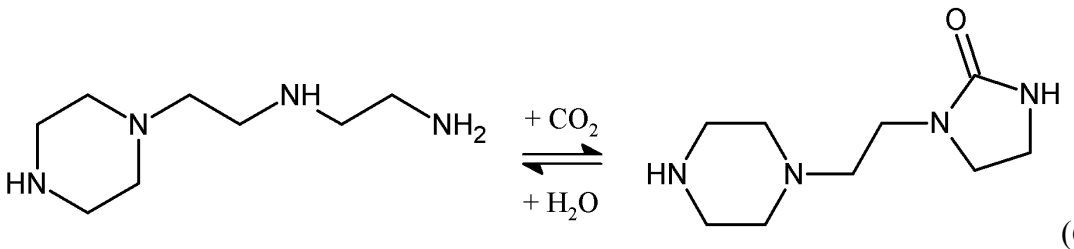

(6.2)

CO_2 will also populate the solution with the carbamates formed by reversible reaction with primary and secondary amine functions. The carbamates rapidly equilibrate so that the respective free amine is still available for S_N2 reactions and free CO_2 is available for urea formation.

Once AEAEPZ and its urea are formed, a variety of other S_N2 type reactions can occur to produce degradation products. The reaction mixture can be complicated very quickly when all of the potential nucleophiles and attack sites are considered. First, only PZ will be considered as the attacking nucleophile, but analogous reactions could potentially be occurring by other nucleophiles in solution such as amine degradation products (e.g. ethylenediamine (EDA)). Until a significant amount of PZ has been lost to degradation, it is the most likely nucleophile due to its abundance in solution.

At the elevated temperature of thermal degradation, the urea of AEAEPZ will be in equilibrium with AEAEPZ itself. S_N2 reactions involving both AEAEPZ and the urea of AEAEPZ are suspected to proceed in a similar fashion. One example of S_N2 reaction of the urea of AEAEPZ will be provided (Equation 6.3) while the remaining examples will be shown using AEAEPZ. All of the potential reactions are not laid out here, but could be predicted to produce the same molecules plus a CO_2 molecule.

PZ can attack and cause an S_N2 substitution at multiple points on the AEAEPZ molecule, assuming the amino function can be protonated. If the terminal amino function is protonated on the urea of AEAEPZ, an ammonia (NH_4^+), CO_2, and quintamine molecule are produced (Equation 6.3). This is an example of the reaction occurring on with urea of AEAEPZ while the remaining reactions occur with AEAEPZ. For the following examples of S_N2 reactions, the residual proton is shown on the original nitrogen to clarify the structures produced and maintain a charge balance, rather than to suggest a specific detailed mechanism

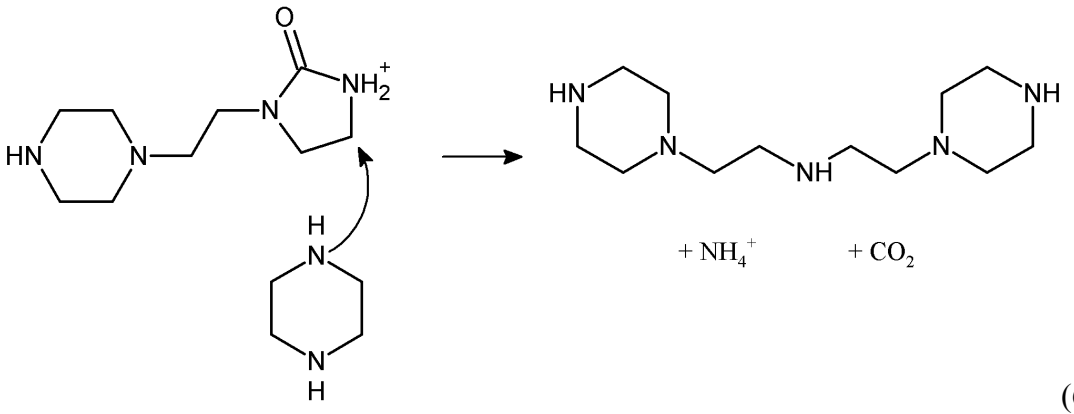

(6.3)

If the internal secondary amino function is protonated, or exists as the cyclic urea, either of its α-carbons can be attacked to produced different molecules. First, if the carbon on the right is attacked, two N-(2-aminoethyl) piperazine (AEP) molecules are produced (Equation 6.4).

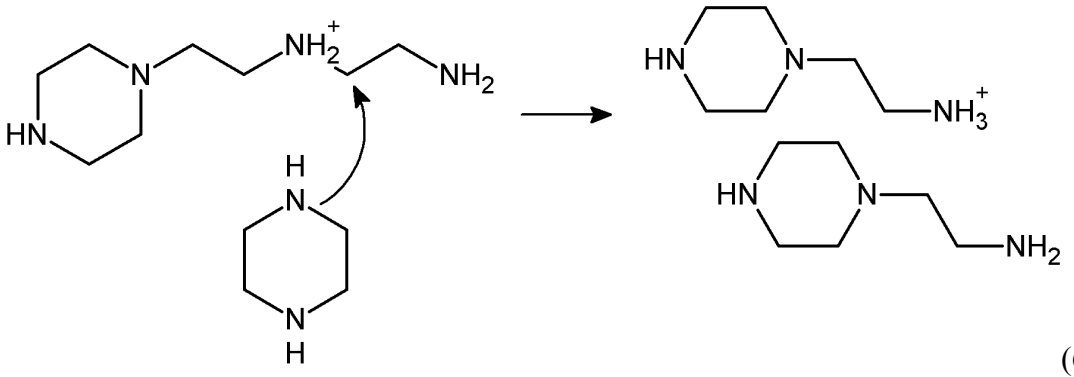

(6.4)

If the carbon on the left is attacked, an EDA and 1,1'-(1,2-ethanediyl)bis-PZ (PEP) are produced (Equation 6.5).

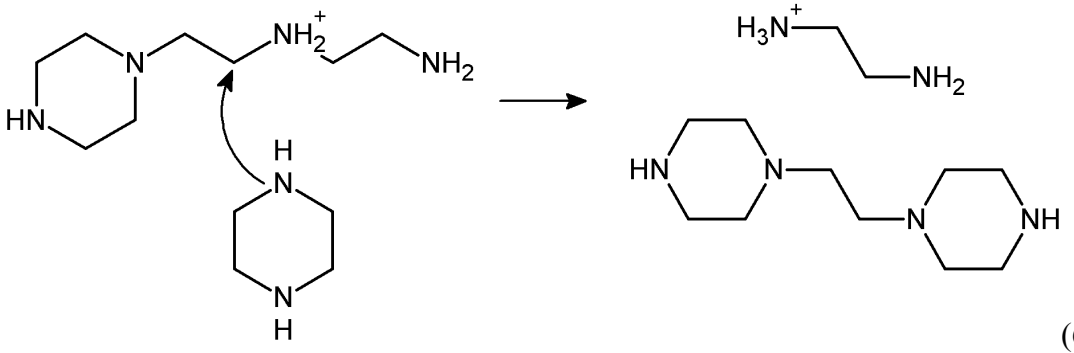

(6.5)

If either of the amino functions within the cyclic PZ structure are protonated, which is less likely, either the reactants are regenerated (Equation 6.6) or long chain PZ hexamines are produced (Equations 6.7 and 6.8). The long chain PZ hexamines are expected to be only minor products if they are produced. It could be further hypothesized that these types of long-chain monoamines could react further to create molecules such as diethylenetriamine (DETA), triethylenetetramine (TETA), tetraethylenepentamine (TEPA), or other polymeric ethylenediamine molecules.

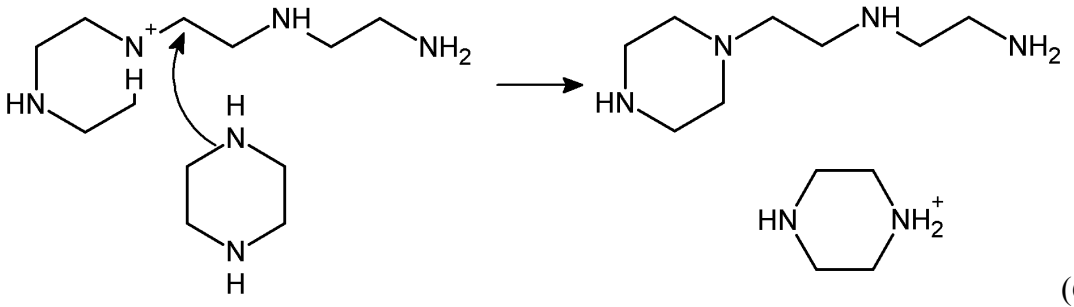

(6.6)

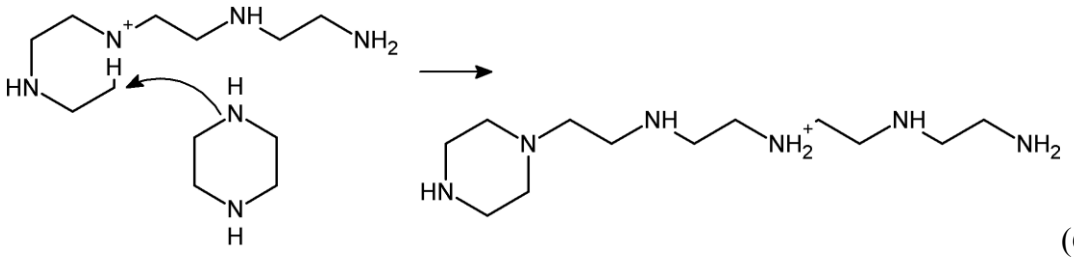

(6.7)

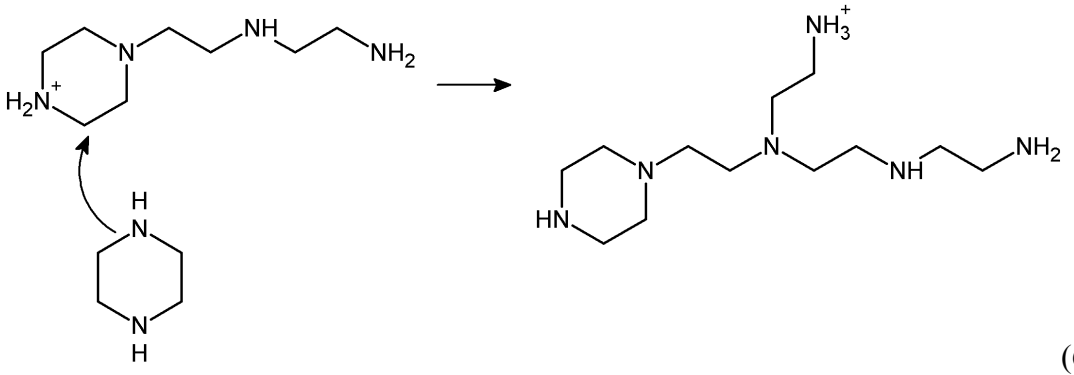

(6.8)

Further S_N2 reaction of the quadramine produced in Equation 6.3 could be proposed that produces AEP and PEP (Equation 6.9)

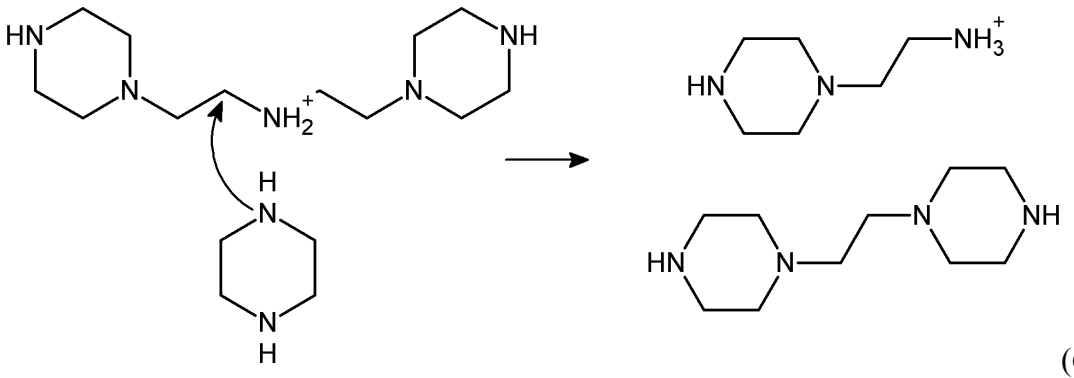

(6.9)

All of the above reactions consider PZ as the attacking nucleophile in S_N2 substitution reactions. EDA, AEP, N-(2-hydroxyethyl)piperazine (HEP), or any of the other degradation products could also act as a nucleophile. The tendency to attack depends on the pKa of the attacking amino group and the concentration in solution. The following reactions are examples of the products that could be formed if AEP was the attacking nucleophile. First, if AEP attacked another AEP molecule, PZ and N,N'-di(2-aminoethyl) piperazine (DAEP) are produced (Equation 6.10). DAEP is expected to be only a minor product and could be generated with this type of reaction which is essentially an arm-switching reaction.

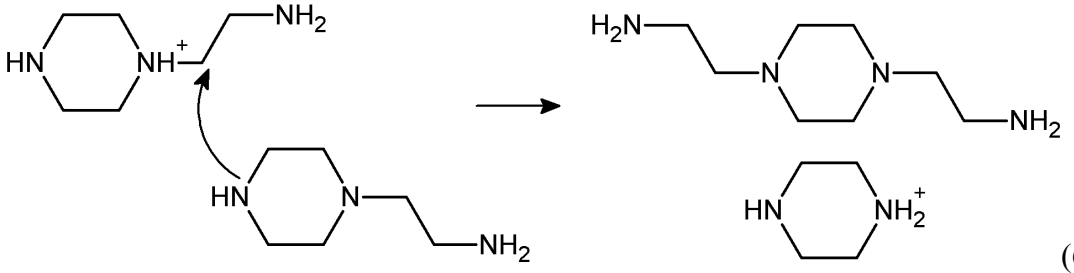

(6.10)

If PZ was the attacking molecule in the above reaction (Equation 6.10), the reactants would be generated again. If the terminal amino function on AEP was protonated instead, an ammonia and a polyAEP structure would be produced (Equation 6.11). This could be another route to generate the NH_4^+ quantified in solution.

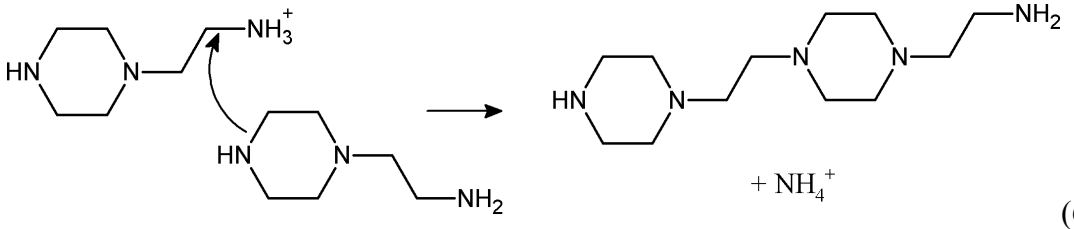

(6.11)

S_N2 type reactions in the presence of PZ can generate a variety of products as shown in the reactions above. Those shown are likely only a subset of the potential reactions and an extrapolation of the reactions here could be proposed that included every kind of attacking nucleophile and molecule being attacked. Included in the reactions shown are plausible routes to produce EDA, AEP, and NH_4^+, quantified degradation products in thermally degraded PZ. Also, AEAEPZ, the urea of AEAEPZ, and PEP were produced, which are all important suspected intermediates.

6.1.2 Elimination reactions

Another type of reaction that is believed to be occurring in thermally degraded PZ is elimination at a tertiary amine. In elimination reactions, two substituents are removed from a molecule, usually to produce an alkane, and rely on the presence of a good leaving group (McMurry, 2000). It is not known whether the one-step, second order E2 mechanism or two-step, first order E1 mechanism dominates in the case of high temperature PZ degradation. Since this is the case, a specific mechanism with the appropriate intermediate molecules will not be hypothesized, only the products. S_N2 reactions are usually favored over E2 eliminations except when basicity increases, at higher temperatures or when the nucleophile is poor, among other circumstances (McMurry, 2000). In the case of PZ thermal degradation, it is possible that both S_N2 and E2 eliminations are occurring simultaneously because of the high temperature and mix of nucleophiles and leaving groups.

An elimination reaction of AEP, could produce PZ and ethenamine (CAS: 593-67-9; vinylamine) (Equation 6.12). In another example, an elimination reaction of PEP would produce 1-ethylenyl-piperazine and PZ (Equation 6.13).

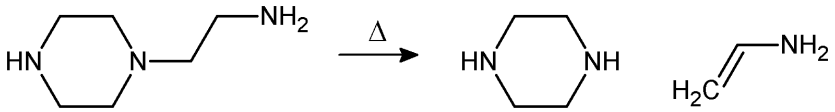

(6.12)

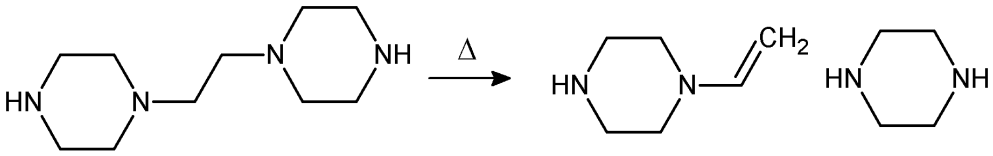

(6.13)

Hofmann elimination takes place at a quaternary amine function to form an alkyl and a tertiary amine. This could take place on PEP, for example if one of the interior amino functions was protonated (Equation 6.14).

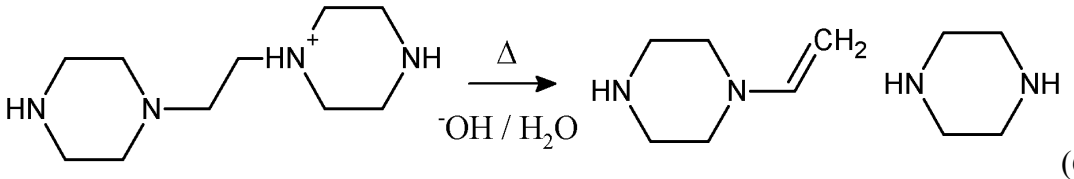

(6.14)

Once the alkene or olefin compound has been generated, the double bond could be hydrated. Hydrations usually occur in acidic conditions, but it could be reasoned that under these high temperature conditions, hydrations are possible. Anti-Markovnikov hydration of 1-ethylenyl-piperazine would produce N-(2-hydroxyethyl) piperazine (HEP) (Equation 6.15). Markovnikov hydration of 1-ethylenyl-piperazine would produce α-methyl-1-piperazinemethanol, (CAS: 65703-81-3), a hemiaminal form of N-ethyl piperazine (Equation 6.16).

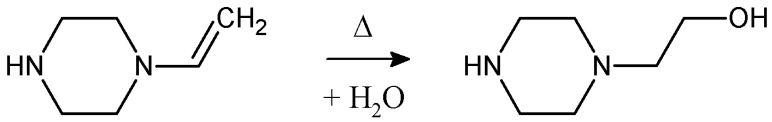

(6.15)

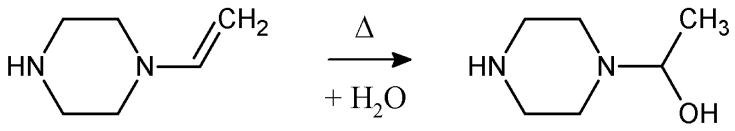

(6.16)

6.1.3 Urea generation

Ureas are a particular subset of amides that contain two amino functions connected by a carbonyl. Ureas can be readily formed in the presence of CO_2 and amines under alkaline conditions. For example, EDA in the presence of CO_2 can form $EDACOO^-$ (EDA carbamate), and the terminal amino function can react to form the cyclic, internal urea of EDA, 2-Imidiazolidone (2-Imid) (Equation 6.17).

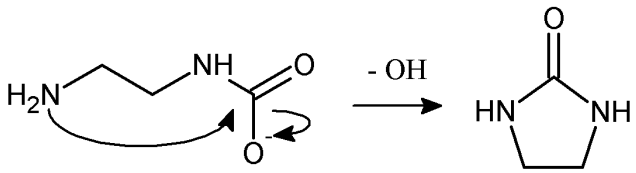

(6.17)

This reaction is known to take place readily under thermal degradation conditions as has been described previously and discussed in section 6.5 of this chapter (Zhou et al., 2010). Provided the rapid reaction of EDA to 2-Imid at high temperature, it appears the proximity of the terminal nitrogen in $EDACOO^-$ accelerates reactions. It is not expected, for example, that the formation of the diPZ urea would proceed as rapidly from $PZCOO^-$ in loaded solutions (Equation 6.18).

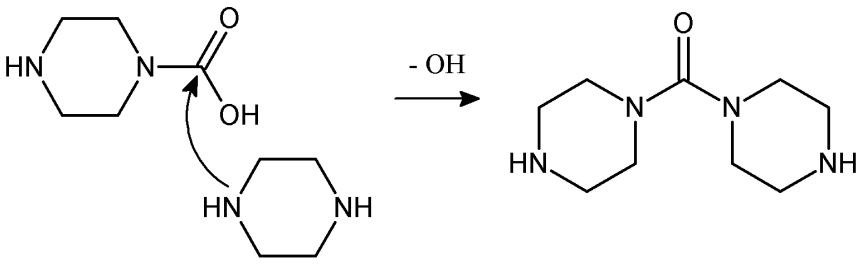

(6.18)

Ureas are believed to be important molecules for PZ thermal degradation because they are stable, contain a CO_2 molecule, and are rapidly generated at high temperatures. Since the ureas contain a CO_2 molecule, they could prove to be important in the reaction of CO_2 to form formate, which is not yet understood. Ureas are expected to be important in the overall study of thermal degradation of CO_2 capture amines due to the fact that reactive amino functions and CO_2 molecules are readily present in nearly all amine-based solvents under study for this application.

6.1.4 Formate generation from CO_2-containing molecules

As the discussion in section 6.4 will show, formate is generated from CO_2 or CO_2-containing molecules. The reduction of CO_2 to formate was not predicted and there are not any obvious pathways for this to occur. It is also not clear if the formate or a formyl amide is first produced. These molecules establish an equilibrium once they are present in solution and it was not clear in any experiment which was produced first. In terms of the actual generation mechanism, it is also not clear if free CO_2 or a CO_2-containing molecule such as $PZCOO^-$ or H^+PZCOO^- reacts to form the first formate or formyl amide molecule.

If formate is generated through the reduction of CO_2 to formate, it is expected that another molecule would be oxidized in the process as a companion redox reaction. At this point, there have not been any specific oxidation products identified in thermally degraded solutions, but a few possible species are discussed in this chapter.

Another possibility is the generation of formate or formyl amides from ureas. Ureas, as discussed in the preceding section, are generated during thermal degradation due to the presence of CO_2 molecules in solution. Ureas, as with other amides, have a delocalization of electrons between the nitrogens and the carbons and oxygens that create

resonance forms (Brown, 1994). For example, the resonance forms of the urea of AEAEPZ are shown in Equation 6.19.

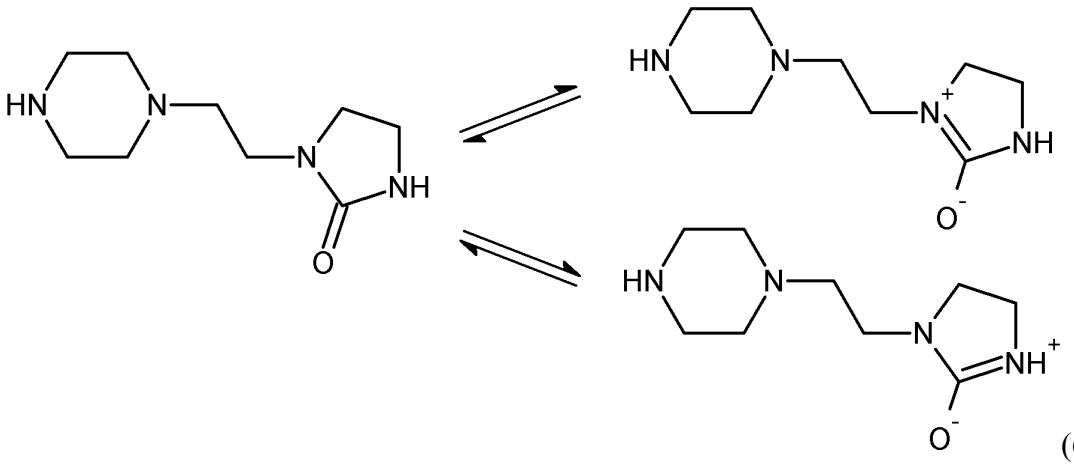

(6.19)

Another concept for formate generation is through free radical mechanisms. Similar to those expected to be occurring in oxidation, free radicals of peroxides or other oxygen containing molecules could be generated due to pyrolysis at high temperature. When formate is produced, it exists at high temperature in equilibrium with formyl amides such as N-formylpiperazine (FPZ).

6.2 THE GENERATION OF THERMAL DEGRADATION PRODUCTS

A variety of molecules are generated when concentrated, loaded PZ is exposed to high temperature. Elevated temperature accelerates reactions that would otherwise be slow or undetectable at a decreased temperature. Experiments were performed with the intention of accelerating or maximizing thermal degradation in order to more easily quantify the reactions occurring. Because of this, the experimental conditions do not directly represent a real CO_2 capture system. In reference to the focus of this chapter, solutions were allowed to degrade significantly beyond what would be normally seen in an amine-based absorption-stripping system, producing large concentrations of

degradation products. Operations resulting in 30 to 70% PZ degradation would not be observed in industry as is typical of the experiments discussed here. The approach is to understand this high level of degradation and then apply that knowledge to the initial rates and causes of degradation in real systems. A summary of degradation products successfully identified and quantified as well as suspected new products are summarized in Table A.3 (Appendix A).

6.2.1 Representative thermal degradation product mix

A typical thermally degraded PZ sample includes amines, amides, carboxylate ions, imidazolidones, and ureas. This sample could also include aldehydes, oxazolidones, and polymeric compounds, although these have not been positively quantified in degraded PZ. As an example of what would be expected in a typical thermal degradation experiment for concentrated, loaded PZ, a representative experiment will be discussed in detail. For this example, the thermal degradation of 8 molal (m) PZ with 0.3 mole CO_2 per mole alkalinity degraded at 165 °C for 20 weeks (TE44) will be used. This experiment was performed toward the end of this project and was subjected to the most advanced analytical techniques developed. This temperature is also of specific interest to new PZ projects that call for stripper or two-stage flash operation around 150 °C.

In this experiment, 10 major degradation products were identified and quantified. In order to simplify the results, the concentration profiles are split among multiple figures. First, the loss of PZ and CO_2 during the 20 weeks of degradation is shown in Figure 6.1. Over the course of 20 weeks, 1730 mmole PZ per kg solution was degraded or 40.8% of the initial concentration. In that same time period, 888 mmole CO_2 per kg solution was lost or 32.3% of the initial concentration. The significance of the PZ and CO_2 losses will be discussed it the following sections.

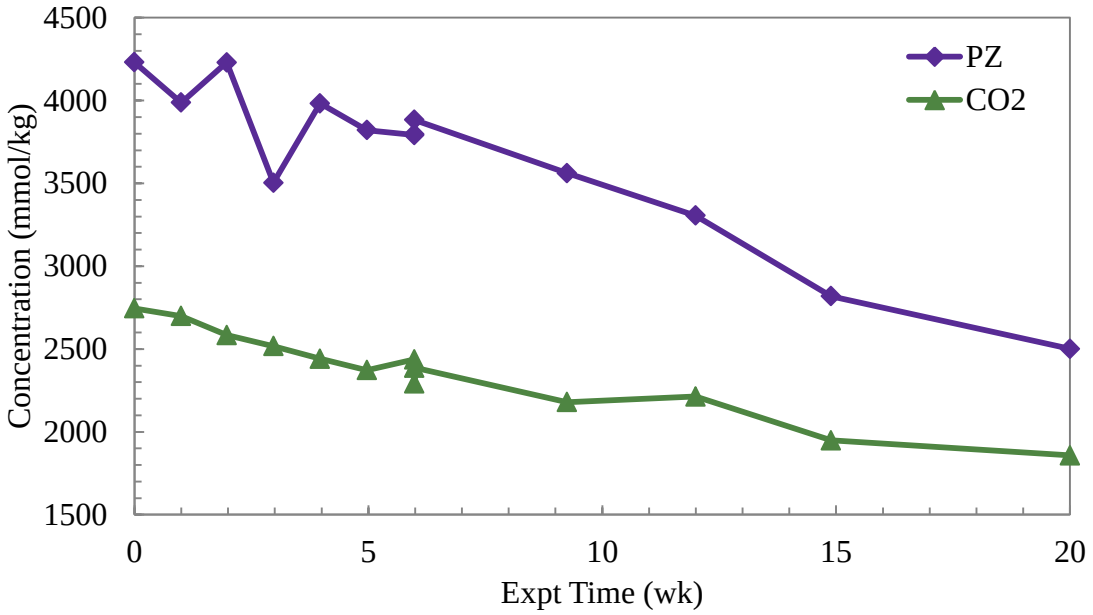

Figure 6.1: Loss of PZ and CO_2 during thermal degradation of 8 m PZ with 0.3 mole CO_2 per mole alkalinity at 165 °C (TE44)

Carboxylate ions, also known as heat stable salts, are commonly produced in thermal degradation experiments and are quantified using anion IC. Anion IC can also quantify non-carboxylate degradation products such as nitrite or nitrate, as well as other ions that are not degradation products such as sulfate, chloride, or thiosulfate. Nitrite and nitrate were not found to be dominant degradation products in any thermal degradation experiment. Due to the importance of nitrite in nitrosamine formation, it is important to be clear on this point. An unidentified anion IC peak has been misidentified in the past as nitrite, as discussed in section 6.1.4. The carboxylate ions produced in TE44 are shown in Figure 6.2. The concentrations of the basic carboxylate ions (glycolate, acetate, formate, and oxalate) are shown in this figure along with their concentrations after NaOH treatment. This value, labeled "Total [Ion]" represents the concentration of the original ion and the concentration increase that may have resulted from the reversal of any amide

formation (see Section 3.1.6 for details). The difference between the two values would represent the concentration of amides of that carboxylate ion.

Formate was the dominant carboxylate ion produced in every PZ thermal degradation experiment and the differences in magnitude between formate and the other carboxylate ions shown in Figure 6.2 is representative of most experiments. The concentration range is magnified in Figure 6.3 to highlight the behavior of the non-formate carboxylate ions. It is important to note that all of the data series shown contain non-zero values.

Amine products, including substituted PZ molecules, account for a majority of both the carbon and nitrogen mass recovered after thermal degradation. The concentration profiles for the amines positively identified and quantified using cation IC are shown in Figure 6.4 and include NH_4^+, EDA, FPZ, 1-methylpiperazine (1-MPZ), HEP, and AEP. A magnified view of the same figure is shown in Figure 6.5. NH_4^+ was found to have one of the largest concentrations in thermally degraded experiments. N-formyl PZ, although an amide, is included in this figure since N-Formyl PZ can be quantified directly with cation IC and is a substituted PZ. The previous graphs showed the total formyl amides quantified through alkaline treatment.

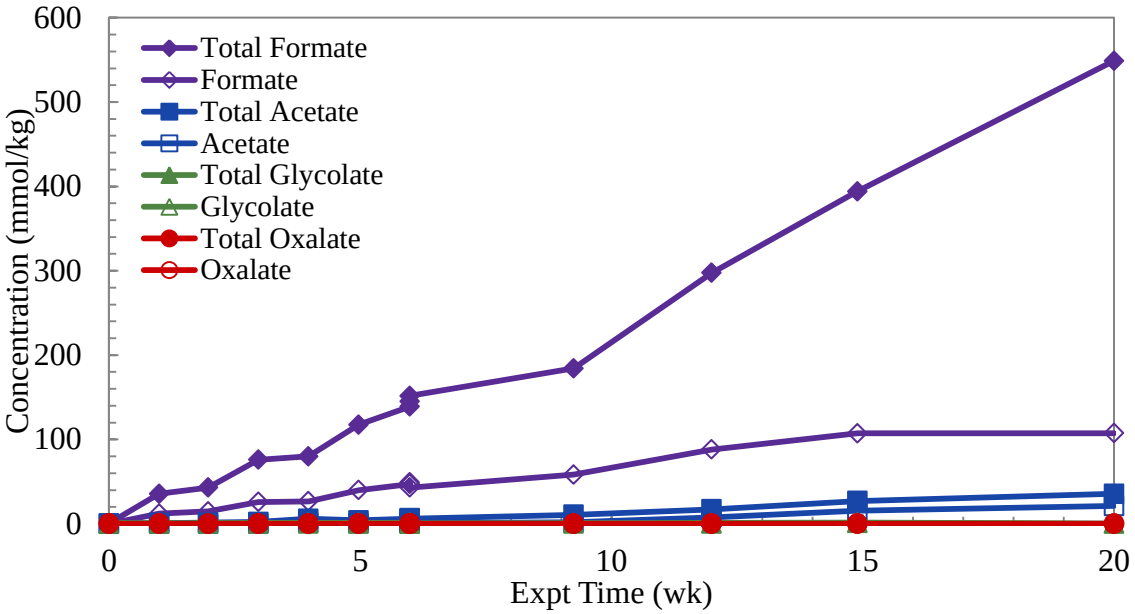

Figure 6.2: Production of carboxylate ions during thermal degradation of 8 m PZ with 0.3 mole CO_2 per mole alkalinity at 165 °C (TE44) (legend matches order of curves)

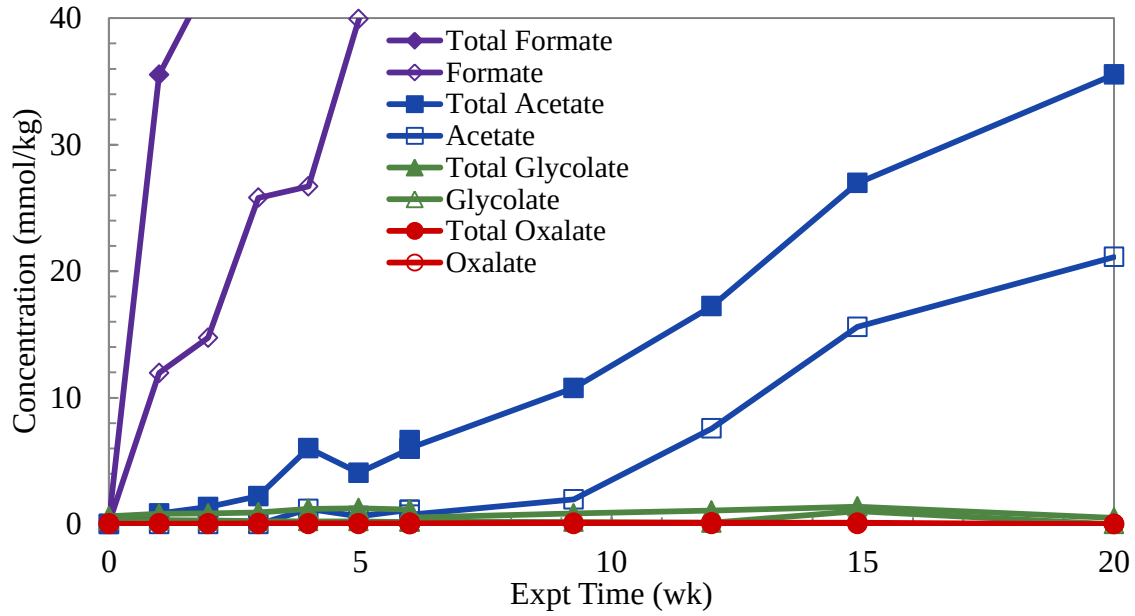

Figure 6.3: A magnified view of the production of carboxylate ions during thermal degradation of 8 m PZ with 0.3 mole CO_2 per mole alkalinity at 165 °C (TE44) (legend matches order of curves)

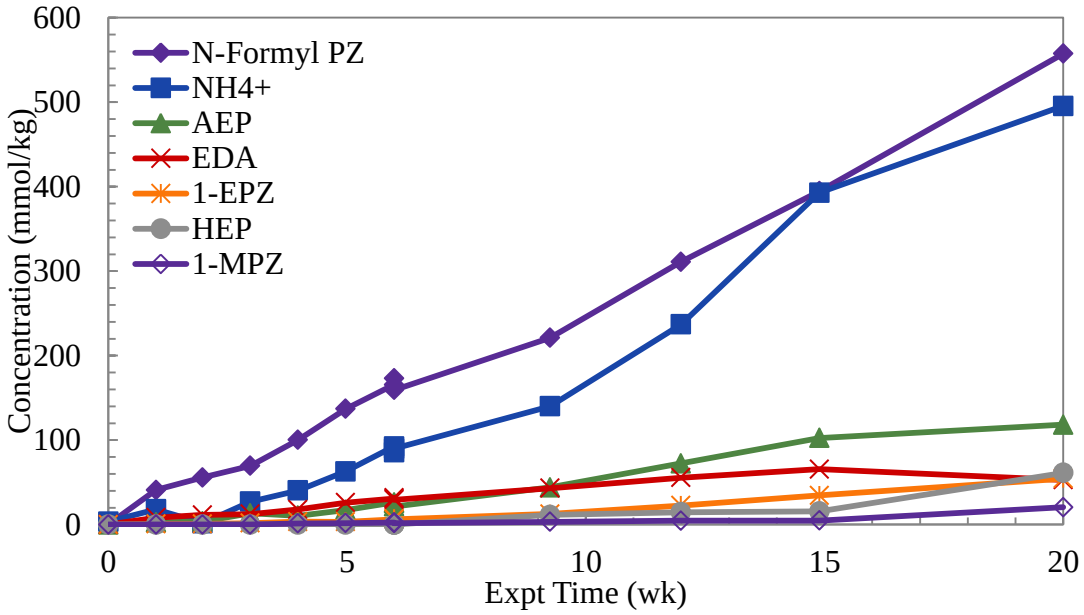

Figure 6.4: Production of amine degradation products during thermal degradation of 8 m PZ with 0.3 mole CO_2 per mole alkalinity at 165 °C (TE44) (legend matches order of curves)

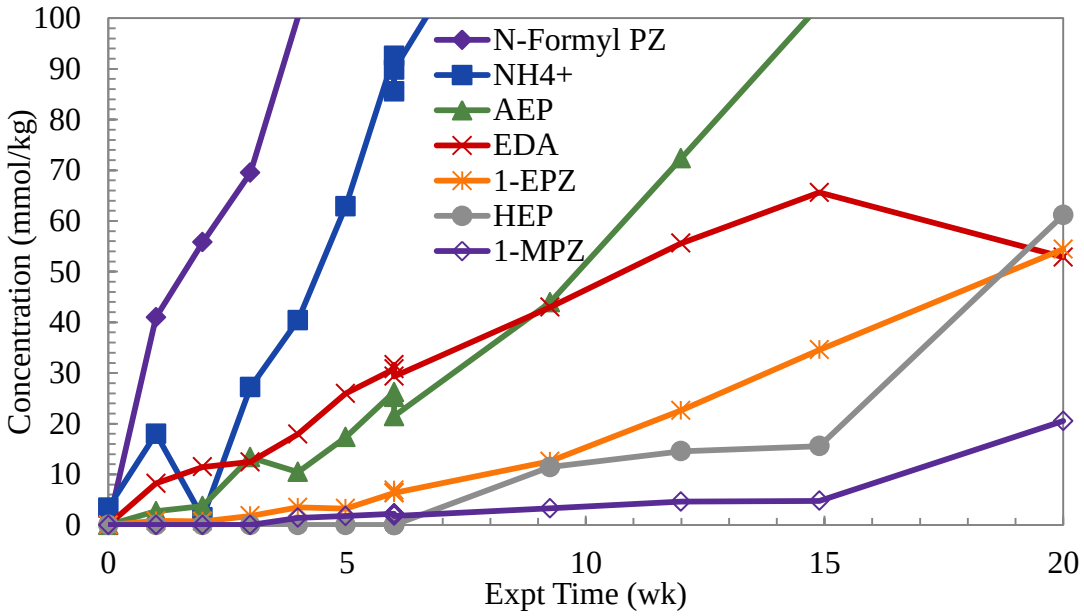

Figure 6.5: A magnified view of the production of amine degradation products during thermal degradation of 8 m PZ with 0.3 mole CO_2 per mole alkalinity at 165 °C (TE44) (legend matches order of curves)

Only one compound was positively identified and quantified using HPLC. The generation of 2-Imid is compared with that of formate, NH_4^+, FPZ and AEP in Figure 6.6 to put the 2-Imid concentration in perspective in the total degradation mix. Also, this plot demonstrates how formate, AEP, and 2-Imid were generated in concentrations very similar to each other.

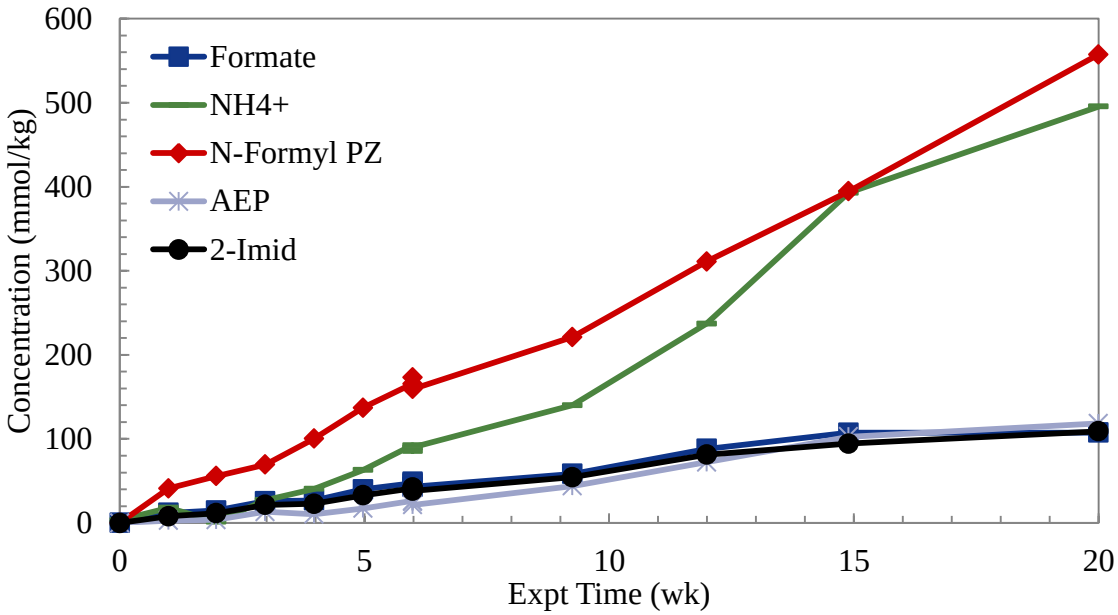

Figure 6.6: Production of 2-Imid during thermal degradation of 8 m PZ with 0.3 mole CO_2 per mole alkalinity at 165 °C (TE44)

6.2.2 Total Nitrogen (TN) and Total Organic Carbon (TOC) analysis

The samples from this experiment were analyzed for total organic carbon (TOC) and total nitrogen (TN). The fraction of both TOC and TN as a function of the initial concentration are shown in Figure 6.7. Over the 20 weeks of degradation, the TOC concentration remained steady while the TN concentration decreased by 13%. The error associated with both measurements is high, between 2 and 6.5%, as demonstrated by the error bars on each data point, but a downward trend in TN is observable. This loss of N

indicates the generation of volatile products during degradation beginning after approximately 10 weeks. This loss of volatile N may correlate with the delay in production of some of the minor liquid phase products such as 1-EPZ, 1-MPZ, HEP, and acetate. Since the TOC did not decrease during the experiment, it is expected that the loss of TN is in the form of volatile ammonia (NH_3), NO_X (NO and N_2O), or molecular nitrogen (N_2). These volatile species would have escaped from the liquid phase once the thermal cylinders were opened and the samples were stored for analysis. The presence of detectable NH_4^+ in solution supports the conclusion that volatile NH_3 was lost in the gas phase in some concentration. The absence of nitrite or nitrate in the liquid phase makes NO_X less probable

The loss of total alkalinity, PZ, and TN is compared for this experiment in Figure 6.8. The effect of PZ thermal degradation is clear as all three quantities decrease. As PZ is degraded, there is generation of amine products that maintain alkalinity, indicated by the higher concentration of alkalinity than PZ. The difference between total alkalinity and TN is likely the concentration of ureas, amides, and amino acids that would be detected as TN, but are not detected by acid titration as alkalinity. The presence of carboxylic acids may also underestimate alkalinity measurements using acid titration, although the concentration of free carboxylate ions is low compared to the concentration of carboxylate tied up as amides.

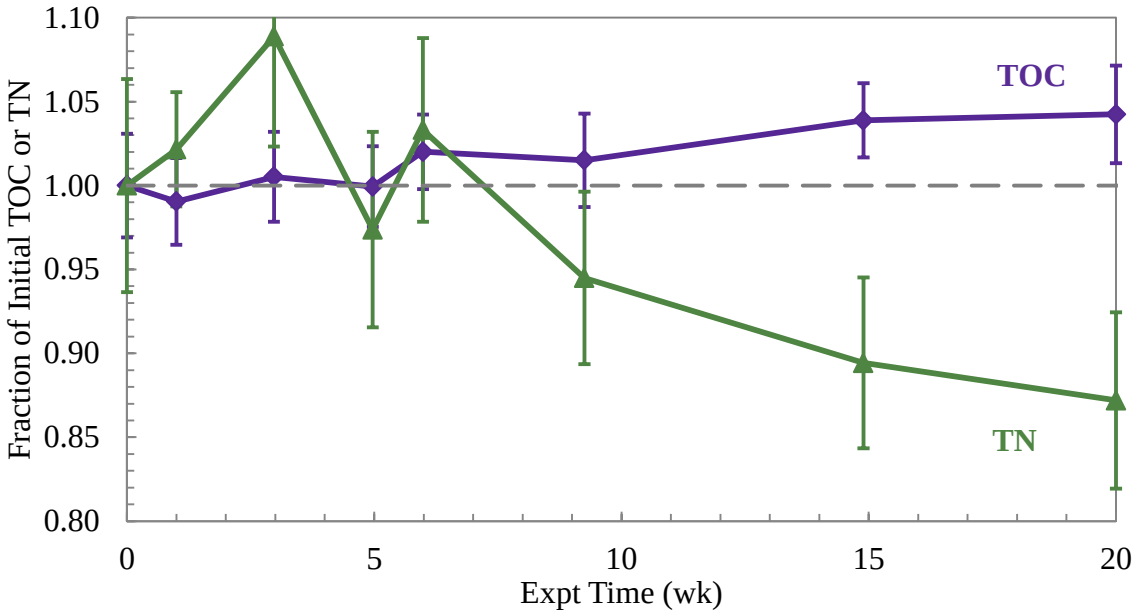

Figure 6.7: Fraction of initial TOC and TN during thermal degradation of 8 m PZ with 0.3 mole CO_2 per mole alkalinity at 165 °C

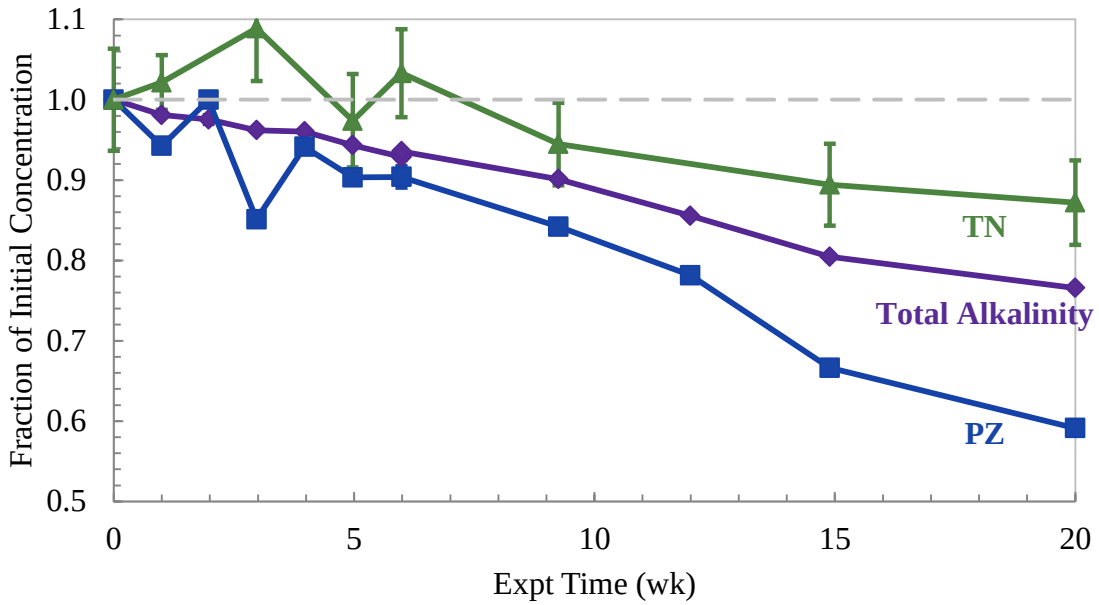

Figure 6.8: Comparison of the fraction of initial total alkalinity, PZ, and TN for thermal degradation of 8 m PZ with 0.3 mole CO_2 per mole alkalinity at 165 °C (TE44)

6.2.3 Carbon and nitrogen mass balance

Using the concentrations of PZ, CO_2, and degradation products, the recovery of mass during this sample thermal degradation experiment can be analyzed as an example of a typical mass balance in concentrated PZ thermal degradation experiments. The nitrogen and carbon balance achieved in TE44, the sample experiment, is shown in Table 6.1. These balances were calculated for the final sample of TE44 after 20 weeks of degradation at 165 °C and do not include any unidentified peaks discussed in the next section. Two molecules, 1-MPZ, and HEP, saw distinct increase in concentration in the final sample (t = 20 weeks), so their concentrations may be overestimated in the mass balances. Formyl amides calculated from alkaline amide reversal were not included in the balances while N-Formyl PZ quantified using cation IC was included. Glycolate, glycolyl amides, oxalate, and oxalyl amides were not included in the balances due to their negligible concentrations. This table, as well as the following two tables that contain balances, show the raw concentration of each molecule in solution in the first column for reference. The degradation products are listed in decreasing N concentration and the order is maintained for all tables in this section.

After 20 weeks, 1730 mmole PZ per kg and 887 mmole CO_2 per kg were lost to thermal degradation pathways. The mass recovered after 20 weeks of degradation is fairly high with 74% of the nitrogen and 63% of the carbon recovered. N-Formyl PZ, NH_4^+, AEP, and 2-Imid are the most prominent degradation products of thermally degraded PZ. These four molecules account for 63 and 49%, respectively of the N and C mass lost as PZ and CO_2 during degradation.

The apparent loss of TN over the course of the experiment should correspond to a volatile N product that does not contain C. Ammonia (NH_3) may be volatile enough to be lost to the atmosphere when the cylinders were opened. Other possible volatile N

products include nitrogen (N_2) and NO_X (NO, NO_2), none of which were quantified. NH_4^+ was quantified in liquid solution so volatile NH_3 is expected. TN analysis indicates a 13% loss of TN where the initial concentration was 8500 mmole N per kg. The difference in the N and C balance also indicates that there are C-containing liquid phase degradation products that have not been identified that do not contain N.

Table 6.1: Nitrogen and carbon mass balance closure for thermally degraded PZ at 165 °C for 20 weeks

		Nitrogen Balance		Carbon Balance	
	Conc. mmol/kg	N Conc. mmol/kg	Lost N %	C Conc. mmol/kg	Lost C %
PZ Lost in 20 weeks	1729	3458	-	6916	-
CO_2 Lost in 20 weeks	888	-	-	888	-
TOTAL Lost		3458		7804	
DEGRADATION PRODUCTS:					
N-Formyl PZ	558	1115	32.2	2787	35.7
NH_4^+	496	496	14.3	0	-
AEP	118	355	10.3	710	9.1
2-Imid	109	218	6.3	327	4.2
HEP	61	122	3.5	367	4.7
1-EPZ	54	109	3.1	327	4.2
EDA	53	106	3.1	106	1.4
1-MPZ	21	41	1.2	103	1.3
Formate	108	0	-	108	1.4
Total Acetate	36	0	-	71	0.9
TOTAL		2561.1	74.1	4904.0	62.8

The distribution of N-containing degradation products is compared with the unrecovered (or "missing") N from the degradation of PZ in Figure 6.9. In this figure, the generation of each of the prominent N-containing degradation products is shown through the course of the experiment. HEP, 1-EPZ, EDA, and 1-MPZ are plotted together in order to see their concentration on this scale. At 1 and 3 weeks, the PZ data had some scatter, creating an excess of missing PZ N. All of the major degradation products are continually increasing without any delay indicating a secondary mechanism.

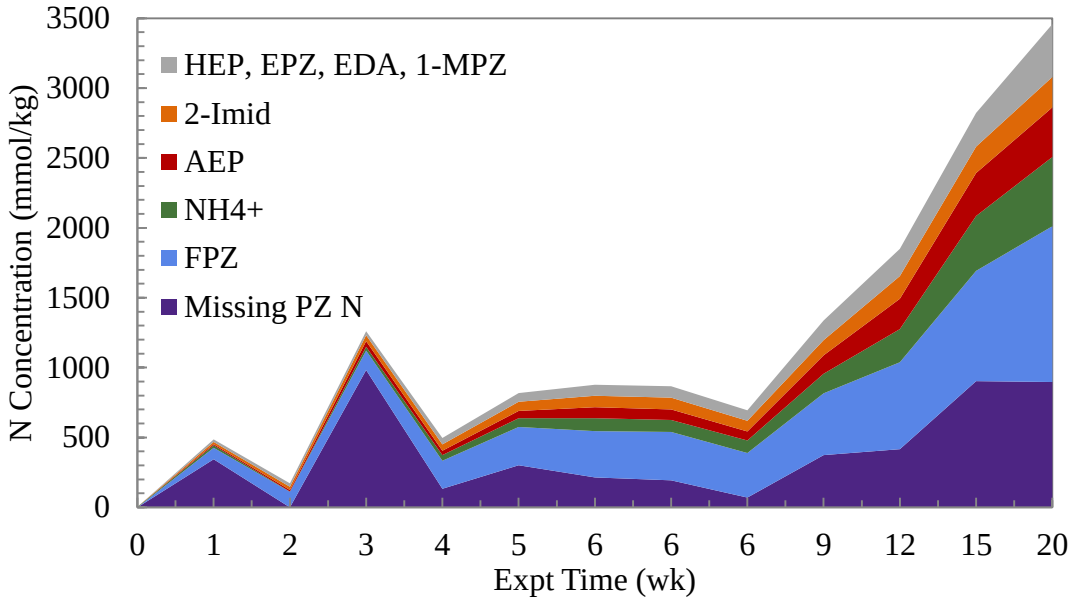

Figure 6.9: Distribution of recovered N during thermal degradation of 8 m PZ with 0.3 mole CO_2 per mole alkalinity at 165 °C (TE44)

The loss of CO_2 is a unique observation that has not be seen for amine thermal degradation before. CO_2 is lost during thermal degradation of PZ to generate formate, formyl amides, and ureas, as will be discussed in greater detail in section 6.4. A mass balance, shown in Table 6.2, can be made for all CO_2 containing degradation products in an attempt to trace CO_2 loss. Formate, N-formyl PZ, and 2-Imid all contain one CO_2 function in their structure and account for 87.2% of the lost CO_2. This balance indicates that there are likely unidentified molecules with urea or formyl amide structures that contain functionalities originally derived from CO_2.

Finally, a fourth balance on the alkyl portion of the PZ molecule can be estimated. This balance accounts for where the backbone carbons of the PZ end up and is shown in Table 6.3. This was calculated as an "ethyl" balance where the every two-carbon chain was calculated separately. For example, every mole of EDA, 2-Imid, and acetate had one "ethyl", each mole of PZ and FPZ had two "ethyls", and each mole of HEP and AEP had

three “ethyls”. 1-MPZ was considered to have 2.5 “ethyls” for the balance. After 20 weeks of degradation, 60% of the lost backbone carbons of PZ are recovered in degradation products. This is similar to the overall C balance and has much worse closure than the overall N and CO_2 balances. This indicates that there are likely numerous carbon-based degradation products that have yet to be identified in the liquid phase.

6.2.4 Unidentified or unquantified products

Unfortunately, there were unidentified and unquantified peaks on all three of the major analytical tools used to analyze this example experiment. The mass balances discussed indicate that the major degradation products have been identified, but there is still room for further identification and mass balance closure. A comparison of the anion IC chromatogram for the initial and final sample for this experiment is shown in Figure 6.10 and with a magnified signal in Figure 6.11. From the magnified chromatogram, six unknown peaks are visible labeled with a “U” on the chromatogram. The peak at a retention time of 24 minutes is not nitrite, although the nitrite peak eludes just after it. The unidentified peaks are spread throughout the chromatogram and do not correspond to peaks identified in Chapter 8 as possible mono-amides of oxalate.

A comparison of the anion IC chromatogram for the original and NaOH treated final sample with a magnified signal is shown in Figure 6.12. The only change visible in the non-magnified chromatogram is the sizable increase in the formate peak. The alkaline treatment produced more formate and oxalate, but did not change the unidentified peaks. It is unlikely at this point that any of the unidentified peaks seen through anion IC are parts of amides.

Table 6.2: CO_2 mass balance for 8 m PZ with 0.3 mole CO_2 per mole alkalinity degraded at 165 °C for 20 weeks (TE44)

		CO_2 Balance	
	Conc. mmol/kg	CO_2 Conc. mmol/kg	Lost CO_2 %
PZ Lost in 20 weeks	1729	0	-
CO_2 Lost in 20 weeks	888	888	-
TOTAL Lost		888	
DEGRADATION PRODUCTS:			
N-Formyl PZ	557	557	62.8
NH_4^+	496	0	-
AEP	118	0	-
2-Imid	109	109	12.3
HEP	61	0	-
1-EPZ	54	0	-
EDA	53	0	-
1-MPZ	21	0	-
Formate	108	108	12.1
Total Acetate	36	0	-
TOTAL		774	87.2

Table 6.3: "Ethyl" mass balance for 8 m PZ with 0.3 mole CO_2 per mole alkalinity degraded at 165 °C for 20 weeks (TE44)

		Ethyl Balance	
	Conc. mmol/kg	Ethyl Conc. mmol/kg	Lost Ethyl %
PZ Lost in 20 weeks	1729	3458.1	-
CO_2 Lost in 20 weeks	888	0	-
TOTAL Lost			
DEGRADATION PRODUCTS:			
N-Formyl PZ	557	1115	32.2
NH_4^+	496	0	-
AEP	118	355	10.3
2-Imid	109	109	3.2
HEP	61	184	5.3
1-EPZ	54	163	4.7
EDA	53	53	1.5
1-MPZ	21	51	1.5
Formate	108	0	-
Total Acetate	36	36	1.0
TOTAL		2065	**59.7**

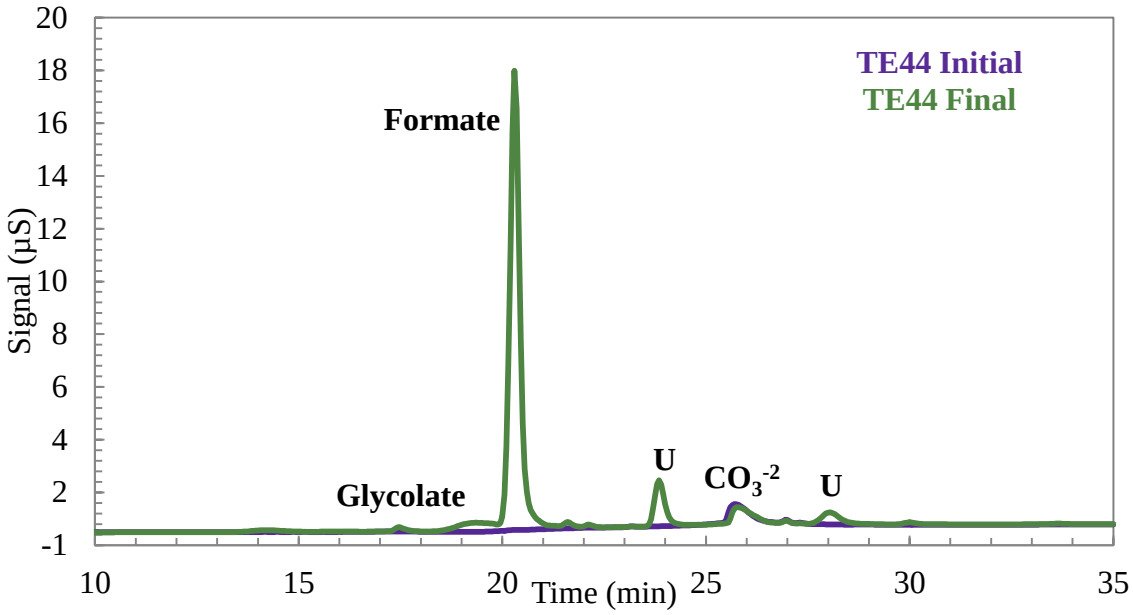

Figure 6.10: Anion IC chromatogram of initial and final sample of 8 m PZ with 0.3 mole CO_2 per mole alkalinity degraded at 165 °C (TE44)

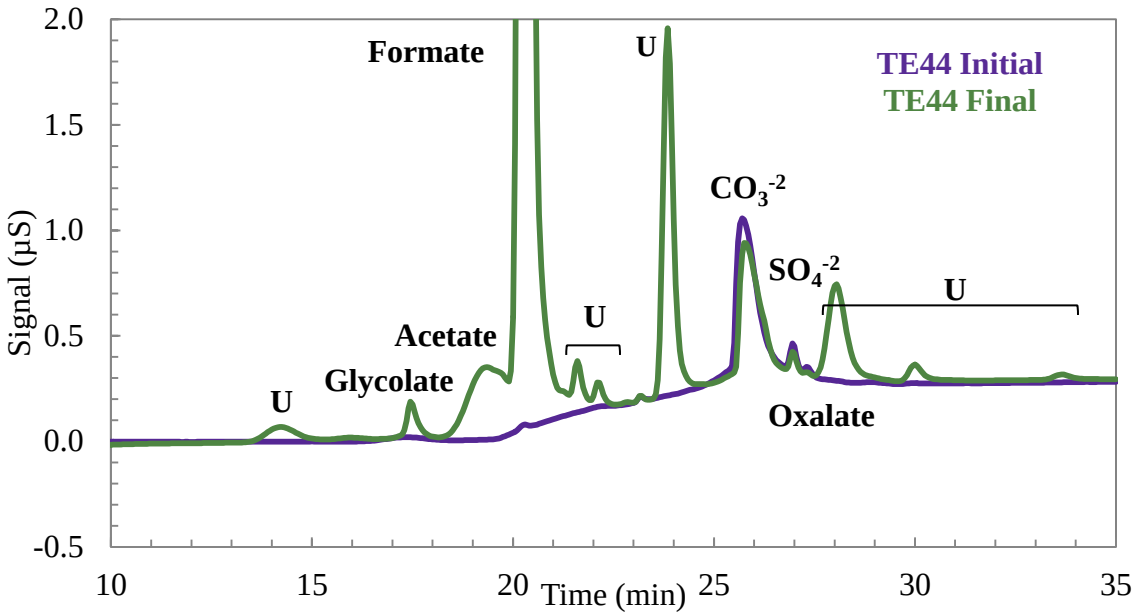

Figure 6.11: Anion IC chromatogram of initial and final sample of 8 m PZ with 0.3 mole CO_2 per mole alkalinity degraded at 165 °C with magnified signal (TE44)

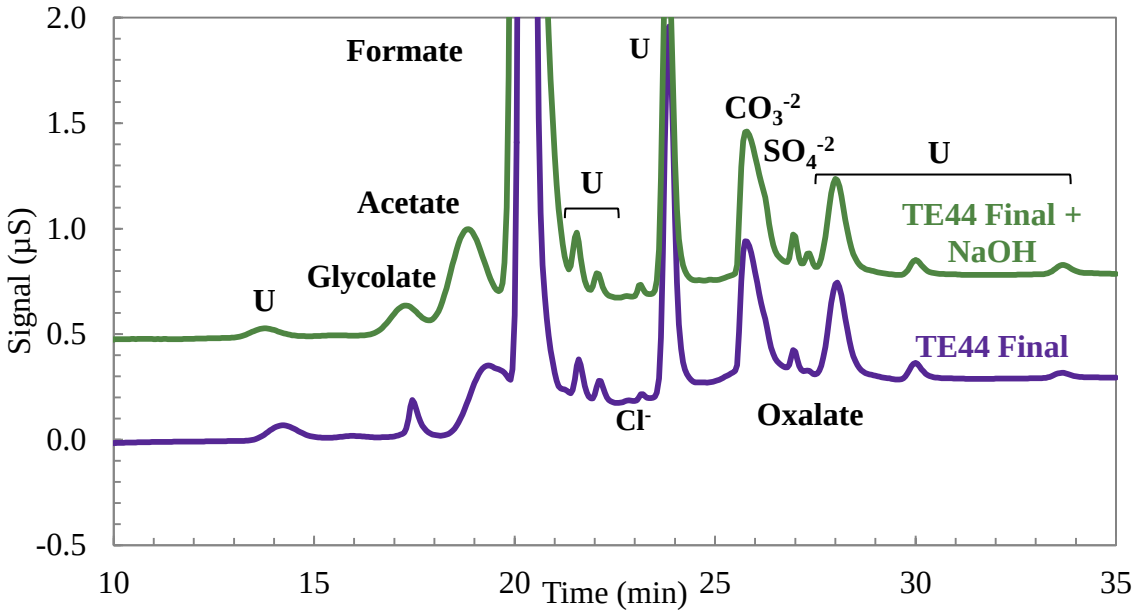

Figure 6.12: Anion IC chromatogram of original and NaOH treated final sample of 8 m PZ with 0.3 mole CO_2 per mole alkalinity degraded at 165 °C with magnified signal (Signal offset of 0.5 µS) (TE44)

There were also unidentified peaks on the Cation IC. The chromatogram for the final sample after 20 weeks of thermal degradation is shown in with a magnified signal in Figure 6.13. There were 5 major peaks at retention times of 18.0, 39.7, 42.0, 42.5, and 43.3 minutes that have yet to be positively identified and quantified. Suspected identities of these peaks are discussed in the following section. A comparison of the cation IC chromatograms for the original and NaOH treated final sample is made in Figure 6.14. The peak for N-formyl PZ is the only peak to disappear between the chromatograms indicating that none of the major unidentified peaks are also amides.

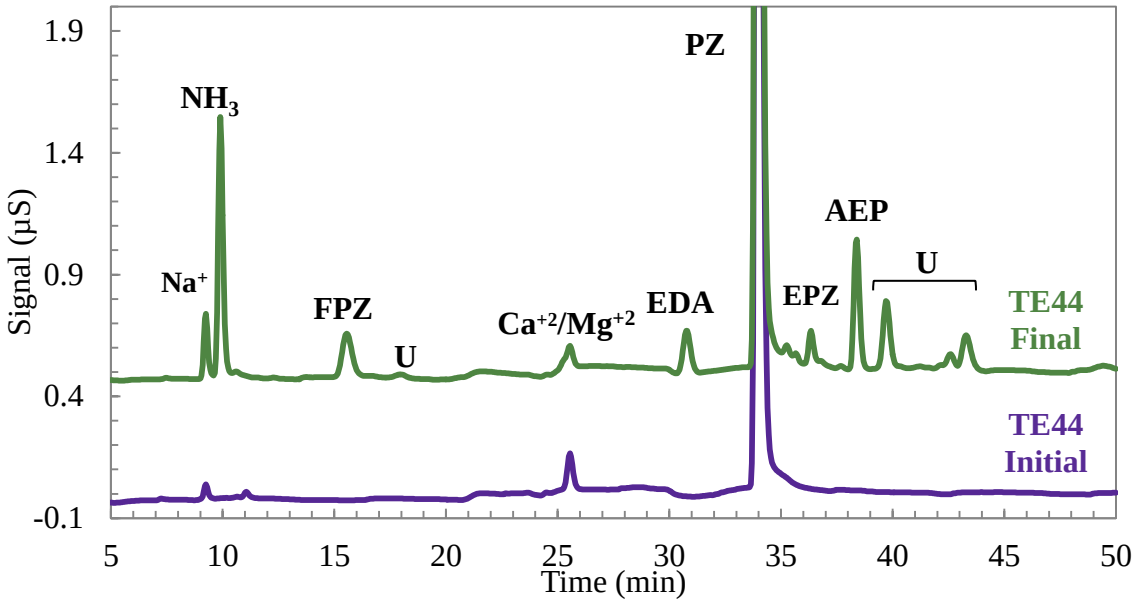

Figure 6.13: Cation IC chromatogram of the initial and final sample of 8 m PZ with 0.3 mole CO_2 per mole alkalinity degraded at 165 °C with magnified signal (Signal offset 0.5 µS) (TE44)

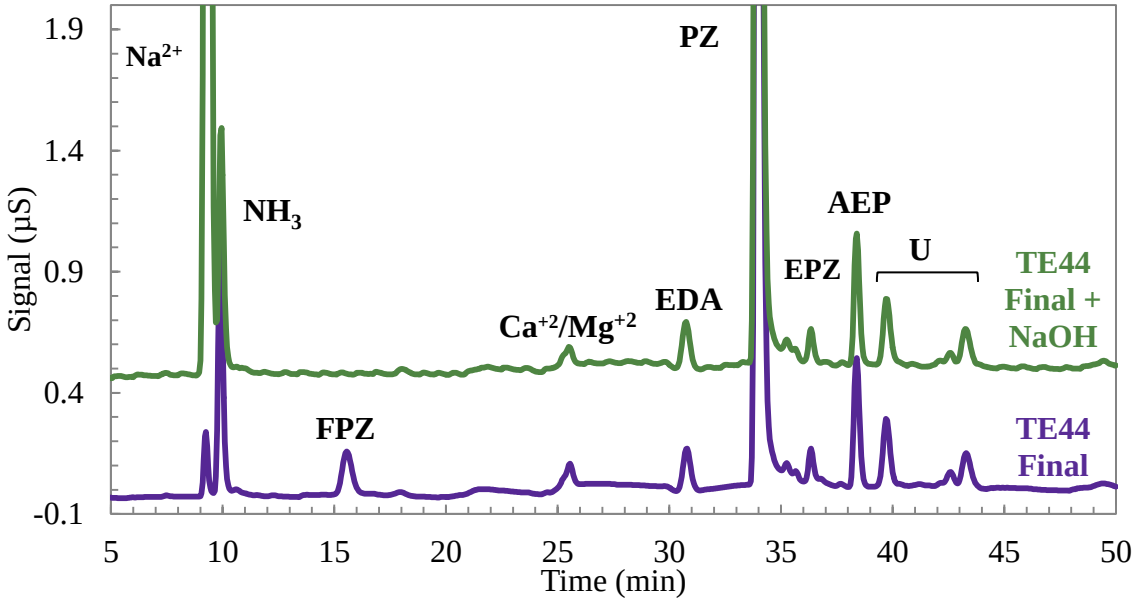

Figure 6.14: Cation IC chromatogram of original and NaOH treated final sample of 8 m PZ with 0.3 mole CO_2 per mole alkalinity degraded at 165 °C with magnified signal (Signal offset 0.5 µS) (TE44)

Finally, the HPLC also revealed multiple unidentified peaks that could correspond to major degradation products of PZ thermal degradation, as demonstrated in Figure 6.15. The only peak that was positively identified was 2-Imidazolidone (2-Imid), as labeled. The large peak between 16.5 and 22 minutes is an artifact of this particular run and did not occur in typical thermally degraded PZ samples. There are at least 8 significant, unidentified peaks but the relative importance in terms of concentration is not known due to possible differences in the response factor of each molecule with UV detection.

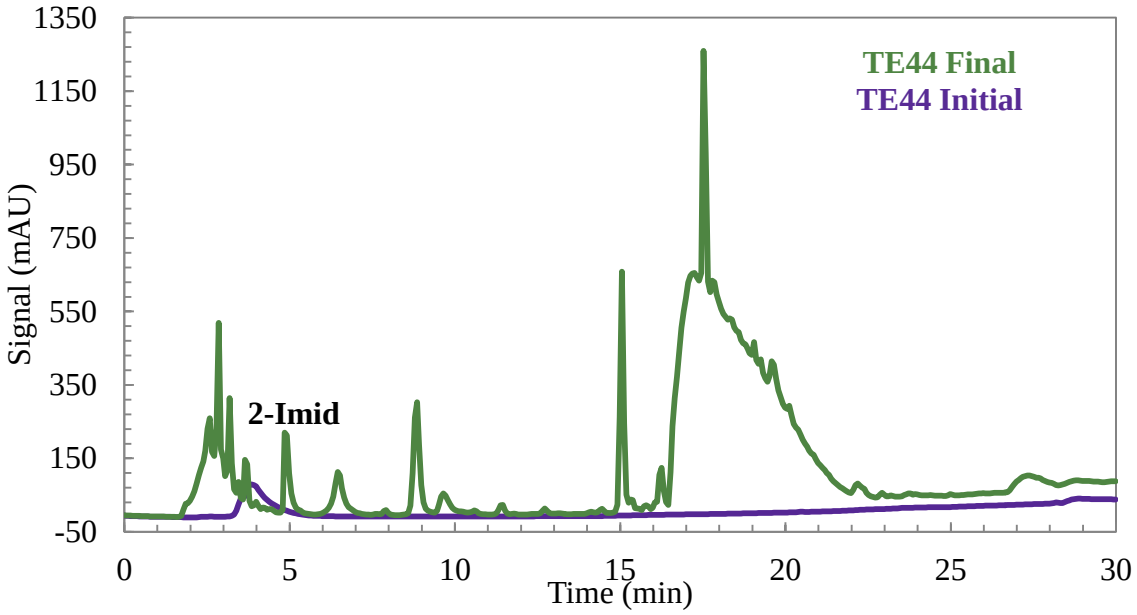

Figure 6.15: HPLC chromatogram of final sample of 8 m PZ with 0.3 mole CO_2 per mole alkalinity degraded at 165 °C (TE44)

6.2.5 Suspected thermal degradation products

The degradation products discussed in the previous sections have all been confirmed using commercially available standards and in the case of cations, confirmed with cation IC coupled with mass spectroscopy (IC-MS). An additional set of products have been suspected based on IC-MS or GC-MS results, but cannot be fully identified

due to a lack of a commercially available standard. Finally, a third category of molecules are suspected based on supposed mechanisms or other conjectures. In this project, no peak assignments were made without a positive match with a commercial standard, even if a GC-MS library match existed.

A number of molecules were unsuccessfully screened in an attempt to match unidentified peaks. Some molecules, such as 2-piperazinone, were screened on numerous analytical techniques to see if any response was registered. In a discussion of unknowns in regards to peak assignments, it is important to list what has been eliminated. All of these were tested as standards without alkaline reversal. For the anion analysis, common anions were screened to eliminate possible contamination. The anions screened included carbonate, bicarbonate, phosphate, thiosulfate, sulfite, persulfate, fluoride, iodine, iodate, bromide, bromate, metavanadate, permanganate, and borate. For cation IC, diethanolamine (DEA), methyldiethanolamine (MDEA), triethanolamine (TEA), dimethylaminoethanol (DMAE), methylaminoethanol (MAE), monoethanolamine (MEA), N,N'-bis(2-hydroxyethyl)piperazine (bHEP), diethylenetriamine (DETA), N,N'-diethylpiperazine (DEPZ), N-(2-Hydroxyethyl)-N'-methylpiperazine (HEMP), N-(2-aminoethyl)-N'-methylpiperazine (AEMP), N-(2-Hyroxyethyl)ethylenediamine (HEEDA), N,N'-diformylpiperazine (DFPZ), N-acetylpiperazine (AcPZ), 2-piperazinone, 2,5-piperazinedione, 2-imidazolidone (2-Imid), 2-methyl-2-imidazolidone, pyrazine, and N-(2-aminoethyl)glycine (AEG) were among those compounds tested as standards but not found as peaks in thermal degraded PZ.

6.2.5.1 Molecules identified through MS techniques

In this section, molecules that are suspected based on results from IC-MS and GC-MS techniques are discussed in terms of their possible contribution to the thermal

degradation mixture. LC-MS analyses were not successful at identifying any unique molecules. All of the molecules suspected, as discussed below, are shown with their structure and pertinent data in Table 6.4. An example of IC-MS analysis for a thermally degraded sample is shown in Appendix G. The technique used for each suspected molecule is specified in the last column and refer to either IC-MS with chromatographic separation in single quad mode with electrospray ionization (IC), GC-MS with chromatographic separation on a semi-polar column with electron ionization (GC), GC-MS with chromatographic separation, chemical ionization, and high resolution mass readings (HRGC). No results were obtained using direct injection into an MS in this project.

The most important unknown cation peaks are those at retention times of 39.7 and 43.3 minutes, as demonstrated in the magnified chromatogram shown in Figure 6.16 below. The first peak at 39.7 is suspected to be 1,1'-carbonyl-bis-piperazine (diPZ urea; CAS 17159-16-9) or 1-[2-(piperazinyl)ethyl]-2-imidazolidinone (the urea of AEAEPZ; CAS 104087-61-8). The IC-MS results indicated a molecule with a molecular weight of 198.2 grams per mole (m/z 199.2) which could be either of these molecules. Both are ureas and are suspected because of the known reaction of CO_2 with amines to create imidazolidones or oxazolidones as part of degradation pathways in other amines. There is also an abundance of PZ and CO_2 in solution due to the high PZ concentration and CO_2 loading in most solutions. Both of these ureas have two active amino functions that will respond in the diamine region of the cation. The results of acidified PZ experiments discussed in section 6.3 shed light on the identity of this peak and the urea of AEAEPZ is more likely. Pharmacological studies have investigated molecules with AEAEPZ side chains that react to form a side chain of AEAEPZ urea in the presence of urea and heat,

similar to the high temperature reactions in the presence of CO_2 studied in this project, so this product is highly likely (Bøgesø et al., 1988).

Table 6.4: Molecules identified with various MS-based techniques for thermally degraded concentrated PZ

Name	Abb.	Structure	CAS No.	MW (g/mol)	Basis*
1,1'-carbonylbis-piperazine	diPZ urea	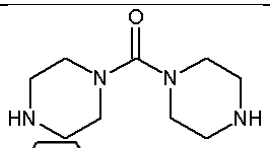	17159-16-9	198.2654	HRGC
1-[2-(piperazinyl)ethyl]-2-imidazolidinone	AEAEPZ Urea	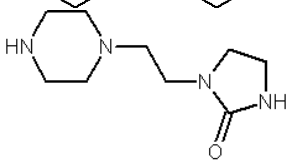	104087-61-8	198.2654	IC
1,1'-(1,2-ethanediyl)bis-piperazine	PEP	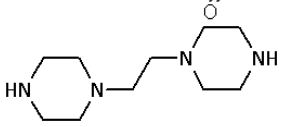	19479-83-5	198.3085	HRGC
1-[2-[(2-aminoethyl)amino] ethyl] piperazine	AEAEPZ	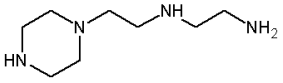	24028-46-4	172.2736	IC
N,N'-di(2-aminoethyl) piperazine	DAEP	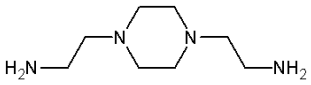	6531-38-0	172.2736	IC
1,1'-(1,2-dioxo-1,2-ethanediyl)bis-piperazine		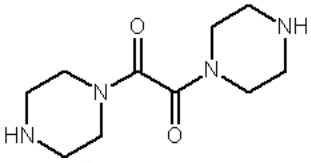	105807-56-5	226.28	IC
1-(2-Aminoethyl)-2-imidazolidone	AEI	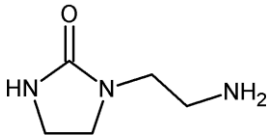	6281-42-1	129.16	IC
1,3-bis(N-hydroxymethyl) urea		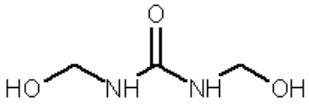	140-95-4	120.11	IC
N,N'-di(2-hydroxymethyl) EDA		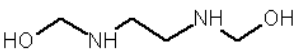	70495-38-4	120.15	IC
Triethylenediamine	TEDA	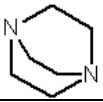	280-57-9	112.17	GC

*IC = Ion chromatography separation coupled with mass spectroscopy; GC = gas chromatography separation coupled with mass spectroscopy; HRGC = High Resolution GC-MS

Another molecule that shares this molecular weight (198.2 gram per mole) is 1,1'-(1,2-ethanediyl)bis-PZ (PEP; CAS 19479-83-5), a polymeric quadramine of two PZ molecules. High resolution GC-MS analysis of thermally degraded 8 m PZ confirmed that the molecular weight for this molecule (198.3085 gram per mole) or an isomer and either of the other two molecules (diPZ urea and AEAEPZ; both 198.2654 gram per mole) are present in degraded solution. It is not expected that this molecule is present in any significant concentration.

The small peak at 42.0 minutes was found to have a molecular weight of 172.2 grams per mole (m/z 173.2) and likely corresponds to 1-[2-[(2-aminoethyl) amino]ethyl] PZ (AEAEPZ; CAS 24028-46-4). In loaded PZ degradation, this peak is minor, but is prominent in acidified PZ degradation and is discussed further in section 6.3. Another suspected degradation product with that molecular weight is N,N'-di(2-aminoethyl) piperazine (DAEP; CAS 6531-38-0) which was suspected in the degradation of AEP, but a standard was not available. In solution, a small concentration of this molecule is expected through S_N2 arm switching mechanism, similar to those discussed in section 7.3.1, but not at any great concentration.

The larger peak at 43.3 minutes was found to have strong signals corresponding to molecular weights of 99.2 and 198.2 grams per mole (m/z 100.2 and 198.2) and a weaker signal indicating a molecular weight of 226.2 grams per mole (m/z 227.2) on the IC-MS analysis. A molecular weight of 198.2 grams per mole could indicate any of the three molecules described above with this molecular weight (AEAEPZ, diPZ urea, or PEP). Given the retention time of the molecule, the best candidate is PEP, a quadramine. AEAEPZ has already been assigned as the most likely candidate for the peak at 39.7 minutes and the diPZ urea would respond as a diamine on the cation. The trace of a 226.2 gram per mole could correspond to 1,1'-(1,2-dioxo-1,2-ethanediyl)bis PZ (CAS:

105807-56-5), which is the oxalyl diPZ amide, although this would be expected to elude as a diamine, usually before this peak retention time. A good candidate for the mass of 99.2 gram per mole that co-elutes is not known.

The peak at 18.0 minutes was found to have a molecular weight of 129.2 gram per mole (m/z 130.2), according to IC-MS, and elutes in the region of monoamines. The peak grows with time, indicating it is a degradation product but not an amide. It was found that this peak corresponds to 1-(2-aminoethyl)-2-imidazolidone (AEI; CAS 6281-42-1), the internal amide of DETA. Despite being a triamine, the urea function makes only the terminal amino function responsive to cation IC and it should elute in this region of the chromatogram. This peak was identified, but not quantified for any experiment.

Finally, the peak at 42.5 minutes was determined to have a molecular weight of 120.7 grams per mole (m/z 121.7) on IC-MS. This does not correspond to any strong candidates for likely degradation products. The molecular weight matches N,N'-di(2-hydroxymethyl) EDA (CAS 70495-38-4) and N,N'-bis(2-hydroxymethyl urea (CAS 140-95-5), but neither of these are strongly suspected.

Triethylenediamine (TEDA) is a molecule is suspected to be present based on proposed reactions and was identified with low resolution GC-MS with library matching of a thermally degraded PZ sample. TEDA elutes just after 1-EPZ on the IC-MS, but was not matched to any major peaks. It is suspected that TEDA is being produced and may react to other related forms, such as 1-piperazineacetic acid (1-PA), as is discussed in the next section.

High resolution MS of thermally degraded PZ also found peaks corresponding to N,N'-diformylpiperazine (DFPZ, CAS 4164-39-0), a molecular formulas of $C_7H_{14}N_2O$, and a molecular formula of $C_9H_{19}N_3O$. These molecular formulas to not match any suspected products and are not present in large concentrations. Standard (low resolution)

GC-MS analysis of thermally degraded 8 m PZ confirmed the presence of AEP, FPZ, and 1-MPZ through library matching. The same data also suggested TEDA, 2-methyl piperazine (2-MPZ), 2,5-dimethyl piperazine, and tetraethylenepentamine (TEPA, CAS 112-57-2), but only TEDA is believed to be a potentially important product based on the proposed mechanisms.

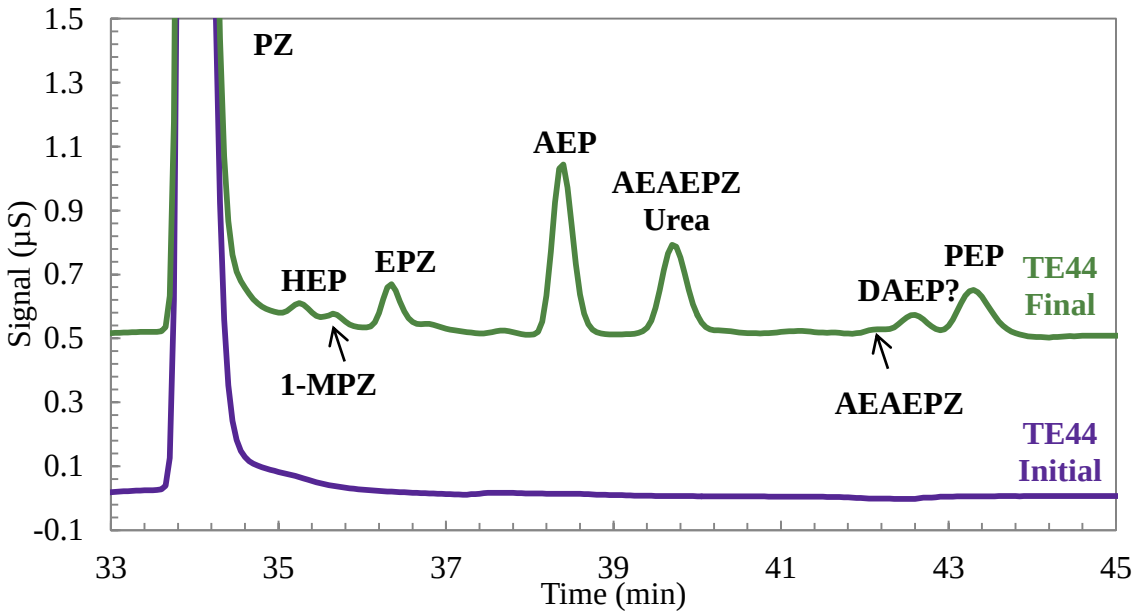

Figure 6.16: Cation IC chromatogram of initial and final sample of 8 m PZ with 0.3 mole CO_2 per mole alkalinity degraded at 165 °C with magnified signal (Signal offset 0.5 µS) (TE44)

6.2.5.2 Relative abundance of suspected products

For the unknown peaks that have suspected identities, the relative abundance of each can be approximated by analyzing the peak area from the cation IC chromatograms. The molecules tentatively assigned to the important unquantified peaks are the urea of AEAEPZ, AEAEPZ, PEP, and DAEP, although the assignment of DAEP is the least confident. The area of each unknown peak is compared to the peak area of AEP, a prominent degradation product, in Figure 6.17. This comparison should provide the

relative importance of each peak and give an idea as to the impact of the unknown molecules on the mass balances. It is important to note that molecules can have varying response factors during chromatography, so for the same concentration, peaks areas could be significantly different. This analysis does not attempt to predict the response factors of each molecule, but assume they are similar to the response factor of AEP to allow a relative comparison. This assumption could be disproven by running standards of each molecule to allow direct calibration and quantification of each molecule.

The urea of AEAEPZ is a prominent degradation product that appears with a larger peak area, and therefore larger assumed concentration than AEP. This molecule is expected to have a large impact on the mass balance based on relative peak area and the size of the molecule, which includes nine carbons and four nitrogens. The PEP peak area is very similar to the AEP peak area throughout the experiment indicating this may also be significant to the mass balance due to the importance of AEP to the mass balance. The concentration of AEAEPZ remains low throughout the experiment as it is suspected to react quickly with CO_2 to form its internal urea. The peak assigned to DAEP, if that is correct, is generated at low concentrations after an initial lag in production. This peak represents a product that is generated after initial degradation mechanisms by second order processes.

6.2.5.3 Other molecules suspected based on reactions

Additional reaction products are suspected to be formed during thermal degradation despite a lack of analytical evidence of their presence. These suspected molecules are summarized in Figure 6.18. Formaldehyde and other reactive aldehydes such as acetaldehyde or hydroxyethylacetaldehyde are suspected to be present and active

in the thermal degradation of concentrated PZ. A colorimetric approach to quantify aldehydes in thermally degraded PZ was attempted without success (Fregert et al., 1984).

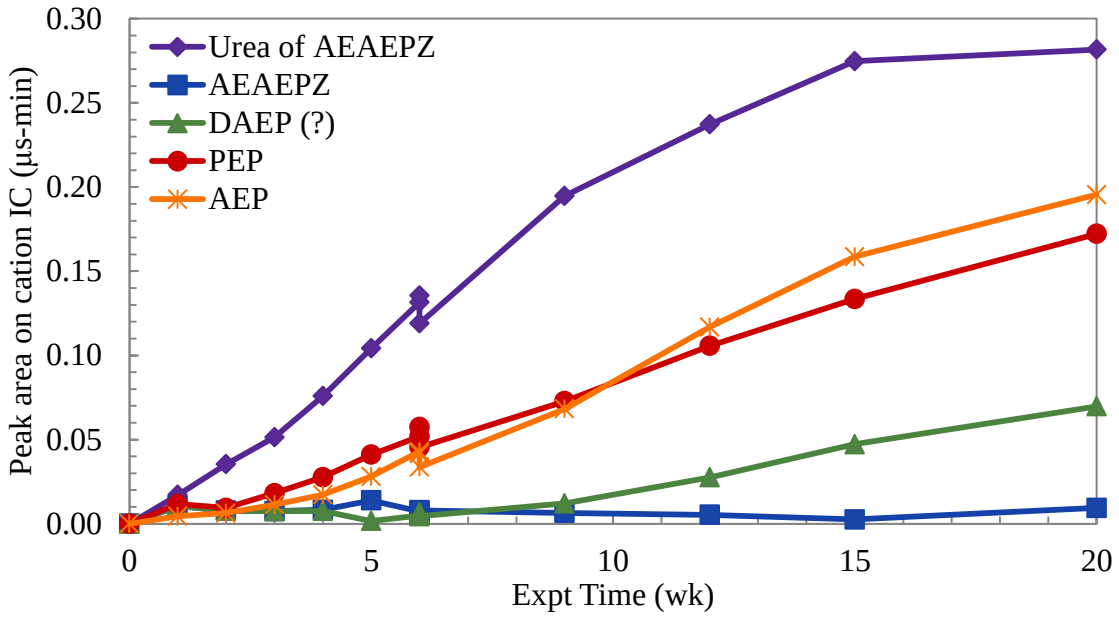

Figure 6.17: Relative abundance of suspected degradation products in the thermal degradation of 8 m PZ with 0.3 mole CO_2 per mole alkalinity at 165 °C (TE44)

A variety of oxidized forms of PZ are suspected because of the formate generation mechanism. In some way, CO_2 is reduced to formate or formyl species and it is believed that another molecule must be oxidized at the same time in a redox-type reaction scheme. Possible oxidized forms of PZ or substituted PZ include 1-PA, the ketone form of TEDA, the enamine form of TEDA, or the hemiaminal (carbinolamine) form of TEDA, which is the hydrated form of the enamine. If 1-PA is produced, it is also possible to imagine two amide forms of that molecule, 1,4-Diazabicyclo[2.2.2]octan-2-one and 1-(1-Piperazinylacetyl)-piperazine. The discussion of oxidized products in Chapter 8 can be extended to thermal degradation because of the suspected redox reaction responsible for formate and formyl amide production.

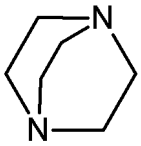

Triethylenediamine
MW: 112.17
(CAS: 280-57-9)

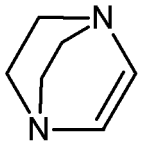

1,4-Diazabicyclo[2.2.2]oct-2-ene
(TEDA enamine)
MW: 110.16
(CAS: 122883-12-9)

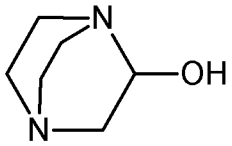

1,4-Diazabicyclo[2.2.2]octan-2-ol
(TEDA hemiaminal)
MW: 128.17
(CAS: 146562-84-7)

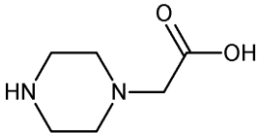

1-Piperazineacetic acid
(1-PA)
MW: 144.17
(CAS: 37478-58-3)

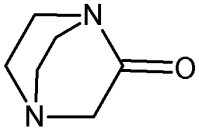

1,4-Diazabicyclo[2.2.2]octan-2-one (Amide of 1-PA)
MW: 126.16
(CAS: 146562-83-6)

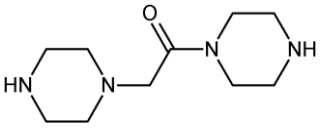

1-(1-Piperazinylacetyl)-piperazine
(Amide of 1-PZ)
MW: 212.29
(CAS: 69253-90-3)

Formaldehyde
MW: 30.03
(CAS: 50-00-0)

Acetaldehyde
MW: 44.05
(CAS: 75-07-0)

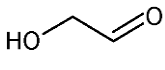

Hydroxyacetaldehyde
MW: 60.05
(CAS: 141-46-8)

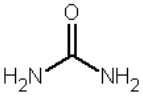

Urea
MW: 60.06
(CAS: 57-13-6)

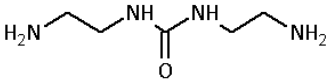

N,N'-bis(2-aminoethyl)-urea
(diEDA urea)
MW:146.19
(CAS: 940866-61-5)

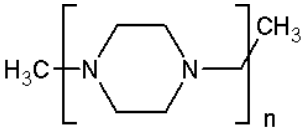

Poly(methylene)PZs

Figure 6.18: Structures of other suspected thermal degradation products

The presence of CO_2 and quantified production of 2-Imid indicate that other ureas are likely being created in solution. Simple urea (the urea of ammonia), PZ urea structures, or additional EDA urea structures are possible since there is a significant concentration of CO_2 left in solution after degradation.

Polymeric PZ structures are also suspected to be formed during thermal degradation of concentrated PZ. If formaldehyde is present, as believed, PZ and formaldehyde can react and form polymerized PZ products through condensation reactions (Iovu et al., 1994; Sandler and Delgado, 1969). Sandler and Delgado found that changing the ratio of formaldehyde to PZ could produce either polymethylene PZs or N,N'-(2-hyroxymethyl) PZ in water (Sandler and Delgado, 1969). Later research suggested that PZ and formaldehyde polymerization was catalyzed by metals such as complexes of nickel and other amines, which is pertinent since thermal degradation experiments were performed in stainless steel cylinders where iron (II), chromium (III), and nickel (II) are expected to be present due to mild corrosion (Ukraintsev and Krasnov, 1997).

6.3 Role of H^+PZ as an Active Species

Concentrated, loaded PZ solutions contain numerous species that could participate in thermal degradation reactions over a range of CO_2 loadings. Protonated PZ (H^+PZ) and PZ carbamate ($PZCOO^-$) are created from the initial reaction of PZ with CO_2. A series of experiments were performed in order to determine if H^+PZ or $PZCOO^-$ is the active species for degradation. It is hypothesized, and shown in section 6.1 above, that H^+PZ plays an important role in the initial thermal degradation pathways. When PZ is protonated, the α-carbon is subject to attack by another nucleophilic PZ, creating ring-opening products. The suspected reaction is shown below in Equation 6.19. Other products are possible through a similar reaction or series of reactions where the α-carbon next to a protonated amino function is subject to attack by any nucleophile in solutions.

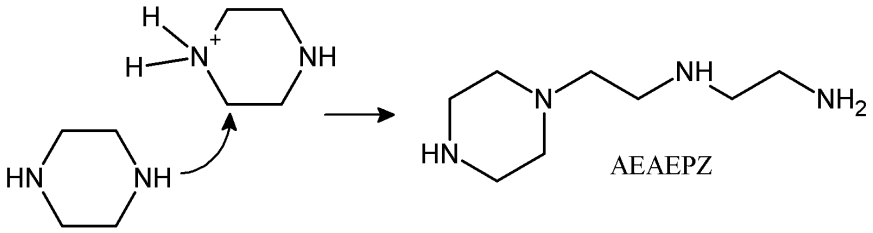

(6.19)

To test the behavior of H^+PZ, concentrated PZ in the absence of CO_2 was acidified to generate H^+PZ and then degraded under standard conditions. The goal was to examine H^+PZ degradation in the absence of any CO_2-containing species such as $PZCOO^-$, H^+PZOO^-, or $PZ(COO^-)_2$. Experiments exploring the effects of temperature, PZ concentration, and acid concentration were performed. Oppositely, to test the behavior of $PZCOO^-$, concentrated PZ was spiked with $KHCO_3$ to generate $PZCOO^-$ in the absence of H^+PZ and then degraded under standard conditions.

6.3.1 Thermal degradation of acidified, concentrated PZ

The baseline experiment for acidified PZ was 8 m PZ with 0.3 mole H^+ per mole alkalinity degraded at 175 °C. This H^+ concentration was chosen to mimic the concentration of H^+PZ in 8 m PZ with CO_2 loading of 0.3 moles CO_2 per mole alkalinity is used. The experimental design assumed that loading created the same concentration of H^+PZ and $PZCOO^-$ at this lean loading. Modeling of the system shows that this assumption is valid, as there is only slightly more H^+PZ than $PZCOO^-$ at this CO_2 loading because $PZCOO^-$ is beginning to react to form H^+PZCOO^- (Frailie and Rochelle, 2011).

The PZ loss and generation of total formate and EDA are compared in Figure 6.19, Figure 6.20, and Figure 6.21, respectively, for 8 m PZ with 0.3 moles CO_2 or H^+ mole per alkalinity degraded at 175 °C. In the acidified experiment, PZ loss is decreased to only 34% of the initial PZ compared to 68% in the loaded experiment after 15 weeks. CO_2 is known catalyst for thermal degradation (section 5.3.3), and these results indicate

that degradation can occur in the absence of CO_2 with H^+PZ present. H^+PZ is, therefore, an active species for thermal degradation and may initiate the first mechanisms for PZ thermal degradation. Degradation in loaded PZ solutions is likely a combination of the initiating action of H^+PZ and the reaction of CO_2-containing species with the products of H^+PZ initiated reactions.

The production of total formate and EDA in acidified solutions indicates the importance of CO_2 in degradation product generation. Negligible concentrations of formate were produced in the absence of CO_2 while EDA concentrations were higher than loaded solutions. As discussed in the next section, formate is generated directly from CO_2 or CO_2-containing species during thermal degradation and in the acidified experiments, no CO_2 was available to be reduced to formate. During loaded degradation of PZ, EDA is generated through initial degradation mechanisms and then reacts with CO_2 to form 2-Imid. In the acidified experiments, no CO_2 is available to form 2-Imid so EDA accumulates and acquires larger concentrations, even with less overall degradation. EDA appears to have a slightly higher initial rate of generation in the presence of CO_2 which may indicate the fact that PZ degradation is occurring faster, or that the formate generation mechanism may help stimulate EDA generation in some way.

6.3.2 Effect of temperature, PZ concentration, and H^+ concentration

The degradation of acidified PZ was investigated from 150 to 175 °C, 4 to 12 m PZ, and 0.2 to 0.6 mole H^+ per mole alkalinity. These experiments were intended to determine if H^+PZ initiated degradation in the absence of CO_2 responded similarly to changes in temperature, PZ concentration, and H^+ concentration as CO_2-loaded degradation.

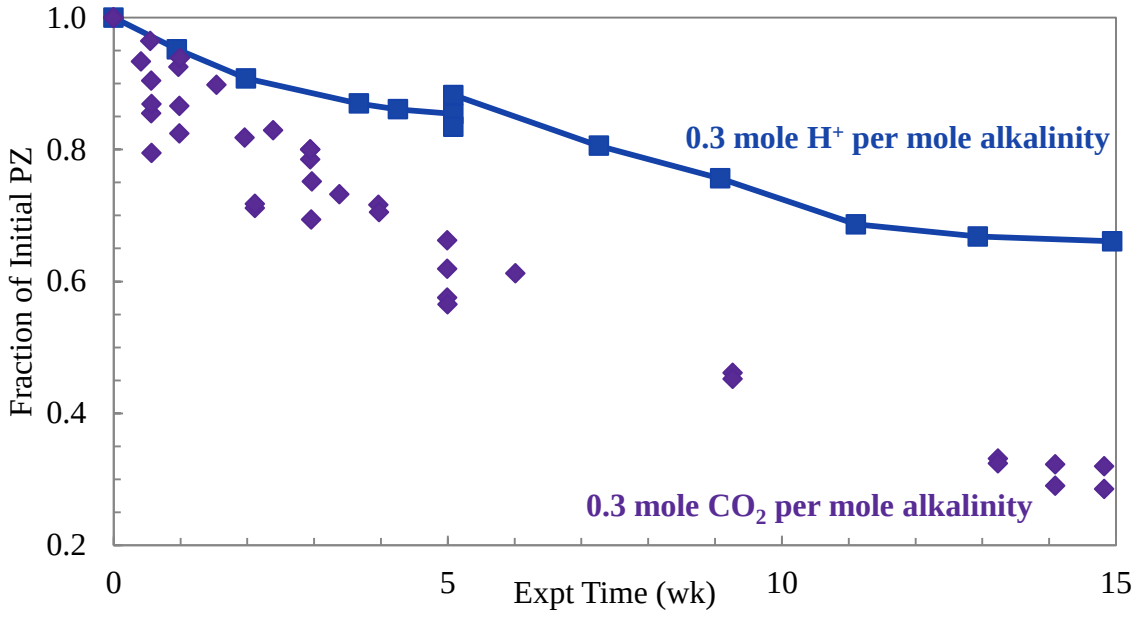

Figure 6.19: PZ loss in 8 m PZ at 175 °C with 0.3 mole CO_2 or H^+ per mole alkalinity

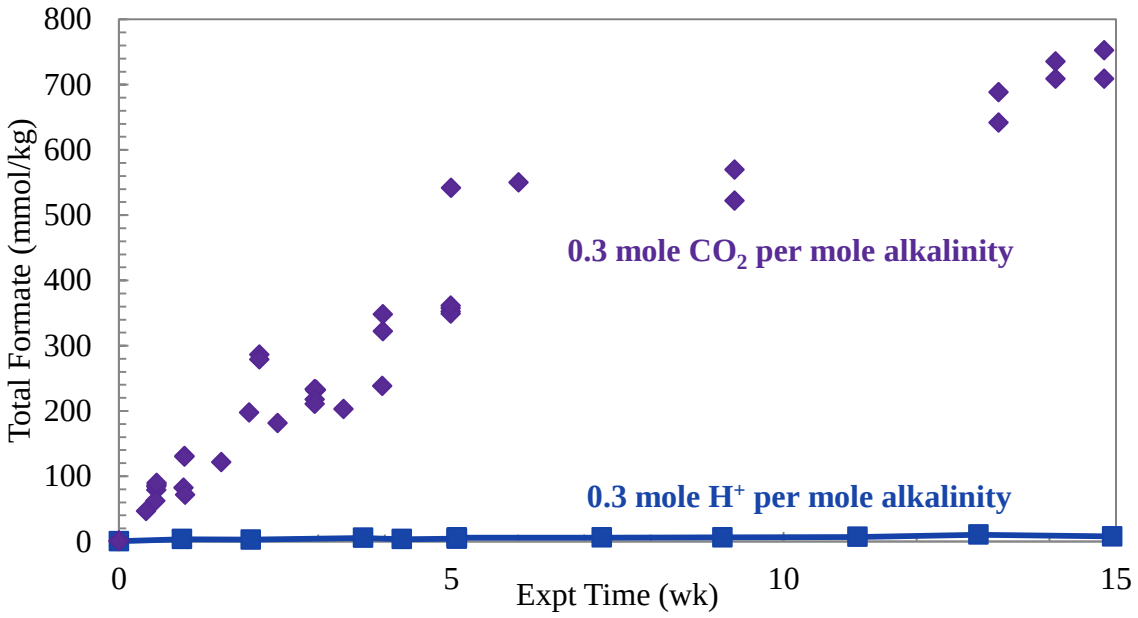

Figure 6.20: Generation of total formate in 8 m PZ at 175 °C with 0.3 mole CO_2 or H^+ per mole alkalinity

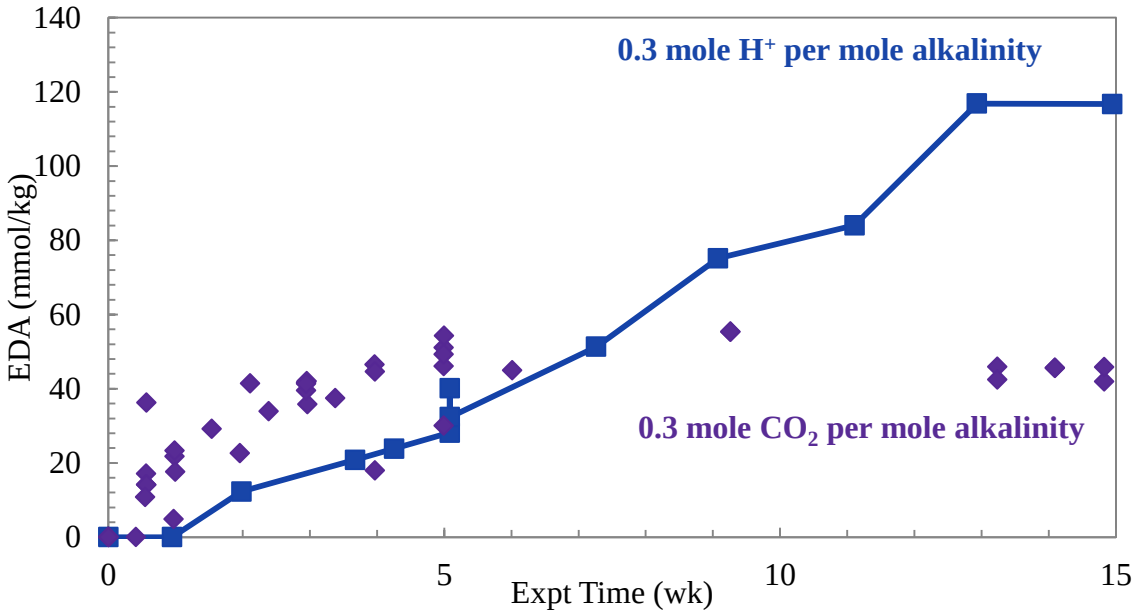

Figure 6.21: Generation of EDA in 8 m PZ at 175 °C with 0.3 mole CO_2 or H^+ per mole alkalinity

6.3.2.1 Effect of temperature on acidified PZ degradation

The k_1 for PZ loss in acidified PZ is compared to loaded solutions over 150 to 175 °C in Figure 6.22. At each temperature, the CO_2-loaded solution degrades at least twice as fast as the acidified experiment. The production of EDA for the same six experiments is compared in Figure 6.23. The three CO_2-loaded experiments have larger initial rates of EDA generation due to enhanced rates of thermal degradation. As EDA accumulates, it reacts with CO_2 in these loaded cases to form 2-Imid and EDA reaches a maximum concentration. In the acidified experiments, the EDA is generated faster as temperature increases, as expected and accumulates as a final product of thermal degradation.

This observation of the acidified production of EDA can shed light on the suspected mechanisms involved. First, CO_2 is not required to make EDA. The presence of CO_2, however, may accelerate its production or just accelerates the overall thermal

degradation rate. This could indicate, for example, that EDA is more readily produced from the urea of AEAEPZ than from AEAEPZ itself. Secondly, there appears to be a slight delay in the production of EDA in the absence of CO_2, so the generation of EDA may be a second order reaction. There was not enough data at very short times in the loaded experiments to confirm that in EDA generation is a second order product in the presence of CO_2.

6.3.2.2 Effect of PZ concentration on acidified PZ degradation

The k_1 for PZ loss in acidified 4 to 12 m PZ is compared to loaded solutions from 150 to 175 °C in Figure 6.24. As with 8 m PZ, both 4 and 12 m PZ with 0.3 mole H^+ per mole alkalinity degrade more than twice as slow as the loaded solutions. The PZ concentration behavior is similar for both CO_2-loaded and acidified solutions as the rates are slightly more than first order in PZ concentration. The production of EDA for the same six conditions at 175 °C is compared in Figure 6.25. As expected, the three loaded experiments have higher initial rates of EDA generation. In the acidified experiments, the EDA is generated at the same initial rate from 4 to 12 m PZ, while the experiments with CO_2 had increasing initial EDA production rates with increased PZ concentration. This indicates that the mechanism for EDA generation is rate limited by something other than PZ concentration because increasing the concentration of free PZ does not accelerate the EDA generation mechanism in the absence of CO_2.

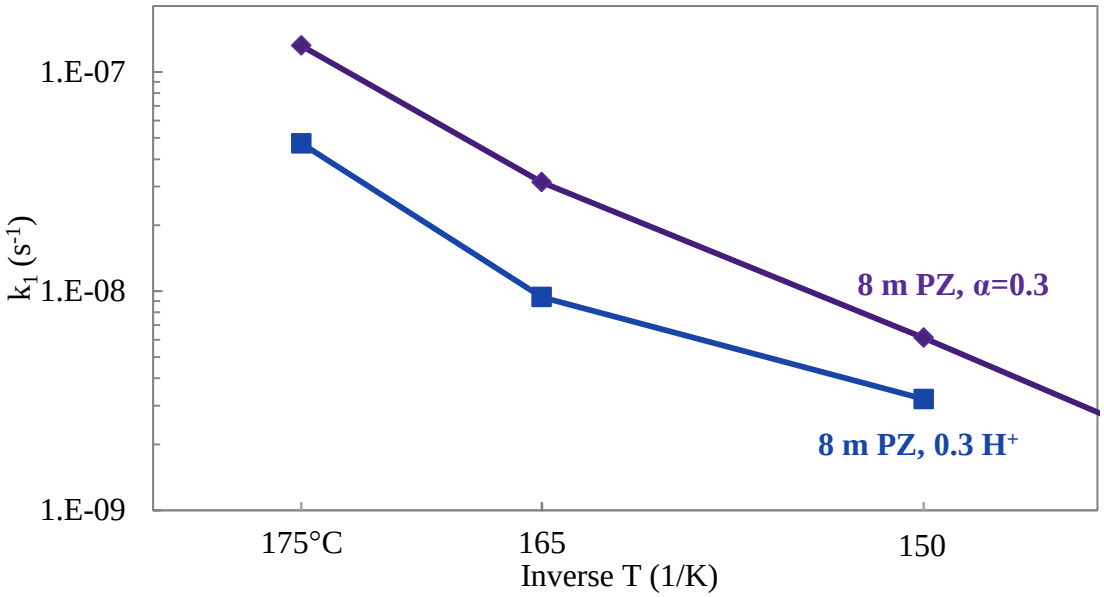

Figure 6.22: Comparison of k_1 values for PZ thermal degradation of acidified and loaded 8 m PZ

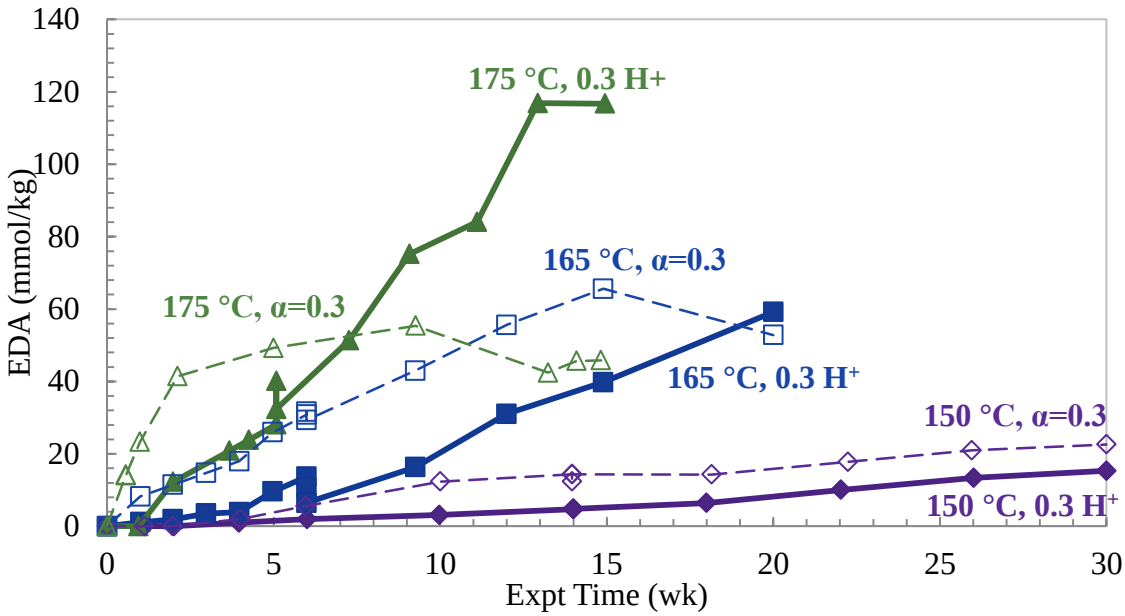

Figure 6.23: Generation of EDA for thermal degradation of 8 m PZ with 0.3 mole H^+ (solid) or CO_2 (dashed) per mole alkalinity from 150 to 175 °C

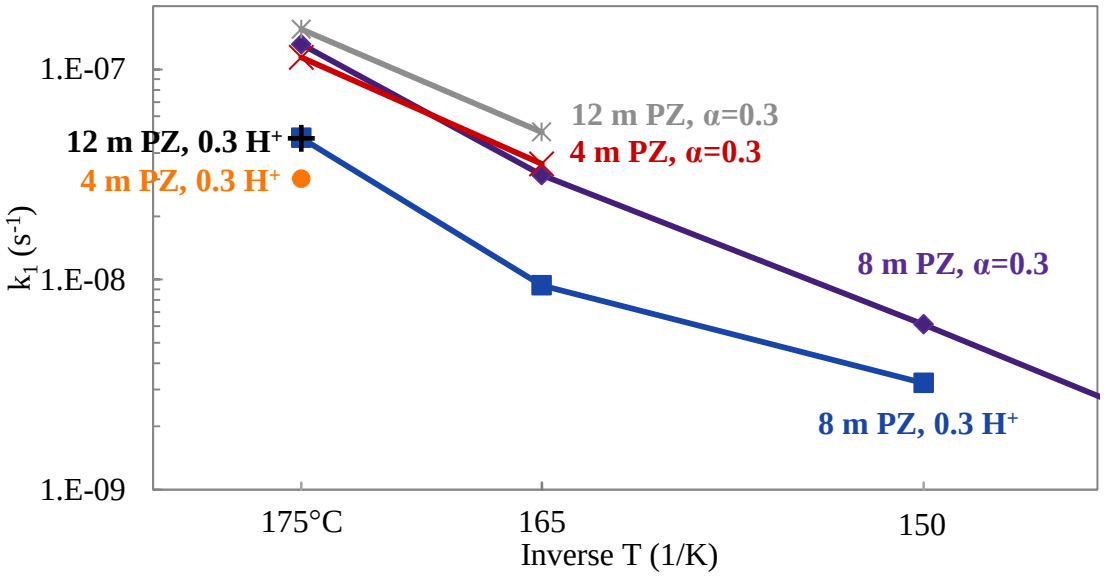

Figure 6.24: Comparison of k_1 values for thermal degradation of acidified and loaded 4 to 12 m PZ

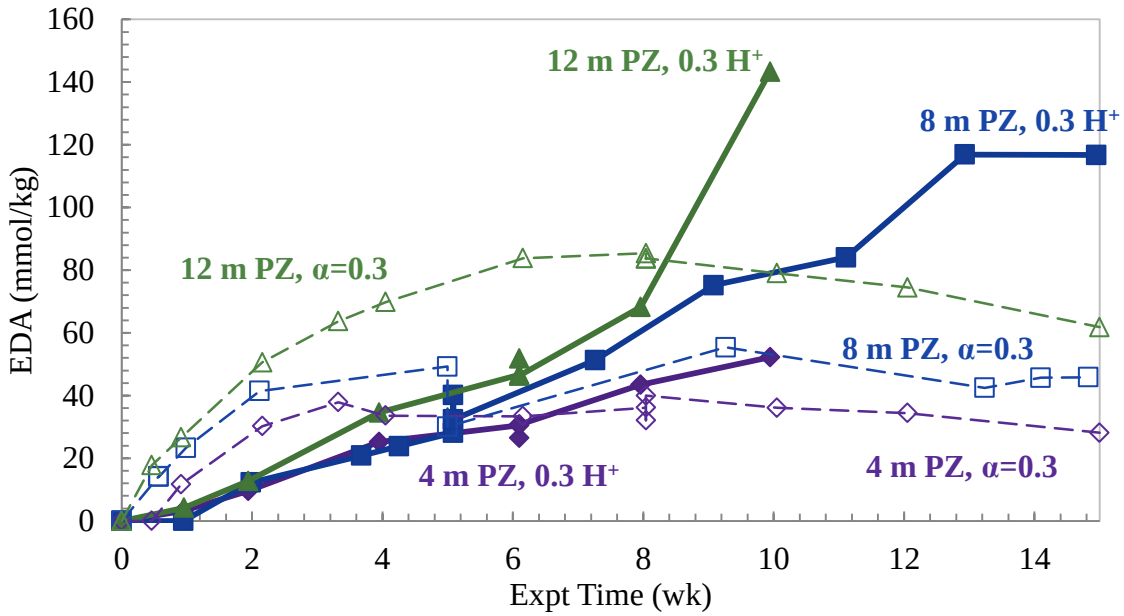

Figure 6.25: Generation of EDA for thermal degradation of 4 to 12 m PZ with 0.3 mole H^+ (solid) or CO_2 (dashed) per mole alkalinity at 175 °C

6.3.2.3 Effect of H^+ concentration on acidified PZ degradation

Finally, the k_1 for PZ loss in 8 m PZ with 0.2 to 0.6 mole H^+ per mole alkalinity and 0.3 mole CO_2 per mole alkalinity are compared in Figure 6.26. Both concentrations of 0.2 and 0.6 mole H^+ per mole alkalinity decreased PZ loss compared with 0.3 mole H^+ per mole alkalinity. A maximum in PZ loss was also observed in loaded experiments and the acidified data appear to mimic that behavior. The production of EDA for the same three H^+ concentrations at 175 °C is compared in Figure 6.27. Interestingly, the generation of EDA proceeds at the same initial rate in the presence of all three H^+ concentrations, indicating that the EDA generation mechanism is not directly dependent on the concentration of H^+PZ in solution.

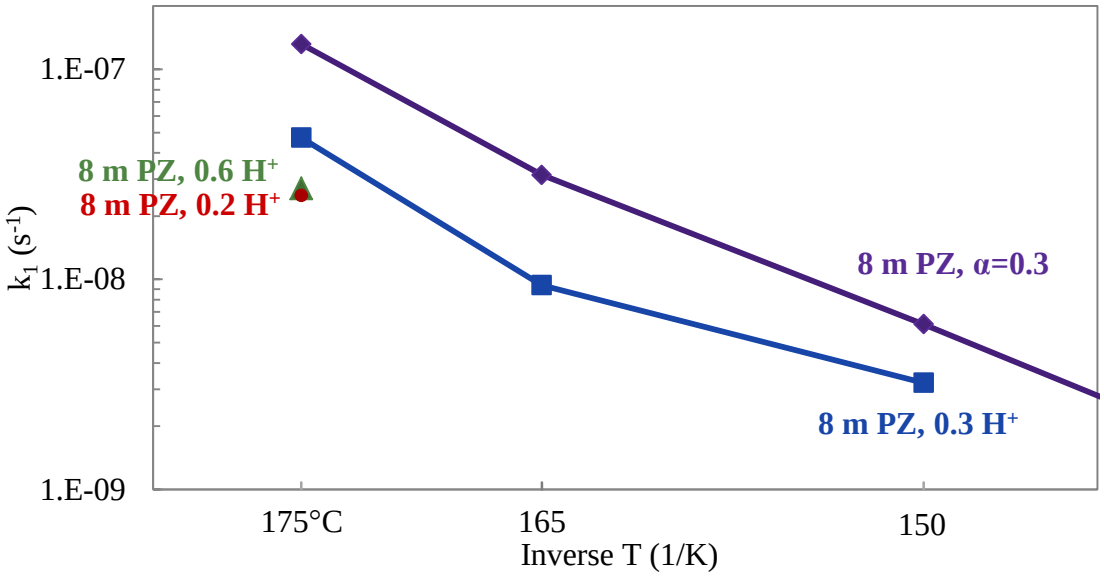

Figure 6.26: Comparison of k_1 values for thermal degradation of 8 m PZ with 0.2 to 0.6 mole H^+ or 0.3 mole CO_2 per mole alkalinity

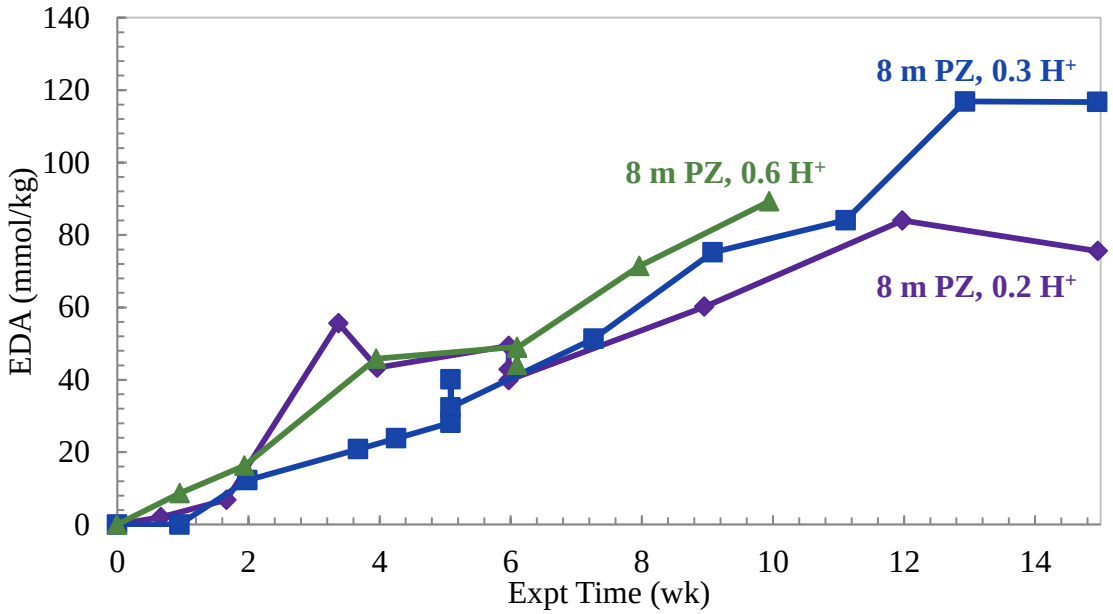

Figure 6.27: Generation of EDA for thermal degradation of 8 m PZ with 0.2 to 0.6 mole H^+ per mole alkalinity at 175 °C

6.3.3 Thermal degradation of PZ with $KHCO_3$

A solution of 8 m PZ with 0.1 mole $KHCO_3^-$ per mole alkalinity was degraded at 175 °C in an effort to determine if degradation would occur in the absence of H^+PZ. It was assumed that the present of $KHCO_3^-$ would react to create PZ carbamate ($PZCOO^-$) and other CO_2-containing molecules without significant concentrations of H^+PZ. The PZ loss in this experiment is compared to the complementary loaded experiment (0.1 mole CO_2 per mole alkalinity) in Figure 6.28. The generation of formate and EDA in these two experiments is compared in Figure 6.29. The absence of H^+PZ severely limits overall degradation of PZ and generation of both formate and EDA compared to a loaded solution. H^+PZ is a crucial species in the degradation mechanisms for PZ.

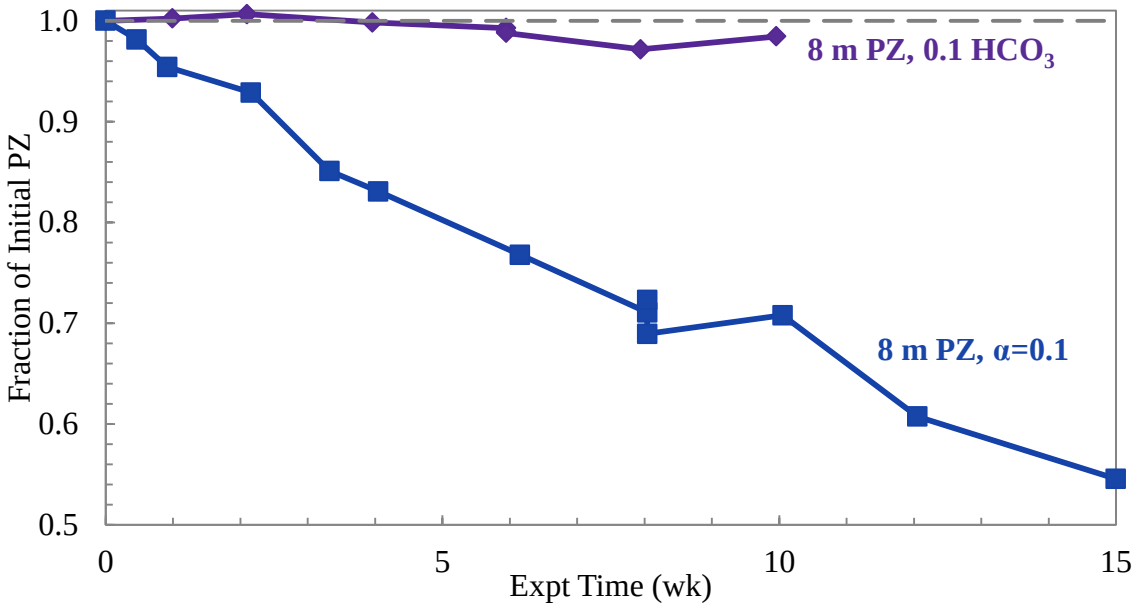

Figure 6.28: PZ Loss for thermal degradation of 8 m PZ with 0.1 mole CO_2 or $KHCO_3^-$ per mole alkalinity at 175 °C

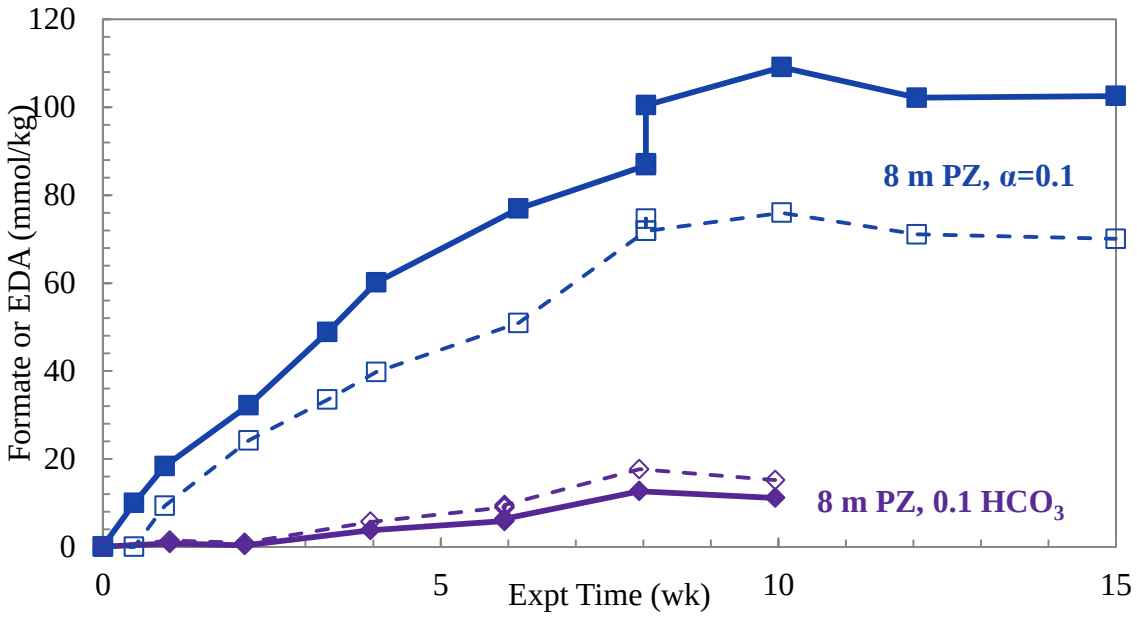

Figure 6.29: Generation of formate (solid) and EDA (dashed) for thermal degradation of 8 m PZ with 0.1 mole CO_2 or $KHCO_3^-$ per mole alkalinity at 175 °C

6.3.4 Difference in degradation products in acidified PZ

Changes in EDA and formate generation during acidified PZ degradation were discussed in the preceeding sections. Additional changes occur to the other degradation products in the absence of CO_2 that are observable when the cation IC chromatograms for 8 m PZ with 0.3 mole CO_2 (TE44) or H^+ (TE48) per mole alkalinity degraded at 175 °C are compared. A 15-minute portion of the cation IC chromatograms for the final samples of these two experiments are compared in Figure 6.30. The acidified experiment had half as much degradation as the loaded experiment, so peak sizes are reflective of product rates relative to the overall level of degradation. EDA was shown to accumulate in the acidified degradation experiments due to a lack of CO_2 to react with and this observation will be extended to other species in solution. As an additional note, there were not significant changes between the original and alkaline treated samples for the acidified experiment, indicating that amides were not produced in any significant concentration.

The unidentified peaks in both samples can be analyzed in terms of the known reactions occurring in each sample and the MS results discussed above in section 6.1.4. The major unidentified peaks occur at retention times of 39.7, 42.0, 42.5, and 43.3 minutes. The peak at 42.0 minutes is a large peak in the acidified experiment, indicating it is a species that does not contain CO_2 (i.e. not an urea or imidazolidone) and not generated from a mechanism that requires CO_2 or CO_2-containing species. The peaks at 39.7 and 42.5 minutes are only significant in the loaded experiment, indicating CO_2 is involved in their structure or generation mechanisms. Based on the aforementioned observations and IC-MS data, suspected identities of these peaks can be assigned.

The peak at 42.0 minutes is believed to be 1-[2-[(2-aminoethyl)amino]ethyl] piperazine (AEAEPZ) (CAS 24028-46-4; N1-[2-(1-piperazinyl)ethyl]-1,2-Ethanediamine). This molecule is believed to be created from the S_N2 reaction of PZ

with H^+PZ in the initial stages of degradation. This molecule was also suspected for a peak in this region during thermal degradation screening of AEP performed by Davis (2009) and was supported by IC-MS molecular weight measurements.

The peak 39.7 is suspected to be the urea of AEAEPZ urea, which is dominant in CO_2-loaded degradation. It is believed that in the presence of CO_2, AEAEPZ would rapidly react with CO_2 to form the AEAEPZ urea leaving only trace amounts of unreacted AEAEPZ. The molecular weight of the peak at 39.7 minutes was also determined to be 198.2 gram per mole using IC-MS, which matches the AEAEPZ urea. It is possible that this peak is the diPZ urea since the molecular weights are the same, but provided the presence of an AEAEPZ peak in the acidified experiment and the elution position in the quadamine region of the chromatogram, AEAEPZ urea is a more likely molecule. The last two peaks at 42.5 and 43.3 minutes have not been positively identified but their suspected molecules are discussed in section 6.1.4.

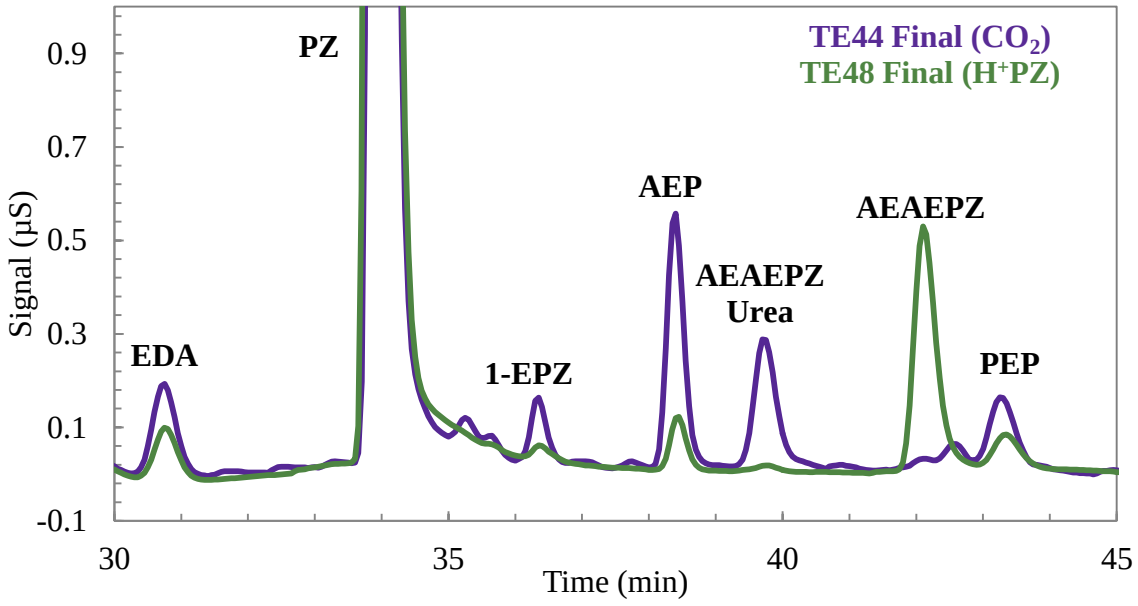

Figure 6.30: Cation IC chromatogram for the final sample of TE44 and TE48

6.4 MECHANISM FOR THE GENERATION OF FORMATE

6.4.1 Degradation of 8 m PZ in the presence of $^{13}CO_2$

In order to understand the generation of formate in oxygen-poor thermal degradation of concentrated PZ, an experiment was devised using ^{13}C-labelled CO_2 ($^{13}CO_2$) and NMR analysis. A solution of 8 m PZ was loaded with 0.3 mole CO_2 per mole alkalinity with $^{13}CO_2$. This solution was then degraded at 175 °C in thermal cylinders for six weeks. The degraded solutions were analyzed using ^{1}H and ^{13}C NMR in order to determine if the CO_2 lost during degradation ends up as formate or other products. A complimentary experiment with 8 m PZ with 0.3 mole natural CO_2 per mole alkalinity was performed in parallel as a control. Both sets of cylinders were degraded under the same conditions and analyzed in parallel.

The PZ loss and formate generation for the $^{13}CO_2$-loaded and natural CO_2 experiments are compared to collated data for 8 m PZ with 0.3 mole CO_2 degraded at 175 °C (TE4, TE12, and TE18) in Figure 6.31 and Figure 6.32, respectively. The PZ loss is consistent between the collated reference data, $^{13}CO_2$ experiment, and natural CO_2 experiment, while the formate data contains some scatter in the collated reference data. These comparisons demonstrate that the $^{13}CO_2$ and natural CO_2 reference experiments match previously collected data for thermal degradation at these conditions and NMR analysis of these samples should be representative of expected degradation.

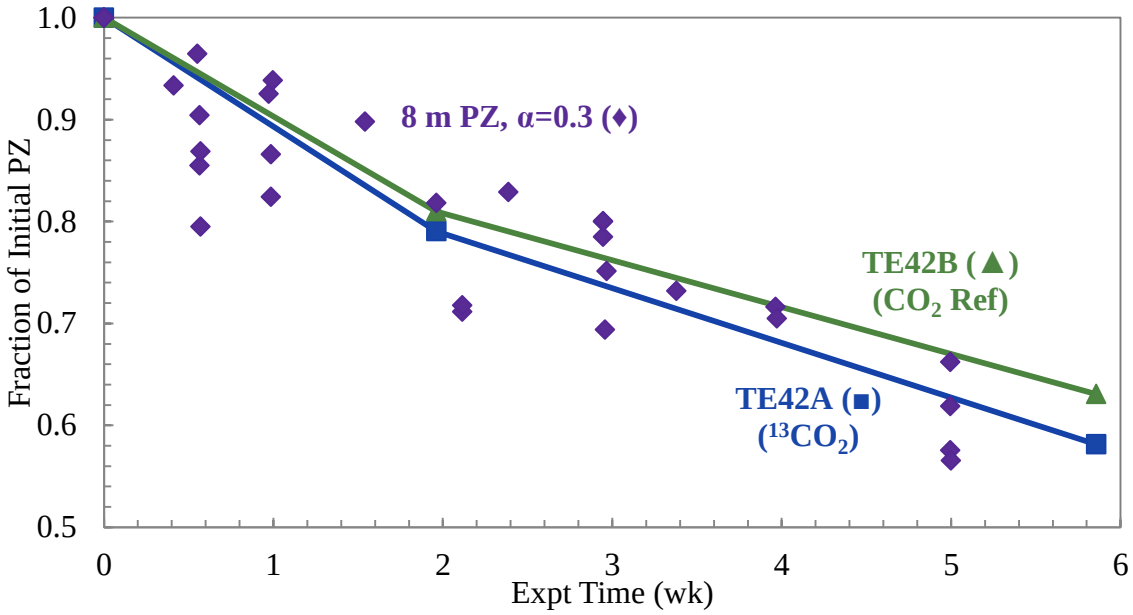

Figure 6.31: Comparison of PZ loss for 8 m PZ with 0.3 mole CO_2 or $^{13}CO_2$ per mole alkalinity at 175 °C

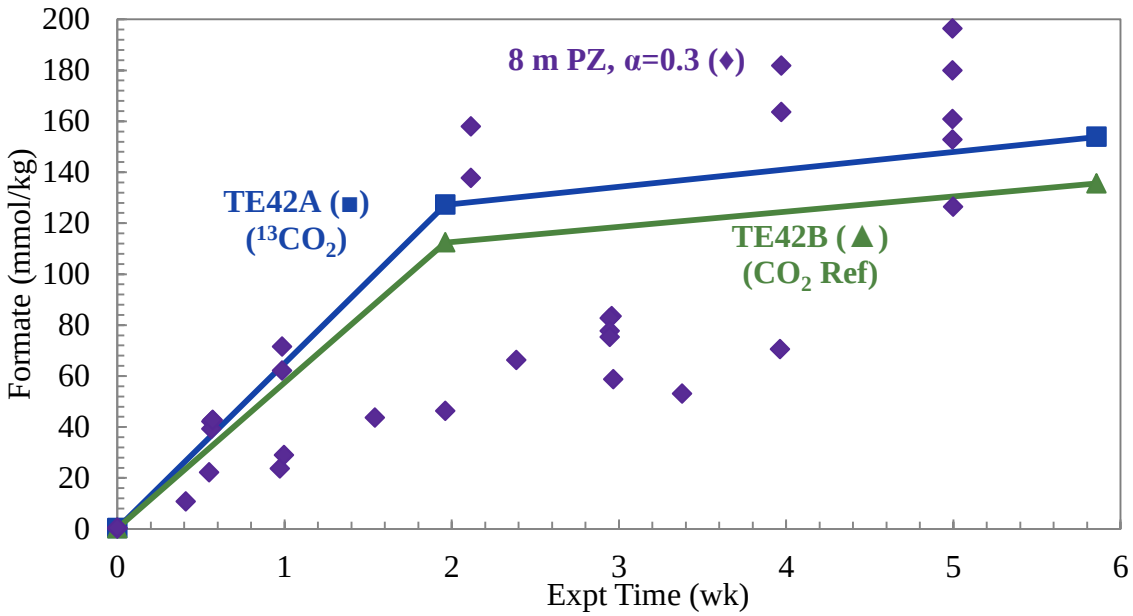

Figure 6.32: Comparison of formate generation for 8 m PZ with 0.3 mole CO_2 or $^{13}CO_2$ per mole alkalinity at 175 °C

6.4.2 NMR analysis of $^{13}CO_2$ degradation study

Degraded samples from the $^{13}CO_2$ and natural CO_2 experiments were analyzed using ^{1}H and ^{13}C NMR. The goal of the NMR work was to confirm the hypothesis that formate is generated during degradation from CO_2, not carbons of the PZ backbone. The NMR results would indicate if formate contained ^{13}C from ^{13}C-labelled CO_2, therefore indicating a mechanism for formate generation in an oxygen-poor environment. All NMR analysis was conducted at the NMR Laboratory at the University of Texas at Austin (Wallin and Storey, 2010).

To prepare for the NMR, background samples were analyzed to determine where formate generally appears in NMR spectra. The Spectral Database for Organic Compounds (SDBS) has a ^{13}C reference spectrum for formic acid (AIST, 2010). This spectrum was analyzed in the presence of $CDCl_3$ and shows the formic acid peak at 166.22 ppm (Figure 6.33). The peak expected for sodium formate in D_2O would be at 171.67 ppm (Gottlieb et al., 1997). The difference between these two chemical shifts is due to the pH of the solution in which formate was detected and demonstrates the range of shift for formate ions in aqueous solution that may be expected. The region where formate is seen is the downfield range of the ^{13}C spectrum where carbons that are part of a carbonyl (C=O) generally appear. In loaded PZ samples, the carbons of carbamate carbonyls and carbonate/bicarbonate carbonyls will also appear. In degraded solutions, it is expected that carbons of aldehyde carbonyls, ketone carbonyls, and amide carbonyls would appear in the same downfield area of the spectrum.

In order to anticipate what may be seen in degraded PZ solutions, two aliquots of loaded 8 m PZ were spiked with 38 and 305 mM formic acid and analyzed. The resulting downfield ^{13}C NMR spectra are shown in Figure 6.34 and Figure 6.35 below. In these two samples, the formate peak appears at a chemical shift of 170.191 and 170.296 ppm,

respectively. Both spectra also show peaks for the carbonyl in $PZCOO^-$ (162.334 and 162.375 ppm, respectively) and the carbonyl in CO_3^-/HCO_3^- (162.796 and 162.838 ppm, respectively) in the same downfield view. The sample with 38 mM also registered a peak for the $PZ(COO^-)_2$ at 163.135 ppm and it is not clear why that did not show up in the 305 mM sample. In loaded PZ solutions, the chemical shift of the carbon in formate is not quite as great as that of sodium formate reference spectrum, but should occur around 170 ppm. This test also demonstrates that the formate peak does not overlap with any of the carbonyl peaks expected in neat and CO_2-loaded PZ.

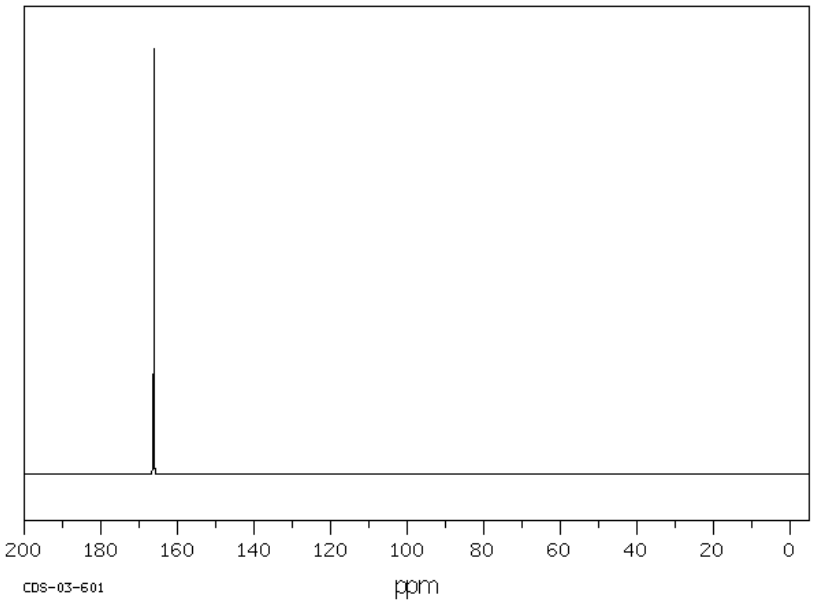

Figure 6.33: Reference ^{13}C spectrum for formic acid showing a major peak at 166.22 ppm (AIST, 2010)

In the degradation experiments, the ^{13}C-labelled CO_2 is used to amplify the NMR signal. ^{13}C NMR, as the name indicates, only detects ^{13}C isotopes of carbon. In standard samples, the signal is generated from the naturally occurring ^{13}C that is present in all matter, approximately 1% of all carbon. The effect of loading a PZ solution with $^{13}CO_2$

is seen when panels A and B of Figure 6.36 are compared. Panel A is a ^{13}C NMR spectrum of loaded PZ with natural CO_2 while Panel B is a ^{13}C NMR spectrum of $^{13}CO_2$-loaded PZ. It is important to note the relative size of the group of peaks upfield (right side of spectrum, ~40 ppm) and downfield (left side of spectrum, ~160 ppm). The upfield peaks represent naturally occurring ^{13}C in the carbons on the PZ backbone and are the same size in Panels A and B, despite the difference in the ordinate scale. The downfield peaks represent carbonyl carbons ($PZCOO^-$, $PZ(COO^-)_2$, and CO_3^-/HCO_3^-). The effect of $^{13}CO_2$ is clearly visible in the increased size of the carbonyl peaks.

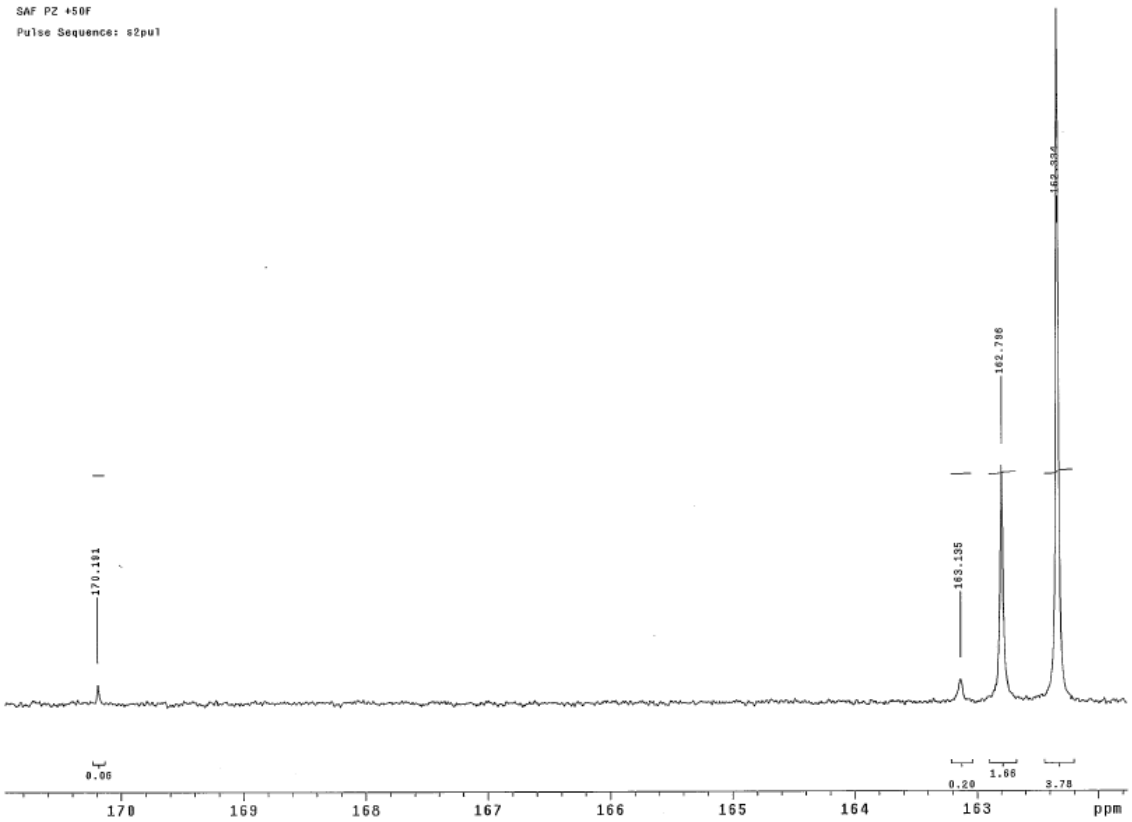

Figure 6.34: Downfield ^{13}C NMR spectrum for 8 m PZ with 0.3 mole CO_2 per mole alkalinity spiked with 38 mM formate

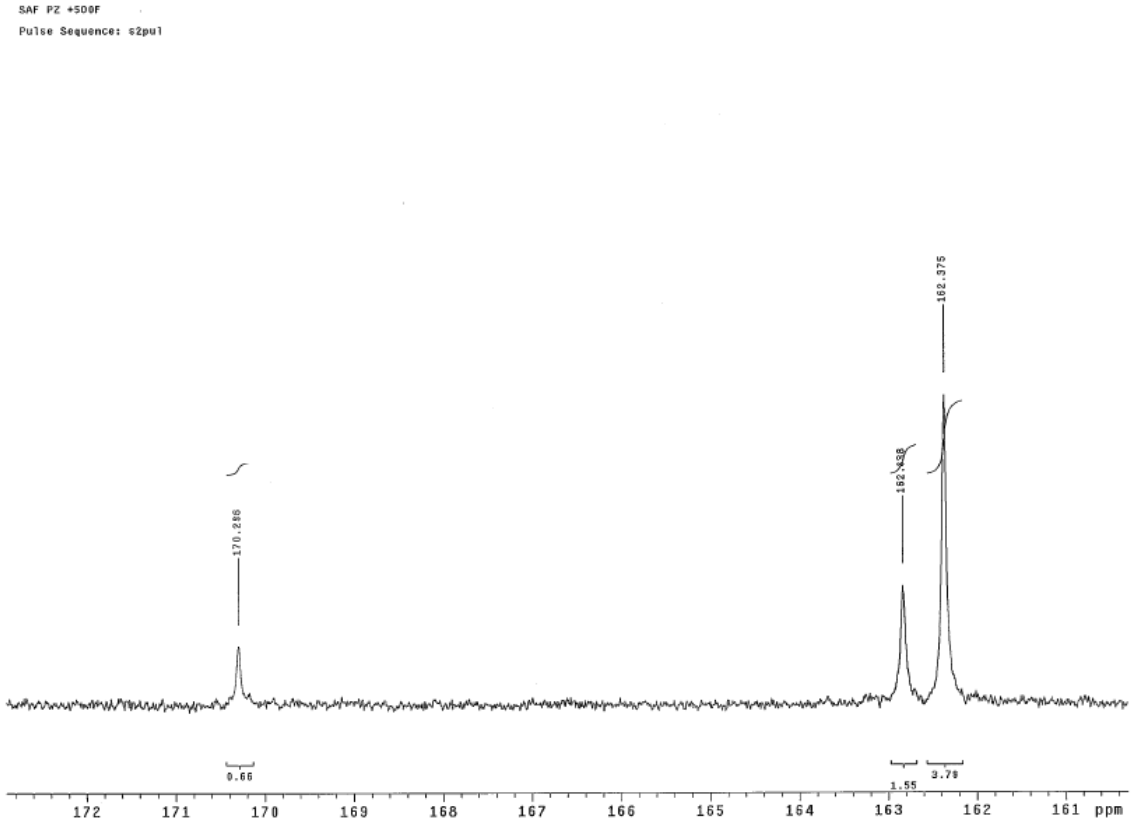

Figure 6.35: Downfield ^{13}C NMR spectrum for 8 m PZ with 0.3 mole CO_2 per mole alkalinity spiked with 305 mM formate

Samples of degraded PZ after 2 and 6 weeks of degradation at 175 °C were analyzed with quantitative ^{13}C NMR. As expected, the ^{13}C NMR spectra for degraded PZ samples were very complex due to the high level of degradation. Examples of the downfield ^{13}C NMR spectrum for degraded solutions containing $^{13}CO_2$ and natural CO_2 after 6 weeks of degradation are shown in Figure 6.37 and Figure 6.38. The spectra are cropped to show between 160 and 172 ppm of the downfield ^{13}C spectrum for comparison purposes. The peak at the far left at 170.1 ppm in both figures correspond to formate based on the background spectra analyzed above.

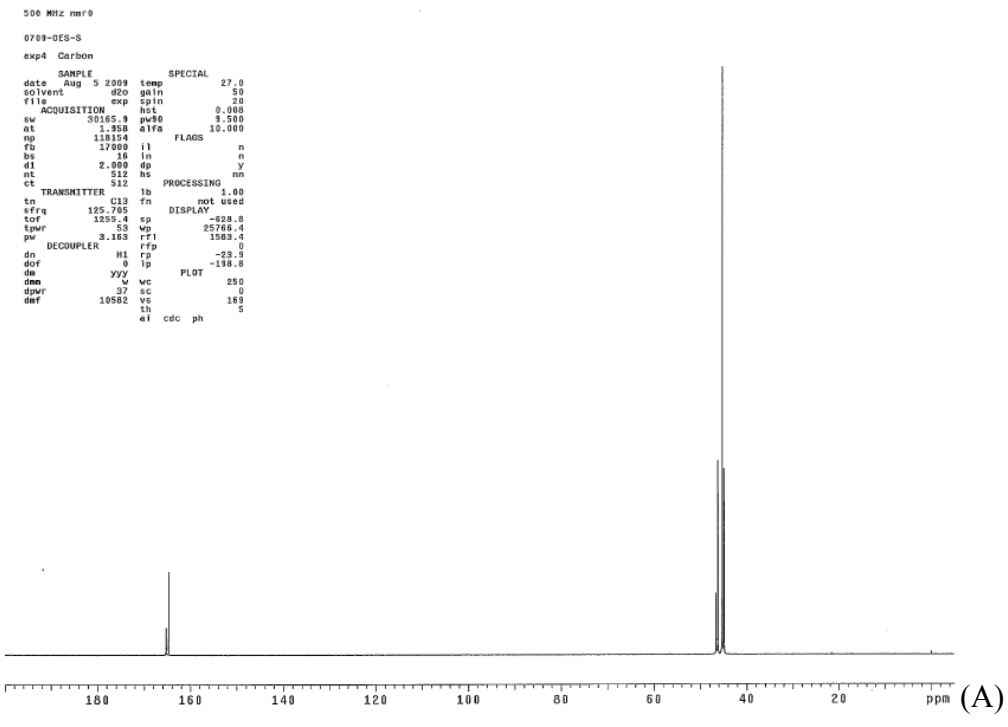

(A)

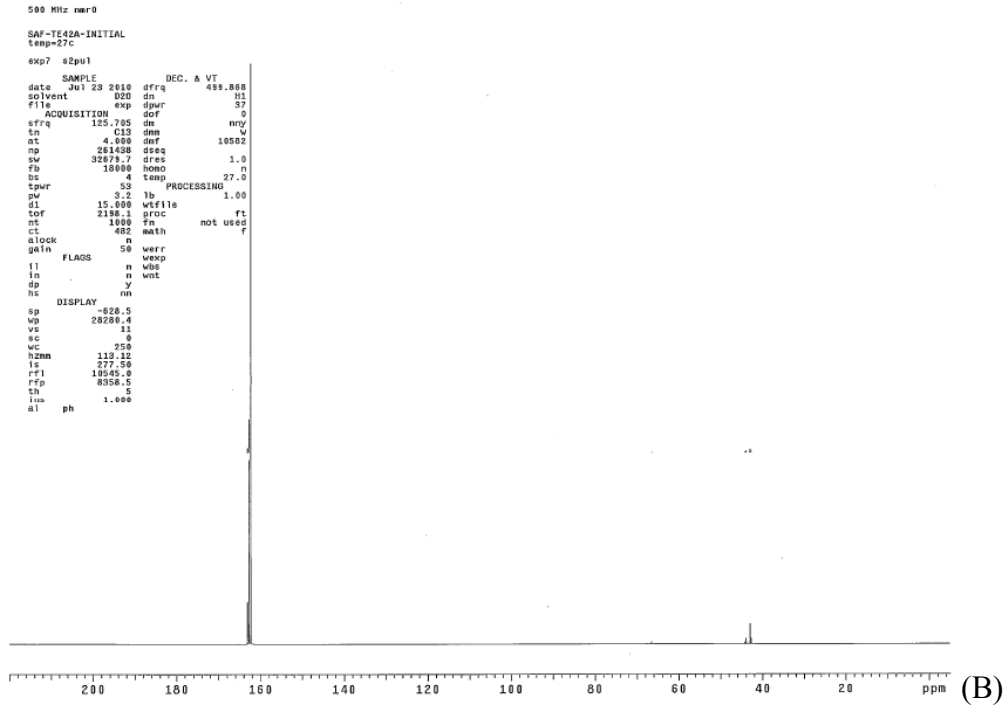

(B)

Figure 6.36: Comparison of ^{13}C NMR spectrums for 8 m PZ loaded with (A) natural or (B) ^{13}C-labelled CO_2 (aligned on horizontal ppm scale)

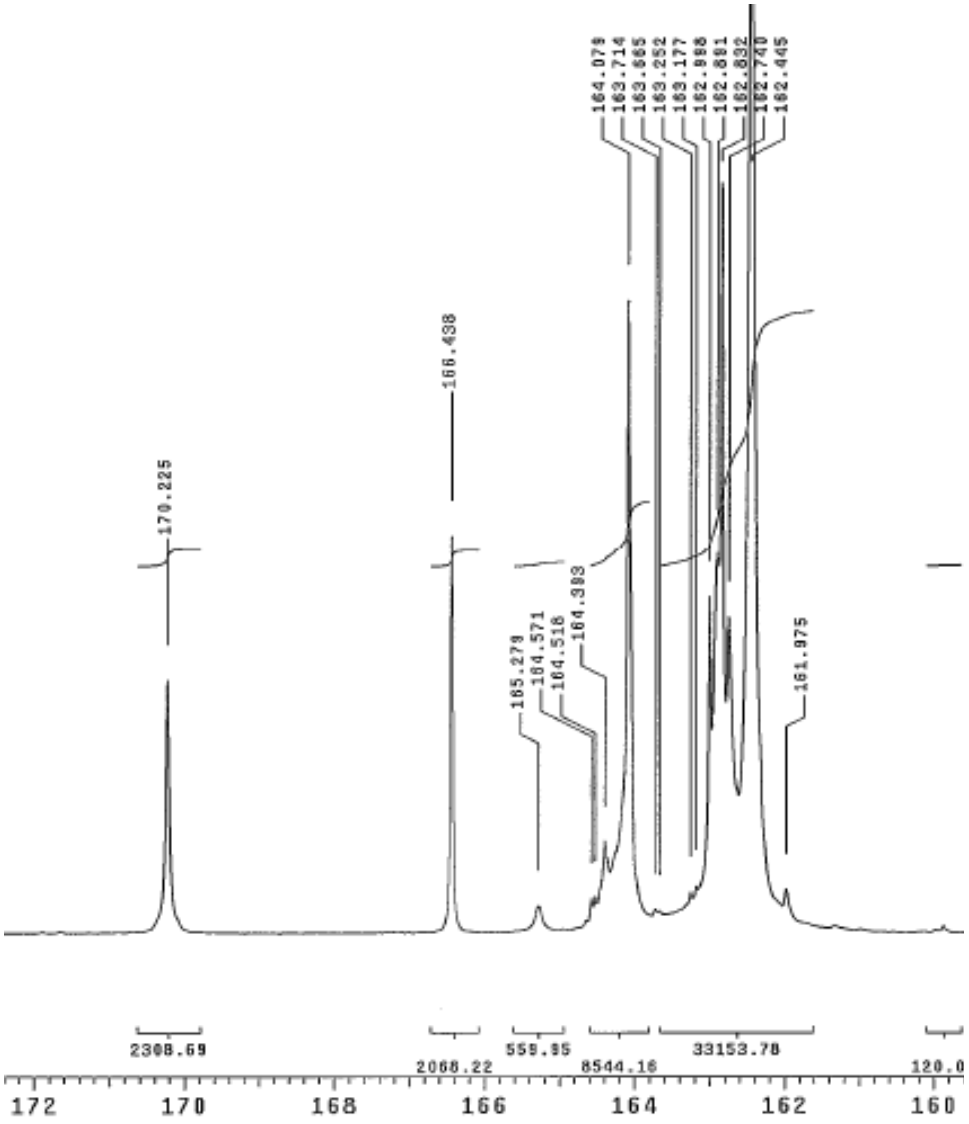

Figure 6.37: Downfield ^{13}C NMR spectrum for $^{13}CO_2$ loaded 8 m PZ after 6 weeks at 175 °C

From these spectra, the concentration of formate was estimated using a reference standard of 1 wt % dioxane. The peak areas associated with dioxane (~3.5 ppm in ^{1}H and 66.5 ppm in ^{13}C) were then used to estimate the concentration of other species in solution. The calculation started by determining the concentration of dioxane, $C_{Dioxane}$, in the submitted sample in units of moles dioxane per kg of total solution (Equation 6.20).

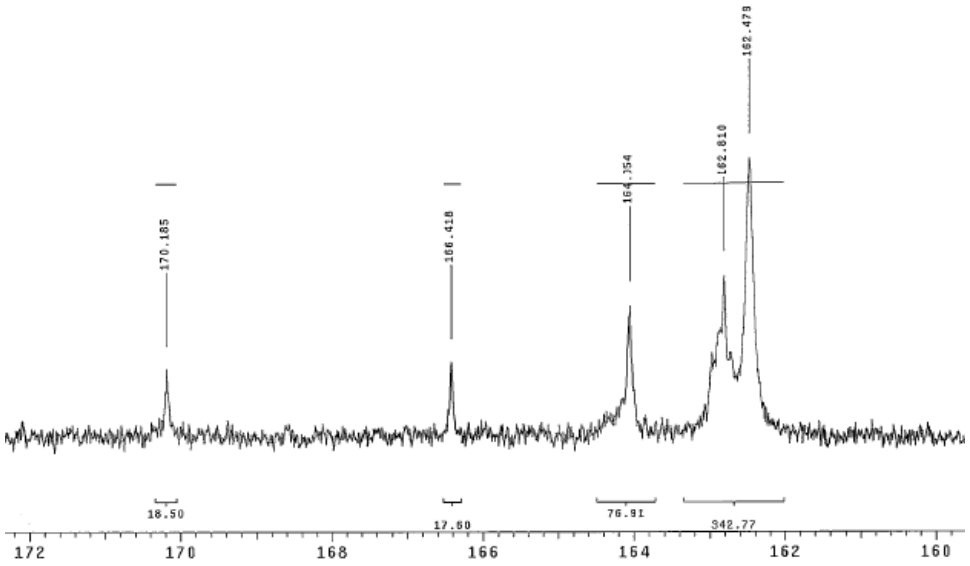

Figure 6.38: Downfield ^{13}C NMR spectrum for natural CO_2 loaded 8 m PZ after 6 weeks at 175 °C

$$C_{Dioxane} = \frac{\text{g Dioxane}}{\text{g total}} \times \frac{\text{mol Dioxane}}{\text{88.11 g Dioxane}} \times \frac{\text{1000 g total}}{\text{1 kg total}} \tag{6.20}$$

Then, a response factor, $RF_{Dioxane}$, was calculated using that concentration of dioxane, the number of carbons in dioxane, and the area from the ^{13}C NMR spectrum, $Area_{Dioxane}$ (Equation 6.21).

$$RF_{Dioxane} = \frac{\text{mole Dioxane}}{\text{kg soln}} \times \frac{\text{4 Carbons}}{\text{mole Dioxane}} \times \frac{1}{Area_{Dioxane}} \tag{6.21}$$

Finally, the concentration of the species of interest was calculated using $RF_{Dioxane}$, the area of the peak, and the number of carbons of the species. When calculating concentrations for species that are assumed to contain only ^{13}C, the ratio of ^{13}C to ^{12}C must be applied since the reference chemical, dioxane contains only naturally occurring

^{13}C. The concentration of formate, $C_{Formate}$, which is assumed to contain only ^{13}C, was calculated using Equation 6.22.

$$C_{Formate} = RF_{Dioxane} \times Area_{Formate} \times \frac{\text{mole Formate}}{1\,\text{Carbon}} \times \underbrace{\frac{0.0107\ \text{mole}\ ^{13}C}{0.9893\ \text{mole}\ ^{12}C}}_{\text{Ratio of natural } CO_2} \qquad (6.22)$$

Using Equation 6.22, the concentration of formate was calculated from the ^{13}C NMR spectrum for the degraded PZ. The calculated concentrations are compared with anion IC data of the same samples in Table 6.5. The formate concentration, not the total formate or formyl amide concentration was used because any amides would appear as separate peaks in the downfield region of the ^{13}C NMR. One set of calculations assumed that the formate peak in the $^{13}CO_2$ experiment contained all ^{13}C to match the hypothesis of the experiment. The final column in the table estimates the formate concentration from assuming it only contained natural ^{13}C. This would indicate a scenario where the formate carbon was produced from the PZ carbon backbone, rather than CO_2. It is clear from comparing the last two columns of Table 6.5 that the assumption that formate contains only ^{13}C is valid. The formate estimated from assuming only naturally occurring carbon is up to 80X larger than the anion IC measurement. This comparison confirms the hypothesis that formate is generated from CO_2, not the carbons on the PZ backbone.

Overall, the NMR analysis underestimated the formate concentration compared to the anion IC results. The NMR estimate is within 15% of the anion IC results for the final sample after 6 weeks of degradation. Given the nature of the NMR estimate, it is expected that the formate concentration contains more error when calculated this way compared to the direct measurement through anion IC.

Table 6.5: Comparison of formate quantified using anion IC and NMR in degraded PZ with $^{13}CO_2$ and natural CO_2

Expt.	Deg. Time	Formate Concentration		
		Anion IC	NMR – ^{13}C	NMR – Natural C
	weeks	mmol/kg	mmol/kg	mmol/kg
$^{13}CO_2$ (TE42A)	0	0.27	0	0
	2	127.2	66	6120
	6	153.9	132	12,160
Natural CO_2 (TE42B)	0	0.21	0	0
	2	112.4	-	-
	6	135.6	-	101

The NMR analysis shows conclusively that the formate generated in degraded PZ solutions is from the CO_2 molecule. Formate contains the CO_2 carbon and is not generated through break-up of the PZ molecule itself. The mechanism for this CO_2-reduction is not clear at this time.

This finding is notable since CO_2 is the only significant source of oxygen besides water in oxygen-poor thermal degradation. In addition, formate and formyl amides are found as a dominant degradation product in the thermal degradation of a variety of amines. This is primarily true in systems that do not undergo carbamate polymerization since that pathway uses the CO_2 molecule to create oxazolidones (Davis, 2009). The amines that produce significant formate concentrations during thermal degradation include: cyclic diamines (PZ, 1-MPZ, 2-MPZ), cyclic amines (piperidine, morpholine, pyrrolidine, hexamethyleneimine), straight chain amines (EDA, hexamethylenediamine), and some alkanolamines (MDEA). The presence of CO_2 is common in every experiment while the structures of the amine are very different including primary, secondary, and tertiary amines, linear amines, cyclic amines, monoamines, and diamines.

To demonstrate this, the generation of formate and total formate are compared for a variety of amines in Figure 6.39 and Figure 6.40, respectively. The degradation

conditions for the amines shown are different, but demonstrate the generation of formate and formyl amides in all solutions where data is available. The amines plotted are 8 m PZ, 7 m MEA (Davis, 2009), 8 m EDA (Zhou et al., 2010), 9 m 3-(methylamino) propylamine (MAPA) (Vevelstad, 2010), 8 m Mor, 7 m MDEA, 7/2 MDEA/PZ (Closmann, 2011), and 8 m 1-MPZ. CO_2 loadings were 0.2 mole per mole alkalinity for MDEA and MDEA/PZ, 0.3 mole per mole alkalinity for PZ, Mor, and 1-MPZ, and 0.4 mole CO_2 per mole alkalinity for MEA, EDA, and MAPA. Data shown represents thermal degradation at 135 °C for MEA, EDA, MAPA, MDEA, and MDEA/PZ, 150 °C for 1-MPZ, and 175 °C for PZ, Mor, and 1-MPZ. It is expected that all amines thermally degraded in the presence of CO_2 will produce both formate and formyl species, even if these products have not yet been quantified.

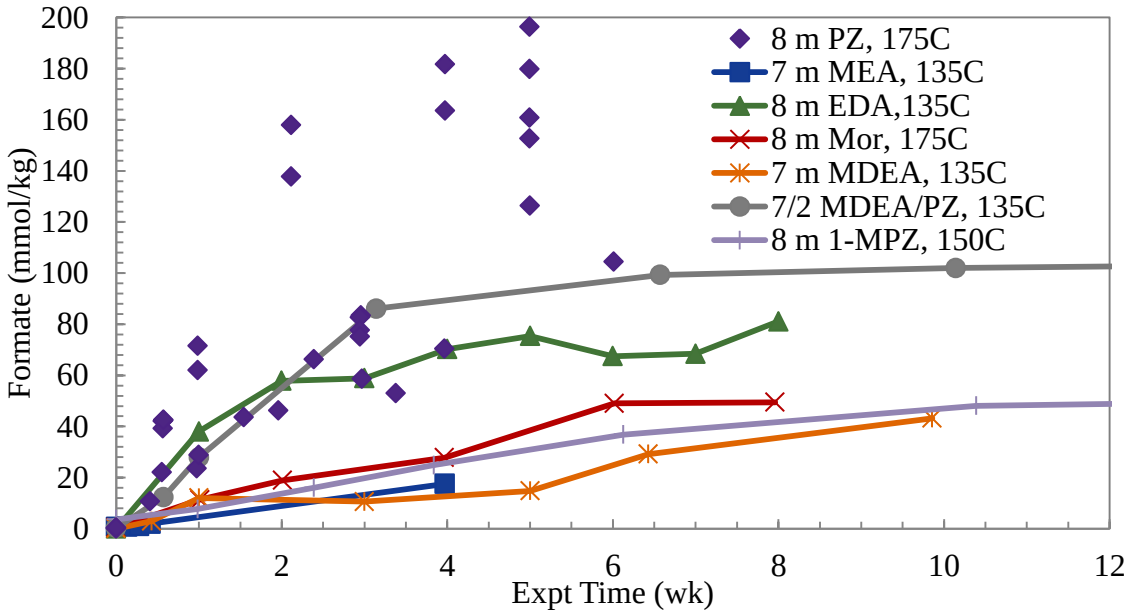

Figure 6.39: Comparison of formate generation for a variety of CO_2 capture amines

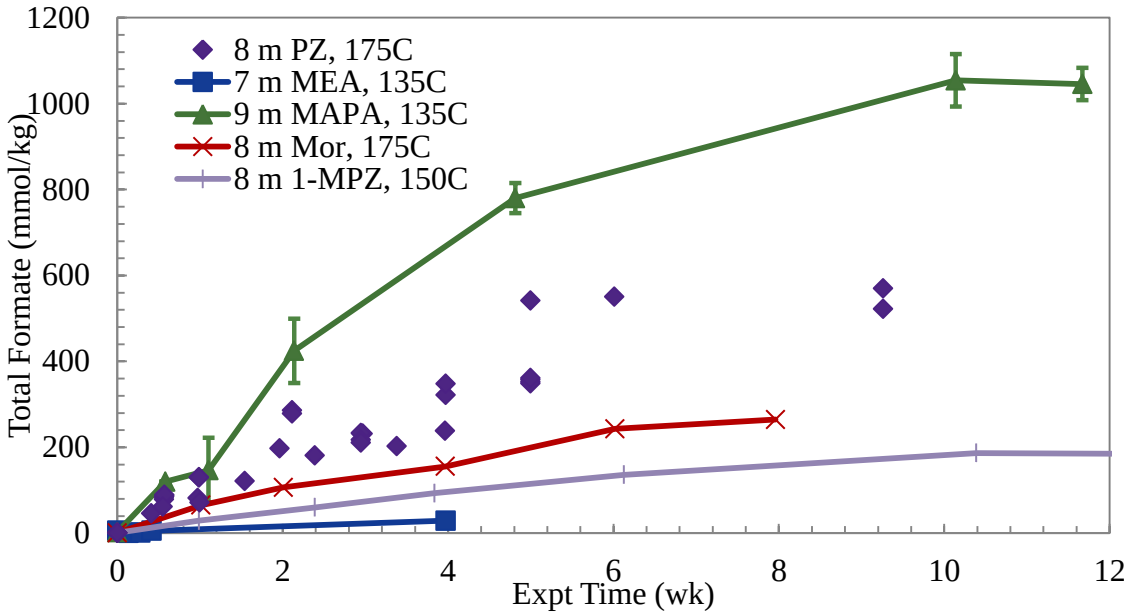

Figure 6.40: Comparison of total formate generation for a variety of CO_2 capture amines

6.4.3 Relationship of formate, PZ, and N-formyl PZ

The generation of formate, formyl amides, and FPZ is a crucial part of the thermal degradation of concentrated, aqueous PZ. Formate and formyl amides were generated in every thermally degraded solution containing CO_2 and are used a tracer compounds to track PZ degradation. The mechanism for the generation of formate from CO_2 has not been elucidated and it is not known whether formate ion or FPZ is produced first. All that is known is that both species are generated in the initial mechanisms of degradation products without a lag in the production. Most likely, one is generated first and reacts quickly with water or PZ to produce the complementary species. An equilibrium reaction appears to be occurring between the molecules where both are final products and the concentrations depend on degradation conditions (Equation 6.23). This equilibrium is complicated by the speciation of PZ into a variety of molecules including H^+PZ and $PZCOO^-$. It is not clear which form prefers to take part in the equilibrium.

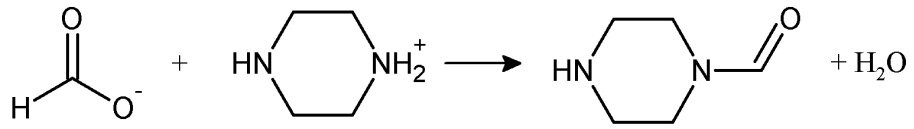

(6.23)

Amides can be converted to their respective carboxylate ion and amine through a hydrolysis, which is the basis of the alkaline treatment for quantifying amides (Koike et al., 1987). This reaction can be catalyzed by either acid or base and could occur readily in either direction at high temperature (Brown, 1994). It well established that FPZ can be produced through the reaction of PZ with active reactants in high temperature environments. For example, Horrom and colleagues produced FPZ by combining methyl formate and PZ while Duranleau reacted CO with catalyst at high temperature to produce FPZ and N,N'-diformyl PZ (Duranleau et al., 1986; Horrom et al., 1954). The same has been observed for other amides where research has shown that equimolar amounts of oxalate and PZ react to create N-oxalyl PZ (Mislyuk et al., 1985).

The interconversion of formate and FPZ was tested by spiking loaded 8 m PZ with either 200 mM formate or FPZ. The ratio of these species was monitored over 5 days at 175 °C, as shown in Figure 6.41. In both solutions, the spiked component reacted with either PZ or water to produce the other, indicating that neither is an intermediate for the other, but both are final products that can interconvert.

Other amides are created during thermal degradation of PZ, but FPZ is the first amine created and accumulates to significant concentrations before additional amides are formed. This is illustrated in Figure 6.42 where the concentration of formyl amides quantified using alkaline reversal and the anion IC tracks with the concentration of FPZ for the first 6 weeks of degradation. After that, the concentration of FPZ plateaued while the total formyl amides concentration continues to increase, indicating the production of different amides.

In all thermal degradation experiments with concentrated PZ, more formyl amides are generated than formate. The ratio of formyl amides to formate that is generated, however, appears to depend on solution speciation. The ratio of formyl amides to formate in degraded 4 to 20 m PZ with 0.3 mole CO_2 per mole alkalinity is compared in Figure 6.43. The ratio increases with increased PZ concentration, which is expected with higher concentrations of free PZ according to Le Chatelier's principle. The ratio of formyl amides to formate in degraded 8 m PZ with 0 to 0.47 mole CO_2 per mole alkalinity are compared in Figure 6.44. Increased CO_2 concentration also increases the ratio of formyl amides to formate. There is a larger amount of CO_2 in solution at higher loadings which can lead to more formate or formyl amides through the formate generation mechanism. Interestingly, the high loading experiment with 0.47 mole CO_2 per mole alkalinity did not lose as much PZ as lower loadings, but produced larger ratios of formyl amides to formate.

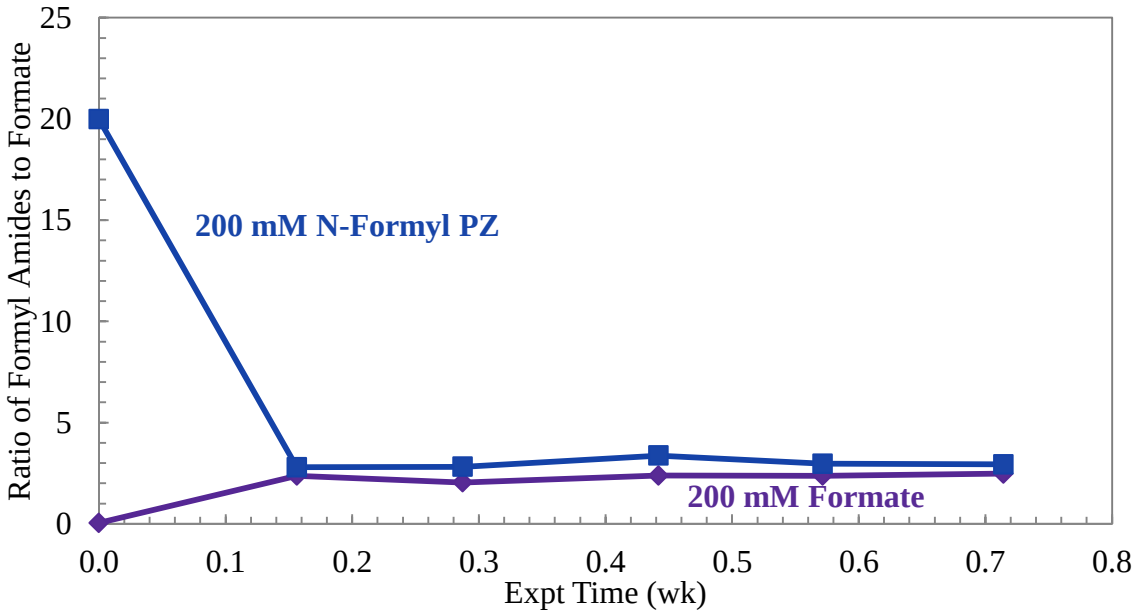

Figure 6.41: Equilibrium of formyl amides and formate at 175 °C in 8 m PZ spiked with 200 mM formate (TE66) or N-formyl PZ (TE67)

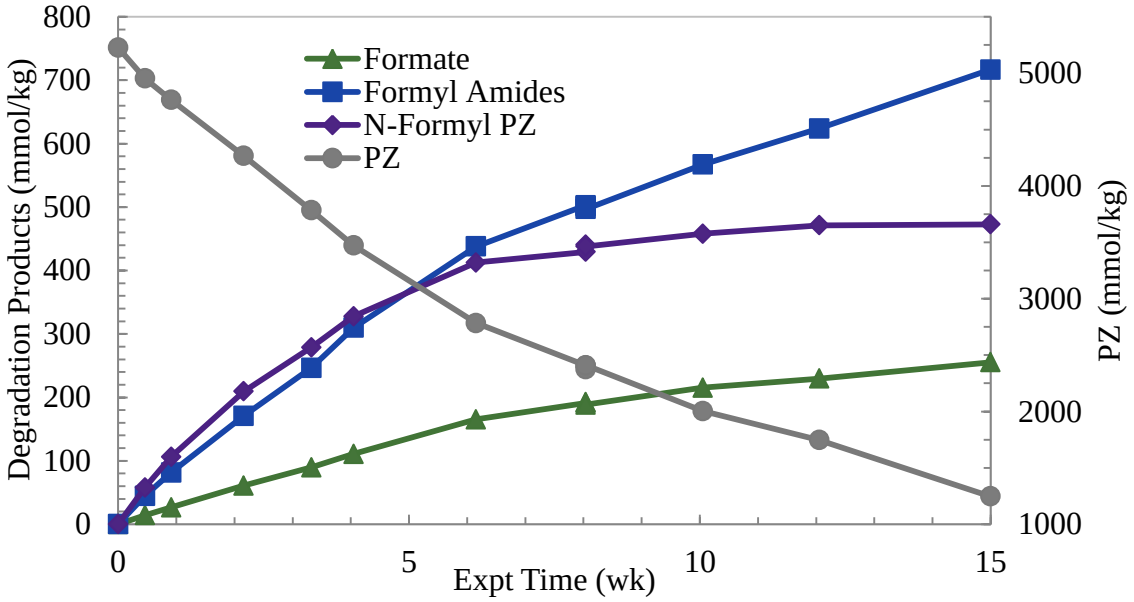

Figure 6.42: Concentration profiles for PZ loss and generation of degradation products for 12 m PZ with 0.3 mole CO_2 per mole alkalinity at 175 °C (TE33)

The effect of temperature on the equilibrium ratio of formyl amides to formate from 55 to 175 °C is shown in Figure 6.45. The experiment at 55 °C is oxidation of 8 m PZ with 0.3 mole CO_2 per mole alkalinity in the presence of 4 mM Cu^{2+} (OE25) while the remaining data sets are thermal degradation of 8 m PZ with 0.3 mole CO_2 per mole alkalinity (TE10, TE12, TE14, and TE44). Although oxidation and thermal degradation occur through different processes and under different conditions, the equilibrium ratio of formyl amides to formate is not strikingly different. The oxidation experiment was not as long in duration, but the data obtain indicate the ratio is very similar to the range of data obtained with thermal degradation. There is not a clear trend in the ratio with changing temperature. In all cases discussed, it is clear that the equilibrium ratio for each condition is reached quickly and persists, despite changing levels of overall degradation.

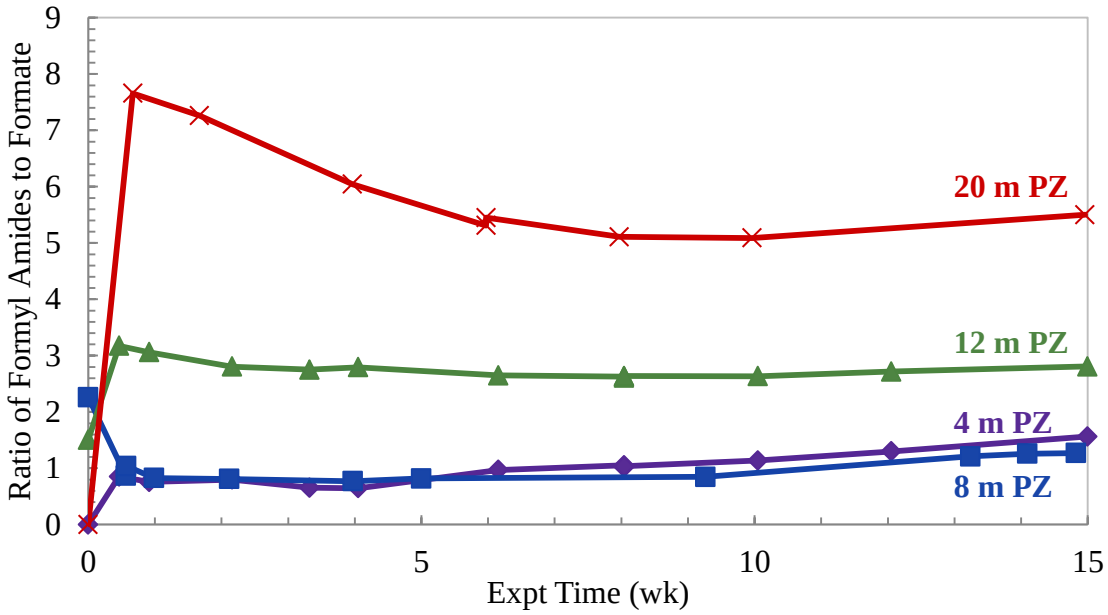

Figure 6.43: Ratio of formyl amides to formate produced during degradation of 4 to 20 m PZ with 0.3 mole CO_2 per mole alkalinity at 175 °C

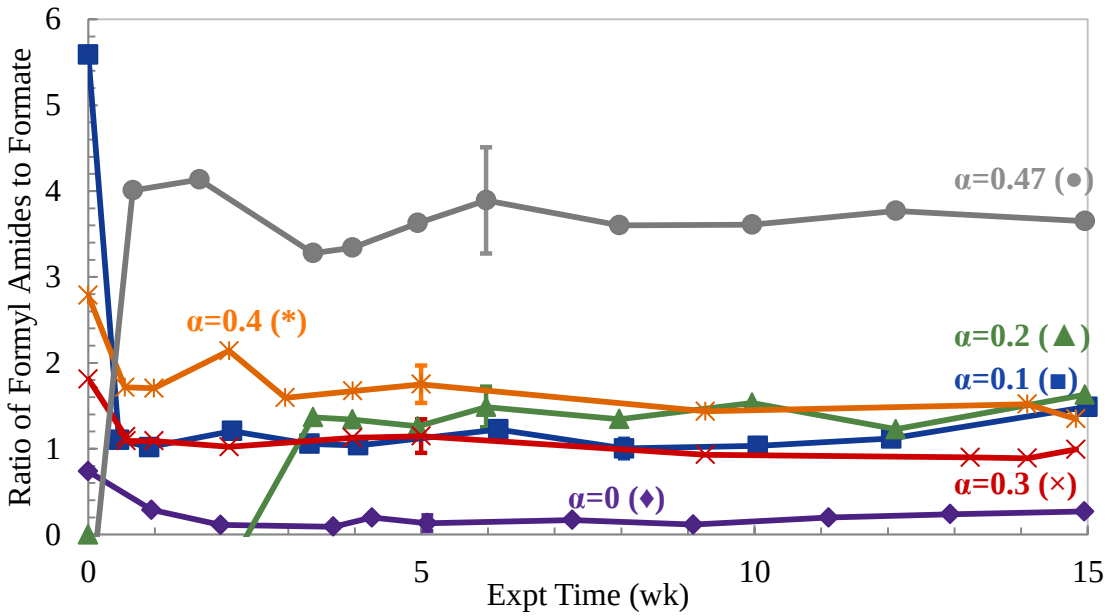

Figure 6.44: Ratio of formyl amides to formate produced during degradation of 8 m PZ with 0 to 0.47 mole CO_2 per mole alkalinity at 175 °C

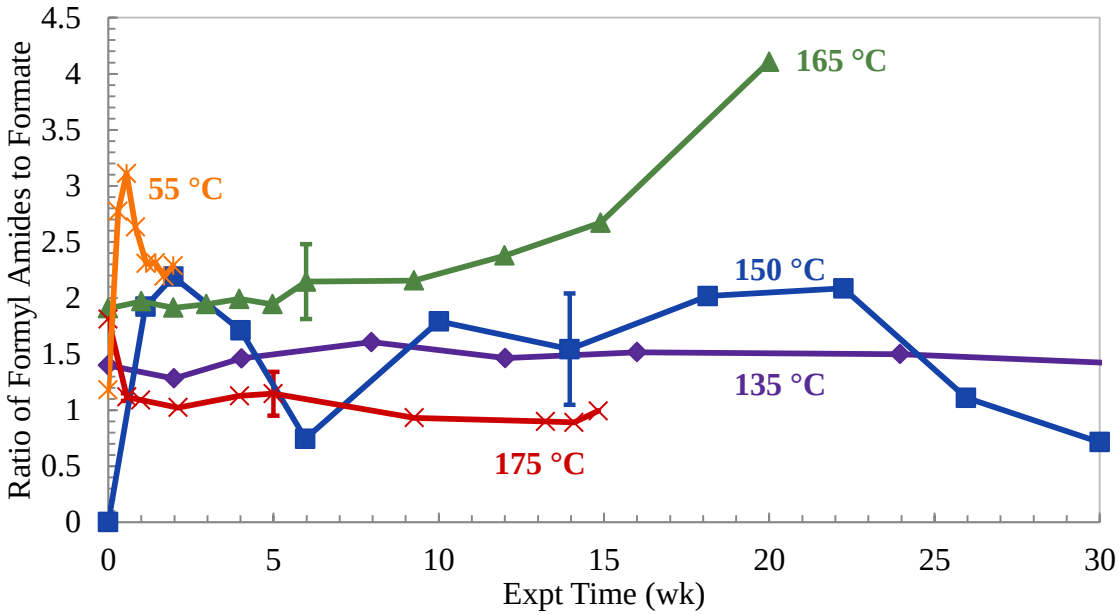

Figure 6.45: Ratio of formyl amides to formate produced during degradation of 8 m PZ with 0.3 mole CO_2 per mole alkalinity from 55 to 175 °C (OE25, TE10, TE12, TE14, and TE44

In order to understand the behavior of formyl amides and formate during thermal degradation, the average of the equilibrium ratio of formyl amides to formate was calculated for experiments ranging from 4 to 20 m PZ, 0 to 0.47 mole CO_2 per mole alkalinity, and 55 to 175 °C. As with Figure 6.45, the 55 °C data is from oxidation in the presence of 5 mM Cu^{2+} (OE25). If the ratio varied with time, the ratio toward the end of the experiment was taken to represent the equilibrium ratio expected. The ratios are shown for all conditions over a range of CO_2 loadings in Figure 6.46. The ratio increases with both PZ and CO_2 concentration, indicating a preference for producing amides at high PZ concentration and CO_2 loading. This result could be expected because increased concentrations of either free PZ or CO_2 would be expected to produce more amides.

Surprisingly, the effect of temperature is minimal, except for the two data points for 12 m PZ at 165 and 175 °C. This fact is demonstrated in Figure 6.47 where all of the

8 m PZ data are plotted as the same data set. In fact, a linear fit of all of the 8 m PZ data provides a reasonable regression that could predict the expected ratio of formyl amides to formate over a range of CO_2 loadings. The regression is shown in the figure and is as follows where the concentration of formyl amides, C_{FA}, and concentration of formate, C_F, are related to the CO_2 loading, α (mole CO_2 per mole alkalinity), by Equation 6.24. For 20 m PZ at 175 °C, the ratio can be described by Equation 6.25). Data for 4 and 12 m PZ were not gathered at varied CO_2 concentrations so the same regression cannot be performed.

$$\frac{C_{FA}}{C_F} = 5.54 \times \alpha + 0.30 \tag{6.24}$$

$$\frac{C_{FA}}{C_F} = 7.73 \times \alpha + 3.10 \tag{6.25}$$

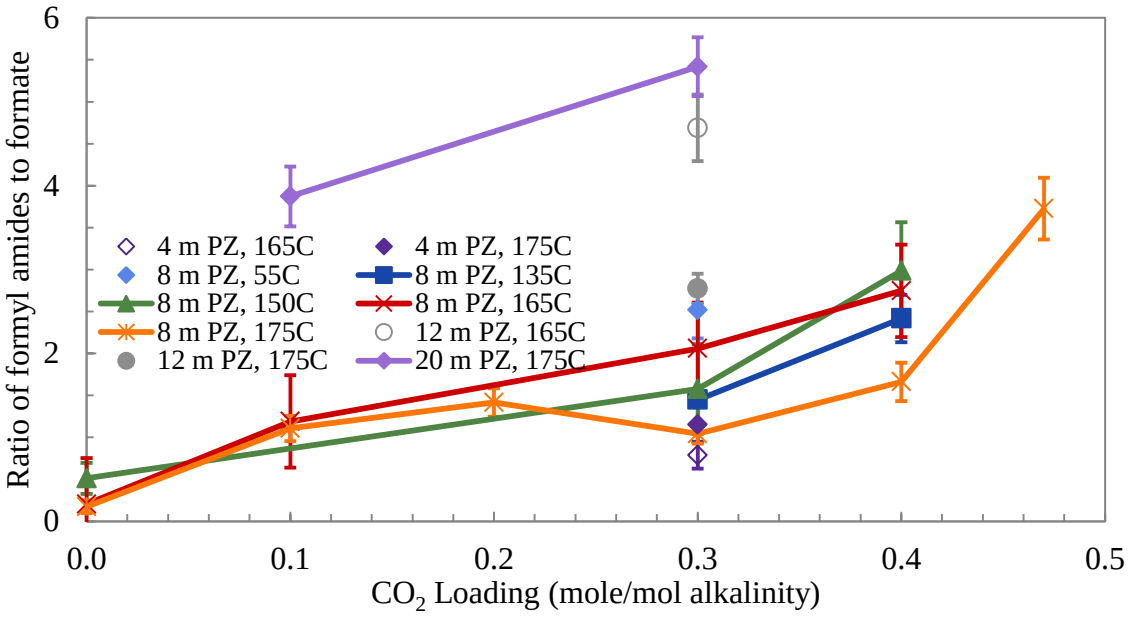

Figure 6.46: Ratio of formyl amides to formate generated during PZ thermal degradation of 4 to 12 m PZ at 135 to 175 °C

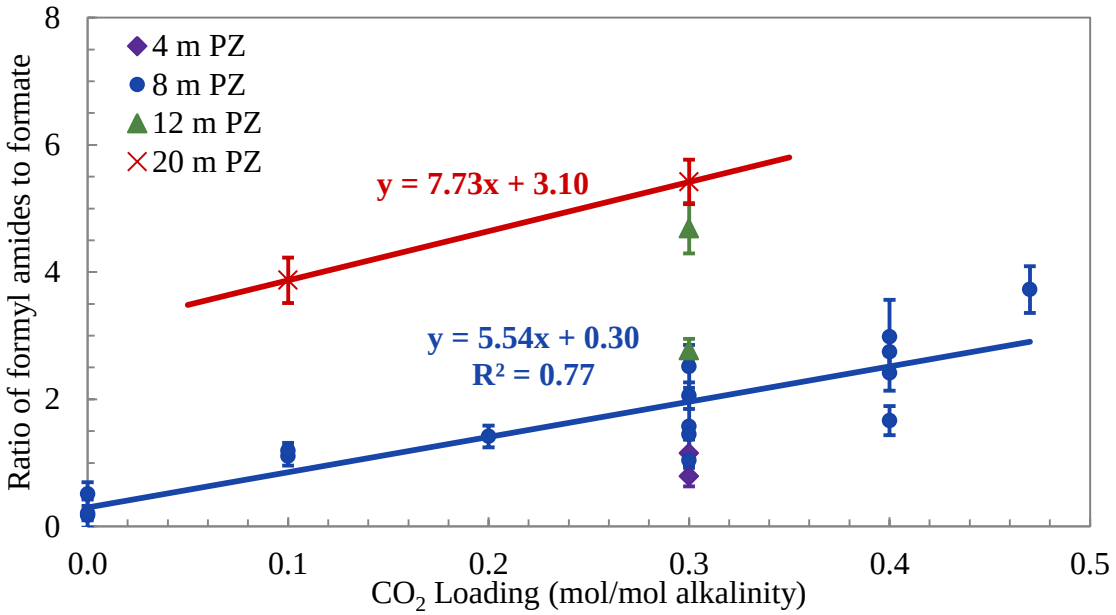

Figure 6.47: Ratio of formyl amides to formate generated during PZ thermal degradation of 4 to 12 m PZ without the effect of temperature

6.5 Role of EDA in PZ thermal degradation

EDA is a prominent thermal degradation product of PZ, but is known to degrade rapidly at temperatures lower than normal PZ degradation experiments (Zhou et al., 2010). During degradation, EDA produces both the cyclic EDA urea, 2-Imidazolidone (2-Imid), and the linear diEDA urea, N,N'-bis(2-aminoethyl)urea, whose chemical structures are shown in Figure 6.48 below. Zhou quantified 2-Imid using HPLC with UV detection while N,N'-bis(2-aminoethyl)urea was identified using cation IC-MS (Rochelle, 2009b). Since EDA is generated during PZ degradation, the thermal degradation of EDA is important to understand.

Three experiments were performed with the aim of highlighting the behavior of EDA in thermally degraded PZ. Blends of 8 m PZ and 1 m EDA were degraded at 150 and 175 °C and 8 m PZ spiked with 1 m 2-Imid was degraded at 175 °C. It was

hypothesized that EDA reacts with CO_2 to rapidly form 2-Imid, so the equilibrium between the two molecules in the presence of high concentration PZ was investigated.

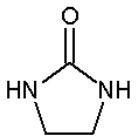

2-Imidazolidone (2-Imid)
MW = 86.09 g/mol
(Cyclic EDA)

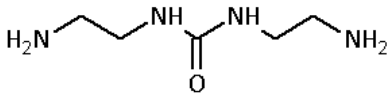

N,N'-bis(2-aminoethyl)urea
MW = 146.19 g/mol
(Linear diEDA urea)

Figure 6.48: Chemical structures of EDA ureas produced during thermal degradation

The concentrations of PZ, EDA, 2-Imid, and EDA loss for the blend 8 m PZ + 1 m EDA at 150 °C is shown in Figure 6.49. EDA quickly reacted with CO_2 in this blend to form 2-Imid. It is not suspected that EDA reacted from any other product as the EDA loss tracks closely with the generation of 2-Imid, within the expected error of the two analytical methods. During the 4 weeks of degradation, both the EDA loss and 2-Imid generation level out indicating an equilibrium condition may have been reached where the EDA and 2-Imid have nearly the same concentration (approximately 225 mmole per kg). The loss of PZ is consistent through the experiment, with only 4% lost after 4 weeks at 150 °C. The equilibrium of EDA and 2-Imid occurs significantly faster than PZ loss and is likely not strongly affected by other PZ degradation products in this experiment.

The concentrations of PZ, EDA, 2-Imid, and EDA loss for the blend 8 m PZ + 1 m EDA at 175 °C are shown in Figure 6.50. The high reaction temperature produced a rapid equilibrium between EDA, CO_2 and 2-Imid where EDA and 2-Imid reached equilibrium concentrations within 1 week. As found in the lower temperature experiment, the EDA loss tracks closely with the generation of 2-Imid within the expected error of the two analytical methods. The difference in analytical technique used

for quantification or the presence of another EDA-based degradation product may account for the slight difference in the concentration of 2-Imid and EDA loss. After 1 week of degradation, the EDA and 2-Imid concentrations level out, but not to the same value as in the 150 °C experiment. The temperature dependence of the equilibrium or the presence of more degradation products may be influenced these equilibrium concentrations.

In an effort to understand the equilibrium between EDA and 2-Imid, a blend of 8 m PZ + 1 m 2-Imid was degraded at 150 °C. A secondary goal of this experiment was to determine if ureas switched arms rapidly in degrading solutions at high temperature. Since 2-Imid was added, it was hypothesized that PZ, being a stronger nucleophile and more concentrated in solution, would react and take the place of the EDA molecule in the urea structure to generate PZ-based ureas.

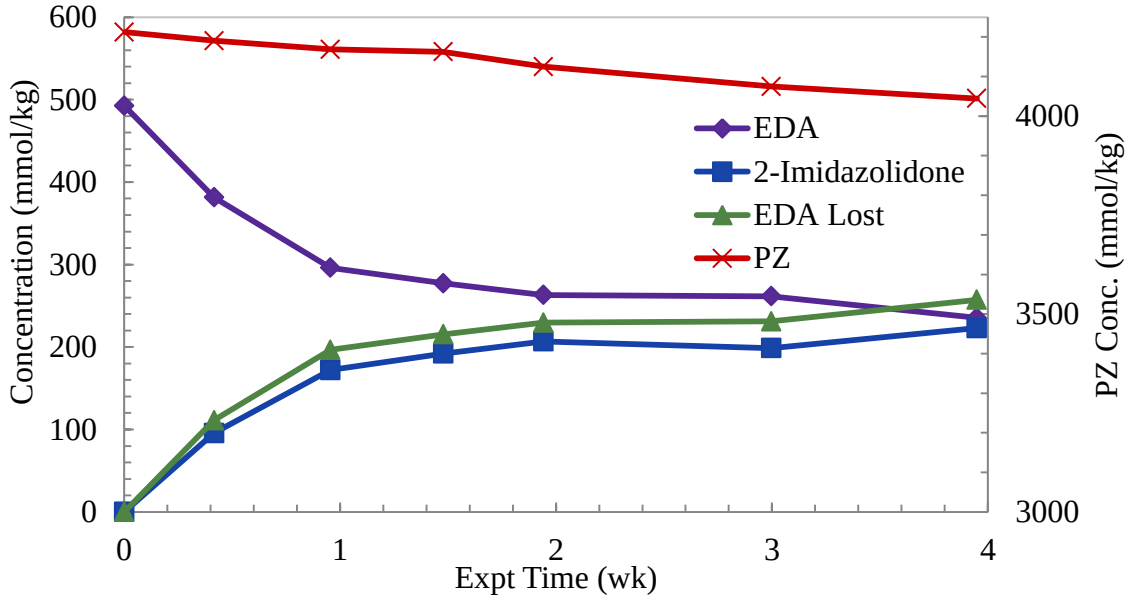

Figure 6.49: Concentration profiles for prominent amines in thermal degradation of 8 m PZ + 1 m EDA (α = 0.3) at 150 °C

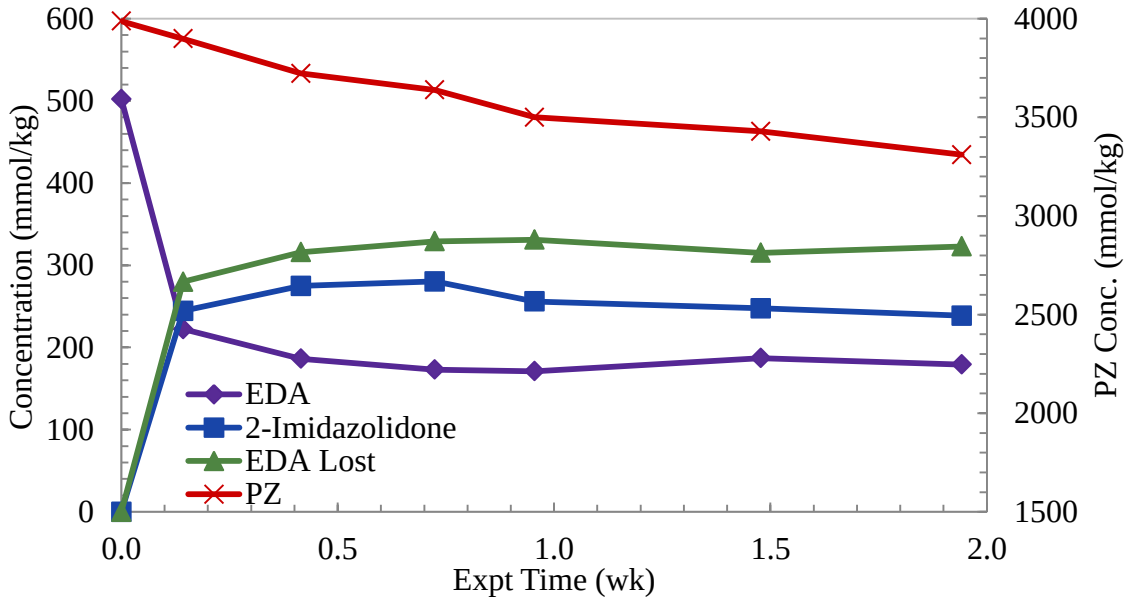

Figure 6.50: Concentration profiles for prominent amines in thermal degradation of 8 m PZ + 1 m EDA (α = 0.3) at 175 °C

The concentrations for PZ, 2-Imid, EDA, CO_2, and lost 2-Imid are shown in Figure 6.51. As hypothesized, the loss of 2-Imid correlates with the production of EDA. A majority of 2-Imid loss ends up as EDA directly, with a smaller fraction being lost to other products or due to differences in analytical technique. The experiment was not long enough to establish equilibrium between the two compounds, if this would have occurred. A rise in CO_2 concentration is noticeable, but not as large as would be expected from the reaction of 2-Imid into EDA and CO_2, indicating that CO_2 is participating in other reactions as well. The cation IC did not show new, unidentified peaks indicating the presence of new ureas. The experiment was short, but it is clear that although PZ is a stronger nucleophile, it does not act to displace the EDA and form new ureas which would be seen on the cation IC due to second amino function on PZ. The 5-membered, cyclic urea structure of 2-Imid is like more thermodynamically stable than any other di-amine urea that may be produced from other amines, rather than internal ureas.

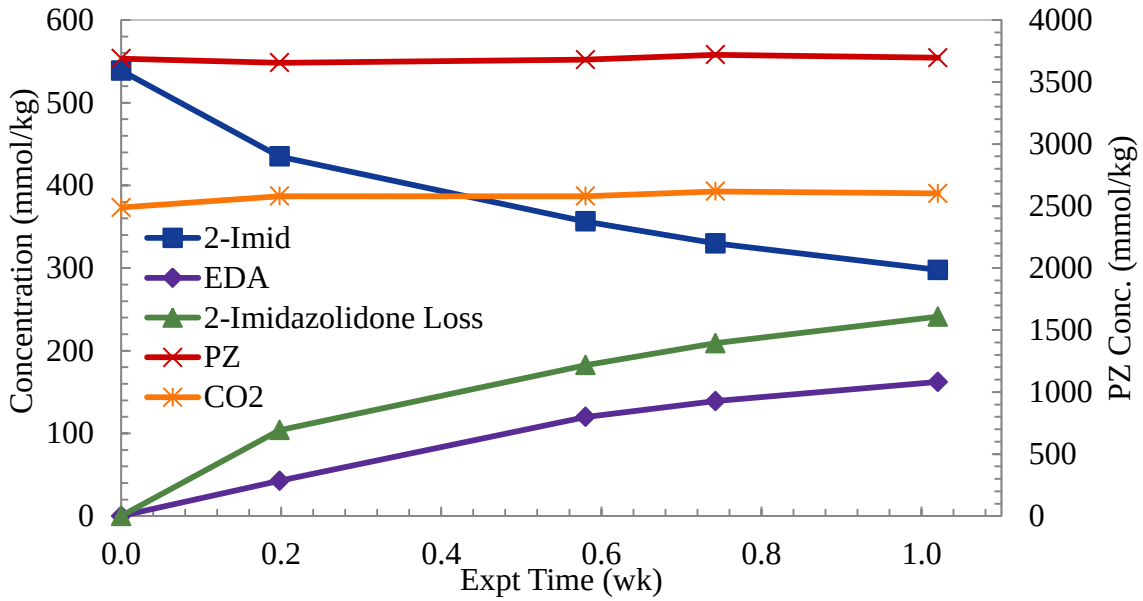

Figure 6.51: Concentration profiles for thermal degradation of 8 m PZ + 1 m 2-Imid (α = 0.3) at 175 °C

The formate generation pathways discussed in section 6.1 suggested that formate and formyl amides could be produced from ureas in solution rather than carbamate species. This set of experiments with added EDA or 2-Imid would have increased concentrations of urea earlier in the experiment than PZ degrading on its own. If formate is generated from ureas like 2-Imid, the generation of formate should be increased, at least initially. The generation of total formate is compared for thermal degradation of 8 m PZ (represented as collated data from TE4, TE12, and TE18) and 8 m PZ/1 m EDA (TE59) at 175 °C in Figure 6.52. Formate is generated at the same rate as the experiment not spiked with EDA. At this temperature, 2-Imid and EDA reached equilibrium within 1 day, so there was an enhanced concentration of 2-Imid past this point in the spiked experiment. The presence of 2-Imid does not appear to enhance formate production at 175 °C.

Unexpectedly, this same observation was not made for the 150 °C data. The generation of total formate is compared for thermal degradation of 8 m PZ (represented as collated data from TE4, TE12, and TE18), 8 m PZ/1 m EDA (TE64), and 8 m PZ/1 m 2-Imid (TE64) at 175 °C in Figure 6.53. In this case, the addition of EDA enhanced formate generation compared to unspiked PZ and PZ spiked with 2-Imid. There are too few data to make a conclusive statement about the 2-Imid spiked experiment, but the enhancement due to EDA is unexpected. If formate is generated from 2-Imid, the EDA spiked experiment certainly has more 2-Imid present for the duration of the experiment. It is possible that at 150 °C PZ degradation is slow and does not produce significant 2-Imid within this time period. At 175 °C, PZ degradation is fast and makes 2-Imid at a rate that can compete with the spiked concentration of 2-Imid, so an enhancement in formate generation is not observed. The data is inconclusive at this point to determine if the presence of 2-Imid enhances formate generation across all temperatures.

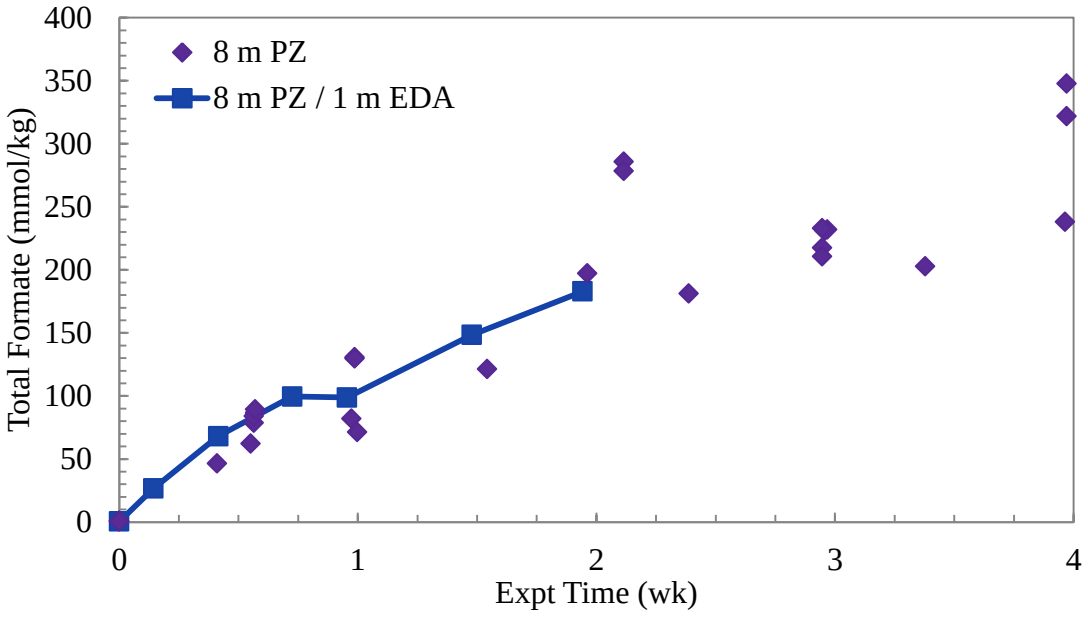

Figure 6.52: Comparison of total formate generation in thermal degradation of 8 m PZ and 8 m PZ/1 m EDA with 0.3 mole CO_2 per mole alkalinity at 175 °C

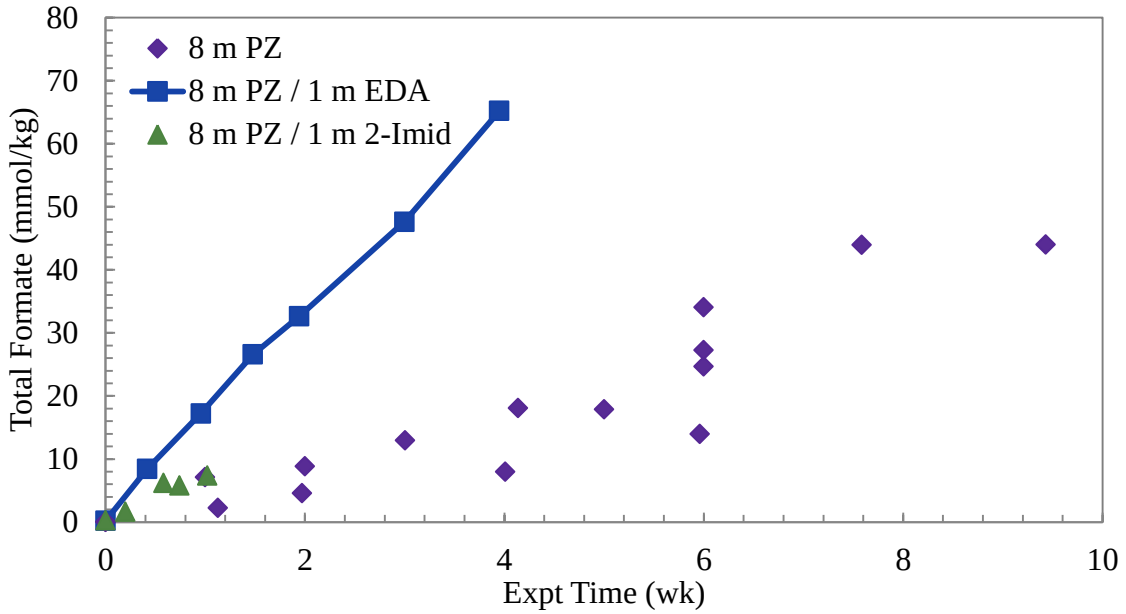

Figure 6.53: Comparison of total formate generation in thermal degradation of 8 m PZ, 8 m PZ/1 m EDA, and 8 m PZ/1 m 2-Imid with 0.3 mole CO_2 per mole alkalinity at 175 °C

The results of these experiments indicate that an equilibrium is occurring between EDA, CO_2 and 2-Imid. These match observations seen in all thermally degraded, loaded PZ where EDA is produced, but does not accumulate like other products. The reaction to form 2-Imid was written as follows (Equation 6.26).

$$EDA + CO_2 \leftrightarrow 2\text{-Imid} + H_2O \tag{6.26}$$

The equilibrium constant, K_{EQ}, for the reaction could then be written to relate the concentrations of each species, indicated by brackets (Equation 6.27). In this equilibrium equation, the concentration of water is ignored since this reaction occurs in aqueous solution and its concentration is not limited.

$$K_{EQ} = \frac{[2-\text{Imid}]}{[\text{EDA}]\cdot[CO_2]} \tag{6.27}$$

The K_{EQ} was calculated at each time point for the three experiments discussed in this section and one baseline 8 m PZ experiment (TE44). The K_{EQ} is compared for all four in Figure 6.54 and the tabulated values are shown in Table 6.6. All four experiments demonstrate similar behavior of tending toward a K_{EQ} value of approximately 0.0005 kg per mole, even though experiments were performed at various temperatures.

Data past 12 weeks for the baseline 8 m PZ experiment show an increase in this value where the equilibrium is likely affected by the high levels of PZ degradation and presence of other degradation products. This analysis shows that the conversion of EDA to 2-Imid in loaded PZ solutions occurs with predictable behavior and makes 2-Imid an important final product of degradation while EDA is simply an initial indicator and intermediate product. Longer term experiments would be needed to differentiate the temperature dependence of the K_{EQ}.

Table 6.6: Calculated K_{EQ} for 8 m PZ with either 1 m EDA or 1 m 2-Imid with 0.3 mole CO_2 per mole alkalinity (TE59, TE60, and TE64)

	8 m PZ / 1 m EDA		8 m PZ / 1 m 2-Imid	
Temp °C	Time wk	K_{EQ} kg/mol	Time wk	K_{EQ} kg/mol
150	0.0	0	0.0	0
	0.4	0.000092	0.2	0.003702
	1.0	0.000215	0.6	0.001143
	1.5	0.000261	0.7	0.000839
	1.9	0.000307	1.0	0.000683
	3.0	0.000096		
	3.9	0.000377		
175	0.0	0		
	0.1	0.000248		
	0.4	0.000377		
	0.7	0.000411		
	1.0	0.000404		
	1.5	0.000391		
	1.9	0.000437		

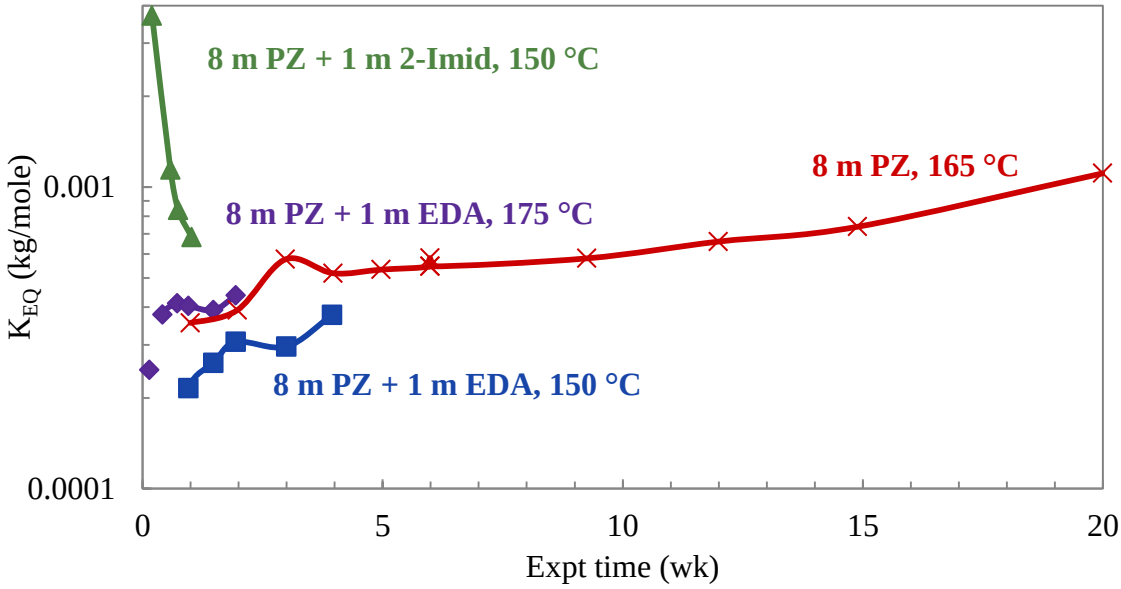

Figure 6.54: Equilibrium of EDA, CO_2, and 2-Imid in spiked thermal degradation experiments

6.6 Absence of Oxygen and CO_2 through Nitrogen Purge

It has been suggested that the production of formate during thermal degradation experiments is due to the presence of oxygen (O_2) in the headspace of the thermal cylinders and dissolved O_2 in the amine solution at the start of thermal degradation experiments. The argument has been that the O_2 molecules in the formate and formyl amides must be due in part to the dissolved O_2 and water, rather than CO_2 as suggested by the mechanism discussed in section 6.3 above. A complimentary concept is that the presence of molecular O_2 activates or initiates the mechanisms that lead to PZ thermal degradation and the production of degradation products such as formate and formyl amides. In an effort to address these arguments, two thermal degradation experiments, one unloaded and one lean loaded (0.3 mole CO_2 per mole alkalinity), were conducted with an inert headspace in the cylinders at the start of the experiment. This circumstance was achieved by filling and sealing the thermal cylinders in a glove bag filled with

nitrogen (N_2) gas. The hypothesis of these experiments was that the replacement of O_2 and CO_2 in the headspace with inert N_2 would demonstrate the effect of those molecules, especially O_2.

To create an inert environment, all of the materials needed for the task were first placed into the glove bag. Then, the glove bag was flushed with N_2, sealed, and inflated to a reasonable working pressure with N_2. The PZ solutions were not specifically purged or sparged with N_2 to remove O_2 since the process of loading the solution with CO_2 acts to strip out most of the other gases present in solution. The cylinders were filled in the glove bag and sealed according Swagelok® specifications while under the presence of N_2. The tightness of the cylinders was checked out of the glove bag to ensure the success of the experiment. For the unloaded experiment, cylinders were filled in the same fashion but with warm solution to maintain a liquid phase solution.

The PZ loss for the high temperature degradation of standard unloaded 8 m PZ is compared to the N_2 purged experiment in Figure 6.55. A third set of data from three separate repeated experiments exploring thermal degradation of 8 m PZ with 0.3 mole CO_2 per mole alkalinity at 175 °C is also included to place the unloaded degradation data in context. Both unloaded experiments suffered only a very slight loss of PZ compared with the loaded degradation rate. There was a small decrease in the PZ loss in the N_2 purged experiment indicating that ambient O_2 may, in fact, affect the overall degradation rate of thermal degradation experiments.

In order to further see the effect of the N_2 headspace, the production of total formate and EDA are compared in Figure 6.56 and Figure 6.57, respectively, for the same three conditions. There is a noticeable decrease in rate of total formate generated during the experiments as the concentration is decreased by 56 % from 18.3 to 8.1 mmole per kg. The loaded experiment generates formate concentration quickly due to the formate

generation mechanism discussed above. Total formate concentration is decreased under a N_2 atmosphere compared to the baseline unloaded experiment. The presence of O_2 could have activated mechanisms responsible for both the degradation of PZ and production of total formate. A decrease in rate can be observed in both PZ loss and formate production when O_2 was removed from the headspace. The O_2 does not appear to be required for either mechanism, since both proceed without it, but likely acts to activate or catalyze the mechanisms of degradation.

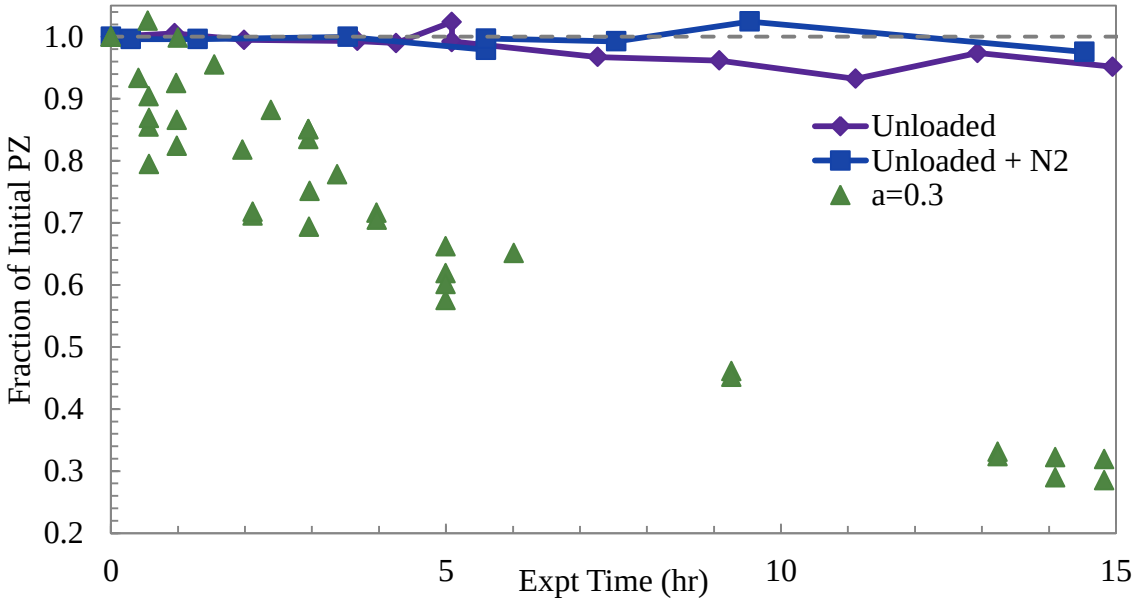

Figure 6.55: Comparison of PZ loss for degradation at 175 °C for unloaded 8 m PZ, unloaded and N_2-purged 8 m PZ, and 8 m PZ with 0.3 mole CO_2 per mole alkalinity

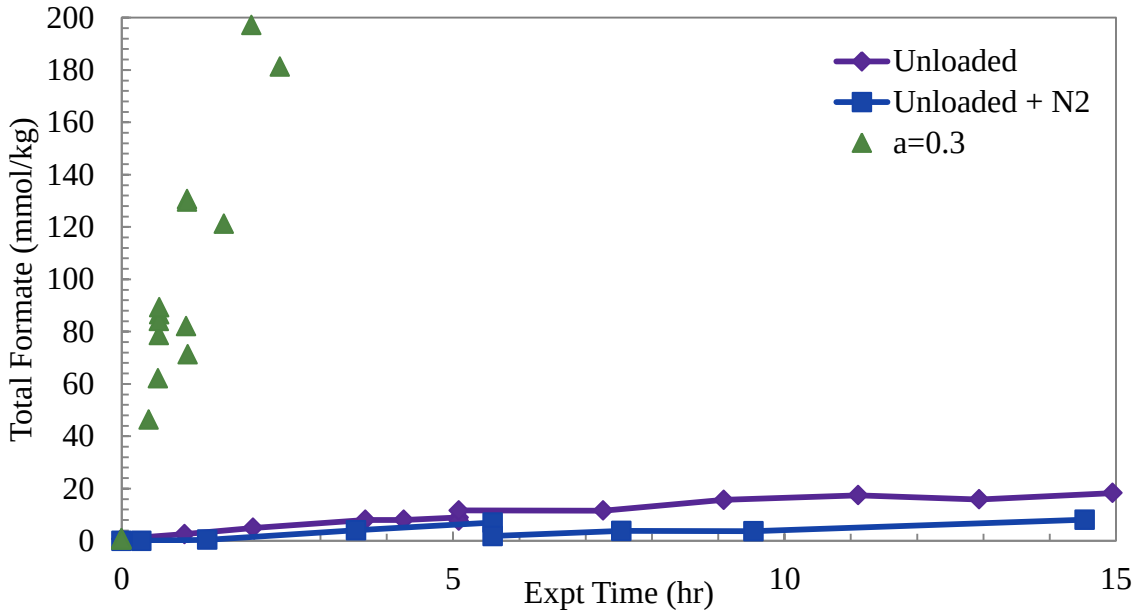

Figure 6.56: Generation of total formate in degradation at 175 °C for unloaded 8 m PZ, unloaded and N_2-purged 8 m PZ, and 8 m PZ with 0.3 mole CO_2 per mole alkalinity

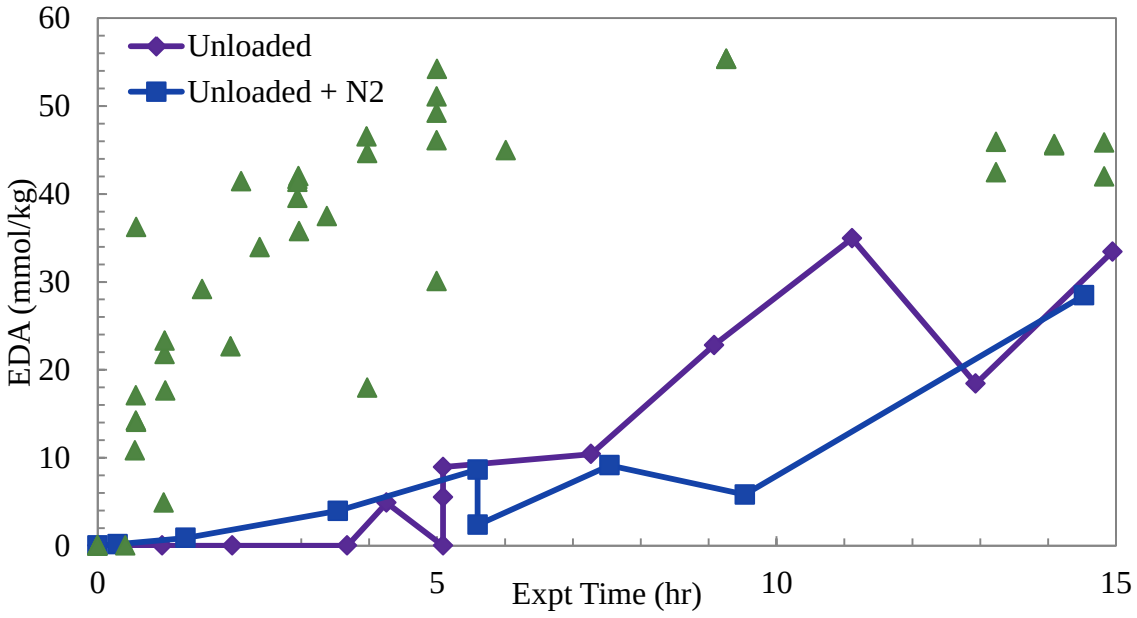

Figure 6.57: Generation of EDA in degradation at 175 °C for unloaded 8 m PZ, unloaded and N_2-purged 8 m PZ, and 8 m PZ with 0.3 mole CO_2 per mole alkalinity

A second important observation can be made from the EDA data in Figure 6.57. The generation of EDA between the standard and N_2-purged experiments is nearly identical, indicating the lack of O_2 and CO_2 in the headspace did not affect EDA formation. As detailed in previous sections, it is believed that EDA generation is due to the action of the H^+PZ molecule and is separate from the formate generation mechanism. In these experiments, the concentration of H^+PZ and, therefore, the production of EDA, should not have been affected by the presence or lack of O_2 or CO_2 in the headspace.

The PZ loss for 8 m PZ with 0.3 mole CO_2 per mole alkalinity with a N_2 purged headspace is compared to a standard experiment in Figure 6.58. The standard data are collated points from repeated experiments on 8 m PZ with 0.3 mole CO_2 per mole alkalinity degraded at 175 °C. The PZ loss is close between the two sets of data except for a slight deviation at the latter time points. After seven weeks, the loss of PZ in the N_2 experiment is less than the CO_2-loaded experiment. Again, this indicates that a lack of O_2 does decrease the loss of PZ during thermal degradation significantly.

The generation of total formate and EDA are compared in Figure 6.59 and Figure 6.60, respectively. The concentration of total formate is the same between the standard and N_2 experiments, while the EDA concentration is slightly increased the N_2 case. This is not expected given the decreased PZ loss. The reaction of EDA with CO_2 to form 2-Imid may be impacted and slowed by the reaction mixture present in the N_2 experiment. If that reaction were slowed by the lack of O_2 in some way, EDA would be allowed to accumulate to slightly higher concentrations than would be expected in a standard experiment. If O_2 typically activates or accelerates various mechanisms during degradation, the EDA/2-Imid equilibrium may rely on the presence of another species that is at a lower concentration due to the lack of O_2.

The N_2-purged experiments demonstrated that the presence of O_2 in the headspace of the thermal degradation experiments has a slight, but noticeable effect of PZ loss and the generation of degradation products in the absence of CO_2. The degradation mechanisms are not dependent on the presence of O_2 and are only minimally enhanced by O_2. It is not surprising that O_2 is reactive at these extreme temperatures. A likely hypothesis is that the small initial concentration of O_2 present from the headspace and any dissolved O_2 in solution react with the metal surfaces or dissolved metals in solutions through free radical mechanisms. Once the O_2 molecules are used up, the effect is lost and rates proceed as they would in the absence of O_2. Changes in the initial degradation rates were not directly observed in the aforementioned experiments, as would be expected with this hypothesis, but the expected error of the analytical tools would likely preclude this observation with the given data sets.

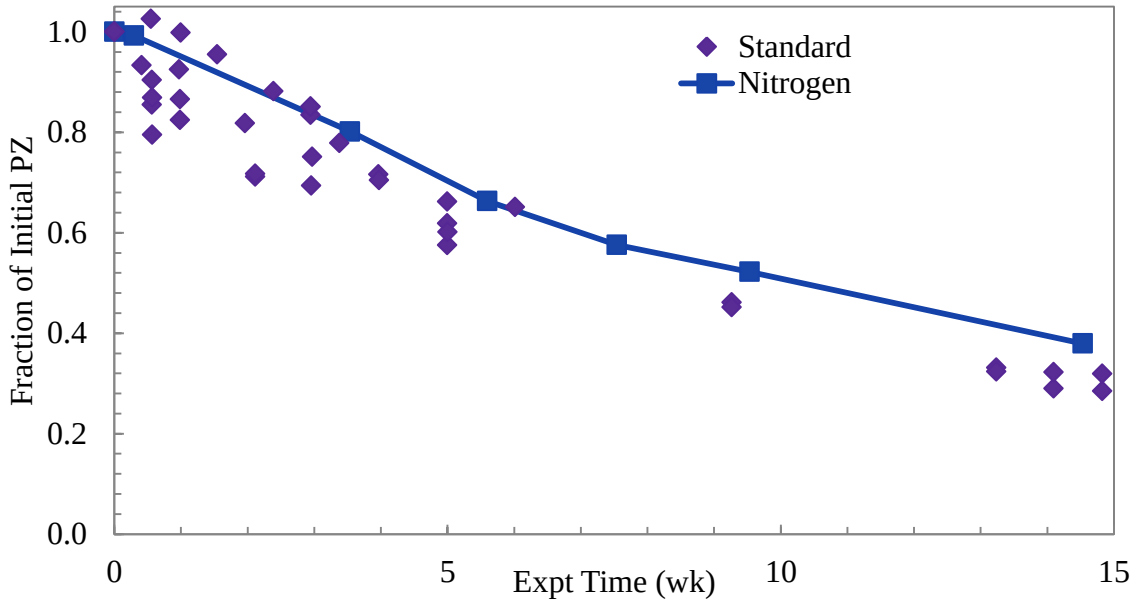

Figure 6.58: Comparison of PZ loss in degradation of 8 m PZ with 0.3 mole CO_2 per mole alkalinity at 175 °C with a standard or N_2 headspace

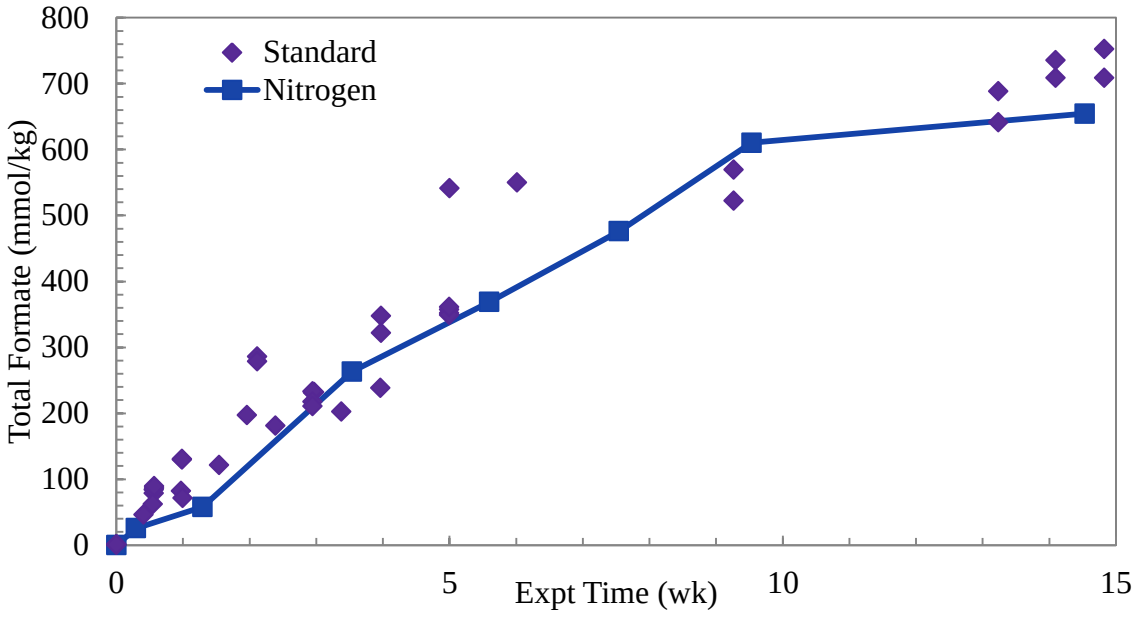

Figure 6.59: Generation of total formate in degradation of 8 m PZ with 0.3 mole CO_2 per mole alkalinity at 175 °C with a standard or N_2 headspace

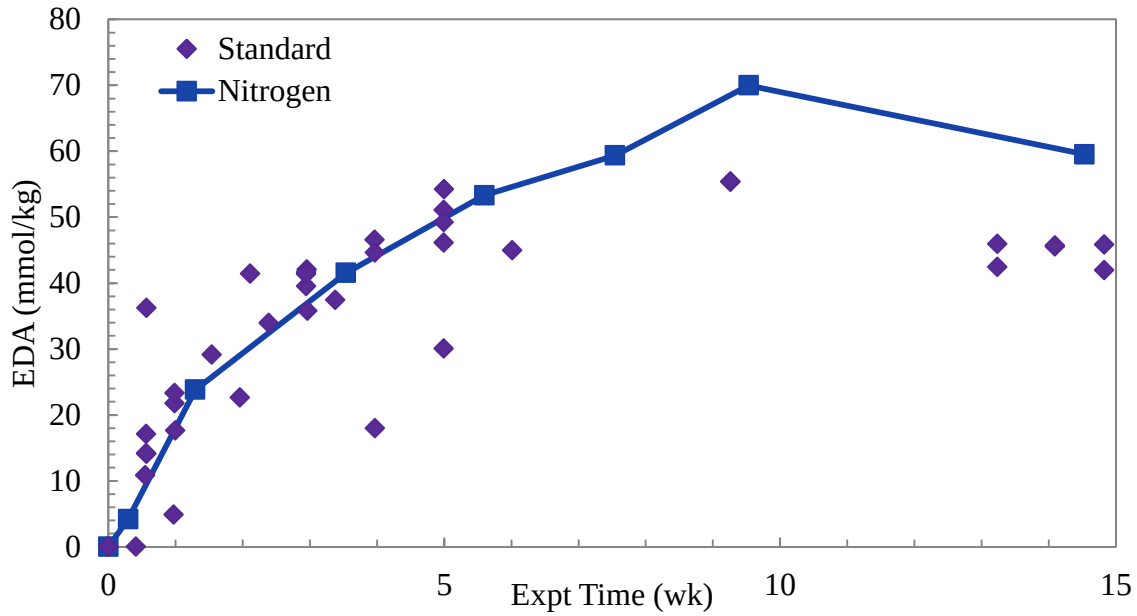

Figure 6.60: Generation of EDA in degradation of 8 m PZ with 0.3 mole CO_2 per mole alkalinity at 175 °C with a standard or N_2 headspace

6.7 CONCLUSIONS

The most abundant degradation products of thermally degraded 8 m PZ are N-formyl PZ (FPZ), ammonium (NH_4^+), and N-(2-aminoethyl)PZ (AEP). These molecules account for 57% of nitrogen and 45% of carbon lost during degradation as PZ and CO_2. Other prominent products include, in order of decreasing impact on the nitrogen and carbon balance, 2-imidazolidone (2-Imid), N-(2-hydroxyethyl)piperazine (HEP), N-ethylpiperazine, ethylenediamine (EDA), 1-Methylpiperazine (1-MPZ), formate, acetate, and other heat stable salts (glycolate and oxalate) in small concentrations.

After 20 weeks of thermal degradation at 165 °C, 74% and 63%, respectively, of the nitrogen and carbon lost in the form of PZ and CO_2 was recovered in the form of quantifiable degradation products. For the same experiment, 87% and 60% of the lost CO_2 molecules and "ethyls" were recovered.

In the first step of the mechanism, 1-[2-[(2-aminoethyl) amino]ethyl] PZ (AEAEPZ) is believed to be formed from a ring opening S_N2 reaction of PZ with H^+PZ. The limiting rate was found to require protonated amine, but not CO_2, which agrees with the proposed production of AEAEPZ from H^+PZ and PZ. Degradation of concentrated PZ in the presence of HCO_3^- demonstrated that PZ loss and generation of formate and EDA depend on the presence of H^+PZ to proceed. In the presence of CO_2, AEAEPZ is expected to react to form its internal urea. Both molecules, AEAEPZ and its urea, are suspected to play major roles in thermal degradation pathways for concentrated PZ.

At 150 °C, EDA is in equilibrium with 2-Imid, the internal urea of EDA. The equilibrium constant, K_{EQ}, tends toward a value between 0.0004 and 0.0006 kg solution per mole.

Degradation of acidified PZ was shown to mimic what would occur in the absence of CO_2 and explained some behavior of the EDA generation mechanism. EDA

accumulates in the absence of CO_2 because it does not react to form the more preferred 2-Imid structure. CO_2 is not required in the degradation mechanism that generates EDA. EDA generation is not directly dependent on either PZ or H^+PZ concentration.

NMR analysis of degraded $^{13}CO_2$-loaded PZ solutions conclusively showed that formate is generated directly from the CO_2 in solution. The mechanism is not clear at this point. Formate is not generated from the break-up of the PZ backbone itself. Formate is generated consistently as a major product in all oxygen-poor, CO_2 loaded amine thermal degradation where carbamate polymerization is not the major degradation mechanism.

During thermal degradation from 135 to 175 °C, and oxidation at 55 °C, formyl amides are in equilibrium with formate. Formyl amides were consistently produced at higher concentrations that formate. The ratio of formyl amides to formate produced was a strong function of PZ concentration and CO_2 concentration, but not temperature. For 8 m PZ from 55 to 175 °C, the ratio can be described as follows where the CO_2 loading, α, is in units of mole CO_2 per mole alkalinity (Equation 6.24). For 20 m PZ at 175 °C, the ratio can be described as follows (Equation 6.25).

$$\frac{C_{FA}}{C_F} = 5.54 \times \alpha + 0.30 \tag{6.24}$$

$$\frac{C_{FA}}{C_F} = 7.73 \times \alpha + 3.10 \tag{6.25}$$

The oxygen present as dissolved oxygen or in the headspace of the thermal cylinders was found to have a minimal effect that could not account for all quantified formate and formyl amides generated in typical thermal degradation experiments.

Chapter 7 – Thermal Degradation of Structural Analogs of Piperazine and Substituted Piperazines

The thermal degradation of structural analogs of PZ, substituted PZs, and PZ blends were explored in this chapter. Structural analogs of PZ were examined in an effort to understand the thermal stability of PZ. Substituted PZs were investigated as potential new solvents with advantageous characteristics for CO_2 capture applications. Blends of PZ with substituted PZs were also studied as a new solvent system with advantageous thermal equilibrium characteristics. Portions of this chapter are excerpted from a previous article (Freeman and Rochelle, 2011).

7.1 Structural Analogs of Piperazine

One of the most important advantages of concentrated PZ over other well-studied, baseline alkanolamine solvents such as monoethanolamine (MEA), 2-amino-2-methyl-1-

propanol (AMP), or methyldiethanolamine (MDEA) is its exceptional resistance to thermal degradation. PZ has been found to be resistant to degradation up to 150 °C, well above the standard stripper operating conditions, as demonstrated in Chapter 5 of this dissertation and previously (Freeman et al., 2010a). At temperatures above 150 °C, PZ begins to degrade at rates similar to alkanolamines at temperatures between 100 and 135 °C.

The structural reasons for the resistance of PZ to thermal degradation is not clear when analyzing the degradation data obtained previously. PZ is 6-membered ring with two secondary amino functions. Six-membered cyclic alkanes are known to be stable due to minimized angle or torsional strain and six-member heterocycles, such as PZ, would benefit as well (McMurry, 2000). PZ does not have an alcohol function, which is known to enhance thermal degradation through well understood pathways (Davis, 2009; Dawodu and Meisen, 1996; Kennard and Melsen, 1985). It is also lacking any steric hindrance from alkane or hydroxyl groups on the amine or α-carbon that would interfere with reactions at the position of the amino function. The library of thermal degradation data available in literature includes studies on primary amines, secondary amines, tertiary amines, alkanolamines, hindered amines, long-chain amines, and other amines of interest to CO_2 capture applications. Despite the wide range of degradation data available, it is difficult to draw conclusions about the structural strength of PZ.

Thermal degradation of seven structural analogs of PZ was performed to determine the structural characteristics that provide thermal resistance. The structures of PZ, piperidine (PD), morpholine (Mor), pyrrolidine (Pyr), hexamethyleneimine (HMI), homopiperazine (HomoPZ), ethylenediamine (EDA), and hexamethylenediamine (HMDA) are shown in Figure 7.1. The molecules are arranged to demonstrate the comparisons developed in this paper. The effect of changing a secondary heteroatom,

ring size in monoamines, ring size in diamines, and methylene chain length are each analyzed using thermal degradation data. Thermal degradation data for EDA was taken from the work of Shan Zhou (Zhou et al., 2010). The first order rate, k_1, constant analysis developed in section 5.2 will be used for comparison. The k_1 was calculated using the entire time series of data, unless otherwise indicated. When comparisons are made to 8 molal (m) PZ with 0.3 mole CO_2 per mole alkalinity, the data shown are collated from three separate, repeated experiments.

COMPARISON	Molecules Investigated		
Secondary Heteroatom	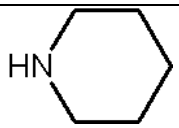 Piperidine (PD)	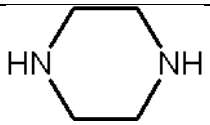 PZ	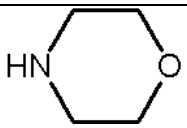 Morpholine (Mor)
Ring Size in Monoamines	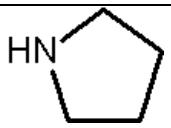 Pyrrolidine (Pyr)	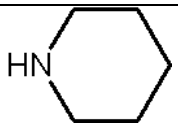 Piperidine (PD)	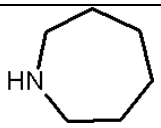 Hexamethyleneimine (HMI)
Ring Size in Diamines	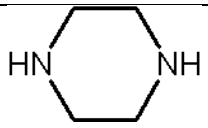 PZ	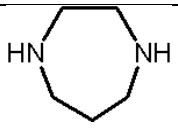 Homopiperazine (PZ)	
Methylene Chain Length	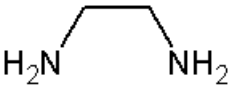 Ethylenediamine (EDA)	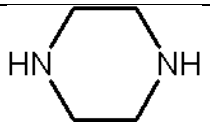 PZ	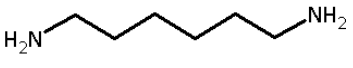 Hexamethylenediamine (HMDA)

Figure 7.1: Structures of amines investigated in thermal screening

7.1.1 Effect of second heteroatom in 6-member ring

The effect of changing the heteroatom in a six-member ring containing one amino function was investigated by degrading 8 m PD, 8 m PZ, and 8 m Mor with 0.3 mole CO_2 per mole alkalinity at 175 °C. This analysis compares the degradation rate achieved when the methylene group in the 4 position on PD is changed to an amino group (PZ) or oxygen (Mor). The fraction of the initial amine remaining after degradation at 175 °C is shown in Figure 7.2. Data were fit with an exponential regression and the calculated k_1 value is shown for each amine. For all three amines, total formate was a dominant degradation product and is compared in Figure 7.3.

Mor and PD both degraded more slowly than PZ. These are the first amines to be found to be more thermally stable than PZ, although Mor has been previously identified as thermally stable (Davis, 2009). The presence of a second amino function in the 6-member ring increases the thermal degradation rate of PZ. The k_1 value of PD, 8.41×10^{-8} s^{-1}, is 1.7 times that of Mor, 4.97×10^{-8} s^{-1}, while the k_1 of PZ, 1.32×10^{-7} s^{-1}, is over 2.6 times that of Mor. The presence of multiple amino functions allows for more nucleophilic attack which increases degradation. This is especially important since PZ is unique in that even when PZ has reacted with CO_2 to form protonated PZ (H^+PZ) and PZ carbamate ($PZCOO^-$), there is another amino group that can be an attacking nucleophile or be subject to nucleophilic attack. The concentration of total formate in the PD and Mor experiments is half of that produced in the PZ experiments. The raw CO_2 concentration in the PZ experiment was double that of the other experiments due to the definition of CO_2 loading and directly caused the doubling of total formate generation.

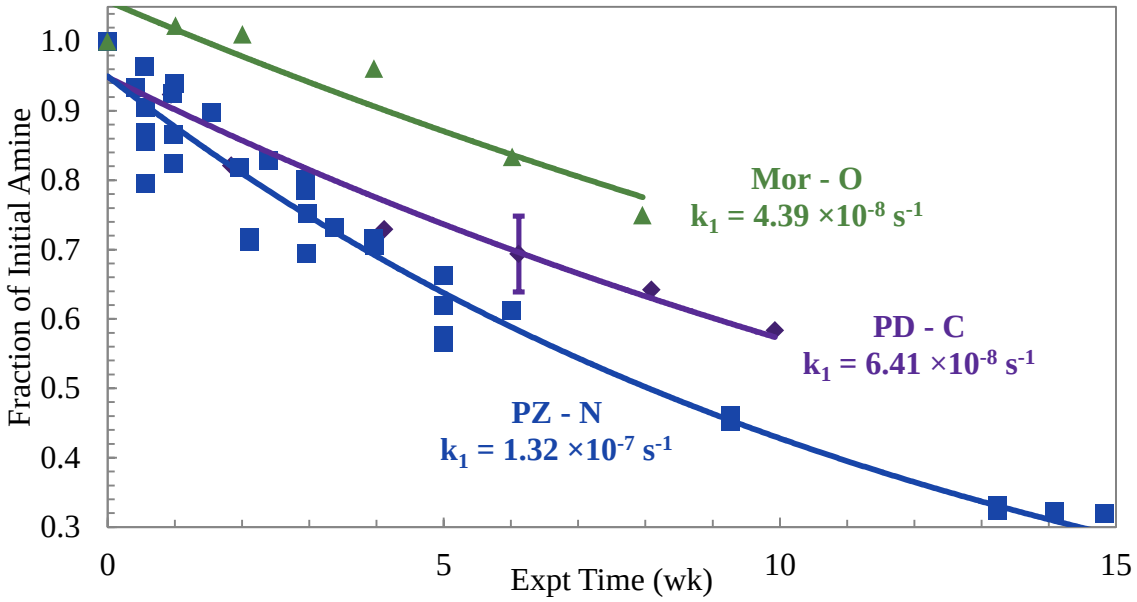

Figure 7.2: Amine loss in thermal degradation of 6-membered rings with varying heteroatoms at 175 °C

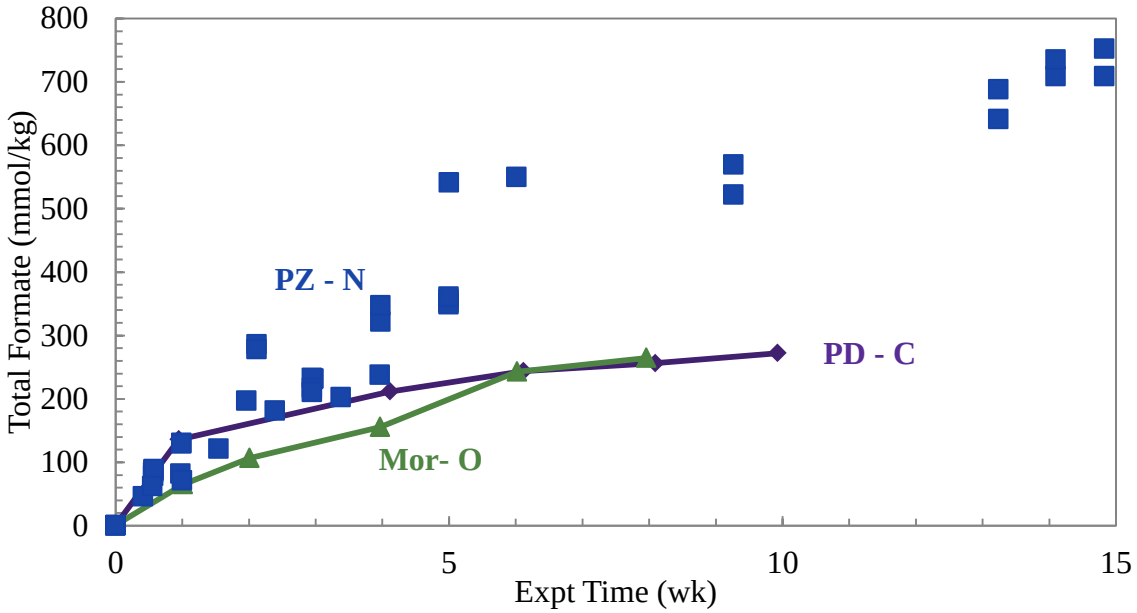

Figure 7.3: Production of total formate in thermal degradation of 6-membered rings with varying heteroatoms at 175 °C

The pK_a values for the amines studied in this paper are shown in Table 7.1. The pK_a values reported for PD, PZ, and Mor in Table 7.1 indicate that PZ has an intermediate base strength with PD having the highest pK_a for the amino group. From the low pK_a value of Mor, it was expected that it would act as a weak attacking group and have a lower degradation rate than PZ. Although PD has a higher pK_a than PZ, indicating it is a stronger base, the higher degradation rate in PZ is likely just due to the additional amino function available for nucleophilic attack reactions whereas PD has a portion of its molecules tied up as protonated PD (H^+PD) and PD carbamate ($PDCOO^-$) after reaction with CO_2.

Table 7.1: pKa values at 298 K

Molecule	$pK_{a,1}$	$pK_{a,2}$	Reference[b]
PD	11.22	-	S
PZ	9.71 - 9.73	5.33 - 5.41	Ha, He, K
Mor	8.36	-	H, Pa
Pyr	11.12-11.27	-	AS, S
HMI	11.07	-	Pe
HomoPZ[a]	10.09	6.67	Pa
1-MPZ	9.14	4.63	K
2-MPZ	9.57	5.24	K

[a] Values listed for HomoPZ are at 303 K
[b] Reference: AS = (Albert and Serjeant, 1971); H = (Hall, 1956); Ha = (Hamborg and Versteeg, 2009); He = (Hetzer et al., 1968); K = (Khalili et al., 2009); Pa = (Pagano et al., 1961); Pe = (Perrin, 1965); S = (Searles et al., 1956)

7.1.2 Effect of ring size in monoamines

The effect of ring size on thermal degradation of a monoamine was investigated by degrading 8 m Pyr, 8 m PD, and 8 m HMI with 0.3 mole CO_2 per mole alkalinity at 175 °C. The fraction of the initial amine remaining after 10 weeks at 175 °C is compared in Figure 7.4. An exponential regression was fit to each set of data and the calculated k_1 values are shown. For Pyr and HMI, where the degradation rate is clearly more than first

order in amine concentration, the k_1 was calculated using only the first week of data and should be considered an apparent k_1. For all three amines, total formate was one of the dominant degradation product identified and the concentration is compared in Figure 7.5.

The most thermally stable amine of the three, as expected, is the six-membered PD. It is well known that 5- and 7-membered rings are not as stable as 6 membered rings and the thermal stability of these amines follows suit. Comparing the simplest cyclic alkanes, cyclopentane, cyclohexane, and cycloheptane, cyclohexane is considered to be free of strain while the cyclopentane and cycloheptane have 6.2 and 6.1 kcal/mol of torsional strain, respectively (McMurry, 2000). In amine heterocycles, the 7-membered HMI appears to be the least stable, losing nearly all the initial amine after one week of degradation compared to only 55% and 8% loss of Pyr and PD, respectively.

The production of total formate (Figure 7.5) does not track with the amount of amine lost for each despite having the same CO_2 concentration. PD produced the most formate while the least amount of amine was lost. Degraded solutions of both Pyr and HMI were found to contain polymeric substances. This was not observed thermally degraded PD or PZ. The mechanism for thermal degradation is certainly quite different from previous amines studied and the presence of polymeric substances after degradation does not lend itself for further study in the field of CO_2 capture.

7.1.3 Effect of ring size in diamines

The effect of ring size on thermal degradation of a diamine was investigated by thermally degrading 8 m PZ and 8 m HomoPZ with 0.3 mole CO_2 per mole alkalinity at 175 °C. The loss of amine and production of total formate is shown in Figure 7.6 and Figure 7.7. HomoPZ degrades rapidly in comparison with PZ, losing 98% of the initial amine within 4 weeks while PZ loses only 30%. Total formate is a dominant degradation

product for both amines, but in HomoPZ it is an intermediate. All previous work on PZ showed steady increases of total formate, indicating it was a final product of degradation (Freeman et al., 2010a).

The addition of one methylene group to a PZ molecule (HomoPZ) weakens the structure and the thermal resistance seen in PZ is lost. The degradation also proceeds through a different mechanism, as demonstrated by the presence of formate and formyl amides as intermediates, rather than final products. Although there are few data points in the region where HomoPZ is initially being degraded, the data indicates that the reaction is not first order in amine, as has been hypothesized for PZ thermal degradation (Freeman et al., 2010a).

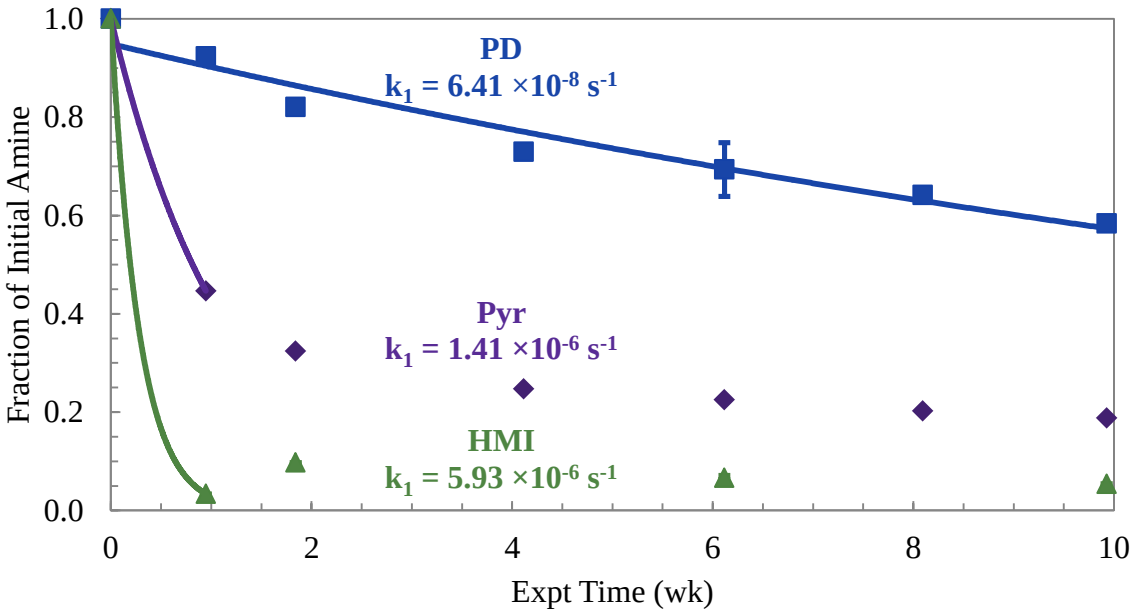

Figure 7.4: Amine loss in thermal degradation of monoamines at 175 °C

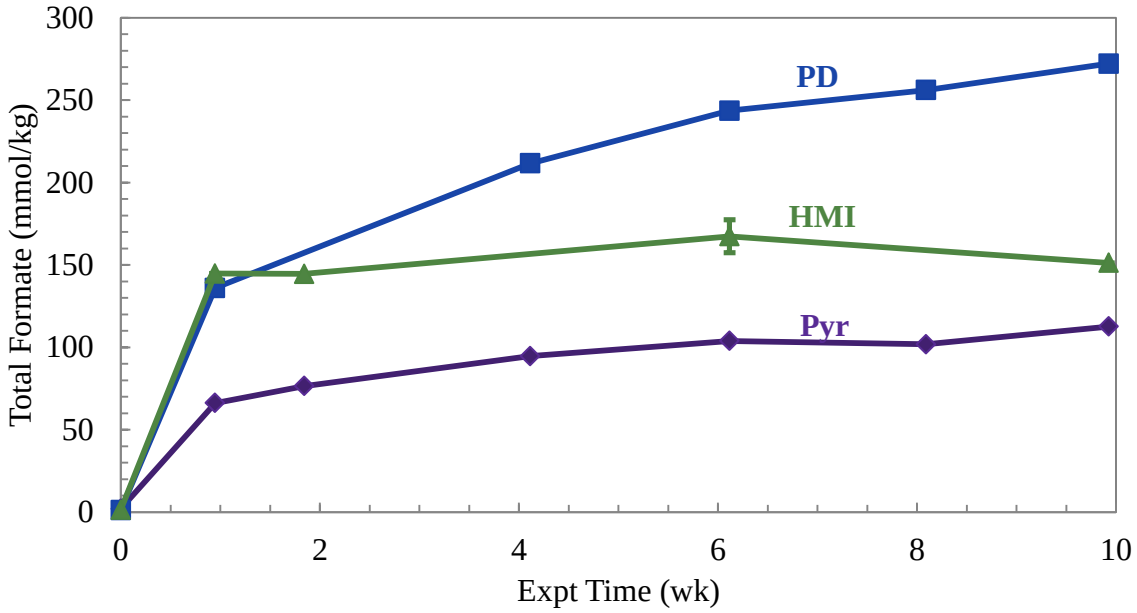

Figure 7.5: Production of total formate in thermal degradation of monoamines at 175 °C

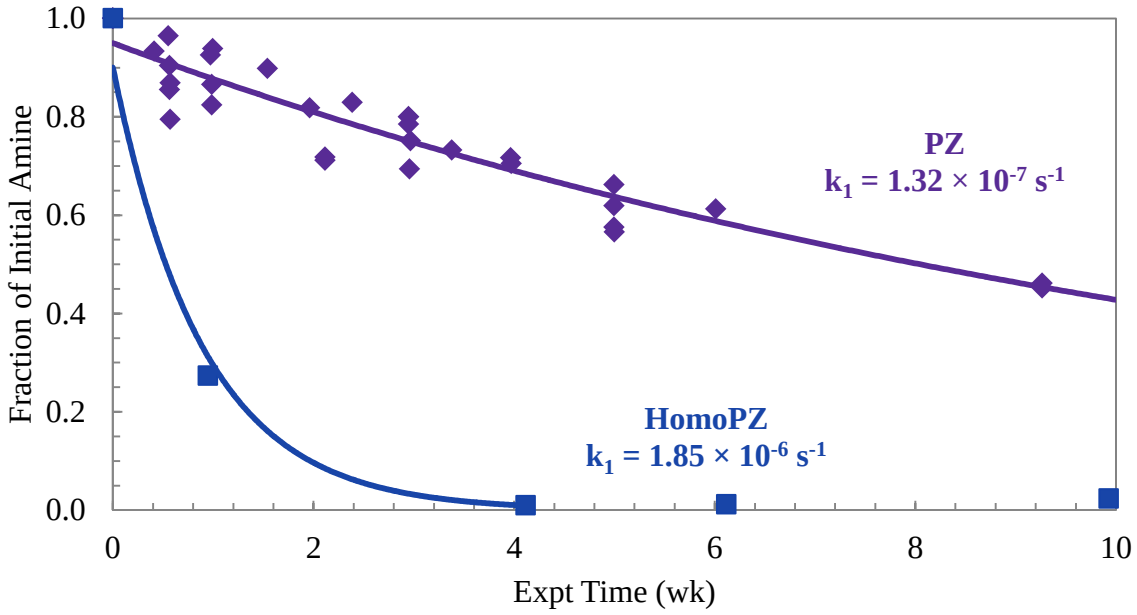

Figure 7.6: Amine loss in thermal degradation of diamines at 175 °C

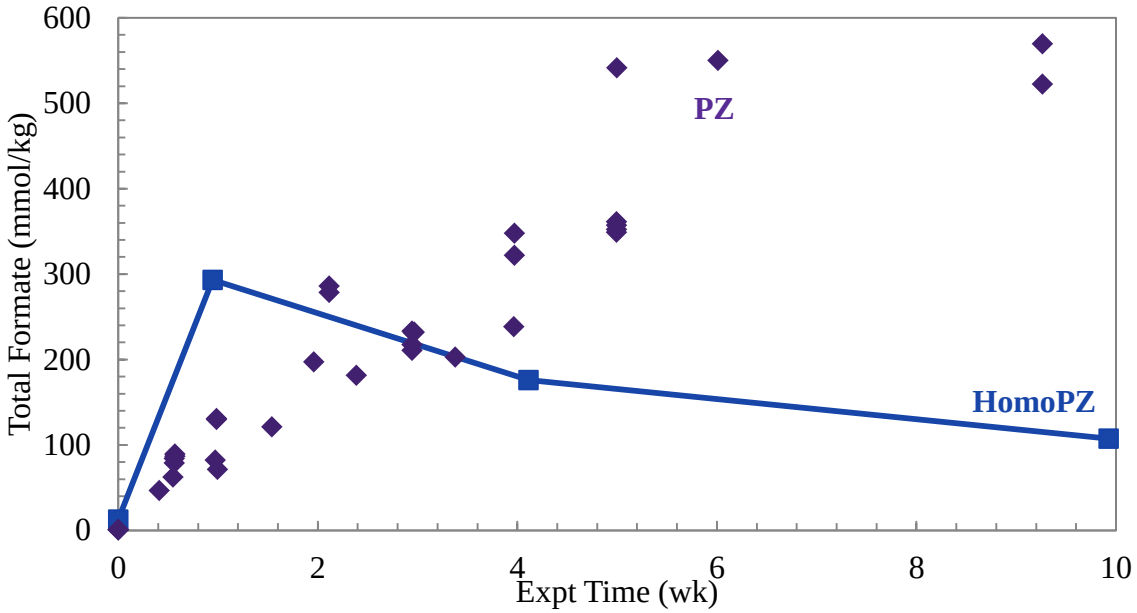

Figure 7.7: Production of total formate in thermal degradation of diamines at 175 °C

7.1.4 Effect of methylene chain length

The effect of methylene chain length on thermal stability of amines was investigated by degrading 8 m PZ and 8 m HMDA with 0.3 moles CO_2 per mole alkalinity at 175 °C. The thermal degradation of concentrated EDA was also investigated previously by Zhou and Eide-Haugmo (Eide-Haugmo et al., 2011; Zhou et al., 2010). The EDA data collected at various CO_2 loadings and lower temperatures due to the instability of EDA. Zhou (2010) investigated 8 m EDA with 0.2 or 0.4 mole CO_2 per mole alkalinity at 135 °C (Zhou et al., 2010). The study of Eide-Haugmo investigated 7.13 m EDA with 0.25 moles CO_2 per mole alkalinity degraded at 135 °C (Eide-Haugmo et al., 2011). Due to the differences in CO_2 concentration and temperature, the three amines will be analyzed using k_1 values alone, rather than the raw concentration data in order to understand the overall degradation effects.

Previous work on structural analogs of MEA found that amine stability was dependent on the stability of or inability to create the initial oxazolidone ring product (Davis, 2009). Davis found that increasing the length of the amine, and therefore, the ring size of the initial oxazolidone product, decreased degradation rates and prevented the carbamate polymerization pathway from proceeding past this initial product.

The k_1 values calculated from exponential regression of amine concentration data are compared in Figure 7.8 for all relevant data. PZ and HMDA demonstrate thermal stability compared to all three sets of EDA data. At 135 °C, where data overlaps, EDA degrades between 31 and 172 faster than PZ. HMDA is primarily stable because the internal urea that could be created with reaction with CO_2 would be an unstable 9-member ring. On the other hand, EDA can readily react with CO_2 to create the internal urea, 2-Imid (discussed in section 6.5). The cyclic structure of PZ prevents the formation of the internal urea of PZ, which would be too sterically strained to exist at significant concentrations. As with the conclusions of Davis, changes in amine structure that prevent the formation of stable or fast reacting intermediates slows overall thermal degradation rates.

7.2 METHYL-SUBSTITUTED PIPERAZINES

Four mono- and dimethyl substituted PZ structural analogs were analyzed for their thermal stability. The methyl-substituted PZs investigated were 1-methylpiperazine (1-MPZ), 1,4-dimethylpiperazine (1,4-DMPZ), 2-methylpiperazine (2-MPZ), and *trans*-2,5-dimethylpiperazine (t2,5-DMPZ), whose structures provided in Figure 7.9. Two enantiomers of 2-MPZ, (R)-(-)-2-MPZ and (S)-(+)-2-MPZ exist and the form used in this study was assumed to be a racemic mixture because it was not specified by the

manufacturer. The *trans* isomer of 2,5-DMPZ was used due to it availability compared to the *cis* isomer.

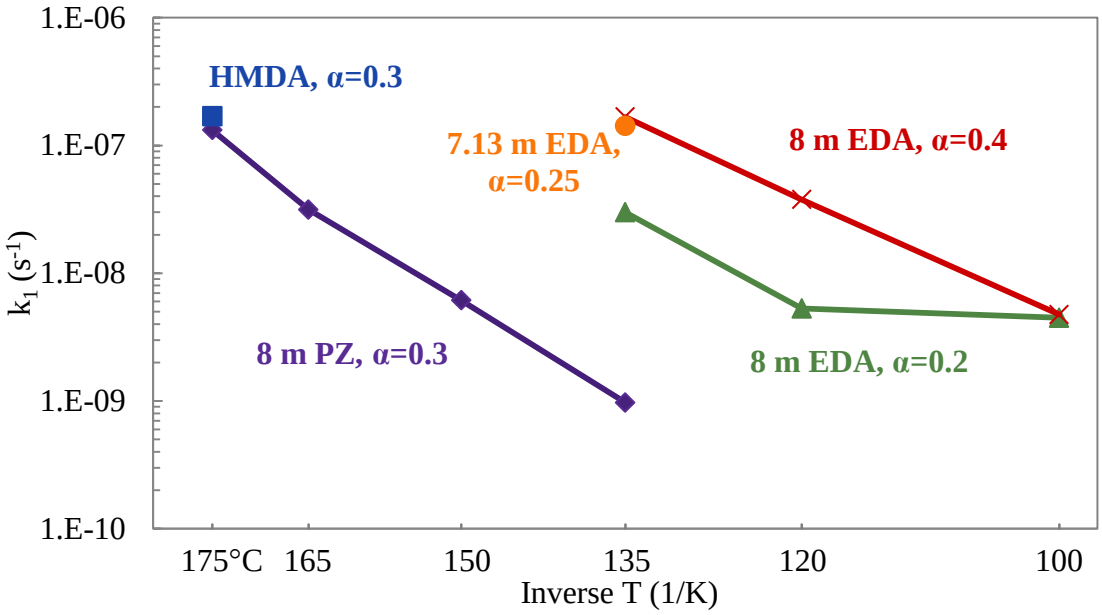

Figure 7.8: Comparison of k_1 values for thermal degradation of PZ, HMDA, and EDA from 100 to 175 °C

1-MPZ and 2-MPZ were both studied as 8 m solutions, and in a 4 m/4 m blend with PZ. 1,4-DMPZ was not studied alone or as a blend with PZ due to its inability to absorb CO_2. This amine was investigated as part of a blend of PZ, 1-MPZ, and 1,4-DMPZ that is discussed in detail in the next section. t2,5-DMPZ was studied as a 2 m solution, much lower than the other methyl-substituted amines, due to severe solubility issues and was studied in a 4 m /4 m blend with PZ. This blend also had solubility issues, but they were manageable using the same techniques used to investigate unloaded 8 m PZ.

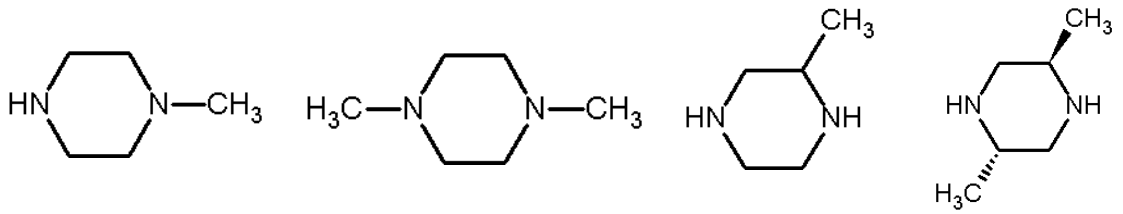

1-MPZ 1,4-DMPZ 2-MPZ *t*2,5-DMPZ

Figure 7.9: Structures of methyl-substituted PZs

Davis found that blending of amines caused more degradation of each constituent, in general (Davis, 2009). For example, when PZ is blended with another amine such as MEA or AMP, both the other amine and PZ are degraded faster than each alone. This has also recently been confirmed for blends of MDEA and PZ where degradation occurs at a ratio of one mole PZ alkalinity to one mole MDEA alkalinity until PZ is completely degraded (Closmann, 2011; Closmann et al., 2009). PZ is a strong nucleophile and can attack the other amines in solution and cause degradation outside of the usual pathways associated with MEA or AMP degradation. PZ can also attack itself, as it does in a solution by itself, but weaker nucleophiles such as MEA or AMP are more susceptible to PZ's attack, causing faster degradation for each than separate.

7.2.1 1-Methylpiperazine (1-MPZ) and PZ + 1-MPZ blend

The thermal degradation of 8 m 1-MPZ and 4 m PZ / 4 m 1-MPZ were studied at 150 °C. The loss of total starting amine in these experiments is compared with 8 m PZ with exponential regressions and the calculated k_1 values in Figure 7.10. For the blend, the sum of PZ and 1-MPZ at each time point is taken as a fraction of the initial total amine concentration to show the overall degradation during the experiment. The main degradation products of 1-MPZ degradation were found to be PZ, 1,4-DMPZ, formyl amides such as N-formyl PZ, and formate. Acetate and oxalate were found in very small, non-zero concentrations. Unfortunately, the blend experiment suffered from a large

percentage of failed cylinders so data was only obtained for the first 10 weeks. The main degradation products generated in the blend were formate, formyl amides, 1,4-DMPZ, and EDA. The generation of total formate and EDA are compared for degradation of PZ, 1-MPZ, and the blend in Figure 7.11 and Figure 7.12, respectively.

The effect of blending PZ with 1-MPZ in comparison to the thermal stability of the amines by themselves can be observed directly. Degradation occurs rapidly in the solution of 1-MPZ alone compared to both the blend and PZ alone. This is due to an equilibrium being established between PZ, 1-MPZ, and 1,4-DMPZ that is discussed in more detail in section 7.3 below. EDA was not produced in the degradation of 1-MPZ, which supports the presence of a separate, equilibrium mechanism that dominates reactions in this solution.

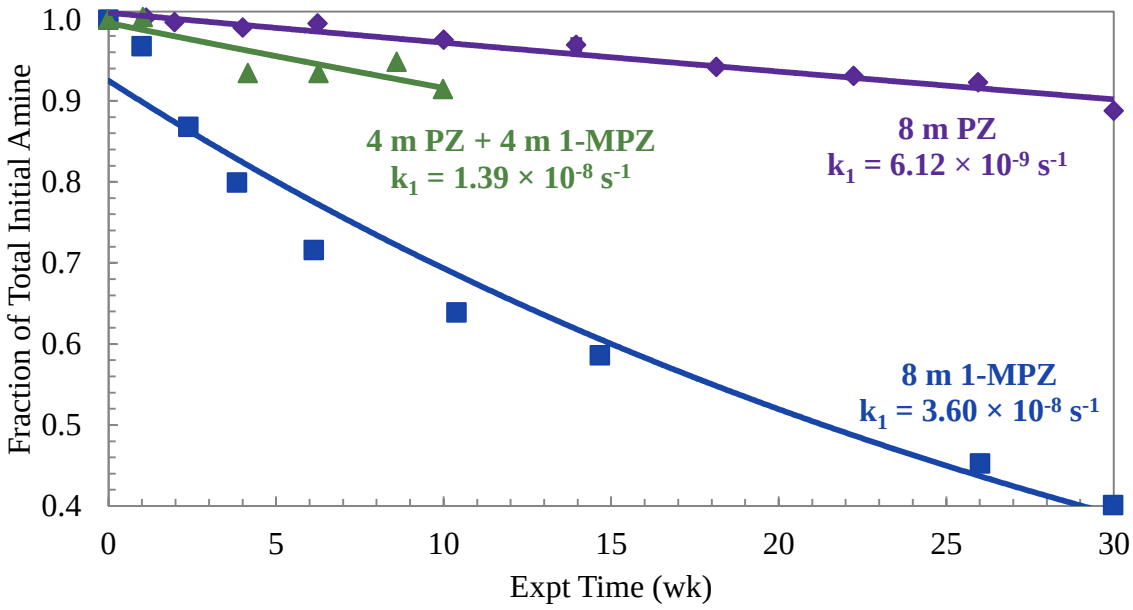

Figure 7.10: Total amine loss during degradation of 8 m PZ, 8 m 1-MPZ, and 4 m PZ + 4 m 1-MPZ blend at 150 °C

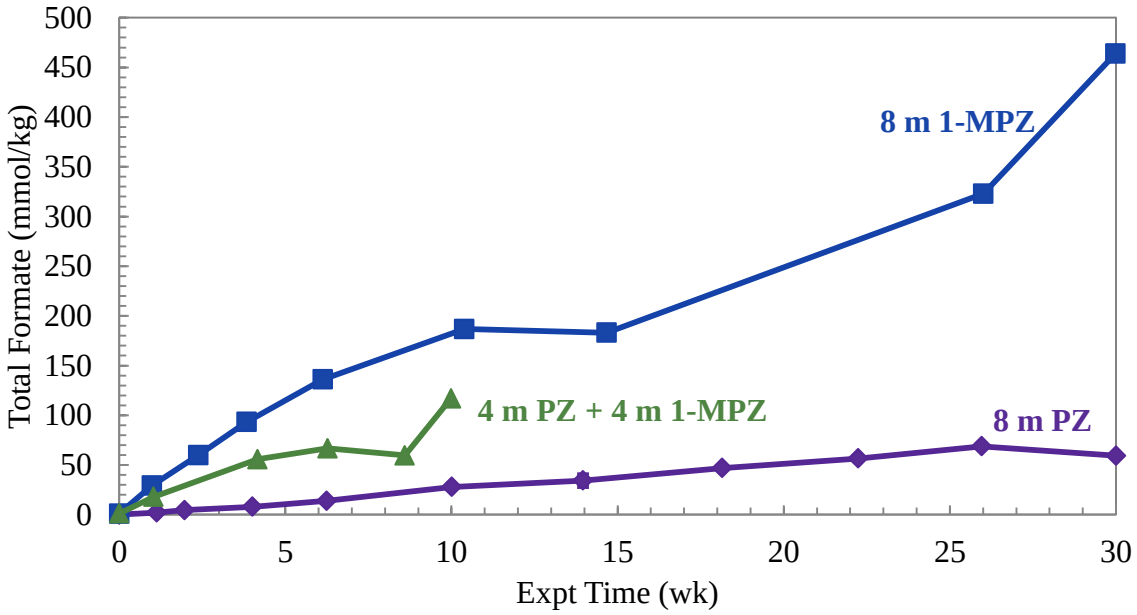

Figure 7.11: Generation of total formate in thermal degradation of 8 m PZ, 8 m 1-MPZ, and 4 m PZ + 4 m 1-MPZ blend at 150 °C

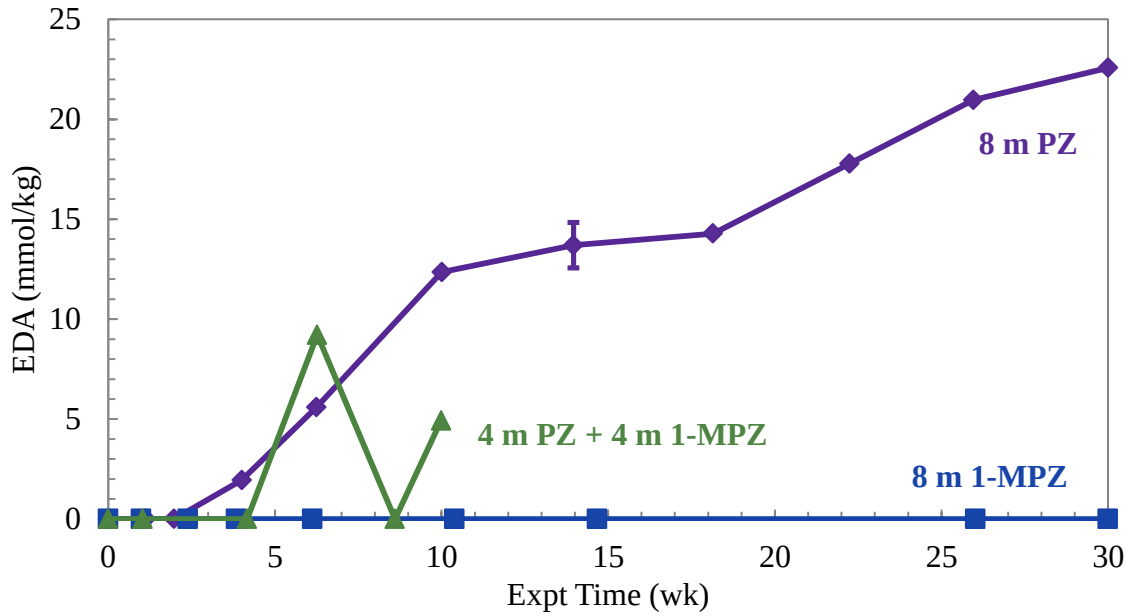

Figure 7.12: Generation of EDA in thermal degradation of 8 m PZ, 8 m 1-MPZ, and 4 m PZ + 4 m 1-MPZ blend at 150 °C

The recovery of carbon and nitrogen in the degradation of 1-MPZ was exceptionally good compared to traditional PZ degradation experiments because two major amine based degradation products were recovered and quantified (PZ and 1,4-DMPZ). The overall recovery of carbon during the experiment is shown in Figure 7.13 below. At the end of the experiment, 21% of the initial carbon as 1-MPZ was not recovered in the form of the products listed. The concentration of N-formyl PZ from the cation IC was used and no further addition to the mass balance was made from the formyl amides concentration since the specific speciation is not clear. Concentrations of oxalate, acetate, and EDA were not included in the figure. This closure of the carbon mass balance indicates the presence of a rapid equilibrium between 1-MPZ and it two major products: PZ and 1,4-DMPZ. This is a unique case of thermal degradation that has not been observed in other amines.

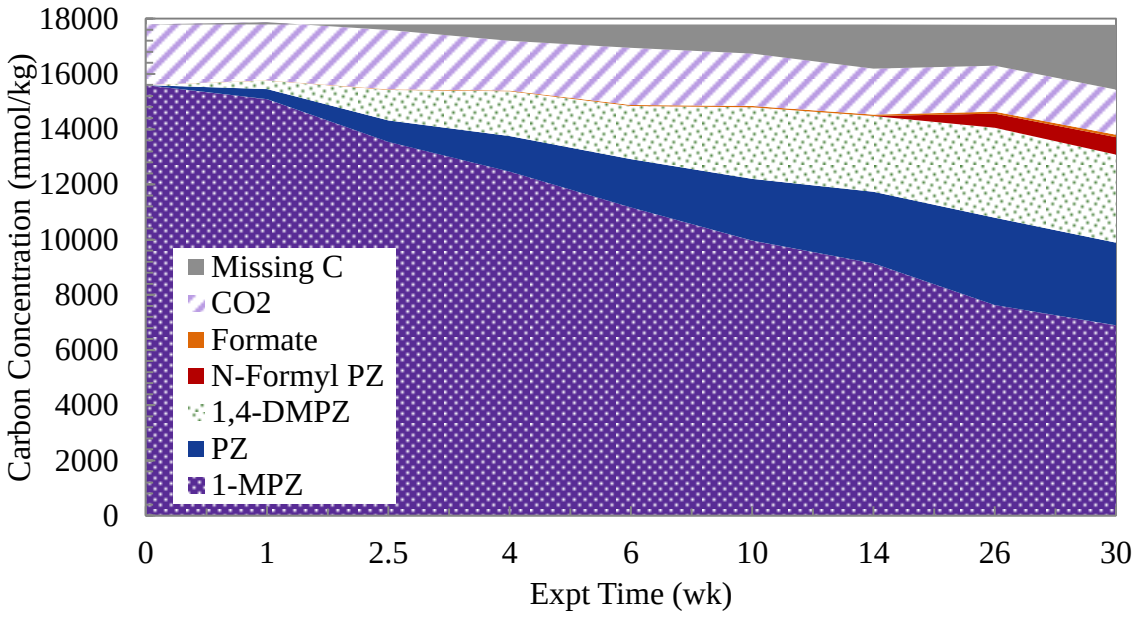

Figure 7.13: Carbon Mass Balance for 8 m 1-MPZ Degraded at 150 °C for 30 weeks

Although a unique equilibrium is being established, some conclusions can still be gleaned from the amine loss data. The fraction of amine remaining for each amine alone and in the blend is compared in Figure 7.14. The results are plotted as fraction of initial amine, despite the differences in starting concentration. The PZ results are difficult to interpret since little PZ is lost. The 1-MPZ data show that the loss of 1-MPZ is slower when blended than alone. This effect may be explained by the combination of two effects. First, the concentration is half that of when the amine is alone, 8 m versus 4 m 1-MPZ. Amine concentration is known to have a minimal effect on overall degradation rate for PZ, but the effect may be stronger in 1-MPZ systems. Secondly, the results could represent the nucleophilicity of 1-MPZ compared to other amines that have been blended with PZ. The presence of the methyl group on the amino function of 1-MPZ decreases the pKa, and therefore reactivity, of the molecule. The first and second pKa values for 1-MPZ are 9.14 and 4.63 compared to 9.73 and 5.35 for PZ (at 298K) (Khalili et al., 2009). When PZ undergoes a nucleophilic attack of 1-MPZ, this proceeds slower than when PZ is blended with MEA or AMP which it attacks readily. The decreased pKa of 1-MPZ makes it attractive for PZ to attack compared with attacking itself during thermal degradation of 8 m PZ.

7.2.2 2-Methylpiperazine (2-MPZ) and PZ + 2-MPZ

The thermal degradation of 8 m 2-MPZ and the blend of 4 m PZ + 4 m 2-MPZ were studied with 0.3 mole CO_2 per mole alkalinity at 150 °C. The loss of total initial amine in these experiments is compared with 8 m PZ in Figure 7.15. PZ and 2-MPZ were not able to be separated on the cation IC and the total area was calibrated with a PZ standard and reported as a single concentration. The k_1 values calculated with an exponential regression are included on the figure. The main degradation products of 2-

MPZ and blend degradation were EDA, formyl amides, and formate. The generation of total formate and EDA are compared for degradation of PZ, 2-MPZ, and the blend in Figure 7.16 and Figure 7.17, respectively. A standard of 2-methyl derivative of EDA, 1,2-diaminopropane, was tested on the cation IC and eluted near EDA, but was not identified as a dominant product for the thermal degradation of 2-MPZ.

The effect of blending PZ with 2-MPZ in comparison to the thermal stability of the amines by themselves can be observed directly. As with the previous comparison, the methylated PZ degrades faster than PZ alone while the blend falls in between. The generation of total formate increases with increased degradation, as expected. EDA is a contaminant in 2-MPZ solutions as it is present in initial samples containing 2-MPZ, but generation of EDA increases with further degradation.

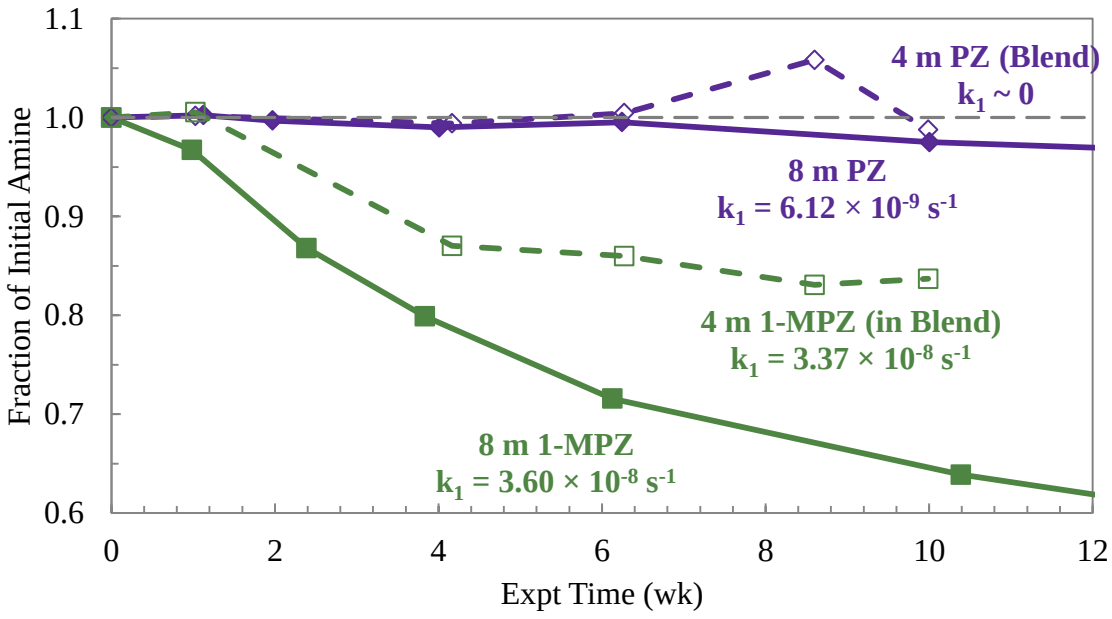

Figure 7.14: Loss of amine for degradation of PZ or 1-MPZ alone and in a 4 m PZ + 4 m 1-MPZ blend at 150 °C

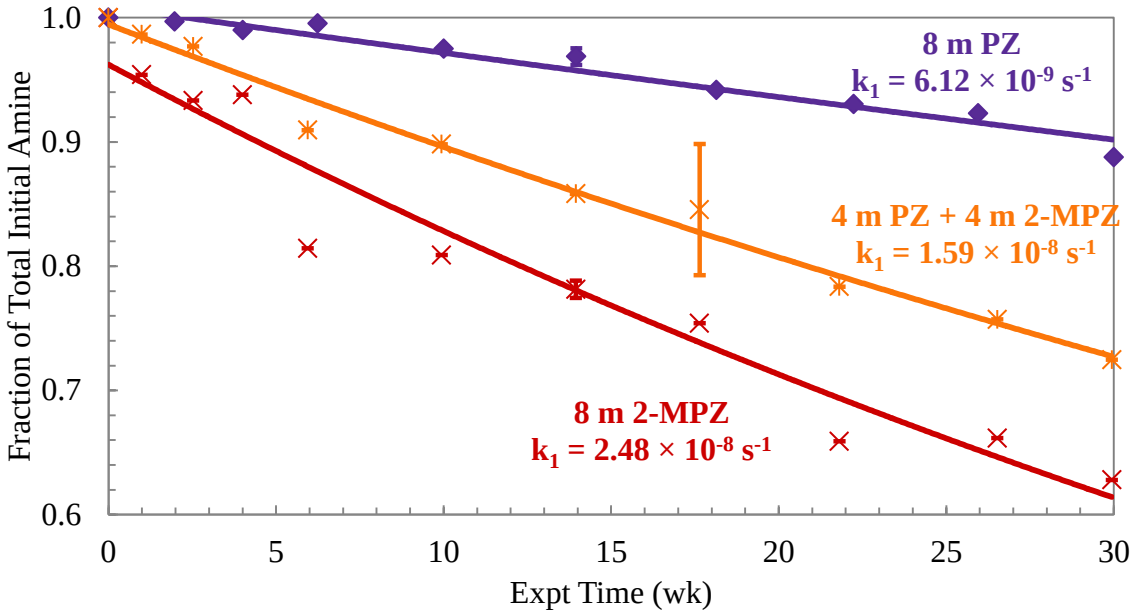

Figure 7.15: Total amine loss during degradation of 8 m PZ, 8 m 2-MPZ, and 4 m PZ + 4 m 2-MPZ blend at 150 °C

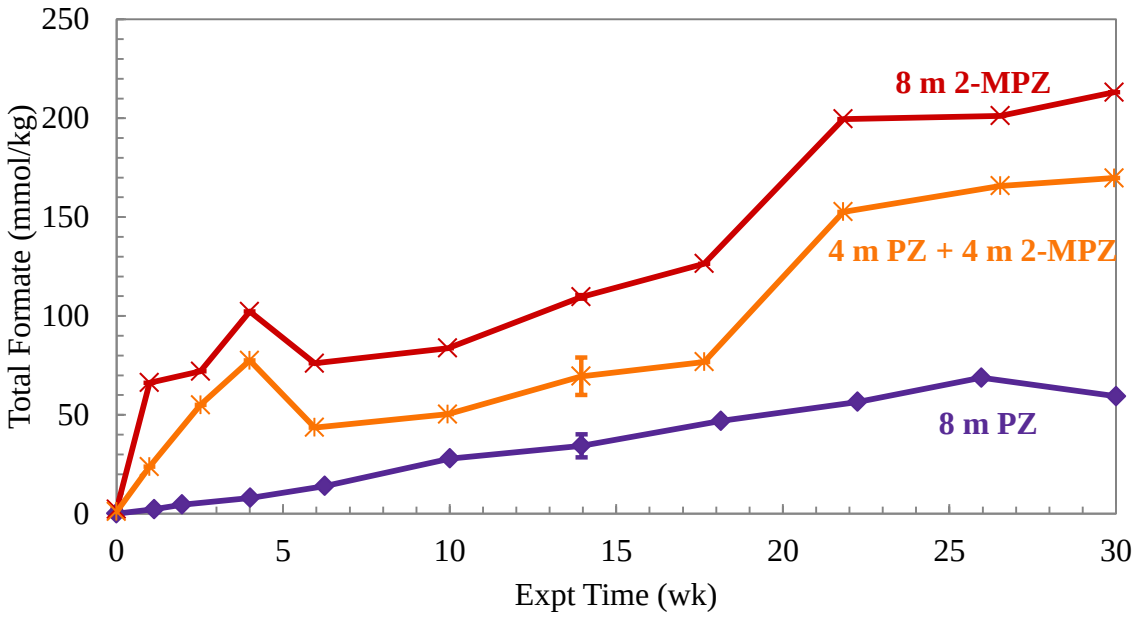

Figure 7.16: Generation of total formate in thermal degradation of 8 m PZ, 8 m 2-MPZ, and 4 m PZ + 4 m 2-MPZ blend at 150 °C

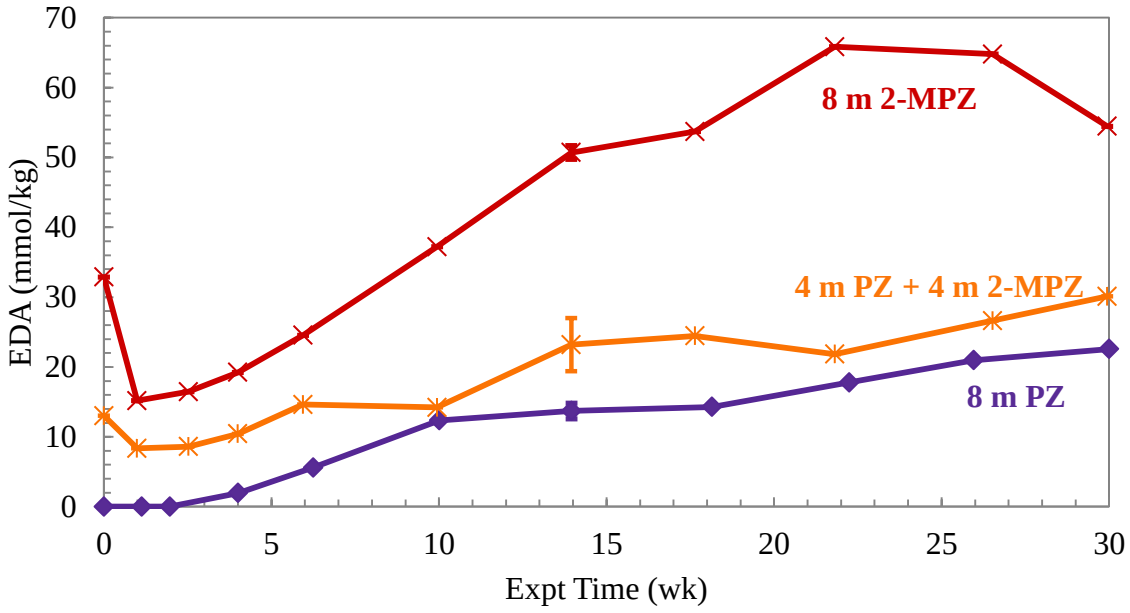

Figure 7.17: Generation of EDA in thermal degradation of 8 m PZ, 8 m 2-MPZ, and 4 m PZ + 4 m 2-MPZ blend at 150 °C

7.2.3 trans-2,5-Dimethylpiperazine (t2,5-DMPZ) and PZ + t2,5-DMPZ blend

The thermal degradation of 2 m t2,5-DMPZ and the blend of 4 m PZ + 4 m t2,5-DMPZ were studied with 0.3 mole CO_2 per mole alkalinity at 150 °C. The loss of total starting amine in these experiments fit with an exponential regression and compared with 8 m PZ in Figure 7.18. As with 2-MPZ, t2,5-DMPZ was not able to be separated on the cation IC from PZ and the total area was calibrated with a PZ standard and reported as a single concentration. The main degradation products of t2,5-DMPZ and blend degradation were EDA, formyl amides, and formate, as with previous methylated PZ experiments. The generation of total formate and EDA are compared for degradation of PZ, t2,5-DMPZ, and the blend in Figure 7.19 and Figure 7.20, respectively. There were additional peaks on the cation IC chromatogram that were not identified.

The k_1 data indicates that 2 m t2,5-DMPZ degrades 1.5 times faster than 8 m PZ while the blend is almost 3 times faster. This is the only comparison where the

methylated molecule was more stable than the blend, but this is likely due to the low concentration of t2,5-DMPZ. The generation of total formate and EDA behaved as expected, with higher rates of amine degradation producing higher concentrations of products. One exception was the t2,5-DMPZ case where EDA was rapidly generated, then maintained at an equilibrium concentration of 10 to 14 mmole per kg.

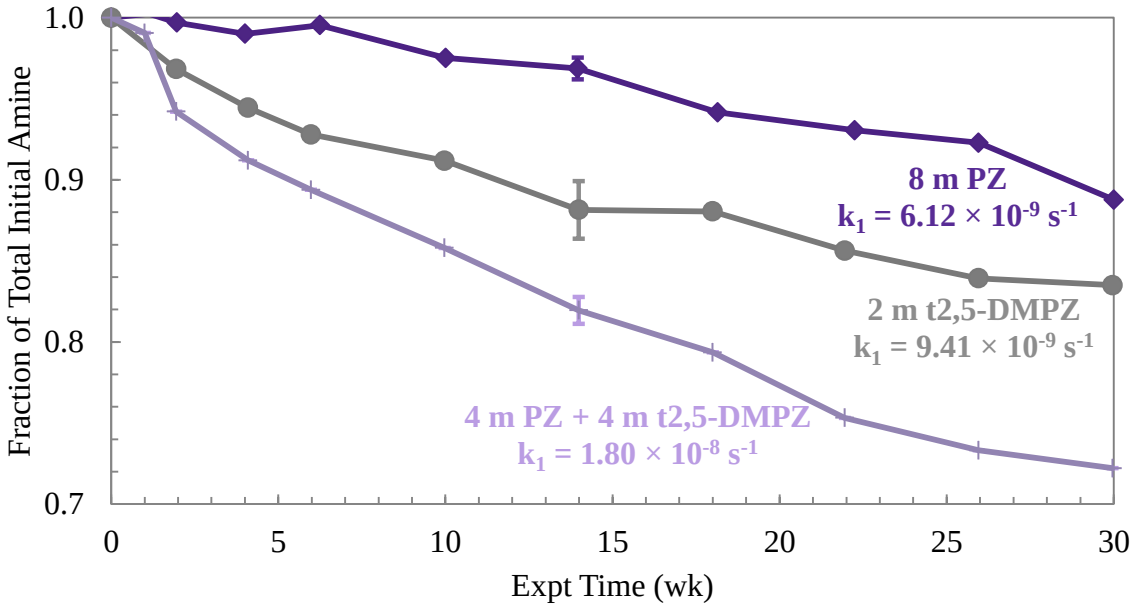

Figure 7.18: Total amine loss during degradation of 8 m PZ, 2 m t2,5-DMPZ, and 4 m PZ + 4 m t2,5-DMPZ blend at 150 °C

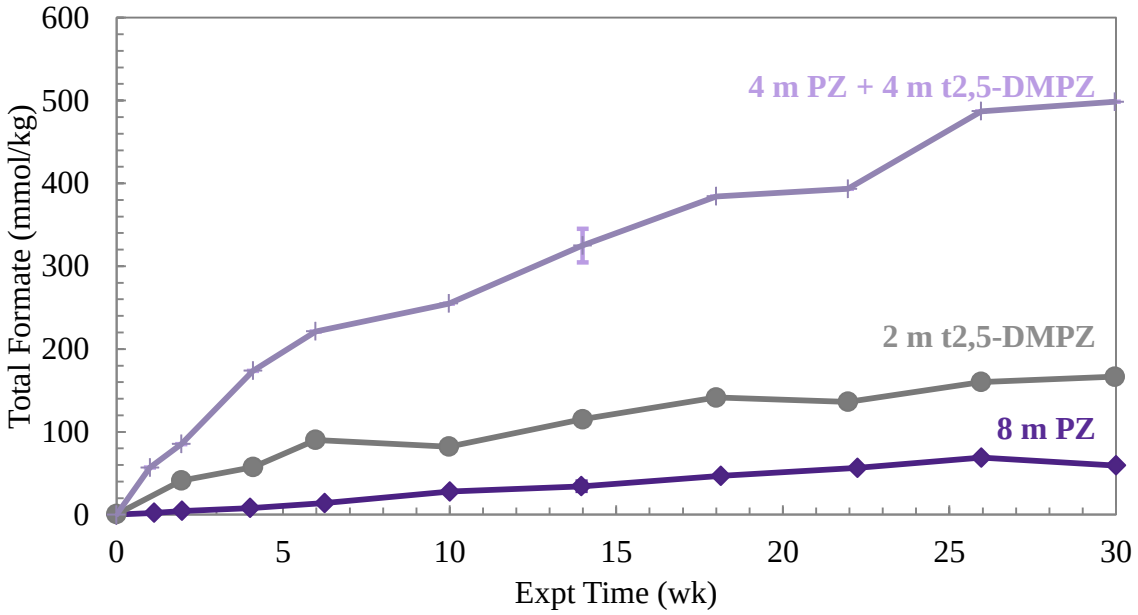

Figure 7.19: Generation of total formate in thermal degradation of 8 m PZ, 8 m t2,5-DMPZ, and 4 m PZ + 4 m t2,5-DMPZ blend at 150 °C

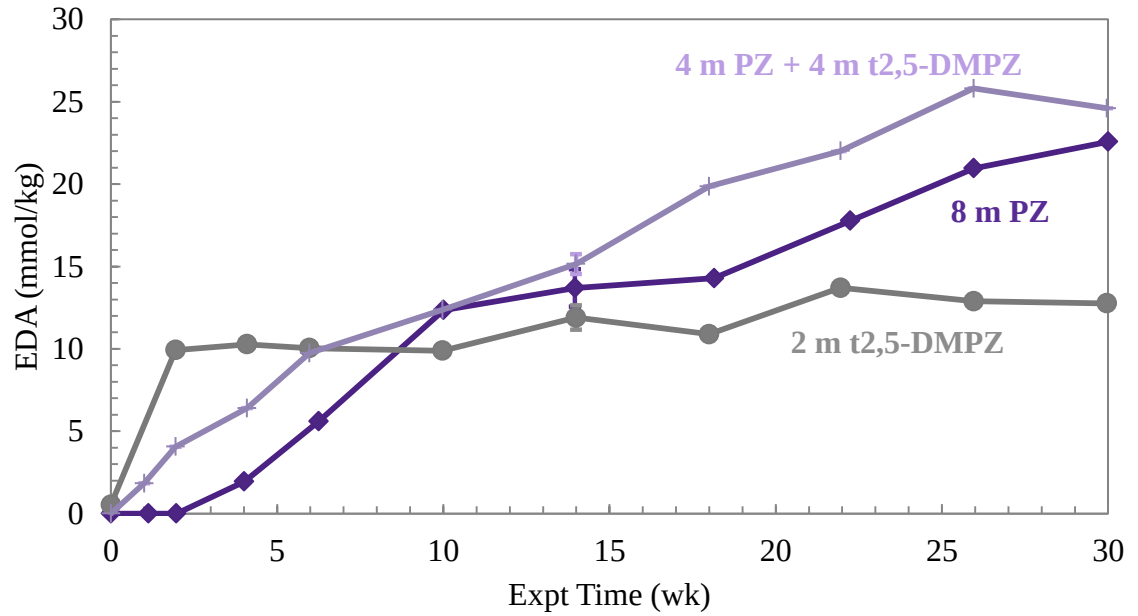

Figure 7.20: Generation of EDA in thermal degradation of 8 m PZ, 8 m t2,5-DMPZ, and 4 m PZ + 4 m t2,5-DMPZ blend at 150 °C

7.2.4 Effect of methyl substitution

The effect of methylation on PZ was assessed at 150 °C and a first order rate constant, k_1, was regressed for all experiments. The addition of a methyl group at either the 1- or 2-position on PZ weakens the molecule to thermal degradation reactions. The data discussed in the previous section indicate that an amino methyl, rather than an α-methyl, enhances degradation, but a discussion of the 1-MPZ thermal equilibrium discussed in the following section negates this conclusion. Blending either 1-MPZ or 2-MPZ will decrease the thermal stability of PZ, although to a lesser extent than when blended with MEA, AMP, and MDEA (Closmann et al., 2009; Davis, 2009). Despite the degradation measured, the overall rate of degradation in blends of PZ with 1-MPZ and 2-MPZ is slow compared to other CO_2 capture solvents of interest and should prove to be valuable replacements for thermally instable solvents.

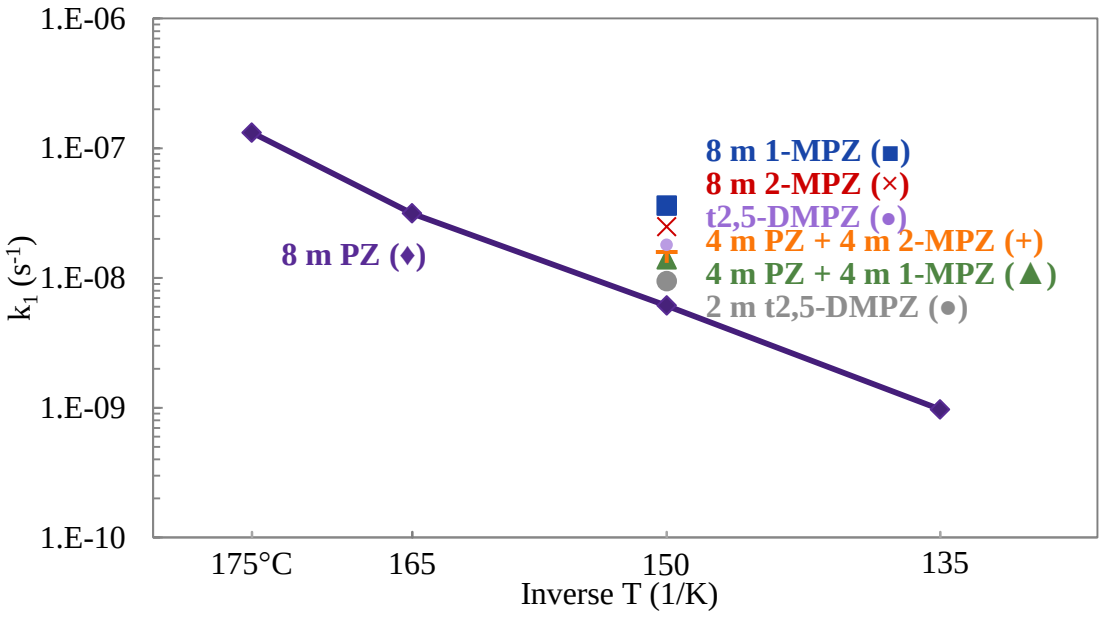

Figure 7.21: Amine loss in thermal degradation of methyl substituted PZs at 150 °C

7.3 THERMAL EQUILIBRIUM OF METHYL-SUBSTITUTED PZS

A new solvent concept in the field of post-combustion CO_2 capture is the use amines that demonstrate noticeable levels of overall thermal degradation, but degrade to useful products that can react with CO_2 and maintain alkalinity of the solution. One example of this solvent concept is the use of a blend of PZ, 1-MPZ, and 1,4-DMPZ (Rochelle et al., 2010). As described above in section 7.2.1, 1-MPZ degrades to form nearly equimolar concentrations of PZ and 1,4-DMPZ. PZ as a degradation product is an obvious advantage of any 1-MPZ-based solvent system. If 1-MPZ is the starting solvent, appreciable concentrations of PZ and 1,4-DMPZ will eventually accumulate due to degradation. Observations indicate that systems of this nature will tend toward an equilibrium set of concentrations as they interconvert.

To demonstrate this concept, blends of PZ + 1-MPZ + 1,4-DMPZ were thermally degraded in an attempt to understand the equilibrium between the three amines. Solutions with varying amine compositions with 0.3 mole CO_2 per mole alkalinity were degraded at 150 °C for up to 15 weeks. At this temperature, some degradation will occur, but the interconversion of PZ, 1-MPZ, and 1,4-DMPZ is assumed to occur more rapidly than degradation processes based on the slow degradation rates discussed in the previous section. The concentration combinations studied, listed as the molal concentrations of PZ, 1-MPZ, and 1,4-DMPZ, were 5 m PZ + 2 m 1-MPZ + 1 m 1,4-DMPZ, or 5/2/1, 5/2.5/0.5, 5/1.5/1.5, 3.9/3.9/0.2, and 3.75/3.75/0.5 blends. In addition to these blends, information can be gleaned from previously discussed experiments performed on 8 m 1-MPZ and the blend of 4 m PZ + 4 m 1-MPZ.

It is important to note that the interconversion of PZ, 1-MPZ, and 1,4-DMPZ represents multiple arm-switching reactions between molecules. The change of substituent groups, or ‘arms’, has been observed previously for 2-hydroxyethyl and

methyl arms attached directly to a reactive amine center such as the conversion of MDEA to diethanolamine (DEA), triethanolamine (TEA), or N,N-dimethylethanolamine (DMEA) (Bedell et al., 2010; Closmann and Rochelle, 2011). Similar reactions are seen in blends of MDEA and PZ where the protonated MDEA reacts with a PZ molecule to produce DEA and 1-MPZ (Closmann et al., 2009). This reaction is commonly called 'arm-switching', but likely occurs as a S_N2 substitution or nucleophilic attack reaction similar to that described in section 6.1. In this reaction, a strong nucleophile, such as one of the amine functions on PZ or 1-MPZ, reacts with the α-carbon of the substituent to be transferred from another molecule. In traditional S_N2 reactions, this α-carbon must have a strong leaving group such as a halide or other weak base (McMurry, 2000). The amine functions on PZ act as good nucleophiles since strong bases are generally considered strong nucleophiles and given the first pKa of PZ and 1-MPZ, either could act as a good nucleophile. In this particular reaction, an amine function is both a leaving group and a nucleophile. The lower pKa of the tertiary amino function of 1-MPZ makes this group a willing leaving group since it is a weaker base than other secondary amine functions.

An example of this type of reaction for the solvent system under discussion is provided in Figure 7.22. In this example, a methyl group from 1,4-DMPZ is transferred to a PZ to produce two 1-MPZ molecules through a quaternary intermediate complex. The carbon that is transferred is highlighted in blue to distinguish the main reaction. The reaction is initiated when the tertiary amine attached to the arm to be transferred is protonated. Given the complex speciation of a mixture of PZ-based it is likely that the tertiary amine would be protonated to a small degree, even if not the dominant protonated molecule. A strong nucleophile at this point can attack the α-carbon and initiate the arm switch.

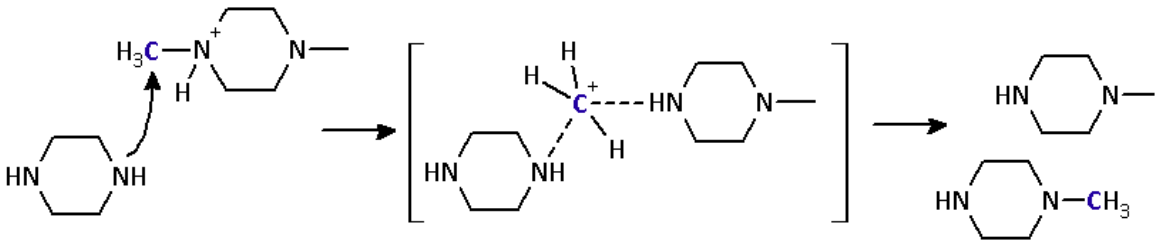

Figure 7.22: Mechanism for S_N2 nucleophilic attack to transfer a methyl group

The expected equilibrium reaction of 1-MPZ is as follows, where the brackets indicate the concentration of the given species in units of mmole per kg (Equation 7.1). The equilibrium constant, K_{EQ}, of Equation 1 can then be calculated (Equation 7.2)

$$2[\text{1-MPZ}] \leftrightarrow [\text{PZ}] + [\text{1.4-DMPZ}] \tag{7.1}$$

$$K_{eq} = \frac{[\text{PZ}][1,4-\text{DMPZ}]}{[1-\text{MPZ}]^2} \tag{7.2}$$

The goal of this K_{EQ} analysis is to determine the concentrations of the three amine species in equilibrium at 150 °C. These concentrations would be what were expected to be stable in a system with a reboiler temperature of 150 °C. The K_{EQ} values for the thermal equilibrium of PZ, 1-MPZ, and 1,4-DMPZ are shown in Figure 7.23. In each case, the K_{eq} was calculated at each time point according to Equation 7.2 and plotted against degradation time.

All of the experiments were found to tend toward a K_{EQ} value of 0.27-0.30, indicating the equilibrium concentrations of amine expected at 150 °C. The long term blend experiments containing 3.9/3.9/0.2 and 3.75/3.75/0.5 demonstrate this tendency toward a K_{EQ} of 0.29. Even the two experiments with only limited data demonstrate the trend toward the same approximate K_{EQ} value as the other blends.

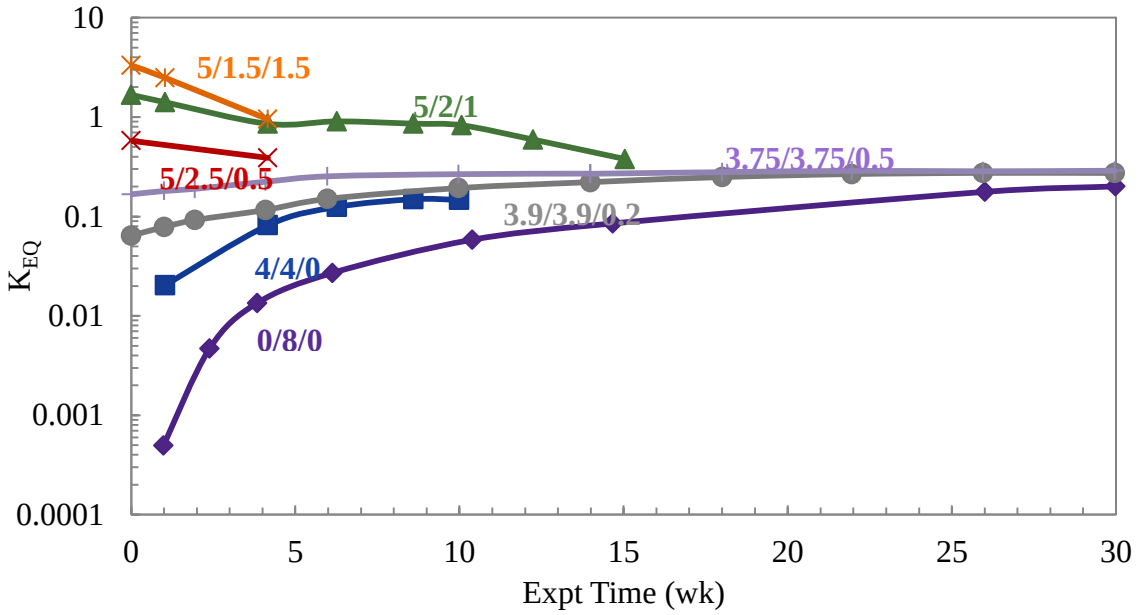

Figure 7.23: K_{eq} for PZ + 1-MPZ + 1,4-DMPZ Solutions Thermally Degraded at 150 °C (α=0.3). Labels indicate the concentrations of PZ, 1-MPZ, and 1,4-DMPZ in solution in molal (m)

Degradation of PZ alone will not yield these results as 1-MPZ and 1,4-DMPZ are minor products. However, when a blend begins with at least some 1-methylated PZs (i.e., 1-MPZ or 1,4-DMPZ), these methyl groups can easily undergo a straightforward nucleophilic attack and disproportionation, resulting in switching of the methyl groups between molecules. Overall, the data suggest that any system starting with 1-MPZ will tend toward a K_{eq} of 0.28 to 0.30 at 150 °C.

7.3.1 Implications for other CO_2 capture solvents

The interconversion and equilibrium of methylated PZs is an important concept for blended CO_2 capture amines. The results demonstrate the advantages of starting with a blended solvent rather than a monosubstituted solvent that is likely to react to form its corresponding unsubstituted and disubstituted counterparts during degradation. This

concept can be applied to a number of solvents already being used or being suggested for industrial application.

As an example, N-(2-hydoxyethyl)piperazine (HEP) is being suggested as a novel CO_2 capture solvent. Given the structure of this molecule, it is likely that when exposed to stripping temperatures, HEP will react to form its unsubstituted form (PZ) and its disubstituted form (bis-(2-hydroxyethyl)piperazine, bHEP). In order to establish this equilibrium quickly, it could be advantageous to being with a blend of these three molecules, whose structures are shown in Figure 7.24. Depending on the route of manufacturing of the parent molecule, HEP, an additional advantage could be gained by decreasing the purification needed if the contaminants are PZ or bHEP. In that way, the cost of the amine itself can be decreased while higher levels of contamination could be tolerated if the equilibrium between the molecules were understood.

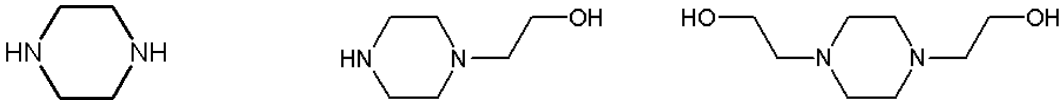

PZ | N-(2-hydroxyethyl) PZ (HEP) | bis-(2-hydroxyethyl) PZ (bHEP)

Figure 7.24: Molecules present in an equilibrium mixture of HEP

There could be numerous advantages to a solvent with equilibrium distribution of related molecules. Another system that may be of interest is that based on N-Ethyl PZ (1-EPZ) where its complementary unsubstituted and disubstituted molecules are PZ and N,N'-diethyl PZ (1,4-DEPZ) whose structures are shown in Figure 7.25. Since 1-EPZ is a common product of PZ thermal degradation, there already exists routes of reaction between the molecules. The ease of transfer of ethyl groups has not yet been observed but can be assumed to be slightly more sterically hindered than methyl arm switching.

The fact that 2-hydroxyethyl groups arm switch readily indicates that ethyl arm switching should be possible.

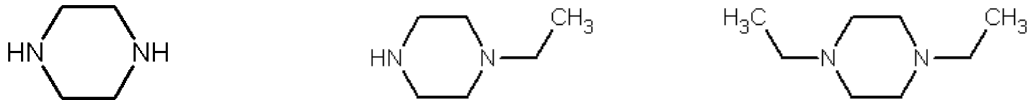

PZ | N-Ethyl PZ (1-EPZ) | N,N'-Diethyl PZ (1,4-DEPZ)

Figure 7.25: Molecules present in an equilibrium mixture of 1-EPZ

7.4 THERMAL STABILITY OF CO_2 CAPTURE AMINES

The thermal stability of a PZ, PZ structural analogs, and substituted PZs has been analyzed during the course of this work. The degradation behavior of amines is a notoriously complex issue which is complicated to compare directly because of differences in temperature, CO_2 concentration, CO_2 partial pressure, and amine concentration. The comparison presented in this section utilizes first order rate constants, k_1, regressed from raw amine data. A second analysis based on this will be presented that calculates the maximum operating stripper temperature for a given amine solvent.

7.4.1 Comparisons of first-order rate constants for thermal amine loss

The methodology for calculating first-order rate constants, k_1, was developed in section 5.2 of this dissertation. A k_1 was calculated for each amine studied in this thesis and those found in literature. Data for 7 m MEA, 7 m AMP, 7 m Diglycolamine® (DGA®), 3.5 m HEP, 2.33 m diethylenetriamine (DETA), 2.33 m N-(2-aminoethyl) PZ (AEP), N-(2-hyroxyethyl) EDA (HEEDA), and 7 m MEA / 2 m PZ blend were reported previously (Davis, 2009). Data for EDA and 2-piperidineethanol (2-PE) were reported previously by Zhou while data for MDEA and the blend of MDEA and PZ were reported previously by Closmann (Closmann, 2011; Closmann et al., 2009; Zhou et al., 2010).

Data for thermal degradation of 3-(methylamino)propylamine (MAPA) were obtained from unpublished work of Vevelstad (Vevelstad, 2010). Eide-Haugmo tested a variety of amines including MEA, EDA, and DETA using a CO_2 concentration of 0.5 mole CO_2 per mole amine for all amines (Eide-Haugmo et al., 2011). Lepaumier investigated numerous amines but used continuously stirred cells with constant CO_2 partial pressure in the headspace, rather than a constant CO_2 loading in the liquid phase (Lepaumier et al., 2010; Lepaumier et al., 2009a). These data are included, although difficult to compare since the initial loading is unknown and CO_2 solubility for these specialized amines is not available. Data from Chakma and Meisen are included but their data was also obtained at constant CO_2 partial pressure, rather than loading (Chakma and Meisen, 1997).

A summary of k_1 values for thermal degradation are compared in the next three tables. In Table 7.2, PZ is compared with PZ structural analogs and substituted PZs. In Table 7.3, PZ-based blends are compared with some MEA-based blends. Finally, PZ is compared with other CO_2 capture amines in Table 7.4. In all three tables, amines are listed in approximate order of decreasing resistance to thermal degradation. This order is based on the analysis presented in the next section. The data for 8 m PZ with 0.3 mole CO_2 per mole alkalinity and 7 m MEA with 0.4 mole CO_2 per mole alkalinity are highlighted with bold text in the tables. For Pyr, HMI, HomoPZ, and 20 m PZ, where amine loss is initially drastic and certainly not first order in amine, the initial rate demonstrated after 1-6 weeks of degradation was used to calculate an apparent k_1. For some literature data with limited data, an apparent k_1 was calculated using the available data.

Table 7.2: Apparent first order rate constant (k_1) for thermal degradation of PZ, structural analogs of PZ, and substituted PZs

Amine	Conc.	Loading	$k_1 \times 10^9$ (s^{-1})						Ref*
	m	mol/mol alk	100 °C	120	135	150	165	175	
Piperazine (PZ)	8	0				0.1	0.8	7	
PZ	8	0.47						24	
PZ	20	0.1						45	
Morpholine	8	0.3						50	
PZ	8	0.1					18	66	
PZ	8	0.2						79	
Piperidine	8	0.3						84	
PZ	4	0.3					36	114	
PZ	**8**	**0.3**			**1**	**6**	**31**	**132**	
PZ	8	0.4			0.5	8	41	171	
t2,5-DimethylPZ	2	0.3				9			
PZ	12	0.3					50	156	
Hexamethylenediamine	8	0.3						169	
PZ	10	0.3			5	9			
PZ	20	0.3				24		168	
2-MethylPZ	8	0.3				25			
1-MethylPZ	8	0.3				36			
PZ	10	0.4				6			
Ethylenediamine (EDA)	8	0.2	5	5	30				Z
Pyrrolidine	8	0.3						1400	
EDA	8	0.4	5	38	167				Z
Homopiperazine	8	0.3						1850	
N-(2-Hydroxyethyl) PZ	3.5	0.4			58				D
Hexamethyleneimine	8	0.3						5900	
EDA	3.5	0.4			247	339			D
N-(2-Aminoethyl) PZ	2.33	0.4			191				D
EDA	7.13	0.25			143				EH

* If not specified, from this work; D = (Davis, 2009); EH = (Eide-Haugmo et al., 2011); Z = (Zhou et al., 2010).

Table 7.3: Apparent first order rate constant (k_1) for thermal degradation of blended solvents CO_2 capture amines

Amine	Blend Components	Conc.	Loading	$k_1 \times 10^9$ (s^{-1})					Ref*
		m	mol/mol alk	100 °C	120	135	150	200	
PZ	PZ/1-MPZ	4/4	0.3				~0		
3.9/3.9/0.2 (TA)	PZ/1-MPZ/1,4-DMPZ	-	0.3				8		
3.75/3.75/0.5 (TA)	PZ/1-MPZ/1,4-DMPZ	-	0.3				10		
5/2/1 (TA)	PZ/1-MPZ/1,4-DMPZ	-	0.3				14		
PZ + 1-MPZ (TA)	PZ/1-MPZ	4/4	0.3				14		
5/2.5/0.5 (TA)	PZ/1-MPZ/1,4-DMPZ	-	0.3				14		
PZ + 2-MPZ (TA)	PZ/2-MPZ	4/4	0.3				16		
MDEA	MDEA/DEA	5.3/1.7	0.27					1550	RT
PZ + t2,5-DMPZ (TA)	PZ/t2,5-DMPZ	4/4	0.3				18		
MDEA + DEA (TA)	MDEA/DEA	5.3/1.7	0.27					2200	RT
1-MPZ	PZ/1-MPZ	4/4	0.3				34		
MDEA	MDEA/PZ	7/2	0			34	19		C
MDEA + PZ (TA)	MDEA/PZ	7/2	0			33	21		C
PZ	MDEA/PZ	7/2	0			32	27		C
5/1.5/1.5 (TA)	PZ/1-MPZ/1,4-DMPZ	-	0.3				75		
MDEA	MDEA/PZ	7/2	0.11			25	42		C
PZ	PZ/AMP	6/4	0.4			32	92		Z
MDEA + PZ (TA)	MDEA/PZ	7/2	0.11			49	61		C
PZ + AMP (TA)	PZ/AMP	6/4	0.4			46	144		Z
DEA	MDEA/DEA	5.3/1.7	0.27					13700	RT
AMP	MEA/AMP	7/2	0.4	5		6	85		D
AMP	PZ/AMP	6/4	0.4			67	249		Z

Table 7.3: Apparent first order rate constant (k_1) for thermal degradation of blended solvents CO_2 capture amines (continued)

Amine	Blend Components	Conc.	Loading	$k_1 \times 10^9$ (s^{-1})					Ref*
		m	mol/mol alk	100 °C	120	135	150	200	
MDEA	MDEA/PZ	7/2	0.25		11	58	284		C
MEA + AMP (TA)	MEA/AMP	7/2	0.4	2	23	123	408		D
MEA	MEA/AMP	7/2	.04	0.8	31	1890	686		D
PZ	MDEA/PZ	7/2	0.11			378	486		C
MDEA + PZ (TA)	MDEA/PZ	7/2	0.25		27	110	297		C
PZ	MDEA/PZ	7/2	0.25		118	780	2050		C
MEA + DGA® (TA)	MEA/DGA®	7/2	0.4	19	20	162	551		D
MEA	MEA/DGA®	7/2	0.4	19	26	190	716		D
DGA®	MEA/DGA®	7/2	0.4	17	3	92	289		D
Mor	MEA/Mor	7/2	0.4	14	64	248	532		D
MEA + Mor (TA)	MEA/Mor	7/2	0.4	16	62	237	592		D
MEA	MEA/Mor	7/2	0.4	16	62	234	612		D
MEA	MEA/PZ	7/2	0.4	26	56	238	683		D
MEA + PZ (TA)	MEA/PZ	7/2	0.4	27	62	251	608		D
PZ	MEA/PZ	7/2	0.4	31	84	316	1200		D

* If not specified, from this work; C = (Closmann et al., 2009); D = (Davis, 2009); RT = (Reza and Trejo, 2006); Z = (Zhou et al., 2010)

Table 7.4: Apparent first order rate constant (k_1) for thermal degradation of CO_2 capture amines

Amine	Abbreviation[a]	Conc.[b]	Loading	$k_1 \times 10^9$ (s^{-1})[c]								Ref.[d]
		m	mol/mol alk	100 °C	120	135	140	150	160/165	175	180/200	
Morpholine	Mor	8	0.3							50		
Piperidine	PD	8	0.3							84		
Piperazine	**PZ**	**8**	**0.3**			**1**		**6**	**31**	**132**		
Piperazine	PZ	8	0.4			0.5		8	41	171		
3.9 / 3.9 / 0.2 (TA)	PZ/MPZ/DMPZ	8	0.3					8				
Hexamethylenediamine	HMDA	8	0.3							19		
trans-2,5-Dimethylpiperazine	t2,5-DMPZ	2	0.3					9				
3.75 / 3.75 / 0.5 (TA)	PZ/MPZ/DMPZ	8	0.3					10				
5 / 2 / 1 (TA)	PZ/MPZ/DMPZ	8	0.3					14				
PZ / 1-MPZ (TA)	PZ/1-MPZ	4/4	0.3					14				
5 / 2.5 / 0.5 (TA)	PZ/MPZ/DMPZ	8	0.3					14				
PZ / 2-MPZ (TA)	PZ/2-MPZ	4/4	0.3					16				
PZ / t2,5-DMPZ (TA)	PZ/t2,5-DMPZ	4/4	0.3					18				
2-Methylpiperazine	2-MPZ	8	0.3					25				
MDEA / DEA (TA)	MDEA/DEA	5.3/1.7	0.27								2250	RT
1-Methylpiperazine	1-MPZ	8	0.3					36				
5-amino-1-pentanol	5a1p	7	0.4			13		43				D
MDEA / PZ (TA)	MDEA/PZ	7/2	0			33		21				C
Pyrrolidine	Pyr	8	0.3							1400		
Homopiperazine	HomoPZ	8	0.3							1850		
2-Amino-2-methyl-1-propanol	AMP	4.81	0.5			17						EH
1,4-Dimethylpiperazine	DMPZ	4*	2 MPa				35.5					L1
MDEA / PZ (TA)	MDEA/PZ	7/2	0.11			49		61				C
2-amino-2-methyl-1-propanol	AMP	7	0.4		8	21		86				D
PZ + AMP (TA)	PZ/AMP	6/4	0.4			46		144				Z
4-amino-1-butanol	4a1b	7	0.4		6	37		195				D

Table 7.4: Apparent first order rate constant (k_1) for thermal degradation of CO_2 capture amines (Continued)

Amine	Abbreviation[a]	Conc.[b]	Loading	$k_1 \times 10^9$ (s^{-1})[c]								Ref.[d]
		m	mol/mol alk	100 °C	120	135	140	150	160/165	175	180/200	
Diglycolamine®	DGA	7	0.4			39						D
Hexamethyleneimine	HMI	8	0.3							5950		
N-(2-Hydroxyethyl)piperazine	HEP	7	0.4			58						D
N-Methyldiethanolamine	MDEA	4*	2 MPa				90					L1
N,N,N',N',N''-pentamethyldipropylenetriamine	PMDPTA	2.5*	2 MPa				99					L3
Methyldiethanolamine	MDEA	7	0.1					283				C
Ethylenediamine	EDA	8	0.2	5	5	30						Z
Methyldiethanolamine	MDEA	7	0.2			42		438				C
3-amino-1-propanol	3a1p	7	0.4	2	17	47		221				D
2-Piperidineethanol	2-PE	8	0.4			80		293				Z
N,N,N',N'-Tetramethylethylenediamine	TMEDA	4*	2 MPa				125					L1
3-aminopropanol	AP	5.71	0.5			82						EH
Monoethanolamine	MEA	11	0.2		19	69						D
Ethylenediamine	EDA	3.5	0.4			247		339.4				D
Monoethanolamine	MEA	3.5	0.2	8	33	41						D
N,N,N',N'-Tetramethypropylenediamine	TMPDA	4*	2 MPa				182					L3
2-Amino-2-methyl-1-propanol	AMP	4*	2 MPa				182					L1
MEA / AMP (TA)	MEA/AMP	7/2	0.4	2	23	123		408				D
DL-1-amino-2-propanol		7	0.4	5	17	70		282				D
N,N-Dimethylethanolamine	DMMEA	4.81	0.5			118						EH
Monoethanolamine	MEA	3.5	0.4	3	22	109						D
N-(2-Aminoethyl)piperazine	AEP	2.33	0.4			191						D
Monoethanolamine	MEA	7	0.2		28	90		397				D
Monoethanolamine	**MEA**	**7**	**0.4**	**2**	**29**	**134**		**828**				**D**

Table 7.4: Apparent first order rate constant (k_1) for thermal degradation of CO_2 capture amines (Continued)

Amine	Abbreviation[a]	Conc.[b]	Loading	$k_1 \times 10^9$ (s^{-1})[c]								Ref.[d]
		m	mol/mol alk	100 °C	120	135	140	150	160/165	175	180/200	
Ethylenediamine	EDA	7.14	0.25			143						EH
MDEA / PZ (TA)	MDEA/PZ	7/2	0.25		27	110		297				C
N-Methyldiethanolamine	MDEA	3.6	0.5			153						EH
N-Methyldiethanolamine	MDEA	8.4	0.4			166						D
Diethylenetriamine	DETA	4.15	0.17			186						EH
N,N-Dimethylethanolamine	DMAE	4*	2 MPa				321					L1
Monoethanolamine	MEA	7	0.5	2	68	201		1300				D
Ethylenediamine	EDA	8	0.4	5	38	167						Z
3-(Methylamino)propylamine	MAPA	4.81	0.25			229						EH
6-amino-1-hexanol	6a1h	7	0.4	3		590		541				D
Monoethanolamine	MEA	11	0.4		61	174						D
Monoethanolamine	MEA	4*	2 MPa				420					L1
Monoethanolamine	MEA	7.01	0.5			264						EH
N,N-Dimethylethylenediamine	N,N-diMEDA	4*	2 MPa				46					L1
N-(2-Hydroxyethyl) ethylenediamine	HEEDA	4.12	0.25			303						EH
3-(Methylamino)propylamine	MAPA	9	0.4			313						V
DL-2-amino-1-propanol	MIPA	7	0.4	9		131		523				D
MEA / DGA® (TA)	MEA/DGA®	7/2	0.4	19	20	162		551				D
N,N,N'-Trimethylethylenediamine	triMEDA	4*	2 MPa				651					L1
Monoethanolamine	MEA	11	0.5		112	249						D
Monoethanolamine	MEA	3.5	0.5	13	58	137						D
2-Piperidinemethanol	2-PM	7	0.4			541						D
Diethylenetriamine	DETA	7	0.4			1150		1600				D
MEA / Mor (TA)	MEA/Mor	7/2	0.4	16	62	237		592				D
N,N,N',N'-tetramethylbutylenediamine	TMBDA	4*	2 MPa				1250					L3

Table 7.4: Apparent first order rate constant (k_1) for thermal degradation of CO_2 capture amines (Continued)

Amine	Abbreviation[a]	Conc.[b]	Loading	$k_1 \times 10^9$ (s^{-1})[c]								Ref.[d]
		m	mol/mol alk	100 °C	120	135	140	150	160/165	175	180/200	
N,N,N',N',N''-pentamethyldiethylenetriamine	PMDETA	2.5*	2 MPa				1550					L3
N-Methylethanolamine	MAE	4*	2 MPa				1650					L1
Diethanolamine	DEA	4.08	0.5			991						EH
N,N'-Dimethylethylenediamine	N,N'-diMEDA	4*	2 MPa				1700					L1
MEA / PZ (TA)	MEA/PZ	7/2	0.4	27	62	251.3		608				D
Diethanolamine	DEA	4*	2 MPa				2050					L1
N-Methyldiethanolamine	MDEA	8.39	2.59 MPa	49	83		333		611		25000	CM
2-Methylaminoethanol	MMEA	5.71	0.5			1300						EH
N-(2-Hydroxyethyl) ethylenediamine	HEEDA	3.5	0.4			1600						D
N-(2-Hydroxyethyl) ethylenediamine	HEEDA	4*	2 MPa				3550					L1

[a] MPZ = 1-MPZ; DMPZ = 1,4-DMPZ
[b] Asterisk (*) indicates unites of moles amine per kg solution
[c] Data from this study was at 165 °C; Chakma and Meisen (CM) data was at 160 and 180 °C; Reza and Trejo (RT) data was at 200 °C,
[d] If not specified, from this work; CM = (Chakma and Meisen, 1997); C = (Closmann et al., 2009); D = (Davis, 2009); EH = (Eide-Haugmo et al., 2011); L1 = (Lepaumier et al., 2009a); L3 = (Lepaumier et al., 2010); RT = (Reza and Trejo, 2006); V = (Vevelstad, 2010); Z = (Zhou et al., 2010).

The data presented in the previous tables can be shown graphically with a plot of k_1 against T^{-1}. This comparison is made for PZ related compounds, blends, and CO_2 capture amines in Figure 7.26, Figure 7.27, and Figure 7.28, respectively. With these plots, the trends and differences in magnitude of k_1 can readily be observed.

PZ is highly resistant to thermal degradation, as evidenced by the low k_1 values associated with a variety of experimental conditions. The least stable PZ conditions were 10, 12 and 20 m PZ while unloaded and lean loaded PZ was the most stable. Mor and PD are the only amines found to be more resistant to thermal degradation than PZ. The k_1 values of Mor and PD were found to be 2.7 and 1.6 times lower than PZ at 175 °C. Mor was previously identified as highly stable to thermal degradation at 135 °C (Davis, 2009).

The k_1 analysis for the blended PZ solvents demonstrates that PZ is preferentially degraded. The PZ / 1-MPZ blend is omitted from the figure since it is in equilibrium, rather than just degrading. In blends with MDEA, PZ is preferentially degraded 12 to 15 times faster than MDEA and 4 to 8 times faster than the total amine concentration. In this case, PZ reacts faster with CO_2 and exists mostly as $PZCOO^-$. PZ is a stronger nucleophile than MDEA and is degraded through S_N2 nucleophilic substitution reactions where PZ is the preferred accepting molecule when reacting with protonated MDEA. In blends with MEA, PZ degrades only 1.2 to 1.7 times faster than MEA and 1.1 to 1.9 times faster than the total amine concentration. The effect of blending is not as extreme with MEA as with MDEA.

The k_1 values for MEA and AMP were found to be 132 and 14 times higher, respectively, than 8 m PZ with 0.3 mole CO_2 per mole alkalinity. This is a significant advantage for concentrated, aqueous PZ CO_2 capture systems. All PZ structural analogs (Mor, PD, HMDA) and substituted PZs (1-MPZ, 2-MPZ) compared in Table 7.4 and Figure 7.28 are all more thermally stable than MEA, AMP, EDA, DGA, or MDEA.

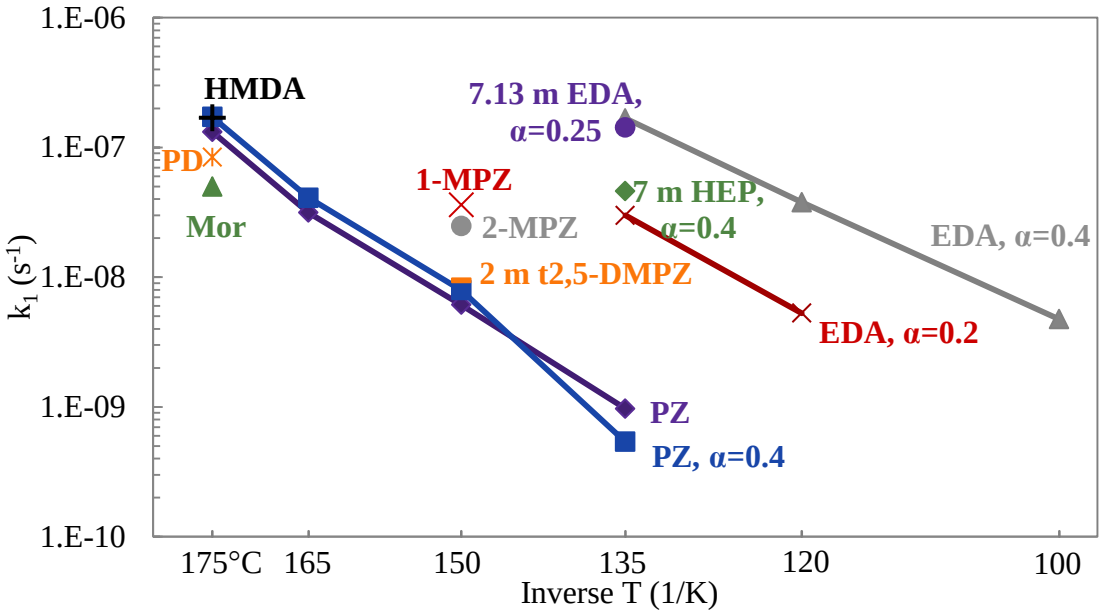

Figure 7.26: Comparison of k_1 values for PZ, PZ structural analogs, and substituted PZ; all solutions are 8 m amine with 0.3 mole CO_2 per mole alkalinity, unless noted (7.13 m EDA data from (Eide-Haugmo et al., 2011))

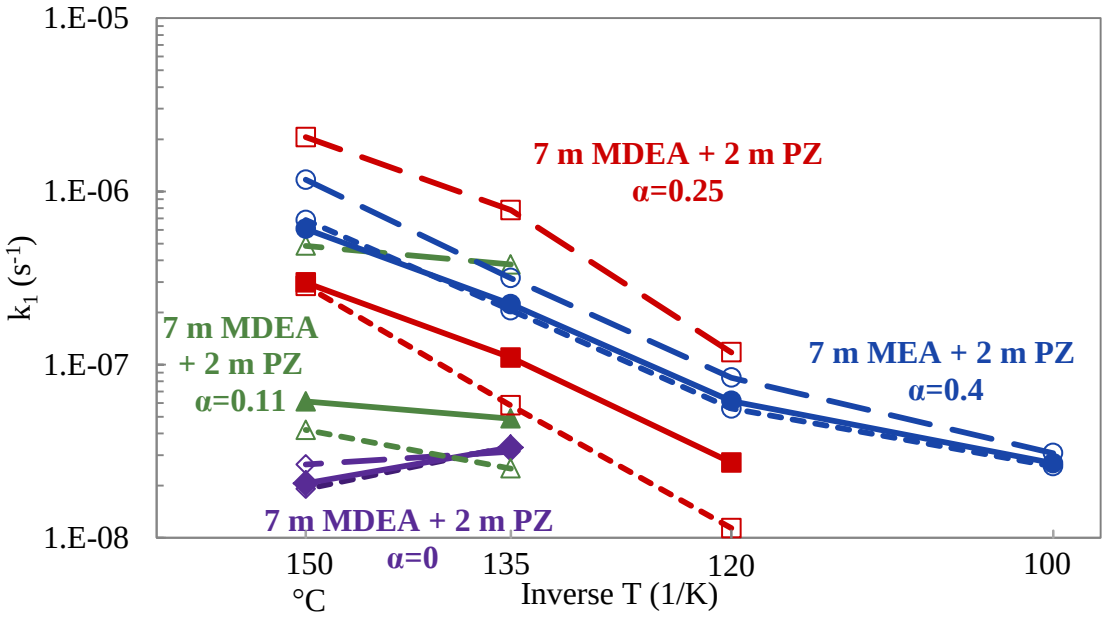

Figure 7.27: Comparison of k_1 values for 7 m MDEA + 2 m PZ (Closmann, 2011) and 7 m MEA + 2 m PZ blends (Davis, 2009). Lines: solid, total amine; short dash, MDEA or MEA; long dash, PZ

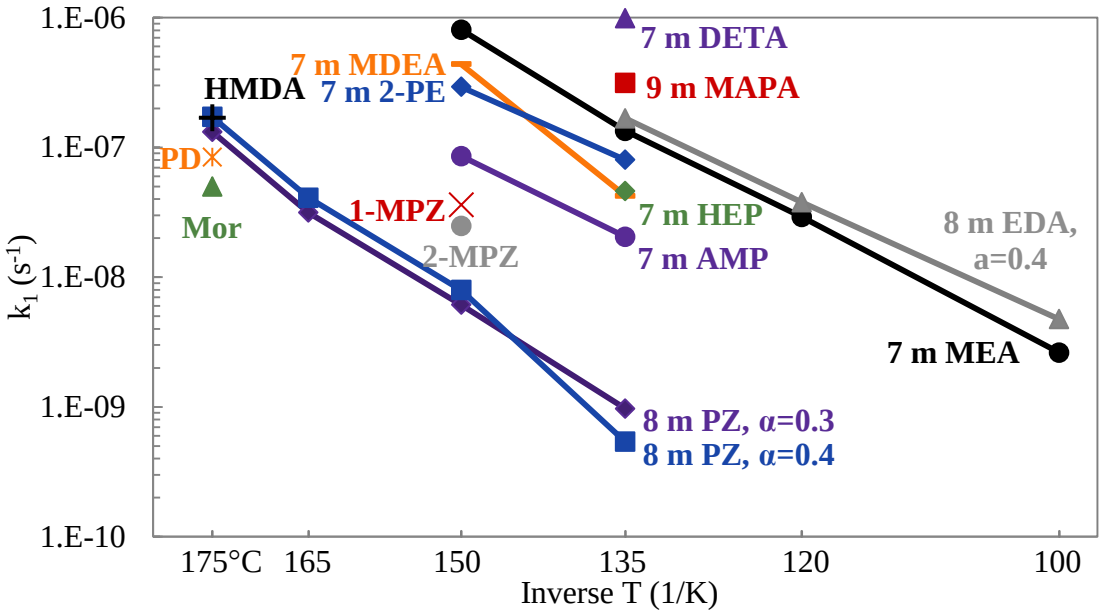

Figure 7.28: Comparison of k_1 values for CO_2 capture amines (Closmann et al., 2009; Davis, 2009; Vevelstad, 2010; Zhou et al., 2010)

7.4.2 Maximum operating stripper temperature

Although a powerful representation of thermal stability of each amine, the k_1-analysis is limited because any figure developed for comparisons can quickly become cluttered. Additionally, extending the data to predict behavior outside the tested temperature range is not easily accomplished. A second analysis to understand and compare the thermal stability of amines used for CO_2 capture is presented that calculates the maximum allowable stripper temperature. This analysis provides a real number that can be used and understood by the reader who only has cursory knowledge of the fundamentals of thermal degradation of amines.

The work of Davis determined that the optimal or acceptable operating temperature for a 7 m MEA solution was 122 °C (Davis, 2009). This determination was based on an optimization and balance of energy savings from higher temperature operation with the cost of thermal degradation including amine replacement, reclaiming,

and disposal costs. Based on his data for 7 m MEA, this temperature corresponds to a loss of approximately 2% of the initial amine per week (Davis, 2009). This also corresponds to an apparent first order rate constant (k_1) value of 2.91×10^{-8} s^{-1} (1.05×10^{-4} hr^{-1}, 2.51×10^{-3} d^{-1}, or 1.76×10^{-2} wk^{-1}). The cost of this loss rate of MEA was deemed acceptable and balanced by the advantageous of high temperature and pressure operation of the stripper. This conclusion is supported by the fact that numerous MEA based absorption-stripping systems for CO_2 scrubbing have operated successfully and economically at 115 to 120 °C for extended periods of time (Arnold et al., 1982; St.Clair and Simister, 1983).

Based on the acceptable loss rate for 7 m MEA, a tolerable stripper temperature can be determined for any amine. The k_1 values for 8 m PZ with 0.3 mole CO_2 per mole alkalinity and 7 m MEA with 0.4 mole CO_2 per mole alkalinity are compared from 100 to 175 °C in Figure 7.29. A stripper temperature of 122 °C for MEA corresponds to a k_1 value of 2.91×10^{-8} s^{-1}, as indicated by the dashed line in the figure. Using this k_1 value as a basis, the temperature at which any amine meets this value can be determined from the available k_1 data and an activation energy. For the 8 m PZ data shown in the figure, the regressed fit provided an activation energy of 183.5 kJ per mole was used to determine that at 162.8 °C the k_1 value would be 2.91×10^{-8} s^{-1}. This procedure can be used for the amines with multiple k_1 values at a given condition such as PZ, EDA and AMP where a well behaved regression for k_1 can be created to determine the activation energy.

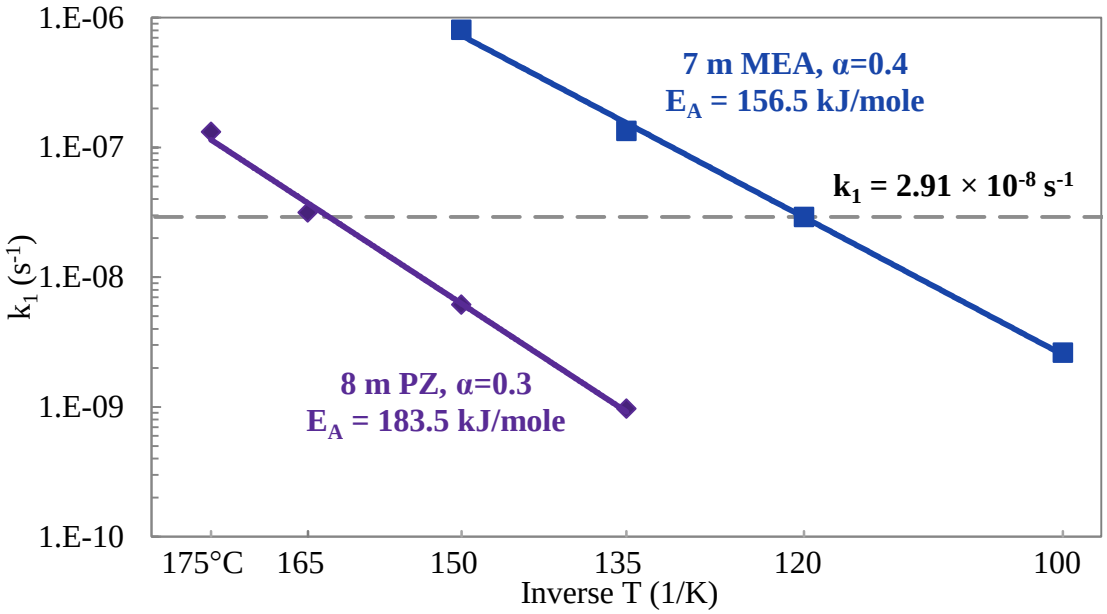

Figure 7.29: Analysis of k_1 values for 8 m PZ (α=0.3) and 7 m MEA (α=0.4) (Davis, 2009)

For numerous amines, only one or two data points exist so a regression for activation energy cannot be performed. The activation energy, and therefore, slope of the Arrhenius k_1 plot, does not fluctuate greatly between amine systems, as demonstrated by Figure 7.28 above. Amines shown in this figure vary greatly in structure and include primary amines, secondary amines, monoamines, diamines, hindered amines, and alkanolamines. These diverse molecules all demonstrate similar k_1 behavior so it can be safely assumed that a majority of amines would behave likewise. For amines with only one data point, the slope of the data for 7 m MEA with 0.4 mole CO_2 per mole alkalinity, and therefore the activation energy of 156.5 kJ per mole, was used for extrapolation. For amines with two data points, the prediction was done using the slope of MEA independently and then the average stripper temperature calculated from each point was averaged to provide the final temperature. For amines with at least three temperatures, an activation energy was calculated and used for that data. For PZ experiments with less

than three points, the slope of the data for 8 m PZ with 0.3 mole CO_2 per mole alkalinity was used, rather than the MEA data, in the same fashion. When the lowest temperature data of a given amine data set was too high, showing a difficultly at accurately detecting small changes in amine concentration, the lowest temperature data point was not used in the prediction of stripper temperature. A summary of the activation energies calculated and used is given in Table 7.5.

The raw material cost for the amines compared in this section is not included in this analysis and would have a great impact on the results if included. Costs can vary greatly between amines by factors as much as 10 or 50 and will impact the level of tolerable thermal degradation for an operator. For many of the amines compared in this work, reliable bulk prices are not easily obtained and laboratory or small quantity prices are not necessarily reflective of bulk pricing. This analysis could easily be amended if the amine of interest has known bulk pricing. The objective k_1 value could be adjusted by a factor representative of the relative difference between the price of MEA and the amine of interest. In that way, an estimate of the stripper temperature could still be obtained.

A summary table of the calculated stripper temperatures that correspond to a loss of 2% of the initial amine per week is shown in Table 7.6. All of the amines screened in this work and previous works are included for completeness and are listed in order of decreasing stripper temperature (Chakma and Meisen, 1997; Closmann et al., 2009; Davis, 2009; Eide-Haugmo et al., 2011; Lepaumier et al., 2010; Lepaumier et al., 2009a; Reza and Trejo, 2006; Vevelstad, 2010; Zhou et al., 2010). This analysis provides a very clear ranking of amines in terms of their thermal stability. A summary of only MEA and MEA blends is shown in Table 7.7 to demonstrate the range of values due to differences in amine concentration, CO_2 loading, and data source. Over a range of 3.5 to 11 m MEA

with 0.2 to 0.5 mole CO_2 per mole alkalinity, the estimated stripper temperature varies from 111 to 126 °C. Similar ranges are present for amines that have been degraded under varying conditions by different authors such as EDA, AMP, and HEEDA.

Table 7.5: Summary of activation energies used for the calculation of maximum stripper temperatures

Amine	Conc. m	Loading mol/mol alk	Act. Energy kJ/mol	Temperatures °C	Ref. [a]
Piperazine (PZ)	**8**	**0.3**	**184**	**135, 150, 165, 175**	
Piperazine (PZ)	8	0.4	191	150, 165, 175	
Monoethanolamine (MEA)	3.5	0.2	60	100, 120, 135	D
Monoethanolamine (MEA)	3.5	0.4	129	100, 120, 135	D
Monoethanolamine (MEA)	3.5	0.5	86	100, 120, 135	D
Monoethanolamine (MEA)	7	0.2	123	120, 135, 150	D
Monoethanolamine (MEA)	**7**	**0.4**	**157**	**100, 120, 135, 150**	**D**
Monoethanolamine (MEA)	7	0.5	162	100, 120, 135, 150	D
2-amino-2-methyl-1-propanol (AMP)	7	0.4	112	120, 135, 150	D
3-amino-1-propanol (3a1p)	7	0.4	117	100, 120, 135, 150	D
4-amino-1-butanol (4a1b)	7	0.4	161	120, 135, 150	D
6-amino-1-hexanol (6a1h)	7	0.4	148	100, 135, 150	D
DL-2-amino-1-propanol (MIPA)	7	0.4	105	100, 135, 150	D
DL-1-amino-2-propanol	7	0.4	106	100, 120, 135, 150	D
MEA in MEA/AMP Blend	7/2	0.4	179	100, 120, 135, 150	D
AMP in MEA/AMP Blend	7/2	0.4	623	100, 135, 150	D
Total Amine in MEA/AMP Blend	7/2	0.4	146	100, 120, 135, 150	D
MEA in MEA/Mor Blend	7/2	0.4	97	100, 120, 135, 150	D
Mor in MEA/Mor Blend	7/2	0.4	99	100, 120, 135, 150	D
Total Amine in MEA/Mor Blend	7/2	0.4	97	100, 120, 135, 150	D
MEA in MEA/PZ Blend	7/2	0.4	88	100, 120, 135, 150	D
PZ in MEA/PZ Blend	7/2	0.4	96	100, 120, 135, 150	D
Total Amine in MEA/PZ Blend	7/2	0.4	84	100, 120, 135, 150	D
MEA in MEA/DGA® Blend	7/2	0.4	99	100, 120, 135, 150	D
DGA® in MEA/DGA® Blend	7/2	0.4	72	100, 135, 150	D
Total Amine in MEA/DGA® Blend	7/2	0.4	94	100, 120, 135, 150	D
N-Methyldiethanolamine (MDEA)	8.39	2.6 MPa	100	100, 120, 140, 160, 180	CM
Ethylenediamine (EDA)	8	0.4	154	100, 120, 135	Z
MDEA in MDEA/PZ Blend	7/2	0.25	148	120, 135, 150	C
PZ in MDEA/PZ Blend	7/2	0.25	132	120, 135, 150	C
Total Amine in MDEA/PZ Blend	7/2	0.25	111	120, 135, 150	C

[a] If not specified, from this work; CM =(Chakma and Meisen, 1997); C = (Closmann et al., 2009); D = (Davis, 2009); Z = (Zhou et al., 2010)

The most thermally stable amine tested to date is 8 m Mor which can tolerate a stripper temperature of 169 °C. Davis found no loss of Mor after 4 weeks at 135 °C, confirming the stability of Mor found in this project (Davis, 2009). The top rows of Table 7.6, indicating the most stability, are dominated by PZ, cyclic PZ analogs, and PZ blends. Towards the middle of the ranking, tertiary amines, sterically hindered amines and unique functionalities, such as esters, are present. The most instable, or bottom of the table, is dominated by straight-chain alkanolamine and amines. The only straight chain molecule with appreciable stability is HMDA, which draws its stability from an inability to form a stable 9-membered oxazolidone.

The most instable amines measured, MMEA, DEA, DETA, and MAPA, are longer straight-chain alkyl amines with at least one secondary amino function and either hydroxyl groups or multiple amino function. DEA, DETA, and MAPA degrade to N-(2-aminoethyl) imidazolidone (CAS 6281-41-1), tetrahydro-1-methyl-2(1H)-Pyrimidinone (CAS 10166-54-8), and 3-(2-hydroxyethyl)-2-Oxazolidone (HEOD, CAS 3356-88-5), respectively, all very stable 5 and 6-member urea structures. As with MEA, the stability of the initial cyclic urea intermediate or reaction product dictates the extent of thermal degradation.

Table 7.6: Estimated stripper temperature at $k_1 = 2.91 \times 10^{-8}$ s^{-1}

Amine	Abbreviation	Structure(s)	Conc.[a] m	Loading mol/mol alk	T Range of Data °C	Act. Energy[b] kJ/mol	Stripper Temp °C	Ref. [c]
Morpholine	Mor	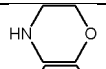	8	0.3	175	PZ	170	
Piperidine	PD		8	0.3	175	PZ	166	
Piperazine	**PZ**	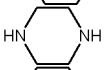	**8**	**0.3**	**135-175**	**184**	**163**	
Piperazine	PZ	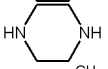	8	0.4	135-175	191	162	
Piperazine / 1-Methylpiperazine / 1,4-Dimethylpiperazine (TA)	PZ/ 1-MPZ/ 1,4-DMPZ	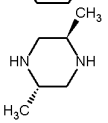	3.9/ 3.9/ 0.2	0.3	150	PZ	160	
Hexamethylenediamine	HMDA	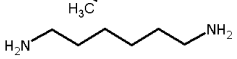	8	0.3	175	PZ	160	
trans-2,5-Dimethylpiperazine	t2,5-DMPZ	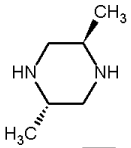	2	0.3	150	PZ	159	
Piperazine / 1-Methylpiperazine / 1,4-Dimethylpiperazine (TA)	PZ/ 1-MPZ/ 1,4-DMPZ	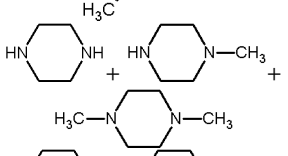	3.75/ 3.75/ 0.5	0.3	150	PZ	159	
Piperazine / 1-Methylpiperazine / 1,4-Dimethylpiperazine (TA)	PZ/ 1-MPZ/ 1,4-DMPZ	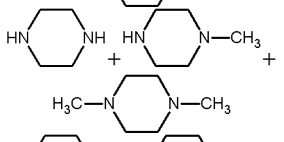	5/ 2/ 1	0.3	150	PZ	156	
Piperazine / 1-Methylpiperazine (TA)	PZ /1-MPZ	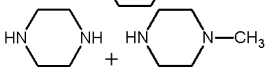	4 /4	0.3	150	PZ	156	

Table 7.6: Estimated stripper temperature at $k_1 = 2.91 \times 10^{-8}$ s^{-1} (Continued)

Amine	Abbreviation	Structure(s)	Conc.[a] m	Loading mol/mol alk	T Range of Data °C	Act. Energy[b] kJ/mol	Stripper Temp °C	Ref. [c]
Piperazine / 1-Methylpiperazine / 1,4-Dimethylpiperazine (TA)	PZ/ 1-MPZ/ 1,4-DMPZ	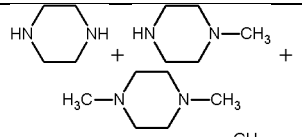	5/ 2.5/ 0.5	0.3	150	PZ	156	
Piperazine / 2-Methylpiperazine (TA)	PZ/ 2-MPZ	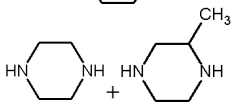	4/ 4	0.3	150	PZ	155	
Piperazine / *trans*-2,5-Dimethylpiperazine (TA)	PZ/ t2,5-DMPZ	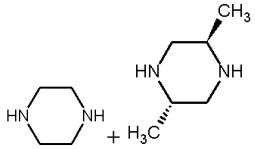	4/ 4	0.3	150	PZ	154	
2-Methylpiperazine	2-MPZ	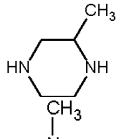	8	0.3	150	PZ	151	
N-Methyldiethanolamine / Diethanolamine (TA)	MDEA/ DEA	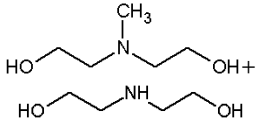	5.3/ 1.7	0.27	200	MEA	151	RT
1-Methylpiperazine	1-MPZ	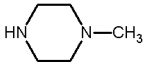	8	0.3	150	PZ	148	
5-amino-1-pentanol	5a1p	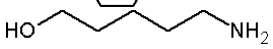	7	0.4	135-150	MEA	145	D
N-Methyldiethanolamine / Piperazine (TA)	MDEA/ PZ	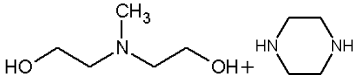	7/ 2	0	135-150	PZ	143	C
Pyrrolidine	Pyr		8	0.3	175	PZ	142	
Homopiperazine	HomoPZ	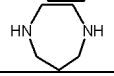	8	0.3	175	PZ	140	

Table 7.6: Estimated stripper temperature at $k_1 = 2.91 \times 10^{-8}$ s^{-1} (Continued)

Amine	Abbreviation	Structure(s)	Conc.[a] m	Loading mol/mol alk	T Range of Data °C	Act. Energy[b] kJ/mol	Stripper Temp °C	Ref. [c]
2-Amino-2-methyl-1-propanol	AMP	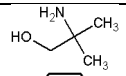	4.81	0.5	135	MEA	140	EH
1,4-Dimethylpiperazine	1,4-DMPZ	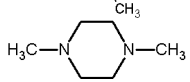	4*	2 MPa	140	PZ	138	L1
N-Methyldiethanolamine / Piperazine (TA)	MDEA/ PZ	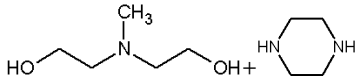	7/ 2	0.11	135-150	PZ	138	C
2-amino-2-methyl-1-propanol	AMP	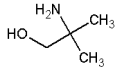	7	0.4	120-150	112	137	D
Piperazine / 2-amino-2-methyl-1-propanol (TA)	PZ/ AMP	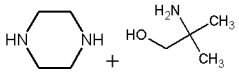	6/ 4	0.4	135-150	PZ	134	Z
4-amino-1-butanol	4a1b	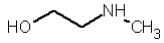	7	0.4	120-150	161	133	D
Diglycolamine®	DGA	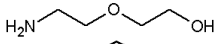	7	0.4	135	MEA	132	D
Hexamethyleneimine	HMI		8	0.3	175	PZ	131	
N-(2-Hydroxyethyl)piperazine	HEP	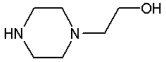	7	0.4	135	PZ	130	D
N-Methyldiethanolamine	MDEA	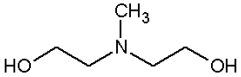	4*	2 MPa	140	MEA	129	L1
N,N,N',N',N''-pentamethyldipropylenetriamine	PMDPTA	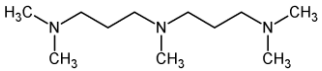	2.5*	2 MPa	140	MEA	129	L3
Methyldiethanolamine	MDEA	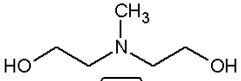	7	0.1	150	MEA	128	C
Ethylenediamine	EDA	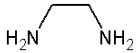	8	0.2	100-135	MEA	128	Z
Methyldiethanolamine	MDEA	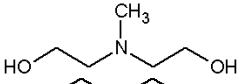	7	0.2	135-150	MEA	128	C
3-amino-1-propanol	3a1p	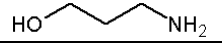	7	0.4	100-150	117	127	D

Table 7.6: Estimated stripper temperature at $k_1 = 2.91 \times 10^{-8}$ s^{-1} (Continued)

Amine	Abbreviation	Structure(s)	Conc.[a] m	Loading mol/mol alk	T Range of Data °C	Act. Energy[b] kJ/mol	Stripper Temp °C	Ref. [c]
2-Piperidineethanol	2-PE	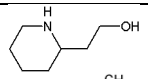	8	0.4	135-150	MEA	127	Z
N,N,N',N'-Tetramethylethylenediamine	TMEDA	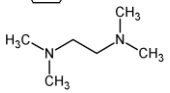	4*	2 MPa	140	MEA	127	L1
3-aminopropanol	AP		5.71	0.5	135	MEA	126	EH
Monoethanolamine	MEA		11	0.2	120-135	MEA	125	D
Ethylenediamine	EDA	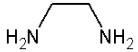	3.5	0.4	135-150	PZ	125	D
Monoethanolamine	MEA	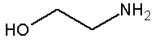	3.5	0.2	100-135	60	123	D
N,N,N',N'-Tetramethypropylenediamine	TMPDA	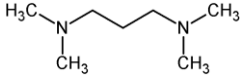	4*	2 MPa	140	MEA	123	L3
2-Amino-2-methyl-1-propanol	AMP	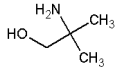		2 MPa	140	MEA	123	L1
Monoethanolamine / 2-Amino-2-methyl-1-propanol (TA)	MEA/ AMP	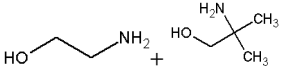	7/ 2	0.4	100-150	146	123	D
DL-1-amino-2-propanol		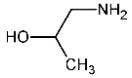	7	0.4	100-150	106	123	D
N,N-Dimethylethanolamine	DMMEA	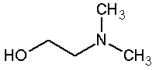	4.81	0.5	135	MEA	122	EH
Monoethanolamine	MEA	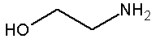	3.5	0.4	100-135	129	122	D
N-(2-Aminoethyl)piperazine	AEP	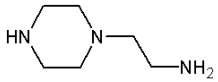	2.33	0.4	135	PZ	121	D
Monoethanolamine	MEA	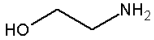	7	0.2	120-150	123	121	D
Monoethanolamine	**MEA**	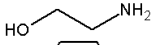	**7**	**0.4**	**100-150**	**157**	**121**	**D**
Ethylenediamine	EDA	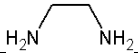	7.14	0.25	135	MEA	121	EH

Table 7.6: Estimated stripper temperature at $k_1 = 2.91 \times 10^{-8}$ s^{-1} (Continued)

Amine	Abbreviation	Structure(s)	Conc.[a] m	Loading mol/mol alk	T Range of Data °C	Act. Energy[b] kJ/mol	Stripper Temp °C	Ref. [c]
N-Methyldiethanolamine / Piperazine (TA)	MDEA/ PZ	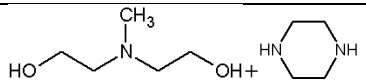	7/ 2	0.25	120-150	111	120	C
N-Methyldiethanolamine	MDEA	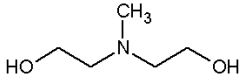	3.60	0.5	135	MEA	120	EH
N-Methyldiethanolamine	MDEA	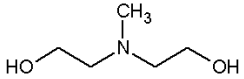	8.4	0.4	135	MEA	119	D
Diethylenetriamine	DETA	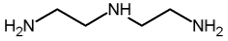	4.15	0.17	135	MEA	118	EH
N,N-Dimethylethanolamine	DMAE	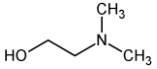	4*	2 MPa	140	MEA	118	L1
Monoethanolamine	MEA	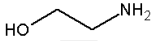	7	0.5	100-150	162	117	D
Ethylenediamine	EDA		8	0.4	100-135	154	117	Z
3-(Methylamino)propylamine	MAPA	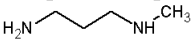	4.81	0.25	135	MEA	117	EH
6-amino-1-hexanol	6a1h	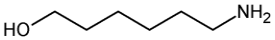	7	0.4	100-150	148	117	D
Monoethanolamine	MEA	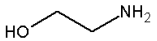	11	0.4	120-135	MEA	116	D
Monoethanolamine	MEA	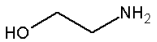	4*	2 MPa	140	MEA	116	L1
Monoethanolamine	MEA	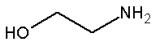	7.01	0.5	135	MEA	115	EH
N,N-Dimethylethylenediamine	N,N-diMEDA	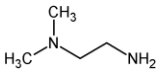	4*	2 MPa	140	MEA	115	L1
N-(2-Hydroxyethyl)ethylenediamine	HEEDA	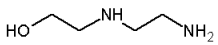	4.12	0.25	135	MEA	114	EH
3-(Methylamino)propylamine	MAPA	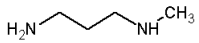	9	0.4	135	MEA	114	V
DL-2-amino-1-propanol (MIPA)	MIPA	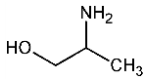	7	0.4	100-150	105	114	D

Table 7.6: Estimated stripper temperature at $k_1 = 2.91 \times 10^{-8}$ s^{-1} (Continued)

Amine	Abbreviation	Structure(s)	Conc.[a] m	Loading mol/mol alk	T Range of Data °C	Act. Energy[b] kJ/mol	Stripper Temp °C	Ref. [c]
Monoethanolamine / Diglycolamine® (TA)	MEA/ DGA®	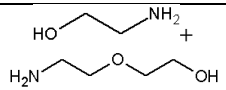	7/ 2	0.4	100-150	94	112	D
N,N,N'-Trimethylethylenediamine	triMEDA	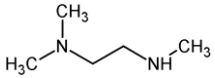	4*	2 MPa	140	MEA	112	L1
Monoethanolamine	MEA	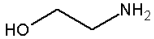	11	0.5	120-135	MEA	112	D
Monoethanolamine	MEA	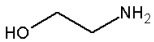	3.5	0.5	100-135	86	111	D
2-Piperidinemethanol	2-PM	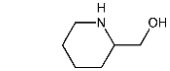	7	0.4	135	MEA	109	D
Diethylenetriamine	DETA	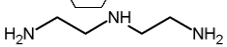	7	0.4	135-150	MEA	108	D
Monoethanolamine / Morpholine (TA)	MEA/ Mor	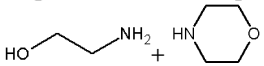	7/ 2	0.4	100-150	97	108	D
N,N,N',N'-tetramethylbutylenediamine	TMBDA	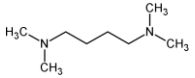	4*	2 MPa	140	MEA	107	L3
N,N,N',N',N''-pentamethyldiethylenetriamine	PMDETA	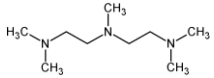	2.5*	2 MPa	140	MEA	105	L3
N-Methylethanolamine	MAE	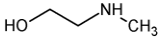	4*	2 MPa	140	MEA	105	L1
Diethanolamine	DEA	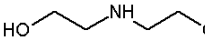	4.08	0.5	135	MEA	105	EH
N,N'-Dimethylethylenediamine	N,N'-diMEDA	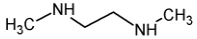	4*	2 MPa	140	MEA	104	L1
Monoethanolamine / Piperazine (TA)	MEA/ PZ	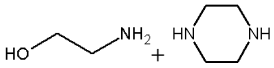	7/ 2	0.4	100-150	84	104	D
Diethanolamine	DEA	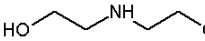	4*	2 MPa	140	MEA	103	L1
N-Methyldiethanolamine	MDEA	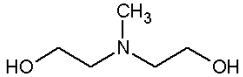	8.39	2.6 MPa	100-180	100	103	CM
2-Methylaminoethanol	MMEA	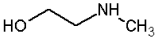	5.71	0.5	135	MEA	102	EH

Table 7.6: Estimated stripper temperature at $k_1 = 2.91 \times 10^{-8}$ s^{-1} (Continued)

Amine	Abbreviation	Structure(s)	Conc.[a] m	Loading mol/mol alk	T Range of Data °C	Act. Energy[b] kJ/mol	Stripper Temp °C	Ref. [c]
N-(2-Hydroxyethyl) ethylenediamine	HEEDA	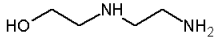	3.5	0.4	135	MEA	101	D
N-(2-Hydroxyethyl) ethylenediamine	HEEDA	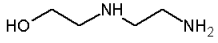	4*	2 MPa	140	MEA	99	L1

[a] Concentrations indicated with asterisks (*) are in units of mole amine per kg solution, not molal (m)

[b] Activation Energy used to estimate stripper temperature is noted; PZ indicates that the activation energy of 184 kJ/mole was used based on data at 8 m PZ, α=0.3; MEA indicates that the activation energy of 157 kJ/mole was used based on data at 7 m MEA, α=0.4.

[c] Reference: If blank, data is from this work, otherwise: CM = (Chakma and Meisen, 1997); C = (Closmann et al., 2009); D = (Davis, 2009); EH = (Eide-Haugmo et al., 2011); L1 = (Lepaumier et al., 2009a); L3 = (Lepaumier et al., 2010); RT = (Reza and Trejo, 2006); V = (Vevelstad, 2010); Z = (Zhou et al., 2010).

Table 7.7: Comparison of estimated stripper temperature at $k_1 = 2.91 \times 10^{-8}$ s^{-1} for a variety of MEA conditions

Amine	Abbreviation	Structure(s)	Conc.[a] m	Loading mol/mol alk	T Range of Data °C	Act. Energy[b] kJ/mol	Stripper Temp. °C	Ref.[c]
Monoethanolamine	MEA	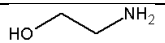	11	0.2	120-135	MEA	126	D
Monoethanolamine	MEA	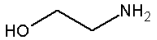	3.5	0.2	100-135	60	123	D
Monoethanolamine / 2-Amino-2-methyl-1-propanol (TA)	MEA/ AMP	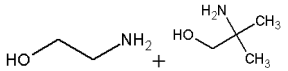	7/ 2	0.4	100-150	146	123	D
Monoethanolamine	MEA	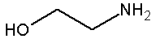	3.5	0.4	100-135	129	122	D
Monoethanolamine	MEA	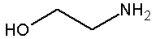	7	0.2	120-150	123	121	D
Monoethanolamine	MEA	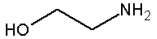	7	0.4	100-150	157	121	D
Monoethanolamine	MEA	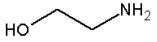	7	0.5	100-150	162	117	D
Monoethanolamine	MEA	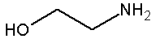	11	0.4	120-135	MEA	117	D
Monoethanolamine	MEA	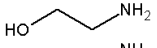	4*	2 MPa	140	MEA	116	L1
Monoethanolamine	MEA	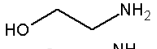	7.01	0.5	135	MEA	115	EH
Monoethanolamine / Diglycolamine® (TA)	MEA/ DGA®	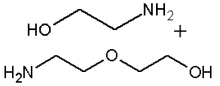	7/ 2	0.4	100-150	94	112	D
Monoethanolamine	MEA	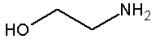	11	0.5	120-135	MEA	112	D
Monoethanolamine	MEA	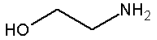	3.5	0.5	100-135	86	111	D
Monoethanolamine / Morpholine (TA)	MEA/ Mor	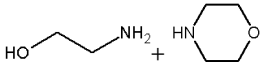	7/ 2	0.4	100-150	97	108	D

[a] Concentrations indicated with asterisks (*) are in units of mole amine per kg solution, not molal (m)

[b] Activation Energy used to estimate stripper temperature is noted; MEA indicates that the activation energy of 156.5 kJ/mole was used based on data at 7 m MEA, α=0.4.

[c] Reference: D = (Davis, 2009); EH = (Eide-Haugmo et al., 2011); L1 = (Lepaumier et al., 2009a).

7.5 CONCLUSIONS

The calculated k_1 values for thermal degradation were successfully translated into predicted stripper temperatures that represent a maximum acceptable degradation rate. Morpholine (Mor) was determined to be the most stable amine tested to date with a predicted stripper temperature of 170 °C. Piperidine (PD) and piperazine (PZ) and with 0.3 mole CO_2 per mole alkalinity were the next most stable amines with estimated stripper temperatures of 166 and 163 °C, respectively. Cyclic, 6-membered amines such as PZ, Mor, and PD were determined to be exceptionally resistant to thermal degradation.

Substituted PZs such as 1-methylpiperazine (1-MPZ), 2-methylpiperazine (2-MPZ) and PZ analogs such as hexamethylenediamine (HMDA) were shown to be stable, tolerating temperatures between 148 and 160 °C. PZ structural analogs with 5- or 7-membered rings such as pyrrolidine (Pyr), hexamethyleneimine (HMI), and homopiperazine (HomoPZ), were found to have diminished stability. Methylation of the PZ structure at the 1- or 2-position also decreased stability of the PZ molecule to thermal degradation.

The most instable amines measured, such as N-(2-hydroxyethyl)ethylenediamine (HEEDA), 2-methylaminoethanol (MMEA), diethanolamine (DEA), N-methylethanolamine (MAE), diethanoltriamine (DETA), and 3-(methylamino) propylamine (MAPA), which will all degrade significantly at temperatures above 120 °C, are longer straight-chain alkyl amines with at least one secondary amino function and either hydroxyl groups, methyl groups, or multiple amino function. The estimated stripper temperature for 3.5 to 11 m MEA solutions with 0.2 to 0.5 mole CO_2 per mole alkalinity ranged from 111 to 126 °C.

A thermal equilibrium between PZ, 1-MPZ, and 1,4-DMPZ was discovered that offers the opportunity for a blended solvent that is resistant to overall thermal degradation. At 150 °C, the equilibrium constant for the disproportionation of 1-MPZ into PZ and 1,4-DMPZ with 0.3 mole CO_2 per mole alkalinity was found to be 0.28. A tertiary blend designed around this constant, 3.9 m PZ / 3.9 m 1-MPZ / 0.2 m 1,4-DMPZ degraded with a k_1 value of 8.44×10^{-9} s^{-1}, only 37% higher than the k_1 for 8 m PZ with 0.3 mole CO_2 per mole alkalinity.

PZ was not found to preferentially degrade in a blend of 4 m PZ + 4 m 1-MPZ since an equilibrium is being established that occurs more rapidly that thermal degradation. PZ is preferentially degraded in blends with MDEA and MEA. In the presence of MDEA, PZ degrades up to 15 times faster than MDEA. The stability of PZ when blended with another amine depends heavily on the pKa or nucleophilic strength of the amine. Blending PZ has been previously stated as inadvisable, but could be advantageous when matched with a similarly stable molecule, such as 1-MPZ or 2-MPZ.

Chapter 8 – Oxidation of Concentrated, Aqueous PZ

The oxidation of concentrated PZ was investigated over a variety of conditions to understand oxidative degradation expected in absorption-stripping CO_2 capture systems. Previous work on concentrated PZ demonstrated a resistance to oxidation that was identified as an advantageous characteristic of the solvent (Sexton, 2008). This chapter details the experiments performed that analyzed the effect of oxygen (O_2), temperature, CO_2, and PZ. The effect of CO_2 was not fully analyzed due to the compounding effect of changing both CO_2 and O_2 at the same time. The reactor used to perform the oxidation experiments is analyzed in detail for possible sources of error. All of the oxidation products that have been identified are described in detail along with carbon and nitrogen balances typically achieved in concentrated PZ oxidation experiments.

8.1 SUMMARY OF OXIDATION EXPERIMENTS PERFORMED

A summary of the experiments performed investigating the oxidation of concentrated PZ is shown in Table 8.1. All experiments were performed with 8 molal (m) PZ, except for the first two. After the first 16 experiments, the reactor was redesigned as described in Section 3.2.3, and the remaining experiments were carried out in the new reactor. The temperature of the reactor was varied between 55 and 70 °C through the addition of an oil bath as a way to further accelerate oxidation. O_2 content was varied between 40 and 98 kPa in the headspace with CO_2 loadings varying from 0.2 to 0.4 mole CO_2 per mole alkalinity. A variety of metal catalysts including iron (II) (Fe^{2+}), chromium (III) (Cr^{3+}), nickel (II) (Ni^{2+}), copper (II) (Cu^{2+}), and vanadium (V) (V^{5+}) were used to induce oxidation. Three inhibitors, Inhibitor A, Inhibitor B, and Inhibitor C, were also tested for their efficacy at inhibiting metal-catalyzed PZ oxidation. The effects of metal catalysts and inhibitors are discussed in detail in Chapter 9. The tabulated results of each experiment can be found in Appendix E of this dissertation.

8.2 MECHANICAL LIMITATIONS OF EXPERIMENTAL APPARATUS

Oxidation of concentrated PZ was first attempted by Sexton when 2.5 and 5 m PZ were oxidized using a low gas flow reactor (Sexton, 2008). Sexton found that oxidation occurred, but at significantly slower rates than MEA under similar conditions. The slow oxidation was difficult to quantify accurately with the analytical equipment utilized at the time. Experiments performed in this project matched the work of Sexton and confirmed his observations on the resistance of PZ to oxidation.

Table 8.1: Summary of PZ oxidation experiments performed

Expt.	Rxtr.	PZ m	T °C	P_{CO2} kPa	CO_2 Ldg mol/mol alk	P_{O2} kPa	Additives* mM
OE1	OOR	10	55	2	0.3	98	Fe (0.23), Cr (1.6), Ni (0.2)
OE2	OOR	10	55	2	0.3	98	Cu (4)
OE3	OOR	8	55	2	0.3	98	Fe (0.1), V (0.1)
OE4	OOR	8	55	2	0.3	98	Fe (0.1), Cu (5), A (100)
OE5	OOR	8	55	2	0.3	98	Fe (1)
OE6	OOR	8	55	2	0.3	98	Fe (1), A (100)
OE7	OOR	8	55	2	0.3	98	Fe (1), B (20)
OE8	OOR	8	55	2	0.3	98	Fe (1), C (30)
OE9	OOR	8	55	2	0.3	0	-
OE10	OOR	8	55	2	0.3	0	-
OE11	OOR	8	55	2	0.3	98	-
OE12	OOR	8	55	2	0.3	98	-
OE13	OOR	8	55	2	0.3	98	Fe (1)
OE14	OOR	8	55	2	0.3	98	Fe (1), A (100)
OE15	OOR	8	55	2	0.3	98	SSM
OE16	OOR	8	55	2	0.3	98	SSM, A (10)
OE17	TOR	8	55	2	0.3	98	Fe (1)
OE18	TOR	8	55	2	0.3	98	SSM
OE19	TOR	8	70	2	0.2	98	SSM
OE20	TOR	8	70	2	0.2	98	SSM, Formate (500)
OE21	TOR	8	70	2	0.2	98	SSM, Formaldehyde (500)
OE22	TOR	8	70	60	0.4	40	SSM
OE23	TOR	8	70	6	0.3	40	Cu (4)
OE24	TOR	8	70	6	0.3	40	Cu (4), A (100)
OE25	TOR	8	70	6	0.3	94	Cu (4)
OE26	TOR	8	70	6	0.3	94	SSM
OE27	TOR	8	55	2	0.3	40	Cu (4)
OE28	TOR	8	55	2	0.3	40	SSM

* Abbreviations are as follows: Fe is Fe^{2+} added as $FeSO_4 \cdot 7H_2O$; Cr is Cr^{3+} added as $CrK(SO_4)_2 \cdot 12H_2O$; Ni is Ni^{2+} added as $NiSO_4 \cdot 6H_2O$; Cu is Cu^{2+} added as $CuSO_4 \cdot 5H_2O$; V is V^{5+} added as $NaVO_3$; A is Inhibitor A; B is Inhibitor B; C is Inhibitor C; SSM indicates the standard stainless steel metals mixture (0.4 mM Fe^{2+} + 0.1 mM Cr^{3+} + 0.05 mM Ni^{2+})

There were mechanical limitations of both low gas flow reactors used to oxidize PZ in this project. The Original Oxidation Reactor (OOR), which was used previously and had a rubber stopper as a lid, and the Teflon® Oxidation Reactor (TOR), which was

designed for this work from a jacketed glass reactor with flange and Teflon® lid, were subject to similar limitations. The primary difficulty encountered in both was in maintaining the water balance during the experiment. Water and amine are primarily lost during experiments through the annular space surrounding the agitator. In order to maintain the water balance, the assumption was made that liquid loss between sampling was all water, which agrees with an analysis of the relative volatility of water and PZ (see section 8.2.4 for more details). The water balance is also influenced by the pre-saturator and the amount of water that enters the reactor system in the gas phase.

Another operational concern is the mechanical stability of the agitator, which vibrates due to the fast agitation rate (1400 rpm). The agitator shaft can catch on the lid, causing catastrophic failure of the reactor which is a serious safety concern due the presence of glass and hot liquid amine.

The quality of data obtained from either reactor (OOR or TOR) is subjective and depends heavily on the individual conditions of each experiment. The goal during each experiment was to minimize the error in an effort to make the data as smooth and understandable as possible. There are many times, however, when data is scattered and does not behave as expected. It is assumed that there were influences from the reactor and water balance on these occasions. For instance, if a sampling port was left uncovered overnight or the flange was not fully tightened, extra liquid can evaporate due to this opening and cause a drastic shift in the water balance. A small operational change or error can greatly influence the data obtained from these types of reactors.

All of these operational concerns are only of critical importance for amine systems that do not degrade readily, like PZ. The same conditions were present for the work of Sexton but were not as influential because MEA, AMP, and other amines tested easily degraded with short experiments. Errors due to the water balance were likely

overshadowed in most cases by the loss of amine due to rapid oxidation. PZ presents a unique problem of attempting to measure oxidation that occurs very slowly and requires longer experiments. Small fluctuations in the operation of the reactor impacted the data immensely causing more scatter and difficulty in quantifying only small changes in concentration of either PZ or the degradation products.

An issue discussed throughout this chapter is the fact that oxidation experiments show PZ losses in the range of 2 to 10% of the initial PZ while producing few quantified degradation products, usually accounting for less than 1% of the lost PZ. The most likely explanation is that the products to which PZ is degrading are not able to be detected, identified, or quantified with the analytical techniques employed for PZ oxidation thus far. The techniques regularly employed for PZ thermal degradation (i.e. anion IC and cation IC) may not capture the most important oxidation products. In a similar vein, it is possible that one or more major degradation products are volatile and escape the reactor without retaining a significant concentration in the liquid phase for analysis. The impact of this possibility was not assessed because the current reactor design does not support gas phase analysis. There may also be additional mechanical issues relating to the reactor itself, which does not exclude the presence of unidentified volatile or non-volatile degradation products. All of these options for explaining the mass balance disparity are discussed in detail in the next sections.

8.2.1 Baseline oxidation experiments

A series of baseline oxidation experiments were performed in an attempt to assess both the repeatability of the entire experimental procedure and the impact of the reactor itself of PZ losses in the absence of catalyst. The first two baseline experiments (OE9 and OE10) were performed at 55 °C with agitation at 1400 rpm and with a gas stream of

100 mL per minute of 98% N_2/2% CO_2 in the absence of any metal catalyst or inhibitors. These conditions were meant to measure the loss of PZ that was due to mechanical losses from volatility at 55 °C, entrainment, or water balance inconsistencies due to the air stream exiting the reactor around the agitator opening. The second two baseline experiments (OE11 and OE12) were performed at the same conditions, except for a change in the gas phase composition to 98% O_2/2% CO_2. These conditions were intended to provide a baseline level of degradation due to O_2 alone, in the absence of metal catalysts. The agitator shaft is constructed of stainless steel, however, so the solutions may have been exposed to a small amount of leached metal. Each of these conditions was duplicated to observe the repeatability in oxidation experiments.

The raw and sulfate adjusted data for PZ loss in the presence of N_2/CO_2 is compared in Figure 8.1. Sulfate adjustment of the data is used in to take into account the water balance of the reactor at any given time through the use of a tracer compound (Sexton, 2008). Sulfate added as potassium sulfate (K_2SO_4) was used as a tracer and all concentrations are adjusted based on the ratio of sulfate in the current sample to that of the initial sample. Since the analysis of the baseline experiments deals with how well the water balance is maintained, both the raw and sulfate adjusted data are shown.

The repeatability in these oxidation experiments was poor. For either the raw or adjusted data, the PZ loss for OE9 and OE10 were substantially different over the course of the experiment. After 150 hours, OE9 has lost 5% of the initial PZ while OE10 has lost only 0.5%. The data were more similar at 240 hours where they have lost 4 and 2%, respectively. The sulfate adjusted data show even stronger disagreement in both the values and the trends of each experiment. The overall range of values is not large and both experiments lose 3 to 7% of the initial PZ during the experiment in the absence of O_2 due to mechanical losses. From these results, it was determined that the sulfate

adjusted data were not providing any insight into the water balance of the reactor. The trends of the raw data are more regular and proceed as expected without rapid changes.

The generation of formate, total formate, and EDA are compared between the two experiments in Figure 8.2. It was not expected that detectable and increasing levels of degradation products would be produced in the absence of O_2, but small concentrations were quantified. The concentration profiles for each species do not track closely between the two experiments, but the overall quantity of formate and total formate are approximately the same at the end of the experiments. The concentrations themselves are small, all being less than 6 mmole per kg at the most.

The raw and sulfate adjusted PZ loss data in the O_2/CO_2 baseline experiments are compared in Figure 8.3. Unlike the previous set of experiments, it was expected that a small amount of oxidation would occur in these experiments due to the presence of O_2 and trace amount of metals from the agitator. The repeatability between the two experiments is similar to the previous set, but the sulfate adjustment appears to skew the data into unexpected trends and added scatter. The raw data is well behaved and produced the expected trend of a small rate of oxidation. After about 300 hours, each experiment has lost between 3.5 and 6.5% of the initial PZ. The repeatability of the two experiments is approximately the same as that between OE9 and OE10.

The degradation products generated during the O_2/CO_2 baseline experiments are compared in Figure 8.4. Detectable and increasing levels of formate and formyl amides were found in both experiments while EDA was only detected in OE11. The concentration profiles for formate track closely to each other while there is appreciable deviation in the EDA and total formate concentrations. As with the N_2/CO_2 baseline experiments, the maximum concentrations of all degradation products are small, all being less than 6 mmole per kg at their maximum.

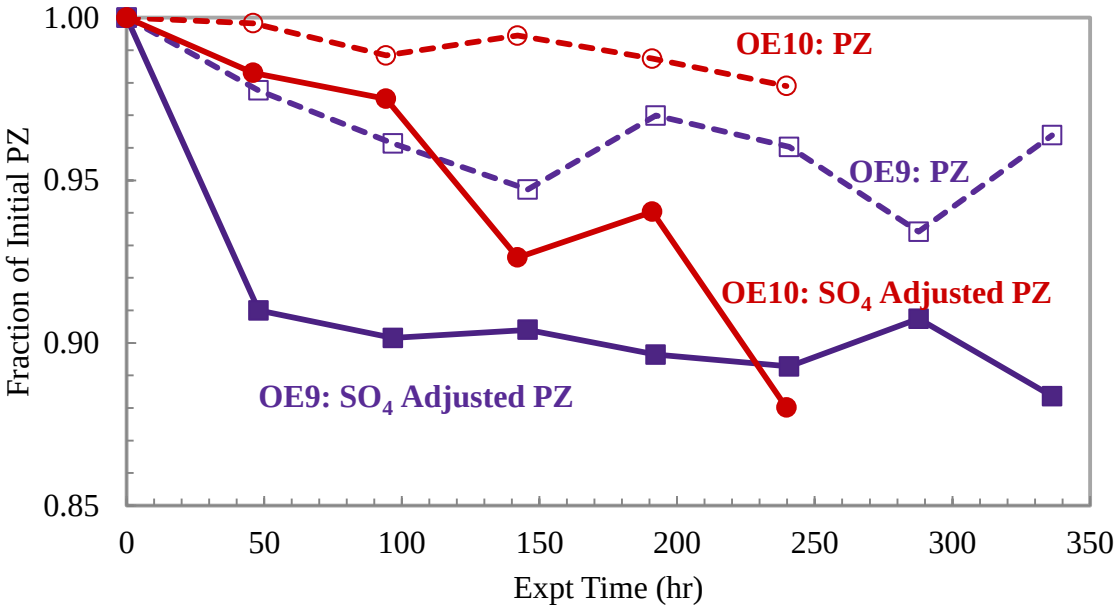

Figure 8.1: Comparison of PZ loss in N_2/CO_2 baseline experiments with original (dashed) and sulfate adjusted (solid) data (8 m PZ, 55 °C, 1400 rpm, 100 mL per minute of 98% N_2/2% CO_2, no catalyst)

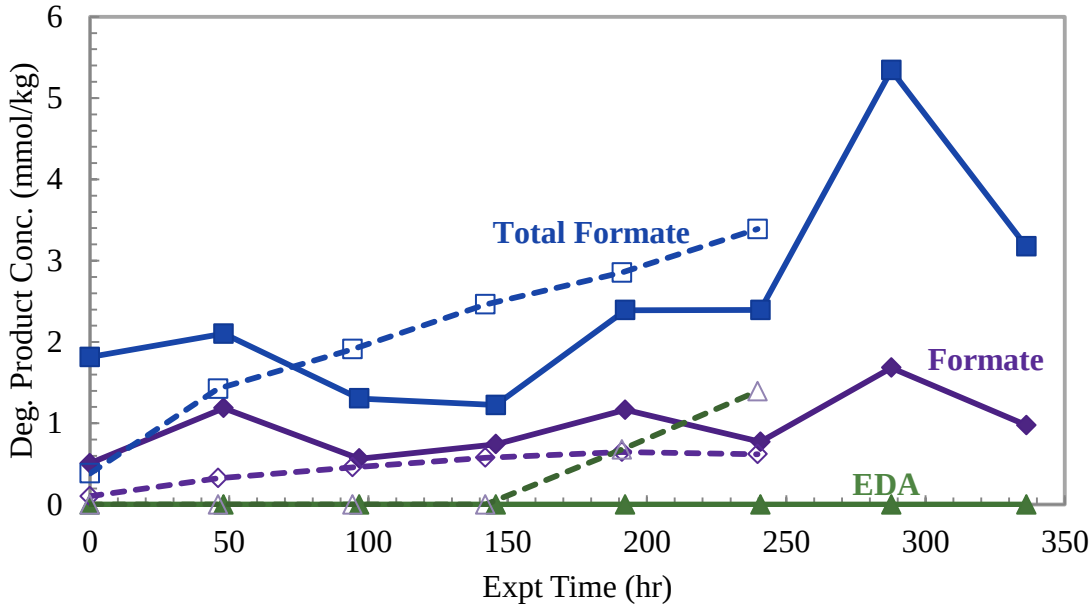

Figure 8.2: Generation of formate (♦), total formate (■), and EDA (▲) in N_2/CO_2 baseline experiments for OE9 (filled points) and OE10 (open points) (8 m PZ, 55 °C, 1400 rpm, 100 mL per minute of 98% N_2/2% CO_2, no catalyst)

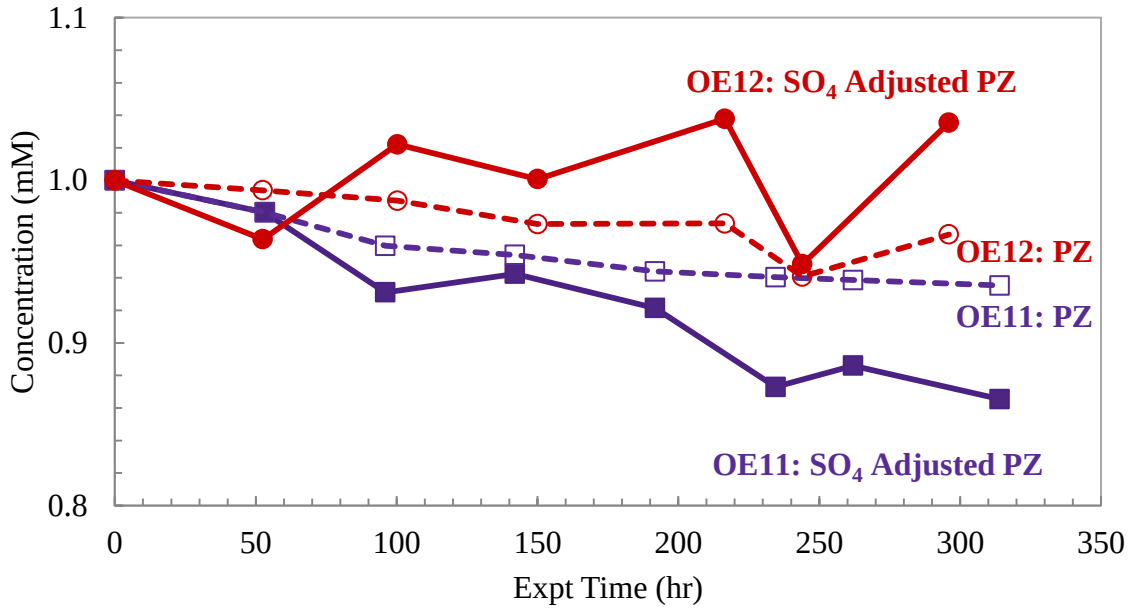

Figure 8.3: Comparison of PZ loss in O_2/CO_2 baseline experiments with original (dashed) and sulfate adjusted (solid) data (8 m PZ, 55 °C, 1400 rpm, 100 mL per minute of 98% O_2/2% CO_2, no catalyst)

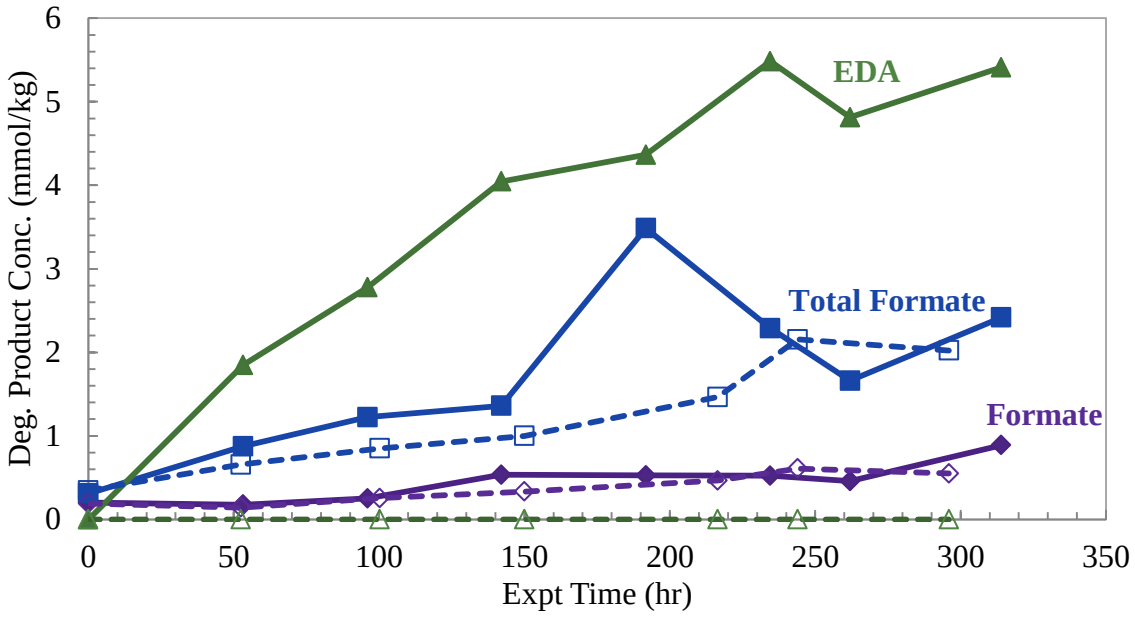

Figure 8.4: Comparison of formate (♦), total formate (■), and EDA (▲) in O_2/CO_2 baseline experiments for OE11 (filled points) and OE12 (open points) (8 m PZ, 55 °C, 1400 rpm, 100 mL per minute of 98% O_2/2% CO_2, no catalyst)

8.2.2 Repeatability and error

These baseline experiments quantify repeatability and show a systematic loss of PZ without corresponding concentrations of oxidation products. The repeatability of the oxidation experiments is not as high as preferred and is assumed to be primarily to the low level of oxidation occurring and, to a lesser extent, due to limitations in the analytical equipment. The quantification of PZ and EDA is performed on cation IC with a 10000X dilution prepared from a set of serial 100X dilutions. Since serial dilutions are used, there is more opportunity for error and inconsistency. EDA and PZ have nearly identical response factors on the cation IC, so the small expected concentration of EDA is problematic with this high dilution. Also, there is a bump in the baseline due to a change in the eluent gradient in the cation IC method where EDA elutes, adding to the difficulty. The concentration of degradation products are expected to be within the detection limit of the analytical equipment, generally understood to be near 1-2 mmole per kg, but the disparity in concentration creates additional error.

Comparing PZ loss in all four baseline experiments demonstrates a loss of 2 to 7% of the initial PZ due to all of sources of error discussed (Figure 8.5). This includes PZ losses due to oxidation, volatility, entrainment, dilution or concentration of PZ due to water balance issues, the addition of water or loss of water through the pre-saturator, losses experienced during start-up, sampling, and the clean-up of the reactor, and analytical error. All oxidation experiments discussed in this chapter and the next should be examined in light of this conclusion. PZ losses of less than or close to 7% over a two week standard experiment length should be cautiously described as oxidation. Oxidation above and beyond 7% in two weeks is needed to positively identify PZ oxidation versus the losses due to experimental considerations. A majority of figures showing PZ loss presented in these two chapters include these baseline curves in light gray. These data

are included to allow more accurate interpretation of data in light of the conclusions from the baseline experiments. The data for the generation of degradation products during the baseline experiments are also included on figures when data is difficult to interpret due to low oxidation rates.

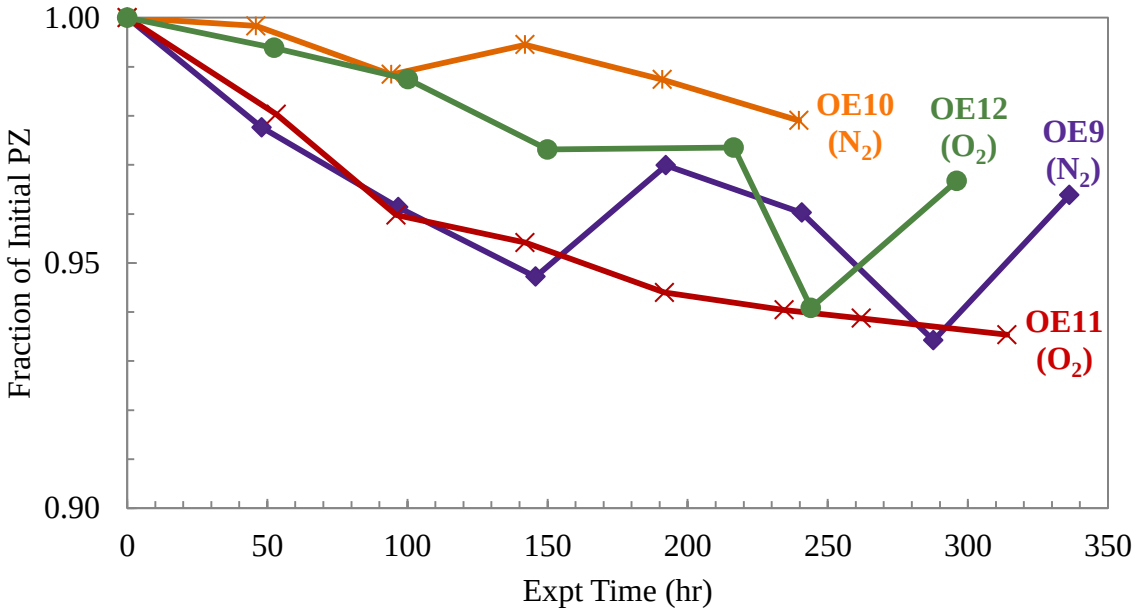

Figure 8.5: Comparison of PZ loss for all baseline experiments (8 m PZ, 55 °C, 1400 rpm, 100 mL per minute of 98% N_2 or O_2/2% CO_2, no catalyst)

8.2.3 Comparison of OOR and TOR

Once the Teflon® Oxidation Reactor (TOR) was built to replace the Original Oxidation Reactor (OOR), a baseline Fe^{2+}-catalyzed experiment was performed in the new reactor. Solutions of 8 m PZ were oxidized in each reactor at 55 °C with 100 mL per minute of 98% O_2/2% CO_2, agitation at 1400 rpm, and 1 mM Fe^{2+}. The PZ loss and generation of dominant degradation products is compared between the OOR (OE13) and TOR (OE17) experiments in Figure 8.6 and Figure 8.7, respectively. The results, unfortunately, do not demonstrate strong agreement in PZ loss (Figure 8.6). The trend in

the OE17 data, however, shows a clear dip in the initial sample and then a leveling off of the data to a subtle downward slope. This behavior is typical of a period of time where the reactor was open to the environment in some way and experienced a high rate of water loss. Since this was the first experiment in the TOR, the flange clamp holding the top of the reactor to the Teflon® lid was not fully tightened, allowing water loss. The clamp was not tightened fully because the appropriate tightness to obtain a secure connection without damaging the flange was not yet known. An accumulation of water between the lid and the glass flange was observed during the first sample and the clamp was then tightened, the slope in the PZ data after this point, excluding the initial point, likely demonstrate the expected loss of PZ under these conditions. The slope of the data in this region agrees with that of the OOR experiment which shows about 8% loss of the initial PZ after 450 hours.

The generation of degradation products mostly agrees between the two experiments (Figure 8.7). Formate and total formate generation rates agree, but with some scatter in the data. EDA, on the other hand, was not detected in the earlier experiment in the OOR. This may be similar error as was seen with EDA detection in the baseline experiments, or analysis done later in OE17 was more advanced. In both cases, oxidation was slow and degradation products did not accumulate to significant concentrations during the course of the 450 hour experiment.

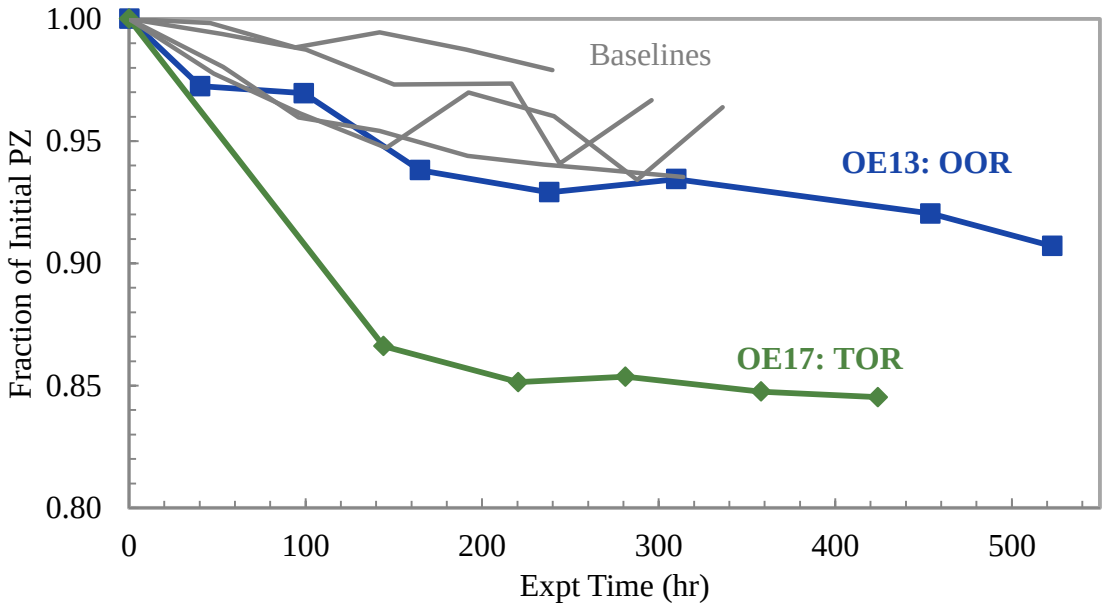

Figure 8.6: Comparison of PZ loss during oxidation in the OOR and TOR (8 m PZ, 55 °C, 1400 rpm, 100 mL per minute of 98% O_2/2% CO_2, 1 mM Fe^{2+})

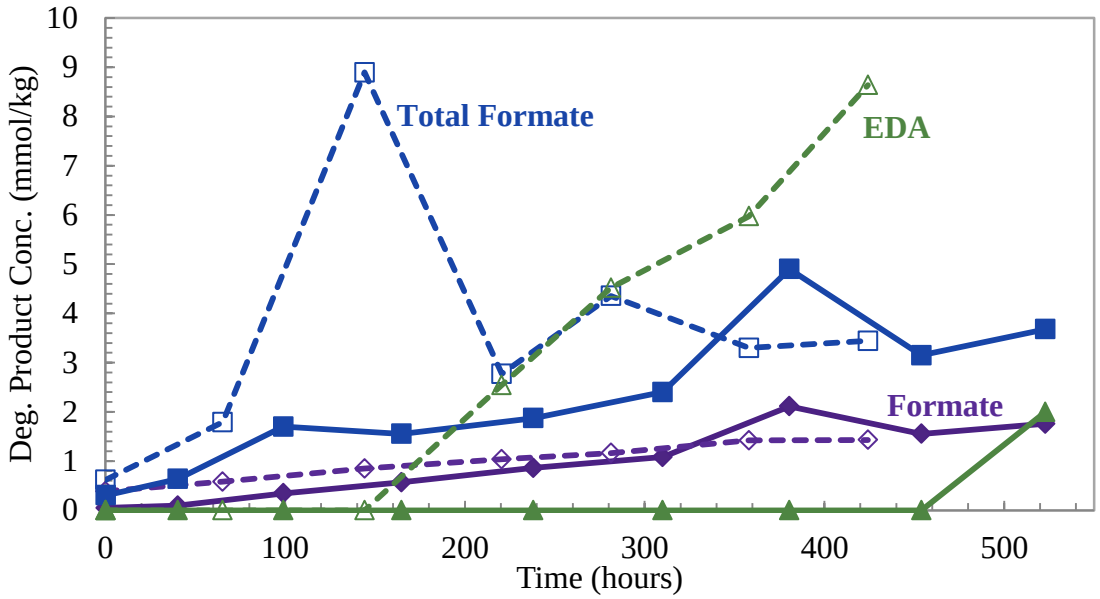

Figure 8.7: Generation of formate (♦), total formate (■), and EDA (▲) during PZ oxidation in the OOR (filled points, OE13) and TOR (open points, OE17) (8 m PZ, 55 °C, 1400 rpm, 100 mL per minute of 98% O_2/2% CO_2, 1 mM Fe^{2+})

8.2.4 Volatility of PZ in oxidation experiments

The volatility of PZ is a concern for all oxidation experiments because the reactors are open to the atmosphere around the agitator and have with 100 mL per minute of gas flowing in and out of the headspace of the reactor. The volatility of PZ and water in loaded 8 m PZ has been accurately measured by Nguyen using a multi-component FTIR, as discussed in section 2.3.5 (Nguyen et al., 2010). Using this information, an estimation of the PZ and water loss due to volatility during operation of the TOR reactors was made to determine the effect of volatility to the PZ mass balance. The partial pressure of PZ in 8 m PZ with a loading of 0.29 moles CO_2 per mole alkalinity is shown at 40 and 60 °C in Figure 8.8. The two data points were regressed with a linear trendline and the partial pressure of PZ was extrapolated to 55 and 70 °C. The partial pressure of PZ in a lean loaded (0.3 mole CO_2 per mole alkalinity) solution was estimated to be 0.00438 and 0.00798 kPa at 55 and 70 °C, respectively. This value was then converted to parts per million (ppm) using atmospheric pressure of 1 atm.

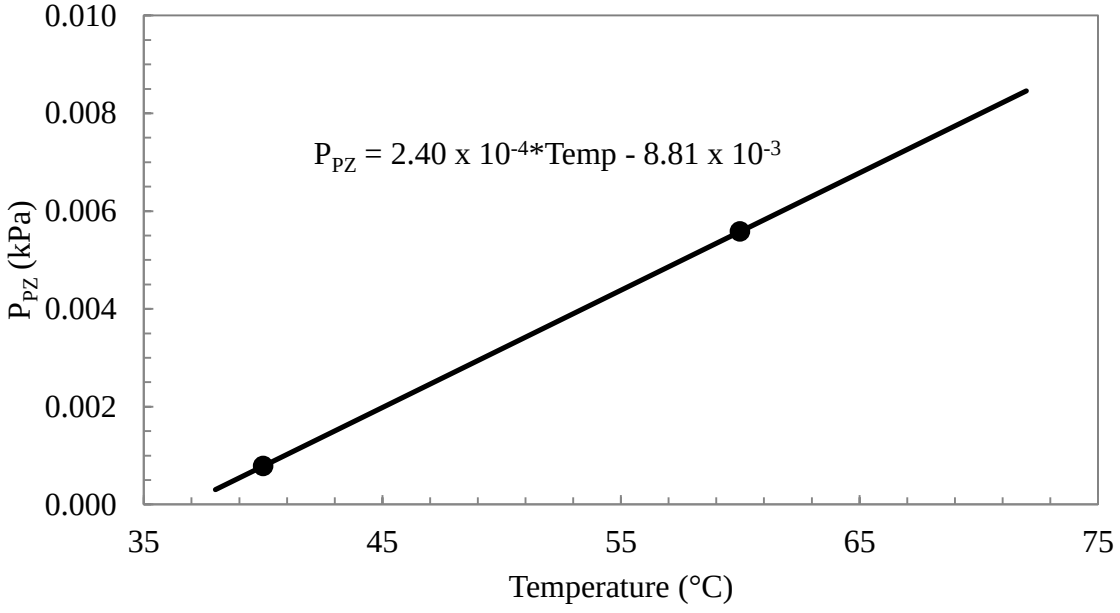

Figure 8.8: Volatility of 8 m PZ with 0.29 mole CO_2 per mole alkalinity

The concentration in ppm estimated for each temperature was then converted to a volumetric flow rate using the total gas flow rate. First, the molar volume of an ideal gas (V_M), was calculated using the ideal gas law (Equation 8.1) for each temperature using the ideal gas constant, R, system temperature, T, and system pressure, P.

$$PV = nRT \tag{8.1}$$

$$\frac{V}{n} = \frac{RT}{P} = V_M \tag{8.2}$$

The molar volume of an ideal gas at 55 and 70 °C are calculated in Equation 8.3 and Equation 8.4, respectively.

$$V_{M,\,55^\circ C} = \frac{\left(0.08206\,\frac{L\cdot atm}{mol\cdot K}\right)\times\left(55^\circ C + 273.15\right)K}{\left(1\,atm\right)} = 26.93\,\frac{L}{mol} \tag{8.3}$$

$$V_{M,\,70^\circ C} = \frac{\left(0.08206\,\frac{L\cdot atm}{mol\cdot K}\right)\times\left(70^\circ C + 273.15\right)K}{\left(1\,atm\right)} = 28.16\,\frac{L}{mol} \tag{8.4}$$

Using the calculated values for the molar volume at each temperature, the concentration in ppm can be converted to a volumetric concentration, C_V, in each case using the following equation (Equation 8.5).

$$C_V = \frac{ppm\times MW}{V_M} \tag{8.5}$$

The estimated volumetric concentration of PZ exiting the reactor at 55 and 70 °C are calculated in Equation 8.6 and Equation 8.7, respectively.

$$C_{V,55^\circ C} = \frac{\left(\frac{43.24\,\mu g}{g}\right)\times\left(\frac{1\,g}{10^6\,\mu g}\right)}{\left(26.93\frac{L}{mole}\right)\times\left(\frac{1\,mole}{1000\,mmole}\right)\times\left(\frac{1000\,mL}{1\,L}\right)} = 1.61\times10^{-6}\,\frac{mmole}{mL} \quad (8.6)$$

$$C_{V,70^\circ C} = \frac{\left(\frac{78.74\,\mu g}{g}\right)\times\left(\frac{1\,g}{10^6\,\mu g}\right)}{\left(28.16\frac{L}{mole}\right)\times\left(\frac{1\,mole}{1000\,mmole}\right)\times\left(\frac{1000\,mL}{1\,L}\right)} = 2.80\times10^{-6}\,\frac{mmole}{mL} \quad (8.7)$$

Using the total flow rate of gas entering and exiting the reactor, the loss of PZ can be calculated per unit time. The loss of PZ per hour of operation has been estimated for operation at 55 °C in units of mmole and mg per hour in Equation 8.8 and Equation 8.9, respectively. The same has been calculated for operation at 70 °C in Equation 8.10 and Equation 8.11, respectively.

$$\text{Loss}(55^\circ C) = \left(\frac{1.61\times10^{-6}\,mmole}{mL}\right)\times\left(\frac{100\,mL}{min}\right)\times\left(\frac{60\,min}{hr}\right) = 0.00963\,\frac{mmole}{hr} \quad (8.8)$$

$$\text{Loss}(55^\circ C) = \left(\frac{1.38\times10^{-4}\,mg}{mL}\right)\times\left(\frac{100\,mL}{min}\right)\times\left(\frac{60\,min}{hr}\right) = 0.83\,\frac{mg}{hr} \quad (8.9)$$

$$\text{Loss}(70^\circ C) = \left(\frac{2.80\times10^{-6}\,mmole}{mL}\right)\times\left(\frac{100\,mL}{min}\right)\times\left(\frac{60\,min}{hr}\right) = 0.0168\,\frac{mmole}{hr} \quad (8.10)$$

$$\text{Loss}(70^\circ C) = \left(\frac{2.41\times10^{-4}\,mg}{mL}\right)\times\left(\frac{100\,mL}{min}\right)\times\left(\frac{60\,min}{hr}\right) = 1.45\,\frac{mg}{hr} \quad (8.11)$$

These loss rates lead to daily losses of only 0.23 and 0.40 mmole PZ per day, or 0.020 and 0.035 gram of PZ at 55 and 70 °C. At 55 °C, this loss rate could account for the experiments with minimum or even negligible loss rates of PZ, such as OE6, OE15,

or OE18. At 70 °C, this volatility accounts for only 11.6% of the minimum loss rate of PZ observed (OE19). At worst, volatility accounts for only 0.3 and 0.2%, respectively, of the PZ loss rate in heavily oxidized experiments at 55 and 70 °C (OE2 and OE25, for example). This indicates that PZ losses due to volatility are not an important portion of the PZ loss seen over the course of an experiment. Volatility is on the same order as PZ loss only in experiments with difficult to detect levels of oxidation due to weak catalysts. In the reactor, PZ may also leave the reactor through entrainment, or the effect of liquid drops leaving the reactor through splashing of the liquid or aerosolization, which is not included in this calculation. This phenomenon is not well understood and would be dictated by the temperature of the reactor, gas flow in the headspace, agitation rate, and agitator shaft position relative to the liquid surface. Entrainment and aerosolization could cause more PZ to leave than by simple volatility, but the effect is not definitively known.

This same analysis was performed for water using water volatility measurements obtained during the same experiments used to determine PZ volatility. Water volatility is strictly dependent on temperature, not CO_2 loading as with PZ volatility. The partial pressure measurements for water at 40 and 60 °C were extrapolated to determine those at 55 and 70 °C. The estimated values are partial pressures of 13.17 and 20.46 kPa water, or 130002 and 201875 ppm water, at each temperature respectively. Using the same analysis presented above for PZ, the loss of water at each temperature was determined to be 12.51 and 18.58 gram water per day at 55 and 70 °C. These high loss rates are comparable with the water replacement rates quantitatively observed with experiments at each temperature.

For seven experiments performed at 70 °C in the TOR, an average of 11.51 g of water (range of 8.1 to 18.9 grams) was added per day to the reactor and the saturator in total (OE19 through OE25). This represents the total amount of replacement water that

was needed in the system to maintain system levels. The actual water additions are of a similar magnitude to the theoretical volatility of water that indicates that 18.58 grams of water should volatilize per day. During operation of the TOR at 55 °C, an average of 5.36 grams of water (range of 4.3 to 6.4 grams) was added to the reactor per day (OE17 and OE18) compared to the theoretical value of 12.51 grams, but this did not included additions to the saturator (which was not recorded). In the high temperature experiments, the water added to the saturator is nearly identical to that added to the reactor itself (average of 5.63 grams to saturator compared to 5.89 grams to the reactor). If the same ratio held for the low temperature experiments, the total water added to the low temperature experiments may have been closer to 10.7 grams of water, closely matching the theoretical water volatility calculations.

Another issue related to PZ volatility is the volatility of oxidation products that will be produced during the reactions. The volatility of some degradation products, such as EDA, is well understood (Zhou et al., 2010). On the other hand, the volatility of other degradation products are either not well understood in this particular solvent system, as is the case of ammonia volatility, or not understood at all, as in the case of PZ-based amides. The use of the low gas flow reactor, either the OOR or TOR, assumes that the solvent under investigation produces dominantly liquid phase degradation products since it is not equipped with gas phase analysis. The dominant oxidation pathways for PZ are not fully understood, but volatile products are certainly expected, such as NH_3/NH_4^+, NO_X, and formaldehyde, and will not be captured with this experimental procedure.

8.2.5 Total Nitrogen (TN) and Total Organic Carbon (TOC) analysis

The final explanation for mass balance issues during oxidation experiments is the inability to identify and quantify all of the degradation products generated from PZ

oxidation. One universal method to determine if the liquid phase contains additional degradation products is a total organic carbon (TOC) and total nitrogen (TN) analysis. The total organic carbon assay measures the concentration of C contained in all organic liquid phase components. This excludes inorganic C such as in carbonate or bicarbonate. Inorganic C is quantified by a separate total inorganic carbon (TIC) assay. The TN analysis quantifies all N in the liquid phase in a similar fashion. TOC and TN were not performed on all experiments, but a select few to highlight the role of unidentified degradation products. Error bars shown represent the standard deviation in five replicates of either a TOC or TN measurement. The expected overall error of both analyses is at least 5%.

OE11, one of the baseline experiments performed in the presence of O_2/CO_2 but without metal catalysts, was analyzed for TOC and TN. The TOC and TN during the course of the experiment are shown as a fraction of the initial concentration in Figure 8.9. The data show that while the concentration of organic C is maintained during the experiment, there is a statistically significant loss of N. In OE11, 6.5% of the initial PZ was lost during the experiment. Since the error in the TOC and TN analysis is expected to be around 5%, a loss of 6.5% in either assay would be observable. The error bars on the last TN data points suggest up to 8.5% of the N is lost after 350 hours of oxidation. This suggests that there are N-based products lost in the gas phase during the experiment. On the other hand, the TOC concentration is relatively constant, suggesting C-containing degradation products in solution that have yet to be identified. The TOC results indicate that the PZ loss is primarily due to the production of unidentified degradation products that remain in solution, as hypothesized.

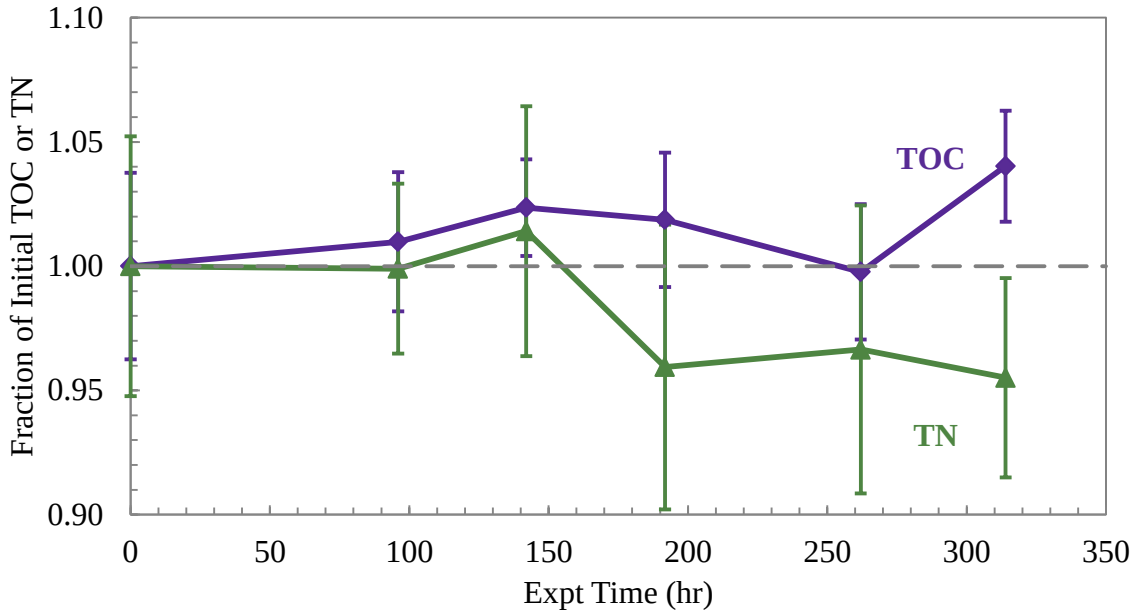

Figure 8.9: TOC and TN in the liquid phase during OE11 (8 m PZ, 55 °C, 1400 rpm, 100 mL per minute of 98% O_2/2% CO_2, no catalyst)

OE25, an oxidation experiment with a very high rate of oxidation due to the presence of Cu^{2+} catalyst and high temperature, was also analyzed for TOC and TN. The TOC and TN are presented as a fraction of the initial value in Figure 8.10. Although the reaction conditions were very different, both OE11 and OE25 had similar results for the TOC data with no appreciable loss or change of the TOC data after 350 hours. This confirms the presence of unidentified C-based degradation products at both low and high rates of oxidation. The TN data for this experiment is striking in that 27% of the initial N is lost after 350 hours. This loss of N, 2650 mmole per kg after 350 hours, is significant and well outside the analytical error. This loss of N while maintaining overall the C concentration suggests, as with OE11 discussed previously, volatile N-based compounds without attached C.

The concentrations of PZ, total alkalinity, and total N for OE25 are compared in Figure 8.11. There is a decrease in all three measurements and the extent of PZ oxidation

is clearly demonstrated. PZ is lost rapidly and degradation products are generated that retain alkalinity in solution, indicated by the higher concentration in total alkalinity. Of these products, some retain N functions and keep the TN concentration higher than either PZ or total alkalinity in the liquid phase. This comparison confirms the detection of products such as ammonium and EDA in the liquid phase that retain alkalinity. The difference between the alkalinity and TN curves represent products that retain N but would not alkalinity, like ureas or amides. The TN results clearly suggest volatile, non-C products which must be ammonia (NH_3), nitrogen oxides (NO_X; NO or NO_2), or molecular nitrogen (N_2). Ammonia is known to be volatile and the presence of small concentrations of ammonium in the liquid suggests lost ammonia in the gas phase. Ammonia was found as an oxidation product of PZ previously in a high-gas flow reactor using multi-component FT-IR while NO_X was not mentioned as a gaseous product (Sexton, 2008).

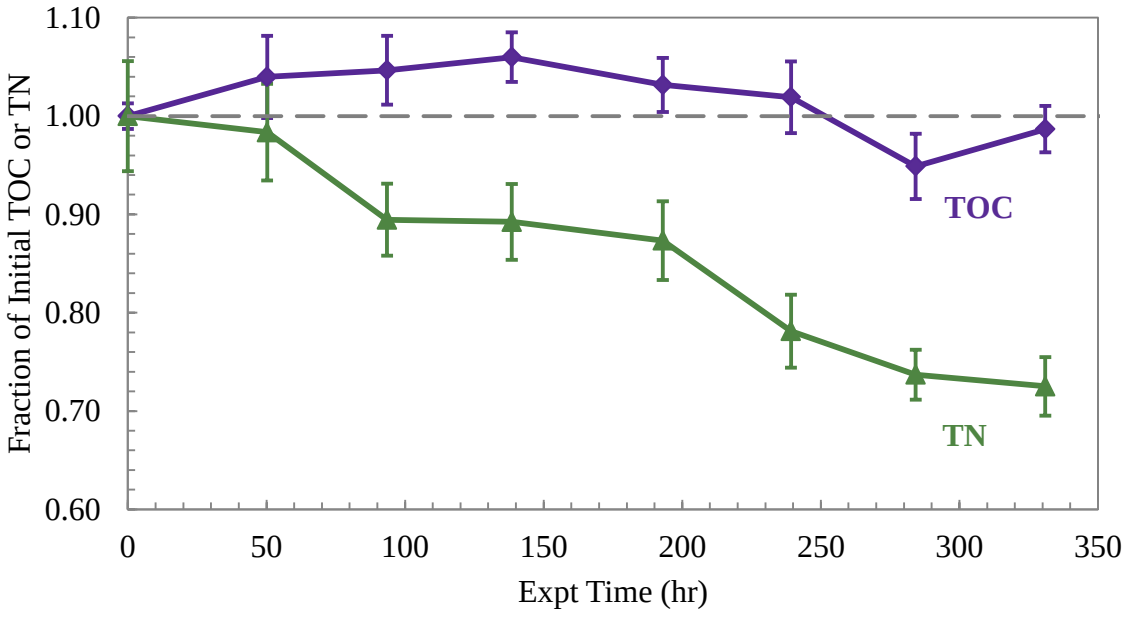

Figure 8.10: TOC and TN in the liquid phase during OE25 (8 m PZ, 70 °C, 1400 rpm, 100 mL per minute of 94% O_2/2% CO_2, 4 mM Cu^{2+})

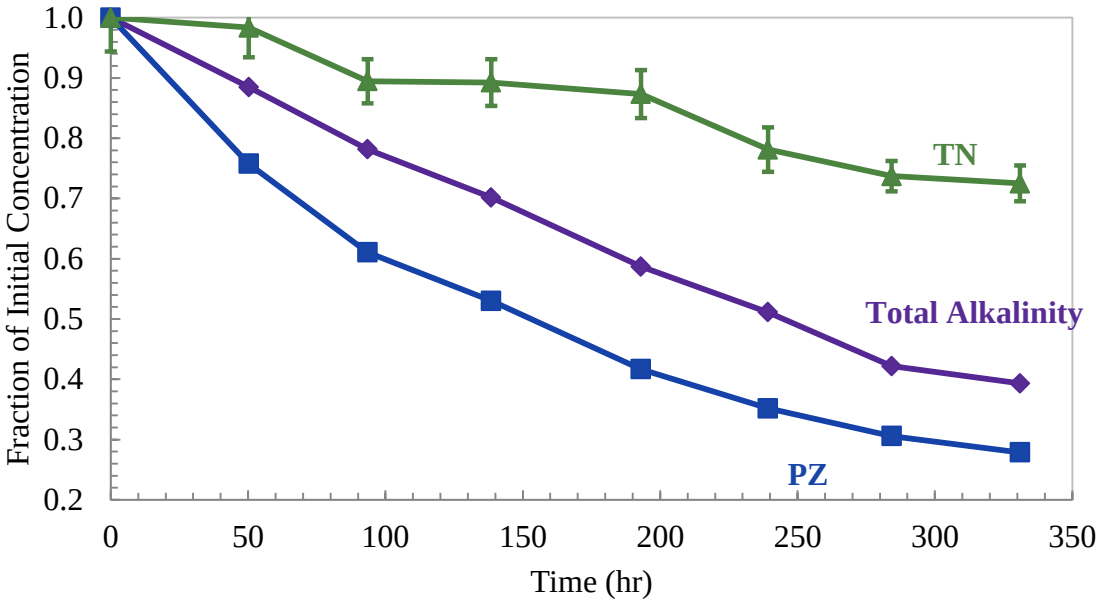

Figure 8.11: Comparison of PZ, total alkalinity, and total N for OE25 (8 m PZ, 70 °C, 1400 rpm, 100 mL per minute of 94% O_2/2% CO_2, 4 mM Cu^{2+})

The TOC results suggest the need for more sophisticated analytical techniques to effectively identify and quantify liquid-phase oxidation products of PZ. In the next section, the degradation products that have been identified and quantified are discussed along with unknown products that have been observed, but not yet identified. There are clearly many products remaining to identify, and some are observable on the current analytical tools including anion IC, cation IC, and amino acid detection.

8.2.5.1 Estimated volatility of ammonia during oxidation

The volatility of ammonia during PZ oxidation can be estimated to determine the impact of this species on the TN analysis. To estimate volatility, a Henry's constant is first estimated based on NH_3 solubility data in water (Perry and Green, 1997). An assumption will be made that NH_3 solubility in 8 m PZ is similar to that of water since data in PZ is not available. Solubility data for a solution of 2.91 mass percent NH_3 were

available at 50 and 60 °C and those points were used to estimate values for 55 and 70 °C (Table 8.2). With this data, the Henry's constant can be estimated at the two temperatures of interest using Henry's Law shown in Equation 8.12. Henry's Law relates the partial pressure of a species such as ammonia, P_{NH3}, to its liquid phase concentration, C_{NH3}, at a constant temperature using Henry's constant, H_{NH3}. The mass percent concentration of the data is converted to the more useful units of mmole NH_3 per kg solution in Equation 8.13. The Henry's constant for is then calculated for 55 and 70 °C in Equation 8.14 and 8.15.

Table 8.2: Partial pressure of NH_3 over 2.91 mass percent NH_3 in water (Perry and Green, 1997)

Temp °C	P_{NH3} mmHg
50	67.1
55	80.7
60	94.3
70	121.5

$$P_{NH3} = H_{T,NH3} \cdot C_{NH3} \tag{8.12}$$

$$\frac{2.91\,\text{g NH}_3}{\text{g soln}} \times \frac{1000\,\text{g}}{1\,\text{kg}} \times \frac{1\,\text{mole}}{17\,\text{g NH}_3} \times \frac{1000\,\text{mmole}}{1\,\text{mole}} = 1713.3 \frac{\text{mmole NH}_3}{\text{kg soln}} \tag{8.13}$$

$$H_{55C,NH3} = \frac{80.7\,\text{mm Hg} \times \dfrac{1\,\text{atm}}{760\,\text{mm Hg}}}{\dfrac{1713.3\,\text{mmole}}{\text{kg soln}}} = 6.20 \times 10^{-5}\,\frac{\text{atm} \cdot \text{kg}}{\text{mmole}} \tag{8.14}$$

$$H_{70C,NH3} = \frac{121.5\,\text{mm Hg} \times \dfrac{1\,\text{atm}}{760\,\text{mm Hg}}}{\dfrac{1713.3\,\text{mmole}}{\text{kg soln}}} = 9.33 \times 10^{-5}\,\frac{\text{atm} \cdot \text{kg}}{\text{mmole}} \tag{8.15}$$

At the end of OE25, which was performed at 70 °C, nearly 4 mmole free NH_4^+ per kg and 131 mmole total NH_4^+ per kg was quantified. In order to address the issues in the TN results and the overall N balance, the potential quantity of NH_3 that volatilized during the experiment will be estimated and reported as the concentration if it had all remained in solution. This estimation will be done in order to bracket the two extremes, with both the minimum and maximum possible volatile NH_3 loss estimated. The minimum amount of volatile NH_3 lost would be a calculation based on the 4 mmole NH_4^+ per kg. The maximum loss would be calculated based on the concentration of total NH_4^+ and assuming that it is not all bound as amide, but represents other NH_3 containing species. Another quantity, an intermediate value, will also be calculated based on the total NH_4^+ data which reach a plateau around 70 mmole per kg.

An interesting observation is the behavior of the free NH_4^+ compared to the total NH_4^+ after alkaline treatment. Free NH_4^+ is only detected in the last few samples of OE25, which may indicated a sample stability issue. This experiment was highly oxidized and even at room temperature, active species such as aldehydes, peroxides, if present, and even ureas may have reacted with the free NH_4^+ before analysis in the cation IC. The NH_{4+} released during alkaline treatment would be analyzed directly, without time for additional reactions and may reflect a more representative level of NH_4^+ in the solution than the free NH_4^+.

For any of the liquid phase concentrations, the amount of NH_3 in the gas phase can be calculated using the Henry's constant for that condition. This calculation does not take into account the change of liquid phase NH_3 production with time and assumes a constant rate of NH_3 production. If NH_3 were being generated a constant rate, which is believed to be occurring, it would like accumulate in the liquid phase before it was then

stripped into the gas phase as concentration increases and eventually an equilibrium is reached where the generation rate and volatilization rate are equal.

For each liquid phase concentration, the gas phase partial pressure can be calculated using Equation 8.12 and the Henry's constant calculated in Equation 8.14, as demonstrated in Equation 8.16.

$$P_{NH3} = \frac{9.33\times10^{-5}\,\text{atm}\cdot\text{kg}}{\text{mmole}} \times \frac{4\,\text{mmole}}{\text{kg}} = 3.73\times10^{-4}\,\text{atm} \qquad (8.16)$$

For the low NH_4^+ concentration case, the partial pressure of NH_3 was calculated to be 3.73×10^{-4} atm, or 373 ppm. Based on 2 weeks of operation and a gas flow rate of 100 mL per min, the overall loss of NH_3 can be estimated using the ideal gas law (Equation 8.17).

$$n_{NH3} = \frac{\left(3.73\times10^{-4}\,\text{atm}\right)\times\left(2\,\text{wk}\times\frac{10080\,\text{min}}{\text{wk}}\times\frac{0.1\,\text{mL}}{\text{min}}\right)}{\left(70^{\circ}\text{C}+273.15\right)\text{K}\times\left(0.08206\,\frac{\text{L}\cdot\text{atm}}{\text{mole}\cdot\text{K}}\right)} = 0.027\,\text{mole NH}_3 \qquad (8.17)$$

This amount of moles can then be converted to the liquid phase concentration if all of this volatile NH_3 had remained in solution based on the overall solution mass in the reactor (Equation 8.18).

$$C_{NH3} = \frac{0.027\,\text{mole NH}_3 \times \frac{1000\,\text{mmole}}{1\,\text{mole}}}{390\,\text{g soln}\times\frac{1\,\text{kg}}{1000\,\text{g soln}}} = 68.5\,\frac{\text{mmole}}{\text{kg}} \qquad (8.18)$$

This calculation estimates that if all of the volatilized NH_3 were retained in solution, the concentration of NH_3 would be 68.5 mmole per kg higher. If the same

calculation is done for the measured liquid phase concentrations of 70 and 131 mmole NH_4^+ per kg, the volatile NH_3 would have added 1200 and 2244 mmole NH_3 per kg, respectively, to the solution if no volatilization occurred.

The TN measurements discussed earlier in this section suggested a N loss of 2650 mmole per kg throughout the course of the experiment. Volatile NH_3 is a strong candidate to explain a significant portion of this N loss, but even a calculation expected to predict the maximum amount of NH_3 lost cannot account for the entire N loss. It is not expected that NO_X species are made in significant quantities based on previous FT-IR experiments (Sexton, 2008).

8.3 Degradation products of concentrated PZ oxidation

The generation of degradation products was monitored with the best available techniques for all oxidation experiments. Anion and cation IC were performed on all experimental samples while amino acid detection, a newer technique, was only performed on select experiments. IC-MS and GC-MS techniques were also performed on some samples in an effort to find missing degradation products with limited success. A summary of degradation products successfully identified and quantified as well as suspected new products are summarized in Table A.3 (Appendix A).

In all experiments regarding the oxidation of concentrated PZ, the quantified degradation products accounted for very little of the loss PZ, with only a few exceptions. The inability to detect the most prominent degradation products, as highlighted by the TOC and TN results in the preceding section, is the most important issue regarding the study of PZ oxidation. The unidentified products are not being quantified because they are either volatile, non-ionic (i.e., not detectable on anion or cation IC), polymeric (not seen with current cation IC method), or undetectable with IC due to their molecular

structure or stability issues (e.g., aldehydes, ureas, and others). The volatility of degradation products is only a minor issue based on the TOC and TN results. It is likely that all of the abovementioned concerns are cumulatively producing poor overall mass balance results.

Despite an unsatisfactory mass balance, the products that were consistently detected can be discussed. The most prominent degradation products of oxidation were formate, oxalate, formyl amides, oxalyl amides, and EDA. Smaller concentrations of acetate and glycolate were found inconsistently while NH_4^+, nitrite, and nitrate were found only in heavily oxidized solutions. The volatility analysis presented in the previous section suggests that volatile NH_3 and instable NH_4^+ in solution may be more important than the liquid analysis has shown. In order to demonstrate the typical, expected generation of degradation products during oxidation, two experiments will be analyzed in detail. The first experiment represents a low oxidation condition that should be similar to an absorber system which is run at moderate temperatures, without a Cu^{2+}-based corrosion inhibitor and with appropriate pre-treatment to remove a majority of SO_X and NO_X in a coal fired flue gas stream. The second experiment will examine the degradation profile of a heavily oxidized PZ solution at the absorber temperature bulge (70 °C) with a Cu^{2+}-based corrosion inhibitor and without an oxidation inhibitor.

As a representative experiment for the low oxidation condition, 8 m PZ was oxidized at 55 °C with a lean loading (0.3 moles CO_2 per mole alkalinity) with agitation at 1400 rpm in the presence of the typical SSM mixture (0.4 mM Fe^{2+}, 0.1 mM Cr^{3+}, and 0.05 mM Ni^{2+}) with 100 mL per minute of inlet gas with 98% O_2 (OE18). For the highly oxidized solution, 8 m PZ was oxidized at 70 °C with a lean loading (0.3 moles CO_2 per mole alkalinity) with agitation at 1400 rpm in the presence of 4 mM Cu^{2+} with 100 mL per minute of inlet gas with 94% O_2 (OE25). These two cases will be examined in terms

of the types of products generated, the unknowns observed in solution, and the overall mass balance at the end of the experiment.

8.3.1 Types of oxidation products

8.3.1.1 Degradation products found in experiments with low PZ oxidation rates

In OE18, 8 m PZ was oxidized at 55 °C with a lean loading (0.3 moles CO_2 per mole alkalinity) with agitation at 1400 rpm in the presence of the typical SSM mixture (0.4 mM Fe^{2+}, 0.1 mM Cr^{3+}, and 0.05 mM Ni^{2+}) with 100 mL per minute of inlet gas with 98% O_2. Very low rates of PZ loss and product generation were observed, as shown in Figure 8.12. Essentially no PZ loss was observed in this experiment as the amine concentration changed by 135 mmole per kg compared to the initial sample. Degradation products were primarily formate and total formate. No EDA or oxalyl amides were detected in this experiment.

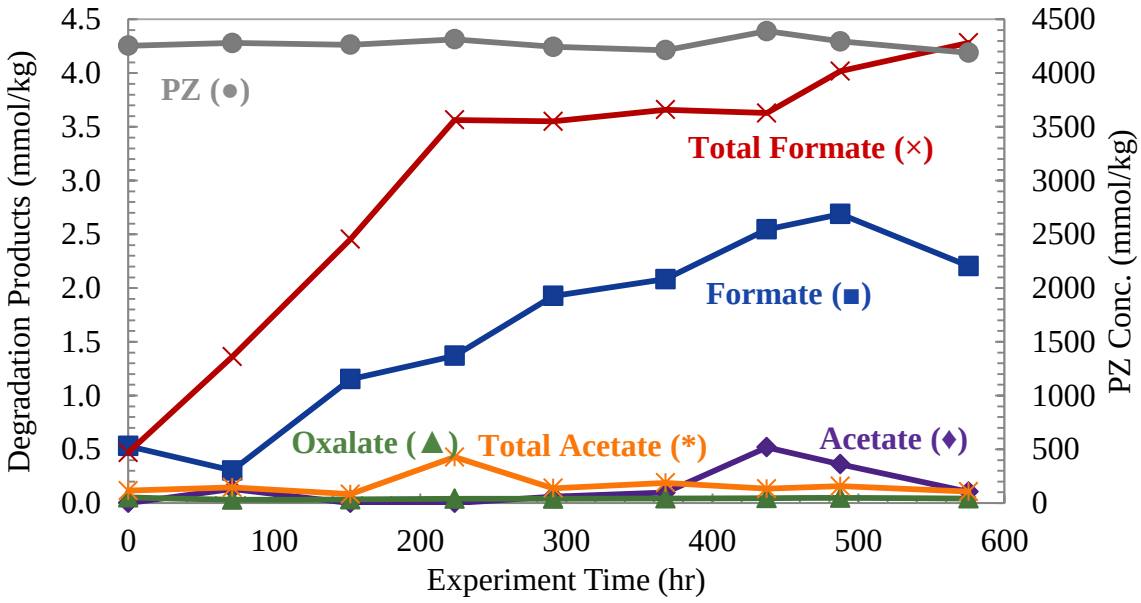

Figure 8.12: Profiles for PZ and degradation products for typical low oxidation experiment (OE18) (8 m PZ, 55 °C, 1400 rpm, 100 mL/min 98% O_2, SSM)

The cation and anion IC chromatograms from the initial and final samples are compared in Figure 8.13 and Figure 8.14, respectively. The lack of degradation is demonstrated by the similarity of the two chromatograms after 24 days of oxidation. The cation IC chromatogram only contains a strong peak for PZ (retention time of 13.9 minutes) outside of the background peaks for K^+, Na^+, and either Ca^{2+} or Mg^{2+} that also appear. The PZ peak does not appreciably decrease during the course of the experiment, indicating a very low level of oxidation occurred. The anion IC chromatogram contains only one strong product peak for formate (20.9 minutes), outside of background peaks for CO_3^- and SO_4^{-2}. Oxalate, acetate and glycolate were also detected in this sample at very low levels. There are no significant unknown peaks present on either chromatogram that would indicate an important, unidentified degradation product.

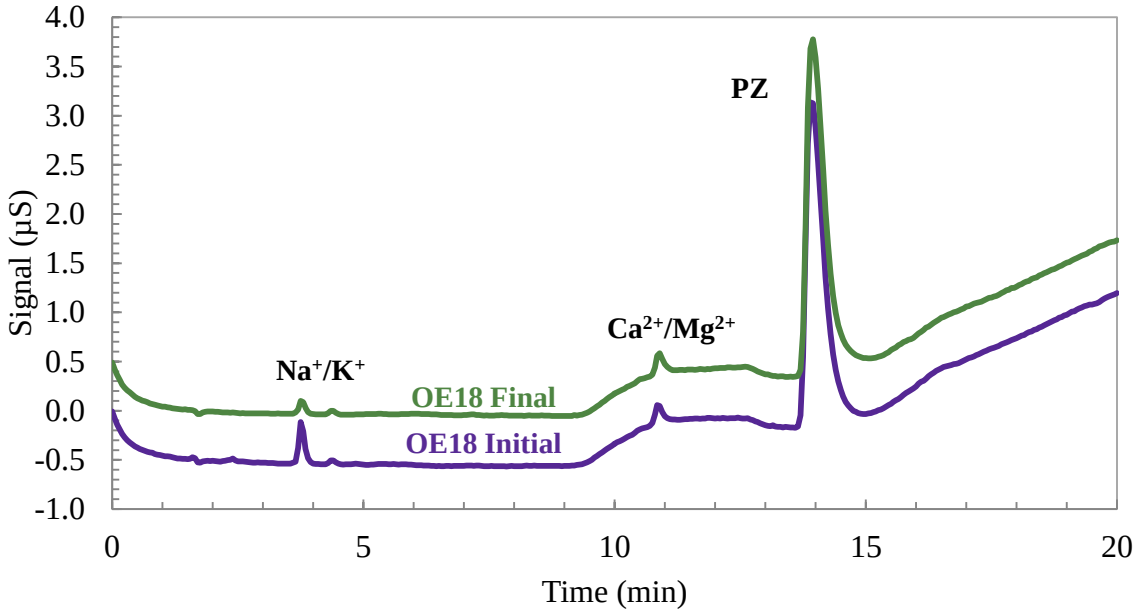

Figure 8.13: Comparison of cation IC chromatograms at the start and end of OE18 demonstrating low oxidation (signals are offset 0.5 µS for clarity) (8 m PZ, 55 °C, 1400 rpm, 100 mL/min 98% O_2, SSM, 24 days)

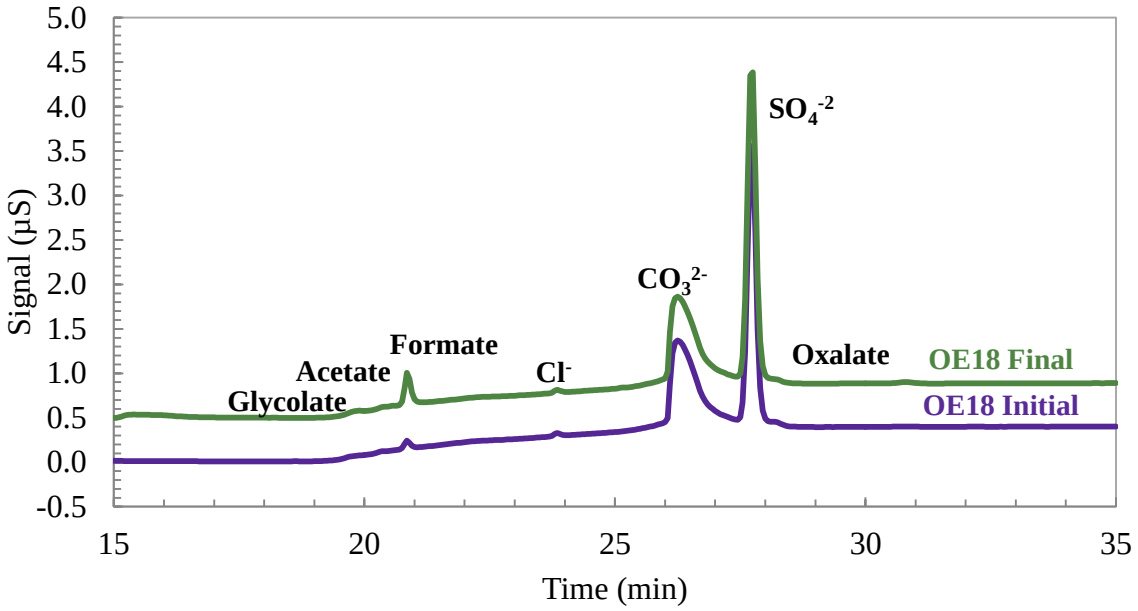

Figure 8.14: Comparison of anion IC chromatograms at the start and end of OE18 demonstrating low oxidation (signals are offset 0.5 µS for clarity) (8 m PZ, 55 °C, 1400 rpm, 100 mL/min 98% O_2, SSM, 24 days)

Analysis of OE18 provides a representative view of the types of degradation products seen in experiments with low rates of PZ oxidation. In this project, only three Cu^{2+}-catalyzed experiments showed high rates of oxidation, so a majority of oxidation data is of this nature. Despite the seeming lack of data, some conclusions can still be drawn from low PZ oxidation rates by examining production rates of formate, total formate, and EDA. Throughout this chapter and the following chapter (Chapter 9), comparisons of PZ loss and the generation of formate, total formate, and EDA will be used in order to draw conclusions on overall PZ oxidation rate. For the degradation products, an assumption is made that these three products represent the total mix of degradation products produced, either identified or unidentified. This assumption could be incorrect or an oversimplification, but appears to hold true given the data gathered in this project, especially for low oxidation experiments where there is little other data. This

type of analysis leads to inconclusive evidence in some experiments, especially in the case of EDA data. EDA is difficult to accurately detect at low levels due to the dilution required for cation IC. In cases of low oxidation, only low levels of EDA would be expected and were quantified. Formate and formyl amides are more accurately measured in the anion IC method and are considered the best overall indicators of oxidation of the degradation products quantified.

A second assumption made throughout this project is that catalysis by one metal generates the same product mix as catalysis by another metal. That is to say, that Cu^{2+}-catalyzed oxidation of PZ will lead to generation of the same degradation products as stainless steel metal-catalyzed oxidation, but at different overall rates. This assumption is supported by the fact that the same dominant products, formate, total formate, and EDA, are found across the board in both types of experiments. This assumption could be disproven when additional degradation products are identified in the various metal catalyzed systems. In the meantime, those three degradation products will be used to quantify and compare overall oxidation between experiments catalyzed in varying ways.

8.3.1.2 Degradation products found in experiments with high PZ oxidation rates

In OE25, 8 m PZ was oxidized at 70 °C with a lean loading (0.3 moles CO_2 per mole alkalinity), agitation at 1400 rpm with 4 mM Cu^{2+} and 100 mL per minute 94% O_2. This experiment had the highest rate of PZ oxidation of all oxidation experiments. The loss of PZ and generation of carboxylate ions and their corresponding amides are shown in Figure 8.15. The loss of PZ is compared with the generation of the dominant amine-based products in Figure 8.16. The two sets of products are separated to more clearly see trends. Formyl amides are included in both figures in order to demonstrate the congruity between the concentration of formyl amides and N-formyl PZ (FPZ).

The loss of PZ is severe in this experiment, with 72% of the initial PZ lost after 350 hours of oxidation. In accordance with the high level of PZ oxidation, high concentrations of degradation products were quantified. High concentrations of formate and formyl amides were generated, reaching up to 168 and 386 mmole per kg, respectively. These are significantly higher than those concentrations found in low oxidation experiments where formyl amides, also the most dominant product, usually reached only 10 to 20 mmole per kg. Oxalate, oxalyl amides, and acetyl amides were also generated at significant quantities compared to low oxidation experiments. There was no acetate quantified in the original samples while small concentrations were detected in the NaOH treated samples indicating the presence of acetyl amides.

For amine-based products, EDA and FPZ were quantified with the highest concentration. The agreement between the formyl amides quantified on the anion IC through alkaline reversal and N-formyl PZ quantified directly on cation IC indicates that N-formyl PZ is likely the only formyl amide in solution, within experiment error of the two instruments. Total NH_4^+ concentration quantified after alkaline treatment is produced at a level similar to that of formate.

This is the only experiment where EDA concentration increased, reached a maximum and then decreased. In other oxidation experiments with appreciable degradation (e.g., OE2), the EDA concentration grew and reached a plateau, but did not decrease. The behavior of EDA clearly indicates it is a reaction intermediate. Analyzing the alkaline treated sample indicates that EDA is reacting to form amides. The total EDA concentration (Figure 8.16) grows and maintains a relatively level concentration. This shows that EDA is produced and form amides in the initial phases of PZ oxidation. Then, the generation of EDA slows due to the lower concentration of PZ, while the EDA in solution continues to form amides due to the presence of reactive carboxylate ions.

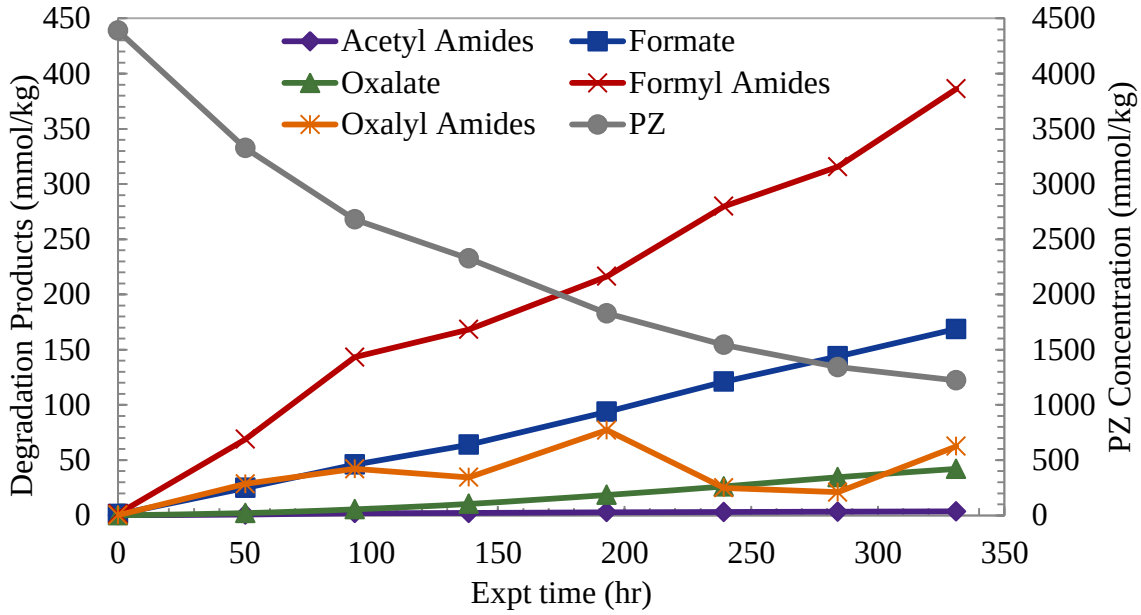

Figure 8.15: Profiles for PZ and heat stable salt products for experiment with high oxidation rates (OE25) (8 m PZ, 70 °C, 1400 rpm, 100 mL/min 94% O_2, 4 mM Cu^{2+})

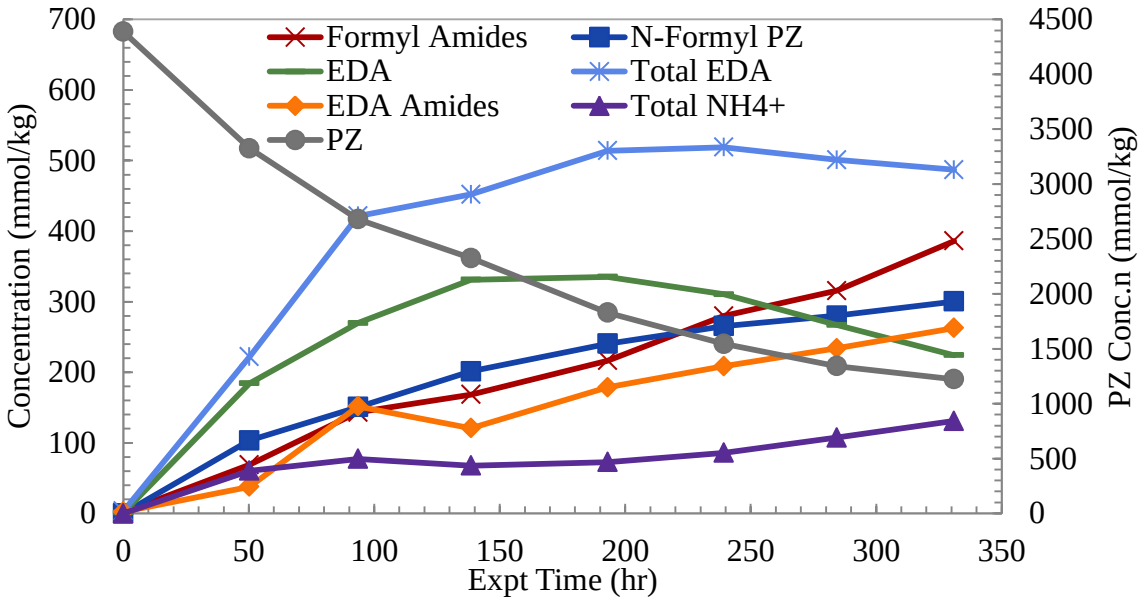

Figure 8.16: Profiles for PZ and amine products for experiment with high oxidation rates (OE25) (8 m PZ, 70 °C, 1400 rpm, 100 mL/min 94% O_2, 4 mM Cu^{2+})

The cation and anion IC chromatograms from the initial and final sample are compared in Figure 8.17 and Figure 8.20, respectively, while an enlarged view of the cation IC chromatogram is shown in Figure 8.18 to show detail. Cation and anion IC chromatograms for the final sample before and after alkaline treatment for amide reversal are shown in Figure 8.19 and Figure 8.21, respectively, to examine the impact of amide degradation products. This set of chromatograms is by far the most interesting achieved for oxidized PZ, showing numerous unidentified peaks on both anion and cation IC.

In the cation IC chromatograms, there are clear peaks for PZ, EDA, FPZ, and NH_4^+ that are visible in the expanded view (Figure 8.17). A significant decrease in the PZ peak is also visible, showing the 72% loss of PZ found in this experiment. Upon closer inspection (Figure 8.18), there are also numerous, smaller unidentified peaks that are detected on the cation IC after oxidation. There are five peaks that are likely monoamines (labeled as unidentified monoamines (UM)), and 5 peaks that are likely di-, tri-, or quadamines (labeled as unidentified polyamines (UP)). Although the peaks are small in comparison with EDA and PZ, they represent new oxidation products that were not found in previous experiments with lower oxidation rates. IC-MS work was attempted to identify the peaks, but did not prove conclusive to render identification.

Observing the changes to the cation IC chromatogram after treatment with NaOH also provides insight into the possible structure of the unidentified peaks (Figure 8.19). After treatment, which is intended to convert amides back to their respective amine and carboxylate ion portions, the peaks of two of the unidentified monoamines and the two dominant unidentified polyamines are decreased significantly. This indicates that these peaks, like the peak for FPZ, represent amides that are eliminated after alkaline treatment. These peaks are labeled as unidentified amides (UA) in the figure. Three monoamines peaks and smaller concentration polyamine peaks remain after alkaline treatment. This

sample is highly oxidized and numerous types of amides involving PZ, EDA, NH_3, formate, acetate, or oxalate, could hypothetically be formed and mono-amides of PZ and EDA should respond on the cation IC because of the second amino function

The anion IC chromatograms from this experiment are also interesting due to the appearance of new degradation product peaks. Comparing the initial and final sample in Figure 8.20, it is clear that several degradation products were generated. The only peaks in the initial sample represent CO_3^{-2} and SO_4^{-2}. It should be noted that the position and shape of the CO_3^{-2} peak shifted in the degraded sample, as has been observed previously with significant changes in speciation or pH. After oxidation, there are still peaks for these two background compounds, but they have been swamped by the peaks representing degradation products. Formate and oxalate are the two largest peaks at retention times of approximately 20 and 27 minutes, respectively. There is not a peak for acetate, since acetate was not found in the original samples. Small concentrations of nitrite (NO_2^-) and nitrate (NO_3^-) were detected in this experiment and those peaks are labeled accordingly. This is the only experiment where appreciable quantities of either of these N-based ions were detected.

The peak eluting at approximately 20.5 minutes, right after formate, has been tentatively identified as the mono-oxalyl amide of PZ, also known as N-oxalyl PZ. Since N-oxalyl PZ has an exposed anionic functionality on the oxalate, it should be detected by anion IC. Chromatograms from the original and NaOH treated final samples from OE25 are compared in Figure 8.21. The peak thought to be N-oxalyl PZ and the third unidentified peak (labeled UA) disappear when treated with NaOH, indicating they are both amides. This confirms the possible identity of the N-oxalyl peak, although either peak could represent this molecule since a standard is not available to analyze. Mono-amides have been seen in previous work on other amines where the NaOH treatment

requires more time to fully reverse the dioxalyl amide of certain amines (Voice, 2010). The slower recovery of oxalate was also explored in the analysis of the NaOH treatment procedure discussed in section 3.1.6. The amide reaction of PZ with oxalate is especially complex given that PZ has two functional amino groups and oxalate has two carbonyl functional groups that can form a double amide. The same is true for EDA, the dominant amine degradation product for PZ oxidation, which complicates the amide generation and analysis process. The three possible amide structures of the reaction of PZ or EDA with oxalate are shown in Figure 8.22. This adds a third possible amide compared to formate and acetyl-based amides which cannot form an amide that is observable through anion IC. The identity of the last unknown anion peak (labeled U) is not known at this time.

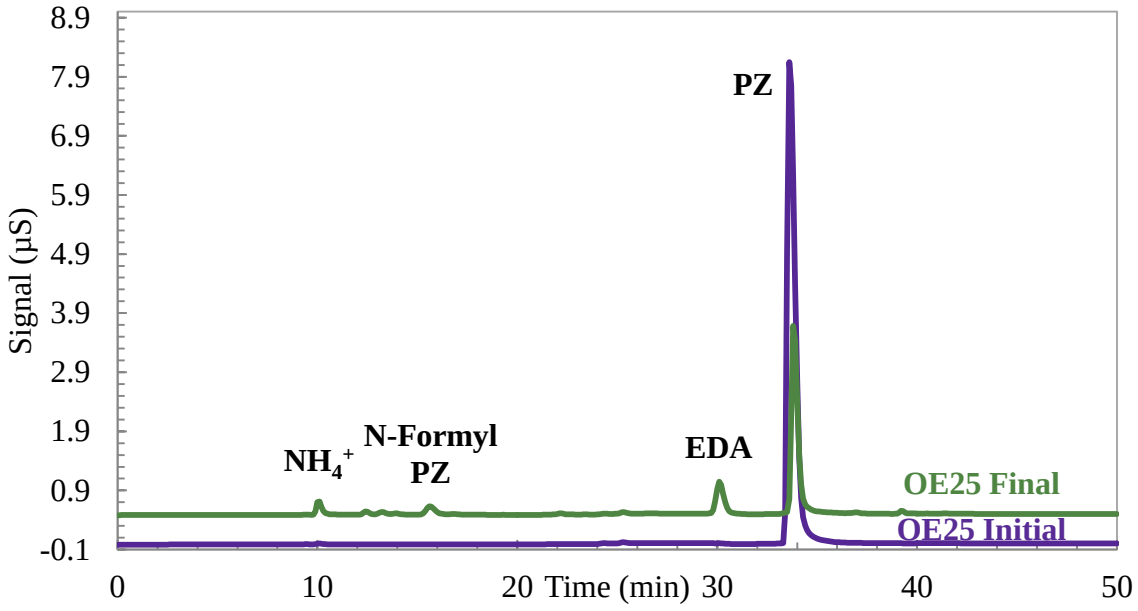

Figure 8.17: Comparison of cation IC chromatograms at the start and end of OE25 demonstrating high oxidation rates (signals are offset 0.5 µS for clarity) (8 m PZ, 70 °C, 1400 rpm, 100 mL/min 94% O_2, 4 mM Cu^{2+}, 14 days)

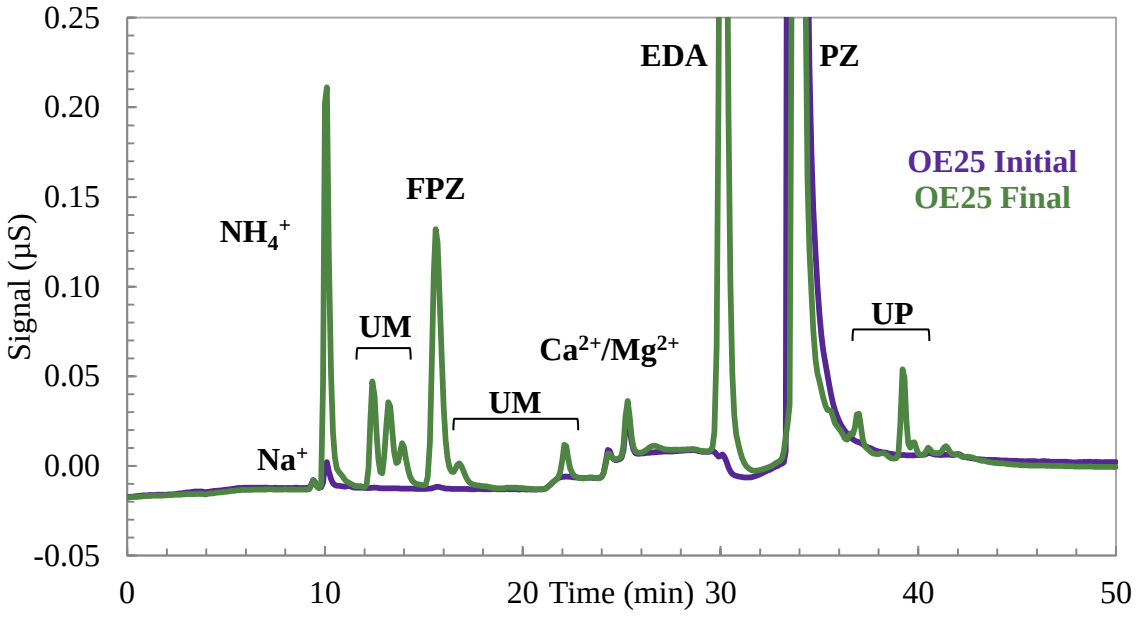

Figure 8.18: Comparison of cation IC chromatograms at the start and end of OE25 demonstrating high oxidation rates (enlarged); abbreviations: UM, unidentified monoamines; UP, unidentified polyamines (8 m PZ, 70 °C, 1400 rpm, 100 mL/min 94% O_2, 4 mM Cu^{2+}, 14 days)

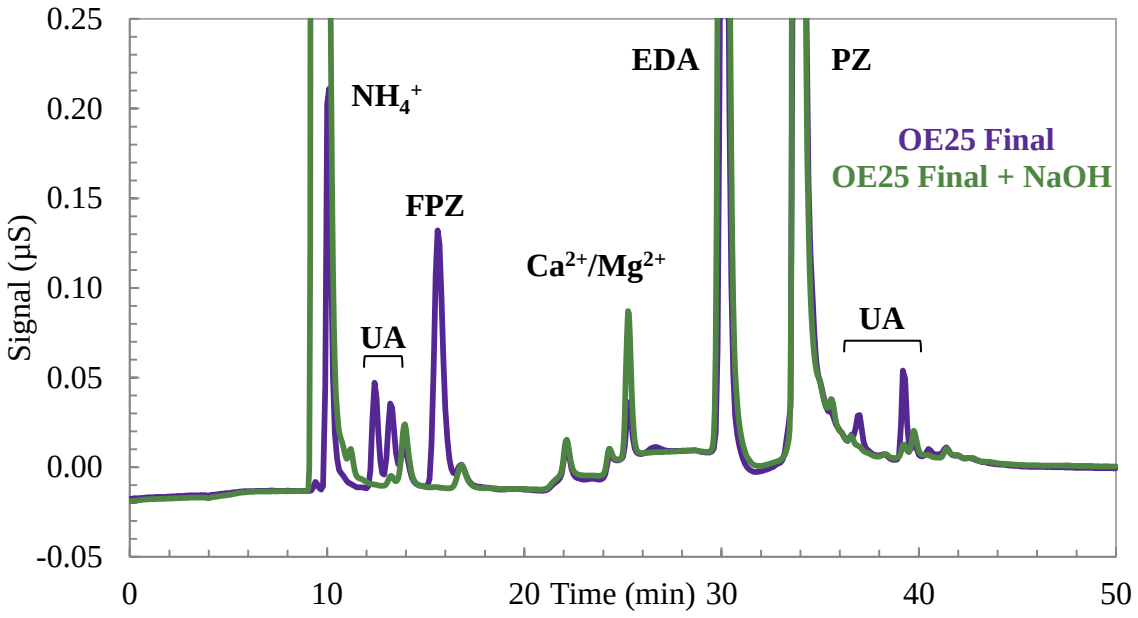

Figure 8.19: Comparison of cation IC chromatograms for the final sample of OE25 before and after NaOH treatment (enlarged); UA indicates unidentified amides (8 m PZ, 70 °C, 1400 rpm, 100 mL/min 94% O_2, 4 mM Cu^{2+}, 14 days)

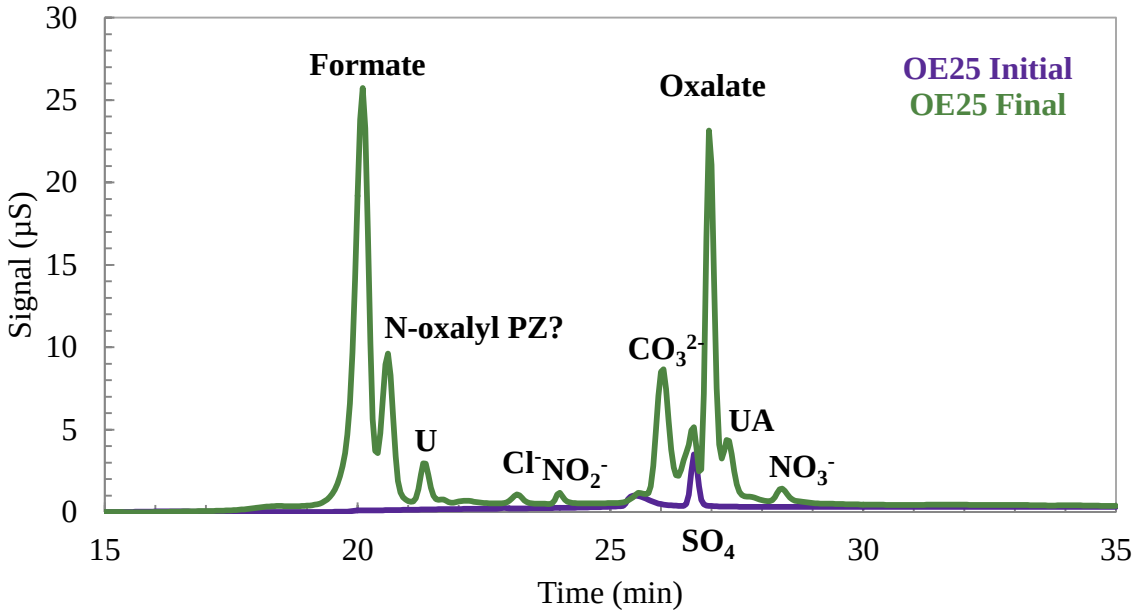

Figure 8.20: Comparison of anion IC chromatograms at the start and end of OE25 demonstrating high oxidation rates; abbreviations: U, unidentified; UA, unidentified amide (8 m PZ, 70 °C, 1400 rpm, 100 mL/min 94% O_2, 4 mM Cu^{2+}, 14 days)

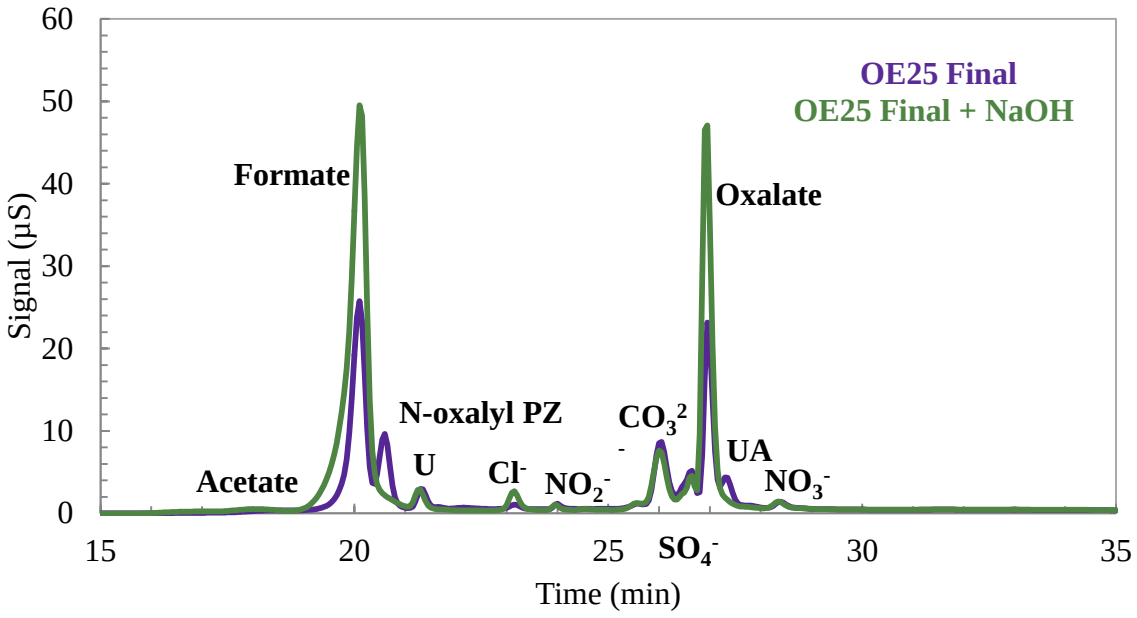

Figure 8.21: Comparison of anion IC chromatograms for the final sample of OE25 before and after NaOH treatment; abbreviations: U, unidentified; UA, unidentified amide (8 m PZ, 70 °C, 1400 rpm, 100 mL/min 94% O_2, 4 mM Cu^{2+}, 14 days)

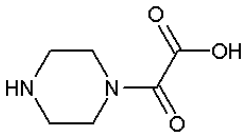

N-oxalyl PZ
(CAS: 691394-09-9)

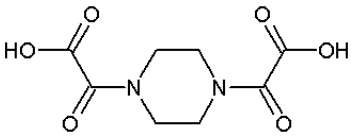

N,N-dioxalyl PZ

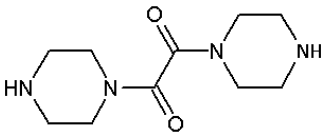

1,1'-(1,2-dioxo-1,2-ethanediyl)bis PZ
(CAS: 105807-56-5)

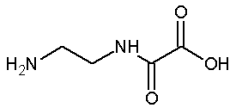

N-oxalyl EDA
(2-[(2-aminoethyl)amino]-2-oxo-acetic acid
(CAS: 5238-84-6)

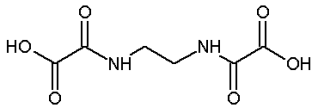

N,N-dioxalyl EDA

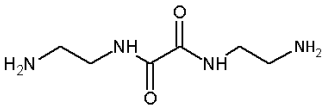

N,N'-bis(2-aminoethyl)-ethanediamide
(CAS: 4312-20-3)

Figure 8.22: Chemical structures of products of reaction of oxalate with PZ or EDA

This experiment represents a new area of PZ study where highly oxidized PZ solutions can be analyzed in a sophisticated way to identify more degradation products than just carboxylate ions, EDA, and N-formyl PZ. Identification of these peaks could lead to new understanding of the PZ oxidation pathways that are not well understood at this point due to the lack of overall PZ oxidation usually observed under conditions that are representative of anticipated absorber conditions. On the other hand, this type of study may not be useful since PZ solutions in service would not be expected to reach this level of oxidation, even in the presence of a Cu^{2+}-based corrosion inhibitor.

8.3.2 Mass balances achieved in PZ oxidation

The oxidation experiments described in this project all suffer from a common failure to close the overall mass balance. The PZ loss observed through cation IC is not balanced with the generation of degradation products. This was true of both the nitrogen (N) and carbon (C) balance and was observed in every experiment, without fail. Three example mass balances are discussed in this section to provide an example of the mass

balanced closure usually achieved. The two experiments representing the low (OE18) and high (OE25) level of oxidation are each discussed, as well as one of the baseline experiments (OE11). The range of mass balance closure observed in all 28 oxidation experiments can be represented by these three experiments.

In the following three tables (Table 8.3 to Table 8.5) the amount of N and C in PZ lost during each oxidation experiment is shown along with the final concentrations of the quantified degradation products. For the degradation products, the percentage that each represents in terms of the amount of PZ lost is also shown as a percentage. This represents the percent of PZ lost that was recovered in each of the products in terms of either N or C. The last row of the table shows the total N or C recovered in degradation products as a percent of the overall PZ loss. If all of the lost PZ was recovered in degradation products, as in the ideal scenario, this last row would be 100. Degradation products not containing either N or C are indicated as not applicable (NA) in each case. When a listed product was tested for but not found, a concentration and percentage of zero are shown in the table.

The N and C mass balanced achieved in the experiment showing low levels of oxidation, OE18, is shown in Table 8.3. During the experiment, only 65.9 mmole per kg of PZ was lost or 131.7 mmole N from PZ per kg and 263.4 mmole C from PZ per kg. Small concentrations of formate (2.1 mmole per kg) and formyl amides (2.2 mmole per kg) were produced while no EDA was detected. Based on observations in previous oxidation experiments, this concentration of formyl amides was assumed to all be N-formyl PZ and the appropriate N and C concentrations, 4.4 and 11.1 mmole per kg, respectively, were included in the mass balance. No other N containing degradation products were detected. Very low levels of glycolate, acetate, and oxalate were also

found that accounted for a total of only 0.5 mmole per kg. Overall, only 3.4% and 5.2 % of the lost PZ N and C were recovered, respectively, in detectable degradation products.

Table 8.3: Nitrogen and Carbon Mass Balance in OE18 (8 m PZ, 55 °C, 1400 rpm, 100 mL/min 98% O_2, SSM, 24 days)

		Nitrogen Balance		Carbon Balance	
	Conc.	N Conc.	PZ N Loss	C Conc.	PZ C Loss
	mmol/kg	mmol/kg	%	mmol/kg	%
PZ Lost	65.9	131.7	-	263.4	-
DEGRADATION PRODUCTS:					
N-Formyl PZ	2.2	4.4	3.4	11.1	4.2
Formate	2.1	NA	-	2.1	0.8
Oxalate, Acetate, and Glycolate	0.2	NA	-	0.5	0.2
Total PZ Mass Recovered in Products		4.4	**3.4**	13.6	**5.2**

This experiment exhibited a very low level of PZ loss during oxidation, even lower than all four baseline experiments. In order to put this experiment in perspective, the baseline experiment with the most PZ loss, OE11, is also analyzed for its mass balance closure. Numerous PZ oxidation experiments suffered from PZ loss rates that fell between OE18 and OE11, so the analysis of these two mass balances should give a representative picture of what would be expected in experiments with low or even negligible PZ loss rates. The experiments with these low rates of oxidation are essentially all experiments performed in the absence of Cu^{2+} and at low temperature (55 °C), as is discussed in this chapter and the subsequent chapter.

The N and C mass balances achieved in this baseline experiment, OE11, are shown in Table 8.4. In this experiment, 292.9 mmole PZ per kg was lost, accounting for 585.7 and 1171.5 mmole N and C per kg, respectively. The generation of degradation products was similar to the previously example as formate (1.0 mmole per kg) and formyl amides (1.44 mmole per kg) were detected along with a low concentration of EDA (11.7

mmole per kg). As with the previous example, all of the formyl amides were assumed to be N-formyl PZ for the mass balance. Glycolate, acetate, and oxalate were not detected. Based on the TOC and TN results discussed above, the concentration of volatile N from that analysis, 426.4 mmole N per kg, was included in the mass balance. With this inclusion, the N mass balance improves significantly from 2.5 to 75.3% of the lost PZ recovered as products. On the other hand, only 1.7 % of the loss PZ C was recovered in products. The generation of degradation products was of a similar magnitude in this experiment compared with OE18, while the overall PZ loss was higher, leading to worse mass balance closure. The TOC analysis discussed in section 8.2.5 demonstrated that there are unidentified C-based degradation products that have not been quantified that could help with the overall mass balance closure. Missing degradation products will also contain N functionality based on the 24.7% of N that is yet to be recovered.

Table 8.4: Nitrogen and carbon mass balance in OE11 (8 m PZ, 55 °C, 1400 rpm, 100 mL/min 98% O_2, no catalyst, 13 days)

		Nitrogen Balance		Carbon Balance	
	Conc.	N Conc.	PZ N Loss	C Conc.	PZ C Loss
	mmol/kg	mmol/kg	%	mmol/kg	%
PZ Lost	292.9	585.7	-	1171.5	-
DEGRADATION PRODUCTS:					
N-Formyl PZ	1.4	2.9	0.5	7.2	0.6
EDA	5.8	11.7	2.0	11.7	1.0
Formate	1.0	NA	-	1.0	0.1
Oxalate, acetate, and glycolate	0	NA	-	0	-
Volatile N	426.4	426.4	72.8	NA	-
Total PZ Mass Recovered in Products		441.0	**75.3**	19.8	**1.7**

On the opposite extreme, the mass balance in an experiment where a high rate of oxidation was achieved (OE25) can be examined. As discussed previously in this section, the conditions of OE25 represent the maximum acceleration of oxidation through

the addition of Cu^{2+}, the most potent catalyst for PZ degradation (discussed in further detail in section 9.1.3), high temperature, and high O_2 content. This experiment had the highest concentrations of degradation products detected in any experiment and represent the best chance for mass balance closure in this study.

The N and C balances for OE25 are shown in Table 8.5. In this experiment, 3166.6 mmole PZ per kg was lost or 6333.3 mmole N from PZ per kg and 12666.5 mmole C from PZ per kg. EDA and FPZ were the most dominant products with 974.0 and 300.3 mmole per kg at the end of the experiment, respectively. Ammonium (NH_4^+), nitrite (NO_2^-), and nitrate (NO_3^-) were also found in small quantities. It should be noted that for cationic molecules, such as EDA and NH_4^+, the total concentrations quantified after alkaline treatment were used in the mass balance to include the portion as the free molecule and the portion that was tied up as an unidentified amide. Concentrations of oxalate and acetate after alkaline treatment, representing both free carboxylate ions and carboxylate as amides, were included in the mass balance. For formate, free formate from the original sample was included in the mass balance. The concentration of formyl amides determined from alkaline treatment was adjusted to remove the concentration of FPZ quantified directly from cation IC to leave non-PZ formyl amides. Based on the results of the TOC and TN analysis for this experiment, the volatile N is also included in the mass balance although the specific species are not known. The inclusion of volatile N determined from the TN analysis improved the N balance from only 27% of the lost PZ N recovered to nearly 69%. Only 23.3% of the loss PZ C was recovered in detectable degradation products. There is still unidentified degradation products that contain both C and N based on the lack of mass balance closure in either cases.

The amide data for this experiment is especially interesting and represents how anion and cation pairs that form amides can distribute themselves in solution. The

concentrations of the anion and cation portions of potential amides are shown in Table 8.6 for the final sample of OE25. All values are the increase in concentration between the alkaline treated and original samples. All six species shown, formate, acetate, oxalate, PZ, EDA, and NH_4^+, were all present in the oxidized solution as some form of an amide since their concentration increased after alkaline treatment. FPZ can be quantified directly and had a concentration of 300.3 mmole per kg at the conclusion of the experiment. Unfortunately, the PZ concentration was not increased by this value during the reversal, indicating some disparity in the data. This is not surprising given that PZ is the most dominant species in solution and the error in measuring a small increase in a large peak on the cation IC is high based on many analytical factors.

Table 8.5: Nitrogen and Carbon Mass Balance in OE25 (8 m PZ, 70 °C, 1400 rpm, 100 mL/min 94% O_2, 4 mM Cu^{2+}, 14 days)

		Nitrogen Balance		Carbon Balance	
	Conc. mmol/kg	N Conc. mmol/kg	PZ N Loss %	C Conc. mmol/kg	PZ C Loss %
PZ Lost	3167	6333	-	12667	-
DEGRADATION PRODUCTS:					
EDA	487.0	974.0	15.4	974	7.7
N-Formyl PZ	300.3	600.6	9.5	1501.6	11.9
Formate	168.7	NA	-	168.7	1.3
NH_4^+	130.9	130.9	2.1	NA	-
Oxalate and oxalyl amides	104.6	NA	-	209.1	1.7
Formyl amides (non-PZ)	85.8	NA	-	85.8	0.7
NO_2^- and NO_3^-	4.7	4.7	0.1	NA	-
Acetate and acetyl amides	3.6	NA	-	7.2	0.1
Volatile N (unknown species)	2649	2649	41.8	NA	-
Total PZ Mass Recovered in Products		4359	**68.8**	2947	**23.3**

Assuming that FPZ was the only PZ-based amide, this leaves only 85.8 mmole formate per kg that exists in another amide form. This form could be either formamide (the amide of formate and NH_3) or N-formyl EDA, based on the cation data. The

quantified increase of EDA and NH_4^+ is much higher in concentration than the recovered anions and indicates additional unidentified anion portions of amines. One explanation could be unidentified peaks on the anion IC chromatogram or anion amide pairs that would not be detected on the anion IC. The oxalyl amides of EDA or NH_4^+ with two amines forming two amide functions on one oxalyl group are also possibilities. The oxalyl amides of PZ and EDA were discussed in the preceding section, and the mono-oxalyl EDA (N-oxalyl EDA) could also exist and account for one of the unidentified peaks on the anion IC chromatogram for this sample. Although the amide mass balance also does not close for this experiment, the detected molecules indicate a complicated reaction scheme and distribution of amide reactants that could see amides representing every combination of the detected anion and cation portions of amides present in a highly oxidized solution.

Table 8.6: Amide balance in final sample of OE25 (8 m PZ, 70 °C, 1400 rpm, 100 mL/min 94% O_2, 4 mM Cu^{2+}, 14 days)

Anion	Concentration mmol/kg	Cation	Concentration mmol/kg
Formyl	386.1	PZ	230.7
Acetyl	3.6	EDA	262.7
Oxalyl	62.5	NH_3	127.8
TOTAL	452.2	TOTAL	621.2

This highly oxidized sample represents the best mass balance closure of any oxidized PZ experiment. This represents where PZ oxidation research lies in terms of degradation rates and the production of degradation products. Although high concentrations of products were quantified, there is still work to be done to identify the additional products. A vast majority of experiments in this project were performed on solutions that were very slow to oxidize, complicating the problem of closing a mass balance due to very low concentrations of detectable degradation products.

8.3.3 Amino Acid (AA-LC) analysis of oxidized PZ

One additional advanced chromatographic technique was employed in an effort to find degradation products. Amino acid LC (AA-LC) was used to analyze oxidized PZ samples in an effort to identify and quantify new oxidation products that would satisfy the mass balance. An experiment with a very low level of oxidation (OE26) and one highly oxidized experiment (OE25) were analyzed using AA-LC. The initial and final chromatograms for the low level of oxidation experiment are shown in Figure 8.23. Chromatograms from the highly oxidized experiment at the start, after 4 days, and at the end of the experiment are compared Figure 8.24. The large peak between retention times of 5 and 13 minutes is the initial PZ charge in each figure. The bump between 25 and 29 minutes is part of the eluent ramp and is seen in each initial sample.

As with other techniques, the low level of oxidation seen in OE26 did not produce peaks on the AA-LC chromatogram. There are few changes in the chromatogram after 14 days of degradation and there were not significant amino acids produced during oxidation. On the other hand, the highly oxidized OE25 experiment shows the generation of numerous peaks on the AA-LC chromatogram, along with a significant decrease in the PZ peak. The shape of the chromatogram changes significantly over 14 days and multiple peaks are seen to grow with time, indicating the presence of amino acid-based degradation products. Unfortunately, none of the peaks matched standards of glycine, bicine, 2-piperazinone, 2,5-pipearzinone (glycine anhydride), or N-(2-aminoethyl) glycine. None of the peaks on the AA-LC chromatogram have been identified.

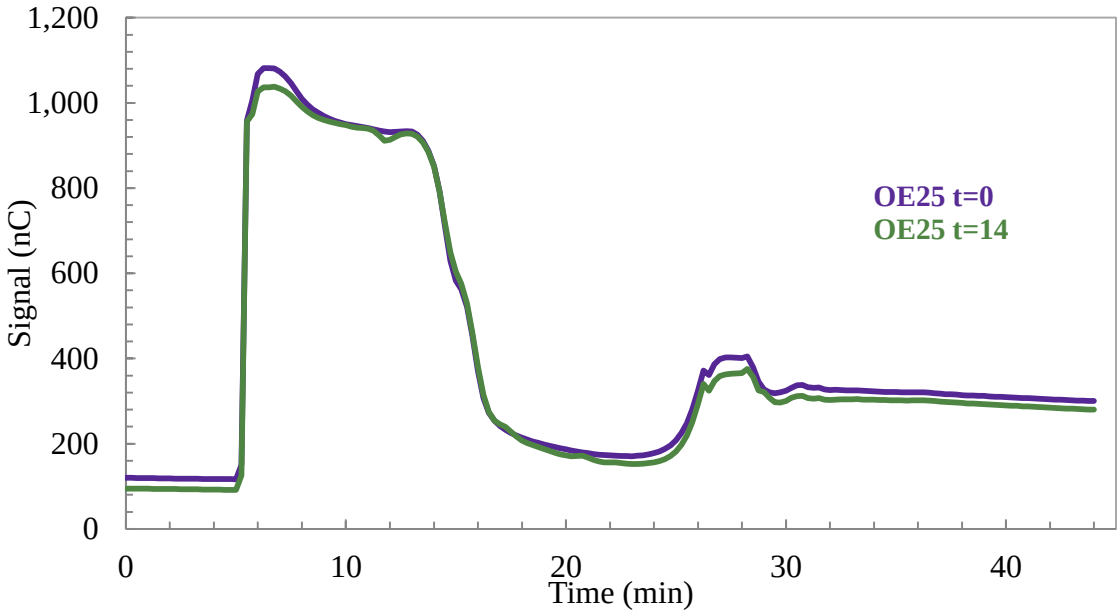

Figure 8.23: Amino acid (AA-LC) analysis of low level oxidation of PZ (OE26) showing little evidence of oxidation (8 m PZ, 70 °C, 1400 rpm, 100 mL/min 94% O_2, SSM, 14 days)

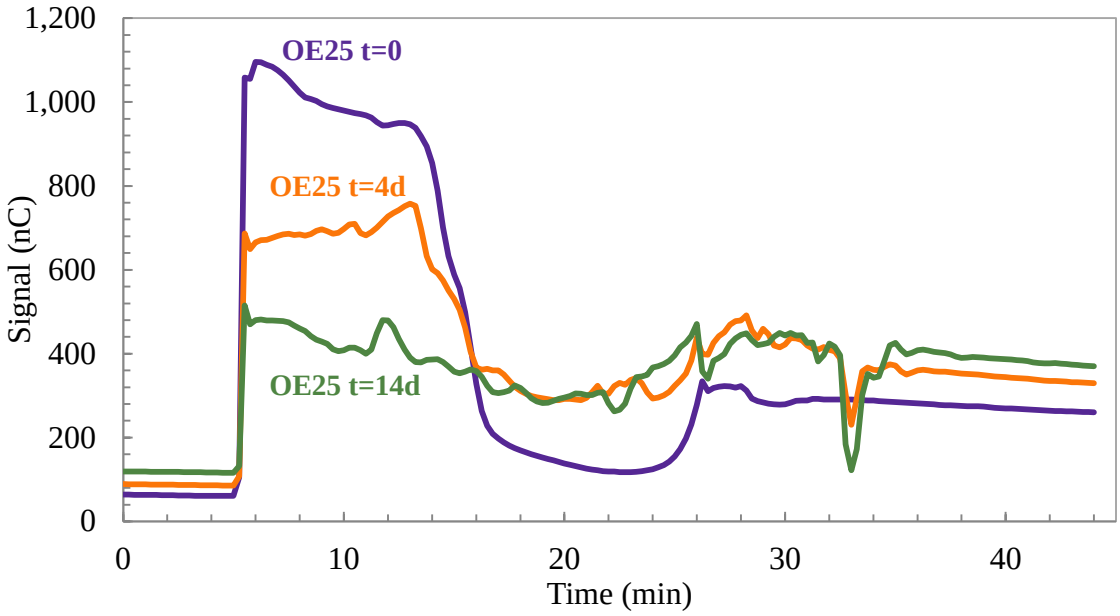

Figure 8.24: Amino acid (AA-LC) analysis of highly oxidized PZ (OE25) showing unidentified peaks (8 m PZ, 70 °C, 1400 rpm, 100 mL/min 94% O_2, 4 mM Cu^{2+}, 14 days)

8.3.4 Postulated oxidation products not detected

A variety of molecules have been postulated as potential oxidation products of concentrated PZ that have not been conclusively confirmed in degraded solutions. Oxidation typically entails fragmentation of the original amine along with condensation of fragments to produce a host of possible molecules. Although PZ oxidation has not been well studied on its own, analogies to both the oxidation of the PZ moiety in larger molecules and the oxidation of alkanolamines can be made to provide suspected oxidation products for concentrated PZ. Predicting basic mechanisms of oxidation can also allow for new oxidation products to be postulated. The suspected oxidation products discussed in the following paragraphs are shown in Figure 8.25. In general, aldehydes, alcohols, ureas, amino acids, and oxidized PZ molecules are suspected.

Formaldehyde is an important aldehyde that is suspected to play an important role in the oxidation mechanisms of PZ. Formaldehyde is likely produced as an oxidized fragment of the PZ ring structure and is highly reacted. Previous oxidation experiments performed on PZ using chloride dioxide (ClO_2) as the oxidant were found to produce EDA and formaldehyde (Dennis et al., 1967). Generation of EDA is common to all medium to highly oxidized PZ solutions and in the most basic oxidative mechanism, it is expected that for each PZ oxidized, an EDA and two formaldehyde-type molecules are formed. EDA is stable and persists to be quantified, while formaldehyde reacts to other products. Attempts were made to quantify formaldehyde in liquid solution using a colorimetric method, but were unsuccessful due to the reliance on response in the visible range when degraded solutions containing metal are usually highly colored (Fregert et al., 1984; Miksch et al., 1981). Although not successfully identified and quantified, it is very likely that formaldehyde plays an important role in the production of formate and other fragmented or condensed oxidation reactants. Formaldehyde and PZ are known to react

to form polymeric PZ structures, as discussed in section 6.1.5. Other suspected aldehydes and alcohols include, but are not limited to acetaldehyde, hydroxyacetaldehyde, methanol, ethanol, and ethylene glycol.

The analogy of ciprofloxacin oxidation was discussed in section 2.4.4 where the PZ moiety was oxidized using ozone, permanganate, or photo-oxidation. The oxidation products found in that study would, by extension, be expected in this type of PZ oxidation. The analogous PZ-based oxidation products would be EDA, ammonia or ammonium, 2-piperazinone, 2,5-piperazinedione, 2-piperazinol (the carbinolamine or hemiaminal form of PZ), and N-oxide piperazine. EDA and ammonium have been identified and quantified and are not included in the figure for this reason. Both 2-piperazinone and 2,5-piperazinedione were obtained as standards and tested on all the analytical methods (anion IC, cation IC, AA-LC, and HPLC) but were not matched to unknown peaks. N-oxide PZ and 2-piperazinol were not able to be obtained as standards, likely due to their reactive, unstable nature. It is believed that either would react during analysis in the cation IC and be detected as PZ or very near it in retention time.

Finally, a few other molecules are suspected based on specific suspected oxidation pathways. Reduction-oxidation pairs of reactions are believed to be occurring which could include a reaction at the amino function of a PZ molecule where the bond between the N and the α-carbon is reduced to a double bond while a separate reaction occurs to create an oxidized product. This would leave the imine form of PZ placing a double bond at the amino function (1,2,3,6-tetrahydro pyrazine), which could also be transferred to a double bond between the two carbons on the backbone of the molecule or the enamine form of PZ (1,2,3,4-tetrahydro pyrazine). Both the imine and enamine form of PZ should be detectable as a mono or diamine, if stable. Finally, molecules are suspected that would result from a ring opening of the PZ at the α-carbon. One such

molecule would be N-(2-aminoethyl) glycine, which is the oxidized, open form of the PZ molecule.

Formaldehyde
MW: 30.03
(CAS: 50-00-0)

Acetaldehyde
MW: 44.05
(CAS: 75-07-0)

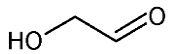

Hydroxyacetaldehyde
MW: 60.05
(CAS: 141-46-8)

Methanol
MW: 32.04
(CAS: 67-56-1)

Ethanol
MW: 46.07
(CAS: 64-17-5)

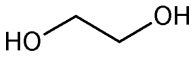

Ethylene Glycol
MW: 62.07
(CAS: 107-21-1)

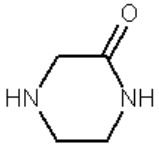

2-piperazinone
MW: 100.12
(CAS: 5625-67-2)

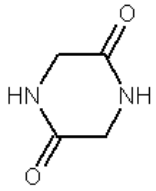

2,5-piperazinedione
MW: 114.10
(CAS: 106-57-0)

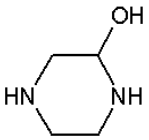

2-piperazinol (hemiaminal of PZ)
MW:102.14
(CAS: 1104858-53-8)

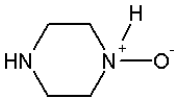

N-oxide PZ

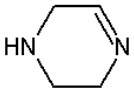

1,2,3,6-tetrahydro pyrazine
(imine of PZ)
MW: 84.12
(CAS: 77253-83-9)

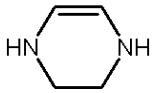

1,2,3,4-tetrahydro pyrazine
(enamine of PZ)
MW: 84.12
(CAS: 5194-05-8)

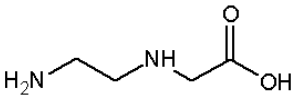

N-(2-aminoethyl)glycine
(AEG)
MW: 118.13
(CAS: 24123-14-6)

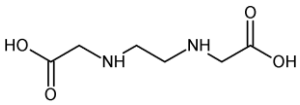

N,N'-1,2-ethanediylbis-
glycine
MW:176.17
(CAS: 5657-17-0)

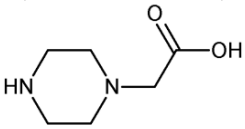

1-Piperazineaceticacid
MW: 144.17
(CAS: 37478-58-3)

Figure 8.25: Additional suspected oxidation products

Another category of possible oxidation products are triethylenediamine (TEDA) and its oxidized forms, shown in Figure 8.26. TEDA is suspected in both oxidation and thermal degradation and its oxidized forms include 1,4-Diazabicyclo[2.2.2]octan-2-one (an amide), 1,4-Diazabicyclo[2.2.2]oct-2-ene (an enamine), and 1,4-Diazabicyclo[2.2.2]octan-2-ol (a hemiaminal). TEDA has not been found in oxidized solutions, but is suspected to be present.

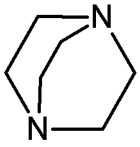

Triethylenediamine
MW: 112.17
(CAS: 280-57-9)

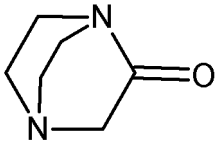

1,4-Diazabicyclo[2.2.2]octan-2-one (TEDA Amide)
MW: 126.16
(CAS: 146562-83-6)

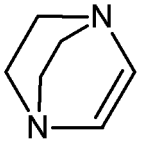

1,4-Diazabicyclo[2.2.2]oct-2-ene
(TEDA enamine)
MW: 110.16
(CAS: 122883-12-9)

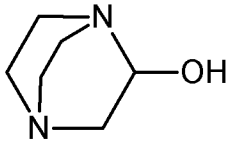

1,4-Diazabicyclo[2.2.2]octan-2-ol
(TEDA hemiaminal)
MS: 128.17
(CAS: 146562-84-7)

Figure 8.26: Suspected triethylenediamine-based oxidation products

8.4 EFFECT OF OXYGEN CONCENTRATION

The effect of O_2 concentration, or O_2 partial pressure, on the overall amine oxidation rate of concentrated PZ is a crucial parameter. CO_2 capture systems retrofitted to treat coal-fired power plant flue gas can expect between 5-7% O_2 entering the absorber between the bottom of the packing and the sump (Arnold et al., 1982). O_2 is absorbed by the amine solution as the flue gas rises through the packing and while retained in liquid residing in the sump. CO_2 capture systems treating natural gas flue gas can expect up to

12-15% O_2, making the amine choice in these systems very selective for oxidative resistance. The effect of O_2 concentration was examined in the presence of both stainless steel metals and Cu^{2+} for 8 m PZ.

8.4.1 Effect of oxygen on stainless-steel catalyzed oxidation

The oxidation of 8 m PZ was studied in the TOR with the standard SSM mixture (0.4 mM Fe^{2+}, 0.1 mM Cr^{3+}, and 0.05 mM Ni^{2+}) at 55 °C, agitation at 1400 rpm and 100 mL of mixed gas with 2% CO_2, maintaining a loading of 0.3 mole CO_2 per mole alkalinity. The inlet gas also contained either 40 (OE28) or 98% O_2 (OE18), with the balance made up with N_2 in the low O_2 case.

The PZ loss and generation of degradation products for both the low and high O_2 cases are compared in Figure 8.27 and Figure 8.28, respectively. The PZ loss in both experiments is within the expected error in the oxidation experiment, as demonstrated by the baseline data shown in gray. A conclusion on the effect of O_2 is, therefore, not able to be conclusively made from the PZ loss data. On the other hand, the generation of degradation products shows an enhancement in the production of formate and total formate in high O_2 case although no EDA was detected. This enhancement demonstrates an increased rate of production of formate and formyl amides with increased O_2. Based on formate and total formate, the oxidation of PZ shows a tendency to oxidize by mechanisms that are at least first order in O_2 partial pressure. The low level of oxidation due to the weakness of stainless steel as a catalyst disallows more precise conclusions.

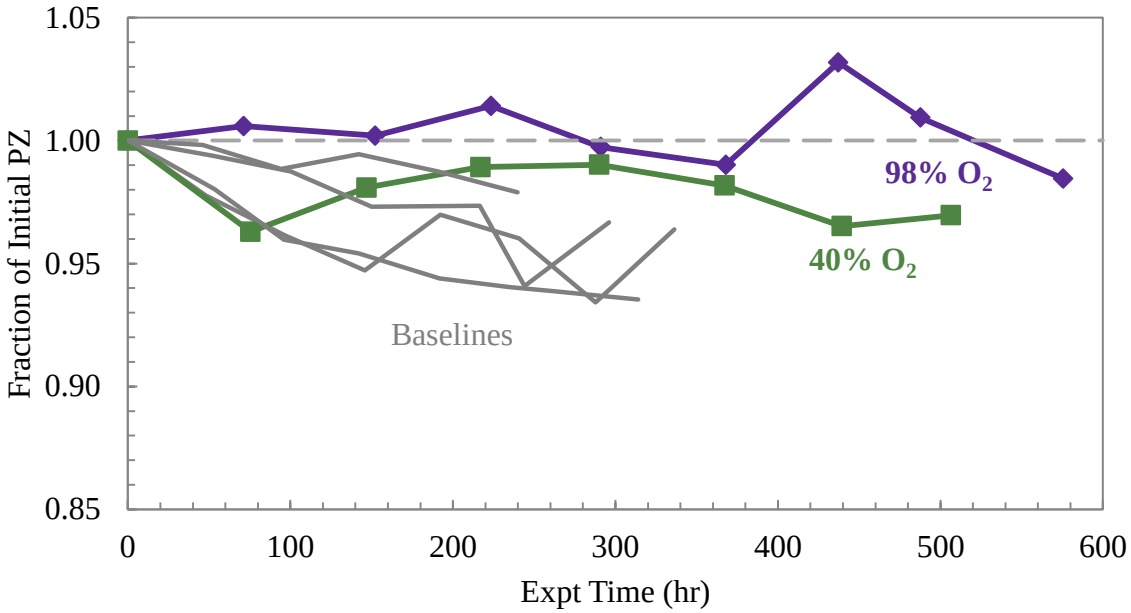

Figure 8.27: Effect of O_2 on PZ loss (TOR, 8 m PZ, 55 °C, 1400 rpm, 100 mL/min inlet gas with 40 (OE28) or 98% (OE18) O_2/2% CO_2 (α=0.3), SSM)

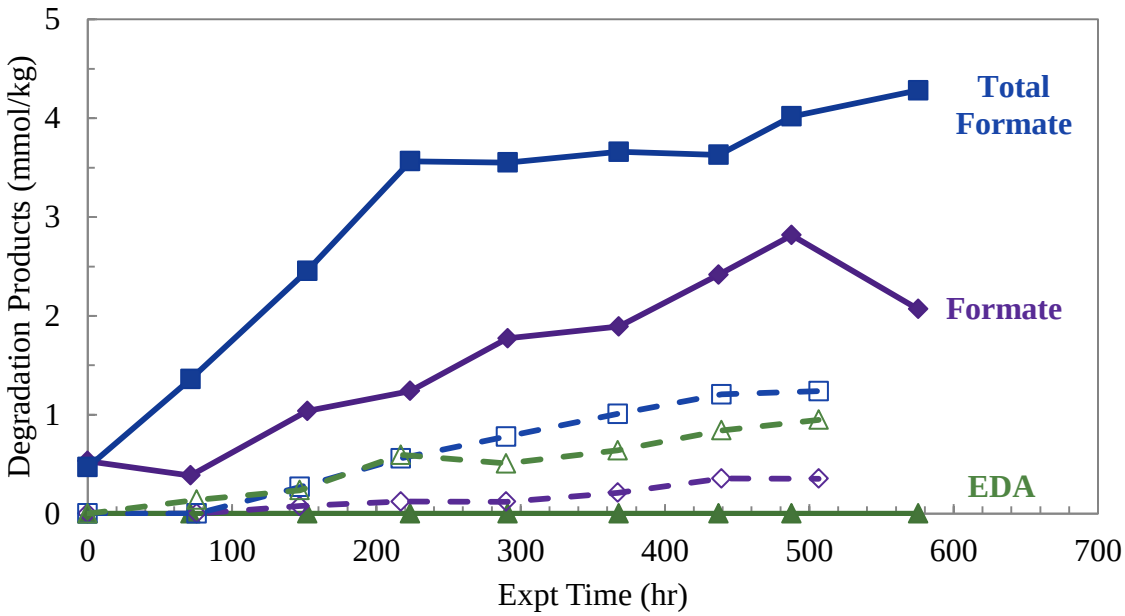

Figure 8.28: Effect of O_2 on generation of formate (♦), total formate (■), and EDA (▲) with 40% (open points, OE28) or 98% O_2 (filled points, OE18) (TOR, 8 m PZ, 55 °C, 1400 rpm, 100 mL/min inlet gas with 2% CO_2 (α=0.3), SSM)

8.4.2 Effect of oxygen on copper-catalyzed oxidation

8.4.2.1 Effect of oxygen on copper-catalyzed oxidation at 55 °C

The oxidation of 8 m PZ was also investigated in the OOR and TOR with 4 mM Cu^{2+} at 55 °C, agitation at 1400 rpm and 100 mL of mixed gas with 2% CO_2, maintaining a loading of 0.3 mole CO_2 per mole alkalinity. The inlet gas also contained either 40 (OE27, TOR) or 98% O_2 (OE2, OOR), with the balance N_2 in the low O_2 case. Provided that copper is a stronger catalyst for amine oxidation (see 9.1.3 for more detail), the effects of O_2 should be readily observable with a higher rate of oxidation.

The PZ loss and generation of degradation products for both the low and high O_2 cases are shown in Figure 8.29 and Figure 8.30, respectively. PZ loss and the generation of all three of the major degradation products are strongly enhanced by an increase in O_2 content. After 450 hours of oxidation, an increase in O_2 content from 40 to 98%, or 245%, enhanced PZ loss by approximately 240% in terms of the fraction of initial loss. PZ loss at 55 °C is therefore approximately first order in O_2 content in the inlet gas. Formate, total formate, and EDA generation were all increased with the higher O_2 content. After 450 hours of oxidation, EDA, total formate, and formate production were increased 180, 340, and 370%, respectively, as the O_2 content increased 250%. The generation of these products is not in the same ratio in each case, indicating that the O_2 content or rate of oxidation may impact the mixture of degradation products generated.

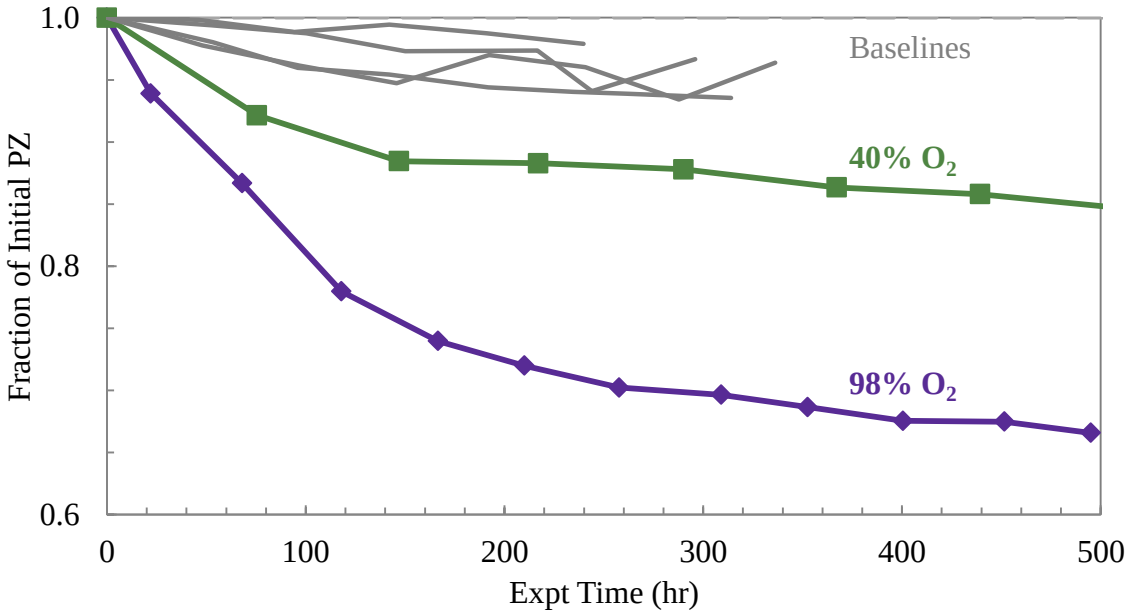

Figure 8.29: Effect of O_2 on PZ loss (8 m PZ, 55 °C, 1400 rpm, 100 mL/min inlet gas with 40 (OE27) or 98% (OE2) O_2/2% CO_2 (α=0.3), 4 mM Cu^{2+})

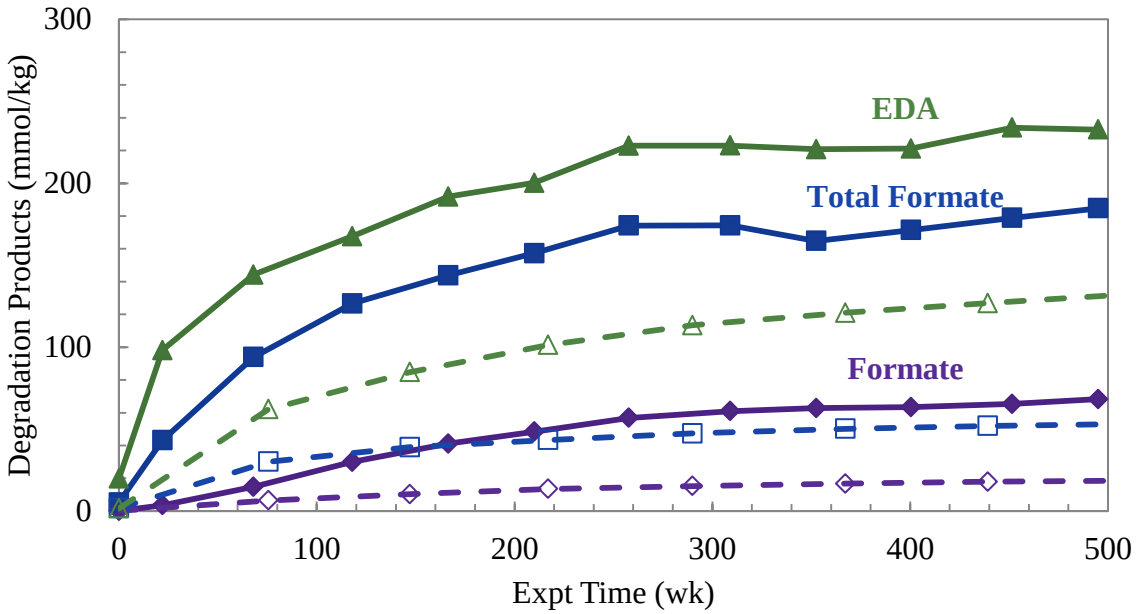

Figure 8.30: Effect of O_2 on generation of formate (♦), total formate (■), and EDA (▲) with 40% (open points, OE27) or 98% O_2 (filled points, OE2) (8 m PZ, 55 °C, 1400 rpm, 100 mL/min inlet gas with 2% CO_2 (α=0.3), 4 mM Cu^{2+})

8.4.2.2 Effect of oxygen on copper-catalyzed oxidation at 70 °C

Finally, the effect of oxidation at high temperature was investigated. Solutions of 8 m PZ were oxidized in the TOR with 4 mM Cu^{2+} at 70 °C, agitation at 1400 rpm and 100 mL of mixed gas with 6% CO_2, maintaining a loading of 0.3 mole CO_2 per mole alkalinity at this elevated temperature. The inlet gas also contained either 40 (OE23) or 94% O_2 (OE25), with the balance N_2 in the low O_2 case.

The PZ loss and generation of degradation products for both the low and high O_2 cases are shown in Figure 8.31 and Figure 8.32, respectively. As found in the low temperature Cu^{2+}-catalyzed experiments, the concentration of O_2 has strong effect on both PZ loss and product generation. The PZ loss is nearly doubled from 35 to 72% of the initial PZ degraded after 350 hours when the O_2 partial pressure is increased from 40 to 94% of the inlet gas. That is to say, a 235% increase in O_2 partial pressure increased PZ loss by 206%. As with the low temperature experiment, the ratio of increase in O_2 content and PZ loss is roughly the same, indicating that PZ oxidation is first order in O_2 under these conditions. For this case, however, this observation may not fully represent the system because of data quality issues in the 40% O_2 experiment (OE23). The change in PZ concentration in the initial sample was thought to be due to additional water loss because the TOR flange clamp was not fully tightened. It also may represent real PZ loss since the concentration profile for the degradation products does not seem affected. An increase in the generation of degradation products in the high O_2 experiment was observed for all three major products, supporting findings from the PZ loss data.

This direct dependence on O_2 concentration found at 55 and 70 °C indicates that for Cu^{2+}-catalyzed oxidation, the degradation could be O_2 mass transfer controlled. The PZ oxidation process uses as much O_2 as it can find in solution. The data is also consistent with a kinetic mechanism that is first order in O_2.

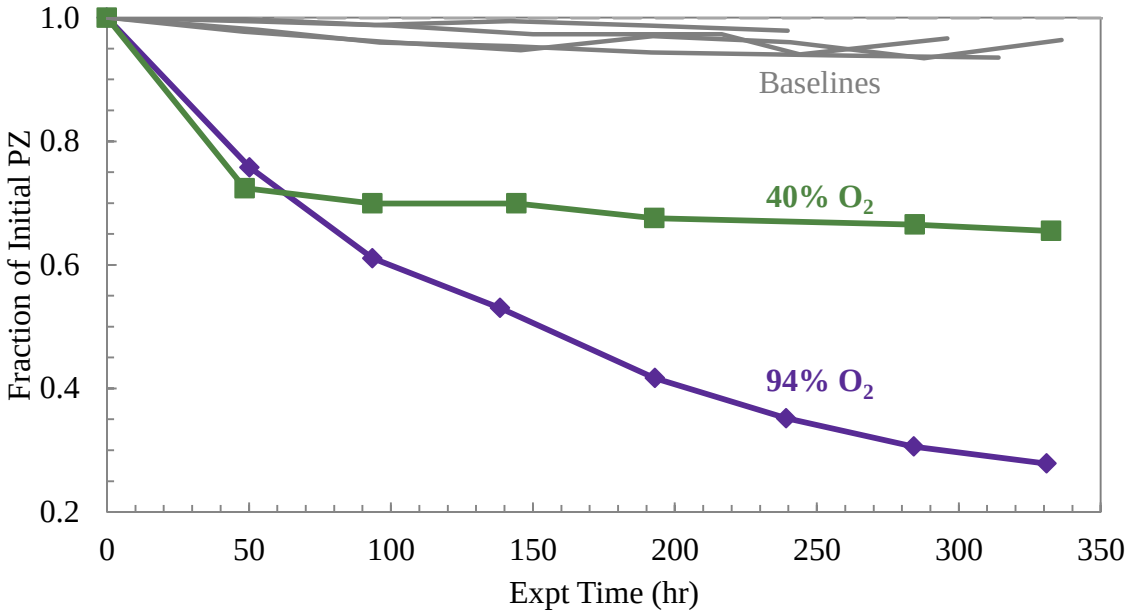

Figure 8.31: Effect of O_2 on PZ loss (TOR, 8 m PZ, 70 °C, 1400 rpm, 100 mL/min inlet gas with 40 (OE23) or 94% (OE25) O_2/6% CO_2 (α=0.3), 4 mM Cu^{2+})

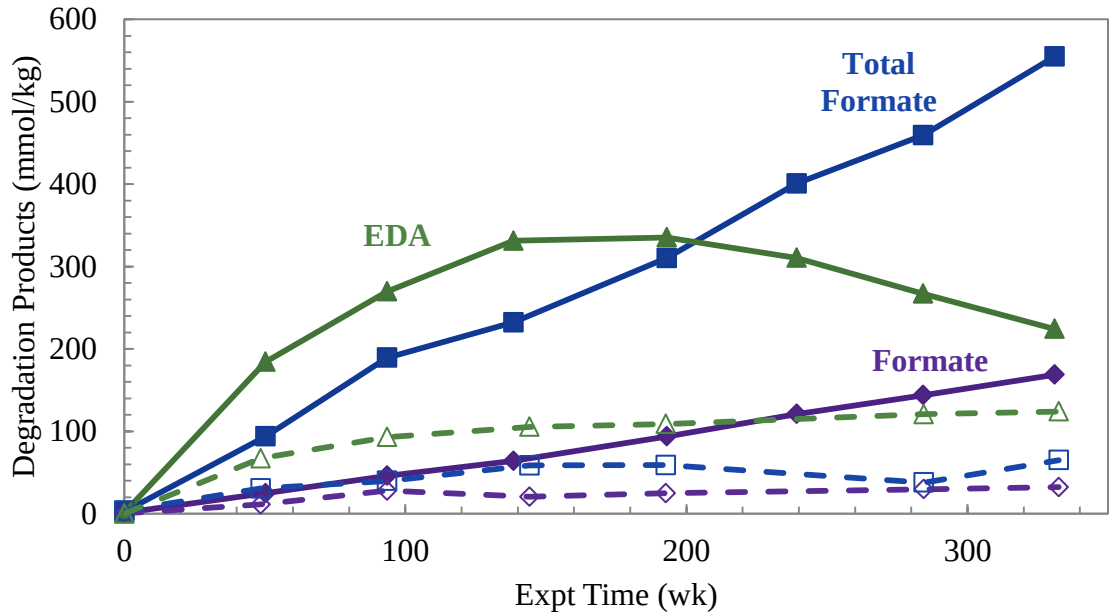

Figure 8.32: Effect of O_2 on generation of formate (♦), total formate (■), and EDA (▲) with 40% (open points, OE23) or 94% O_2 (solid points, OE25) (TOR, 8 m PZ, 70 °C, 1400 rpm, 100 mL/min inlet gas with 6% CO_2 (α=0.3), 4 mM Cu^{2+})

8.5 EFFECT OF TEMPERATURE

PZ oxidation is expected to accelerate with increased temperature. The temperature bulge in the absorber is predicted to reach up to 70 °C, making the overall temperature range in the absorber and absorber sump 40 to 70 °C (Plaza et al., 2009). The absorber sump, where the most residence time and liquid hold up occurs, should be maintained at the lower end of the temperature range, which will minimize oxidation effects. The sump, however, is where the concentration of O_2 is likely to remain high since the sumps position directly below the flue gas inlet.

The acceleration of oxidation due to increased temperature was independently investigated in the presence of stainless steel metals and copper. For both catalysts, temperatures of 55 and 70 °C were investigated to represent the average and maximum expected temperatures.

8.5.1 Effect of temperature on stainless steel catalyzed oxidation

The oxidation of 8 m PZ was studied in the TOR with the standard SSM mixture (0.4 mM Fe^{2+}, 0.1 mM Cr^{3+}, and 0.05 mM Ni^{2+}), agitation at 1400 rpm and 100 mL of O_2/CO_2 mixed gas. The CO_2 concentration of the inlet gas was adjusted based on the reactor temperature in order to maintain a CO_2 loading of 0.3 mole CO_2 per mole alkalinity at 55 °C (OE18: 98% O_2/2% CO_2) and 70 °C (OE25: 94% O_2/6% CO_2).

The loss of PZ and the generation of degradation products in both experiments are compared in Figure 8.33 and Figure 8.34, respectively. The higher temperature noticeably increased the loss of PZ, although both sets of data lie within the error limits established by the baseline experiments. Although perhaps not statistically significant, the increase in temperature does increase PZ loss. For the degradation products, higher concentrations of total formate and EDA were observed in the higher concentration experiment while formate production was nearly identical. It is important to note that no

EDA was observed in the 55 °C experiment while EDA levels reached nearly 30 mmole per kg in the 70 °C experiment. The undetected EDA may be a true observation, or an artifact of the difficulty in quantifying low levels of EDA while more substantial concentrations found in the high temperature experiment were more readily detected. These results indicate that the enhanced loss of PZ at 70 °C is potentially a true increase in oxidation which is also reflected in increased concentrations of degradation products.

8.5.2 Activation energy of stainless steel-catalyzed oxidation

Given the two experimental temperatures, an activation energy for PZ oxidation can be calculated for stainless-steel catalyzed oxidation. Linear rates of loss or generation of PZ, formate, total formate, and EDA have been regressed for all stainless steel experiments. This procedure is detailed in section 9.4 of the following chapter. Using the rates of experiments catalyzed by SSM, activation energies for each rate can be extracted based on an Arrhenius behavior of rate with temperature, as shown for k_1 of thermal degradation in section 5.2.

The rates for PZ loss and generation of formate, total formate, and EDA for the seven SSM containing experiments (OE1, OE15, OE18, OE19, OE22, OE26, and OE28) are shown in Figure 8.35. One experiment had loss rate of zero for PZ (OE15) while two experiments were not found to produce EDA (OE1 and OE18). For each species, an exponential trendline has been regressed through all the experimental rates and the equation shown on the graph. From the value of the constant in the exponential, the activation energy for loss or generation of that species can be calculated over this temperature range. Standard error in the activation energies were calculated based on the standard error of a linear least-squares fit of the natural log of each rate.

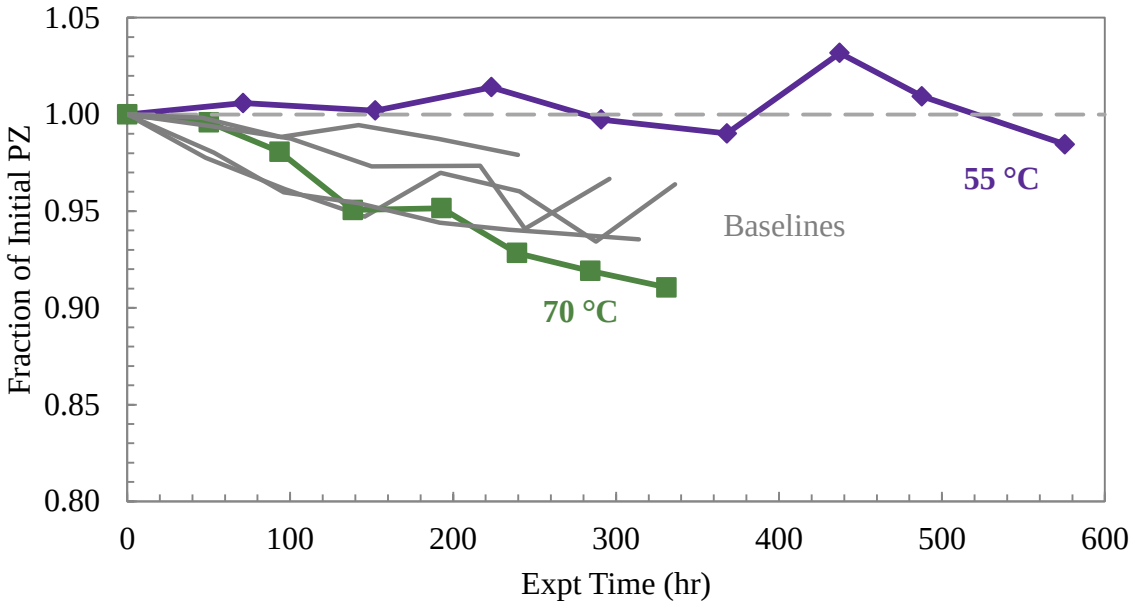

Figure 8.33: Effect of temperature on PZ loss (TOR, 8 m PZ, 1400 rpm, 100 mL/min with 2 (OE18) or 6% (OE28) CO_2 with balance O_2, α=0.3, SSM)

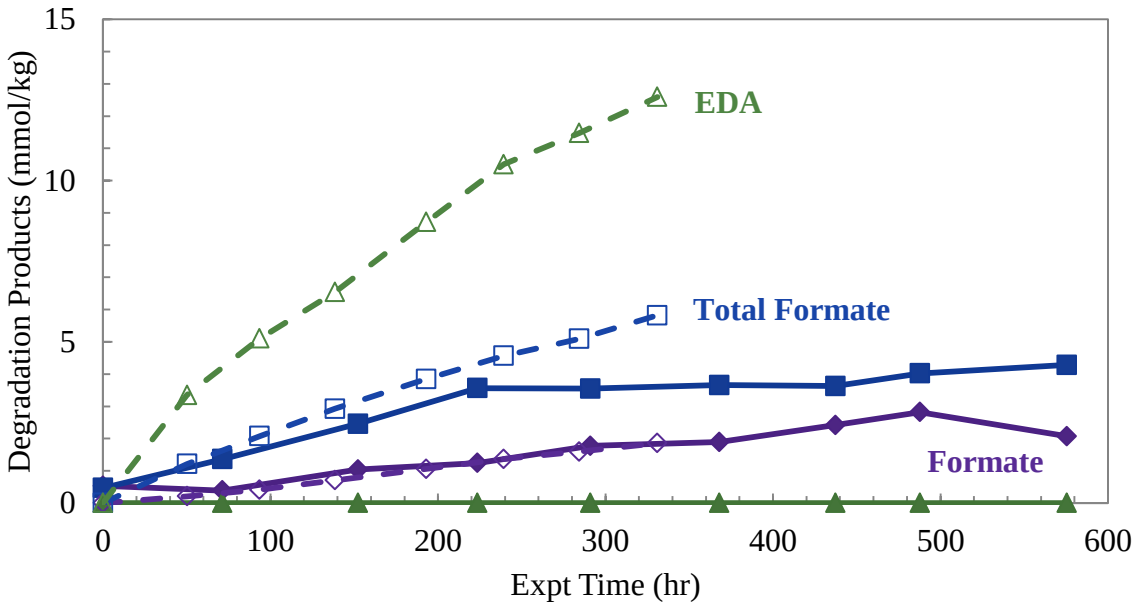

Figure 8.34: Effect of temperature on generation of formate (♦), total formate (■), and EDA (▲) at 55 (solid points, OE18) or 70 °C (open points, OE28) (TOR, 8 m PZ, 1400 rpm, 100 mL/min with 2 (OE18) or 6% (OE28) CO_2 with balance O_2, α=0.3, SSM)

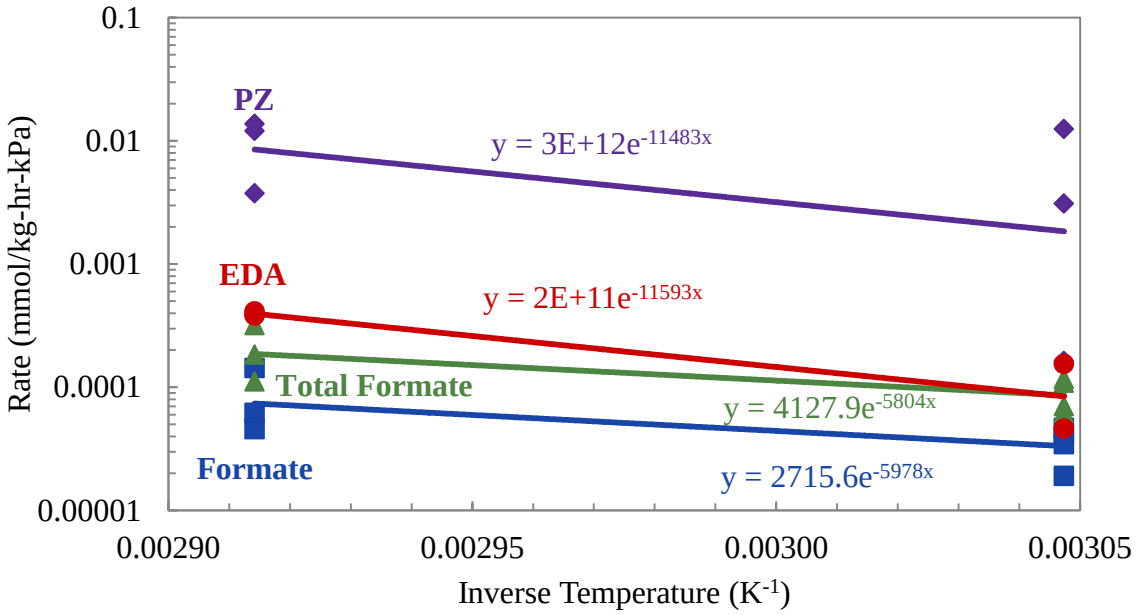

Figure 8.35: Rates of loss or production for PZ (♦), formate (■), total formate (▲), and EDA (●) for stainless-steel catalyzed oxidation

The calculated activation energies with their associated error are compared for the four species in Table 8.7. The loss of PZ and the generation of EDA were found to have very similar activation energies of 96 kJ per mole, while both formate and total formate had activation energies near 50 kJ per mole. This similarity of activation energies indicates that EDA could be generated directly at the rate of PZ oxidation. The similarity of activation energies between total formate and formate indicate that they are likely generated at a constant ratio, no matter the temperature.

Table 8.7: Activation energies for PZ loss and generation of products for stainless steel-catalyzed oxidation

Rate	Activation Energy (kJ/mol)
PZ Loss	96 ± 84
Formate Generation	50 ± 23
Total Formate Generation	48 ± 20
EDA Generation	96 ± 28

8.5.3 Effect of temperature on copper-catalyzed oxidation

A second investigation on the effect of temperature on concentrated PZ oxidation was performed in the presence of Cu^{2+}. Oxidation of 8 m PZ was performed in the OOR and TOR with 4 mM Cu^{2+}, agitation at 1400 rpm and 100 mL of O_2/CO_2 mixed gas. The CO_2 concentration of the inlet gas was adjusted based on the reactor temperature in order to maintain a CO_2 loading of 0.3 mole CO_2 per mole alkalinity at 55 °C (OE2: 98% O_2/2% CO_2) and 70 °C (OE25: 94% O_2/6% CO_2). These experiments were performed in the presence of high O_2 content (94-98% O_2). This condition would accelerate oxidation, as discussed in the previous section, making the effect of temperature more readily observed in PZ oxidation. For the interested reader, a comparison of OE23 and OE27 can be made to investigate the effect of Cu^{2+}-catalyzed oxidation between 55 and 70 °C but with low O_2 content (40%) (See Appendix E for experimental data).

The loss of PZ and generation of degradation products are compared in Figure 8.36 and Figure 8.37, respectively. The loss of PZ is markedly enhanced at the higher temperature. After 350 hours, 72% of the initial PZ is lost in the high temperature experiment compared to only 31% loss in the 55 °C experiment. This is an increase of 230% in PZ loss for an increase of 15 °C. Both experiments demonstrate statistically significant PZ loss compared to the baseline experiments.

The generation of formate, total formate, and EDA were all enhanced at higher temperature as well, as expected with increased PZ oxidation. The formate and total formate are initially generated in a linear fashion in both experiments while a leveling off effect can be seen in these products at 55 °C. This same behavior is mimicked in the low temperature PZ loss data where the oxidation has slowed due to mass transfer or kinetic limitations of the oxidation reactions. On the other hand, the formate and total formate in the 70 °C experiment continue to increase linearly without leveling off. After 350 hours,

formate and total formate concentrations reach 168.7 and 554.9 mmole per kg, respectively, compared to only 62.8 and 164.8 mmole per kg, respectively, at 55 °C. This is an increase of 270 and 340% for formate and total formate, respectively, for an increase of 15 °C. The EDA, however, demonstrates a unique behavior where a clear maximum is achieved after 150 hours at 70 °C. This behavior was not observed in other oxidation experiments and indicates that EDA is an intermediate that is generated from PZ, but then reacts to form other products. As discussed in section 8.3.1.1, it was observed that free EDA was reacting to form EDA-based amides at this point, decreasing the concentration of free EDA quantified. At the maximum of EDA concentration, at 150 hours, the EDA concentration is 170% higher than that of the low temperature experiment.

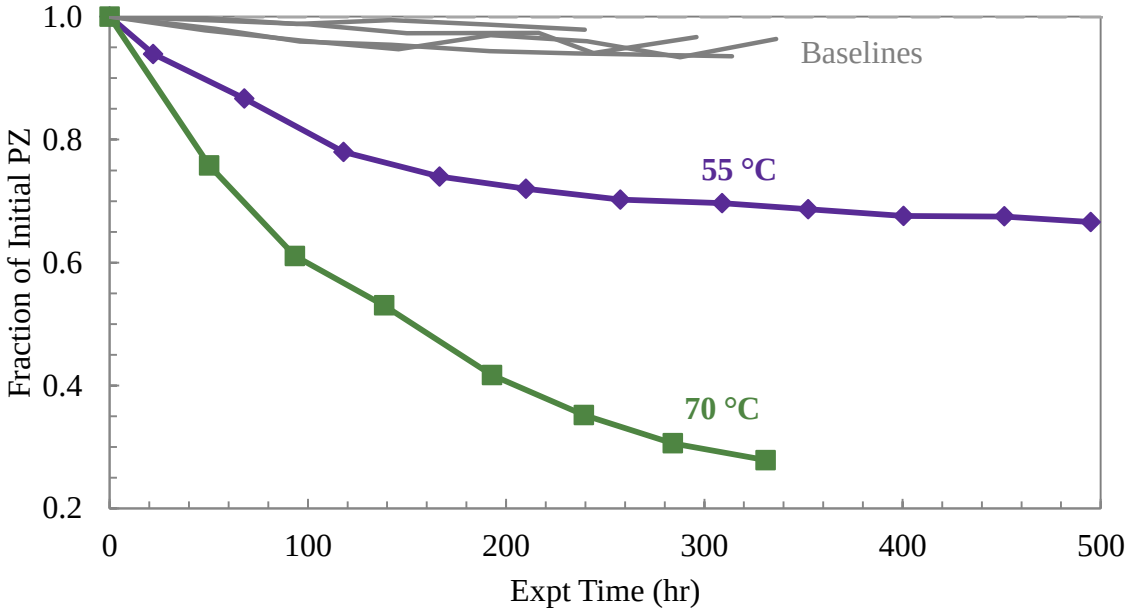

Figure 8.36: Effect of temperature on PZ loss (TOR, 8 m PZ, 1400 rpm, 100 mL/min with 2 (OE2) or 6% (OE25) CO_2 with balance O_2, α=0.3, 4 mM Cu^{2+})

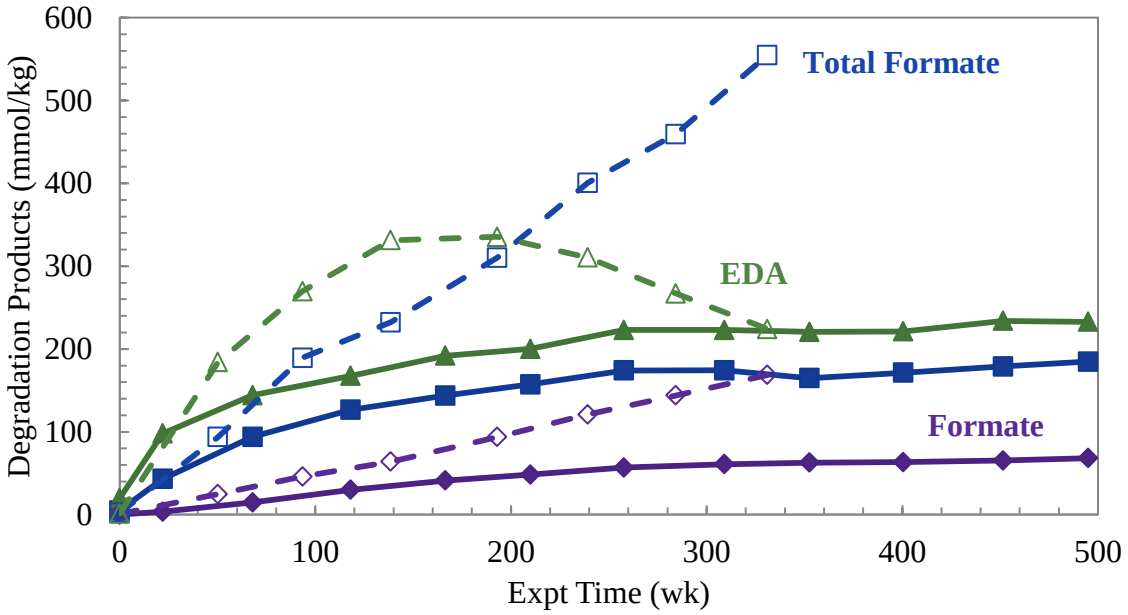

Figure 8.37: Effect of temperature on generation of formate (♦), total formate (■), and EDA (▲) at 55 (solid, OE2) or 70 °C (open, OE25) (8 m PZ, 1400 rpm, 100 mL/min with 2 (OE2) or 6% (OE25) CO_2 with balance O_2, α=0.3, 4 mM Cu^{2+})

8.5.4 Activation energy for copper-catalyzed oxidation

That activation energy for the loss of PZ and generation of formate, total formate, and EDA during Cu^{2+}-catalyzed oxidation were calculated in the same way as SSM-catalyzed oxidation (section 8.5.2). The rates for the four species are compared for four Cu^{2+}-catalyzed experiments (OE2, OE23, OE25, and OE27) in Figure 8.38 and the calculated activation energies with the expected error are shown in Table 8.8.

In this case, the loss of PZ and the generation of total formate were found to have very similar activation energies of 27-29 kJ per mole, while both EDA and total formate had slightly higher activation energies of 36 and 47 kJ per mole, respectively. In comparison with SSM-catalyzed oxidation, the PZ activation energy is three times lower showing the propensity for rapid oxidation that is characteristic of Cu^{2+} catalysis. The activation energy for formate is nearly identical at around 47-49 kJ per mole while both

total formate and EDA have lower energies in the presence of Cu^{2+}. This may indicate that formate generation is not dependent on catalyst while total formate and EDA rates are more subjective to the type and concentration of catalyst. This may also suggest that formate is the best oxidation product to represent overall degradation if its behavior is more similar between catalysts. There is a more complicated equilibrium between formate and formyl amides, so these energies may indicate that the generation of formate is the dominant mechanism associated with oxidation while the generation of amides is an equilibrium phenomena based on formate concentration, not oxidation directly.

Table 8.8: Activation energies for PZ loss and generation of products for Cu^{2+}-catalyzed oxidation

Rate	Activation Energy (kJ/mol)
PZ Loss	27 ± 29
Formate Generation	47 ± 15
Total Formate Generation	29 ± 33
EDA Generation	36 ± 9

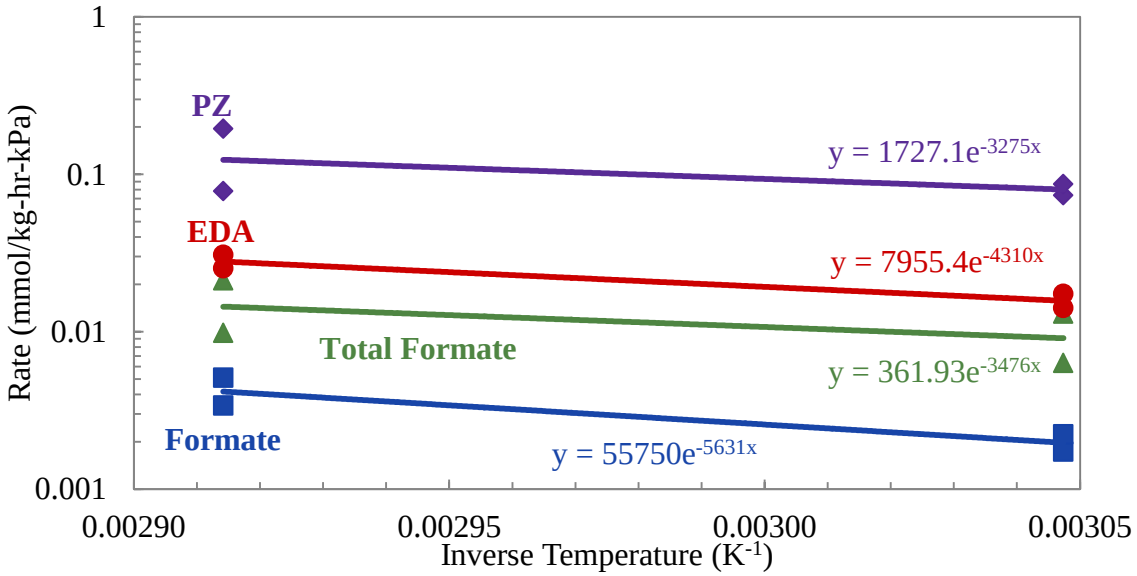

Figure 8.38: Rates of loss or production for PZ (♦), formate (■), total formate (▲), and EDA (●) for Cu^{2+}-catalyzed oxidation

8.6 EFFECT OF CO_2 CONCENTRATION

Most of the oxidation experiments in this project were performed with inlet gas streams containing the partial pressure of CO_2 needed to maintain a lean loading of approximately 0.3 to 0.32 mole CO_2 per mole alkalinity based on CO_2 solubility data. Four of the 28 experiments performed did not maintain this lean loading and the effect of CO_2 concentration can be seen in examining these four experiments. Two of these four experiments contained additives (formate and formaldehyde) that are discussed in section 8.8 below. Of the remaining two experiments, one was performed at a very lean loading of 0.26 mole CO_2 per alkalinity while the last was performed at rich loading of 0.42 mole CO_2 per mole alkalinity. The very lean experiment was performed at conditions similar to a representative lean experiment, except for an increased O_2 concentration (98 vs. 94% O_2 in the inlet gas).

The rich loaded experiment is difficult to compare directly to another lean experiment because of the reaction conditions. The rich experiment contained only 40% O_2 because 60% CO_2 was needed to achieve the rich loading at 70 °C. The two most similar experiments are not easy to compare because they differ either in temperature (55 °C instead of 70 °C) or O_2 concentration (96% instead of 40%). In the sections above, it was shown that for SSM-catalyzed oxidation, an increase of 15 °C had a stronger effect on both PZ loss and product generation in the presence of SSM than an increase from 40 to 98% O_2 (comparison of Figure 8.27 and Figure 8.33). Based on this observation, the rich loading experiment will be compared to an experiment conducted at the same temperature (70 °C) rather than the same O_2 content (40%), in an attempt to highlight the effect of CO_2 concentration. Therefore, the effect of CO_2 concentration on oxidation will be discussed in the presence of SSM at 70 °C with loadings ranging from 0.2 to 0.4 and O_2 contents ranging from 40 to 98%. This comparison does not fully

exclude the effect of O_2, but should limit the interference of the other variables (O_2 and temperature) on the effect of CO_2 loading.

The oxidation of 8 m PZ was studied in the TOR with the standard stainless steel metals mixture (0.4 mM Fe^{2+}, 0.1 mM Cr^{3+}, and 0.05 mM Ni^{2+}) at 70 °C with agitation at 1400 rpm and 100 mL of O_2/CO_2 mixed gas. The CO_2 concentration of the inlet gas was adjusted based on the reactor temperature to produce a CO_2 loading of 0.2 (OE19: 2% CO_2), 0.3 (OE26: 6% CO_2), and 0.4 mole CO_2 per mole alkalinity (OE22: 60% CO_2). The balance of the inlet gas was O_2 in all three cases.

The PZ loss, generation of formate, and generation of total formate are compared in Figure 8.39, Figure 8.40, and Figure 8.41, respectively. The loss of PZ data indicate that increased CO_2 loadings enhance PZ oxidation, although all three data sets are within or near the boundary on error established by the baseline experiments. On the other hand, the production of both formate and total formate indicate the opposite, with the lean solution producing the highest concentrations of both species after oxidation. There is much more confidence in the accurate quantification of the degradation products, so this effect is likely more representative of the effect of loading than any observations based on the PZ loss rate. The lower O_2 content of the rich (α=0.4) experiment will also affect interpretation. At 70 °C, a doubling of O_2 partial pressure will produce approximately a 300% increase in the production of formate and total formate based on the conclusions of section 8.5.2. This would place the rich data in line with the lean (α=0.3) data and an enhanced rate of product generation at very lean loading (α=0.2) would still be observed.

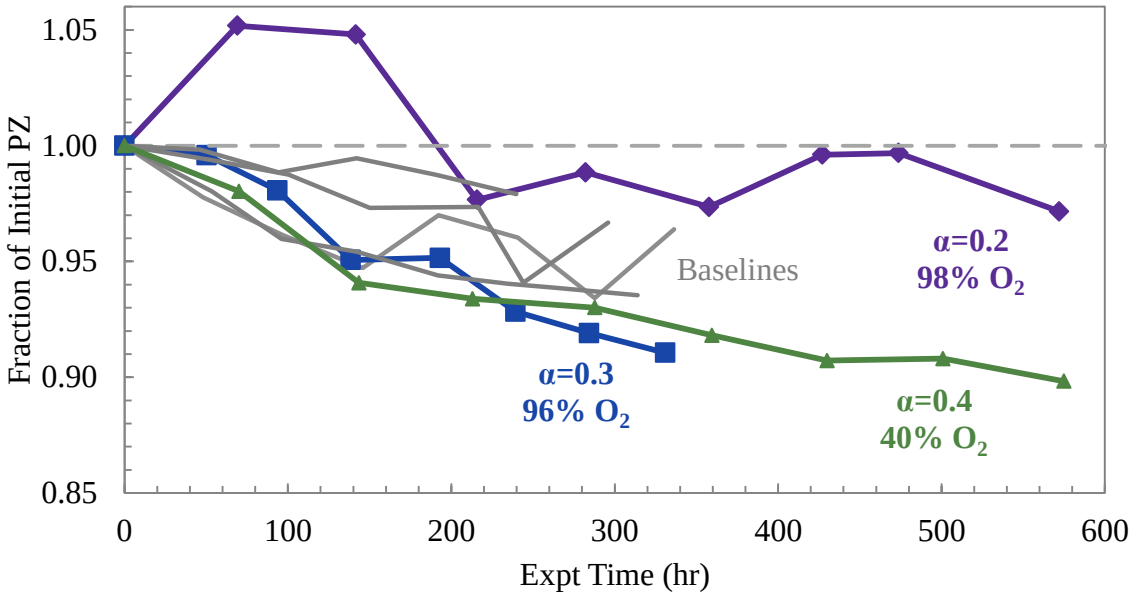

Figure 8.39: Effect of CO_2 on PZ loss (TOR, 70 °C, 8 m PZ, 1400 rpm, 100 mL/min with 2 (OE19), 6 (OE26), or 60% (OE22) CO_2 with balance O_2, SSM)

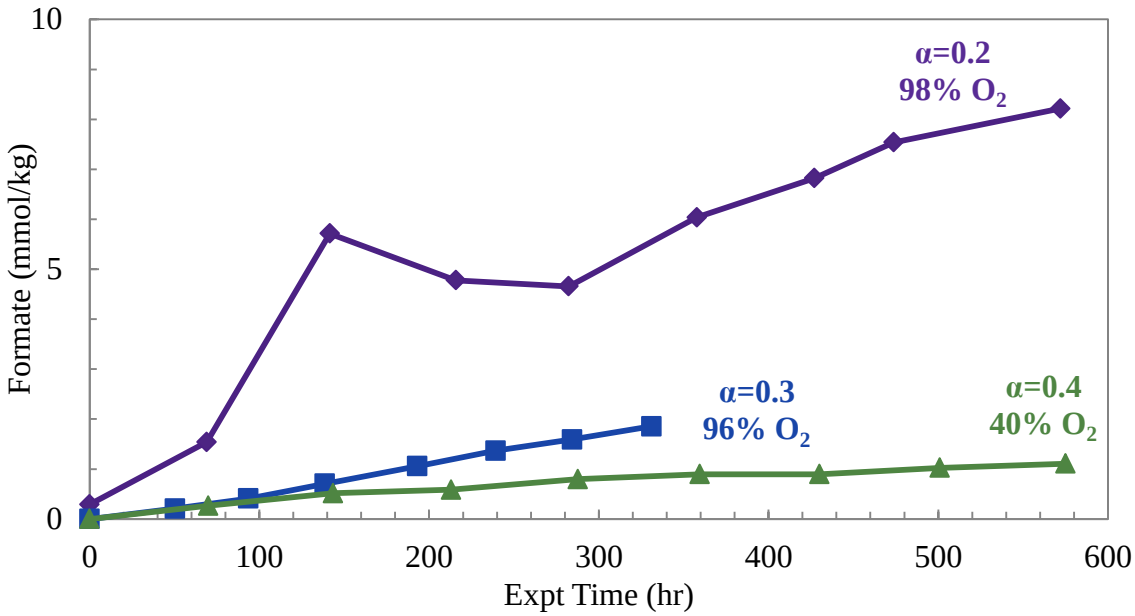

Figure 8.40: Effect of CO_2 on formate generation (TOR, 70 °C, 8 m PZ, 1400 rpm, 100 mL/min with 2 (OE19), 6 (OE26), or 60% (OE22) CO_2 with balance O_2, SSM)

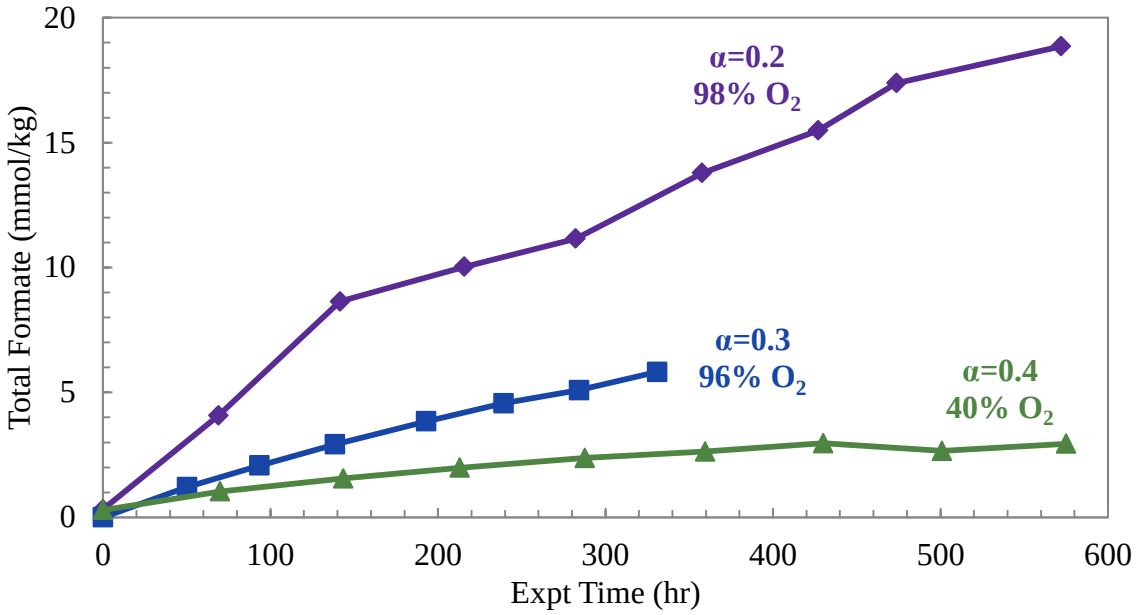

Figure 8.41: Effect of CO_2 on total formate generation (TOR, 70 °C, 8 m PZ, 1400 rpm, 100 mL/min with 2 (OE19), 6 (OE26), or 60% (OE22) CO_2 with balance O_2, SSM)

8.7 Effect of PZ concentration

Another factor explored in this chapter is the effect of PZ concentration on the oxidation of concentrated PZ. The effect of amine concentration on the oxidation of MEA has been explored previously, but not for concentrated PZ (Goff, 2005; Sexton, 2008). Within this project, the effect was not developed fully due to the importance and likely application of 8 m PZ in industrial experiments. However, a few experiments did observe the differences between 8 and 10 m PZ. In addition, previous work on PZ oxidation contains some data for 5 m PZ that will be interpreted as well. All of the experiments discussed in this section were performed at 55 °C with 100 mL per min of 98% O_2/2% CO_2 in a low gas flow reactor (OOR or TOR) with agitation at 1400 rpm. These conditions were maintained for experiments performed in this project and those

performed previously (Sexton, 2008). Only differences in PZ, catalyst, or inhibitor concentrations will be highlighted during the discussions in the rest of the section.

8.7.1 Effect of PZ concentration in stainless-steel catalyzed oxidation

With the available data, there is only one comparison to make for oxidation in the presence of stainless steel metals. Both 8 and 10 m PZ were oxidized in the presence of stainless steel metals under the abovementioned temperature, CO_2, and O_2 conditions. The experiments contained slightly different concentrations of Fe^{2+}, Cr^{3+}, and Ni^{2+}. The 8 m PZ solution (OE18) contained 0.4, 0.1, and 0.05 mM of each metal, respectively, while the 10 m PZ solution (OE1) contained 0.23, 1.6, and 0.2 mM of each metal, respectively. It is assumed that the difference in catalyst concentration would not affect the overall conclusions of the comparison.

The loss of PZ and generation of formate and total formate are compared in Figure 8.42 and Figure 8.43, respectively. The PZ concentrations compared are close to each other and it was not expected that a large change would be seen given this small difference. However, a slightly enhanced loss of PZ and generation of degradation product can be seen in the higher concentration experiment. With 10 m PZ, the amine is steadily lost over the course of the experiment with some scatter in the data. Although the formate concentration profiles are similar between the 8 and 10 m PZ, the 10 m PZ produced roughly 3 mmole per kg more total formate. These differences are small in light of the expected experimental and analytical error demonstrated by the baseline data, but the overall picture seems to indicate that oxidation is a slight function of PZ concentration.

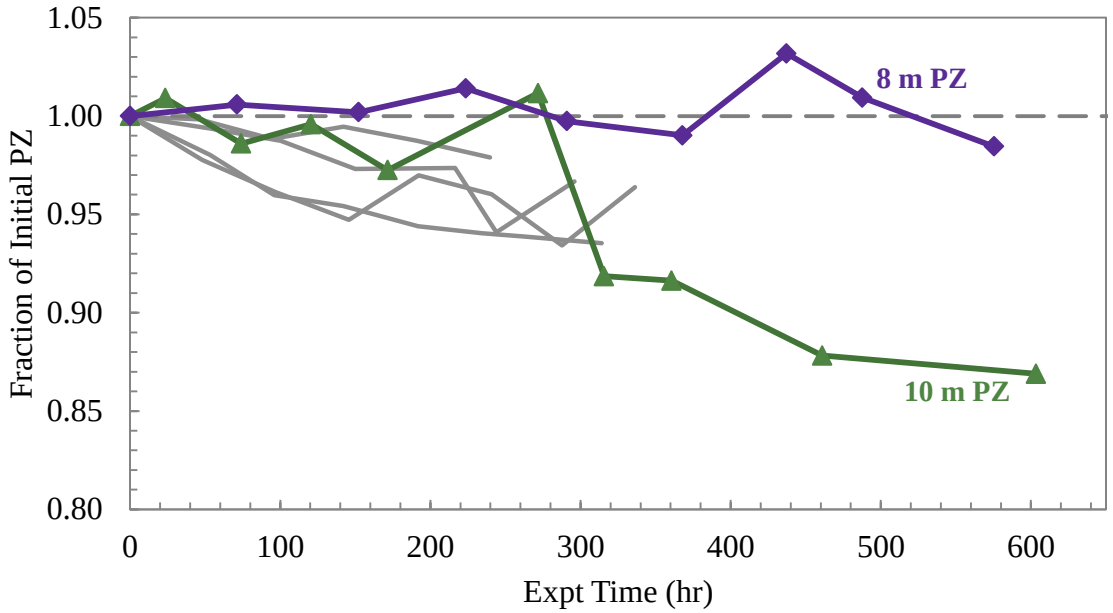

Figure 8.42: Effect of PZ concentration on PZ loss (8 m PZ (OE18) or 10 m PZ (OE1), 55 °C, 1400 rpm, 100 mL/min 98% O_2/2% CO_2, SSM)

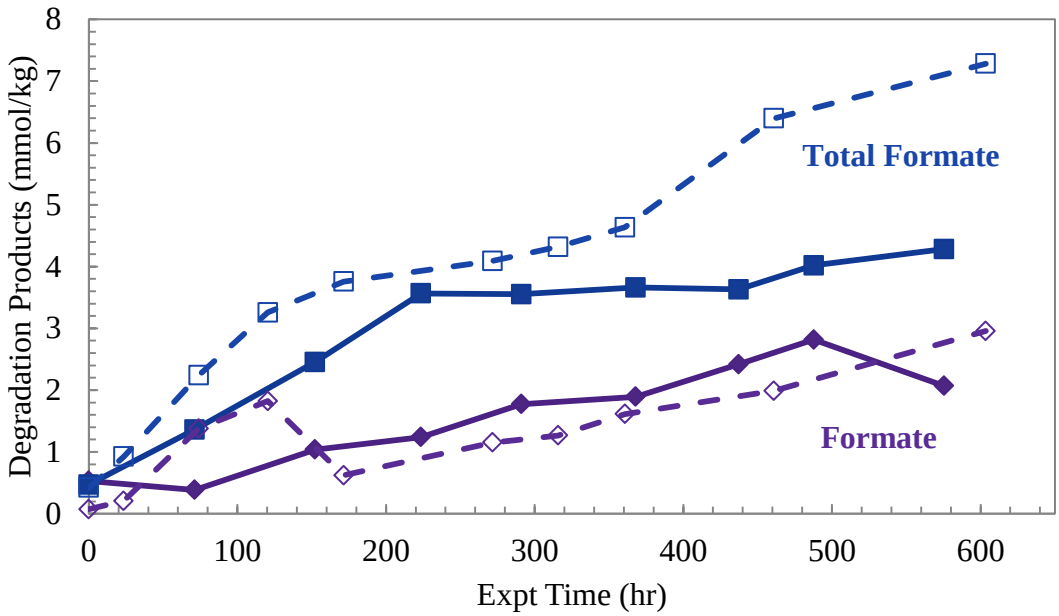

Figure 8.43: Effect of PZ concentration on generation of formate (♦) and total formate (■) for 8 m PZ (OE18, solid) and 10 m PZ (OE1, dashed) with SSM (55 °C, 1400 rpm, 100 mL/min 98% O_2/2% CO_2)

8.7.2 Effect of PZ concentration in copper-catalyzed oxidation

The effect of PZ concentration on copper-catalyzed oxidation can be observed through comparing two sets of experiments. From this project, copper-catalyzed oxidation was measured in 8 and 10 m PZ. Secondly, Sexton performed screening experiments on the oxidation of 5 m PZ in the presence of combinations of Fe^{2+}, Cu^{2+}, and Inhibitor A (Sexton, 2008). Unfortunately, the analysis performed on liquid samples was not completed to the same extent and only a few species, not including PZ in some cases, were measured. Some information can still be garnered from the degradation products that were measured. The experiments containing Cu^{2+} will be the focus since they were the most likely to produce appreciable levels of oxidation.

The oxidation of 5 m PZ in the presence of Cu^{2+} was measured by Sexton (2008) and although the data does not include PZ concentration, multiple dominant degradation products were observed and quantified. The generation of major degradation products is compared in Figure 8.44 to a 10 m PZ experiment with similar catalysts (OE2). The results from the 10 m PZ experiment are shown with filled points and solid lines while the 5 m PZ experiment is shown with open points and dashed lines. Formate (for), oxalate (oxa), total formate, total oxalate, and EDA are compared in Figure 8.44. Amides, it should be noted, were only quantified in the final sample, likely well after the initial quantification due to the development of the amine quantification procedure. The 5 m PZ experiment contained both 0.1 mM Fe^{2+} and 5 mM Cu^{2+} while the 10 m PZ experiment contained only 4 mM Cu^{2+}. The 10 m PZ experiment does not contain any Fe^{2+} but, as will be demonstrated in the next chapter, the catalytic effect of copper far outweighs the presence of 0.1 mM Fe^{2+} so these experiments are approximately comparable (section 9.1.1).

It is expected that an increase in PZ concentration would enhancement oxidation and, therefore, enhance the rates of generation of degradation products. The 10 m PZ experiment produces, roughly double the EDA concentration and slightly higher total formate and total oxalate concentrations as the 5 m PZ experiment, but the production of formate is one-third less. The equilibrium between formate and formyl amides has not been well studied in highly oxidized PZ solutions, but higher concentration PZ solutions appear to favor amides over carboxylate ions. This result matches that seen in thermally degraded PZ where the ratio of formyl amides to formate increases with PZ concentration likely due to the increased free PZ concentration (section 6.4.3).

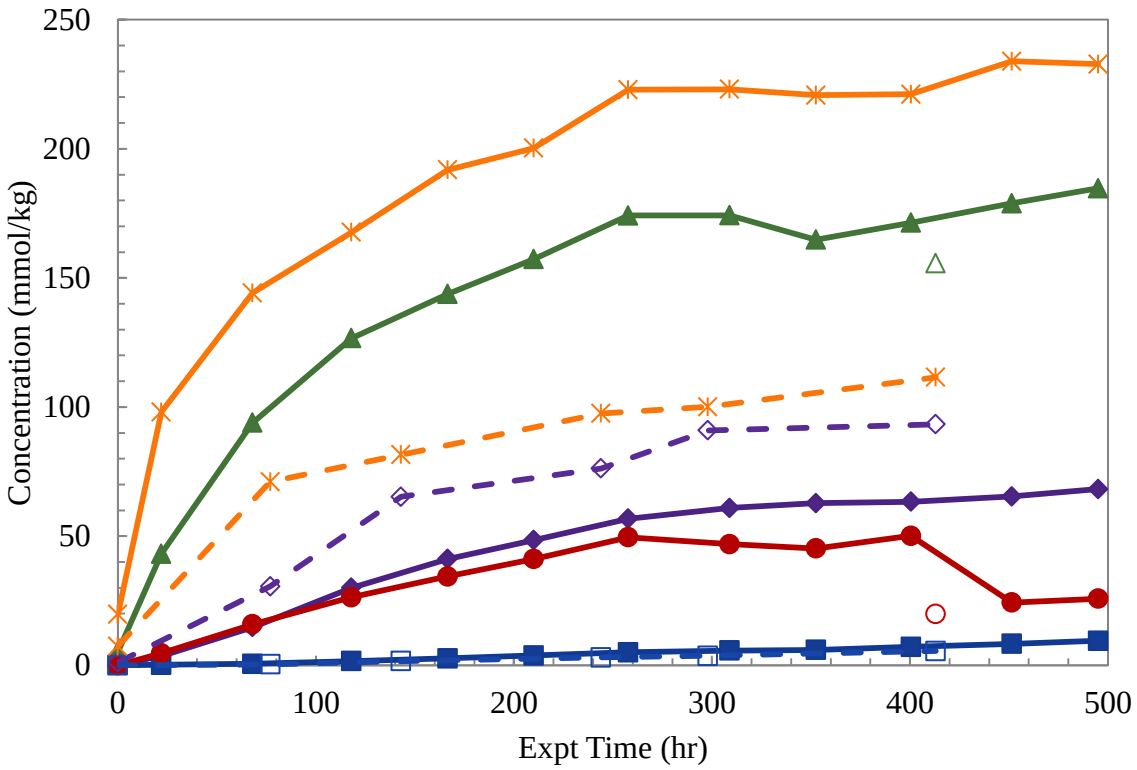

Figure 8.44: Effect of PZ concentration on generation of formate (♦), oxalate (■), total formate (▲), total oxalate (●), and EDA (*) during oxidation of 5 m PZ (open/dashed, (Sexton, 2008)) and 10 m PZ (solid, OE2) (55 °C, 1400 rpm, 100 mL/min 98% O_2/2% CO_2, 4-5 mM Cu^{2+})

A third comparison exploring PZ concentration can be made by evaluating 5 and 8 m PZ oxidation in the presence of Fe^{2+}, Cu^{2+}, and Inhibitor A. As with the previous example, the PZ concentration was not measured in the 5 m PZ experiment, and in this case neither was the total formate, oxalate, or total oxalate. Therefore, the degradation products where data is available are compared for these two experiments in Figure 8.45. In this comparison, the catalyst and inhibitor concentrations were the same at 0.1 mM Fe^{2+}, 5 mM Cu^{2+}, and 100 mM Inhibitor A. Unfortunately, the results are not easily interpreted due to the lack of low concentration data, lack of overall oxidation in PZ systems, and conflicting concentration profiles. The 5 m PZ experiment produced lower concentrations of formate, except in its final point, while it consistently produced more EDA. It was expected that the 8 m PZ experiment would demonstrate enhanced oxidation, but that conclusion cannot be drawn from this data.

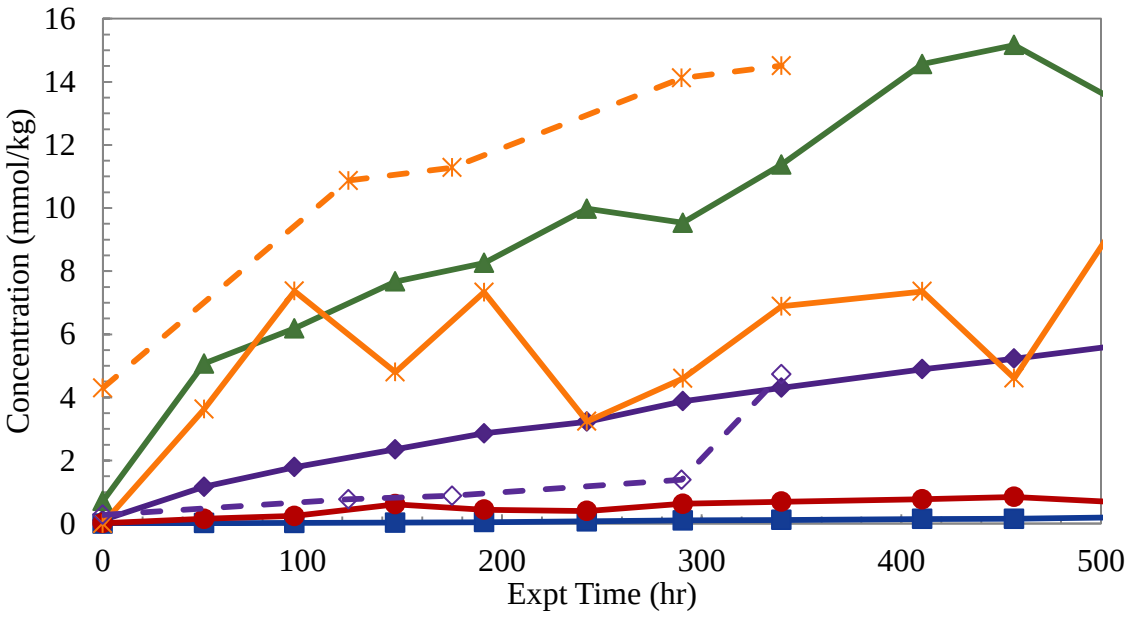

Figure 8.45: Effect of PZ concentration on generation of formate (♦), oxalate (■), total formate (▲), total oxalate (●), and EDA (*) during oxidation of 5 m PZ (open/dashed, (Sexton, 2008)) and 8 m PZ (solid, OE4) (55 °C, 1400 rpm, 100 mL/min 98% O_2/2% CO_2, 0.1 mM Fe^{2+}, 5 mM Cu^{2+}, 100 mM Inhibitor A)

8.8 EFFECT OF ADDITIVES

One final variable that was adjusted during this study of PZ oxidation was the use of additives to catalyze degradation, inhibit degradation or attempt to elucidate degradation pathways. The study of catalysts and inhibitors for PZ oxidation is extensively covered in Chapter 9. Other additives investigated are discussed here in terms of the individual goal of the experiment and the eventual outcome.

8.8.1 Addition of formate

An oxidation experiment was performed in the presence of the SSM (0.4 mM Fe^{2+}, 0.1 mM Cr^{3+}, and 0.05 mM Ni^{2+}) and 500 mmole per kg formate at 70 °C with agitation at 1400 rpm and 0.2 mole CO_2 per mole alkalinity. It was hypothesized that formate may be a reaction intermediate or act as an oxidation inhibitor. Previous oxidation results showed a lack of dominant degradation products and it was hypothesized that formate may be generated through oxidation of PZ and then further oxidized to CO_2, which would not be seen in our typical analysis. If CO_2 was being generated, the loading would not necessarily change because of the agitation and constant influx of CO_2 in the headspace of the reactor. This would explain some of the gap in the C mass balance, if found to be true.

There were three predicted outcomes of this experiment. First, formate might convert to formyl amides and the total formate (500 mmole per kg) would be conserved during the experiment. In this case, the experiment would just test the equilibrium between formate and formyl amides at 70 °C. Second, formate would be oxidized to CO_2 and the total formate concentration would decrease as CO_2 is generated and lost to the headspace of the reactor. Finally, it was suspected that formate may act as an oxidation inhibitor and would also be conserved and decreased the overall PZ loss rate. As a corollary, Sexton tested formate as a potential oxidation inhibitor for 7 m MEA and

found that the addition of 500 mM formate actually accelerated MEA loss by nearly 20% in the presence of 1 mM Fe^{2+} at 55 °C (Sexton, 2008).

The concentrations of PZ, CO_2, formate, and formyl amides for this oxidation experiment (OE20) are shown below in Figure 8.46. Trace concentrations of acetate, acetyl amides, oxalate, oxalyl amides, nitrite and nitrate were detected but are not shown in the figure. No EDA, glycolate, or glycolyl amides were detected. Over the course of 350 hours, approximately 8.8% of the initial PZ was lost. Formate acted as an inhibitor for the generation of oxidation products.

During the experiment, the overall concentration of formate was essentially conserved at 500 mmole per kg (red (×) data in Figure 8.46). The formate added to the solution at the beginning of the experiment quickly reacted with PZ in solution to form FPZ, even in the initial reactor sample. Since the initial sample was taken a few minutes after the addition of formate, there was already very quick equilibrium between formate and FPZ that manifested as formyl amides being present in the initial sample. The PZ loss is compared to an analogous experiment without formate in Figure 8.47. Outside of the second time point, the PZ loss was slightly decreased in the spiked experiment, although the error in the cation may be larger than the difference observed. This observation may indicate that formate is weak oxidation inhibitor, which is the opposite of the findings of Sexton (2008) who found formate addition accelerated MEA oxidation.

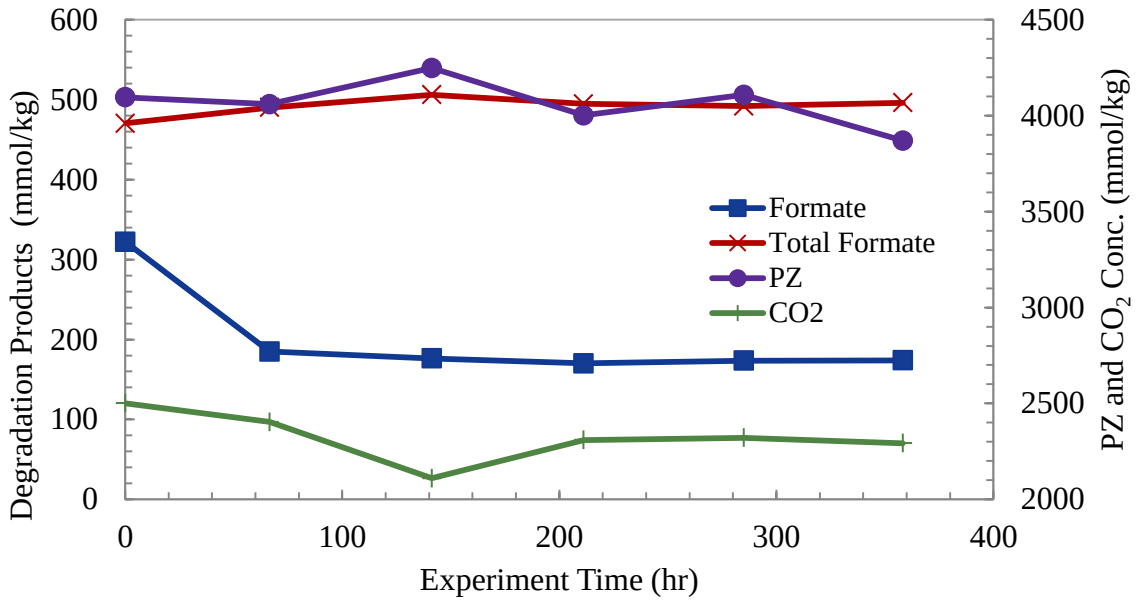

Figure 8.46: Concentration curves for OE20 (8 m PZ, 70 °C, 100 mL/min 98% O_2/2% CO_2, α=0.3, SSM, 500 mmol/kg formate)

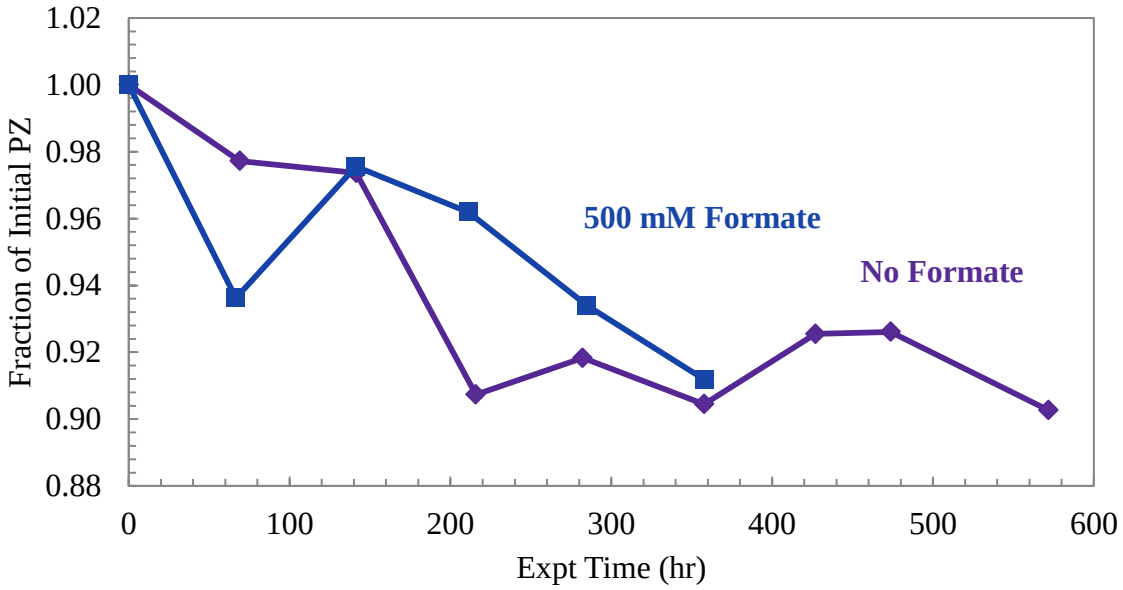

Figure 8.47: Effect of formate addition on PZ loss (8 m PZ, 70 °C, 100 mL/min 98% O_2/2% CO_2, α=0.3, SSM,)

8.8.2 Addition of formaldehyde

As a complementary experiment to OE20, an oxidation experiment was performed in the presence of SSM (0.4 mM Fe^{2+}, 0.1 mM Cr^{3+}, and 0.05 mM Ni^{2+}) and 500 mmole per kg formaldehyde at 70 °C with agitation at 1400 rpm and 2% CO_2 (OE21). Formaldehyde was chosen as a spike in an attempt to accelerate oxidation of PZ. This species is suspected to be an important intermediate in the oxidation of PZ and it was hypothesized that the addition of this high concentration would catalyze the PZ degradation. In this way, oxidation could be more easily and confidently quantified. Sexton investigated formaldehyde as a potential oxidation inhibitor for MEA, but found the addition of 500 mM formaldehyde increased MEA loss by nearly 35% in the presence of 1 mM Fe^{2+} at 55 °C (Sexton, 2008). Since PZ is difficult to oxidize, the use of formaldehyde was tested as an accelerant of SSM-catalyzed oxidation.

Unfortunately, the concentration was much too high and generated an operational issue. When it was added, it reacted quickly to form very stable, dense, white foam on the surface of the reactor. This foam persisted even with agitation and the experiment was continued for 5 days to see how the formaldehyde and the foam would affect the results. At the conclusion of the experiment, the experimental solution was transferred to a bottle for storage. The foam persisted for at least 10 months and is shown in Figure 8.48 next to a neat PZ solution without foam

The concentrations of PZ, CO_2, formate, formyl amides, acetyl amides, oxalyl amides, and FPZ are shown in Figure 8.49 below. No glycolate, acetate, nitrite, or nitrate was found in appreciable quantities. The concentration of FPZ tracks in agreement with that of formyl amides quantified via amide reversal indicating that FPZ is the only formyl amide of appreciable quantity. Two samples were taken at the beginning of the experiment, one before (t = 0A) and one after (t = 0B) the addition of formaldehyde. The

decrease in PZ between sample 0A and 0B indicates that PZ may have been taken up in the dense white foam that was created from the addition of formaldehyde as only the liquid below the foam was sampled for 0B.

Panel A: Neat loaded PZ solution with SSM

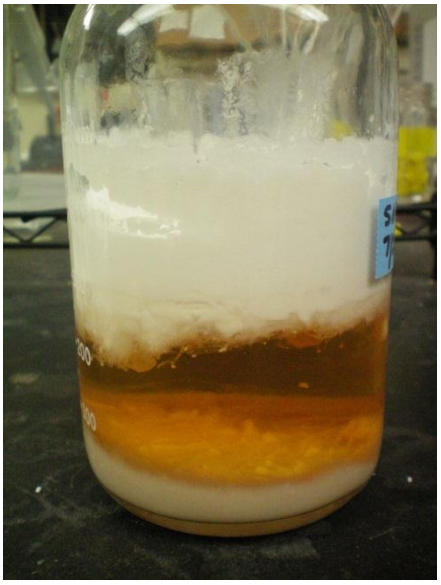

Panel B: OE21 final solution with SSM and stable foam

Figure 8.48: Foam created in OE21 compared with a neat PZ solution

Through the course of the 5 day experiment, 7.8% or 2.3% of the initial PZ was lost if either sample 0A or 0B, respectively, was regarded as the initial sample. FPZ was the only amide produced, which is expected with such a large addition of formaldehyde. The production of formate and total formate in an analogous experiment without formaldehyde addition is compared with this experiment in Figure 8.50. The production of formate and formyl amides was found to be decreased with the large addition of formaldehyde. Initially, the rates are similar for the two experiments but those for the spiked experiment then slow down. This was not expected since formaldehyde has been

assumed to be a very reactive intermediate in the oxidation process, and was expected to rapidly oxidize to formate under the O_2-rich conditions of the reactor.

The presence of the foam complicates the experiment since the concentration of formaldehyde in solution is not actually 500 mM. The exact composition of the foam is not known, but it is probable that it is a polymer of formaldehyde and PZ so the concentration of formaldehyde could be significantly lower than the 500 mM added. The fact that less formate was produced than a comparable solution is still unexpected even with a lower formaldehyde concentration than thought. It was anticipated that any spike of formaldehyde would increase the concentration of formate and formyl amides. The presence of the foam likely limited the amount of O_2 that was successfully absorbed into solution. Even with agitation, the foam was present and likely interfered with the mass transfer of O_2 into solution.

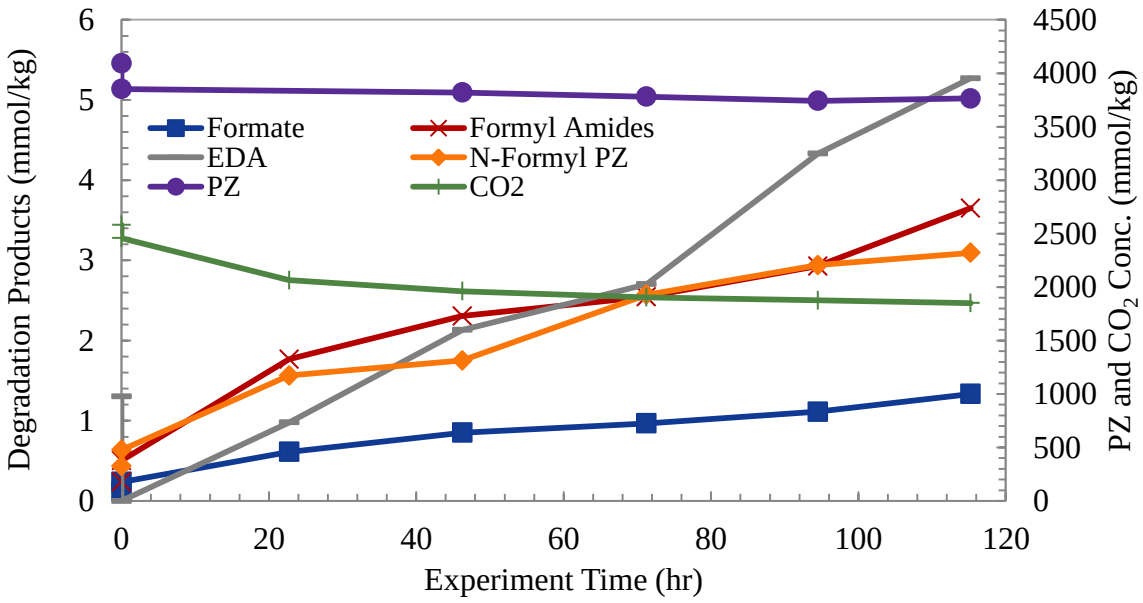

Figure 8.49: Concentration curves for OE21 (8 m PZ, 70 °C, 100 mL/min 98% O_2/2% CO_2, α=0.3, SSM, 500 mmol/kg formaldehyde)

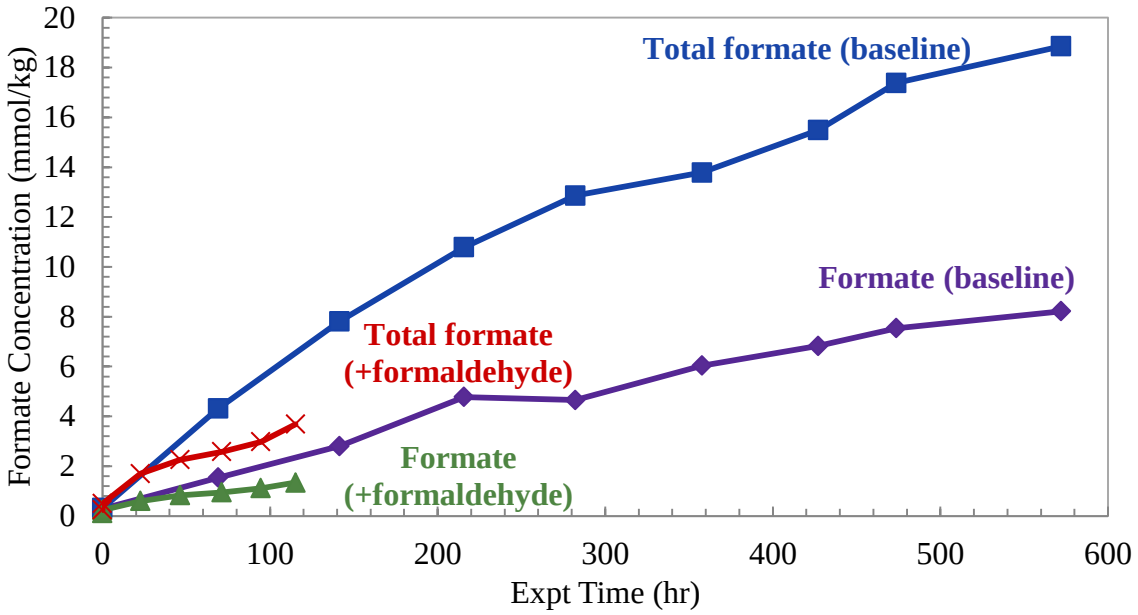

Figure 8.50: Effect of 500 mM formaldehyde addition on formate and formyl amide production (8 m PZ, 70 °C, 100 mL/min 98% O_2/2% CO_2, α=0.3, SSM)

8.9 Analysis of Foaming in Relation to Oxidation

Foaming in amine systems can be a significant problem for the effective mass transfer area in the absorber and, to a lesser extent, in the stripper. Previous work has analyzed the extent of foaming in experimental and neat solutions through the measurement of a foaminess coefficient (Chen et al., 2011; Thitakamol and Veawab, 2007). The method used was that of Thitakamol and Veawab (2007) which was adapted from a standard ASTM method to measure foaminess of lubricating oils (ASTM, 2000). The foaminess (F) is defined in Equation 8.12 as the ratio of volume of foam (V_g) to the superficial gas velocity (G). The volume of foam is calculated as the difference between the total steady volume (V_t) and the original liquid volume (V_0).

$$F = \frac{V_t - V_0}{G} = \frac{V_g}{G} \qquad (8.12)$$

The foaminess coefficient of solutions has been measured on every PZ oxidation experiment to date, except for a few cases where the solution was not available for testing. A summary of the foaming results for all the oxidation experiments performed during this project are shown in Table 8.9. A neat solution of 8 m PZ was analyzed by Chen and is included as the first entry in the table (Chen et al., 2011). All experiments were performed on 8 m PZ except for OE1 and OE2 which were 10 m PZ. The type of reactor was changed from the OOR to the TOR starting with OE17. Experiments OE1, OE2, OE3, and OE14 were not tested because the solutions were discarded before the apparatus was built or there was no final solution. The foam stability of OE4 was not measured. OE21 was not tested because the addition of 500 mM formaldehyde to the reactor created very stable white foam that persists in the final solution. The total formate at the end of the experiment is included in the table as an indication of the overall level of degradation.

Foaminess results have been used in some cases to make the argument for PZ oxidation where the analysis of products was not conclusive. Unfortunately, the results have been contradictory and all of the foaming results are analyzed to determine the reliability of the measurements for oxidized PZ solutions.

Foaminess to this point has been fairly inconclusive. Earlier researchers have had some success with the comparison of foaming between solutions (Chen et al., 2011). Qualitatively, PZ solutions are frequently difficult to test because the same solution can foam differently on a different day for unknown reasons between the same or different researchers. As evidence of this unknown variability, oxidation experiments performed with the same experimental conditions sometimes have different foaminess coefficients. This is demonstrated in Table 8.9 as OE9 and OE10 are the same experiment but the foaminess ranges from 2.5 to 20 x 10^{-3} m^2-s. These two values differ and are also wildly

different from the neat PZ solution value 78.8 x 10^{-3} m^2-s. This experiment was a blank solution where a loaded PZ solution was exposed to a gas mixture of 98% N_2/2% CO_2 at 55 °C for 3 weeks. There should not have been any oxidation with this experiment and the foaminess should have been similar to that of neat, loaded PZ.

As another example of the inconsistency of foaminess as a measure of oxidation, the results from OE15 and OE16 are not conclusive. Inhibitor A has been previously shown to decrease degradation and, therefore, foaming of oxidized PZ solutions (Chen et al., 2011). Thus it was expected that the foaminess coefficient would be lower in OE16 where 10 mM of Inhibitor A was present. The experimental results, however, were opposite with the foaminess coefficient of OE16 being 50% higher than that of OE15 while neither experiment had significant oxidation.

The inconsistencies noticed in the foaming data can be demonstrated further when looking at the four experiments that were degraded only in the presence of Fe^{2+}: OE5, OE5B, OE13, and OE17 under similar conditions. These experiments are highlighted in bold in Table 8.9. The foaminess coefficients for these four experiments are 85, 300, 8, and 17 × 10^{-3} m^2-s, respectively, while the foam stability is >600, >600, 8, and 19 seconds, respectively. The experiments have differences such as reactor type and degradation time, but the range in the data is striking and suggests that all the foaming data should be reconsidered. The high foaminess coefficient found for OE5B has been used as a rationale for the hypothesis that PZ is oxidizing while degradation products cannot be found in solution. This assumption is questionable in light of the other foaming results for oxidation, with 1.0 mM Fe^{2+} yielding similar concentrations of total formate (OE5, OE13, and OE17).

Table 8.9: Summary of foaming tests performed on oxidized PZ

Expt.	Expt. Additives [a]	Rxtr. Temp.	Deg. Time	Total Formate	Before Foaming [c]	Foaminess Coefficient [c]	Foam Stability [c]
	mM	°C	hr	mmol/kg	day	10^{-3} m^2-s	sec
Neat	-	-	-			78.8-86	29
PP	100 A	-	-			43.8	12
OE1	0.2 Fe, 1.6 Cr, 0.2 Ni	55	606	7.3	NT	NT	NT
OE2	4 Cu	55	495	184.7	NT	NT	NT
OE3	0.1 Fe, 0.1 V	55	381	10.5	NT	NT	NT
OE4	1 Fe, 5 Cu, 100 A	55	742	20.5	195	300	NT
OE5	1 Fe	55	70	2.4	1	85	>600
OE5B	1 Fe	55	163	2.1	0	300	>600
OE6	1 Fe, 100A	55	70	1.3	1	92	>600
OE6B	1 Fe, 100A	55	163	1.4	0	68	>600
OE7	30 B	55	164	0.6	1	380	>600
OE8	30 C	55	168	18.4	1	88	>600
OE9	-	55	336	2.5	283	3	10
OE10	-	55	336	4.7	207	20	40
OE11	-	55	314	2.4	198	11	37
OE12	-	55	296	1.8	225	18	19
OE13	1 Fe	55	523	3.7	112	8	18
OE14	1 Fe, 100A	55	381	3.6	NT	NT	NT
OE15	0.4 Fe, 0.1 Cr, 0.05 Ni	55	427	4.8	82	10	22
OE16	0.4 Fe, 0.1 Cr, 0.05 Ni, 10 A	55	427	1.3	82	16	25
OE17	1 Fe	55	424	3.4	156	17	19
OE18	0.4 Fe, 0.1 Cr, 0.05 Ni	55	576	4.3	49	117	45
OE19	0.4 Fe, 0.1 Cr, 0.05 Ni	70	572	18.9	11	195	35
OE20	0.4 Fe, 0.1 Cr, 0.05 Ni, 500 Formate	70	358	NA [b]	1	110	140
OE21	0.4 Fe, 0.1 Cr, 0.05 Ni, 500 Formaldehyde	70	115	3.7	NT	NT	NT
OE22	0.4 Fe, 0.1 Cr, 0.05 Ni	70	575	3.0	32	26.25	85

[a] Abbreviations: Fe is Fe^{2+}, Cr is Cr^{3+}, Ni is Ni^{2+}, Cu is Cu+, V is V^{5+}, A is Inhibitor A, B is Inhibitor B, C is Inhibitor C.
[b] NA = Not applicable since formate was an additive
[c] NT = not tested

The difficulty of understanding the oxidation of PZ has been discussed in regards to the lack of detectable degradation products. Only formate, total formate, and

occasionally EDA are present most oxidized solutions. It has been hypothesized separately that either the total formate concentration or foaminess of a solution should represent the overall PZ oxidation rate in lieu of accurately quantifying PZ loss during the experiment. The foaminess coefficient is plotted against the total formate concentration at the end of the experiment in Figure 8.51 below. The experiments with the same additives have been indicated using different colored data points. The experiments with 1.0 mM Fe^{2+} have blue squares while those with 0.4 mM Fe^{2+}, 0.1 mM Cr^{3+}, and 0.05 mM Ni^{2+} are indicated with green triangles. The inconsistency of the data can easily be seen in this figure.

Unfortunately, there is not a dependable relationship between the two variables and this inconsistency indicates that both cannot represent PZ oxidation as a whole. The three experiments with the highest concentrations of total formate (OE4, OE8, and OE19) have foaminess coefficients ranging from 88 to 300 $\times 10^{-3}$ m^2-s. However, what does not seem to make sense is that two of the experiments with the highest foaminess coefficients (OE5B and OE7) have very low total formate concentrations of 2.4 and 0.6 mmole per kg, respectively, at the end of each experiment. The four experiments with 1.0 mM Fe^{2+} (blue squares) have a wide range of foaminess coefficients with consistent levels of total formate at the end of the experiment.

The stability or shelf-life of oxidized PZ solutions after the conclusion of an experiment was a primary concern considering the conflicting foaminess data. To analyze this, the number of days between the end of the oxidation experiment and the foaminess test was calculated for all the foaming tests performed. The number of days between the experiment end and the test are plotted against the foaminess coefficient in Figure 8.52.

With the exception of the data from OE4 (195 days, 300 $\times 10^{-3}$ m^2-s), there is a correlation between the number of days and the overall foaminess coefficient. No measurements past 60 days resulted in foaminess coefficients of more than 25 $\times$ 10^{-3} m^2-s, except OE4. This suggests that the contaminants or degradation products in solution that cause foaming during the foaming tests continue to react while on the shelf and can greatly affect test results. If this is the case, there is significant error in the foaminess test since the protocol does not require the test be performed consistently. Comparing the number of days between the experiment end and the foaming test as a function of the foam stability also produces a very clear correlation (Figure 8.53). High foam stability values cannot be achieved with longer wait times. It is important to note that the foam stability was not measured for OE4.

The measurement of foaminess coefficient is not a reliable or consistent analytical technique. It varies widely for similar solutions and any conclusions taken from foaminess data should be considered qualitative at best. Since the degradation products that are responsible for foaming have not been determined, it is not known which variables in these experiments most affect the measured foaminess coefficient. At this point, the time between the experiment end and the measurement has the most impact on the results.

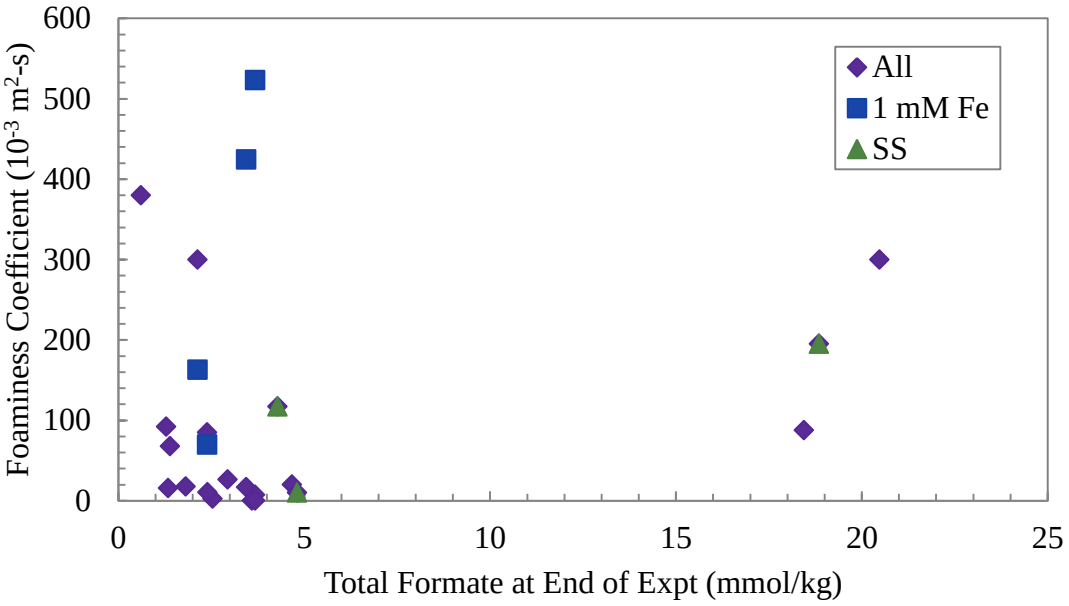

Figure 8.51: Relationship between the foaminess coefficient and total formate production

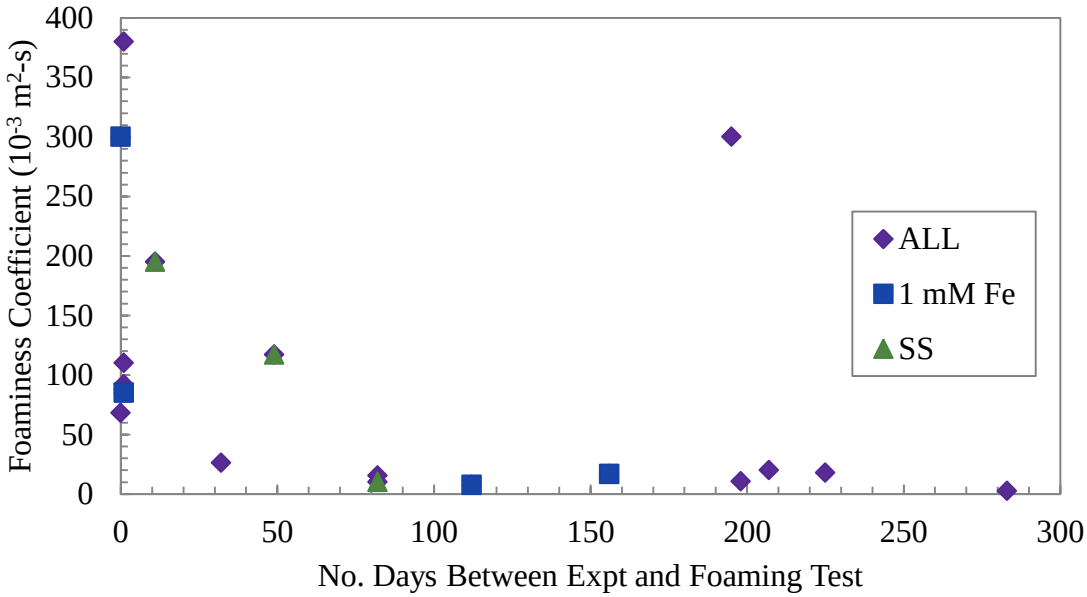

Figure 8.52: Relationship of foaminess coefficient and the delay in measurement

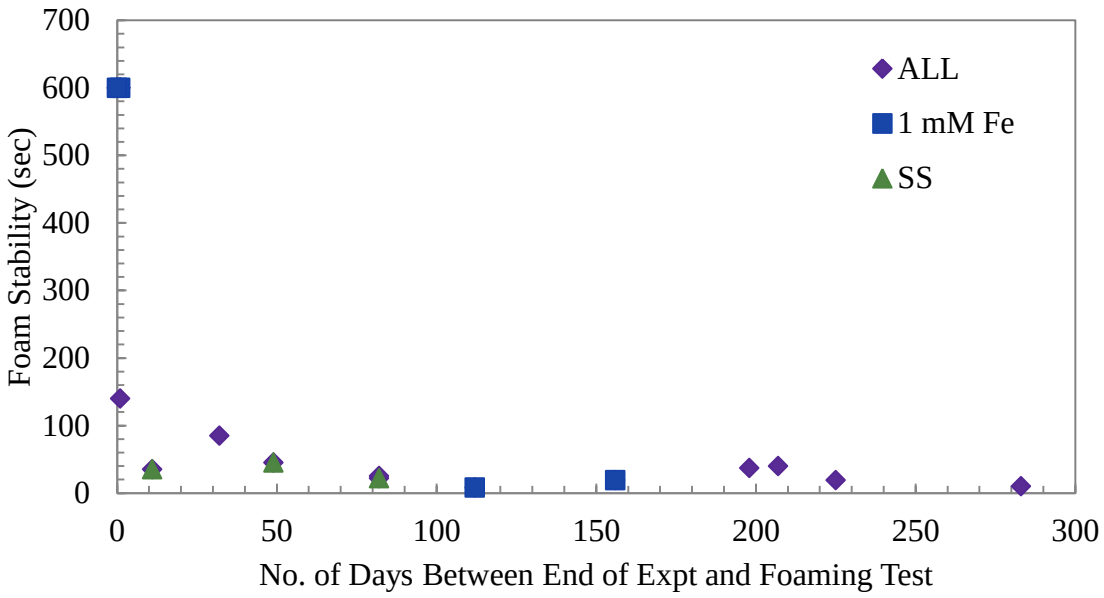

Figure 8.53: Relationship of foam stability and the delay in measurement

8.11 CONCLUSIONS

Oxidation of concentrated PZ from 55 to 70 °C in the presence of Cu^{2+} was found to be consistent with a mechanism that is first order in O_2 partial pressure. A 245% increase in O_2 partial pressure from 40 to 98 kPa enhanced PZ loss by 240% at 55 °C. The production of formate, total formate, and EDA increased by 180, 340, and 370%, respectively, for the same increase in O_2 partial pressure. At 70 °C in the presence of Cu^{2+}, PZ loss was enhanced 206% with a 235% increase in O_2 partial pressure. This data indicates a first order dependence of PZ oxidation on O_2. In the presence of SSM, the oxidation rate was too slow to see a large change in PZ loss, but the generation rate of degradation products increased with higher O_2 partial pressures, consistent with the Cu^{2+} experiments.

In Cu^{2+}-catalyzed systems, an increase in reactor temperature from 55 to 70 °C increased the PZ loss rate by 230%. A change of 15 °C in reactor temperature, therefore,

has the same effect as an increase in O_2 content by 245% in Cu^{2+}-catalyzed systems. At the same time, the production of formate, total formate, and EDA increased by 270, 340, and 170%, respectively. The activation energy for PZ loss in this temperature range was determined to be 27.2 kJ per mole in Cu^{2+}-catalyzed systems. This low activation energy indicates the propensity of PZ to degrade in the presence of Cu^{2+}. Activation energies for the generation of formate, total formate, and EDA were calculated to be 47, 29, and 36 kJ per mole, respectively, in the presence of Cu^{2+}. Since the activation energy for formate generation is higher than that of total formate, it is likely that formate generation is an oxidation mechanism while the formation of amides is dependent on formate concentration, rather than oxidation directly.

In SSM-catalyzed systems, an increase of 15 °C, from 55 to 70 °C, produced a small but noticeable increase in PZ loss. The activation energy for PZ loss in SSM-catalyzed systems was determined to be 96 kJ per mole, 3.5 times higher than in the presence of Cu^{2+}. Activation energies for the generation of formate, total formate, and EDA were calculated to be 50, 48, and 96 kJ per mole, respectively, in the presence of SSM.

The activation energy for the generation of formate is approximately the same in the presence of Cu^{2+} and SSM at 47-49 kJ per mole. The oxidation mechanism that is responsible for formate may not be dependent on the catalyst type. Formate is likely the most representative product to indicate oxidation when PZ data is unreliable.

CO_2 concentration was found to have a weak effect on PZ oxidation compared to O_2 and temperature. A decrease from 0.3 to 0.2 mole CO_2 per mole alkalinity produced a decreased PZ loss rate, but enhanced rate of generation of formate and total formate. Data with a high loading (0.4 mole CO_2 per mole alkalinity) demonstrated counteractive effect of low O_2 partial pressure and was not conclusive.

PZ concentration was also found to have only a weak effect on PZ oxidation from 5 to 10 m PZ. Higher concentration PZ was found to preferentially produce amides over the corresponding free carboxylate ion, matching observations in thermally degraded PZ experiments. The effect of PZ concentration is small compared to that of O_2 and temperature.

Baseline oxidation experiments performed in the absence of metal catalysts experienced 2 to 7% PZ loss over 350 hours, representing the PZ loss due to overall experimental error. Tracers were not effective at maintaining the water balance in the reactor.

The identified oxidation products of PZ include EDA, carboxylate ions (formate, oxalate, acetate), amides (formyl amides, oxalyl amides, and acetyl amides of PZ, EDA, and ammonia), and ammonium (NH_4^+). Glycolate, nitrite and nitrate are minor products that were inconsistently generated. In highly oxidized solutions, unidentified peaks on both anion IC and cation IC have been classified as either monoamines, polyamines, and amides, but are significantly smaller in area to the primary degradation products.

Analysis of TOC and TN indicated the presence of unidentified liquid phase degradation products. Both a baseline experiment and a heavily oxidized solution in the presence of Cu^{2+} were found to have maintained the TOC concentration in the liquid phase during the experiment, indicating unquantified liquid phase oxidation products. Both experiments also experienced a quantifiable decrease in TN concentration, indicating the loss of volatile N compounds not containing C. Ammonia (NH_3) has been confirmed as one volatile product while NO_X species are also suspected.

N and C mass balances on oxidized solutions were poor, especially with low rates of oxidation. In OE11, a baseline experiment, only 2.5% and 1.7% of the N and C, respectively, lost as PZ was recovered. Inclusion of an estimate of the volatile N from

the TN analysis increased the N balance to 75% of the lost PZ. For OE18, an experiment with SSM, only 3.4% and 5.2% of the N and C lost as PZ was recovered in products. In OE25, the most heavily oxidized PZ solution in the study, 27% and 23% of the N and C, respectively, from the lost PZ was recovered as liquid phase products. With the inclusion of an estimate of 2650 mmole volatile N per kg from TN, 69% of the lost PZ N was recovered.

A combination of the mass balance and TOC results suggest a significant concentration of degradation products that have not been identified in the liquid phase. More sophisticated liquid phase analyses are needed to identify the important oxidation products of concentrated PZ. Amino acid detection indicates that this may be an important function group in oxidation products, but no amino acids were identified. It is suspected that aldehydes (e.g. formaldehyde, acetaldehyde, and hydroxyacetaldehyde), alcohols (e.g. methanol, ethanol, and, ethylene glycol), ureas of PZ, amino acids (e.g. N-(2-aminoethyl) glycine, N,N'-1,2-ethanediylbis-glycine), and oxidized PZ molecules (2-piperazinone, 2,5-piperazinedione, 2-piperazinol, 1,2,3,6-tetrahydro pyrazine, 1,2,3,4,-tetrahydro pyrazine, 1-piperazineaceticacid) are a significant portion of the unidentified products.

The addition of 500 mM formate to 8 m PZ eliminated the production of EDA, suggesting that PZ oxidation was significantly decreased. However, the change in the loss rate of PZ was small and possibly not statistically significant. Formate is not oxidized to CO_2 in PZ oxidation experiments but may act as a weak oxidation inhibitor for PZ.

The addition of 500 mM formaldehyde to 8 m PZ created stable, dense, white foam that persisted through the oxidation experiment. The foam is likely a polymer of formaldehyde and PZ that was stable for over 10 months.

The foaminess coefficient is not a consistent measurement technique and does not produce repeatable results. The amount of time between the end of an experiment and the foaminess test appears to impact results, which is an unforeseen problem in the assay. The foaminess coefficient also does not accurately represent the overall degradation of an oxidized PZ solution.

Chapter 9 – Catalysts and Inhibitors for the Oxidation of Concentrated, Aqueous PZ

The oxidation of concentrated PZ systems can be greatly affected by the presence of metal catalysts or inhibitors. Metal catalysts are likely to be present in industrial CO_2 capture systems due to corrosion of the materials of construction, presence of metals in industrial chemicals, and through the use of inhibitors or other additives. This chapter explores the catalytic effect iron (II) (Fe^{2+}), copper (II) (Cu^{2+}), a combination of Fe^{2+}, chromium (III) (Cr^{3+}), nickel (II) (Ni^{2+}), and a combination of Fe^{2+} and vanadium (V) (V^{5+}). Three inhibitors are investigated to determine their efficacy at decreasing metal-catalyzed oxidation. Portions of this chapter are excerpted from a previous publication relating to PZ oxidation (Freeman et al., 2010a).

9.1 METAL CATALYSTS FOR OXIDATION OF PIPERAZINE

Metal catalysts are known to enhance oxidation rates of amines in the presence of elemental oxygen (O_2) (Goff, 2005; Sexton, 2008). The effect of metal catalysts on the oxidation of PZ has only been studied to a small degree by Sexton. Sexton focused on low concentration solutions, always below 5 molal (m) PZ (Sexton, 2008). The work in this section focuses on metal catalysis of oxidation of 8 m PZ.

The discussion of catalytic impact of metals will rely on comparisons to the four baseline experiments discussed in section 8.2.1. These experiments in the absence of metal catalysts or inhibitors represent the range of expected experimental error over the course of a typical experiment. Any loss of PZ in a catalyzed experiment that is close the level shown in the baseline experiments indicates a weak catalyst for PZ oxidation or data that should be interpreted with caution. Strong catalysts and conditions will demonstrate PZ losses that are noticeably faster that the baseline experiments. Differences in experiments in terms of O_2 concentration, CO_2 concentration, and PZ concentration will be noted, but the data will be plotted together for efficiency. Only experiments with differences in metal catalyst and temperature will be presented separately in this chapter.

9.1.1 Effect of iron (Fe^{2+})

In industrial CO_2 capture systems constructed of carbon steel, aqueous iron or iron particulates are expected to be present in amine solutions due to corrosion of the columns, column internals, storage tanks, and piping. If carbon steel is to be used for PZ-based CO_2 capture systems, the catalytic effect of aqueous iron on the oxidation of PZ needs to be understood in order to mitigate the effect, if possible. This concentration of iron was based on concentrations observed to accumulate in commercial acid gas treating systems lacking a corrosion inhibitor. Reports of CO_2 capture systems in service without corrosion inhibition using a variety of amines, typically alkanolamines such as

monoethanolamine (MEA) or diethanolamine (DEA), have reported concentrations up to 6000 ppm iron (Hall and Barron, 1981; Holub et al., 1998). Sexton had previously studied lower concentration PZ oxidation found that Fe^{2+}-catalyzed oxidation of PZ was very slow compared to 7 m MEA (Sexton, 2008). Sexton also observed no difference in oxidation when the Fe^{2+} was varied from 0.1 to 5 mM.

To simulate the effects of carbon steel corrosion, 8 m PZ was oxidized in the presence of 1 mM Fe^{2+}. Three experiments, OE4, OE13, and OE17, were performed on 8 m PZ in the presence of 1 mM Fe^{2+} at 55 °C with agitation at 1400 rpm and 100 mL per minute of 98% O_2/2% CO_2 in the headspace. The PZ loss data from these three experiments are compared to the baseline experiments in Figure 9.1. Sexton performed an experiment in 5 m PZ with 5 mM Fe^{2+} under similar reactor conditions in an attempt to maximize Fe^{2+}-catalytic impact and these data are compared as well.

Initially, the PZ loss rates in all four experiments appear to be faster than the baseline experiments. After 100 hours, however, the data for the high Fe^{2+} experiment becomes more scattered and the final points recover the initial PZ concentration. The remaining three experiments demonstrate some disagreement but all oxidize faster than the baseline experiment. After 160 hours, the loss of PZ ranges from 7 to 14%, above the baseline cases ranging from of 1 to 5%. There is a significant level of scatter in the high Fe^{2+} data, but the high level of Fe^{2+} does not enhance oxidation above the levels seen in the 1 mM experiments.

The production of total formate and ethylenediamine (EDA) are compared for the same four experiments and four baseline experiments in Figure 9.2 and Figure 9.3, respectively. The productions of both of these major degradation products are close to the four baseline experiments and do not demonstrate repeatability. There is significant scatter in the total formate data for OE5 and the high Fe^{2+} experiment. The other two

experiments have the expected trend, but are not statistically significant compared to the baseline experiments. EDA, which is difficult to quantify accurately at low concentrations, was detected in all four experiments, but not consistently or at levels above the baseline experiments.

Overall, Fe^{2+} appears to be only a very weak catalyst for PZ oxidation, even up to 5 mM Fe^{2+}, based on PZ loss. The generation of degradation products is not consistent between experiments and is within the concentrations produced in the baseline experiments. Fe^{2+} may catalyze PZ oxidation to a small extent, but no more than a 7% loss of PZ after 300 hours as found in the baseline experiments.

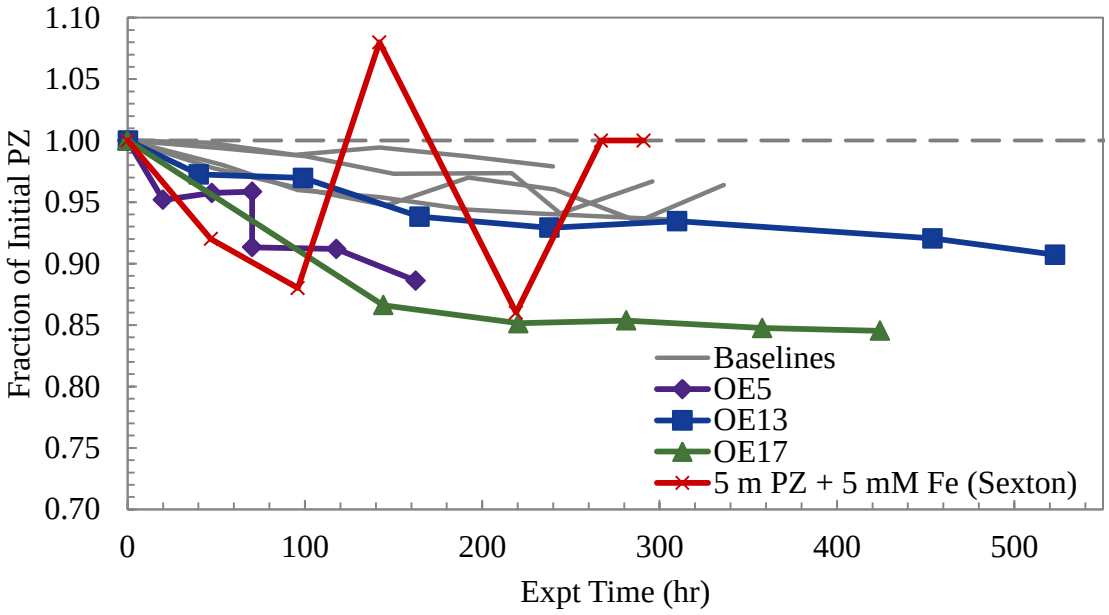

Figure 9.1: Catalytic effect of Fe^{2+} on PZ Loss (8 m PZ, 55 °C, 1400 rpm, 100 mL/min 98% O_2/2% CO_2, 1 or 5 mM (×) Fe^{2+})

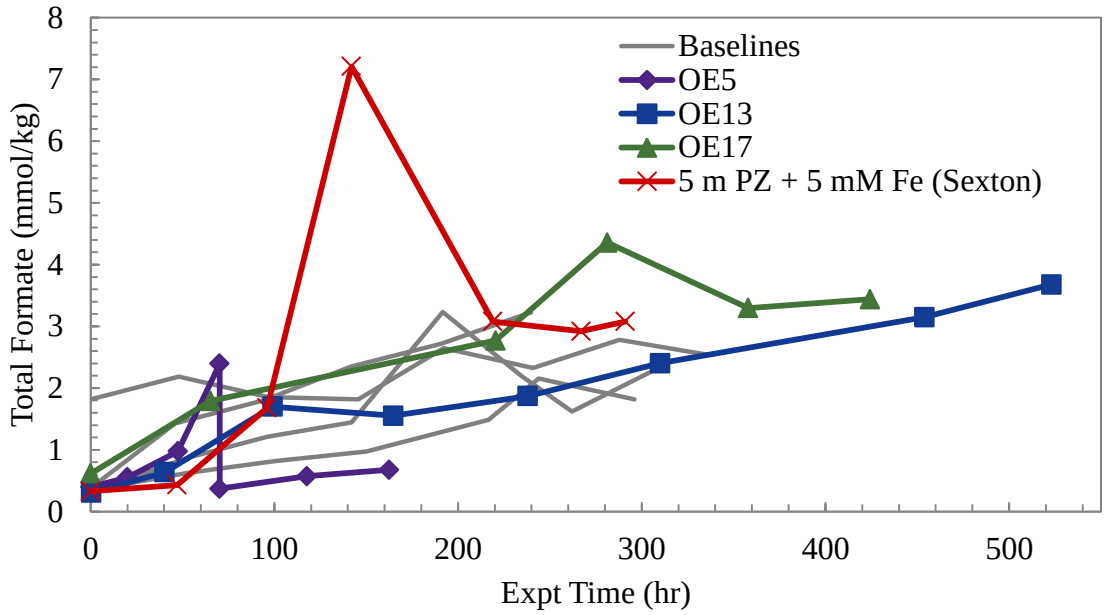

Figure 9.2: Production of total formate in the presence of 1 or 5 mM (×) Fe^{2+} (8 m PZ, 55 °C, 1400 rpm, 100 mL/min 98% O_2/2% CO_2)

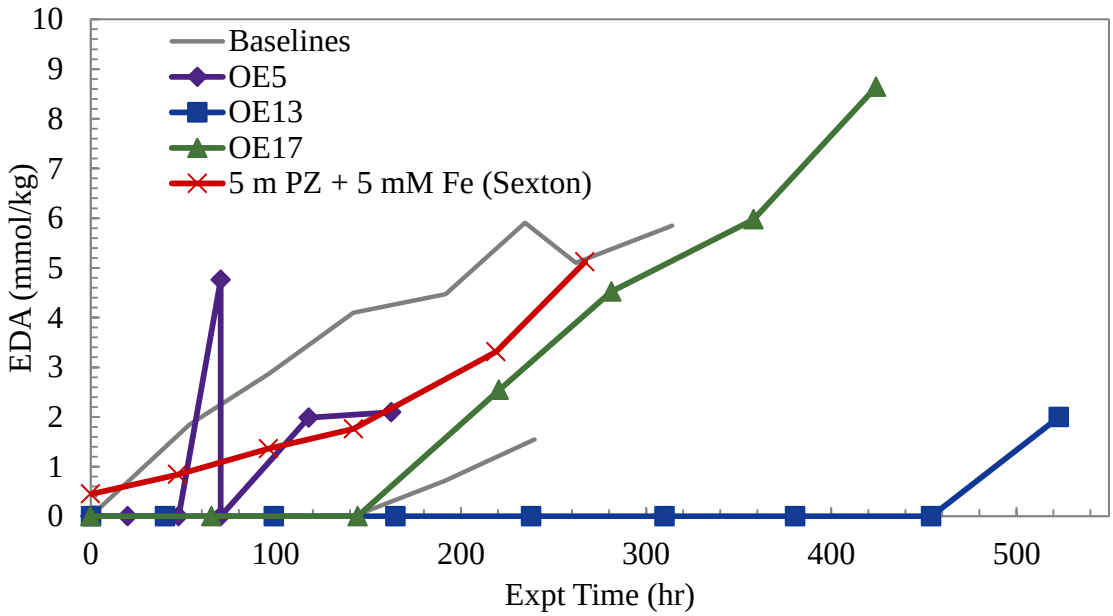

Figure 9.3: Production of EDA in the presence of 1 or 5 mM (×) Fe^{2+} (8 m PZ, 55 °C, 1400 rpm, 100 mL/min 98% O_2/2% CO_2)

9.1.2 Effect of stainless steel metals (Fe^{2+}, Cr^{3+}, and Ni^{2+})

Stainless steel will more likely be used as the material of construction for absorber-stripper systems due to its enhanced resistivity to corrosion. If any corrosion does occur, low concentrations of Fe^{2+}, Cr^{3+}, and Ni^{2+} can exist as aqueous species in amine solutions. To simulate the catalytic effect of stainless steel metals, concentrated PZ was oxidized in the presence of 0.4 mM Fe^{2+}, 0.1 mM Cr^{3+}, and 0.05 mM Ni^{2+}, also known as the standard stainless steel metal (SSM) mixture. This combination was determined to be representative of the expected concentrations of each species and relative concentrations to each other in a stainless steel system without corrosion inhibitors. This concentration mixture was maintained for all of the experiments containing SSM, with one exception. In the first oxidation experiment, 10 m PZ was oxidized in the presence of 0.26 mM Fe^{2+}, 1.6 mM Cr^{3+}, and 0.26 mM Ni^{2+} before the standard SSM mixture was developed.

9.1.2.1 Effect of stainless steel metals at 55 °C

In total, four concentrated PZ experiment were performed in the presence of SSM at 55 °C. Three experiments, OE15, OE18, and OE18, were performed on 8 m PZ with the standard SSM mixture, while a fourth, OE1, was a 10 m PZ experiment with varied concentrations of metals, as described above. The PZ loss for these four experiments is compared to the four baseline experiments in Figure 9.4. The 10 m PZ experiment is indicated in the figure to highlight the difference in PZ and metals concentrations. The experiments with 8 m PZ and the SSM mixture demonstrated PZ loss data well within the range of the four baseline experiments and appear to demonstrate a small level of oxidation inhibition. The 10 m PZ experiment demonstrated slightly enhanced PZ loss after 300 hours of oxidation that was statistically significant above the baseline experiments.

The generation of total formate and EDA for the four experiments and four baseline experiments is compared in Figure 9.5 and Figure 9.6, respectively. As was expected after analyzing the PZ loss, the generation rate of total formate and EDA in all four experiments is low and falls within the boundaries established by the baseline experiments. The generation of products at similar levels as the baseline indicates there is not inhibition, but very low rates of oxidation. Overall, the SSM are a weak catalyst for PZ oxidation when examined in terms of both PZ loss and the generation of degradation products. As with Fe^{2+}-catalysis, SSM may catalyze PZ oxidation to some extent, but no more than the baseline 7% loss of PZ after 300 hours as found in the baseline experiments.

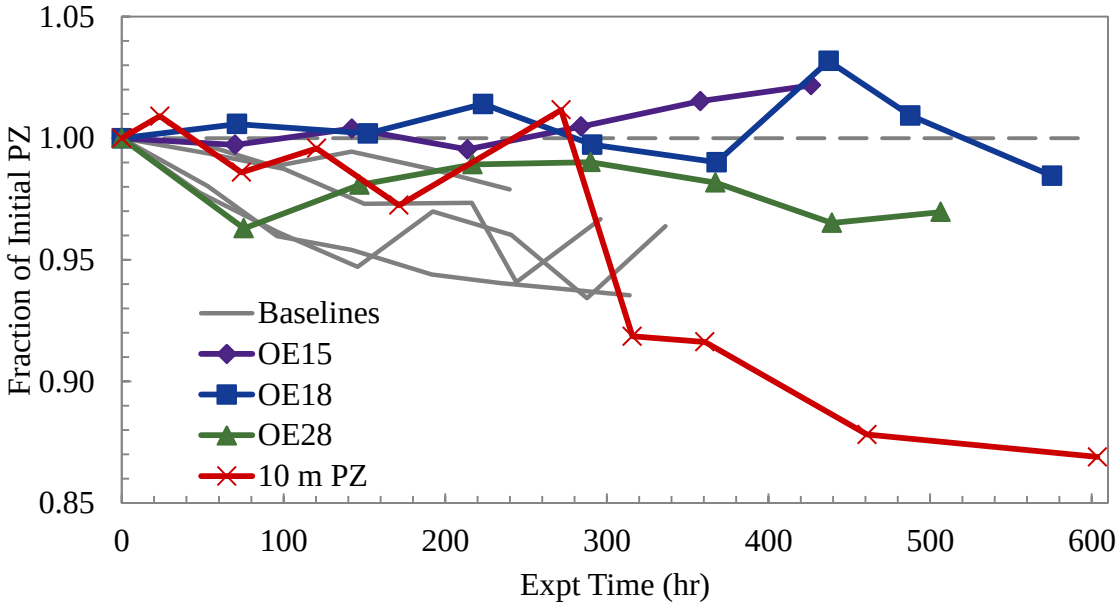

Figure 9.4: Catalytic effect of SSM on PZ Loss (8 m PZ, 55 °C, 1400 rpm, 100 mL/min 98% O_2/2% CO_2, 0.4 mM Fe^{2+}, 0.1 mM Cr^{3+}, 0.05 mM Ni^{2+})

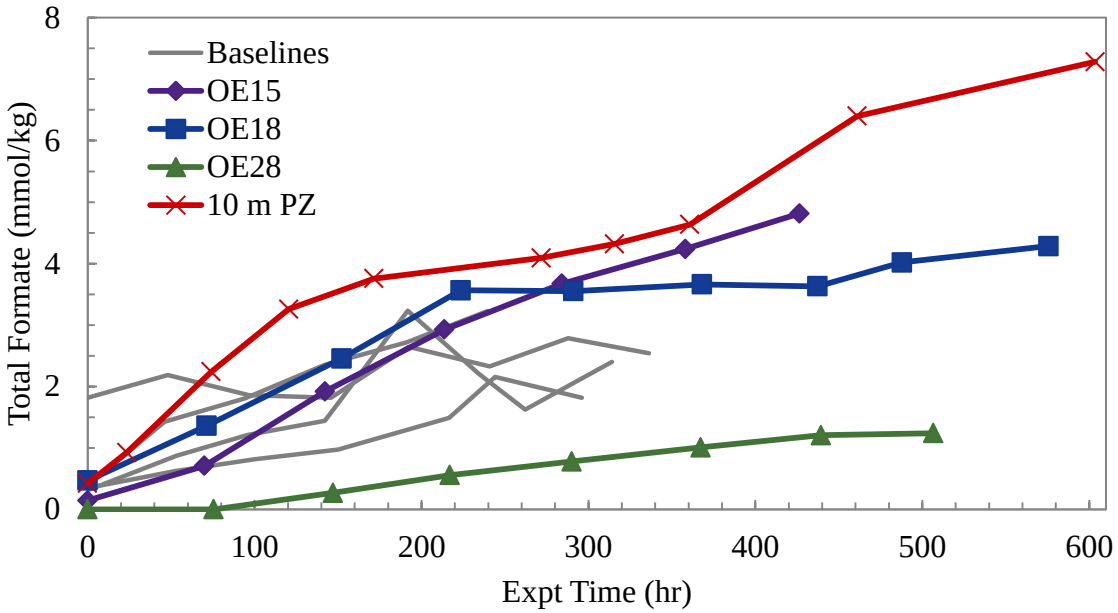

Figure 9.5: Production of total formate in the presence of SSM (8 m PZ, 55 °C, 1400 rpm, 100 mL/min 98% O_2/2% CO_2, 0.4 mM Fe^{2+}, 0.1 mM Cr^{3+}, 0.05 mM Ni^{2+})

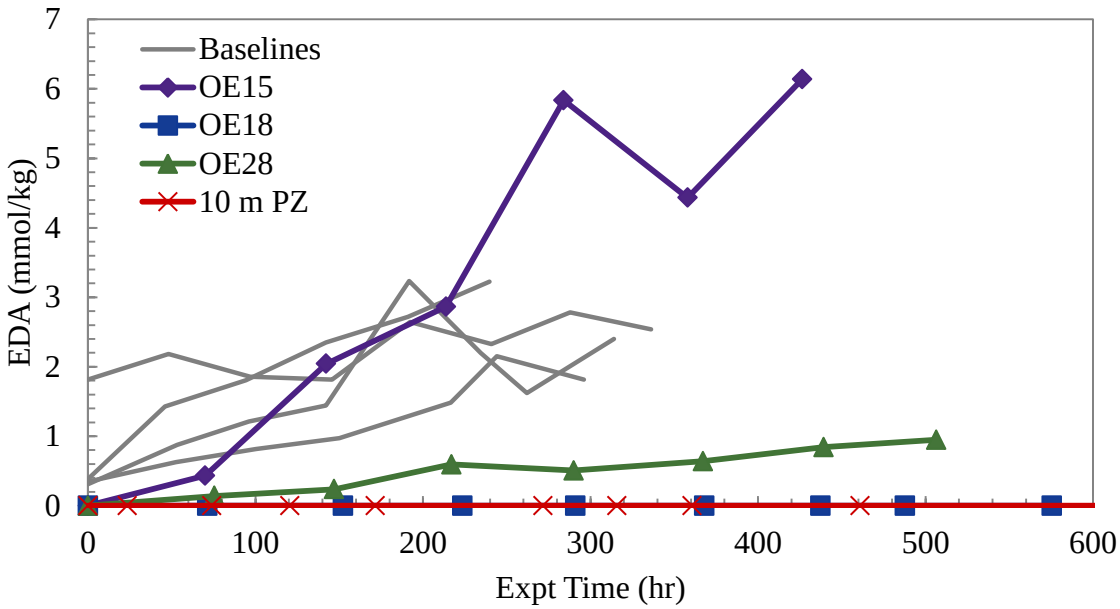

Figure 9.6: Production of EDA in the presence of SSM (8 m PZ, 55 °C, 1400 rpm, 100 mL/min 98% O_2/2% CO_2, 0.4 mM Fe^{2+}, 0.1 mM Cr^{3+}, 0.05 mM Ni^{2+})

9.1.2.2 Effect of stainless steel metals at 70 °C

The catalytic effect of stainless steel metals was also investigated at the higher temperature of 70 °C. High temperature experiments were performed in order to accelerate degradation in order to analyze PZ oxidation more accurately. Unfortunately, no baseline experiments were performed at 70 °C, so it is not possible to understand if there are any mechanistic differences in the reactor operation or water balance due to the increased temperature. Since the water and amine volatility will increase at 70 °C, the water balance will be strongly affected due to increased water losses. The water balances were carefully monitored for high temperature experiments and the water added to the pre-saturator was also monitored starting with OE19, the first high temperature experiment. This was done in an effort to maintain the water balance as closely as possible.

In total, three concentrated PZ experiment, OE19, OE22, and OE26, were performed in the presence of the standard stainless steel metal mixture at 70 °C. PZ loss for these three experiments is compared to the four baseline experiments at 55 °C in Figure 9.7. Unfortunately, the three experiments do not demonstrate a high degree of repeatability in terms of the PZ loss data. Both OE22 and OE26 demonstrate PZ loss that is slightly more than that observed in the baseline experiments, indicating that the presence of SSM at 70 °C may enhance PZ oxidation rates above the baseline noise of the experiment, while OE19 falls within the range of the baselines. OE22 had a lower O_2 content (40%) than the other two experiments (96-98%), but the PZ loss data shows that OE19 had the lowest loss rate of PZ.

The generation of total formate and EDA for the four experiments and four baseline experiments are compared in Figure 9.8 and Figure 9.9, respectively. The total formate and EDA data have opposite trends as those seen in the PZ loss data for

experiments OE19 and OE22. For OE22, where PZ loss up to 10% was observed, the total formate concentration is within the noise of the baselines. For OE19, which did not have significant PZ loss, the highest concentration of both products was observed. Overall, SSM are not a strong catalyst for concentrated PZ oxidation, even at the elevated temperature of 70 °C. There is some evidence that at this temperature, oxidation is starting to be accelerated, but more data at even higher temperatures would be needed to fully confirm this observation. The loss of PZ in this condition is at most 10% of the initial PZ after 400 hours.

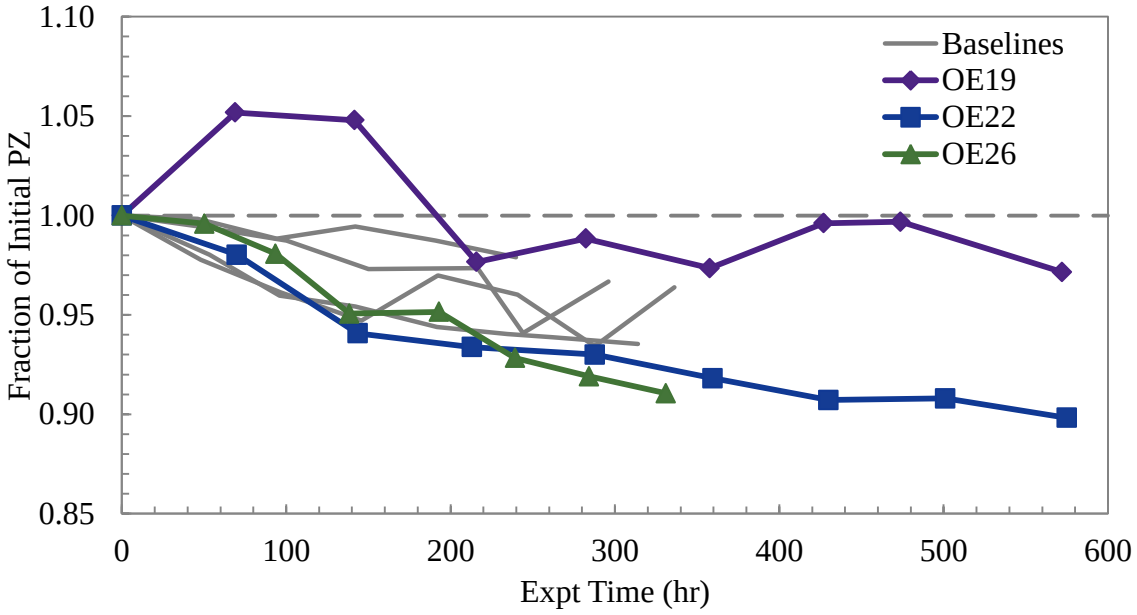

Figure 9.7: Catalytic effect of SSM on PZ Loss (8 m PZ, 70 °C, 1400 rpm, 100 mL/min 40-98% O_2/2-6% CO_2, 0.4 mM Fe^{2+}, 0.1 mM Cr^{3+}, 0.05 mM Ni^{2+})

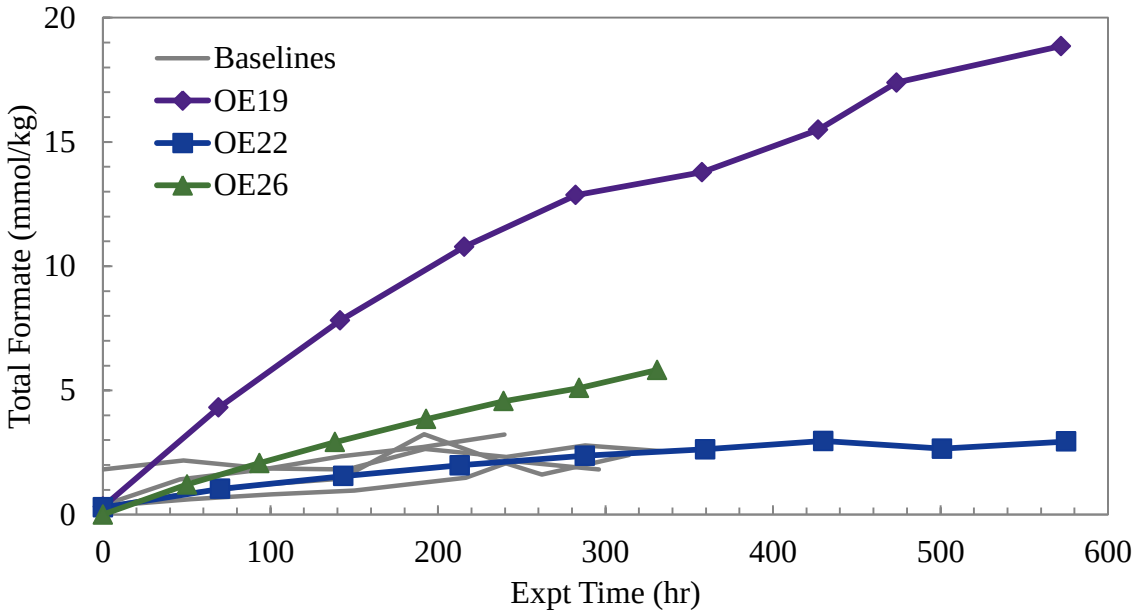

Figure 9.8: Production of total formate in the presence of SSM (8 m PZ, 70 °C, 1400 rpm, 100 mL/min 40-98% O_2/2-6% CO_2, 0.4 mM Fe^{2+}, 0.1 mM Cr^{3+}, 0.05 mM Ni^{2+})

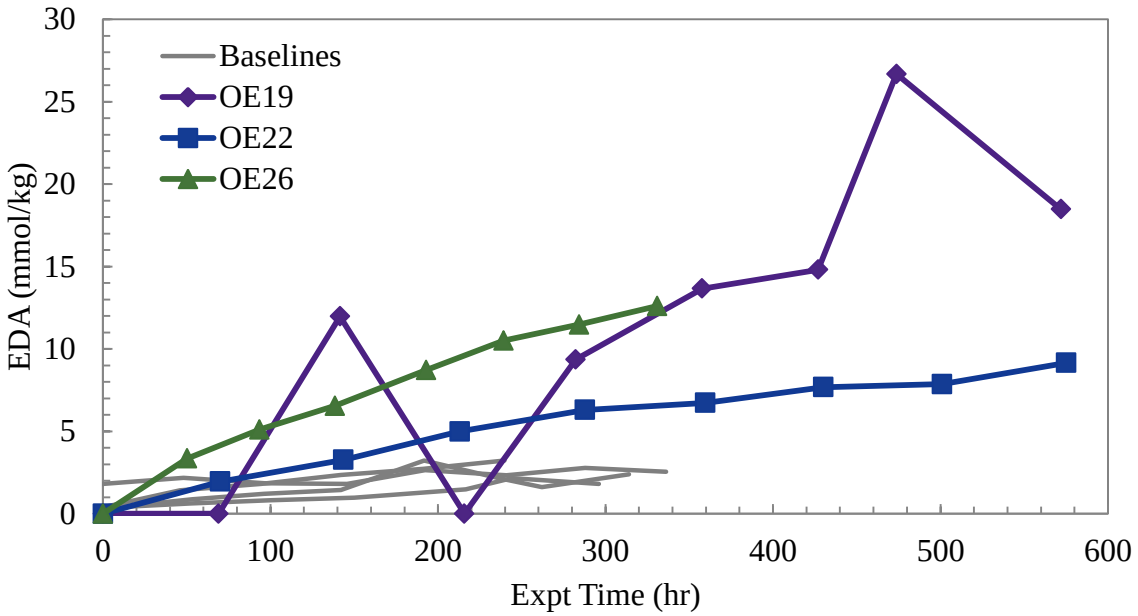

Figure 9.9: Production of EDA in the presence of SSM (8 m PZ, 70 °C, 1400 rpm, 100 mL/min 40-98% O_2/2-6% CO_2, 0.4 mM Fe^{2+}, 0.1 mM Cr^{3+}, 0.05 mM Ni^{2+})

9.1.3 Effect of copper (Cu^{2+})

Copper salts have been used as a corrosion inhibitor in industrial gas treating systems and are also a well-known catalyst for amine degradation. To determine the extent of copper-catalyzed oxidation, 8 m PZ was degraded in the presence of 4.0 mM Cu^{2+}, or roughly 250 ppm Cu^{2+}. This concentration of Cu^{2+} was chosen to match those proposed for Cu^{2+}-based corrosion inhibitors (Pearce, 1984; Reed, 1945). Cu^{2+} has been identified previously to have the strongest catalytic effect on oxidation of MEA and the same behavior was expected for concentrated PZ (Goff and Rochelle, 2006; Sexton and Rochelle, 2009b). As demonstrated in the previous two sub-sections, PZ degradation is slow in the presence of either Fe^{2+} or SSM and Cu^{2+}-catalyzed degradation was used to rapidly achieve oxidation with the purposes of identifying degradation products.

9.1.3.1 Effect of copper (Cu^{2+}) at 55 °C

The effect of Cu^{2+} on PZ oxidation at 55 °C was explored in two experiments, OE2 and OE27. These two experiments were compared in section 8.4.2.1 to demonstrate the effect of O_2 partial pressure. The PZ loss for these two experiments is compared to the baseline data in Figure 8.29 while the generation of degradation products in both experiments is compared to the baselines in Figure 8.30.

Copper is clearly an exceedingly strong catalyst for PZ oxidation under both low (OE27) and high O_2 (OE2) conditions. After 500 hours of oxidation, either 16 or 33% of the initial PZ is lost for the low and high O_2 conditions, respectively. In agreement with the PZ loss data, the generation of formate, total formate, and EDA are all well above that of the baseline experiments, demonstrating the strength of Cu^{2+} as a PZ oxidation catalyst at 55 °C.

9.1.3.2 Effect of copper (Cu^{2+}) at 70 °C

The effect of Cu^{2+} on PZ oxidation at 70 °C was explored in two experiments, OE23 and OE25, with either 40 or 94% O_2. These experiments were discussed in section 8.4.2.2 to demonstrate the effect of O_2 partial pressure on high temperature, Cu^{2+}-catalyzed oxidation. The PZ loss for these two experiments is compared to the baseline data in Figure 8.31 while the generation of formate, total formate, and EDA are compared in Figure 8.32.

As expected, Cu^{2+} is a very strong catalyst for PZ oxidation under both low and high O_2 conditions at 70 °C. Between 35 and 72% of the initial PZ is oxidized in these experiments, indicating the superior efficacy of Cu^{2+} as an oxidation catalyst. The generation of total formate and EDA are in agreement with the PZ loss data. High concentrations of the degradation products were seen in both experiments, with up to 170, 555, and 335 mmole per kg of formate, total formate, and EDA, respectively, seen in the high O_2 experiment. The low O_2 experiment also demonstrates the generation of significant concentrations of both products, well above what was quantified in the baseline experiments. Aqueous Cu^{2+} is a clear catalyst for oxidation of concentrated PZ at 70 °C.

9.1.4 Effect of vanadium (V^{5+})

V^{5+} is a component of some corrosion inhibitors and can be used at variable concentrations (Ranney, 1976). The potential catalytic effect of low concentration V^{5+} was assessed for concentrated PZ. A solution of 8 m PZ with 0.1 mM V^{5+} and 0.1 mM Fe^{2+} was oxidized at 55 °C with agitation at 1400 rpm with 100 mL per minute 98%O_2/2% CO_2 in the headspace (OE3). This low concentration was chosen to match the expected concentration of V^{5+} based corrosion inhibitors (Mago, 1974; Mago and West, 1976; Nieh, 1983). Fe^{2+} was added to simulate a system where corrosion would

lead to small concentrations of Fe^{2+} in solution. Sexton observed a strong catalytic effect of V^{5+} on MEA oxidation, where MEA was oxidized half as fast as when in the presence of Fe^{2+}, a strong catalyst for MEA oxidation (Sexton, 2008). V^{5+}-catalyzed oxidation has not been studied for concentrated PZ systems.

The PZ loss for the V^{5+} experiment is compared with the four baseline PZ oxidation experiments in Figure 9.10. The PZ loss is virtually negligible and falls well within the error experienced in the baseline experiments. The generation of total formate, the dominant degradation product in the V^{5+} experiment, is compared with the baseline experiments in Figure 9.11. As with PZ loss, the total formate data is very close to the baseline data. After 200-250 hours of oxidation, the concentration of total formate continues to climb, indicating an enhanced production of this product compared to the baseline cases. There may be a delay in total formate production in the presence of this catalyst and a longer experiment would clarify this phenomenon.

Both the PZ and total formate data appear to indicate that V^{5+} is a weak catalyst for PZ oxidation at 55 °C. Sexton observed that V^{5+} had a stronger catalytic effect on PZ than Fe^{2+}, but his observations were based on experiments at 2.5 m PZ and 5 mM V^{5+} (Sexton, 2008). The effect of V^{5+} on 8 m PZ is difficult to assess with only low concentration V^{5+} data available. Oxidation performed with 5 mM V^{5+} may demonstrate that a high concentration of V^{5+} is required to observe a catalytic effect. Based on the data obtained in this project, V^{5+}-catalyzed oxidation occurs slower than a loss of 7% of the initial PZ after 300 hours, the baseline rate.

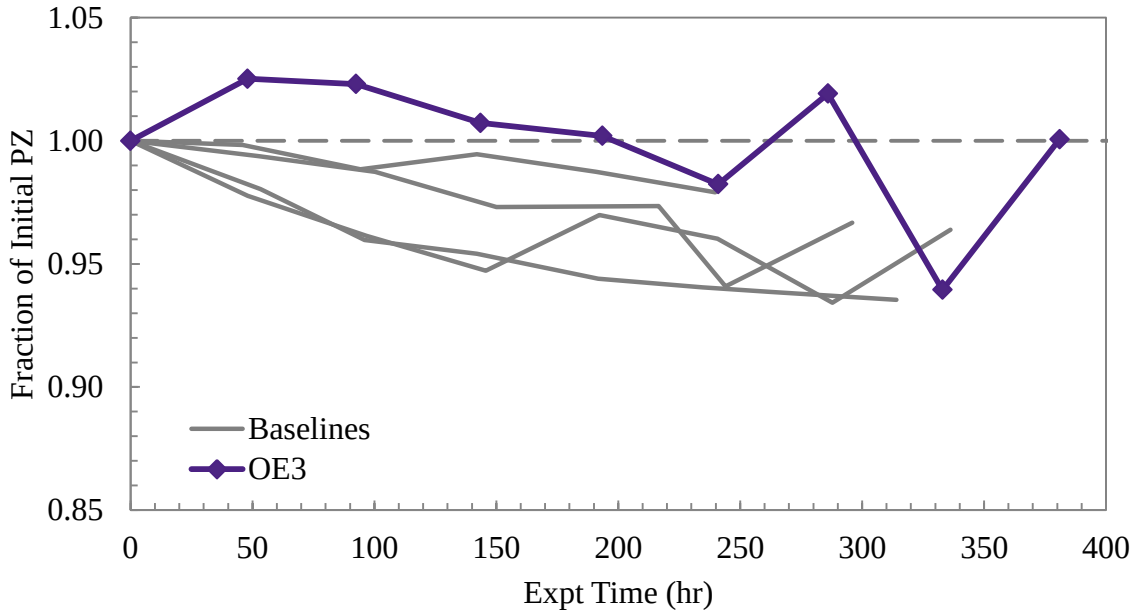

Figure 9.10: Catalytic effect of 0.1 mM V^{5+} and 0.1 mM Fe^{2+} (8 m PZ, 55 °C, 1400 rpm, 100 mL/min 98% O_2/2% CO_2)

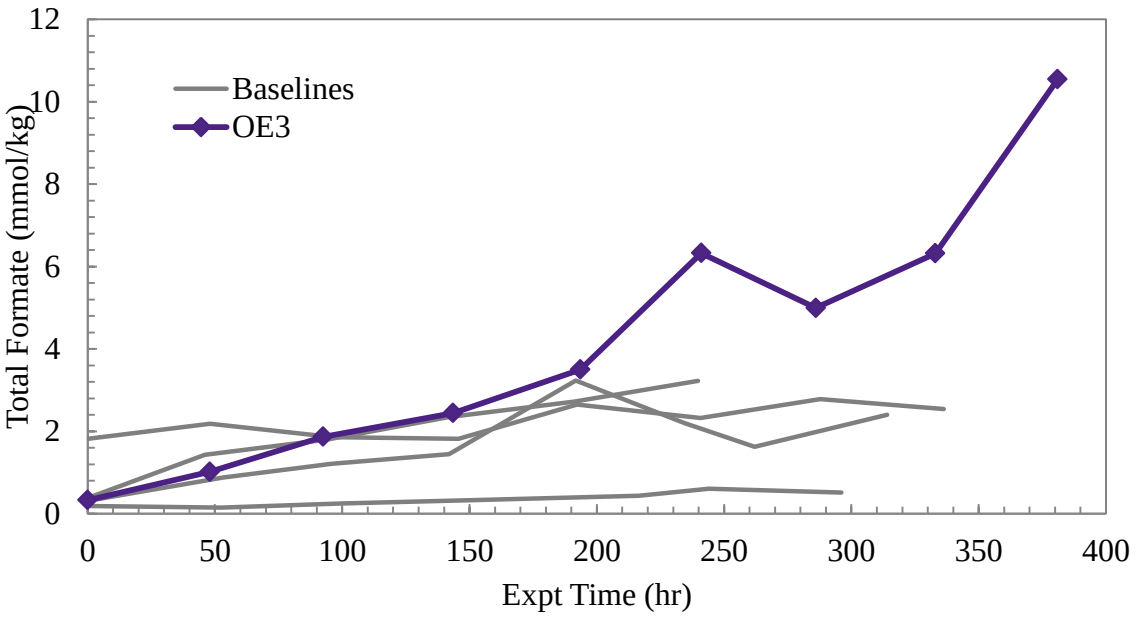

Figure 9.11: Production of total formate in the presence of 0.1 mM V^{5+} and 0.1 mM Fe^{2+} (8 m PZ, 55 °C, 1400 rpm, 100 mL/min 98% O_2/2% CO_2)

9.2 COMPARISON OF METAL CATALYZED OXIDATION OF CO_2 CAPTURE AMINES

9.2.1 Iron-catalyzed oxidation of CO_2 capture amines

In the presence of iron, many amines are known to oxidize readily, especially as the iron concentration increases (Goff, 2005; Sexton, 2008). Oxidation of PZ has been performed in the presence of 1 mM Fe^{2+} while previous amine oxidation studies went as high as 5 mM Fe^{2+} in order to rapidly catalyze oxidation (Goff, 2005; Sexton, 2008). PZ, MEA, EDA, Diglycolamine® (DGA), and DEA have all been oxidized at similar conditions in the low gas flow reactor with 1 mM Fe^{2+} at 55 °C with agitation at 1400 rpm and a flow of 100 mL per minute of 98% O_2/2% CO_2 in the headspace (Sexton, 2008; Zhou et al., 2010). The amine loss is compared between all five amines in Figure 9.12. Amine solutions discussed were 8 m PZ, 7 m MEA, 8 m EDA, 4 m DGA, or 4 m DEA, where concentrations differed based on the individual solvent system (Sexton, 2008; Zhou et al., 2010).

In the absence of any other metal catalyst or inhibitor, 8 m PZ loses 8% of the original amine after 450 hours. In the same time, 44% of 7 m MEA is lost. PZ is 5.5 times more resistant to Fe^{2+}-catalyzed degradation than the comparable MEA system. EDA oxidizes slowly at first, and then suffers Fe^{2+}-catalyzed oxidation after an initial lag of 50 hours. Although the experiment was shorter than that for PZ, EDA would be expected to have more oxidation than PZ after the initial lag phase based on the slope of the data. DGA is very resistant to Fe^{2+}-catalyzed oxidation. Some error in the water balance or analytical techniques led to an increase of DGA through the course of the experiment which can be interpreted as an overall lack of oxidation. Finally, DEA rapidly oxidized in the presence of Fe^{2+} catalyst and has initial oxidation rates similar to that of MEA.

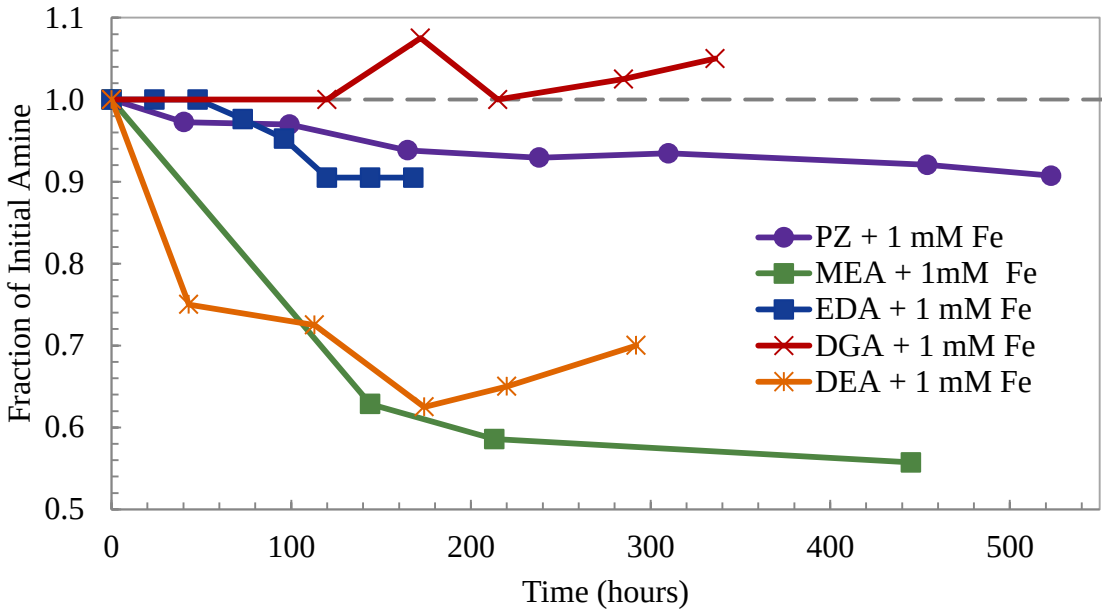

Figure 9.12: Comparison of PZ, MEA, EDA, DGA, and DEA loss in the presence of 1 mM Fe^{2+} (55 °C, 1400 rpm, 100 mL/min 98% O_2/2% CO_2) (Sexton, 2008; Zhou et al., 2010)

9.2.2 Stainless steel metal-catalyzed oxidation of CO_2 capture amines

Understanding the catalytic impact of SSM on amines is valuable because stainless steel is the expected material of construction for industrial CO_2 capture applications. PZ, MEA, and 3-(methylamino)propylamine (MAPA) have been oxidized in the same manner in the presence of the standard stainless steel SSM mixture (0.4 mM Fe^{2+}, 0.1 mM Cr^{3+}, and 0.05 mM Ni^{2+}) at 55 °C with agitation at 1400 rpm and 100 mL per minute of 98% O_2/2% CO_2 in the headspace (Sexton, 2008; Vevelstad, 2010). The amine loss is compared in Figure 9.13. Experiments compared in this figure were performed on 8 m PZ, 7 m MEA, and 9 m MAPA (Sexton, 2008; Vevelstad, 2010). The amine concentrations differed slightly as each amine has a preferred concentration for CO_2 capture applications (Rochelle, 2010a). After 350 hours, only 1%, of the original PZ has oxidized while the MEA experiment shows a loss of 35%. MAPA is completely

oxidized within 120 hours. The resistance of PZ and, to a lesser extent, MEA, to oxidation catalyzed by stainless steel metals is clearly demonstrated.

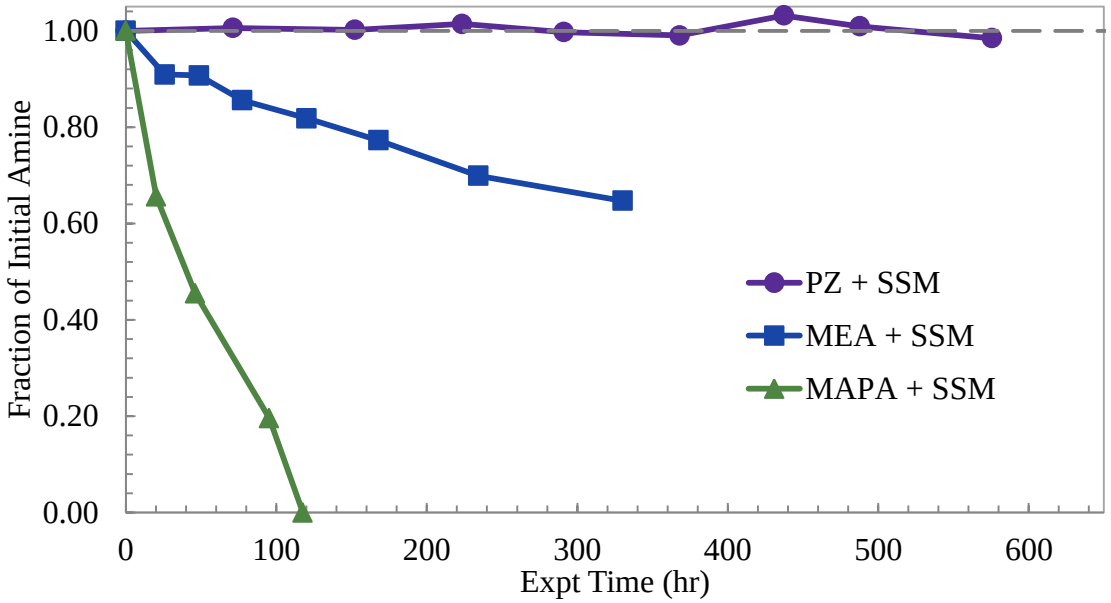

Figure 9.13: Comparison of PZ and MEA loss in the presence of SSM (55 °C, 1400 rpm, 100 mL/min 98% O_2/2% CO_2) (Sexton, 2008; Vevelstad, 2010)

9.2.3 Copper-catalyzed oxidation of CO_2 capture amines

Finally, Cu^{2+} is a well-studied oxidation catalyst that may be present in system utilizing a Cu^{2+}-based corrosion inhibitor. PZ, MEA, 2-amino-2-methyl-1-propanol (AMP), and EDA have been oxidized in the presence of Cu^{2+} at 55 °C with agitation at 1400 rpm and 100 mL per minute of 98% O_2/2%CO_2 in the headspace. The concentration of metals was slightly different between the experiments. The PZ, AMP, and EDA experiments contained 4, 5, and 5 mM Cu^{2+}, respectively, while the MEA experiment contained both 1 mM Fe^{2+} and 5 mM Cu^{2+} (Sexton, 2008). A comparable MEA experiment was not performed with only Cu^{2+} present. The concentration of amines also differed slightly depending on the solvent system. The experiments

discussed were performed on 8 m PZ, 7 m MEA, 4 m AMP, and 3.5 m EDA (Sexton, 2008).

The loss of amine for each of these experiments is compared in Figure 9.14. Although the metals concentrations are not exactly the same, the effect of copper on amine oxidation is clearly demonstrated. After 220 hours, 28% of the PZ had been degraded while 73% of the MEA was degraded. Even though PZ showed 2.6 times less degradation than 7 m MEA, the 28% degradation observed was nearly four times more than both Fe^{2+}- and SSM-catalyzed PZ oxidation. AMP and EDA, as observed by Sexton (2008), are both more stable to Cu^{2+}-catalyzed oxidation than both PZ and MEA. The EDA concentration studied is lower than would be typically used in a CO_2 capture system, but the resistance to Cu^{2+}-catalyzed oxidation can be assumed to extend to higher EDA concentrations. At higher EDA concentrations, the oxidation rate may increase slightly, but it would still be more resistant to oxidation than either PZ or MEA.

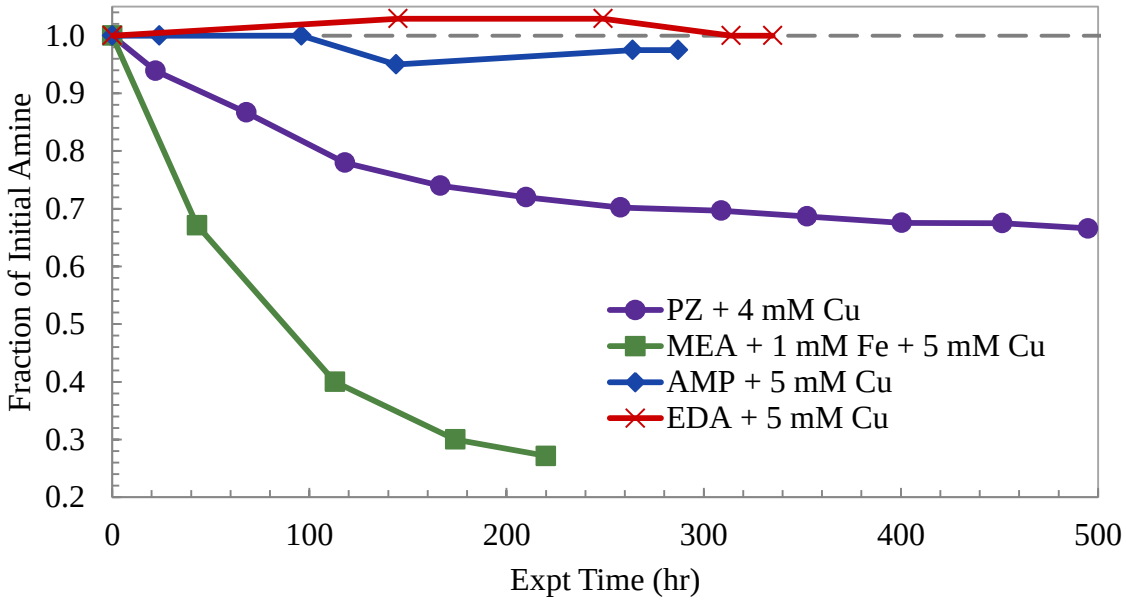

Figure 9.14: Comparison of PZ, MEA, AMP, and EDA loss in the presence of 4-5 mM Cu^{2+} (55 °C, 1400 rpm, 100 mL/min 98% O_2/2% CO_2) (Sexton, 2008)

9.3 INHIBITION OF THE OXIDATION OF PIPERAZINE

Inhibition of oxidation is a topic closely related to metal-catalyzed oxidation. In industrial systems, corrosion that leads to metals contamination of the amine solution can be mitigated with an inhibitor that can effectively decrease the catalytic effect of the metals. One of the most potent inhibitors investigated in the Rochelle group is Inhibitor A. Inhibitor A is a trade secret compound that can be added to concentrations of up to 100 mM. Inhibitor A has been proven effective at impeding both Fe^{2+}- and Cu^{2+}-catalyzed degradation in other amines such as MEA and 7 m MEA/2 m PZ blends (Goff and Rochelle, 2006; Sexton, 2008). Sexton also demonstrated that Inhibitor A decreased the production of degradation products for 2.5 and 5 m PZ. The efficacy of Inhibitor A to inhibit Fe^{2+}-, stainless steel metal, and Cu^{2+}-catalyzed oxidation was tested with 8 m PZ during the course of this project. Two alternative inhibitors, Inhibitor B and Inhibitor C were also tested for their efficacy at decreasing Fe^{2+}-catalyzed oxidation.

9.3.1 Efficacy of Inhibitor A with Iron (Fe^{2+})

Inhibitor A was tested on 8 m PZ containing 1 mM Fe^{2+} and either 0 or 100 mM Inhibitor A. The first set of experiments exploring the inhibitor was conducted in connection with analysis for foaming characteristics. In these experiments, both solutions were oxidized at 55 °C with 1400 rpm and 100 mL per min of 98% O_2/2% CO_2 for 70 hours, then removed from the low gas flow reactor and subjected to foaming tests (see section 8.9). Then, both solutions were returned to their respectively reactors to be further oxidized for another 93 hours. This was an unusual experiment and the effect of removing the solution from the reactor and returning it was not known at that time. There was a period of 5 days where the solution sat before the foaming tests were performed. The solutions were then returned to the reactors and restarted shortly after completing the foaming tests.

The efficacy of Inhibitor A to decrease Fe^{2+}-catalyzed oxidation is demonstrated in Figure 9.15 when comparing the uninhibited (OE5) and inhibited (OE6) experiments. Fe^{2+}-catalyzed oxidation of concentrated PZ is a slow process and Inhibitor A effectively inhibits the oxidation further. In the inhibited system, no degradation was statistically observable. The PZ concentration actually slightly increased during the course of the experiment. This increase reveals the experimental error due to the water balance in the reactor changing during the experiment and the cumulative error involved in the analytical process. The baseline Fe^{2+}-catalyzed oxidation with 1 mM Fe^{2+} had a 10% loss of PZ after 500 hours of oxidation and the addition of Inhibitor A makes oxidation negligible.

The multiple points present at 70 hours indicate the last point before the solutions were removed for the foaming test and the first point when the solutions were returned to the reactors. The difference between the two points for the 1 mM Fe^{2+} experiment is unfortunately quite large. The solutions were handled with care when transferred, but some changes to the composition of the solution may have occurred. During the foaming test itself, N_2 is sparged through the system and may impact the composition of the solution. It is likely that the water content of the solution was affected by evaporation and any degradation compounds with appreciable volatility would have escaped from solution due to gas sparging.

The formate, total formate, and EDA quantified in these experiments are compared in Figure 9.16. Overall, the formate concentration tracks very well between the experiments with and without Inhibitor A, which was not expected. No EDA was detected in the inhibited solution, indicating effectiveness at decreasing the generation of EDA during oxidation. Both the total formate and EDA concentrations, however, appeared to have been affected by the transfer of the solutions for the foaming test. Both

appear to be building up prior to the solutions removal from the reactor and then are diminished when the oxidation test is restarted. This may indicate that the N_2 sparging stripped out some of the volatile degradation products or shifted the degradation reactions during the foaming test. The lowering of total formate indicates that the formyl amides were strongly affected, which have unknown volatility in comparison to non-volatile heat stable salts. The impact of the foaming test, unfortunately, compounds the fact the experiments were short and produced low concentrations of degradation products that are near the error limits of the anion and cation IC. Despite the impact of the foaming test, the change in PZ loss and lack of EDA production indicate that Inhibitor A is effective at decreasing Fe^{2+}-catalyzed oxidation.

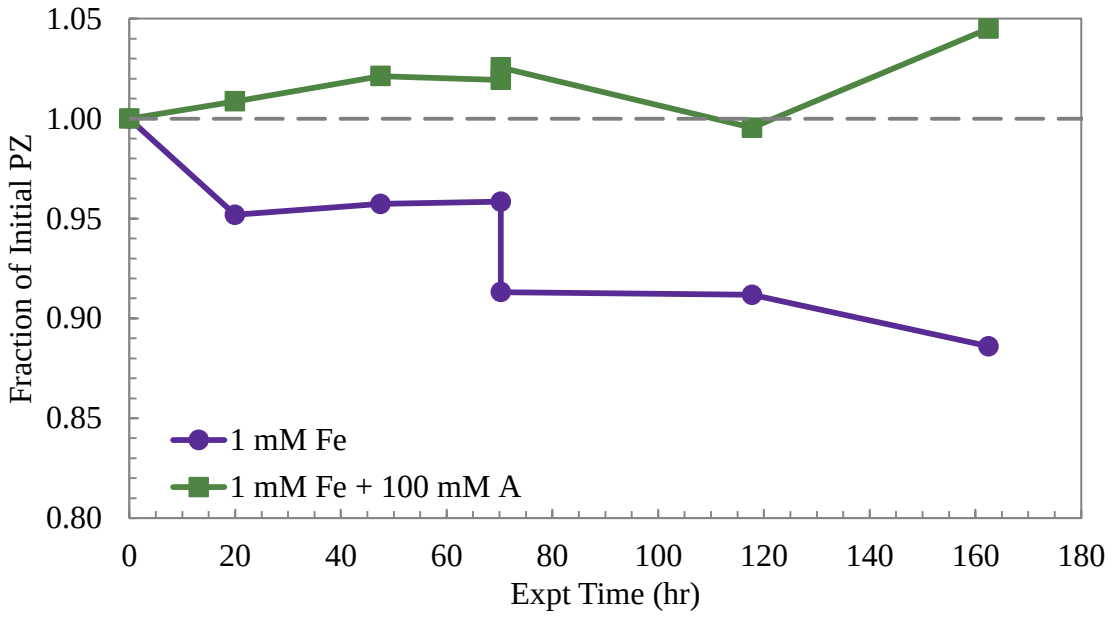

Figure 9.15: Effect of 100 mM Inhibitor A on PZ loss either uninhibited (●) or inhibited (■) (8 m PZ, 55 °C, 1400 rpm, 100 mL/min 98% O_2/2% CO_2, 1 mM Fe^{2+})

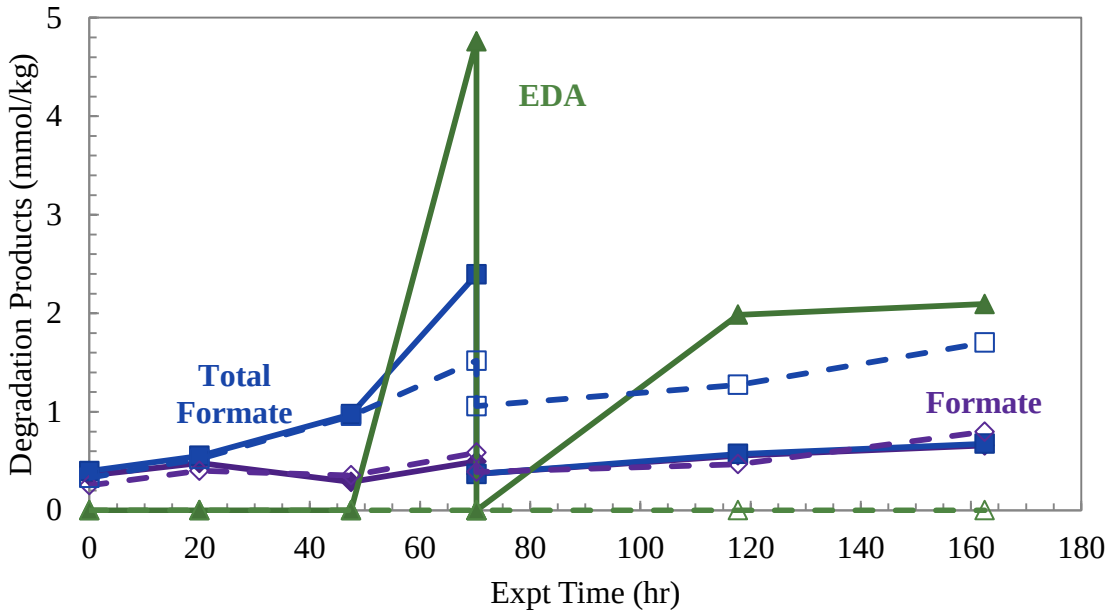

Figure 9.16: Effect of 100 mM Inhibitor A on generation of formate (♦), total formate (■), and EDA (▲) either uninhibited (solid) or inhibited (open) (8 m PZ, 55 °C, 1400 rpm, 100 mL/min 98% O_2/2% CO_2, 1 mM Fe^{2+})

In a second set of experiments, 8 m PZ was oxidized at 55 °C with 1400 rpm and 100 mL per min of 98% O_2/2% CO_2 with either 0 (OE13) or 100 mM Inhibitor A (OE14). This set of experiments was a repeat of the previous set with the goal of avoiding the issues experimenced due to the mid-experiment foaming test. The PZ loss during the experiments is shown in Figure 9.17 while the production of formate and total formate are compared in Figure 9.18. The PZ loss data indicates that Inhibitor A is successful at inhibiting Fe^{2+}-catalyzed oxidation in 8 m PZ. There is significant scatter in the inhibited solution that demonstrates the overall error in the experiment. No EDA was detected in either experiment, unlike the previous comparison. Unexpectedly, more formate and total formate were generated in the inhibited solution. The concentrations overall are very low, and some error is expected as demonstrated by the outliers. The cause for this higher level of degradation products in the inhibited solution is unknown.

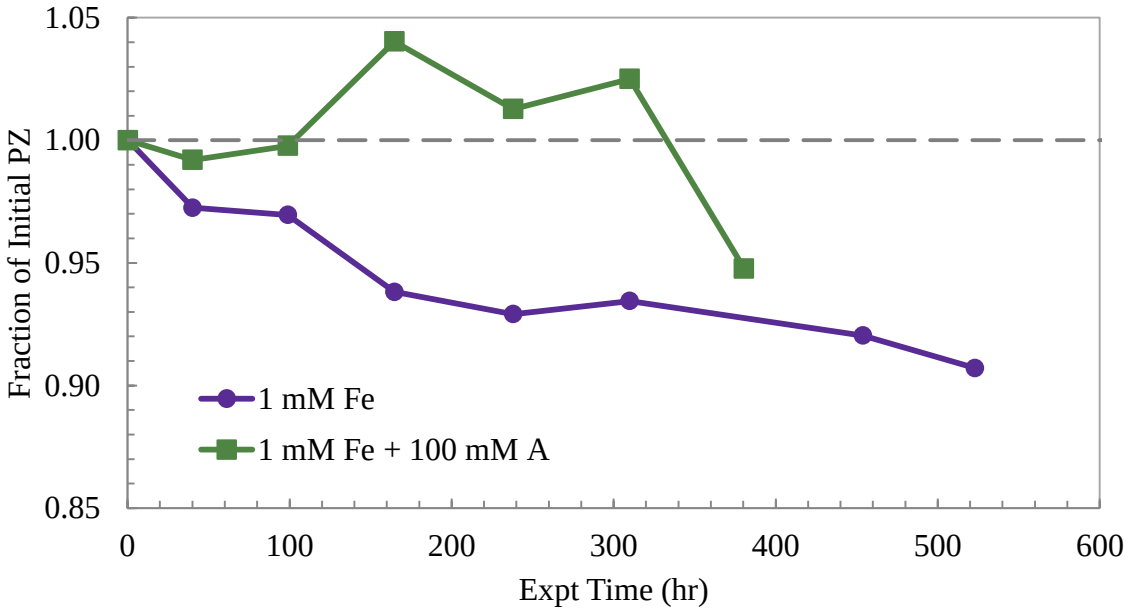

Figure 9.17: Effect of 100 mM Inhibitor A on PZ Loss either uninhibited (●) or inhibited (■) (8 m PZ, 55 °C, 1400 rpm, 100 mL/min 98% O_2/2% CO_2, 1 mM Fe^{2+})

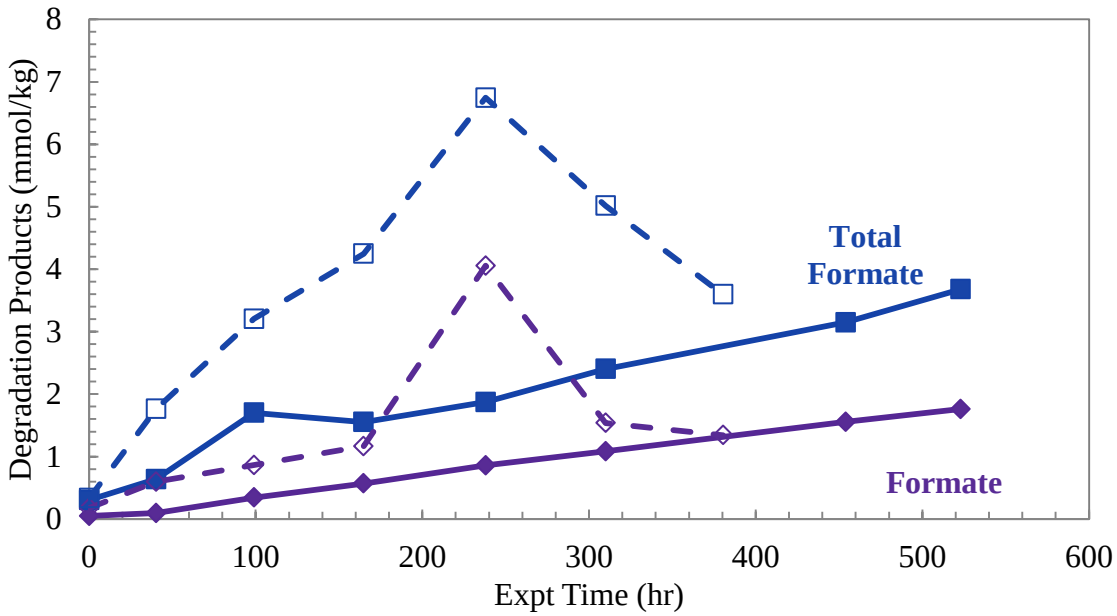

Figure 9.18: Effect of 100 mM Inhibitor A on generation of formate (♦) and total formate (■) either uninhibited (solid) or inhibited (open) (8 m PZ, 55 °C, 1400 rpm, 100 mL/min 98% O_2/2% CO_2, 1 mM Fe^{2+})

Oxidation can be detected either by the loss of PZ or the production of degradation products. In the case of these four experiments, some of the results are contradictory. Overall, Inhibitor A does appear to inhibit Fe^{2+}-catalyzed PZ oxidation, although the production of degradation products is not always substantially decreased in every case. The weak catalytic effect of Fe^{2+} made observing the effect of Inhibitor A on PZ oxidation difficult.

9.3.2 Efficacy of Inhibitor A with Stainless Steel Metals (Fe^{2+}, Cr^{3+}, and Ni^{2+})

The effectiveness of Inhibitor A to mitigate stainless steel metal catalyzed corrosion has not been tested previously on concentrated PZ. In order to determine the efficacy of Inhibitor A, 8 m PZ with the standard SSM mixture (0.4 mM Fe^{2+}, 0.1 mM Cr^{3+}, and 0.05 mM Ni^{2+}) was oxidized at 55 °C with 1400 rpm and 100 mL per min of 98% O_2/2% CO_2 with either 0 (OE15) or 10 mM Inhibitor A (OE16). The loss of PZ is shown in Figure 9.19 while the generation of degradation products is compared in Figure 9.20. Both solutions lose very little PZ during the course of the 420 hour experiment, with the inhibited experiment actually losing more PZ than the uninhibited case. It is important to remember that the baseline experiments described in Section 8.2.1 showed 3 to 7% PZ loss simply due to the operation error of the experiment.

In this case with little overall oxidation the production of degradation products is more informative. The inhibited solution has lower concentrations of formate and total formate and no detected EDA. A significant drop in the total formate is seen, but the concentrations are all below 7 mmole per kg. Although only 10 mM of Inhibitor A was used it noticeably decreased the generation of degradation products. The degradation products clearly indicates that Inhibitor A is successful in hindering SSM-catalyzed oxidation where PZ loss data is not statistically significant due to low oxidation rates.

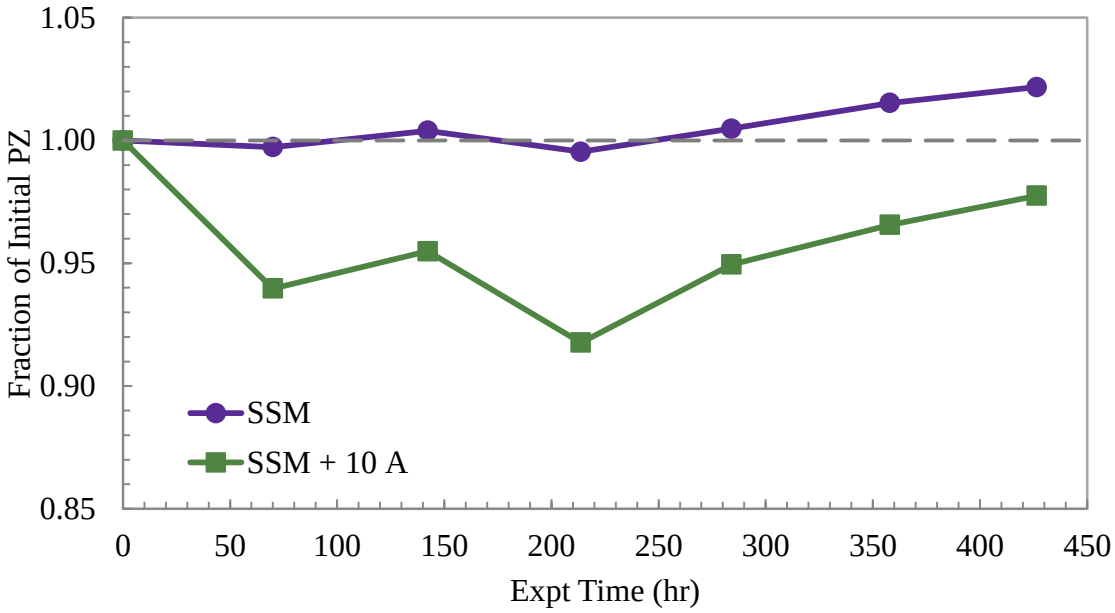

Figure 9.19: Effect of 10 mM Inhibitor A on PZ Loss either uninhibited (●) or inhibited (■) (8 m PZ, 55 °C, 1400 rpm, 100 mL/min 98% O_2/2% CO_2, SSM)

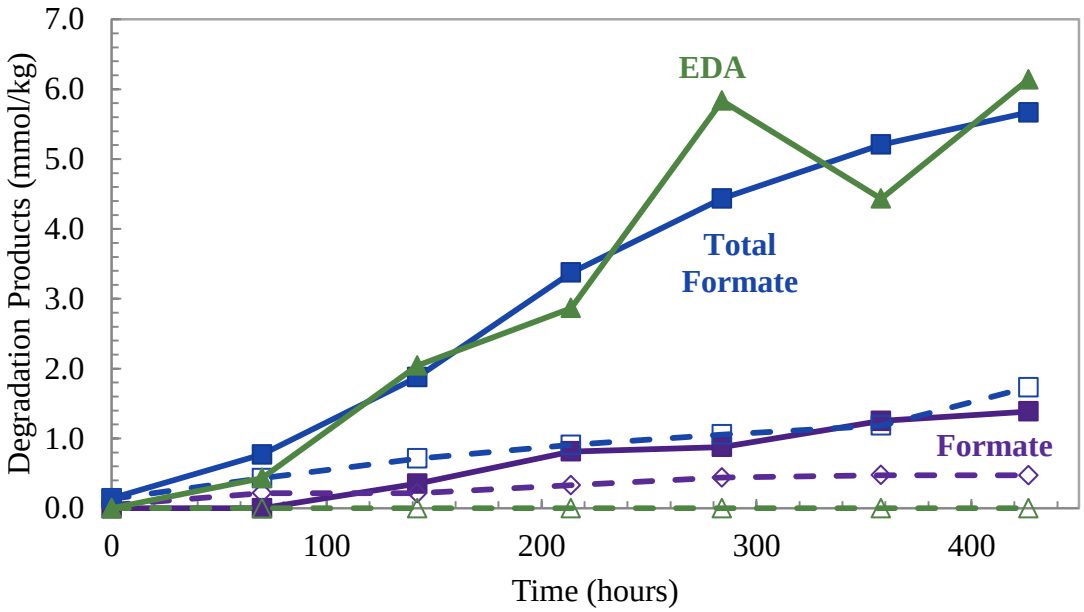

Figure 9.20: Effect of 10 mM Inhibitor A on generation of formate (♦), total formate (■), and EDA (▲) either uninhibited (solid) or inhibited (open) (8 m PZ, 55 °C, 1400 rpm, 100 mL/min 98% O_2/2% CO_2, SSM)

9.3.3 Efficacy of Inhibitor A with Copper (Cu^{2+})

Inhibitor A has previously been investigated for its ability to inhibit Cu^{2+}-catalyzed oxidation of low concentration PZ. Sexton observed that 100 mM Inhibitor A was highly effective and decreased the generation of formate and EDA by 90% in 5 m PZ at 55 °C with 5 mM Cu^{2+} (Sexton, 2008). PZ concentrations were not measured for the experiments discussed by Sexton, but it can be assumed that PZ loss was also decreased by a similar degree through the addition of Inhibitor A.

9.3.3.1 Efficacy of Inhibitor A with Copper (Cu^{2+}) at 55 °C

The effectiveness of Inhibitor A was tested on 8 m PZ in the presence of Cu^{2+} at 55 °C. Two experiments were performed in which PZ was oxidized uninhibited in the presence of 4 mM Cu^{2+} (OE2) or in the presence of 5 mM Cu^{2+}, 0.1 mM Fe^{2+}, and 100 mM Inhibitor A (OE4). The metals concentrations differed both in Cu^{2+} concentration and in the addition of Fe^{2+} to the inhibited experiment. As discussed in section 9.2 above, the catalytic impact of 0.1 mM Fe^{2+} is minimal in comparison with the presence of any concentration of Cu^{2+}. The higher concentration present in the inhibited solution will only further test the efficacy of Inhibitor A at decreasing Fe^{2+} and Cu^{2+}-catalyzed degradation.

The efficacy of Inhibitor A at decreasing Cu^{2+}-catalyzed PZ oxidation is clearly demonstrated in the PZ loss data in Figure 9.21. After 500 hours, PZ loss is decreased by three times as 34% PZ was lost in the uninhibited case compared to 11% in the inhibited case. The higher starting concentration of Cu^{2+} did not decrease the inhibitory power of Inhibitor A. The generation of formate, total formate, and EDA are compared in Figure 9.22 for the uninhibited and inhibited experiments. In concurrence with the PZ loss data, the generation of all three dominant degradation products is significantly decreased in the inhibited solution. After 500 hours, the concentration of formate, total formate, and EDA

were decreased by 92, 93, and 96%, respectively. These decreases mimic what was observed for 5 m PZ (Sexton, 2008).

In order to gauge the full effectiveness of Inhibitor A on Cu^{2+}-catalyzed oxidation, the two experiments were performed at high temperature. Solutions of 8 m PZ were oxidized in the presence of 4 mM Cu^{2+} at 70 °C agitated at 1400 rpm with 100 mL per minute of 40% O_2/6% CO_2 either uninhibited (OE23) or with 100 mM Inhibitor A (OE24). The PZ loss in each case is compared in Figure 9.23. As with the lower temperature experiments, the effectiveness of Inhibitor A at decreasing PZ loss in the presence of Cu^{2+} is clear. Inhibitor A decreased the loss of PZ by five times as the uninhibited experiment lost 35% of the initial PZ while the inhibited experiment lost only 6%.

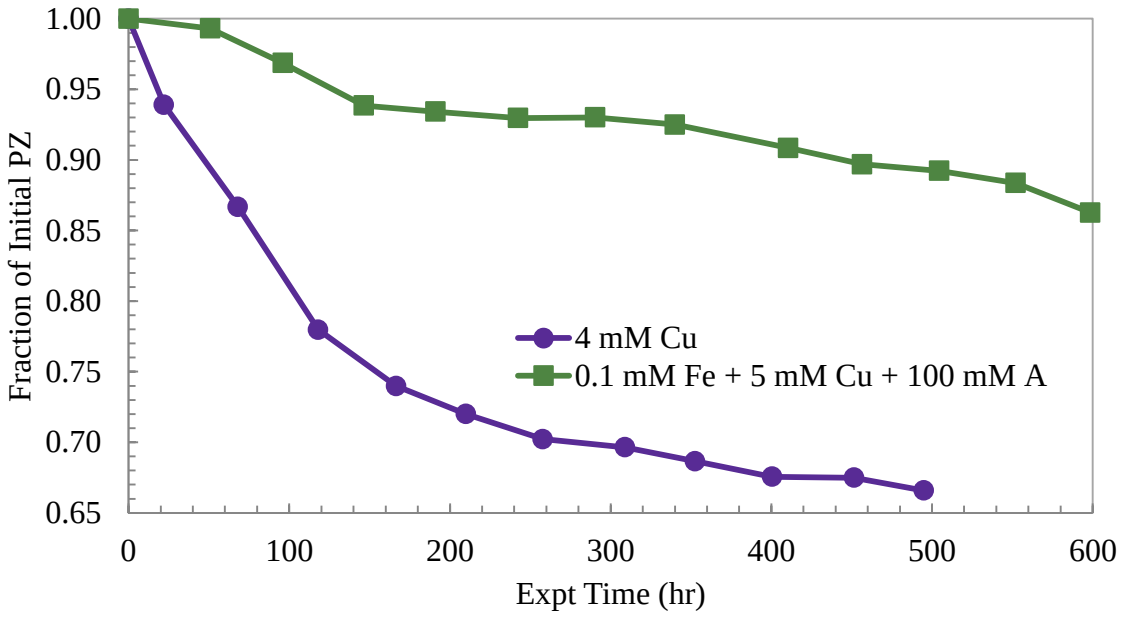

Figure 9.21: Effect of 100 mM Inhibitor A on PZ loss either uninhibited (●) or inhibited (8 m PZ, 55 °C, 1400 rpm, 100 mL/min 98% O_2/2% CO_2, 4 mM Cu^{2+}(uninhibited) or 0.1 mM Fe^{2+} and 5 mM Cu^{2+} (inhibited))

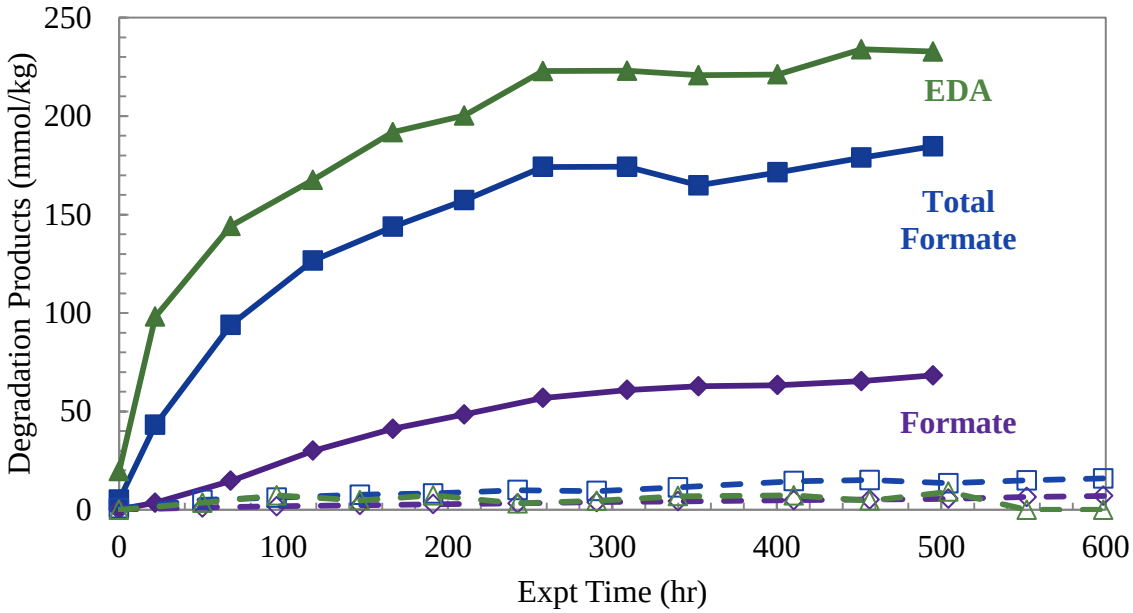

Figure 9.22: Effect of 100 mM Inhibitor A on generation of formate (♦), total formate (■), and EDA (▲) either uninhibited (solid) or inhibited (open) (8 m PZ, 55 °C, 1400 rpm, 100 mL/min 98% O_2/2% CO_2, 4 mM Cu^{2+})

9.3.3.2 Efficacy of Inhibitor A with Copper (Cu^{2+}) at 70 °C

The production of formate, total formate, and EDA, the major degradation products are compared in Figure 9.24 for the uninhibited and inhibited experiments. In agreement with the PZ data, the production of all three degradation products is visibly decreased by the presence of Inhibitor A. After 330 hours, the production of formate, total formate, and EDA were each decreased by 87, 81, and 90%, respectively. This decrease is very similar to the decrease seen with both 5 and 8 m PZ at 55 °C. Inhibitor A is extremely effective at decreasing high temperature oxidation of PZ in the presence of Cu^{2+}.

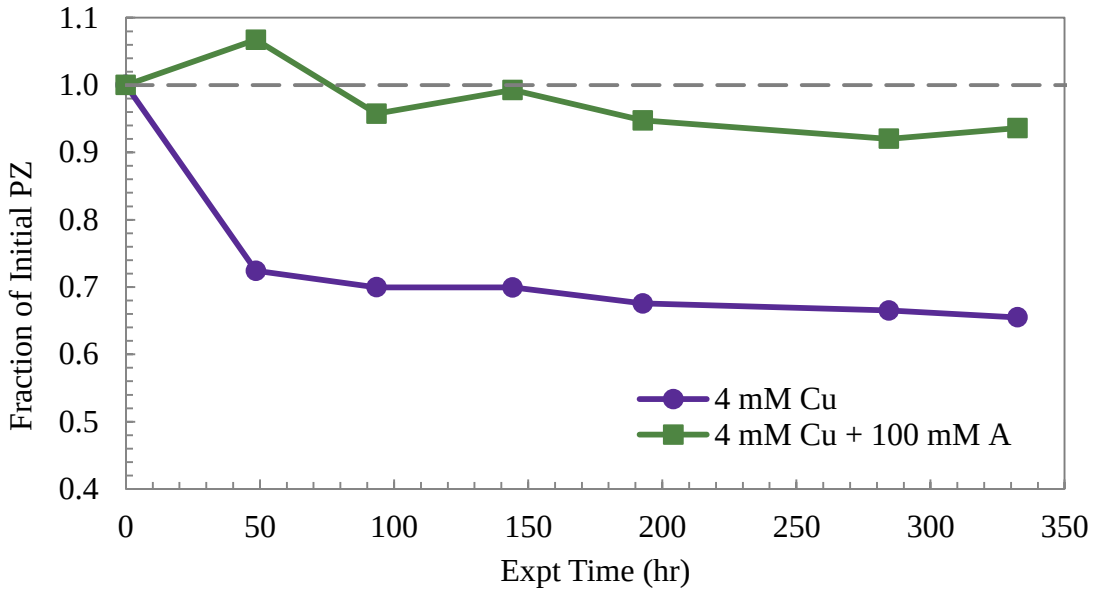

Figure 9.23: Effect of 100 mM Inhibitor A on PZ loss either uninhibited (●) or inhibited (■) (8 m PZ, 70 °C, 1400 rpm, 100 mL/min 40% O_2/2% CO_2, 4 mM Cu^{2+})

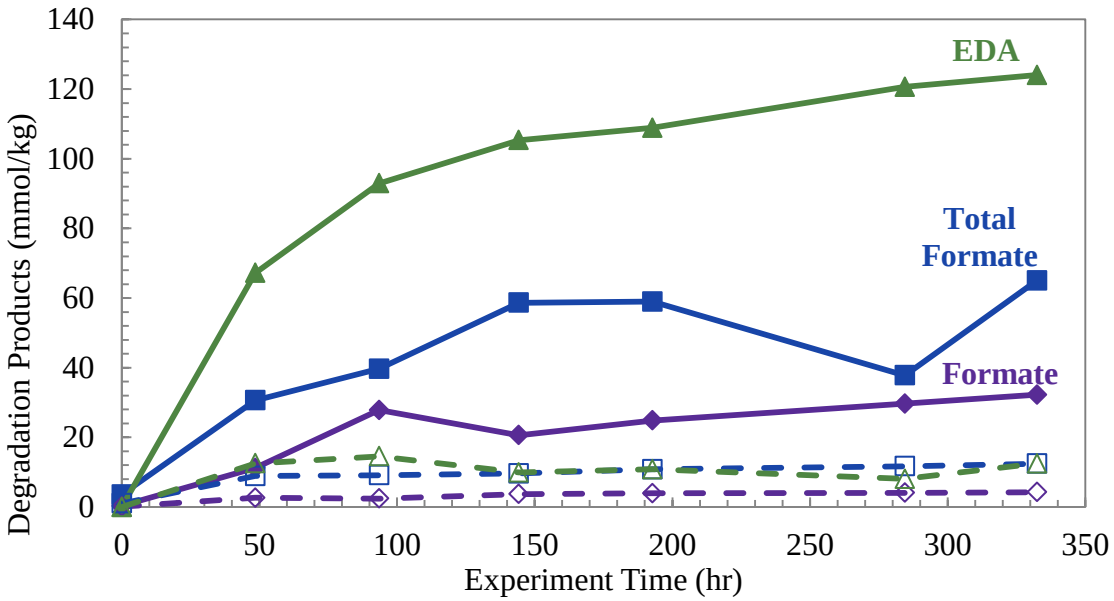

Figure 9.24: Effect of 100 mM Inhibitor A on generation of formate (♦), total formate (■), and EDA (▲) either uninhibited (solid) or inhibited (open) (8 m PZ, 70 °C, 1400 rpm, 100 mL/min 40% O_2/2% CO_2, 4 mM Cu^{2+})

9.3.3.2 Activation energy of copper-catalyzed oxidation with Inhibitor A

That activation energies for the loss of PZ and generation of formate, total formate, and EDA during Cu^{2+}-catalyzed oxidation with 100 mM Inhibitor A were also calculated in the same way as SSM- and Cu^{2+}-catalyzed experiments in sections 8.5.2 and 8.5.4. The rates for the four species are compared for two Cu^{2+}-catalyzed experiments (OE4 and OE24) in Figure 9.25. An estimation of error was not able to be performed because there were only two data points for the regression, making the degrees of freedom zero for the calculation of activation energy.

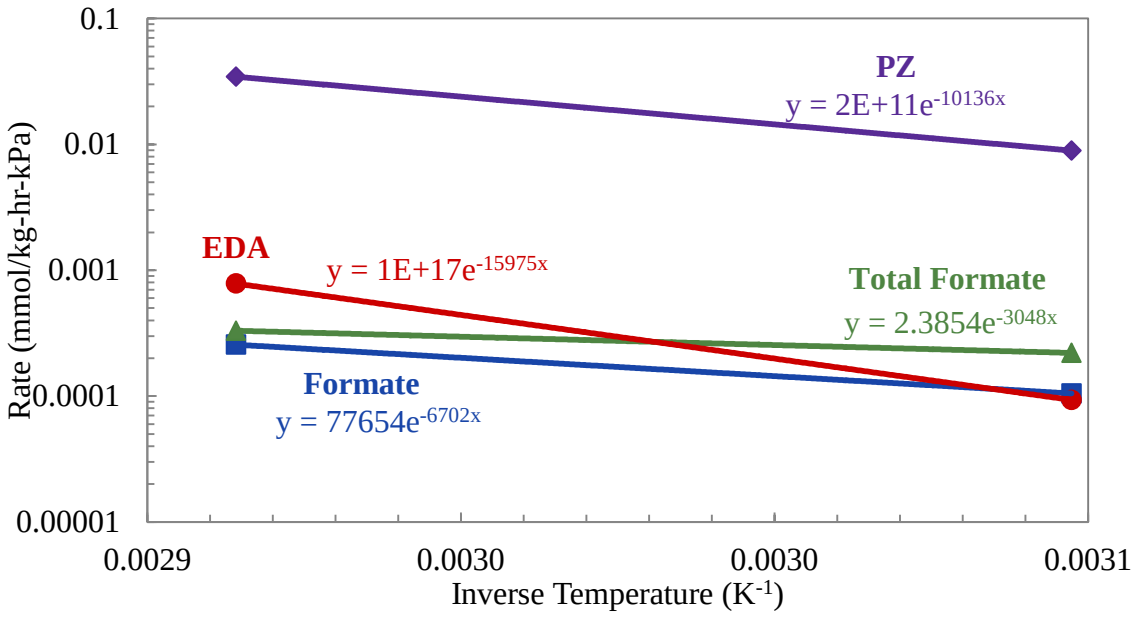

Figure 9.25: Rates of loss or production for PZ (♦), formate (■), total formate (▲), and EDA (●) for Cu^{2+}-catalyzed oxidation with 100 mM Inhibitor A

The calculated activation energies are compared for the four species in the presence of Cu^{2+} and with and without 100 mM Inhibitor A in Table 9.1. The first column of data is taken from Table 8.8. The most striking effect of Inhibitor A is the sharp increase in the activation energy for EDA. Inhibitor A may work directly to minimize the reactions responsible for EDA production in Cu^{2+}-catalyzed oxidation of

PZ. The activation energy for PZ itself is increased by three times, to a level almost as high as SSM-catalyzed oxidation. The formate generation energy is slightly high, but in the same range as that of both SSM- and Cu^{2+}-catalyzed oxidation suggesting that Inhibitor A may not be effective at interfering with the mechanisms that generate formate.

Table 9.1: Activation energies for PZ loss and generation of products for Cu^{2+}-catalyzed oxidation with and without 100 mM Inhibitor A

Rate	Cu^{2+} Activation Energy (kJ/mol)	Cu^{2+} + 100 mM Inhibitor A Activation Energy (kJ/mol)
PZ Loss	27 ± 29	84
Formate Generation	47 ± 15	56
Total Formate Generation	29 ± 33	25
EDA Generation	36 ± 9	133

9.3.4 Efficacy of Inhibitor B with Iron (Fe^{2+})

Inhibitor B is a trade secret oxidation inhibitor that has been classified as a reaction mechanism inhibitor. Previous work by Sexton has shown the effectiveness Inhibitor B at inhibiting oxidation of MEA in the presence of Fe^{2+} by decreasing MEA loss by up to 75% (Sexton, 2008). Unpublished work of the Rochelle group has indicated that Inhibitor B may enhance oxidation of MEA in the presence of both Fe^{2+} and Cu^{2+}. Inhibitor B was tested for its effectiveness at inhibiting Fe^{2+}-catalyzed oxidation of 8 m PZ. A solution of 8 m PZ was oxidized at 55 °C with 1 mM Fe^{2+} and 20 mM Inhibitor B with agitation at 1400 rpm and 100 mL per minute 98% O_2/2%CO_2.

The loss of PZ is compared for this inhibited experiment and a comparable uninhibited experiment in Figure 9.26. The loss of PZ is very similar in both experiments, with and without Inhibitor B. There is scatter in the inhibited data that leads to the increase in the final data point. Overall, the loss of PZ is very small in both

experiments over this short time range. Then generation of formate and total formate are compared in Figure 9.27. No EDA was detected in either experiment. The degradation product data appears to conclusively show that Inhibitor B does, in fact, decrease the production of formate and formyl amides in concentrated PZ. Both concentrations in the inhibited solution are almost negligible after 170 hours of degradation, reaching only 0.6 mmole per kg. A longer experiment would be needed to confirm the decrease in PZ loss that should accompany this decrease in degradation production formation.

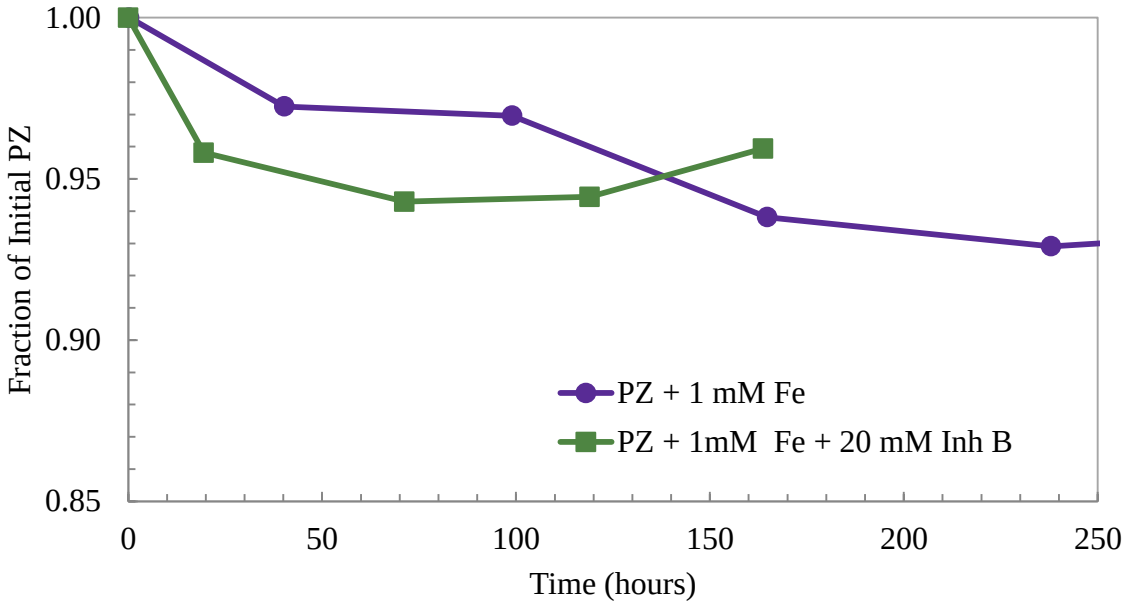

Figure 9.26: Effect of 20 mM Inhibitor B on PZ loss either uninhibited (●) or inhibited (■) (8 m PZ, 55 °C, 1400 rpm, 100 mL/min 98% O_2/2% CO_2, 1 mM Fe^{2+})

9.3.5 Efficacy of Inhibitor C with Iron (Fe^{2+})

Inhibitor C is another trade secret inhibitor that is classified as a chelating agent. Unpublished work from within the Rochelle group has shown that Inhibitor C is effective at decreasing both Fe^{2+}- and Cu^{2+}-catalyzed oxidation of MEA. The effectiveness of Inhibitor C to decrease PZ oxidation was investigated in the presence of 1 mM Fe^{2+}

through the oxidation of 8 m PZ was oxidized at 55 °C with 30 mM Inhibitor C, agitation at 1400 rpm and 100 mL per minute 98% O_2/2%CO_2.

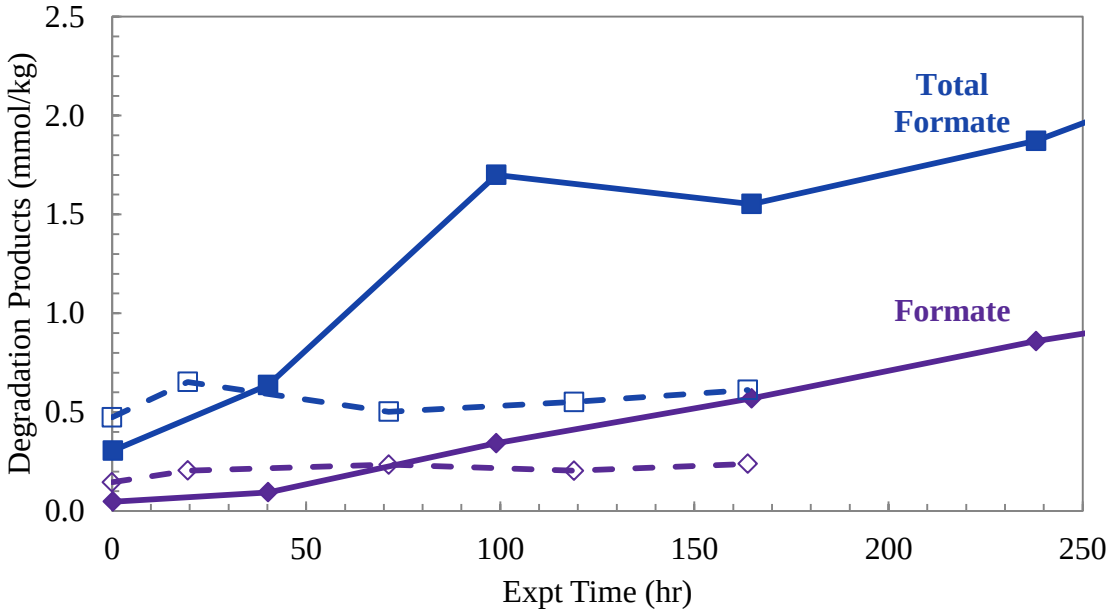

Figure 9.27: Effect of 20 mM Inhibitor B on generation of formate (♦) and total formate (■) either uninhibited (solid) or inhibited (open) (8 m PZ, 55 °C, 1400 rpm, 100 mL/min 98% O_2/2% CO_2, 1 mM Fe^{2+})

The loss of PZ for the inhibited and uninhibited experiments is compared in Figure 9.28. The PZ data suggests that Inhibitor C has no effect on PZ loss. The production of formate, total formate, and EDA is compared for the two experiments in Figure 9.29. There is a striking increase in the production of all three of the dominant degradation products, formate, formyl amides, and EDA, in the presence of 30 mM Inhibitor C. This observation does not match the PZ loss data which suggests a similar rate of oxidation. It is possible that the inhibitor itself is oxidizing and this is reflected in the increased product generation. Despite the uncertainty of the fate of Inhibitor C in solution, it is clear that Inhibitor C is not a useful inhibitor of oxidation in concentrated PZ solutions and may, in fact, catalyze the generation of oxidation products.

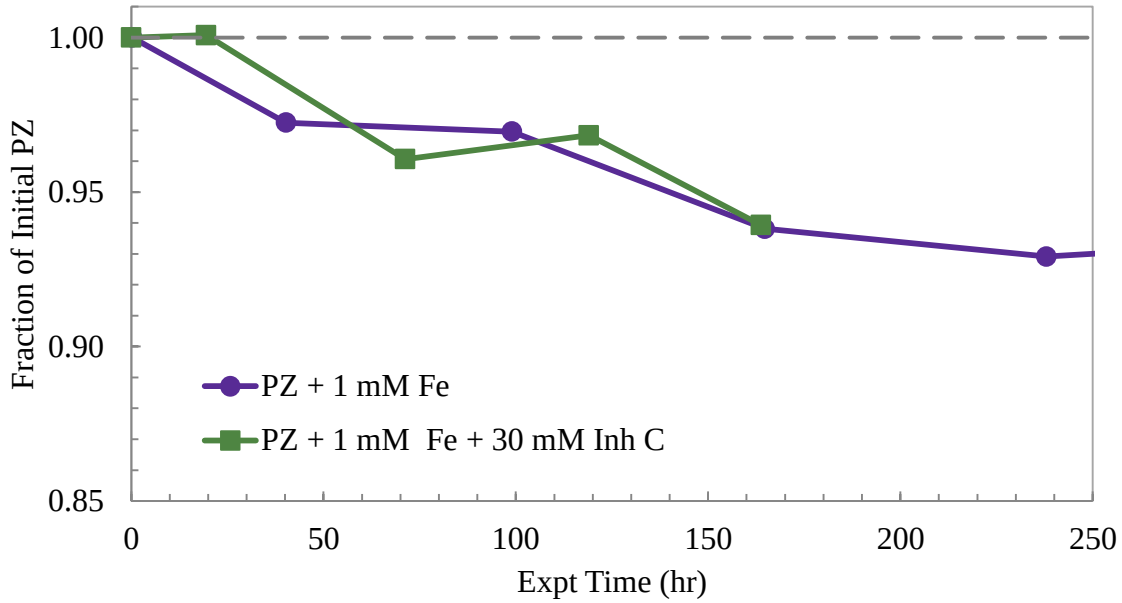

Figure 9.28: Effect of 30 mM Inhibitor C on PZ loss either uninhibited (●) or uninhibited (■) (8 m PZ, 55 °C, 1400 rpm, 100 mL/min 98% O_2/2% CO_2, 1 mM Fe^{2+})

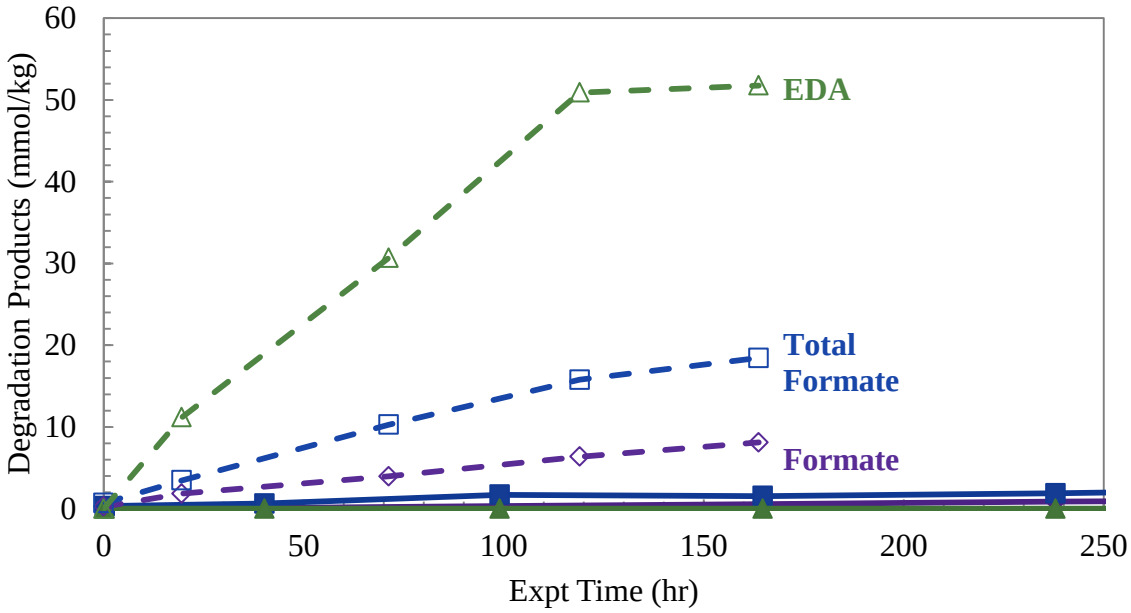

Figure 9.29: Effect of 30 mM Inhibitor C on generation of formate (♦), total formate (■), and EDA (▲) either uninhibited (solid) or inhibited (open) (8 m PZ, 55 °C, 1400 rpm, 100 mL/min 98% O_2/2% CO_2, 1 mM Fe^{2+})

9.4 COMPREHENSIVE OXIDATION RATE ANALYSIS FOR CONCENTRATED PZ

A comprehensive analysis of the oxidation rate of concentrated PZ can be performed using the loss rate of PZ and generation rate for the marker degradation products. In all of the oxidation experiments, the loss rate of PZ (R_{PZ}) and generation rate of formate ($R_{formate}$), total formate (R_{TF}), and EDA (R_{EDA}) have been calculated from the raw data. Linear rates were used except for data from OE2, OE23, OE25 and OE27 where very fast oxidation rates were measured that leveled out over time. In these four experiments, a linear rate was determined using the first three time points in order to estimate initial rates of oxidation. A summary of the calculated rates is provided in Table 9.3 along with the pertinent experimental conditions. All rates are calculated in units of mmole per kg per hr per kPa O_2. The slope of the raw experimental data is divided by the partial pressure of O_2 in the experiment to normalize the effect of O_2 partial pressure and to match previous analyses. In two cases, OE6 and OE15, the PZ concentration increased with time giving a positive slope, so these rates were assumed to be zero.

The effect of process parameters on PZ oxidation can be well understood by comparing the overall oxidation rates. In the following analysis, all oxidation data is used except for OE7, OE8, OE20, and OE21, which were spiked with Inhibitor B, Inhibitor C, formate, or formaldehyde, respectively. For the remaining experiments, $R_{formate}$, R_{TF}, or R_{EDA} are compared to R_{PZ} in Figure 9.30, Figure 9.31, and Figure 9.32, respectively. In all of the figures, the different catalysts and inhibitor conditions are indicated with different data shapes, but no distinction is made for experiments at 55 and 70 °C. All three graphs are plotted with log-log coordinates in order to spread the data because rates extend over four orders of magnitude. A linear regression is shown that fits all of the data and a coefficient of determination (r^2) is indicated for each regression.

Analyzing the oxidation rates with this approach will highlight the oxidation behavior of PZ. As expected, all three degradation products are generated as PZ is lost to oxidation, as indicated by the increasing slope of the data. The catalytic effect of Cu^{2+} on PZ oxidation is also emphasized in these figures. For all three degradation products, the Cu^{2+} experiments have the highest product generation rates and PZ loss rates. These data points heavily influence the data regressions because they are one to two orders of magnitude higher than most of the data. The baseline, SSM, SSM with Inhibitor A, Fe, and Fe with Inhibitor A experiments all have PZ loss rates and product generation rates that are in the very low ranges of each graph. Although the log-log coordinates highlight this data be stretching it out across multiple orders of magnitude, the highest rate of PZ loss seen in any condition without Cu^{2+} is below all of the Cu^{2+} data. The same can be said for all product generation rates in the absence of Cu^{2+}. The slopes of the linear regressions shown in the Figure 9.30, Figure 9.31, and Figure 9.32 suggest the interactions between PZ and the degradation products. The slopes indicate that for each mole of PZ oxidized, 0.03 mole formate, 0.11 mole total formate, and 0.18 mole EDA are produced.

The degradation product generation rates are of particular interest in this project because, on a whole, they were more accurately quantified than PZ loss rates. The rates of production of formate and total formate are correlated in Figure 9.33. The same type of correlation is done for formate and EDA in Figure 9.34 and total formate and EDA in Figure 9.35. In each of these three figures, a linear regression has been performed with all of the oxidation data and for only the non-Cu^{2+} data. In this way, any differences in the generation of products in Cu^{2+}-catalyzed degradation can be assessed since the regression for all of the data is essentially only heavily influenced by the copper data because of its magnitude.

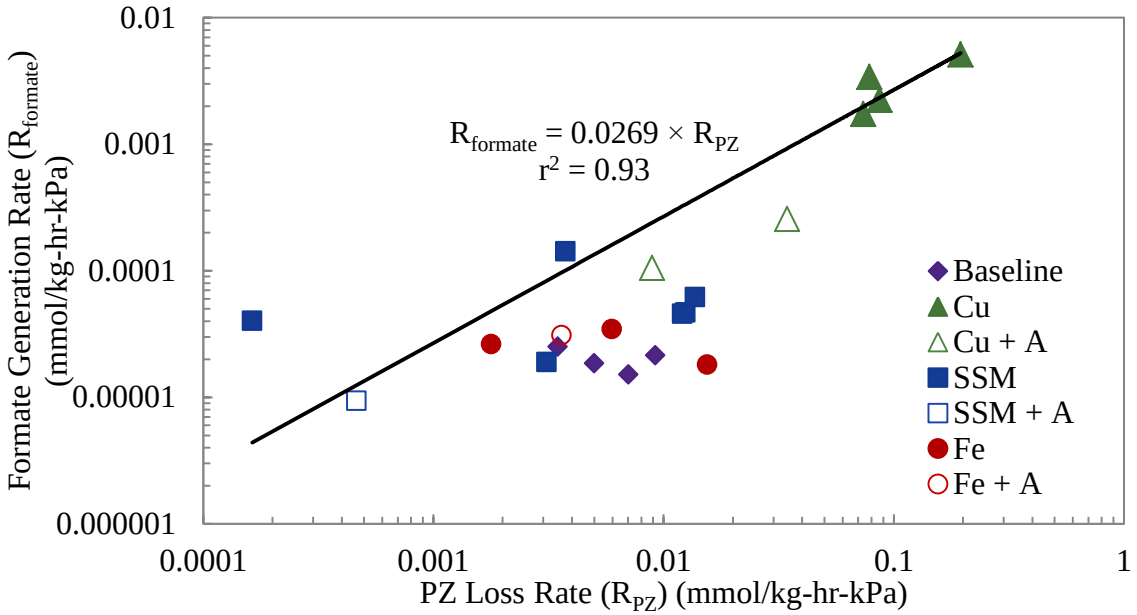

Figure 9.30: Correlation of R_{PZ} and $R_{formate}$ for all PZ oxidation experiments with a linear regression

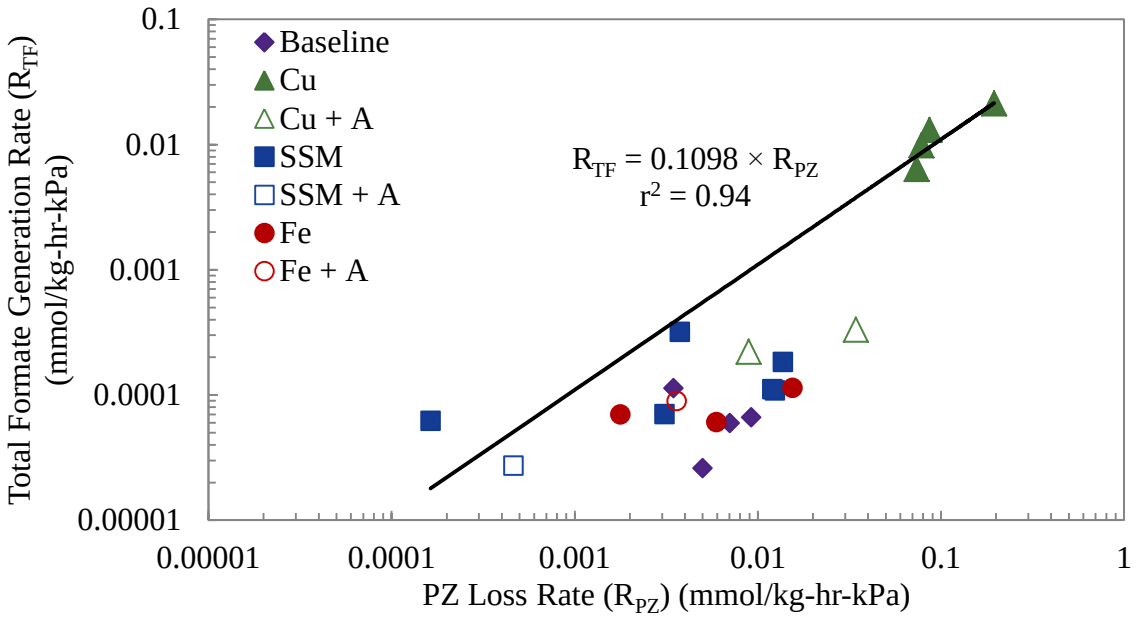

Figure 9.31: Correlation of R_{PZ} and R_{TF} for all PZ oxidation experiments with a linear regression

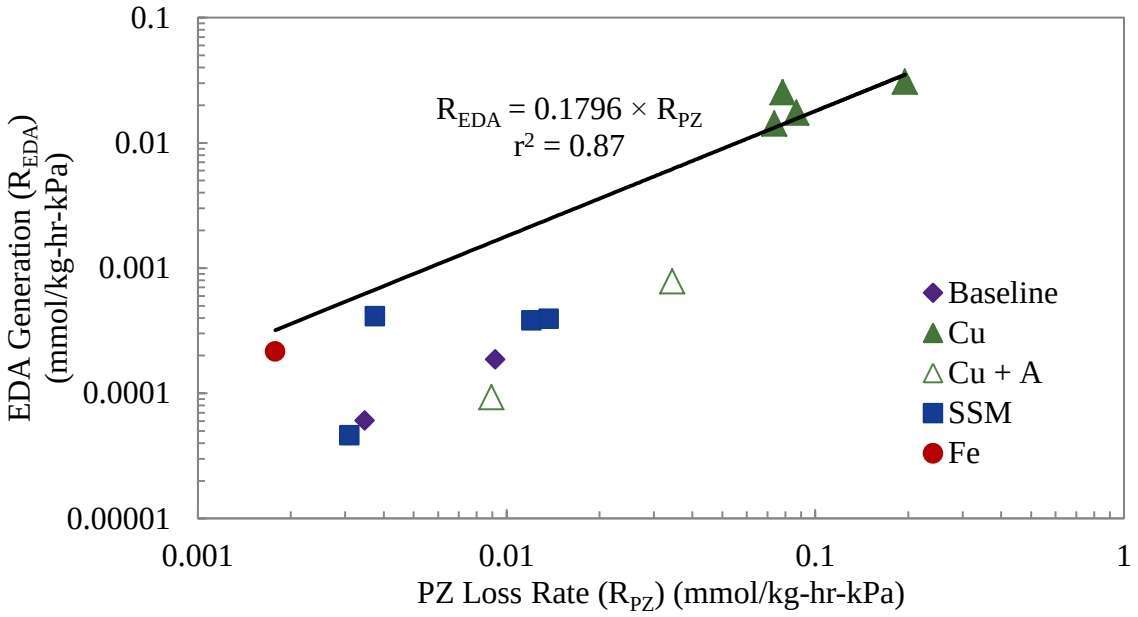

Figure 9.32: Correlation of R_{PZ} and R_{EDA} for all PZ oxidation experiments with a linear regression

The slopes of the correlation between formate and total formate suggest that there is an appreciable difference between the apparent equilibrium of formate and formyl amides in the presence of Cu^{2+}-catalyzed degradation (Figure 9.33). In more heavily oxidized solutions (i.e. with Cu^{2+} present), the equilibrium of formate and formyl amides favors amides and only a quarter of the total formate is usually in the form of free formate. In poorly oxidized solutions (i.e. in the absence of Cu^{2+}), the equilibrium shifts toward producing more formate where roughly 40% of the total formate in is the form of free formate.

The slopes of the correlation between total formate and EDA are also enlightening (Figure 9.35). The correlation based on the Cu^{2+} data or the non-Cu^{2+} data yielded the same slope of 1.6, within expected error. This indicates that regardless of the rate of oxidation or the strength of the catalyst, total formate and EDA will be generated in approximately the same ratio in all cases. There will always 1.6 moles of EDA generated

for every mole of total formate. This conclusion suggests that EDA and total formate are generated either at the same time or with mechanisms that are interdependent on each other and not influenced by the type of catalyst.

The slopes of the correlation of formate and EDA reflect the conclusions made in the two previous paragraphs (Figure 9.34). Since EDA and TF are produced at a constant ratio, the relationship between formate and EDA is dependent on the relationship or equilibrium between formate and formyl amides. In the presence of Cu^{2+}, 6.7 moles of EDA will be generated for each mole of formate. Without Cu^{2+}, 4.0 moles of EDA will be generated for each mole of formate.

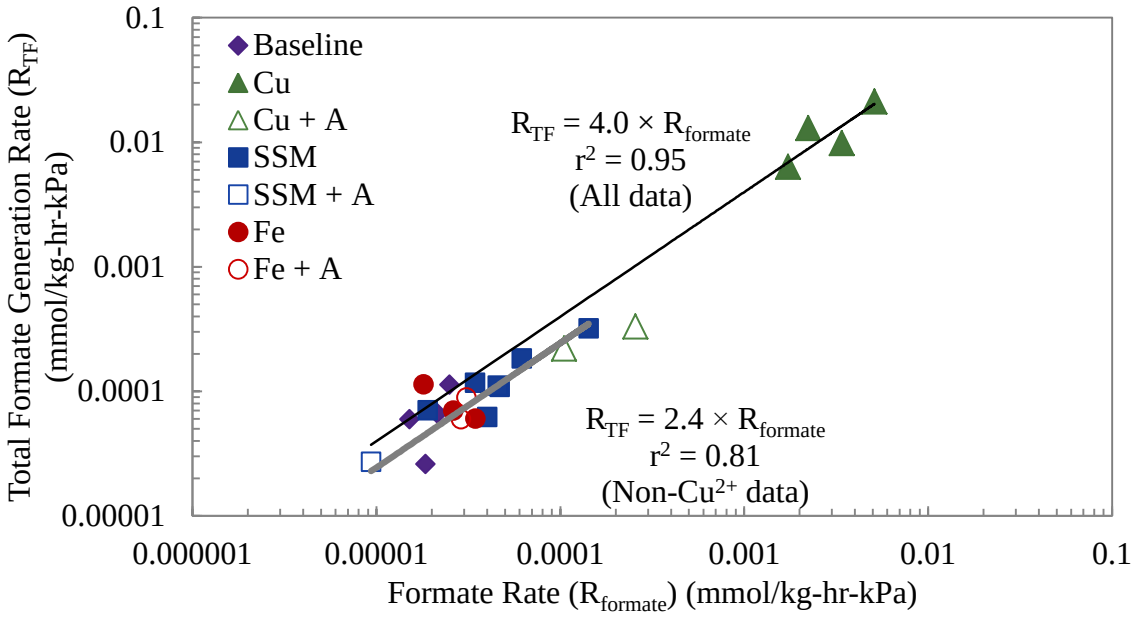

Figure 9.33: Correlation of $R_{formate}$ and R_{TF} including linear regressions for all data (thin, black line) and only non-Cu^{2+} data (thick, gray line)

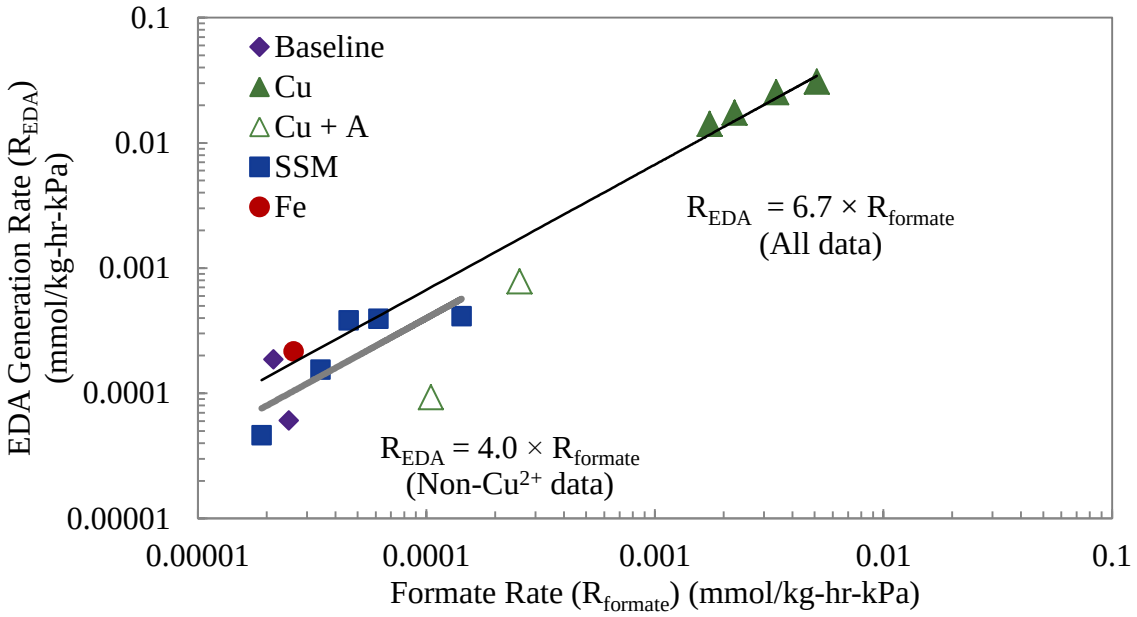

Figure 9.34: Correlation of $R_{formate}$ and R_{EDA} including linear regressions for all data (thin, black line) and only non-Cu^{2+} data (thick, gray line)

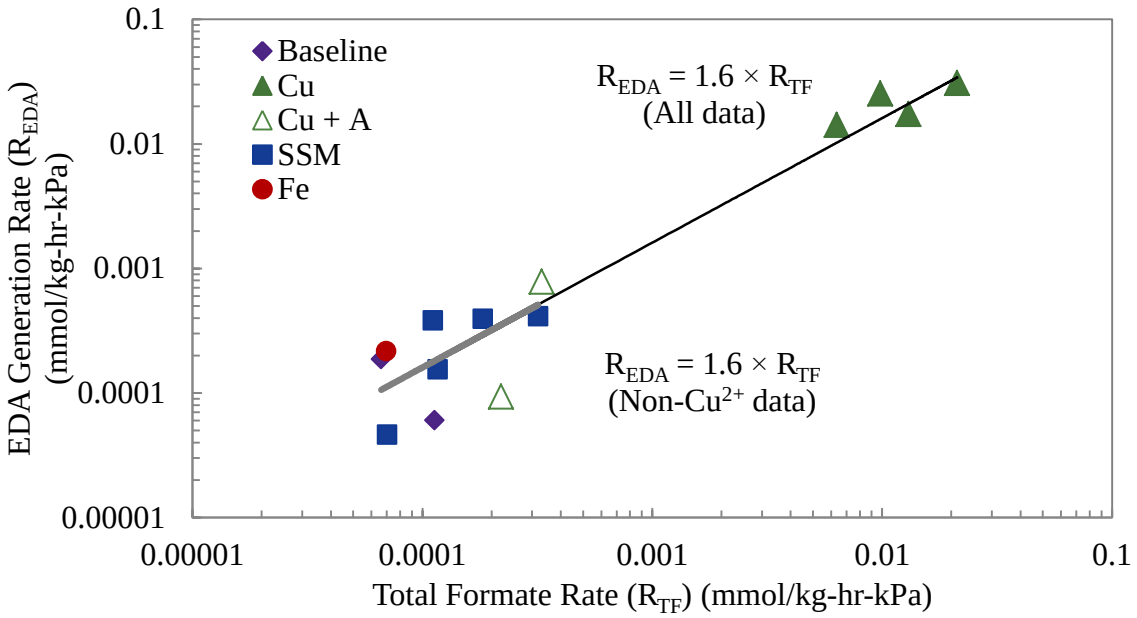

Figure 9.35: Correlation of R_{TF} and R_{EDA} including linear regressions for all data (thin, black line) and only non-Cu^{2+} data (thick, gray line)

Given the inconsistency and unreliability of PZ measurements, an estimation of the PZ loss rate based on the generation of degradation products can be performed. This will allow further understanding of the influence of metal catalysts on oxidation and allow estimation of PZ loss rates when rates based on cation IC showed significant error or positive slopes. Since total formate is consistently generated with EDA, it serves as a good marker for overall PZ oxidation. Using the R_{TF} data for all experiments and the slope of the correlation in Figure 9.31, an estimated PZ loss rate ($R_{PZ,est}$) can be calculated. This procedure essentially removes the scatter and places all data on the regressed correlation.

The $R_{PZ,est}$ based on the R_{TF} is compared to the R_{TF} in Figure 9.36. This figure is comparable to Figure 9.31, but with scatter in the PZ rate removed. From this figure, a few important new conclusions can be made. First of all, SSM have a slightly higher catalytic impact than Fe^{2+} based on the higher rates of SSM-catalyzed oxidation. There is scatter in both sets of data, and this may just be due to a lack of data for Fe^{2+}-catalyzed oxidation at higher temperature. Secondly, inhibitor is highly effective at decreasing SSM-catalyzed degradation. The experiment with both SSM and inhibitor A has the lowest PZ loss rate except for a baseline experiment. Finally, Inhibitor A is not effective at decreasing Fe^{2+}-catalyzed degradation. The experiment including both Fe^{2+} and Inhibitor A is in the middle of all of the Fe^{2+} experiments. Neither SSM or Fe^{2+} are strong catalysts for oxidation of PZ, but inhibitor A is able to decrease oxidation to extremely low levels in the SSM experiment. The same conclusions can be made when R_{PZ} is estimated from formate or EDA data. The estimation of a R_{PZ} allows for more information to be minded from degradation product data. Since that is obtained with more confidence than PZ data, conclusions can be drawn that are not apparent when looking at the raw concentration curves for each experiment.

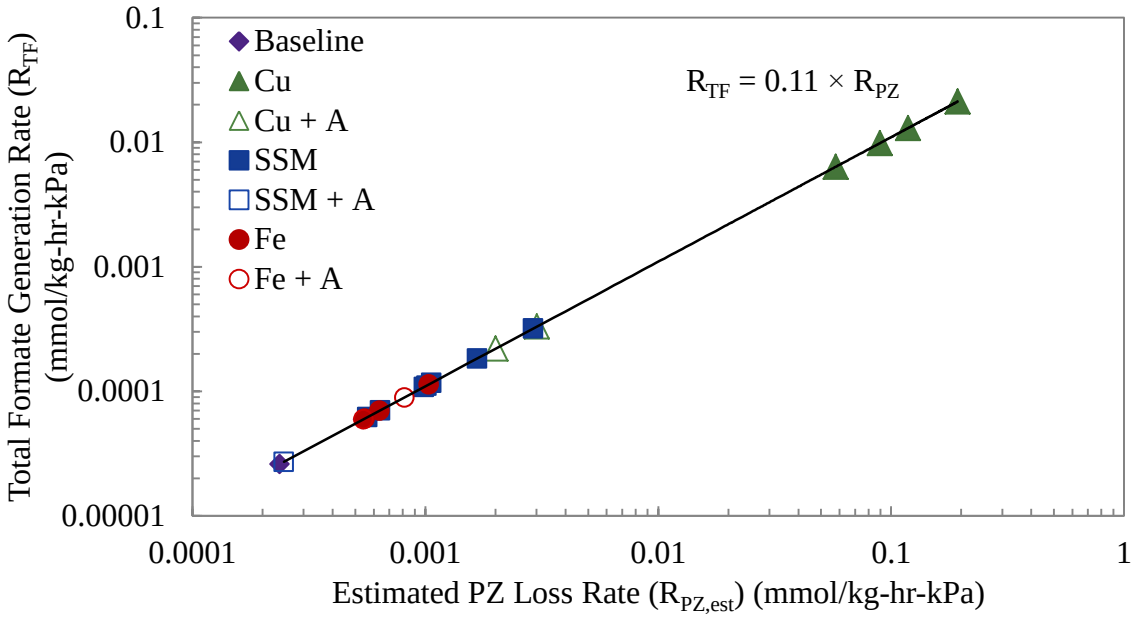

Figure 9.36: Correlation of the estimated PZ loss rate ($R_{PZ,est}$) with R_{TF}

A summary of the average rates in the presence of varying catalysts for the four species of interest is provided in Table 9.2. For the six experiments performed at 70 °C, each rate was extrapolated to the expected rate at 55 °C using the activation energy for each condition and species calculated in sections 8.5.2, 8.5.4, and 9.3.3.2. With the Cu^{2+} + Inhibitor A experiments, there was only one experiment at each temperature so the activation energy predicted exactly the conditions found in the 55 °C, so there is no standard deviation for the rates. Only one experiment was performed in the presence of SSM and 10 mM Inhibitor A, so there is also no standard deviation for this condition. The estimated PZ rate in the final column of Table 9.2 is an average rate based on the analysis shown in Figure 9.36 with the 70 °C adjusted to 55 °C using the activation energy for total formate for each catalyst condition. The total formate activation energy was used, rather than the PZ activation energy because this analysis is based on the idea that the total formate data is more reliable and indicates true PZ oxidation.

The rates from Table 9.2 for all of the catalysts conditions are also compared using a log scale in Figure 9.37, with just the formate compared in Figure 9.38. This analysis shows that although PZ oxidation is occurring in the presence of Fe^{2+} and SSM, the rate of PZ loss is likely below 0.0077 mmole PZ loss per kg per hr per kPa, well below levels seen with Cu^{2+}. The difficulty in accurately measuring the PZ loss rate, as detailed in Chapter 8, is evident by the standard deviation error bars in Figure 9.37 and Figure 9.38 and the difference between the raw PZ loss rate and the estimated PZ rate. In every case except Cu^{2+}, the estimated rate based on total formate production was lower than the raw PZ loss rate, indicating the error associated with accurately quantifying PZ oxidation. At low overall rates of oxidation, the quantification of degradation products is also subject to large standard deviations, as shown in Table 9.2. The large standard deviation of the PZ loss rate in the presence of Cu^{2+} is due to the influence of O_2 concentration, despite the normalization by O_2 partial pressure. The estimated PZ loss rates also indicate that Inhibitor A is not effective at reducing Fe^{2+}-catalyzed oxidation as the PZ loss rates and product rates are nearly the same.

Table 9.2: Average loss or generation rates for each catalyst condition during PZ oxidation with 70 °C data adjusted to 55 °C rates

Catalyst or Inhibitor (mM) [a]	Loss or Generation Rate × 10^3 (mmol/kg-hr-kPa O_2)				
	PZ	Formate	Total Formate	EDA	PZ (est) [b]
4 Cu^{2+}	84.4 ± 31	2.0 ± 0.39	9.7 ± 4.0	15.8 ± 1.8	107 ± 65
4 Cu^{2+} + 100 A	8.9	0.11	0.22	0.09	2.0
SSM	3.1 ± 4.3	0.03 ± 0.02	0.09 ± 0.03	0.07 ± 0.06	1.2 ± 0.9
SSM + 10 A	0.46	0.01	0.03	0	0.2
1 Fe^{2+}	7.7 ± 7.0	0.03 ±0.01	0.08 ± 0.03	0.07 ± 0.12	0.7 ± 0.3
1 Fe^{2+} + 100 A	1.8 ± 2.6	0.03 ± 0.001	0.07 ± 0.02	0	0.7 ± 0.2
Baseline	6.2 ± 2.5	0.02 ± 0.004	0.07 ± 0.04	0.06 ± 0.09	0.6 ± 0.3

[a] SSM = stainless steel metal mixture, 0.4 mM Fe^{2+}, 0.1 mM Cr^{3+}, 0.05 mM Ni^{2+}; Baseline indicates no added metal catalysts

[b] PZ (est) = the average PZ loss rate estimated from the total formate generation rate as shown in Figure 9.36

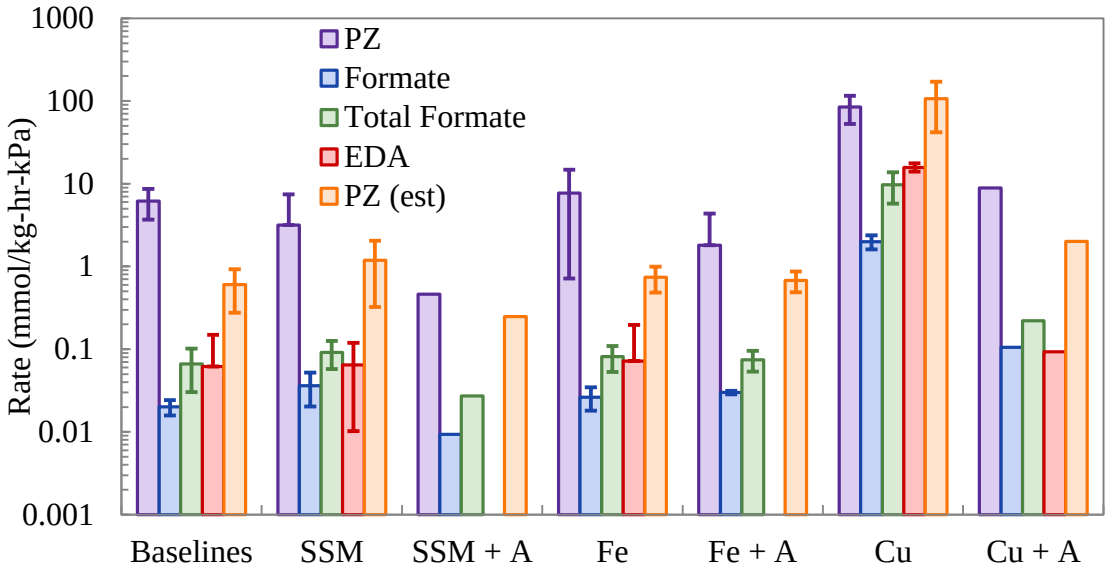

Figure 9.37: Comparison of PZ loss and product generation rates for catalysts systems tested

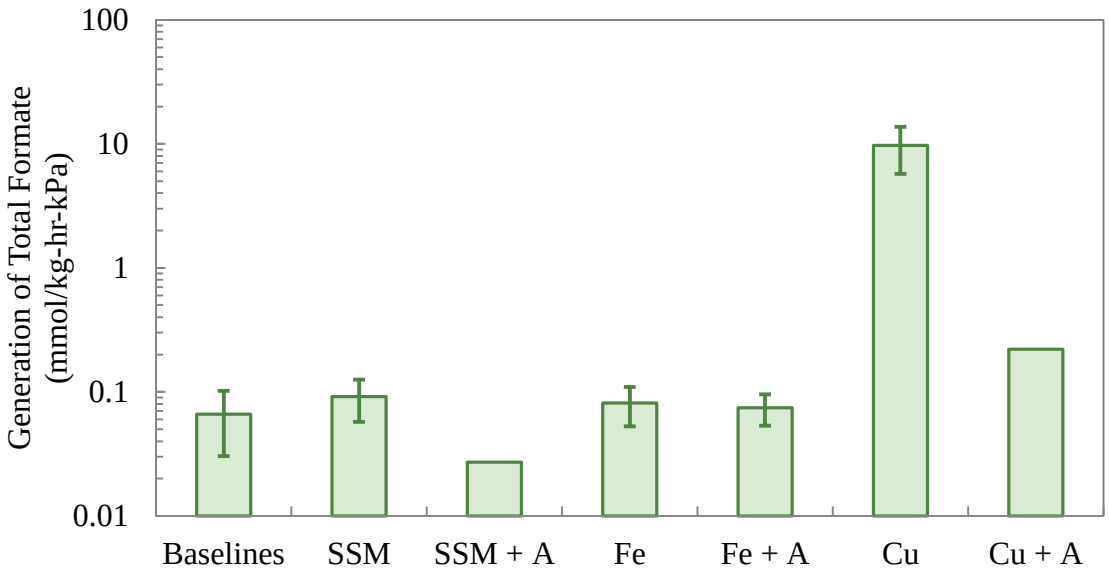

Figure 9.38: Comparison of total formate generation rates for catalysts systems tested

As an estimate of what may be expected in a real system, a rate of PZ loss and product generation can be calculated based on the expected conditions. With an inlet partial pressure of 5 kPa O_2 and absorber operation at 55 °C, the loss rate of PZ for Fe^{2+} or SSM conditions would be 0.0226 mmole per kg per hr. This estimate is based on the average rate, 0.0045 mmole per kg per hr per kPa, seen with either Fe^{2+} or SSM conditions at 55 °C, or 70 °C rates extrapolated to 55 °C. A residence time can be assumed where the solution spends only one third of its time exposed to O_2 in the absorber, absorber sump, and piping. If this rate is extrapolated, including the residence time, a loss of 66 mmole PZ per kg, or 0.066 mole PZ per kg, would be expected in one year of operation. This loss rate is likely an overestimate which provides a reasonable design specification for PZ-based absorber-stripper designs. Using the maximum rate seen in any Fe^{2+} or SSM experiment predicts roughly 0.23 mole PZ per kg loss in one year of operation. A better estimate of the residence time of the solvent when exposed to O_2 would make the estimate more accurate. This rate was based on PZ loss measurements, which may overestimate PZ loss due to the reasons discussed in this chapter and the previous one.

Performing the same estimate using the average PZ loss rate when 5 mM Cu^{2+}-based corrosion inhibitor is present (5 kPa O_2, 55 °C absorber, solution exposed to O_2 one third of residence time), the loss rate of PZ is predicted to be 0.14 mmole per kg per hr or 1.23 mole PZ per kg in one year of operation. This is approximately 19 times more oxidation than seen in a Fe^{2+} or SSM system. With the addition of 100 mM of inhibitor A, the data suggest that this rate could be decreased to 0.015 mmole per kg per hr or 0.13 mole PZ per kg in one year of operation. This level of oxidation is 2 times higher than when only Fe^{2+} or SSM are present, but represent a workable level of oxidation if Cu^{2+} corrosion inhibitors are required based on the material of construction.

Table 9.3: Summary of PZ Loss and generation of degradation products in oxidation experiments on concentrated PZ

Expt.	PZ	Temp.	P_{CO2}	CO_2 Ldg	P_{O2}	Additives	Loss or generation rate × 10^3 (mmol/kg-hr-kPa O_2)			
	m	°C	Pa	mol/mol alk	Pa	mM	PZ Loss	Formate	T. Formate	EDA
OE1	10	55	2	0.3	98	Fe (0.23), Cr (1.6), Ni (0.2)	12.44	0.047	0.108	0
OE2	10	55	2	0.3	98	Cu (4)	86.89	2.234	13.011	17.385
OE3	8	55	2	0.3	98	Fe (0.1), V (0.1)	4.49	0.065	0.194	0
OE4	8	55	2	0.3	98	Fe (0.1), Cu (5), A (100)	8.93	0.105	0.220	0.093
OE5	8	55	2	0.3	98	Fe (1)	15.46	0.018	0.113	0
OE6	8	55	2	0.3	98	Fe (1), A (100)	0	0.029	0.060	0
OE7	8	55	2	0.3	98	Fe (1), B (20)	8.63	0.004	0.003	0
OE8	8	55	2	0.3	98	Fe (1), C (30)	15.64	0.479	1.136	3.382
OE9	8	55	2	0.3	0	-	5.00	0.019	0.026	0
OE10	8	55	2	0.3	0	-	3.47	0.025	0.113	0.060
OE11	8	55	2	0.3	98	-	9.20	0.021	0.066	0.186
OE12	8	55	2	0.3	98	-	7.03	0.015	0.059	0
OE13	8	55	2	0.3	98	Fe (1)	5.95	0.035	0.060	0
OE14	8	55	2	0.3	98	Fe (1), A (100)	3.61	0.031	0.089	0
OE15	8	55	2	0.3	98	SSM	0	0.034	0.117	0.154
OE16	8	55	2	0.3	98	SSM, A (10)	0.46	0.009	0.027	0
OE17	8	55	2	0.3	98	Fe (1)	1.78	0.026	0.070	0.216
OE18	8	55	2	0.3	98	SSM	0.16	0.040	0.062	0
OE19	8	70	2	0.2	98	SSM	3.75	0.143	0.319	0.412
OE20	8	70	2	0.2	98	SSM, Formate (500)	4.99	NA	NA	0
OE21	8	70	2	0.2	98	SSM, Formaldehyde (500)	9.52	0.098	0.276	0.233
OE22	8	70	60	0.4	40	SSM	12.04	0.046	0.111	0.381
OE23	8	70	6	0.3	40	Cu (4)	78.46	3.401	9.830	25.295
OE24	8	70	6	0.3	40	Cu (4), A (100)	34.44	0.256	0.331	0.782

Table 9.3: Summary of PZ Loss and generation of degradation products in oxidation experiments on concentrated PZ (Continued)

Expt.	PZ	Temp.	P_{CO2}	CO_2 Ldg	P_{O2}	Additives	Loss or generation rate × 10^3 (mmol/kg-hr-kPa O_2)			
	m	°C	Pa	mol/mol alk	Pa	mM	PZ Loss	Formate	T. Formate	EDA
OE25	8	70	6	0.3	94	Cu (4)	195.30	5.109	21.210	30.778
OE26	8	70	6	0.3	94	SSM	13.71	0.062	0.183	0.394
OE27	8	55	2	0.3	40	Cu (4)	73.70	1.735	6.348	14.203
OE28	8	55	2	0.3	40	SSM	3.10	0.019	0.070	0.046

9.5 CONCLUSIONS

The a system with Fe^{2+} or SSM, 5 kPa O_2 in the inlet glue gas, an absorber operated at 55 °C, and with the solution exposed to O_2 approximately one third of the total residence time of the system, the maximum loss rate of PZ is expected to be 0.026 mmole per kg per hr or 0.23 mole PZ per kg solvent in one year of operation. This represents a maximum rate that is a reasonable estimate for design purposes and oxidation may occur even slower in real systems. Based on an average rate of PZ loss in the presence of Fe^{2+} or SSM, the expected rate of PZ loss is only 0.066 mole PZ per kg solvent in one year of operation.

In a similar system with 5 mM Cu^{2+}-based corrosion inhibitor, 5 kPa O_2 inlet gas, 55 °C absorber, and the same residence time, the loss rate of PZ is predicted to be 0.14 mmole per kg per hr or 1.23 mole PZ per kg solvent in one year of operation. With 100 mM of inhibitor A, this rate could be decreased to 0.015 mmole per kg per hr or 0.13 mole PZ per kg solvent in one year of operation. Oxidation in a system with a Cu^{2+}-based corrosion inhibitor could be controlled with an effective oxidation inhibitor like Inhibitor A.

Aqueous iron (Fe^{2+}) is only a weak catalyst for concentrated PZ oxidation up to a concentration of 5 mM. The rate of PZ loss in the presence of Fe^{2+} was found to be only 0.0077 ± 0.007 mmole PZ per kg per hr per kPa O_2. For the generation of formate, total formate and EDA, average rates of only 0.00003 ± 0.000008 mmole formate, 0.00008 ±0.00003 mmole total formate, and 0.0007 ± 0.0001 mmole EDA per kg per hr per kPa O_2, respectively, were observed. V^{5+} is also a weak catalyst that cannot increase oxidation above the baseline experimental levels.

PZ is resistant to Fe^{2+}-catalyzed degradation in comparison with other well-known amines used for CO_2 capture processes. Only DGA oxidized noticeably slower than PZ while EDA, MEA and DEA degraded more rapidly in the presence of Fe^{2+}. Concentrated PZ was roughly 5.5 times more resistant to oxidation than 7 m MEA.

The combination of stainless steel metals (SSM), Fe^{2+}, Cr^{3+}, and Ni^{2+}, is only a weak catalyst for concentrated PZ oxidation. In the presence of SSM, the average rate of PZ loss was calculated to be only 0.0065 ± 0.006 mmole PZ per kg per hr per kPa O_2. For the generation of formate, total formate and EDA, average rates of only 0.00006 ± 0.00004 mmole formate, 0.0001 ± 0.00009 mmole total formate, and 0.0002 ± 0.0002 mmole EDA per kg per hr per kPa O_2, respectively, were observed.

PZ has enhanced resistance to SSM-catalyzed oxidation compared to 7 m MEA and 9 m MAPA. After 350 hours of oxidation, no PZ loss was observed compared to a loss of 35% for a comparable 7 m MEA experiment and complete oxidation of MAPA.

Cu^{2+} is a robust and effective catalyst for oxidation of concentrated PZ at both 55 and 70 °C. In the presence of Cu^{2+}, oxidation occurs rapidly with a loss rate of 0.109 ± 0.058 mmole PZ loss per kg per hr per kPa O_2. Formate, total formate, and EDA were generated at rates of 0.0031 ± 0.001 mmole formate, 0.013 ± 0.006 mmole total formate, or 0.022 ± 0.008 mmole EDA per kg per hr per kPa O_2, respectively. The rapid rate of Cu^{2+}-catalyzed degradation disallows the use of Cu^{2+}-based corrosion inhibitors in concentrated PZ systems without the presence of a separate oxidation inhibitor.

PZ was found to be 2.6 times more resistant to Cu^{2+}-catalyzed oxidation compared to 7 m MEA, but PZ was more easily oxidized by Cu^{2+} than both EDA and AMP.

Inhibitor A was effective at decreasing the PZ loss rate in both Fe^{2+} and SSM-catalyzed systems. Fe^{2+} and SSM cause only low levels of oxidation, as discussed above,

and Inhibitor A limits oxidation further through the decreased generation of degradation products. In systems examined with either 1 mM Fe^{2+} and 100 mM Inhibitor A or the standard SSM mixture and 10 mM Inhibitor A, almost no degradation was detected.

Inhibitor A is highly effective at inhibiting Cu^{2+}-catalyzed oxidation at 55 and 70 °C. Overall, the average PZ loss rate was decreased 10 times from 0.084 to 0.0089 mmole per kg per hr per kPa through the addition of 100 mM Inhibitor A. Oxidation was decreased to levels observed in the Fe^{2+}-catalyzed experiment.

The activation energy for PZ loss in the presence of Cu^{2+} and 100 mM Inhibitor A is 84 kJ per mole, three times higher than in the presence of Cu^{2+} alone. The activation energy for the generation of EDA is also increased 3.7 times indicating that Inhibitor A may work to inhibit the EDA generation mechanism specifically. The formate activation energy is very similar with and without Inhibitor A.

In the presence of 1 mM Fe^{2+}, Inhibitor B was effective at decreasing the concentration of degradation products formed during oxidation while Inhibitor C greatly increased degradation product concentrations. Neither Inhibitor B nor C was as effective as Inhibitor A for mitigating concentrated PZ oxidation.

Chapter 10 – Conclusions and Recommendations

The thermal degradation, oxidation, and physical properties of concentrated, aqueous PZ have been evaluated under conditions expected in industrial absorber-stripper systems for CO_2 capture from coal-fired flue gas. The conclusions developed in this thesis will be summarized with particular emphasis on what would be expected in a full scale system. Recommendations will be made for further study of the topics discussed. Additional study will be recommended where vital gaps in knowledge exist.

10.1 CONCLUSIONS

10.1.1 Thermal degradation of PZ

10.1.1.1 Expected rate of thermal degradation of PZ

At 150 °C, 8 molal (m) PZ with 0.3 mole CO_2 per mole alkalinity thermally degrades with a first order rate constant of 6.12×10^{-9} s^{-1}, or approximately 500 mmole per kg after 30 weeks.

PZ thermal degradation can be described effectively with a first rate constant, k_1, relating to a first order loss of PZ. For 8 m PZ with the expected lean loading of 0.3 mole CO per mole alkalinity, the fraction of PZ remaining (F_{PZ}) is provided by the following set of equations.

$$F_{PZ} = F_{PZ,0} \cdot \exp(-k_1 \cdot t) \tag{5.4}$$

$$k_1 = 2.78 \times 10^{14} \cdot \exp\left(\frac{183.5\,\text{kJ}}{\text{mole}} \cdot \frac{1}{RT}\right) \tag{5.13}$$

The activation energy of the system was determined to be 183.5 kJ per mole. At the rich loading condition, 8 m PZ with 0.4 mole CO_2 per mole alkalinity experiences slightly faster PZ loss according the following equation.

$$k_1 = 3.19 \times 10^{15} \cdot \exp\left(\frac{191.4\,\text{kJ}}{\text{mole}} \cdot \frac{1}{RT}\right) \tag{5.14}$$

The activation of the rich loaded condition was determined to be 191.1 kJ per mole.

The concentration of CO_2 generally increases the thermal degradation of concentrated PZ. At 175 °C, PZ degradation increased as a linear function of CO_2 loading up to 0.3 mole CO_2 per mole alkalinity. A maximum rate of degradation was observed between 0.3 and 0.4 mole CO_2 per mole alkalinity and then a decreased rate at

the very rich loading of 0.47 mole CO_2 per mole alkalinity. This behavior suggests that solution speciation with changes in CO_2 loading strongly affect thermal degradation. Model predictions of speciation at 175 °C do not indicate one species is solely responsible for this behavior, but it is rather a combination of H^+PZ, $PZCOO^-$, and H^+PZCOO^- concentrations.

On the whole, PZ loss during thermal degradation is first order in PZ, as is the basis of the k_1 analysis. A slight effect of increasing PZ concentration was observed that increases the k_1 value approximately 30% from 4 to 12 m PZ at the same conditions (0.3 mole CO_2 per mole alkalinity, 175 °C). Highly concentrated PZ solutions do not match this behavior and degradation kinetics of more than first order was observed in 20 m PZ with 0.3 mole CO_2 per mole alkalinity.

The addition of Cu^{2+}, Fe^{2+}, Cr^{3+}, or Ni^{2+} did not affect the rate of PZ thermal degradation. Solutions degraded in the absence of metals were found to have slightly repressed rates of generation of formate and formyl amides, indicating it is likely that the mechanisms responsible for generation of products are catalyzed by metals. Concentrated PZ has decreased tendency to corrode stainless steel metals in comparison to MEA, EDA, and MAPA based on the concentration of leached metals during thermal degradation.

The addition of 100 mM of Inhibitor A decreased PZ loss during thermal degradation by approximately 20% and decreased the production of total formate and EDA.

10.1.1.2 Degradation products of thermal degradation of PZ

The most abundant degradation products of thermally degraded 8 m PZ are N-formyl PZ (FPZ), NH_4^+, and N-(2-aminoethyl) piperazine (AEP). These three molecules account for 57% of nitrogen and 45% of carbon lost during degradation as PZ and CO_2.

Other prominent products include, in order of decreasing impact on the nitrogen and carbon balance, 2-imidazolidone (2-Imid), N-(2-hydroxyethyl) piperazine (HEP), N-ethylpiperazine (EPZ), ethylenediamine (EDA), 1-Methylpiperazine (1-MPZ), formate, acetate, and other heat stable salts such as oxalate and glycolate.

After 20 weeks of thermal degradation at 165 °C, 74% and 63%, respectively, of the nitrogen and carbon lost in the form of PZ and CO_2 was recovered in the form of quantifiable degradation products. For the same experiment, 87% and 60% of the lost CO_2 molecules and "ethyls" were recovered.

10.1.1.3 Postulated pathways for the generation of thermal degradation products

It is postulated that thermal degradation of PZ proceeds through a variety of S_N2 type substitution reactions that result in ring opening and polymerization products. In the first step of the mechanism, 1-[2-[(2-aminoethyl) amino]ethyl] PZ (AEAEPZ) is believed to be formed from a ring opening S_N2 reaction of PZ with H^+PZ.

The limiting rate was found to require protonated amine, but not CO_2, which agrees with the proposed production of AEAEPZ from H^+PZ and PZ. Further reaction of AEAEPZ with CO_2 is predicted to form the internal urea of AEAEPZ.

AEAEPZ is believed to also react with PZ or other amines through S_N2 substitution to produce AEP, EDA, and NH_4^+. Elimination reactions of AEAEPZ could produce HEP and other products. Two of the most important suspected species, AEAEPZ and the urea of AEAEPZ, have not been confirmed to be present, but are believed to represent two major, unidentified peaks on the cation IC.

Degradation of concentrated PZ in the presence of HCO_3^- demonstrated that PZ loss and generation of formate and EDA depend on the presence of H^+PZ to proceed.

NMR analysis of degraded $^{13}CO_2$-loaded PZ solutions conclusively showed that formate is generated directly from the CO_2 in solution. The mechanism is separate from the primary degradation of PZ through substitution reactions and is not clear at this point. Formate is not generated from the break-up of the PZ backbone itself. Formate is generated consistently as a major product in all oxygen-poor, CO_2 loaded amine thermal degradation where carbamate polymerization is not the major degradation mechanism.

At 150 °C, EDA is in equilibrium with 2-Imidazolidone, the cyclic urea of EDA. The equilibrium constant, K_{EQ}, tends toward a value between 0.0004 and 0.0006 kg solution per mole. EDA is produced during the thermal degradation of PZ through reactions that do not require CO_2. In the presence of CO_2, EDA reacts to form 2-Imid, a stable product. In the absence of CO_2, EDA accumulates in solution.

During thermal degradation from 135 to 175 °C, and oxidation at 55 °C, formyl amides are in equilibrium with formate. Formyl amides were consistently produced at higher concentrations that formate. The ratio of formyl amides to formate produced was a strong function of PZ concentration and CO_2 concentration, but not temperature. For 8 m PZ from 55 to 175 °C, the ratio can be described as follows where the CO_2 loading, α, is in units of mole CO_2 per mole alkalinity (Equation 6.24). For 20 m PZ at 175 °C, the ratio can be described as follows (Equation 6.25).

$$\frac{C_{FA}}{C_F} = 5.54 \times \alpha + 0.30 \tag{6.24}$$

$$\frac{C_{FA}}{C_F} = 7.73 \times \alpha + 3.10 \tag{6.25}$$

The O_2 present as dissolved O_2 or in the headspace of the thermal cylinders was found to have a minimal effect that could not account for all quantified formate and formyl amides generated in typical thermal degradation experiments.

10.1.2 Oxidation of PZ

10.1.2.1 Expected oxidation rate of concentrated PZ

A system with Fe^{2+} or SSM, 5 kPa O_2 in the inlet glue gas, an absorber operated at 55 °C, and the solution exposed to O_2 approximately one third of the total residence time of the system, the maximum loss rate of PZ is expected to be 0.026 mmole per kg per hr or 0.23 mole PZ per kg solvent in one year of operation. This represents a maximum rate that is a reasonable estimate for design purposes and oxidation may occur even slower in real systems. Based on the average rate of PZ loss in the presence of Fe^{2+} or SSM, the expected rate of PZ loss is only 0.066 mole PZ per kg solvent in one year of operation.

In a similar system with 5 mM Cu^{2+}-based corrosion inhibitor, 5 kPa O_2 inlet gas, 55 °C absorber, and the same residence time, the loss rate of PZ is predicted to be 0.14 mmole per kg per hr or 1.23 mole PZ per kg solvent in one year of operation. With 100 mM of inhibitor A, this rate could be decreased to 0.015 mmole per kg per hr or 0.13 mole PZ per kg solvent in one year of operation. Oxidation in a system with a Cu^{2+}-based corrosion inhibitor could be controlled with an effective oxidation inhibitor like Inhibitor A.

10.1.2.2 Catalysis and inhibition of oxidation of concentrated PZ

Aqueous iron (Fe^{2+}) is only a weak catalyst for concentrated PZ oxidation up to a concentration of 5 mM. The rate of PZ loss in the presence of Fe^{2+} was found to be only

0.0077 ± 0.007 mmole PZ per kg per hr per kPa O_2. V^{5+} is also a weak catalyst that cannot increase oxidation above the baseline experimental levels.

Concentrated PZ is 5.5 times more resistant to Fe^{2+}-catalyzed degradation than 7 m MEA. DGA® oxidized noticeably slower than PZ while EDA and DEA degraded more rapidly in the presence of Fe^{2+}.

The combination of stainless steel metals (SSM), Fe^{2+}, Cr^{3+}, and Ni^{2+}, is only a weak catalyst for concentrated PZ oxidation. In the presence of SSM, the average rate of PZ loss was calculated to be only 0.0065 ± 0.006 mmole PZ per kg per hr per kPa O_2.

Cu^{2+} is a robust and effective catalyst for oxidation of concentrated PZ at both 55 and 70 °C. In the presence of Cu^{2+}, oxidation occurs rapidly with a loss rate of 0.109 ± 0.058 mmole PZ loss per kg per hr per kPa O_2.

The rapid rate of Cu^{2+}-catalyzed degradation disallows the use of Cu^{2+}-based corrosion inhibitors in concentrated PZ systems without the presence of a separate oxidation inhibitor.

PZ has enhanced resistance to SSM-catalyzed oxidation compared to 7 m MEA and 9 m MAPA. After 350 hours of oxidation, no PZ loss was observed compared to a loss of 35% for a comparable 7 m MEA experiment and complete oxidation of MAPA. PZ was 2.6 times more resistant to Cu^{2+}-catalyzed oxidation compared to 7 m MEA, but PZ was more easily oxidized by Cu^{2+} than both EDA and AMP.

Inhibitor A is highly effective at inhibiting Cu^{2+}-catalyzed oxidation at 55 and 70 °C. Overall, the average PZ loss rate was decreased 10 times from 0.084 to 0.0089 mmole per kg per hr per kPa through the addition of 100 mM Inhibitor A. Oxidation was decreased to levels observed in the Fe^{2+}-catalyzed experiment. Inhibitor A was effective at decreasing the PZ loss rate in both Fe^{2+} and SSM-catalyzed systems.

The activation energy for PZ loss in the presence of Cu^{2+} and 100 mM Inhibitor A is 84 kJ per mole, three times higher than in the presence of Cu^{2+} alone. The activation energy for the generation of EDA is also increased 3.7 times indicating that Inhibitor A may work to inhibit the EDA generation mechanism specifically. The formate activation energy is very similar with and without Inhibitor A.

10.1.2.3 Oxidation products of concentrated PZ

The identified oxidation products of PZ include EDA, carboxylate ions (formate, oxalate, acetate), amides (formyl amides, oxalyl amides, and acetyl amides of PZ or EDA), and ammonium (NH_4^+). Glycolate, nitrite and nitrate are minor products that were inconsistently generated.

TOC and TN analysis indicated the presence of unidentified liquid phase degradation products. Both a baseline experiment and a heavily oxidized solution in the presence of Cu^{2+} were found to have maintained the TOC concentration in the liquid phase during the experiment, indicating unquantified liquid phase oxidation products. Both experiments also experienced a quantifiable decrease in TN concentration, indicating the loss of volatile molecules such as ammonia, NO_X, or N_2.

N and C mass balances on oxidized solutions were poor, especially with low rates of oxidation. In OE11, a baseline experiment, only 2.5% and 0.7% of the N and C, respectively, lost as PZ was recovered. Inclusion of an estimate of the volatile N from the TN analysis increased the N balance to 73% of the lost PZ. For OE18, an experiment with SSM, only 3.4% and 5.2% of the N and C lost as PZ was recovered in products. In OE25, the most heavily oxidized PZ solution in the study, 27% and 23% of the N and C, respectively, from the lost PZ was recovered as liquid phase products. With the inclusion

of an estimate of 2650 mmole volatile N per kg from TN, 69% of the lost PZ N was recovered.

It is suspected that aldehydes (e.g. formaldehyde, acetaldehyde, and hydroxyacetaldehyde), alcohols (e.g. methanol, ethanol, and, ethylene glycol), ureas of PZ, amino acids (e.g. N-(2-aminoethyl) glycine, N,N'-1,2-ethanediylbis-glycine), and oxidized PZ molecules (2-piperazinone, 2,5-piperazinedione, 2-piperazinol, 1,2,3,6-tetrahydro pyrazine, 1,2,3,4,-tetrahydro pyrazine, 1-piperazineaceticacid) are a significant portion of the unidentified products. Amino acid liquid chromatography indicates that this may be an important functional group in oxidation products, but no amino acids were able to be identified.

The addition of 500 mM formate to 8 m PZ eliminated the production of EDA, suggesting that PZ oxidation was significantly decreased. Formate is not oxidized to CO_2 in PZ oxidation experiments but may act as a weak oxidation inhibitor for PZ.

The addition of 500 mM formaldehyde to 8 m PZ created stable, dense, white foam that persisted through the oxidation experiment. The foam is likely a polymer of formaldehyde and PZ that was stable for over 10 months.

The foaminess coefficient is not a consistent measurement technique and does not produce repeatable results. The amount of time between the end of an experiment and the foaminess test appears to impact results, which is an unforeseen problem in the assay.

10.1.3 Thermal degradation of PZ structural analogs and other CO_2 capture amines

Calculated first order rate constants for amine thermal degradation, k_1, were successfully translated into predicted stripper temperatures that represent a maximum acceptable degradation rate. Morpholine (Mor) was determined to be the most stable amine tested to date with a predicted stripper temperature of 170 °C. Piperidine (PD) and

piperazine (PZ) and with 0.3 mole CO_2 per mole alkalinity were the next most stable amines with estimated stripper temperatures of 166 and 163 °C, respectively. Cyclic, 6-membered amines such as PZ, Mor, and PD were determined to be exceptionally resistant to thermal degradation.

Substituted PZs such as 1-methylpiperazine (1-MPZ), 2-methylpiperazine (2-MPZ) and PZ analogs such as hexamethylenediamine (HMDA) were shown to be stable, tolerating temperatures between 148 and 160 °C. PZ structural analogs with 5- or 7-membered rings such as pyrrolidine (Pyr), hexamethyleneimine (HMI), and homopiperazine (HomoPZ), were found to have diminished stability. Methylation of the PZ structure at the 1- or 2-position also decreased stability of the PZ molecule to thermal degradation.

The most instable amines measured, such as N-(2-hydroxyethyl) ethylenediamine (HEEDA), 2-methylaminoethanol (MMEA), diethanolamine (DEA), N-methylethanolamine (MAE), diethanoltriamine (DETA), and 3-(methylamino) propylamine (MAPA), which will all degrade significantly at temperatures above 120 °C, are longer straight-chain alkyl amines with at least one secondary amino function and either hydroxyl groups, methyl groups, or multiple amino function. The estimated stripper temperature for 3.5 to 11 m MEA solutions with 0.2 to 0.5 mole CO_2 per mole alkalinity ranged from 111 to 126 °C.

A thermal equilibrium between PZ, 1-MPZ, and 1,4-DMPZ was discovered that offers the opportunity for a blended solvent that is resistant to overall thermal degradation. At 150 °C, the equilibrium constant for the disproportionation of 1-MPZ into PZ and 1,4-DMPZ with 0.3 mole CO_2 per mole alkalinity was found to be 0.28. A tertiary blend designed around this constant, 3.9 m PZ / 3.9 m 1-MPZ / 0.2 m 1,4-DMPZ

degraded with a k_1 value of 8.44×10^{-9} s^{-1}, only 37% higher than the k_1 for 8 m PZ with 0.3 mole CO_2 per mole alkalinity.

PZ was not found to preferentially degrade in a blend of 4 m PZ + 4 m 1-MPZ since an equilibrium is being established that occurs more rapidly that thermal degradation. PZ is preferentially degraded in blends with MDEA and MEA. In the presence of MDEA, PZ thermally degrades up to 15 times faster than MDEA. The stability of PZ when blended with another amine depends heavily on the pKa or nucleophilic strength of the amine. Blending PZ has been previously stated as inadvisable, but could be advantageous when matched with a similarly stable molecule, such as 1-MPZ or 2-MPZ.

10.1.4 Physical properties of PZ

At 0 °C, 8 m PZ will not precipitate solids between 0.32 and 0.44 mole CO_2 per mole alkalinity. At an operating temperature of 40 °C, 8 m PZ will be an aqueous solution between 0.1 and 0.45 mole CO_2 per mole alkalinity. The room temperature (20 °C) solubility of unloaded PZ is 14 weight %, or 1.9 m PZ, while the soluble loading range is approximately 0.25 to 0.4 mole CO_2 per mole alkalinity at this temperature. Transition temperatures for concentrated PZ were measured over a range of CO_2 loading and hysteresis was observed in the temperature at which crystals formed when cooled or precipitation melted when heated.

The viscosity of 8 m PZ at 40 °C with 0.4 mole CO_2 per mole alkalinity is 11.4 cP, higher than that of 9 m MEA with 0.5 mole CO_2 per mole alkalinity (3 cP). Solutions of 60wt% DGA® with 0.4 mole CO_2 per mole alkalinity, a commercial gas treating solvent, has a viscosity 13.7 cP, even higher than PZ. The viscosity of 8 m PZ is given

by Equation 4.9 in terms of the viscosity of water (cP), μ_{water}, concentration of CO_2 (mole per kg), C_{CO2}, concentration of PZ (mole per kg), C_{PZ}, and temperature (K), T.

$$\ln\left(\frac{\mu}{\mu_{water}}\right) = 1.723 + 2.63 \cdot C_{CO2} - 1.019 \cdot C_{PZ} - 0.527 \cdot C_{CO2} \cdot C_{PZ} + \frac{-778 \cdot C_{CO2} + 355.2 \cdot C_{PZ} + 169.3 \cdot C_{CO2} \cdot C_{PZ}}{T} \quad (4.9)$$

Density of 5 to 12 m PZ solutions was regressed in terms of the density of water, ρ_{water}, C_{CO2}, and C_{PZ}, and the resulting regression is shown in Equation 4.1. The effect of temperature on density was eliminated by including ρ_{water} at a given temperature.

$$\frac{\rho}{\rho_{water}} = 0.0407 \cdot C_{CO2} + 0.008 \cdot C_{PZ} + 0.991 \quad (4.1)$$

Online measurement of density and viscosity will permit accurate on-line estimates of PZ concentration and CO_2 loading. On-line viscosity and density monitors can be employed in a pilot plant, demonstration plant, or full scale CO_2 capture application as an inexpensive, easy, and effective way to continually monitor the condition of a PZ solvent. Both PZ concentration and CO_2 loading have traditionally been offline analyses that take on the order of minutes or hours to complete. Online monitoring allows for instant feedback and constant monitoring of the solvent conditions where maintaining the solution within physical solubility windows is a crucial operational concern.

The regression for viscosity was developed with only 8 m PZ data and this limits its application. Viscosity of PZ solutions is complicated and regressions across large PZ concentration ranges generally contain unacceptable levels of error for online monitoring

applications. The density regression should be very robust in applications centering around 8 m PZ, the most likely concentration of concentrated PZ systems.

A blend of 4 m PZ / 4 m 2-MPZ, being developed for its beneficial physical solubility, has density less than 1% higher than an 8 m PZ solution with the same alkalinity. On the other hand, a blend of 5 m PZ / 2 m 1-MPZ / 1 m 1,4-DMPZ has up to a 3% lower density but 23% higher viscosity. All blends of PZ with substituted PZ molecules had very similar density values to PZ itself, but up to 30% higher viscosity. Blends can have advantageous characteristics, but can also result in unfavorable changes to density and viscosity.

10.2 RECOMMENDATIONS

Absorption-stripping with aqueous, concentrated piperazine (PZ) is a viable retrofit technology for post-combustion CO_2 capture from coal-fired power plants. The low thermal degradation and oxidation rates observed under conditions similar to those expected in industry are an important advantage of this solvent. Stability to temperature and oxidation, along with fast rates of CO_2 absorption, high CO_2 capacity, and a moderate heat of absorption recommend aqueous, concentrated PZ as the solvent of choice for absorption-stripping for CO_2 capture.

Before deployment of this solvent, there are some unanswered questions that could be investigated to understand the solvent more fully. There is further work recommended on specific lab-scale degradation experiments that will allow more rigorous explanation of the degradation seen in this dissertation. Recommendations for understanding factors important to the responsible implementation of this type of system are also discussed. The following recommendations are listed in order of importance to

indicate what must be more fully understood before full-scale implementation of a PZ system.

10.2.1 Environmental implications of PZ use at a large scale

One area where this project did not focus is the environmental implications of a full-scale PZ-based CO_2 capture system. This is a crucial issue that needs priority attention before any full-scale realization of PZ systems. One of the primary issues is the unknown environmental impact and fate of the thermal degradation and oxidation products. The issues involved with environmental impact include volatility of PZ, volatility of degradation products, reactions of these products in the atmosphere, and handling and storage of liquid and solid wastes created during reclaiming activities. The volatilities of many of the products are unknown, such as amides, or are already know to be high, such as ammonia and 1,4-dimethylpiperazine (1,4-DMPZ) (Rochelle, 2011). Reclaiming is another area where environmental concerns must be considered when designing a PZ reclaiming system. The overall degradation rate of PZ is expected to be low, but the issues surrounding the environmental impact of degradation products should be thoroughly researched before full-scale implementation of PZ.

10.2.1.1 Nitrosamine generation during PZ use

Another important topic related to the environmental impact of PZ is the generation, identification, and quantification of nitrosamines produced during PZ degradation. Nitrosamines are a class of compounds with a $R_1N(-R_2)-N=O$ functional group. A majority of nitrosamines are carcinogenic or potentially carcinogenic to humans, demonstrating the importance of identifying any nitrosamines created during PZ degradation. During the degradation of amines like PZ, nitrite (NO_2^-) and nitrate (NO_3^-) can be produced in small quantities. In highly oxidative environments, significant

quantities can be created, such as in the Cu^{2+}-catalyzed oxidation of PZ. Secondary amines can react to form an amine free radical species with can react with NO to form nitrosamines (Challis and Challis 1982).

Toxicological studies on animals have shown that N-mononitrosopiperazine (MNPZ), N,N'-dinitrosopiperazine (DNPZ), N-Nitroso-3-hydroxypyrrolidine, and N-nitrosodiethanolamine can all derived from PZ in vivo (Tricker et al. 1991). MNPZ has been reported to be mutagenic and carcinogenic in animals although it this may be attributed to the rapid conversion to DNPZ which is highly mutagenic and carcinogenic (Elespuru and Lijinsky 1976; Love et al. 1977). Given these few nitrosamines as a starting point, the importance of finding nitrosamines as degradation products is crucial to fully understanding the PZ solvent system and appreciating its full safety and environmental impact.

Large concentrations of nitrosamines are not expected to be produced under standard operating conditions of a PZ-based CO_2 capture system. NO_2^-, which can produce NO in solution, is only found in trace quantities outside of heavily oxidized PZ solutions. In real systems, oxidation will not be allowed to progress this far in any case due to loss of CO_2 capture capacity and cost. Also, any nitrosamine created is not expected to be stable at high temperatures, so any reaching the stripping section of the system will not persist. A real concern though is the generation of nitrosamines either in the absorber itself, where they could volatilize and reach the atmosphere, or the photolytic reaction of volatile PZ in the atmosphere with NO_X molecules to create nitrosamines in the atmosphere, after leaving the CO_2 capture system. Any of these possibilities need to be fully understood before any application of PZ at a large scale.

10.2.2 Identification of degradation products

One of the most important recommendations of this dissertation is the need for more sophisticated analytical methods to detect unknown degradation products. In both thermal degradation and oxidation of PZ, there is significant gap in the mass balance that was determined to be liquid phase, unknown degradation products. Identifying these products is important for a variety of reasons including understanding their environmental impact, understanding the degradation mechanisms that produce them, studying the best way to reclaim them, and learning how to mitigate or prevent their production.

Important classes of compounds that have not been identified and quantified at this point are aldehydes, alcohols, and ureas. These types of molecules are suspected in both oxidation and thermal degradation of PZ and could represent significant portions of the overall degraded mass balance. Only one significant urea (2-Imid) has been positively identified and many others are suspected, such as the urea of AEAEPZ. No aldehydes or alcohols have been identified yet, but many such as formaldehyde, acetaldehyde, and methanol and strongly suspected.

10.2.3 Further investigation of thermal degradation

Although the rate of thermal degradation with respect to temperature, PZ concentration, and CO_2 concentration is fairly well understood as a result of this dissertation, the specific mechanisms responsible for degradation are not well known. More work is needed to determine exactly which mechanisms are responsible for the loss of PZ observed. In collaboration with this work will be the identification of thermal degradation products, as discussed above, and a better understanding of speciation at high temperature.

High temperature speciation of any amine system is needed to fully grasp the mechanisms that are occurring during degradation. High temperature speciation can be predicted based on current models, but are mostly extrapolations of low temperature NMR speciation results. Medium or high temperature experimental data (80-175 °C) for PZ speciation would make the speciation predicted by the thermodynamic models more robust and could add insight into the mechanisms responsible for thermal degradation.

More thermal degradation experiments are also recommended to determine the details of the dominant mechanisms. Some experiments were performed with the express intention of learning about the mechanisms, but more would be needed to solidify the hypothesized reactions. Work focused on speciation, such as the acidified experiments in section 6.3, could be extended to investigate the role of specific species during degradation. Also, more spiked experiments, like those performed with EDA and 2-Imid, could be done with other degradation products to determine their behavior.

10.2.4 Further investigation of oxidation

There are many effects related to PZ oxidation that were not fully explored in this project due to time or equipment constraints. First, differences in the generation of degradation products due to various metal catalysts should be further explored. With the application of novel techniques to identify and quantify degradation products, the products expected in each particular system can be identified. This will allow a more directed analysis of systems in the field using each catalyst set based on knowledge of what is expected to be the most dominant product or which indicates overall oxidation rates.

If inhibition is needed, further tests should be performed that isolate the exact concentration of Inhibitor A, for example, which is needed to see inhibition. The use of

100 mM Inhibitor A is likely more concentrated than needed and an optimization should be performed based on the catalyst system expected to be present.

The catalytic effect of Fe^{2+} and SSM should be further investigated. Significant error and poor repeatability were observed in these experiments due to very low rates of PZ oxidation. If an experiment was developed to accurately measure low rates of PZ oxidation, the effect of each catalyst could be determined with better accuracy. This is an important point since the use of stainless steel as a material of construction is the most likely choice of CO_2 capture systems.

The effect of CO_2 concentration on PZ oxidation was not fully understood during the course of this project. Additional experiments could determine if a large difference in oxidation rate is expected across the absorber and absorber sump due to differences in CO_2 concentration.

10.2.5 Monitoring of PZ degradation in pilot, demonstration, or full-scale plants

When PZ is used in pilot or demonstration plants, a number of monitoring tools are recommended to fully track the progress of PZ as a solvent. First, the PZ and CO_2 concentrations should be monitored regularly to maintain alkalinity and the appropriate CO_2 loading range. This can be achieved through online density and viscosity measuring, as discussed in Chapter 4. This is also important in order to maintain an aqueous solution to avoid solubility issues with PZ. This represents the very minimal level of monitoring needed to use PZ. Other techniques such as acid titration or total inorganic carbon (TIC) should also be employed offline to ensure the accuracy of the online measurements.

A second level of monitoring for degradation is suggested for longer term pilot plant tests, demonstration plants, and full-scale application. With longer term tests, the

rate of degradation, either from oxidation or thermal degradation, is very useful in order to understand changes in CO_2 capacity or shifts in the loading range that can be seen in degraded solution. This project has identified some of the major degradation products that can be quantified through chromatographic techniques. A basic level of monitoring for degradation products would include a dual IC system (or two separate systems) that can test for liquid phase concentrations of anions and cations. This will allow quantification of heat stable salts (formate, oxalate, acetate, glycolate), potential nitrosamine precursors (nitrate and nitrate), ammonium, amine based degradation products (EDA, AEP, and others), and quantify the parent amine itself. The methods employed in this project, as detailed in Appendix C, could be replicated on any ion chromatography system and would allow monitoring of some of the important liquid phase products.

A third level of monitoring should be used for very long-term experiments where the effect of degradation of PZ would be the most pronounced. This implies the use of high performance liquid chromatography (HPLC), nuclear magnetic resonance (NMR) or other advanced techniques to extend the quantification of degradation products. HPLC techniques were only used in this project to quantify 2-imidazolidone, but can be extended to include more amine products and amino acids. Developments in the quantification of amides, ureas, aldehydes, and alcohols will hopefully lead to chromatographic techniques that can monitor these important species in solution.

Appendix A – Nomenclature, Abbreviations, and Glossary of Degradation Products

The first two tables in this appendix detail the nomenclature and abbreviations used throughout this thesis. This includes symbols used for variables (rate constants, μ, ρ), symbols representing units (g, kg, m), abbreviations for molecules (PZ, EDA, CO_2), and abbreviations for equipment and materials (LGF, TOR). The final table in this appendix is a summary of the degradation products discussed frequently in chapters 5 through 9. This summary includes identified and quantified products as well as suspected products and includes pertinent identifying data. A more detailed list of the chemicals used including their purity, source, and synonyms is given in Appendix B.

Table A.1: List of Abbreviations

Symbol	Units	Definition
1-EPZ	-	1-Ethyl piperazine
1-MPZ	-	1-Methyl piperazine
1-PA	-	1-Piperazineacetic acid
1,4-DMPZ	-	1,4-Dimethyl piperazine
1,4-DEPZ	-	1,4-Diethyl piperazine
2-MPZ	-	2-Methyl piperazine
2-PE	-	2-Piperidineethanol
2-PM	-	2-Piperidinemethanol
2,5-PZdione	-	2,5-Piperazinedione
3a1p	-	3-Amino-1-propanol
4a1b	-	4-Amino-1-butanol
5a1p	-	5-Amino-1-propanol
6a1h	-	6-Amino-1-hexanol
AEAEPZ	-	1-[2-[(2-aminoethyl) amino]ethyl] piperazine
AEI	-	1-(2-Aminoethyl)-2-imidazolidone
AEP	-	1-(2-Aminoethyl) piperazine
AMP	-	2-Amino-2-methyl-1-propanol
AP	-	3-Aminopropanol
bHEP	-	N,N'-bis(2-hydroxyethyl) piperazine
C	-	Carbon; a carbon atom within a molecule
CO_2	-	Carbon dioxide
Cr or Cr^{3+}	-	Chromium, chromic (usually in aqueous solution)
Cu or Cu^{2+}	-	Copper (usually in aqueous solution)
D_2O	-	Deuterium oxide: used in mass spectrometry analyses
DAEP	-	1,4-di(2-aminoethyl) piperazine
DEA	-	Diethanolamine
DETA	-	Diethylenetriamine
DGA®	-	Diglycolamine
DOF	-	Degrees of freedom, statistically
diPZ urea	-	1,1'-carbonylbis-PZ
DMAE	-	N,N-Dimethylethanolamine
DMMEA	-	N,N-Dimethylethanolamine
EDA	-	Ethylenediamine
Fe or Fe^{2+}	-	Iron, ferrous (usually in aqueous solution)
FPZ	-	N-Formyl Piperazine
g	gram	Mass in units of gram
GC-MS	-	Gas chromatography coupled with mass spectroscopy
HEEDA	-	N-(2-hydroxyethyl) ethylenediamine
HEIA	-	1-(2-Hydroxyethyl)-2-Imidazolidone
HEOD	-	3-(2-Hydroxyethyl)-2-Oxazolidone

Table A.1: List of Abbreviations (Continued)

Symbol	Units	Definition
HEP	-	N-(2-Hydroxyethyl) Piperazine
HMDA	-	Hexamethylenediamine
HMI	-	Hexamethyleneimine
HomoPZ	-	Homopiperazine
IC	-	Ion chromatography, anion or cation
IC-MS	-	Cation IC coupled with mass spectroscopy
k_1	-	First order rate constant for amine loss during thermal degradation
KOH	-	Potassium hydroxide: eluent for anion IC analysis
kg	kilogram	Mass in units of kilogram
LGF	-	Low Gas Flow Reactor
m	Mole·(kg H_2O)$^{-1}$	Molal, concentration unit based on kg H_2O
m/z	-	Mass to charge ratio of ions detected during mass spectroscopy
MAPA	-	3-(Methylamino)propylamine
MDEA	-	N-Methyldiethanolamine
MEA	-	Monoethanolamine
MIPA	-	DL-2-Amino-1-propanol
mM	mmol·L^{-1}	Millimolar, concentration unit
MMEA	-	2-Methylaminoethanol
Mor	-	Morpholine
MS	-	Mass spectrometry: analytical technique to determine the molecular weight of a molecule of interest
MSA	-	Methanesulfonic acid: eluent for cation IC analysis
N	-	Nitrogen; a nitrogen atom within a molecule
Ni or Ni^{2+}	-	Nickel (usually in aqueous solution)
N,N'-diMEDA	-	N,N'-Dimethylethylenediamine
N,N-diMEDA	-	N,N-Dimethylethylenediamine
O_2	-	Oxygen
OOR	-	Original oxidation reactor
PD	-	Piperidine
PMDETA	-	N,N,N',N',N''-pentamethyldiethylenetriamine
PMDPTA	-	N,N,N',N',N''-pentamethyldipropylenetriamine
PEP	-	1,1'-(1,2-ethanediyl)bis-PZ
Pyr	-	Pyrrolidine
PZ	-	Piperazine
t2,5-DMPZ	-	*trans*-2,5-Dimethyl piperazine
TEDA	-	Triethylenediamine

Table A.1: List of Abbreviations (Continued)

Symbol	Units	Definition
TEPA	-	Tetraethylenediamine
TIC	-	Total Inorganic Carbon: assay to measure CO_2 concentration
TIC	-	Total Ion Current: raw signal output of mass spectrometer
TMBDA	-	N,N,N',N'-tetramethylbutylenediamine
TMEDA	-	N,N,N',N'-Tetramethylethylenediamine
TMPDA	-	N,N,N',N'-Tetramethypropylenediamine
TriMEDA	-	N,N,N'-Trimethylethylenediamine
TOR	-	Teflon oxidative reactor

Table A.2: List of Greek Symbols

Symbol	Units	Definition
α	mole CO_2/mole alkalinity	CO_2 loading in terms of moles of CO_2 per mole alkalinity (equivalent to mole CO_2 per mole amine functions)
α-	-	The first carbon or other molecule away from a dominant atom (i.e. nitrogen). The α-carbon is the carbon nearest to the nitrogen in a PZ molecule
ρ	g mL^{-1}	Density of a solution
μ	mPa-s	Viscosity of a solution

The following table (Table A.3) is a summary of the degradation products identified or suspected for either thermal degradation or oxidation. The table is sorted alphabetically by abbreviation and then chemical name. Those molecules that have been positively identified and can be quantified readily with techniques described in this dissertation are indicated with a "Q". Those that are suspected and not yet confirmed due to a lack of a commercial standard or an appropriate method to identify them are indicated with an "S".

Table A.3: Glossary of Degradation Products

Chemical Name	Abbreviation	Structure	CAS Number	MW (g/mol)	Status*	Deg. Type+
1,4-Dimethylpiperazine	1,4-DMPZ	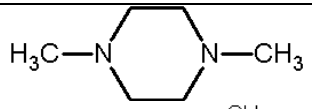	106-58-1	114.2	Q	T
1-Ethylpiperazine	1-EPZ	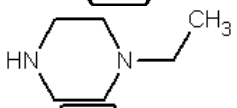	5308-25-8	114.2	Q	T
1-Methylpiperazine	1-MPZ	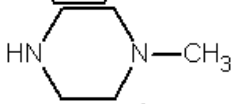	109-01-3	100.2	Q	T
1-Piperazineacetic acid	1-PA	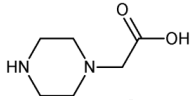	37478-58-3	144.17	S	O, T
2,5-Piperazinedone	2,5dione	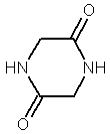	106-57-0	114.10	S	O
2-Imidazolidone	2-Imid	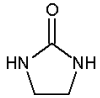	120-93-4	86.09	Q	T
1-Acetylpiperazine	AcPZ	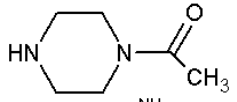	13889-98-0	128.17	S	O, T
1-[2-[(2-Aminoethyl)amino] ethyl] piperazine	AEAEPZ	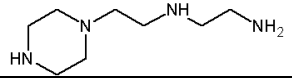	24028-46-4	172.27	S	T

Table A.3: Glossary of Degradation Products (Continued)

Chemical Name	Abbreviation	Structure	CAS Number	MW (g/mol)	Status*	Deg. Type+
1-[2-(Piperazinyl)ethyl]-2-imidazolidinone	AEAEPZ Urea	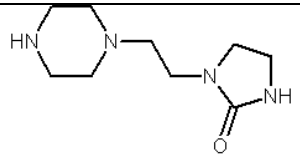	104087-61-8	198.27	S	T
1-(2-Aminoethyl)glycine	AEG	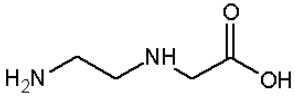	24123-14-6	118.13	S	O
1-(2-Aminoethyl)-2-imidazolidone	AEI	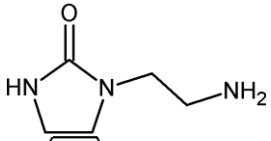	6281-42-1	129.16	S	T
1-(2-Aminoethyl)piperazine	AEP	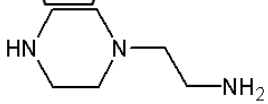	140-31-8	129.2	Q	T
Glycolate	$C_2H_4O_3$	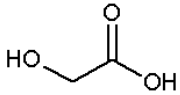	79-14-1	75.1	Q	O, T
Oxalate	$C_2O_4^{2-}$	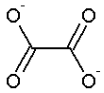	NA	88.0	Q	O, T
Acetate	CH_3COO	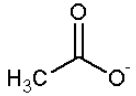	NA	59.1	Q	O, T
Formaldehyde	CHO		50-00-0	30.03	S	O, T
Formate	CHO_2	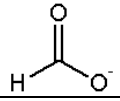	NA	45.0	Q	O, T

Table A.3: Glossary of Degradation Products (Continued)

Chemical Name	Abbreviation	Structure	CAS Number	MW (g/mol)	Status*	Deg. Type+
1,4-di(2-aminoethyl) piperazine	DAEP	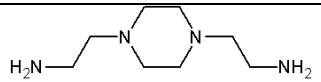	6531-38-0	172.2736	S	T
N,N'-bis(2-aminoethyl)-urea (diEDA urea)	diEDA urea	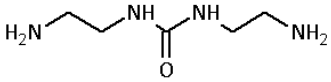	940866-61-5	146.19	S	T
1,1'-carbonylbis-piperazine	diPZ urea	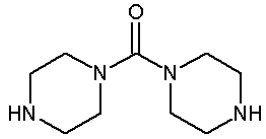	17159-16-9	198.2654	S	T
Ethylenediamine	EDA	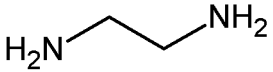	107-15-3	60.1	Q	O, T
Ethanol	EtOH		64-17-5	46.07	S	O
1-Formylpiperazine	FPZ	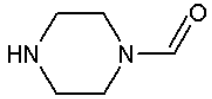	7755-92-2	114.2	Q	O, T
1-(2-Hydroxyethyl)piperazine	HEP	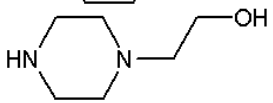	103-76-4	130.19	Q	T
Methanol	MeOH		67-56-1	32.04	S	O
Nitrite	NO_2^-		NA	46.0	Q	O
Nitrate	NO_3^-	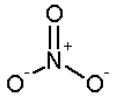	NA	62.0	Q	O
1,1'-(1,2-Ethanediyl)bis-piperazine	PEP	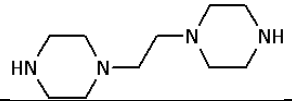	19479-83-5	198.3085	S	T

Table A.3: Glossary of Degradation Products (Continued)

Chemical Name	Abbreviation	Structure	CAS Number	MW (g/mol)	Status*	Deg. Type+
2-Piperazinone	PZone	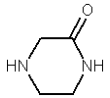	5625-67-2	100.12	S	O
Triethylenediamine	TEDA	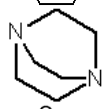	280-57-9	112.17	S	T
1-(1-Piperazinylacetyl)-piperazine (Amide of 1-PZ)		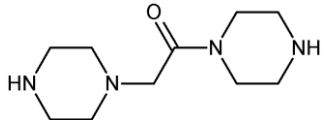	69253-90-3	212.29	S	T
1,1'-(1,2-dioxo-1,2-ethanediyl)bis-piperazine (diPZ oxalyl amide)		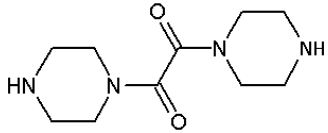	105807-56-5	226.28	S	O, T
1,2,3,4-tetrahydro pyrazine (enamine of PZ)		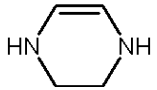	5194-05-8	84.12	S	O
1,2,3,6-tetrahydro pyrazine (imine of PZ)		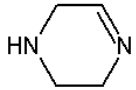	77253-83-9	84.12	S	O
1,3-bis(N-hydroxymethyl) urea		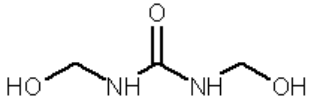	140-95-4	120.11	S	T
1,4-di(2-hydroxymethyl) EDA		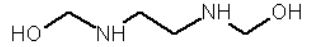	70495-38-4	120.15	S	T
1,4-Diacetylpiperazine		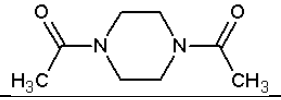	18940-57-3	170.21	S	O, T

Table A.3: Glossary of Degradation Products (Continued)

Chemical Name	Abbreviation	Structure	CAS Number	MW (g/mol)	Status*	Deg. Type+
1,4-Diazabicyclo[2.2.2]oct-2-ene (TEDA enamine)		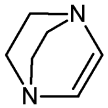	122883-12-9	110.16	S	O, T
1,4-Diazabicyclo[2.2.2]octan-2-ol (TEDA hemiaminal)		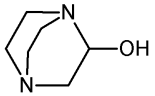	146562-84-7	128.17	S	O, T
1,4-Diazabicyclo[2.2.2]octan-2-one (Amide of 1-PA)		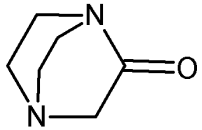	146562-83-6	126.16	S	O, T
1,4-Dioxalylpiperazine		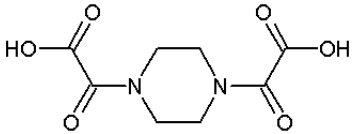	None	230.17	S	O, T
1-Oxalylpiperazine (α-oxo-1-piperazineacetic acid)		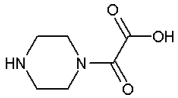	691394-09-9	158.16	S	O, T
2-piperazinol (hemiaminal of PZ)		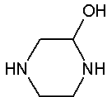	1104858-53-8	102.14	S	O
Acetaldehyde			75-07-0	44.05	S	O, T
Ethylene glycol		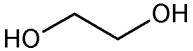	107-21-1	62.07	S	O
Hydroxyacetaldehyde		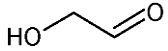	141-46-8	60.05	S	O, T
N,N'-1,2-ethanediylbis-glycine		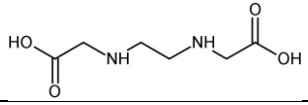	5657-17-0	176.17	S	O

Table A.3: Glossary of Degradation Products (Continued)

Chemical Name	Abbreviation	Structure	CAS Number	MW (g/mol)	Status*	Deg. Type+
N-oxidepiperazine		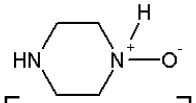	NA	102.1	S	O
Poly(methylene)piperazine		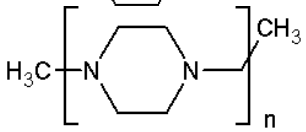	NA	NA	S	T
Urea		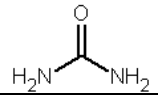	57-13-6	60.06	S	T

* S: Suspected; Q: positively identified and quantified
+ O: Oxidation; T: thermal degradation

Appendix B – List of Chemicals

All chemicals used for experimentation or analytical techniques were laboratory grade or purer. Details of the materials used in this thesis are included in Table B.1.

Table B.1: Details of All Chemicals Used

Chemical Name [Synonyms]	Abbreviation	Manufacturer*	CAS No.^	Purity^{+}	MW (g/mol)
1-(2-Aminoethyl) piperazine [N-(2-Aminoethyl) piperazine]	AEP	Acros	140-31-8	99%	129.2
1-(2-Hydroxyethyl)-2-Imidazolidone [N-(2-Hydroxyethyl) imidazolidinone	HEI	Aldrich	3699-54-5	75% Soln.	130.2
1-(2-Hydroxyethyl)-4-methyl piperazine [N-(2-Hydroxyethyl)-N'-methyl piperazine]	HEMP	Acros	5464-12-0	98%	144.2
1-(2-Hydroxyethyl) ethylenediamine [N-(2-Hyroxyethyl) ethylenediamine] [2-(2-Aminoethylamino) ethanol]	HEEDA	Acros	111-41-1	>99%	104.2
1-(2-Hydroxyethyl) piperazine [N-(2-Hydroxyethyl) piperazine] [1-piperazineethanol]	HEP	TCI	103-76-4	>99.0%	130.19
1,4-bis(β-hydroxyethyl)piperazine [N,N'-bis(2-hydroxyethyl) piperazine] [1,4-piperazinediethanol]	bHEP	Aldrich	122-96-3	99%	174.24
1,4-Diethyl piperazine [N,N'-Diethyl PZ]	DEPZ	Acros	229-341-5	98%	142.24
1,4-Diformyl piperazine [N,N'-Diformyl PZ]	DFPZ	TCI	4164-39-0	>98.0%	142.2
1,4-Dimethyl piperazine [N,N'-Dimethyl PZ]	1,4-DMPZ	Acros	106-58-1	98.5%	114.2
1,4-Dioxane, stabilized	Dioxane	Acros	123-91-1	99+%	88.11
1-Acetyl piperazine [N-Acetyl piperazine]	AcPZ	TCI	13889-98-0	>98.0%	128.2

Table B.1: Details of All Chemicals Used (Continued)

Chemical Name [Synonyms]	Abbreviation	Manufacturer*	CAS No.^	Purity^{+}	MW (g/mol)
1-Amino-4-methyl piperazine [N-Amino-N'-methyl piperazine]	AMPZ	Acros	6928-85-4	99%	115.2
1-Ethyl piperazine [N-Ethyl piperazine]	EPZ	TCI	5308-25-8	99	114.2
1-Formyl piperazine [N-Formyl piperazine]	FPZ	TCI	7755-92-2	>98.0%	114.2
1-Formyl piperazine [N-Formyl piperazine]	FPZ	Acros Organics	7755-92-2	98%	114.2
1-Methyl piperazine [N-Methyl piperazine]	1-MPZ	Acros	109-01-3	>99%	100.2
2,5-Dimethyl piperazine [*trans*-2,5-Dimethyl piperazine]	t2,5-DMPZ	AK Scientific	3815-34-1	99%	114.19
2,5-Piperazinedione [Glycine anhydride]	2,5-PZdione	Acros	106-57-0	98%	114.1
2-Imidazolidone	2-Imid	Aldrich	120-93-4	96%	86.09
2-Imidazolidone Hemihydrate		Acros	121325-67-5	>99%	86.1
2-Methyl-2-imidazoline		TCI	534-26-9	>97.0%	84.16
2-Methyl piperazine	2-MPZ	Acros	109-07-9		100.16
3-(2-Hydroxyethyl)-2-Oxazolidone	HEOD	MP	3356-88-5		131.1
3-(Trimethylsilyl)-1-propanesulfonic acid, sodium salt [Sodium 2,2-dimethyl-2-silapentane-5-sulfonate]	DDS	Aldrich	2039-96-5	97%	218.3
Acetic Acid, glacial	CH_3COOH	Fisher	64-19-7	100%	60.1

Table B.1: Details of All Chemicals Used (Continued)

Chemical Name [Synonyms]	Abbreviation	Manufacturer*	CAS No.^	Purity^{+}	MW (g/mol)
Ammonium Chloride	NH_4Cl	Fisher	12125-02-9	99.6%	53.49
Ammonium Sulfate	$(NH_4)_2SO_4$	EM	7783-20-2	99.0%	132.15
Carbon, Inorganic Standard (Na_2CO_3 /$NaHCO_3$)	NA	Ricca	None	1000 ppm	NA
Carbon Dioxide	CO_2	Matheson	124-38-9	99.5%	44.01
Carbon Dioxide (2%)/Oxygen (98%)	CO_2/O_2	Matheson	None	NA	NA
Chromic (III) Sulfate Hydrate	$Cr_2(SO_4)_3$ xH_2O	Pfaltz & Bauer	15244-38-9	NA	392.16
Chromium in 3% Nitric Acid	Cr	Ricca	NA	1000 ppm	NA
Chromium Potassium Sulfate Dodecahydrate	$CrK(SO_4)_2 \cdot 12H_2O$	Acros	7788-99-0	99%	499.25
Copper in 3% Nitric Acid	Cu	Ricca	NA	1000 ppm	NA
Cupric (II) Sulfate Pentahydrate	$CuSO_4 \cdot 5H_2O$	Mallinckrodt	7758-99-8	99.5%	249.68
Deuterium oxide	D_2O	Cambridge	7789-20-0	99.9%	20.04
Ethylenediamine	EDA	Strem	107-15-3	99%	60.10
Ferric (III) Chloride	$FeCl_3 \cdot 6H_2O$	Fisher	10025-77-1	99.4%	270.3
Ferrous (II) Sulfate Heptahydrate	$FeSO_4 \cdot 7H_2O$	Spectrum	7782-63-0	99.0%	278.05
Formaldehyde	CH_2O	Fisher	50-00-0	37 wt%	30.0
Formic Acid	CH_2O_2	Fisher	None	90.4%	46.03
Glycolic Acid, 67% solution in water	$C_2H_4O_3$	Acros	79-14-1	67%	76.05
Homopiperazine [1,4-Diazacycloheptane] [Hexahydro-1H-1,4-Diazepine]	HomoPZ	Acros	505-66-8	98%	100.16
Hexamethylenediamine [1,6-Hexanediamine]	HMDA	Sigma Aldrich	124-09-4	98%	100.16

Table B.1: Details of All Chemicals Used (Continued)

Chemical Name [Synonyms]	Abbreviation	Manufacturer*	CAS No.^	Purity^{+}	MW (g/mol)
Hexamethyleneimine [Azacycloheptane] [Azepane] [Perhydroazepine]	HMI	Acros	111-49-9	99%	99.15
Iodine (Iodide/Iodine)	I_2	Ricca	NA	0.1 N	NA
Inhibitor A	-	-	-	99%	-
Inhibitor B	-	-	-		-
Inhibitor C	-	-	-		-
Iron in 3% Nitric Acid	Fe	Ricca	NA	1000 ppm Fe	NA
Methanesulfonic Acid	MSA	Acros	75-75-2	99%	96.1
Morpholine	Mor	Aldrich	110-91-8	99.5+%	87.12
Nickel (II) Sulfate Hexahydrate	$NiSO_4 \cdot 6H_2O$	Alfa Aesar	10101-97-0	>98.0%	237.72
Nitric Acid	HNO_3	Fisher	7697-37-2	68-71%	63.01
Nitric Acid	HNO_3	Fisher	NA	6M	NA
Nitrogen	N_2	Praxair	7727-37-9	97	28.01
Oxygen	O_2	Matheson	7782-44-7	99.9	32.00
Piperazine, anhydrous [1,4-diazacyclohexane]	PZ	Fluka	110-85-0	>99.0%	86.14
Piperazine, anhydrous [1,4-diazacyclohexane]	PZ	Sigma Aldrich	110-85-0	99%	86.14
Piperidine [Azacyclohexane] [Pentamethyleneimine]	PD	Sigma Aldrich	110-89-4	99%	85.15
Phosphoric Acid	H_3PO_4	Acros	7664-38-2	85%	98.00

Table B.1: Details of All Chemicals Used (Continued)

Chemical Name [Synonyms]	Abbreviation	Manufacturer*	CAS No.^	Purity^{+}	MW (g/mol)
Potassium Formate	$KCHO_2$	Alfa Aesar	590-29-4	99%	84.12
Potassium Iodate	KIO_3	Acros	758-05-6	-	214.0
Pyrazine	$C_4H_4N_2$	Acros	290-37-9	99+%	80.09
Pyrrolidine [Azacyclopentane] [Tetramethyleneimine]	Pyr	Fluka	123-75-1	>99%	71.12
Sodium Chloride	NaCl	EM Science	7647-14-5	99.0%	58.44
Sodium Hydroxide Solution	NaOH	Fisher	None	5 N	40.00
Sodium Metavanadate	$NaVO_3$	Acros	13718-26-8	96.%	121.93
Sodium Nitrate	$NaNO_3$	Fisher	7631-99-4	>99%	84.99
Sodium Nitrite	$NaNO_2$	Fisher	7632-00-0	97.0%	69.00
Sodium Oxalate	$Na_2C_2O_4$	JT Baker	62-76-0	99.9%	134.0
Sodium Sulfate	$NaSO_4$	Spectrum	7757-82-6	>99%	142.04
Sodium Sulfide Nonahydrate	$Na_2S \cdot 9H_2O$	Ricca	1313-84-4	5% (m/v)	240.18
Sulfuric Acid, Concentrated	H_2SO_4	Fisher	None	36 N	98.07
Sulfuric Acid Solution	H_2SO_4	Fisher	None	0.2 N	98.07
Triethylenediamine [1,4-Diazabicyclo[2.2.2]octane]	TEDA	Acros	280-57-9	97%	112.17

* Manufacturer abbreviations are as follows:
Acros: Acros Organics N.V., Geel, Belgium
AK Scientific: AK Scientific Incorporated, Mountain View, CA
Alfa Aesar: Alfa Aesar, Ward Hill, MA
Cambridge: Cambridge Isotope Laboratories, Andover, MA
EM Science: Division of EM Industries, Gibbstown, NJ
Fisher: Fisher Scientific Worldwide, Hampton, NH

Fluka: Sigma-Aldrich Corporation, St. Louis, MO
JT Baker: Mallinkrodt Baker Inc., Phillipsburg, NJ
Matheson: Matheson Tri-Gas Inc., Basking Ridge, NJ
Mallinckrodt: Mallinkrodt Baker Inc., Phillipsburg, NJ
MP: MP Biomedicals LLC, Solon, OH
Pfaltz & Bauer: Pfaltz & Bauer, Waterbury, CT
Praxair: Praxair, Inc., Danbury, CT
Ricca: Ricca Chemical Company, Pequannock, NJ
Sigma-Aldrich: Sigma-Aldrich Corporation, St. Louis, MO
Spectrum: Spectrum Chemical Manufacturing Company, Gardena, CA
Strem Chemicals: Strem Chemicals, Inc., Newburyport, MA
TCI: Tokyo Chemical Industry (TCI) America, Portland, OR

^ CAS Number: "none" is listed for items that do not have a CAS number because it is a mixture of more than one chemical or because it is a specialty item

[+] Purity: The concentration is listed for chemical solutions; NA is listed when chemical purity is not available from supplier

Appendix C – Details of Analytical Methods Used

The details of the analytical techniques methods used throughout this dissertation are included in this appendix. The program methods that were used on the anion IC, cation IC, cation IC-MS, HPLC, and amino acid liquid chromatography (AA-LC) are described in this chapter.

C.1 ANION IC

The anion IC was used to quantify the concentration of formate, acetate, glycolate, oxalate, sulfate, chlorine, nitrite, and nitrate in experimental samples. The 35 minute method used a gradient ranging from 2 to 45 mM KOH and a 6 minute equilibration time at the start of the program. The program used, "Anions.pgm", was as follows:

Anions.pgm

Sampler.AcquireExclusiveAccess
Sampler_DiverterValve.Position_2
Column_TC.AcquireExclusiveAccess
Compartment_TC.AcquireExclusiveAccess
Pressure.LowerLimit = 200 [psi]
Pressure.UpperLimit = 3000 [psi]
MaximumFlowRamp = 6.00 [ml/min²]
%A.Equate = "%A"
CR_TC = On
Flush Volume = 250
Wait FlushState
NeedleHeight = 2 [mm]
CutSegmentVolume = 10 [µl]
SyringeSpeed = 2
CycleTime = 0 [min]
WaitForTemperature = False
Data_Collection_Rate = 5.0 [Hz]
Temperature_Compensation = 1.7 [%/°C]
CellHeater.Mode = On
CellHeater.TemperatureSet = 35.00 [°C]
Column_TC.Mode = On
Column_TC.TemperatureSet = 30.00 [°C]
Compartment_TC.Mode = On
Compartment_TC.TemperatureSet = 30.00 [°C]
Suppressor2.Type = ASRS_4mm
Suppressor2.CurrentSet = 179 [mA]
Flow = 1.600 [ml/min]
Pump_2.Curve = 5
Wait SampleReady

-6.10 Concentration = 45.00 [mM]
EGC_1.Curve = 5

-6.00 Concentration = 2.00 [mM]
EGC_1.Curve = 5

0.00 CDet1.Autozero
Load
Wait CycleTimeState
Inject
Wait InjectState

CD_1.AcqOn
CD_1_Total.AcqOn
Sampler.ReleaseExclusiveAccess
Compartment_TC.ReleaseExclusiveAccess
Column_TC.ReleaseExclusiveAccess

17.00 Concentration = 2.00 [mM]
EGC_1.Curve = 5

25.00 Concentration = 45.00 [mM]
EGC_1.Curve = 5

35.00 Concentration = 45.00 [mM]
CD_1.AcqOff
CD_1_Total.AcqOff
EGC_1.Curve = 5
End

C.2 CATION IC

Two different methods were used for cation IC analysis. The first method used was a short method that was used to quantify the concentration of PZ, EDA, FPZ, other amines, Na^+, and K^+ in experimental samples. The 20 minute method used a gradient ranging from 5.5 to 38.5 mM MSA and a 3 minute equilibration time at the start of the program. The gradient was delivered by assigning a percentage of the eluent that was either analytical grade water (Channel B) or 55 mM MSA (Channel C). The program used, "Jason3Auto.pgm", was as follows:

Jason3Auto.pgm

Pressure.LowerLimit = 200
Pressure.UpperLimit = 4000
%A.Equate = "6"
%B.Equate = "8"
%C.Equate = "55"
%D.Equate = "%D"
Pump_InjectValve.LoadPosition
Data_Collection_Rate = 2.0

Temperature_Compensation = 1.7
Oven_Temperature = 40
Suppressor_Type = CSRS_4mm
Suppressor_Current = 136

-3.00 Flow = 1.20
%B = 90.0
%C = 10.0
%D = 0.0
Curve = 5

-2.40 Pump_relay_1.open

-2.30 Pump_Relay_1.Closed duration = 120
Flow = 1.20
%B = 90.0
%C = 10.0
%D = 0.0
Curve = 5

0.00 Autozero
Flow = 1.20
%B = 90.0
%C = 10.0
%D = 0.0
Curve = 5
ECD_1.AcqOn
Pump_InjectValve.InjectPosition Duration= 30
Flow = 1.20
%B = 90.0
%C = 10.0
%D = 0.0
Curve = 5

7.00 Flow = 1.20
%B = 90.0
%C = 10.0
%D = 0.0
Curve = 5

7.001 Flow = 1.20
%B = 80.0
%C = 20.0

%D = 0.0
Curve = 5

12.0 Flow = 1.20
%B = 80.0
%C = 20.0
%D = 0.0
Curve = 5

17.0 Flow = 1.20
%B = 30.0
%C = 70.0
%D = 0.0
Curve = 5

20.0 ECD_1.AcqOff
Flow = 1.20
%B = 30.0
%C = 70.0
%D = 0.0
Curve = 5
End

A second, longer method was used to quantify complex, degraded amine mixtures. It mimicked the method used for cation IC-MS (detailed in the next section), but was performed on the IC not connected to the MS. The flow rate was lower than "Jason3Auto.pgm" to enhance separation. The details of the "Stephanie3Auto.pgm" method are as follows:

Stephanie3Auto.pgm

Pressure.LowerLimit = 200 [psi]
Pressure.UpperLimit = 3000 [psi]
%A.Equate = "%A"
CR_TC = On
DeliverSpeed = 4.0 [ml/min]
DelayVolume = 125 [µl]
FlushFactor = 10
Sampler.LoadPosition
DeliverSampleVolume=1666

```
        EndSamplePrep
        Data_Collection_Rate =        5.0 [Hz]
        CellTemperature.Nominal =  30.0 [°C]
        ColumnTemperature.Nominal =       30.0 [°C]
        Suppressor_Type =    CSRS_4mm
        Suppressor_Current =          77 [mA]
        Channel_Pressure.Average = On
        Flow =          0.50 [ml/min]

 0.000  Autozero
        Concentration =        5.50 [mM]
        Curve =        5
        Wait    CycleTimeState
        Inject
        ECD_1.AcqOn
        Channel_Pressure.AcqOn
        Concentration =        5.50 [mM]
        Curve =        5

 0.500  BeginOverlap

16.400  Concentration =        5.50 [mM]
        Curve =        5

16.501  Concentration =        11.00 [mM]
        Curve =        5

26.400  Concentration =        11.00 [mM]
        Curve =        5

36.400  Concentration =        38.50 [mM]
        Curve =        5

47.400  Concentration =        38.50 [mM]
        Curve =        5

47.500  Concentration =        5.50 [mM]
        Curve =        5

50.000  ECD_1.AcqOff
        Concentration =        5.50 [mM]
        Curve =        5
        Channel_Pressure.AcqOff
```

End

C.3 HIGH PERFORMANCE LIQUID CHROMATOGRAPHY (HPLC)

The HPLC was used to quantify organic molecules that were not easily quantified using anion or cation IC. A 30 minute method, PA2-MeOH-CAN-2.pgm, was used that contained a gradient of water, methanol, and acetonitrile. It was developed for the Polar Advantage 2 analytical separation column (Dionex Corporation) as described in section 3.1.12. It is important to note that in the HPLC set-up, eluent A was a buffer, eluent B was acetonitrile, eluent C was methanol, and eluent D was water. The details of PA2-MeOH-CAN-2.pgm are as follows:

PA2-MeOH-ACN-2.pgm

```
Column_A.ActiveColumn =  No
TempCtrl =     On
Temperature.Nominal =        30.0 [°C]
Column_B.ActiveColumn =  No
Pressure.LowerLimit =        5 [bar]
Pressure.UpperLimit =        300 [bar]
MaximumFlowRampDown =          Infinite
MaximumFlowRampUp =     Infinite
%A.Equate =  "%A"
%B.Equate =  "%B"
%C.Equate =  "%C"
%D.Equate =  "%D"
DrawSpeed =  5.000 [µl/s]
DrawDelay =  3000 [ms]
DispSpeed =  20.000 [µl/s]
DispenseDelay =       0 [ms]
WasteSpeed =          32.000 [µl/s]
SampleHeight =        2.000 [mm]
InjectWash =  NoWash
LoopWashFactor =     2.000
PunctureOffset =      0.0 [mm]
PumpDevice =          "Pump"
InjectMode =  Normal
SyncWithPump =       On
```

Data_Collection_Rate = 2.5 [Hz]
TimeConstant = 0.60 [s]
ELS_1.Step = 0.10 [s]
ELS_1.Average = Off
UV_VIS_1.Wavelength = 210 [nm]
EvaporatorTemperature.Nominal = 50 [°C]
NebuliserTemperature = 90 [°C]
LightSourceIntensity = 85 [%]
CarrierFlow.Nominal = 1.60 [slm]
SmoothWidth = 20
PMTGain = 1.0
UV.LeakSensorMode = Disabled

-4.000 Flow = 1.000 [ml/min]
%B = 0.0 [%]
%C = 0.0 [%]
%D = 100.0 [%]

0.000
UV.Autozero
ELSD.Autozero
Wait AZ_Done
Wait UV.Ready and ELSD.Ready
Inject
ELS_1.AcqOn
UV_VIS_1.AcqOn

3.000 Flow = 1.000 [ml/min]
%B = 0.0 [%]
%C = 0.0 [%]
%D = 100.0 [%]

10.000 Flow = 1.000 [ml/min]
%B = 0.0 [%]
%C = 5.0 [%]
%D = 95.0 [%]

20.000 Flow = 1.000 [ml/min]
%B = 0.0 [%]
%C = 50.0 [%]
%D = 50.0 [%]

30.000 Flow = 1.000 [ml/min]

%B = 20.0 [%]
%C = 50.0 [%]
%D = 30.0 [%]

ELS_1.AcqOff
UV_VIS_1.AcqOff
End

NOTE:
A=NH4Ac
B=Acetonitrile
C=Methanol
D=Water

C.4 CATION IC-MS

The cation IC-MS was used to identify unknown peaks observed on the cation IC. The method used was essentially the same as "Jason3Auto.pgm" described above, except the timing was stretched out to accommodate a lower flowrate required for the MS. The 50 minute method used a gradient ranging from 5.5 to 38.5 mM MSA and a 2.4 minute equilibration and injection time at the start of the program. The Xcalibur® program which operates the IC-MS cannot accept negative time, so the equilibration and injection time are in positive time with the injection of the sample at 2.4 minutes. The gradient was delivered by an eluent generator for MSA. The program used, "Jason3Auto-HalfmL_min.pgm", was as follows:

Jason3Auto-HalfmL_min.pgm:

Pressure.LowerLimit = 200 [psi]
Pressure.UpperLimit = 3000 [psi]
%A.Equate = "%A"
CR_TC = On
WaitForTemperature = False
Data_Collection_Rate = 5.0 [Hz]
CellTemperature.Nominal = 30.0 [°C]
ColumnTemperature.Nominal = 30.0 [°C]
Suppressor_Type = CSRS_4mm
Suppressor_Current = 77 [mA]

```
        ECD_Total.Step = 0.20 [s]
        ECD_Total.Average = Off
        Pump_InjectValve.LoadPosition
        Flow = 0.50 [ml/min]

 0.000  Concentration = 5.50 [mM]
        Autozero
        Inject
        ECD_1.AcqOn
        ECD_Total.AcqOn
        Concentration = 5.50 [mM]
        Pump_ECD_Relay_2.Closed Duration=10.00

 0.100  Pump_ECD_Relay_1.State    Closed

 1.000  Pump_ECD_Relay_1.State    Open

 2.300  Pump_InjectValve.InjectPosition      Duration=60.00

16.400  Concentration = 5.50 [mM]

16.501  Concentration = 11.00 [mM]

26.400  Concentration = 11.00 [mM]

36.400  Concentration = 38.50 [mM]

47.400  Concentration = 38.50 [mM]

47.500  Concentration = 5.50 [mM]

50.000  ECD_1.AcqOff
        ECD_Total.AcqOff
        Concentration = 5.50 [mM]

End
```

C.5 AA-LC

The amino acid liquid chromatography (AA-LC) analysis was used to identify amino acid-based degradation products. The 50 minute method used a gradient ranging from 5.5 to 38.5 mM MSA and a 2.4 minute equilibration and injection time at the start

of the program. The Xcalibur® program which operates the IC-MS cannot accept negative time, so the equilibration and injection time are in positive time with the injection of the sample at 2.4 minutes. The gradient was delivered by an eluent generator for MSA. The program used, “Voice-1.pgm”, was as follows:

“Voice-1.pgm”

```
Sampler.AcquireExclusiveAccess
Sampler_DiverterValve.Position_1
Column_TC.AcquireExclusiveAccess
Compartment_TC.AcquireExclusiveAccess
Pressure.LowerLimit =          200 [psi]
Pressure.UpperLimit =          3900 [psi]
MaximumFlowRamp =          1.00 [ml/min²]
%A.Equate =   "%A"
%B.Equate =   "%B"
%C.Equate =   "%C"
%D.Equate =   "%D"
Flush    Volume = 250
Wait    FlushState
NeedleHeight =          2 [mm]
CutSegmentVolume =          10 [µl]
SyringeSpeed =          4
CycleTime =   0 [min]
WaitForTemperature =          False
EDet1.Mode =          IntAmp
EDet1.CellControl      = On
Data_Collection_Rate =          1.00 [Hz]
pH.UpperLimit =       13.00
pH.LowerLimit =       10.00
WaveformName = "amino acids (ph,ag,agcl reference)"
WaveformDescription = "Amino Acids (pH/Ag/AgCl Ref.)"
Electrode = pH
Waveform Time = 0.000, Potential = 0.130, GainRegion = Off, Ramp = On,
        Integration = Off
Waveform Time = 0.040, Potential = 0.130, GainRegion = Off, Ramp = On,
        Integration = Off
Waveform Time = 0.050, Potential = 0.330, GainRegion = Off, Ramp = On,
        Integration = Off
Waveform Time = 0.210, Potential = 0.330, GainRegion = On, Ramp = On,
```

```
        Integration = On
      Waveform Time = 0.220, Potential = 0.550, GainRegion = On, Ramp = On,
        Integration = On
      Waveform Time = 0.460, Potential = 0.550, GainRegion = On, Ramp = On,
        Integration = On
      Waveform Time = 0.470, Potential = 0.330, GainRegion = On, Ramp = On,
        Integration = On
      Waveform Time = 0.560, Potential = 0.330, GainRegion = Off, Ramp = On,
        Integration = Off
      Waveform Time = 0.570, Potential = -1.670, GainRegion = Off, Ramp = On,
        Integration = Off
      Waveform Time = 0.580, Potential = -1.670, GainRegion = Off, Ramp = On,
        Integration = Off
      Waveform Time = 0.590, Potential = 0.930, GainRegion = Off, Ramp = On,
        Integration = Off
      Waveform Time = 0.600, Potential = 0.130, GainRegion = Off, Ramp = On,
        Integration = Off, LastStep = On
      Column_TC.Mode =   On
      Column_TC.TemperatureSet =          30.00 [°C]
      Compartment_TC.Mode =     On
      Compartment_TC.TemperatureSet = 30.00 [°C]
      Wait    SampleReady

-1.000 Flow =           0.250 [ml/min]
      %B =   24.0 [%]
      %C =   0.0 [%]
      %D =   0.0 [%]
      Curve =         5

 0.000 Load
      Inject
      InjectValve_1.InjectPosition  Duration=120.00
      ED_1.AcqOn
      ED_1_Total.AcqOn
      Sampler.ReleaseExclusiveAccess
      Compartment_TC.ReleaseExclusiveAccess
      Column_TC.ReleaseExclusiveAccess

8.000  Flow =           0.250 [ml/min]
      %B =   36.0 [%]
      %C =   0.0 [%]
      %D =   0.0 [%]
      Curve =         8
```

11.000 Flow = 0.250 [ml/min]
%B = 36.0 [%]
%C = 0.0 [%]
%D = 0.0 [%]
Curve = 8

18.000 Flow = 0.250 [ml/min]
%B = 20.0 [%]
%C = 40.0 [%]
%D = 0.0 [%]
Curve = 8

21.000 Flow = 0.250 [ml/min]
%B = 16.0 [%]
%C = 44.0 [%]
%D = 0.0 [%]
Curve = 5

23.000 Flow = 0.250 [ml/min]
%B = 16.0 [%]
%C = 70.0 [%]
%D = 0.0 [%]
Curve = 8

42.000 Flow = 0.250 [ml/min]
%B = 16.0 [%]
%C = 70.0 [%]
%D = 0.0 [%]
Curve = 8

42.100 Flow = 0.250 [ml/min]
%B = 80.0 [%]
%C = 0.0 [%]
%D = 0.0 [%]
Curve = 5

44.100 Flow = 0.250 [ml/min]
%B = 80.0 [%]
%C = 0.0 [%]
%D = 0.0 [%]
Curve = 5

44.200 ED_1.AcqOff
ED_1_Total.AcqOff
Flow = 0.250 [ml/min]
%B = 24.0 [%]
%C = 0.0 [%]
%D = 0.0 [%]
Curve = 5

75.000 Flow = 0.250 [ml/min]
%B = 24.0 [%]
%C = 0.0 [%]
%D = 0.0 [%]
Curve = 5
End

Note:
A: Water
B: 250 mM sodium hydroxide
C: 1.0 M sodium acetate

Appendix D – Tabulated From Thermal Degradation Experiments

All tabulated experimental data that follows maintains the same format. Original sample data are the experimental sample while the base hydrolyzed data is the post-NaOH treatment data. Nitrite (NO_2^-) and nitrate (NO_3^-) were not found in thermally degraded PZ solutions. Abbreviations are as follows:

Gly, Glycolate (Anion IC)
Ace, Acetate (Anion IC)
Form, Formate (Anion IC)
Oxa, Oxalate (Anion IC)
Sulf, Sulfate (Anion IC)
Cl^-, Chloride (Anion IC)
NH_4^+, ammonium (Cation IC)
FPZ, N-formyl PZ (Cation IC)
EDA, Ethylenediamine (Cation IC)
PZ, Piperazine (Cation IC)
HEP, N-(2-Hydroxyethyl) piperazine (Cation IC)

1-MPZ, N-Methylpiperazine (Cation IC)
1-EPZ, N-Ethylpiperazine (Cation IC)
1,4-DMPZ, N,N'-dimethylpiperazine (Cation IC)
AEP, N-(2-Aminoethyl)piperazine (Cation IC)
CO_2, Carbon Dioxide (TIC)
SD_{CO2}, standard deviation of three CO_2 measurements
Alk, total alkalinity (Acid Titration), calculation assumes diamine is present, raw alkalinity would be twice this number
SD_{Alk}, standard deviation of two total alkalinity titrations
Fe^{2+}, aqueous iron (ICP-OES)
Cr^{3+}, aqueous chromium (ICP-OES)
Ni^{2+}, aqueous nickel (ICP-OES)
NT, value not tested
NA, not applicable; when only one measurement was made, calculation of standard deviation was not possible

Table D.1A: Tabulated Experimental Data for TE1A (10 m PZ, 0.3 mole CO_2 per mole alkalinity initially, 135 °C)

	Time (wk)	0	499	1008	2008
Original Samples (mmol/kg)	Gly	0.013	0.039	0.072	0.021
	Ace	0.051	0.115	0.480	0.298
	Form	0.113	2.790	3.474	1.937
	Oxa	0	0	0.244	0.019
	EDA	0	0	0	0
	PZ	4901.1	4727.7	4829.4	4733.5
	CO_2	NT	NT	NT	NT
	SD_{CO2}	NT	NT	NT	NT
	Alk	4682.8	4629.4	4706.8	4710.1
	SD_{Alk}	32.9	NT	NT	14.2
Hydrolyzed Samples (mmol/kg)	Gly	0	0.472	0.225	0.134
	Ace	0	0.340	1.087	0.486
	Form	0.462	13.709	11.404	10.326
	Oxa	0.057	0.124	0.048	0.026
	EDA	NT	7.3	0	0
	PZ	NT	4668.2	4947.1	4701.6

Table D.1B: Tabulated Experimental Data for TE1B (10 m PZ, 0.4 mole CO_2 per mole alkalinity initially, 135 °C)

	Time (wk)	499	1008	1504.5	2008	2521
Original Samples (mmol/kg)	Gly	0	0.019	0.052	0.017	0.013
	Ace	0.105	0.052	0.086	0.030	0.064
	Form	0.223	3.710	4.567	2.742	3.472
	Oxa	0	0	0.203	0.010	0.005
	EDA	0	0	0	0	0
	PZ	4577.7	4366.2	4431.1	4596.7	4130.7
	CO_2	NT	NT	NT	NT	NT
	SD_{CO2}	NT	NT	NT	NT	NT
	Alk	4446.1	4223.7	NT	NT	4390.2
	SD_{Alk}	20.7	NT	NT	NT	16.2
Hydrolyzed Samples (mmol/kg)	Gly	NT	0.108	NT	0.048	0.024
	Ace	NT	0.184	NT	0.117	0.168
	Form	NT	20.360	NT	17.248	21.157
	Oxa	NT	0.018	NT	0.009	0.008
	EDA	NT	6.0	NT	0	0
	PZ	NT	4021.5	NT	4772.4	4431.5

Table D.2A: Tabulated Experimental Data for TE2A (10 m PZ, 0.3 mole CO_2 per mole alkalinity initially, 150 °C)

	Time (wk)	0.0	1.0	2.0	3.0	3.8	5.2
Original Samples (mmol/kg)	Gly	0.01	0.06	0.03	0.05	0	0.02
	Ace	0.05	0.15	0.11	0.70	0.58	0.10
	Form	0.11	1.11	1.88	2.65	3.54	8.41
	Oxa	0	0.09	0	0.03	0.03	0.23
	EDA	0	0	0	0	10.41	0
	PZ	4901.2	4723.2	4760.5	4755.0	4721.4	4716.2
	CO_2	NT	NT	NT	NT	NT	NT
	SD_{CO2}	NT	NT	NT	NT	NT	NT
	Alk	4659.6	4758.4	4659.3	4653.2	4597.3	4887.0
	SD_{Alk}	32.90	NA	11.87	NA	NA	NA
Hydrolyzed Samples (mmol/kg)	Gly	0	0	0	0	0.11	0.13
	Ace	0	0.33	0	1.32	1.03	0.20
	Form	0.46	3.08	4.68	4.84	23.76	22.17
	Oxa	0.06	0.18	0	0.09	0.04	0.11
	EDA	NT	NT	NT	NT	NT	NT
	PZ	NT	NT	NT	NT	NT	NT

Table D.2B: Tabulated Experimental Data for TE2B (10 m PZ, 0.4 mole CO_2 per mole alkalinity initially, 150 °C)

	Time (wk)	0.0	1.0	2.0	3.8	5.2
Original Samples (mmol/kg)	Gly	0.0	0.0	0.1	0.0	0.0
	Ace	0.10	0.13	0.14	0.20	0.12
	Form	0.22	1.45	3.72	4.12	13.70
	Oxa	0	0	0	0.03	0.23
	EDA	0	0	0	9.34	0
	PZ	4577.7	4614.3	4310.0	4555.8	4500.6
	CO_2	NT	NT	NT	NT	NT
	SD_{CO2}	NT	NT	NT	NT	NT
	Alk	4431.5	4414.2	4402.5	4468.9	4679.8
	SD_{Alk}	32.90	NA	11.87	NA	NA
Hydrolyzed Samples (mmol/kg)	Gly	NT	0	0	0.05	0.05
	Ace	NT	0.12	0.29	0.16	0.17
	Form	NT	3.58	9.95	30.60	38.81
	Oxa	NT	0	0.09	0.07	0.04
	EDA	NT	NT	NT	NT	NT
	PZ	NT	NT	NT	NT	NT

Table D.3A: Tabulated Experimental Data for TE3A (15 m PZ, 0.3 mole CO_2 per mole alkalinity initially, 150 °C)

	Time (wk)	0.0	1.0	2.0	3.0	4.0	4.8
Original Samples (mmol/kg)	Gly	0	0.01	0.01	0.01	0.02	0.02
	Ace	0.32	0.03	0.02	0.07	0.07	0.11
	Form	0.37	0.44	0.98	5.73	8.06	8.09
	Oxa	0	0.02	0.02	0.39	0.25	0.19
	EDA	0	0	0	0	0	0
	PZ	5560.9	5626.0	5568.7	5721.9	5796.4	5699.4
	CO_2	NT	NT	NT	NT	NT	NT
	SD_{CO2}	NT	NT	NT	NT	NT	NT
	Alk	5478.4	5455.0	5416.2	5839.0	5668.8	5652.9
	SD_{Alk}	27.10	NA	NA	NA	NA	NA
Hydrolyzed Samples (mmol/kg)	Gly	0.17	0	0.05	0.05	0.04	0.06
	Ace	0.29	0.10	0.17	0.18	0.15	0.17
	Form	0.57	3.78	14.81	19.00	25.72	29.29
	Oxa	0.03	0	0.05	0.02	0.02	0.04
	EDA	NT	NT	NT	NT	NT	NT
	PZ	NT	NT	NT	NT	NT	NT

Table D.3B: Tabulated Experimental Data for TE3B (20 m PZ, 0.3 mole CO_2 per mole alkalinity initially, 150 °C)

	Time (wk)	0.0	1.0	2.0	3.0	4.0	4.8
Original Samples (mmol/kg)	Gly	0	0.01	0.01	0	0.03	0.02
	Ace	0.14	0.03	0.03	0.10	0.11	0.09
	Form	0.17	0.29	0.64	5.55	6.04	9.28
	Oxa	0	0.03	0.02	0.27	0.22	0.21
	EDA	0	0	0	0	0	0
	PZ	6232.4	7140.2	6122.8	6337.1	6018.2	6246.7
	CO_2	NT	NT	NT	NT	NT	NT
	SD_{CO2}	NT	NT	NT	NT	NT	NT
	Alk	6065.6	6116.5	6124.9	6491.9	NT	6369.0
	SD_{Alk}	59.37	NA	NA	NA	NT	NA
Hydrolyzed Samples (mmol/kg)	Gly	0.37	0	0.06	0.06	NT	0.08
	Ace	0.10	0.24	0.09	0.29	NT	0.18
	Form	0.67	3.53	16.00	27.39	NT	45.30
	Oxa	0.03	0	0.05	0.07	NT	0.04
	EDA	NT	NT	NT	NT	NT	NT
	PZ	NT	NT	NT	NT	NT	NT

Table D.4: Tabulated Experimental Data for TE4 (8 m PZ, 0.3 mole CO_2 per mole alkalinity initially, 175 °C)

	Time (wk)	0	0.4	1.0	2.0	3.0	4.0
Original Samples (mmol/kg)	Gly	0	0.02	0.02	0	0.02	0.02
	Ace	0.02	0.33	1.19	3.45	6.60	9.72
	Form	0.06	10.65	23.60	46.25	58.68	70.43
	Oxa	0	0.01	0.01	0.00	0.00	0.00
	Sulf	0.18	0.18	1.85	0.52	0.20	0.15
	EDA	0	0	4.88	22.64	35.77	46.54
	PZ	4307.5	4020.6	3985.4	3523.9	3236.3	3085.2
	CO_2	2831.5	2710.8	2691.8	2483.2	2227.2	2289.8
	SD_{CO2}	12.56	32.13	5.45	18.87	37.60	5.71
	Alk	4126.2	4045.8	3951.9	3771.5	3627.7	3615.1
	SD_{Alk}	NA	NA	NA	NA	NA	NA
Hydrolyzed Samples (mmol/kg)	Gly	0.06	0.21	2.07	0.41	2.22	3.11
	Ace	0.46	0.83	2.28	6.39	12.46	15.72
	Form	0.52	46.34	82.04	197.19	231.92	238.18
	Oxa	0.03	0.01	0.07	0.02	0.10	0.06
	Sulf	0.34	0.22	1.11	0.34	2.16	0.19
	EDA	7.81	3.21	3.63	38.72	42.54	50.03
	PZ	4151.9	4081.1	4000.2	3652.5	3405.0	3297.0

Table D.5: Tabulated Experimental Data for TE5 (8 m PZ, 0.3 mole CO_2 per mole alkalinity initially, 175 °C, 5.0 mM Cu^{2+}, 1.0 mM Fe^{2+})

	Time (wk)	0	0.4	1.0	2.0	3.0	4.0
Original Samples (mmol/kg)	Gly	0.35	0.04	0.04	0.05	0.02	0.04
	Ace	0	0.38	1.30	3.22	6.67	10.84
	Form	0.12	11.63	24.52	45.24	58.12	75.31
	Oxa	0	0.01	0.00	0	0.00	0
	Sulf	8.43	8.00	10.35	8.19	7.77	7.72
	EDA	0	0	4.94	17.54	37.53	41.89
	PZ	4140.9	3876.7	3877.3	3439.6	3237.0	2948.1
	CO_2	2767.5	2619.3	2619.0	2396.8	2222.3	2083.1
	SD_{CO2}	41.93	37.48	7.30	23.80	23.99	21.14
	Alk	4005.3	3915.3	3852.6	3676.8	3573.7	3387.7
	SD_{Alk}	NA	NA	NA	NA	NA	NA
Hydrolyzed Samples (mmol/kg)	Gly	0.85	0.27	2.11	0.70	3.51	4.19
	Ace	0.38	0.85	3.04	5.51	12.25	22.07
	Form	3.04	43.69	86.62	189.16	214.48	284.24
	Oxa	0.86	0.03	0.05	0.04	0.06	0.07
	Sulf	7.89	8.21	9.69	6.80	7.62	8.07
	EDA	27.46	3.45	4.23	38.29	41.76	46.12
	PZ	3909.2	3875.3	3983.9	3647.5	3384.5	3115.4

Table D.6: Tabulated Experimental Data for TE6 (8 m PZ, 0.3 mole CO_2 per mole alkalinity initially, 175 °C, 5.0 mM Cu^{2+}, 1.0 mM Fe^{2+}, 100 mM Inhibitor A)

	Time (wk)	0	0.4	1.0	2.0	3.0	4.0	5.0
Original Samples (mmol/kg)	Gly	0	0.03	0.06	0	0.03	0.04	NT
	Ace	0	0.31	1.28	2.50	5.29	7.28	NT
	Form	0.06	9.22	22.15	35.38	47.94	57.12	NT
	Oxa	0	0.01	0.01	0	0.00	0	NT
	Sulf	8.17	8.11	9.89	7.81	7.41	6.33	NT
	EDA	0	0	2.64	15.72	28.77	30.62	NT
	PZ	4075.4	3802.3	3746.9	3472.6	3226.4	2673.1	NT
	CO_2	2714.2	2536.6	2533.6	2409.4	2202.3	1882.1	2165.1
	SD_{CO2}	19.04	47.26	16.44	20.84	29.79	16.67	16.15
	Alk	3934.8	3849.5	3761.1	3665.2	3523.0	2986.0	3394.2
	SD_{Alk}	NA	NA	NA	NA	NA	NA	NA
Hydrolyzed Samples (mmol/kg)	Gly	0.04	0.24	2.37	0.87	2.82	3.99	NT
	Ace	0.34	1.05	2.83	4.46	8.74	13.00	NT
	Form	0.76	37.27	83.91	131.52	171.96	168.69	NT
	Oxa	0.01	0.02	0.06	0.01	0.06	0.05	NT
	Sulf	8.22	7.93	9.13	6.84	7.35	6.52	NT
	EDA	25.53	7.86	1.70	32.90	34.50	31.17	NT
	PZ	4041.1	3899.2	3826.2	3628.9	3333.8	2736.5	NT

Table D.7: Tabulated Experimental Data for TE7 (8 m PZ, 0.3 mole CO_2 per mole alkalinity initially, 175 °C, 1000 mM formate, 100 mM oxalate, 150 mM EDA)

	Time (wk)	0	0.4	1.0	2.0	4.0
Original Samples (mmol/kg)	Gly	0.02	0	0.00	0	0
	Ace	8.12	5.39	7.21	7.44	9.86
	Form	1342.7	396.7	429.3	358.6	628.0
	Oxa	66.29	0.07	0.07	0.03	0.02
	Sulf	0.19	0.26	1.56	0.22	0.34
	EDA	125.76	36.48	32.45	33.37	35.27
	PZ	3965.6	2773.8	2904.0	2589.4	1938.3
	CO_2	2380.5	2209.0	2264.2	2146.8	1704.1
	SD_{CO2}	11.49	25.99	6.58	20.86	14.67
	Alk	3442.5	3185.3	3243.6	3106.8	2442.5
	SD_{Alk}	NA	NA	NA	NA	NA
Hydrolyzed Samples (mmol/kg)	Gly	0.03	0	0.13	0.18	3.12
	Ace	9.80	8.85	10.86	12.16	17.37
	Form	1343.1	1397.0	1417.5	1475.4	1233.8
	Oxa	101.69	0.08	0.13	0.07	0.11
	Sulf	0.25	0.27	0.92	0.20	0.47
	EDA	111.46	34.62	32.84	51.79	42.24
	PZ	3968.7	3721.3	3747.5	3584.3	2618.3

Table D.8: Tabulated Experimental Data for TE8 (8 m PZ, 0.3 mole CO_2 per mole alkalinity initially, 175 °C, 0.1 Fe^{2+}, 0.6 mM Cr^{3+}, 0.1 mM Ni^{2+})

	Time (wk)	0	0.4	1.0	2.0	3.0	4.0	5.0
Original Samples (mmol/kg)	Gly	0.01	0.02	0.02	0	0.03	0.02	NT
	Ace	0.03	0.26	0.91	2.31	5.56	8.29	NT
	Form	0.59	7.35	21.14	37.05	49.99	65.28	NT
	Oxa	0	0.01	0.01	0.00	0.00	0	NT
	Sulf	1.30	1.64	2.69	1.37	1.51	1.63	NT
	EDA	0	0	3.48	18.32	32.01	39.91	NT
	PZ	4223.3	4062.0	3927.7	3641.8	3318.1	3139.7	NT
	CO_2	2722.5	2674.1	2598.7	2468.6	2345.9	2250.3	2150.1
	SD_{CO2}	19.90	17.60	8.64	17.44	31.24	8.71	1.80
	Alk	4070.7	3998.3	3911.5	3823.6	3749.1	3542.2	3442.2
	SD_{Alk}	NA	NA	NA	NA	NA	NA	NA
Hydrolyzed Samples (mmol/kg)	Gly	0	0.24	1.79	1.21	3.56	3.96	NT
	Ace	0	1.30	2.72	4.89	7.18	16.99	NT
	Form	0.83	29.37	81.36	148.78	186.22	258.34	NT
	Oxa	0.02	0.02	0.07	0.03	0.05	0.06	NT
	Sulf	1.46	1.68	2.31	1.26	1.52	1.78	NT
	EDA	5.87	6.27	2.16	36.32	37.12	41.08	NT
	PZ	4206.7	4018.4	3968.5	3837.4	3585.1	3344.9	NT

Table D.9: Tabulated Experimental Data for TE9 (8 m PZ, 0.3 mole CO_2 per mole alkalinity initially, 150 °C)

	Time (wk)	0	1.0	2.0	3.0	4.1	5.0	6.0	6.0	6.0	7.6	9.4	12.3	13.3	16.0	17.2	18.0
Original Samples (mmol/kg)	Gly	0	0	0	0	0	0	0	0	0	0	0	0	0	0	0	0
	Ace	0	0	0	0	0	0	2.82	1.30	0	0	0	0	0	0.47	0	0
	Form	0	3.09	4.02	4.07	5.85	5.96	11.84	9.02	11.99	15.20	15.45	21.86	20.58	18.90	18.94	17.05
	Oxa	0	0	0	0	0	0.01	0.07	0.05	0	0	0.01	0.01	0	0.00	0.01	0
	Sulf	0	0.80	0.79	0.69	0.61	0.24	0.97	0.20	0.52	0.26	0.16	0.18	0.85	0.20	0.13	1.46
	Cl^-	0	1.69	1.87	1.82	1.23	0.04	1.58	0.03	1.46	0.04	0.04	0.03	2.12	0.02	0.02	3.84
	EDA	0	4.33	4.50	5.03	6.93	7.21	9.23	10.39	10.03	15.68	17.13	20.23	19.53	20.40	21.55	22.63
	PZ	4400.0	4378.1	4327.7	4348.3	4329.8	4326.5	4285.8	4282.2	4202.9	4216.4	4206.9	4113.0	4072.5	4037.3	4037.3	4028.5
	CO_2	2626.7	2798.2	2715.8	2620.8	2634.8	2424.7	2635.9	2692.9	2659.2	2639.1	2627.2	2549.1	2602.4	2587.5	2573.5	2550.9
	SD_{CO2}	29.73	22.53	16.48	81.97	16.29	130.45	41.19	34.31	23.94	12.01	13.77	45.98	9.64	9.89	6.69	29.36
	Alk	4163.7	4151.9	4160.0	4124.5	4114.9	4143.7	4101.4	4096.2	4079.5	4069.3	4071.4	4033.6	4016.7	4025.1	4010.2	4022.5
	SD_{Alk}	2.85	2.29	30.70	7.25	1.48	41.72	2.37	9.76	2.74	26.96	11.10	28.33	7.88	22.40	9.29	3.94
Hydrolyzed Samples (mmol/kg)	Gly	0	0	0	0	0	0	0	0	0	0	0	0	0	0	0	0
	Ace	0	0	0	0	0	0	0	0	0.28	0	0.18	0.31	0.36	0	0.20	0.34
	Form	0	7.13	8.82	12.93	18.07	17.88	24.68	27.24	34.08	43.95	44.01	65.94	62.74	62.53	65.61	58.57
	Oxa	0	0.01	0.00	0.00	0.01	0.00	0	0.00	0.01	0.00	0.01	0.01	0.01	0.01	0.04	0.02
	Sulf	0	0.28	0.27	0.28	0.26	0.25	0.26	0.24	0.16	0.25	0.26	0.22	0.25	0.23	0.18	0.42
	Cl^-	0	0.28	0.22	0.45	0.05	0.23	0.18	0.10	0.02	0.17	0.17	0.12	0.09	0.14	0.08	0.08
	EDA	0	4.72	5.11	6.85	6.81	7.75	9.48	9.84	10.84	13.35	14.27	18.06	19.02	21.20	21.61	22.12
	PZ	4400.0	4409.1	4387.3	4371.5	4199.2	4328.6	4330.8	4283.4	4303.0	4269.9	4280.5	4212.3	4185.6	4176.5	4197.2	4185.5

Table D.10: Tabulated Experimental Data for TE10 (8 m PZ, 0.3 mole CO_2 per mole alkalinity initially, 135 °C)

	Time (wk)	0	2.0	4.0	8.0	12.0	16.0	24.0	32.1	39.0	39.0	39.0	39.0	48.1	56.0	64.0	72.0
Original Samples (mmol/kg) (Metals are in units of µg/g)	Gly	0.42	0.43	0.44	0.42	0.42	0.42	0.41	0.39	0.39	0.40	0.35	0.39	0.39	0.40	0.38	0.38
	Ace	0	0	0	0	0	0	0	0	0	0	0	0	0	0	0	0
	Form	0.17	0.84	1.34	1.68	3.12	4.32	5.31	7.69	7.39	8.62	9.09	7.40	8.12	9.30	10.62	10.02
	Oxa	0	0.01	0.02	0.01	0.02	0.02	0.01	0.01	0.01	0.01	0.01	0.01	0.00	0.01	0.01	0.01
	Sulf	0.11	0.21	0.19	0.12	0.25	1.15	0.41	0.14	0.09	0.09	0.10	0.15	0.09	0.15	0.19	0.14
	Cl^-	0	0.04	0.03	0.04	0.12	0.04	0.07	0.04	0.04	0.02	0.05	0.04	0.04	0.04	0.05	0.05
	NH_4^+	0	0	1.51	0	0	18.76	3.07	0	3.71	0	4.32	0.88	4.67	3.67	10.11	20.45
	FPZ	0	2.07	3.89	4.06	6.85	12.65	14.91	20.35	20.04	23.12	22.56	20.50	24.19	25.91	30.79	36.84
	EDA	0	0	0	0	0.67	1.49	1.86	2.56	2.62	3.62	3.85	2.29	3.55	3.72	4.43	5.42
	PZ	4087.8	4122.0	4241.1	4092.9	4072.6	4099.1	4075.9	4124.6	4056.4	4089.0	4072.6	4051.6	4101.4	4022.5	3991.9	3894.9
	1-EPZ	0	0	0	0	0	0.15	0.23	0.43	0.41	0.42	0.54	0.24	0.55	0.75	0.84	1.11
	AEP	0	0	0	0	0	0.22	0.17	0.34	0.51	0.72	0.72	0.54	0.84	1.03	1.10	1.55
	CO_2	2394.0	2379.8	2350.2	2315.1	2272.6	2275.9	2271.5	2223.7	2219.7	2215.4	2190.5	2199.4	2183.8	2197.8	2207.1	2280.8
	SD_{CO2}	3.46	63.67	6.59	13.05	8.15	22.80	10.80	12.52	3.75	28.00	14.53	20.90	2.55	3.42	22.22	27.10
	Alk	4166.1	4152.3	4255.8	4153.5	4134.6	4142.9	4154.6	4115.0	4102.4	4093.7	4100.9	4100.1	4087.0	4093.1	4072.7	4055.3
	SD_{Alk}	23.57	12.44	57.05	15.37	8.64	11.59	11.24	1.09	2.00	6.45	15.51	3.06	5.05	10.59	8.51	1.47
	Fe^{2+}	0.13	10.21	3.07	21.56	28.19	24.17	10.49	19.79	8.83	8.58	9.94	9.45	16.05	14.21	10.23	8.79
	Ni^{2+}	0.06	17.65	14.87	15.36	20.65	29.68	39.40	40.94	40.86	43.49	46.36	42.14	41.75	57.80	60.18	67.76
	Cr^{3+}	0.07	7.52	10.20	14.60	12.27	8.07	5.30	7.29	6.08	7.14	6.23	6.63	6.56	6.23	5.21	5.07
Hydrolyzed Samples (mmol/kg)	Gly	0.26	0.29	0.32	0.32	0.29	0.30	0.34	0.28	0.35	0.36	0.33	0.35	0.34	0.42	0.38	0.53
	Ace	0	0	0	0	0	0	0	0	0	0	0	0	0	0	0	0
	Form	0.40	1.92	3.30	4.37	7.70	10.88	13.26	18.43	18.45	21.23	22.23	17.56	19.58	22.61	26.46	31.33
	Oxa	0.00	0.02	0.04	0.19	0.03	0.04	0.03	0.03	0.03	0.02	0.03	0.02	0.02	0.01	0.02	0.02
	Sulf	0.16	0.48	0.40	0.28	0.18	1.21	0.50	0.18	0.25	0.18	0.16	0.16	0.28	0.16	0.37	0.12
	Cl^-	0.05	0.59	0.48	0.37	0.16	0.04	0.09	0.06	0.13	0.05	0.06	0.11	0.34	0.08	0.53	0.07
	NH_4^+	0	0	0	0	0	0	0	0	0	0	0	0	0	0	0	0
	FPZ	0	0	0	0	0	0	0	0	0	0	0	0	0	0	0	0
	EDA	0	2.25	2.50	3.24	4.67	6.13	6.98	8.53	7.11	9.25	10.89	8.19	9.44	10.28	20.74	13.37
	PZ	4150.7	4134.3	4177.6	4112.8	4108.6	4116.3	4114.5	4036.8	3356.2	4017.5	4187.5	4092.2	3932.4	4007.9	7197.7	3924.3
	1-EPZ	NT	NT	NT	NT	NT	NT	NT	NT	NT	NT	NT	NT	NT	NT	NT	NT
	AEP	0	0	0.43	0.53	1.32	1.82	2.55	3.34	2.81	4.05	4.57	3.32	3.87	4.53	10.22	7.16

Table D.11: Tabulated Experimental Data for TE11 (8 m PZ, 0.4 mole CO_2 per mole alkalinity initially, 135 °C)

	Time (wk)	0	2.0	4.0	8.0	16.0	24.0	32.1	39.0	39.0	39.0	48.1	56.0	64.0	72.0
Original Samples (mmol/kg) (Metals are in units of µg/g)	Gly	0.47	0.46	0.46	0.46	0.44	0.51	0.42	0.41	0.42	0.42	0.37	0.34	0.39	0.37
	Ace	0	0	0	0	0	0	0	0	0	0	0	0	0	0
	Form	0.09	0.88	1.52	2.67	5.96	8.43	7.08	8.75	9.39	8.01	11.52	12.91	14.34	13.30
	Oxa	0	0	0.01	0.01	0.02	0.03	0	0.02	0.01	0.02	0.01	0.01	0.01	0.01
	Sulf	0.09	0.33	0.10	0.19	0.10	0.11	0.29	0.22	0.14	0.10	0.11	0.12	0.15	0.11
	Cl^-	0	0.37	0.06	0.03	0.04	0.05	0.05	0.03	0.04	0.04	0.04	0.03	0.03	0.03
	NH_4^+	0	0	0.27	0	0	0	8.00	6.50	0	0.37	2.65	1.42	9.95	20.79
	FPZ	0	1.47	7.09	13.07	25.73	40.61	40.34	46.51	41.85	37.54	51.56	48.07	67.81	69.37
	EDA	0	0	0	1.00	1.42	3.99	1.99	3.00	3.12	2.58	5.31	5.07	6.04	7.43
	PZ	3922.4	3908.3	3940.9	3884.2	3872.1	4587.1	3898.3	3884.3	3864.2	3848.0	3857.7	3844.5	3846.5	3815.7
	1-EPZ	0	0	0	0	0	0.40	0.48	0.61	0.49	0.55	0.67	0.61	1.09	1.23
	AEP	0	0	0	0	0	0.56	0.38	0.62	0.52	0.53	0.91	1.43	1.40	1.69
	CO_2	3463.4	3478.6	3447.7	3411.2	3362.3	3056.5	3532.1	3511.6	3403.6	3440.4	3209.8	3340.7	3064.4	3228.2
	SD_{CO2}	48.21	14.47	9.73	17.90	17.28	26.54	25.94	61.59	10.00	5.10	12.71	9.89	23.40	4.84
	Alk	3973.1	3974.5	3974.4	3977.9	3967.0	3973.5	3969.9	3955.6	3966.0	3934.1	3908.4	3915.6	3903.6	3881.8
	SD_{Alk}	7.83	7.94	17.85	17.84	22.63	39.88	19.58	0.15	17.27	0.68	3.79	1.93	13.71	4.06
	Fe^{2+}	0.22	5.83	4.22	3.80	16.77	14.30	9.46	10.58	10.42	12.66	51.22	48.83	30.69	25.84
	Ni^{2+}	0.05	21.30	21.99	20.82	38.06	70.33	88.51	75.96	77.91	67.33	59.73	77.98	101.42	84.85
	Cr^{3+}	0.14	34.15	33.65	34.81	56.10	60.26	30.47	43.10	62.38	44.70	83.86	60.36	54.01	68.90
Hydrolyzed Samples (mmol/kg)	Gly	0.52	0.50	0.48	0.47	0.48	0.54	0.47	0.46	0.47	0.48	0.46	0.47	0.51	0.48
	Ace	0	0	0	0	0	0	0	0	0	0	0	0	0	0
	Form	0.31	2.68	5.46	9.72	19.97	26.87	27.33	30.55	30.84	28.00	36.84	37.42	48.32	51.12
	Oxa	0	0.02	0.02	0.02	0.03	0.08	0.06	0.03	0.02	0.04	0.01	0.02	0.02	0.01
	Sulf	0.28	0.24	0.46	0.38	0.18	0.22	0.30	0.30	0.21	0.19	0.15	0.22	0.25	0.14
	Cl^-	0.25	0.36	1.18	0.49	0.22	0.31	0.12	0.08	0.16	0.09	0.04	0.13	0.31	0.03
	NH_4^+	0	0	0	0	0	0	0	0	0	0	0	0	0	0
	FPZ	0	0	0	0	0	0	0	0	0	0	0	0	0	0
	EDA	0	1.83	2.58	3.96	51.88	9.39	8.93	9.87	9.42	9.17	12.26	14.76	14.85	16.03
	PZ	3991.5	3855.0	3917.4	3929.3	12941	4625.0	3872.5	3859.5	3859.6	3836.6	3798.5	3806.1	3800.4	3828.4
	1-EPZ	NT	NT	NT	NT	NT	NT	NT	NT	NT	NT	NT	NT	NT	NT
	AEP	0	0.31	0.38	0.70	1.30	2.41	3.14	3.75	3.37	3.28	4.63	4.99	6.25	7.56

Table D.12: Tabulated Experimental Data for TE12 (8 m PZ, 0.3 mole CO_2 per mole alkalinity initially, 175 °C)

	Time (wk)	0	0.6	0.6	1.0	2.1	4.0	5.0	5.0	9.3	13.2	14.1	14.8
Original Samples (mmol/kg) (Metals are in units of µg/g)	Gly	0	0	0	0	0	0	0	0	0	0	0	0
	Ace	0	0.93	1.08	1.93	6.00	9.20	15.64	13.48	33.14	46.32	45.74	48.70
	Form	0.34	39.23	42.67	62.04	137.74	163.51	152.70	179.85	294.95	362.56	389.05	377.75
	Oxa	0	0.14	0.06	0.10	0.15	0.16	0.34	0.21	0.17	0.33	0.21	0.19
	Sulf	0	0	0.04	0.24	0	0.21	0.60	0.19	0	0.08	0	0
	Cl^-	0.17	0.14	0.42	0.17	0.17	0.95	0.34	0.12	0.13	0.73	0.09	0.74
	NH_4^+	94.61	53.78	54.71	79.80	147.09	66.98	332.83	130.36	542.82	667.69	754.24	651.80
	FPZ	0	51.09	53.80	76.84	153.36	54.21	186.40	112.42	201.17	182.72	183.22	185.44
	EDA	0	14.20	14.07	23.30	41.43	17.94	49.24	30.07	55.38	42.45	45.67	45.83
	PZ	4204.4	3594.5	3652.7	3465.0	3017.0	898.99	2419.6	1640.5	1899.8	1361.5	1354.5	1342.7
	HEP	0	0	0	0	19.57	49.75	72.80	57.67	72.77	81.12	84.66	83.32
	1-MPZ	0	0	0	0	13.02	0	19.35	8.09	17.18	21.21	22.39	18.59
	AEP	0	7.65	8.71	15.20	45.92	18.83	72.86	44.08	106.63	101.89	105.78	114.26
	CO_2	2501.9	2614.4	2144.8	2409.0	2148.7	1994.9	2369.5	1897.3	1489.3	1280.0	1188.4	1216.6
	SD_{CO2}	186.48	10.02	9.90	40.08	12.00	5.51	8.27	1.32	12.65	4.53	23.64	4.32
	Alk	4130.8	3921.1	3989.3	3803.1	3725.5	3495.0	3280.4	3361.4	2818.9	2580.6	2511.1	2529.1
	SD_{Alk}	2.08	63.65	5.93	142.61	173.66	14.08	30.15	24.55	131.48	102.08	3.69	40.32
	Fe^{2+}	0	57.28	46.02	84.82	120.66	82.35	133.12	121.55	133.70	84.48	105.20	86.21
	Ni^{2+}	0	84.99	32.98	74.44	132.89	429.69	148.18	419.30	240.22	312.14	439.57	380.21
	Cr^{3+}	0	9.30	13.54	19.39	22.97	0	22.90	4.54	11.83	6.18	4.12	0
Hydrolyzed Samples (mmol/kg)	Gly	0.22	0.87	1.45	1.94	2.19	2.35	3.14	2.41	3.69	3.04	4.28	2.96
	Ace	0	3.24	2.14	2.90	8.81	14.95	25.80	19.45	47.40	70.42	72.56	73.31
	Form	0.96	83.97	89.25	129.67	278.49	347.69	348.90	361.07	569.57	688.20	735.20	752.48
	Oxa	0	0.55	0.32	0.43	0.47	0.60	2.14	0.83	0.77	2.31	1.49	1.26
	Sulf	0.70	0.85	1.98	0.69	0.69	1.09	0.51	0.53	0.54	0.44	3.02	1.20
	Cl^-	0.16	1.31	0.26	0.44	0.18	0.25	0.27	0.20	0.30	0.13	0.34	1.52
	NH_4^+	0	88.93	69.62	101.04	199.35	302.37	359.75	374.51	584.99	747.82	804.47	792.42
	FPZ	0	0	0	0	0	0	0	0	0	0	0	0
	EDA	0	21.40	18.66	27.85	50.10	60.85	56.15	59.77	71.08	59.00	62.49	65.38
	PZ	4027.8	3871.3	3897.2	3370.1	3056.4	2755.1	2548.5	2907.3	2224.0	1656.1	1625.6	1757.6
	HEP	0	0	0	51.36	60.27	68.16	70.57	66.51	84.78	90.22	90.99	95.51
	1-MPZ	0	0	0	7.50	12.28	13.46	16.75	12.72	16.95	20.04	20.52	23.33
	AEP	0	7.36	8.22	13.03	43.36	69.31	75.99	79.17	126.59	127.64	129.83	150.66

Table D.13: Tabulated Experimental Data for TE13 (8 m PZ, 0.4 mole CO_2 per mole alkalinity initially, 175 °C)

	Time (wk)	0	0.5	1.0	2.1	3.0	4.0	5.0	5.0	9.3	14.1	14.8
Original Samples (mmol/kg) (Metals are in units of µg/g)	Gly	0	0	0	0	0	0	0	0	0	0	0
	Ace	0	1.17	1.00	3.34	6.63	6.71	9.06	7.60	31.69	43.50	47.44
	Form	0.52	36.14	56.28	62.59	136.81	148.63	164.12	126.73	268.20	281.49	398.65
	Oxa	0	0.09	0.10	0.34	0.14	0.18	0.15	0.40	0.19	0.38	0.22
	Sulf	0.67	0.57	0.70	0.80	0.44	0.56	0.80	0.56	0.53	0.65	0.76
	Cl^-	0.52	0.36	0.43	1.07	0.15	0.15	0.26	0.24	0.13	0.26	0.57
	NH_4^+	0.00	26.75	50.04	131.59	180.96	225.61	282.25	277.17	521.19	859.50	848.45
	FPZ	0	59.30	89.15	127.22	184.54	182.84	210.97	199.21	241.20	247.02	265.21
	EDA	0	20.82	27.47	38.72	52.20	52.22	58.96	55.83	59.43	49.30	52.81
	PZ	4012.9	3743.9	3552.4	3148.3	2826.1	2406.4	2577.7	2719.3	1814.4	1328.6	1211.3
	HEP	0	0	51.51	54.88	48.94	58.63	59.75	61.08	61.61	75.03	73.68
	1-MPZ	0	0	7.92	8.61	9.11	15.32	14.90	12.20	17.97	20.34	20.46
	AEP	0	6.33	12.51	30.34	50.55	58.53	72.99	69.88	97.10	103.52	95.44
	CO_2	3171.7	3044.2	2993.6	3256.9	2598.9	2636.2	2441.0	2290.9	2209.5	2378.9	1690.6
	SD_{CO2}	15.94	18.08	2.86	28.05	16.11	40.42	75.50	12.60	16.10	5.15	7.42
	Alk	3952.5	3817.7	3730.0	3478.1	3344.9	3224.8	3164.6	3205.6	2705.3	2332.9	2204.5
	SD_{Alk}	NA	NA	NA	NA	NA	NA	NA	NA	NA	NA	NA
	Fe^{2+}	0	23.63	44.80	81.82	124.23	153.55	128.07	110.95	141.96	71.12	81.26
	Ni^{2+}	0	25.50	39.05	162.52	104.80	190.20	157.31	208.41	274.03	765.10	532.61
	Cr^{3+}	0	40.61	62.03	15.13	118.41	73.33	48.82	26.24	48.24	0	0
Hydrolyzed Samples (mmol/kg)	Gly	0	0.38	0.40	0.23	0.37	0.26	0.21	0.13	0.36	0.31	1.08
	Ace	0	1.44	2.96	4.78	13.86	20.08	22.26	16.88	50.47	68.26	79.74
	Form	1.96	98.12	152.15	196.55	354.76	397.30	426.16	368.12	653.46	709.43	935.74
	Oxa	0.02	0.14	0.19	0.45	0.27	0.69	0.38	0.63	0.59	1.46	1.16
	Sulf	0.76	0.51	0.62	0.82	0.40	0.77	0.72	0.53	0.72	0.59	0.84
	Cl^-	0.31	0.12	0.52	0.57	0.28	0.52	0.24	0.88	0.50	0.21	0.71
	NH_4^+	0.00	68.64	68.27	161.37	262.65	325.85	347.15	260.31	585.61	873.83	908.83
	FPZ	0	0	0	0	0	0	0	0	0	0	0
	EDA	0	19.04	30.09	42.25	56.49	59.89	60.73	41.01	68.14	58.58	62.03
	PZ	4276.4	3707.7	3710.6	3362.9	3184.3	3085.1	2837.6	2177.1	2202.1	1591.7	1523.2
	HEP	0	0	42.46	49.68	57.98	59.56	64.42	56.25	70.21	85.01	86.30
	1-MPZ	0	0	4.68	10.21	14.24	16.41	16.99	8.80	18.42	22.82	22.56
	AEP	0	6.26	14.42	31.94	56.30	71.97	79.27	55.28	115.93	119.95	117.76

Table D.14: Tabulated Experimental Data for TE14 (8 m PZ, 0.3 mole CO_2 per mole alkalinity initially, 150 °C)

	Time (wk)	0	1.1	2.0	4.0	6.0	10.0	14.0	14.0	14.0	18.1	22.2	26.0	30.0
Original Samples (mmol/kg) (Metals are in units of µg/g)	Gly	0	0	0	0	0	0	0	0	0	0	0	0	0
	Ace	0	0	0	0	0.08	0.16	0.18	0.15	0.18	0.20	0.27	1.11	1.37
	Form	0.16	0.76	1.44	2.95	8.01	9.99	13.70	12.89	14.10	15.54	18.32	32.61	34.62
	Oxa	0.06	0.05	0.05	0.06	0	0.05	0.05	0.06	0.05	0.05	0.05	0.02	0.02
	Sulf	0.32	0.35	0.34	0.33	0.29	0.40	0.35	0.34	0.33	0.33	0.32	0.15	0.16
	Cl^-	0.14	0.09	0.04	0.08	0.07	0.05	0.07	0.05	0	0.06	0	0.06	0.04
	EDA	0	0	0	1.95	5.59	12.35	14.34	12.39	14.36	14.28	17.78	20.96	22.58
	PZ	4300.9	4311.7	4287.8	4258.0	4281.1	4193.9	4146.2	4153.6	4199.5	4049.9	4002.2	3969.2	3817.8
	CO_2	2632.9	2602.2	2600.2	2573.9	2516.5	2456.1	2434.0	2521.8	2485.6	2456.7	2417.6	2400.9	2368.1
	SD_{CO2}	14.37	7.46	62.05	26.40	23.33	26.56	18.75	8.11	10.53	11.67	25.43	32.89	28.99
	Alk	4117.3	4132.7	4118.8	4093.9	4136.2	4041.8	4021.6	4038.2	4017.3	3990.1	3994.1	4004.6	3882.8
	SD_{Alk}	1.10	11.58	12.69	14.53	32.27	7.10	35.61	26.92	15.23	21.75	4.52	13.49	6.02
	Fe^{2+}	0.53	5.79	17.12	25.80	24.91	28.81	35.16	33.94	25.15	32.84	29.81	35.52	57.52
	Ni^{2+}	0.93	13.87	21.48	21.03	34.91	48.38	59.50	52.92	60.89	60.14	66.74	82.66	76.39
	Cr^{3+}	1.54	6.59	26.66	23.84	15.57	14.38	14.82	17.13	15.41	15.94	12.94	12.95	13.97
Hydrolyzed Samples (mmol/kg)	Gly	0	0.17	0.08	0.12	0.18	0.23	0.22	0.22	0.49	0.38	1.03	0.42	0.43
	Ace	0.06	0.08	0.09	0.11	0.15	0.22	0.38	0.34	0.20	0.48	0.65	0.87	0.63
	Form	0.06	2.23	4.59	7.99	13.98	27.89	38.62	36.62	27.78	46.88	56.54	68.79	59.34
	Oxa	0.04	0.06	0.07	0.06	0.08	0.09	0.11	0.10	0.13	0.10	0.12	0.12	0.12
	Sulf	0.34	0.41	0.41	0.34	0.49	0.46	0.43	0.40	0.40	0.38	0.42	0.43	0.41
	Cl^-	0.07	0.21	0.12	0.11	0.13	0.18	0.16	0.15	0.11	0.12	0.12	0.14	0.13
	EDA	0	0	2.41	2.65	5.90	10.24	11.39	9.94	14.08	15.95	20.32	20.18	12.19
	PZ	4311.6	4314.3	4280.5	4269.6	4222.4	4154.2	4109.6	4141.6	4154.6	4044.4	3999.8	3916.9	3159.3

Table D.15: Tabulated Experimental Data for TE15 (8 m PZ, 0.4 mole CO_2 per mole alkalinity initially, 150 °C)

	Time (wk)	0	1.1	2.0	4.0	6.0	10.0	14.0	14.0	14.0	18.1	22.2	26.0	30.0
Original Samples (mmol/kg) (Metals are in units of µg/g)	Gly	0	0	0	0	0	0	0	0	0	0	0	0	0
	Ace	0.63	0.04	0.05	0.09	0.10	0.13	0.23	0.20	0.18	0.29	0.48	1.56	2.05
	Form	0.30	1.76	5.66	7.20	10.61	17.60	18.72	19.65	15.88	22.22	23.47	39.82	44.18
	Oxa	0.02	0.04	0.03	0.03	0.03	0.02	0.03	0.06	0.03	0.03	0.03	0.03	0.03
	Sulf	0.26	0.28	0.27	0.26	0.28	0.25	0.25	0.30	0.25	0.27	0.25	0.17	0.12
	Cl^-	0.16	0.06	0.04	0.05	0.06	0.03	0.04	0.05	0.04	0.05	0.02	0.12	0.08
	EDA	0	0	2.93	8.39	11.41	16.01	17.80	17.31	16.69	18.29	24.61	25.48	32.80
	PZ	4174.7	4166.6	4087.7	4061.8	3997.8	3913.6	3879.9	3886.2	3928.9	3832.4	3813.7	3516.7	3538.2
	CO_2	3203.3	3177.5	3224.8	3148.3	3080.8	3249.5	3213.3	3180.8	3260.4	3157.3	3158.5	3121.8	2992.7
	SD_{CO2}	15.64	10.27	69.48	54.60	15.74	33.01	12.77	39.51	20.19	31.91	31.55	5.50	4.25
	Alk	3961.3	3961.9	3933.7	3914.5	3945.1	3919.3	3910.8	3998.9	3884.1	3796.0	3900.7	3778.6	3904.2
	SD_{Alk}	24.05	5.30	8.39	20.46	112.32	51.25	30.86	14.60	17.67	31.93	136.98	21.01	86.15
	Fe^{2+}	0.31	14.74	45.41	41.12	37.77	72.15	82.14	43.38	36.93	59.61	79.18	113.05	72.01
	Ni^{2+}	0.74	18.68	51.87	35.41	47.39	80.86	77.30	85.87	93.85	104.70	107.21	119.22	123.98
	Cr^{3+}	1.23	31.66	79.05	53.70	70.00	109.48	111.39	70.34	73.33	109.31	131.78	150.36	132.18
Hydrolyzed Samples (mmol/kg)	Gly	0	0	0	0	0	0	0.38	0.07	0.05	0.08	0.04	0.05	0.08
	Ace	0	0.08	0.11	0.17	0.22	0.44	0.56	0.55	0.59	0.70	0.99	1.21	1.80
	Form	0.08	8.19	22.22	30.16	41.98	67.46	72.56	75.36	79.99	88.43	104.63	115.30	140.73
	Oxa	0.02	0.05	0.07	0.05	0.05	0.07	0.10	0.10	0.08	0.09	0.09	0.09	0.09
	Sulf	0.34	0.37	0.39	0.39	0.39	0.35	0.39	0.35	0.29	0.41	0.36	0.38	0.38
	Cl^-	0.15	0.08	0.12	0.13	0.11	0.08	0.10	0.11	0.13	0.13	0.12	0.11	0.09
	EDA	0	1.97	4.75	9.94	11.56	15.28	16.59	17.01	15.63	20.96	23.96	31.86	33.72
	PZ	4101.4	4098.3	4104.9	4040.0	4030.1	3899.5	3892.7	3874.7	3877.6	3840.9	3821.5	3796.5	3692.9

Table D.16: Tabulated Experimental Data for TE16 (8 m 2-Methylpiperazine, 0.3 mole CO_2 per mole alkalinity initially, 150 °C)

	Time (wk)	0	1.0	2.5	4.0	5.9	9.9	13.9	13.9	13.9	17.6	21.8	26.5	29.9
Original Samples (mmol/kg) (Metals are in units of µg/g)	Gly	0	0	0	0	0	0	0	0	0	0	0	0	0
	Ace	0	1.11	2.04	3.09	3.15	4.10	5.54	5.53	5.81	6.52	20.95	24.41	25.61
	Form	0.19	10.36	22.77	32.19	32.33	36.09	44.43	43.77	43.98	44.26	112.77	121.23	117.50
	Oxa	0.33	0.13	0.12	0.10	0.21	0.12	0.11	0.09	0.10	0.10	0.15	0.14	0.14
	Sulf	0.24	0.24	0.27	0.24	0.38	0.38	0.39	0.37	0.42	1.03	0.19	0.18	0.19
	Cl^-	0.13	0.09	0.08	0.07	0.09	0.03	0.06	0.08	0.02	0.03	0.03	0.08	0.02
	EDA	32.88	15.17	16.45	19.24	24.55	37.20	51.21	49.58	51.31	53.69	65.83	64.77	54.46
	2-MPZ	3908.1	3728.4	3647.3	3665.8	3182.6	3161.4	3084.3	3032.5	3044.9	2946.8	2575.7	2585.9	2454.4
	CO_2	2345.6	2424.9	2383.1	2388.7	2352.4	2316.2	2280.2	2277.2	2170.0	2077.7	1987.1	1889.3	1891.9
	SD_{CO2}	16.39	25.99	18.92	10.86	17.96	17.29	0.41	30.10	7.89	9.18	15.46	26.81	10.95
	Alk	3865.9	3832.0	3780.0	3772.3	3692.8	3636.0	3603.9	3569.3	3571.8	3472.0	3431.6	3352.7	3347.9
	SD_{Alk}	0.76	8.33	0.89	58.03	28.03	3.69	31.10	12.90	14.34	6.82	0.86	83.13	15.64
	Fe^{2+}	1.82	30.45	24.13	26.05	31.35	26.68	29.36	29.62	29.12	32.22	31.64	35.20	34.85
	Ni^{2+}	0	75.11	95.89	120.65	139.45	157.36	185.00	177.47	175.31	189.77	197.26	199.35	198.11
	Cr^{3+}	0	69.41	38.75	34.12	32.50	24.81	23.88	19.68	16.32	16.52	14.85	16.41	16.65
Hydrolyzed Samples (mmol/kg)	Gly	0	0	0	0	0	0	0	0	0	0	0	0	0
	Ace	0.45	4.12	3.68	5.11	5.78	6.31	8.25	8.41	8.54	9.29	31.25	33.17	36.31
	Form	2.23	66.27	71.96	102.28	76.06	83.69	108.69	109.76	110.47	126.47	199.62	201.21	213.10
	Oxa	0.28	0.22	0.12	0.14	0.11	0.10	0.11	0.11	0.13	0.14	0.25	0.24	0.27
	Sulf	0.25	0.77	0.34	0.31	0.39	0.39	0.44	0.42	0.52	0.41	0.19	0.21	0.28
	Cl^-	0	0.40	0.18	0.17	0.12	0.06	0.17	0.06	0.18	0.09	0.15	0.12	0.31
	EDA	29.15	15.35	14.77	20.32	26.73	32.59	42.33	35.55	40.07	50.34	60.87	57.16	56.06
	2-MPZ	3788.1	3772.5	3641.9	3629.1	3401.2	3232.1	3146.7	3098.0	3103.1	3102.3	2736.3	2577.5	2550.1

Table D.17: Tabulated Experimental Data for TE17 (4 m PZ + 4 m 2-Methylpiperazine, 0.3 mole CO_2 per mole alkalinity initially, 150 °C)

	Time (wk)	0	1.0	2.5	4.0	5.9	9.9	13.9	13.9	13.9	17.6	21.8	26.5	29.9
Original Samples (mmol/kg) (Metals are in units of µg/g)	Gly	0	0	0	0	0	0	0	0	0	0	0	0	0
	Ace	0	0.52	1.11	1.01	1.55	1.89	1.99	2.40	3.51	3.37	13.63	15.50	16.43
	Form	0	6.98	15.47	18.20	18.65	22.08	25.31	21.18	32.53	24.82	86.04	89.25	84.40
	Oxa	0	0.03	0.04	0.10	0.12	0.10	0.10	0.10	0.09	0.10	0.09	0.10	0.10
	Sulf	0.27	0.23	0.20	0.28	0.40	0.36	0.37	0.37	0.38	0.37	0.19	0.36	0.17
	Cl^-	0.04	0.03	0.02	0.57	0.08	0.04	0.09	0.09	0.07	0.02	0.03	0.15	0
	EDA	13.03	8.35	8.60	10.43	14.63	14.21	23.07	19.45	27.07	24.45	21.84	26.63	30.11
	PZ + 2-MPZ	4205.6	4148.9	4108.1	3565.7	3824.7	3777.5	3407.5	3847.4	3573.1	3556.0	3295.3	3184.2	3047.8
	CO_2	2380.4	2321.8	2315.0	2234.0	2533.0	2477.6	2352.7	2469.6	2341.5	2755.2	2312.3	2224.8	2197.4
	SD_{CO2}	18.17	1.73	9.54	29.26	22.33	32.60	23.61	10.20	4.50	57.26	77.42	54.98	13.20
	Alk	4007.0	4028.9	3943.8	3835.2	3860.3	3853.8	3761.3	3978.6	3750.4	3755.6	3726.0	3667.6	3641.3
	SD_{Alk}	6.30	99.09	11.49	20.12	0.83	7.56	19.14	7.92	22.59	4.36	13.43	6.59	5.38
	Fe^{2+}	0.20	84.83	70.52	103.55	49.48	60.16	99.51	58.84	55.09	56.04	56.77	64.77	71.61
	Ni^{2+}	0	69.48	123.25	119.54	197.91	189.40	219.63	184.05	242.27	190.25	216.00	245.10	346.97
	Cr^{3+}	0	87.27	47.43	18.96	16.43	26.16	22.66	20.25	13.98	16.76	14.18	19.60	15.98
Hydrolyzed Samples (mmol/kg)	Gly	0	0	0	0	0	0	0	0	0	0	0.70	0.73	0.69
	Ace	0.29	1.11	2.25	2.40	3.21	3.33	3.92	4.00	5.26	5.39	21.31	23.98	24.85
	Form	1.01	23.76	54.97	77.48	43.62	50.32	70.26	59.75	78.55	76.75	152.69	165.77	169.77
	Oxa	0.12	0.05	0.09	0.12	0.14	0.16	0.11	0.11	0.12	0.08	0.16	0.17	0.15
	Sulf	0.35	0.33	0.37	0.36	0.48	0.47	0.54	0.44	0.41	0.46	0.23	0.26	0.23
	Cl^-	0	0	0.09	0.63	0.14	0.18	0.27	0.13	0.09	0.18	0.18	0.22	0.09
	EDA	13.89	7.54	8.83	7.99	13.62	16.38	22.93	18.32	26.05	25.79	19.63	28.20	23.94
	PZ	4096.7	4161.7	3866.7	3656.9	3962.3	3894.8	3550.5	3822.7	3663.3	3669.4	3264.2	3132.7	3274.6

Table D.18: Tabulated Experimental Data for TE18 (8 m PZ, 0.3 mole CO_2 per mole alkalinity initially, 175 °C)

	Time (wk)	0	0.6	1.0	1.5	2.4	2.9	2.9	2.9	3.4	5.0	6.0
Original Samples (mmol/kg) (Metals are in units of µg/g)	Gly	0.07	0.11	0.16	0.07	0.24	0.27	0.24	0.25	0.08	0.12	0.25
	Ace	0.07	0.29	1.26	1.48	3.16	5.68	5.34	5.11	4.44	12.42	9.79
	Form	0.35	22.13	28.87	43.59	66.23	82.71	77.67	75.20	53.07	126.35	104.47
	Oxa	0.08	0.07	0.10	0.06	0.06	0.08	0.07	0.07	0.08	0.13	0.09
	Sulf	0.17	0.16	0.16	0.18	0.20	0.16	0.16	0.16	0.19	0.17	0.16
	Cl^-	0.13	0.18	0.16	0.11	0.19	0.18	0.13	0.09	0.12	0.10	0.17
	EDA	0	10.81	17.61	29.15	33.94	39.52	41.67	41.34	37.45	54.22	44.95
	PZ	3352.8	4312.8	4197.2	4015.5	3706.7	3509.7	3577.0	3578.3	3272.7	2527.8	2737.4
	CO_2	2497.3	2386.7	2317.7	2269.5	2103.7	2102.7	2177.9	2186.4	2977.8	2427.6	1863.3
	SD_{CO2}	17.67	4.78	5.81	10.33	1.42	63.84	15.74	13.88	29.05	33.29	14.30
	Alk	4129.1	4024.9	3966.8	3884.6	3813.7	3630.4	3650.7	3729.1	3419.7	3037.2	3347.9
	SD_{Alk}	13.39	0.85	0.23	13.91	85.21	10.40	2.69	83.50	18.20	37.78	6.66
	Fe^{2+}	0	27.89	72.41	91.55	74.18	110.23	109.62	127.41	96.68	222.06	126.69
	Ni^{2+}	0	54.10	40.24	65.55	91.20	103.58	94.38	91.41	305.54	199.41	205.86
	Cr^{3+}	0.67	38.54	35.63	31.54	12.03	24.24	25.54	39.79	10.16	174.49	24.19
Hydrolyzed Samples (mmol/kg)	Gly	0.17	0.28	0.32	0.70	0.72	0.75	0.58	0.44	1.61	0.30	0.30
	Ace	0.13	0.61	1.62	2.99	5.21	6.99	6.45	6.40	7.86	19.07	18.92
	Form	0.45	62.18	71.28	121.23	181.32	233.05	217.43	210.52	202.68	541.41	550.08
	Oxa	0.04	0.10	0.08	0.09	0.10	0.11	0.10	0.13	0.40	0.15	0.15
	Sulf	0.30	0.31	0.28	0.25	0.31	0.32	0.31	0.33	0.45	0.27	0.32
	Cl^-	0.43	0.48	0.39	0.17	0.23	0.40	0.55	0.59	0.42	0.42	0.66
	EDA	0	8.41	19.64	22.06	39.58	44.97	44.27	42.64	42.73	68.83	64.99
	PZ	4472.0	4295.8	4031.3	4041.8	3839.6	3708.7	3704.2	3725.6	3588.9	2924.7	2917.0

Table D.19: Tabulated Experimental Data for TE19 (8 m PZ, 0.4 mole CO_2 per mole alkalinity initially, 175 °C)

	Time (wk)	0	0.6	1.0	1.5	2.4	2.9	2.9	2.9	3.4	5.0	6.0
Original Samples (mmol/kg) (Metals are in units of µg/g)	Gly	0.09	0.12	0.11	0.11	0.11	0.12	0.08	0.10	0.13	0.08	0.15
	Ace	0.04	1.78	2.69	3.99	7.09	8.44	7.75	7.17	9.58	8.07	15.01
	Form	0.19	32.09	48.34	72.84	88.98	102.15	93.59	89.00	108.66	99.49	143.15
	Oxa	0.01	0.06	0.07	0.10	0.11	0.11	0.10	0.10	0.10	0.08	0.14
	Sulf	0.13	0.15	0.13	0.16	0.15	0.15	0.14	0.14	0.15	0.14	0.13
	Cl^-	0.29	0.14	0.13	0.29	0.11	0.30	0.13	0.11	0.12	0.05	0.07
	EDA	0	21.72	30.08	44.06	53.03	56.29	51.86	51.94	56.05	57.56	61.05
	PZ	4332.9	3880.1	3802.9	3464.3	3235.0	3072.8	3164.1	3092.4	2869.7	3147.5	2273.4
	CO_2	3245.0	3048.2	2930.7	2903.5	2670.5	2656.3	2752.9	2789.8	2653.6	1965.2	1829.7
	SD_{CO2}	5.93	15.84	15.06	236.90	30.47	18.77	11.06	6.38	10.63	5.34	17.44
	Alk	3960.7	3761.0	3649.7	3477.5	3343.3	3372.6	3389.6	3329.4	3145.3	3222.4	2811.2
	SD_{Alk}	3.27	28.14	10.30	19.16	13.76	167.76	118.64	5.73	6.48	317.87	3.72
	Fe^{2+}	0	72.56	94.12	123.15	156.45	128.98	135.62	154.74	175.07	142.15	192.94
	Ni^{2+}	0	34.79	54.25	69.18	92.41	152.70	115.78	113.24	203.89	153.48	299.46
	Cr^{3+}	0	46.11	74.66	89.36	111.11	74.72	78.74	115.42	75.08	34.89	144.34
Hydrolyzed Samples (mmol/kg)	Gly	0.18	0.20	0.19	0.22	0.20	0.41	0.36	0.26	0.39	1.02	0.49
	Ace	0.12	2.06	3.68	6.66	9.47	12.43	11.22	9.99	15.02	11.51	25.13
	Form	0.31	122.82	183.49	272.14	341.50	405.06	364.09	344.05	448.48	309.93	705.08
	Oxa	0.02	0.08	0.09	0.17	0.11	0.14	0.14	0.11	0.16	0.14	0.20
	Sulf	0.31	0.33	0.38	0.38	0.38	0.36	0.37	0.36	0.32	0.36	0.40
	Cl^-	0.22	0.27	0.73	0.55	0.52	0.57	0.31	0.35	0.47	0.30	0.39
	EDA	0	23.30	30.02	48.23	50.83	56.33	57.74	56.86	65.36	57.93	66.01
	PZ	4313.9	4003.0	3892.8	3623.7	3452.8	3316.9	3333.2	3422.8	3187.3	3372.6	2637.7

Table D.20: Tabulated Experimental Data for TE20 (8 m 1-Methylpiperazine, 0.3 mole CO_2 per mole alkalinity initially, 150 °C)

	Time (wk)	0	1.0	2.4	3.8	6.1	10.4	14.7	17.9	22.4	26.0	30.0
Original Samples (mmol/kg) (Metals are in units of µg/g)	Gly	0	0	0	0	0	0	0	0	0	0	0
	Ace	0.64	0	0.28	0.43	0.71	1.11	1.09	0.06	0.26	3.52	4.82
	Form	3.63	7.73	16.08	24.85	36.86	48.08	50.11	4.13	18.08	72.44	90.12
	Oxa	0.05	0.04	0.04	0.05	0.04	0.04	0	0.02	0.02	0	0
	Sulf	0.14	0.12	0.14	0.14	0.12	0.13	0.12	0.18	0.13	0.10	0.10
	Cl^-	0.27	0.04	0.05	0.05	0.04	0.05	0.02	0.02	0.07	0.02	0.04
	FPZ	0	0	0	0	0	0	0	0	17.39	102.10	126.26
	EDA	0	0	0	0	0	0	0	0.32	0.66	1.53	1.69
	PZ	0	90.68	194.33	321.83	437.19	559.20	648.09	284.03	719.01	790.14	748.42
	1-MPZ	3899.5	3771.5	3384.3	3115.3	2790.9	2491.0	2284.5	4672.9	3165.5	1907.4	1723.8
	1,4-DMPZ	0	77.98	276.78	405.88	481.76	647.85	686.34	317.64	689.12	815.32	797.18
	CO_2	2189.8	2104.5	2153.7	1802.6	2069.1	1895.9	1666.4	157.5	575.61	1664.3	1633.6
	SD_{CO2}	5.42	10.41	17.12	4.25	2.24	19.14	3.95	1.62	3.47	5.61	7.65
	Alk	3947.7	3959.0	3901.4	4041.9	3804.5	3752.7	3727.1	4631.3	4251.7	3583.0	3359.0
	SD_{Alk}	7.33	2.54	8.79	5.55	24.92	9.78	29.03	17.97	19.31	45.35	1.36
	Fe^{2+}	0	10.08	9.33	10.99	13.85	13.10	9.51	0	2.67	11.41	13.49
	Ni^{2+}	0	21.79	14.71	27.28	41.19	54.18	55.99	6.96	36.52	98.46	110.34
	Cr^{3+}	0	35.81	14.54	13.35	25.20	16.55	7.07	0	0	9.23	14.95
Hydrolyzed Samples (mmol/kg)	Gly	0	0	0	0.29	0.18	0.29	0.39	0	0	1.00	1.00
	Ace	0	0.51	1.55	1.88	2.42	3.34	3.36	0.24	1.42	6.72	9.31
	Form	1.02	29.34	59.99	93.28	136.05	186.86	183.14	11.76	59.17	322.99	464.04
	Oxa	0.03	0.11	0.12	0.21	0.10	0.15	0.08	0.11	0.07	0.10	0.07
	Sulf	0.11	0.12	0.16	0.16	0.14	0.14	0.15	0.21	0.31	0.29	0.14
	Cl^-	0.06	0.18	0.10	0.09	0.10	0.08	0.05	0.05	0.11	0.40	0.08
	FPZ	0	0	0	0	0	0	0	0	0	0	0
	EDA	0	0	0	0	0	0	0	0.44	0.80	2.15	2.37
	PZ	0	70.38	178.85	332.86	448.59	470.39	644.85	285.10	730.72	857.71	746.12
	1-MPZ	4081.2	3628.7	3299.3	3058.4	2792.6	2281.3	2211.0	4447.9	3157.3	1951.7	1628.7
	1,4-DMPZ	0	70.05	231.27	305.28	434.51	470.93	586.89	292.84	689.26	781.34	707.57

Table D.21: Tabulated Experimental Data for TE21 (8 m PZ, unloaded, 175 °C)

	Time (wk)	0	1.0	2.0	3.7	4.3	5.1	5.1	5.1	7.3	9.1	11.1	12.9	14.9
Original Samples (mmol/kg) (Metals are in units of µg/g)	Gly	0	0.17	0.12	0.20	0.13	0.15	0.17	0.15	0.22	0.16	0.10	0.16	0.12
	Ace	0	0.12	0.14	0.26	0.26	0.18	0.22	0.44	0.32	0.72	1.61	0.83	1.07
	Form	0.44	1.98	4.44	7.35	6.71	7.24	7.33	10.30	9.86	14.02	14.58	12.81	14.40
	Oxa	0.05	0.05	0.06	0.05	0.08	0.04	0.08	0.07	0.06	0.07	0.06	0.09	0.07
	Sulf	0.19	0.21	0.12	0.14	0.20	0.19	0.22	0.20	0.20	0.18	0.19	0.16	0.14
	Cl^-	0.15	0.11	0.05	0.05	0.06	0.05	0.16	0.11	0.04	0.08	0	0.04	0.10
	EDA	0	0	0	0	4.88	0	5.50	8.92	10.41	22.80	34.93	18.42	33.43
	PZ	4826.8	4852.8	4801.8	4793.6	4776.8	4941.3	4784.0	4790.9	4669.0	4641.1	4500.1	4700.0	4593.6
	Alk	4715.2	4688.0	4685.0	4661.0	4655.2	4671.7	4655.0	4680.0	4660.8	4667.1	4629.7	4653.3	4626.1
	SD_{Alk}	NA	NA	NA	NA	NA	NA	NA	NA	NA	NA	NA	NA	NA
	Fe^{2+}	0	0	1.15	0.11	1.31	0.09	0.47	0.77	4.50	2.66	1.77	0	7.68
	Ni^{2+}	0	0	1.57	0	0.14	0	0	0.28	1.40	1.09	2.91	1.08	1.66
	Cr^{3+}	0	0	0.12	0	0	0	0	0	0.16	0.12	0.04	0	1.43
Hydrolyzed Samples (mmol/kg)	Gly	0	0	0	0	0	0	0	0	0	0	0	0	0
	Ace	0.16	0.25	0.26	0.54	0.41	0.51	0.44	0.85	0.88	1.91	3.22	1.46	1.50
	Form	0.76	2.56	4.94	8.02	8.04	8.91	7.66	11.60	11.54	15.65	17.46	15.85	18.28
	Oxa	0.13	0.06	0.06	0.07	0.23	0.06	0.09	0.14	0.08	0.10	0.12	0.10	0.08
	Sulf	0.20	0.19	0.22	0.21	0.23	0.23	0.26	0.21	0.23	0.28	0.21	0.36	0.23
	Cl^-	0.18	0.32	0.24	0.22	0.23	0.38	0.26	0.27	0.23	0.27	0.21	0.27	0.26
	EDA	0	0	0	0	4.68	9.75	9.20	11.27	11.31	25.47	33.08	15.21	20.45
	PZ	5575.1	4962.6	4877.2	4777.9	4855.0	4721.5	4915.5	5019.1	4787.9	4716.3	4647.3	4764.5	4665.7

Table D.22: Tabulated Experimental Data for TE22 (8 m PZ, 0.3 mole CO_2 per mole alkalinity initially, 175 °C, glass-lined cylinders)

	Time (wk)	0.0	1.0	3.7	4.3	5.1	5.1	5.1	7.3	12.9	14.9
Original Samples (mmol/kg) (Metals are in units of µg/g)	Gly	0	0	0	0	0	0	0	0	0	0
	Ace	0	0.64	6.72	4.15	10.87	8.80	9.45	13.18	19.77	23.07
	Form	0.16	6.78	79.91	46.67	141.02	110.62	119.64	180.37	304.73	373.02
	Oxa	0.04	0.09	0.10	0.08	0.14	0.10	0.10	0.12	0.12	0.04
	Sulf	0.21	0.24	0.27	0.23	0.27	0.22	0.27	0.24	0.23	0.26
	Cl^-	0.09	0.13	0.06	0.14	0.05	0.08	0.06	0.14	0.09	0.06
	EDA	0	20.11	36.99	42.46	53.02	35.78	27.86	48.59	41.52	46.20
	PZ	4301.1	6767.4	3750.0	4296.9	3047.9	3129.0	3106.5	2716.3	1901.4	1457.3
	CO_2	2803.0	915.8	2175.5	1378.8	2276.9	2199.1	2107.7	2125.6	1305.0	NT
	SD_{CO2}	4.71	52.02	139.01	14.44	51.17	12.81	35.49	62.77	51.28	NT
	Alk	4.15	6.87	3.67	4.61	3.48	3.49	3.46	3.32	2.97	2.66
	SD_{Alk}	0.01	NA	0.13	0.03	0.02	0.05	0.02	0.02	0.01	0.11
	Fe^{2+}	0	0	0	NT	NT	1.19	NT	NT	0	0
	Ni^{2+}	0	0	0	NT	NT	0	NT	NT	0	0
	Cr^{3+}	0	0	0	NT	NT	0	NT	NT	0	0
Hydrolyzed Samples (mmol/kg)	Gly	0	1.78	1.24	1.48	0	0	0	0	0.66	0.25
	Ace	0.35	3.81	10.00	6.69	15.13	12.63	13.50	18.19	28.14	29.57
	Form	3.72	42.59	128.06	79.61	213.34	170.27	185.54	272.67	492.00	538.00
	Oxa	0.03	0.57	0.21	0.30	0.36	0.22	0.28	0.34	0.34	0.15
	Sulf	0.27	0.58	0.24	0.31	0.26	0.26	0.22	0.22	0.44	0.26
	Cl^-	0.26	0.27	0.20	0.52	0.23	0.17	0.19	0.22	0.23	0.21
	EDA	0	13.72	34.82	42.31	48.50	46.49	38.38	47.04	53.78	50.73
	PZ	4370.2	6789.7	3693.9	4355.0	3252.2	3317.7	3259.0	2960.6	2201.3	1786.9

Table D.23: Tabulated Experimental Data for TE23 (8 m PZ, 0.3 mole H+ per mole alkalinity initially, 175 °C)

	Time (wk)	0	0.9	2.0	3.7	4.3	5.1	5.1	5.1	7.3	9.1	11.1	12.9	14.9
Original Samples (mmol/kg) (Metals are in units of μg/g)	Gly	0	0	0	0	0	0	0	0	0	0	0	0	0
	Ace	0	0.22	0.21	1.86	0.30	0.44	0.77	0.81	1.09	1.60	2.46	3.42	3.05
	Form	0.24	1.44	1.37	6.02	1.49	1.85	2.20	2.62	2.78	2.70	3.51	4.58	2.75
	Oxa	0	0	0	0	0	0	0	0	0	0	0	0	0
	Sulf	1641.1	1685.2	1631.0	5073.7	1604.6	1564.1	1638.4	1619.2	1626.1	1624.3	1575.3	1645.4	1427.3
	Cl^-	0.05	0.08	0.15	0.51	0.05	0.05	0.08	0.10	0.06	0.14	0.08	0.06	0.08
	EDA	0	0	12.26	20.82	23.85	28.14	40.11	32.35	51.31	75.17	84.05	116.87	116.73
	PZ	4341.8	4133.5	3941.2	3775.8	3738.1	3707.4	3622.0	3832.4	3497.9	3282.8	2980.5	2900.6	2868.5
	CO_2	0	0	0	0	0	0	0	0	0	0	0	0	0
	SD_{CO2}	0	0	0	0	0	0	0	0	0	0	0	0	0
	Alk	2858.0	2833.6	2710.8	2753.1	2707.6	2726.1	2702.6	2718.7	2656.3	2609.3	2491.4	2535.0	2506.0
	SD_{Alk}	5.10	13.88	3.97	11.84	25.40	2.40	11.01	16.24	29.54	12.36	1.06	37.73	17.51
	Fe^{2+}	0	16.98	31.29	55.69	63.75	51.30	60.07	74.94	65.16	177.14	221.06	243.79	374.71
	Ni^{2+}	0	9.72	18.68	52.46	19.48	25.64	28.12	65.34	76.99	106.15	131.19	243.79	151.36
	Cr^{3+}	0	0	0.01	0	0.14	0.06	0	0	0.19	0	0	0.54	0.23
Hydrolyzed Samples (mmol/kg)	Gly	0	0	0	0	0	0	0	0	0	0	0	0	0
	Ace	0	0.95	0.74	1.70	1.10	1.14	1.36	1.61	1.88	2.84	3.37	5.46	4.98
	Form	0.33	3.55	2.89	5.42	3.56	4.21	4.77	6.08	5.90	6.26	6.90	10.46	7.72
	Oxa	0	0	0	0	0	0	0	0	0	0	0	0	0
	Sulf	1686.0	1597.1	1492.5	917.1	1545.2	980.9	1742.0	1129.8	978.7	1618.7	1575.3	1449.7	1674.5
	Cl^-	0.09	0.25	0.15	0.20	0.12	0.10	0.10	0.28	0.18	0.08	0.08	0.14	0.13
	EDA	0	4.33	7.98	25.15	36.37	35.62	34.22	39.51	61.80	73.47	85.18	114.97	110.65
	PZ	4479.7	4168.4	3931.4	3958.1	3617.4	3848.3	3559.0	3801.6	3641.4	3442.5	3061.7	2995.3	2872.6

Table D.24: Tabulated Experimental Data for TE24 (8 m Homopiperazine (HomoPZ), 0.3 mole CO_2 per mole alkalinity initially, 175 °C)

	Time (wk)	0	0.9	4.1	6.1	9.9
Original Samples (mmol/kg) (Metals are in units of µg/g)	Gly	0	0	0	0	0
	Ace	0	9.37	17.57	23.13	23.20
	Form	0.51	38.02	59.11	26.36	54.49
	Oxa	0	0.25	0.32	0.47	0.15
	Sulf	15.67	16.60	17.29	19.15	16.70
	Cl^-	0.64	0.59	0.70	1.14	0.74
	HomoPZ	3770.2	1029.7	35.37	44.26	86.94
	CO_2	2546.0	1243.7	806.6	1274.8	483.2
	SD_{CO2}	22.03	12.73	8.26	8.18	4.46
	Alk	3933.9	2455.0	1345.1	1705.0	1380.9
	SD_{Alk}	2.84	0.98	12.61	6.91	172.74
	Fe^{2+}	0	NT	100.75	NT	35.01
	Ni^{2+}	0	NT	1136.6	NT	1628.1
	Cr^{3+}	0	NT	14.70	NT	4.72
Hydrolyzed Samples (mmol/kg)	Gly	0	0	0.44	NT	0.34
	Ace	0	9.40	30.77	NT	43.42
	Form	12.54	293.16	175.81	NT	107.23
	Oxa	0.33	0.53	0.84	NT	0.84
	Sulf	17.07	19.59	18.25	NT	17.40
	Cl^-	0.77	0.60	0.63	NT	0.60
	HomoPZ	2978.9	1106.1	106.9	NT	0

Table D.25: Tabulated Experimental Data for TE25 (8 m Pyrrolidine (Pyr), 0.3 mole CO_2 per mole alkalinity initially, 175 °C)

	Time (wk)	0	0.9	1.8	4.1	6.1	6.1	6.1	8.1	9.9
Original Samples (mmol/kg) (Metals are in units of µg/g)	Gly	0	0	0	0	0	0	0	0	0
	Ace	0	0.81	0	0	0	0	0	0	0
	Form	1.07	45.46	43.72	72.24	80.27	81.58	77.89	88.35	82.13
	Oxa	0.21	0.14	0	0	0.10	0.12	0.16	0.15	0.13
	Sulf	17.12	16.37	17.57	10.47	12.90	14.41	14.12	16.24	17.33
	Cl^-	0.38	0	0.11	0.06	0.07	0.21	0.10	0.06	0.40
	Pyr	4354.9	1945.0	1410.5	1077.3	989.58	981.07	967.15	880.55	817.47
	CO_2	1400.7	1454.4	1413.7	1438.8	1439.3	1436.4	1414.5	1341.4	1288.3
	SD_{CO2}	10.88	1.42	4.02	11.32	7.98	49.02	12.20	13.07	30.72
	Alk	4725.2	4366.1	4316.5	3988.5	4019.6	4032.7	3972.8	4021.7	4156.0
	SD_{Alk}	24.32	97.63	375.76	18.89	64.73	26.96	28.28	33.85	59.81
	Fe^{2+}	0	NT	NT	5.92	NT	NT	NT	NT	3.69
	Ni^{2+}	0	NT	NT	5.74	NT	NT	NT	NT	7.02
	Cr^{3+}	0	NT	NT	0.96	NT	NT	NT	NT	0.29
Hydrolyzed Samples (mmol/kg)	Gly	0	0	0	0	0	0	0	0	0
	Ace	0	1.31	0	0	0	0	0	0	0
	Form	2.00	66.22	76.55	94.71	103.69	103.26	104.59	101.88	112.63
	Oxa	0.59	0.19	0.18	0.17	0.20	0.26	0.17	0.12	0
	Sulf	29.45	17.94	17.74	18.29	18.36	29.78	15.01	13.75	13.72
	Cl^-	0.73	0.22	0.19	0.23	0.20	0.16	0.23	0.11	0.10
	Pyr	1501.2	2206.8	1453.2	955.71	800.70	570.09	890.41	871.87	841.00

Table D.26: Tabulated Experimental Data for TE26 (8 m Piperidine (PD), 0.3 mole CO_2 per mole alkalinity initially, 175 °C)

	Time (wk)	0	0.9	1.8	4.1	6.1	6.1	6.1	8.1	9.9
Original Samples (mmol/kg) (Metals are in units of µg/g)	Gly	0	0	0	0	0	0	0	0	0
	Ace	0	0	0	0	0	0	0.25	0	0
	Form	0.46	65.44	71.31	89.69	100.09	95.54	36.57	95.06	95.83
	Oxa	0	0	0	0	0	0	0	0	0
	Sulf	6.92	5.12	7.40	7.52	7.40	3.42	2.27	2.78	2.55
	Cl^-	0.13	0.12	0.07	0.10	0.06	0.07	0.27	0.06	0.14
	PD	4489.3	4146.1	3685.6	3274.2	3054.3	2903.7	3382.7	2882.0	2619.5
	CO_2	1645.7	1475.9	1483.7	1456.0	1417.1	1402.8	2323.4	1357.4	1338.1
	SD_{CO2}	11.30	6.94	7.07	12.91	26.39	14.57	8.96	5.73	3.45
	Alk	4375.7	4281.0	4261.7	4246.9	4136.2	4142.5	4476.1	4107.8	4081.7
	SD_{Alk}	17.76	6.02	1.79	57.24	108.70	14.60	NA	34.67	59.80
	Fe^{2+}	0	NT	NT	4.11	NT	NT	NT	NT	5.60
	Ni^{2+}	0	NT	NT	1.48	NT	NT	NT	NT	1.47
	Cr^{3+}	0	NT	NT	1.56	NT	NT	NT	NT	0.88
Hydrolyzed Samples (mmol/kg)	Gly	0	0	0	0	0	0	0	0	0
	Ace	0	0	0	0	0	0	0.37	0	0.10
	Form	1.24	136.02	0	211.69	244.61	242.61	94.09	256.17	272.21
	Oxa	0.08	0.07	0	0.06	0.06	0.07	0.06	0.06	0.06
	Sulf	1.07	3.58	2.54	0.53	0.65	0.53	0.69	0.60	0.60
	Cl^-	0.17	0.24	0	0.24	0.24	0.23	0.52	0.22	0.22
	PD	797.36	701.34	689.18	631.66	620.89	565.34	3221.2	1203.9	1146.3

Table D.27: Tabulated Experimental Data for TE27 (8 m Hexamethyleneimine (HMI), 0.3 mole CO_2 per mole alkalinity initially, 175 °C)

	Time (wk)	0	0.9	1.8	6.1	6.1	9.9
Original Samples (mmol/kg) (Metals are in units of μg/g)	Gly	0	0	0	0	0	0
	Ace	0	0	0	0	0	0
	Form	0.34	41.73	56.51	65.64	71.93	71.06
	Oxa	0	0	0.44	0.02	0.04	0.03
	Sulf	0.46	7.37	7.62	0.27	0.75	0.54
	Cl^-	0.17	0.70	1.13	0.14	0.10	0.04
	HMI	4282.2	143.93	416.96	299.19	270.46	231.56
	CO_2	1355.6	1077.3	1176.1	1138.2	1210.0	1104.8
	SD_{CO2}	23.18	8.01	14.04	11.38	7.92	8.29
	Alk	4196.3	3392.9	3085.2	2668.6	2698.6	2668.1
	SD_{Alk}	37.71	30.41	31.93	46.20	24.97	49.49
	Fe^{2+}	0	NT	NT	4.93	NT	5.23
	Ni^{2+}	0	NT	NT	4.54	NT	5.27
	Cr^{3+}	0	NT	NT	0.33	NT	0.67
Hydrolyzed Samples (mmol/kg)	Gly	0	0	0	0	0	0
	Ace	0	0	0	0.21	0	0.14
	Form	1.40	144.77	144.58	174.49	160.38	151.25
	Oxa	0.05	0.07	0.07	0.09	0.06	0.05
	Sulf	0.59	0.58	0.69	0.88	0.46	0.45
	Cl^-	0.31	0.26	0.26	0.47	0.28	0.19
	HMI	376.12	233.33	101.91	54.23	42.59	47.19

Table D.28: Tabulated Experimental Data for TE28 (4 m PZ + 4 m 1-Methylpiperazine (1-MPZ), 0.3 mole CO_2 per mole alkalinity initially, 175 °C)

	Time (wk)	0	1.0	4.2	6.3	8.6	10.0
Original Samples (mmol/kg) (Metals are in units of µg/g)	Gly	0	0	0	0	0	0
	Ace	0.12	0	0.09	0.24	0.16	1.13
	Form	0.20	4.16	14.44	16.16	17.16	28.65
	Oxa	0	0	0	0	0	0.02
	Sulf	0.22	0.17	0.17	0.25	0.19	0.21
	Cl^-	0	0.14	0	0	0	0.01
	FPZ	0	0	0	0	0.62	1.02
	EDA	0	0	0	9.21	0	4.92
	PZ	2027.6	2030.8	2015.6	2036.4	2145.8	2002.4
	1-MPZ	1910.6	1920.8	1662.7	1642.8	1587.3	1598.9
	1,4-DMPZ	0	36.85	111.98	165.19	175.22	187.75
	CO_2	2575.9	2582.3	2429.7	NT	1601.7	2470.9
	SD_{CO2}	13.05	24.15	63.75	NT	9.95	23.02
	Alk	3989.8	3974.1	3966.1	NT	4145.0	3812.6
	SD_{Alk}	2.92	11.14	27.94	NT	NA	17.71
	Fe^{2+}	0	13.95	23.94	18.51	1.60	25.85
	Ni^{2+}	0	10.28	62.70	107.96	103.87	85.07
	Cr^{3+}	0	19.86	43.57	5.89	3.70	28.03
Hydrolyzed Samples (mmol/kg)	Gly	0	0	0	0	0	0
	Ace	0.07	0.09	0.51	0.59	1.17	2.76
	Form	1.23	17.98	55.68	66.68	59.62	116.97
	Oxa	0	0	0	0	0.07	0.07
	Sulf	0.23	0.21	0.20	0.43	0.23	0.24
	Cl^-	0.08	0.06	0.04	0.42	0.04	0.04
	FPZ	0	0	0	0	0	0
	EDA	0	6.28	0	0	0	5.40
	PZ	2040.1	2027.6	2069.7	2025.7	2237.2	2200.7
	1-MPZ	1877.4	1844.2	1763.3	1680.7	1610.2	1753.3
	1,4-DMPZ	0	74.37	108.48	201.95	303.46	200.89

Table D.29: Tabulated Experimental Data for TE29 (5 m PZ + 2 m 1-Methylpiperazine (1-MPZ) + 1 m 1,4-Dimethylpiperazine (1,4-DMPZ), 0.3 mole CO_2 per mole alkalinity initially, 150 °C)

	Time (wk)	0	1.0	4.2	6.3	8.6	10.1	12.2	15.0
Original Samples (mmol/kg) (Metals are in units of µg/g)	Gly	0	0	0	0	0	0	0	0
	Ace	0	0	0	0.15	0.19	2.01	1.72	0.83
	Form	0.49	4.34	13.66	11.55	16.48	33.77	29.20	30.83
	Oxa	0	0	0	0	0	0.03	0.02	0
	Sulf	0.31	0.26	0	0.30	0.24	0.22	0.19	0.11
	Cl^-	0.06	0.07	0.04	0.16	0.04	0.02	0	0.02
	FPZ	0	0	0	0	0	1.52	1.43	0
	EDA	0	0	0	2.91	3.08	0	0	7.39
	PZ	2626.6	2536.8	2410.7	2282.8	2342.8	2163.7	2197.9	2152.1
	1-MPZ	988.78	1159.6	1345.4	1223.6	1257.4	1124.0	1228.4	1388.7
	1,4-DMPZ	622.97	748.35	642.64	594.15	579.76	483.01	408.11	291.18
	CO_2	NT	NT	NT	NT	NT	NT	NT	NT
	Alk	4038.5	4043.0	3999.1	NT	3973.5	3856.8	3889.0	3849.1
	SD_{Alk}	9.57	15.80	20.03	NT	18.31	15.97	12.60	14.67
	Fe^{2+}	0	7.91	23.80	NT	9.76	24.33	17.31	NT
	Ni^{2+}	0	19.98	33.88	NT	87.01	71.36	63.06	NT
	Cr^{3+}	0	2.03	32.06	NT	0	20.86	7.39	NT
Hydrolyzed Samples (mmol/kg)	Gly	0	0	0	0	0	0	0	0.79
	Ace	0	0	0	0.23	0.40	3.74	0.65	2.31
	Form	2.40	15.73	49.13	48.79	64.18	125.85	107.74	135.66
	Oxa	0.07	0.29	0	0.07	0.01	0.06	0	0.03
	Sulf	0.42	0.27	0.30	0.29	0.20	0.28	0.18	0.14
	Cl^-	0.18	0.10	0.06	0.14	0.04	0.06	0	0.06
	FPZ	0	0	0	0	0	0	0	0
	EDA	0	0	0	0	0	0	2.00	0
	PZ	2522.4	2526.9	2427.1	2315.1	2380.2	2292.5	2224.5	2157.0
	1-MPZ	1144.1	1116.0	1219.4	1240.4	1229.7	1275.6	1234.5	1326.4
	1,4-DMPZ	736.22	737.75	621.61	589.96	429.04	483.09	543.50	348.70

Table D.30: Tabulated Experimental Data for TE30 (5 m PZ + 2.5 m 1-Methylpiperazine (1-MPZ)+ 0.5 m 1,4-Dimethylpiperazine (1,4-DMPZ), 0.3 mole CO_2 per mole alkalinity initially, 150 °C)

	Time (wk)	0	4.2
Original Samples (mmol/kg)	Gly	0	0
	Ace	0	0.09
	Form	0.38	11.42
	Oxa	0	0.05
	Sulf	0.25	0.23
	Cl^-	0.10	0
	EDA	0	0
	PZ	2775.9	2530.9
	1-MPZ	1252.5	1376.9
	1,4-DMPZ	326.56	291.51
	CO_2	2485.1	2399.5
	SD_{CO2}	11.82	19.22
	Alk	4084.5	4038.3
	SD_{Alk}	15.14	15.29
Hydrolyzed Samples (mmol/kg)	Gly	0	0
	Ace	0.22	0.25
	Form	1.70	42.72
	Oxa	0.06	0.06
	Sulf	0.30	0.27
	Cl^-	0.09	0
	EDA	0	0
	PZ	2759.8	2528.0
	1-MPZ	1330.3	1288.5
	1,4-DMPZ	436.88	356.84

Table D.31: Tabulated Experimental Data for TE31 (5 m PZ + 1.5 m 1-Methylpiperazine (1-MPZ) + 1.5 m 1,4-Dimethylpiperazine (1,4-DMPZ), 0.3 mole CO_2 per mole alkalinity initially, 150 °C)

	Time (wk)	0	1.0	4.2
Original Samples (mmol/kg)	Gly	0	0	0
	Ace	0.13	0.54	0.48
	Form	0.68	4.12	15.39
	Oxa	0	0.07	0.04
	Sulf	0.25	0.24	0.30
	Cl^-	0.07	0.06	0.34
	EDA	0	0	0
	PZ	2570.0	2419.7	2128.4
	1-MPZ	840.48	888.19	1000.0
	1,4-DMPZ	912.95	811.22	446.24
	CO_2	2337.6	2449.5	2261.7
	SD_{CO2}	15.86	15.26	9.49
	Alk	3932.1	3897.6	3861.6
	SD_{Alk}	15.16	27.05	23.87
Hydrolyzed Samples (mmol/kg)	Gly	0	0	0
	Ace	0.05	0.22	0.69
	Form	3.80	14.82	57.01
	Oxa	0.12	0.13	0.07
	Sulf	0.21	0.28	0.33
	Cl^-	0.17	0	0
	EDA	0	0	0
	PZ	2470.0	2408.6	2276.3
	1-MPZ	749.86	798.15	1072.04
	1,4-DMPZ	678.61	730.74	551.52

Table D.32: Tabulated Experimental Data for TE32 (4 m PZ, 0.3 mole CO_2 per mole alkalinity initially, 175 °C)

	Time (wk)	0	0.5	0.9	2.2	3.3	4.0	6.2	8.0	8.0	8.0	10.1	12.1	15.0
Original Samples (mmol/kg) (Metals are in units of µg/g)	Gly	0	0	0	0	0	0	0	0	0	0	0	0	0
	Ace	0	0	0.62	1.97	4.23	4.27	7.83	9.14	12.43	12.32	15.07	18.67	23.66
	Form	0	14.08	30.67	76.51	106.00	111.12	147.69	157.21	151.91	149.82	164.73	179.33	191.42
	Oxa	0	0.24	0	0	0	0	0	0	0	0	0	0	0
	Sulf	0.09	0.09	0.09	0.12	0.11	0.09	0.08	0.07	0.10	0.09	0.09	0.11	0.08
	Cl^-	0	0	0	0	0	0	0	0	0	0	0	0	0
	EDA	0	0	11.69	30.23	37.88	33.61	33.39	36.15	32.09	39.97	36.08	34.38	28.12
	PZ	3031.3	2843.5	2850.6	2444.7	2396.7	2188.2	1815.6	1562.2	1664.2	1737.3	1567.9	1346.9	1018.7
	CO_2	2667.3	2342.9	2289.5	2180.5	1959.4	1962.6	1765.1	1693.3	1683.8	1681.8	1774.3	1216.1	1133.8
	SD_{CO2}	16.73	2.54	18.89	152.20	15.18	8.93	7.38	17.18	13.36	11.83	33.50	8.41	35.36
	Alk	2715.3	2658.0	2611.2	2458.2	2364.7	2327.0	2168.7	2091.1	2117.9	2105.5	2036.6	1914.0	1759.0
	SD_{Alk}	0.44	5.88	1.48	1.88	19.56	3.51	4.41	8.01	1.49	1.57	10.88	7.07	4.34
	Fe^{2+}	0.76	8.04	15.22	25.64	28.99	28.25	30.29	30.40	26.26	28.24	32.86	31.37	30.93
	Ni^{2+}	0.25	9.21	17.44	44.74	62.93	66.92	97.84	104.90	111.22	103.37	119.49	141.98	169.60
	Cr^{3+}	1.22	9.69	9.18	11.86	12.12	11.35	8.82	7.70	7.48	7.58	10.47	7.43	5.69
Hydrolyzed Samples (mmol/kg)	Gly	0	1.09	0.79	1.42	1.71	1.40	2.16	1.52	2.96	1.32	2.54	2.50	2.83
	Ace	0	0.13	0.71	3.29	5.41	6.37	15.12	18.18	16.93	17.09	20.70	26.43	34.31
	Form	0.20	26.10	53.89	137.56	175.49	182.94	290.93	322.46	306.22	304.74	352.14	412.35	490.51
	Oxa	0	0.06	0.07	0.09	0.09	0.10	0.12	0.16	0.12	0.21	0.10	0.15	0.13
	Sulf	0.12	0.16	0.12	0.12	0.17	0.20	0.14	0.11	0.13	0.13	0.15	0.16	0.13
	Cl^-	0	0.07	0.13	0.07	0.20	0.32	0.08	0.06	0.13	0.05	0.18	0.07	0.10
	EDA	0	8.44	10.85	26.69	38.00	34.71	45.19	35.17	36.38	42.82	38.55	37.54	33.06
	PZ	2915.4	2752.9	2777.4	2540.4	2275.7	2201.2	1921.0	1764.3	1785.5	1848.5	1668.1	1455.5	1210.0

Table D.33: Tabulated Experimental Data for TE33 (12 m PZ, 0.3 mole CO_2 per mole alkalinity initially, 175 °C)

	Time (wk)	0	0.5	0.9	2.2	3.3	4.0	6.2	8.0	8.0	8.0	10.1	12.1	15.0
Original Samples (mmol/kg) (Metals are in units of μg/g)	Gly	0	0	0	0	0	0	0	0	0	0	0	0	0
	Ace	0	0.08	0.39	2.08	4.63	6.23	10.85	13.10	13.52	13.19	16.25	18.50	22.57
	Form	0.08	14.11	26.66	60.96	89.60	110.91	165.40	191.31	192.22	188.43	215.34	229.57	255.31
	Oxa	0	0.02	0.02	0.03	0.03	0.04	0.05	0.04	0.05	0	0.05	0.05	0
	Sulf	0.20	0.15	0.13	0.19	0.16	0.17	0.18	0.15	0.19	0.15	0.19	0.17	0.23
	Cl^-	0	0.03	0.03	0.04	0.12	0.03	0.06	0.04	0.02	0.02	0.03	0.02	0.03
	FPZ	0	57.87	106.33	209.36	278.81	327.67	412.56	429.47	440.39	438.03	457.88	471.24	472.87
	EDA	0	17.75	26.64	50.58	63.68	69.84	83.79	85.38	83.62	83.75	78.99	74.46	61.80
	PZ	5226.6	4953.2	4763.1	4267.2	3784.1	3471.8	2784.0	2406.2	2375.6	2409.4	2003.1	1746.3	1247.7
	CO_2	3005.1	2853.3	2909.2	2508.8	2281.8	2149.0	1798.7	1655.9	1649.9	1948.9	1468.7	1692.4	1408.9
	SD_{CO2}	5.06	13.80	4.56	14.94	5.77	17.34	5.59	9.04	11.89	8.33	12.79	4.00	3.69
	Alk	5106.4	4986.6	4899.9	4629.1	4368.1	4118.0	3807.4	3640.0	3634.8	3611.0	3385.3	3247.1	2906.2
	SD_{Alk}	4.64	11.08	48.36	15.93	6.50	19.67	25.58	59.91	12.41	16.61	39.18	142.42	125.17
	Fe^{2+}	0.22	120.09	159.35	320.23	486.65	561.14	494.03	454.06	437.68	454.93	396.09	416.61	293.47
	Ni^{2+}	0.16	21.14	26.77	58.11	110.09	174.82	291.87	374.15	374.47	372.57	451.00	507.92	552.33
	Cr^{3+}	0.29	31.46	40.87	79.80	114.90	124.68	87.84	70.55	68.22	68.00	52.83	41.99	24.60
Hydrolyzed Samples (mmol/kg)	Gly	0	0	0	0	0	0	0	0	0	0	0	0	0.44
	Ace	0	0.20	0.88	4.06	7.23	10.76	18.31	22.50	22.83	22.60	28.17	31.78	40.06
	Form	0.21	58.92	108.29	231.90	336.06	420.69	603.39	694.11	693.44	685.40	782.54	853.46	971.95
	Oxa	0.02	0.05	0.08	0.10	0.13	0.21	0.17	0.21	0.19	0.18	0.23	0.24	0.28
	Sulf	0.11	0.20	0.13	0.17	0.20	0.16	0.25	0.18	0.21	0.20	0.23	0.21	0.26
	Cl^-	0.06	0.07	0.05	0.05	0.18	0.09	0.12	0.09	0.05	0.07	0.07	0.09	0.16
	FPZ	0	0	0	0	0	0	0	0	0	0	0	0	0
	EDA	0	16.51	26.22	51.18	65.78	71.45	87.85	90.17	89.63	89.65	89.46	84.20	71.91
	PZ	5054.7	4809.2	4659.0	4239.5	3868.8	3648.4	3036.7	2713.8	2722.1	2788.6	2468.0	2192.0	1694.5

Table D.34: Tabulated Experimental Data for TE34 (8 m PZ, 0.1 mole CO_2 per mole alkalinity initially, 175 °C)

	Time (wk)	0	0.5	0.9	2.2	3.3	4.0	6.2	8.0	8.0	8.0	10.1	12.1	15.0
Original Samples (mmol/kg) (Metals are in units of μg/g)	Gly	0	0	0	0	0	0	0	0	0	0	0	0	0
	Ace	0	0	0	0.37	1.34	1.66	2.54	3.39	3.20	9.17	10.43	10.83	12.65
	Form	0.10	9.95	18.34	32.19	48.86	60.16	76.96	86.78	87.26	100.45	109.12	102.18	102.58
	Oxa	0	0	0	0	0	0	0	0	0	0.05	0.03	0	0.04
	Sulf	0.13	0.10	0.12	0.11	0.12	0.11	0.11	0.16	0.11	0.16	0.18	0.17	0.17
	Cl^-	0	0.06	0.01	0.04	0.05	0.04	0.04	0.06	0.08	0.02	0.02	0.09	0.02
	FPZ	0	0	0	0	20.89	16.60	16.74	51.41	50.20	35.06	0	0	30.03
	EDA	0	0	9.30	24.21	33.50	39.76	50.92	71.86	74.67	71.86	75.98	71.07	70.08
	PZ	4497.3	4413.7	4291.1	4177.3	3827.0	3735.6	3453.0	3196.5	3252.1	3100.6	3183.0	2731.2	2453.6
	CO_2	1221.8	3202.0	1145.4	1023.1	2649.5	942.2	864.5	758.3	785.2	783.9	1272.5	812.8	2165.4
	SD_{CO2}	1.96	13.87	3.34	1.65	3.45	2.77	6.96	2.97	3.41	2.12	5.49	0.30	3.17
	Alk	4446.7	4415.7	4350.6	4219.4	4114.0	4025.0	3906.9	3836.7	3810.8	3761.6	3673.4	3638.2	3526.5
	SD_{Alk}	6.30	29.63	13.58	10.45	4.63	7.92	20.77	15.42	3.16	15.66	7.50	5.44	13.11
	Fe^{2+}	0.23	31.39	35.42	49.51	45.35	37.88	51.87	49.67	48.62	48.21	36.13	53.87	68.57
	Ni^{2+}	0.23	12.09	19.09	36.93	60.66	67.62	98.35	123.93	133.05	133.19	159.39	154.26	196.96
	Cr^{3+}	0.37	0.97	1.19	1.90	0.85	0.54	0.83	0.37	1.00	0.42	0.53	0.41	0.46
Hydrolyzed Samples (mmol/kg)	Gly	0	0.28	0.42	1.04	1.53	1.98	1.61	2.22	1.68	1.56	1.47	0	0
	Ace	0	0	0.45	1.66	2.50	3.28	5.16	6.23	6.08	6.67	8.61	14.58	16.95
	Form	0.67	20.93	37.00	71.05	100.53	122.60	171.20	183.11	175.43	189.51	221.95	216.44	255.25
	Oxa	0.04	0.06	0.07	0.05	0.14	0.12	0.13	0.11	0.10	0.10	0.24	0.10	0.09
	Sulf	0.33	0.14	0.25	0.32	0.16	0.24	0.14	0.18	0.16	0.16	0.24	0.22	0.21
	Cl^-	0.46	0.14	0.12	0.55	0.06	0.11	0.09	0.09	0.10	0.04	0.08	0.12	0.06
	FPZ	0	0	0	0	0	0	0	0	0	0	0	0	0
	EDA	0	0	11.36	28.76	42.31	43.84	42.76	56.21	56.29	76.61	80.62	66.27	70.16
	PZ	4386.4	4298.4	4169.1	4073.9	3905.5	3702.8	2839.0	3253.3	3259.5	2754.6	2923.7	2854.6	2492.7

Table D.35: Tabulated Experimental Data for TE35 (8 m Morpholine (Mor), 0.3 mole CO_2 per mole alkalinity initially, 175 °C)

	Time (wk)	0	1.0	2.0	4.0	6.0	6.0	8.0	10.0	15.0
Original Samples (mmol/kg)	Gly	0	0	0	0	0	0	0	0	0
	Ace	0	0.94	1.78	2.55	2.87	4.86	4.93	3.70	2.79
	Form	0.38	11.34	18.93	27.79	18.03	49.05	49.47	24.71	35.62
	Oxa	0	0.09	0.08	0.06	0.11	0.03	0.01	0.02	0.04
	Sulf	0.33	0.25	0.16	0.28	0.19	0.38	0.22	0.15	0.36
	Cl^-	0.45	0.14	0.02	0.41	0.02	0.49	0.04	0.03	0.61
	Mor	3594.1	4260.6	4207.4	4001.8	3724.7	3471.5	3121.9	3414.3	2957.9
	CO_2	1178.3	1185.9	1374.2	1354.8	1568.8	1173.6	981.6	1679.3	1540.1
	SD_{CO2}	2.54	4.80	5.67	7.81	7.36	1.84	2.82	8.85	14.42
	Alk	4330.5	4238.2	4165.7	4051.0	4061.9	3879.8	3811.3	3968.1	3823.1
	SD_{Alk}	1.30	13.25	9.16	3.34	NA	10.85	1.03	5.34	1.76
Hydrolyzed Samples (mmol/kg)	Gly	0	0	0	0	0	0	0	0	0
	Ace	0	1.54	4.81	6.24	6.77	9.28	10.08	7.53	5.99
	Form	0.87	65.30	106.64	155.61	128.21	242.93	264.71	161.28	212.19
	Oxa	0.01	0.47	0.45	0.36	0.87	0.36	0.11	0.21	0.20
	Sulf	0.21	0.19	0.30	0.08	0.15	0.21	0.12	0.13	0.23
	Cl^-	0.27	0.05	0.69	0.12	0.05	0.24	0.24	0.13	0.27
	Mor	4166.3	4181.6	4165.3	3750.9	3571.5	2781.6	3315.5	3200.8	2997.5

Table D.36: Tabulated Experimental Data for TE36 (8 m Hexamethylenediamine (HMDA), 0.3 mole CO_2 per mole alkalinity initially, 175 °C)

	Time (wk)	0	0.7	1.0	2.0	3.0	4.0	6.0	6.0	6.0	8.0	10.0	12.0	15.0
Original Samples (mmol/kg)	Gly	0	0	0	0	0	0	0	0	0	0	0	0	0
	Ace	0	0	0	0	0	0	0	0	0	0	0	0	0
	Form	0.26	9.44	12.51	18.10	31.02	28.97	36.92	39.53	42.52	41.94	50.69	58.90	71.43
	Oxa	0.01	0.01	0.02	0.01	0.03	0.03	0.02	0.02	0.03	0.03	0.03	0.04	0.03
	Sulf	0.43	0.31	0.23	0.28	0.22	0.22	0.20	0.23	0.24	0.20	0.24	0.19	0.19
	Cl^-	0.09	0.08	0.08	0.20	0.24	0.15	0.12	0.08	0.14	0.12	0.11	0.11	0.08
	HMDA	2500*	1930.6	1749.5	1407.5	1540.5	975.39	701.36	708.66	648.86	641.01	575.60	494.82	492.53
	CO_2	752.89	2019.3	2030.7	2033.8	2001.7	2191.5	2093.6	2026.3	1975.1	2007.8	2025.1	2007.5	2060.8
	SD_{CO2}	3.04	16.71	24.75	16.72	8.24	24.86	13.72	11.62	11.96	8.96	8.24	3.34	5.06
	Alk	3404.4	3033.5	2998.4	3043.2	2953.1	3087.0	3114.3	3108.1	3093.4	3133.9	3168.4	3100.4	3183.5
	SD_{Alk}	22.64	7.39	4.96	9.30	5.09	12.98	10.09	8.10	0.96	0.39	11.44	22.82	7.98
Hydrolyzed Samples (mmol/kg)	Gly	0	0	0	0	0	0	0	0	0	0	0	0	0
	Ace	0	0	0	0	0	0	0	0	0	0	0	0	0
	Form	0.89	19.96	27.91	43.00	70.45	72.33	93.44	99.75	108.37	108.27	119.44	147.12	1.90
	Oxa	0.02	0.04	0.03	0.04	0.11	0.05	0.04	0.04	0.04	0.05	0.04	0.05	0.03
	Sulf	0.45	0.35	0.22	0.20	0.19	0.18	0.20	0.18	0.21	0.18	0.21	0.17	0.22
	Cl^-	0.14	0.10	0.15	0.08	0.18	0.04	0.08	0.07	0.07	0.07	0.04	0.04	0.17
	HMDA	2500*	1883.7	1715.8	1405.9	1541.1	983.1	733.6	738.1	677.5	660.2	594.6	517.5	520.3

* Concentration inferred due to broken sample vial

Table D.37: Tabulated Experimental Data for TE37 (8 m PZ, 0.3 mole H^+ per mole alkalinity initially, 150 °C)

	Time (wk)	0	1.0	2.0	4.0	6.0	10.0	14.0	14.0	14.0	18.0	22.0	26.0	30.0
Original Samples (mmol/kg)	Gly	0	0	0.03	0.02	0.02	0.03	0.04	0.02	0.04	0.01	0.01	0.02	0
	Ace	0	0	0.19	0.09	0.12	0.21	0.44	0.19	0.18	1.08	0.27	0.24	0.21
	Form	0.37	1.26	0.65	0.46	0.93	0.78	1.82	0.64	0.62	0.77	0.79	0.78	0.49
	Oxa	0	0	0	0	0	0	0	0	0	0	0	0	0
	Sulf	0	0	0	0	0	0	0	0	0	0	0	0	0
	Cl^-	0.02	0.05	0.02	0.04	0.04	0.04	0.06	0.04	0.04	0.09	0.06	0.03	0.04
	NH_4^+	0	0.10	0	1.69	1.26	1.40	11.27	5.07	5.44	10.51	9.74	14.00	16.84
	FPZ	0	1.17	0.75	0.62	0.35	0.99	1.70	2.99	0.52	1.56	0.66	1.25	1.35
	EDA	0	0	0	1.00	1.98	3.10	4.72	4.81	4.80	6.42	10.06	13.38	15.30
	PZ	3803.8	3813.1	3814.3	3781.1	3781.8	3731.1	3687.0	3706.0	3716.0	3707.3	3687.8	3594.9	3675.9
	HEP	0	0	0	0	0	0	0	0	0	0	0	0	0
	1-MPZ	0	0	0	0	0	0	0	0	0	0	0	0	0
	1-EPZ	0	0	0	0	0.39	0.78	1.50	1.17	1.27	1.76	2.37	3.16	3.86
	1,4-DMPZ	0	0	0	0.62	1.09	2.40	4.57	2.29	2.72	5.22	4.96	7.71	9.50
	AEP	0	0	0	0	0	0	0	0	0	0	0	0	0
	CO_2	0	0	0	0	0	0	0	0	0	0	0	0	0
	SD_{CO2}	0	0	0	0	0	0	0	0	0	0	0	0	0
	Alk	2693.5	2668.2	2746.0	2674.2	2669.7	2678.7	2608.5	2694.0	2705.0	2693.3	2676.0	2678.4	2620.7
	SD_{Alk}	14.94	11.72	86.50	12.70	27.25	6.27	101.06	73.00	31.37	25.84	28.88	2.21	2.28
Hydrolyzed Samples (mmol/kg)	Gly	0.04	0.36	0.27	0.18	0.20	0.26	0.32	0.37	0.14	0.17	0.21	0.24	0.51
	Ace	0.23	0.59	0.38	0.35	0.29	0.45	0.85	0.34	0.44	0.57	0.68	0.77	0.39
	Form	0.36	2.14	1.26	1.31	0.72	1.53	3.13	1.22	1.33	1.81	1.75	2.06	1.51
	Oxa	0	0	0	0	0	0	0	0	0	0	0	0	0
	Sulf	0	0	0	0	0	0	0	0	0	0	0	0	0
	Cl^-	0.09	0.07	0.14	0.18	0.13	0.09	0.08	0.08	0.26	0.11	0.15	0.08	0.08
	NH_4^+	NT	NT	NT	NT	NT	NT	NT	NT	NT	NT	NT	NT	50.1
	FPZ	NT	NT	NT	NT	NT	NT	NT	NT	NT	NT	NT	NT	0
	EDA	0	0.90	0.46	1.30	1.17	4.54	7.79	7.68	7.12	7.54	13.39	16.87	17.42
	PZ	4384.2	4207.7	3802.9	4337.4	2959.2	4185.3	4296.9	4216.9	3790.2	2584.4	3306.3	5230.0	3517.1
	HEP	NT	NT	NT	NT	NT	NT	NT	NT	NT	NT	NT	NT	0
	1-MPZ	NT	NT	NT	NT	NT	NT	NT	NT	NT	NT	NT	NT	0
	1-EPZ	NT	NT	NT	NT	NT	NT	NT	NT	NT	NT	NT	NT	3.75
	1,4-DMPZ	NT	NT	NT	NT	NT	NT	NT	NT	NT	NT	NT	NT	0
	AEP	NT	NT	NT	NT	NT	NT	NT	NT	NT	NT	NT	NT	13.02

Table D.38: Tabulated Experimental Data for TE38 (2 m *trans*-2,5-Dimethylpiperazine (t2,5-DMPZ), 0.3 mole CO_2 per mole alkalinity initially, 150 °C)

	Time (wk)	0	1.9	4.1	6.0	10.0	14.0	14.0	18.0	22.0	26.0	30.0	0	1.9
Original Samples (mmol/kg)	Gly	0	0	0	0	0	0	0	0	0	0	0	0	0
	Ace	0.82	7.68	10.87	15.27	19.14	27.15	24.49	27.39	33.09	35.29	36.54	0.82	7.68
	Form	0.34	36.11	51.30	79.84	91.73	101.84	99.51	122.80	117.59	138.95	139.77	0.34	36.11
	Oxa	0.02	0.09	0.06	0.04	0.03	0.03	0.03	0.03	0.02	0.01	0.01	0.02	0.09
	Sulf	0.11	0.10	0.09	0.09	0.09	0.09	0.11	0.08	0.12	0.09	0.06	0.11	0.10
	Cl^-	0.03	0.05	0.05	0.02	0.06	0.06	0.07	0.04	0.05	0.07	0.03	0.03	0.05
	NH_4^+	0	15.42	30.37	35.45	62.83	76.35	72.06	97.92	101.74	133.74	136.81	0	15.42
	FPZ	0	0	0	0	0	0	0	0	0	0	0	0	0
	EDA	0.54	9.93	10.27	10.05	9.88	12.42	11.38	10.89	13.70	12.89	12.76	0.54	9.93
	t2,5-DMPZ	1438.0	1392.5	1358.1	1334.4	1311.2	1249.4	1285.7	1266.2	1231.4	1206.9	1200.7	1438.0	1392.5
	HEP	0	0	0	0	0	0	0	0	0	0	0	0	0
	1-MPZ	0	0	0	1.58	2.71	10.16	8.81	9.58	13.60	13.94	12.60	0	0
	1-EPZ	0	0	0	0	0	0	0	0	0	0	0	0	0
	1,4-DMPZ	0	0	0	1.38	2.38	8.91	7.73	8.40	11.93	12.23	11.06	0	0
	AEP	0	0	0	0	0	0	0	0	0	0	0	0	0
	CO_2	923.44	778.50	925.94	774.09	746.57	730.11	742.54	751.04	689.50	727.69	701.96	923.44	778.50
	SD_{CO2}	2.27	3.69	34.65	2.56	4.51	3.80	3.53	4.77	0.80	33.35	2.69	2.27	3.69
	Alk	1610.6	1586.8	1572.8	1583.1	1499.0	1421.8	1453.5	1396.2	1396.2	1365.0	1369.3	1610.6	1586.8
	SD_{Alk}	NA	NA	NA	NA	NA	NA	NA	NA	NA	NA	NA	NA	NA
Hydrolyzed Samples (mmol/kg)	Gly	0	0	0	0	0	0	0	0	0	0	0	0	0
	Ace	1.47	10.32	13.84	18.32	17.44	30.41	28.23	30.77	36.53	38.46	40.03	1.47	10.32
	Form	0.72	41.14	57.48	90.33	82.19	115.19	115.03	141.51	136.29	160.14	166.53	0.72	41.14
	Oxa	0.02	0.15	0.07	0.05	0.04	0.05	0.05	0.05	0.03	0.03	0.03	0.02	0.15
	Sulf	0.16	0.15	0.13	0.21	0.08	0.18	0.14	0.14	0.19	0.17	0.13	0.16	0.15
	Cl^-	0.12	0.08	0.13	0.14	0.08	0.12	0.13	0.12	0.10	0.16	0.08	0.12	0.08
	NH_4^+	0	0	0	77.12	65.76	99.52	95.36	120.15	114.63	159.15	151.96	0	0
	FPZ	0	0	0	0	0	0	0	0	0	0	0	0	0
	EDA	1.28	11.76	11.70	11.71	8.78	14.27	13.33	12.17	15.10	13.71	14.09	1.28	11.76
	t2,5-DMPZ	1445.1	1402.2	1364.0	1336.9	1049.5	1272.2	1306.4	1270.9	1240.7	1224.6	1213.5	1445.1	1402.2
	HEP	0	0	0	0	0	0	0	0	0	0	0	0	0
	1-MPZ	0	0	1.38	5.13	4.56	10.51	8.52	9.74	14.61	14.81	14.62	0	0
	1-EPZ	0	0	0	0	0	0	0	0	0	0	0	0	0
	1,4-DMPZ	0	0	1.21	4.50	4.00	9.22	7.48	8.54	12.82	12.99	12.82	0	0
	AEP	0	0	0	0	0	0	0	0	0	0	0	0	0

Table D.39: Tabulated Experimental Data for TE39 (4 m PZ + 4 m *trans*-2,5-Dimethylpiperazine (t2,5-DMPZ), 0.3 mole CO_2 per mole alkalinity initially, 150 °C)

	Time (wk)	0	1.0	1.9	4.1	6.0	10.0	14.0	14.0	18.0	22.0	26.0	30.0	0
Original Samples (mmol/kg)	Gly	0	0	0	0	0	0	0	0	0	0	0	0	0
	Ace	0	1.28	1.00	2.81	3.75	5.53	7.21	7.42	9.20	10.66	12.24	13.16	0
	Form	0	26.34	40.27	83.39	102.74	108.96	127.17	137.77	155.79	157.67	185.62	155.30	0
	Oxa	0	0.26	0.03	0.03	0.02	0.04	0.03	0.02	0.01	0.01	0.05	0.03	0
	Sulf	0.07	0.17	0.09	0.19	0.13	0.12	0.11	0.12	0.09	0.12	0.12	0.09	0.07
	Cl^-	0.02	0.10	0.06	0.07	0.07	0.05	0.03	0.06	0.06	0.07	0.08	0.04	0.02
	NH_4^+	0	12.45	56.01	120.87	165.55	227.22	282.77	285.18	334.08	374.43	451.49	457.76	0
	FPZ	0	42.74	69.74	144.58	184.45	214.78	256.93	265.15	307.55	329.76	337.24	392.06	0
	EDA	0	1.84	4.06	6.40	9.75	12.38	14.73	15.57	19.86	22.01	25.81	24.60	0
	PZ + t2,5-DMPZ	3698.4	3663.3	3484.1	3372.8	3305.7	3173.3	3052.6	3008.9	2934.9	2785.5	2711.6	2670.7	3698.4
	HEP	0	0	0	0	0	0	0	0	0	0	0	0	0
	1-MPZ	0	0	0	0.70	1.25	1.80	2.54	2.42	3.45	3.84	4.29	4.83	0
	1-EPZ	0	0.37	0.86	3.32	5.32	8.98	13.61	14.08	19.47	23.72	31.57	31.63	0
	1,4-DMPZ	0	0	0	0.61	1.10	1.58	2.23	2.12	3.03	3.37	3.76	4.24	0
	AEP	0	0.19	0.26	0.35	0.47	0.64	0.93	0.85	1.13	1.34	4.42	4.41	0
	CO_2	2495.7	2429.8	2348.4	2262.9	2227.6	2236.8	2168.1	2030.5	2009.3	2069.3	1898.1	1914.1	2495.7
	SD_{CO2}	32.87	14.18	8.35	2.79	9.99	12.85	17.09	20.23	17.21	86.17	28.65	13.18	32.87
	Alk	4098.0	4064.8	3830.4	3844.9	3754.9	3675.3	3630.4	3523.6	3543.3	3396.5	3420.6	3310.3	4098.0
	SD_{Alk}	NA	NA	NA	NA	NA	NA	NA	NA	NA	NA	NA	NA	NA
Hydrolyzed Samples (mmol/kg)	Gly	0	0	0	0	0	0	0	0	0	0	0	0	0
	Ace	0.14	2.23	1.92	4.67	6.94	8.76	11.41	12.28	11.31	14.57	19.87	21.06	0.14
	Form	0	56.84	85.33	173.80	221.26	254.79	310.65	339.19	384.32	393.30	487.07	498.40	0
	Oxa	0	0.48	0.05	0.05	0.04	0.06	0.07	0.05	0.05	0.06	0.09	0.08	0
	Sulf	0.13	0.13	0.12	0.13	0.11	0.11	0.10	0.14	0.11	0.09	0.14	0.11	0.13
	Cl^-	0.08	0.12	0.09	0.12	0.08	0.13	0.07	0.10	0.10	0.11	0.21	0.32	0.08
	NH_4^+	0	0	76.36	138.63	174.38	217.62	275.54	284.15	296.85	322.20	410.71	402.30	0
	FPZ	0	0	0	0	0	0	0	0	0	0	0	0	0
	EDA	0	3.60	5.15	9.12	11.60	14.48	16.65	17.74	17.42	21.03	27.68	26.99	0
	PZ + t2,5-DMPZ	3682.4	3646.9	3574.9	3429.9	3370.6	3282.6	3182.7	3159.0	2552.3	3053.5	2861.9	2849.0	3682.4
	HEP	0	0	0	0	0	0	0	0	0	0	0	0	0
	1-MPZ	0	0	0	0	1.12	1.81	2.35	2.18	2.54	3.14	4.05	4.10	0
	1-EPZ	0	0.45	1.17	3.87	6.27	9.95	15.09	15.86	17.57	21.47	34.80	35.75	0
	1,4-DMPZ	0	0	0	0	0.99	1.59	2.06	1.92	2.23	2.75	3.56	3.59	0
	AEP	0	0.25	0.28	0.32	0.49	0.65	0.97	0.96	0.94	1.16	5.05	5.08	0

Table D.40: Tabulated Experimental Data for TE40 (3.9 m PZ + 3.9 m 1-Methylpiperazine (1-MPZ) + 0.2 m 1,4-Dimethylpiperazine (1,4-DMPZ), 0.3 mole CO_2 per mole alkalinity initially, 150 °C)

	Time (wk)	0	1.0	1.9	4.1	6.0	10.0	14.0	14.0	18.0	22.0	26.0	30.0
Original Samples (mmol/kg)	Gly	0.34	0.21	0.21	0.22	0.16	0.14	0.15	0.16	0.12	0.09	0.07	0.07
	Ace	0	0	0	0	0	0	0	0	0	0	0	0
	Form	0.30	4.48	7.68	10.78	25.40	18.20	29.86	17.72	38.93	47.77	50.54	54.44
	Oxa	0.02	0.05	0.05	0.06	0.03	0.13	0.06	0.05	0.05	0.03	0.03	0.03
	Sulf	0.13	0.13	0.14	0.15	0.13	0.19	0.15	0.15	0.13	0.15	0.13	0.12
	Cl^-	0.05	0.06	0.06	0.06	0.07	0.06	0.05	0.07	0.07	0.07	0.08	0.05
	NH_4^+	0	0	0	0	18.03	27.31	36.14	22.47	48.93	53.55	66.79	77.96
	FPZ	0	13.57	22.46	33.05	71.86	76.31	109.62	44.26	139.55	164.84	185.62	217.30
	EDA	0	0	0	0.24	0.61	0.72	1.55	1.12	2.61	2.82	4.09	3.61
	PZ	1985.3	1991.8	2006.1	1994.8	1998.4	1954.4	1937.9	2061.2	1918.0	1892.0	1863.8	1822.7
	HEP	0	0	0	0	0	0	0	0	0	0	0	0
	1-MPZ	1972.9	1910.4	1877.8	1803.2	1716.1	1631.7	1531.6	1783.9	1476.5	1421.0	1397.4	1360.0
	1-EPZ	0	0	0	0	0	0	14.19	0	12.58	12.47	19.30	20.39
	1,4-DMPZ	125.95	143.82	161.77	189.65	221.32	263.16	268.48	247.71	283.46	285.23	287.66	278.15
	AEP	0	0	0	0	0	1.09	3.33	0	4.14	8.17	16.44	14.48
	CO_2	2386.9	2331.1	2421.2	2540.6	2362.9	2869.8	2556.5	1683.9	2401.7	2207.3	2167.6	2097.8
	SD_{CO2}	37.81	35.13	6.65	12.24	14.37	17.83	3.69	15.69	39.41	35.84	18.61	3.64
	Alk	4011.2	3991.3	3997.0	3937.8	3892.6	NT	NT	4049.3	3695.3	3675.0	3692.3	3619.1
	SD_{Alk}	8.58	27.27	19.12	0.36	4.03	NT	NT	13.67	43.10	1.44	26.94	34.06
Hydrolyzed Samples (mmol/kg)	Gly	0	0.54	2.51	0.81	2.25	0.32	3.90	11.48	3.97	3.96	5.59	5.93
	Ace	0	0	0	0.19	0.38	1.47	1.25	1.87	1.53	2.20	2.71	3.36
	Form	0.53	12.92	25.44	37.13	85.39	75.30	117.38	54.19	145.78	181.14	208.87	242.38
	Oxa	0.08	0.23	0.17	0.24	0.12	0.28	0.33	0.32	0.29	0.15	0.23	0.18
	Sulf	0.17	0.21	0.19	0.16	0.16	0.18	0.24	0.37	0.44	0.30	0.18	0.16
	Cl^-	0.13	0.11	0.13	0.10	0.16	0.17	0.28	0.91	1.27	0.71	0.18	0.16
	NH_4^+	0	0	0	0	0	0	0	0	0	0	0	0
	FPZ	0	0	0	0	0	0	0	0	0	0	0	0
	EDA	0	0	0.80	0.71	1.67	2.02	3.09	6.10	4.47	5.65	7.78	7.47
	PZ	1752.1	1060.0	1708.5	1771.2	2000.8	1950.9	1968.7	2068.5	1777.2	1960.0	1905.9	1911.1
	HEP	0	0	0	0	0	0	0	0	0	0	0	0
	1-MPZ	1705.5	937.6	1562.1	1549.5	1690.1	1586.2	1519.6	1750.8	1319.4	1450.3	1395.1	1377.4
	1-EPZ	0	0	0	0	0	0	14.95	11.41	17.50	17.29	21.04	22.64
	1,4-DMPZ	111.48	70.67	137.23	164.42	214.07	243.85	265.92	241.55	250.84	281.06	280.43	278.90
	AEP	0	0	0	0	1.28	1.75	1.85	0.93	3.22	10.10	14.22	15.84

Table D.41: Tabulated Experimental Data for TE41 (3.75 m PZ + 3.75 m 1-Methylpiperazine (1-MPZ) + 0.5 m 1,4-Dimethylpiperazine (1,4-DMPZ), 0.3 mole CO_2 per mole alkalinity initially, 150 °C)

	Time (wk)	0	1.0	1.9	6.0	10.0	14.0	14.0	14.0	18.0	22.0	26.0	30.0
Original Samples (mmol/kg)	Gly	0.30	0.19	0.23	0.13	0.10	0.09	0.09	0.11	0.08	0.05	0.04	0.04
	Ace	0	0	0	0.54	0.82	1.22	1.31	1.10	1.43	1.81	2.55	3.16
	Form	0.31	5.98	11.23	23.77	38.70	48.64	50.78	41.39	52.59	57.82	68.17	72.18
	Oxa	0.02	0.07	0.06	0.04	0.03	0.02	0.04	0.07	0.04	0.03	0.03	0.05
	Sulf	0.12	0.12	0.13	0.13	0.13	0.92	0.19	0.15	0.11	0.20	0.14	0.13
	Cl^-	0.03	0.03	0.10	0.06	0.05	0.08	0.05	0.10	0.07	0.06	0.06	0.06
	NH_4^+	0	0	0	16.28	23.47	42.98	49.41	39.06	71.29	88.00	91.12	98.99
	FPZ	0	19.91	32.58	73.15	122.13	155.93	159.29	128.78	173.22	197.13	242.74	269.59
	EDA	0	0	0	0	0.49	0.79	0.84	0.88	1.46	1.50	2.23	2.65
	PZ	1937.8	1933.3	1910.4	1906.6	1856.1	1821.4	1809.2	1861.8	1774.8	1740.3	1661.6	1594.2
	HEP	0	0	0	0	0	0	0	0	0	0	0	0
	1-MPZ	1853.1	1801.3	1761.2	1685.5	1577.3	1527.4	1508.9	1559.8	1470.9	1444.2	1374.4	1323.5
	1-EPZ	0	0	0	0	14.13	16.74	18.88	17.16	21.77	22.46	23.85	29.92
	1,4-DMPZ	296.20	302.96	308.28	333.48	339.91	341.70	339.76	351.79	340.58	345.17	324.08	317.45
	AEP	0	0	0	0	3.18	5.37	4.62	3.92	10.16	13.92	16.86	18.13
	CO_2	2472.6	2495.6	2404.7	2386.4	2314.2	2236.2	2231.8	2149.1	2208.4	2078.9	2057.4	1981.2
	SD_{CO2}	25.09	34.59	12.10	10.12	9.37	15.11	19.41	18.79	14.69	13.93	11.37	17.98
	Alk	4008.4	3995.3	3926.9	3880.4	3810.7	3744.1	3736.4	3817.4	3699.1	3638.1	3577.9	3488.3
	SD_{Alk}	23.75	11.45	3.20	2.76	4.89	15.82	26.49	17.39	15.41	24.68	5.53	4.27
Hydrolyzed Samples (mmol/kg)	Gly	0	0.43	1.88	2.13	2.55	2.81	2.89	4.58	3.77	4.29	4.21	4.94
	Ace	0	0.37	0	0.99	1.43	2.04	2.12	1.11	1.26	2.97	4.76	5.43
	Form	3.07	22.05	31.90	85.09	139.16	180.39	183.81	133.27	184.62	228.53	299.50	346.97
	Oxa	0.08	0.19	0.29	0.17	0.17	0.17	0.24	0.49	0.35	0.55	0.22	0.25
	Sulf	0.17	0.16	0.24	0.20	0.16	0.98	0.19	0.15	0.25	0.42	0.16	0.09
	Cl^-	0.18	0.15	0.16	0.24	0.11	0.16	0.18	0.18	0.92	0.15	0.14	0.15
	NH_4^+	0	0	0	0	0	0	0	0	0	0	0	0
	FPZ	0	0	0	0	0	0	0	0	0	0	0	0
	EDA	0	0	0	1.11	2.35	3.09	2.90	2.06	2.27	5.45	6.10	7.79
	PZ	2090.1	1873.2	1027.9	1916.2	1878.1	1857.1	1794.2	1171.0	1070.8	1807.1	1775.0	1720.9
	HEP	0	0	0	0	0	0	0	0	0	0	0	0
	1-MPZ	2069.3	1753.1	889.5	1700.7	1613.3	1544.4	1484.9	926.1	833.6	1478.9	1431.4	1387.9
	1-EPZ	0	0	0	0	0	18.71	18.20	9.54	10.25	23.71	27.67	31.59
	1,4-DMPZ	318.7	294.7	161.9	333.2	336.1	340.2	329.8	212.3	196.7	341.2	328.4	321.4
	AEP	0	0	0	0	2.83	4.58	3.59	0.81	1.54	12.53	16.10	21.08

Table D.42A: Tabulated Experimental Data for TE42A (8 m PZ, 0.3 mole $^{13}CO_2$ per mole alkalinity initially, 175 °C)

	Time (wk)	0	2.0	5.9
Original Samples (mmol/kg)	Gly	0	0	0
	Ace	0	0	10.22
	Form	0.27	127.24	153.87
	Oxa	0.01	0.21	0.03
	Sulf	0.18	0.20	0.28
	Cl^-	0.02	0	0
	FPZ	0	200.07	307.10
	EDA	0	54.22	64.90
	PZ	2891.5	2285.5	1680.8
	CO_2	NT	NT	NT
	SD_{CO2}	NT	NT	NT
	Alk	NT	NT	NT
	SD_{Alk}	NT	NT	NT
Hydrolyzed Samples (mmol/kg)	Gly	0	0	0
	Ace	0	6.87	16.20
	Form	0.42	255.25	458.15
	Oxa	0.02	0.27	0.15
	Sulf	0.26	0.26	0.24
	Cl^-	0.09	0.26	0
	FPZ	0	0	0
	EDA	0.91	53.56	71.83
	PZ	2894.5	2406.2	1844.9

Table D.42B: Tabulated Experimental Data for TE42B (8 m PZ, 0.3 mole CO_2 per mole alkalinity initially, 175 °C)

	Time (wk)	0	2.0	5.9
Original Samples (mmol/kg)	Gly	0	0	0
	Ace	0	5.38	8.22
	Form	0.21	112.44	135.60
	Oxa	0	0.19	0.03
	Sulf	0.24	0.20	0.19
	Cl^-	0	0	0
	FPZ	0	210.57	280.61
	EDA	0	52.80	66.51
	PZ	2979.1	2412.9	1878.5
	CO_2	NT	NT	NT
	SD_{CO2}	NT	NT	NT
	Alk	NT	NT	NT
	SD_{Alk}	NT	NT	NT
Hydrolyzed Samples (mmol/kg)	Gly	0	0	0
	Ace	0	6.81	12.21
	Form	0.22	294.80	402.94
	Oxa	0	0.27	0.16
	Sulf	0.02	0.32	0.25
	Cl^-	0	0.25	0
	FPZ	0	0	0
	EDA	0	55.42	73.16
	PZ	3019.8	2555.4	2054.2

Table D.43: Tabulated Experimental Data for TE43 (8 m PZ, unloaded, 150 °C)

	Time (wk)	0	1.0	2.0	6.3	8.0	10.0	14.0	14.0	14.0	17.9	22.1	25.9	30.0
Original Samples (mmol/kg)	Gly	0	0.19	0.42	0.21	0.15	0.21	0.17	0.14	0.15	0.14	0.12	0.23	0.17
	Ace	0	0	0	0	0.20	0.28	0.32	0.36	0.30	0.55	0.37	0.33	0.12
	Form	0	0.41	0.59	1.24	1.25	1.51	1.51	1.86	1.51	1.84	2.06	1.28	0.57
	Oxa	0.03	0.02	0.04	0.07	0.08	0.12	0.09	0.06	0.06	0.05	0.04	0.03	0.01
	Sulf	0.12	0.09	0.14	0.15	0.15	0.19	0.14	0.14	0.12	0.12	0.17	0.10	0.18
	Cl^-	0	0.02	0.03	0	0	0	0	0	0	0	0	0	0
	NH_4^+	0	1.00	12.23	1.66	1.74	2.50	3.54	3.82	4.84	5.27	5.74	4.39	0
	FPZ	0	0	0	0	0.26	0.17	0.35	0.72	0.33	0.65	0.22	0.60	0
	EDA	0	0	0.07	0.21	0.62	1.05	0.66	0.64	0.75	1.18	0.94	1.03	1.34
	PZ	4355.7	4342.8	4396.5	4384.8	4350.6	4383.5	4378.5	4367.7	4368.2	4332.9	4385.0	4350.7	4359.9
	HEP	0	0	0	0	0	0	0	0	0	0	0	0	0
	1-MPZ	0	0	0	0	0	0	0	0	0	0	0	0	0
	1-EPZ	0	0	0	0	0	0	0	0	0	0	0	0	0
	1,4-DMPZ	0	0	0	0	0	0	0	0	0	0	0	0	0
	AEP	0	0	0	0	0	0	0.19	0.44	0.24	0.53	0.18	0.27	0
	Alk	4826.0	4799.5	4806.4	5145.1	4826.8	4853.1	4798.6	4818.3	4755.0	4866.9	4904.4	4805.6	4816.1
	SD_{Alk}	NA	NA	NA	NA	NA	NA	NA	NA	NA	NA	NA	NA	NA
Hydrolyzed Samples (mmol/kg)	Gly	0.05	0.37	0.67	1.06	0.99	1.19	1.57	1.03	1.20	1.95	2.02	2.20	1.76
	Ace	0.08	0.10	0.09	0.13	0.32	0.23	0.28	0.39	0.31	0.29	0.39	0.26	0.14
	Form	0.28	0.74	1.01	1.77	1.95	2.14	2.13	2.38	2.12	2.20	3.19	2.17	0.97
	Oxa	0.01	0.05	0.11	0.23	0.22	0.23	0.22	0.20	0.20	0.17	0.16	0.13	0.03
	Sulf	0.24	0.19	0.23	0.20	0.28	0.38	0.29	0.26	0.20	0.32	0.31	0.24	0.20
	Cl^-	0	0	0	0	0	0	0	0	0	0	0	0	0
	NH_4^+	0	0	0	0	0	0	0	0	0	0	0	0	0
	FPZ	0	0	0	0	0	0	0	0	0	0	0	0	0
	EDA	0	0.26	0.19	0.43	1.53	1.76	1.46	1.11	1.25	2.27	2.34	1.87	1.97
	PZ	4339.5	4375.8	4398.4	4365.0	4362.1	4401.8	4305.0	4308.6	4271.9	4286.3	4246.5	4261.8	4277.4
	HEP	0	0	0	0	0	0	0	0	0	0	0	0	0
	1-MPZ	0	0	0	0	0	0	0	0	0	0	0	0	0
	1-EPZ	0	0	0	0	0	0	0	0	0	0	0	0	0
	1,4-DMPZ	0	0	0	0	0	0	0	0	0	0	0	0	0
	AEP	0	0	0	0	0	0.08	0.19	0.47	0.27	0.50	0.33	0.26	0

Table D.44: Tabulated Experimental Data for TE44 (8 m PZ, 0.3 mole CO_2 per mole alkalinity initially, 165 °C)

	Time (wk)	0	1.0	2.0	3.0	4.0	5.0	6.0	6.0	6.0	9.3	12.0	14.9	20.0
Original Samples (mmol/kg) (Metals are in units of µg/g)	Gly	0.32	0.32	0.30	0.24	0.24	0.24	0.18	0.19	0.21	0.18	0.12	1.03	0
	Ace	0	0	0	0	1.21	0.63	1.13	1.14	0.76	1.97	7.57	15.59	21.12
	Form	0.07	11.96	14.74	25.81	26.69	39.92	47.17	49.09	42.93	58.39	88.10	107.31	107.47
	Oxa	0.05	0.03	0.02	0.02	0.01	0.02	0.02	0.02	0.02	0.02	0.02	0.02	0
	Sulf	0.14	0.16	0.14	0.16	0.14	0.15	0.15	0.12	0.15	0.15	0.13	0.12	0.39
	Cl^-	0.05	0.06	0.05	0.07	0.07	0.05	0.06	0.04	0.06	0.06	0.06	0.05	0.05
	NH_4^+	3.43	17.99	1.49	27.19	40.42	62.89	92.52	85.55	89.85	140.04	237.07	392.88	495.57
	FPZ	0	40.99	55.77	69.49	100.25	137.02	165.65	173.15	159.32	221.14	311.10	394.61	557.36
	EDA	0	8.23	11.47	12.44	17.95	25.97	30.80	31.61	29.32	42.97	55.60	65.61	52.84
	PZ	3883.5	3987.3	4229.6	3600.4	3982.3	3821.6	3791.8	3797.1	3883.2	3561.9	3305.6	2819.2	2501.4
	HEP	0	0	0	0	0	0	0	0	0	11.45	14.55	15.57	61.16
	1-MPZ	0	0	0	0	1.43	1.79	2.24	2.24	1.82	3.29	4.62	4.77	20.53
	1-EPZ	0	0.83	0.75	1.81	3.47	3.25	6.35	6.87	6.33	12.58	22.62	34.56	54.44
	1,4-DMPZ	0	0	0	0	0	0	0	0	0	0	0	0	0
	AEP	0	2.74	3.72	13.36	10.45	17.35	26.20	25.23	21.49	43.93	72.32	102.48	118.27
	2-Imid	0	7.88	11.59	21.38	22.70	32.82	40.97	42.15	38.21	54.33	81.20	94.44	109.04
	CO_2	2745.1	2699.2	2583.7	2517.4	2441.4	2372.7	2437.3	2292.4	2387.2	2179.2	2213.5	1948.1	1857.4
	SD_{CO2}	10.69	25.11	18.61	9.89	26.17	10.59	4.11	76.71	290.70	150.88	129.13	70.09	64.44
	Alk	4134.3	4055.3	4032.3	3977.7	3970.7	3899.9	3839.5	3839.8	3868.8	3725.3	3537.1	3326.3	3165.5
	SD_{Alk}	12.56	9.55	22.54	2.88	10.36	3.26	1.68	13.93	1.65	3.59	5.50	8.12	10.22
	Fe^{2+}	0	48.97	21.61	40.15	36.05	36.13	40.92	43.36	46.14	NT	69.23	107.57	106.66
	Ni^{2+}	0	33.91	24.75	47.28	57.71	72.67	72.74	74.69	74.96	NT	156.98	267.18	240.23
	Cr^{3+}	0	34.51	26.68	50.99	28.96	41.37	23.28	57.10	34.00	NT	46.83	32.72	56.20
Hydrolyzed Samples (mmol/kg)	Gly	0.63	0.83	0.85	0.94	1.23	1.27	1.17	0.60	0.52	0.85	1.08	1.40	0.52
	Ace	0	0.85	1.36	2.22	6.01	4.07	5.95	6.63	6.02	10.77	17.23	26.97	35.54
	Form	0.21	35.53	42.95	76.01	79.86	117.56	138.98	145.26	151.62	184.23	297.59	393.99	548.86
	Oxa	0	0.05	0.05	0.08	0.07	0.07	0.07	0.10	0.08	0.13	0.13	0.11	0
	Sulf	0.60	0.21	0.22	0.19	0.18	0.14	0.16	0.15	1.34	0.19	0.20	0.17	0.31
	Cl^-	0.03	0.06	0.07	0.06	0.06	0	0.09	0.08	1.21	0.16	0.19	0.12	0.05
	NH_4^+	0	36.72	43.28	29.41	32.47	32.02	107.82	104.53	60.88	166.26	254.93	379.83	501.52
	FPZ	0	0	0	0	0	0	0	0	0	0	0	0	0
	EDA	0	9.74	12.09	20.43	21.95	30.08	31.14	35.90	34.65	46.01	61.43	77.16	60.30
	PZ	4230.5	4166.0	4118.5	4075.4	4058.4	3967.5	3830.7	3844.7	2596.8	3626.3	3374.4	3022.7	2797.4
	HEP	0	0	0	0	9.90	7.60	10.68	10.66	11.02	13.82	13.78	15.56	58.88
	1-MPZ	0	0	0	0.96	1.24	1.80	2.43	2.66	1.96	2.34	4.67	4.56	20.28
	1-EPZ	0	0	1.43	2.18	3.52	4.86	6.35	6.92	6.67	8.00	27.80	41.64	58.01
	1,4-DMPZ	0	0	0	0	0	0	0	0	0	0	0	0	0
	AEP	0	2.75	4.39	8.84	11.16	21.32	26.66	25.68	26.45	44.93	74.37	108.99	130.51

Table D.45: Tabulated Experimental Data for TE45 (8 m PZ, 0.4 mole CO_2 per mole alkalinity initially, 165 °C)

	Time (wk)	0	1.0	2.0	3.0	4.0	5.0	6.0	6.0	6.0	9.3	12.0	14.9	20.0
Original Samples (mmol/kg) (Metals are in units of µg/g)	Gly	0.33	0.33	0.28	0.23	0.21	0.20	0.15	0.17	0.16	0.13	0.10	0.11	0
	Ace	0	0	0.15	0.61	1.33	1.77	2.85	2.32	2.80	11.54	14.41	18.58	26.55
	Form	0.09	12.74	26.28	36.76	52.71	51.48	73.33	61.98	67.04	93.13	97.00	105.09	107.56
	Oxa	0	0.01	0.02	0.02	0.02	0.01	0.03	0.02	0.02	0.03	0.02	0.01	0
	Sulf	0.13	0.13	0.10	0.13	0.13	0.14	0.06	0.11	0.11	0.13	0.12	0.12	0.16
	Cl^-	0.09	0.05	0.05	0.03	0.27	0.05	0.01	0.04	0.01	0.05	0.04	0.03	0.02
	NH_4^+	1.70	20.24	32.63	61.62	101.88	110.25	158.41	122.62	139.76	258.96	312.14	402.35	601.28
	FPZ	0	64.68	124.22	171.81	225.15	227.70	317.13	271.53	279.33	386.03	421.17	436.11	539.02
	EDA	0	10.30	18.18	26.69	37.92	38.24	49.63	43.17	47.48	59.50	63.57	65.30	60.38
	PZ	4225.4	4063.9	3925.5	3800.8	3607.0	3558.7	3295.0	3444.5	3456.0	3067.0	2893.9	2658.5	2173.1
	HEP	0	0	0	0	0	7.51	9.47	9.97	11.06	13.95	7.18	15.70	62.11
	1-MPZ	0	0	1.53	2.71	3.67	3.43	4.80	5.56	4.76	5.68	5.04	5.45	20.93
	1-EPZ	0	1.92	1.36	5.08	8.07	9.01	15.73	11.80	14.14	23.52	27.51	34.97	63.86
	1,4-DMPZ	0	0	0	0	0	0	0	0	0	0	0	0	0
	AEP	0	3.28	7.40	14.25	25.73	29.14	47.19	36.78	42.24	70.42	81.41	97.47	113.71
	2-Imid	0	12.56	25.67	40.72	57.01	59.92	83.54	71.83	77.08	102.75	107.65	129.94	131.81
	CO_2	2877.1	3000.2	2716.7	2837.3	2721.5	2681.5	2564.2	2736.2	2682.1	2546.7	2268.2	2426.8	2141.4
	SD_{CO2}	223.93	26.80	27.69	18.41	79.23	23.48	52.83	60.40	22.71	31.37	48.34	21.01	28.37
	Alk	3988.8	3918.2	3881.9	3762.1	3715.1	3615.9	3596.1	3646.0	3613.4	3419.3	3289.6	3229.7	2785.1
	SD_{Alk}	2.79	7.47	3.16	35.73	44.84	16.53	19.56	14.01	2.47	10.96	19.04	52.03	16.79
	Fe^{2+}	0	41.47	45.53	48.52	85.56	54.55	105.21	57.85	111.10	148.83	119.24	NT	223.42
	Ni^{2+}	0	50.33	102.70	92.90	118.36	71.84	117.82	90.66	99.86	138.76	160.35	NT	283.52
	Cr^{3+}	0	51.94	141.77	64.80	135.42	96.43	154.98	114.09	128.50	158.29	125.85	NT	184.80
Hydrolyzed Samples (mmol/kg)	Gly	0.77	0.39	0.33	0.31	0.27	0.14	0.21	0.23	0.21	0.17	0.02	0.08	0
	Ace	0	1.11	4.39	3.88	7.18	7.37	12.46	9.61	10.45	22.53	24.17	29.99	36.14
	Form	0.49	46.86	93.73	131.43	189.89	186.93	276.18	225.98	245.27	369.49	425.03	480.63	584.56
	Oxa	0.01	0.04	0.03	0.04	0.05	0.03	0.08	0.04	0.05	0.06	0.05	0.04	0
	Sulf	0.17	0.20	0.17	0.18	0.19	0.17	0.17	0.18	0.18	0.16	0.58	0.20	0.17
	Cl^-	0.04	0.08	0.05	0.05	0.06	0.05	0.05	0.04	0.05	0.04	0.06	0.03	0.04
	NH_4^+	0	40.76	62.63	92.19	129.40	134.25	210.28	162.95	191.51	280.99	328.60	413.94	608.52
	FPZ	0	0	0	0	0	0	0	0	0	0	0	0	0
	EDA	0	12.26	17.18	27.45	37.60	39.53	54.85	44.30	53.96	63.90	67.93	71.35	72.03
	PZ	4123.5	4051.9	3964.9	3852.7	3738.7	3687.0	3505.9	3596.7	3543.6	3271.6	3148.4	2916.8	2666.7
	HEP	0	0	0	0	0	0	2.90	3.14	3.19	9.80	5.50	9.62	59.11
	1-MPZ	0	0	0	4.14	3.48	3.01	3.26	5.27	2.84	6.39	6.62	8.13	25.61
	1-EPZ	0	0	3.61	7.31	10.01	10.53	15.10	14.41	16.11	25.42	29.39	40.39	67.85
	1,4-DMPZ	0	0	0	0	0	0	0	0	0	0	0	0	0
	AEP	0	0	6.73	14.85	25.99	29.77	51.16	40.05	44.03	78.73	91.41	106.29	137.26

Table D.46: Tabulated Experimental Data for TE46 (8 m PZ, unloaded, 165 °C)

	Time (wk)	0	1.0	2.0	4.0	6.0	6.0	14.9	20.0
Original Samples (mmol/kg)	Gly	0	0.25	0.20	0.14	0.17	0.13	0.17	0.23
	Ace	0	0	0.10	0.10	0.14	0.14	1.00	0.96
	Form	0	0.34	0.41	1.11	1.77	0.90	5.62	8.75
	Oxa	0.05	0.04	0.04	0.04	0.04	0.04	0.05	0.05
	Sulf	0.23	0.15	0.15	0.12	0.11	0.14	0.16	0.12
	Cl^-	0.81	0.07	0.04	0.04	0.07	0.05	0.03	0.03
	NH_4^+	0	0	0	0	0	0	51.61	31.91
	FPZ	0	0	0	0	0	0	2.11	4.05
	EDA	0	0	0	0	0	0	38.35	26.26
	PZ	4676.48	4696.405	4641.452	4656.684	4617.498	4641.684	4452.838	4748.591
	HEP	0	0	0	0	0	0	0	0
	1-MPZ	0	0	0	0	0	0	0	0
	1-EPZ	0	0	0	0	0	0	4.92	4.13
	1,4-DMPZ	0	0	0	0	0	0	0	0
	AEP	0	0	0	0	0	0	1.15	1.87
	Alk	4720.8	4598.7	4747.6	4698.9	4718.5	4610.4	4641.4	4972.5
	SD_{Alk}	3.47							
Hydrolyzed Samples (mmol/kg)	Gly	0.09	0.63	0.52	0.65	0.99	0.57	1.34	3.13
	Ace	0	0	0.13	0.12	0.35	0.31	1.40	1.73
	Form	0	0.26	0.35	1.01	1.86	0.90	7.13	13.02
	Oxa	0.04	0.05	0.05	0.07	0.10	0.08	0.35	0.58
	Sulf	0.13	0.17	0.15	0.14	0.18	0.15	0.14	0.16
	Cl^-	0.05	0.12	0.06	0.10	0.10	0.10	2.79	0.09
	NH_4^+	0	0	0	0	0	0	91.96	83.82
	FPZ	0	0	0	0	0	0	0	0
	EDA	0	0	0	0	3.89	1.68	47.66	31.37
	PZ	4712.3	4705.4	4714.4	4738.1	4764.2	4769.5	4558.1	4851.4
	HEP	0	0	0	0	0	0	0	0
	1-MPZ	0	0	0	0	0	0	0	0
	1-EPZ	0	0	0	0	0	0	4.24	3.93
	1,4-DMPZ	0	0	0	0	0	0	0	0
	AEP	0	0	0	0	0	0	2.98	2.60

Table D.47: Tabulated Experimental Data for TE47 (8 m PZ, 0.1 mole CO_2 per mole alkalinity initially, 165 °C)

	Time (wk)	0	1.0	2.0	4.0	6.0	6.0	15.0	19.9
Original Samples (mmol/kg)	Gly	0.40	0.43	0.39	0.36	0.29	0.32	0.17	0.22
	Ace	0	0	0.06	0.14	0.37	0.22	2.81	2.10
	Form	0	1.56	4.27	11.87	21.30	15.07	37.44	46.35
	Oxa	0.01	0.01	0.02	0.02	0.03	0.02	0.03	0.01
	Sulf	0.09	0.11	0.11	0.09	0.28	0.10	0.04	0.07
	Cl^-	0.02	0.09	0.03	0.03	0.07	0.02	0.02	0.04
	NH_4^+	0	0	0	0	17.06	0	102.14	98.59
	FPZ	0	4.26	9.53	20.12	40.07	29.54	71.28	54.45
	EDA	0	0	3.95	10.78	18.35	13.97	57.11	51.03
	PZ	4540.3	4452.2	4409.8	4331.6	4194.9	4229.4	3804.2	3629.5
	HEP	0	0	0	0	0	0	0	0
	1-MPZ	0	0	0	0	3.46	0	3.26	1.46
	1-EPZ	0	0	0	0.97	2.41	1.96	24.69	16.46
	1,4-DMPZ	0	0	0	0	0	0	0	0
	AEP	0	1.61	0.59	3.51	7.65	5.81	44.34	55.68
	CO_2	939.6	927.3	917.1	891.6	876.6	824.0	875.7	709.6
	SD_{CO2}	12.93	4.96	16.49	7.98	10.76	12.36	20.60	10.82
	Alk	4476.1	4489.0	4441.2	4376.5	4440.8	4362.0	NT	4150.7
	SD_{Alk}	NA	NA	NA	NA	NA	NA	NA	NA
Hydrolyzed Samples (mmol/kg)	Gly	0.07	0.93	1.25	1.17	2.08	1.92	1.76	2.59
	Ace	0	0	0.08	0.31	0.68	0.25	5.66	3.45
	Form	0	3.58	9.60	23.25	45.59	32.24	87.87	102.15
	Oxa	0.03	0.07	0.07	0.10	0.13	0.10	1.10	0.30
	Sulf	0.16	0.13	0.14	0.17	0.34	0.14	0.26	0.18
	Cl^-	0.08	0.07	0.10	0.10	0.19	0.12	0.28	0.21
	NH_4^+	0	0	0	0	78.82	69.00	107.90	94.82
	FPZ	0	0	0	0	0	0	0	0
	EDA	0	3.36	6.68	13.28	23.13	18.56	68.91	58.31
	PZ	4505.7	4545.7	4508.7	4438.4	4272.3	4341.9	4279.6	3824.5
	HEP	0	0	0	0	0	0	0	0
	1-MPZ	0	0	0	0	2.84	0	2.48	0
	1-EPZ	0	0	0	0.89	2.82	1.91	23.04	16.58
	1,4-DMPZ	0	0	0	0	0	0	0	0
	AEP	0	0	1.32	4.88	9.83	8.92	51.05	61.03

Table D.48: Tabulated Experimental Data for TE48 (8 m PZ, 0.3 mole H^+ per mole alkalinity initially, 165 °C)

	Time (wk)	0.0	1.0	2.0	3.0	4.0	5.0	6.0	6.0	6.0	9.3	12.0	14.9	19.9
Original Samples (mmol/kg)	Gly	0.00	0.03	0.03	0.03	0.02	0.01	0.01	0.02	0.04	0.01	0.02	0.02	0.00
	Ace	0.11	0.13	0.11	0.10	0.19	0.20	0.30	0.22	0.12	0.36	0.52	0.76	1.40
	Form	0.19	0.53	0.52	0.46	0.72	0.83	1.35	1.08	0.45	1.57	1.56	1.99	2.07
	Oxa	0	0	0	0	0	0	0	0	0	0	0	0	0
	Sulf	0	0	0	0	0	0	0	0	0	0	0	0	0
	Cl^-	0.02	0.01	0.04	0.02	0.03	0.07	0.07	0.04	0.04	0.05	0.07	0.04	0.06
	NH_4^+	0	0	9.44	0	0	8.68	24.16	20.62	17.29	39.42	27.50	75.26	141.69
	FPZ	0	0	0	0	0	0	0	0	0	0	5.37	5.63	0
	EDA	0	1.14	1.92	3.49	3.91	9.59	13.67	10.67	6.46	16.31	31.03	39.79	59.20
	PZ	4357.3	4278.0	4236.9	4216.4	4259.5	4163.4	4070.2	4127.6	4064.8	4018.4	4069.4	3978.1	3623.0
	HEP	0	0	0	0	0	0	0	0	0	0	0	0	0
	1-MPZ	0	0	0	0	0	0	0	0	0	0	0	0	0
	1-EPZ	0.00	0.00	0.00	0.00	0.96	1.06	2.96	1.43	1.65	3.02	6.99	8.70	18.09
	1,4-DMPZ	0	0	0	0	0	0	0	0	0	0	0	0	0
	AEP	0.00	0.51	0.32	1.36	1.51	2.26	4.17	2.64	2.31	5.64	14.41	20.73	46.51
	CO_2	NT	NT	NT	NT	NT	NT	NT	NT	NT	NT	NT	NT	NT
	SD_{CO2}	NT	NT	NT	NT	NT	NT	NT	NT	NT	NT	NT	NT	NT
	Alk	2881.7	2916.5	2916.5	2834.6	2825.9	2888.0	2799.1	2804.3	2814.1	2814.4	2758.5	2741.9	2690.4
	SD_{Alk}	85.35	6.81	14.90	10.20	10.81	9.78	0.42	3.08	3.62	3.56	6.07	3.79	8.63
Hydrolyzed Samples (mmol/kg)	Gly	0.22	0.13	0.17	0.33	0.30	0.48	0.41	0.33	0.74	0.50	0.38	0.42	0.18
	Ace	0.32	0.39	0.39	0.36	0.49	0.45	0.71	0.64	0.28	1.35	1.23	1.76	2.64
	Form	0.37	0.76	0.68	0.95	1.40	1.94	3.11	2.95	0.88	4.76	3.92	5.69	6.85
	Oxa	0	0	0	0	0	0	0	0	0	0	0	0	0
	Sulf	0	0	0	0	0	0	0	0	0	0	0	0	0
	Cl^-	0.05	0.07	0.07	0.05	0.08	0.07	0.11	0.09	0.08	0.07	0.06	0.08	0.06
	NH_4^+	0	0	0	0	0	0	8.32	6.77	2.46	18.86	33.99	34.34	145.33
	FPZ	0	0	0	0	0	0	0	0	0	0	0	0	0
	EDA	0.00	1.62	2.43	4.11	4.54	10.32	14.73	11.10	6.34	18.11	34.78	39.46	59.03
	PZ	4465.83	4335.27	4405.46	4358.19	4269.55	4101.30	4184.36	4294.50	4318.63	4154.12	4085.68	3977.15	3620.53
	HEP	0	0	0	0	0	0	0	0	0	0	0	0	0
	1-MPZ	0	0	0	0	0	0	0	0	0	0	0	0	0
	1-EPZ	0	0.35	0.25	0.84	0.92	1.29	2.68	1.47	1.93	3.00	7.40	8.68	17.80
	1,4-DMPZ	0	0	0	0	0	0	0	0	0	0	0	0	0
	AEP	0	0.68	0.58	1.79	2.27	2.56	4.30	3.08	2.49	6.99	15.56	21.25	46.18

Table D.49: Tabulated Experimental Data for TE49 (4 m PZ, 0.3 mole CO_2 per mole alkalinity initially, 165 °C)

	Time (wk)	0.0	0.9	5.8
Original Samples (mmol/kg)	Gly	0.39	0.21	0.12
	Ace	0	0	0.86
	Form	0.08	6.90	40.69
	Oxa	0	0.03	0.03
	Sulf	0.30	0.27	0.23
	Cl^-	0	0	0
	NH_4^+	0	0	0
	FPZ	0	10.92	69.59
	EDA	0	1.23	13.90
	PZ	2757.0	2714.6	2434.5
	HEP	0	0	0
	1-MPZ	0	0	0
	1-EPZ	0	0.25	5.89
	1,4-DMPZ	0	0	0
	AEP	0	0	8.87
	CO_2	1613.7	1612.5	1465.8
	SD_{CO2}	8.91	11.07	26.68
	Alk	2757.6	2733.0	2584.7
	SD_{Alk}	4.52	18.29	6.31
Hydrolyzed Samples (mmol/kg)	Gly	0	0.27	0.24
	Ace	0.05	0.12	1.72
	Form	0.09	11.57	77.34
	Oxa	0	0.05	0.11
	Sulf	0	0	0
	Cl^-	0	0	0
	NH_4^+	0	34.47	109.17
	FPZ	0	0	0
	EDA	0	3.65	21.42
	PZ	3204.1	2496.7	2506.0
	HEP	0	0	30.32
	1-MPZ	0	0	0
	1-EPZ	0	0	8.27
	1,4-DMPZ	0	0	3.57
	AEP	0	0	24.90

Table D.50: Tabulated Experimental Data for TE50 (12 m PZ, 0.3 mole CO_2 per mole alkalinity initially, 165 °C)

	Time (wk)	0.0	0.9	1.8	3.8	5.8	5.8	9.9	14.8	19.8
Original Samples (mmol/kg)	Gly	0.40	0.42	0.33	0.25	0.21	0.24	0.14	0.12	0.09
	Ace	0	0	0	0.34	0.60	0.59	1.31	2.60	3.48
	Form	0.05	8.26	12.88	26.92	34.32	36.47	55.07	77.24	68.59
	Oxa	0	0.01	0	0.01	0.01	0	0.01	0	0
	Sulf	0.10	0.16	0.14	0.17	0.15	0.13	0.46	0.11	0.11
	Cl^-	0	0	0	0	0	0	0	0	0
	NH_4^+	0	19.00	45.91	55.98	87.29	132.52	214.17	328.33	464.01
	FPZ	0	85.77	117.24	185.72	252.85	257.55	373.62	451.96	603.17
	EDA	0	10.18	19.28	23.87	34.68	35.27	56.98	64.58	64.39
	PZ	5572.6	5172.6	4913.8	4157.6	3963.6	4417.2	3953.0	3466.0	2916.8
	HEP	0	0	0	4.27	7.48	26.18	46.26	50.69	53.05
	1-MPZ	0	0	8.22	2.24	3.79	27.49	19.25	27.43	25.40
	1-EPZ	0	0	2.11	4.52	7.90	8.70	20.34	34.87	52.81
	1,4-DMPZ	0	0	2.91	3.26	3.06	9.94	0	3.27	20.39
	AEP	0	2.27	8.63	33.09	47.37	34.48	61.77	90.23	111.08
	CO_2	3358.9	3349.4	3192.2	2838.0	2756.0	2943.0	2644.8	2394.0	2008.7
	SD_{CO2}	65.87	20.31	15.37	58.42	37.25	46.61	36.78	36.78	32.04
	Alk	4991.5	4912.6	4860.0	4703.1	4562.7	4579.9	4332.8	4097.7	3778.7
	SD_{Alk}	6.56	8.71	2.16	7.81	14.59	2.35	17.37	4.35	15.86
Hydrolyzed Samples (mmol/kg)	Gly	0.45	0.32	0.25	0.26	0.22	0.29	0.16	0.07	0.04
	Ace	0	0.16	0.28	0.80	1.55	1.19	3.17	5.37	6.37
	Form	0.11	36.97	50.50	142.68	202.89	186.83	336.99	440.42	409.89
	Oxa	0	0.02	0	0.03	0.02	0.03	0.02	0.04	0.01
	Sulf	0.16	0.13	0.15	0.11	0.12	0.09	0.09	0.10	0.10
	Cl^-	0	0	0	0	0	0	0	0	0
	NH_4^+	0	22.90	46.06	97.22	134.60	134.82	52.76	325.26	484.80
	FPZ	0	0	0	0	0	0	0	0	0
	EDA	0	3.53	7.31	29.12	41.61	42.72	12.55	65.98	80.41
	PZ	3701.4	3888.9	3548.3	4672.3	4560.0	4613.3	1076.0	3637.9	3500.0
	HEP	0	0	0	0	0	0	34.49	46.05	64.10
	1-MPZ	0	0	8.60	18.43	16.79	23.99	6.84	30.06	23.75
	1-EPZ	0	2.76	1.32	10.52	10.93	9.25	3.89	36.49	62.38
	1,4-DMPZ	0	3.44	6.71	1.96	9.95	10.33	0	0	4.58
	AEP	0	1.60	8.45	21.82	34.64	31.82	16.04	94.10	135.07

Table D.51: Tabulated Experimental Data for TE51 (8 m PZ, 0.3 mole CO_2 per mole alkalinity initially, 175 °C, N_2 headspace)

	Time (wk)	0.0	0.3	1.3	3.5	5.6	7.5	9.5	14.5
Original Samples (mmol/kg)	Gly	0.68	0.54	0.24	0.20	0.12	0.07	0.05	0.02
	Ace	0	0	0.35	2.23	5.50	8.83	12.13	18.38
	Form	0	9.86	21.01	92.72	126.69	166.37	214.10	198.77
	Oxa	0.02	0.03	0.04	0.02	0.03	1.59	0.04	0.05
	Sulf	0.14	0.13	0.10	0.30	0.10	0.10	0.12	0.13
	Cl^-	0.03	0.04	0.03	0.10	0.06	0.03	0.04	0.03
	NH_4^+	0	0	10.70	115.73	250.27	382.76	450.19	745.28
	FPZ	0	28.30	63.59	256.60	302.59	354.14	415.66	434.70
	EDA	0	4.18	23.83	41.55	53.30	59.35	69.99	59.53
	PZ	4096.1	4064.7	4686.8	3283.0	2715.8	2358.0	2139.1	1554.4
	HEP	0	0	0	6.99	10.69	0	13.80	31.34
	1-MPZ	0	0	0	2.39	8.65	5.19	5.51	18.18
	1-EPZ	0	0	2.68	18.26	33.57	48.84	56.07	90.27
	1,4-DMPZ	0	0	0	0	0	0	0	0
	AEP	0	0	6.82	44.12	91.88	120.74	132.87	143.71
	CO_2	2350.8	2308.7	NT	1889.0	1902.9	1632.8	1368.2	1209.0
	SD_{CO2}	7.47	46.48	NT	7.94	5.95	28.97	6.18	3.29
	Alk	4219.5	4162.8	NT	3673.2	3409.0	3207.9	3116.8	2804.8
	SD_{Alk}	46.67	33.37	NT	3.14	10.49	51.88	100.25	5.55
Hydrolyzed Samples (mmol/kg)	Gly	0	0.45	1.66	0.52	0.42	0.87	1.73	1.63
	Ace	0	0.16	0.86	3.58	8.74	15.40	20.07	31.88
	Form	0	25.56	57.95	263.14	368.83	476.10	610.32	654.40
	Oxa	0.02	0.07	0.39	0.22	0.35	0.35	0.24	0.28
	Sulf	0.18	0.16	0.21	0.44	0.16	0.18	0.24	0.18
	Cl^-	0.21	0.09	0.20	0.80	0.14	0.11	0.12	0.15
	NH_4^+	0	0	0	74.13	180.25	293.20	346.66	596.57
	FPZ	0	0	0	0	0	0	0	0
	EDA	0	5.78	27.13	46.60	59.08	66.29	78.86	69.58
	PZ	4126.7	4090.3	4794.5	3413.3	2903.0	2544.6	2380.5	1816.5
	HEP	0	0	0	11.14	11.32	14.45	12.52	18.97
	1-MPZ	0	0	0	3.16	9.68	5.76	5.09	4.93
	1-EPZ	0	0	2.64	19.47	39.13	59.52	72.95	101.36
	1,4-DMPZ	0	0	0	0	0	0	0	0
	AEP	0	1.27	19.58	57.49	101.76	133.61	151.33	168.13

Table D.52: Tabulated Experimental Data for TE52 (8 m PZ, unloaded, 175 °C, N_2 headspace)

	Time (wk)	0	0.3	1.3	3.5	5.6	5.6	7.5	9.5	14.5
Original Samples (mmol/kg)	Gly	0	0.17	0.03	0.23	0.16	0.33	0.03	0.24	0.02
	Ace	0	0	0.06	0.21	0.35	0.29	0.31	0.26	0.66
	Form	0.05	0.25	0.39	3.39	5.69	1.72	3.52	3.17	7.19
	Oxa	0.03	0.01	0.02	0.02	0.02	0.02	0.01	0.02	0.02
	Sulf	0.13	0.11	0.13	0.14	0.14	0.10	0.16	0.37	1.03
	Cl^-	0.02	0.04	0.05	0.03	0.08	0.04	0.05	0.04	0.34
	NH_4^+	0	0	0	0	0	0	0	0	19.97
	FPZ	0	0	0	1.06	1.95	1.01	0.94	1.10	2.66
	EDA	0	0.16	0.86	3.94	8.64	2.36	9.13	5.80	28.49
	PZ	4678.7	4661.2	4661.1	4677.8	4579.6	4664.5	4643.5	4793.3	4564.3
	HEP	0	0	0	0	0	0	0	0	0
	1-MPZ	0	0	0	0	0	0	0	0	0
	1-EPZ	0	0	0	0	0	0	0	0	2.34
	1,4-DMPZ	0	0	0	0	0	0	0	0	0
	AEP	0	0	0	0	0.74	0	0.63	0.69	2.56
	Alk	4751.1	4858.4	4806.0	4794.1	4808.9	4856.0	4783.3	5034.3	4738.6
	SD_{Alk}	47.02	NA	NA	NA	NA	NA	NA	NA	NA
Hydrolyzed Samples (mmol/kg)	Gly	0	0	0.35	0.98	1.48	0.91	0.80	1.04	1.35
	Ace	0	0	0.12	0.52	0.68	0.25	0.48	0.45	0.75
	Form	0	0	0.42	4.06	6.99	1.85	3.79	3.68	8.09
	Oxa	0.02	0.03	0.05	0.17	0.17	0.07	0.08	0.07	0.07
	Sulf	0.11	0.24	0.18	0.17	0.19	0.18	0.20	0.42	1.00
	Cl^-	0.06	0.16	0.13	0.10	0.15	0.12	0.23	0.13	0.45
	NH_4^+	0	0	0	0	0	0	0	0	0
	FPZ	0	0	0	0	0	0	0	0	0
	EDA	0	0	2.08	5.97	13.06	3.59	10.75	7.87	29.19
	PZ	4682.1	4634.3	4827.9	4873.9	4700.7	4774.3	4699.9	5018.6	4416.4
	HEP	0	0	0	0	0	0	0	0	0
	1-MPZ	0	0	0	0	0	0	0	0	0
	1-EPZ	0	0	0	0	0	0	0	1.09	2.05
	1,4-DMPZ	0	0	0	0	0	0	0	0	0
	AEP	0	0	0	1.19	1.64	0	0.98	1.23	3.00

Table D.53: Tabulated Experimental Data for TE53 (8 m PZ, 0.2 mole CO_2 per mole alkalinity initially, 175 °C)

	Time (wk)	0	1.7	3.4	4.0	4.9	6.0	6.0	6.0	8.0	10.0	12.1	15.0
Original Samples (mmol/kg) (Metals are in units of µg/g)	Gly	0	0.29	0.25	0.25	0.18	0.16	0.15	0.19	0.11	0.08	0.06	0.04
	Ace	0	1.12	1.30	1.24	2.44	2.39	3.34	3.96	4.51	7.10	11.02	11.70
	Form	0	28.15	64.55	65.62	99.44	80.55	105.69	87.61	137.15	155.34	203.97	174.03
	Oxa	0.00	0.15	0.01	0.01	0.00	0.01	0.00	0.05	0.00	0.00	0.00	0.00
	Sulf	0.08	24.83	0.26	0.15	0.23	0.84	0.19	2.63	0.13	0.07	0.08	0.07
	Cl^-	0.08	0.05	0.06	0.05	0.04	0.02	0.01	0.02	0.02	0.02	0.02	0.02
	NH_4^+	5.09	90.40	94.30	101.16	176.53	163.28	236.66	80.70	300.58	388.37	562.26	606.21
	FPZ	0	118.95	139.90	140.63	201.25	169.64	210.22	214.27	259.06	283.12	320.09	345.33
	EDA	0	42.78	33.96	37.94	53.57	48.44	57.58	55.82	63.67	71.04	73.11	80.04
	PZ	4535.1	3634.3	3731.9	3668.5	3425.3	3505.3	3213.7	3350.8	2903.1	2655.6	2320.0	2205.5
	HEP	0	0	0	0	10.87	9.32	8.78	5.50	6.46	9.68	14.38	27.72
	1-MPZ	0	0	0	0	0	0	0	0	0	3.51	10.60	13.83
	1-EPZ	0	11.07	10.06	10.47	20.93	18.93	25.00	31.52	36.90	45.28	81.78	62.32
	1,4-DMPZ	0	0	0	0	0	0	0	0	0	0	0	0
	AEP	0	24.52	39.05	43.38	75.55	66.78	88.08	82.49	115.94	146.81	168.30	174.16
	CO_2	1708.4	2575.1	1309.0	1292.2	1137.5	1218.3	1116.3	1215.3	948.39	934.48	768.92	770.11
	SD_{CO2}	27.66	27.21	14.02	3.24	8.79	7.79	25.37	30.07	14.20	9.78	7.91	12.48
	Alk	4407.8	NT	4083.8	4084.9	3920.7	3881.2	3810.1	4054.4	3661.3	3571.4	3302.5	3297.4
	SD_{Alk}	30.32	NT	89.80	15.13	46.81	29.36	16.03	NA	28.90	NA	83.17	51.00
	Fe^{2+}	0	NT	12.61	14.51	17.52	NT	NT	NT	22.36	13.58	41.03	75.62
	Ni^{2+}	0	NT	74.03	75.38	117.79	NT	NT	NT	195.13	218.85	270.28	302.73
	Cr^{3+}	0	NT	0	0	0	NT	NT	NT	0.09	0	1.54	1.75
Hydrolyzed Samples (mmol/kg)	Gly	0.11	NT	0.63	1.00	1.10	0.75	0.69	1.91	1.38	0.94	2.17	2.00
	Ace	0	NT	2.19	1.94	3.83	3.67	5.09	8.44	7.58	11.31	17.06	17.76
	Form	0	NT	152.76	153.60	224.78	188.90	248.90	241.79	321.54	393.66	454.14	457.73
	Oxa	0.01	NT	0.15	0.05	0.05	0.15	0.16	1.43	0.08	0.08	0.09	0.08
	Sulf	1.72	NT	0.31	0.22	0.26	0.82	0.26	2.88	0.20	0.14	0.13	0.14
	Cl^-	0.09	NT	0.26	0.11	0.08	0.08	0.06	0.20	0.11	0.13	0.09	0.08
	NH_4^+	0	NT	95.05	109.75	164.36	157.71	205.43	67.42	283.18	384.95	483.05	538.29
	FPZ	0	NT	0	0	0	0	0	0	0	0	0	0
	EDA	0	NT	36.52	41.61	56.05	51.41	59.68	66.75	68.28	78.56	76.71	85.48
	PZ	4539.1	NT	3834.1	3800.5	3437.7	3510.5	3248.8	3489.6	3111.5	2954.9	2403.9	2404.7
	HEP	0	NT	0	0	0	0	0	2.33	6.85	10.60	14.62	28.46
	1-MPZ	0	NT	0	0	0	0	0	0	0	3.33	12.13	13.08
	1-EPZ	0	NT	10.78	11.47	21.26	19.68	27.55	33.31	39.90	52.57	71.11	76.36
	1,4-DMPZ	0	NT	0	0	0	0	0	0	0	0	0	0
	AEP	0	NT	42.05	46.57	77.25	70.68	91.05	90.42	123.65	164.10	174.53	186.25

Table D.54: Tabulated Experimental Data for TE54 (8 m PZ, 0.47 mole CO_2 per mole alkalinity initially, 175 °C)

	Time (wk)	0	0.7	1.7	3.4	4.0	4.9	6.0	6.0	6.0	8.0	10.0	12.1	15.0
Original Samples (mmol/kg) (Metals are in units of µg/g)	Gly	0.70	0.56	0.34	0.39	0.35	0.27	0.28	0.22	0.28	0.21	0.11	0.07	0.08
	Ace	0	0	0.49	0.55	0.71	1.16	1.00	1.81	1.06	1.97	6.02	10.05	15.34
	Form	0.96	5.29	24.28	31.96	37.53	44.53	42.13	65.63	34.58	67.32	108.76	147.13	190.47
	Oxa	0.01	0.03	0.03	0.01	0.01	0.02	0.01	0.00	0.02	0.01	0.01	0.01	0.01
	Sulf	0.17	0.09	0.05	0.05	0.09	0.09	0.08	0.07	0.09	0.11	0.09	0.08	0.10
	Cl^-	0.34	0.03	0.05	0.04	0.04	0.05	0.05	0.05	0.06	0.05	0.05	0.04	0.07
	NH_4^+	7.65	8.16	57.27	51.80	59.88	95.48	79.22	129.46	81.11	102.72	291.15	441.44	644.66
	FPZ	0	41.50	176.30	186.40	214.60	258.53	238.53	344.01	253.36	356.58	493.20	599.57	679.04
	EDA	0	5.40	22.72	24.11	28.75	35.91	32.75	46.48	36.52	45.60	60.70	61.99	65.95
	PZ	4125.2	4021.3	3632.1	3705.9	3666.1	3532.6	3500.5	3299.1	3309.0	3227.6	2647.0	2134.6	1685.7
	HEP	0	0	0	0	0	0	0	8.50	7.67	9.06	8.59	8.27	12.30
	1-MPZ	0	0	0	0	0	0	0	0	0	3.86	5.25	6.06	5.07
	1-EPZ	0	0	4.65	4.09	6.09	9.73	8.27	14.97	9.58	15.41	32.51	46.05	56.22
	1,4-DMPZ	0	0	0	0	0	0	0	0	0	0	0	0	0
	AEP	0	2.04	15.63	16.64	21.71	36.07	32.38	51.03	36.71	53.45	96.35	111.54	126.40
	CO_2	3022.2	3223.3	3005.1	2781.7	2785.5	2714.3	2768.4	2666.0	3042.3	2664.4	2416.6	2138.2	1901.3
	SD_{CO2}	28.70	42.18	27.75	40.06	8.47	29.39	44.85	20.20	37.76	12.03	10.02	23.84	15.93
	Alk	4183.1	4034.9	3797.6	3821.4	3883.9	3822.9	3739.9	3589.9	3668.9	3572.9	3235.2	2938.2	2623.8
	SD_{Alk}	37.60	53.09	40.92	29.74	8.55	50.22	10.07	42.38	3.78	4.80	67.84	16.58	2.94
	Fe^{2+}	0	NT	NT	69.90	78.26	NT	93.10	89.67	NT	98.55	174.76	206.43	195.06
	Ni^{2+}	0	NT	NT	40.01	55.01	NT	79.14	95.97	NT	84.51	190.74	229.93	286.11
	Cr^{3+}	0	NT	NT	45.75	74.22	NT	85.41	127.39	NT	97.16	113.40	120.75	154.70
Hydrolyzed Samples (mmol/kg)	Gly	0.84	0.63	0.41	0.40	0.35	0.27	0.31	0.22	0.29	0.22	0.09	0.02	0.00
	Ace	0	0	0.53	0.63	0.86	1.65	1.17	2.47	1.34	2.35	9.62	16.37	25.53
	Form	0	26.48	124.69	136.74	162.90	206.12	188.29	302.33	193.80	309.85	501.48	701.82	886.01
	Oxa	0.00	0.03	0.05	0.02	0.02	0.07	0.02	0.02	0.05	0.02	0.04	0.08	0.10
	Sulf	0.12	0.15	0.13	0.14	0.14	0.14	0.10	0.12	0.12	0.14	0.14	0.12	0.15
	Cl^-	0.07	0.08	0.09	0.09	0.11	0.12	0.09	0.08	0.11	0.09	0.08	0.09	0.12
	NH_4^+	0	0	66.83	66.12	54.31	88.29	76.91	124.53	87.67	130.92	280.21	417.68	586.15
	FPZ	0	0	0	0	0	0	0	0	0	0	0	0	0
	EDA	0	5.85	22.55	24.61	29.31	36.94	34.34	47.48	36.80	47.68	63.89	68.01	74.73
	PZ	4142.0	4039.8	3701.0	3753.7	3685.4	3622.3	3600.3	3422.0	3506.9	3454.4	2922.7	2516.8	2115.0
	HEP	0	0	0	0	0	0	0	0	0	9.48	5.66	9.15	14.40
	1-MPZ	0	0	0	0	0	0	0	3.79	2.53	4.26	5.42	7.16	5.74
	1-EPZ	0	0	4.56	4.64	5.64	10.29	9.18	16.40	10.09	17.37	40.71	62.47	83.36
	1,4-DMPZ	0	0	0	0	0	0	0	0	0	0	0	0	0
	AEP	0	1.90	15.89	17.04	22.62	37.98	34.29	54.01	38.56	57.61	106.34	131.14	155.62

Table D.55: Tabulated Experimental Data for TE55 (8 m PZ, 0.2 mole H^+ per mole alkalinity initially, 175 °C)

	Time (wk)	0	0.7	1.7	3.4	4.0	6.0	6.0	6.0	9.0	12.0	15.0
Original Samples (mmol/kg)	Gly	0	0	0	0	0	0	0	0	0	0	0
	Ace	0	0	0	0.23	0.50	0.44	0.34	0.31	0.53	0.77	0.47
	Form	0	0.2	0.5	2.2	3.7	3.9	3.7	3.3	3.7	4.8	2.6
	Oxa	0	0	0	0	0	0	0	0	0	0	0
	Sulf	0	0	0	0	0	0	0	0	0	0	0
	Cl^-	0.03	0.03	0.04	0.03	0.04	0.04	0.02	0.05	0.06	0.03	0.01
	NH_4^+	1.00	3.37	6.36	22.60	47.16	81.70	64.91	45.51	78.70	98.60	116.69
	FPZ	0	0.77	0.36	2.53	4.91	4.04	3.56	7.33	4.97	4.43	3.70
	EDA	0	2.07	6.80	55.60	43.30	49.34	42.83	39.90	60.18	83.98	75.53
	PZ	4729.6	4629.1	4428.0	4378.4	4297.9	4116.0	4258.1	4165.7	3965.6	3842.5	3753.1
	HEP	0	0	0	0	0	0	0	0	0	0	0
	1-MPZ	0	0	0	0	0	0	0	0	0	0	0
	1-EPZ	0	0	0	4.02	6.11	8.73	8.23	7.89	12.86	16.54	18.10
	1,4-DMPZ	0	0	0	0	0	0	0	0	0	0	0
	AEP	0	1.04	2.89	9.55	17.74	23.98	21.45	20.49	35.47	49.24	55.21
	Alk	NT	NT	NT	NT	NT	NT	NT	NT	NT	NT	NT
Hydrolyzed Samples (mmol/kg)	Gly	0	0	0.64	0.31	0.66	0.34	0.38	0.66	0.40	0.28	0.70
	Ace	0	0	0	0.44	1.00	0.83	0.73	0.61	0.89	1.49	0.85
	Form	0	0.01	0.15	0.85	1.21	1.06	1.27	1.06	1.04	1.43	0.68
	Oxa	0	0	0	0	0	0	0	0	0	0	0
	Sulf	0	0	0	0	0	0	0	0	0	0	0
	Cl^-	0.08	0.07	0.09	0.05	0.09	0.07	0.66	0.11	0.09	0.14	0.08
	NH_4^+	0	0	0	0	66.94	47.85	69.17	71.98	55.88	85.65	94.25
	FPZ	0	0	0	0	0	0	0	0	0	0	0
	EDA	0	2.47	7.98	26.63	45.25	51.78	43.99	41.82	62.39	85.64	78.66
	PZ	4702.3	4641.6	4569.3	4398.9	4283.9	4114.0	4160.3	4274.5	3932.1	3866.1	3730.0
	HEP	0	0	0	0	0	0	0	0	0	0	0
	1-MPZ	0	0	0	0	0	0	0	0	0	0	0
	1-EPZ	0	0	0	3.93	6.41	9.29	8.23	8.31	12.90	16.77	18.07
	1,4-DMPZ	0	0	0	0	0	0	0	0	0	0	0
	AEP	0	0.97	3.07	10.10	18.93	25.52	22.17	22.33	37.30	51.80	56.84

Table D.56: Tabulated Experimental Data for TE56 (8 m PZ, 0.3 mole CO_2 per mole alkalinity initially, 175 °C, 100 mM Inhibitor A)

	Time (wk)	0	0.7	1.7	3.4	4.0	6.0	6.0	6.0	9.0	12.0	15.0
Original Samples (mmol/kg)	Gly	0.62	0.55	0.43	0.45	0.40	0.41	0.42	0.43	0.10	0.06	0.04
	Ace	0	0	0.40	0.38	0.68	0.95	0.76	0.77	4.21	9.12	11.43
	Form	1.00	6.15	32.76	32.92	34.93	55.51	46.96	47.38	117.84	185.78	191.64
	Oxa	0.01	0.02	0.01	0.00	0.00	0.00	0.00	0.00	0.00	0.01	0.01
	Sulf	0.11	0.13	0.16	0.10	0.11	0.15	0.11	0.15	0.13	0.20	0.13
	Cl^-	0.04	0.03	0.07	0.04	0.03	0.08	0.04	0.08	0.03	0.04	0.03
	NH_4^+	1.78	6.35	40.83	45.43	49.67	79.99	73.51	81.64	322.21	494.87	567.58
	FPZ	0	16.86	105.11	103.96	110.92	158.90	146.88	147.77	337.96	447.98	480.49
	EDA	0	4.26	17.70	23.95	24.58	34.46	31.15	29.63	58.79	60.43	63.62
	PZ	4425.1	4294.6	4075.0	4021.7	3956.7	3627.4	3814.9	3815.5	2828.5	2272.7	2041.8
	HEP	0	0	0	0	0	0	0	0	32.62	42.41	48.49
	1-MPZ	0	0	0	11.04	16.02	15.36	13.60	12.21	14.62	23.08	23.46
	1-EPZ	0	0	3.72	3.90	5.17	8.45	7.22	7.29	34.00	65.15	73.42
	1,4-DMPZ	0	0	0	0	0	0	0	0	0	0	0
	AEP	0	1.88	14.90	18.74	21.59	39.98	35.11	35.19	101.73	139.30	148.16
	CO_2	2300.6	2247.1	2224.2	2193.4	2268.6	1972.6	2060.3	2058.6	1969.5	1414.0	1315.9
	SD_{CO2}	39.65	25.12	13.48	24.37	4.65	13.03	18.64	55.10	2.54	17.18	11.75
	Alk	4157.2	4143.5	4140.4	4067.0	4074.6	3802.1	3952.8	3945.4	3286.1	3094.5	3012.9
	SD_{Alk}	51.07	0.84	36.51	64.78	112.59	268.09	33.25	46.51	NA	13.00	0.68
Hydrolyzed Samples (mmol/kg)	Gly	0.33	0.56	0.85	0.81	0.95	1.07	0.97	0.98	0.44	1.12	1.61
	Ace	0	0	0.79	0.80	1.30	1.62	1.37	1.31	8.53	15.53	19.12
	Form	0	12.13	91.39	90.85	98.28	153.62	134.41	134.56	376.29	567.18	607.76
	Oxa	0.01	0.05	0.06	0.07	0.07	0.05	0.07	0.05	0.31	0.22	0.15
	Sulf	0.07	0.15	0.13	0.20	0.18	0.21	0.17	0.14	0.15	0.22	0.22
	Cl^-	0.06	0.10	0.10	0.37	0.11	0.43	0.13	0.10	0.09	0.13	0.33
	NH_4^+	0	0	73.67	76.64	83.18	118.14	107.84	104.37	352.09	527.31	590.72
	FPZ	0	0	0	0	0	0	0	0	0	0	0
	EDA	0	5.71	22.09	23.75	27.17	35.99	32.39	32.64	62.26	69.26	71.42
	PZ	4341.5	4251.2	4081.6	4035.8	3967.6	3739.3	3865.0	3862.2	3033.5	2534.4	2294.2
	HEP	0	0	0	0	0	0	0	0	31.54	42.36	45.89
	1-MPZ	0	0	0	0	7.40	9.82	8.69	8.80	17.73	23.29	21.65
	1-EPZ	0	0	3.68	4.40	5.39	8.94	8.02	7.96	39.15	67.68	75.49
	1,4-DMPZ	0	0	0	0	0	0	0	0	0	0	0
	AEP	0	2.34	15.51	19.28	22.23	41.85	35.79	35.94	111.04	156.52	165.38

Table D.57: Tabulated Experimental Data for TE57 (20 m PZ, 0.3 mole CO_2 per mole alkalinity initially, 175 °C)

	Time (wk)	0	0.7	1.7	4.0	6.0	6.0	8.0	10.0	15.0
Original Samples (mmol/kg)	Gly	0.79	0.36	0.29	0.09	0.05	0.06	0	0	0
	Ace	0	0.31	0.79	3.75	7.40	6.92	9.08	11.10	11.64
	Form	0	23.37	45.67	133.75	182.85	175.30	206.74	216.23	199.91
	Oxa	0.05	0.02	0.07	0	0	0	0	0	0
	Sulf	0.10	0.08	0.12	0.12	0.16	0.13	0.15	0.16	0.12
	Cl^-	0.06	0.06	0.03	0.20	0.04	0.03	0.04	0.38	0.13
	NH_4^+	0	45.74	96.74	354.79	511.80	533.09	647.85	754.75	809.11
	FPZ	0	293.89	491.51	920.07	967.37	986.01	1005.0	975.47	950.12
	EDA	0	25.13	43.26	84.90	87.14	88.50	91.29	102.49	90.16
	PZ	5663.9	4925.4	4396.4	2783.6	2124.2	2173.1	1764.2	1525.9	1385.3
	HEP	0	0	0	9.60	17.93	18.32	24.66	29.07	31.82
	1-MPZ	0	7.42	16.22	31.09	31.87	32.30	31.11	29.32	26.90
	1-EPZ	0	4.23	10.68	50.01	80.79	80.87	89.10	101.63	104.83
	1,4-DMPZ	0	10.23	9.19	0	0	0	0	0	0
	AEP	0	11.01	27.56	84.45	101.54	101.04	111.43	118.82	123.06
	CO_2	4042.2	3581.3	3178.2	2042.6	1570.0	1643.4	1318.6	1208.6	1148.1
	SD_{CO2}	61.25	71.78	44.38	24.65	9.05	11.99	12.62	15.17	16.70
	Alk	6121.5	5863.9	5452.0	4439.1	3910.5	3891.8	3761.8	3712.0	3559.7
	SD_{Alk}	NA	NA	NA	NA	NA	NA	NA	NA	NA
Hydrolyzed Samples (mmol/kg)	Gly	1.05	0.47	0.31	0.05	0	0	0	0	0
	Ace	0	0.54	1.59	12.92	20.65	21.36	27.07	30.49	33.25
	Form	0	202.37	377.33	942.12	1153.83	1130.80	1263.22	1316.40	1299.36
	Oxa	0	0.07	0.18	0	0	0	0	0	0
	Sulf	0.15	0.11	0.14	0.13	0.13	0.15	0.09	0.10	0.20
	Cl^-	0	0	0	0	0	0	0	0	0
	NH_4^+	0	61.39	90.15	320.08	457.20	464.33	570.34	696.79	750.44
	FPZ	0	0	0	0	0	0	0	0	0
	EDA	0.22	26.70	47.35	95.93	101.04	102.49	108.68	122.77	109.63
	PZ	5671.7	5041.1	4634.6	3280.8	2665.4	2721.5	2344.3	2098.5	1945.3
	HEP	0	0	0	9.54	21.10	18.52	29.43	35.91	39.13
	1-MPZ	0	9.53	17.17	33.98	35.00	38.32	36.54	35.29	35.06
	1-EPZ	0	4.27	12.50	63.59	92.30	94.03	113.13	125.60	133.57
	1,4-DMPZ	0	11.44	9.70	5.03	0	0	0	0	0
	AEP	0	12.07	29.81	97.89	125.76	125.75	143.08	155.52	163.95

Table D.58: Tabulated Experimental Data for TE58 (20 m PZ, 0.1 mole CO_2 per mole alkalinity initially, 175 °C)

	Time (wk)	0	0.7	1.7	4.0	6.0	6.0	8.0	10.0	15.0
Original Samples (mmol/kg)	Gly	0.52	0.43	0.33	0.22	0.20	0.20	0.14	0.13	0.09
	Ace	0	0	0.22	0.50	0.56	0.56	0.99	1.07	1.69
	Form	0.02	8.77	29.23	50.86	51.54	52.55	73.33	67.84	81.14
	Oxa	0.01	0.03	0.06	0.04	0.06	0.06	0.06	0.05	0.06
	Sulf	0.08	0.10	0.09	0.10	0.09	0.12	0.11	0.14	0.09
	Cl^-	0.03	0.16	0.04	0.05	0.06	0.04	0.04	0.04	0.06
	NH_4^+	0	8.57	26.67	71.44	85.87	85.14	139.53	150.20	225.89
	FPZ	0	58.96	191.78	298.84	300.81	304.66	385.63	367.47	425.74
	EDA	0.01	14.16	30.59	61.95	66.29	67.78	91.73	97.47	119.63
	PZ	6368.0	6097.8	5660.2	5178.7	5053.3	5054.5	4643.8	4668.9	4184.0
	HEP	0	0	0	0	0	0	9.39	9.41	4.80
	1-MPZ	0	0	3.68	7.64	12.25	8.48	9.87	9.27	12.38
	1-EPZ	0	0.81	3.75	10.78	12.57	12.62	22.69	21.65	35.35
	1,4-DMPZ	0	3.40	6.87	5.38	4.40	4.51	3.15	2.65	0.66
	AEP	0	2.97	11.78	29.82	33.58	33.95	55.91	54.20	83.80
	CO_2	1441.7	1345.8	1191.9	1075.0	1400.0	853.2	917.6	730.9	1228.6
	SD_{CO2}	12.73	4.60	4.42	1.64	13.43	7.61	8.32	8.75	9.34
	Alk	6977.6	6912.6	6645.7	6464.9	6367.7	6362.2	6102.7	6152.5	5903.8
	SD_{Alk}	NA	NA	NA	NA	NA	NA	NA	NA	NA
Hydrolyzed Samples (mmol/kg)	Gly	6.46	2.41	4.26	5.11	0.90	0.79	3.35	0.79	0.73
	Ace	0	0.60	1.04	2.24	2.00	2.02	3.18	3.42	5.52
	Form	0.55	142.42	151.83	252.83	232.98	243.07	401.41	309.55	385.67
	Oxa	0.01	0.77	0.46	0.89	0.36	0.31	0.85	0.31	0.36
	Sulf	0.11	0.20	0.13	0.09	0.18	0.12	0.09	0.13	0.08
	Cl^-	0.12	0	0	0	0	0	0	0	0
	NH_4^+	0	0	33.58	60.91	88.16	83.63	71.79	151.05	206.48
	FPZ	0	0	0	0	0	0	0	0	0
	EDA	4.12	23.44	46.06	66.60	69.44	71.34	71.24	103.41	129.42
	PZ	7345.6	3758.5	6820.3	4979.5	5204.3	5216.4	2982.2	4875.1	4497.5
	HEP	0	0	0	0	0	0	6.46	10.85	12.20
	1-MPZ	0	2.82	4.75	7.66	13.43	8.71	5.45	9.50	10.48
	1-EPZ	0	1.93	4.42	9.15	13.00	13.09	12.45	22.93	38.46
	1,4-DMPZ	0.99	3.78	7.69	4.80	4.38	4.35	1.56	3.15	1.75
	AEP	0	7.59	14.17	28.65	34.92	35.04	34.65	56.45	88.28

Table D.59: Tabulated Experimental Data for TE59 (8 m PZ + 1 m Ethylenediamine, 0.3 mole CO_2 per mole alkalinity initially, 175 °C)

	Time (wk)	0	0.1	0.4	0.7	1.0	1.5	1.9
Original Samples (mmol/kg)	Gly	0.13	0.14	0.13	0.13	0.10	0.10	0.10
	Ace	0	0	1.46	3.81	6.10	5.65	8.51
	Form	0.13	7.55	15.03	28.05	39.53	32.40	49.00
	Oxa	0	0.01	0.01	0.01	0.01	0.01	0.01
	Sulf	0.10	0.10	0.14	0.12	0.09	0.10	0.09
	Cl^-	0.03	0.02	0.04	0.04	0.02	0.02	0.02
	NH_4^+	6.05	38.46	89.22	134.46	198.12	229.15	273.45
	FPZ	0	30.04	78.13	154.91	162.62	193.82	224.89
	EDA	502.16	222.32	186.27	173.01	171.09	187.12	179.25
	PZ	3987.6	3898.5	3722.3	3638.7	3499.8	3428.8	3310.3
	HEP	0	0	0	0	0	0	0
	1-MPZ	0	16.28	16.04	16.35	14.24	13.63	13.18
	1-EPZ	0	0	1.22	2.40	5.09	5.07	7.49
	1,4-DMPZ	0	0	5.63	7.59	2.85	1.94	1.82
	AEP	0	17.80	48.13	67.69	90.74	105.34	119.76
	2-Imid	0	244.41	274.86	280.38	255.96	247.51	238.58
	CO_2	2849.9	2588.2	2459.9	2461.4	2411.1	2419.8	2319.7
	SD_{CO2}	28.51	14.61	27.75	18.45	23.24	19.37	18.08
	Alk	4517.2	4282.0	4140.9	4175.6	4024.1	4016.3	3934.9
	SD_{Alk}	10.33	90.93	0.82	126.45	44.79	56.87	5.09
Hydrolyzed Samples (mmol/kg)	Gly	0	0.21	0.27	0.39	0.41	0.62	0.58
	Ace	0	1.26	4.72	8.13	9.10	13.37	0
	Form	0.50	26.54	68.09	99.61	98.84	148.47	182.89
	Oxa	0.02	0.04	0.05	0.07	0.05	0.06	0.06
	Sulf	0.14	0.11	0.14	0.16	0.10	0.14	0.12
	Cl^-	0.03	0.05	0.08	0.09	0.02	0.10	0.04
	NH_4^+	0	14.40	53.55	85.48	137.80	160.41	192.29
	FPZ	0	0	0	0	0	0	0
	EDA	486.9	223.5	188.8	168.6	174.0	185.6	183.7
	PZ	3935.9	3851.8	3718.4	3622.2	3551.9	3506.5	3355.4
	HEP	0	0	0	0	0	0	0
	1-MPZ	0	13.83	17.20	15.66	14.10	13.46	12.52
	1-EPZ	0	0	1.54	2.89	5.39	5.73	11.53
	1,4-DMPZ	0	0	2.06	3.78	2.23	1.72	1.92
	AEP	0	21.18	50.66	63.80	98.62	105.05	124.59

Table D.60: Tabulated Experimental Data for TE60 (8 m PZ + 1 m Ethylenediamine, 0.3 mole CO_2 per mole alkalinity initially, 150 °C)

	Time (wk)	0	0.4	1.0	1.5	1.9	3.0	3.9
Original Samples (mmol/kg)	Gly	0.15	0.19	0.22	0.32	0.19	0.15	0.18
	Ace	0	0	0	0	0	0	0
	Form	0.07	2.28	5.02	7.25	8.86	8.62	14.82
	Oxa	0	0.00	0.01	0.00	0.01	0.01	0.00
	Sulf	0.11	0.14	0.13	0.15	0.18	0.13	0.13
	Cl^-	0	0	0	0	0	0	0
	NH_4^+	6.21	15.77	22.94	28.18	38.52	46.03	61.09
	FPZ	0	10.04	19.31	42.46	64.41	104.65	102.01
	EDA	492.62	381.42	296.09	277.19	263.03	261.63	235.42
	PZ	4212.1	4190.3	4168.8	4162.3	4125.1	4074.9	4044.7
	HEP	0	0	0	0	0	0	0
	1-MPZ	0	12.00	19.34	22.41	26.64	25.33	29.06
	1-EPZ	0	0	0	0	0	0	0
	1,4-DMPZ	0	0	0	0	0	0	0
	AEP	0	7.41	9.78	14.94	17.77	25.41	33.03
	2-Imid	0	95.68	172.00	192.16	206.89	198.73	222.89
	CO_2	2884.6	2718.1	2699.2	2654.4	2564.5	2566.8	2511.5
	SD_{CO2}	15.87	57.01	5.72	32.54	22.93	38.01	71.39
	Alk	4551.1	4429.5	4345.6	4376.7	4267.9	4246.5	4208.6
	SD_{Alk}	33.21	3.95	21.87	131.54	37.21	1.42	19.54
Hydrolyzed Samples (mmol/kg)	Gly	0.14	0.17	0.16	0.15	0.16	0.15	0.17
	Ace	0	0.05	0.08	0.12	0.15	0.24	0.34
	Form	0.20	8.43	17.22	26.58	32.63	47.62	65.22
	Oxa	0.01	0.01	0.01	0.01	0.01	0.01	0.02
	Sulf	0.11	0.15	0.13	0.15	0.16	0.14	0.16
	Cl^-	0	0	0	0	0	0	0
	NH_4^+	0	2.86	33.18	42.86	71.10	62.83	68.52
	FPZ	0	0	0	0	0	0	0
	EDA	492.17	384.59	300.21	278.85	258.17	260.77	238.64
	PZ	4186.3	4188.9	4159.9	4132.9	4125.4	4106.2	4124.2
	HEP	0	0	0	0	0	0	0
	1-MPZ	0	19.64	20.08	26.16	23.09	21.05	27.62
	1-EPZ	0	0	0	0	0	0	0
	1,4-DMPZ	0	0	0	0	3.23	3.90	4.31
	AEP	0	3.63	10.01	16.01	16.24	28.65	37.05

Table D.61: Tabulated Experimental Data for TE61 (4 m PZ, 0.3 mole H^+ per mole alkalinity initially, 175 °C)

	Time (wk)	0	1.0	1.9	3.9	6.1	6.1	6.1	8.0	9.9
Original Samples (mmol/kg)	Gly	0	0	0	0	0	0	0	0	0
	Ace	0	0	0.1	0.3	0.6	0.5	0.6	1.0	1.3
	Form	0	0.3	0.4	0.8	1.0	0.8	1.1	1.5	1.6
	Oxa	0	0	0	0	0	0	0	0	0
	Sulf	0	0	0	0	0	0	0	0	0
	Cl^-	0.0	0.0	0.0	0.0	0.0	0.0	0.0	0.0	0.0
	NH_4^+	1.1	3.6	9.0	33.7	51.3	39.4	51.5	113.1	162.8
	FPZ	0	0	0.8	1.6	1.8	1.4	1.6	2.7	3.0
	EDA	0	3.3	9.5	25.2	30.5	26.5	30.7	43.4	52.2
	PZ	2515.8	2481.9	2441.3	2305.1	2280.6	2323.4	2286.4	2167.1	2077.6
	HEP	0	0	0	0	0	0	0	0	0
	1-MPZ	0	0	0	0	0	0	0	0	0
	1-EPZ	0	0	3.1	8.7	11.6	9.5	11.4	20.2	26.8
	1,4-DMPZ	0	0	0	0	0	0	0	0	0
	AEP	0	1.1	3.8	15.1	22.1	17.1	22.0	38.1	49.0
	Alk	NT	NT	NT	NT	NT	NT	NT	NT	NT

Table D.62: Tabulated Experimental Data for TE62 (12 m PZ, 0.3 mole H^+ per mole alkalinity initially, 175 °C)

	Time (wk)	0	1.0	1.9	3.9	6.1	6.1	6.1	8.0	9.9
Original Samples (mmol/kg)	Gly	0	0	0	0	0	0	0	0	0
	Ace	0	0	0	0.12	0.20	0.21	0.21	0.45	0.80
	Form	0.57	0.12	0.33	0.90	1.00	0.77	1.04	1.64	2.41
	Oxa	0	0	0	0	0	0	0	0	0
	Sulf	0	0	0	0	0	0	0	0	0
	Cl^-	0.03	0.03	0.04	0.03	0.04	0.05	0.03	0.04	0.03
	NH_4^+	0.77	3.02	9.10	39.42	69.64	70.09	71.80	122.52	315.37
	FPZ	0	1.12	1.61	2.62	4.06	3.57	3.89	19.41	9.56
	EDA	0	4.16	12.69	34.55	46.66	51.81	46.32	68.24	143.27
	PZ	4568.2	4459.3	4310.9	4076.9	3945.6	3893.8	3871.8	4056.9	3185.4
	HEP	0	0	0	0	0	0	0	0	0
	1-MPZ	0	0	0	0	0	0	0	0	0
	1-EPZ	0	0.90	3.21	8.21	12.55	13.20	13.43	24.31	42.13
	1,4-DMPZ	0	0	0	0	0	0	0	0	0
	AEP	0	1.14	4.94	21.41	32.58	35.72	36.22	75.59	130.05
	Alk	NT	NT	NT	NT	NT	NT	NT	NT	NT

Table D.63: Tabulated Experimental Data for TE63 (8 m PZ, 0.6 mole H^+ per mole alkalinity initially, 175 °C)

	Time (wk)	0	1.0	1.9	3.9	6.1	6.1	6.1	8.0	9.9
Original Samples (mmol/kg)	Gly	0	0	0	0	0	0	0	0	0
	Ace	0	0	0	0.21	0.26	0.23	0.23	0.46	0.58
	Form	0	0.25	0.07	0.14	0.14	0.10	0.21	0.16	0.66
	Oxa	0	0	0	0	0	0	0	0	0
	Sulf	0	0	0	0	0	0	0	0	0
	Cl^-	0.01	0.03	0.03	0.04	0.06	0.02	0.04	0.05	0.04
	NH_4^+	0.96	5.25	10.25	48.85	58.47	51.71	56.81	115.67	181.34
	FPZ	0	1.12	1.55	2.23	2.93	2.66	3.52	3.83	5.41
	EDA	0	8.66	16.29	45.81	49.05	44.08	48.82	71.36	89.28
	PZ	3398.7	3331.7	3284.4	3207.9	3097.2	3127.4	3090.3	2995.3	2850.3
	HEP	0	0	0	0	0	0	0	0	0
	1-MPZ	0	0	0	0	0	0	0	0	0
	1-EPZ	0	2.16	3.81	11.05	12.19	10.40	12.17	18.50	25.80
	1,4-DMPZ	0	0	0	0	0	0	0	0	0
	AEP	0	2.89	6.90	26.72	32.26	26.89	31.52	55.79	79.59
	Alk	NT	NT	NT	NT	NT	NT	NT	NT	NT

Table D.64: Tabulated Experimental Data for TE64 (8 m PZ + 1 m 2-Imidazolidone, 0.3 mole CO_2 per mole alkalinity initially, 150 °C)

	Time (wk)	0	0.2	0.6	0.7	1.0
Original Samples (mmol/kg)	Gly	0.30	0.24	0.19	0.25	0.15
	Ace	0	0	0	0	0
	Form	0.16	0.29	1.31	1.43	1.49
	Oxa	0.00	0.01	0.01	0.01	0.01
	Sulf	0.14	0.13	0.09	0.31	0.17
	Cl^-	0.04	0.03	0.02	0.51	0.07
	NH_4^+	0	4.63	4.62	6.25	8.19
	FPZ	0.19	1.59	4.23	4.46	5.81
	EDA	0	42.61	119.82	139.12	162.33
	PZ	3688.2	3654.8	3679.3	3719.2	3695.5
	HEP	0	0	0	0	0
	1-MPZ	0	42.05	36.47	35.56	32.99
	1-EPZ	0	0	0	0	0
	1,4-DMPZ	0	0	0	0	0
	AEP	0	0	1.17	1.82	3.10
	2-Imid	538.89	434.94	356.42	329.90	297.73
	CO_2	2488.3	2579.4	2579.0	2617.6	2601.5
	SD_{CO2}	48.53	18.23	7.39	31.84	5.95
	Alk	3957.4	4032.2	4121.0	4121.6	4210.5
	SD_{Alk}	7.99	35.72	18.12	54.01	158.71
Hydrolyzed Samples (mmol/kg)	Gly	0.29	0.24	0.25	0.26	0.25
	Ace	0	0	0	0	0
	Form	0.26	1.64	6.19	5.78	7.35
	Oxa	0.02	0.03	0.01	0.02	0.02
	Sulf	0.19	0.17	0.11	0.13	0.20
	Cl^-	0.05	0.12	0.03	0.06	0.11
	NH_4^+	0	0	0	0	0
	FPZ	0	0	0	0	0
	EDA	0	51.38	122.23	141.27	168.24
	PZ	3794.6	3713.2	3747.5	3790.0	3795.3
	HEP	0	0	0	0	0
	1-MPZ	0	25.76	20.60	19.97	17.97
	1-EPZ	0	0	0	0	0
	1,4-DMPZ	0	0	0	0	0
	AEP	0	0	1.75	1.60	3.33

Table D.65: Tabulated Experimental Data for TE65 (8 m PZ, 0.1 mole HCO_3^- per mole alkalinity initially, 175 °C)

	Time (wk)	0	1.0	2.1	4.0	5.9	5.9	5.9	7.9	10.0
Original Samples (mmol/kg)	Gly	0.19	0.27	0.36	0.35	0.23	0.24	0.27	0.25	0.24
	Ace	0	0	0	0.08	0.11	0.12	0.12	0.31	0.22
	Form	0.01	0.79	0.35	3.79	5.84	5.98	6.38	12.66	11.13
	Oxa	0	0	0.02	0.02	0.01	0.02	0.02	0.02	0.01
	Sulf	0.61	0.49	0.43	0.39	0.31	0.27	0.30	0.21	0.28
	Cl^-	0.01	0.01	0.02	0.02	0.01	0.02	0.02	0.03	0.03
	NH_4^+	1.31	1.68	1.45	4.01	7.04	7.17	6.95	29.86	16.90
	FPZ	0	0	0	0.62	1.04	0.98	0.94	1.88	1.33
	EDA	0	1.40	0.89	5.68	8.98	8.90	9.50	17.64	15.19
	PZ	3962.2	3971.2	3988.1	3955.5	3933.3	3919.8	3914.8	3849.5	3900.6
	HEP	0	0	0	0	0	0	0	0	0
	1-MPZ	0	0	0	0	0	0	0	0	0
	1-EPZ	0	0	0	0.14	0.21	0.18	0.20	1.96	0.51
	1,4-DMPZ	0	0	0	0	0	0	0	0	0
	AEP	0	0.12	0.09	0.67	1.20	1.20	1.11	4.55	2.73
	CO_2	NT	NT	NT	NT	NT	NT	NT	NT	NT
	Alk	NT	NT	NT	NT	NT	NT	NT	NT	NT

Table D.66: Tabulated Experimental Data for TE66 (8 m PZ, 0.3 mole CO_2 per mole alkalinity initially, 175 °C, 200 mM formate)

	Time (wk)	0	0.2	0.3	0.4	0.6	0.7
Original Samples (mmol/kg)	Gly	0.09	0.11	0.13	0.13	0.10	0.12
	Ace	0.14	0.14	0.15	0.17	0.17	0.21
	Form	153.64	50.12	54.22	51.10	52.00	52.83
	Oxa	0.02	0.01	0.01	0.01	0.01	0.02
	Sulf	0.07	0.14	0.12	0.16	0.14	0.15
	Cl^-	0.05	0.03	0.04	0.08	0.06	0.07
	NH_4^+	0.40	1.21	1.97	2.88	4.21	5.89
	FPZ	1.73	203.74	205.94	214.79	220.29	230.77
	EDA	0	3.03	4.09	4.82	6.26	7.95
	PZ	3578.1	3429.2	3473.7	3402.6	3399.8	3345.7
	HEP	0	0	0	0	0	0
	1-MPZ	0	0	0	0	0	0
	1-EPZ	0	0.11	0.28	0.41	0.54	0.88
	1,4-DMPZ	0	0	0	0	0	0
	AEP	0	0.31	0.66	1.03	1.50	2.42
	CO_2	NT	NT	NT	NT	NT	NT
	Alk	NT	NT	NT	NT	NT	NT
Hydrolyzed Samples (mmol/kg)	Gly	0.35	0.61	0.70	0.73	1.05	0.98
	Ace	0.25	0.25	0.25	0.30	0.31	0.40
	Form	160.79	169.16	164.95	172.93	175.62	183.62
	Oxa	0.02	0.02	0.03	0.03	0.03	0.03
	Sulf	0.06	0.13	0.12	0.30	0.08	0.16
	Cl^-	0.04	0.04	0.04	0.64	0.04	0.08
	NH_4^+	0	0	0	0	0	0
	FPZ	0	0	0	0	0	0
	EDA	0	3.21	4.50	5.73	8.89	9.41
	PZ	3669.1	3603.6	3541.4	3556.4	3474.4	3485.9
	HEP	0	0	0	0	0	0
	1-MPZ	0	0	0	0	0	0
	1-EPZ	0	0.13	0.31	0.47	0.58	0.98
	1,4-DMPZ	0	0	0	0	0	0
	AEP	0	0.38	0.72	1.13	1.60	2.76

Table D.67: Tabulated Experimental Data for TE67 (8 m PZ, 0.3 mole CO_2 per mole alkalinity initially, 175 °C, 200 mM FPZ)

	Time (wk)	0	0.2	0.3	0.4	0.6	0.7
Original Samples (mmol/kg)	Gly	0.13	0.11	0.13	0.12	0.10	0.11
	Ace	0.04	0.06	0.11	0.09	0.11	0.11
	Form	8.71	49.90	50.07	44.36	49.73	50.60
	Oxa	0.00	0.02	0.02	0.02	0.02	0.01
	Sulf	0.12	0.08	0.12	0.11	0.18	1.26
	Cl^-	0.08	0.03	0.04	0.06	0.10	0.11
	NH_4^+	0.60	1.01	2.87	3.51	4.52	4.90
	FPZ	276.11	232.87	240.58	238.46	251.89	256.17
	EDA	0	3.32	4.55	4.59	5.74	6.74
	PZ	3738.7	3727.9	3716.7	3600.7	3688.3	3671.5
	HEP	0	0	0	0	0	0
	1-MPZ	0	0	0	0	0	0
	1-EPZ	0	0.10	0.27	0.34	0.43	0.61
	1,4-DMPZ	0	0	0	0	0	0
	AEP	0	0.30	0.89	0.98	1.34	1.98
	CO_2	NT	NT	NT	NT	NT	NT
	Alk	NT	NT	NT	NT	NT	NT
Hydrolyzed Samples (mmol/kg)	Gly	1.40	0.43	0.60	0.73	0.90	0.99
	Ace	0.05	0.12	0.15	0.15	0.20	0.23
	Form	182.86	189.43	191.19	194.03	197.17	199.02
	Oxa	0	0.04	0.04	0.03	0.04	0.03
	Sulf	0.13	0.11	0.12	0.12	0.17	1.32
	Cl^-	0.03	0.05	0.12	0.12	0.10	0.12
	NH_4^+	0	0	0	0	0	0
	FPZ	0	0	0	0	0	0
	EDA	0.44	4.23	5.29	5.94	7.24	8.28
	PZ	3902.6	3976.9	3944.3	3997.8	3909.7	3874.3
	HEP	0	0	0	0	0	0
	1-MPZ	0	0	0	0	0	0
	1-EPZ	0	0	0	0.31	0.55	0.75
	1,4-DMPZ	0	0	0	0	0	0
	AEP	0	0.50	0.99	1.21	1.61	2.13

Appendix E – Tabulated Data from Oxidation Experiments

All tabulated experimental data that follows maintains the same format. Original sample data are the raw values from the experimental samples. The base hydrolyzed data is the post-NaOH treatment data where the difference between the two would represent amide concentrations. Data shown are not sulfate-adjusted. Outlier data have not been removed. Abbreviations are as follows:

Fe^{2+}, iron added as $FeSO_4 \cdot 7H_2O$
Cu^{2+}, copper added as $CuSO_4 \cdot 5H_2O$
Cr^{3+}, chromium added as $Cr_2(SO_4)_3 \cdot 3.8H_2O$ or $CrK(SO_4)_2 \cdot 12H_2O$
Ni^{2+}, nickel added as $NiSO_4 \cdot 6H_2O$
V^{4+}, vanadium added as $NaVO_3$
A, Inhibitor A
B, Inhibitor B
OOR, Original Oxidation Reactor
TOR, Teflon Oxidation Reactor
Gly, Glycolate (Anion IC)
Ace, Acetate (Anion IC)

Form, Formate (Anion IC)
NO_2^-, Nitrite (Anion IC)
Oxa, Oxalate (Anion IC)
NO_3^-, Nitrate (Anion IC)
Sulf, Sulfate (Anion IC)
Cl^-, Chloride (Anion IC)
NH_4^+, Ammonium (Cation IC)
FPZ, N-Formyl PZ (Cation IC)
EDA, Ethylenediamine (Cation IC)
PZ, Piperazine (Cation IC)
CO_2 (TIC), Carbon Dioxide
SD_{CO2}, standard deviation of three CO_2 measurements
Alk, total alkalinity (Acid Titration)
SD_{Alk}, standard deviation of two total alkalinity titrations
NT, value not tested
NA, not applicable; when only one measurement was made, calculation of standard deviation was not possible

Table E.1: Tabulated Experimental Data for OE1 (10 m PZ, 2 kPa CO_2, 98 kPa O_2, 55 °C, 0.27 mM Fe^{2+}, 0.65 mM Cr^{3+}, 0.26 mM Ni^{2+}, OOR)

		10 m PZ + Fe + Cr + Ni									
	Time (hr)	0	23.5	74.0	120.5	171.5	271.8	315.8	360.8	461.0	603.5
Original Samples (mmol/kg)	Gly	0	0	0	0	0	0	0	0	0	0
	Ace	0	0	0	0	0	0	0	0	0	0
	Form	0.07	0.21	1.38	1.82	0.62	1.15	1.26	1.61	1.99	2.96
	NO_2^-	0	0	0	0	0	0	0	0	0	0
	Oxa	0.13	0.02	0	0.02	0.00	0.09	0.05	0.05	0.06	0.08
	NO_3^-	0	0	0	0	0	0	0	0.22	0.26	0.23
	EDA	0	0	0	0	0	0	0	0	0	0
	PZ	4915.2	4959.9	4846.4	4894.9	4779.8	4972.4	4515.0	4503.5	4316.4	4271.0
	CO_2	NT	NT	NT	NT	NT	NT	NT	NT	NT	NT
	Alk	NT	NT	NT	NT	NT	NT	NT	NT	NT	NT
Hydrolyzed Samples (mmol/kg)	Gly	0	0.05	0	0.11	0.10	0.09	0.08	0.03	0.08	0.11
	Ace	0	0.09	0.11	0.11	0.13	0.16	0.13	0.12	0.17	0.20
	Form	0.42	0.92	2.24	3.26	3.76	4.09	4.32	4.63	6.40	7.28
	NO_2^-	0	0	0	0	0	0.10	0.04	0.06	0.06	0.11
	Oxa	0	0	0.08	0.06	0.09	0.08	0.06	0.11	0.15	0.22
	NO_3^-	0	0	0	0	0.12	0.08	0.07	0.10	0.18	0.10
	EDA	NT	NT	NT	NT	NT	NT	NT	NT	NT	NT
	PZ	NT	NT	NT	NT	NT	NT	NT	NT	NT	NT

Table E.2: Tabulated Experimental Data for OE2 (10 m PZ, 2 kPa CO_2, 98 kPa O_2, 55 °C, 3.94 mM Cu^{2+}, OOR)

		10 m PZ + Cu											
	Time (hr)	0.0	22.0	68.0	118.0	166.5	210.0	257.8	309.0	352.5	400.5	451.5	495.0
Original Samples (mmol/kg)	Gly	0.26	0	0	0	0	0	0	0	0	0	0.04	0.05
	Ace	0	0.38	0.69	2.11	2.20	1.21	1.24	1.25	1.27	0.90	1.05	1.01
	Form	0.17	3.56	14.76	30.02	41.14	48.46	56.79	60.89	62.79	63.35	65.36	68.25
	NO_2^-	0	0.46	1.83	3.33	3.28	3.63	3.01	2.96	2.85	2.93	2.88	2.80
	Oxa	0	0.19	0.59	1.62	2.66	3.80	5.00	5.68	5.95	7.14	8.33	9.49
	NO_3^-	0	0.61	1.12	0	0	2.10	2.25	2.23	2.20	2.54	2.36	2.00
	EDA	19.71	98.10	144.18	167.64	191.81	200.29	222.90	223.04	220.76	221.16	233.92	232.77
	PZ	4480.5	4207.3	3883.4	3493.4	3314.7	3225.9	3146.4	3120.5	3076.4	3026.9	3023.9	2983.2
	CO_2	NT	NT	NT	NT	NT	NT	NT	NT	NT	NT	NT	NT
	Alk	4496.1	4274.5	4058.3	3822.1	3684.8	3543.6	3548.7	3461.5	3367.3	3330.5	3315.7	3294.3
	SD_{Alk}	NA	NA	NA	NA	NA	NA	NA	NA	NA	NA	NA	NA
Hydrolyzed Samples (mmol/kg)	Gly	0.40	0.59	0.72	0.98	0.28	0.41	0.53	0.32	0.59	0.52	0.39	0.41
	Ace	0.14	0.41	1.08	1.65	0.96	1.32	1.28	1.36	2.32	2.53	2.40	2.44
	Form	5.17	43.17	93.97	126.65	143.78	157.24	174.20	174.26	164.84	171.42	178.89	184.68
	NO_2^-	0	0.19	1.28	2.00	2.90	2.83	2.94	2.65	2.89	2.91	1.73	1.67
	Oxa	0	4.66	15.86	26.31	34.39	41.15	49.57	46.93	45.22	50.10	24.29	25.77
	NO_3^-	0	0.47	0.52	1.71	2.00	2.32	1.67	1.95	2.19	2.22	1.24	1.35
	EDA	NT	NT	NT	NT	NT	NT	NT	NT	261.79	296.64	NT	309.45
	PZ	NT	NT	NT	NT	NT	NT	NT	NT	3199.7	3489.8	NT	3212.7

Table E.3: Tabulated Experimental Data for OE3 (8 m PZ, 2 kPa CO_2, 98 kPa O_2, 55 °C, 0.10 mM Fe^{2+}, 0.10 mM V^{4+}, OOR)

		8 m PZ + Fe + V								
	Time (hr)	0	48.0	92.5	143.5	193.5	241.0	286.0	333.0	381.0
Original Samples (mmol/kg)	Gly	0	0	0.01	0.02	0.02	0.03	0.03	0.04	0.07
	Ace	0	0.01	0	0.01	0.03	0.03	0.01	0.01	0.13
	Form	0.05	0.26	0.40	0.64	1.01	1.46	1.79	2.12	5.05
	NO_2^-	0	0.04	0.09	0.12	0.21	0.30	0.36	0.44	0.65
	Oxa	0	0.02	0.01	0.02	0.04	0.03	0.04	0.05	0.07
	NO_3^-	0	0.17	0.28	0.41	0.45	0.49	0.58	0.64	0.99
	Sulf	0.34	0.36	0.28	0.41	0.40	0.48	0.49	0.34	8.57
	EDA	0	0	0	0	0	0	0	0	0
	PZ	4371.5	4481.6	4472.3	4403.3	4380.3	4294.4	4455.2	4106.9	4374.1
	CO_2	2563.4	NT	2291.9	NT	2050.5	NT	1886.8	NT	1752.6
	SD_{CO2}	22.72	NT	48.32	NT	47.19	NT	30.44	NT	12.86
	Alk	4157.5	4338.3	4262.2	4182.6	4185.8	4126.1	4075.2	4019.7	3963.8
	SD_{Alk}	8.94	51.58	12.66	5.47	12.74	1.42	3.42	9.86	14.95
Hydrolyzed Samples (mmol/kg)	Gly	0.11	0.07	0.07	0.08	0.13	0.18	0.14	0.18	0.23
	Ace	0.10	0.08	0.13	0.09	0.12	0.57	0.16	0.18	0.62
	Form	0.33	1.02	1.87	2.44	3.50	6.33	4.99	6.32	10.54
	NO_2^-	0	0.03	0.09	0.13	0.14	0.40	0.36	0.44	0.70
	Oxa	0.02	0.04	0.05	0.07	0.04	0.14	0.15	0.18	0.25
	NO_3^-	0	0.11	0.30	0.39	0.27	0.60	0.59	0.66	0.95
	Sulf	0.39	0.37	0.30	0.39	0.24	0.54	0.43	0.41	0.55
	EDA	0	0	0	0	0	0	0	0	0
	PZ	4432.2	4613.6	4415.5	4370.7	4347.3	4241.5	4209.1	4039.8	4323.9

Table E.4: Tabulated Experimental Data for OE4 (8 m PZ, 2 kPa CO_2, 98 kPa O_2, 55 °C, 0.1 mM Fe^{2+}, 5.02 mM Cu^{2+}, 100.15 mM Inhibitor A, OOR)

	8 m PZ + Fe + Cu + A															
	Time (hr)	0	50.8	96.0	146.5	191.0	242.5	290.5	340.0	410.5	456.5	504.5	552.0	598.5	670.3	742.3
Original Samples (mmol/kg)	Gly	0.07	0.01	0.01	0.00	0.02	0.03	0.03	0.03	0.04	0.04	0.03	0.01	0.02	0.05	0.01
	Ace	0.02	0.09	0.08	0.09	0.04	0.03	0.11	0.10	0.07	0.10	0.06	0.10	0.06	0.14	0.11
	Form	0.11	1.17	1.79	2.35	2.86	3.23	3.88	4.30	4.89	5.23	5.61	6.49	7.05	7.71	7.91
	NO_2^-	0	0.26	0.32	0.30	0.39	0.42	0.36	0.37	0.39	0.35	0.37	0.48	0.52	0.51	0.43
	Oxa	0	0.01	0.02	0.03	0.05	0.07	0.10	0.12	0.15	0.15	0.19	0.26	0.30	0.34	0.34
	NO_3^-	0.04	0.10	0.16	0.25	0.24	0.19	0.33	0.35	0.36	0.32	0.36	0.54	0.67	0.58	0.41
	Sulf	8.13	8.05	8.09	7.79	8.07	7.93	8.16	8.08	8.41	7.74	7.75	11.05	11.14	10.39	7.35
	EDA	0	3.62	7.36	4.80	7.33	3.24	4.60	6.88	7.36	4.61	9.20	0	0	0	6.68
	PZ	4378.2	4347.8	4240.8	4109.1	4089.9	4070.2	4072.2	4050.1	3977.7	3926.8	3906.6	3869.0	3777.1	3660.9	3744.1
	CO_2	2437.3	2213.5	2089.1	2049.9	1914.2	1828.9	1768.3	1711.3	1616.3	1627.1	1547.8	1462.6	1299.1	1352.3	1347.5
	SD_{CO2}	41.71	40.28	36.34	31.23	33.65	20.65	51.30	45.35	10.74	27.43	27.54	24.20	8.25	4.98	2.79
	Alk	4002.5	3999.9	3983.1	3937.2	3925.4	3896.6	3843.2	3833.7	3833.6	3809.3	3746.5	3713.0	3628.2	3532.1	3589.2
	SD_{Alk}	0.82	0.14	0.23	10.50	0.05	2.93	6.00	5.26	5.35	0.33	0.38	1.00	8.54	105.49	44.35
Hydrolyzed Samples (mmol/kg)	Gly	0.35	0.09	0.08	0.11	0.15	0.15	0.12	0.11	0	0.06	0.04	0.06	0.10	0.06	0.03
	Ace	0.52	0.30	0.30	0.46	0.43	1.15	0.47	0.45	0	0.68	0.44	0.50	0.42	0.53	0.63
	Form	0.71	5.07	6.18	7.67	8.26	9.98	9.53	11.38	14.56	15.17	13.50	15.00	15.90	16.13	20.48
	NO_2^-	0.05	0.40	0.46	0.41	0.42	0.43	0.52	0.51	0.49	0.43	0.38	0.49	0.55	0.43	0.51
	Oxa	0.01	0.15	0.25	0.61	0.44	0.40	0.63	0.70	0.77	0.85	0.70	0.84	1.01	0.93	1.27
	NO_3^-	0	0.19	0.19	0.24	0.27	0.55	0.23	0.25	0.39	0.38	0.36	0.55	0.40	0.39	0.50
	Sulf	8.15	8.20	8.32	8.15	8.08	8.19	8.66	9.27	9.40	9.04	7.64	10.13	12.07	7.46	9.05
	EDA	0	3.52	6.81	3.16	3.65	0	0	0	8.07	9.02	2.82	0	0	2.97	4.33
	PZ	4369.8	4155.5	4273.8	4151.7	4062.5	3987.1	3981.7	4026.0	2708.3	2590.2	3859.7	3840.0	3742.5	3442.0	2415.6

Table E.5: Tabulated Experimental Data for OE5/OE5B (8 m PZ, 2 kPa CO_2, 98 kPa O_2, 55 °C, 1.03 mM Fe^{2+}, OOR)

	8 m PZ + Fe							
	Time (hr)	0	20.0	47.5	70.3		70.3	117.8	162.5
Original Samples (mmol/kg)	Gly	0.045	0.010	0.021	0.077	Reactor contents removed for foaming test, and then restarted.	0.073	0.116	0.107
	Ace	0.145	0.274	0.174	0.052		0.073	0.147	0.054
	Form	0.353	0.480	0.288	0.496		0.369	0.555	0.658
	NO_2^-	0	0.044	0.024	0.027		0	0.010	0.012
	Oxa	0.077	0.068	0.051	0		0	0	0
	NO_3^-	0.062	0.026	0.023	0.062		0	0	0
	Sulf	2.924	3.009	3.006	2.988		0.966	0.969	0.940
	Cl^-	0.266	0.123	0.153	0.154		0.031	0.040	0.044
	EDA	0	0	0	4.759		0	0	0
	PZ	4243.0	4038.6	4061.9	4066.4		4159.4	3973.1	3924.8
	CO_2	2520.0	2457.6	2512.9	2502.0		2477.0	2344.2	2296.9
	SD_{CO2}	23.857	12.908	24.298	14.499		8.673	9.545	6.324
	Alk	4083.6	3940.2	3888.4	3832.1		3812.4	3605.3	3575.9
	SD_{Alk}	28.186	8.822	7.624	13.337		19.238	11.016	14.935
Hydrolyzed Samples (mmol/kg)	Gly	0.104	0.243	0.612	0.564		0	0	0
	Ace	0	0	0	0.645		0.065	0.012	0
	Form	0.399	0.553	0.975	2.393		1.461	1.798	2.132
	NO_2^-	0.033	0.015	0.016	0.055		0	0.018	0.019
	Oxa	0.033	0.034	0.004	0.053		0.041	0.043	0.057
	NO_3^-	0.011	0.024	0.024	0.091		0.190	0.010	0.014
	Sulf	1.784	1.649	1.630	1.991		1.003	0.952	1.062
	Cl^-	0.198	0.067	0.042	0.598		0.044	0.055	0.076
	EDA	0	0	0	0		0	0	0
	PZ	4211.8	4583.0	4754.8	4030.2		4030.5	4342.1	3934.4

Table E.6: Tabulated Experimental Data for OE6/OE6B (8 m PZ, 2 kPa CO_2, 98 kPa O_2, 55 °C, 1.03 mM Fe^{2+}, 100.36 mM Inhibitor A, OOR)

	8 m PZ + Fe + A							
	Time (hr)	0	20.0	47.5	70.3	70.3	117.8	162.5
Original Samples (mmol/kg)	Gly	0.06	0.04	0.04	0.02	0.03	0	0
	Ace	0.24	0.02	0.02	0.03	0.17	0.02	0
	Form	0.25	0.37	0.34	0.53	0.38	0.53	0.76
	NO_2^-	0.01	0.01	0.01	0.01	0.05	0.02	0.04
	Oxa	0.01	0.01	0.03	0	0.02	0.01	0.04
	NO_3^-	0.02	0.20	0.03	0	0	0	0.03
	Sulf	1.59	1.74	1.65	1.76	1.64	1.41	1.67
	Cl^-	0.17	0.43	0.12	0.04	0.29	0.08	0.17
	EDA	0	0	0	0	0	0	0
	PZ	4251.8	4288.3	4342.4	4333.9	4360.5	4232.2	4443.5
	CO_2	2481.5	2267.4	2258.5	2231.0	2227.3	2514.7	2687.4
	SD_{CO2}	21.15	5.14	8.83	13.39	4.67	6.89	30.69
	Alk	4049.3	4121.2	4153.1	4169.8	4178.1	4023.1	4307.7
	SD_{Alk}	21.38	22.20	6.85	11.90	11.38	5.07	7.33
Hydrolyzed Samples (mmol/kg)	Gly	0.21	0.08	0.07	0.20	0	0	0
	Ace	0	0	0	0	0	0	0.01
	Form	0.33	0.55	0.98	1.29	0.79	1.07	1.39
	NO_2^-	0	0.01	0.01	0.02	0.03	0.03	0.03
	Oxa	0	0	0.03	0.12	0.03	0.03	0.04
	NO_3^-	0	0	0	0	0	0.14	0
	Sulf	1.54	1.46	1.51	1.81	2.05	1.83	1.88
	Cl^-	0.06	0	0	0.26	0.48	0.17	0.20
	EDA	0	0	0	0	0	0	0
	PZ	4542.0	4808.3	4912.7	4260.2	4406.9	4297.5	4496.4

Reactor contents removed for foaming test, and then restarted.

Table E.7: Tabulated Experimental Data for OE7 (8 m PZ, 2 kPa CO_2, 98 kPa O_2, 55 °C, 1.00 mM Fe^{2+}, 20.82 mM Inhibitor B, OOR)

	8 m PZ + Fe + Inh B					
	Time (hr)	0.0	19.5	71.3	119.0	163.8
Original Samples (mmol/kg)	Gly	0	0.01	0.02	0.01	0.02
	Ace	0.01	0.01	0.00	0.03	0.03
	Form	0.15	0.20	0.23	0.20	0.24
	NO_2^-	0	0	0	0	0
	Oxa	0	0	0	0	0
	NO_3^-	0	0	0.01	0.01	0.01
	Sulf	16.95	18.50	17.87	17.98	18.23
	Cl^-	0.04	0.10	0.07	0.14	0.05
	EDA	0	0	0	0	0
	PZ	4396.3	4212.2	4145.3	4152.1	4217.8
	CO_2	2709.1	2710.6	2665.7	2686.2	2667.3
	SD_{CO2}	5.60	11.76	24.49	25.68	9.48
	Alk	4082.2	4042.3	3978.5	3998.5	4020.8
	SD_{Alk}	21.35	0.15	0.96	11.94	3.42
Hydrolyzed Samples (mmol/kg)	Gly	0.24	0	0	0.04	0.08
	Ace	0.01	0.02	0.01	0	0
	Form	0.47	0.65	0.50	0.55	0.61
	NO_2^-	0.02	0.06	0.00	0	0
	Oxa	0	0	0	0	0
	NO_3^-	0	0	0.01	0	0
	Sulf	16.53	18.94	17.92	17.95	18.25
	Cl^-	0.06	0.50	0.04	0.06	0.03
	EDA	0	0	0	0	0
	PZ	4516.2	4275.7	4159.6	4135.6	4177.8

Table E.8: Tabulated Experimental Data for OE8 (8 m PZ, 2 kPa CO_2, 98 kPa O_2, 55 °C, 1.0 mM Fe^{2+}, 29.89 mM Inhibitor C, OOR)

	8 m PZ + Fe + Inh C					
	Time (hr)	0	19.5	71.3	119.0	163.8
Original Samples (mmol/kg)	Gly	0.02	0	0	0	0
	Ace	0.06	0.10	0.04	0	0
	Form	0.25	1.83	3.95	6.37	8.10
	NO_2^-	0	0.05	0.04	0.09	0.09
	Oxa	0	0	0.08	0.29	0.32
	NO_3^-	0	0.04	0	0	0
	Sulf	1.37	1.26	1.04	1.15	1.16
	Cl^-	0.13	0.11	0.26	0.42	0.16
	EDA	0	11.17	30.67	50.90	51.76
	PZ	4231.7	4235.0	4065.2	4097.9	3974.9
	CO_2	2680.9	2582.8	2497.5	2517.5	2547.9
	SD_{CO2}	34.76	33.03	36.82	3.06	28.56
	Alk	4027.4	4012.6	3944.3	3935.9	3927.3
	SD_{Alk}	1.93	3.97	3.07	3.63	19.35
Hydrolyzed Samples (mmol/kg)	Gly	0	0	0	0	0
	Ace	0	0	0	0	0.07
	Form	0.68	3.46	10.28	15.77	18.44
	NO_2^-	0.06	0.05	0.07	0.11	0.10
	Oxa	0.02	0.12	1.35	2.70	4.36
	NO_3^-	0.12	0	0	0.08	0
	Sulf	1.43	1.18	1.20	1.11	1.18
	Cl^-	0.26	0.23	0.24	0.33	0.32
	EDA	0	15.64	33.08	50.30	70.50
	PZ	4269.9	4382.0	4058.6	4117.2	4041.0

Table E.9: Tabulated Experimental Data for OE9 (8 m PZ, 2 kPa CO_2, 98 kPa N_2, OOR)

		8 m PZ + N_2							
	Time (hr)	0	48.0	96.8	145.8	192.3	240.8	287.8	336.3
Original Samples (mmol/kg)	Gly	0.38	0.42	0.43	0.25	0.40	1.46	0.37	0.50
	Ace	0	0	0	0	0	0	1.92	0
	Form	0.51	1.28	0.60	0.78	1.26	0.83	1.73	1.07
	NO_2^-	0	0	0	0	0	0	0	0
	Oxa	0	0	0	0	0	0	0	0.02
	NO_3^-	0	0	0	0	0	0	0	0
	Sulf	0.44	0.41	0.41	0.42	0.41	0.41	0.43	0.40
	Cl^-	0.09	0.05	0.08	0.09	0.07	0.08	0.07	0.10
	EDA	0	0	0	0	0	0	0	0
	PZ	4368.7	4271.0	4199.9	4138.0	4237.2	4195.1	4081.3	4210.7
	CO_2	2733.8	2671.3	2597.3	2605.5	2696.1	2599.1	2551.0	2665.3
	SD_{CO2}	5.04	9.94	20.02	1.49	5.22	11.40	4.70	11.79
	Alk	4108.7	3987.4	3916.6	3869.7	3989.5	3856.4	3753.2	3915.5
	SD_{Alk}	5.32	9.67	3.13	4.25	5.04	0.35	3.99	4.54
Hydrolyzed Samples (mmol/kg)	Gly	0.18	0.18	0.18	0	0	0.30	0	0
	Ace	0	1.37	0	0	0	0	0	0
	Form	1.82	2.18	1.86	1.82	2.65	2.32	2.78	2.54
	NO_2^-	0	0	0	0	0	0	0	0
	Oxa	0	0	0	0	0.01	0.01	0.01	0.03
	NO_3^-	0	0	0	0	0	0	0	0
	Sulf	0.28	0.27	0.20	0.19	0.26	0.29	0.55	0.36
	Cl^-	0.08	0.07	0.04	0.10	0.06	0.07	0.09	0.26
	EDA	0	0	0	0	0	0	0	0
	PZ	4402.0	4317.1	4176.2	4094.1	4234.8	4188.8	4069.9	4142.3

Table E.10: Tabulated Experimental Data for OE10 (8 m PZ, 2 kPa CO_2, 98 kPa N_2, 55 °C, 19.77 mM K_2SO_4, OOR)

		8 m PZ + N_2							
	Time (hr)	0	46.0	94.3	142.0	191.0	239.8	293.8	336.3
Original Samples (mmol/kg)	Gly	0	0	0	0	0	0	0	0
	Ace	0	0	0	0	0	0	0	0
	Form	0.10	0.33	0.47	0.62	0.68	0.69	1.06	1.07
	NO_2^-	0	0	0	0	0	0	0	0
	Oxa	0	0	0	0	0	0	0	0
	NO_3^-	0	0	0	0	0	0.01	0.01	0.03
	Sulf	16.99	16.73	16.76	15.83	16.18	15.28	18.93	19.33
	Cl^-	0.03	0.06	0.04	0.03	0.06	0.03	0.04	0.03
	EDA	0	0	0	0	0.71	1.55	3.24	3.60
	PZ	4343.5	4336.1	4293.2	4319.6	4288.8	4252.4	4750.2	4862.7
	CO_2	2639.8	2733.5	2681.5	2645.5	2638.6	2612.7	2628.0	2877.1
	SD_{CO2}	6.06	6.38	40.69	6.44	6.15	10.28	17.85	2.76
	Alk	4100.3	4056.1	4040.3	4038.3	4090.5	4013.3	4522.1	4611.1
	SD_{Alk}	40.31	11.31	6.36	0.00	476.59	0.71	2.83	45.25
Hydrolyzed Samples (mmol/kg)	Gly	0	0	0	0	0	0	0	0
	Ace	0	0	0	0	0	0	0	0
	Form	0.38	1.43	1.80	2.35	2.72	3.23	4.55	4.67
	NO_2^-	0	0	0.01	0.02	0.03	0.07	0.09	0.10
	Oxa	0	0.04	0.06	0.08	0.09	0.08	0.13	0.14
	NO_3^-	0	0.02	0.05	0.02	0.03	0.04	0.09	0.07
	Sulf	16.69	16.66	17.67	17.48	17.52	17.53	20.14	20.47
	Cl^-	0.03	0.05	0.08	0.05	0.08	0.06	0.40	0.09
	EDA	0	0	0	0	0	0.93	2.59	3.06
	PZ	4371.4	4344.1	4270.0	4335.0	4277.2	4276.3	4767.5	4852.8

Table E.11: Tabulated Experimental Data for OE11 (8 m PZ, 2 kPa CO_2, 98 kPa O_2, 55 °C, 20.12 mM K_2SO_4, OOR)

		8 m PZ + O_2							
	Time (hr)	0	53.3	96.0	142.0	191.8	234.5	262.0	314.0
Original Samples (mmol/kg)	Gly	0	0	0	0	0	0	0	0
	Ace	0	0.08	0	0	0	0	0	0
	Form	0.20	0.18	0.26	0.54	0.54	0.56	0.48	0.96
	NO_2^-	0.06	0.06	0.06	0.05	0.05	0.05	0.06	0.06
	Oxa	0.03	0	0	0	0	0.05	0	0
	NO_3^-	0.01	0.02	0.06	0.01	0	0.01	0.02	0.01
	Sulf	0.59	18.01	17.47	17.79	17.58	16.72	17.00	16.66
	Cl^-	0.09	0.02	0.02	0.03	0.02	0.02	0.02	0.03
	EDA	0	1.85	2.86	4.10	4.47	5.91	5.10	5.85
	PZ	4531.5	4442.4	4349.1	4323.8	4277.7	4261.6	4253.8	4238.7
	CO_2	2582.9	2669.3	2658.6	2614.9	2576.7	2556.5	2567.6	2466.6
	SD_{CO2}	12.86	20.20	7.84	6.90	6.12	28.99	5.97	13.21
	Alk	4134.8	4114.4	4015.3	4035.8	4006.2	3957.4	3992.8	3883.0
	SD_{Alk}	19.80	9.19	28.28	44.55	10.61	19.09	8.49	14.85
Hydrolyzed Samples (mmol/kg)	Gly	0	0	0	0	0	0	0	0
	Ace	0	0	0	0	0	0	0	0
	Form	0.31	0.88	1.21	1.44	3.23	2.20	1.62	2.40
	NO_2^-	0.04	0.05	0.05	0.05	0.21	0.07	0.06	0.06
	Oxa	0.03	0.01	0.02	0.03	0.05	0.05	0.03	0.09
	NO_3^-	0.03	0.01	0.01	0.02	0.06	0.02	0.02	0.02
	Sulf	0.41	16.85	16.97	15.87	18.16	17.54	17.25	16.97
	Cl^-	0.17	0.03	0.06	0.03	3.80	0.09	0.04	0.09
	EDA	3.26	2.27	10.57	5.49	294.65	4.78	3.50	14.17
	PZ	4464.2	4408.9	4340.8	4331.7	4303.4	4217.6	4232.4	4174.3

Table E.12: Tabulated Experimental Data for OE12 (8 m PZ, 2 kPa CO_2, 98 kPa O_2, 55 °C, 20.09 mM K_2SO_4, OOR)

	8 m PZ + O_2							
	Time (hr)	0	52.5	100.3	150.0	216.5	244.0	296.0
Original Samples (mmol/kg)	Gly	0	0	0	0	0	0	0
	Ace	0	0	0	0	0	0	0
	Form	0.19	0.15	0.25	0.32	0.44	0.60	0.51
	NO_2^-	0	0	0	0	0	0	0
	Oxa	0	0	0	0	0.07	0.08	0.09
	NO_3^-	0	0	0	0	0	0	0
	Sulf	16.74	16.23	17.33	17.21	17.85	16.87	17.93
	Cl^-	0	0	0	0	0	0	0.22
	EDA	0	0	0	0	0	0	0
	PZ	4431.9	4404.6	4376.3	4312.8	4314.5	4169.6	4284.4
	CO_2	2390.8	2564.8	2531.9	2563.8	2579.0	2434.0	2560.5
	SD_{CO2}	14.19	17.86	3.66	31.61	30.21	13.41	11.51
	Alk	4114.2	4097.8	4074.3	4055.8	4077.1	3863.9	4049.4
	SD_{Alk}	3.77	0.46	1.83	11.29	4.79	1.95	1.72
Hydrolyzed Samples (mmol/kg)	Gly	0	0	0	0	0	0	0
	Ace	0	0	0	0	0	0	0
	Form	0.35	0.63	0.82	0.97	1.49	2.15	1.82
	NO_2^-	0	0	0	0	0	0	0
	Oxa	0	0.10	0.12	0.12	0.13	0.22	0.17
	NO_3^-	0	0	0	0	0	0	0
	Sulf	16.85	17.65	17.51	17.32	16.62	16.86	18.75
	Cl^-	0	0.55	0	0	0.07	0	4.55
	EDA	0	0	0	0	0	0	0
	PZ	4384.0	4368.8	4328.7	4324.4	4082.6	4159.4	4278.4

Table E.13: Tabulated Experimental Data for OE13 (8 m PZ, 2 kPa CO_2, 98 kPa O_2, 55 °C, 1.00 mM Fe^{2+}, OOR)

		8 m PZ + Fe + Cu + A								
	Time (hr)	0.3	40.3	99.0	164.8	238.0	310.0	380.5	454.0	523.0
Original Samples (mmol/kg)	Gly	0.66	0.63	0.59	0.58	0.56	0.56	0.72	0.52	0.52
	Ace	0.11	0.23	0.45	0.52	0.53	0.53	0.14	0.49	0.55
	Form	0.05	0.09	0.34	0.57	0.86	1.08	2.11	1.55	1.76
	NO_2^-	0	0	0.01	0.01	0.01	0.01	0.01	0.01	0.01
	Oxa	0.01	0.01	0.01	0.02	0.02	0.03	0.03	0.04	0.07
	NO_3^-	0	0.01	0.03	0.02	0.02	0.02	0.03	0.03	0.03
	Sulf	1.08	0.98	0.93	0.99	0.98	1.00	1.11	0.94	1.00
	Cl^-	0.02	0.06	0.08	0.08	0.10	0.15	0.04	0.11	0.04
	EDA	0	0	0	0	0	0	0	0	2.00
	PZ	3855.6	3749.4	3738.2	3617.1	3582.2	3602.7	3786.8	3548.6	3497.3
	CO_2	2632.7	2558.7	2585.6	2536.3	2504.3	2513.7	2706.2	2409.5	2413.6
	SD_{CO2}	43.10	33.40	10.85	20.61	6.35	22.25	7.53	20.26	6.35
	Alk	4094.0	3979.5	3986.0	3838.7	3830.5	3784.4	4104.5	3710.0	3696.0
	SD_{Alk}	6.28	4.65	2.34	10.55	25.00	0.90	8.97	3.62	10.49
Hydrolyzed Samples (mmol/kg)	Gly	0	0	0	0	0	0	0	0	0
	Ace	0.80	1.80	2.72	3.86	4.63	5.81	9.70	7.16	8.51
	Form	0	0	0	0	0	0	0	0	0
	NO_2^-	0.00	0	0	0.01	0.01	0.01	0.01	0.01	0.01
	Oxa	0.02	0.02	0.04	0.06	0.08	0.11	0.17	0.14	0.18
	NO_3^-	0.00	0.03	0.01	0.02	0.04	0.06	0.03	0.03	0.04
	Sulf	1.11	1.18	0.98	1.04	1.01	1.06	1.03	1.05	1.04
	Cl^-	0.27	0.26	0.15	0.20	0.17	0.20	0.11	0.13	0.34
	EDA	0	0	0	0	0	0	0	0	0
	PZ	3791.1	3635.6	3699.2	3580.6	3532.9	3570.9	3698.3	3438.7	3443.1

Table E.14: Tabulated Experimental Data for OE14 (8 m PZ, 2 kPa CO_2, 98 kPa O_2, 55 °C, 1.00 mM Fe^{2+}, 100.11 mM Inhibitor A, OOR)

		8 m PZ + Fe + A						
	Time (hr)	0.3	40.3	99.0	164.8	238.0	310.0	380.5
Original Samples (mmol/kg)	Gly	0	0	0	0	0	0	0
	Ace	0	0.03	0.03	0.04	0.19	0.03	0.06
	Form	0.18	0.60	0.86	1.17	4.05	1.54	1.34
	NO_2^-	0	0	0	0	0.04	0	0
	Oxa	0	0	0	0.34	0.05	0.06	0.11
	NO_3^-	0	0	0	0	0.14	0	0
	Sulf	1.21	1.13	1.15	1.84	1.19	1.16	1.50
	Cl^-	0.03	0.44	0.04	0.03	0.04	0.02	0.02
	FPZ	0.52	1.67	2.56	3.75	5.28	4.38	3.42
	EDA	0	0	0	0	0	0	6.24
	PZ	3952.8	3894.2	4001.3	4055.5	4027.5	4014.0	3669.3
	CO_2	2465.0	2531.8	2622.5	2674.1	2635.2	2662.3	2424.4
	SD_{CO2}	20.44	14.67	0.33	19.75	7.89	3.43	11.63
	Alk	4027.6	3982.6	4080.7	4121.2	4102.0	4099.3	3729.7
	SD_{Alk}	3.73	1.16	7.56	14.74	2.32	4.11	6.08
Hydrolyzed Samples (mmol/kg)	Gly	0	0	0	0	0	0	0
	Ace	0	0.08	0.28	0.06	2.25	0.09	0.40
	Form	0.34	1.76	3.20	4.25	6.75	5.02	3.60
	NO_2^-	0	0	0	0	0.24	0	0
	Oxa	0.01	0.04	0.09	0.19	0	0.15	0.11
	NO_3^-	0	0	0	0	0	0	0
	Sulf	1.25	1.17	1.25	1.67	0.19	1.35	1.34
	Cl^-	0.14	0.50	0.11	0.07	0.06	0.05	0.07
	FPZ	0	0	0	0	0	0	0
	EDA	0	0	0	0	0	0	0
	PZ	3939.9	3902.4	4003.2	4079.9	4128.2	4135.9	3760.2

Table E.15: Tabulated Experimental Data for OE15 (8 m PZ, 2 kPa CO_2, 98 kPa O_2, 55 °C, 0.41 mM Fe^{2+}, 0.10 mM Cr^{3+}, 0.05 mM Ni^{2+}, OOR)

		8 m PZ + Fe + Cr + Ni						
	Time (hr)	0	70.0	142.3	213.8	284.0	358.0	426.5
Original Samples (mmol/kg)	Gly	0.52	0.48	0.54	0.54	0.55	0.55	0.56
	Ace	0	0	0.32	0.36	0.40	0.41	0.43
	Form	0	0	0.37	0.73	0.94	1.15	1.29
	NO_2^-	0.02	0.01	0.02	0.02	0.02	0.02	0.02
	Oxa	0.07	0.05	0.09	0.06	0.10	0.13	0.14
	NO_3^-	0	0.03	0.03	0.06	0.05	0.06	0.05
	Sulf	0.66	0.65	0.64	0.73	0.62	0.72	0.71
	Cl^-	0.16	0.12	0.04	0.24	0.13	0.07	0.06
	EDA	0	0.43	2.04	2.87	5.83	4.43	6.14
	PZ	4342.4	4330.6	4359.5	4322.4	4363.3	4408.8	4436.9
	CO_2	2681.7	2766.5	2717.7	2714.2	2849.0	2838.4	2719.9
	SD_{CO2}	16.60	34.41	100.00	8.17	96.88	75.33	154.21
	Alk	4122.5	4069.4	4095.7	4085.7	4112.1	4172.6	4205.8
	SD_{Alk}	NA	NA	NA	NA	NA	NA	NA
Hydrolyzed Samples (mmol/kg)	Gly	0.02	0.31	0.20	0.06	0.05	0.04	0.04
	Ace	0	0.03	0.07	0	0.11	0.12	0.14
	Form	0.14	0.71	1.92	2.93	3.67	4.24	4.81
	NO_2^-	0	0.01	0.02	0.02	0.02	0.02	0.02
	Oxa	0	0.04	0.08	0.14	0.18	0.27	0.30
	NO_3^-	0	0	0	0.04	0.05	0.06	0.06
	Sulf	0.64	0.70	0.63	0.74	0.77	0.79	0.75
	Cl^-	0.08	0.09	0.13	0.11	0.15	0.11	0.09
	EDA	0	1.12	2.65	3.19	3.82	4.61	5.55
	PZ	4328.8	4261.3	4373.5	4318.4	4315.5	4352.1	4411.8

Table E.16: Tabulated Experimental Data for OE16 (8 m PZ, 2 kPa CO_2, 98 kPa O_2, 55 °C, 0.40 mM Fe^{2+}, 0.10 mM Cr^{3+}, 0.05 mM Ni^{2+}, 10.06 mM Inhibitor A, OOR)

	8 m PZ + Fe + Cr + Ni + A							
	Time (hr)	0	70.0	142.3	213.8	284.0	358.0	426.5
Original Samples (mmol/kg)	Gly	0	0	0	0	0	0	0
	Ace	0.06	0.34	0.09	0.08	0.10	0.11	0.10
	Form	0.06	0.36	0.23	0.35	0.47	0.49	0.50
	NO_2^-	0	0.01	0.01	0.01	0.02	0.02	0.02
	Oxa	0	0.02	0.02	0.03	0.03	0.04	0.04
	NO_3^-	0	0	0.02	0.02	0.02	0.03	0.02
	Sulf	0.56	0.39	0.62	0.62	0.62	0.63	0.62
	Cl^-	0.16	0.03	0.09	0.17	0.15	0.28	0.14
	EDA	0	0	0	0	0	0	0
	PZ	4398.8	4133.6	4200.2	4036.6	4176.5	4247.6	4299.9
	CO_2	2603.3	2682.6	2632.8	2592.1	2598.0	2664.4	2573.8
	SD_{CO2}	57.60	120.35	14.52	14.65	18.89	61.48	199.56
	Alk	4137.1	3959.3	3928.0	3919.2	3919.5	3983.3	4036.4
	SD_{Alk}	2.46	2.56	3.94	4.42	4.26	13.84	1.58
Hydrolyzed Samples (mmol/kg)	Gly	0	0.01	0.01	0.02	0.02	0.03	0.03
	Ace	0.05	0.05	0.05	0.08	0.04	0.04	0.06
	Form	0.11	0.38	0.62	0.77	0.93	1.03	1.34
	NO_2^-	0	0.01	0.01	0.02	0.02	0.02	0.02
	Oxa	0	0.04	0.05	0.07	0.07	0.08	0.09
	NO_3^-	0	0.03	0.02	0.03	0.04	0.03	0.03
	Sulf	0.76	0.73	0.73	0.75	0.73	0.73	0.83
	Cl^-	0.11	0.18	0.17	0.26	0.17	0.16	0.16
	EDA	0	0	0	0	0	0	0
	PZ	4374.9	4220.5	4186.7	4196.4	4185.0	3772.1	3907.4

Table E.17: Tabulated Experimental Data for OE17 (8 m PZ, 2 kPa CO_2, 98 kPa O_2, 55 °C, 1.0 mM Fe^{2+}, TOR)

	8 m PZ + Fe (1st TOR)							
	Time (hr)	0	65.3	144.3	220.5	281.3	358.0	424.3
Original Samples (mmol/kg)	Gly	0.11	0.09	0.16	0.12	0.12	0.11	0.12
	Ace	0.10	0.11	0.18	0.18	0.16	0.33	0.17
	Form	0.39	0.58	0.85	1.04	1.16	1.42	1.43
	NO_2^-	0	0	0	0	0	0.00	0.01
	Oxa	0.19	0.09	0.06	0.06	0.07	0.05	0.06
	NO_3^-	0	0	0.03	0.13	0.05	0.04	0.08
	Sulf	5.73	5.70	5.68	5.67	5.55	5.58	5.63
	Cl^-	0.28	0.26	0.24	0.16	0.09	0.30	0.10
	EDA	0	0	0	2.54	4.52	5.97	8.64
	PZ	4857.3	3174.3	4207.0	4135.5	4146.5	4116.7	4105.7
	CO_2	2658.9	2614.9	2598.7	2612.0	2562.1	2581.8	2604.2
	SD_{CO2}	6.19	27.06	33.04	18.72	22.04	35.07	13.10
	Alk	4070.7	4021.9	3993.6	3934.6	3911.6	3962.4	4006.3
	SD_{Alk}	33.09	1.72	8.92	3.95	13.48	20.98	12.06
Hydrolyzed Samples (mmol/kg)	Gly	0.53	0.61	1.46	0.32	4.20	0.13	0.14
	Ace	0.09	0.15	0.86	0.12	0.34	0.16	0.14
	Form	0.62	1.79	8.90	2.77	4.36	3.30	3.44
	NO_2^-	0.00	0.08	0.08	0.06	0.03	0.02	0.07
	Oxa	0.06	0.07	0.12	0.16	0.14	0.15	0.16
	NO_3^-	0.03	0.02	0.09	0.08	0.09	0.06	0.21
	Sulf	5.66	5.71	5.82	5.55	5.56	5.58	5.64
	Cl^-	0.30	0.33	0.13	0.09	0.11	0.47	0.19
	EDA	0	0	4.18	5.63	7.25	6.66	7.88
	PZ	4256.6	4211.9	4044.2	4117.5	3965.7	4136.8	4217.3

Table E.18: Tabulated Experimental Data for OE18 (8 m PZ, 2 kPa CO_2, 98 kPa O_2, 55 °C, 0.40 mM Fe^{2+}, 0.10 mM Cr^{3+}, 0.05 mM Ni^{2+}, TOR)

		8 m PZ + Fe + Cr + Ni								
	Time (hr)	0	71.3	152.3	223.5	291.0	368.0	437.3	487.8	575.5
Original Samples (mmol/kg)	Gly	0	0.03	0.05	0.04	0.08	0.10	0.11	0.10	0.10
	Ace	0	0.17	0	0	0.06	0.09	0.49	0.38	0.10
	Form	0.53	0.39	1.04	1.24	1.77	1.89	2.42	2.82	2.07
	NO_2^-	0	0	0	0	0	0	0	0	0
	Oxa	0.05	0.04	0.03	0.04	0.04	0.04	0.04	0.05	0.04
	NO_3^-	0	0	0	0	0	0	0	0	0
	Sulf	4.35	3.42	4.83	4.80	4.73	4.79	4.58	4.15	4.64
	Cl^-	0.07	0.06	0.10	0.16	0.15	0.14	0.07	0.54	0.07
	EDA	0	0	0	0	0	0	0	0	0
	PZ	4255.1	4280.1	4263.5	4315.0	4243.9	4213.3	4390.4	4294.8	4189.3
	CO_2	3140.6	3187.8	3186.5	3181.4	3140.5	3018.6	2955.6	2606.6	2844.3
	SD_{CO2}	976.81	143.15	765.20	750.81	170.68	137.53	126.69	741.42	165.79
	Alk	4131.6	4180.6	4172.8	4202.3	4201.0	4158.4	4296.8	4179.0	4037.1
	SD_{Alk}	12.75	26.93	25.92	18.49	0.56	7.99	49.96	68.98	19.39
Hydrolyzed Samples (mmol/kg)	Gly	0.05	0.25	0.09	0.06	0.06	0.06	0.06	0.08	0.04
	Ace	0.12	0.14	0.08	0.43	0.14	0.19	0.13	0.16	0.11
	Form	0.47	1.36	2.46	3.56	3.55	3.66	3.63	4.02	4.28
	NO_2^-	0	0	0	0	0	0	0	0	0
	Oxa	0	0	0	0	0	0	0	0	0
	NO_3^-	0	0.05	0.05	0.07	0.14	0.05	0.04	0.07	0.05
	Sulf	6.79	6.98	6.87	7.38	6.89	6.86	6.44	6.88	6.98
	Cl^-	0.26	0.33	0.16	0.37	0.28	0.21	0.23	0.25	0.24
	EDA	0	0	0	0	0	0	0	0	0
	PZ	3890.3	3893.8	3926.3	3939.5	3870.1	3912.6	3830.9	3896.2	3794.7

Table E.19: Tabulated Experimental Data for OE19 (8 m PZ, 2 kPa CO_2, 98 kPa O_2, 70 °C, 0.40 mM Fe^{2+}, 0.10 mM Cr^{3+}, 0.05 mM Ni^{2+}, TOR)

	8 m PZ + Fe + Cr + Ni (70 °C)									
	Time (hr)	0	69.0	141.5	215.8	282.3	357.8	427.0	473.8	572.0
Original Samples (mmol/kg)	Gly	0	0	0	0	0	0	0	0	0
	Ace	0	0	0	0	0	0	0.29	0.27	0.24
	Form	0.29	1.54	2.81	4.78	4.66	6.04	6.82	7.54	8.21
	NO_2^-	0	0	0.08	0	0	0	0	0	0
	Oxa	0	0	0.07	0	0	0	0	0	0
	NO_3^-	0	0	0	0.33	1.78	0.16	0.17	0.21	0.24
	Sulf	4.66	5.90	5.00	5.77	5.70	5.73	5.49	5.45	5.39
	Cl^-	0	0	0.07	0.02	0.12	0.01	0	0	0
	EDA	0	0	11.97	0	9.36	13.66	14.80	26.68	18.48
	PZ	3943.0	4147.2	4132.2	3850.8	3897.3	3838.6	3927.7	3930.4	3830.9
	CO_2	2677.1	2302.4	2143.1	2078.5	2655.8	1977.4	2717.9	2266.1	2202.7
	SD_{CO2}	13.83	23.60	6.83	5.69	2.59	6.83	14.85	9.38	8.64
	Alk	4103.9	4213.9	4142.1	4121.5	4046.4	4035.6	4014.0	3967.1	3920.6
	SD_{Alk}	4.08	34.88	14.18	35.18	4.76	18.93	62.62	3.78	6.37
Hydrolyzed Samples (mmol/kg)	Gly	0	0	0	0	0	0	0	0	0
	Ace	0.09	0	0.12	0.25	0.36	0.38	0.38	0.37	0.52
	Form	0.32	4.31	7.81	10.78	12.86	13.78	15.49	17.38	18.85
	NO_2^-	0	0	0.08	0.09	0.08	0	0	0	0
	Oxa	0	0.09	0.09	0.17	0.20	0	0	0	0
	NO_3^-	0	0	0	0	0	0.21	0.20	0.23	0.22
	Sulf	4.71	5.06	4.96	5.12	4.88	5.39	5.35	5.31	5.35
	Cl^-	0.40	0.12	0.05	0.24	0.14	0.03	0.08	0.14	0.04
	EDA	0	0	0	0	40.92	11.45	11.67	14.54	16.59
	PZ	4244.0	4329.0	4246.9	4348.7	4076.1	3906.9	3868.1	3884.0	3814.1

Table E.20: Tabulated Experimental Data for OE20 (8 m PZ, 2 kPa CO_2, 98 kPa O_2, 70 °C, 0.40 mM Fe^{2+}, 0.10 mM Cr^{3+}, 0.05 mM Ni^{2+}, 500 mM Formate, TOR)

8 m PZ + Fe + Cr + Ni + Formate (70 °C)							
	Time (hr)	0	66.5	141.3	211.3	285.0	358.3
Original Samples (mmol/kg)	Gly	0	0	0	0	0	0
	Ace	0.85	1.10	0.98	1.04	0.86	0.97
	Form	322.14	184.95	176.24	170.14	173.44	173.99
	NO_2^-	0.00	0.01	0.03	0.04	0.05	0.04
	Oxa	0	0	0	0.04	0.05	0.04
	NO_3^-	0.08	0.08	0.09	0.10	0.09	0.10
	Sulf	0.89	0.93	0.87	0.90	0.86	0.89
	Cl^-	0.05	0.07	0.05	0.10	0.07	0.07
	EDA	0	0	0	0	0	0
	PZ	4095.6	4060.1	4248.4	4001.6	4108.5	3869.7
	CO_2	2501.2	2403.9	2110.0	2309.6	2321.2	2292.7
	SD_{CO2}	12.07	14.04	8.92	1.84	6.84	9.53
	Alk	4051.9	4100.1	4239.7	4193.0	4090.7	4099.0
	SD_{Alk}	17.59	5.61	2.03	73.86	9.29	0.90
Hydrolyzed Samples (mmol/kg)	Gly	0	0	0	0	0	0
	Ace	1.07	1.42	2.42	0.93	0.92	1.03
	Form	470.39	490.12	506.12	494.88	491.92	496.09
	NO_2^-	0.01	0.03	0.05	0.05	0.05	0.06
	Oxa	0.03	0.05	0.06	0.08	0.10	0.12
	NO_3^-	0.09	0.09	0.09	0.09	0.11	0.11
	Sulf	0.92	1.01	1.06	0.97	0.92	1.01
	Cl^-	0.14	0.15	0.19	0.09	0.12	0.23
	EDA	0	0	0	0	0	0
	PZ	3663.5	4133.4	4003.5	3998.7	3988.5	4071.3

Table E.21: Tabulated Experimental Data for OE21 (8 m PZ, 2 kPa CO_2, 98 kPa O_2, 70 °C, 0.40 mM Fe^{2+}, 0.10 mM Cr^{3+}, 0.05 mM Ni^{2+}, 500 mM Formaldehyde, TOR)

8 m PZ + Fe + Cr + Ni + Formaldehyde (70 °C)									
	Time (hr)	0		0	22.8	46.3	71.3	94.5	115.3
Original Samples (mmol/kg)	Gly	0	500 mM Formaldehyde Added to reactor	0	0	0	0	0	0
	Ace	0		0	0	0	0	0	0
	Form	0.12		0.24	0.60	0.83	0.95	1.12	1.34
	NO_2^-	0		0	0	0	0	0.00	0.00
	Oxa	0		0	0	0	0	0	0.03
	NO_3^-	0		0	0	0	0	0	0
	Sulf	5.39		5.24	5.48	5.52	5.50	5.37	5.36
	Cl^-	0.04		0.02	0.03	0.03	0.03	0.03	0.02
	FPZ	0.43		0.64	1.56	1.75	2.57	2.94	3.09
	EDA	1.30		0	0.98	2.13	2.70	4.33	5.27
	PZ	4093.4		3853.3	NT	3819.2	3780.6	3741.8	3763.7
	CO_2	2582.3		2458.8	2064.9	1961.6	1904.4	1876.7	1850.8
	SD_{CO2}	13.94		4.80	5.22	9.57	2.46	6.48	12.50
	Alk	4132.4		3950.6	4061.3	3925.1	3848.4	3845.1	3794.9
	SD_{Alk}	33.74		0.23	13.72	17.77	5.14	24.00	2.24
Hydrolyzed Samples (mmol/kg)	Gly	0		0	0	0	0	0	0
	Ace	0		0	0	0.18	0.10	0.05	0.10
	Form	0.24		0.50	1.70	2.26	2.58	2.98	3.69
	NO_2^-	0.01		0.01	0.01	0.01	0.01	0.01	0.00
	Oxa	0		0	0	0.04	0.05	0.07	0.07
	NO_3^-	0		0	0	0	0	0	0
	Sulf	5.41		5.44	5.63	5.52	5.33	5.32	5.36
	Cl^-	0.05		0.03	0.04	0.06	0.07	0.04	0.08
	FPZ	0		0	0	0	0	0	0
	EDA	0		0	1.19	1.98	3.05	4.38	4.65
	PZ	4021.3		3882.9	3900.7	3796.2	3729.0	3714.4	3647.8

Table E.22: Tabulated Experimental Data for OE22 (8 m PZ, 60 kPa CO_2, 40 kPa O_2, 70 °C, 0.40 mM Fe^{2+}, 0.10 mM Cr^{3+}, 0.05 mM Ni^{2+}, TOR)

	8 m PZ + Fe + Cr + Ni (70 °C)									
	Time (hr)	0	70.0	143.5	213.0	287.8	359.5	430.0	501.0	575.0
Original Samples (mmol/kg)	Gly	0	0	0	0	0	0	0	0	0
	Ace	0	0	0	0	0	0	0	0	0
	Form	0	0.26	0.52	0.59	0.80	0.90	0.90	1.03	1.11
	NO_2^-	0	0.01	0.01	0	0.00	0.00	0.00	0.00	0.00
	Oxa	0	0	0	0	0	0	0	0	0
	NO_3^-	0	0.04	0.07	0.10	0.07	0.06	0.06	0.16	0.10
	Sulf	5.23	5.11	4.93	4.95	4.97	5.03	4.84	4.96	4.80
	Cl^-	0.01	0.01	0.02	0.02	0.03	0.34	0.02	0.13	0.02
	EDA	0	1.95	3.27	4.99	6.30	6.72	7.67	7.86	9.16
	PZ	2902.3	2845.0	2730.4	2710.3	2699.3	2664.7	2632.9	2635.3	2607.0
	CO_2	3073.7	2812.6	2717.3	2624.8	2702.7	2643.8	2642.1	2782.5	2804.3
	SD_{CO2}	11.15	12.44	8.74	5.26	0.90	2.43	14.82	8.23	11.44
	Alk	3947.6	3841.3	3689.8	3662.2	3643.4	3580.2	3561.6	3573.1	3531.2
	SD_{Alk}	18.51	3.15	4.22	2.51	6.75	4.93	0.08	7.01	5.48
Hydrolyzed Samples (mmol/kg)	Gly	0	0	0	0	0	0	0	0	0
	Ace	0	0	0	0	0	0	0	0	0
	Form	0.29	1.04	1.56	1.98	2.37	2.63	2.96	2.66	2.95
	NO_2^-	0	0.00	0.00	0.00	0.00	0	0.01	0.00	0.00
	Oxa	0	0	0	0	0	0	0	0	0
	NO_3^-	0	0.03	0	0	0.08	0.08	0.07	0.06	0.10
	Sulf	5.31	5.17	5.02	5.06	5.04	5.00	5.00	4.84	4.85
	Cl^-	0.07	0.05	0.05	0.04	0.05	0.05	0.05	0.11	0.03
	EDA	0	2.07	3.48	4.80	6.44	0	6.43	8.75	9.39
	PZ	2866.7	2796.8	2686.0	2666.0	2611.1	1791.1	NT	2574.6	2604.3

Table E.23: Tabulated Experimental Data for OE23 (8 m PZ, 6 kPa CO_2, 40 kPa O_2, 70 °C, 4.0 mM Cu^{2+}, TOR)

	8 m PZ + Cu (70 °C)							
	Time (hr)	0	48.5	93.5	144.3	192.8	284.5	332.5
Original Samples (mmol/kg)	Gly	0.29	0.15	0.28	0.14	0.16	0.19	0.14
	Ace	0	0	0	0	0	0	0
	Form	0.39	11.17	27.82	20.61	24.85	29.67	32.24
	NO_2^-	0	0.05	0.28	0.03	0.02	0.02	0.02
	Oxa	0	0.54	1.32	1.53	2.31	3.91	4.41
	NO_3^-	0	0.08	0.19	0.11	0.13	0.21	0.17
	Sulf	3.68	2.89	3.94	2.26	2.41	2.77	2.64
	Cl^-	0.02	0.04	0.06	0.01	0.00	0.02	0.02
	NH_4^+	0.16	4.96	9.54	4.07	2.91	3.05	3.29
	FPZ	0	43.52	55.83	61.45	69.68	76.57	76.24
	EDA	0	67.19	92.95	105.32	108.88	120.65	124.04
	PZ	4389.1	3178.3	3070.3	3069.4	2965.7	2919.6	2874.5
	CO_2	2596.9	1947.1	1899.6	1833.3	1788.4	1755.8	1718.5
	SD_{CO2}	13.99	6.54	5.93	20.31	20.63	11.85	7.96
	Alk	4147.8	3096.6	3039.0	3045.2	2962.6	2954.6	2930.3
	SD_{Alk}	NA	NA	NA	NA	NA	NA	NA
Hydrolyzed Samples (mmol/kg)	Gly	0.64	0.81	0.40	0.45	0.39	0.22	0.36
	Ace	0.30	1.07	2.31	3.23	3.59	2.46	4.23
	Form	3.58	30.64	39.67	58.68	58.98	37.80	65.06
	NO_2^-	0.02	0.06	0.06	0.05	0.02	0.01	0.02
	Oxa	0.15	6.66	8.75	13.31	13.26	8.08	14.78
	NO_3^-	0	0.07	0.11	0.18	0.16	0.15	0.19
	Sulf	2.77	2.40	2.11	2.98	2.77	1.44	2.54
	Cl^-	0.07	0.04	0.02	0.06	0.02	0.06	0.03
	NH_4^+	0	0	0	0	0	0	0
	FPZ	0	0	0	0	0	0	0
	EDA	9.37	81.61	105.30	122.16	127.17	130.06	135.02
	PZ	4349.5	3166.2	3009.6	2737.3	3045.2	2855.8	2951.6

Table E.24: Tabulated Experimental Data for OE24 (8 m PZ, 6 kPa CO_2, 40 kPa O_2, 70 °C, 4.0 mM Cu^{2+}, 100 mM Inhibitor A, TOR)

	8 m PZ + Cu + A (70 °C)							
	Time (hr)	0	48.5	93.5	144.3	192.8	284.5	332.5
Original Samples (mmol/kg)	Gly	0.26	0.34	0.31	0.36	0.30	0.34	0.28
	Ace	0	0	0	0	0	0	0
	Form	0.14	2.67	2.41	3.69	3.95	4.07	4.24
	NO_2^-	0.02	0.10	0.04	0.03	0.01	0.01	0.01
	Oxa	0	0.11	0.14	0.29	0.37	0.53	0.51
	NO_3^-	0	0.26	0.23	0.30	0.31	0.37	0.31
	Sulf	2.68	3.86	2.65	3.57	3.40	3.35	2.73
	Cl^-	0.03	0.04	0.03	0.03	0.04	0.26	0.16
	NH_4^+	1.31	2.62	1.10	1.43	1.75	1.12	0.84
	FPZ	0	0	0	0	0	0	0
	EDA	0	12.55	14.53	9.91	10.83	8.06	12.49
	PZ	4341.3	4633.4	4156.6	4309.5	4113.3	3994.7	4063.4
	CO_2	2464.0	2786.1	2466.1	2413.9	2414.5	2405.4	2347.7
	SD_{CO2}	12.59	26.08	26.51	13.55	32.19	44.55	10.96
	Alk	4080.6	4044.3	3958.9	3938.8	3875.0	3786.7	3809.3
	SD_{Alk}	NA	NA	NA	NA	NA	NA	NA
Hydrolyzed Samples (mmol/kg)	Gly	0.26	0.49	0.39	0.40	0.35	0.27	0.28
	Ace	0	0	0	0	0.19	0.42	0.42
	Form	1.06	8.90	9.13	9.64	10.82	11.72	12.44
	NO_2^-	0.03	0.09	0.04	0.03	0.02	0.01	0.01
	Oxa	0	1.01	1.24	1.49	1.88	2.19	2.58
	NO_3^-	0	0.25	0.26	0.28	0.32	0.32	0.34
	Sulf	3.47	3.78	3.32	3.04	3.38	3.15	3.29
	Cl^-	0	0.10	0.14	0.05	0.08	0.04	0.05
	NH_4^+	0	0	0	0	0	0	0
	FPZ	0	0	0	0	0	0	0
	EDA	5.05	10.60	12.08	11.52	10.28	11.89	13.64
	PZ	4261.5	4219.0	4153.2	4128.0	4049.7	4015.2	3935.0

Table E.25: Tabulated Experimental Data for OE25 (8 m PZ, 6 kPa CO_2, 94 kPa O_2, 70 °C, 4.0 mM Cu^{2+}, TOR)

	8 m PZ + Cu (70 °C)								
	Time (hr)	0	50.3	93.5	138.5	193.0	239.3	284.3	331.0
Original Samples (mmol/kg)	Gly	0.64	0	0	0	0	0	0	0
	Ace	0	0	0	0	0	0	0	0
	Form	1.13	24.84	46.06	63.96	93.84	120.99	143.91	168.74
	NO_2^-	0	0.26	0.45	0.66	0.97	1.18	1.71	1.90
	Oxa	0	2.04	5.46	10.34	18.42	26.19	34.54	42.10
	NO_3^-	0	0.31	0.62	0.94	1.80	2.31	2.80	2.81
	Sulf	3.67	3.76	4.29	5.12	6.23	7.33	8.08	9.08
	Cl^-	0.07	10.44	0	0	0	0	0	0
	NH_4^+	0	0	0	0	0	3.77	3.56	3.13
	FPZ	0	103.33	150.60	201.22	240.57	265.50	280.16	300.32
	EDA	1.15	184.21	269.73	331.27	335.37	310.54	267.05	224.24
	PZ	4389.0	3325.2	2679.8	2326.3	1828.7	1543.9	1342.3	1222.4
	1-MPZ	0	0	0	0	0	0.68	0.64	0.56
	1-EPZ	0	0	0	0	0	0	0	0
	1,4-DMPZ	0	0	0	0	0	0	0	0
	AEP	0	0	0	0	0	0	0	0
	CO_2	2479.1	1986.8	1630.5	1420.5	993.6	760.2	580.7	442.4
	SD_{CO2}	16.38	26.68	10.46	17.13	9.77	6.50	5.53	0.78
	Alk	4117.7	3643.3	3217.9	2888.8	2416.2	2105.2	1736.7	1618.4
	SD_{Alk}	NA	NA	NA	NA	NA	NA	NA	NA
Hydrolyzed Samples (mmol/kg)	Gly	0	1.21	0	0	0	0	0	0
	Ace	0	0.66	1.92	2.17	2.86	2.98	3.29	3.62
	Form	2.47	93.74	189.35	232.30	310.27	400.78	459.50	554.88
	NO_2^-	0	0.36	0.60	0.78	1.06	1.57	1.76	1.94
	Oxa	0.23	30.59	47.55	44.75	95.52	51.08	55.53	104.56
	NO_3^-	0	0.32	0.79	1.02	1.47	1.98	2.42	2.98
	Sulf	3.74	3.63	4.48	4.53	4.60	6.01	6.54	6.83
	Cl^-	0.10	0	0	0	0	0	0	0
	NH_4^+	0	60.50	77.16	67.76	72.64	85.79	107.50	130.90
	FPZ	0	0	0	0	0	0	0	0
	EDA	3.34	221.93	421.42	452.06	514.02	518.96	501.01	486.98
	PZ	4370.5	3548.7	2178.2	2430.0	2009.0	1747.5	1565.3	1453.1
	1-MPZ	0	0	0	0	1.99	2.34	2.90	3.27
	1-EPZ	0	0	0	0	0	0	0	0
	1,4-DMPZ	0	0	0	0	0	0	0	0
	AEP	0	0	0	0	0	0	0	0

Table E.26: Tabulated Experimental Data for OE26 (8 m PZ, 6 kPa CO_2, 94 kPa O_2, 70 °C, 0.40 mM Fe^{2+}, 0.10 mM Cr^{3+}, 0.05 mM Ni^{2+}, TOR)

	8 m PZ + Fe + Cr + Ni (70 °C)								
	Time (hr)	0	50.3	93.5	138.5	193.0	239.3	284.3	331.0
Original Samples (mmol/kg)	Gly	0.52	0.55	0.56	0.56	0.56	0.54	0.52	0.50
	Ace	0	0	0	0	0	0.06	0.08	0.14
	Form	0	0.21	0.41	0.70	1.06	1.37	1.59	1.85
	NO_2^-	0	0.03	0.03	0.02	0.02	0.02	0.02	0.02
	Oxa	0	0	0	0.00	0.00	0.01	0.01	0.01
	NO_3^-	0	0.03	0.05	0.05	0.07	0.07	0.06	0.08
	Sulf	5.16	5.19	5.09	4.95	4.99	4.90	4.77	4.80
	Cl^-	0.03	0.03	0.06	0.03	0.18	0.04	0.05	0.04
	NH_4^+	1.78	0	0.43	1.46	0	0	0	2.19
	FPZ	0	2.94	3.44	4.32	4.61	5.16	5.98	6.96
	EDA	0	3.35	5.10	6.54	8.72	10.50	11.47	12.60
	PZ	4406.7	4388.5	4321.8	4189.1	4193.1	4091.0	4050.1	4012.5
	1-MPZ	0	0	0	0	0	0	0	0
	1-EPZ	0	0	0	0	0	0	0	0
	1,4-DMPZ	0	0	0	0	0	0	0	0
	AEP	0	0	0	0	0	0	0	0
	CO_2	2439.1	2500.4	2465.6	2472.3	2415.4	2409.5	2361.9	2336.5
	SD_{CO2}	7.66	46.29	5.83	15.88	11.82	29.25	22.34	20.55
	Alk	4238.4	4220.1	4187.0	4045.5	4047.3	3987.8	3957.2	3858.4
	SD_{Alk}	NA	NA	NA	NA	NA	NA	NA	NA
Hydrolyzed Samples (mmol/kg)	Gly	0.37	0.36	0.43	0.39	0.38	0.22	0.24	0.22
	Ace	0	0	0	0	0	0	0	0
	Form	0	1.21	2.07	2.92	3.85	4.57	5.09	5.82
	NO_2^-	0	0.02	0.03	0.02	0.02	0.02	0.02	0.02
	Oxa	0	0.02	0.03	0.10	0.11	0.17	0.19	0.21
	NO_3^-	0	0.03	0.04	0.05	0.06	0.07	0.10	0.08
	Sulf	5.20	5.19	5.12	4.94	5.00	4.91	4.89	4.72
	Cl^-	0.09	0.06	0.07	0.09	0.08	0.10	0.38	0.08
	NH_4^+	0	0	0	0	0	0	0	0
	FPZ	0	0	0	0	0	0	0	0
	EDA	0	3.57	5.14	6.90	8.45	10.14	11.76	12.99
	PZ	4431.9	4320.9	4325.8	4175.5	4211.4	4122.5	4099.1	4008.3
	1-MPZ	0	0	0	0	0	0	0	0
	1-EPZ	0	0	0	0	0	0	0	0
	1,4-DMPZ	0	0	0	0	0	0	0	0
	AEP	0	0	0	0	0	0	0	0

Table E.27: Tabulated Experimental Data for OE27 (8 m PZ, 2 kPa CO_2, 40 kPa O_2, 55 °C, 4.0 mM Cu^{2+}, TOR)

		8 m PZ + Cu							
	Time (hr)	0	75.5	147.0	217.0	290.0	367.3	439.3	506.5
Original Samples (mmol/kg)	Gly	0.51	0.40	0.21	0.29	0.25	0.15	0.13	0.12
	Ace	0	0	0	0	0	0	0	0
	Form	0.11	6.43	10.29	13.44	15.27	16.72	17.83	18.43
	NO_2^-	0	0.14	0.18	0.17	0.18	0.17	0.14	0.13
	Oxa	0	0.21	0.48	0.68	1.00	1.23	1.52	1.79
	NO_3^-	0	0	0.12	0.13	0.14	0.16	0.16	0.16
	Sulf	3.74	3.84	3.67	3.69	3.64	3.67	3.62	3.52
	Cl^-	0	0	0	0	0	0	0	0
	NH_4^+	0	2.42	1.61	1.33	0.77	1.17	0.96	2.58
	FPZ	2.06	27.14	34.80	39.63	41.93	43.77	44.93	45.75
	EDA	1.55	62.09	84.74	101.34	113.35	120.96	126.82	131.88
	PZ	3740.8	3446.9	3308.7	3302.6	3284.0	3229.9	3209.4	3169.6
	1-MPZ	0	0	0	0	0	0	0	0
	1-EPZ	0	0	0	0	0	0	0	0
	1,4-DMPZ	0	0	0	0	0	0	0	0
	AEP	0	0.84	1.12	1.03	0.98	0.84	0.74	0.79
	CO_2	2479.8	2228.6	2194.8	2106.6	2048.8	2001.9	1947.2	1916.6
	SD_{CO2}	29.70	8.15	11.01	18.49	17.74	6.00	4.26	2.16
	Alk	4080.7	4002.7	3953.5	3935.3	3984.3	3977.2	3803.3	3655.9
	SD_{Alk}	NA	NA	NA	NA	NA	NA	NA	NA
Hydrolyzed Samples (mmol/kg)	Gly	1.03	1.49	1.03	0.62	0.85	0.40	0.31	0.32
	Ace	0	0	0	0.27	0.71	0.47	0.47	0.46
	Form	1.81	30.11	38.96	43.31	47.37	50.19	51.96	53.06
	NO_2^-	0	0.20	0.23	0.22	0.21	0.20	0.18	0.17
	Oxa	0.20	6.12	9.40	9.27	10.15	11.26	11.22	11.29
	NO_3^-	0	0.11	0.13	0.15	0.23	0.18	0.17	0.18
	Sulf	3.78	3.83	3.73	3.68	3.81	3.97	3.63	3.65
	Cl^-	0	0	0	0	0	0	0	0
	NH_4^+	0	0	0	0	0	0	0	0
	FPZ	0	0	0	0	0	0	0	0
	EDA	3.37	73.11	100.99	115.29	128.79	137.11	143.14	145.98
	PZ	3793.9	3517.5	4821.9	3759.5	3402.4	3329.4	3278.7	3208.9
	1-MPZ	0	0	0	0	0	0	0	0
	1-EPZ	0	0	0	0	0	0	0	0
	1,4-DMPZ	0	0	0	0	0	0	0	0
	AEP	0	0.40	0.33	0.35	0.37	0.33	0.31	0.28

Table E.28: Tabulated Experimental Data for OE28 (8 m PZ, 2 kPa CO_2, 98 kPa O_2, 55 °C, 0.40 mM Fe^{2+}, 0.10 mM Cr^{3+}, 0.05 mM Ni^{2+}, TOR)

		8 m PZ + Fe + Cr + Ni							
	Time (hr)	0	75.5	147.0	217.0	290.0	367.3	439.3	506.5
Original Samples (mmol/kg)	Gly	0.49	0.41	0.48	0.50	0.48	0.50	0.48	0.42
	Ace	0	0	0	0	0	0	0	0
	Form	0	0	0.08	0.12	0.12	0.21	0.35	0.35
	NO_2^-	0	0	0	0	0	0	0	0
	Oxa	0	0	0	0	0	0	0	0
	NO_3^-	0	0	0	0	0	0	0	0
	Sulf	5.03	5.03	5.07	5.12	5.01	4.99	4.96	4.95
	Cl^-	0.04	0.03	0.02	0.03	0	0	0	0
	NH_4^+	0	0	0.20	0	0.36	0.10	0.30	1.69
	FPZ	0	0	0	0.91	0.82	1.21	1.28	1.35
	EDA	0	0.14	0.24	0.59	0.51	0.64	0.84	0.95
	PZ	3780.4	3640.3	3708.1	3739.8	3743.4	3711.4	3648.9	3665.7
	1-MPZ	0	0	0	0	0	0	0	0
	1-EPZ	0	0	0	0	0	0	0	0
	1,4-DMPZ	0	0	0	0	0	0	0	0
	AEP	0	0	0	0	0	0	0	0
	CO_2	2362.2	2267.2	2179.6	2229.9	2165.0	2148.1	2108.1	2111.6
	SD_{CO2}	26.77	12.67	238.88	13.95	10.31	23.17	23.49	35.11
	Alk	4225.2	4114.6	4136.7	4247.9	4198.6	4154.1	4046.6	4082.1
	SD_{Alk}	NA	NA	NA	NA	NA	NA	NA	NA
Hydrolyzed Samples (mmol/kg)	Gly	0	0	0	0	0	0	0	0
	Ace	0	0	0	0	0	0	0	0
	Form	0	0	0.27	0.56	0.78	1.01	1.21	1.24
	NO_2^-	0	0	0	0	0	0	0	0
	Oxa	0	0	0	0	0	0	0	0
	NO_3^-	0	0	0	0	0	0	0	0
	Sulf	5.01	5.70	5.14	5.17	5.02	5.10	6.07	5.04
	Cl^-	0	0	0	0	0	0	0	0
	NH_4^+	0	0	0	0	0	0	0	0
	FPZ	0	0	0	0	0	0	0	0
	EDA	0	0	0.13	0.31	0.50	0.70	0.90	1.02
	PZ	3816.8	4179.1	3779.3	3808.3	3775.6	3747.0	3697.3	3775.3
	1-MPZ	0	0	0	0	0	0	0	0
	1-EPZ	0	0	0	0	0	0	0	0
	1,4-DMPZ	0	0	0	0	0	0	0	0
	AEP	0	0	0	0	0	0	0	0

Appendix F – Measurements of Heat of Absorption of CO_2 into Concentrated PZ

The heat of absorption of 8 m PZ was measured at Norges Teknish-Naturvitenshapelige Universitet (The Norwegian University of Science and Technology – NTNU) under the guidance of Dr. Inna Kim and Prof. Hallvard Svendsen. NTNU has a well-developed method for determining the heat of absorption of CO_2 into amine solutions using a reaction calorimeter. Numerous amines have been tested by their group with success (Kim and Svendsen, 2007).

F.1 REACTION CALORIMETER

F.1.1 Apparatus description

The reaction calorimeter (ChemiSens AB, Lund, Sweden) is a 2 L stainless steel jacketed vessel as shown in Figure F.1. There is a top mounted stainless steel stirrer operated by a separate stirrer motor. The heating/cooling system, or recirculator, uses cooling water (process water from the fume hood) and electrical power to heat and cool the silicon oil that circulates in the jacket around the reactor. There is a small electrical heater sticking into the vessel for calibration (not shown on figure). The CO_2 and solvent inlets are on the top of the vessel, as is the outlet for the vacuum pump system. The CO_2 flow is controlled by a mass flow controller attached to two small CO_2 tanks whose temperature is controlled in a water bath. The control box links the stirrer, recirculator, mass flow controller, temperature gauges, and pressure gauges to the computer. The InTouch program (ChemiSens AB) is used to control all the aspects of the system.

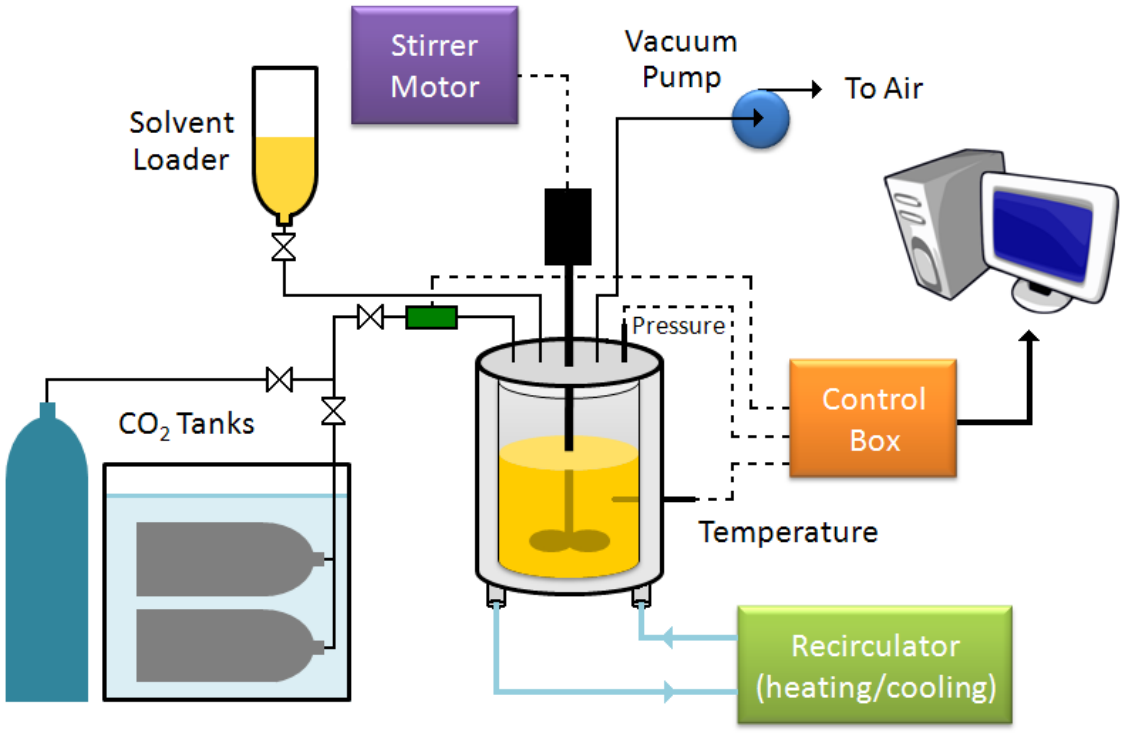

Figure F.1: Simplified Schematic of Reaction Calorimeter (ChemiSens AB)

F.1.2 Measurement procedure

To perform a heat of absorption measurement, the reactor is first evacuated to a gauge pressure of -0.9 to -0.95 bar. Then, CO_2 is then added to the reactor to a gauge pressure of approximately 2 bar to ensure that no air is in the reactor. The CO_2 is again evacuated to a reactor pressure of -0.9 to -0.95 bar. The solvent loader is flushed with N_2 and filled with solvent. The solvent loader is attached to the solvent inlet on the top of the reactor and the vacuum in the reactor is used as suction to draw the solvent into the calorimeter. The desired temperature and stirring speed are then set for the experiment. Once an initial equilibrium has been achieved, a small amount of CO_2 is added to the reactor, usually between 0.2 and 0.3 moles CO_2. The system is allowed time to reach an equilibrium before another pulse of CO_2. This process is repeated until the pressure in the reactor builds up as to not allow further addition of CO_2. The maximum total pressure of the calorimeter can be varied from 3 to 10 bars. All experiments were performed with a maximum pressure of 10 bars.

F.1.3 Data recording

The InTouch software allows the user to control nearly every aspect of the calorimeter operation. During an experiment, data is logged continuously every 10 seconds. For the calculation of heat of absorption, nine variables are of particular importance while other parameters are useful for seeing the stability of the experiment. The following variables are needed for the calculations:

Reactor_temp – temperature of the reactor

Reference_temp – temperature of the thermostatting fluid (silicon oil)

HB_dT_reactor – temperature difference in the thermostatting fluid entrance and exit

HLoss_dT_reactor – temperature difference across the insulation

dT_dt_reactor – instantaneous time derivative of the reactor temperature (°C/s)

Total_power – online measurement of power provided by recirculator (W)

Pressure_A – pressure of the reactor

Pressure_B – pressure of one of the two CO_2 cylinder

Convert_B2 – temperature of one of the CO_2 cylinders

During the experiment, the following variables are also of use to observe the stability of the system and to estimate the progress.

Lin_in_A1 – CO_2 mass flow controller reading

Calibration_power – power imparted by calibration electric heater, up to 30 W

Convert_A2 – temperature of the second CO_2 cylinder

F.1.4 Theory of heat of absorption measurements

The heat of absorption of CO_2 into amine systems is measured by directly measuring the heat released from the reaction. This is accomplished by measuring the heat need to be added to the system in order to maintain a constant temperature during reaction. The online power (recorded as Total_power in the InTouch software) is calculated using calibration parameters as discussed in detail in the next section. The calculation is based on the heat balance principle. The heat produced during the reaction creates an increase in temperature in the reactor contents. In order to maintain the experimental temperature, the thermostatting media (silicon oil), must change in temperature to accommodate the energy balance. The basic heat balance equation applied to this calorimeter in is shown in the following equation (ChemiSens).

$$\text{Total Energy} = m_{oil} C_{P,oil} \left(T_{oil,\,out} - T_{oil,\,in} \right)$$

In order to relate to the calorimeter system, this equation can be rewritten in terms of time and power instead of energy.

$$\text{Total Power} = \dot{m}_{oil} C_{P,oil} \left(T_{oil,\,out} - T_{oil,\,in} \right)$$

This expression is described by the manufacturer, ChemiSens AB, as describing the system at a steady state operation in the absence of heat losses (ChemiSens). The product ($\dot{m}_{oil} C_{P,oil}$) are not measured separately, but the product is fitted during calibration as a parameter named FlowCp.

The heat loss from the calorimeter to the surroundings is estimated as the heat flow through the insulation out of the reactor. This is captured by a term multiplying a heat conductivity coefficient (HlossC, a calibrated parameter) and the difference in temperature across the insulation. Including this heat loss term results in the following equation which fully characterizes the steady state heat balance on the calorimeter.

$$\text{Total Power} = \dot{m}_{oil} C_{P,oil} \times \left(T_{oil,\,out} - T_{oil,\,in} \right) + \text{HlossC} \left(T_{HL(inner)} - T_{HL(outer)} \right)$$

The difference in temperature across the insulation is a measured variable (Hloss_DT_reactor) which represents ($T_{HL(inner)} - T_{HL(outer)}$) in the total power equation.

When the calorimeter is actively controlling temperature, heat 'accumulates' in the reactor contents and various metallic parts on the inside of the reactor before it can be compensated for with the thermostatting fluid. This dynamic heat is accounted for in a separate term in the total power equation. This dynamic term includes a heat capacity term (C_R, a calibrated parameter) that is a total heat capacity for the solvent in the reactor, stirrer, and interior reactor walls that interact with the solvent multiplied by the time derivative of the reactor temperature. This time derivative of the reactor temperature is a

measured parameter (dT_dt_reactor) and it is assumed that the internal metallic parts of the calorimeter follow the same dT/dt behavior as the solution.

$$\text{Total Power} = \dot{m}_{oil} C_{P,oil} \times \left(T_{oil,\,out} - T_{oil,\,in}\right) + \text{HlossC}\left(T_{HL(inner)} - T_{HL(outer)}\right) + C_R \frac{dT}{dt}$$

The final term in the power equation is a term representing the dynamic changes in the reactor jacket. This term is represented as the heat flow from the thermostatting media to the outer reactor jacket including a coefficient the average total heat transfer (BKA, a calibrated parameter). This term is important because the external metallic parts of the jacket have a significantly higher heat capacity than the solution itself, so its contribution could be significant during CO_2 pulses.

$$\text{Total Power} = \dot{m}_{oil} C_{P,oil} \times \left(T_{oil,\,out} - T_{oil,\,in}\right) + \text{HlossC}\left(T_{HL(inner)} - T_{HL(outer)}\right) + C_R \frac{dT}{dt} + \text{BKA} \times \left(T_{ref} - T_j\right)$$

The final part of the Total Power equation is an adjustment made to capture any final heat leakages from the system. In addition, the small pressure drop across the jacket produces a small amount of heat that will cause an offset in the experimental heat measured. These phenomena are fixed through the addition of a baseline correction through a calibrated parameter (Baseline) (ChemiSens).

The complete equation for the total power with descriptions of each term is included below (ChemiSens).

$$\text{Total Power} = \underbrace{\overbrace{\dot{m}_{oil} C_{P,oil}}^{\text{Calibration constant}} \times \left(T_{oil,\,out} - T_{oil,\,in} - \overbrace{\text{Baseline}}^{\text{Calibration Constant}} \right)}_{\text{heat exchange with thermostatting media}} + \underbrace{\overbrace{\text{HlossC}}^{\text{Calibration Constant}} \times \left(T_{HL(inner)} - T_{HL(outer)}\right)}_{\text{heat loss through the jacket}}$$

$$+ \underbrace{\overbrace{C_R}^{\text{Calibration constant}} \frac{dT}{dt}}_{\text{dynamic heat of reactor}} + \underbrace{\overbrace{BKA}^{\text{Calibration constant}} \times \left(T_{ref} - T_j\right)}_{\text{dynamic heat of jacket}}$$

F.1.5 Data analysis

For each experiment, it is advisable to begin with a calibration procedure. There are 5 calibrated parameters and one constant as described in Table F.1. All of the calibrated parameters are strong functions of temperature and functions of the solvent system in use to a lesser extent. After the reactor is loaded with the solvent and brought up to the experimental temperature, the electrical calibration heater inside the reactor is set to generate 30W of power for 15 to 20 minutes. After the system has regained equilibrium (approximately 1 hour later), the parameters are fitted by matching a calculated power curve to the curve showing the calibration power (Calibration_power). The calculated power curve, or Calc_power, is produced with the equation described in the preceding section for the Total_power. In the Graph window of the InTouch program, the calibrated parameters can be adjusted to visually fit the two curves. An additional check is to verify that the area under both the Calc_power and Calibration_power curves are the same. When the curves are as similar as possible, the new values of the calibrated parameters are found.

Once the calibration is complete, the experiment can proceed. After each differential addition of CO_2, the system is allowed to reach equilibrium where the reactor temperature (T_r), reactor pressure (P_r), CO_2 tank temperature (T_{CO2}), CO_2 tank pressure (P_{CO2}), and the recirculator system power (Total_power) have all reached a steady value. The heat given or taken away from the reactor by the silicon oil during the pulse of CO_2 and subsequent time for equilibrium is continually measured and recorded. The Total_power measurement is directly in Watts of power. Integration of the time vs.

Total_power curve produces Joules of energy exchanged over a specified time range, known as the dH_{online}, or online energy measurement.

Table F.1: Description of calibration parameters for calorimeter

Parameter	Description
FlowCp	Product of the volumetric flow rate, density, and heat capacity of the silicon oil, usually 600 – 900 W/°C
Baseline	Establishes a baseline power
HlossC	Heat conductivity coefficient to characterize heat losses through the thermal shield, usually 1 – 1.4 W/°C
BKA	Average total heat transfer coefficient, represents heat transfer between the thermostatting media (silicon oil) and the outer reactor jacket, calibrated parameter based on dynamic system response during calibration
CB	Heat capacity of the reactor jacket, constant for this calorimeter at 1500 J/°C
CR	Heat capacity of the reactor contents, including the solution, contributions from the stirrer, reactor base, and interior walls; calibrated parameter based on solvent and temperature in use, usually 5500 – 7800 J/°C.

Once the dH_{online} is calculated, it can be directly associated with the amount of CO_2 or amine to calculated the heat of absorption per mol CO_2 or per mol amine. The amount of amine charged is known from when the solvent was loaded into the system at the beginning of the experiment. The amount of CO_2 added to the calorimeter during each differential addition is calculated using the Peng-Robinson equation of state. The pressure explicit version of the Peng-Robinson equation is used, whose terms are shown below (Smith et al., 1995; Tester and Modell, 1997).

$$P = \frac{nRT}{V - nb} - \frac{n^2 a\alpha}{V^2 + 2bnV - (nb)^2}$$

$$a = \frac{0.45724\ R^2 T_C^2}{P_C}$$

$$b = \frac{0.07780\ RT_C}{P_C}$$

$$\alpha = \left[1 + (0.37464 + 1.54226\omega - 0.26952\omega^2)\left(1 - \sqrt{T_R}\right)\right]^2$$

The critical constants for CO_2 used in the Peng-Robinson calculations are listed in Table F.2.

Table F.2: Critical constants for CO_2 (Perry and Green, 1997)

Constant	Value
T_C	304.21 K
P_C	73.9 bar
ω	0.224

The moles of CO_2 present in the CO_2 storage tanks are calculated before and after each CO_2 injection and the difference is the amount injected into the reactor. In the instances where the reactor pressure increased after a CO_2 pulse, the change in vapor pressure of CO_2 is calculated based on this pressure increase. The increase in reactor pressure is due to a portion of the CO_2 not being absorbed into the liquid because an equilibrium limit had been reached. The amount of CO_2 remaining in the vapor phase is subtracted from the total amount added to the reactor to calculate the moles of CO_2 that have been absorbed into the solvent during each CO_2 pulse. Once the moles absorbed into the solvent are known, the loading at each point can be calculated based on the known amount of amine charged initially.

During the experiment, the progress can be estimated by using the mass flow controller reading to estimate the amount of CO_2 inputted into the reactor during each impulse. A calibration equation is used to produce a curve of the CO_2 flow in liters per second. Integration of this curve over time produces a rough estimate of the liters of CO_2 entering the reactor.

To perform these calculations, a MATLAB program written by Inna Kim is used (Kim, 2008). An input file for each experiment contains the P_{CO2}, T_{CO2}, and P_r before

and after each impulse as well as the integrated values for dH_{online} and the estimate for liters of CO_2. The amount of CO_2 added to the reactor during each impulse is more accurately calculated as described above and the final values for the heat of absorption as a function of CO_2 loading are produced.

F.2 RESULTS OF HEAT OF ABSORPTION MEASUREMENTS

My efforts for the latter half of the second quarter of 2008 were focused on measuring the heat of absorption of CO_2 in aqueous concentrated PZ solutions. These experiments were performed in collaboration with Inna Kim and Hallvard Svendsen of the Norwegian Technical University (NTNU) in Trondheim, Norway.

The first series of experiments were calibration and verification tests performed on 30wt% (7 m MEA) and 2.4 m (2.0 M) PZ. The heats of absorption for these solutions were compared to the previous work of Inna Kim and Marcus Hilliard to verify my experimental procedure.

The first measurements conducted were with 7m MEA at 40˚C and 80˚C. The results of both are shown in Figure F.2 and Figure F.3 below. Only a few points were taken since the data seemed to match well with the previous work of Kim and Svendsen.(Kim and Svendsen, 2007) After the completion of testing with 8 m PZ, a short test with 7 m MEA was conducted at 120C since this temperature was not testing with 40 and 80 in the beginning. This test was also important to validate the data obtained for PZ at 100 and 120C where more data scatter was observed. The results for 7 m MEA at 120 compared to the data of Kim are shown in Figure F.4.(Kim and Svendsen, 2007)

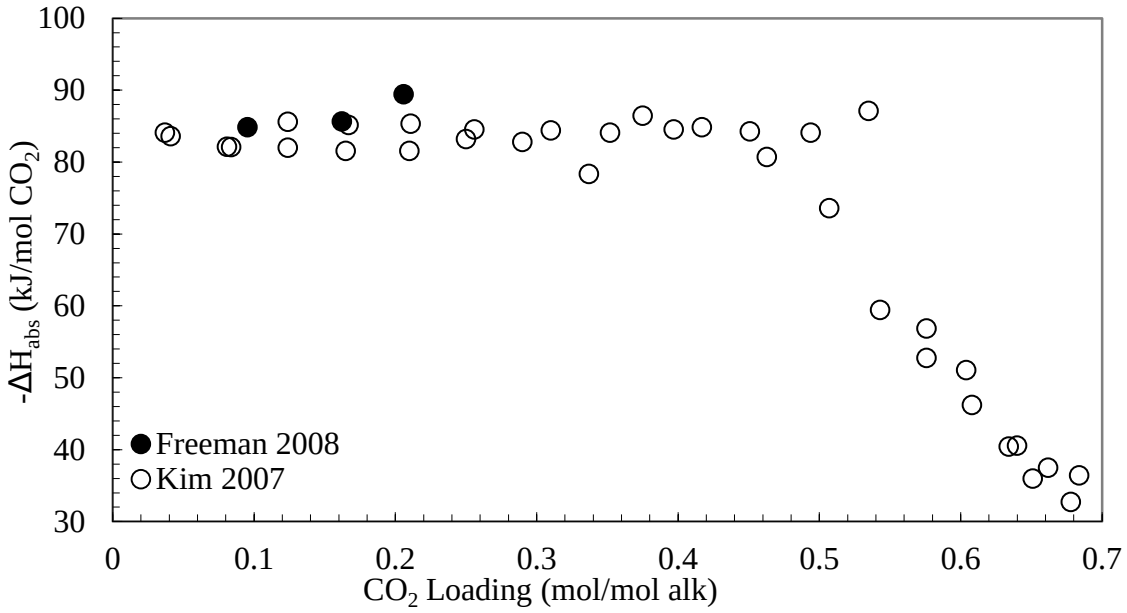

Figure F.2: Heat of absorption of 7 m MEA at 40˚C (Kim and Svendsen, 2007)

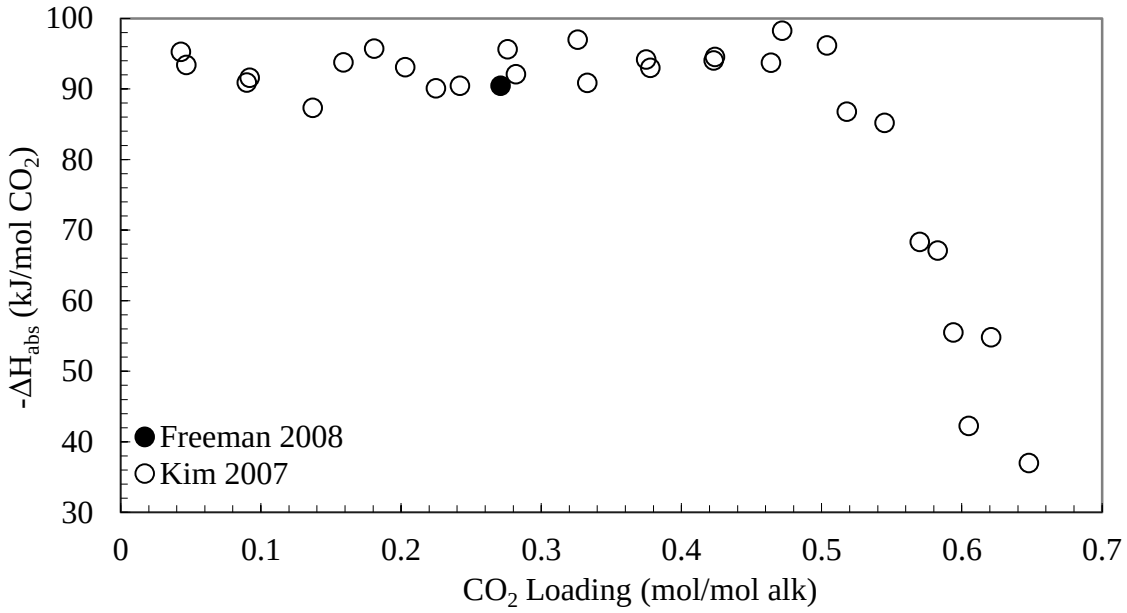

Figure F.3: Heat of absorption of 7 m MEA at 80˚C (Kim and Svendsen, 2007)

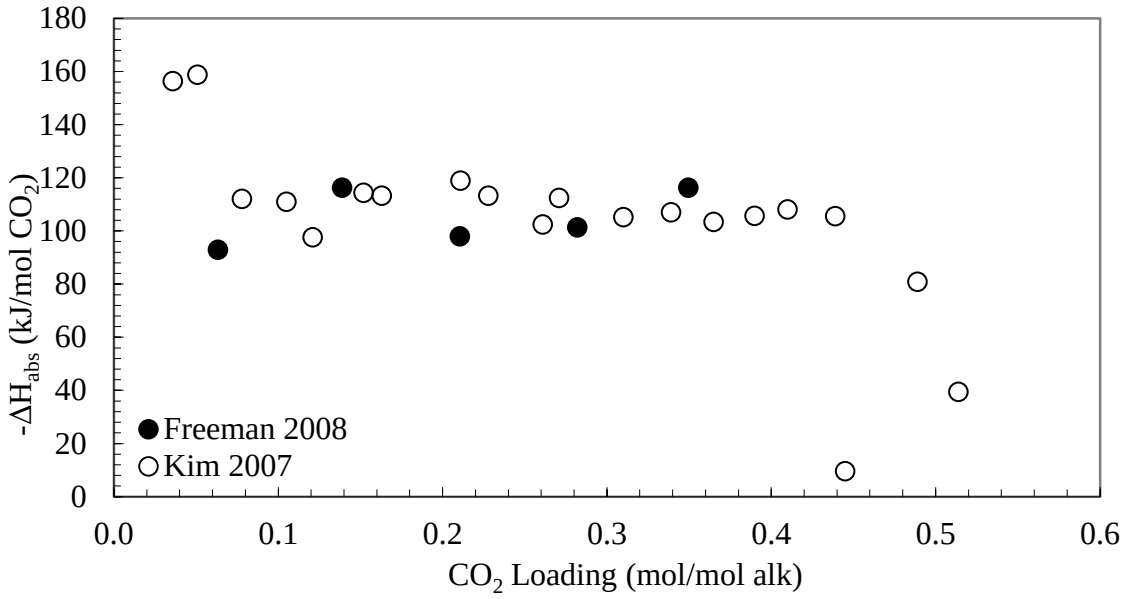

Figure F.4: Heat of absorption of 7 m MEA at 120˚C (Kim and Svendsen, 2007)

After the short tests with MEA, the work with PZ was started. The comparison between my data and that from Hilliard's thesis for 2.4 m PZ at 40˚C is shown below in Figure F.5 (Hilliard, 2008). The experiment performed on 2.4 m PZ took larger differential elements in CO_2 loading so the procedure could be quickly verified by reproducing Hilliard's results. With the exception of the very first point, the new data are close to that of Hilliard, although not within the ± 2% error that was reported. The first point was an accident as valve was open and letting CO_2 into the reaction vessel before the test was due to begin. The small amount of CO_2 let into the vessel and the heat released from the reaction was recorded. Since the areas of both were so small, the integration was flawed and not representative of the actual heat of reaction.

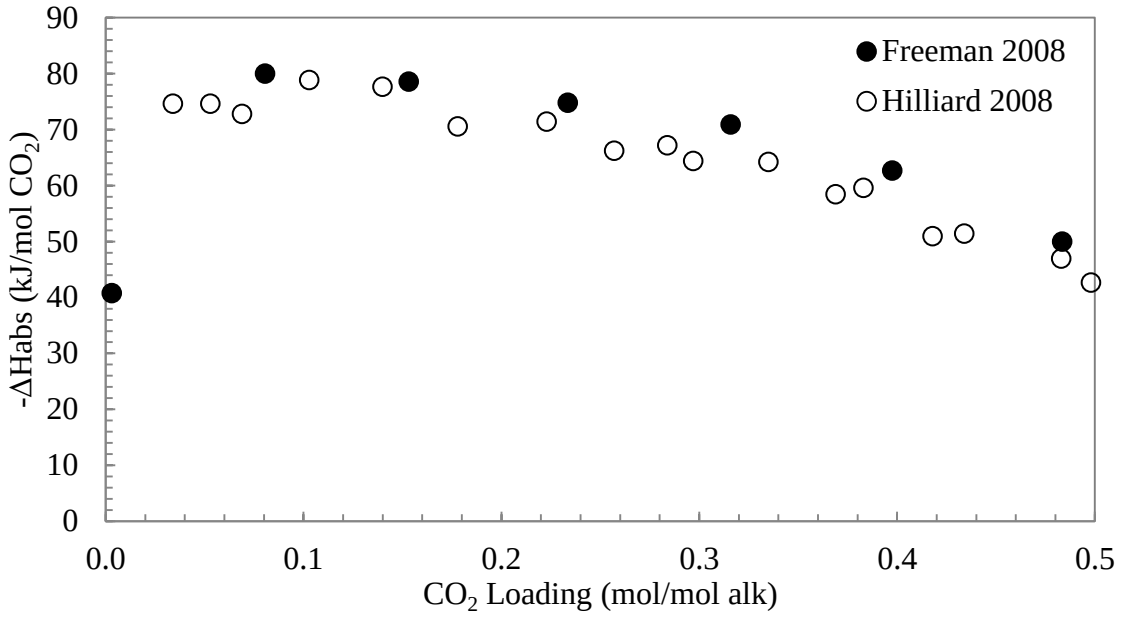

Figure F.5: Heat of absorption of CO_2 in 2.4 m PZ at 40˚C

After it was concluded that the experimental procedure and data analysis matched that of previous experiments, solutions of 8 m PZ were analyzed.

Measurements of the heat of absorption of CO_2 into aqueous 8 m PZ were conducted at 60, 80, 100, and 120˚C. At each temperature, two separate runs were performed and both runs are shown in Figure F.6, Figure F.7, Figure F.8, and Figure F.9 for 60, 80, 100, and 120˚C, respectively.

From the data collected, the cumulative heat of absorption of CO_2 per mole of amine could also be calculated as a function of loading.

$$\Delta H_{abs} = \frac{\int_0^{a_{final}} \text{Total Power } (\alpha')d\alpha'}{\text{mol PZ initially fed}}$$

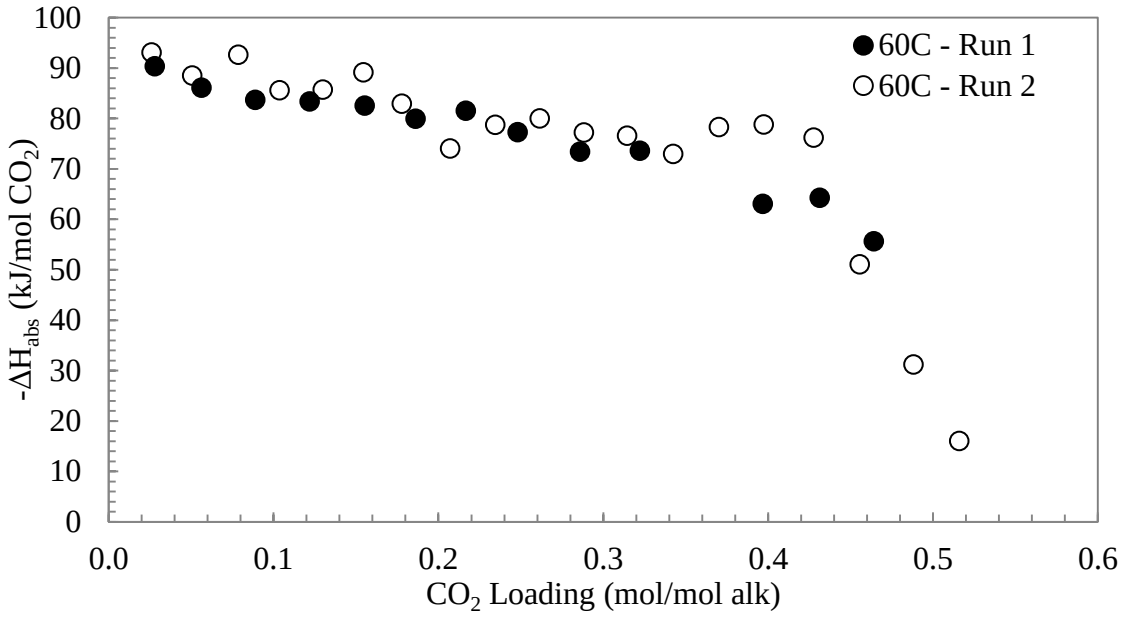

Figure F.6: Heat of absorption of CO_2 in 8 m PZ at 60˚C

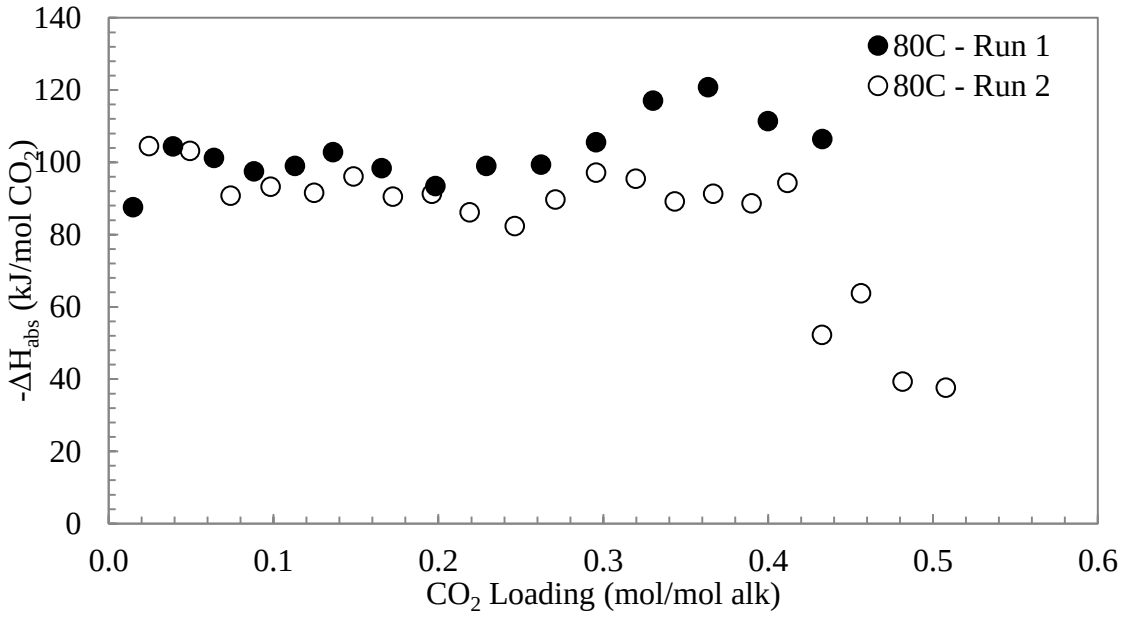

Figure F.7: Heat of absorption of CO_2 in 8 m PZ at 80°C

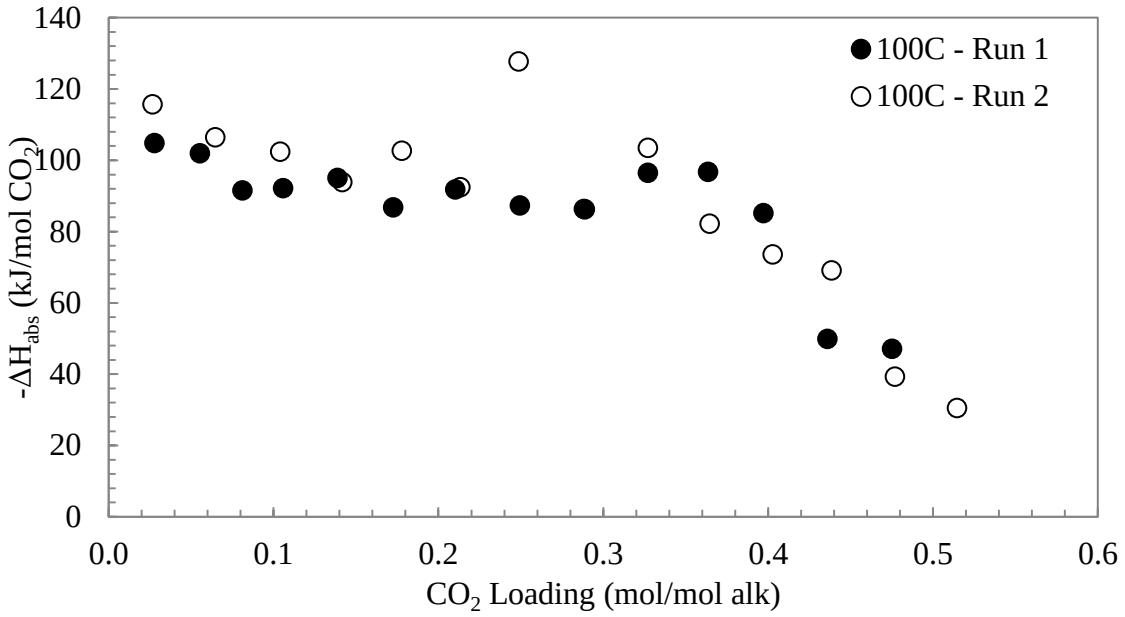

Figure F.8: Heat of absorption of CO_2 in 8 m PZ at 100˚C

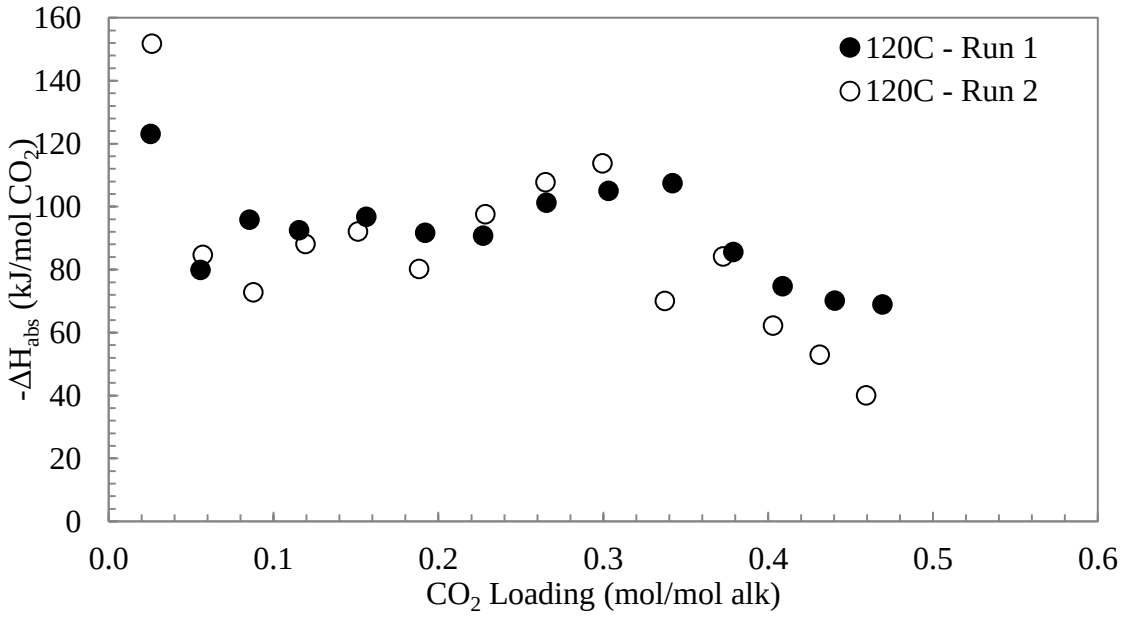

Figure F.9: Heat of absorption of CO_2 in 8 m PZ at 120˚C

The results for all eight runs are shown in Figure F.10. There is a good agreement between the two runs for 60˚C and the 120˚C at low loadings. In the 80˚C runs, the

results are quite separated indicating a lack of repeatability which was also observed in Figure F.7. In the 100˚C runs, the results also seem separated like the 80˚C, but the heat of absorption per mol of CO_2 data in Figure F.10 were much better than that of 80˚C. The 120˚C data fit very well between the two runs from a loading of zero until around 0.3 and then there is a deviation as run2 is lower than run 3. The cause of this deviation is unknown. Overall, the heat of absorption in terms of the total moles of amine does not change significantly with temperature until a loading of above 0.2 to 0.3 is reached. The temperature dependence is significant in the region of higher loading, approximately 0.25 to 0.50, which is the industrially relevant loading region as well.

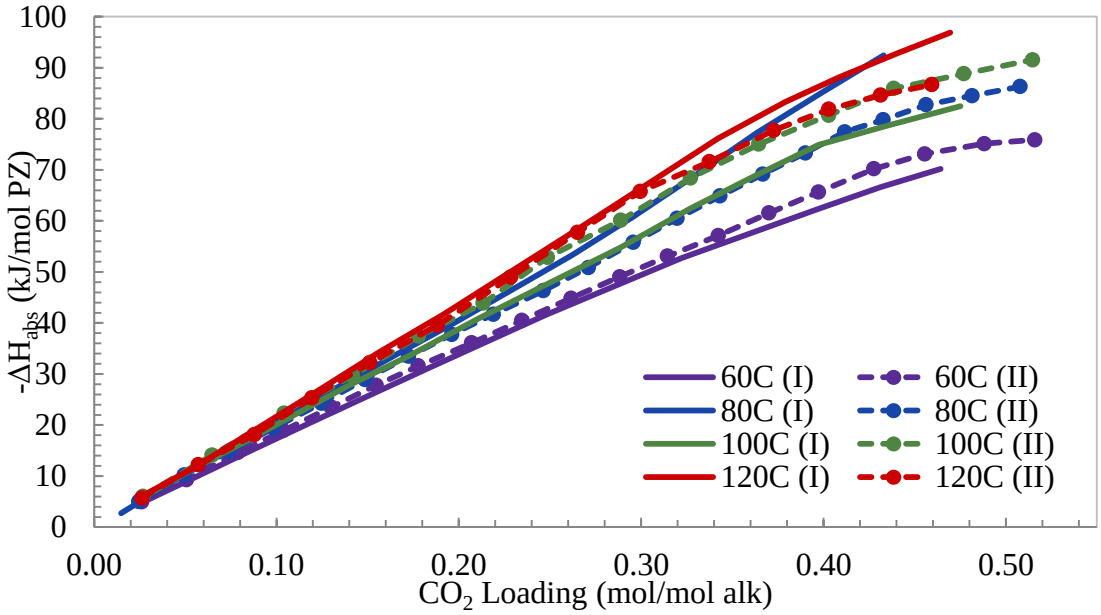

Figure F.10: Heat of absorption per mole of PZ at all temperatures

F.3 COMPLICATIONS WITH THE HEAT OF ABSORPTION MEASUREMENT

The measurement of the heat of absorption for concentrated PZ solutions is very complex because the solutions are not soluble at room temperature while unloaded. The calorimeter is designed so that the vessel is sealed and all solutions must enter through

the designated solvent inlet port. The solutions are loaded via suction created by pulling a vacuum in the reaction vessel prior to solvent loading. In addition, the inlet and outlet tubing is all ¼ inch stainless steel piping and Swagelok® valves. These narrow pipes are also highly susceptible to being clogged because of PZ precipitation.

To overcome these obstacles, numerous modifications were required to the original procedure developed at used at NTNU. First of all, the solutions were still prepared unloaded but were kept warm using a water bath maintained between 45 and 50 °C. The first unsuccessful attempt at adding 8 m PZ to the reactor demonstrated that the solvent inlet line needed to be heated to receive the warm solution. Electrical heating tape was wrapped around the entire inlet line with a thermocouple to monitor the temperature of the pipe. The temperature of the heating tape could not be controlled, so the tape was only plugged in a few minutes before loading to ensure that the temperature did not go above 90 °C. This allowed the solution to be successfully added to the reactor.

The first time 8 m PZ was used in the reactor, the temperature in the reactor could not come to equilibrium at 40 °C. The temperature was very slow to respond, slower than had been observed before. The experiment was abandoned and precipitated PZ was found to be clogging the entire outlet line. It was believed that the low temperature of 40°C was not high enough to prevent precipitation under vacuum and the precipitation may have interfered with the temperature sensor in the reactor that was unresponsive. The decision was made to only attempt measurements at 60 °C and above for 8 m PZ solutions.

In addition to heating the inlet line, it was found that warming the entire glass solution loader before attempting to load the solution into the reactor made it much more likely to succeed. After the solution was added to the glass loader, the connection piece was added to the top, the entire bottle was weighed, and then the bottle was ran under

warm water for about 3 minutes. Special attention was made to ensure that the connection piece was warmed before any attempt to load the solution as undertaken. Also, the rest of the bottle was warmed continuously to ensure that the glass did not crack due to thermal shock since some sections were cold after the solvent was added. Warming the connection piece and connecting it to the inlet line warmed by the heating tape ensured that there was not precipitation in the inlet line and that the solution successfully entered the reactor.

F.4 DISCUSSION OF HEAT OF ABSORPTION RESULTS

Two types of heat of absorption data can be measured experimentally, the integral and the differential heats of absorption. The integral heat of absorption is the more standard measurement in literature and is commonly measured using a flow calorimeter.(Carson et al., 2000; Mathonat et al., 1998) In flow calorimeters, two inlet streams of the amine and the CO_2 are fed continuously at defined ratios and the heat released over the course of the apparatus to absorb the CO_2 into the liquid is measured on-line. In this way, the heat need to absorb all of the CO_2 fed is measured. On the other hand, differential calorimetry measures the heat needed to absorb a small, differential amount of CO_2 added to the system. In this way, the same solution is utilized to cover the entire range of CO_2 loadings rather than a separate experiment to obtain each loading point, as with integral heats of absorption. When differential heats are measured, the integral heat can be calculated afterward according to the following equation for each loading point.

$$-\Delta H_{int} = \int_0^{\alpha} -\Delta H_{diff}(\alpha')d\alpha'$$

The reverse, calculating differential heats from integral heats is more difficult and usually contains more error. The calorimeter at NTNU is set-up for differential heat of absorption measurements. The integral heats of absorption were calculated from the collected differential heat data and are shown for all eight runs in Figure F.11.

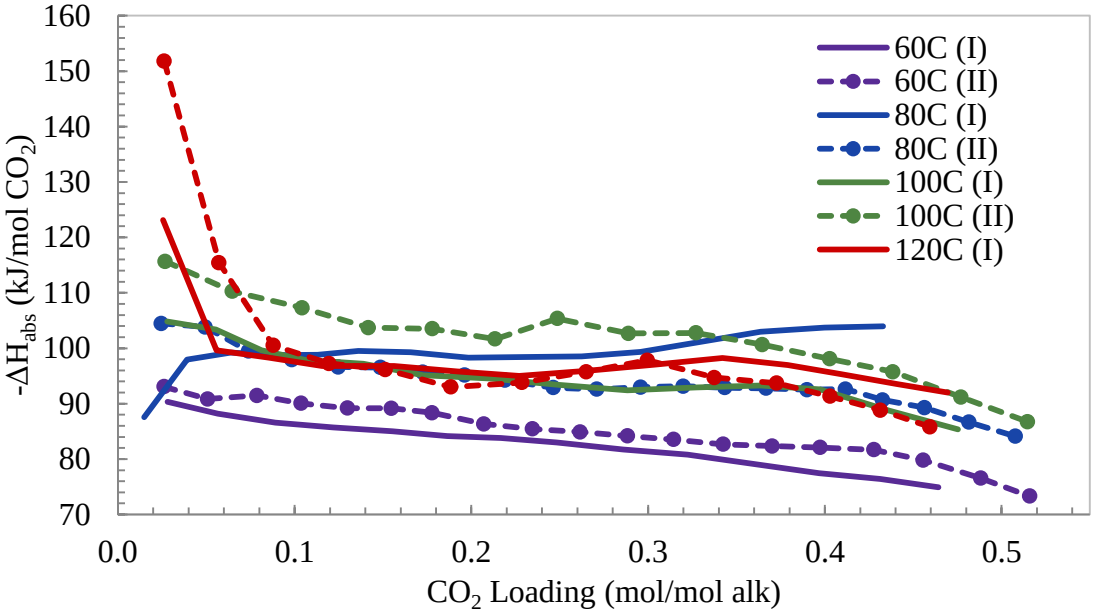

Figure F.11: Integral Heat of Absorption at 60, 80, 100, and 120˚C

As shown in Figure F.11, calculating the integral heats of absorption evens out the differential data and produces easier trends to interpret. Unfortunately, information is lost in performing the integral calculation. As with the heats of absorption in terms of moles of amine (Figure F.10), the data for 80 and 100 °C are quite different between the two runs performed at each temperature. Additionally, the large heat of absorption measured at the first loading for the two runs at 120 °C distort the trends for those runs. As mentioned before, the reason for this larger first measurement is not clear.

The heat of absorption measurements proved to be problematic for 8 m PZ. The data obtained at higher temperatures, primarily 80 and 120 °C, are very scattered within

each individual run and also between the two repeated runs. The cause of the high level of scatter in the higher temperature measurements is not well understood. It was observed that the baseline obtained after each CO_2 pulse was not as steady for the higher temperatures. This unsteady baseline was more difficult to manually integrate and likely resulted in higher errors than in the lower temperature measurements where the baseline was flat and well behaved. The response of the total power measurement over time is shown in Figure F.12 for multiple CO_2 pulses at 60 °C (panel A) and at 120 °C (panel B). This is a representative curve that demonstrates the difficulties encountered while integrating the higher temperature data. The chaotic baselines obtained at higher temperature seem to indicate that the calorimeter had more difficulty keeping a stable temperature, perhaps because of the thermostatting oil having too low of a viscosity. All the experiments reported here were conducted with oil with a viscosity of 10 cP, but an oil with 50 cP may have been more able to maintain higher temperatures.

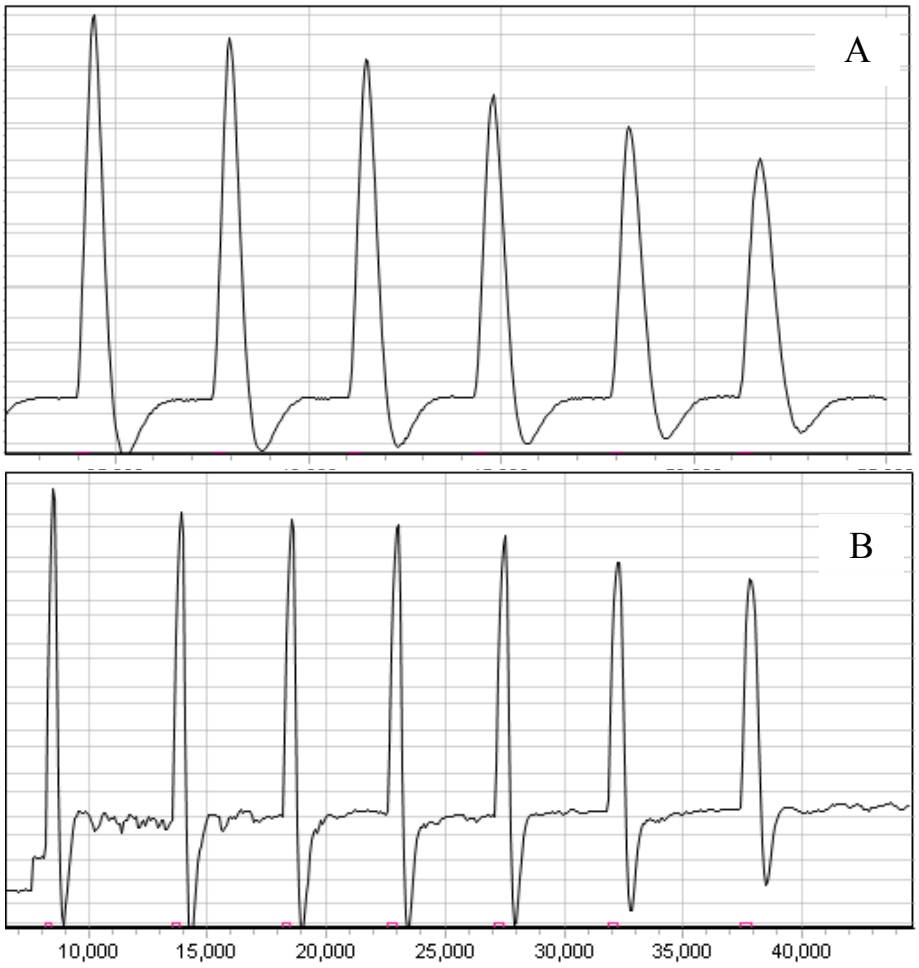

Figure F.12: Comparison of total power baselines for ΔH_{abs} measurements at 60 (panel A) and 120˚C (panel B)

The thesis of Hilliard is the only other source of heat of absorption data for aqueous PZ solutions (Hilliard, 2008). His work analyzed 2.4 m PZ and the results for 40, 80 and 120°C are shown below in Figure F.13. As expected, the heat of absorption increased with temperature while, as with other amine solvents, the heat of absorption decreased with increased CO_2 loading. The data at 120°C did not reach as high of a loading as the other data, so the data maintain approximately the same value from a loading of zero to 0.4.

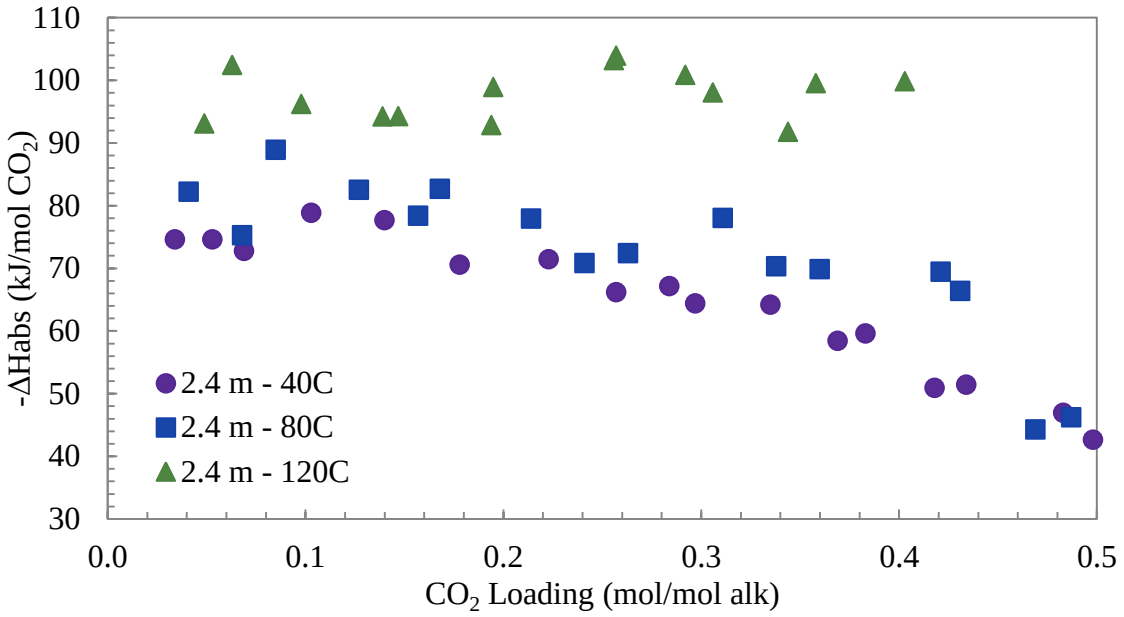

Figure F.13: Heat of absorption of CO_2 for 2.4 m PZ at 40, 80, and 120˚C (Hilliard, 2008)

The data for 8.0 m PZ shown above in the results section demonstrates similar trends, although the quality of data at higher temperatures is still under review.

In this initial phase of experimentation, the addition of lid heating since Kim's previous work was questioned. When the calorimeter was serviced (after the conclusion of most of Kim's work and before that of Hilliard), the lid of the vessel was modified to include an additional metal plate for insulation and a separate lid heating system. The specifics of the lid heating are not known and the control of the small electrical heater in the lid is not integrated with the rest of the calorimeter. Tests with the lid heating apparatus unplugged showed greater similarity with previous data on MEA and PZ so it was determined that lid heating should be abandoned. Calibration points were re-run at the experimental temperatures in the absence of lid heating to ensure complete elimination of the influence of lid heating from the system. Since lid heating was not integrated with the rest of the heat data collected by the calorimeter, it was decided that

this did not adequately reflect the heat of absorption and data collected with lid heating in place most likely had additional error.

F.5 Conclusions and Recommendations

The heat of absorption measurements proved difficult due to solubility issues with the PZ and due to the differences in instrument stability at varying temperatures. Overall, the heat of absorption of PZ follows similar trends to other amines, such as MEA and MDEA, in that the heat of absorption trend stays relative constant over a range of low loadings until a threshold loading is reached, when the value decreases rapidly. For PZ, this decreased was observed to begin around a loading of 0.4 mole CO_2 per mole alkalinity or a loading of 0.9 to 1.0 mole CO_2 per mole PZ. In PZ, the data actually decrease slightly until the threshold where in MEA, the data remains quite constant until the threshold of 0.5 mole CO_2 per mole alkalinity is reached. For 8 m PZ at a loading of 0.025 mole CO_2 per mole alkalinity, the heat of absorption was 90.3, 104.5, 115.7, and 123.1 kJ per mole CO_2, respectively, at temperatures of 60, 80, 100, and 120˚C. After the initial loadings, there was little difference in the values for the heat of absorption between 80, 100, and 120˚C.

The nomenclature and abbreviations used throughout this section are summarized in Table F.3.

Table F.3: Nomenclature and abbreviations for heat of absorption calculations

Symbol	Units	Description
a	m^3atm/mol	Parameter used in the Peng-Robinson equation of state; function of the gas constant, critical temperature, and critical pressure of a substance.
b	m^3/mol	Parameter used in the Peng-Robinson equation of state; function of the gas constant, critical temperature, and critical pressure of a substance.
BKA	W/°C	Average total heat transfer between the thermostatting media (silicon oil) and the outer reactor jacket, calibrated parameter based on dynamic system response during calibration
Calc_power	W	The power outputted by the recirculator to heat and cool the reactor contents as calculated using the six calibration parameters
CB	J/°C	Heat capacity of the outer reactor jacket, fixed at 1500 for this calorimeter
CR	J/°C	Heat capacity of the reactor contents, including the solution, contributions from the stirrer, reactor base, and interior walls; calibrated parameter based on solvent and temperature in use
dF_DT_reactor	°C	Difference in temperature between jacket (taken at the inlet) and the reactor ($T_r - T_j$); recorded variable during calorimeter experiments
dH_{online}	J	Heat exchanged between the circulator and the reactor contents, calculated as the area under a curve of time (s) vs. Total_power (W)
dH_{calc}	J	Heat exchanged between the circulator and the reactor contents, calculated as the area under a curve of time (s) vs. Calc_power (W), used for comparison to dH_{online} and calibration
dT/dt	°C/sec	Change in reactor temperature with time; recorded variable during calorimeter experiments.
FlowCp	W/°C	Product of the volumetric flow rate, density, and heat capacity of the thermostatting media (silicon oil), usually 600 – 900 W/°C, calibrated parameter based on temperature
HB_DT_reactor	°C	Temperature difference in silicon oil between entering and exiting the reactor ($T_{j(out)} - T_{j(in)}$); recorded variable during calorimeter experiments

Table F.3: Nomenclature and abbreviations for heat of absorption calculations (Continued)

Symbol	Units	Description
HLoss_DT_reactor	°C	Average temperature gradient across the insulation between the reactor jacket and the outer metal shield ($T_{HL(inner)} - T_{HL(outer)}$); recorded variable during calorimeter experiments
HlossC	W/°C	Heat Conductivity coefficient to characterize heat losses through the thermal shield, usually 1 – 1.4 W/°C, calibrated parameter based on temperature
n	mol	Number of moles
P_C	Bar	Critical pressure
PZ	-	Piperazine (abbreviation)
R	J/mol-K	Universal gas constant
T_C	K	Critical temperature
T_j	°C	Calculated Temperature of the jacket of the calorimeter; function of T_{ref}, BKA, and CB
$T_{j(in)}$	°C	Temperature of the jacket at the inlet of the thermostatting media
$T_{j(out)}$	°C	Temperature of the jacket at the exit of the thermostatting media
$T_{j, i}$	°C	Temperature of the jacket of the calorimeter at point i
$T_{j, (i-1)}$	°C	Temperature of the jacket of the calorimeter at point (i-1)
T_r	°C	Temperature of the reactor contents
T_R	K	Reduced temperature, ratio of temperature and the critical temperature of a substance
T_{ref}	°C	Measured temperature of the thermostatting media (silicon oil)
Total_power	W	The power directly outputted by the recirculator to heat and cool the reactor contents through the silicon oil; recorded variable during calorimeter experiments
V	m^3	Volume, used in Peng-Robinson equation of state
α	-	Parameter used in the Peng-Robinson equation of state; function of temperature and ω, the Pitzer acentric factor
ω	-	Pitzer acentric factor, used for Peng-Robinson equation of state

Appendix G – Details of IC-MS Analysis

An example of the type of details MS work that was done during this project tis provided in this appendix. The details of each degraded sample analyzed with IC-MS in this project are not provided anywhere due to space constraints. In this appendix, a full IC-MS analysis is shown for a set of standards and one thermally degraded sample, the final sample of TE12. These are provided an example of the type of work done to identify degradation products in oxidized and thermally degraded PZ samples.

G.1 IC-MS ANALYSIS OF STANDARDS

PZ derivatives that are suspected degradation products were analyzed with cation IC-MS. IC-MS was used to identify where the compounds would show up on a cation IC chromatogram and what mass-to-charge (m/z) ratios would be shown for each compound. It is expected that each compound would acquire one proton making its m/z equal to the

molecular weight plus one. However, it is possible that each molecule could behave differently than expected. For example, two molecules can attach to the same charge (m/z = 2×MW + 1) or a molecule attaching to potassium or sodium ion in the system (m/z = MW + 23 or 40) to represent their mass differently from expected.

The compounds tested are shown below in Table G.1. The molecular weight and expected m/z for each compound is shown as well as its chemical structure. The cation IC-MS chromatograms for a 1000 ppm solution of each species are shown in Figure G.1 through G.16. In each figure, the top panel is the total MS signal over the course of the chromatographic separation. The bottom panel is the cation IC chromatogram total conductivity signal. The panels are aligned so that they correspond in time.

Table G.1: Summary of PZ Derivatives Analyzed by Cation IC-MS

Compound	Abb.	MW (g/mol)	Expected m/z	Chemical Structure
2-Imidazolidone	-	86.1	87.1	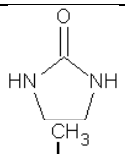
2-Methyl-2-imidazoline	-	84.1	85.1	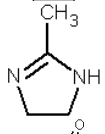
2,5-piperazindione	-	114.1	115.1	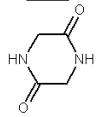
N-Acetyl PZ	AcPZ	128.2	129.2	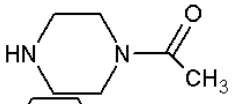
N-(2-Aminoethyl) PZ	AEPZ	129.2	130.2	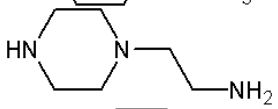
N-Amino-N'-Methyl-PZ	AMPZ	115.2	116.2	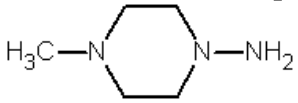
N,N'-Diformyl PZ	DFPZ	142.2	143.2	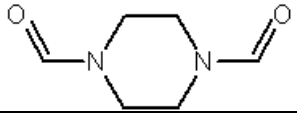

Table G.1: Summary of PZ Derivatives Analyzed by Cation IC-MS (Continued)

Compound	Abb.	MW (g/mol)	Expected m/z	Chemical Structure
N,N'-Dimethyl PZ	DMPZ	114.2	115.2	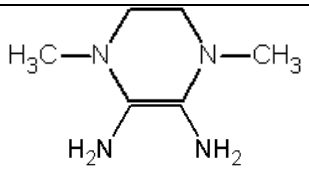
Ethylenediamine	EDA	60.1	61.1	
N-Ethyl PZ	EPZ	114.2	115.2	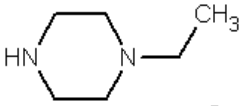
N-Formyl PZ	FPZ	114.2	115.2	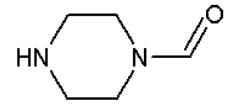
N-(2-Hydroxyethyl) EDA	HEEDA	104.2	105.2	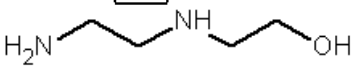
N-Hydroxyethyl PZ	HEP	130.2	131.2	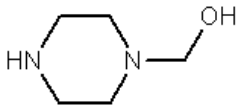
N-(2-Hydroxyethyl)-N'-Methyl PZ	HEMP	144.2	145.2	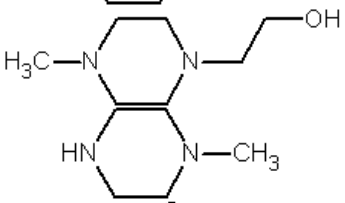
N-Methyl PZ	1-MPZ	100.2	101.2	
Triethylenediamine	TEDA	112.2	113.2	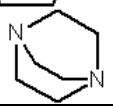

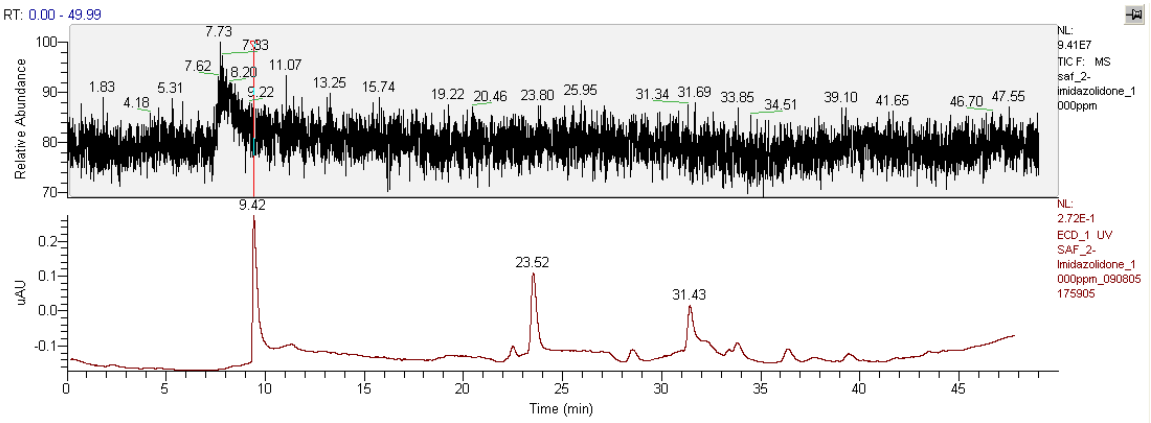

Figure G.1: Cation IC-MS chromatogram for 1000 ppm 2-Imidazolidone (2-Imid)

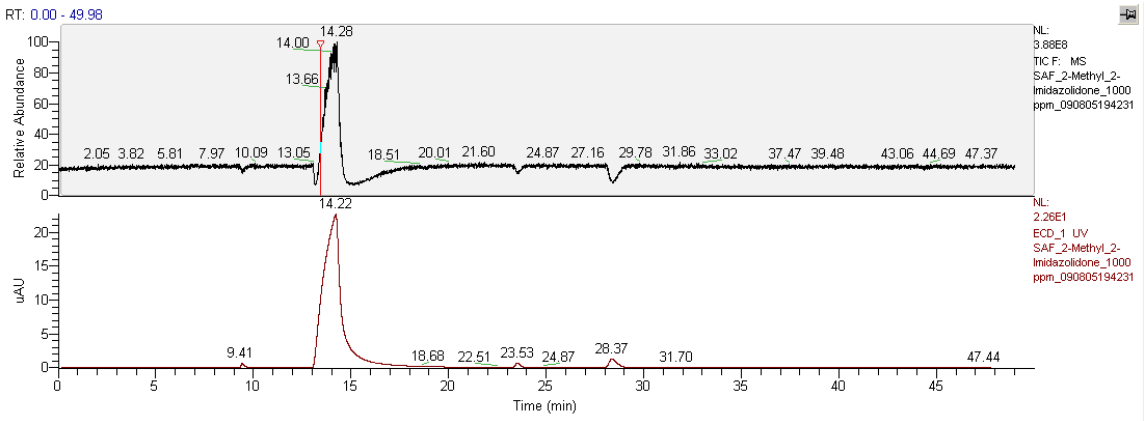

Figure G.2: Cation IC-MS chromatogram for 1000 ppm 2-Methyl-2-Imidazoline

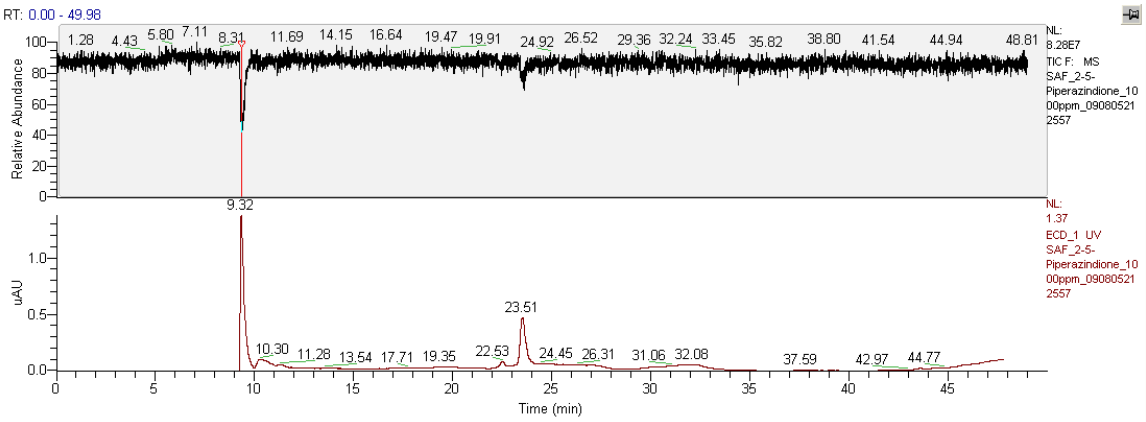

Figure G.3: Cation IC-MS chromatogram for 1000 ppm 2,5-Piperazindione

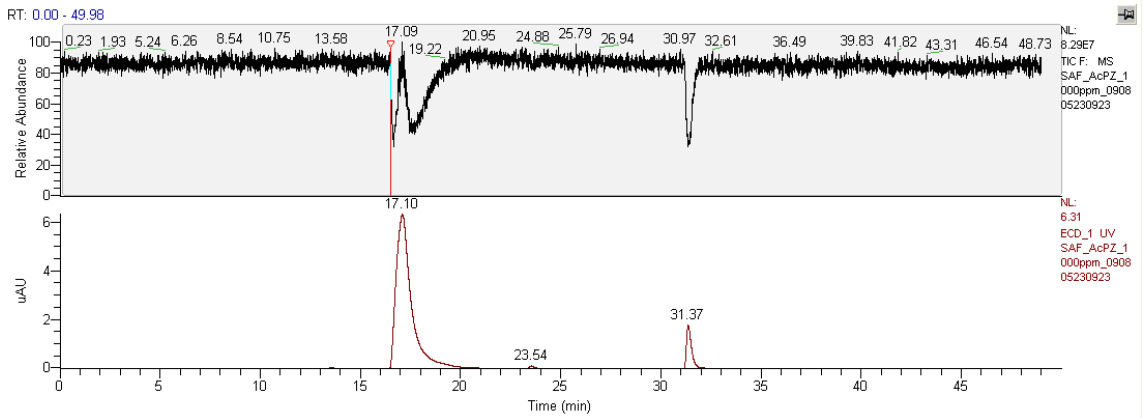

Figure G.4: Cation IC-MS chromatogram for 1000 ppm N-Acetyl PZ (AcPZ)

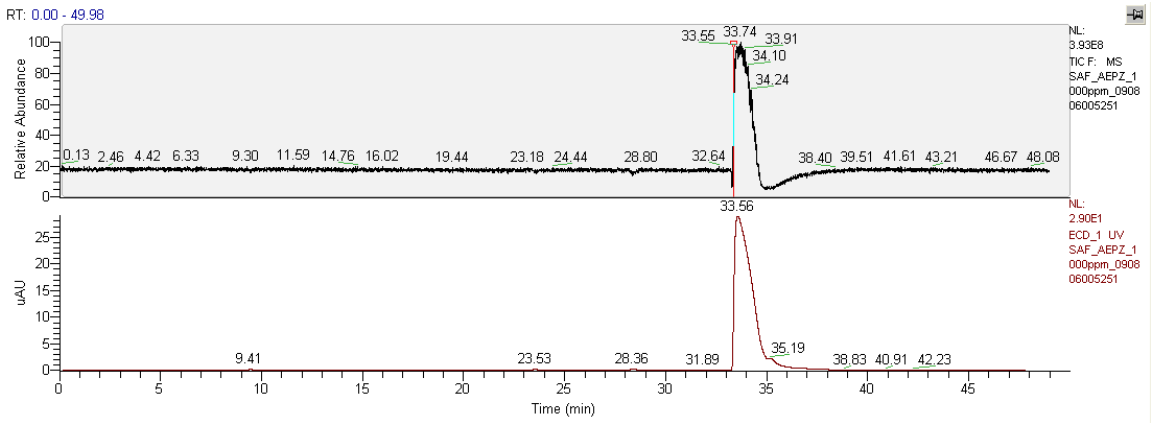

Figure G.5: Cation IC-MS chromatogram for 1000 ppm AEP

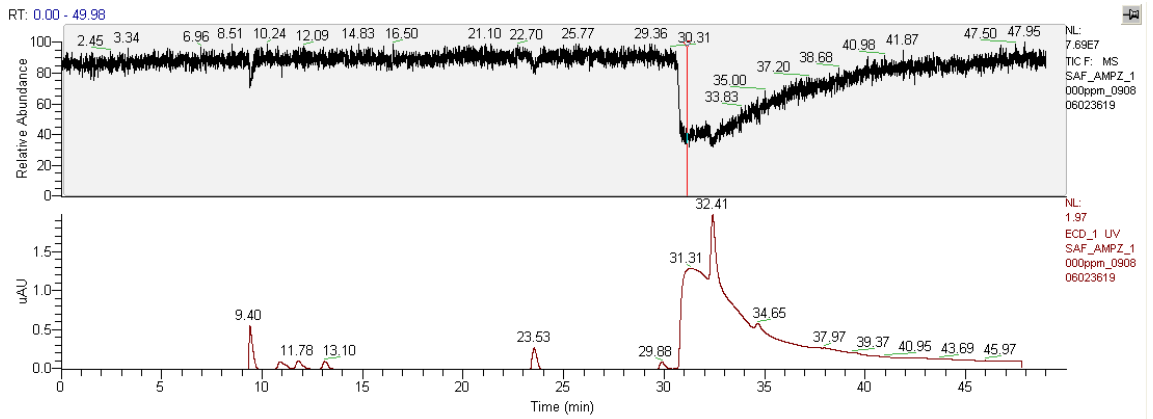

Figure G.6: Cation IC-MS chromatogram for 1000 ppm AMPZ

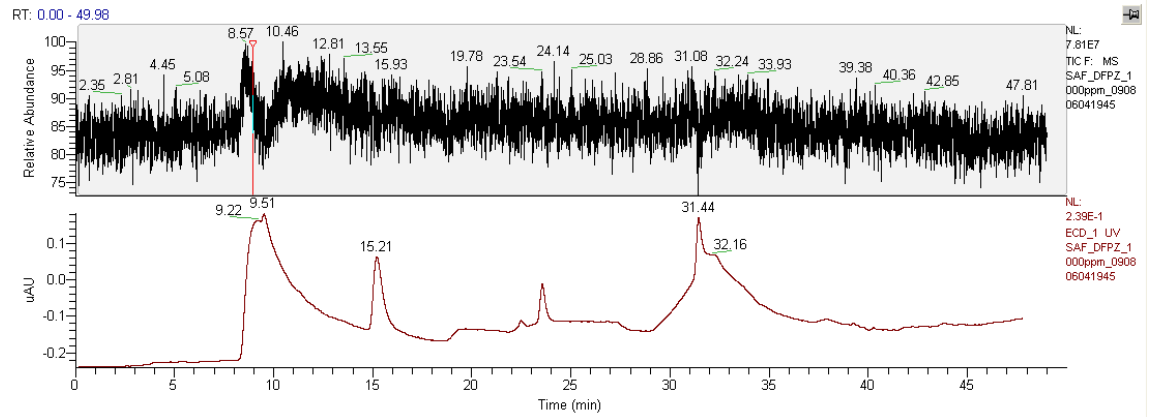

Figure G.7: Cation IC-MS chromatogram for 1000 ppm N,N'-Diformyl PZ (DFPZ)

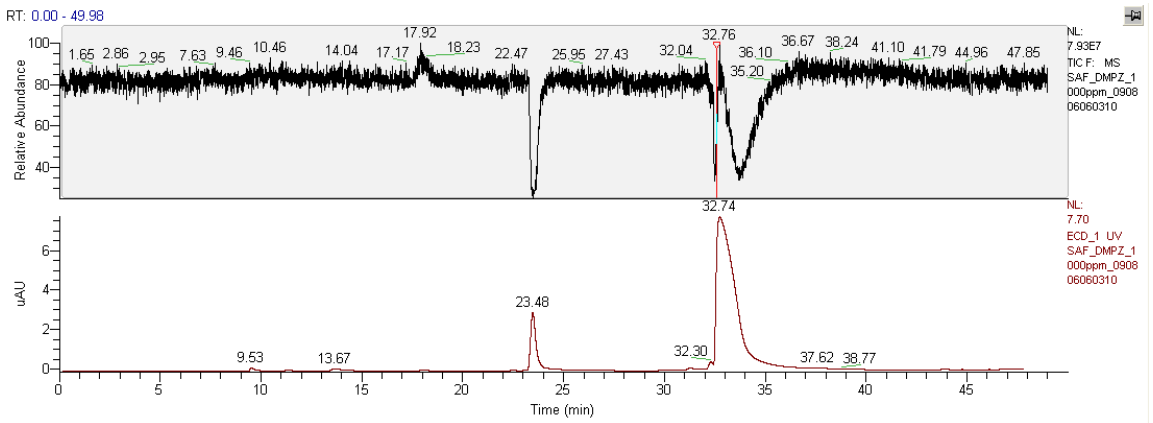

Figure G.8: Cation IC-MS chromatogram for 1000 ppm 1,4-DMPZ

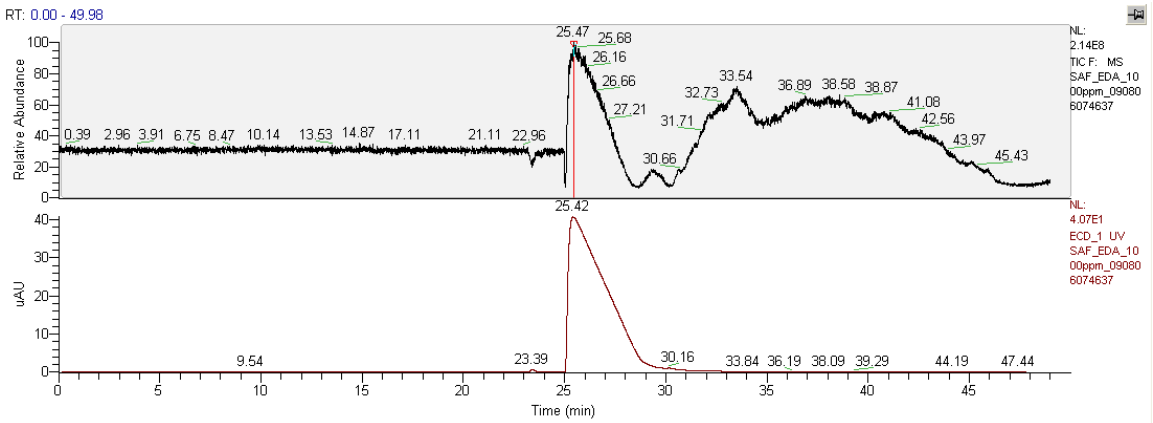

Figure G.9: Cation IC-MS chromatogram for 1000 ppm EDA

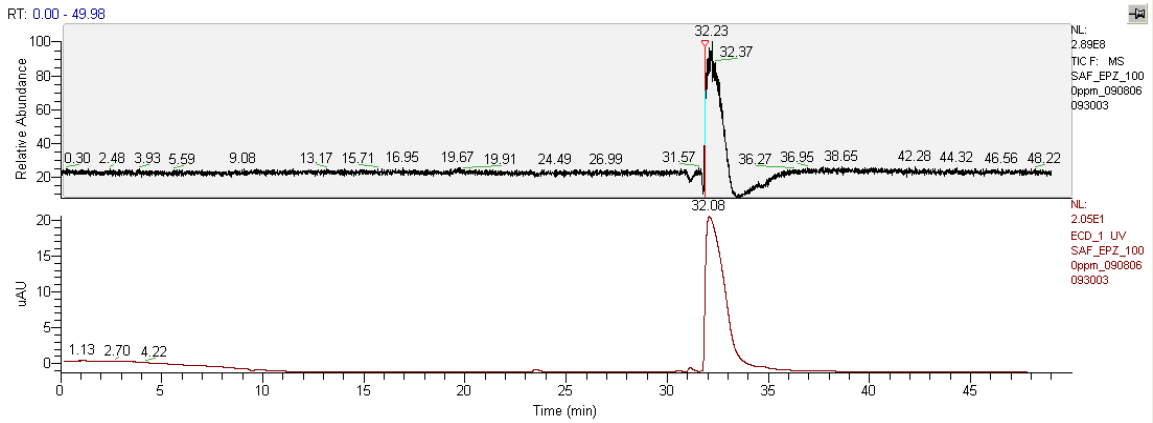

Figure G.10: Cation IC-MS chromatogram for 1000 ppm N-Ethyl PZ (1-EPZ)

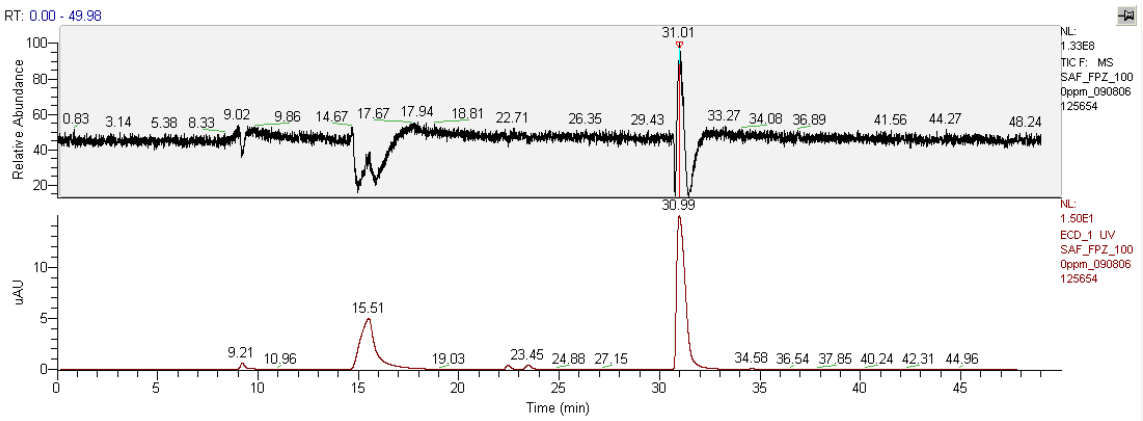

Figure G.11: Cation IC-MS chromatogram for 1000 ppm N-formylpiperazine (FPZ)

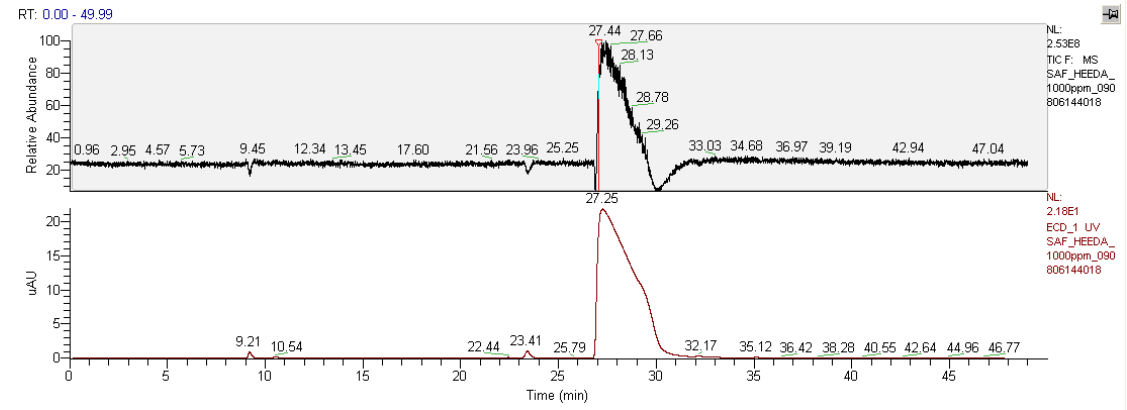

Figure G.12: Cation IC-MS chromatogram for 1000 ppm HEEDA

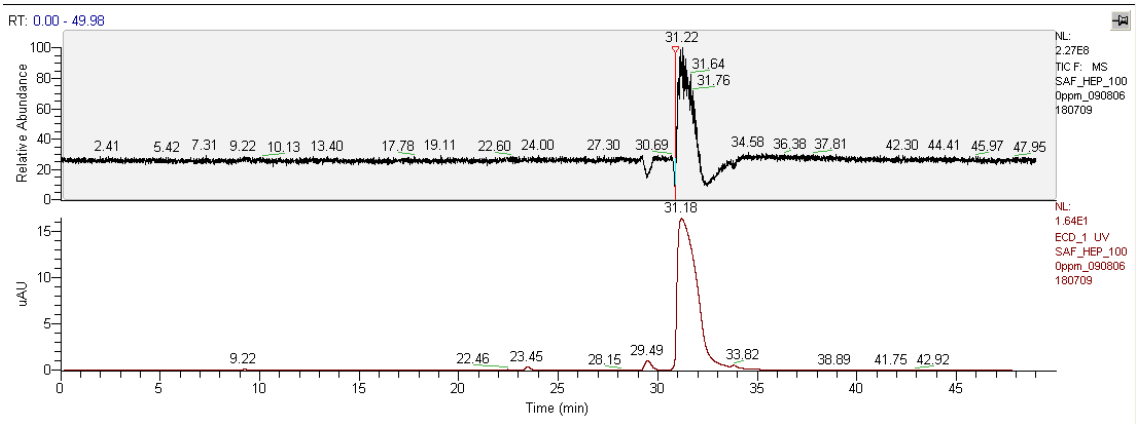

Figure G.13: Cation IC-MS chromatogram for 1000 ppm HEP

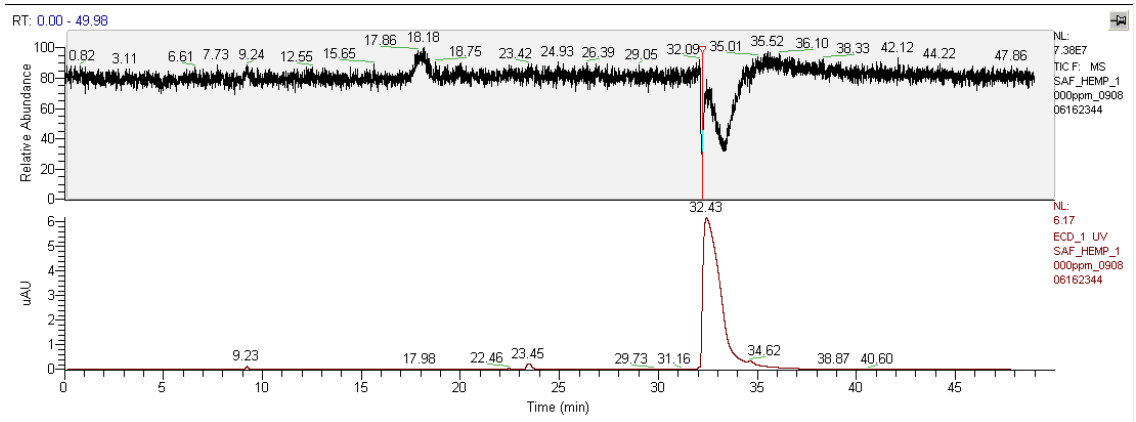

Figure G.14: Cation IC-MS chromatogram for 1000 ppm HEMP

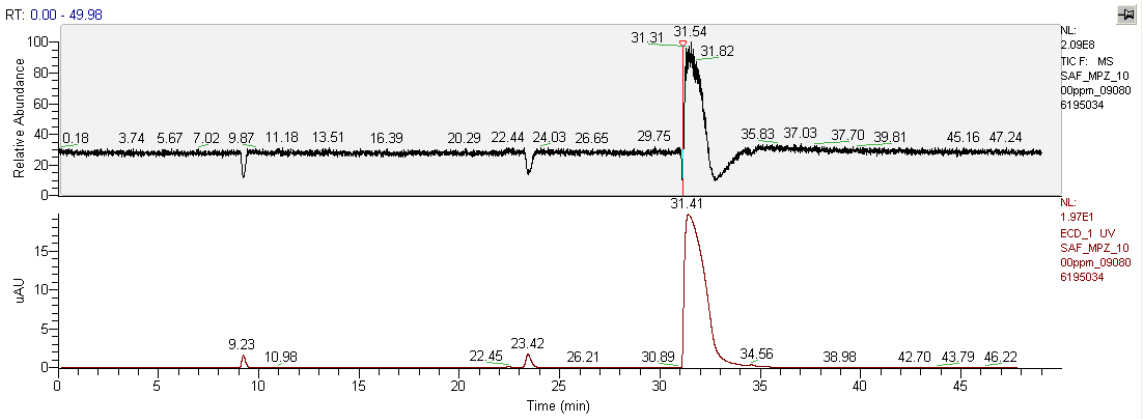

Figure G.15: Cation IC-MS chromatogram for 1000 ppm N-methyl PZ (1-MPZ)

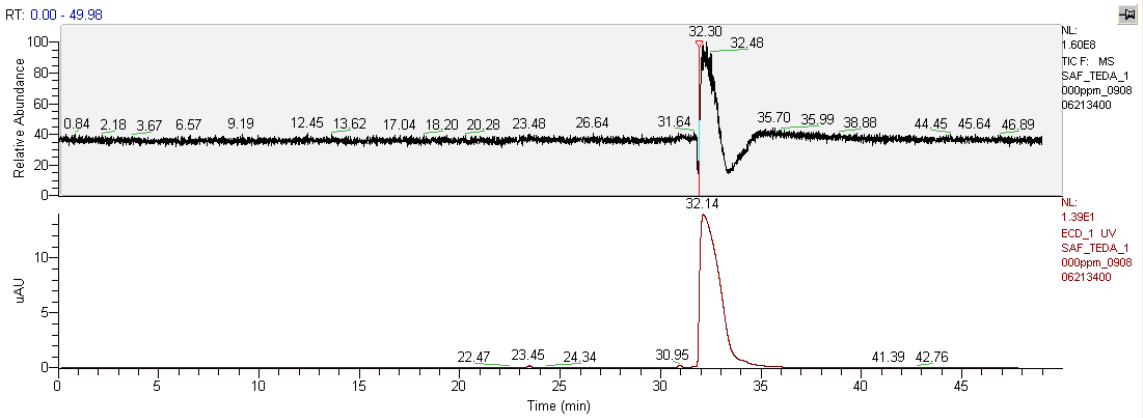

Figure G.16: Cation IC-MS chromatogram for 1000 ppm TEDA

Of the 16 derivatives analyzed by Cation IC-MS, 13 of the species (AcPZ, AEP, AMPZ, DFPZ, 1,4-DMPZ, EDA, 1-EPZ, FPZ, HEEDA, HEP, HEMP, 1-MPZ and TEDA) all gave clear chromatograms with good responses from the primary analyte. Each of these chromatograms had a primary peak that is significantly larger than any secondary peaks and contained the expected m/z value for the given compound. The retention times varied and a few, such as FPZ, had visible PZ contamination peaks. It is not believed that 2-Imid, 2,5-piperazindione, and DFPZ have any significant cation IC response and any peaks shown in the figures above are just background or contaminant species that respond to cation IC.

A comparison of the analytes and their performance on cation IC-MS is shown below in Table G.2. For each analyte, the retention time of the main peak, any other m/z ratios found in that peak, and the maximum signal response of the main peak is shown. The other m/z ratios found in the main peak are indicated because seven of the analytes formed doublets in the main peak (indicated by * in the table). Doublets occur when two analyte molecules attach to one charge, giving a m/z ratio that corresponds to 2×MW+1. Two analytes, 1,4-DMPZ and 1-EPZ behaved differently as the main secondary m/z in the primary peak corresponded to 2×MW-1. It is not clear time how this m/z resulted or how the structure of 1,4-DMPZ and 1-EPZ led to this difference. Also, since all the analytes were 1000 ppm, the maximum response gives an indication of the response factor a particular analyte has for the cation IC conductivity detector.

The results shown in Table G.2 reveal important information on where PZ derivatives are expected cation IC chromatograms of degraded PZ samples. First off, the differences in maximum response are very helpful. For the same concentration (1000 ppm), the responses vary from 0.2 to 40. This explains why EDA is one of the most easy degradation products to detect with cation IC. EDA has a retention time separate from

most of the other analytes and has a large response factor. Analytes that have small response factors (AMPZ, and DFPZ) are not likely to be detected in experimental samples unless their concentrations are very high. The retention times also indicate that quite a few analytes overlap and elude at similar times, therefore making it difficult to distinguish between the two (or more) analytes. One set of analytes, HEP, AMPZ, and 1-MPZ, elude within 0.2 minutes of each other. EDA and HEEDA are within 1.8 minutes of each other while are all within only 0.2 minutes. Finally, EPZ, HEMP, and 1,4-DMPZ are all within 0.6 minutes of each other.

Table G.2: Summary of PZ Derivative Cation IC-MS Results

Compound	Abb.	RT (min)	Also in Main Peak (m/z)	Maximum Response (uAU)	Notes
2-Imidazolidone		9.43	105.1	0.2	
2-Methyl-2-imidazoline		14.22	103.1, 205.1	23	+
2,5-piperazindione		9.32	77.0, 129.2	1.4	+
N-Acetyl PZ	AcPZ	17.10	257.2*	6	^
N-(2-Aminoethyl) PZ	AEP	33.56	130.1	28	
N-Amino-N'-Methyl-PZ	AMPZ	~31-32	114.1	2	
N,N'-Diformyl PZ	DFPZ	9.22	161.1	0.2	
N,N'-Dimethyl PZ	1,4-DMPZ	32.74	227.2*	8	
Ethylenediamine	EDA	25.42	121.1*	40	
N-Ethyl PZ	1-EPZ	32.08	227.2*	20	^
N-Formyl PZ	FPZ	15.51	229.1*****, 87.1	15	^
N-(2-Hydroxyethyl) EDA	HEEDA	27.25	209.1*****	22	
N-Hydroxyethyl PZ	HEP	31.18	129.1	16	
N-(2-Hydroxyethyl)-N'-Methyl PZ	HEMP	32.43	145.1, 287.1*	6	
N-Methyl PZ	1-MPZ	31.41	101.1, 119.1	16	
Triethylenediamine	TEDA	32.14	113.1, 225.2*	15	

* Secondary m/z found in peak is doublet of analyte

+ Primary analyte is not in main peak. Details of main peak are still given.

^ PZ contamination is present at PZ RT of ~30.5 to 31 min

G.2 CONFIRMATION OF PZ CARBAMATE WITH IC-MS

The presence of piperazine carbamate in aqueous, loaded PZ solutions was confirmed using MS with direct injection. This confirmation was made in both positive

and negative ion mode. In positive ion mode, the PZ carbamate exists as its protonated acid form. In negative ion mode, PZ carbamate usually exists as drawn ($PZCOO^-$). Both structures are shown in Figure G.17.

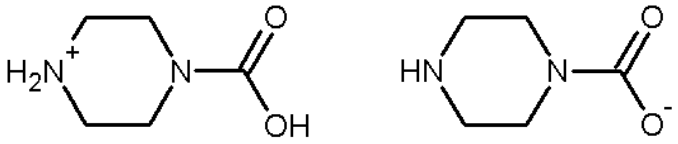

(A) Positive Ion Mode (B) Negative Ion Mode

Figure G.17: Structure of PZ carbamate as seen in (A) positive and (B) negative ion modes of the MS

To confirm this species was present, an 8 m PZ solution with a loading of 0.3 mole CO_2 per mole alkalinity was tested on the MS using direct infusion (i.e., not utilizing any chromatographic separation). In positive mode, the species of interest (Figure G.17, panel A) has a mass-to-charge (m/z) ratio of 131.15. In order to verify the molecule, a total scan of m/z of 30 to 150 was done to see the prevalence of 131.2. The peak at 87.1 for PZ was dominant, so collision-induced disassociation (CID) was performed to isolate the molecule of interest. In CID, a filter is applied between the first and second quadrapoles of the instrument that only allows the particular m/z of interest (known as the parent molecule) to reach the second quadrapole. All other masses are deflected to the waste stream. A voltage (0 to 50 eV) is applied to the second quadrapole to induce disassociation of the parent molecule. The fragments then travel to the third quadrapole and are detected.

The CID for m/z 131.2 is shown in Figure G.18 for positive mode of the MS. The parent fragment of 131.2 is clearly visible as well as fragments at 114.3 and 85.3. The

fragment at 114.3 is a loss of 16.9 (~17) which is likely a loss of NH_3 during fragmentation. The fragment at 85.3 is a loss of 45.9 (~46) or a loss of HCOOH.

In negative mode, the same procedure of direct infusion was followed and the m/z of interest was 129.1. The CID for m/z 129.1 is shown in Figure G.19 for negative mode of the MS. The parent fragment of 129.1 is clearly visible as well as primary fragment at 84.8 and a small fragment at 45.2. The fragment at 84.8 is a loss of 44.3 or COO^-.

The fact that 131.2 and 129.1 m/z could be isolated and fragmented in positive and negative mode, respectively, indicates the presence of PZ carbamate in solution. Also, in both modes a dominant fragment was the loss of a carbamate piece of the structure (either -44 or -46). Both allude to the presence of PZ carbamate.

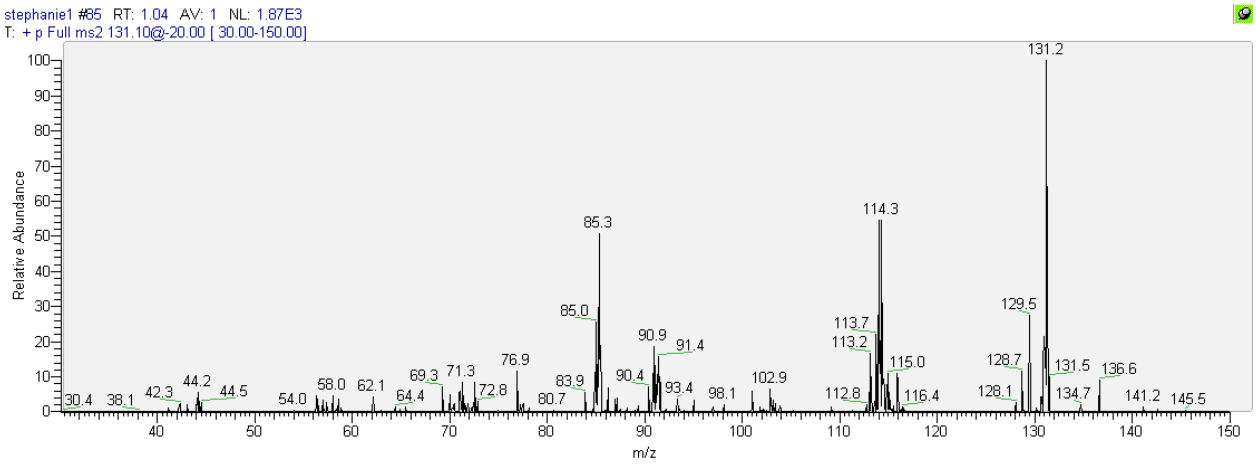

Figure G.18: Total Ion Current (TIC) graph for CID of 131.1 in positive mode

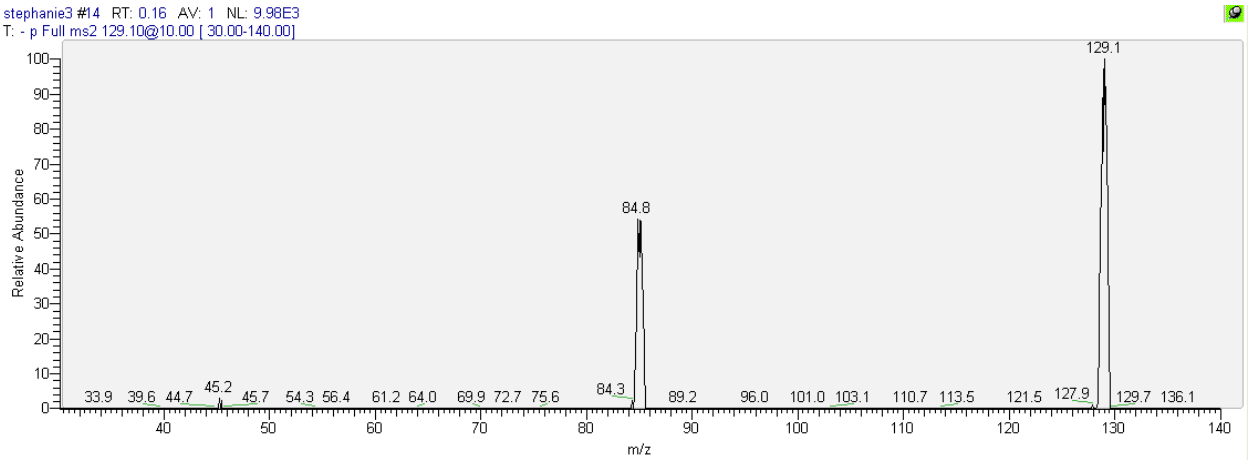

Figure G.19: Total Ion Current (TIC) graph for CID of 129.1 in negative mode

A common m/z ratio that co-elutes with PZ at a retention time of 30.5 minutes was also identified. The m/z of 105.1 is always found with the large PZ peak on the cation IC-MS and has the second highest response in terms of ion current, after PZ. This m/z has been identified as the hydrated form of protonated PZ, or $PZH^+ \cdot H_2O$. During electrospray ionization (ESI), both a PZ and a water molecule are co-coordinated with one proton. The mass of this molecule is 105.1 with one charge, giving a m/z of 105.1. A representation of this molecule is shown below in Figure G.20.

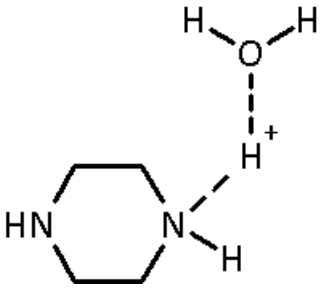

Figure G.20: Representation of $PZH^+ \cdot H_2O$ as it would appear after ESI

G.3 IC-MS ANALYSIS OF THERMALLY DEGRADED PZ (TE12, T=15 WEEKS)

A detailed cation IC-MS analysis was performed for the final sample of TE12. In TE12, 8 m PZ with 0.3 mole CO_2 per mole alkalinity was degraded for 15 weeks. This sample was chosen to represent the most heavily degraded sample and, therefore, most likely to contain all of the important species of interest. This solution was analyzed with cation IC-MS and the resulting data was analyzed for the possible identity of the unknown peaks.

The raw data for the final sample of TE12 (t=15 weeks) is shown in Figure G.21. The top portion of the figure is the Total Ion Current from the MS while the IC chromatograph is shown in the bottom half of the figure. The two signals are adjusted so the timing of the horizontal axis matches. This sample is heavily degraded and there are numerous peaks in both panels. Peaks in the TIC signal sometimes appear with negative deflection if the sample hitting the sensor is relatively small. When higher concentrations of ions hit the sensor, the negative deflection revers to create a positive deflection, as with the PZ peak at 30.86 minutes.

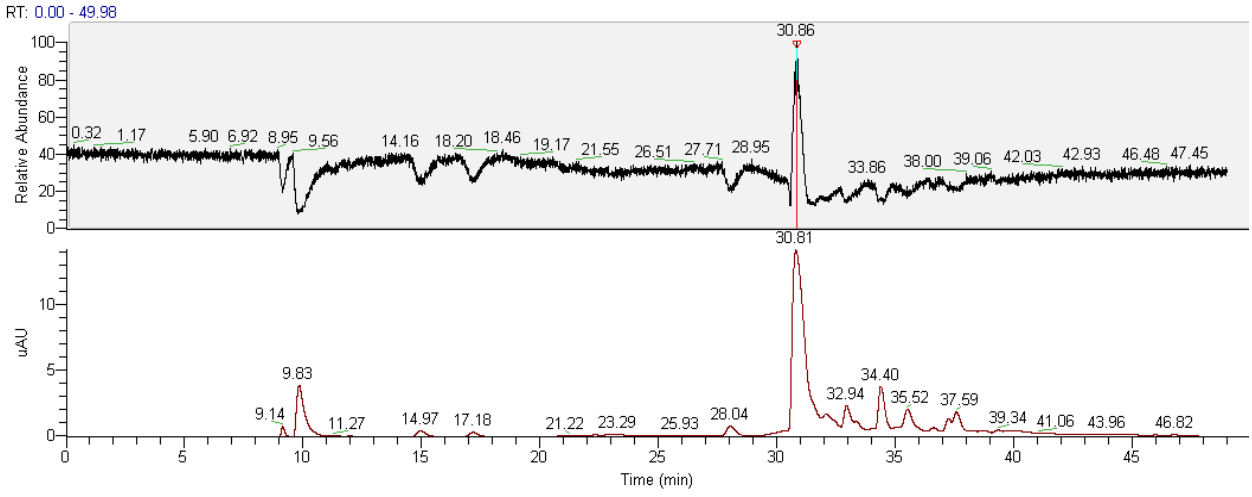

Figure G.21: Total Ion Current for m/z 50.0-300.0 and Cation IC Chromatograph for TE12 t=15 weeks

In the Xcalibur software where data analysis occurs, the TIC signal can be analyzed in two ways. First, the signal can be scanned over time to determine the most abundant m/z values for any given position in the chromatogram. Second, a particular mass range of ions can be isolated to see where a particular ion elutes in relation to the IC chromatogram. This is a powerful way to relate a particular ion of interest to a peak on the IC chromatogram. To demonstrate this technique, Figure G.22 through G.24 show three different isolated m/z or mass ranges.

In G.22, the mass range for PZ (87.1 ± 0.5 m/z) is isolated. The peak corresponding to where PZ elutes is clearly distinguished in both the Total Ion Current and the cation IC. The peak assigned to PZ at a retention time of 30.8 minutes is confirmed to have the expected m/z of 87.1 (MW+1).

For smaller, unknown IC peaks, the next two figures demonstrate the utility of this type of data analysis. In Figure G.23, the mass range of 115.1 ± 0.5 m/z is isolated and three distinct peaks are shown that correspond to smaller peaks on the IC chromatograph. Multiple possible species are suspected with this molecular weight (114 g/mol) including N-formylpiperazine (FPZ), N-ethylpiperazine (1-EPZ), N,N'-dimethylpiperazine (1,4-DMPZ), 2,5-piperazindione, and 2,5-dimethylpiperazine. By matching to the standard curves presented in section G.1, it is clear from Figure G.10 and G.11 that the first and third peaks correspond to FPZ and 1-EPZ, respectively. The retention times are slightly off because of the differences in analysis unrelated to the chromatogram.

In Figure G.24, the mass range of 130.2 ± 0.5 m/z is isolated and it is clear that two peaks on the IC chromatogram have been identified as molecules with a molecular weight of 129.2 g/mol. By matching to Figure G.5, the peak at a retention time of 34.4

minutes corresponds to AEP. The identity of the peak at 17.2 minutes is not know at this time but one strong candidate is 1-(2-aminoethyl)-2-imidazolidone (CAS 6281-42-1).

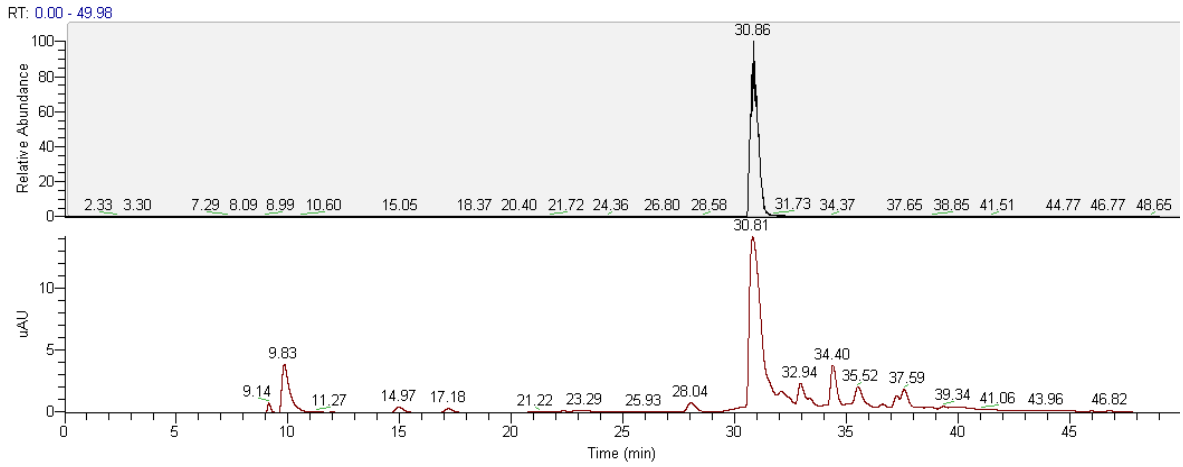

Figure G.22: Total Ion Current for m/z 86.6–87.6 and cation IC chromatograph for TE12 t=15 weeks

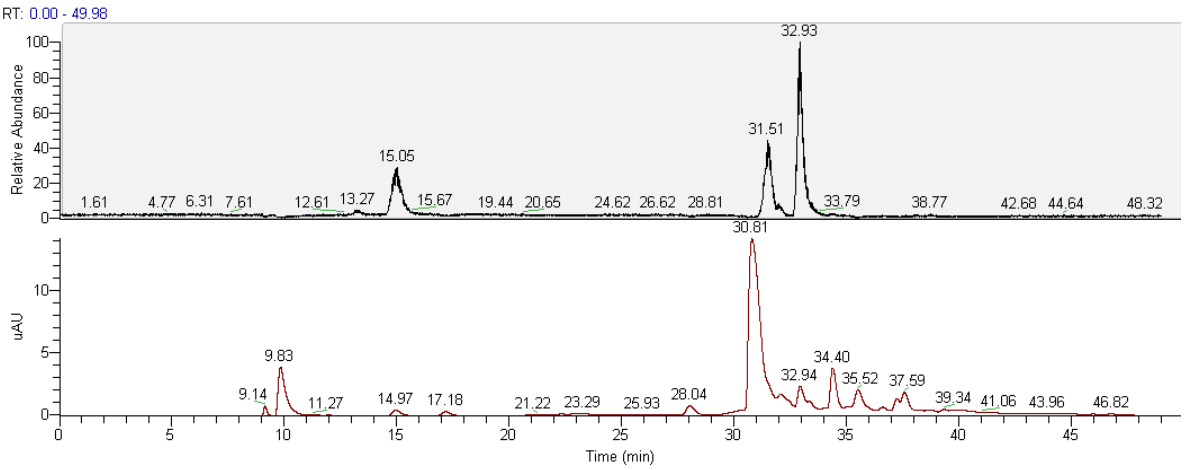

Figure G.23: Total Ion Current for m/z 114.7–115.7 and cation IC chromatograph for TE12 t=15 weeks

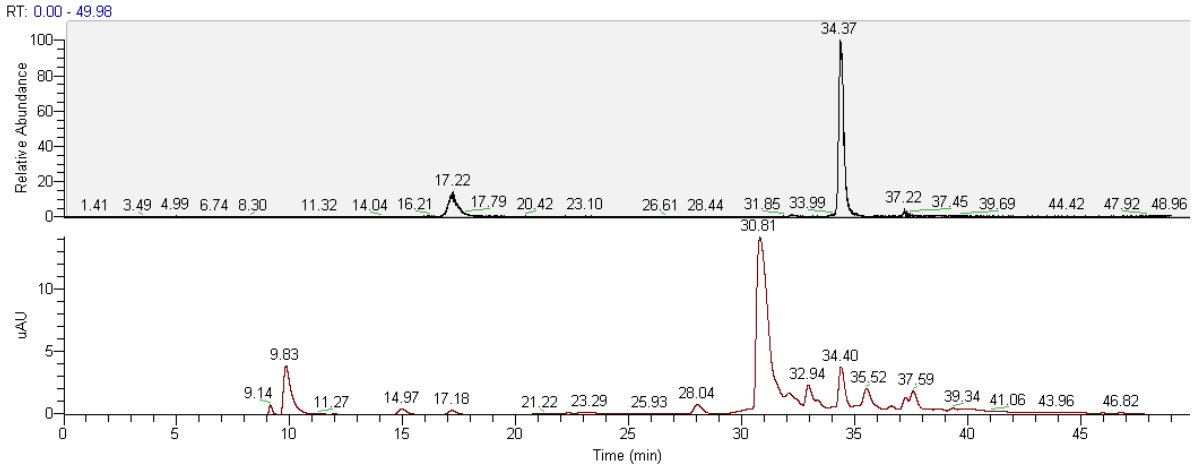

Figure G.24: Total Ion Current for m/z 129.7–130.7 and Cation IC Chromatograph for TE12 t=15 weeks

The utility of isolating a specific m/z ratio makes a complicated spectrum more accessible. For degraded PZ solutions, the diamine and triamine section of the cation IC chromatograph will always be complicated as degradation increases. First pass analysis of the raw data determines which m/z values are of interest to isolate. Isolation helps with identification and quantification that would otherwise not be possible in such a crowded part of the IC chromatogram.

This final sample of TE12 is further analyzed below by isolating all of the dominant m/z ratios found any point in the total ion current raw data. The total ion current was isolated for those m/z ratios ± 0.5 m/z to determine the time at which species eluted off the IC column. The isolated total ion current graphs for all of the m/z ratios of interest are compared to the total ion current for 50–300 m/z in Table G.3. This allows the reader to see which molecular weights are co-eluting and which molecular weights are responsible for each of the dominant peaks. The total ion current for 50–300 m/z with the corresponding IC chromatograph is repeated at the top of each page of Table G.3.

A summary of the important m/z ratios is given in Table G.4 along with potential molecules that correspond to the indicated molecular weight.

Table G.3: Isolated m/z ± 0.5 for degradation products of TE12 on Cation IC-MS

Total Ion Current Graph	m/z
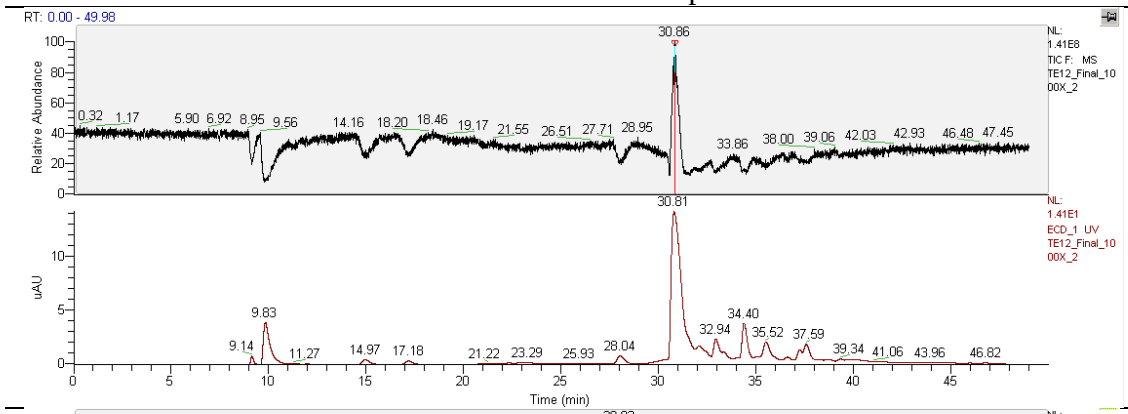	Total Scan with IC
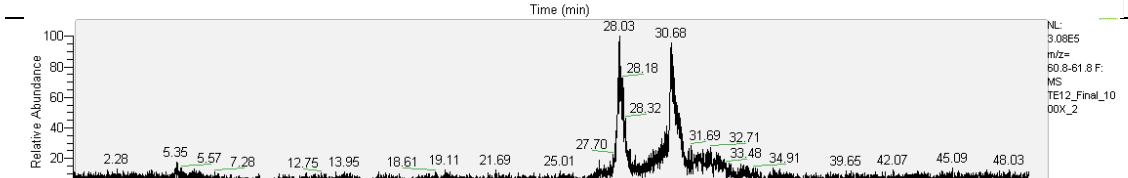	61.2
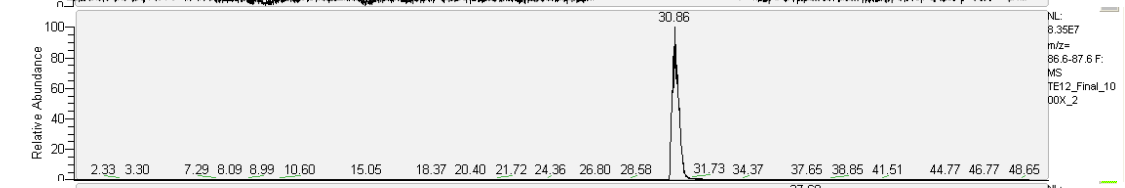	87.1
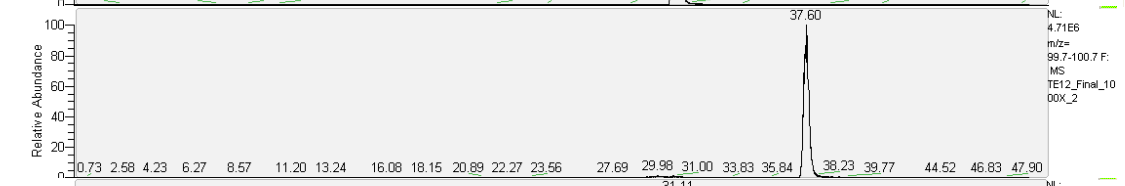	100.2
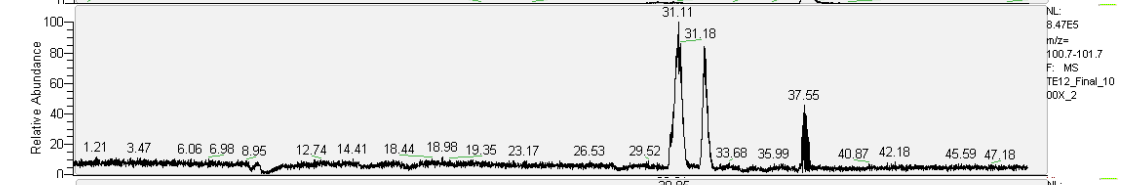	101.2
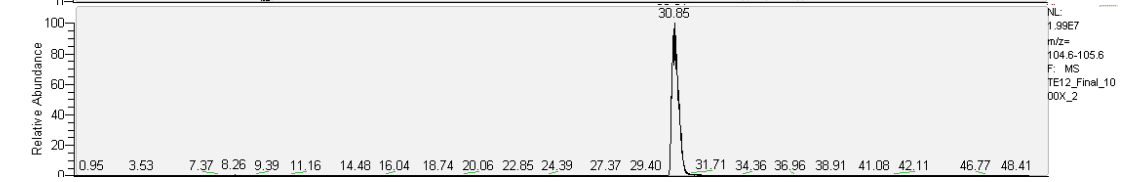	105.1

Total Ion Current Graph	m/z
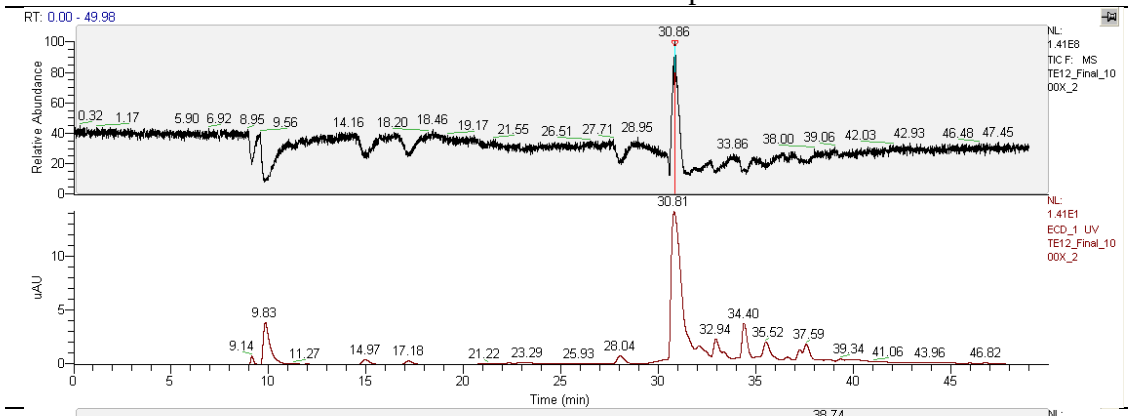	Total Scan with IC
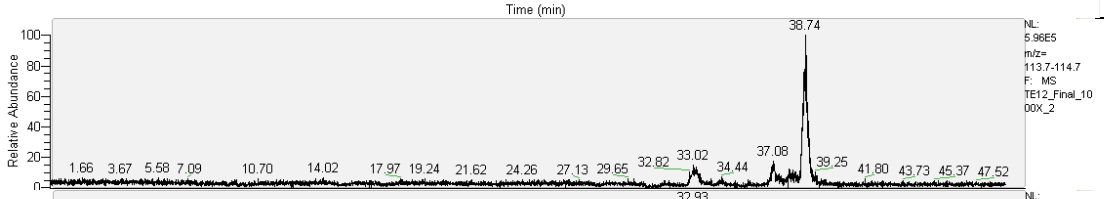	114.2
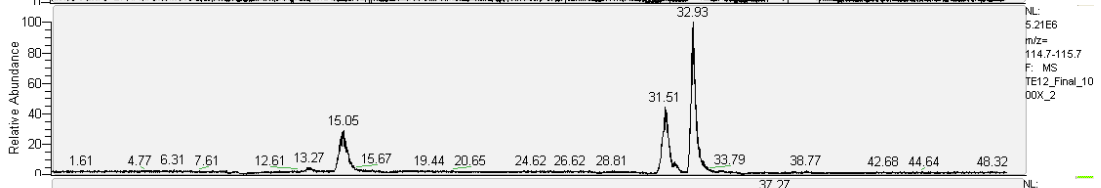	115.2
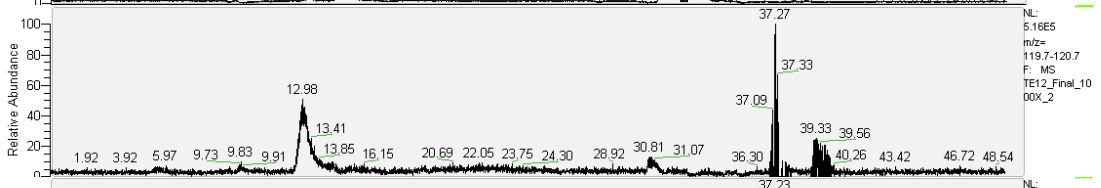	120.2
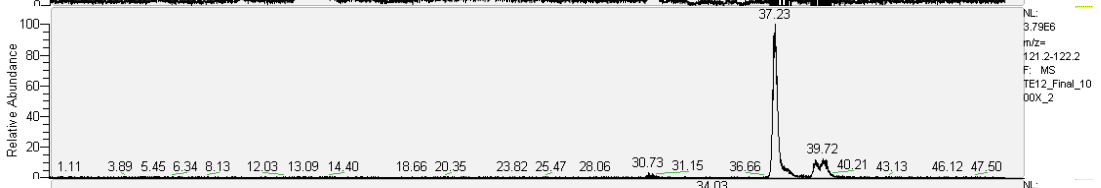	121.7
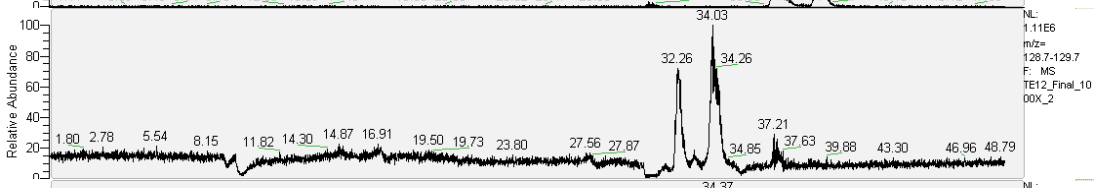	129.2
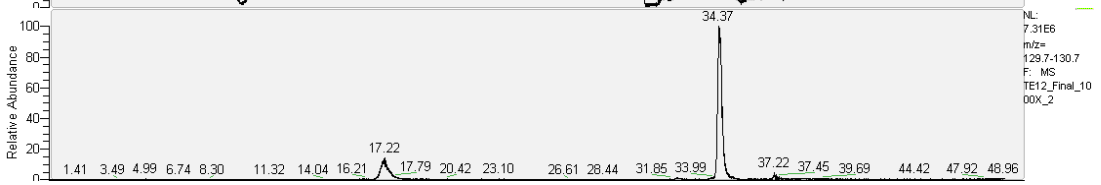	130.2

Total Ion Current Graph	m/z
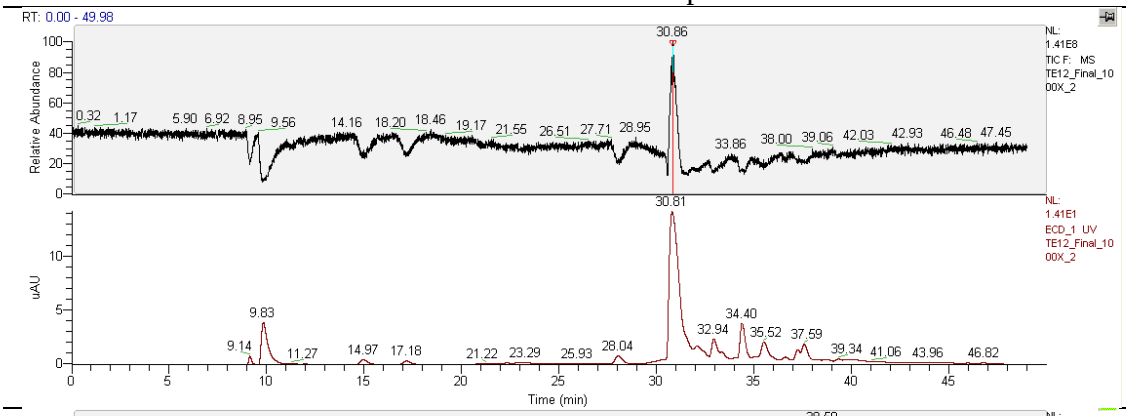	Total Scan with IC
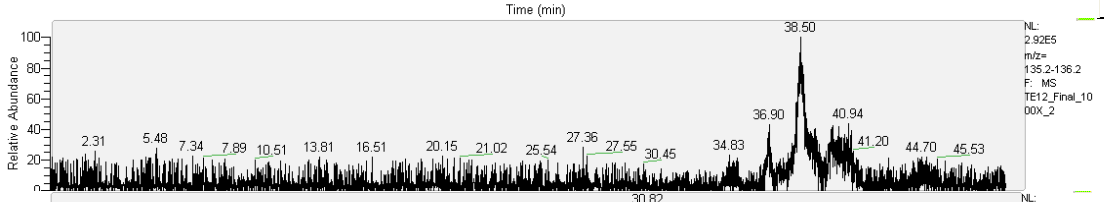	135.7
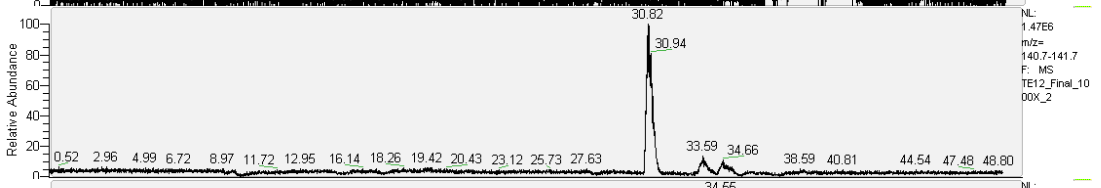	141.2
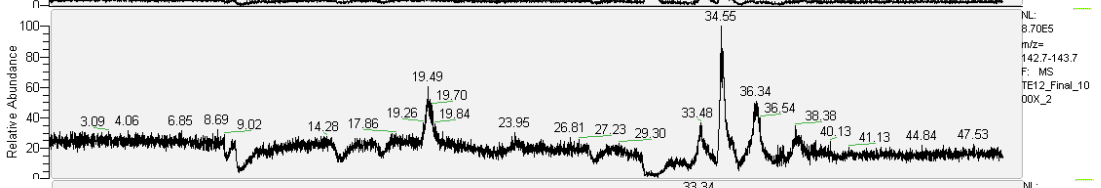	143.2
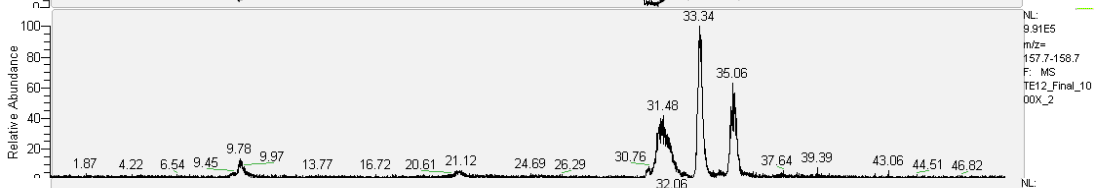	158.2
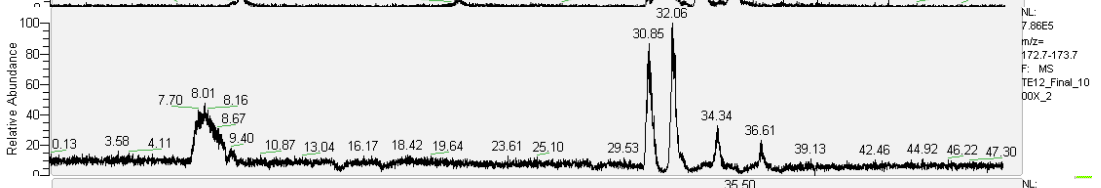	173.2
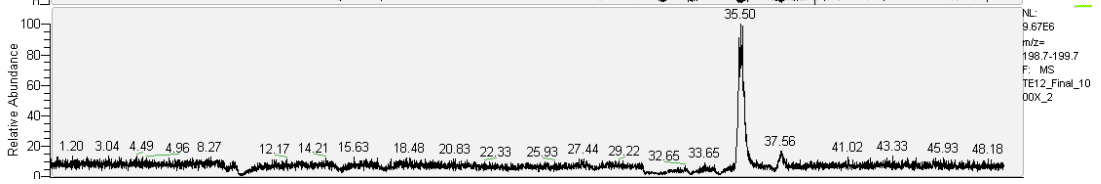	199.2

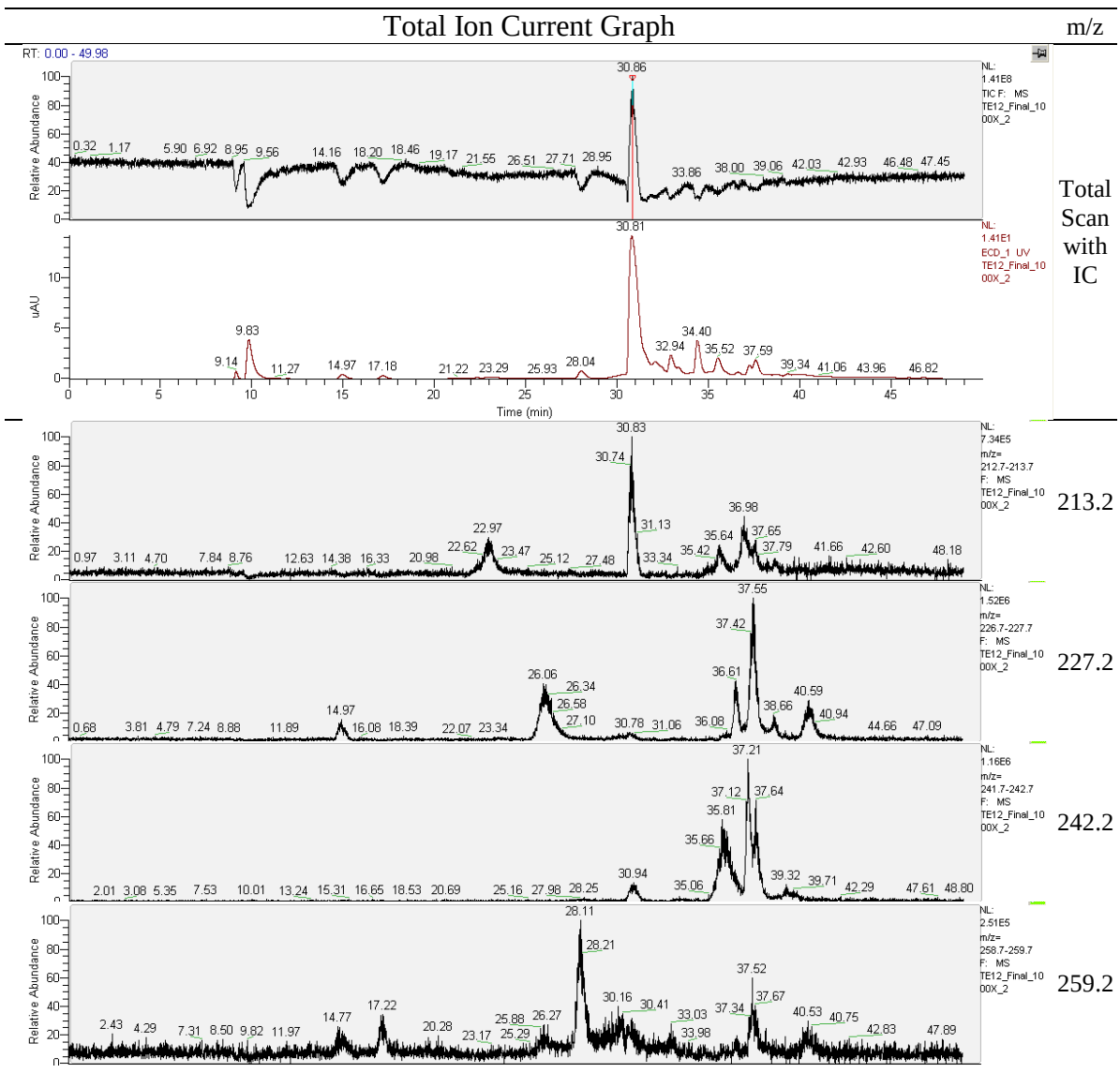

The complexity of heavily degraded PZ samples is demonstrated by the sheer volume of information shown in Tables G.3 and G.4. For each sample run on IC-MS, there is a wealth of information that is complicated to reduce to usable information. All peaks that could be identified so far are indicated. A few have suspected matches where a standard was not commercially available (e.g. AEAEPZ and the urea of AEAEPZ)

Table G.4: Possible identification of the major peaks from isolated m/z ratios in TE12

m/z	MW	Possible Species (**Confirmed**) (RT of Standard)	Major Peaks (**Dominant**)
61.3	60.2	**EDA** (27.80 mins)	**28.0**, **30.7**
87.1	86.1	**PZ** (30.9 mins)	**30.9**
100.2	99.2		**37.6**
101.2	100.2	N-methyl PZ (31.41 mins) 2-methyl PZ 2-piperazinone	**31.1**, **32.2**, 37.55
105.1	104.1	**PZ·H_2O**	**30.9**
114.2	113.1		**38.8**
115.2	114.2	2,5-piperazinedione **N-Formyl PZ** (15.5 mins) 1,4-Dimethyl PZ (32.79 mins) 2,5-Dimethyl PZ **N-Ethyl PZ** (32.08 mins)	**15.0**, **31.5**, **32.9**
120.2	119.2	MDEA N1-(2-aminoethyl)-N1-hydroxy-1,2-Ethanediamine	**13.0**, 37.3
121.7	120.7	N,N'-bis(Hydroxymethyl) urea N,N'-di(hydroxymethyl) EDA	**37.2**, 39.7
129.2	128.2	N-Acetyl PZ (ruled out due to NaOH treatment)	**32.3**, **34.0**
130.2	129.2	$PZCOO^-$ 1-(2-Aminoethyl)-2-imidazolidone (17.10 min) 1,4,7-Triazacyclononane N-(2-aminoethyl) PZ (33.56 mins)	**17.2**, **34.4**
135.7	134.7		38.5
141.2	140.2		**30.8**, 33.6, 34.7
143.2	142.2	N,N'-Diformyl PZ **N'N-Diethyl PZ** (34.4) (v. small concentration)	19.5, 34.6
158.2	157.2		**31.5**, **33.3**, **35.0**
173.2	172.2	$PZ(COO^-)_2$ 1-[2-[(2-aminoethyl)amino]ethyl] PZ (AEAEPZ) (suspected at 36.6 mins) N,N'-bis(2-aminoethyl) PZ (DAEP)	8.0, **30.9**, **32.0**, 34.3, 36.6
199.2	198.2	1,1'-carbonylbis-PZ (diPZ urea) Urea of AEAEPZ (suspected at 35.5 mins) 1,1'-(1,2-ethanediyl)bis-PZ (PEP) (suspected at 37.6 mins)	**35.5**, 37.6
213.2	212.2		23.0, **30.8**, 37.0
227.2	226.2	1,1'-(1,2-dioxo-1,2-ethanediyl)bis PZ 1-ethyl-4-[2-(1-piperazinyl)ethyl] piperazine	15.0, **26.0**, 36.6, **37.6**, 40.6
242.2	241.2		30.9, 35.8, 37.2
259.2	258.2		14.7, 17.2, 28.1, 37.5

G.4 MS ANALYSIS OF OXIDATION SAMPLES

The final samples of some oxidation experiments were analyzed by cation IC-MS and the results are shown here to demonstrate the range of IC-MS data obtained. The samples shown range from barely degraded (e.g. OE3, OE5) to fairly heavily degraded (e.g.OE2). The cation IC-MS chromatograms for OE1 through OE10 are shown below in Figure G.25 to Figure G.35. The chromatographs are displayed in the same way as the PZ derivatives panels above (Figure G.1 to Figure G.16) in that the top panel is the total MS signal while the bottom panel is the cation IC chromatogram total conductivity signal. The panels are aligned so that they correspond in time. In each of these chromatographs, peaks that are known to correspond to a particular species are indicated. They all contain PZ, the primary peak at ~30.5 minutes. Other peaks positively identified are EDA and N-Formyl PZ. Contamination from MEA, and MDEA during cation IC analysis was suspected in a few samples. Other peaks with well-established m/z values are shown and tentative identifications of peaks are shown with a question mark. Further analysis of oxidation samples were not performed due to the lack of unidentified peaks of a significant size.

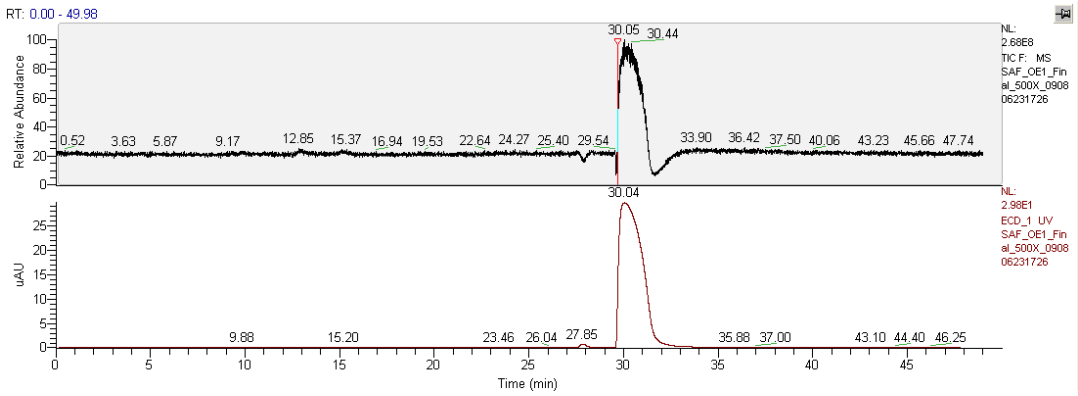

Figure G.25: Cation IC-MS chromatogram for the Final Sample of OE1 (10 m PZ, 55 °C, 2% CO_2, 0.26 mM Fe^{2+}, 0.65 mM Cr^{3+}, 0.26 mM Ni^{2+})

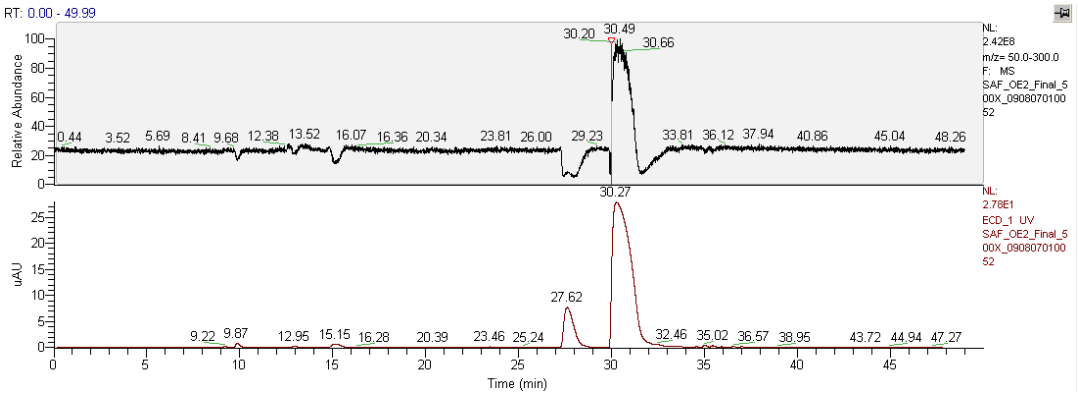

Figure G.26: Cation IC-MS Chromatogram for the Final Sample of OE2 (10 m PZ, 55 °C, 2% CO_2, 4.0 mM Cu^{2+})

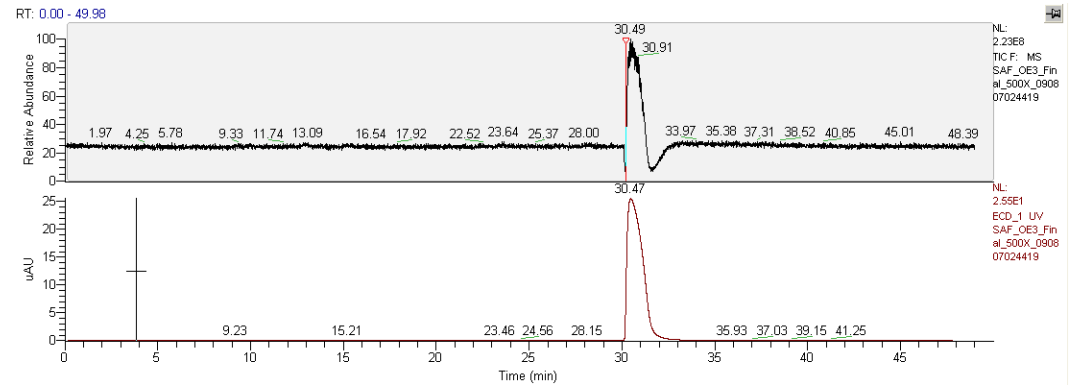

Figure G.27: Cation IC-MS Chromatogram for the Final Sample of OE3 (8 m PZ, 55 °C, 2% CO_2, 0.1 mM Fe^{2+}, 0.1 mM V^{5+})

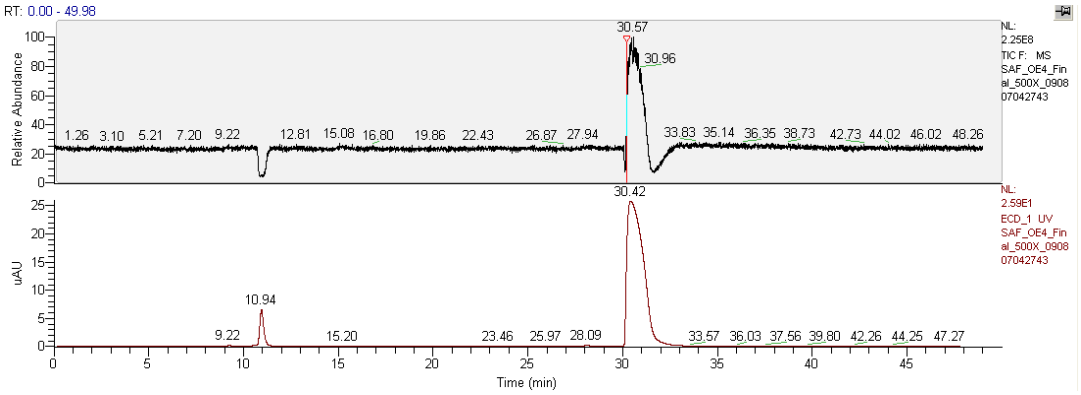

Figure G.28: Cation IC-MS Chromatogram for the Final Sample of OE4 (8 m PZ, 55 °C, 2% CO_2, 5.0 mM Cu^{2+}, 0.1 mM Fe^{2+}, 100 mM Inhibitor A)

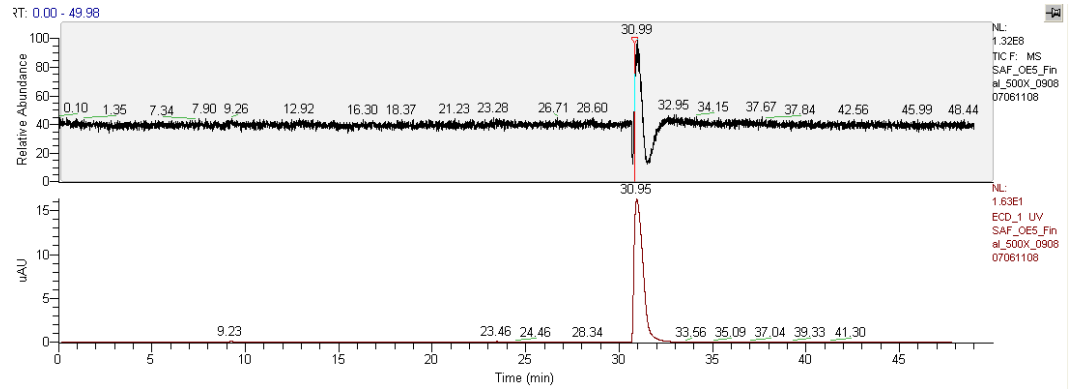

Figure G.29: Cation IC-MS Chromatogram for the Final Sample of OE5B (8 m PZ, 55 °C, 2% CO_2, 1.0 mM Fe^{2+})

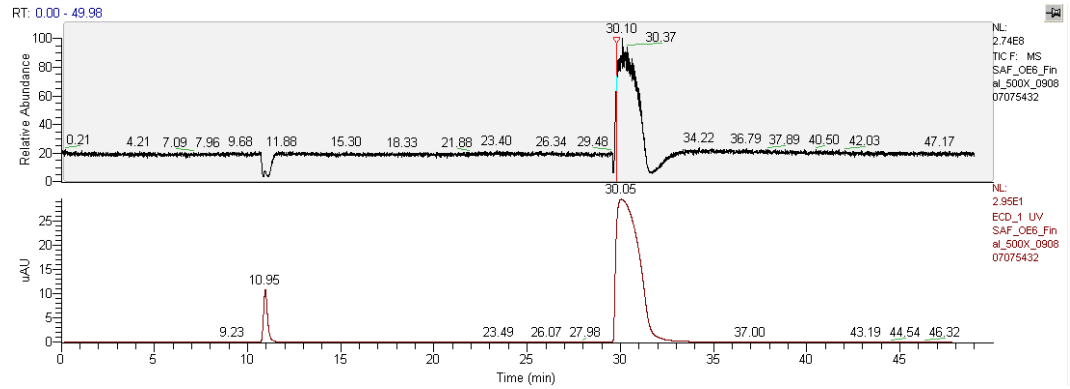

Figure G.30: Cation IC-MS Chromatogram for the Final Sample of OE6B (8 m PZ, 55 °C, 2% CO_2, 1.0 mM Fe^{2+}, 100 mM Inhibitor A)

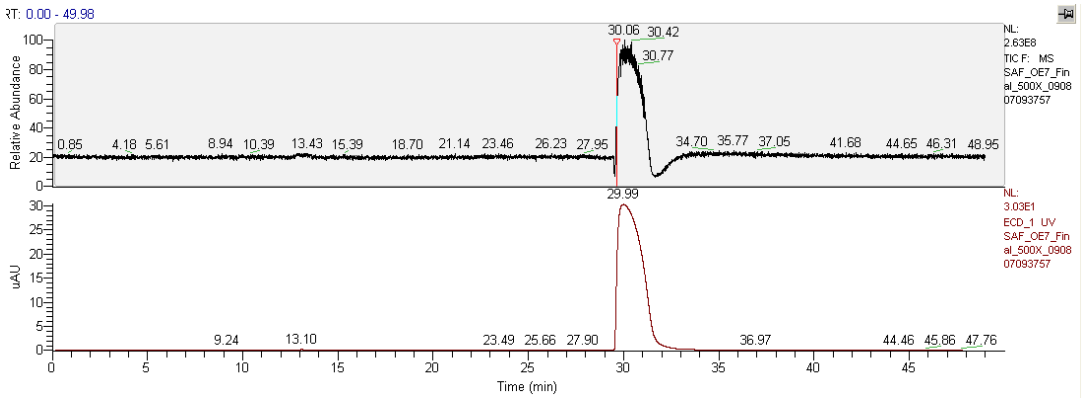

Figure G.31: Cation IC-MS Chromatogram for the Final Sample of OE7 (8 m PZ, 55 °C, 2% CO_2, 1.0 mM Fe^{2+}, 20 mM Inhibitor B)

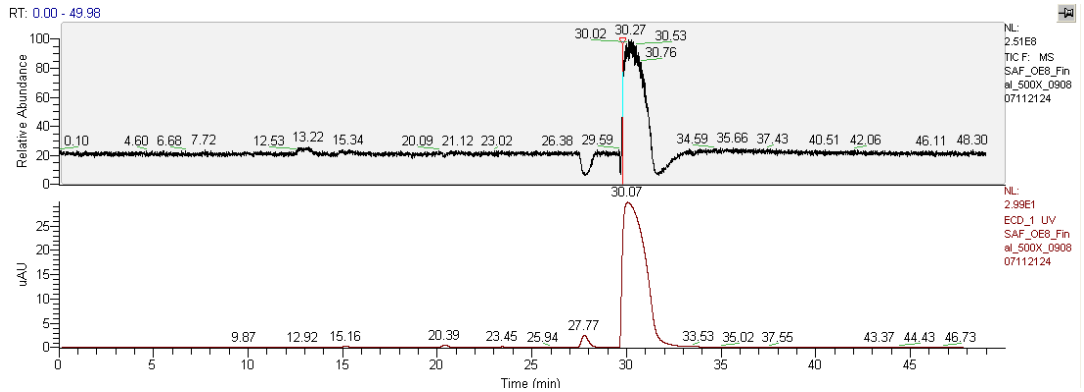

Figure G.32: Cation IC-MS Chromatogram for the Final Sample of OE8 (8 m PZ, 55 °C, 2% CO_2, 1.0 mM Fe^{2+}, 30 mM EDTA)

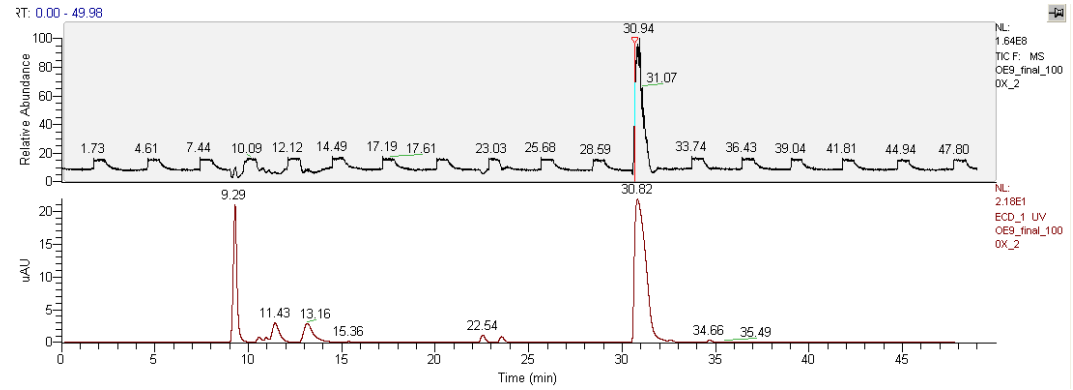

Figure G.33: Cation IC-MS Chromatogram for the Final Sample of OE9 (8 m PZ, 55 °C, 2% CO_2 in N_2)

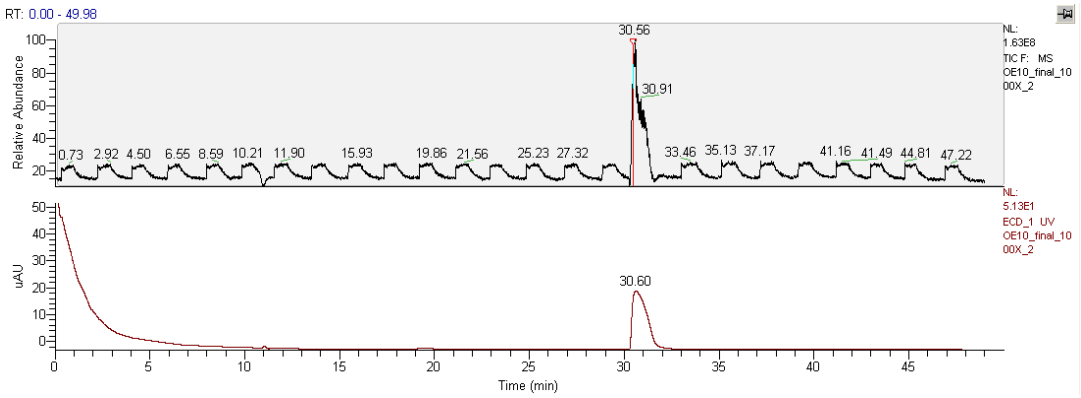

Figure G.34: Cation IC-MS Chromatogram for the Final Sample of OE10 (8 m PZ, 55 °C, 2% CO_2 in N_2)

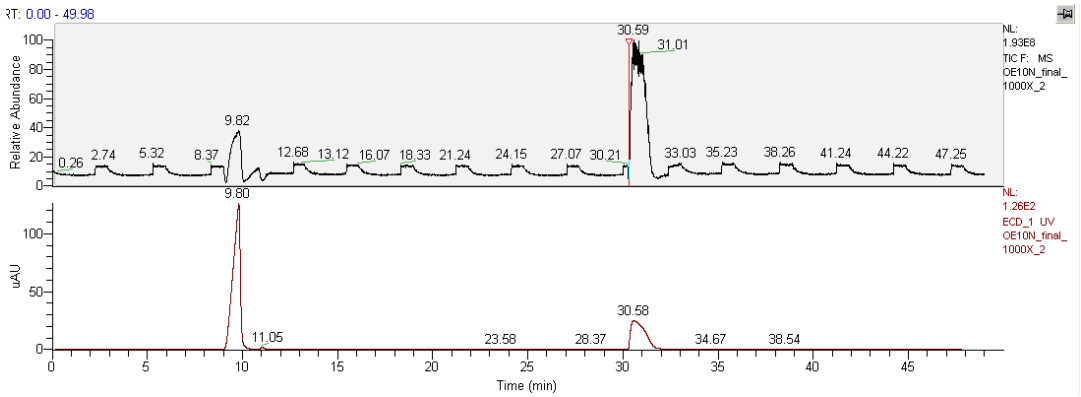

Figure G.35: Cation IC-MS Chromatogram for the Final Sample of OE10 Treated with 5N NaOH (8 m PZ, 55 °C, 2% CO_2 in N_2)

References

Aaron D, Tsouris C (2005). "Separation of CO_2 from Flue Gas: A Review." *Separation Science and Technology*. **40**: 321-348.

AIST (2010). Spectral Database for Organic Compounds (SDBS). National Institute of Advanced Industrial Science and Technology (AIST). Accessed October 5th, 2010.

Al-Juaied M, Rochelle GT (2006a). "Absorption of CO_2 in aqueous blends of diglycolamine® and morpholine." *Chemical Engineering Science*. **61** (12): 3830-3837.

Al-Juaied M, Rochelle GT (2006b). "Absorption of CO_2 in aqueous diglycolamine." *Industrial & Engineering Chemistry Research*. **45** (8): 2473-2482.

Al-Juaied M, Rochelle GT (2006c). "Thermodynamics and equilibrium solubility of carbon dioxide in diglycolamine/morpholine/water." *Journal of Chemical and Engineering Data*. **51** (2): 708-717.

Al-Juaied MA. *Carbon Dioxide Removal from Natural Gas by Membranes in the Presence of Heavy Hydrocarbons and by Aqueous Diglycolamine®/Morpholine*. The University of Texas at Austin. Ph.D. Dissertation. 2004:

Alawode AO. *Oxidative Degradation of Piperazine in the Absorption of Carbon Dioxide*. The University of Texas at Austin. MS Thesis. 2005: 82.

Albert A, Serjeant EP(1971). The determination of ionization constants: A laboratory manual. Edinburg, Chapman and Hall.

Appl M, Wagner U, Henrici HJ, Kuessner K, Volkamer K, Fuerst E (1982). "Removal of CO_2 and/or H_2S and/or COS from Gases Containing These Constituents." BASF GmbH, Germany. US Patent 4,336,233.

Arcis H, Rodier L, Coxam JY (2007). "Enthalpy of solution of CO_2 in aqueous solutions of 2-amino-2-methyl-1-propanol." *Journal of Chemical Thermodynamics*. **39** (6): 878-887.

Arnold DS, Barrett DA, Isom RH (1982). "CO_2 production from coal-fired boiler flue gas by MEA process". Presented at Gas Conditioning Conference, Oklahoma City, OK.

ASTM (2000). "ASTM D 892: Standard Test Method for Foaming Characteristics of Lubricating Oils." ASTM International: West Conshohocken, Pa.

Bedell SA, Worley CM, Darst K, Simmons K (2010). "Thermal and oxidative disproportionation in amine degradation - O_2 stoichiometry and mechanistic implications." *International Journal of Greenhouse Gas Control*. **In print**.

Bishnoi S. *Carbon Dioxide Absorption and Solution Equilibrium in Piperazine Activated Methyldiethanolamine*. The University of Texas at Austin. Ph.D. dissertation. 2000: 292.

Bishnoi S, Rochelle GT (2000a). "Absorption of carbon dioxide into aqueous piperazine: reaction kinetics, mass transfer and solubility." *Chemical Engineering Science*. **55** (22): 5531-5543.

Bishnoi S, Rochelle GT (2000b). "Physical and chemical solubility of carbon dioxide in aqueous methyldiethanolamine." *Fluid Phase Equilibria*. **168** (2): 241-258.

Bishnoi S, Rochelle GT (2002a). "Absorption of carbon dioxide in aqueous piperazine/methyldiethanolamine." *AIChE Journal*. **48** (12): 2788-2799.

Bishnoi S, Rochelle GT (2002b). "Thermodynamics of piperazine/methyldiethanolamine/water/carbon dioxide." *Industrial & Engineering Chemistry Research*. **41** (3): 604-612.

Blachly CH, Ravner H (1964). "The stabilization of monoethanolamine solutions for submarine carbon dioxide scrubbers." AD609888, NRL-6189; US Naval Research Laboratory: Washington D.C. U. S. Naval Research Laboratory: Washington D.C.

Blachly CH, Ravner H (1965). "Studies of Submarine Carbon Dioxide Scrubber Operation: Effect of an Additive Package for the Stabilization of Monoethanolamine Solutions." NRL Memorandum Report 1598. Naval Research Laboratory: Washington D.C.

Blachly CH, Ravner H (1966). "Stabilization of Monoethanolamine Solutions in Carbon Dioxide Scrubbers." *Journal of Chemical and Engineering Data*. **11** (3): 401-403.

Bøgesø KP, Arnt J, Boeck V, Christensen AV, Hyttel J, Jensen KG (1988). "Antihypertensive activity in a series of 1-piperazino-3-phenylidans with potent 5-HT2-antaganistic activity." *Journal of Medical Chemistry*. **31**: 2247-2256.

Bottoms RR (1930). "Separating acid gases." Girdler Corporation, Louisville, KY. US Patent 1,783,901.

Bradsher K, Barboza D (2006). Pollution from Chinese coal casts a global shadow. The New York Times. New York City, NY.

Brown BR(1994). The Organic Chemistry of Aliphatic Nitrogen Compounds. Oxford, Clarendon Press.

Brown HW, Chan KF (1955). "Treatment of *Enterobius Vermicularis* Infections with Piperazine." *American Journal of Tropical Medical Hygiene*. **4** (2): 321-325.

Brown HW, Sterman MM (1954). "Treatment of *Ascaris Lumbricoides* Infections with Piperazine Citrate." *American Journal of Tropical Medical Hygiene*. **3** (4): 750-754.

Burhenne J, Ludwig M, Nikoloudis P, Spiteller M (1997). "Photolytic degradation of fluoroquinolone carboxylic acids in aqueous solution .1. Primary photoproducts and half-lives." *Environmental Science and Pollution Research*. **4** (1): 10-15.

Carson JK, Marsh KN, Mather AE (2000). "Enthalpy of solution of carbon dioxide in (water plus monoethanolamine, or diethanolamine, or N-methyldiethanolamine) and (water plus monoethanolamine plus N-methyldiethanolamine) at T=298.15 K." *Journal of Chemical Thermodynamics*, **32** (9):1285-1296.

Chakma A, Meisen A (1997). "Methyl-diethanolamine degradation - Mechanism and kinetics." *Canadian Journal of Chemical Engineering*. **75** (5): 861-871.

Challis, BC, Challis JA (1982). N-nitrosamines and N-nitrosoimines. The chemistry of amino, nitroso and nitro compounds and their derivatives, Supplement F, Part 2. Ed. S. Patai. New York, John Wiley and Sons**:** 1151-1223.

ChemiSens A. "ChemiSens CPA 122 System Manual." ChemiSens AB: Lund, Sweden.

Chen E. *Carbon Dioxide Absorption into Promoted Potassium Carbonate in Structured Packing*. The University of Texas at Austin. Ph.D. Dissertation. 2007: 505.

Chen X, Freeman SA, Rochelle GT (2011). "Foaming of aqueous piperazine and monoethanolamine for CO_2 Capture." *International Journal of Greenhouse Gas Control*. **5** (2): 381-386.

Chi SQ. *Oxidative Degradation of Monoethanolamine*. The University of Texas at Austin. Ph.D. Dissertation. 2002:

Closmann F (2011). Thermal degradation data for 7 m MDEA and 7/2 MDEA/PZ and cycling data for 8 m PZ. Personal communication to S. A. Freeman.

Closmann F, Nguyen T, Rochelle GT (2009). "MDEA/Piperazine as a solvent for CO_2 capture." *Energy Procedia*. **1** (1): 1351-1357.

Closmann F, Rochelle GT (2011). "Degradation of aqueous methyldiethanolamine by temperature and oxygen cycling." *Energy Procedia*. **4**: 23-28.

Cook HL, Lowe BM (1976). "Viscosity B-Coefficients for Pinacol and Piperazine in Aqueous-Solution at 25 and 35°C." *Electrochimica Acta*. **21** (2): 153-154.

Critchfield JE. *CO_2 absorption/desorption in methyldiethanolamine solutions promoted with monoethanolamine and diethanolamine: mass transfer and reaction kinetics* The University of Texas at Austin. Ph.D. Dissertation. 1988: 155.

Crossley LJ (1991). "Thermal degradation of aqueous oxalate species." *Geochimica et Cosmochimica acta*. **55**: 1515-1527.

Cullinane JT, Rochelle GT (2004). "Carbon dioxide absorption with aqueous potassium carbonate promoted by piperazine." *Chemical Engineering Science*. **59** (17): 3619-3630.

Cullinane JT, Rochelle GT (2005). "Thermodynamics of aqueous potassium carbonate, piperazine, and carbon dioxide." *Fluid Phase Equilibria*. **227** (2): 197-213.

Cullinane JT, Rochelle GT (2006). "Kinetics of carbon dioxide absorption into aqueous potassium carbonate and piperazine." *Industrial & Engineering Chemistry Research*. **45** (8): 2531-2545.

Davis GT, Rosenblatt DH, Demek MM (1972). "Oxidations of Amines .X. Detailed Kinetics in Reaction of Chlorine Dioxide with Triethylenediamine." *Journal of the American Chemical Society*. **94** (10): 3321-&.

Davis J (2008). "Thermal degradation of monoethanolamine at stripper conditions". Presention at GHGT-9, Washington D.C.

Davis J. *Thermal Degradation of Aqueous Amines Used for Carbon Dioxide Capture*. The University of Texas at Austin. Ph.D. Dissertation. 2009: 278.

Davis J, Rochelle GT (2009). "Thermal degradation of monoethanolamine at stripper conditions." *Energy Procedia*. **1** (1): 327-333.

Dawodu OF, Meisen A (1996). "Degradation of alkanolamine blends by carbon dioxide." *Canadian Journal of Chemical Engineering*. **74** (6): 960-966.

Dennis WH, Hull LA, Rosenblatt DH (1967). "Oxidations of Amines. IV. Oxidative Fragmentation." *Journal of Organic Chemistry*. **32** (12): 3783-&.

Derks PW, Hogendoorn KJ, Versteeg GF (2005). "Solubility of N_2O in and density, viscosity, and surface tension of aqueous piperazine solutions." *Journal of Chemical and Engineering Data*. **50** (6): 1947-1950.

Derks PWJ, Hamborg ES, Hogendoorn JA, Niederer JPM, Versteeg GF (2008). "Densities, viscosities, and liquid diffusivities in aqueous piperazine and aqueous (piperazine plus N-methyldiethanolamine) solutions." *Journal of Chemical and Engineering Data*. **53** (5): 1179-1185.

Dewitte B, Dewulf J, Demeestere K, De Vyvere VV, De Wispelaere P, Van Langenhove H (2008). "Ozonation of ciprofloxacin in water: HRMS identification of reaction products and pathways." *Environmental Science & Technology*. **42** (13): 4889-4895.

Dionex Corporation (2007). "Product Manual: ASRS 300 and CSRS 300." 031956. Dionex Corporation: Sunnyvale, CA.

DIPPR (2010). "DIPPR 801 Database of Physical and Thermodynamic Properties of Pure Chemicals." Brigham Young University.

Dodd MC, Buffle MO, Von Gunten U (2006). "Oxidation of antibacterial molecules by aqueous ozone: Moiety-specific reaction kinetics and application to ozone-based wastewater treatment." *Environmental Science & Technology*. **40** (6): 1969-1977.

Dugas RE (2008). "Absorption and desorption rates of carbon dioxide with monoethanolamine and piperazine". Presented at GHGT-9, Washington D.C.

Dugas R, Rochelle GT (2009). "Absorption and desorption rates of carbon dioxide with monoethanolamine and piperazine." *Energy Procedia*. **1** (1): 1163-1169

Dugas RE. *Carbon Dioxide Absorption, Desorption, and Diffusion in Aqueous Piperazine and Monoethanolamine*. The University of Texas at Austin. Ph.D. Dissertation. 2009: 253.

Duranleau RG, Knifton JF, Speranza GP (1986). "Method for the Preparation of Formamides." Texaco Inc., White Plains, NY. US Patent 4,565,866.

EIA (2007a). "(CO_2) - History from 1949." Retrieved October 1, 2008, from www.eia.doe.gov/oiaf/1605/ggrpt/excel/historical_co2.xls.

EIA (2007b). "Electric power annual - net generation by energy source by type of producer." Retrieved October 1, 2008, from http://www.eia.doe.gov/cneaf/electricity/epa/epat1p1.html

Eide-Haugmo I, Lepaumier H, Einbu A, Vernstad K, da Silva EF, Svendsen HF (2011). "Chemical stability and biodegradability of new solvents for CO_2 capture." *Energy Procedia*. **4**: 1631-1636.

Elespuru, RK, Lijinsky W (1976). "Mutagenicity of Cyclic Nitrosamines in Escherichia coli following Activation with Rat Liver Microsomes " *Cancer Research* **36**: 4099-4101.

Enea O, Houngbossa K, Berton G (1972). "Chaleurs de protonation de la piperazine et de quelques-uns de ses derives." *Electrochimica Acta*. **17** (9): 1585-1594.

Ermatchkov V, Kamps APS, Speyer D, Maurer G (2006). "Solubility of carbon dioxide in aqueous solutions of piperazine in the low gas loading region." *Journal of Chemical and Engineering Data*. **51** (5): 1788-1796.

Frailie P, Rochelle GT, Chen X, Xu Q, Nguyen T (2011). "Modeling energy performance of aqueous methyldiethanolamine/piperazine for CO_2 capture". Presented at Trondheim CO_2 Capture, Transport, and Storage Conference., Trondheim, NO. June 14-16, 2011.

Freeman SA, Davis J, Rochelle GT (2010a). "Degradation of aqueous piperazine in carbon dioxide capture." *International Journal of Greenhouse Gas Control*. **4** (5): 756-761.

Freeman SA, Dugas R, VanWagener D, Nguyen T, Rochelle GT (2010b). "Carbon dioxide capture with concentrated, aqueous piperazine." *International Journal of Greenhouse Gas Control*. **4** (2): 119-124.

Freeman SA, Rochelle GT (2011). "Thermal Degradation of Piperazine and its Structural Analogs." *Energy Procedia*. **4**: 43-50.

Freeman SA, Rochelle GT (2011). "Density and Viscosity of Aqueous (Piperazine + Carbon Dioxide) Solutions." *Journal of Chemical and Engineering Data*. **56** (3): 574-581.

Fregert S, Dahlquist I, Gruvberger B (1984). "A Simple Method for the Detection of Formaldehyde." *Contact Dermatitis*. **10** (3): 132-134.

Girdler Corporation (1950). "Carbon Dioxide Absorbents." Contract No. 50023. Girdler Corporation, Gas Processing Division: Louisville, KY.

Goff GS. *Oxidative Degradation of Aqueous Monoethanolamine in CO_2 Capture Processes: Iron and Copper Catalysts, Inhibition, and O_2 Mass Transfer*. The University of Texas at Austin. Ph.D. Dissertation. 2005: 263.

Goff GS, Rochelle GT (2006). "Oxidation inhibitors for copper and iron catalyzed degradation of monoethanolamine in CO_2 capture processes." *Industrial & Engineering Chemistry Research*. **45** (8): 2513-2521.

Górski A, Kraśnicka AD (1987a). "Formation of oxalates and carbonates in the thermal decompositions of alkali metal formates." *Journal of Thermal Analysis*. **32**: 1895-1904.

Górski A, Kraśnicka AD (1987b). "The importance of CO_2^{2-} anion in the mechanism for the thermal decomposition of oxalates." *Journal of Thermal Analysis*. **32**: 1229-1241.

Gottlieb HE, Kotlyar V, Nudelman A (1997). "NMR Chemical Shifts of Common Laboratory Solvents as Trace Impurities." *Journal of Organic Chemistry*. **62**: 7512-7515.

Hall HK (1956). "Field and Inductive Effects on the Base Strengths of Amines." *Journal of the American Chemical Society*. **78** (11): 2570-2572.

Hall WD, Barron JG (1981). "Solving Gas Treating Problems - A Different Approach". Presented at Laurence Reid Gas Conditioning Conference, Norman, OK.

Hamborg ES, Derks PWJ, Kersten SRA, Niederer JPM, Versteeg GF (2008). "Diffusion coefficients of N_2O in aqueous piperazine solutions using the Taylor dispersion

technique from (293 to 333) K and (0.3 to 1.4) mol.dm(-3)." *Journal of Chemical and Engineering Data*. **53** (7): 1462-1466.

Hamborg ES, Versteeg GF (2009). "Dissociation Constants and Thermodynamic Properties of Amines and Alkanolamines from (293 to 353) K." *Journal of Chemical and Engineering Data*. **54** (4): 1318-1328.

Hetzer HB, Robinson RA, Bates RG (1968). "Dissociation Constants of Piperazinium Ion and Related Thermodynamic Quantities from 0 to 50°C." *Journal of Physical Chemistry*. **72** (6): 2081-2086.

Hilliard MD. *A Predictive Thermodynamic Model for an Aqueous Blend of Potassium Carbonate, Piperazine, and Monoethanolamine for Carbon Dioxide Capture from Flue Gas*. The University of Texas at Austin. Ph.D. Dissertation. 2008: 1083.

Hofmeyer BG, Scholten HG, Lloyd WG (1956). Contamination and corrosion in monoethanolamine gas treating systems. National Meeting of the American Chemical Society. Dallas, TX.

Hoigné J, Bader H (1983). "Rate Constants of Reactions of Ozone with Organic and Inorganic-Compounds in Water - II: Dissociating Organic-Compounds." *Water Research*. **17** (2): 185-194.

Holub PE, Critchfield JE, Su W-Y (1998). "Amine Degradation Chemistry in CO_2 Service". Presented at Laurence Reid Gas Conditioning Conference, Norman, OK.

Horrom BW, Freifelder M, Stone GR (1954). "1-Formylpiperazine and Related Compounds." *Journal of the American Chemical Society*. **77**: 753-754.

Hull LA, Davis GT, Rosenblatt DH (1969a). "Oxidations of Amines .IX. Correlation of Rate Constants for Reversible One-Electron Transfer in Amine Oxidation with Reactant Potentials." *Journal of the American Chemical Society*. **91** (23): 6247-&.

Hull LA, Davis GT, Rosenblatt DH (1969b). "Oxidations of Amines. IX. Correlation of Rate Constants for Reversible One-Electron Transfer in Amine Oxidation with Reactants Potentials." *Journal of the American Chemical Society*. **91**: 6247.

Hull LA, Davis GT, Rosenblatt DH, Mann CK (1969c). "Oxidations of Amines. VII. Chemical and Electrochemical Correlations." *Journal of Physical Chemistry*. **73** (7): 2142-&.

Hull LA, Davis GT, Rosenblatt DH, Williams HKR, Weglein RC (1967). "Oxidations of Amines. III. Duality of Mechanism in the Reaction of Amines with Chlorine Dioxide." *Journal of the American Chemical Society*. **89**: 1163.

Hull LA, Giordano WP, Rosenblatt DH, Davis GT, Mann CK, Milliken SB (1969d). "Oxidations of Amines. VIII. Role of Cation Radical in Oxidation of Triethylenediamine by Chlorine Dioxide and Hypochlorous Acid." *Journal of Physical Chemistry*. **73** (7): 2147-&.

Huntsman Corporation (2005). "Diglycolamine® Agent - Product Information." Huntsman Corporation: The Woodlands, TX.

Iovu H, Teodorescu M, Calinescu I (1994). "New Compounds Obtained by Condensation of Piperazine with Formaldehyde." *Revue Roumaine De Chimie*. **39** (6): 653-657.

IPCC (2001). "Climate Change 2001: The Scientific Basis. Contribution of Working Group I to the Third Assessment Report of the Intergovernmental Panel on Climate Change." Cambridge University Press: Cambridge, United Kingdom.

Jones TL. *Oxidative degradation of piperazine in aqueous potassium carbonate*. The University of Texas at Austin. M. S. 2003:

Kennard ML, Melsen A (1985). "Mechanisms and Kinetics of Diethanolamine Degradation." *Industrial & Engineering Chemistry Fundamentals*. **24** (2): 129-140.

Khalili F, Henni A, East ALL (2009). "pK_a Values of Some Piperazines at (298, 303, 313, and 323) K." *Journal of Chemical and Engineering Data*. **54** (10): 2914-2917.

Khounlavong L, Ganesan V (2009). Influence of interfacial layers upon the barrier properties of polymer nanocomposites. *Journal of Chemical Physics*. **130**(10), article number 104901.

Khounlavong L, Pryamitsyn V, Ganesan V (2010). Many-body interactions and coarse-grained simulations of structure of nanoparticle-polymer melt mixtures. *Journal of Chemical Physics*. **133**(14), article number 144904.

Kim I (2008). Data Analysis for Reaction Calorimeter. Personal communication to S. A. Freeman.

Kim I, Svendsen HF (2007). "Heat of absorption of carbon dioxide (CO_2) in monoethanolamine (MEA) and 2-(Aminoethyl)ethanolamine (AEEA) solutions." *Industrial & Engineering Chemistry Research*, **46** (17):5803-5809.

Kim I, Svendsen HF, Borresen E (2008). "Ebulliometric Determination of Vapor-Liquid Equilibria for Pure Water, Monoethanolamine, N-Methyldiethanolamine, 3-(Methylamino)-propylamine, and Their Binary and Ternary Solutions." *Journal of Chemical and Engineering Data*. **53** (11): 2521-2531.

Kleinbaum DG, Kupper LL, Muller KE (1988). Applied Regression Analysis and Other Multivariable Methods, 2nd Edition. Boston, BWS-KENT Publishing Company.

Koike L, Barone JS, Godinho OES, Aleixo LM, Reis FDM, Fernandes EC, Barbosa JB (1987). "N-Formyldiethanolamine - A New Artifact in Diethanolamine Solutions." *Chemistry & Industry*. (17): 626-627.

Lee YJ. *Oxidative Degradation of Organic Acids Conjugated with Sulfite Oxidation in Flue Gas Desulfurization*. The University of Texas at Austin. Ph.D. Dissertation. 1986: 170.

Lepaumier H, Martin S, Picq D, Delfort B, Carrette PL (2010). "New Amines for CO_2 Capture. III. Effect of Alkyl Chain Length between Amine Functions on Polyamines Degradation." *Industrial & Engineering Chemistry Research*. **49** (10): 4553-4560.

Lepaumier H, Picq D, Carrette P-L (2009a). "New Amines for CO_2 Capture. I. Mechanisms of Amine Degradation in the Presence of CO_2." *Industrial & Engineering Chemistry Research*. **48**: 9061-9067.

Lepaumier H, Picq D, Carrette P-L (2009b). "New Amines for CO_2 Capture. II. Oxidative Degradation Mechanisms." *Industrial & Engineering Chemistry Research*. **48**: 9068-9075.

Liu H-B, Zhang C-F, Xu G-W (1999). "A Study on Equilibrium Solubility for Carbon Dioxide in Methyldiethanolamine-Piperazine-Water Solution." *Industrial & Engineering Chemistry Research*. **38** (10): 4032-4036.

Love, LA, Lijinsky W, Keefer L, Garcia H (1977). "Chronic oral administration of 1-nitrosopiperazine in high doses to MRC rats." *Zeitschrift Fur Krebsforschung*: 69-73.

Mago BF (1974). "Antimony-Vanadium Corrosion inhibitors for alkanolamine gas treating system." Union Carbide Corporation, New York, NY. US Patent 3,808,140.

Mago BF, West CW (1976). "Corrosion inhibitors for alkanolamine gas treating systems." Union Carbide Corporation, New York, NY. US Patent 3,959,170.

Mandal BP, Bandyopadhyay SS (2006). "Absorption of carbon dioxide into aqueous blends of 2-amino-2-methyl-1-propanol and monoethanolamine." *Chemical Engineering Science*. **61** (16): 5440-5447.

Mandal BP, Kundu M, Bandyopadhyay SS (2005). "Physical solubility and diffusivity of N_2O and CO_2 into aqueous solutions of (2-amino-2-methyl-1-propanol plus monoethanolamine) and (N-methyldiethanolamine plus monoethanolamine)." *Journal of Chemical and Engineering Data*. **50** (2): 352-358.

Mathonat C, Majer V, Mather AE, Grolier JPE (1998). "Use of flow calorimetry for determining enthalpies of absorption and the solubility of CO_2 in aqueous monoethanolamine solutions." *Industrial & Engineering Chemistry Research*, **37** (10):4136-4141.

McMurry J(2000). Organic Chemistry. Pacific Grove, Brooks/Cole.

Merck Corporation (2009). "MSDS Anhydrous Piperazine." Merck Corporation: Whitehouse Station, NJ.

Miksch RR, Anthon DW, Fanning LZ, Hollowell CD, Revzan K, Glanville J (1981). "Modified Pararosaniline Method for the Determination of Formaldehyde in Air." *Analytical Chemistry*. **53** (13): 2118-2123.

Mislyuk OA, Shibaev VI, Ponomareva RP, Vyunov KA (1985). "Decarboxylation of Piperazinium Monooxalate and Dioxalate." *Khimiya Geterotsiklicheskikh Soedinenii*. (6): 851-852.

Mouriquand G, Roman E, Coisnard J (1951). **32**: 189.

Muhammad A, Mutalib MIA, Murugesan T, Shafeeq A (2009). "Thermophysical Properties of Aqueous Piperazine and Aqueous (N-Methyldiethanolamine plus Piperazine) Solutions at Temperatures (298.15 to 338.15) K." *Journal of Chemical and Engineering Data*. **54** (8): 2317-2321.

Nguyen T, Hilliard MD, Rochelle GT (2010). "Amine volatility in CO_2 capture." *International Journal of Greenhouse Gas Control*. **4** (5): 707-715.

Nieh ECY (1983). "Vanadium-amine corrosion inhibitor system for sour gas conditioning solutions." Texaco Inc., White Plains, NY. US Patent 4,372,873.

Oyenekan BA, Rochelle GT (2009). "Rate modeling of CO_2 stripping from potassium carbonate promoted by piperazine." *International Journal of Greenhouse Gas Control*. **3** (2): 121-132.

Pagano JM, Golberg DE, Fernelius WC (1961). "A Thermodynamic Study of Homopiperazine, Piperazine, and N-(2-Aminoethyl)-Piperazine and their Complexes with Copper (II) Ion." *Journal of Physical Chemistry*. **65**: 1062-1064.

Paul S, Mandal B (2006a). "Density and viscosity of aqueous solutions of (2-piperidineethanol plus piperazine) from (288 to 333) K and surface tension of aqueous solutions of (N-methyldiethanolamine plus piperazine), (2-amino-2-methyl-1-propanol plus piperazine), and (2-piperidineethanol plus piperazine) from (293 to 323) K." *Journal of Chemical and Engineering Data*. **51** (6): 2242-2245.

Paul S, Mandal B (2006b). "Density and viscosity of aqueous solutions of (N-methyldiethanolamine plus piperazine) and (2-amino-2-methyl-1-propanol plus piperazine) from (288 to 333) K." *Journal of Chemical and Engineering Data*. **51** (5): 1808-1810.

Pearce RL (1984). "Process for Removal of Carbon Dioxide from Industrial Gases." The Dow Chemical Company, Midland, MI. US Patent 4,440,731.

Perrin DD(1965). Dissociation constants of organic bases in aqueous solution. London, Buttersworth.

Perry RH, Green DW (1997). Perry's Chemical Engineers' Handbook. New York, McGraw-Hill.

Pietsch J, Sacher F, Schmidt W, Brauch HJ (2001). "Polar nitrogen compounds and their behavior in the drinking water treatment process." *Water Research*. **35** (15): 3537-3544.

Plaza JM, Chen E, Rochelle GT (2009). "Absorber intercooling in CO_2 absorption by piperazine-promoted potassium carbonate." *AIChE Journal*. **56** (4): 905-914.

Plaza JM, Rochelle G (2010). "Modeling pilot plant results for CO_2 capture by aqueous piperazine." *Energy Procedia*. **4**: 1593-1600.

Ranney MW (1976). "Corrosion Inhibitors - Manufacture and Technology." Noyes Data Corporation: Park Ridge, NJ.

Reed RM (1945). "Stabilization of Monoethanolamine Solutions." The Girdler Corporation, Louisville, KY. US Patent 2,377,966.

Reza J, Trejo A (2006). "Degradation of aqueous solutions of alkanolamine blends at high temperature, under the presence of CO_2 and H_2S." *Chemical Engineering Communications*. **193** (1): 129-138.

Rochelle GT (2009). "Amine Scrubbing for CO_2 Capture." *Science*. **325** (5948): 1652-1654.

Rochelle GT (2009a). "CO_2 Capture by Aqueous Absorption, First Quarterly Progress Report 2009." Luminant Carbon Management Program. The University of Texas at Austin.

Rochelle GT (2009b). "CO_2 Capture by Aqueous Absorption, Second Quarterly Progress Report 2009." Luminant Carbon Management Program. The University of Texas at Austin.

Rochelle GT (2010a). "CO_2 Capture by Aqueous Absorption, First Quarterly Progress Report 2010." Luminant Carbon Management Program. The University of Texas at Austin.

Rochelle GT (2010b). "CO_2 Capture by Aqueous Absorption, Third Quarterly Progress Report 2010." Luminant Carbon Management Program. The University of Texas at Austin.

Rochelle GT (2011). "CO_2 Capture by Aqueous Absorption, Fourth Quarterly Progress Report 2010." Luminant Carbon Management Program. The University of Texas at Austin.

Rochelle GT (2001). "Research Needs for CO_2 Capture from Flue Gas by Aqueous Absorption/Stripping." DE-AF26-99FT01029.

Rochelle GT, Freeman SA, Chen X, Nguyen T, Rafique H (2010). "CO_2 Scrubbing by a soluble amine blend." Patent disclosure filed August 2010.

Ronalter M (2009). UT Chemistry Department Glass Shop. Personal communication to S. A. Freeman.

Rooney PC, DuPart MS, Bacon TR (1998). "Oxygen's role in alkanolamine degradation." *Hydrocarbon Processing*. **77** (7): 109-113.

Rosenblatt DH, Albert J. Hayes J, Harrison BL, Streaty RA, Moore KA (1963). "The Reaction of Chlorine Dioxide with Triethylamine in Aqueous Solution." *Journal of Organic Chemistry*. **28**: 2790-2794.

Rosenblatt DH, Davis GT, Hull LA, Forberg GD (1968). "Oxidations of Amines. V. Duality of Mechanism in Reactions of Aliphatic Amines with Permanganate." *Journal of Organic Chemistry*. **33** (4): 1649.

Rosenblatt DH, Deme MM, Davis GT (1972). "Oxidations of Amines .XI. Kinetics of Fragmentation of Triethylenediamine Chlorammonium Cation in Aqueous-Solution." *Journal of Organic Chemistry*. **37** (25): 4148-4151.

Rosenblatt DH, Hull LA, Deluca DC, Davis GT, Weglein RC, Williams HK (1967). "Oxidations of Amines. II. Substituent Effects in Chlorine Dioxide Oxidations." *Journal of the American Chemical Society*. **89** (5): 1158-&.

Samanta A, Bandyopadhyay SS (2006). "Density and viscosity of aqueous solutions of piperazine and (2-amino-2-methyl-1-propanol + piperazine) from 298 to 333 K." *Journal of Chemical and Engineering Data*. **51** (2): 467-470.

Samanta A, Bandyopadhyay SS (2009). "Absorption of carbon dioxide into aqueous solutions of piperazine activated 2-amino-2-methyl-1-propanol." *Chemical Engineering Science*. **64** (6): 1185-1194.

Samanta A, Roy S, Bandyopadhyay SS (2007). "Physical solubility and diffusivity of N_2O and CO_2 in aqueous solutions of piperazine and (N-methyldiethanolamine plus piperazine)." *Journal of Chemical and Engineering Data*. **52** (4): 1381-1385.

Sandler SR, Delgado ML (1969). "Reinvestigation of Reaction of Piperazine with Aldehydes." *Journal of Polymer Science Part A-1: Polymer Chemistry*. **7** (5): 1373-1378.

Scheiman MA (1962). "A review of monoethanolamine chemistry." Report No. 5746. U. S. Naval Research Laboratory.

Searles S, Tamres M, Block F, Quarterman LA (1956). "Hydrogen Bonding and Basicity of Cyclic Imines." *Journal of the American Chemical Society*. **78**: 4917-4920.

Sexton AJ. *Amine Oxidation in CO_2 Capture Processes*. The University of Texas at Austin. Ph.D. Dissertation. 2008: 262.

Sexton AJ, Rochelle GT (2009a). "Catalysts and inhibitors for MEA oxidation." *Energy Procedia*. **1** (1): 1179-1185.

Sexton AJ, Rochelle GT (2009b). "Catalysts and Inhibitors for Oxidative Degradation of Monoethanolamine " *International Journal of Greenhouse Gas Control*. **3** (6): 704-711.

Sexton AJ, Rochelle GT (2009c). "Reaction Products from the Oxidative Degradation of Monoethanolamine." *Industrial & Engineering Chemistry Research*. **In print**.

Smith JM, Van Ness HC, Abbott M (1995). Introduction to Chemical Engineering Thermodynamics. New York, McGraw-Hill.

St.Clair JH, Simister WF (1983). "Process to remove carbon dioxide from flue gas gets first large-scale tryout in Texas." *Oil & Gas Journal*. **81** (6): 109-110.

Sun WC, Yong CB, Li MH (2005). "Kinetics of the absorption of carbon dioxide into mixed aqueous solutions of 2-amino-2-methyl-l-propanol and piperazine." *Chemical Engineering Science*. **60** (2): 503-516.

Tester JW, Modell M (1997). Thermodynamics and Its Applications. Upper Saddle River, Prentice Hall PTR.

Thabaj KA, Kulkarni SD, Chimatadar SA, Nandibewoor ST (2007). "Oxidative transformation of ciprofloxacin by alkaline permanganate - A kinetic and mechanistic study." *Polyhedron*. **26** (17): 4877-4885.

The Dow Chemical Company (2001). "Ethyleneamines." The Dow Chemical Company: Midland, MI.

Thieleman T, Schmidt S, Gerling JP (2007). "Lignite and hard coal: Energy suppliers for world needs until the year 2100." *International Journal of Coal Geology*. **72** (1): 1-14.

Thitakamol B, Veawab A (2007). "Foaming Behavior in CO_2 Absorption Process Using Aqueous Solutions of Single and Blended Alkanolamines." *Industrial & Engineering Chemistry Research*. **47**: 216-225.

Tricker, AR, Kumar R, Siddiqi M, Khuroo MS, Preussmann R (1991). "Endogenous formation of N-nitrosamines from piperazine and their urinary excretion following antihelmintic treatment with piperazine citrate " *Carcinogenesis* **12** (9): 1595-1599.

Tsai RE, Seibert AF, Eldridge RB, Rochelle GT (2011). A dimensionless model for predicting the mass-transfer area of structured packing. *AIChE Journal*. **57**(5): 1173-1184.

Tsai RE, Schultheiss P, Kettner A, Lewis JC, Seibert AF, Eldridge RB, Rochelle GT (2008). Influence of surface tension on effective packing area. *Industrial & Engineering Chemistry Researc*h. **47**(4): 1253-1260.

Ukraintsev VB, Krasnov BA (1997). "Initiation of piperazine cycle formation through formaldehyde due to its interaction with N-(2-aminoethyl)aziridine and N-(2-halogenoethyl)ethylenediamine nickel(II) complexes." *Zhurnal Obshchei Khimii*. **67** (1): 134-137.

VanWagener D, Rochelle GT (2011). "Stripper configurations for CO_2 capture by aqueous monoethanolamine." *Chemical Engineering Research and Design*. **In print**.

Vevelstad S (2010). "Thermal Degradation of 3-(Methylamino)propylamine (MAPA)."

Voice AK (2010). Identification of mono-oxalyl MEA compound on anion IC chromatogram. Personal communication to S. Freeman.

Wallin J, Storey S (2010). NMR Measurements. Personal communication to

Watts S (2005). "A coal-dependent future?" BBC News Corporation Retrieved October 1, 2008, from http://news.bbc.co.uk/2/hi/programmes/newsnight/4330469.stm.

Weiland RH, Dingman JC, Cronin DB, Browning GJ (1998). "Density and viscosity of some partially carbonated aqueous alkanolamine solutions and their blends." *Journal of Chemical and Engineering Data*. **43** (3): 378-382.

White RHR, Standen OD (1953). "Piperazine in the Treatment of Threadworms in Children." *British Medical Journal*. **2** (4839): 755-757.

Xu GW, Zhang CF, Qin SJ, Wang YW (1992). "Kinetics Study on Absorption of Carbon-Dioxide into Solutions of Activated Methyldiethanolamine." *Industrial & Engineering Chemistry Research*. **31** (3): 921-927.

Xu Q (2008). XRD analysis of rich loaded PZ precipitation. Personal communication to S. A. Freeman.

Xu Q, Rochelle GT (2011). "Pressure and CO_2 Solubility at High Temperature in Aqueous Amines." *Energy Procedia*. **4**: 117-124.

Yang Z-Y, Soriano AN, Caparanga AR, Li M-H (2010). "Equilibrium solubility of carbon dioxide in (2-amino-2-methyl-1-propanol + piperazine + water)." *Journal of Chemical Thermodynamics*. **42** (5): 659-665.

Zhang X, Zhang CF, Qin SJ, Zheng ZS (2001). "A kinetics study on the absorption of carbon dioxide into a mixed aqueous solution of methyldiethanolamine and piperazine." *Industrial & Engineering Chemistry Research*. **40** (17): 3785-3791.

Zhou S, Chen X, Nguyen T, Voice Alexander K, Rochelle GT (2010). "Aqueous Ethylenediamine for CO_2 Capture." *ChemSusChem*. **3** (8): 913-918.

Vita

Stephanie Anne Freeman was born in Phoenix, AZ and graduated from Centennial High School in Peoria, AZ, in May of 2001. She entered The University of Arizona in the fall of 2001 to pursue a degree in chemical engineering. The author spent the fall of 2004 doing research abroad at Wageningen University in Wageningen, The Netherlands. Upon returning to the US, she completed her degree and graduated in December of 2005 with a B. S. in chemical engineering with an emphasis in environmental engineering and a minor in chemistry. Ms. Freeman then returned to Wageningen University to continue prior research efforts. During her undergraduate education, she worked with ExxonMobil in Houston, TX, and Joliet, IL, and Idaho National Laboratory in Idaho Falls, ID. In September of 2006, she entered the master's program at the Massachusetts Institute of Technology in Cambridge, MA. In September of 2007, Ms. Freeman completed her M. S. in chemical engineering practice with internships at Cabot Corporation in Billerica, MA, and Novartis Pharmaceuticals in East Hanover, NJ. She entered the graduate chemical engineering program at The University of Texas at Austin in September of 2007. She spent June of 2009 at the laboratories of Prof. Hallvard Svendsen at the Norges Teknisk-Naturvitenskapelige Universitet (Norwegian University of Science and Technology, NTNU) in Trondheim, Norway.

Permanent email: stephanie.a.freeman@gmail.com

This dissertation was typed by the author.